#7

PROBABILISTIC SEISMIC HAZARD ANALYSES FOR FAULT DISPLACEMENT AND VIBRATORY GROUND MOTION AT YUCCA MOUNTAIN, NEVADA

FINAL REPORT
VOLUME 1
TEXT

Prepared for the U.S. Geological Survey

by the

Civilian Radioactive Waste Management System
Management & Operating Contractor

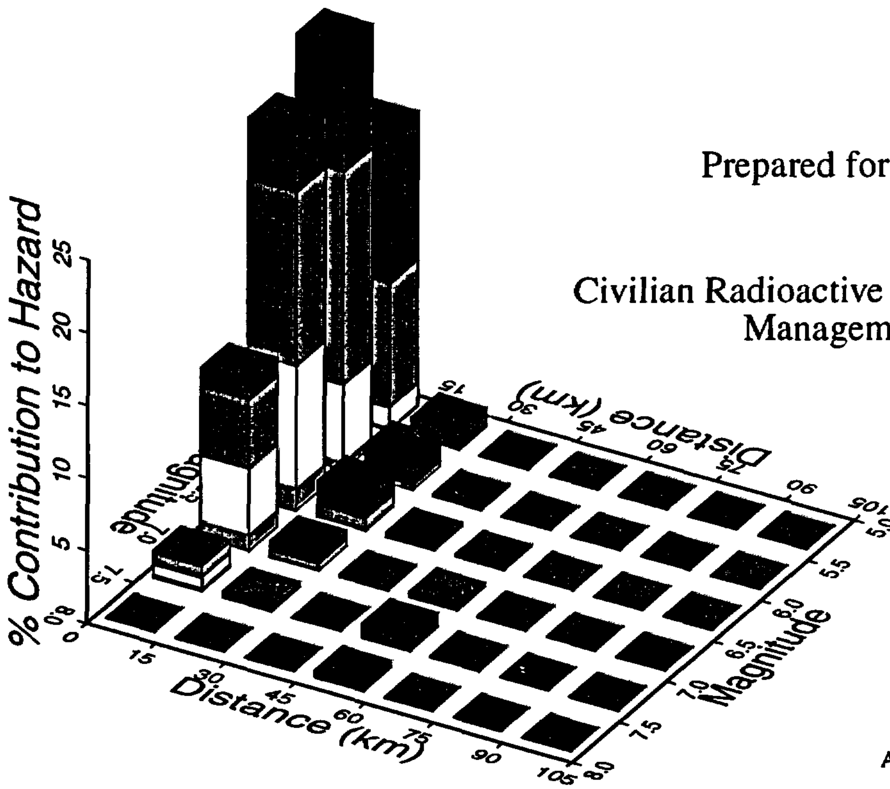

Ivan G. Wong and J. Carl Stepp
Report Coordinators

A report to the U.S. Department of Energy
that fulfills Level 3 Milestone SP32IM3
WBS Number 1.2.3.2.8.3.6

Prepared in cooperation with the U.S. Department of Energy
under Interagency Agreement DE-AI08-92NV 10874
Contract DE-AC04-94AL85000

Oakland, California
23 February 1998

PDF 03 1/ 102 WM-11

DRAFT DISCLAIMER

This contractor document was prepared for the U.S. Department of Energy (DOE), but has not undergone programmatic, policy, or publication review, and is provided for information only. The document provides preliminary information that may change based on new information or analysis, and is not intended for publication or wide distribution; it is a lower level contractor document that may or may not directly contribute to a published DOE report. Although this document has undergone technical reviews at the contractor organization, it has not undergone a DOE policy review. Therefore, the views and opinions of authors expressed do not necessarily state or reflect those of the DOE. However, in the interest of the rapid transfer of information, we are providing this document for your information.

PROBABILISTIC SEISMIC HAZARD ANALYSES FOR FAULT DISPLACEMENT AND VIBRATORY GROUND MOTION AT YUCCA MOUNTAIN, NEVADA

FINAL REPORT
VOLUME 1 TEXT

Prepared for the

U.S. Geological Survey

by the

Civilian Radioactive Waste Management System
Management & Operating Contractor

Ivan G. Wong and J. Carl Stepp
Report Coordinators

A report to the U.S. Department of Energy
that fulfills Level 3 Milestone SP32IM3
WBS Number 1.2.3.2.8.3.6

Prepared in cooperation with the
U.S. Department of Energy under
Interagency Agreement DE-AI08-92NV10874
Contract DE-AC04-94AL85000

Oakland, California
23 February 1998

PROBABILISTIC SEISMIC HAZARD ANALYSIS (PSHA)
FINAL REPORT

TABLE OF CONTENTS

TABLE OF CONTENTS (Continued)

TABLE OF CONTENTS (Continued)

TABLE OF CONTENTS (Continued)

TABLE OF CONTENTS (Continued)

LIST OF APPENDICES

TABLE OF CONTENTS (Continued)

TABLE OF CONTENTS (Continued)

LIST OF TABLES (Follow Sections)

TABLE OF CONTENTS (Continued)

TABLE OF CONTENTS (Continued)

LIST OF FIGURES (Follow Sections)

LIST OF ACRONYMS

AAR	Arabasz, Anderson, Ramelli team
ASM	Ake, Slemmons, McCalpin team
CNWRA	Center for Nuclear Waste Regulatory Analysis
CRWMS	Civilian Radioactive Waste Management System
DOE	U.S. Department of Energy
DSR	Doser, Fridrich, Swan team
EPRI	Electric Power Research Institute
ESF	Exploratory Studies Facility
GM	Ground Motion
IAEA	International Atomic Energy Agency
M_{max}	maximum magnitude
M_w	moment magnitude
M&O	Management and Operating (Contractor)
NRC	U.S. Nuclear Regulatory Commission
NTS	Nevada Test Site
PGA	peak ground acceleration
PSHA	Probabilistic Seismic Hazard Analyses
QA	quality assurance
QARD	Quality Assurance Requirements and Description
RVT	Random Vibration Theory
RYA	Rogers, Yount, Anderson team
SBK	Smith, Bruhn, Knuepfer team
SDO	Smith, de Polo, O'Leary team
SSCs	structures, systems, and components
SSFD	Seismic Source and Fault Displacement
SSHAC	Senior Seismic Hazard Analysis Committee
UHS	uniform hazard spectrum
UNE	underground nuclear explosion
USBR	U.S. Bureau of Reclamation
USGS	U.S. Geological Survey
WCFS	Woodward-Clyde Federal Services

ACKNOWLEDGMENTS

This technical report is the result of many individuals' efforts over the past three plus years beginning in August 1994. We would like to acknowledge the many contributions of the Project participants described in Chapter 1 whose hard work and conscientious efforts are reflected in this report. Many individuals provided us tremendous support in the performance of the project, particularly in the workshop logistics and preparation of the Activity and Final Reports. In particular, we would like to express our gratitude to Sue Penn of Woodward-Clyde Federal Services (WCFS) and Kathryn Hanson and Nancy Iacono of Geomatrix Consultants, Inc. Other individuals who provided valuable assistance included Tom Statton, Jacqueline Bott, Anna Sojourner, Doug Wright, Rein Dillon, Sadako McInerney, Fumiko Goss, Ron Goss, Melinda Lee, Rachel Griener, and Roger Ocampo of WCFS; Nick Gregor, consultant, Patricia Sheaffer, Martha Mustard, Bruce Parks, John Stuckless, Tom Chaney, and Dan Soeder of the U.S. Geological Survey; Robin McGuire, John Vlasity, and Katherine Morgan of Risk Engineering, Inc., John Savino of Golder Associates, and John Stamatakos of the CNWRA.

This project was performed under the auspices of the U.S. Geological Survey with support from the Civilian Radioactive Waste Management System Management and Operating Contractor TRW Environmental Safety Systems, Inc. and DOE under contract DE-AC04-94AL85000. Special thanks to Tim Sullivan of DOE for his advice, guidance, and most of all, patience.

John Whitney
Carl Stepp
Ivan Wong
Richard Quittmeyer

As part of the U.S. Department of Energy's (DOE) evaluation of Yucca Mountain as a potential geologic repository for spent nuclear fuel and high-level radioactive waste, two projects related to the repository's seismic performance have been performed: (1) probabilistic seismic hazard analyses (PSHA) and (2) the development of seismic design basis parameters. The U.S. Geological Survey (USGS) has been assigned the primary responsibility for the PSHA Project and Woodward-Clyde Federal Services (WCFS), a member of the Civilian Radioactive Waste Management System (CRWMS) Management and Operating (M&O) Team, has been assigned the task to manage the project. This report describes the PSHA Project. The determination of seismic design basis values is being conducted by the Seismic Design Basis Team under contract to the CRWMS M&O.

The PSHA Project was performed in three strongly integrated parallel activities leading to the determination of fault displacement and vibratory ground motion hazards that form the basis for development of seismic design basis inputs for the Yucca Mountain repository structures, systems, and components (SSCs) and to a full documentation of the technical bases for these determinations. Seismic design basis covers surface and subsurface SSCs. Both the preclosure and postclosure performance periods of the repository (100 and up to 100,000 years, respectively) were addressed in the project. The PSHA results form the basis for developing seismic design basis inputs for the potential repository and support an assessment of the potential repository's long-term performance with respect to waste containment and isolation.

The activities performed were (1) evaluation and characterization of relevant seismic sources including the characterization of potential fault displacement; (2) evaluation and characterization of vibratory ground motion attenuation, including earthquake source, wave propagation path, and rock site effects; and (3) the performance of PSHAs for both fault displacement and vibratory ground motion. The results are in the form of hazard curves that express the annual frequencies with which various levels of fault displacement at locations within the Controlled Area and vibratory ground motion at a reference rock outcrop are estimated to be exceeded. The reference rock outcrop is at the ground surface but at a location at the same elevation of the repository.

The hazard analyses are based on evaluations of seismic source characteristics, earthquake ground motions, and fault displacement that reflect interpretations of different scientific hypotheses and models using available data. These interpretations include uncertainties due to the inability of data to resolve different hypotheses and models. To evaluate scientific uncertainty, seismic source and fault displacement characterizations have been made by six teams composed of three experts each, who in composite are expert in the seismicity, paleoseismology, and regional tectonics and geology of the Yucca Mountain site and region. Ground motion assessments have been made by seven individuals expert in evaluating the generation and attenuation of earthquake ground motions. Interpretations for hazard assessment have been coordinated and facilitated through a series of workshops, direct elicitation meetings, and a feedback process conducted by two facilitation teams.

The Cornell-McGuire PSHA methodology coupled with a logic tree approach was used in the project resulting in uncertainties being propagated through the hazard calculations. The hazard results are presented as mean, median, and fractile hazard curves representing the total uncertainty in input interpretations.

Seismic Sources. Two basic types of seismic sources were considered by the seismic source and fault displacement (SSFD) experts: fault-specific sources and areal source zones. The latter represent areas of distributed seismicity that are not apparently associated with known specific faults. The faults were characterized in terms of probability of activity, their geographic locations, rupture lengths, sense of slip, fault dips, and maximum depth. The geometric characterization depended on the tectonic model(s) adopted by the experts. The approach used to evaluate the maximum earthquake for fault-specific sources (maximum magnitude [M_{max}]) was generally based on empirical relationships between magnitude and the maximum rupture dimensions (e.g., surface rupture length, rupture area, and maximum and average displacement.) Recurrence for the faults was described through the use of either recurrence intervals and/or slip rates. Four recurrence models were considered to characterize the magnitude distributions for faults including the characteristic, truncated exponential, modified truncated exponential, and maximum moment.

Regional faults were treated in a similar fashion by all SSFD expert teams. Regional faults are those faults within about 100 km that were considered to be capable of generating earthquakes of moment magnitude (M_w) 5 or greater based primarily on fault length and histories of multiple surface-rupturing earthquakes in the Quaternary. The number of regional faults included as seismic sources by teams ranged from 11 to 36. This reflects the teams' evaluations regarding the activity of various faults. All teams modeled the regional faults as planar faults to maximum seismogenic depths with generalized dips depending on the style of faulting (90° for strike-slip faults, 60° or 65° for normal-slip faults). Alternative fault lengths were included to express uncertainty in their mapped lengths.

Alternative faulting behavior and structural models were interpreted by the SSFD expert teams to capture the range of complex rupture patterns and fault interactions in the characterization of local faults. A planar-fault block model is preferred by most teams, with linkages along strike or coalescence down dip considered by all teams. Simultaneous rupture of multiple faults was included in all of the teams' interpretations. Some teams considered detachment models to constrain the extent and geometry of the local faults while others included the detachment as being itself seismogenic.

The possibility that dextral shear is being accommodated by a buried strike-slip fault in the Yucca Mountain region was considered by all teams. Several teams included a regional buried strike-slip fault source with low probability while other teams included throughgoing regional dextral shear zones.

Seismicity related to volcanic processes, particularly earthquakes related to basaltic volcanoes and dike-injection, was explicitly modeled in volcanic source zones by only two teams. Volcanic-related earthquakes were not modeled as a separate source by the other teams, but owing to the low magnitude and frequency of volcanic-related seismicity, were accounted for by the areal source zones.

The areal source zones required definition of their boundaries, and assessments of M_{max} and recurrence. The areal zones corresponded to seismotectonic areas or regions defined by the experts. The M_{max} distributions for the areal zones represent uncertainty in the largest random

earthquake in the region (associated with the minimum threshold for surface faulting) and/or estimated for a geologic structure that was not explicitly included as a fault-specific seismic source. Earthquake recurrence for the areal zones was derived from the historical seismicity record. Several alternative historical catalogues, which were provided to the SSFD expert teams, were evaluated for incompleteness, dependent events removed, and underground nuclear explosions and other forms of blasting identified.

Different areal source zones were defined by the experts. Several teams defined a site area or zone representing the area where most detailed investigations have been conducted and the inventory of fault sources is more complete. All teams used the truncated exponential recurrence model to estimate earthquake recurrence rates within the areal source zones. Varying treatments of the background seismicity included (1) uniform smoothing of seismicity and (2) nonuniform smoothing using Gaussian kernels having different smoothing distances.

Ground Motion Attenuation. The ground motion (GM) experts estimated median ground motion, aleatory uncertainty, and associated epistemic uncertainties for a matrix of earthquake magnitudes, source-to-site distances, and faulting styles and for a suite of spectral frequencies. These estimates were based on empirical and numerical simulation-based models and combinations of conversion factors. The matrix of point estimates consisted of 51 combinations of parameters, which was judged to adequately define attenuation for the seismic sources considered by the SSFD expert teams. The matrix covered the range from M_w 5.0 to 8.0, distances from 1 to 160 km, and strike-slip and normal faulting (both hanging wall and footwall). The range of frequencies for which ground motion was evaluated spans the range of interest for all SSCs: 20, 10, 5, 2, 1, 0.5, and 0.3 Hz plus peak ground acceleration (PGA) and peak ground velocity.

The GM experts' point estimates were parameterized by attenuation relations. The regression analysis to develop the attenuation relations was performed by the GM Facilitation Team. Each GM expert defined the distance measure used in the regression analyses for his/her point estimates. They chose whether the footwall and hanging wall point estimates were regressed together, resulting in a single normal faulting attenuation equation, or separately, yielding

separate models for sites on the hanging wall and footwall. In addition, the experts constrained the degree of magnitude saturation at close distances. The GM experts also considered two special cases, multiple parallel fault rupture and a shallow detachment fault, and developed scaling rules to apply to their models to represent these seismic sources.

Vibratory Ground Motion Hazard Results. Based on equally weighted inputs from the six SSFD expert teams and the seven GM experts, the probabilistic hazard for vibratory ground motion was calculated for PGA and spectral accelerations at frequencies of 0.3, 0.5, 1, 2, 5, 10, and 20 Hz and are expressed in terms of hazard curves. The hazard is also expressed in terms of uniform hazard spectra. PGA, 0.3, and 1.0 Hz values are summarized below for the annual exceedance probabilities of 10^{-3} and 10^{-4}. The largest source of epistemic uncertainty in the hazard results is due to the epistemic uncertainty in the ground motion characterization.

Frequency	Horizontal (g)		Vertical (g)	
(Hz)	10^{-3}	10^{-4}	10^{-3}	10^{-4}
PGA	0.169	0.534	0.112	0.391
0.3	0.051	0.168	0.029	0.105
1.0	0.162	0.471	0.073	0.222

Deaggregation of the mean hazard for an annual exceedance probability of 10^{-4} shows that at 5 to 10 Hz (or other high frequencies) ground motions are dominated by earthquakes of smaller than M_w 6.5 occurring at distances less than 15 km. Dominant events for low-frequency ground motions, such as at 1 to 2 Hz, display a bimodal distribution including large nearby events and M_w 7 and larger earthquakes beyond distances of 50 km. The latter contribution is due mainly to the relatively higher activity rates for the Death Valley, Furnace Creek, and Fish Lake Valley faults.

Vibratory Ground Motion Sensitivity Results. Extensive evaluations of parametric sensitivities were performed. The recurrence approach (either slip rates or recurrence intervals) and recurrence model (e.g., characteristic, exponential, or maximum moment) are the parameters that contribute the most to uncertainty in the ground motion hazard, at the design basis hazard: 10^{-3} and 10^{-4} per year. M_{max} has a small effect on uncertainty especially for 10

Hz, because a large fraction of the hazard at this frequency comes from more frequent moderate-magnitude events. Geometric fault parameters (e.g., rupture lengths, dips, maximum depths) are minor contributors to uncertainty. These parameters have a moderate effect on the locations of earthquakes and on M_{max}, but do not affect earthquake recurrence. Although the SSFD expert teams results vary somewhat, the dominant sources for seismic hazard at 10 Hz ground motions are the Paintbrush Canyon-Iron Ridge faults, the Solitario Canyon fault (or coalesced fault systems including these two faults), and the host areal seismic source zone. For 1 Hz ground motions, the dominant seismic sources are the Death Valley-Furnace Creek fault system and the same three sources mentioned above. Multiple-rupture interpretations of the type with comparable seismic moment release on more than one fault (i.e., those requiring modification of the attenuation equations) make a small contribution to the total hazard. Buried strike-slip faults, volcanic seismicity, and seismogenic detachments contribute negligibly to the total hazard.

The major contributor to epistemic uncertainty in the ground motion hazard is the expert's epistemic uncertainty in ground motion amplitude (within-expert epistemic uncertainty). Additional contributions to epistemic uncertainty arise from moderate differences among the SSFD expert teams and among the GM experts as well as expand from the uncertainties expressed by the seismic source logic trees.

Fault Displacement Characterization. Several original approaches to characterize the fault displacement potential were developed by the SSFD expert teams based primarily on empirical observations of the pattern of faulting at the site during past earthquakes determined from data collected during fault studies at Yucca Mountain. Empirical data were fit by statistical models to allow use by the experts.

The potential for fault displacement was categorized as either principal or distributed faulting. Principal faulting is the faulting along the main plane (or planes) of crustal weakness responsible for the release of seismic energy during the earthquake. Where the principal fault rupture extends to the surface, it may be represented by displacement along a single narrow trace or over a zone that is a few to many meters wide. Distributed faulting is defined as rupture that occurs on other faults in the vicinity of the principal rupture in

response to the principal displacement. It is expected that distributed faulting will be discontinuous in nature and occur over a zone that may extend outward several tens of meters to many kilometers from the principal rupture. A fault that can produce principal rupture may also undergo distributed faulting in response to principal rupture on other faults.

Both principal and distributed faulting are important to the assessment of the fault displacement hazard at the Yucca Mountain site. Nine locations within the Controlled Area were identified to demonstrate the fault displacement methodology. Two of the nine sites each had four identified faulting conditions. These locations were chosen to represent the range of potential faulting conditions. Some of these locations lie on faults that may experience both principal faulting and distributed faulting. The other points are sites only of potential distributed faulting.

The basic formulation for the probabilistic evaluation of fault displacement hazard is analogous to that for the ground shaking hazard. The hazard is represented probabilistically by a displacement hazard curve that is analogous to ground motion hazard curves. Thus, the hazard curve is a plot of the frequency of exceeding a fault displacement value d, designated by $\nu(d)$. This frequency can be computed by the expression $\nu(d) = \lambda_{DE} \cdot P(D > d)$ where λ_{DE} is the frequency at which displacement events occur on a feature at the site of interest, and $P(D>d)$ is the conditional probability that the displacement in a single event will exceed value d.

The approaches developed by the SSFD expert teams for characterizing the frequency of displacement events, λ_{DE}, can be divided into two categories: the *displacement approach* and the *earthquake approach*. The displacement approach provides an estimate of the frequency of displacement events directly from observed feature-specific or point-specific data. The earthquake approach involves relating the frequency of slip events to the frequency of earthquakes on the various seismic sources defined by the seismic source characterization models for the ground motion assessment. Both approaches are used for assessing the fault displacement hazard for principal faulting and distributed faulting.

The conditional probability of exceedance, $P(D>d)$, can be considered to contain two-parts: the variability of slip from event to event, and the variability of slip along strike during a single event. The teams developed several approaches for evaluating the distribution of slip at a location given a principal faulting event; others combine them into a single distribution function.

In aggregate, the six SSFD expert teams slightly preferred the displacement approach (aggregate weight ~ 0.6) over the earthquake approach for characterizing fault displacement. For characterizing principal faulting hazard, four of the teams considered only one approach for characterizing the faulting potential. Three of the teams considered only one approach for characterizing distributed faulting potential.

Principal faulting hazard was assessed for sites located on faults that the SSFD expert teams identified as being seismogenic. The preferred approach for estimating the frequency of displacement events is the use of slip rate divided by the average displacement per event. The slip rates were primarily based on the teams' seismic source characterization for the ground motion hazard assessment. The teams used a number of approaches to evaluate the conditional probability of exceedance. These are based on empirical distributions derived from Yucca Mountain trenching data normalized by various parameters, including the expected maximum displacement in the maximum event, the average displacement estimated from displacement data, and the average and maximum displacements estimated from the length of the feature.

To characterize the frequency of displacement events, the teams used the frequency of earthquakes developed for the ground motion hazard assessment multiplied by the conditional probability that an event produces surface rupture at the site of interest. The along-strike intersection probability was computed using the rupture length estimated from the magnitude of the event randomly located along the fault length. Most teams used an empirical model based on historical ruptures to compute the probability of surface rupture. The approach used by most of the teams to assess the conditional probability of exceedance was to define a distribution for the maximum displacement based either on the magnitude or the rupture length of the earthquake. This distribution is then convolved with a

distribution for the ratio of the displacement to the maximum displacement to compute $P(D > d)$.

The majority of the SSFD expert teams considered the frequency of displacement events on features subject to only distributed faulting to be estimated by slip rate divided by the average displacement per event. The slip rates were based on the cumulative displacement and slip history. The teams used similar approaches for evaluating the conditional probability of exceedance to those used in the displacement approach for characterizing principal faulting hazard. The empirical distributions used are correlated with the scaling relationship used to estimate the average displacement per event.

The SSFD expert teams displayed the most variability in characterizing distributed faulting potential using the earthquake approach. The basic assessment of the frequency of earthquakes was derived from the seismic source characterization for ground motion hazard assessment defined by each team. The probability that an earthquake causes slip at the point of interest was assessed in a variety of ways. Most teams utilized the logistic regression model based on analyses of the pattern of historical ruptures. The widest variations in approaches were those for assessing the distribution for displacement per event on the distributed ruptures.

All of the teams considered the points on the Bow Ridge and Solitario Canyon faults as subject to principal faulting hazard. A few teams also considered some potential for principal faulting hazard at two locations on two intrablock faults. The teams varied widely in their assessments of the probability that distributed faulting could occur in future earthquakes at points that are located off of the block-bounding faults. These assessment were based on fault orientation, cumulative slip, and structural relationship. Four teams considered that the probability of displacement at a point in intact rock due to the occurrence of a future earthquake is essentially zero.

Fault Displacement Hazard Results. The probabilistic fault displacement hazard was calculated at nine demonstration sites within the Controlled Area. Two of the sites have four hypothetical conditions representative of the features encountered within the ESF. The

integrated results provide a representation of fault displacement hazard and its uncertainty at the nine sites, based on the interpretations and parameters developed by the six SSFD expert teams. Separate results are obtained for each site in the form of summary hazard curves. The following table summarizes the mean displacement hazard results for the two design basis annual exceedance probabilities, 10^{-4} and 10^{-5}, at the nine demonstration sites.

MEAN DISPLACEMENT HAZARD AT NINE DEMONSTRATION SITES

		Mean Displacement (cm)	
		Annual Exceedance Probability	
Site	Location	10^{-4}	10^{-5}
1	Bow Ridge fault	<0.1	7.8
2	Solitario Canyon fault	<0.1	32
3	Drill Hole Wash fault	<0.1	<0.1
4	Ghost Dance fault	<0.1	<0.1
5	Sundance fault	<0.1	<0.1
6	Unnamed fault west of Dune Wash	<0.1	<0.1
7	100 m east of Solitario Canyon fault		
7a	2-m small fault	<0.1	<0.1
7b	10-cm shear	<0.1	<0.1
7c	fracture	<0.1	<0.1
7d	intact rock	<0.1	<0.1
8	Between Solitario Canyon and Ghost Dance faults		
8a	2-m small fault	<0.1	<0.1
8b	10-cm shear	<0.1	<0.1
8c	fracture	<0.1	<0.1
8d	intact rock	<0.1	<0.1
9	Midway Valley	<0.1	0.1

With the exception of the block-bounding Bow Ridge and Solitario Canyon faults at 10^{-5} annual exceedance probability, the mean displacements are all less than 0.1 cm. At 10^{-5} probability, the mean displacements are 7.8 and 32 cm, respectively for these two faults. Thus sites not located on a block-bounding fault such as sites on the intrablock faults, other small faults, shear fractures, and intact rock are estimated to have displacements significantly less than 0.1 cm for periods up to 100,000 years.

The fault displacement hazard results display significant uncertainty. This uncertainty is indicative of the state of practice in PSHA for fault displacement, which is less mature than PSHA for ground motions. Nonetheless, the results obtained here are considered robust by virtue of the extensive efforts at expert elicitation and feedback, as well as the methodological developments, that were undertaken as part of this study. Sites with the highest fault displacement hazard show uncertainties comparable to those obtained in ground motion PSHA. Sites with low hazard show much higher uncertainties.

There is also a not unexpected correlation between the amount of geologic data available at a site and the uncertainty in the calculated hazard at that site. For sites where there are significant geologic data, the team-to-team uncertainty is less than one order of magnitude. For sites for which there are little or no data, the individual team curves span three orders of magnitude. The larger uncertainty at these sites is considered to be due to data uncertainty, i.e., less certain constraints on the team's fault displacement characterization models.

1.0
INTRODUCTION

In accordance with the Nuclear Waste Policy Amendments Act of 1982, as amended, the U.S. Department of Energy (DOE) is charged with the responsibility of evaluating Yucca Mountain as a potential geologic repository to site the nation's first permanent disposal facility for spent nuclear fuel and high-level radioactive waste. As part of this effort, two projects related to the seismic performance of the repository have been carried out: (1) probabilistic seismic hazard analyses (PSHA) and (2) the development of seismic design basis parameters. Both projects are being performed jointly by the U.S. Geological Survey (USGS) and the Civilian Radioactive Waste Management System (CRWMS) Management and Operating (M&O) contractor. The USGS has been assigned the primary responsibility for the PSHA Project and Woodward-Clyde Federal Services (WCFS), a member of the M&O Team, has been assigned the task to manage the project. This report describes the PSHA Project. The determination of seismic design basis input is being conducted by the Seismic Design Basis Team under contract to the CRWMS M&O.

The PSHA Project was performed in three strongly integrated parallel activities leading to the determination of fault displacement and vibratory ground motion hazards levels that form the basis for development of seismic design basis inputs for the Yucca Mountain repository structures, systems, and components (SSCs) and to a documentation of the technical bases for these determinations. Seismic design basis covers surface and subsurface SSCs. Both the preclosure and postclosure performance periods of the repository (100 and up to 100,000 years, respectively) were addressed in this project. The activities performed were: (1) evaluation and characterization of seismic sources including the characterization of potential fault displacement; (2) evaluation and characterization of vibratory ground motion attenuation, including earthquake source, wave propagation path, and rock site effects; and (3) PSHAs for both fault displacement and vibratory ground motion. This report describes the process followed to carry out the PSHA Project and includes documentation of the interpretations and uncertainties used as input to the hazard calculations from both the seismic source and fault displacement characterization and ground motion characterization.

1.1 PROJECT OBJECTIVES AND SCOPE OF WORK

The overall approach that the DOE has undertaken to address potential seismic hazards at Yucca Mountain is documented in three topical reports: "Methodology to Assess Fault Displacement and Vibratory Ground Motion Hazards at Yucca Mountain" (Topical Report No. 1) (DOE, 1997a) and "Preclosure Seismic Design Methodology for a Geologic Repository at Yucca Mountain" (Topical Report No. 2) (DOE, 1997b). Topical Report No. 3 planned for completion later this fiscal year, will document the results of both the PSHA and Seismic Design Basis Projects. The methodology adopted and used in the PSHA Project is described in Topical Report No. 1. The methodology and acceptance criteria used by the DOE to determine the preclosure seismic design of repository SSCs is described in Topical Report No. 2.

The objectives of the PSHA Project are to: (1) determine the fault displacement and vibratory ground motion hazards at the Yucca Mountain site and (2) provide documentation of the technical basis for determining these hazards. The PSHA also provides quantitative hazard results to support an assessment of the potential repository's long-term performance with respect to waste containment and isolation and forms the basis for developing seismic design inputs for the License Application of the potential repository. The hazards results are in the form of annual frequencies with which various levels of fault displacement at locations within the Controlled Area and vibratory ground motion at a reference rock outcrop are expected to be exceeded. The reference rock outcrop is at the ground surface but at a location at the same elevation of the repository (Point A; Figure 1-1).

The hazard analyses are based on evaluations of seismic source characteristics, earthquake ground motions, and fault displacement that reflect interpretations of different scientific hypotheses and models using available data. These interpretations have associated uncertainties related to the ability of data to resolve different hypotheses and models with certainty. The interpretations described in this study are based on seismological, geological, geophysical, and geotechnical data specific to the Yucca Mountain site and the surrounding region within at least a radius of 100 km. To evaluate scientific uncertainty, seismic source and fault displacement characterizations have been made by six teams of experts, who in composite are expert in the seismicity, tectonics, and geology of the Yucca Mountain site and region. Ground motion

assessments have been made by seven individuals expert in evaluating the generation and attenuation of earthquake ground motions.

Interpretations for hazard assessment have been coordinated and facilitated through a series of workshops. Each workshop was designed to accomplish a specific step in the overall process and to ensure that the relevant data were being fully considered and integrated into the evaluations. This process was designed to ensure that all credible interpretations are considered in the fault displacement and vibratory ground motion hazard assessment.

The seismic hazard computational procedures used for this project allowed quantitative assessments of seismic hazard based on input interpretations provided by the experts. Uncertainty in individual interpretations is captured as weighted alternatives in a logic tree structure and propagated through the hazard calculations. Thus the quantification incorporates uncertainty in the hazard due to scientific uncertainty in the input interpretations as well as to random variability in input parameters. The hazard results are presented as mean, median, and fractile hazard curves representing the total uncertainty in input interpretations.

1.2 RELATIONSHIP OF PSHA PROJECT TO SEISMIC DESIGN BASIS DETERMINATION

The following describes how the PSHA Project results will be used in the development of both preclosure and postclosure seismic design bases.

1.2.1 Preclosure Seismic Design Basis Determination

The PSHA Project provides the needed information base for determining the fault displacement and vibratory ground motion levels appropriate for seismic design of the proposed repository SSCs. The criteria for determining seismic design inputs are described in Topical Report No. 2 and will be used together with the PSHA results by the Seismic Design Basis Team to establish the seismic design basis for fault displacement and ground motions for the proposed repository. The seismic design basis will be documented in a separate report, "Seismic Design Input for a High-Level Waste Repository at Yucca Mountain, Nevada" which is in preparation.

In accordance with Topical Report No. 2, seismic design inputs will be developed for Frequency Categories-1 and 2. For vibratory ground motion, the reference annual probabilities of exceedance for these two categories are 10^{-3} and 10^{-4}, respectively, or return periods of 1,000 and 10,000 years. The corresponding probabilities of exceedance (and return periods) for fault displacement are 10^{-4} (10,000 years) and 10^{-5} (100,000 years), respectively.

Seismic design basis for vibratory ground motion will be in the form of peak values, response spectra, and time histories for acceleration and velocity and for both horizontal and vertical components. These motions will be described at the 300-m level of the proposed underground repository in rock (Point B) and at a rock site on the ground surface above the repository (Point C; Figure 1-1). The methodology for determining seismic design input at a soil site (Point D), where the proposed surface facilities will be located in Midway Valley, will also be presented.

The seismic design basis motions will be developed for four controlling Design Basis Earthquakes: an earthquake controlling high frequencies (5 to 10 Hz) and an earthquake controlling low frequencies (1 to 2 Hz) for the two return periods of 1,000 and 10,000 years. These four controlling earthquakes are derived by deaggregating the probabilistic hazard as determined in the PSHA Project in terms of mean magnitude $(\overline{M})$, mean distance $(\overline{d})$ and ground motion deviation (ε).

For fault displacement, the principal design criterion provided in Topical Report No. 2 is to avoid faults that have the potential for offsets of engineering significance where reasonably feasible. Only in cases, if any, where fault avoidance is not feasible and for which the potential fault displacement is significant, as quantified by the PSHA, will fault displacement design be implemented in the design of the Yucca Mountain SSCs.

1.2.2 Postclosure Design Evaluation

Vibratory ground motion and fault displacement hazard information developed by the PSHA Project will be used to evaluate the effects of disruptive processes during the postclosure period on repository performance. SSCs important to safety must be designed and constructed to meet postclosure as well as preclosure performance requirements (DOE, 1996). The DOE is

employing a systems approach which establishes the life cycle functions of repository SSCs to ensure that they are designed to meet their performance requirements. Postclosure performance requirements are expected to be controlling for some SSCs for which repetitive ground motion or fault displacement may be a factor.

An example is the postclosure performance with respect to rockfalls of emplacement drifts. Presently the DOE does not intend to rely on rockfalls not occurring in emplacement drifts for any period of time to meet postclosure performance (DOE, 1996). Rather, the DOE intends to evaluate the effects of rockfalls, including incremental effects of repetitive seismic loading, on postclosure performance and, if necessary, to design to mitigate their consequences. The seismic hazard curves developed by the PSHA Project will be integrated with consequence curves for this assessment. Other postclosure performance evaluations will make similar use of the PSHA Project results.

Postclosure performance evaluations generally involve integration of hazard curves taking account of uncertainty. The vibratory ground motion and fault displacement hazard curves developed by the PSHA Project contain the necessary information for this evaluation.

1.3 PREVIOUS PSHA STUDIES FOR YUCCA MOUNTAIN

Since the inception of the Yucca Mountain Project, several PSHA studies have been performed. The first analysis by URS/John A. Blume & Associates, Engineers (URS/Blume, 1986) evaluated the ground motion hazard at Yucca Mountain for repository conceptual design. In that study, only areal source zones were considered as seismic sources and they were based on the historical earthquake record and some limited paleoseismic data. Based on a probabilistic analysis, peak horizontal accelerations of 0.25, 0.40, and 0.65 g were calculated for return periods of 500, 2,000, and 10,000 years.

In a subsequent study, URS/Blume (1987) evaluated both ground motion and fault displacement hazards to assess the effects of model and parametric uncertainties on the computed hazards. In that analysis, active faults were specifically characterized and modeled based on the available paleoseismic data. A simplified fault model was used to calculate the fault displacement hazard based on a joint probability for surface rupture displacement, length,

and rupture radius exceedances together with the fault recurrence models. The calculated probabilistic ground motion hazard was dominated by the Paintbrush Canyon and related faults and by background seismicity and was most sensitive to the relationships between slip rate and fault lengths used in the analysis. The surface fault displacement hazard was calculated for the Paintbrush Canyon fault, and related primary faults in the site vicinity. The resulting hazard was also most sensitive to the assumed slip rate-fault length relations.

In a 1994 study for seismic design of the Exploratory Studies Facility (ESF), the CRWMS M&O performed a PSHA for ground shaking (CRWMS M&O, 1994; Wong *et al.*, 1996). In that study, 24 Quaternary faults and a background areal zone were included in the analysis. Characterization of seismic sources included consideration of additional paleoseismic data collected as part of the site characterization activities. Four western U.S. empirical relationships for rock were used to characterize the ground motion attenuation. The resulting peak horizontal accelerations for return periods of 1,000 and 10,000 years were 0.27 g and 0.66 g, respectively.

In a recent PSHA for the preliminary design of the Waste Handling Building (Wong *et al.*, 1998), the ESF study was updated by incorporating available paleoseismic data, particularly on the local faults, and the extensional regime attenuation relationship by Spudich *et al.* (1996). The resulting peak horizontal accelerations were 0.16, 0.21, and 0.50 g, for return periods of 500, 1,000, and 10,000 years, respectively. These motions were significantly lower than the ESF values due to the high weight (0.50) assigned to the Spudich *et al.* (1996) relationship (which results in calculated ground motions about 20% lower than California-based attenuation relations) and lower slip rates for the local faults based on the newer paleoseismic data.

In a demonstration project in 1992, Electric Power Research Institute (EPRI) sponsored an expert elicitation PSHA for fault displacement at Yucca Mountain. The objectives were to (1) demonstrate methods for eliciting expert judgment and (2) to quantify the uncertainties associated with earthquake and tectonic issues for use in the EPRI High-Level Waste performance assessment.

In addition to these site-specific studies, PSHAs have been performed on a national and state basis. Since 1948, ground shaking hazard maps have been developed for the entire U.S. that

form the basis for the zonation in the Uniform Building Code. In the most recent maps (Frankel *et al.*, 1996), the peak horizontal accelerations for return periods of approximately 500, 1,000, and 2,500 years are about 0.16, 0.19, and 0.29 g, respectively, for the Yucca Mountain site. In a study for the Nevada Department of Transportation, Siddharthan *et al.* (1993) developed statewide probabilistic hazard maps. These maps show peak horizontal acceleration values for the Yucca Mountain site of 0.24 g and 0.30 g for return periods of 500 and 1,000 years, respectively. Other PSHAs for vibratory ground motions have been performed for the Nevada Test Site by Rogers *et al.* (1977) and Coats and Murray (1984).

1.4 PROJECT ORGANIZATION

The major components of the project organization included the Principal Investigator, the Project Management Team, Review Panel, technical teams including the facilitation, data management, and calculations teams, and the two expert panels. Team members and experts are shown on Figure 1-1 and in Tables 1-1 to 1-4.

Although not part of the project organization, an important part of the PSHA process was the inclusion of technical specialists. Specialists participated in the project by providing the experts with descriptions of their data, models, and interpretations, during workshops and the field trip. These technical specialists and their affiliations are listed in the summaries of the workshops and the field trip (Appendices C and D). At certain workshops, members of both the facilitation teams and experts also acted as technical specialists of a particular model, data set, or interpretations.

Dr. John Whitney was the Principal Investigator for the Project. In this role, he provided overall technical guidance for the work. In addition, he was responsible for implementing the quality management procedures by which the work was controlled.

1.4.1 Project Management Team

Management of the PSHA Project was provided by the Project Management Team. This team provided overall management of the project, advised on technical issues relating to the project, and oversaw the efforts of the four technical teams. They also ensured consistency with regulatory requirements, DOE policies and guidelines, and program needs. They provided

logistical and organizational management of the workshops and the preparation of reports. Regarding the latter, the Project Management Team ensured that appropriate reviews were implemented to achieve completeness and high technical quality, and that project schedules and milestones were met. The team consisted of Dr. Carl Stepp, Project Director, Deputy Project Directors, Mr. Ivan Wong and Dr. Jean Savy, and Dr. Richard Quittmeyer, Senior Scientist responsible for M&O geoscience activities.

1.4.2 Review Panel

The Review Panel (Figure 1-1) consisted of four individuals who are experts in the range of disciplines and topics that constitute the evaluation of seismic hazards. Each member of the panel was responsible for a specific technical scope of work of the project: Dr. C. Allin Cornell - PSHA methodology and process, Dr. Thomas Hanks - vibratory ground motion, Dr. James N. Brune - seismic source characterization and vibratory ground motion, and Dr. David P. Schwartz - seismic source characterization and fault displacement hazard. The panel attended the workshops and meetings relevant to their assigned scope of review. They provided formal review comments and recommendations within their technical scope following each workshop, and reviewed draft reports and prepared comments and recommendations that were reviewed and implemented by the Project Management Team.

1.4.3 Technical Teams

To plan, organize, and lead the technical workshops, facilitate the experts in their interpretations, and perform the required hazard calculations, four technical teams were assembled: (1) Seismic Source and Fault Displacement (SSFD) Facilitation, (2) Ground Motion (GM) Facilitation, (3) Data Management, and (4) PSHA Calculations (Figure 1-1).

1.4.3.1 Seismic Source and Fault Displacement Facilitation Team. This team facilitated the experts' seismic source and fault displacement evaluations for the hazard analyses. They provided the technical leadership required to facilitate interactions and elicit interpretations by the experts. The SSFD Facilitation Team organized, planned, and led all technical workshops related to characterization of seismic sources and evaluations of the potential for fault displacement. Their responsibilities included (1) planning the technical scope, preparing any necessary white-paper documentation of the state-of-the-art, obtaining input and participation in workshops of data, model, or interpretation proponents, and facilitating

discussion in the workshops; (2) preparing workshop agendas, conducting the workshops, and writing workshop summary reports; (3) eliciting interpretations of the experts; (4) providing feedback to the experts regarding the results of their interpretations; and (5) preparing an Activity Report to describe the process followed to develop the experts' interpretations and to present the interpretations themselves. The team was led by Dr. Kevin Coppersmith. Other members of this team and their principal responsibilities are listed in Table 1-1.

1.4.3.2 Ground Motion Facilitation Team. This team facilitated the characterization of ground motion attenuation by the GM experts for a suite of parameters that was used in the PSHA. The responsibilities of the GM Facilitation Team were the same as those of the SSFD Facilitation Team. Dr. Norm Abrahamson led this team; other members and their principal responsibilities are listed in Table 1-2.

1.4.3.3 Data Management Team. The Data Management Team provided common data sets to the experts. The team compiled relevant data and provided derivative data products and evaluations as identified by the experts during the data needs workshops. The goal was to eliminate differences in interpretations caused by different data and knowledge bases. The historical earthquake catalog was compiled by the Data Management Team. This team was led by Dr. John Whitney and Ivan Wong and support was provided by the USGS and WCFS (Figure 1-1).

1.4.3.4 PSHA Calculations Team. The PSHA Calculations Team performed both preliminary and final seismic hazard computations. The computed seismic hazard is in the form of seismic hazard curves for (1) a range of spectral periods for vibratory ground motions and (2) for locations representing the range of faulting conditions within the Controlled Area. The team also modified the existing seismic hazards computational code for ground shaking to incorporate the code for calculating the hazard from fault displacement. The team was led by Dr. Gabriel Toro and supported by staff at Risk Engineering, Inc. (Figure 1-1).

1.4.4 Experts

The uncertainty in scientific interpretations was incorporated into the probabilistic hazard analyses by including multiple interpretations of scientists with complementary experience and

knowledge. The experts evaluated relevant hypotheses and models and processes using available data and developed and documented interpretations for input into the PSHA calculations. For the seismic source and fault displacement characterizations, six three-person expert teams performed the interpretations. The aggregate expertise of each group covered the seismic geology, geology, tectonics, seismology, and geophysics of Yucca Mountain and the Basin and Range Province. Each SSFD expert team was responsible for identifying and characterizing the seismic sources significant to Yucca Mountain vibratory ground motions or fault displacement hazards. In addition, each SSFD team provided a characterization of the fault displacement potential for calculation of the fault displacement hazard at locations within the Controlled Area.

For ground motion attenuation, seven individual GM experts provided evaluations for input to the PSHA. Each expert provided ground motion point estimates for a specified range of parameters. The GM experts were selected to cover the two principal approaches to estimating ground motions, empirical and numerical modeling, and included one expert in nuclear explosion ground motions. Tables 1-3 and 1-4 list the SSFD and GM experts, respectively, and their affiliations. Biographies of the experts are provided in Appendix A.

1.5 PROJECT ACTIVITIES

Planning of the PSHA Project by the Project Management Team began in August 1994 with the development of Study Plan 8.3.1.17.3.6 "Probabilistic seismic hazard analysis" and the Project Plan, which is entitled "Probabilistic analysis of fault displacement and vibratory ground motion and development of seismic design bases for Yucca Mountain." The latter included the seismic design activities to ensure integration with the PSHA Project. Selection of team members and experts followed in the fall of 1994.

Major elements of the PSHA Project were the workshops conducted by the facilitation teams. These workshops provided the experts with the expert elicitation methodology, facilitated interaction among the experts, defined the data needed to perform their evaluations, provided a forum for discussing the range of relevant technical issues and interpretations, and facilitated the presentation and evaluation of state-of-the-knowledge research as well as proponent models and interpretations. The first workshop was held in April 1995. Due to Yucca Mountain Project

funding limitations, the project was suspended in FY96 and resumed in FY97 with the remaining workshops. A thorough discussion of the workshops and the PSHA process as a whole is presented in Chapters 2.0 to 4.0 and 7.0. The following briefly describes the general aspects of the three primary activities in the PSHA Project: the seismic source and fault displacement and ground motion characterizations and the hazard calculations.

1.5.1 Seismic Source and Fault Displacement Characterization

The purpose of this activity is to characterize all known seismic sources that can generate significant ground shaking at Yucca Mountain. The SSFD expert teams were asked to provide and document in an elicitation summary their interpretations of the location, geometry, probability of activity, maximum magnitude, and recurrence of all seismic sources they identified as being significant to Yucca Mountain both in terms of vibratory ground motions and fault displacement. In addition, they were to provide approaches for characterizing the fault displacement hazard including both primary and distributed faulting.

The process of evaluating and characterizing seismic sources for vibratory ground motion hazard assessment and characterizing potential fault displacement for fault displacement hazard assessment generally followed the guidance in NUREG/CR-6372, *Recommendations for Probabilistic Seismic Hazard Analyses: Guidance on Uncertainty and Use of Experts* (NRC, 1997a) and the NRC guidance in NUREG-1563, *Branch Technical Position on the Use of Expert Elicitation in the High-Level Radioactive Waste Program* (NRC, 1996). The evaluation and characterization of seismic sources for vibratory ground motion hazard assessment generally follow the guidance in Regulatory Guide 1.165, *Identification and Characterization of Seismic Sources and Determination of Safe Shutdown Earthquake Ground Motion* (NRC, 1997b), and NUREG-1451, *Staff Technical Position on Investigations to Identify Fault Displacement Hazards and Seismic Hazards at a Geologic Repository* (NRC, 1992). The evaluation and characterization of the potential for fault displacement made use of the guidance in NUREG-1494, *Staff Technical Position on Consideration of Fault Displacement Hazards in Geologic Repository Design* (NRC, 1994).

A second very important objective of the SSFD characterization was to identify and assess the uncertainties in seismic source and fault displacement characterization. This aspect of the evaluation was designed to capture uncertainty both in the *models* used to characterize seismic

sources, and the *parameter values* used in the models. The experts, who were both from within and outside the Yucca Mountain Project, represented a range of experience and expertise relevant to performing the evaluations. A deliberate process was followed in facilitating interactions among the experts, in training them to express their uncertainties, and in eliciting their interpretations. The resulting evaluations, therefore, provide reasonable assurance that the knowledge and uncertainties about seismic source and fault displacement characterization relevant to PSHA at the Yucca Mountain site has been captured and expressed in the seismic hazard results. The seismic source and fault displacement characterization is described in detail in Chapters 3.0 and 4.0.

1.5.2 Ground Motion Characterization

The goal of this activity was to estimate vibratory ground motion values as a function of frequency at the proposed repository given an earthquake magnitude and distance. The description of ground motion consisted of ground motion attenuation relations specific to the repository site. The relations include earthquake source, propagation path, and site effects specific to Yucca Mountain. The attenuation relations describe ground motions for structural response periods that are required for SSC design. Both horizontal and vertical components of motion were developed. Like the seismic source and fault displacement characterization, the experts evaluated the uncertainties in ground motion as part of their characterizations.

Characterizing ground motions for input into a PSHA required describing motions developed by the various types of seismogenic sources - fault-specific and areal sources. Ground motions resulting from the different styles of faulting (strike-slip, normal, or reverse) were incorporated into the characterization. Thus the seismogenic sources to a degree define the technical issues that the ground motion characterization must address. The ground motion characterization activity thus required coordination with the SSFD Facilitation Team and the PSHA Hazard Calculations Team. A detailed description of the ground motion characterization is contained in Chapters 5.0 and 6.0.

1.5.3 Probabilistic Seismic Hazard Analyses

The PSHA methodology for vibratory ground motions was first developed by Cornell (1968, 1971) and has become standard practice in evaluating seismic hazards. Subsequent to Cornell's work, the basic computational analysis method has changed little, but PSHA

methodology has undergone extensive development principally by the U. S. Nuclear Regulatory Commission (NRC) and utilities that operate nuclear power plants. The extensive developments have been in the area of quantifying necessarily subjective scientific evaluations of seismic sources, source earthquake recurrence characteristics, and ground motion input to seismic hazard assessment. This work has resulted in development of procedures to quantify input interpretations including the experts' uncertainty in their evaluations, and a process for conducting PSHA that provides reasonable assurance that scientific and data uncertainties are properly captured and represented in the hazard results. These procedures and their application have undergone extensive review by the NRC and have been accepted for application to determine seismic design basis for nuclear facilities (EPRI, 1988, 1989; NRC, 1988, 1991, 1997a).

The use of the probabilistic methodology results in calculated annual probabilities that various measures of vibratory ground motion (e.g., peak horizontal acceleration) will be exceeded at a site. The resulting seismic hazard curve represents the integration over all earthquake sources and magnitudes of potential future earthquake occurrence and ground motion variability. The methodology for evaluating fault displacement hazard probabilistically is nearly identical to that for vibratory ground motions.

The calculation of ground motion hazard and fault displacement employs similar processes. For ground motion hazard, three basic inputs are required: (1) the identification of relevant seismic sources and a characterization of their source geometry; (2) an evaluation of the rate of earthquake occurrence, recurrence model, and maximum magnitude distribution for each seismic source; and (3) attenuation relationships that provide for the estimation of a specified ground motion parameter as a function of magnitude, source-to-site distance, and in some cases, seismic source characteristics. Inputs (1) and (2) are developed by the SSFD expert teams and (3) by the GM experts. For assessing fault displacement hazard, the ground motion attenuation relationships are replaced by relationships that describe the distribution, sense, and amounts of displacement with earthquake occurrence. Potentials for both primary and secondary fault displacement are characterized. Uncertainties in these input evaluations are propagated throughout the probabilistic analyses using a logic tree methodology. In this activity, the probabilistic ground shaking hazard was calculated using a quality assurance (QA)-approved computer code developed by Risk Engineering, Inc. For the calculation of

the fault displacement hazard, the evaluations provided by the SSFD experts were coded and incorporated into the basic hazard code. Extensive sensitivity analyses were also performed as part of this activity. A detailed description of the PSHAs and the calculated results are contained in Chapters 7.0 and 8.0.

1.6 QUALITY ASSURANCE

The PSHA Project was performed under the USGS Quality Assurance Program for the Yucca Mountain Project. DOE's Quality Assurance Requirements and Description document (QARD) (DOE/RW-0333P) provides the QA requirements for the Yucca Mountain Project and the USGS Quality Assurance Program is written to meet applicable requirements from the QARD. The key elements of the program applicable to PSHA were personnel qualifications and training, scientific expert elicitation, software controls, records management, and data management.

Personnel qualifications files consisting of position descriptions, resumes, and verification statements have been collected for members of the Project Management Team, the Review Panel, and the technical teams. Training in expert elicitation and in the applicable procedures has been provided via workshops and reading assignments. At the time that the PSHA was performed, the QARD was silent on requirements applicable to scientific expert elicitation; however, the USGS developed a new Quality Management Procedure to include appropriate requirements for scientific expert elicitation. Revision 8 of the QARD, to become effective in June 1998, now includes requirements for scientific expert elicitation based on the *Branch Technical Position on the Use of Expert Elicitation in the High-Level Radioactive Waste Program* (NUREG-1563, NRC, 1996). During a QA audit (USGS-ARP-98-01) of the USGS in October 1997, DOE's Office of Quality Assurance compared the USGS procedure, the PSHA Project Plan, and implementation to the NUREG guidance and to the then-draft QARD requirements. The only significant difference was that the QARD and the NUREG require the experts to provide the reason for any modifications to their interpretations. The Project Management Team disagreed with this position because they thought it could introduce bias, be disruptive to the process, and would negatively impact the end product. The audit team accepted this position and justification.

Software QA requirements were required to be applicable only to the computer codes for ground shaking and fault displacement hazard developed and modified by Risk Engineering. The Risk Engineering code modifications were required to be verified and the released code placed in the USGS Yucca Mountain Project Branch software configuration management system. Software used by the experts in developing their interpretations were exempted from the QARD software requirements.

The report and the information required to support the development will be submitted to the CRWMS records processing center. The hazards curves and logic trees will be submitted to the CRWMS technical data base.

1.7 DOCUMENTATION OF PSHA EXPERT EVALUATIONS

The integrity of a PSHA is considered to rest principally on how it is structured and implemented to derive seismic source and ground motion inputs for hazard computation. For performing the Yucca Mountain PSHA, a structured process was adopted with respect to deriving inputs to insure independent evaluations by recognized experts, representing the scientific community's state of knowledge. Evaluations were elicited through a process involving a series of workshops each structured and implemented to achieve a specifically defined step in the overall evaluation (Sections 3.2 and 5.3), and through individual meetings between the facilitation teams and the experts. All workshops and meetings between the facilitation teams and experts were documented by summaries that are part of the basic documentation of the PSHA Project.

Two defining principles guided the elicitation process: 1) the experts' evaluations should represent the informed scientific community's state of knowledge, and 2) the experts themselves are the owners of their independent evaluations. Thus, the elicitation process continually emphasized the role of the experts as independent evaluators responsible for considering proposed hypotheses and models using available data. It also emphasized that the experts themselves were responsible for describing their final evaluations in a summary report that would become part of the PSHA Project documentation.

Preliminary evaluations were developed by the experts and presented, discussed, and documented in the workshops. In recognition of principle (1), the experts were not asked to

provide written descriptions of these preliminary evaluations beyond their presentation materials in the workshops. Based on the experience base developed over the past decade or more in carrying out seismic hazard assessments, requiring more specific documentation of experts' preliminary evaluations was considered to present an unacceptable risk of anchoring, and thus biasing, the evaluations before completion of the elicitation process. The experts also were provided feedback of hazard results based on their input evaluations. This feedback activity took place after the experts had completed draft expert summaries that described their input evaluations. These draft summaries are part of the PSHA Project basic documentation. Following the feedback activity, the experts were free to make changes in their evaluations before completing and submitting their final summaries for the seismic hazard calculations. The final expert summaries are the only descriptions of their evaluations that are considered to be complete and are intended to be defensible. These are included in this report as Appendices E and F.

1.8 PROJECT PRODUCTS AND REPORT ORGANIZATION

This PSHA Final Report is a DOE Level 3 milestone. It is comprised of three Activity Reports that describe and summarize the three major project activities. These Activity Reports, which are Level 4 documents, are the "Seismic Source and Fault Displacement Characterization Project" (CRWMS M&O, 1997a), "Ground Motion Characterization at Yucca Mountain, Nevada" (CRWMS M&O, 1997b), and "Probabilistic Seismic Hazard Calculations for Yucca Mountain, Nevada" (CRWMS M&O, 1998). In addition, as part of the milestone requirements, for the Final Report, included in Volume 2 are Appendix K, Yucca Mountain Project Records and Data Tracking Information for Data Used and Cited Within the Report, and Appendix L, Milestone SP32IM3 Description/Completion Criteria Compliance Location.

Following this Introduction (Chapter 1.0), there are eight chapters and ten appendices in the Final PSHA Report. Chapter 2.0 describes the process of selecting the experts and provides a general description of the expert elicitation. Chapters 3.0 and 5.0 describe the facilitation approaches taken in the seismic source and fault displacement and ground motion characterizations, respectively. Chapters 4.0 and 6.0 describe the experts' evaluations of seismic source and fault displacement and ground motion, respectively. The probabilistic methodology used to quantify the ground shaking hazard at Yucca Mountain is presented, and

the results along with sensitivity analyses are described, in Chapter 7.0. Chapter 8.0 presents the probabilistic hazard methodology for fault displacement and the results. References cited in the report are contained in Chapter 9.0. Appendix A contains biographies of both the SSFD and GM experts. Data packages distributed to both the SSFD expert teams and GM experts are listed in Appendix B. Appendices C and D contain the workshop summaries. The expert elicitation summaries are contained in Appendices E and F. Appendix G describes the development of the historical seismicity catalog. The development of the fault displacement hazard parameter distributions is discussed in Appendix H. Appendices I and J show the results of the attenuation regression analysis and the development of the hypocentral distance-based models for the areal sources, respectively.

TABLE 1-1

SSFD FACILITATION TEAM MEMBERS AND THEIR PRINCIPAL RESPONSIBILITIES

NAME	AFFILIATION	RESPONSIBILITIES
Kevin J. Coppersmith	Geomatrix Consultants, Inc.	Team leader, project planning and methodology development; facilitating workshops; documentation
Susan S. Olig	Woodward-Clyde Federal Services	Workshop and field trip coordination; workshop summaries; documentation
Roseanne C. Perman	Geomatrix Consultants, Inc.	Project planning and methodology development; documentation
Silvio Pezzopane	U.S. Geological Survey	Project planning and methodology development; data synthesis
Peter A. Morris	Applied Decision Analysis, Inc.	Review of project direction; expert elicitation methodologies and training
Robert R. Youngs	Geomatrix Consultants, Inc.	Project planning and methodology development; eliciting and formulating alternative models; documentation of results/sensitivity

Note: Kathryn L. Hanson, Geomatrix Consultants, Inc., assisted with documentation, review, and report preparation.

TABLE 1-2
GM FACILITATION TEAM MEMBERS AND THEIR PRINCIPAL RESPONSIBILITIES

NAME	AFFILIATION	RESPONSIBILITIES
Norm A. Abrahamson	Consultant	Team leader, project planning and methodology development; facilitating workshops; documentation
Ann M. Becker	Woodward-Clyde Federal Services	Project planning and methodology development; workshop summaries; documentation; data synthesis, elicitation
Peter A. Morris	Applied Decision Analysis, Inc.	Review of project direction; expert elicitation methodologies and training

Note: John Schneider was an original member of the Facilitation Team but left the Project in October 1996.

TABLE 1-3
SSFD EXPERTS

NAME	AFFILIATION	EXPERTISE
Jon P. Ake	U.S. Bureau of Reclamation	Seismology
R. Ernest Anderson	U.S. Geological Survey	Regional Geology and Tectonics
Larry W. Anderson	U.S. Bureau of Reclamation	Paleoseismology
Walter J. Arabasz	University of Utah	Seismology
Ronald Bruhn	University of Utah	Regional Geology and Tectonics
Craig dePolo	Nevada Bureau of Mines & Geology	Paleoseismology
Diane I. Doser	University of Texas, El Paso	Seismology
Christopher J. Fridrich	U.S. Geological Survey	Regional Geology and Tectonics
Peter L.K. Knuepfer	Binghamton University	Paleoseismology
Dennis W. O'Leary	U.S. Geological Survey	Regional Geology and Tectonics
James McCalpin	GEO-HAZ Consulting, Inc.	Paleoseismology
Alan R. Ramelli	Nevada Bureau of Mines & Geology	Paleoseismology
Albert M. Rogers	GeoRisk Associates, Inc.	Seismology
D. Burton Slemmons	Woodward-Clyde Federal Services	Regional Geology, Tectonics, and Paleoseismology
Kenneth D. Smith	University of Nevada, Reno	Seismology
Robert B. Smith	University of Utah	Seismology
Frank H. (Bert) Swan	Geomatrix Consultants, Inc.	Paleoseismology
James C. Yount	U.S. Geological Survey	Regional Geology and Tectonics

Note: Peter Knuepfer and Dennis O'Leary replaced Anthony J. Crone, USGS and Christopher M. Menges, USGS, respectively, during the course of the project.

TABLE 1-4
GM EXPERTS

NAME	AFFILIATION
John G. Anderson	University of Nevada, Reno
David M. Boore	U.S. Geological Survey
Kenneth W. Campbell	EQE International Inc.
Arthur F. McGarr	U.S. Geological Survey
Walter J. Silva	Pacific Engineering & Analysis
Paul G. Somerville	Woodward-Clyde Federal Services
Marianne C. Walck	Sandia National Laboratories

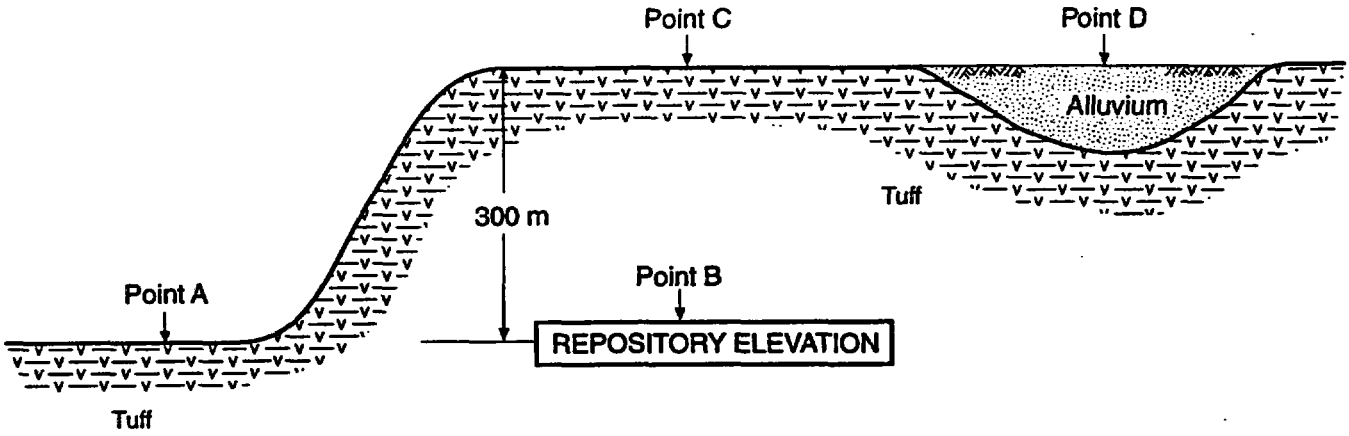

LEGEND

Point A – Reference rock outcrop at repository elevation

Point B – Repository elevation with tuff overburden

Point C – Rock surface

Point D – Soil surface

Figure 1-1 Locations of specified Design Basis Earthquake ground motions

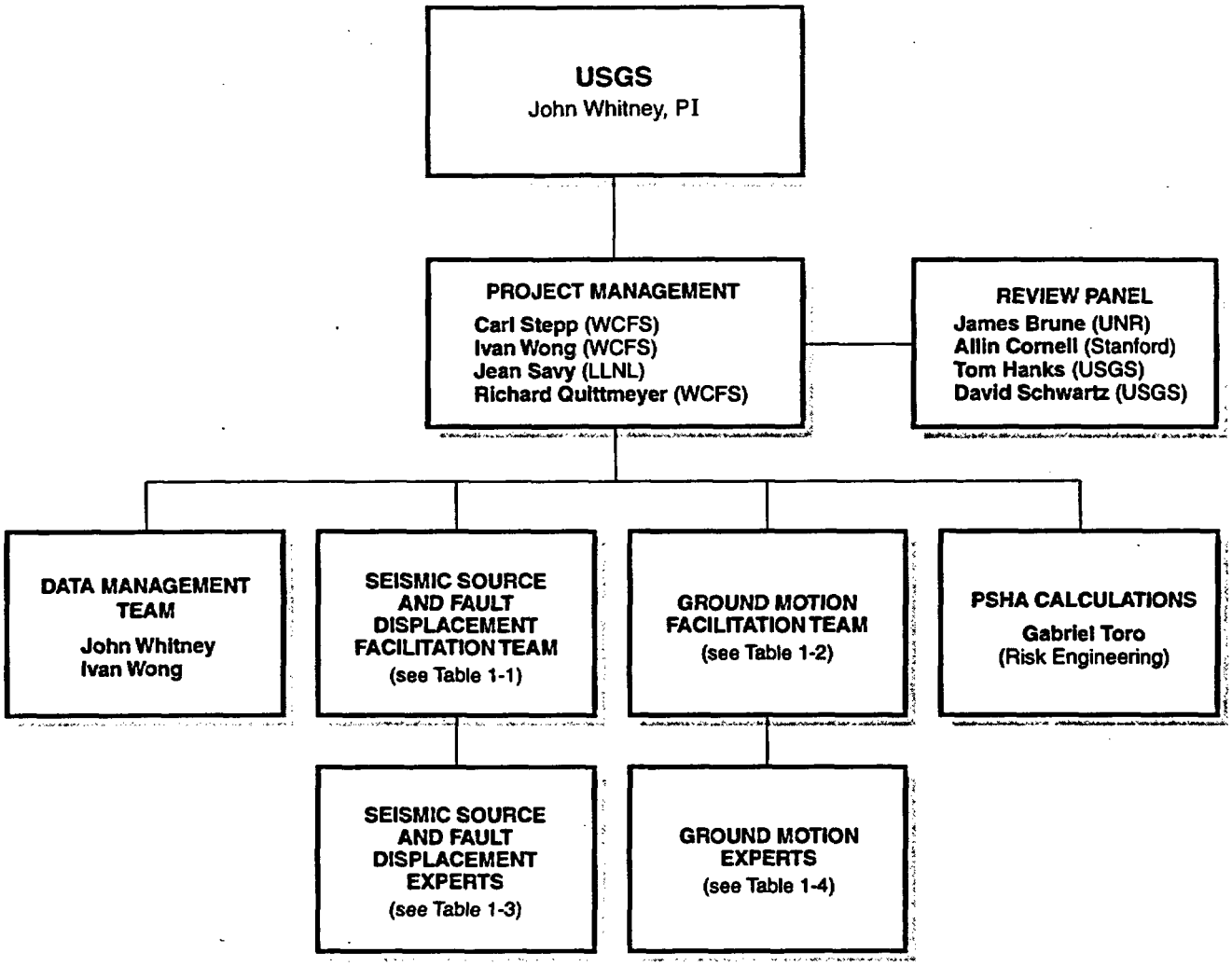

WCFS – Woodward-Clyde Federal Services

LLNL – Lawrence Livermore National Laboratory

UNR – University of Nevada, Reno

USGS – U.S. Geological Survey

Figure 1-2 Project organization

2.0
PROCESS FOR ELICITING EXPERT EVALUATIONS

This chapter describes the criteria for being an expert, the expert selection process, and the methodology followed in eliciting the evaluations of the experts. Experience has shown that to be credible and useful, technical analyses such as those performed for the seismic source fault displacement and ground motion characterizations must (1) be based on sound technical information and interpretations, (2) follow a process that considers all available data, and (3) incorporate uncertainties (SSHAC, 1997). A key mechanism for quantifying uncertainties is the use of multiple expert evaluations. The *process* used to select the experts, facilitate their interaction and mutual training, and elicit and refine their evaluations is as important as the technical content of their interpretations.

In the PSHA Project, the term "elicitation" was used in a broad sense to include all of the processes involved in obtaining the technical judgments of multiple experts. These processes include reviewing available data, debating technical views with colleagues, evaluating the credibility of alternative views, expressing interpretations and uncertainties in interviews, and documenting interpretations. In this sense, the elicitation process began with the first workshops and ended with the finalization of the expert elicitation summaries.

Because of the importance of the entire expert elicitation process, facilitation teams were established at the outset of the project. Facilitation team members had experience in developing guidance for and implementing multiexpert studies and in understanding the technical aspects of the project.

2.1 GUIDANCE REGARDING EXPERT EVALUATIONS

In the evaluation of any complex geological problem, expert interpretation is essential. The data themselves do not usually provide the unique characterization of the processes and outputs needed for subsequent analyses. For example, in the seismic source characterization at Yucca Mountain, data regarding the amounts of displacement and ages of faulted stratigraphic units do not provide direct estimates of the magnitude and recurrence intervals for potential earthquakes on a fault. These data must be interpreted in order to characterize

fault segmentation, rupture lengths, or slip rates. Various conceptual models of rupture behavior and recurrence must be combined with observed data to arrive at results useful to seismic hazard assessment, such as maximum magnitude distributions and frequency-magnitude relationships. Experts integrate and evaluate data to arrive at conclusions that are meaningful to seismic source characterization, including quantitative and qualitative expressions of the uncertainties. In this sense, expert elicitation is **not** a substitute for data, it is the process by which data are evaluated and interpreted. If data are scarce and uncertainties large, the uncertainties expressed by each expert and the range of interpretations across multiple experts should reflect this high degree of uncertainty. This process is the same regardless of the abundance or scarcity of data

The procedures and approaches for expert elicitation, developed through conducting many studies, have been formalized in guidance documents that were followed in the PSHA Project. DOE recently developed guidance for the formal use of expert elicitation by the Yucca Mountain Project (DOE, 1995), and the NRC staff issued a Branch Technical Position on use of expert elicitation in the high-level waste program (NRC, 1996). Comprehensive guidance on expert elicitation for seismic hazards assessments recently was set forth in a study sponsored by the DOE, the EPRI, and the NRC (SSHAC, 1997).

In this project, multidiscipline, multiexpert teams were used to evaluate seismic sources and fault displacements. Individual experts were used in the characterization of ground motion attenuation. Teams were used previously in a large probabilistic evaluation conducted to assess the seismic hazard at 37 commercial nuclear power plant sites in the central and eastern U.S. (EPRI, 1986). In the EPRI study, experts were arranged into six "earth science teams," each having a range of expertise required for characterizing seismic sources, including seismology, geophysics, and geology/tectonics. Multiple workshops were held to discuss technical issues, and each team developed seismic source characterizations and their associated uncertainties. The technical basis for the assessments was documented in a final report (EPRI, 1986), and the study underwent extensive NRC review (EPRI, 1988). As with the EPRI study, each expert team in the seismic source and fault displacement characterization was expected to function as a single "virtual" expert and to express their assessments and uncertainties as an individual expert. Teams were not asked to provide a single consensus assessment—no more than an individual expert is asked to provide a single

estimate. Rather, teams were asked to make assessments with a range of uncertainties, just as individual experts are asked to provide their expressions of uncertainty.

The Senior Seismic Hazard Analysis Committee (SSHAC, 1997) defines the expert roles of *proponent, evaluator,* and *integrator*, roles that were understood and employed by the experts. A proponent advocates a particular technical hypothesis or interpretation, an evaluator considers the support for alternative hypotheses and interpretations in the available data and evaluates the uncertainties associated with the assessments, and an integrator combines the evaluators' alternative interpretations into a composite distribution that includes uncertainties. The experts were informed of their roles as evaluator experts and of the need to forsake the role of proponent in making their interpretations and evaluating uncertainties. Proponents of specific hypotheses or interpretations were engaged as resources and presented their hypotheses or interpretations in workshops. Alternative proponent views were presented to the experts and open scientific debates of alternative views were facilitated among them at the workshops. Some expert evaluators also were engaged temporarily as proponents to describe a particular hypothesis or interpretation in a workshop.

Expert interactions are deemed vital in the SSHAC (1997) process and must be properly facilitated. Experience from numerous seismic hazard studies has shown that experts interact frequently in their professional activities, and that workshops serve to provide information and interaction that facilitate their consideration of hypotheses and data and, ultimately, their evaluations and interpretations. Expert interactions on the PSHA Project were encouraged and facilitated through multiple workshops and, for seismic source and fault displacement characterization, a field trip. Technical challenge and debate of alternative ideas was the focus of these meetings, including discussion of preliminary interpretations made by the experts. Finally, the SSHAC (1997) process emphasizes the need to consider at the outset the strategy for integration or aggregation of the experts' evaluations, so that the analyses are structured in a way that is conducive to aggregation. This project at the outset defined a strategy to combine the evaluations of the experts using equal weights. The key procedural components of the project (ranging from the selection of experts to the dissemination of data sets) were designed to allow the equal-weights strategy to be implemented in a defensible manner. As noted by SSHAC (1997), the goal of any multiexpert study is to identify the

body and range of uncertainty that would be defined by the larger informed technical community if they provided their evaluations.

The PSHA Project followed the procedural guidance set forth in the SSHAC (1997) study, both in spirit (e.g., recognition of the importance of facilitated expert interactions) and, in many cases, in details of implementation (e.g., suggestions for conducting workshops and elicitation interviews). For example, the seismic source and fault displacement characterization process was designed in accordance with SSHAC (1997) guidance to result in probability distributions that represent the range of technical interpretations of the larger informed technical community. The expert teams were informed about and reminded of the need to express this full range of uncertainty in their probability distributions, that is, they were asked to express alternative interpretations permitted by the available data weighted by the degree that each is supported by the data. Inasmuch as SSHAC is nonprescriptive (it avoids specifying a single way of implementing the process), it would be inappropriate to say that the PSHA Project conformed exactly to the SSHAC (1997) process or any other prescription. The goal of all the guidance documents, including the NRC Branch Technical Position (NRC, 1996), is not to establish a rigid set of rules for expert elicitation, rather, it is to draw from experience, both successes and failures, the criteria for when expert elicitation should be used and to outline approaches for motivating, eliciting, and documenting expert evaluations. Other documents in the literature provide complimentary approaches to the formal or informal use of expert elicitation (e.g., Meyer and Booker, 1991).

2.2 GENERAL APPROACH

The general approach implemented in this project for eliciting the evaluations of the experts is described in this section. The principal steps were:

(1) **Selection of Experts.** The Project Management Team established criteria for the selection of experts (See Section 2.3). These criteria were intended to ensure that all the experts had significant professional stature and technical expertise. A list of candidates was developed by the Project Management Team with input from the facilitation team leaders. From this list of candidates, 18 SSFD and 7 GM experts were selected.

(2) **Development of Project Plan.** The Project Management Team developed a Project Plan that outlined the goals and key elements of the project, timing of significant activities such as workshops, and topics to be covered through workshops and the field trip. Throughout the project, management flexibility was maintained to address additional needs as they arose to provide that the project goals were achieved. For example, an additional feedback workshop was implemented to address fault displacement characterization methodologies, and additional feedback teleconferences were held to facilitate the finalization of fault displacement characterization. These additional activities are documented in this report.

(3) **Data Compilation and Dissemination.** The compilation and distribution of pertinent data, including published reference material, began early and continued throughout the project (Appendix B). Before the first workshops, the experts were sent a number of data sets and publications. Important data sets and publications identified during each workshop also were distributed. Experts were provided access, if requested, to all Yucca Mountain data gathered as part of the project and to data gathered by others (for example, the State of Nevada and the Center for Nuclear Waste Regulatory Analyses [CNWRA]).

(4) **Meetings of the Experts.** Structured, facilitated interaction among the experts took place during the workshops (and one field trip for the SSFD experts) and working meetings. The workshops were designed to identify the significant issues, review available data, debate alternative models, and quantify uncertainties related to seismic source and fault displacement and ground motion characterizations. Proponents of particular technical positions provided their interpretations to the experts. Debate and technical challenge of alternative interpretations were encouraged to provide for identifying uncertainties. At these meetings, researchers from a variety of organizations, including for example, USGS, University of Nevada at Reno, Nevada Bureau

of Mines and Geology, CNWRA, and Lawrence Berkeley National Laboratory, presented pertinent data sets and alternative models and methods.

(5) **Elicitation Interviews.** One-day elicitation interviews were held with each of the three-member SSFD expert teams, GM experts, and representatives of the facilitation teams. Each expert or expert team provided their preferred and alternative evaluations, expressed their uncertainties, and specified the technical bases for their assessments. The facilitation teams documented the elicitation during the interview. The experts then independently prepared documentation of their evaluations, included as Appendices E and F in this report.

(6) **Feedback of Preliminary Results.** Following the elicitation interviews, feedback workshops were held. The objectives of these workshops were to review, discuss, and debate the interpretations of each of the experts or expert teams, allowing them to understand and ask questions about the alternative approaches used by others as well as to technically defend their preliminary interpretations. Debate and technical challenge of the interpretations were encouraged to make sure that alternatives were understood and uncertainties were being completely incorporated. Facilitation and calculations team members presented preliminary analysis and sensitivity results. At the final workshops, the aggregation process was discussed.

(7) **Finalization of Expert Assessments.** Following the feedback workshops, the experts revised and refined their interpretations and developed their final elicitation summaries. A series of technical reviews were conducted to ensure that the sequence of models, components, and parameters was logical and complete and that the technical bases for the assessments were clearly provided.

(8) **Preparation of Activity Reports.** Activity Reports for seismic source and fault displacement characterization and ground motion characterization were prepared to document the process followed and the expert elicitation summaries.

2.3 SELECTION OF EXPERTS

The selection of experts involved four steps: (1) developing selection criteria, (2) obtaining a list of candidates, (3) selecting and inviting candidates to participate, and (4) for seismic source and fault displacement characterization, dividing the experts into six multidisciplinary teams. A selection panel, formed from members of the Project Management Team and other selected members of the project including the facilitation team leaders, was responsible for the selection process. The panel included Carl Stepp, John Whitney, Ivan Wong, Tom Hanks, David Schwartz, Silvio Pezzopane, Kevin Coppersmith, and Norm Abrahamson.

Expert selection was based on the following criteria:

- Strong relevant expertise as demonstrated by professional reputation, academic training, experience, and peer-reviewed publications and reports

- Willingness to forsake the role of proponent of any model, hypothesis, or theory and to perform as an impartial expert who considers all hypotheses and theories and evaluates their relative credibility as indicated by the data

- Availability and willingness to commit the time required to perform the evaluations needed to complete the study

- Specific knowledge of the Yucca Mountain area, the Basin and Range Province, or ground motion characterization

- Willingness to participate in a series of open workshops, diligently prepare required evaluations and interpretations, and openly explain and defend technical positions in interactions with other experts participating in the project

- Personal attributes that include strong communications skills, interpersonal skills, flexibility and impartiality, and the ability to explain clearly and succinctly the basis for interpretations and technical positions

In September 1994, the selection panel developed a preliminary list of candidates through a nomination process. Additional candidates were subsequently added to the preliminary list to form the final list of candidate experts. Candidates were nominated to capture the needed breadth of scientific expertise and technical knowledge and to obtain a range of organizational representation. Individuals who had expertise in each of three technical areas for seismic source and fault displacement were also specifically nominated.

From the candidate list, 18 SSFD experts were initially selected in November 1994. Five of the initial seismic source and fault displacement candidates who were invited to become experts declined, stating schedule conflicts or perceived conflicts of interest. Subsequently, additional individuals were contacted until the full complement of 18 experts was attained in January 1995.

In addition to the specific selection criteria, an important general requirement for the GM experts was to ensure that the range of credible ground motion attenuation relations was represented. To that end, GM experts were selected from individuals knowledgeable in both the empirical approach to ground motions as well as numerical modeling techniques. Also, individuals knowledgeable in technical issues such as near-field source effects, crustal attenuation, path effects, site response, and ground motions from nuclear explosions were sought.

From the candidate list, six GM experts were selected by the panel in November 1994. In advance of their selection, the Project Management Team had concluded that the minimum number of experts necessary to provide diversity of knowledge was six. A seventh GM expert was added to complete the representation of various ground motion models. All experts were contacted in late November and early December 1994 to determine whether they could participate in the PSHA Project. All seven selected GM experts agreed to participate.

Of the 18 SSFD experts who attended the initial April 1995 workshop, two subsequently resigned. Before the project resumed in October 1996, Dr. Tony Crone informed the Project Management Team that other commitments prevented him from continuing to serve as an expert. The selection panel chose Dr. Peter Knuepfer as a replacement. In early February 1997, the panel replaced Dr. Chris Menges, who withdrew for health reasons, with Dr. Dennis O'Leary. Dr. O'Leary is a member of the USGS Yucca Mountain geologic team and was an active participant at the seismic source and fault displacement workshops.

The Project Management Team chose to form expert teams for the seismic source and fault displacement characterization portion of the project to incorporate the required scientific disciplines and diversity of knowledge. It was deemed essential that both geologic and seismologic disciplines were represented on the teams. Six three-person teams were formed, consisting of (1) an individual having particular knowledge and expertise about the paleoseismology and Quaternary faulting in the Yucca Mountain area, (2) an individual having particular knowledge and expertise about the regional geology and tectonics of the Yucca Mountain region, and (3) an individual having training or education in seismology and seismicity. The six individuals from each of the three technical areas were selected at random and combined into teams by the SSFD Facilitation Team. The acronyms for each team used in this report are given in order of area of expertise as follows: (1) seismology, (2) regional geology/tectonics, and (3) paleoseismology (e.g., the AAR team is composed of seismologist W. Arabasz, regional geologist E. Anderson, and paleoseismologist A. Ramelli) (see Section 4.3.1.1).

Consistent with the guidance of NUREG-1563 (NRC, 1996), all experts were asked to document any conflicts of interest relating to their roles as evaluators of seismic sources, fault displacement, and ground motion attenuation for Yucca Mountain. Each expert completed a conflict of interest statement, which is included as part of the records of the PSHA Project. None of the selected experts was precluded from participating in the Project on the basis of conflicts of interest.

3.0
SEISMIC SOURCE AND FAULT DISPLACEMENT CHARACTERIZATION FACILITATION APPROACH

In this chapter, the approach utilized by the SSFD Facilitation Team to elicit interpretations from the SSFD experts is described.

3.1 DATA COMPILATION AND DISSEMINATION

Data compilation and dissemination formed an important aspect of the seismic source and fault displacement characterization process. The goal was to ensure that the evaluations by the SSFD expert teams were based on a knowledge of all available data and existing interpretations in the published and unpublished literature. Initially during 1995, the USGS served as a clearinghouse for requests for and dissemination of data. In subsequent stages of the study, the SSFD Facilitation Team and the Data Management Team were responsible for receiving requests for data and for compiling and disseminating the data to the experts. The data distributed included journal articles, preprints of recently completed work, synthesis reports for Yucca Mountain work, digital data bases such as the fracture data base derived from the line-survey for the ESF, and empirical data compiled from literature. In some cases, compilations of data and simple analyses of the data (e.g., linear regressions) were performed by the SSFD Facilitation Team at the specific request of the expert teams. For example, Silvio Pezzopane conducted a number of analyses of empirical data regarding historical surface ruptures to fulfill requests made by the expert teams. These analyses are documented in the workshop summaries.

3.2 SEISMIC SOURCE AND FAULT DISPLACEMENT WORKSHOPS

The following sections summarize the workshops and field trips conducted during the project (Figure 3-1). These activities were the primary vehicles for expert interaction and review of technical issues. Detailed summaries of the workshops and field trip are provided in Appendix C.

3.2.1 Workshop #1-Data Needs

The Workshop on Data Needs, April 17-19, 1995, was the first of six workshops conducted for the seismic source and fault displacement characterization. The primary goals of the workshop were to identify key technical issues of importance to seismic source characterization and to specify the data required to characterize the seismic sources for vibratory ground motion and fault displacement hazards. Other objectives of the workshop were to provide information to the experts on the overall study, the products to be developed, the project schedule, the roles of various participants, alternative expert roles (evaluators, proponents, specialists), basic approaches to PSHAs and expressing uncertainties, and ground rules regarding communication and interaction throughout the study.

To accomplish these goals, the workshop included a series of presentations and discussion sessions that involved scientists from various organizations. The basic approach of the workshop was to (1) identify technical issues of most significance to seismic hazards at Yucca Mountain, (2) link those issues with the data most relevant to addressing the issues, (3) specify the available relevant data for the Yucca Mountain region, and (4) identify the data required by the experts to characterize seismic sources. During a discussion that followed workshop presentations by several technical specialists, the experts identified the issues deemed most important to characterizing seismic sources at Yucca Mountain. The identification of technical issues was essential for identifying the types of data needed, and to help create a common understanding among the experts of the important elements that directly or indirectly influence future seismic hazards at Yucca Mountain.

The major technical issues identified by the experts during the first workshop included (1) defining candidate seismic sources and associated maximum magnitudes for the background earthquake, (2) choosing recurrence models and weights for fault sources, (3) developing models for fault segmentation and multiple fault ruptures, (4) assessing the effects of triggering on earthquake recurrence, (5) characterizing fault geometry and kinematics, (6) characterizing distributive faulting, (7) assessing nonstationary and temporal clustering of earthquakes, and (8) assessing the importance of volcanic earthquakes and characterizing potential sources of such events. A complete list of the technical issues and required data identified by the experts is included as Table 2 in the workshop summary in Appendix C.

Presentations by specialists on technical issues identified from previous studies of historical seismicity and fault sources at Yucca Mountain were the focus of the first day and a half of the workshop. These were followed by a day and a half of presentations on available and forthcoming data sets for the Yucca Mountain region. Topics included historical seismicity, regional and local faults, geologic mapping (both surficial and bedrock), geochronological, structural, and stratigraphic studies, and a variety of geophysical studies. Presentations were given by Yucca Mountain principal investigators who not only provided reference information for published data, but also offered to provide much of the unpublished data to the experts either through personal communications or the USGS Yucca Mountain Project Branch. Before the workshop, the USGS distributed a large amount of available data and lists of relevant data sources to each expert. A complete list of this material is included as Table 3 of the workshop summary (Appendix C).

3.2.2 Workshop #2-Seismic Hazard Methodologies

The workshop on Seismic Hazard Methodologies, October 16-18, 1996, was conducted after the project resumed following a 1-year hiatus. The purpose of this 2½-day workshop was twofold: (1) to review data that had become available since the project had stopped and (2) to identify and evaluate methods and approaches for characterizing seismic sources in the Yucca Mountain region. The workshop also served as a kickoff meeting for restarting the project, and participants were advised of revisions to the Project Plan and schedule.

The approach during the workshop was to divide seismic source characterization into two parts for vibratory ground motion analysis and fault displacement analysis. These parts were then further subdivided into three components: seismic source location and geometry, maximum earthquake magnitude, and earthquake recurrence assessment. Presentations by a variety of technical specialists, many of them experts, were given on each of these topics, first focusing on available methods for characterization and then describing newly available data. A complete list of the data provided is included as Table 1 in the workshop summary (Appendix C).

3.2.3 Workshop #3-Alternative Models and Interpretations and Field Trip

The workshop on Alternative Models and Interpretations, November 18-21, 1996, was combined with a field trip to Yucca Mountain, Crater Flat, and Bare Mountain. The purpose of the 4-day field trip and workshop was to review and evaluate alternative models, hypotheses, and interpretations that are important to the characterization of seismic sources in the Yucca Mountain region. The agenda for the workshop and field trip was developed with the explicit purpose of juxtaposing alternative ideas and views presented by various proponents. Discussions were facilitated to encourage the experts to probe for a better understanding of the technical bases for each model, to debate and listen to the pros and cons of the alternatives, and to quiz the proponents to better understand the uncertainties associated with each model. Additionally, the field trip enabled the experts to observe both surface and subsurface exposures at many key sites, providing first-hand insights into field data and interpretations. In this way they were able to evaluate the limits on resolution and the uncertainties associated with the field data and interpretations.

Throughout the workshop and field trip, a forum was provided for structured debate. Various scientists, including some experts, assumed the role of proponent in presenting arguments in favor of a particular model or interpretation. The experts were then encouraged to act as evaluators by probing the proponent positions in an effort to better understand the interpretations, the supporting data for each interpretation, and the associated uncertainties.

The field trip included 2½ days of field review and discussion focused on (1) the behavior of faults in the Yucca Mountain vicinity, (2) the nature of faulting in the potential repository block, and (3) the behavior of the Bare Mountain fault. John Whitney coordinated the field trip; individual stops were led by a variety of Yucca Mountain investigators. Numerous excavations and natural exposures were reviewed along many faults, including the Bare Mountain, Crater Flat, Windy Wash, Solitario Canyon, Ghost Dance, Bow Ridge, and Paintbrush Canyon faults. At these stops the principal investigators explained the field relationships, provided interpretations of the displacements, their ages, and recurrence, and expressed their uncertainties. A half-day trip into the ESF provided a subsurface view of faults and fractures in the proposed repository block. Highlights of this trip included exposures of (1) the Bow Ridge fault, (2) small intrablock reverse and normal faults, (3) cooling joints and faults, (4) the Drill Hole Wash fault, and (5) breccia zones.

The workshop discussions entailed presentations and debate centered around five key issues to seismic source and fault displacement characterization: tectonic models, three-dimensional geometry of faults, definition and synchronicity of faulting events, characterization of faulting in the proposed repository block, and maximum background earthquakes. Presentations of proponent positions on the five key issues were followed by debate by the experts. Some of the most extensive discussions focused on (1) the possible existence and character of large, buried strike-slip shear zones and detachment faults, (2) structural models of the subsurface geometry of the Bare Mountain and Yucca Mountain faults, (3) the occurrence of distributive faulting on multiple faults, possibly associated with volcanism, (4) slip rates on the Bare Mountain fault and implications to Yucca Mountain faults, (5) the origin of fracturing events observed in many exposures throughout Yucca Mountain, and (6) the age of youngest activity and Quaternary rates of activity for faults in Tertiary bedrock. A more comprehensive summary of the field trip itinerary and the issues discussed throughout the 4-day session is included in the workshop summary (Appendix C).

3.2.4 Workshop #4-Preliminary Interpretations

The goals of the Preliminary Interpretations Workshop, January 6-8, 1997, were to (1) provide an opportunity for the expert teams to receive feedback from their colleagues by presenting and discussing their preliminary interpretations regarding key issues, (2) train the expert teams in the process of elicitation and the characterization of uncertainty, and (3) present and discuss additional information and interpretations of importance to the study. To accomplish these goals, a series of presentations by the experts and group discussions were conducted. Five key issues were identified: (1) tectonic models, (2) potential seismic sources, (3) maximum magnitudes, (4) earthquake recurrence, and (5) fault displacement methodology. Two expert teams were assigned to present their preliminary interpretations of each issue. These presentations were followed by group discussion of each issue, during which the other teams were given the opportunity to debate the credibility of alternative views and to present their preliminary interpretations.

The focus of the presentations and discussions was on understanding the interpretations, their technical bases, their consistency or inconsistency with data, and the expression of uncertainty. Discussion was facilitated so that each team understood the interpretations of others, including the degree to which an interpretation was supported by earthquake and

faulting models and observed data. The experts could then more knowledgeably reevaluate their own team interpretations. The objective was to help teams prepare for the upcoming elicitation interviews so that interpretations would be well-reasoned, technically supported, and complete. Throughout this 2½-day workshop, the facilitator encouraged the experts to explore the issues thoroughly, ask questions that would help them during the elicitations, and continually keep in mind the characterization of uncertainties.

Also included in the workshop was a half-day elicitation training session conducted by normative expert Peter Morris, along with presentations by technical specialists of additional information on some key issues that were highlighted or outstanding from previous workshops. These included presentations on investigations of the Sundance fault, interpretations of seismic reflection lines and relevant geophysical data in the Yucca Mountain vicinity, the southern extent of Yucca Mountain faults, and the seismogenic potential of known or postulated shallow-dipping normal faults. More details on these presentations and those given by the teams on their preliminary interpretations are included in the workshop summary (Appendix C).

3.2.5 Workshop #5-Feedback

The Feedback Workshop, April 14-16, 1997, occurred after the elicitation interviews (discussed below). The purpose of the workshop was to provide feedback to the expert teams by (1) providing an opportunity for the teams to discuss the first round of their interpretations; (2) allowing each team to understand and ask questions about the interpretations made by other teams, (3) providing information on the derivative products of their first-round assessments (i.e., seismic source characteristics), and (4) providing sensitivity analyses to show the relative impact of various assessments on the calculated results. To accomplish these goals, a series of presentations and group discussions were conducted, with emphasis on facilitated interaction among the experts and feedback from the SFFD Facilitation and PSHA Calculations teams. For each of six key issues, two or three expert teams presented their interpretations, followed by a general discussion that included all of the teams. These six key issues, identified by the SSFD Facilitation Team from the preliminary results, included (1) characterization of areal seismic source zones, (2) geometry of local faults, (3) synchronous ruptures of local faults, (4) maximum magnitudes and recurrence on local faults, (5) characterization of other seismic sources, such as buried strike-

slip shear zones, detachments, volcanic zones, and other buried or postulated structures, and (6) methodologies for evaluating fault displacement.

The focus of the presentations and discussion was on understanding the interpretations of others, their technical bases, consistency with data, and expression of uncertainty. Preliminary results and sensitivity analyses were presented, highlighting the sources and parameters most significant to the analyses.

The specific aspects of the six issues discussed were (1) different approaches for defining and determining M_{max} for areal source zones containing Yucca Mountain (i.e., host zones), (2) processing and analysis of the historical seismicity catalog to estimate earthquake recurrence for host zones, (3) different approaches to determining seismogenic depths, (4) the use of structural and tectonic models to constrain subsurface geometries of local faults and potential buried seismic sources, (5) different approaches to developing models of rupture behavior for local faults, (6) the bases for assessing the potential activity of faults, and (7) different approaches to assessing the amounts and rates of fault slip for smaller (not block-bounding) faults in Tertiary bedrock within the Controlled Area. In regard to the latter, the experts extensively discussed the distinction between seismogenic or principal slip, distributive or secondary slip, and nontectonic slip. A clear and common understanding of this distinction is important, because some faults were included as potential sources of fault displacement, but were determined not to be independent seismogenic sources capable of generating earthquakes in the ground motion assessment.

During the workshop, feedback was also provided from the PSHA Calculations Team regarding preliminary results and sensitivity analyses for the first round of seismic source characterization and ground motion interpretations. Feedback included specific results for five teams' characterization models for the ground motion assessment and for four teams' methods and characterization models for the fault displacement assessment. The PSHA Calculations Team sent preliminary hazard curves and results of sensitivity analyses after the workshop to teams that did not complete their input in time to receive feedback at the workshop. At the end of the Feedback Workshop, a joint session was held with the SSFD experts and the GM experts. The purpose of this joint session was to provide an opportunity for interaction between the two groups of experts, specifically to discuss common issues, ask

questions about each other's interpretations and assessments, highlight any inconsistencies between the seismic source and ground motion characterizations, and come to a better common understanding of the linkages between the two groups' input to the seismic source and fault displacement. For example, a subject of considerable discussion was the geometry of seismogenic sources, especially interpretations that call for the simultaneous rupture of multiple Yucca Mountain faults. In addition, interpretations of earthquake stress drop were discussed. The summary of this workshop includes more detail on these and other issues discussed during the Feedback Workshop (Appendix C).

3.2.6 Workshop #6-Fault Displacement

The Fault Displacement Workshop, June 3, 1997, the final workshop conducted for the seismic source and fault displacement characterization, was designed to provide feedback to the teams on their fault displacement approaches and assessments. The threefold purpose of the 1-day workshop was to (1) review and discuss alternative methods and models for assessing fault displacement, (2) discuss uncertainties in parameter values and models, and (3) facilitate the expert teams' discussion of the pros and cons of alternative approaches, models, and submodels. Prior to the workshop, a "white paper" summarizing the fault displacement evaluation approaches developed by the expert teams was prepared by the SSFD Facilitation Team and distributed to the experts. During the workshop, the approaches taken by each expert team to evaluate displacement at nine demonstration points were reviewed in more detail than at the previous workshop. This was followed by extensive discussion and technical challenge about the strengths and weaknesses of all the approaches, data required to apply them, and uncertainties in model parameters.

The methods used for estimating the frequency of displacement events and the expected displacement per event at locations where faults or fractures are present in Tertiary rocks, but Quaternary paleoseismic data are lacking, were discussed extensively. Discussion also focused on the use of data from historical surface faulting events to develop relations for the likelihood of distributive faulting and the pros and cons of approaches using observed displacements versus those that rely on mechanical models of rock deformation. The experts explained different approaches to characterizing both along-strike and event-to-event variations in displacement. Presentations also were given on newly available information from the ESF, as the tunnel boring machine had completed its excavations since Workshop

#5. More details on these presentations and the fault displacement issues discussed are included in this workshop summary (Appendix C).

3.3 ELICITATION OF SSFD EXPERTS

The elicitation interviews involved a series of activities, which can be grouped into two steps: (1) preparation for the interviews and (2) the elicitation interviews.

3.3.1 Preparation for the Elicitation

Peter Morris of the SSFD Facilitation Team provided elicitation training at Workshop #4. The objectives of the training were to demonstrate how to quantify uncertainties using probabilities, to recognize common cognitive biases and compensate for them, and to present examples of the types of assessments that would be made at the elicitation interview (e.g., continuous variables, discrete hypotheses, and associated weights). The training was designed to help the experts be comfortable with the *process* of elicitation, so that the elicitation interview itself could focus on the *technical issues* of importance to the seismic source and fault displacement characterization.

At Workshop #4, the experts had been informed that the seismic source characterization issues presented would be covered in the elicitation interviews. A memo providing guidance for the characterization of fault displacement was provided to the expert teams before the elicitation interviews. The memo described the alternative approaches available to evaluate fault displacement (earthquake-based approaches that rely on the location, frequency, and size of earthquakes, and displacement-based approaches that evaluate the amount and frequency of displacement directly from displacement observations). In addition, the memo identified nine demonstration points within the Controlled Area that would serve as representative points (representing the range of expected conditions) at which all teams' fault displacement methodologies would have to be operative.

3.3.2 Elicitation Interviews

The elicitations of the expert teams took place in separate 1-day interviews in the San Francisco office of Geomatrix Consultants. The interviews were conducted by members of the SSFD Facilitation Team. Dr. Coppersmith (specialist and normative expert) and Dr.

Youngs (generalist and hazard analyst) attended all of the interviews, Dr. Perman, Ms. Olig, and Dr. Morris (normative expert) attended selected interviews. Drs. Whitney and Toro, and an NRC representative, also attended some interviews to observe the process followed.

All data sets provided or made available to the experts during the project were present during the elicitation. The elicitation interview followed a logical sequence from general to more specific assessments. Alternative models, approaches, and hypotheses were discussed, and the logic structure for the assessments and associated probability distributions were developed. Team members discussed the various issues among themselves and arrived at alternative models and probability distributions that they believed spanned the range of views across their team and across the larger technical community. The SSFD Facilitation Team representatives took written notes of all assessments during the interviews.

3.3.3 Documentation and Review

Documentation of the expert elicitations began with documentation and a summary prepared by the SSFD Facilitation Team representatives during the interviews. Experience on several other expert elicitation projects has shown this approach to be preferable to other documentation methods (e.g., written questionnaires, experts writing their interpretations following the interview, or tape recordings). During the 1-day interview, each expert team was asked to make many assessments, to quantify uncertainties, and to provide the technical bases for their interpretations. By having the SSFD Facilitation Team document and summarize, experts were free to focus on thinking through their answers and thoroughly expressing interpretations. The SSFD Facilitation Team was able to be flexible in the elicitation sequence (i.e., following the logic comfortable to the team) while ensuring that all elements were covered.

Following the interviews, the SSFD Facilitation Team provided each expert team with written documentation of the interview, organized by model component. The experts, in accordance with the requirements of the Project Plan, independently prepared a summary that reflected their interpretations. The summaries prepared by each expert team became the first draft document. This draft was reviewed for logical consistency and completeness and returned to the expert team for revision. The revised summary became a second draft that was reviewed by Dr. Stepp. These reviews were conducted to provide for completeness and

clarity of documentation. The teams responded to any requests for further clarifications, and the summaries were finalized. The elicitation summaries are provided in Appendix E.

3.3.4 Feedback and Sensitivity

Feedback to the experts occurred throughout the seismic source and fault displacement characterization, primarily through interaction among experts. By presenting their evaluations of models and associated interpretations at workshops and in general discussions, the experts both provided and received feedback from their peers on the panel.

More formally, feedback was provided to the experts using several approaches.

- At Workshop #4, the expert teams presented their preliminary interpretations regarding the key technical issues to the other teams. The teams were encouraged to understand the alternative views, their technical bases, and uncertainties.

- At Workshops #5 and #6, which occurred after the elicitation interviews, discussion focused on team interpretations. Discussions included the technical bases for the interpretations, the weights assigned to alternative hypotheses, and expressions of uncertainty in parameter values and alternative models (e.g., logic trees).

- Calculations showing the results of each team's initial interpretations were presented at Workshops #5 and #6. Calculations included maximum magnitude distributions, earthquake recurrence relationships for important seismic sources, calculated seismic hazard curves and dominant contributors, and fault displacement hazard curves and dominant contributors.

- Prior to the finalization of the seismic source and fault displacement models, each team was provided with (1) calculations showing the results of their preliminary interpretations, (2) plots showing the sensitivity of their results to alternative maximum magnitude and recurrence approaches or models, and (3) comparison of the calculated seismic hazard curves for all sources combined for all teams to mean recurrence estimates for individual teams. Conference calls with each of the

teams and members of the SSFD Facilitation Team were conducted to provide clarification and additional feedback. Revisions to the seismic source and fault displacement models based on the feedback provided were incorporated into the final results.

- Members of the SSFD Facilitation Team, Project Management Team, and Review Panel reviewed the written elicitation summaries for clarity, adequacy, and completeness of documentation of the technical basis for the evaluations described in them.

The feedback-revision process required the experts to defend/revise their assessments as considered appropriate and to provide appropriate documentation. In all cases, the experts responded positively to critical reviews of their documentation. The resulting assessments and finalized elicitation summaries reflect the significant effort expended by each expert team.

3.3.5 Aggregation of Expert Assessment

The approach taken to combine, or aggregate, the expert evaluations is equal weighting. This approach was not a default but a goal from the start of the project, a goal the experts were apprised of throughout the project. Accordingly, the proper conditions were created throughout the project to allow for using equal weights (SSHAC, 1997). The actions taken to provide these conditions included:

- Carefully selecting highly qualified experts who represent diverse disciplines and experience

- Establishing and confirming the commitment of each expert to provide the required effort throughout the project

- Identifying available data sets and disseminating them to all experts

- Educating the experts in issues important to seismic source and fault displacement characterization and training the experts in elicitation methodologies and the role of experts as evaluators

- Facilitating interaction among the experts in workshops and field trips to foster a free exchange of data and interpretations and scientific debate with respect to hypotheses and resolution of data

- Providing feedback and sensitivity analyses to the experts

- Providing an opportunity for experts to revise their assessments in light of feedback

It should be noted that, in accordance with the guidance provided by SSHAC (1997), conditions could have been such that different weights would have been necessary. For example, if an expert team had been unwilling or unable to devote the required time and effort to develop a complete assessment and documentation, that team would have been removed from the project.

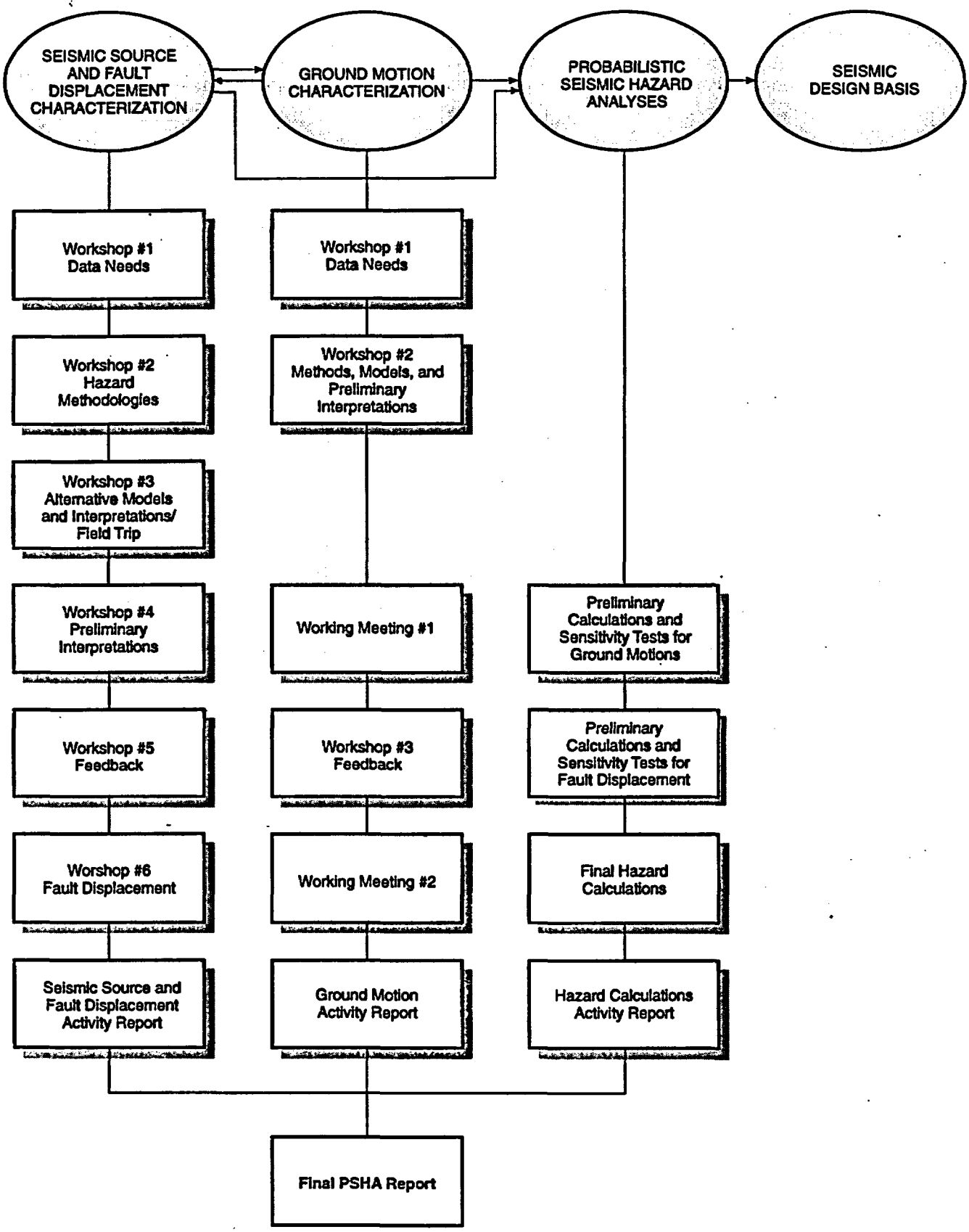

Figure 3-1 Probabilistic Seismic Hazard Analyses Project process for Yucca Mountain

4.0
SEISMIC SOURCE AND FAULT DISPLACEMENT CHARACTERIZATION

This section describes the methodologies used by the expert teams to (1) characterize the sources of potential earthquakes in the vicinity of the Yucca Mountain site for the PSHA for ground shaking hazard and (2) characterize fault displacement hazard within the Controlled Area. Section 4.1 presents the formulations used for seismic source characterization. Section 4.2 presents the formulations used for characterizing fault displacement hazard. The seismic source and fault displacement models developed by the six SSFD expert teams are described in Section 4.3. A detailed description of the PSHA methodology for vibratory ground motions is contained in Section 7.1.

4.1 SEISMIC SOURCE CHARACTERIZATION METHODOLOGY FOR GROUND MOTION HAZARD ASSESSMENT

The role of the SSFD expert teams in the ground motion PSHA is to identify the seismic sources that may produce earthquakes significant to ground motion hazard at the site. Then for each source they are to evaluate the frequency of earthquake occurrence, the maximum earthquake the source can produce, the distribution of earthquake sizes, and the spatial distribution of earthquakes on the source so that the distance to an earthquake of given magnitude can be computed. The methodologies used to assess these characteristics are discussed below.

4.1.1 Logic Trees

The PSHA methodology is formulated to represent the randomness inherent in the natural phenomena of earthquake generation and seismic wave propagation. The randomness in a physical process has come to be called *aleatory* uncertainty (SSHAC, 1997). In all assessments of the effects of rare phenomena, one faces uncertainty in selecting the appropriate models and model parameters because the data are limited and/or there are alternative interpretations of the data. This uncertainty in knowledge has come to be called *epistemic* uncertainty (SSHAC, 1997). The SSFD experts placed a major emphasis on developing a quantitative description of the epistemic uncertainty.

The uncertainty assessment was performed using the *logic tree* methodology. The logic tree formulation for seismic hazard analysis (Kulkarni *et al.*, 1984; Coppersmith and Youngs, 1986; EPRI, 1988; NRC, 1988) involves setting out the sequence of assessments that must be made in order to perform the analysis and then addressing the uncertainties in each assessment sequentially. Thus, it provides a convenient approach for dividing a large, complex assessment into a sequence of smaller, simpler components that can be addressed more easily.

Figure 4-1 shows an example of a logic tree. The logic tree is composed of a series of nodes and branches. Each node represents a state of nature or an input parameter that must be characterized to perform the analysis. Each branch leading from a node represents one possible alternative interpretation of the state of nature or parameter being evaluated. If the variable in question is continuous, it can be discretized at a suitable increment. The branches at each node are intended to represent mutually exclusive and collectively exhaustive states of the input parameter. In practice, a sufficient number of branches are placed at a given node to represent the evaluator's uncertainty in estimating the parameter.

Probabilities are assigned to each branch that represent the expert's evaluation that the branch represents the correct value or state of the input parameter. These probabilities are conditional on the assumption that all the branches leading to that node represent the true state of the preceding parameters. Because they are conditional probabilities for an assumed mutually exclusive and collectively exhaustive set of values, the sum of the conditional probabilities at each node is unity. The probabilities are based on scientific evaluations because the available data are often too limited to allow for objective statistical analysis, and because scientific evaluation is needed to weigh alternative interpretations of the available data. The logic tree simplifies these evaluations, because the uncertainty in each parameter is considered individually, conditional on assumed known states from prior evaluations. The nodes of the logic tree are sequenced to express conditional aspects or dependencies among the parameters and to provide a logical progression of evaluations from general to specific in characterizing the input parameters for PSHA.

The probabilities (relative weights) assigned to the branches at a node of the logic tree represent one of two types of probability assessments. For the first type, the branches at a node define the

range of parameter values; the associated weights define the probability distribution for the parameter. For example, estimates of the slip rate on a fault are uncertain because of uncertainties in the amount of displacement of a particular geologic unit across the fault and the age of the unit. The probability distribution for a parameter value may be characterized in several ways: as a discrete distribution defined by a preferred value and a range of discrete higher and lower values, a cumulative distribution based on scientific evaluations, or by a mean and standard deviation for a specified statistical distribution. Examples of these means of characterization are given below. Continuous distributions can be discretized to form logic tree branches following a number of approaches. Keefer and Bodily (1983) showed that most distributions can be represented reliably by three values: the median estimate (50^{th} percentile), assigned a weight of 0.63, and a higher and lower value, each given weights of 0.185, which represent the 5^{th} and 95^{th} percentiles (± 1.645 standard deviations for a normal distribution). They list other discretization schemes for more points. Another four-point representation of a normal distribution is described in EPRI (1993, Chapter 9). Miller and Rice (1983) present a number of discrete approximations to subjectively defined, continuous cumulative distributions.

In some instances, the uncertainty in assessing parameters can be estimated using formal statistical techniques. In these cases, continuous parameter distributions developed from statistical estimation procedures can be discretized for use in a logic tree formulation. An example of this approach is presented in Section 4.1.3.

A second type of probability assessment, to which logic trees are particularly well suited, is indicating a relative preference for, or degree of belief in, alternative hypotheses. For example, the sense of slip on a fault may be uncertain – two alternatives might be strike-slip or reverse-slip. Based on the pertinent data, a relative preference for these alternatives can be expressed by weights in the logic tree. A very strong preference (i.e., the data strongly support one interpretation over the other) for one alternative over the other usually is represented by weights such as 0.9 and 0.1. If there is no preference (i.e., the data equally support either alternative) for either hypothesis, they are assigned equal weights (0.5 and 0.5 for two hypotheses). Increasing the weight assigned to one alternative from 0.5 to 0.9 (or more) reflects increasing support in the data for that alternative. Because the relative weights ultimately are the result of scientific evaluations based on available information, it is important to document

the data and interpretations that led to the characterization of parameter values and their relative weights so that the process can be reviewed by others.

The example logic tree shown on Figure 4-1 characterizes the uncertainty in assessing the magnitude of paleoearthquakes that have occurred on a fault on the basis of dip-slip offsets observed in a trench placed across the fault. (Such assessments may be one means of characterizing the maximum magnitude [M_{max}] for a seismic source.) There may be multiple sources of uncertainty in the assessment. Stratigraphic relationships in the trench walls may be somewhat ambiguous so that the amount of dip-slip displacement can be estimated only within a factor of two (e.g., 1.0 to 2.0m). One may also be uncertain about the existence of a significant component of lateral slip, which would indicate whether the fault is primarily a normal fault or an oblique-normal fault having a ratio of strike slip to dip slip in the range of 1:1 to 1.5:1. In addition, there is the uncertainty in whether the observed slip is more representative of the maximum slip during the paleoearthquake or the average slip.

The logic tree expresses these uncertainties. The interpretations in the logic tree usually are ordered from general to specific (Figure 4-1). The order of the interpretations, however, is dictated primarily by convenience in dealing with interdependencies in the characterization. For example, the down-dip width of a fault is a function of the thickness of the seismogenic crust and the fault dip. While fault dip may differ from fault to fault in an area, the seismogenic thickness may be the same for all the faults. Therefore, it is more convenient to place the assessment of thickness before the assessment of dip. After the logic tree is constructed, the order of the nodes can be changed. In cases where the interpretation depends on the state of another unknown, then it is placed to the right of that one in the logic tree.

In the example on Figure 4-1, the total amount of fault offset is dependent on whether the fault is a normal fault or an oblique-normal fault. In addition, the evaluation of whether the observed displacement is representative of the maximum or the average displacement may also depend on the style of faulting. The trench may have been placed in an area where the fault scarp was most pronounced, indicative of maximum vertical displacement. However, this may not be the area of maximum slip if the fault is oblique-normal. Because these two interpretations are made more easily given knowledge of the style of faulting, the node for interpretations of the style of faulting is placed first (to the left) in the logic tree. For the example on Figure 4-1, the

evaluation of the assessor is that the interpretation of normal faulting is preferred slightly (0.6) to the interpretation of oblique-normal faulting (0.4). In actual interpretations, the assessor documents the reasons for this evaluation.

Further characterization in the example (Figure 4-1) addresses the amount of displacement. The stratigraphic relationships indicate from 1.0 to 2.0 m of offset. The interpretation of these data may favor displacements in the range of 1.0 to 1.5 m but allow for as much as 2.0 m. Thus, if the fault is a normal fault, the distribution for the observed offset may be specified by three discrete values: 1.0, 1.5, and 2.0 m. The probabilities (relative weights) assigned to these values are 0.4, 0.4, and 0.2, respectively, reflecting that the data more strongly support displacements of 1.0 to 1.5 m.

If the fault is considered an oblique-normal fault, then the observed offsets must be increased to account for unmeasured strike-slip offset to obtain the net slip on the fault plane. The factor of increase is 1.4 for a 1:1 strike-slip/dip-slip ratio, and 1.6 for a 1.5:1 strike-slip/dip-slip ratio. In this example, it is considered twice as likely that the strike-slip to dip-slip ratio is closer to 1:1 than to 1.5:1. Thus the factors are given relative weights of 0.67 and 0.33. The evaluation of the strike-slip to dip-slip ratio is added to the logic tree after the branch for oblique-normal faulting. The evaluation is unnecessary along the normal faulting branch. There the distributions for the amount of net slip are assumed to be equal to those developed for normal faulting multiplied by the appropriate factor.

The final evaluation is whether the observed offsets represent maximum displacements or average displacements. This evaluation is important because separate empirical relationships between magnitude and fault offset are given for maximum and average displacement (e.g., Wells and Coppersmith, 1994). (One could, of course, argue that other interpretations are possible in an exhaustive list of alternatives. It is important that the evaluator considers a sufficiently broad distribution of alternative interpretations to adequately represent the uncertainties in the assessment.) The evaluation of the relative likelihood of the two interpretations is made conditionally on which sense of slip is assumed to be correct—that is, the probability that the observed offset is a maximum given normal faulting is a separate evaluation from the probability that it is a maximum displacement given oblique-normal faulting, and the two probabilities do not have to be equal. In the example the data strongly

support the interpretation that the observed displacements represent maximum (0.8) rather than average (0.2) values if the style of faulting is deemed normal. If the fault is considered oblique-normal, then the maximum and average displacement is considered to be equivocal, and the two alternatives are given equal weight.

Each end branch on the right-hand side of the logic tree (Figure 4-1) specifies one estimate for the magnitude of the paleoearthquake. The magnitude estimate is obtained using the appropriate empirical relationship between fault displacement (either average or maximum) and moment magnitude (M_w) given by Wells and Coppersmith (1994). Their relationships for normal faulting earthquakes were used for the normal style of faulting; their relationships for strike-slip faulting were used for the oblique-normal style of faulting. The resulting magnitudes are listed along the right side of the logic tree. Each magnitude assessment listed on the right-hand side of the logic tree represents a specific set of states of the parameters, and the joint probability of that set is equal to the product of the conditional probabilities assigned to each branch. These probabilities are given in parentheses next to the magnitude assessments. It is possible that two or more end branches may result in the same magnitude estimate (within a specified tolerance), and the joint probabilities can be added together in forming a distribution for the assessed variable. These probabilities are given in parentheses next to the magnitude assessments. The characterization in the logic tree specifies a discrete distribution for the magnitude of the paleoearthquake. This distribution is shown at the right of Figure 4-1 in discrete density and cumulative forms.

The process illustrated above for characterizing magnitude of paleoearthquakes was used to quantitatively express the uncertainty in the seismic source characterization for ground shaking hazard. Each SSFD expert team identified potential seismic sources and then characterized their geometry, M_{max}, frequency of occurrence, and spatial distribution of earthquakes. The scientific uncertainty in all of these evaluations was expressed using the logic tree format. Although it is not necessary that all six teams adopt the same logic tree structure, it was suggested that similar forms be used to facilitate discussion between the teams of the important issues.

Figure 4-2 shows the general structure of a logic tree used to develop the seismic source model to represent faulting within the immediate vicinity of the Yucca Mountain site. The logic tree

begins on the left with consideration of the alternative tectonic/faulting models that may control the number and characteristics of the seismic sources that would be defined for the region. These alternative models may include planar faults extending through the seismogenic crust, a shallow detachment with planar faults above and perhaps a strike-slip source at depth, one or more master faults at depth with coupled surface faults at the surface, or some other model.
The second level of the logic tree expresses the uncertainty in the maximum depth of seismogenic rupture. This is important to the evaluation of M_{max} as well as earthquake recurrence based on fault slip rate .

The next two levels express alternative source configurations for each tectonic model. For example, given the planar fault model, one may have alternative interpretations as to which faults are independent and which faults are coupled. For the detachment model, there may be uncertainty about the depth of the detachment and the underlying driving mechanism. For the master fault, there may be uncertainties about the number of master faults and which of the surface faults are coupled at depth. There may be several levels at this point that express uncertainties in specific attributes of a tectonic/faulting model that are common to all of the seismic sources that will be defined using that model.

At this point, the logic tree lists the individual seismic sources defined by a given tectonic/faulting model and a specific set of model attributes. Here the logic tree branches into subtrees, one subtree for each identified seismic source. We use the convention of a vertical line connecting a series of seismic sources, each with is own subtree, to denote the summation of hazard from multiple sources. No dot is placed at the connecting point, indicating that these are not alternatives but individual, independent sources. The distributions of parameters for each source (defined by the subtree to the right of the source name) are assumed to be independent.

The next level of uncertainty expressed is the likelihood that an individual source is active, that it produces earthquakes in the current tectonic regime. If a source is active, then it is considered a discrete seismic source that contributes to the hazard.

The remaining levels of the logic tree characterize the evaluations of M_{max} and seismicity rate parameters. The approaches that may be used for these evaluations are discussed in Sections 4.1.3 and 4.1.4, respectively.

The logic tree structure shown on Figure 4-2 presents a general framework for representing the uncertainty in defining and characterizing the local seismic sources in the immediate vicinity of the Yucca Mountain block. In addition to these sources, the SSFD expert teams identified and characterized regional sources consisting of specific faults and areal zones of seismicity that cannot be attributed to specific known faults. Figures 4-3 and 4-4 present example logic tree structures used to represent the uncertainties in identifying and characterizing these two types of regional sources.

Figure 4-3 presents an example logic tree structure for the regional fault sources. The first level of the logic tree characterizes interpretations of alternative regional tectonic models that are considered to affect which regional faults are considered potential seismic sources. The logic tree is then expanded into subtrees for each of the individual faults or fault zones considered potential sources. The next level of the logic tree characterizes alternative interpretations of the coupling of individual faults within a particular fault zone or fault system. For example, the evaluator might consider the Furnace Creek and Death Valley faults to be part of a single fault system. They may be a single fault having one set of characteristics, or they may be two separate faults having independent characteristics. The remaining levels of the logic tree characterize the individual fault or fault segment activity, maximum seismogenic depth, M_{max}, and seismicity rate parameters.

Figure 4-4 presents an example logic tree structure for regional areal source zones. Areal source zones are sometimes referred to as "background" sources. Within the framework of this PSHA, areal source zones and background sources are equivalent. Both terms refer to a region where seismicity is not associated with specific geologic structures (faults), but instead is represented by a specified spatial distribution. The first node of the logic tree characterizes alternative approaches for zonation of the region. The alternatives may include defining areal source zones having a uniform spatial density of seismicity, defining areal source zones having a nonuniform spatial density of seismicity, or the spatial smoothing of seismicity without defining specific source zone boundaries. At this point, the logic tree is expanded into subtrees

for each areal source zone. The remaining levels of the logic tree characterize alternative parameters for defining the spatial distribution of seismicity within each zone or within the region, the M_{max}, and the seismicity rate parameters.

4.1.2 Types of Seismic Sources and the Spatial Distribution of Seismicity

Two types of seismic sources were used by the SSFD expert teams, faults and areal source zones. Fault sources are used to represent the occurrence of earthquakes along a known or suspected fault trace or traces. Uncertainty in the definition of fault sources is expressed by considering alternative total lengths, alternative fault dips, and possible linkages with other faults. In addition, an evaluation is made of the probability that a particular fault is active, i.e., the fault produces earthquakes in the current tectonic regime.

Faults were represented in the PSHA by segmented planar features; the fault dip and the minimum and maximum depths of rupture on the fault plane were specified by the SSFD expert teams. Earthquake ruptures typically are considered to occur with equal likelihood at any point on the fault plane, the size of the rupture being specified by an empirical relationship between magnitude and rupture area.

Areal sources represent areas of distributed seismicity that are not apparently associated with specific known faults and, therefore, are considered to be occurring on unidentified and/or unidentifiable faults. Areal source zones may also be used to model the occurrence of earthquakes at great distances from a site when the details of the individual faults are not significant to the hazard assessment. The boundaries of areal zones delineate areas that have relatively uniform seismic potential in terms of earthquake occurrence and maximum earthquake magnitude. Uncertainty in defining areal zones typically was expressed by considering alternative zonations of the region surrounding the Yucca Mountain site.

Two alternative approaches were used by the SSFD expert teams to characterize the spatial distribution of future earthquakes within the areal zones. The first considers that there is equal likelihood of occurrence of earthquakes at all locations within the zone. Under this interpretation the spatial density, $f(x,y)$, of future earthquakes at any point x,y in the areal zone is $1/A_Z$, where A_Z is the area.

The alternative interpretation was nonuniform spatial occurrence expressed by a nonuniform spatial density function for the areal zone using the recorded seismicity estimation of kernel density. This interpretation implies that future seismicity is more likely to occur near where it has in the historical past. This interpretation currently is being used to develop the national seismic hazard maps for the U.S. (Frankel, 1995).

The kernel density estimate of the spatial density function is given by the expression

$$f(x,y) = \frac{\sum_{i=1}^{N} K(d_i,h)}{\iint_Z \sum_{i=1}^{N} K(d_i,h) \cdot dx \cdot dy} \qquad (4\text{-}1)$$

where $K(d_i,h)$ is a kernel density function with characteristic dimension h, and d_i is the distance from point x,y to the i^{th} earthquake in the source zone. The denominator in Equation (4-1) is the integral of the spatial density over the region of the areal zone; this normalizes the kernel density estimate to a proper probability density function.

The SSFD expert teams chose to use a two-dimensional Gaussian kernel function. The form of the kernel function is (Silverman, 1986)

$$K(d_i,h) = \frac{e^{-d_i^2/2h^2}}{2\pi h^2} \qquad (4\text{-}2)$$

The controlling factor in kernel density estimation is the selection of the characteristic dimension h. The SSFD expert teams expressed the uncertainty in defining a nonuniform spatial density by considering various values for h.

4.1.3 Assessment of Maximum Magnitude

The M_{max} for a seismic source represents the largest earthquake for the source, regardless of its frequency of occurrence. Thus, M_{max} defines the upper limit of the earthquake recurrence relationship for the source.

4.1.3.1 Fault-Specific Sources. The approach used to evaluate the M_{max} for a fault source was to estimate the maximum physical dimensions of rupture on the source and use relationships between rupture dimensions and earthquake magnitude to estimate M_{max}. The types of empirical relationships available are magnitude versus rupture length, rupture area, maximum surface displacement, and average surface displacement. Some published empirical relationships include more than one parameter, such as rupture length and slip rate or the product of rupture length and displacement (e.g., Anderson *et al.*, 1996). Estimates of the rupture area and average slip on the fault can also be used to estimate the seismic moment of the maximum event, which then can be converted to M_w using the relationship specified by Hanks and Kanamori (1979). The PSHA was conducted using M_w as the magnitude measure, because this is the scale of choice in ground-motion estimation; all estimates of M_{max} were converted to this scale.

The SSFD expert teams considered multiple sources of uncertainty in estimating M_{max} for fault sources. These include consideration of the (1) relative merit of alternative rupture characteristics for estimating magnitude (such as estimates based on rupture length versus estimates based on maximum displacement), (2) relative merit of alternative published empirical relationships, and (3) uncertainty in estimating the physical dimensions of the maximum rupture on a fault. Figure 4-5 illustrates the approach used to express these uncertainties. In the example, alternative fault widths are assessed by considering a range of permissible maximum depths of rupture and alternative fault dips. Alternative maximum rupture lengths are assessed based on evidence for lasting segmentation points and differences in fault behavior. Alternative empirical relationships are considered: magnitude versus rupture length or rupture area from Wells and Coppersmith (1994), or magnitude versus rupture length and slip rate (Anderson *et al*, 1996). If the Anderson *et al.* (1996) relationship is used, then a distribution of possible fault slip rates is assessed. The example logic tree shown at the top of Figure 4-5 shows only some of the branches to illustrate the various evaluations. The complete logic tree leads to the discrete distribution for M_{max} shown at the bottom of the figure.

4.1.3.2 Areal Source Zones. Different approaches may be used to evaluate the M_{max} for areal zones. In cases where an areal zone is used to model the occurrence of earthquakes at large distances from a site where the details of the individual fault sources are not significant to the

hazard assessment, the M_{max} represents the largest earthquake determined to occur on any of the faults within the areal zone. In cases where areal zones are used to model the occurrence of earthquakes on unknown faults (there may be fault sources within the areal zone that are modeled explicitly as separate sources in the hazard), the M_{max} for the areal zone is determined by the largest fault within the zone that is mapped, or the largest earthquake that is not associated with surface faulting. The size of this fault will depend on the level of detailed mapping of the region and the identification of fault sources. Guidance for this evaluation is provided by studies that examine the frequency at which earthquakes of various magnitudes rupture the surface (e.g., Wells and Coppersmith, 1993, de Polo, 1994, and Pezzopane and Dawson, 1996). The data sets of de Polo (1994) and Pezzopane and Dawson (1996) are specific to the Basin and Range Province.

4.1.4 Assessment of Earthquake Recurrence

Earthquake recurrence relationships for a seismic source describe the frequency at which earthquakes of various magnitudes occur. They are determined by estimating the overall frequency of earthquakes on the source, $\alpha_n(m^0)$, and the relative frequency of earthquakes of various sizes defined by the probability density of earthquake size, $f(m)$, between m^0 (minimum magnitude) and the upperbound magnitude, m^U. Different approaches were used to determine the recurrence relationships for areal source zones and fault sources.

4.1.4.1 Areal Source Zones. The earthquake recurrence relationships for areal zones were determined from the historical seismicity. Appendix G describes the development of the earthquake catalog for the region within 300 km of the Yucca Mountain site. The earthquakes in the catalog are described in terms of a uniform magnitude scale, M_w. The catalog was analyzed to identify dependent events (earthquakes that were aftershocks or foreshocks of larger earthquakes) to produce data sets of earthquakes that can be considered to correspond to a Poisson process. Several alternative methods for identifying dependent events were used to express the uncertainty in the process. The SSFD expert teams used the alternative catalogs (as discussed in Appendix G) to develop alternative recurrence relationships for their areal source zones.

The distribution of earthquake sizes in each areal zone was interpreted to follow the Gutenberg and Richter (1954) exponential recurrence model. Because each source has a defined M_{max}, the

truncated exponential magnitude distribution (Cornell and Van Marke, 1969) was used to define the recurrence relationships. The truncated exponential relationship is of the form

$$N(m) = \alpha(m^0)\frac{10^{-b(m-m^0)} - 10^{-b(m^U-m^0)}}{1-10^{-b(m^U-m^0)}} \tag{4-3}$$

where $N(m)$ is the annual frequency of occurrence of earthquakes of magnitude greater than m, and b is the Gutenberg and Richter (1954, 1956) b-value parameter.

The recurrence parameters needed for each areal zone are $\alpha(m^0)$ and b. The maximum likelihood procedure developed by Weichert (1980) was used to estimate these parameters from the historical catalog. The likelihood function used in this study was modified from that presented by Weichert (1980) to allow for variable periods of complete reporting within the boundaries of the source as well as variable magnitude intervals (Johnston *et al.*, 1994). The source zone is divided into subregions in which the catalog is considered to be homogeneous. The procedure then sorts the catalog by size into a number of magnitude intervals of width Δm. For each magnitude interval, $m_i \leq m < m_i+\Delta m$, and for each of the j subregions of the source, the period of complete reporting, t_{ij}, is identified. Given the truncated exponential recurrence model, the expected frequency of occurrence of earthquakes of magnitude $m_i \leq m < m_i+\Delta m$ within the j^{th} subregion is defined as $\lambda_j(m_i)$ and is given by the expression

$$\lambda_j(m_i) = \alpha(m^0)\frac{e^{-\beta(m_i-m^0)} - e^{-\beta(m_i+\Delta m-m^0)}}{1-e^{-\beta(m^U-m^0)}} \cdot A_j / A_Z \tag{4-4}$$

where $\beta = b \cdot \ln(10)$, A_j is the area of the j^{th} subregion, and A_Z is the total area of the source zone. Interpreting the occurrence of earthquakes within the source to be described by a Poisson process, then the likelihood of observing the recorded catalog is given by

$$L\{\alpha(m^0),\beta\} = \prod_i \prod_j \frac{[\lambda_j(m_i)t_{ij}]^{k_{ij}} e^{-\lambda_j(m_i)t_{ij}}}{k_{ij}!} \tag{4-5}$$

where k_{ij} is the number of earthquakes of magnitude $m_i \leq m < m_i+\Delta m$ that have been recorded in the j^{th} subregion during the period of compete reporting t_{ij}. The maximum likelihood recurrence parameters for the source are found by maximizing $L\{ \alpha(m^0), \beta \}$ over $\alpha(m^0)$ and β.

The uncertainty in the recurrence relationships for the regional sources was characterized as follows. Using the asymptotic standard errors in $\alpha(m^0)$ and β computed from the maximum likelihood fit to the data, five values of $a(m^0)$ and five values of b were defined ranging from -2 standard deviations to +2 standard deviations. These were then used to define 25 recurrence relationships (Figure 4-6) that may have generated the observed data. The likelihood that the observed data were a product of the process defined by each of the recurrence relationships was computed using Equation (4-6). These likelihoods were then normalized to define a discrete distribution for the seismicity parameters. The resulting distribution indicates the degree to which the data constrain the recurrence relationship for the source zone and accounts for the correlation between $\alpha(m^0)$ and β. Figure 4-6 shows an example of the resulting distribution in computed earthquake recurrence frequencies, including the uncertainty in M_{max}. An additional level of uncertainty in the recurrence relationship for the areal source zones was consideration of the alternative catalogs of independent earthquakes generated using the alternative declustering methods.

4.1.4.2 Fault-Specific Sources. Two approaches were used to estimate the earthquake recurrence relationships for faults. The first involved estimating the frequency of large-magnitude surface-rupturing earthquakes on the fault either by dating of paleoearthquakes or by dividing an estimate of the fault slip rate by an estimate of the average slip per event. The complete recurrence relationship for the source is then specified by constraining a particular form of an earthquake recurrence model (magnitude distribution function) to pass through the estimated frequency of large events. The second approach was to translate the estimated fault slip rate into seismic moment rate and then partition the moment into earthquakes of various magnitudes according to the magnitude distribution or recurrence model used. Both of these approaches constrain the earthquake recurrence relationship for the fault at the frequency of magnitudes near the M_{max}. The frequency of smaller-magnitude earthquakes is then extrapolated from this frequency based on the form of the magnitude distribution used.

Several magnitude distribution models were considered by the SSFD expert teams (Figure 4-7). One form is the "characteristic" earthquake magnitude distribution developed by Youngs and Coppersmith (1985). The form of the characteristic magnitude distribution is

$$N(m) = N^e \frac{10^{-b(m-m^o)} - 10^{-b(m^u-\frac{1}{2}-m^o)}}{1-10^{-b(m^u-\frac{1}{2}-m^o)}} + N^c \quad for\, m^o \le m < m^u - \frac{1}{2} \qquad (4\text{-}6)$$

$$N(m) = N^c \frac{m^u - m}{\frac{1}{2}} \quad for\, m^u - \frac{1}{2} \le m < m^u$$

with $$N^e = N^c \frac{1.0 - 10^{-b(m^u-1-m^o)}}{\frac{1}{2} b \ln(10) 10^b 10^{-b(m^u-1-m^o)}}$$

where the terms N^e and N^c represent the rate of exponential and characteristic events, respectively. $N^c = N(m^U\text{-}½)$, the cumulative frequency of characteristic events, and the total seismicity rate equals the sum of the rate for exponential and characteristic events, $\alpha(m^0) = N^e + N^c$. When the rate of large events is specified by the SSFD expert teams, it is assumed to be equal to N^c, and Equation (4-6) is used to define the recurrence relationship. When the recurrence relationship is to be based on slip rate, then the parameters N^e and N^c are given by

$$N^e = \frac{\mu A_f S \left[1 - 10^{-b(m^u-\frac{1}{2}-m^o)}\right]}{M_o(m^u) 10^{-b(m^u-\frac{1}{2}-m^o)} \left[\frac{b \cdot 10^{\frac{-c}{2}}}{c-b} + \frac{b \cdot 10 b (1 - 10^{\frac{-c}{2}})}{c}\right]} \qquad (4\text{-}7)$$

$$N^c = \frac{\frac{1}{2} b \ln(10) N^e 10^{-b(m^u-\frac{3}{2}-m^o)}}{1-10^{-b(m^u-\frac{1}{2}-m^o)}}$$

where μ is the shear modulus of fault zone rock (taken to be 3×10^{11} dyne/cm^2), A_f is the total fault surface area, S is the slip rate, and $M_o(m^U)$ is the seismic moment for the m^U on the fault [$M_o(m)=10^{cm+d}$, with c equal to 1.5 and d equal to 16.1, Hanks and Kanamori (1979)].

The second recurrence model used was the truncated exponential model, Equation (4-3). When the recurrence for the fault is specified to be the recurrence interval for large events, it is interpreted to correspond to the frequency for earthquakes of m^U-½, $N(m^U$-½), and Equation (4-3) is used to define the recurrence relationship for the source. When the recurrence relationship is to be based on slip rate, then the formulation developed by Anderson (1979) is used:

$$\alpha(m^O) = \frac{(c-b)\mu A_f S[1-10^{-b(m^U-m^O)}]}{bM_o(m^U)10^{-b(m^U-m^O)}} \tag{4-8}$$

Youngs *et al.* (1987) introduced a modification to the standard truncated exponential distribution that was used by one of the SSFD expert teams. The modification considers the upperbound magnitude in the density function to be uniformly distributed over the range of m^U-½ to m^U in a similar fashion to the characteristic earthquake model. The effect is to generalize the upper boundary of the magnitude distribution without altering the general shape of the recurrence relationship. The formulation for the modified truncated exponential is:

$$N(m)=\alpha(m^O)\left[1-\frac{\left[1-10^{-b(m-m^O)}\right]-\left[\ln(f^U)-\ln(f^i)\right]}{b\cdot\ln(10)/2}\right] \quad for\ m^O \le m < m^U-\frac{1}{2} \tag{4-9}$$

$$N(m)=\alpha(m^o)\left[1-\frac{\left[1-10^{-b(m-m^o)}\right]\left[\ln(f^u)-\ln(f^i)\right]}{b\cdot\ln(10)/2}-2(m-m^u)\right] \text{ for } m^u-\frac{1}{2}\le m<m^u$$

$$f^i=10^{b(m^u-\frac{1}{2})}-10^{bm^o}$$

$$f^u=10^{bm^u}-10^{bm^o}$$

$$f^i=10^{bm}-10^{bm^o}$$

If the recurrence relationship for a fault is specified by the frequency of large earthquakes, then it is interpreted to equal the cumulative frequency for earthquakes of magnitude m^U-½, $N(m^U$-½), and Equation (4-9) is used to determine the recurrence relationship for the source. If the recurrence relationship is based on slip rate, then the integral of the event frequency derived from Equation (4-9) times the moment for each event is set equal to the moment rate. As a result, $\alpha(m^0)$ is given by

$$\alpha(m^o)=\frac{6\mu A_f S(c-b)}{\frac{M_o(m^u-\frac{1}{2})}{10^{b(m^u-\frac{1}{2}-m^o)}-1}+\frac{4M_o(m^u-\frac{1}{4})}{10^{b(m^u-\frac{1}{4}-m^o)}-1}+\frac{M_o(m^u)}{10^{b(m^u-m^o)}-1}} \qquad (4\text{-}10)$$

The fourth magnitude distribution model the SSFD expert teams considered is the maximum moment model developed by Wesnousky *et al.* (1983), in which only large earthquakes are assumed to occur on the fault. For this model, the recurrence relationships were specified using Equations (4-6) and (4-7) for the characteristic model with N^c set equal to zero (no exponentially distributed events).

Figure 4-7 compares the shape of the exponential, modified exponential, characteristic, and maximum M_w distributions. Shown on the left are the four distributions developed for an assessed fault m^U of M_w 7.5, with the frequency of events larger than M_w 7 set at one per 5000 years. Shown on the right on Figure 4-7 are the magnitude distributions developed on the basis

of a slip rate of 1 mm/yr and a fault area of 1,000 km^2. All the recurrence relationships were developed with a *b*-value of 0.8. As can be seen, the modified truncated exponential distribution is very similar to the truncated exponential distribution. The characteristic magnitude distribution results in about a factor of ten reduction in the frequency of small-magnitude events compared to the exponential model.

Uncertainty in the recurrence relationships for the faults can incorporate alternative recurrence models, alternative methods to constrain the rate of large events (i.e., slip rate versus recurrence interval), uncertainty in the slip rates and recurrence intervals, and alternative *b*-values.

4.2 METHODOLOGY FOR FAULT DISPLACEMENT HAZARD CHARACTERIZATION

At the present time, methodologies for the probabilistic assessment of fault displacement hazard (especially distributed faulting hazard) have not matured to the level of those used for the assessment of ground shaking hazard and there is little relevant literature. As a result, the SSFD expert teams developed a number of original approaches as part of their assessments for the project. These approaches were originated to a significant degree by one of the teams, were discussed in Workshops #4, #5, and #6, and then were refined and modified in the individual team characterizations of fault displacement hazard. The methods are based primarily on empirical observations of the pattern of faulting during earthquakes and on data gathered during studies of the faulting in the Yucca Mountain region. As part of these characterizations, the individual teams developed a number of empirical distributions from data gathered at Yucca Mountain or published in the literature. The SSFD Facilitation Team fit statistical models to these empirical distributions to facilitate numerical calculation of the hazard. Appendix H documents the development of these statistical models.

4.2.1 Principal and Distributed Fault Displacement

The potential for fault rupture within the Controlled Area can be described in terms of two types of fault rupture: *principal faulting* and *distributed faulting*. These are illustrated on Figure 4-8, which shows the surface rupture pattern for the 1959 M_W 7.4 Hebgen Lake earthquake. Principal faulting is the faulting along the main plane (or planes) of crustal weakness responsible for the release of seismic energy during the earthquake. Where the principal fault

rupture extends to the surface, it may be represented by displacement along a single narrow trace or over a zone that is a few to many meters wide. For principal faulting, the faults of concern are those that may produce earthquakes (i.e., are directly related to the primary source of energy release). Repeated large earthquakes on a given fault segment are considered to be produced by repeated principal faulting on the same fault trace or traces, so that faults that are capable of principal rupture can be recognized based on detailed mapping of outcrops and/or in the walls of subsurface excavations (trenches and tunnels).

Distributed faulting is defined as rupture that occurs on other faults in the vicinity of the principal rupture in response to the principal displacement. It is expected that distributed faulting will be discontinuous in nature and occur over a zone that may extend outward several tens of meters to many kilometers from the principal rupture. A fault that can produce principal rupture may also undergo distributed faulting in response to principal rupture on other faults. The extent to which faults that can undergo distributed rupture can be identified depends on the level of detailed mapping but the minimum resolution for detection is generally smaller for distributive faulting than for principal faulting. Interpretation of distributive faulting is more subjective and is, therefore, less certain than for principal faulting.

Both types of faulting are important to the assessment of the fault displacement hazard at the Yucca Mountain site. Figure 4-9 shows the Controlled Area and the nine locations at which the fault displacement methodology is demonstrated. These points were chosen to represent the range of conditions in the Controlled Area. Some of these points lie on faults that may experience principal faulting (the Solitario Canyon fault, the Bow Ridge fault, and possibly some of the intrablock faults) and distributed faulting. The other points are sites of potential distributed faulting. The locations and specific conditions for the nine points are described further in Section 4.3.2. The methodologies described below were developed by the SSFD expert teams to assess the hazard at any location within the Controlled Area, including all of these nine demonstration points.

4.2.2 Basic Formulation

The basic formulation for probabilistic evaluation of the hazard from fault displacement is analogous to that developed for the hazard from ground shaking. The fault displacement PSHA addresses how frequently it occurs and how large the displacements are. The hazard can be

represented probabilistically by a displacement hazard curve that is analogous to ground motion hazard curves. The hazard curve shown on Figure 4-10 represents the hazard at a point within the Controlled Area. It relates the amount of displacement in a *single* event to how often larger displacements occur (i.e., the frequency of exceeding a specified amount of displacement). In the example hazard curve (Figure 4-10), single event displacements larger than 10 cm occur with a frequency of 10^{-4} per year (a return period of 10,000 years); single event displacements larger than 50 cm occur with a frequency of 10^{-5} per year (a return period of 100,000 years). Thus, the hazard curve is a plot of the frequency of exceeding fault displacement value d, designated by $\nu(d)$. This frequency can be computed by the expression:

$$\nu(d) = \lambda_{DE} \cdot P(D > d) \tag{4-11}$$

where λ_{DE} is the frequency at which displacement events occur on the structure located at the point of interest, and $P(D>d)$ is the conditional probability that the displacement in a single event will exceed value d. The SSFD expert teams used different approaches to characterize fault displacement hazard and, thus, different techniques to express these two terms. They also used a variety of data sets to develop the necessary parameters. These approaches and data sets are generally described below. Specific applications of these approaches by each team are described in Section 4.3.2.

The displacement hazard curve can be used to estimate the effective slip rate on the feature of interest. The negative of the slope of the hazard curve, $\partial \nu(d)/\partial d$, provides the rate density of displacements of amount d. Integrating this over displacement provides an estimate of fault slip rate, SR. Specifically:

$$SR = \int_0^{\infty} \left[-\partial \nu(d) / \partial d \times d \right] dd \tag{4-12}$$

4.2.3 Assessment of Scientific Uncertainty

As with the ground motion PSHA methodology, the formulation given by Equation (4-11) represents the randomness in the natural phenomena of earthquake-induced fault displacement (the aleatory uncertainty). The scientific (epistemic) uncertainty is represented in the process of

selecting the appropriate models and model parameters for the fault displacement hazard characterization. The logic tree methodology described in Section 4.1.1 was utilized to characterize the uncertainty in the fault displacement PSHA.

4.2.4 Estimation of Displacement Event Frequency

The approaches for estimating the frequency of displacement events, λ_{DE}, eveloped by the SSFD expert teams can be divided into two categories. The first, designated the *displacement approach*, provides an estimate of the frequency of displacement events directly from observed feature-specific or point-specific data. The second, designated the *earthquake approach*, involves relating the frequency of slip events to the frequency of earthquakes on the various seismic sources defined by the seismic source characterization models developed in Section 4.3.1. Both approaches are used for assessing the fault displacement hazard for principal faulting and distributed faulting.

4.2.4.1 Displacement Approach. The displacement approach estimates the frequency of displacement events, λ_{DE}, from the information available for the specific feature (point) in question. There are two techniques for direct estimation of λ_{DE}, estimation of recurrence intervals and the use of slip rates.

Recurrence Interval Technique. An example of the recurrence interval technique is the assessment of the frequency of displacement events on a source of principal faulting using paleoearthquake data. The SSFD expert teams used such data to estimate the frequency of surface-rupturing events as part of their seismic source characterization models for the ground shaking hazard. This assessment can be used directly in assessing the frequency of faulting events.

Slip-Rate Technique. Fault slip rate, *SR*, is a measure of the amount of slip averaged over a time period that encompasses multiple ruptures. If the slip rate and the average slip in a faulting event, $\bar{D}_E$, are known, then λ_{DE} can be estimated by:

$$\lambda_{DE} = SR / \bar{D}_E \qquad (4\text{-}13)$$

Given *SR*, the use of Equation (4-13) requires an estimate of the average slip in an event, $\bar{D}_E$. For some features (typically those that may be the location of principal faulting), this may be assessed directly from trenching data. For other features, the SSFD expert teams developed scaling relationships that relate $\bar{D}_E$ to fault length, *L*, or cumulative fault displacement, D_{cum}. These are described in the summaries of the models the SSFD expert teams developed for displacement hazard (Section 4.3.2).

The displacement approach does not tie slip events to specific earthquakes, it only evaluates the frequency of slip events. Thus, the displacement approach does not explicitly distinguish between principal and distributed ruptures on a feature.

4.2.4.2 Earthquake Approach. The earthquake approach utilizes the earthquake recurrence models developed for the ground shaking hazard assessment. Each SSFD expert team provided an assessment of the frequency of earthquakes on each seismic source. The occurrence of a slip event (earthquake) on source *j* may induce slip on the feature (point) of interest, point *i*. The probability that slip will occur given an event on source *j*, P_i (*Slip*| *Event on j*), can range from 0 to 1.0. The frequency of displacement events at point *i*, λ_{DE}, is obtained by summing the contributions from all of the seismic sources:

$$\lambda_{DE} = \sum_{j=i}^{n} \lambda_j \,(\text{Events on source } j) \cdot P_i\,(\text{Slip} \mid \text{Event on source } j) \qquad (4\text{-}14)$$

As defined by Equation (4-14), the earthquake approach for assessing the frequency of displacement events consists of two-parts, an evaluation of the opportunity frequency, the frequency of earthquakes, and an evaluation of the probability each opportunity will result in fault slip. Because the earthquake approach is tied directly to the occurrence of earthquakes on various sources, the distinction between principal and distributed faulting events is maintained.

The methods used to evaluate P_i (*Slip*| *Event on j*) depend on whether one is considering principal ($j = i$) or distributed faulting ($j \neq i$).

Probability of Slip for Principal Faulting. In this approach the frequency of principal faulting events is assessed using earthquake recurrence models developed for a seismic source. The models define the frequency of various size earthquakes up to the maximum earthquake assessed for the source. In many cases, the recurrence models were developed by specifying the frequency of surface-rupturing earthquakes from trenching data, interpreting these events to be near the maximum earthquake. For these events, P_i *(Slip| Event on i)* is expected to be 1.0. However, earthquakes smaller than the maximum earthquake may not always rupture to the surface or at shallow depths where the repository is to be located (300 m). They also may have rupture lengths that are shorter than the total fault length. The contribution of these events to the fault displacement hazard will depend on their relative frequency compared to the largest events and the likelihood that they will rupture to near the surface and at the point along the fault where the hazard is being evaluated. Two approaches were developed to assess the probability of surface rupture in a principal faulting event, one based on empirical data on the frequency of surface rupture, and one based on the numerical randomization of the depth of rupture on the fault used in the analysis of ground shaking hazard.

Empirical Probability of Principal Faulting Surface Rupture. Wells and Coppersmith (1993), de Polo (1994), and Pezzopane and Dawson (1996) present data sets that indicate the frequency at which earthquakes of various magnitudes rupture the surface. The data sets of de Polo (1994) and Pezzopane and Dawson (1996) are specific to the Basin and Range Province. These data can be used to develop an empirical model for *Pi (Slip| Event on i)* as a function of magnitude. For example; Wells and Coppersmith (1993) used a *logistic regression* model to evaluate the probability of surface rupture. The logistic regression model (e.g., Hosmer and Lemeshow, 1989) is a commonly used model for assessing the outcome of a dichotomous variable; in this case, surface rupture either occurs or does not occur. The probability of a positive outcome (the occurrence of principal faulting given the occurrence of the event) is given by the expression

$$P(\text{Rupture}) = \frac{e^{a+bm}}{1+e^{a+bm}} \qquad (4\text{-}15)$$

where a and b are constants estimated from data (see Appendix H, Section H4.1). Figure 4-11 presents the results of fitting Equation (4-15) to the various data sets presented by Pezzopane and Dawson (1996) for surface rupture as a function of magnitude.

Focal Depth Distribution. Each SSFD team provided an evaluation of the focal depth distribution for earthquakes in the Yucca Mountain region. Using this distribution along with an assessment of the size of earthquake ruptures as a function of magnitude (e.g., an empirical relationship of rupture area as a function of magnitude) and rupture aspect ratio, the distribution for the down-dip location ruptures on a fault was modeled as part of the calculation of the source-to-site distribution in the ground motion hazard analysis. This process can also be used to calculate the frequency at which earthquakes of a given magnitude occurring on a fault are expected to rupture near the surface, thus providing a fault-specific estimate of P (*surface rupture*).

Probability of Intersection Along Strike. The probability that the earthquake rupture will intersect the point of interest along the fault is computed from the distribution for the location of the rupture along the fault. This distribution is computed for each fault as a part of the ground motion hazard assessment by assuming that earthquake ruptures are equally likely to occur anywhere along the fault. The probability of along-strike intersection of the rupture, $P(intersection)$, times the probability of surface rupture provides the probability of principal faulting in the earthquake, that is:

$$P_i(principal\ faulting\ slip | event\ on\ j) = P(surface\ rupture) \times P(intersection) \qquad (4\text{-}16)$$

Probability of Slip for Distributed Faulting. For distributed faulting, P_i (*Slip| Event on j*) expresses the likelihood that slip on an earthquake source some distance r from the feature of interest will trigger slip locally. Several approaches were considered for assessing P_i (*Slip| Event on j*) for distributed faulting.

Analysis of Historical Distributed Ruptures. Pezzopane and Dawson (1996) developed a data base of distributed ruptures resulting from historical earthquakes in the western U.S. These data were used to assess the density of distributed ruptures as a function of distance from the principal rupture. The process used was to place a 0.5 km × 0.5 km grid on each map of surface ruptures. The number of grid cells that contain a secondary rupture divided by the total number of grid cells at a given distance from the principal rupture provides a measure of the frequency or likelihood that a distributed rupture will occur. Figure 4-12 shows a plot of these data

segregated by magnitude and by location in the hanging wall block and footwall block of the rupture. The data show a decrease in the likelihood of experiencing distributed rupture with increasing distance from the principal rupture. The data also show clear differences between the hanging wall and footwall sides of the rupture. The size (magnitude) of the earthquake appears to provide some control on the maximum distance distributed rupture has been observed away from the principal faulting.

The probability of occurrence of distributed faulting on a feature located r km from a magnitude m earthquake can be determined from these data using the logistic model.

$$P_i \text{ (Slip | Event on } j) = \frac{e^{f(m,r)}}{1+e^{f(m,r)}} \qquad (4\text{-}17)$$

where $f(m,r)$ represents a suitable function of m and r. The data shown on Figure 4-12 indicate that $f(m,r)$ should account for the effect of being on the hanging wall or foot wall sides of the principal rupture. Appendix H, Section H4.2 presents models fit to these data that were used by the expert teams to assess P_i (*Slip| Event on j*) for distributed faulting. This probability is considered an aleatory probability because it defines the likelihood of the occurrence of distributed faulting at a point in a single earthquake.

Slip Tendency. Another approach to estimating the likelihood that a feature will experience distributed faulting is based on characteristics such as feature and orientation. Morris *et al.* (1996) and McKague *et al.* (1996) have performed slip-tendency analyses of faults in the Yucca Mountain region using their orientations with respect to the current stress field. These assessments have been used to either modify P_i (*Slip| Event on j*) (i.e., reduce the probability that distributed slip will occur as the orientation of the feature changes from favorable to unfavorable in the present stress regime) or as an assessment of whether the feature can slip at all in response to earthquakes in the present tectonic stress regime.

Another approach to assessing the likelihood that distributed slip could occur on a feature in response to principal faulting on a seismic source involves evaluating the angle between the strike of the principal fault and the strike of the feature under consideration. Section H4.3 of Appendix H presents an analysis of the pattern of distributed ruptures from mapping data

developed by Pezzopane and Dawson (1996). The relative frequency of rupture orientations with respect to the principal rupture provides an estimate of the likelihood that the feature will slip in response to a principal rupture.

4.2.5 Conditional Probability of Exceedance for Displacement

The conditional probability of exceedance, $P(D>d)$, in Equation 4-11, defines the probability that the amount of displacement occurring at a point during a single displacement event will exceed a specified amount d. The probability can be considered to contain two-parts: the variability of slip from event to event, and the variability of slip along strike during a single event. The first part represents a distribution for the "size" of faulting events and is analogous to an earthquake magnitude distribution model used in the ground shaking hazard analysis. The second part represents the variation of the displacement at a point from the size of the event. This might be considered analogous to the lognormal distribution for peak ground motion about the median value predicted by an attenuation law for a specific magnitude and distance.

The teams developed a variety of approaches for evaluating the distribution of slip at a point in an individual event. Some methods utilize the two-part representation of displacement variability; others combine them into a single distribution function. The various methods are described below as they are applied to principal and distributed faulting. The approaches also differ depending on whether the earthquake or displacement approaches are being used for the assessment.

4.2.5.1 Two-Step Approach for Conditional Probability of Exceedance. The two-part approach for assessing $P(D>d)$ was typically used in the earthquake approach for principal faulting hazard. The size measure used to describe the event was the maximum displacement, *MD*, in an earthquake and was typically assessed using empirical relationships between magnitude and maximum displacement. The value of *MD* in an event was assumed to be distributed according to the empirical regression model, typically lognormal. In some cases, the SSFD expert teams used trenching data to assess *MD* for maximum events on the source.

The second part is an assessment of the variability of slip at a point as a fraction of the maximum displacement in the event. The ASM team analyzed the slip distributions for a number of surface rupturing events. The plot on the left side of Figure 4-13 shows the results in

the form of smoothed curves defining the minimum, median, and maximum values of *D/MD* at a point as a function of location along strike. These values, which can be interpreted as representing a low percentile, the median value, and a high percentile for *D/MD*, can be used to construct a cumulative distribution function for *D/MD*. Shown at the right of Figure 4-13 are examples of cumulative distribution functions for *D/MD* at three values of *x/L*, the location of the point along the rupture. These cumulative functions were made by fitting a beta distribution to the percentiles shown by the solid dots on the plot. The beta distribution was selected because it is a very flexible distribution for modeling variables that are defined over a finite range, in this case $0 \le D/MD \le 1$. The beta distribution has the density function

$$f(y) = y^{a-1}(1-y)^{b-1}\frac{\Gamma(a+b)}{\Gamma(a)\Gamma(b)} \qquad (4\text{-}18)$$

where $\Gamma(\ )$ is the Gamma function. For this application, $y = D/MD$. The cumulative distributions shown on the right of Figure 4-13 were obtained by developing relationships for the parameters a and b as a function of x/L (see Appendix H). The SBK team developed a similar model for the distribution of *D/MD* using numerical simulations of fault rupture patterns (see Appendix H and the SBK elicitation summary in Appendix E).

The conditional probability of exceedance, $P(D>d)$, is then obtained by convolving the distribution for *D/MD* with the distribution for *MD* as a function of the magnitude of the earthquake:

$$P(D > d) = 1 - \int f(MD)\left[\int_0^{d/MD} f(y)\,dy\right] d(MD) \qquad (4\text{-}19)$$

where $f(MD)$ was typically defined by a lognormal distribution and $f(y)$ is given by Equation (4-18).

4.2.5.2 Single-Step Approach for Conditional Probability of Exceedance. The single step approach for assessing $P(D>d)$ involved developing an empirical distribution for the displacement data collected at Yucca Mountain by normalizing the data from each trench location by a normalizing parameter related to the location where the data were obtained. The

resulting distribution of D/D_{norm} were then used to compute $P(D>d)$, given an assessment for D_{norm} at the location of interest. A variety of normalization parameters were developed by the SSFD expert teams, including: the average displacement observed in a trench with multiple displacements, the average or maximum displacement expected for a fault based on its dimension, and the cumulative displacement that has occurred on the feature where the trench was located. These empirical distributions were then fit with statistical models for use in the displacement hazard computation (see Appendix H). Examples of these distributions are shown on Figure 4-14.

4.3 EXPERT TEAM MODELS

The following summarizes the expert team's seismic source characterization and a description of the fault displacement models. Complete expert team elicitation summaries are contained in Appendix E.

4.3.1 Seismic Source Characterization

The previous section describes the type of probabilistic models used to define the spatial location, frequency, and size distribution of earthquakes in the Yucca Mountain region that may generate significant ground motion at the repository. This section describes the seismic source models developed by the SSFD expert teams. Section 4.3.1.1 provides summaries of the individual team models, which are presented in full in each team's elicitation summary in Appendix E. This discussion is followed by a summary in which the assessments of key components of the source characterization models are compared (Section 4.3.1.2).

4.3.1.1 Individual Expert Team Models. The seismic source characterization models for each of the six SSFD teams are summarized in this section using common terminology and format. We do not attempt to summarize the bases for the teams' models, that information is contained in Appendix E. An abbreviated summary of models is given in Table 4-1. Lists of acronyms used to designate fault sources on various source maps referred to in the following sections are given in Table 4-2. The seismic source characterization developed by each SSFD team is described in terms of local faults in the Yucca Mountain region, regional faults within 100 km of the site, and regional areal source zones. Much of the seismic hazard characterization involves assessing seismicity rates and M_{max} for seismic sources. In was the

role of the SSFD Facilitation Team to compute these parameters using the methods and data that the SSFD expert teams specified. The results of these calculations for each team are presented as part of the description of their models. In addition, we employ the expert teams' models to compute the implied rate for future seismicity within 100 km of Yucca Mountain. Figure 4-15 shows the region for which this calculation is made. We present calculated earthquake recurrence rates for local seismic sources, which generally lie within the shaded region at the center of Figure 4-15, the regional faults that lie within a 100-km radius of Yucca Mountain, adjusting for the portions of these faults that may lie outside of this circle, and for those parts of the areal source zones that lie within 100 km of Yucca Mountain. The recurrence rates for the regional faults and the areal zones, as well as the combined recurrence rates for all three types of sources, are compared to the observed seismicity rate within the 100-km circle based on each SSFD team's selection of the appropriate earthquake catalog and catalog completeness periods. Shown on Figure 4-15 are the earthquakes of M_w 5 and larger that have been recorded within the 100-km circle. The choice of a 100 km radius encloses the region containing the seismic sources that will affect the seismic hazard at the Yucca Mountain site.

Arabasz, Anderson, Ramelli (AAR) Team. Tectonic models provide a fundamental framework for the AAR team's seismic source characterization for local sources. Many of their seismic source parameters are dependent on tectonic models, including the geometry of local faults and buried sources, rupture behavioral models for local faults, and the seismogenic potential of hypothesized buried sources. Figure 4-16a and 4-16b show the logic tree that defines the alternative interpretations of local faults developed by the AAR team. These models are based on the inference that the controlling tectonic model for the Crater Flat structural domain is simple shear. Figure 4-16a shows the logic structure for considering alternative models for local faults. The first assessment addresses whether or not a superposed NW-SE dextral shear is manifested as specific structures. If so, three alternative models for these structures are considered: (1) a regional throughgoing dextral shear zone subjacent to Yucca Mountain (Model A), (2) a right-stepping dextral shear zone that produces a pull-apart basin without an underlying cross-basin fault (Model B), and (3) a right-stepping dextral shear zone that produces a pull-apart basin with an underlying cross-basin fault (Model C). The integral structures in all of these models are buried and/or hypothesized, with the possible exception of the Highway 95 (or Carrara) fault, which may form the southern boundary of the pull-apart basin in Models B and C. The locations of these sources are shown on Figure 4-17. The case

with no specific dextral shear source is designated Model D. The Highway 95 fault and the north-bounding fault are assessed to have less than 1.0 probability of being seismogenic.

The possible existence of a local detachment zone was considered, with the likelihood that the detachment exists dependent on the existence of cross-basin shear structures (Figure 4-16a). Although not considered to be seismogenic, the detachment zone controls the down-dip extent of all local faults, except the Bare Mountain fault, and hypothesized buried dextral shear structures. Possible depths for detachments range from 3 km to the maximum thickness of the seismogenic crust. Under the assumption that a detaching layer does not exist, the down-dip extent of the local faults is controlled by the Bare Mountain fault and the thickness of the seismogenic crust.

The AAR team distinguished two parameters for the maximum depth of the seismogenic crust: (1) DMAX1 constrains down-dip extent of fault rupture for calculating rupture area to be used with empirical relations for estimating M_{max} and (2) DMAX2 is the maximum depth of seismogenic rupture during larger earthquakes, in which case rupture area is entered into an equation for seismic moment to estimate M_{max}. DMAX1 was assessed to range from 11 km to 17 km, based on the depth distribution of seismicity in the southern Great Basin, and represents the nominal definition of maximum depth defined in Wells and Coppersmith (1994). DMAX2, ranging from 14 km to 22 km, is based on the assessment that longer ruptures ($\geq$ 25 km) extend below the seismogenic crust into the brittle-ductile transition zone.

Two alternative modes of behavior were assessed for the local fault sources (Figure 4-16b). The first considered the local faults to act as independent sources. Figure 4-18 shows the locations of these faults. Some of these sources were considered to be potentially linked along strike into larger faults (the Paintbrush Canyon-Stagecoach Road system and the Southern, Central, Northern Windy Wash-Fatigue Wash system). The alternative considered that all of the observed normal faults in the Yucca Mountain area coalesce at depth into one to four master faults (Figure 4-19). In general, coalesced behavior is favored over independent behavior, with the specific weight dependent upon the existence and depth of potential detachments. When the number of coalesced faults is less than four, then it is assumed that large earthquakes produce comparable amounts of slip on parallel fault traces during a single earthquake. Under the

assumption of independent fault behavior, the minor faults such as the Ghost Dance, west Dune Wash, and Crater Flat) are assessed to have less than 1.0 probability of being seismogenic.

M_{max} for the local sources was based on empirical relationships between magnitude and rupture length, rupture length and slip rate, rupture area, and on estimation of seismic moment. The assessed distributions for M_{max} are shown on Figure 4-20. The AAR team chose to follow the convention developed by Youngs *et al.* (1987) in developing recurrence relationships for the faults. Following this approach, M_{max} assessed from the various empirical relationships is considered the central value of the characteristic magnitude interval, which is $M_{max} \pm ¼$ magnitude units. The upperbound magnitude of the recurrence relationship, m^U, is thus equal to $M_{max} + ¼$. The magnitudes plotted on Figure 4-20 are m^U.

Earthquake recurrence relationships for the local faults were based on assessments of slip rates and the recurrence intervals of large earthquakes (when data are available for a specific fault), with slip rate slightly favored. Slip rates of individual faults were summed across strike to assess rates for coalesced systems. A characteristic recurrence model was favored over a modified exponential model.

The AAR team identified 19 regional fault sources (Figure 4-21). The potential for two faults to be linked together into a single fault system was considered for the Death Valley and Furnace Creek faults, and for the Amargosa River and Pahrump faults. Preferred dips were generally 65° for normal faults and 90° for strike-slip faults. M_{max} for the regional sources were based on empirical relationships between magnitude and rupture length, rupture length and slip rate, and rupture area. The assessed distributions for M_{max} are shown on Figure 4-22. These values again are $M_{max} + ¼$. Earthquake recurrence relationships for the individual faults were assessed using the approaches outlined above for the local faults.

The AAR team defined regional source zones to account for the potential occurrence of earthquakes on faults not specifically identified as potential sources or unknown faults. Figure 4-23 shows the logic tree that defines the alternative interpretations of regional zones. Three alternatives were considered for defining these zones in which the spatial distribution of seismicity was assessed to be uniform (Figure 4-24). A fourth alternative was to use the kernel density estimation technique (discussed in Section 4.1.2) to define the spatial distribution of

earthquakes within 100 km of Yucca Mountain without imposing source zone boundaries. The potential occurrence of volcanic-related earthquakes was addressed by the regional zones. The M_{max} assessed for the regional zones ranged from M_w 6.6 to 7.3. Because of greater confidence in the identification and characterization of fault sources in the immediate Yucca Mountain vicinity, M_{max} was assessed to range from M_w 6.0 to 6.6 for the areal zone within 20 km of the Yucca Mountain site. The AAR team used the catalog of independent events produced by the declustering method of Veneziano and van Dyck (1985). The recurrence relationships for the individual source zones were estimated using the approach described in Section 4.1.4.1. All earthquakes occurring in the underground nuclear explosion (UNE) zone post-1950 were removed from the recurrence calculation. Figure 4-25 shows the recurrence relationships for each of the regional zones. These relationships were obtained using the maximum likelihood techniques discussed in Section 4.1.4.

The seismic source models developed by the AAR team can be used to calculate earthquake recurrence relationships (Figure 4-26) for the area shown on Figure 4-15. Plot (a) shows the distribution of earthquake frequencies computed using the AAR model for local faults (Figures 4-17 through 4-19). This distribution of earthquake occurrence rates applies to the area approximated by the shaded region around Yucca Mountain shown on Figure 4-15. The AAR local fault model contains about one and one-half orders of magnitude uncertainty in the combined recurrence rate for the local sources.

Plot (b) shows the distribution of earthquake frequencies computed using the AAR model for regional faults (Figure 4-21). Occurrence rates were computed for those portions of the regional faults that lie within 100 km of the Yucca Mountain site. The uncertainty in the recurrence rate for the regional faults is significantly smaller than that for the local faults. It should be noted that for all of the expert team characterizations, the predicted recurrence rates for regional faults are dominated by those estimated for the Death Valley and Furnace Creek faults. Also shown on Plot (b) are the observed frequencies of earthquakes occurring within 100 km of the Yucca Mountain site. Most of the smaller earthquakes are not close to the regional faults.

Plot (c) shows the distribution of earthquake frequencies computed using the AAR model for regional source zones (Figure 4-24). Again, the occurrence rates were computed for those

portions of the regional source zones that lie within 100 km of the Yucca Mountain site. The uncertainty in the recurrence rate for the regional sources zones is also significantly smaller than that for the local fault sources. Also shown on Figure 4-26 are the observed frequencies of earthquakes occurring within the same region. (These are the same frequencies as those shown on Plot [b].) The predicted earthquake frequencies for the regional zones are somewhat greater than the observed frequencies because they are based on larger source areas that include regions of higher seismicity rates that lie beyond the 100-km circle.

Plot (d) shows the distribution of earthquake frequencies computed for all the sources in the AAR seismic source model for the region that lies within 100 km of the Yucca Mountain site compared to the observed earthquake frequencies. There is reasonable agreement between the observed and predicted rates for magnitudes of interest to the ground motion hazard assessment.

Ake, Slemmons, McCalpin (ASM) Team. The ASM team incorporates various aspects of planar fault block, detachment, lateral shear, and volcanic-tectonic models into their characterization of the local seismic sources. Figures 4-27a and 4-27b show their logic tree defining the uncertainties in characterizing the local faults. The locations of these faults are shown on Figures 4-28 and 4-29. The ASM team considers the possibility of the existence of a regional detachment underlying Yucca Mountain, although their preferred tectonic model is that the faults are planar to a depth controlled by the brittle-ductile transition and the Bare Mountain fault. The regional detachment has a very low probability (0.01) of being seismogenic and may lie at three alternative depths: 6 km, halfway between 6 km and the brittle-ductile transition (preferred), and at the brittle-ductile transition. The brittle-ductile transition is assessed to lie in the depth range of 12 to 17 km. They also consider the potential for the existence of a buried strike-slip fault, with the probability that it exists dependent on the existence of a regional detachment. The probability that a buried strike-slip fault is seismogenic depends on its minimum depth, which is controlled by the depth of the detachment (Figure 4-27).

The ASM team identified 10 local faults as seismic sources near Yucca Mountain (Figure 4-28). Five of these faults (Bare Mountain, Windy Wash, Solitario Canyon, and Paintbrush Canyon/Stagecoach Road) are termed major, block-bounding faults, and are assessed to be seismogenic. The remaining faults (Northern and Southern Crater Flat, Fatigue Wash, Iron

Ridge, and Bow Ridge) are interpreted to be minor or secondary faults and have a probability of being seismogenic less than 1.0.

Two alternative geometries are considered for the local faults: planar and merging down dip. Under the planar assumption, the major faults penetrate to the base of the seismogenic crust and the down-dip extent of the minor faults is controlled by an aspect ratio of 1.5. Under the merging down-dip assumption, the major faults are truncated by the Bare Mountain fault or the detachment (if it exists) and the minor faults merge with the major faults. Three alternative geometries are assessed for this merging system: shallow, intermediate, and deep merging depths.

Two alternative behaviors were considered for the case of merging faults: the principal faults always rupture independently (the preferred model) and sometimes the principal faults rupture simultaneously (Figure 4-27b). Specific fault rupture combinations and the fraction of fault ruptures that are simultaneous ruptures were assessed by the ASM team.

The M_{max} for the local fault sources was assessed using empirical relationships between magnitude and surface rupture length, maximum displacement, rupture length times maximum displacement, average displacement, and rupture area (depending upon the available data). Only combined rupture area was used to assess the magnitude of multiple fault ruptures. The resulting M_{max} probability distributions are shown on Figure 4-30.

The ASM team used the convention of Youngs *et al.* (1987) in developing recurrence relationships for the faults, with the upperbound magnitude of the recurrence relationship, m^u, equal to M_{max} obtained from the empirical relationships plus ¼ magnitude units. The magnitudes plotted on Figure 4-30 are m^U. The rates of seismic activity on the local sources were assessed using fault slip rate and large magnitude earthquake recurrence interval approaches (depending on available data). For the mapped normal faults, the characteristic recurrence model was favored (0.7) with lesser weight given to the truncated exponential (0.2) and maximum moment (0.1) recurrence models. Only the characteristic recurrence model was used for the detachment and buried strike-slip sources and the simultaneous rupture of multiple faults was assessed to conform to the maximum moment recurrence model.

Figure 4-31 shows the 26 regional fault sources characterized in the ASM seismic source models. With the exception of the Carrara (Highway 95) fault, these faults are assigned a probability of 1.0 of being seismogenic based on paleoseismic evidence. The sources are modeled as planar faults that extend to the depth of the brittle-ductile transition. Generalized dips of 90° for strike-slip faults and 60° for normal faults were used. M_{max} was assessed based on an assessed distribution for maximum surface rupture length. The resulting M_{max} probability distributions are shown on Figure 4-32. Again, these magnitudes are M_{max} + ¼. Rates of seismicity were assessed based on fault slip rate and estimates of the recurrence intervals for surface-rupturing earthquakes. A maximum moment model was strongly favored (0.8) over a characteristic recurrence model (0.2).

The ASM team defined six regional source zones to account for the potential occurrence of earthquakes on faults not specifically identified as potential sources. Figure 4-33 shows the logic tree that defines the alternative interpretations of the regional source zones shown in Figure 4-34. Volcanic-related earthquakes were not modeled as a separate source, but rather were modeled as part of the earthquakes occurring in the areal source zones.

The M_{max} assessed for the regional zones ranged from M_w 6.5 to 7.2. Because of the greater detail of fault investigations and seismic source characterization in the immediate Yucca Mountain vicinity, M_{max} was assessed to range from M_w 6.0 to 6.6 within 50 km of the Yucca Mountain site. The ASM team used the catalogs of independent events produced by the declustering methods of Youngs *et al.* (1987) and Veneziano and van Dyck (1985). The recurrence relationships for the individual source zones were estimated using the approach described in Section 4.1.4.1. All earthquakes occurring in the UNE zone post-1950 were removed from the recurrence calculation. Figure 4-35 shows the recurrence relationships for each of the source zones.

Figure 4-36 shows the distribution for earthquake recurrence predicted by ASM seismic source characterization for local faults, regional faults, regional zones, and all sources combined compared to the observed frequency of earthquakes occurring within 100 km of the Yucca Mountain site. The ASM local fault model contains about one and one-half orders of magnitude uncertainty in the combined recurrence rates. A significant part of this uncertainty is due to differences between the recurrence rates assessed using fault slip rate and those

assessed using paleoseismic recurrence intervals. The uncertainty in the recurrence rate for large earthquakes occurring on the regional faults is much smaller than that for smaller earthquakes because of the range in earthquake recurrence models used by the ASM team. It should be noted that the use of the maximum moment model for regional fault recurrence does not imply a complete absence of smaller-magnitude earthquakes on or in the immediate vicinity of these faults. The fault sources are superimposed on regional source zones. Thus, the use of a maximum moment recurrence model for the regional faults implies that the occurrence rate for smaller earthquakes is no larger on the fault than at other locations within the regional zone. Within 100 km of Yucca Mountain, the predicted earthquake frequencies for the regional zones are somewhat greater than the observed frequencies, because they are based on larger source areas that include regions of higher seismicity that lie beyond the 100-km circle. The predicted occurrence rates from all sources for earthquakes of interest to the hazard assessment generally fall within the uncertainties in the observed rates.

Doser, Fridrich, Swan (DFS) Team. The DFS team does not specifically address tectonic models in developing an overview model for seismic source characterization, but rather uses aspects of various structural models to estimate the location, style of faulting, and down-dip geometry of local fault sources and hypothetical faults near the site. Figure 4-37 shows the logic tree developed by the DFS team to address uncertainties in defining and characterizing the local faults. Two alternative modes of behavior are considered for the local fault sources: (1) independent fault behavior, which is strongly preferred (weight 0.95), and (2) distributed fault behavior (0.05) (Figure 4-37a). The locations of the independent fault sources are shown on Figure 4-38. The Ghost Dance fault is included as a possible independent fault with a low probability of activity (0.05). The distributed fault behavior model allows for simultaneous rupture on subparallel faults, including faults on either side of Yucca Mountain. The pattern of fault rupture given the distributed fault behavior model varies from single to quadruple parallel ruptures depending on the inferred length of fault rupture. Alternative assessments are defined for the total length of distributed faulting (Figure 4-37b) and for the total length of individual faults (Figure 4-37c). The assessed distributions of maximum rupture length for individual faults depend on the total fault length (Figure 4-37c).

The next assessment in the logic tree addresses the existence of a detachment. The preferred model (weight 0.8) is that the faults are planar to the base of the seismogenic crust (inferred to

be at a depth in the range of 12 to 16 km) The alternative model (weight 0.2) is that the Paintbrush Canyon fault becomes listric at depth, forming a detachment. All of the west-dipping faults at Yucca Mountain are assumed to truncate against the east-dipping Bare Mountain fault. Two alternative structural models are used to define the down-dip geometry of the planar faults and a single model is used to define the down-dip geometries for the detachment model. These geometries are shown in the DFS elicitation summary (Appendix E). The detachment model allows for the possibility of a seismogenic detachment, whereby the Paintbrush Canyon/Stagecoach Road fault is modeled as a shallow-dipping seismogenic source that extends beneath the Crater Flat Basin. The detachment model also allows for the possibility of the existence of a buried strike-slip fault of local (weight 0.5) or regional (weight 0.5) extent. Figure 4-39 shows the location of the hypothesized buried strike-slip fault. The three traces indicate alternative locations for the source. Also shown on Figure 4-39 is the location of the hypothesized Highway 95 fault.

The methods used to calculate M_{max} for the local faults were empirical relations between magnitude and rupture length and area. Figure 4-40 shows the resulting M_{max} probability distributions. The DFS team considered the magnitude estimated from the empirical relationships to be the upperbound magnitude of the recurrence relationships, but included an uncertainty of ±¼ magnitude units about these estimates in forming their M_{max} distributions. The recurrence relationships for the local faults were based on estimates of slip rates. Three recurrence models were used for the local faults: exponential, characteristic, and maximum moment, with the characteristic earthquake model preferred (weight 0.6). The weights assigned to the two other models are conditional on the fault behavior model for the local faults. The maximum moment model is given greater weight in the independent rupture model (Figure 4-37c) and a weight equal to the exponential model in the distributed model (Figure 4-37b).

The DFS team included 18 regional faults that are judged to be capable of generating M_w 5 or larger earthquakes and inferred to have had multiple late Quaternary displacements. These sources are shown on Figure 4-41. All these faults are considered active with a probability of 1.0 and are characterized as planar faults extending to the maximum seismogenic depth with dips dependent on the style of faulting (90° for strike-slip faults, 60° for dip-slip faults). M_{max} were calculated using empirical relationships between magnitude and fault rupture lengths and

rupture areas. Figure 4-42 shows the resulting M_{max} probability distributions. Earthquake recurrence relationships for the regional sources were based on estimates of fault slip rates. The same three earthquake recurrence models used for the local faults were used for the regional sources.

Figure 4-43 shows the logic tree used to define the uncertainty in characterizing the regional source zones. The DFS team considered two alternative source zone models: Model A (weight 0.2), which consists of one regional zone, and Model B (weight 0.8), which has three regional zones. Figure 4-44 shows the configurations of these regional zones. The spatial distribution of earthquakes within these regional zones is interpreted to either conform to the existing pattern of seismicity, estimated using kernel spatial density estimation, or to be uniform, with the nonuniform pattern preferred.

The M_{max} assessed for the regional source zones ranged from M_w 7.0 to 7.7. Because of the greater detail of fault investigations and seismic source characterization in the immediate Yucca Mountain vicinity, M_{max} was assessed to range from M_w 5.6 to 6.0 within the local zone shown on Figure 4-44. The DFS team used the catalogs of independent events produced by the declustering methods of Youngs *et al.* (1987) and Veneziano and van Dyck (1985). The recurrence relationships for the individual source zones were estimated using the approach described above in Section 4.1.4.1. Earthquakes that occurred in close proximity to the regional faults were assumed to be associated with those sources and were not included in the data used to compute the seismicity rates for the regional zones. Figure 4-45 shows the recurrence relationships for each zone.

Figure 4-46 shows the distribution for earthquake recurrence predicted by the DFS team's seismic source characterization for local faults, regional faults, regional source zones, and all sources combined compared to the observed frequency of earthquakes occurring within 100 km of the Yucca Mountain site. The DFS local fault model contains about one and one-half orders of magnitude uncertainty in the combined recurrence rates. A significant part of this uncertainty is due to differences in predicting the frequency of earthquakes smaller than the maximum based on alternative recurrence models. The uncertainty in the recurrence rate for the regional faults is similar to that for the local faults, and also has a significant component contributed by the alternative recurrence models considered to estimate the frequency of

earthquakes smaller than the maximum. Within 100 km of Yucca Mountain, the predicted earthquake frequencies for the regional zones are somewhat higher than the observed frequencies, because they are based in part on larger source areas that include regions of higher seismicity rates that lie beyond the 100-km circle. The predicted occurrence rates from all sources for earthquakes of interest to the hazard assessment generally fall within the uncertainties in the observed rates.

Rogers, Yount, Anderson (RYA) Team. The RYA team states that none of the tectonic models that have been proposed provide a unified explanation of all the available seismic, geologic, and geophysical data for Yucca Mountain and the larger Walker Lane. Therefore, they do not specifically address tectonic models in developing an overview seismic source model. Rather, they use aspects of various structural models to estimate the location, style of faulting, and down-dip geometry of local fault sources and hypothetical faults near the site. Figure 4-47 shows the logic tree used by the RYA team to describe the uncertainty in characterizing the local faults. The basic model is a system of from one to three west-dipping, coalescing faults and the east-dipping Bare Mountain fault (Figure 4-48). The weight assigned to the existence of one, two, or three faults depends upon the thickness of the seismogenic crust, which is assessed to be in the range of 12 to 20 km.

M_{max} for the local faults was estimated using empirical relationships between magnitude and surface rupture length and rupture area. The RYA team considered the magnitude estimated from the empirical relationships to be the upperbound magnitude of the recurrence relationships, but included an uncertainty of ± ½ magnitude units about these estimates in forming their M_{max} distributions. The resulting M_{max} probability distributions are shown on Figure 4-49. Earthquake recurrence rates for the local faults were based on trench recurrence interval data and slip-rate data, with a preference for the slip-rate approach. Characteristic and truncated exponential recurrence models were used. The weight assigned to each model was dependent on the number of coalescing faults, with increasing preference for the exponential model as the number of independent sources decreased.

The RYA team defined 11 regional faults (Figure 4-50). These faults all are considered active with a probability of 1.0. Regional faults are treated as steeply-dipping planar faults penetrating to the maximum thickness of the seismogenic crust, with dips depending on the style of faulting

(90° for strike-slip faults, 60° for normal faults). M_{max} for the regional faults were estimated using empirical relationships between magnitude and surface rupture length, rupture area, and maximum displacement, depending upon the available data. The resulting M_{max} probability distributions are shown on Figure 4-51. Earthquake recurrence relationships for the regional faults were estimated using estimates of fault slip rate . The characteristic and the truncated exponential recurrence models were used, with the characteristic model strongly preferred. In addition, the earthquakes occurring on the regional faults were limited to M_w 6.3 and larger. The occurrence of earthquakes smaller than M_w 6.3 was accounted for by the areal source zones. This approach is based on the concept that earthquakes smaller that M_w 6.3 do not occur on the faults with any greater frequency than elsewhere in the regional source zones.

Figure 4-52 shows the logic tree developed by the RYA team to describe the uncertainty in characterizing regional source zones. The RYA team divided the region within a 100-km radius surrounding Yucca Mountain into three primary seismic source zones with two alternate zonations (Scenarios 1 and 2) used to model a local source (Figure 4-53). The spatial distribution of earthquakes was assessed to be either uniform or nonuniform, with the latter based on a kernel density estimation using historical seismicity.

The M_{max} assigned to each of the areal zones is M_w 6.3 ± 0.3. The recurrence rates for the source zones were estimated by fitting truncated exponential relationships to simulations of the declustered catalogs. The technique used and results are described in the RYA team elicitation summary (Appendix E).

The RYA team also included in their seismic source model a volcanic source that encompasses the area of younger volcanism in the Yucca Mountain region and extends north to include Thirsty Mesa and Buckboard Mesa. They assess the probability that a separate volcanic source exists to be 0.7. The recurrence rate is based on the estimated return period for volcanic events (assessed to be 2×10^5 years to 2×10^6 years) and M_{max} was assessed to be M_w 5.5.

Figure 4-54 shows the distribution for earthquake recurrence predicted by the RYA team's seismic source characterization for local faults, regional faults, regional source zones, and all sources combined compared to the observed frequency of earthquakes occurring within 100 km of the Yucca Mountain site. The RYA local fault source model contains about one order of

magnitude uncertainty in the combined recurrence rates. The uncertainty in the recurrence rate for the regional faults is similar to that for local faults. As discussed above, the regional zones are used to model the occurrence of earthquakes smaller than M_w 6.3 on or near the regional faults. The RYA team used only the recorded earthquakes within 100 km of Yucca Mountain to evaluate the recurrence rate for the regional zones, thus there is good agreement between predicted and observed earthquake frequencies for the regional zones. The predicted occurrence rates for all sources for earthquakes of interest to the hazard assessment generally fall within the uncertainties in observed rates.

Smith, Bruhn, Knuepfer (SBK) Team. The SBK team considered a variety of tectonic models in the development of their seismic source model. Local seismic sources are characterized based on their strongly preferred oblique-rift/planar-fault model, with other tectonic models considered as constraints on source geometry and the potential for existence of hidden seismic sources. In this model, 3-D strain in the Yucca Mountain region is accommodated by normal-slip, strike-slip, and oblique-slip on planar faults. The Bare Mountain (master) and Yucca Mountain (antithetic) faults form a half-graben, whereas the Rock Valley and Highway 95 faults act as accommodation zones. Other potential sources, such as detachment faults, buried dextral shear zones, and volcanic sources related to dike-injection were considered either not to be seismogenic (e.g., detachments) or to be covered by background earthquakes in areal source zones (e.g., buried dextral shear zones and volcanic sources) and, thus, were not explicitly modeled as specific seismic sources.

Figure 4-55 shows the logic tree developed by the SBK team to represent the uncertainty in characterizing the local sources (shown on Figure 4-56). Four alternative behavioral modes were considered for local faults. Independent behavior of the mapped faults was the favored model (weight 0.5). The next most favored behavior mode (weight 0.4) is that the major block-bounding faults are linked along strike to form independent faults along with the Bare Mountain fault. The two additional, less-likely, modes entail all of the Yucca Mountain faults soling into a detachment between 5 km and the base of the seismogenic zone (0.01), and all of the Yucca Mountain faults coalescing at depth into a master block-bounding fault (0.09). For all four modes of behavior, the possibility of simultaneous rupture events triggered by volcanic activity is considered. The likelihood of this simultaneous rupture event is considered greater for the detachment and coalescing fault behavior modes (0.5) than for the linked and independent

modes (0.1). Three alternative geometries that defined the down-dip extent of the Yucca Mountain faults were considered for all four behavior modes.

M_{max} for the local faults was estimated using empirical relationships between magnitude and surface rupture length, rupture area, and maximum displacement, as well as estimates based on evaluation of seismic moment (rupture area times average displacement) and static stress drop. The resulting M_{max} probability distributions are shown on Figure 4-57. The SBK team also used the convention of Youngs *et al.* (1987) in developing recurrence relationships for the faults, with the upperbound magnitude of the recurrence relationship, m^U, equal to M_{max} obtained from the empirical relationships plus ¼ magnitude unit. The magnitudes plotted on Figure 4-57 are m^U. Earthquake recurrence relationships for the local faults were estimated from fault slip rates and recurrence intervals, depending upon the available data. For nonsimultaneous ruptures on coalescing fault and detachment models, slip rates were summed along across-strike transects. Recurrence of simultaneous ruptures was assessed based on recurrence of volcanic eruptions in Crater Flat. The characteristic and truncated exponential recurrence models were used for all but the simultaneous rupture scenarios, with the truncated exponential model generally favored. The maximum moment recurrence model was used for the simultaneous rupture scenarios.

Sixteen regional faults (Figure 4-58) were included with assessed likelihoods of seismogenic activity ranging from 0.01 to 1.0. Regional faults were modeled as independent, planar sources extending to the maximum seismogenic depth (12 to 17 km). Fault dips were based on fault type: 60° for normal, 70° for oblique, and 90° for strike-slip. The SBK team considered the possibility of linked-fault behavior for the Death Valley-Furnace Creek-Fish Lake Valley system of faults. The preferred model is that the four faults, Southern Death Valley, Death Valley, Furnace Creek, and Fish Lake Valley, are independent faults. Approximately 0.05 probability is given to a model with two linked faults, and 0.01 probability is given to a model with all four faults linked. M_{max} for the regional faults was evaluated using empirical relationships between magnitude and surface rupture length, rupture area, and maximum displacement, as well as estimates based on evaluation of seismic moment. The resulting M_{max} probability distributions are shown on Figure 4-59. Again, these are M_{max} + ¼. Both the slip rate and recurrence interval approaches were used to assess rates of seismic activity with the former being favored, but fault-specific weights were assigned depending on available data. A characteristic

recurrence model was favored for range-bounding faults and a truncated exponential model was favored for other fault zones exhibiting distributed faulting on multiple traces.

Figure 4-60 shows the logic tree developed by the SBK team to represent the uncertainty in characterizing the regional source zones. Two alternative zonation models were considered (Figure 4-61): one consisting of three zones and one in which an additional Rock Valley zone is defined. The spatial distribution of seismicity within the source zones was assessed to be uniform.

The M_{max} for regional source zones was assessed to range from M_w 6.2 to 6.6. Because of the greater detail of fault investigations and seismic source characterization in the immediate Yucca Mountain vicinity, M_{max} was assessed to range from M_w 5.6 to 6.2 within the local zone shown on Figure 4-61. The SBK team used the catalogs of independent events produced by the declustering methods of Youngs *et al.* (1987) and Veneziano and van Dyck (1985). The recurrence relationships for the individual source zones were estimated using the approach described above in Section 4.1.4.1. Adjustments for the effects of UNEs were incorporated as an alternative assessment of the recurrence rates. Figure 4-62 shows the recurrence relationships for each of the regional zones.

Figure 4-63 shows the distribution for earthquake recurrence predicted by the SBK team's seismic source characterization for local faults, regional faults, regional source zones, and all sources combined compared to the observed frequency of earthquakes occurring within 100 km of the Yucca Mountain site. The SBK local fault model contains about one order of magnitude uncertainty in the combined recurrence rates. The uncertainty in the recurrence rate for the regional faults is similar to that for the local faults. The SBK team used only the recorded earthquakes within 100 km of Yucca Mountain to evaluate the recurrence rate for the regional zones, thus there is good agreement between predicted and observed earthquake frequencies for the regional zones. The predicted occurrence rates for all sources for earthquakes of interest to the hazard assessment generally fall within the uncertainties in observed rates.

Smith, de Polo, and O'Leary (SDO) Team. The preferred tectonic model for Yucca Mountain proposed by the SDO team is that of a half-graben partly filled by a collapsed volcanic carapace. They acknowledge that the site region also may be experiencing a component of

northwest-directed dextral shear that is either confined to Crater Flat Basin (i.e., the basin itself is becoming distorted because of distributed, regional shear), or less likely, is being accommodated by an external, discrete strike-slip fault. To account for the latter, they assign a relatively high (0.4) probability to a strike-slip fault within or proximal to Crater Flat Basin along the hingeline-Pahrump-Stewart Valley fault zone alignment. They give zero weight to detachment models.

Figure 4-64 shows the logic tree developed by the SDO team to characterize the local faults. The SDO team identified six major faults (Paintbrush Canyon, Stagecoach Road, Solitario Canyon, Iron Ridge, Fatigue Wash, and Windy Wash faults) (Figure 4-65). All of these faults with the exception of the Iron Ridge and Fatigue Wash faults are considered to be "block-bounding" faults, structures that define major tilted panels of the carapace and that probably penetrate to significant seismogenic depth without intersection. Several other faults (Bow Ridge, Ghost Dance, Abandoned Wash, Northern Crater Flat, and Southern Crater Flat faults) might penetrate the carapace, but were deemed not capable of an earthquake larger than the maximum background earthquake (M_w 6.2). Three alternative geometries were defined to represent the interaction between the east-dipping Bare Mountain fault and the west-dipping Yucca Mountain faults. The major faults, as well as the faults that are thought to be confined to the carapace, were included in six individual (single, discrete planes), nine linked (individual planes linked along strike by complex structure) and eight distributed (planes linked across dip) fault rupture scenarios. As indicated on Figure 4-64, these rupture scenarios are not alternatives. All rupture scenarios are assumed to occur. The SDO team established the frequency of rupture on a particular fault, such as Paintbrush Canyon, from paleoseismic data on the occurrence of past ruptures. For each paleoseismic rupture, they evaluated the likelihood that the event corresponded to various rupture scenarios (e.g., rupture of just the northern part of the Paintbrush Canyon fault, versus rupture of all of the Paintbrush Canyon fault, versus rupture of Paintbrush Canyon and Stagecoach Road faults). These assessments for each paleoevent were used to estimate the relative frequency of the various rupture scenarios for each fault. The product of the relative frequencies for the rupture scenarios times the estimates for frequency of ruptures on the fault provide estimates for the frequency of occurrence of the individual rupture scenarios.

M_{max} for the local faults was evaluated based on empirical relationships between magnitude and surface rupture length, maximum displacement, rupture length times maximum displacement, and rupture area, as well as estimates of seismic moment. The resulting M_{max} probability distributions for local faults are shown on Figure 4-66. The SDO team also used the convention of Youngs *et al.* (1987) in developing recurrence relationships for the faults, with the upperbound magnitude of the recurrence relationship, m^U, equal to M_{max} obtained from the empirical relationships plus ¼ magnitude unit. The magnitudes plotted on Figure 4-66 are m^U. A characteristic recurrence model was favored (0.7) over a truncated exponential model (0.3) for predicting the frequency of smaller events. A minimum magnitude of M_w 6.2 was used in the recurrence assessment for the local sources.

As noted above, the SDO seismic source model includes a buried strike-slip fault source. The hingeline, which appears to represent the structural boundary to a zone of features suggestive of distributed dextral shear deformation, is chosen by the SDO team as the best candidate location for a buried strike-slip fault. This fault is shown as fault T6-SS on Figure 4-67. The preferred (27 km) and minimum (20 km) estimates for fault length are based on the postulated length of the hingeline in the Crater Flat area. They also allow for the possibility that the hingeline represents the northwestern extension of the Pahrump-Stewart Valley fault zone. In this case they infer a maximum length of 120 km. The buried strike-slip fault is treated in a similar fashion to the other regional faults discussed below.

Thirty-six regional faults were characterized as separate fault sources by the SDO team (Figure 4-67). Within 50 km of Yucca Mountain, all identified Quaternary and possible Quaternary faults capable of $M_{max} \geq 6.4 \pm 0.2$ were included. In the distance range of 50 to 100 km from Yucca Mountain, faults of lengths of 20 km or more were included. Two faults that generally lie beyond 100 km, the Panamint Valley fault zone and the Ash Hill fault zone, also were included for their potential long-period ground motion contribution. Of the 36 faults included, 24 are judged to be active with a probability of 1.0, and 12 were judged active with probabilities ranging from 0.2 to 0.9. Regional faults are modeled as planar fault sources extending to the maximum seismogenic depth (assessed to be in the range of 14 to 19 km) with dips depending on the style of faulting (90° for strike-slip faults, 60° for normal faults).

M_{max} for the regional faults was assessed using empirical relationships between magnitude and surface rupture length, maximum displacement, rupture length times maximum displacement, and slip rate plus rupture length. Fault weights were assigned depending on available data. The resulting M_{max} probability distributions are shown on Figure 4-68. These are also M_{max} + ¼. A recurrence interval approach was used by the SDO team to assess recurrence for regional faults. Specifically, the method used involved estimating average surface displacement from the minimum, preferred, and maximum fault lengths using relationships from Wells and Coppersmith (1994), dividing average displacement per event by slip rate to get a slip accumulation time (average recurrence interval), and inverting this estimate to obtain an annual earthquake occurrence rate. The characteristic recurrence model was favored over the truncated exponential model. A minimum magnitude of M_w 6.2 was used in the recurrence assessment. The occurrence of earthquakes smaller than M_w 6.2 was accounted for by the areal source zones. This approach is based on the concept that earthquakes smaller that M_w 6.2 do not occur on the faults with any greater frequency than elsewhere in the regional source zones.

Figure 4-69 shows the logic tree developed by the SDO team to represent the uncertainty in characterizing the regional source zones. Eight independent source zones were defined. Three of these zones lie within 100 km of the site (Figure 4-70). The spatial distribution of seismicity within the source zones was assessed to be either uniform or spatially varying, based on the observed pattern of recorded seismicity.

The M_{max} for the regional source zones was assessed to be M_w 6.4 ± 0.2. The SDO team used the catalogs of independent events produced by the declustering methods of Youngs *et al.* (1987) and Veneziano and van Dyck (1985), as well as a specific set of aftershock criteria defined by the team. The recurrence relationships for the individual source zones were estimated using the approach described above in Section 4.1.4.1. Figure 4-71 shows the recurrence relationships for each of the source zones.

The SDO team included two volcanic earthquake sources related to basaltic volcanoes and dike-injection (Figure 4-72): one based on the NE alignment of approximately 1-million-year-old volcanic vents across Crater Flat, and a second based on the vent alignment that encompasses the approximately 70-ka-years-old Lathrop Wells volcanic vent. The M_{max} for a volcanic-related earthquake in these zones was assessed to lie in the range of M_w 5.5 to 6.0. A

recurrence of two to three volcanic events per million years was used to estimate an activity rate for these zones.

Figure 4-73 shows the distribution for earthquake recurrence predicted by the SDO team's seismic source characterization for local faults, regional faults, regional source zones, and all sources combined compared to the observed frequency of earthquakes occurring within 100 km of the Yucca Mountain site. The SDO local fault source model contains about one order of magnitude uncertainty in the combined recurrence rates. The uncertainty in the recurrence rate for the regional faults is similar to that for the local faults. As discussed above, the regional zones are used to model the occurrence of earthquakes smaller than M_w 6.2 on or near the regional faults. The regional zones defined by the SDO team extended beyond the 100-km-radius circle about Yucca Mountain, but did not include the areas of higher seismicity to the northwest that were included by other teams in their Walker Lane regional source zones. Thus, the SDO team's predicted rate of seismicity for the regional source zones within 100 km of Yucca Mountain are in good agreement with the observed earthquake frequencies for the regional zones. The predicted occurrence rates from all sources for earthquakes of interest to the hazard assessment generally fall within the uncertainties in observed rates.

4.3.1.2 Summary of Expert Seismic Source Characterization Assessments. In this section we summarize the range of interpretations made by the expert teams regarding key components of their seismic source characterization models. This section is organized by the various types of sources included in the models: seismic source zones, regional faults, local faults, and other sources (including buried strike-slip fault sources, seismogenic detachment fault, and volcanic sources). A summary of the key components of each of the source models is provided in Table 4-1.

Areal Source Zones. Areal source zones were defined by all teams to account for background earthquakes that occur on potential buried faults or faults not explicitly included in their model. Four teams (AAR, DFS, RYA, and SBK) included alternative models in their characterization of the areal zones within a 100-km radius of the Yucca Mountain site. The RYA team's model always includes three zones, but allows for different configurations of the zone that include the site. The other three teams (AAR, DFS, and SBK) considered models that include one to three areal zones. The ASM and SDO teams each presented a single model that included two and

three zones, respectively. Four teams (AAR, ASM, DFS, and SDO) define areal zones that extend beyond 100 km of the Yucca Mountain site. Four teams (AAR, ASM, DFS, and SBK) defined a site region or zone solely for assigning a lower M_{max} to the area where more detailed investigations have been conducted and the inventory of fault sources is more complete.

All teams used the truncated exponential model to estimate earthquake recurrence rates within the areal source zones. In regard to processing the catalog, the declustering method of Veneziano and van Dyck (1985) (catalog version 7) and the method of Youngs *et al.* (1987 catalog version 5) were both used by five of the teams, one team (AAR) used only catalog version 7 and one team (SDO) also gave some weight to a third catalog (version 8) based on their own analysis of declustering and completeness. Three of the teams (AAR, ASM, and SBK) made adjustments for UNEs in relevant zones. Varying treatments of the background seismicity were included: (1) uniform smoothing of seismicity was used solely or given significant weight by most of the teams, and (2) nonuniform smoothing using Gaussian kernels having different smoothing distances was included by four teams.

The M_{max} distributions for the areal zones were based on the largest earthquake that could occur in the region either randomly and/or on a geologic structure that was not explicitly included in the seismic source model. As noted above, lower values were included in several models for the local area around the Yucca Mountain site.

Regional Fault Sources. Regional faults were treated in a similar fashion by all six teams. Regional faults were defined by most teams as faults within 100 km that were judged to be capable of generating earthquakes of M_w 5 or greater based primarily on fault length and Quaternary histories of multiple surface fault rupturing earthquakes. Paleoseismic data from Piety (1995) was used by all the teams to identify and characterize potential regional faults. Other sources, such as Anderson *et al.* (1995a, 1995b), McKague *et al.* (1996), Keefer and Pezzopane (1996), and Pezzopane (1996) also were used to varying degrees by some of the teams. Many of the faults that McKague *et al.* (1996) consider Type 1 faults were not judged relevant to the hazard analysis and were not included as fault sources by any of the teams because of their short length, distance from Yucca Mountain, and evidence that indicates that many of these faults either have no significant Quaternary displacement or are much shorter than previously thought.

The number of faults included in the seismic source models for the various teams ranged from 11 to as many as 36. This reflects the judgments of the teams regarding the activity of various faults. One team included only faults that were judged to be active with a probability of 1.0, whereas the other five teams also included faults that were judged to be active with probabilities of less than 1.0. All teams modeled the regional faults as simple, planar faults to maximum seismogenic depths with generalized dips depending on the style of faulting (90° for strike-slip faults, 60° or 65° for normal-slip faults). Alternative fault lengths were included for most of the faults by all teams.

A variety of empirical relations were used by the teams to estimate M_{max} for the regional faults. Two teams (ASM and DFS) used only surface rupture length relations, whereas the other four teams incorporated one or more other regression relations based on rupture area, maximum displacement, average displacement, rupture area times maximum displacement, and surface rupture length plus slip rate, depending on available data.

Two general approaches were used to estimate recurrence rates for the regional faults: slip rates and recurrence intervals. Two teams (DFS and RYA) relied strictly on the slip-rate approach, whereas three teams (AAR, ASM, and SBK) used both. The SDO team used only a recurrence interval approach based on dividing the fault slip rate by the displacement for the maximum event. Four different recurrence models were used by the various teams: the characteristic recurrence model was used by all teams with weights ranging from 0.2 to 0.9, four teams used the truncated exponential with weights ranging from 0.1 to 0.3, two teams used a maximum moment model, and one team used a modified exponential.

Local Fault Sources. Varying fault behavioral and structural models were employed by the teams to capture the full range of complex rupture patterns and fault interactions in the characterization of local faults. A planar fault block model is preferred by most teams, with linkages along strike or coalescence down dip considered by all teams. Simultaneous rupture of multiple faults was included in all models and was variously referred to as simultaneous rupture models (ASM and SBK), synchronous behavior (AAR), distributed behavior (DFS and SDO), and coalescing models (AAR, SBK, and RYA). In general, preferred models for multiple fault rupture included two to four coalescing fault systems. Four teams (ASM, AAR, DFS, and

SBK) used detachment models to constrain the extent and geometry of the local faults. Two teams (ASM and DFS) include detachment models in their source model with weights of 0.15 and 0.2, respectively, and use these models to both characterize local faults as well as seismogenic detachment fault sources. In the AAR model, the likelihood of existence of hypothesized, local detachments is dependent on the type of dextral shear structures assumed to be present. The SBK team gave very low weight (0.01) to a model in which the local faults sole into a detachment. The RYA and SDO teams excluded detachments in their source models.

A variety of empirical relations were used by the teams to estimate M_{max} on the local faults. At a minimum, the teams considered rupture length and rupture area relationships. Four teams also considered relationships based on maximum displacement, average displacement, rupture area times maximum displacement, surface rupture length plus slip rate , and seismic moment, depending on available data.

As was done for the regional faults, two general approaches were used to estimate recurrence rates for the local faults: slip rate s and recurrence intervals. Four teams (ASM, AAR, RYA, and SBK) used both approaches with equal weight, or favored the slip-rate approach. The DFS team relied strictly on the slip-rate approach, and the SDO team used only recurrence intervals. Four different recurrence models were used by the various teams: the characteristic recurrence model was used by all teams with weights ranging from 0.2 to 0.9, five teams used the truncated exponential with weights ranging from 0.1 to 0.8, two teams gave weight (0.1 to 0.8) to a maximum moment , and one team used a modified exponential model (weight 0.3).

Buried Strike-Slip Faults. The possibility that dextral shear is being accommodated in the Yucca Mountain region by a buried strike-slip fault was considered by all teams. Four teams included a regional buried strike-slip fault source with low probability. Two teams (AAR and DFS) included throughgoing regional dextral shear zones with fault lengths ranging from 50 to 100 km and 30 to 200 km, respectively. The AAR team included the regional strike-slip fault as part of their throughgoing dextral shear model (0.05). Both the DFS and ASM teams considered the possibility of a buried strike-slip fault source to be conditional upon the existence of a detachment. The ASM team also considered the probability that a buried strike-slip fault was seismogenic conditional upon the depth of the inferred detachment. They used lengths of 25 km (preferred) and 60 km to model their buried fault source. The SDO team

included a discrete buried strike-slip fault, but argued that the hypothesized fault would not extend north of the Crater Flat Basin, they also preferred a relatively short length (27 km), but allowed for a longer rupture (120 km) along the Pahrump/Stewart Valley fault zone to the south. Two teams (RYA and SBK) did not explicitly include buried strike-slip fault sources. Although they do not preclude the possibility of a buried fault, they conclude that this source would be incapable of generating an earthquake larger than those associated with their regional source zones.

Seismogenic Detachment Fault Source. As noted previously five teams incorporated detachment models in their treatment of local fault sources. Only two teams (ASM and DFS) explicitly allow for the existence of a seismogenic detachment fault source in their detachment models, which are given low weights (0.15 and 0.2, respectively). In the DFS model, only a local detachment is considered, whereby the Paintbrush Canyon-Stagecoach Road fault system is modeled as a shallow-dipping seismogenic source. The ASM team allows for a larger detachment source (rupture area of 4000 ± 2000 km^2) in their model, but give very low weight to the possibility of a seismogenic detachment (0.1) given that a detachment exists (0.15).

Volcanic Sources. Seismicity related to volcanic processes, particularly seismicity related to basaltic volcanoes and dike-injection, was explicitly modeled in volcanic source zones by two teams (RYA and SDO). Volcanic-related earthquakes were not modeled as a separate source by the other four teams, but owing to the low magnitude and frequency of volcanic-related seismicity, were accounted for by the areal source zones.

The concept of a volcanic-tectonic earthquake whereby some surface-rupturing earthquakes in Crater Flat Basin are accompanied by dike-injection (i.e., the postulated 70 ka "ash event"), was explicitly modeled by only one team (SBK). All the other teams included the possibility of such an event indirectly as part of their simultaneous rupture models (variously referred to as synchronous [AAR], distributive behavior [DFS], coalescing fault [RYA] rupture models) but did not necessarily tie it to volcanism.

Predicted Recurrence Relationships. Figures 4-74 through 4-77 compare the predicted mean recurrence rates developed by each team to the combined distribution in recurrence rates over all teams for local faults, regional faults, regional source zones, and all sources combined. The

combined distributions were obtained by giving equal weights to the individual team distributions. As was the case for the results presented by each team, the recurrence rate for local sources is for the area approximated by the shaded region on Figure 4-15 and the recurrence rate for the regional faults, regional source zones, and all sources combined is for the region within 100 km of the Yucca Mountain site.

There is approximately an order of magnitude range in the overall uncertainty in recurrence rate for M_w 6 and larger earthquakes on the local faults (Figure 4-74). The range between the mean results for the six teams is about one-half the overall range. The uncertainty in the recurrence rate increases significantly for larger magnitudes, primarily due to differences between the expert teams' assessment of M_{max} for the local faults. Assessments that favor multiple-fault ruptures, the use of displacement-based estimates of M_{max}, and recurrence rates for maximum events based on paleoseismic recurrence intervals tend to produce larger M_{max} and higher overall recurrence rates for the local faults. Assessments that favor the use of M_{max} assessments based on rupture area and recurrence rates based on slip rate tend to produce smaller M_{max} and lower overall recurrence rates. The uncertainty in recurrence rate also increases somewhat for magnitudes less than M_w 6. This increase is due primarily to uncertainty in the form of the recurrence model (truncated exponential versus characteristic versus maximum M_w distributions).

The uncertainty in the recurrence rate for M_w 6 and larger earthquakes on the regional faults (Figure 4-75) is about the same as that for the local faults. However, the uncertainty does not increase for larger magnitudes, because these recurrence rates are controlled by the recurrence for the Death Valley-Furnace Creek system of faults, for which the six teams developed similar characterizations. The very large range in results for smaller magnitudes reflects how the teams characterized the recurrence model (magnitude distribution for the regional sources). The RYA and SDO teams made the assessment that moderate earthquakes would not occur on the regional faults at a greater rate than predicted for the regional source zones and, thus, limited their recurrence models for the regional faults to earthquakes larger than M_w 6.3 and 6.2, respectively. The occurrence of smaller earthquakes on or near the regional faults was modeled by their regional source zones. The remaining four teams considered truncated exponential, characteristic, and M_w distributions, generally favoring the characteristic model. Thus the large range in recurrence rate for M_w 5 and smaller earthquakes shown on Figure 4-75 is somewhat

artificial. The observed rate of earthquakes (Figure 4-75) was not used by any of the teams to characterize the regional faults.

The combined distribution and mean estimates for the individual SSFD teams for recurrence in the regional source zones within 100 km of the Yucca Mountain site is shown on Figure 4-76. The spread in recurrence rates in the M_w 4 to 5.5 range reflects the degree to which the teams based their characterizations on a uniform distribution of seismicity in regional zones that extend beyond the 100-km region. Seismicity zones that included the higher rate of seismicity occurring to the northwest tend to predict higher rates of seismicity than observed in the Yucca Mountain region. This is based on the assumption that larger regions are required to adequately characterize the seismicity rates. The large range in results for magnitudes greater than M_w 6 reflects the differences in how the teams assessed the M_{max} for the regional zones within 100 km of the site. Three teams allowed for the occurrence of earthquakes greater than M_w 7 on sources that were not characterized explicitly as regional or local faults, and three teams considered that the sources of these events were treated explicitly in their characterization of other sources. Thus, the differences between the individual team assessments shown on Figures 4-75 and 4-76 reflect, in part, how each team partitioned the seismic source characterization between regional faults and regional source zones.

Figure 4-77 compares the combined distribution for earthquake recurrence from all seismic sources and the mean results for the six expert team characterizations. There is generally less than an order of magnitude range in uncertainty in the estimation of regional seismicity rates. At smaller magnitudes, the range reflects the differences in how the teams characterize the regional source zones. The overprediction of the observed rate of M_w 4 to 5 earthquakes within 100 km of the site reflects the teams' general assessment that larger regions are needed to characterize the seismicity rates. At larger magnitudes, the assessments from the individual teams lie within the uncertainty in the occurrence rates of earthquakes based on the historical record. As discussed above, the results shown on Figure 4-77 are for the entire region within 100 km of the Yucca Mountain site. It is expected that the ground motion hazard will be influenced largely (at least for high spectral frequency ground motions) by nearby seismic sources. Thus, the larger uncertainty in recurrence rates for the local sources (Figure 4-74) will have a significant effect on the uncertainty in the ground motion hazard.

4.3.2 Fault Displacement Hazard Characterization Models

The instructions given to the SSFD expert teams were to develop a fault displacement hazard characterization model that could be applied to any location within the Controlled Area at the Yucca Mountain site. To demonstrate the application of these models and to provide an estimate of the fault displacement hazard, nine demonstration points were selected (see Figure 4-9) for fault displacement hazard characterization. The points were selected to represent the expected range of fault displacement hazard conditions within the Controlled Area in terms of the types of features that may be encountered: block-bounding faults with greater than 50 m of cumulative offset that may be seismogenic, mapped intrablock faults with north-south and northwest-southeast strikes having a few to tens of meters of cumulative displacement, and features observed within the ESF that are likely to be encountered within the proposed repository block, ranging from small faults uncorrelated with surface feature to intact rock. The selected points are (Figure 4-9):

Point 1. A location on the Bow Ridge fault where it crosses the ESF. The Bow Ridge fault is a block-bounding fault that has been characterized by the SSFD expert teams as being a potentially seismogenic fault and/or to be part of a seismogenic fault system.

Point 2. A location on the block-boundary Solitario Canyon fault, which has been characterized by the expert teams as one of the longer seismogenic faults within the Yucca Mountain site vicinity.

Point 3. A location on the Drill Hole Wash fault where it crosses the ESF, which is one of the longer of the northwest-striking faults within the Yucca Mountain site vicinity.

Point 4. A location on the Ghost Dance fault, which is one of the longer north-south intrablock faults within the Controlled Area.

Point 5. A location on the Sundance fault within the proposed repository footprint west of the ESF. The Sundance fault is an intermediate size, northwest-trending intrablock fault.

Point 6. A location on a small fault mapped in bedrock on the west side of Dune Wash. This point represents a location on one of the many small north-south-striking intrablock faults that have been mapped at the surface of Yucca Mountain.

Point 7. A location approximately 100 m east of Solitario Canyon at the edge of the proposed repository footprint. Any one of four hypothetical conditions were assumed to exist at this location that are representative of features encountered within the ESF that are not directly correlated with specific features observed at the surface:

(a) A small fault having 2 m of cumulative displacement
(b) A shear having 10 cm of cumulative displacement
(c) A fracture having no measurable cumulative displacement
(d) Intact rock

Point 8. A location within the proposed repository footprint midway between the Solitario Canyon and Ghost Dance faults. The same four hypothetical conditions were assumed to exist here as at Point 7.

Point 9. A location in Midway Valley east of the Bow Ridge fault on an observed fracture having no measurable displacement in Quaternary alluvium.

4.3.2.1 Individual Expert Team Models. The fault displacement hazard assessment models developed by the six SSFD expert teams are described in this section along with how the models are to be applied to the nine demonstration points. Table 4-3 summarizes key points of the fault displacement hazard assessment models for each team. Note that many of the terms and parameters used in this section were previously defined in Section 4.2.

Arabasz, Anderson, Ramelli (AAR) Team. The AAR team's characterization of fault displacement hazard differentiates between those sites that are subject to potential principal faulting hazard and those sites that are subject to distributed faulting hazard.

Characterization for Sites of Potential Principal Faulting Hazard. Figure 4-78 presents the AAR team's logic tree for characterization of sites subject to principal faulting hazard. The AAR team considers both the earthquake and displacement approaches.

Earthquake Approach. In the earthquake approach, two contributions to hazard are included (indicated by the vertical line on the logic tree under sources of hazard): hazard from principal faulting due to the occurrence of earthquakes on the fault and distributed faulting hazard from earthquakes occurring on other seismic sources. The first assessment in the earthquake approach is an evaluation of whether or not the feature can experience principal faulting or distributed faulting, $P(C)$. Because the occurrence of principal faulting requires that the feature in question be seismogenic, $P(C)$ for principal faulting is equal to the probability that the fault is seismogenic, $P(S)$, which was assessed as part of the AAR team's seismic source characterization for the ground motion evaluation (see Section 4.3.1.1). The probability that the feature in question can experience distributed slip, $P(C)$, was assessed based on the orientation of the feature in the present stress regime and evidence for past movement.

The next assessment in the earthquake approach is an evaluation of the frequency of occurrence of earthquakes of various magnitudes on each of the seismic sources. The characterization of earthquake recurrence developed by the AAR team for the ground motion hazard assessment was used directly to define the distributions for earthquake occurrence frequency.

Given the occurrence frequency of earthquakes, the next assessment is the approach for evaluating the probability that slip will occur in a given event. For principal faulting, the AAR team assessed P_i(slip|event on i) using the focal depth randomization for each fault developed for the ground motion hazard assessment. Two alternative empirical models for the size of earthquake ruptures as a function of magnitude were used to develop the rupture depth distribution and the distribution for along-strike location of rupture: one that defines rupture length as a function of earthquake magnitude and one that defines rupture area as a function of earthquake magnitude. An empirical distribution for aspect ratio was used to evaluate rupture width given rupture length or rupture area. For distributed faulting, the AAR team assessed P_i(slip|event on j) using the logistic regression model based on the

mapped density of distributed ruptures. The data and resulting model are shown in Figure H-13c. When evaluating the potential distributed faulting events induced by earthquakes occurring within the regional source zones, it is assumed that the point of interest is equally likely to be located in the hanging wall or footwall of the rupture.

The conditional probability of exceeding a specified displacement, $P(D>d)$, was evaluated using the two-part method defined by Equation (4-19). For principal faulting the AAR team considered three alternative empirical relationships for estimating the maximum displacement *MD*: (1) a published empirical model based on earthquake magnitude, (2) a published empirical model based on rupture length, and (3) an empirical model based on fault rupture length developed by the AAR team from Yucca Mountain data. The location of the point of interest was assessed for each rupture to define the parameter *x/L*, and the distribution for *D/MD* was based on the analysis of historical ruptures shown on Figure 4-13. For distributed faulting, an empirical distribution for the ratio of maximum distributed displacement to maximum principal displacement was defined based on published data. This ratio, ranging from 0.2 to 0.7, was used to scale the estimated *MD* for the earthquake source to that for distributed rupture on the fault of interest. The distribution for *D/MD* shown on Figure H-6 was then used to compute the conditional probability of exceedance assuming *x/L* = 0.5 for the distributed rupture.

Displacement Approach. The displacement approach does not distinguish between principal and distributed ruptures. The first assessment in the logic tree (Figure 4-78) is an evaluation of the probability the feature can slip, $P(C)$. This assessment is the same as the assessment of $P(C)$ in the earthquake approach.

The AAR team uses estimates of fault slip rate and average displacement per event to obtain the frequency of displacement events [Equation (4-13)]. The slip-rate estimates are given by the seismic source characterization model developed by the AAR team. The assessment of the average displacement per event, $\bar{D}_E$, is based on the AAR team's evaluation of the displacement data from trenching studies at Yucca Mountain. For each trenching site, they made an estimate of the expected maximum displacement in the maximum event, which they denote by MD^{max}. They then normalized the displacement data from the trench by this value and pooled the data from all trenches. The mean of the pooled data for D/MD^{max} is 0.83. The

AAR team assesses the average displacement per event by estimating MD^{max} for the fault and then uses the expression $\bar{D}_E = 0.83\ MD^{max}$. In applying this approach, they consider three alternative approaches for estimating MD^{max}. The first is based on maximum rupture length and two alternative empirical relationships between rupture length and maximum slip: a published empirical model and an analysis of Yucca Mountain data performed by the AAR team. The second approach uses a scaling relationship between cumulative bedrock offset and average displacement per event developed by the AAR team. The third approach utilized the team's assessments of maximum displacements estimated from paleoseismic data as part of their seismic source characterization of the faults for the ground motion hazard assessment.

The final part of the displacement approach is the model for the conditional probability of exceedance. The AAR team found that the distribution of D/MD^{max} could be modeled by an exponential distribution (see Figure H-5), and utilized this distribution to assess $P(D>d)$.

Characterization for Sites of Only Potential Distributed Faulting Hazard. Figure 4-79 presents the AAR team's logic tree for characterization of sites subject to only distributed faulting hazard. The AAR team considers both the earthquake and displacement approaches and the hazard characterization model is similar to that for sites of principal faulting hazard (Figure 4-78). The differences between the approaches for hazard characterization at the two types of sites primarily reflect the types of data available.

Earthquake Approach. In the earthquake approach, the first assessment is an evaluation of whether or not the feature can experience distributed faulting, $P(C)$, which is assessed based on the orientation of the feature in the present stress regime. The next assessment in the earthquake approach is an evaluation of the frequency of occurrence of earthquakes of various magnitudes on each of the seismic sources. As was the case for sites subject to principal faulting hazard, the characterization of earthquake recurrence developed by the AAR team for the ground motion hazard assessment was used to define the distributions for earthquake occurrence frequency. Given the occurrence frequency of earthquakes, the probability that slip will occur in a given event, P_j(slip|event on j), was assessed using the logistic regression model shown on Figure H-13c.

The conditional probability of exceeding a specified displacement, $P(D>d)$, was evaluated using an assessment of the expected maximum slip in the maximum event, MD^{max}, and the exponential distribution for D/MD^{max} discussed above. Two alternative approaches for estimating MD^{max} were considered, one based on the length of the feature and one based on the cumulative offset. If only one of these types of data were known for a feature, the assessment of MD^{max} was based on a single approach.

Displacement Approach. The displacement approach for sites of only distributed faulting hazard parallels that discussed above for principal faulting hazard. The first assessment in the logic tree (Figure 4-79) is an evaluation of the probability the feature can slip, $P(C)$, which is the same as the assessment of $P(C)$ in the earthquake approach.

The frequency of displacement events again is obtained using Equation (4-13). Three alternative approaches are used to estimate slip rate on the feature: (1) one based on assuming uniform slip for the past 11.6 Ma, (2) one assuming uniform slip for the past 3.7 Ma, and (3) one based on a empirical regression model developed by the AAR team relating Quaternary slip rate to cumulative bedrock offset. For the uniform slip approaches, the AAR team assessed the fraction of the cumulative offset that occurred prior to the period of uniform slip and used only the remaining portion of the cumulative slip to compute the slip rate. For example, one assessment is that 84% of the cumulative slip occurred prior to 3.7 Ma. The fault slip rate then is obtained by the expression: $SR = 0.16 \times D_{cum}/3.7$ Ma. The assessment of the average displacement per event, $\bar{D}_E$, likewise is based on the expression $\bar{D}_E = 0.83\ MD^{max}$, with MD^{max} estimated using either fault length or cumulative displacement in the same way as is done for the earthquake approach. The exponential distribution for D/MD^{max} is used to assess $P(D>d)$. Uncertainty in the cumulative displacement was included in the assessment.

Summary of Application of Model to Nine Demonstration Points. The AAR team interprets Points 1, 2, 4, and 6 to lie on faults that are potentially seismogenic and utilizes the logic tree shown on Figure 4-78 to characterize the hazard at these sites. Point 6 is interpreted to lie on a seismic source that they designated as west Dune Wash fault 1 (WD1 on Figure 4-18). The remaining points are interpreted to be subject to distributed faulting

hazard only and the logic tree shown on Figure 4-79 is used to characterize hazard at these sites. Considering the hypothetical features at points 7 and 8, they utilize the assumed cumulative displacements of 2 m and 10 cm to Characterize the hazard for conditions (a) and (b), respectively; provide a distribution for the length of a fracture to characterize the hazard at point (c); and make the assessment that the potential fault displacement hazard for a point in intact rock is essentially zero.

Ake, Slemmons, McCalpin Team. The ASM team utilizes the earthquake approach to assess the hazard at all locations within the Controlled Area. Their hazard characterization is developed in terms of principal faulting hazard and distributed faulting hazard.

Principal Faulting Hazard Model. Figure 4-80 presents the logic tree that defines the ASM team's characterization of principal faulting hazard. The first assessment is whether the fault can experience principal faulting. This assessment is equal to the probability that the fault is seismogenic, as defined by the ASM team's seismic source characterization for the ground motion hazard assessment.

Conditional on the fault being seismogenic, the frequency of occurrence of earthquakes of various magnitudes on each of the seismic sources is assessed using the characterization of earthquake recurrence developed by the ASM team for the ground motion hazard assessment. Given the occurrence frequency of earthquakes, the next assessment is the probability that surface displacement will occur in a given event. The ASM team assessed P_f(slip|event on i) [Equation (4-16)] using the empirical logistic regression model for the probability of surface rupture, Equation (4-15). Two alternative empirical relationships were considered for the probability of surface rupture: one based on post-1930 Great Basin earthquakes and one based on earthquakes from the extensional Cordillera (see Figure 4-11).

The conditional probability of exceeding a specified displacement, $P(D>d)$, was evaluated using the two-part method defined by Equation (4-19). The distribution for the maximum displacement in an earthquake, MD, was defined using a published empirical model based on earthquake magnitude. The location of the point of interest within the rupture was assessed for each rupture to define the parameter x/L, and the distribution for D/MD was based on the analysis of historical ruptures shown on Figure 4-13.

Distributed Faulting Hazard Model. Figure 4-81 presents the logic tree that defines the ASM team's characterization of distributed faulting hazard. The first assessment is whether the fault can experience slip. This is composed of two assessments. The ASM team categorized the features in the site vicinity into six classes based on their cumulative slip (see Table ASM-9 in Appendix E). For each class of features, an assessment was made of the probability that the feature could undergo slip. The probability the feature can slip was further modified by a factor equal to the cosine of the strike azimuth of the feature, thus reducing the probability that the feature can slip with increasing deviation of its orientation from north-south. The resulting relationship is $P(C) = P(\text{slip}|\text{class})\times\cos(\phi)$, where ϕ is the strike azimuth of the feature of interest.

The frequency of earthquakes on each of the seismic sources that could cause distributed rupture on the feature of interest was assessed using the seismic source characterization developed by the ASM team for the ground motion hazard characterization. The probability that a specific earthquake on source *j* induces slip on feature *i* was assessed using a two-part approach:

$$P_i(\text{slip}|\text{earthquake on } j) = P(\text{surface rupture on } j) \times P_i(\text{distributed slip}|r,h) \qquad (4\text{-}20)$$

The first term to the right of the equal sign is the probability that a earthquake on source *i* will produce surface rupture. This probability is given by the logistic regression model used in the principal faulting hazard characterization, Equation (4-15). The second term is the probability that a surface-rupturing earthquake on source *j* produces distributed slip on the feature of interest at point *i*. This probability is assessed using a form of the logistic regression model defined by Equation (4-17). The ASM team developed two alternative relationships that define the likelihood of the occurrence of distributed slip at a point as functions of distance from the principal rupture and location in the hanging wall (h=1) or footwall (h=0) of the rupture (Figure 4-82). While these relationships are independent of earthquake magnitude, the combined assessment defined by Equation (4-20) depends on the magnitude of the earthquake on source *i* through the probability of principal surface rupture.

The probability defined by Equation (4-20) represents aleatory probability in that it defines the likelihood of distributed slip in an individual earthquake. Epistemic uncertainty in the assessment is represented by the two alternative relationships for the probability of surface rupture and the two alternative relationships for the probability of distributed slip.

The ASM team assesses the distributed faulting displacement as a reduction factor, *RF*, times the principal faulting displacement that occurs on the seismic source at its closest approach to the point of interest. Two approaches are used to define the reduction factor, one based on a displacement potential defined on the basis of an observed ground displacement profile and one based on the relative cumulative slip between the principal fault and the feature of interest.

The displacement potential approach assumes the amount of displacement that can occur decreases with distance from the principal rupture in the same manner as the ground surface displacement decays. The ASM team utilizes the fault-normal geodetic displacement profile for the 1983 Borah Peak earthquake normalized by the displacement at the fault (Figure 4-83) as the basis for defining the net ground surface movement resulting from an earthquake. The normalized displacement profile was fit with the following algebraic expression to provide a relationship for the reduction factor, RF:

$$RF = \varepsilon \times \exp(-0.045 r_n^{1.5}) \text{ for hanging wall}$$
$$RF = \varepsilon \times 0.21 \exp(-0.14 r_n) \text{ for footwall} \qquad (4\text{-}21)$$

where ε is a factor that defines what portion of the displacement potential is realized in an event. The distance term r_n is the distance from the principal rupture normalized to the conditions for the Borah Peak earthquake. The normalizing factor is the crustal depth of the rupture compared to that for the Borah Peak earthquake, such that a decrease in the crustal depth of the rupture decreases the distance extent of the displacement potential. The resulting relationship is $r_n = r \times 16\text{km}/[w \times \sin(\text{dip})]$, where w is the rupture width of the earthquake.

Parameter ε defines how the displacement potential is distributed among the available structures that could slip in the vicinity of the site of interest. Four alternatives are proposed

that are considered to be event-to-event variability in how the displacement potential is distributed. The possibilities include full realization ($\varepsilon = 1.0$), distribution equally among the possible classes of features ($\varepsilon = 0.2$), distribution equally among the estimated number of features of a specific class available ($\varepsilon = 1/N$), or distribution equally among the possible classes of features and the estimated number of features of a specific class ($\varepsilon = 0.2/N$). The expected number of features present, N, is evaluated assuming a power law for feature density, with the relative number of features in two classes proportional to the ratio of their cumulative slip raised to a power of -0.7. The resulting values of N are listed in Table ASM-9 in Appendix E.

The second approach for assessing *RF* involves identification of the portion of the cumulative displacement on the feature of interest at point *i* that resulted from earthquakes occurring on source *j* and using the ratio of this cumulative displacement to the cumulative displacement on earthquake source *j* to estimate the relative amplitude of displacements in individual events. The term within the summation in Equation (4-14), $\lambda_j \times P_i(\text{slip}|\text{event on } j)$, defines the frequency of earthquakes on source *j* producing distributed slip on the feature at point *i*. If all events produce comparable amounts of displacement, then the portion of the cumulative displacement at *i* that is contributed by source *j* is given by $\lambda_j \times P_i(\text{slip}|\text{event on } j) / \sum \lambda_j \times P_i(\text{slip}|\text{event on } j)$. However, the displacements induced by various magnitude earthquakes on the various earthquake sources are not equal. To address this, the ASM team makes the assumption that the relative contribution of each source to the cumulative displacement at point *i* can be estimated from the results of the displacement potential approach. Using Equation (4-12), the displacement hazard curve from each source *j* is used to obtain an effective slip rate from source *j*, ESR_j. The ratio of this effective slip rate to the effective slip rate obtained from the total displacement hazard curve from all sources provides a estimate of the contribution of source *j* to the cumulative slip at point *i*. Thus, the interpretation developed by the ASM team is that the reduction factor to scale, on average, the principal rupture displacement occurring on source *j* to the distributed rupture displacement at point *i* is given by the expression:

$$RF = \frac{ESR_j}{\sum ESR_j} \times \frac{(D_{cum})_i}{(D_{cum})_j \times P_i(\text{slip}|\text{event on } j)} \qquad (4\text{-}22)$$

In Equation (4-22), the cumulative slip on source j is multiplied by P_i(slip|event on j) to account for the fact that not every principal faulting earthquake on source j that contributed to its cumulative slip also produced distributed slip at point i.

Summary of Application of Model to Nine Demonstration Points. The ASM team interprets Points 1 and 2 to lie on faults that are potentially seismogenic and utilizes the logic tree shown on Figure 4-80 to characterize the hazard at these sites. The remaining points are interpreted to be subject to distributed faulting hazard only and the logic tree shown on Figure 4-81 is used to characterize hazard at these sites. Considering the hypothetical features at Points 7 and 8, they utilize the assumed cumulative displacements of 2 m and 10 cm to characterize the hazard for conditions (a) and (b), respectively; provide an assumed maximum cumulative displacement of 1 cm for a fracture with no measurable offset to characterize the hazard at condition (c); and make the assessment that the potential fault displacement hazard for a point in intact rock is essentially zero.

<u>Doser, Fridrich, Swan Team.</u> The DFS team uses the displacement approach for assessing the hazard at all locations.

Principal and Distributed Faulting Hazard Model. Figure 4-84 shows the logic tree used by the DFS team to characterize fault displacement hazard. The first assessment addresses the probability that the feature of interest can slip in a displacement event, $P(C)$. Features that display evidence of Quaternary movement (typically the block-bounding faults) are assigned a probability of 1.0. North-south-striking intrablock faults are assigned a probability of activity of 0.4 and northwest-southeast-trending faults are assigned a probability of activity of 0.01. Minor faults and shears are assigned a probability of activity of 0.05 to 0.01, depending on proximity to block-bounding faults.

The next two assessments are the approaches for estimating the frequency of slip events and the average displacement per event. The DFS team uses the relationship given in Equation (4-13) in two ways. In one approach, a direct estimate of the frequency of slip events is used together with the slip rate on the feature to calculate the average displacement per event. In

the second approach, a direct estimate of the average slip per event together with the slip rate is used to evaluate the frequency of slip events.

Both approaches for estimating slip event frequency and average slip per event require an estimate of the slip rate on the feature. The DFS team considers four alternative approaches for estimating the Quaternary slip rate. The favored approach is the use of paleoseismic data from trenching studies on the feature. The other three approaches estimate the Quaternary slip rate utilizing the cumulative offset of the top of the Tiva Canyon tuff and alternative assumptions for the history of deformation. The first interpretation is that the slip rate has been uniform post-Tiva Canyon and the fault slip rate is $SR=D_{cum(\text{Tiva Canyon})}/12.7\pm1.3$ Ma. The second interpretation is that 80 percent of the post-Tiva Canyon slip occurred prior to deposition of the 11.6±1 Ma Rainier Mesa member of the Timber Mountain tuff and the slip rate has been uniform post-Rainier Mesa, resulting in $SR=0.2D_{cum(\text{Tiva Canyon})}/11.6\pm1$ Ma. The third interpretation is that slip rates have been decreasing through time such that the Quaternary slip rate is in the range of 0.3 to 3.9 percent of the late Miocene slip rate. The late Miocene slip is defined to be the deformation that occurred post-Tiva Canyon and pre-Rainier Mesa and is interpreted to be 80 percent of the post-Tiva Canyon cumulative slip. The resulting relationship for Quaternary slip rate is $SR=RF\times0.8D_{cum(\text{Tiva Canyon})}/1.1\pm0.6$ Ma, where RF is the reduction factor from late Miocene to Quaternary slip rates and ranges from 0.3 to 3.9 percent. If no paleoseismic data are available for a feature, then the DFS team utilizes the three estimates based on the alternative slip history interpretations, giving each equal weight. Uncertainty in the cumulative displacement and age of the units was included in the assessment.

For fractures and unbroken rock, the frequency of displacement events and the average displacement per event are assessed directly. The frequency of events is assessed to lie within a broad range of uncertainty defined from alternative assumptions for the deformation history of Yucca Mountain. The average displacement per event for fractures with no offset and unbroken rock was assessed on the basis of the level of detection for deformation. The assessments for these features are considered to be upperbound values by the DFS team.

The final part of the displacement hazard model is the evaluation of the conditional probability of exceedance. The DFS team developed a triangular probability distribution for

D/AD from the trenching data in the Yucca Mountain region (see Appendix E) As described in Section H.2.1, a gamma distribution provides a better fit to the data and the DFS team actually adopted this distribution for hazard computation. The selected distribution is shown on the left-hand side of Figure 4-14. The probability of exceeding a specified value of d is computed using this distribution together with the estimate of the average displacement per event given for the feature ($\overline{D}_E = AD$).

Summary of Application of Model to Nine Demonstration Points. The DFS team interprets Points 1, 2, 4, and 9 to lie on features that have paleoseismic data for slip rate. Slip rates for the remaining points are evaluated solely from the cumulative slip and alternative interpretations of the deformation history. Considering the hypothetical features at Points 7 and 8, they utilize the assumed cumulative displacements of 2 m and 10 cm to characterize the hazard for conditions (a) and (b), respectively, and estimate the average displacement per event and displacement event frequency for fractures and intact rock, conditions (c) and (d).

Rogers, Yount, Anderson Team. The RYA team uses the displacement approach to characterize the hazard at all locations. Their displacement hazard characterization differs depending on whether or not Quaternary paleoseismic data are available for the location of interest.

Displacement Hazard Characterization for Sites with Quaternary Data. Figure 4-85 shows the logic tree used by the RYA team to characterize the displacement data at locations for which Quaternary paleoseismic data are available. The first assessment is the likelihood that the feature of interest can slip in a displacement event, $P(C)$. This probability is assessed based on evidence for recency of slip and the relationship of the feature to the structural elements of Yucca Mountain. Block-bounding faults with evidence of Quaternary movement are assigned $P(C)=1.0$.

The next assessment is the approach used to assess the frequency of displacement events. The RYA team considers two alternatives: the use of direct estimates of the frequency of displacement events from paleoseismic data, and the use of slip rate and Equation (4-13). The distributions for the average displacement per event, the Quaternary slip rate, and direct estimates of the frequency of displacement events are all based on paleoseismic data.

The final assessment is the approach for estimating the conditional probability of exceedance. Two alternatives are considered. The first is the use of the empirical distribution for *D/AD* developed by the DFS team from Yucca Mountain data. These data were fit with a gamma distribution (see Section H.2.1). The second approach is the distribution for D/MD^{-} developed by the AAR team from Yucca Mountain data. These data were fit by an exponential distribution (see Section H.2.5). The appropriate value of MD^{-} was assessed from paleoseismic data for the feature.

Displacement Hazard Characterization for Sites Without Quaternary Data. Figure 4-86 shows the logic tree used by the RYA team to characterize the displacement data at locations for which no Quaternary paleoseismic data are available. The overall approach parallels are shown on Figure 4-85, except that scaling relationships based on fault length and cumulative displacement are used in place of Quaternary data. The first assessment is the likelihood that the feature of interest can slip in a displacement event, $P(C)$. Intrablock faults with north-south trends are assigned $P(C)$=0.4, and those with northwest-southeast trends are assigned $P(C)$=0.1. Small faults and shears are assigned $P(C)$=0.5 to 0.3.

The frequency of displacement events is assessed using only slip rate and Equation (4-13). The slip rate is assessed based on the cumulative offset of a feature, which is considered to be an uncertain parameter. Three alternative interpretations of the slip history of the faults are considered. The first is that the slip rate has been uniform post deposition of the Tiva Canyon Tuff and the slip rate is given by $SR=D_{cum(\text{Tiva Canyon})}/12.7$ Ma. The second interpretation is that 20 percent of the cumulative deformation on the Yucca Mountain faults occurred after the onset of volcanism in Crater Flat about 3.7 Ma, yielding an estimate of $SR=0.2D_{cum(\text{Tiva Canyon})}/3.7$ Ma. The favored interpretation is that 98 percent of the deformation occurred prior to the Quaternary. The resulting slip-rate estimate is $SR=0.02D_{cum(\text{Tiva Canyon})}/1.6$ Ma. Uncertainty in the cumulative displacement was included in the assessment.

The next assessment is the average displacement per event. The RYA team considers two alternative scaling relationships developed by the AAR team to be appropriate, one based on the length of the feature and one based on the cumulative offset of the feature. These

relationships provide estimates of MD^{max}. The data for D/MD^{max} have a mean value of 0.83 and the RYA team interpreted $\bar{D}_E$ to be equal to 0.83 MD^{max}. If length information is not available for a feature (such as is the case for the hypothetical features at Points 7 and 8), then the assessments are made using only the cumulative offset of the feature.

The final assessment is the approach for estimating the conditional probability of exceedance. The same two alternatives are considered for these sites as were used for sites with Quaternary data (Figure 4-85).

Summary of Application of Model to Nine Demonstration Points. The RYA team interprets Points 1 and 2 to lie on features that have paleoseismic data. Slip rates for the remaining points are evaluated solely from the cumulative slip and alternative interpretations of the deformation history. Considering the hypothetical features at Points 7 and 8, they utilize the assumed cumulative displacements of 2 m and 10 cm to characterize the hazard for conditions (a) and (b), respectively, and interpret the probability of fault slip on a fracture with no measurable offset (c) or in intact rock (d) to be essentially zero.

Smith, Bruhn, Knuepfer Team. The SBK team's characterization of fault displacement hazard differentiates between those sites that are subject to potential principal faulting hazard and those sites that are subject to only distributed faulting hazard.

Characterization for Sites of Potential Principal Faulting Hazard. Figure 4-87 presents the SBK team's logic tree for characterization of sites subject to principal faulting hazard. The SBK team considers both the earthquake and displacement approaches.

Earthquake Approach. In the earthquake approach, two contributions to hazard are included (indicated by the vertical line on the logic tree under sources of hazard): hazard from principal faulting due to the occurrence of earthquakes on the fault and distributed faulting hazard from earthquakes occurring on other seismic sources. The first assessment in the earthquake approach is an evaluation of whether or not the feature can experience principal faulting, $P(C)$. This is interpreted to be equal to the probability that the fault is seismogenic, $P(S)$, which was assessed as part of the SBK team's seismic source characterization (see Section 4.3.1.1). The SBK team's assessment is that all faults can experience distributed slip.

The next assessment in the earthquake approach is an evaluation of the frequency of occurrence of earthquakes of various magnitudes on each of the seismic sources. The characterization of earthquake recurrence developed by the SBK team for the ground motion hazard assessment was used directly to define the distributions for earthquake occurrence frequency.

Given the occurrence frequency of earthquakes, the next assessment is the approach for assessing the probability that slip will occur in a given event. For principal faulting, the SBK team assessed P_i(slip|event on i) using the logistic regression model, Equation (4-15), to assess the probability that surface rupture occurs, selecting the parameters of the model developed from the data base of 32 post-1930 Great Basin earthquakes (Figure 4-11). The probability of intersection with the site was computed by randomization of the rupture length along the fault.

For distributed faulting, the SBK team developed a two-part approach for assessing P_i(slip|event on j):

$$P_i(\text{Slip} \mid \text{event on } j) = P(\theta) \times F(event) \qquad (4\text{-}23)$$

where $P(\theta)$ is a function of the orientation of the feature of interest at point i and $F(event)$ is a function of the earthquake occurring on source j. Two alternatives were used to evaluate the probability $P(\theta)$. The first utilizes an assessment of the slip tendency of the feature with respect to the present stress regime. The slip tendency analysis indicates that features with a north-south orientation are favorably oriented for slip in the present stress regime. Thus, the SBK team considered $P(\theta)$ for these features to be at or near 1.0, if there was evidence of Quaternary displacement. Alternative values of $P(\theta)$ were assessed to account for uncertainty in the interpretation. For features oriented in a northwest-southeast direction, the assessed values for $P(\theta)$ were about 0.5. The second approach for assessing $P(\theta)$ utilized the analysis of the distribution for the angle between the strike azimuths of the principal fault rupture and the associated distributed ruptures presented in Section H.4.3. An evaluation of the focal mechanisms for earthquakes in the immediate Yucca Mountain vicinity (see Chapter 7,

USGS, 1996) indicates that the distribution of nodal plane strike azimuths is approximately uniform and an average value of $P(\theta)$ was computed assuming random strike to apply to earthquakes occurring in the areal source zones.

The second term of Equation (4-23) expresses the probability of slip as a function of the earthquake on the seismic source. The SBK used two alternative approaches for assessing this probability. The first approach is the logistic regression model developed from the analysis of the density of distributed faulting in historical ruptures defined by Equation (4-17) and shown on Figure 4-12. The second approach defines the probability of slip as a function of the peak velocity (*PV* in cm/sec) induced by the earthquake at the site. The relationship developed by the SBK team (see Figure SBK-19 in Appendix E) was fit with the logistic regression model:

$$F(event) = \frac{e^{-7.0+0.14PV}}{1+e^{-7.0+0.14PV}} \qquad (4\text{-}24)$$

The peak velocity induced by the earthquake is estimated using the ground motion models developed for the Yucca Mountain site. The SBK team considers this approach to be valid for underground openings.

The final assessment is the approach for evaluating the conditional probability of exceeding a specified displacement, $P(D>d)$. For principal faulting, this probability was evaluated using the two-part method defined by Equation (4-19). The distribution for *MD* was defined by a published empirical model based on earthquake magnitude. The location of the point of interest was assessed for each rupture to define the parameter *x/L*. Two alternatives are considered for the distribution for *D/MD*. The first is the analysis of data from historical ruptures shown on Figure 4-13. The second is a model developed from numerical simulations of fault displacements (see Section H.3.2). For distributed faulting, an empirical distribution for D/D_{cum} (see Section H.2.6) is used to evaluate the probability of exceeding a specified displacement.

Displacement Approach. The displacement approach does not distinguish between principal and distributed ruptures (Figure 4-87). The first assessment in the logic tree is an evaluation

of the probability the feature can slip, $P(C)$. This assessment is the same as the assessment of $P(C)$ for distributed faulting in the earthquake approach.

The SBK team uses two approaches for estimating the frequency of displacement events. The first method uses a direct estimate of the frequency from paleoseismic data. The second approach uses estimates of fault slip rate and average displacement per event to obtain the frequency of displacement events [Equation (4-13)]. The recurrence rate (inverse of recurrence interval) and slip-rate estimates are given by the seismic source characterization model developed by the SBK team.

The SBK team uses three alternative methods to assess the average displacement per event, $\bar{D}_E$, and the conditional probability of exceedance, $P(D>d)$ that are based on evaluations of the data from Yucca Mountain trenching studies. The first method utilizes the average displacement estimated for paleoearthquakes, designated as AD_{paleo}, to specify $\bar{D}_E$ and uses a distribution for D/AD_{paleo} to compute $P(D>d)$. This distribution is discussed in Appendix H, Section H.2.2. For the second approach, the SBK team used an empirical model between rupture length and average displacement, designated $AD_{F(RL)}$ to develop a distribution for $D/AD_{F(RL)}$ (see Section H.2.3). The mean of this distribution is 1.46 and $\bar{D}_E$ is set equal to $1.46 \times AD_{F(RL)}$. The distribution for $D/AD_{F(RL)}$ is used to compute $P(D>d)$. For the third approach, the SBK team used an empirical model between rupture length and maximum displacement, designated $MD_{F(RL)}$ to develop a distribution for $D/MD_{F(RL)}$ (see Section H.2.4). The mean of this distribution is 0.72 and $\bar{D}_E$ is set equal to $0.72 \times MD_{F(RL)}$. The distribution for $D/MD_{F(RL)}$ is used to compute $P(D>d)$.

Characterization for Sites of Only Potential Distributed Faulting Hazard. Figure 4-88 presents the SBK team's logic tree for characterization of sites subject to only distributed faulting hazard. The SBK team considers both the earthquake and displacement approaches, and the hazard characterization model is similar to that for sites of principal faulting hazard (Figure 4-87). The differences between the approaches for hazard characterization at the two types of sites primarily reflect the different types of data available.

Earthquake Approach. The earthquake approach for sites subject to distributed faulting hazard is identical to that shown on Figure 4-87.

Displacement Approach. The displacement approach for sites of only distributed faulting hazard parallels that discussed above for principal faulting hazard, except that slip rates and average displacements estimated from paleoseismic data are not available and are replaced by scaling relationships utilizing cumulative displacement.

The frequency of displacement events is again obtained using Equation (4-13). Two alternative approaches are used to estimate slip rate on the feature. The first approach is based on the cumulative slip and three alternative interpretations of the history of slip. The first interpretation is uniform slip post-Tiva Canyon. The second interpretation is uniform slip post-Rainier Mesa 11.6 Ma tuff deposition, in which 20 percent of the post-Tiva Canyon deformation has occurred. The third interpretation is that the Quaternary slip rates are 2.1±1.8 percent of the late Miocene slip rates, with the late Miocene rates computed by dividing 80 percent of the post-Tiva Canyon displacement by 0.9 Ma. The second approach for estimating slip rate used by the SBK team involves using the ratio of cumulative slip between the feature of interest and the cumulative slip on those faults with Quaternary slip rate estimates to scale the measured Quaternary slip rates to an estimate for the feature of interest. Uncertainty in the cumulative displacement was included in the assessment.

The SBK team again uses three alternative methods to assess the average displacement per event, $\overline{D}_E$, and the conditional probability of exceedance, $P(D>d)$ that are based on evaluations of the data from Yucca Mountain trenching studies. Two of these are the estimates based on $AD_{F(RL)}$ and $MD_{F(RL)}$ discussed above. For the third approach, the SBK team developed a distribution from the Yucca Mountain data for D/D_{cum} (see Section H.2.6). The mean of this distribution is 0.00176 and $\overline{D}_E$ is set equal to $0.00176 \times D_{cum}$. The distribution for D/D_{cum} is used to compute $P(D>d)$. If the length of the feature is not known, the SBK team uses only the estimate based on cumulative displacement.

Summary of Application of Model to Nine Demonstration Points. The SBK team interprets Points 1 and 2 to lie on faults that are subject to both principal and distributed

faulting hazard and utilizes the logic tree shown on Figure 4-87 to characterize the hazard at these sites. The remaining points are interpreted to be subject to distributed faulting hazard only and the logic tree shown on Figure 4-88 is used to characterize hazard at these sites. Considering the hypothetical features at Points 7 and 8, they utilize the assumed cumulative displacements of 2 m and 10 cm to characterize the hazard for conditions (a) and (b), respectively; provide a distribution for the relative hazard between a fracture, condition (c), and a minor shear, condition (b); and make an estimate of the frequency and amplitude for displacement in intact rock, condition (d).

Smith, de Polo, O'Leary Team. The SDO team's characterization of fault displacement hazard differentiates between those sites that are subject to potential principal faulting hazard and those sites that are subject to only distributed faulting hazard.

Principal Faulting Hazard Model. The SDO team uses the earthquake approach for characterizing the hazard due to principal faulting. Figure 4-89 shows the logic tree that defines their characterization. The frequency of occurrence of earthquakes of various magnitudes on each seismic source are defined by the seismic source characterization model (Section 4.3.1.1). The probability of slip at or near the surface given the occurrence of a magnitude m earthquake is computed using the logistic regression model defined by Equation (4-15). The SDO team uses two alternative data sets to develop the parameters for Equation (4-15): one based on 32 post-1930 Great Basin earthquakes and one based on 47 post-1930 northern Basin and Range earthquakes (Figure 4-11). The probability of intersection of the point of interest is computed by randomizing the location of the rupture length for an earthquake of magnitude m along the fault trace.

The conditional probability of exceeding a specified displacement, $P(D>d)$ for principal faulting was evaluated using two alternative approaches: one based on average displacement, AD, and one based on maximum displacement, MD. The assessment of AD and MD depended upon the size of the earthquake. For earthquakes of magnitude smaller than the characteristic magnitude (defined as $m \leq m^U$-½), the values of AD and MD are assessed using an empirical relationship between displacement per event and earthquake magnitude. For the characteristic magnitude earthquakes (m^U-½ $\leq m \leq m^U$) assessments of AD and MD also are made using the maximum rupture length of the fault and paleoseismic data. Two scaling

relationships are used between *AD* and rupture length: a published empirical model and a scaling model developed by the AAR team. In addition, the SDO team utilized the displacement profile for the Solitario Canyon fault presented by Alan Ramelli in Workshop #6 to characterize the average displacement at Point 2. Given an assessment of *AD*, the distribution for *D/AD* developed by the DFS team (Section H.2.1) was used to compute $P(D>d)$. Given an assessment of *MD*, the two-part method defined by Equation (4-19) was used to compute $P(D>d)$. The distribution for *MD* was defined as lognormal using the standard deviation associated with the empirical model. Two alternatives are considered for the distribution for *D/MD*. The first is the analysis of historical ruptures shown on Figure 4-13. The second is a model developed from numerical simulations of fault displacements (see Section H.3.2).

The SDO team also considered the potential for distributed faulting hazard at sites subject to principal faulting hazard. Their earthquake approach for characterizing distributed faulting hazard, discussed below, was used for these sites.

Distributed Faulting Hazard Model. Figure 4-90 presents the SDO team's logic tree for characterization of distributed faulting hazard. The SDO team considers both the earthquake and displacement approaches for sites subject to only distributed faulting hazard and only the earthquake approach for sites subject to both principal and distributed faulting hazard.

Earthquake Approach. The first assessment is the probability that the feature can slip in the present stress regime, $P(C)$. The SDO team's interpretation is that features oriented in a north-south direction (or are interpreted to be seismogenic) are assigned $P(C) = 1.0$. Features oriented in a northwest-southeast direction are assigned $P(C) = 0.8$.

The frequency of earthquakes occurring on each of the seismic sources is defined as part of the SDO team's seismic source characterization for the ground motion hazard assessment. The probability that slip occurs in an individual earthquake was assessed using the two-part approach defined by Equation (4-23) discussed above for the SBK team. The probability $P(\theta)$, was assessed using the analysis of the distribution of angles between the strikes of principal and distributed ruptures presented in Section H.4.3. An evaluation of the focal mechanisms for earthquakes in the immediate Yucca Mountain vicinity (see Chapter 7 of

USGS, 1996) indicates that the distribution of nodal plane strike azimuths is approximately uniform and an average value of $P(\theta)$ was computed assuming random strike to apply to earthquakes occurring in the areal source zones. The probability $F(event)$ was assessed using the logistic regression model developed from the analysis of the density of distributed faulting in historical ruptures defined by Equation (4-17) and shown on Figure H-13c.

The conditional probability of exceedance, $P(D>d)$, was assessed using two approaches. The first approach defined a reduction factor, RF, equal to the ratio of the cumulative displacements on the feature of interest to the cumulative displacement on the earthquake source. The procedures described above for principal faulting were used to assess the distribution for displacement on the earthquake source at its closest approach to the point of interest. The distribution for displacement at the point of interest then is set equal to RF times the distribution on the earthquake source. The second approach utilized empirical observations of the displacement on distributed ruptures normalized to the maximum displacement on the principal rupture. A curve was defined that approximately enveloped these data (see Figure 4-91). This curve is considered to represent the 95th percentile of the distribution of possible displacements on a distributed rupture. For earthquakes occurring in the areal source zones, the conditional probability of exceedance was computed using only the second approach and the assumption that the point of interest was equally likely to lie in the hanging wall or footwall of the rupture.

Displacement Approach. The first assessment in the displacement approach for characterization of distributed faulting hazard is an assessment of whether or not slip can occur, $P(C)$. This assessment is the same as that for the earthquake approach.
The frequency of displacement events is obtained using Equation (4-13). The slip rate on the feature is estimated from the interpretation that from 0.2 to 2.0 percent of the cumulative post-Tiva Canyon slip has occurred in the Quaternary. The average displacement per event, $\overline{D}_e$, is estimated from the cumulative displacement using two approaches. The first is the scaling relationship developed by the AAR team in which $D_E=0.83\times1.32\times\beta\times D_{cum}$, where β varies from 1.40×10^{-3} to 1.85×10^{-2}. The second approach is the empirical distribution for D/D_{cum} (see Section H.2.6). The mean of this distribution is 0.00176 and $\overline{D}_e$ is set equal to $0.00176\times D_{cum}$.

The conditional probability of exceedance, $P(D>d)$, is assessed using two approaches that correlate with those used to assess D_E. If the scaling relationship developed by the AAR team is used, then $P(D>d)$ is assessed using the distribution for D/MD^{max} (see Section H.2.5) with $MD^{max} = D_E/0.83$. If the mean of the empirical distribution for D/D_{cum} presented in Section H.2.6 is used, then the same distribution is used to assess $P(D>d)$.

Summary of Application of Model to Nine Demonstration Points. The SDO team interprets Points 1 and 2 to lie on faults that are subject to both principal and distributed faulting hazard and utilizes the logic tree shown on Figure 4-89 plus the earthquake approach on the logic tree shown on Figure 4-90 to characterize the hazard at these sites. The remaining points are interpreted to be subject to distributed faulting hazard only and the logic tree shown on Figure 4-90 is used to characterize hazard at these sites. Considering the hypothetical features at Points 7 and 8, they utilize the assumed cumulative displacements of 2 m and 10 cm to characterize the hazard for conditions (a) and (b), respectively, and interpret the probability of fault slip on a fracture with no measurable offset, condition (c), or in intact rock, condition (d), to be essentially zero.

4.3.2.2 Summary of Fault Displacement Hazard Characterization Approaches. In this section we summarize the range of interpretations made by the SSFD expert teams regarding their characterization of fault displacement hazard. A summary of the key components of their models is provided in Table 4-3.

Overall Approach for Characterizing Faulting Hazard. In aggregate, the six SSFD expert teams slightly prefer the displacement approach (aggregate weight ~ 0.6) over the earthquake approach for characterizing fault displacement hazard at sites subject to principal faulting and at sites subject to only distributed faulting. For characterizing principal faulting hazard, four of the teams (ASM, DFS, RYA, and SDO) considered only one approach for characterizing the hazard. Three of the teams (ASM, DFS, and RYA) considered only one approach for characterizing distributed faulting hazard.

Displacement Approach for Principal Faulting Hazard. Principal faulting hazard was assessed for sites located on faults that the SSFD expert teams identified as being seismogenic. The preferred approach for estimating the frequency of displacement events is

the use of slip rate divided by the average displacement per event [Equation (4-13)]. The slip rates were primarily based on the teams' seismic source characterization for the ground motion hazard assessment. One team (DFS) included slip-rate estimates based on cumulative displacement and slip history. The alternative approach used was a direct assessment of the frequency of events from the paleoseismic data applied in the seismic source characterization. The average displacement per event was primarily assessed from paleoseismic data for the sources of principal faulting hazard.

The teams used a variety of approaches to evaluate the conditional probability of exceedance. These are based on empirical distributions derived from Yucca Mountain trenching data normalized by various parameters, including the expected maximum displacement in the maximum event, MD^{max}, the average displacement estimated from displacement data, and the average and maximum displacements estimated from the length of the feature.

Earthquake Approach for Principal Faulting Hazard. The approach used for assessing the frequency of displacement events used by all of the teams was to use the frequency of earthquakes developed for the ground motion hazard assessment multiplied by a probability that each event produces rupture at the site of interest. This probability is the product of the probability of surface rupture times the probability of intersection of the rupture along the strike of the fault. The along-strike intersection probability was computed using the rupture length estimated from the magnitude of the event randomly located along the fault length. Most teams used the empirical model based on historical ruptures (Figure 4-11) to compute the probability of surface rupture. The AAR team used randomization of the rupture location over the down-dip width of the fault to compute the probability of surface rupture.

The approach used by most of the teams to assess the conditional probability of exceedance was to define a distribution for the maximum displacement, *MD*, based either on the magnitude or the rupture length of the earthquake. This distribution is then convolved with a distribution for *D/MD* to compute $P(D>d)$. The preferred distribution of *D/MD* is the empirical model developed by the ASM team from data compiled by Wheeler (1989) on historical ruptures. Some weight was given to a model developed by the SBK team from fractal simulations of fault ruptures. The SDO team also gave some weight to using the

average displacement per event, *AD*, estimated from magnitude, rupture dimensions, and paleoseismic data together with an empirical distribution for *D/AD*.

Displacement Approach for Distributed Faulting Hazard. The majority of the SSFD expert teams specified that the frequency of displacement events on features subject to only distributed faulting be estimated by slip rate divided by the average displacement per event [Equation (4-13)]. The slip rates were primarily based on the cumulative displacement and slip history, though the AAR team developed a correlation between cumulative displacement and Quaternary slip rate from Yucca Mountain data. The interpretations of the slip histories were similar across all teams. The preferred model is that slip has been decreasing with time and the present-day rate is a small percentage of the late Miocene rate. Low weight was given to a uniform slip history for deformation post-12.7 Ma Tiva Canyon tuff deposition. Somewhat higher weight was given to an intermediate model of uniform slip for a time period that ranged from 3.7 to 11.6 Ma. The average displacement per event for features subject to only distributed faulting hazard was estimated using scaling relationships based on either the length of the feature or the cumulative displacement of the feature. If both length and cumulative displacement are known, then the teams gave nearly equal weights to these two approaches.

The teams used similar approaches for evaluating the conditional probability of exceedance to those used in the displacement approach for characterizing principal faulting hazard. The empirical distributions used are typically correlated with the scaling relationship used to estimate the average displacement per event. For example, if the average displacement per event is to be estimated from the cumulative displacement, then the associated distribution for displacement in a single event is based on D/D_{cum}.

Earthquake Approach for Distributed Faulting Hazard. The SSFD expert teams displayed the most variability in characterizing distributed faulting hazard using the earthquake approach. The basic assessment of the frequency of earthquakes was derived from the seismic source characterization for the ground motion hazard assessment defined by each team. The probability that an earthquake causes slip at the point of interest was assessed in a variety of ways. Most teams utilized the logistic regression model based on analyses of the pattern of historical ruptures (e.g., Figure 4-12). Two of the teams (SBK and SDO)

introduced an additional factor based on either the orientation of the feature in the present stress field (slip tendency) or on the angle between the strikes of the feature and the principal rupture. The ASM team introduced a factor that depends on the probability of the earthquake producing principal faulting surface rupture. The SBK team also introduced an approach that is based on the peak velocity induced by the earthquake at the point of interest.

The widest variations in approaches were those for assessing the distribution for displacement per event on the distributed ruptures. Two of the teams (ASM and SDO) used methods defined as a reduction factor, *RF*, times the displacement distribution on the principal rupture. The methods used to assess *RF* were based on (1) the relative cumulative displacement of the feature of interest compared to that of the earthquake source, (2) a scaling relationship defined from the observed ground displacement profile in the 1983 Borah Peak earthquake, and (3) empirical data for the amount of cumulative displacement normalized by the maximum principal faulting displacement. Two other teams (AAR and SBK) used distributions defined by the characteristics of the feature at the point of interest, either length or cumulative displacement. These distributions were the same as those used in the displacement approach.

Application of Models to Nine Demonstration Points. All of the teams considered that Points 1 and 2 are subject to principal faulting hazard. Two of the teams (AAR and DFS) also considered some potential for principal faulting hazard at Point 4 because they had interpreted some probability that the Ghost Dance fault is seismogenic. The AAR team also made the interpretation that Point 6 in Dune Wash lies on their West Dune Wash Number 2 seismic source and may also be subject to principal faulting hazard.

The teams widely varied in their assessments of the probability that distributed faulting could occur in future earthquakes at Points 3 through 9, which are located off of the block bounding faults. These assessment were based on fault orientation, cumulative slip, and structural relationship. The SBK team's interpretation is that all features with some evidence of cumulative displacement are capable of displacement in future earthquakes. The DFS team's interpretation is that for most of these features, the probability that they are capable of displacement in future earthquakes is low. Four of the teams (AAR, ASM, RYA, and SDO)

consider that the probability of displacement at a point in intact rock due to the occurrence of a future earthquake is essentially zero.

TABLE 4-1
SUMMARY OF SEISMIC SOURCE CHARACTERIZATION MODELS

Issue	AAR Team	ASM Team	DFS Team	RYA Team	SBK Team	SDO Team
TECTONIC MODELS						
Overall Approach	Viable models based on observations and inferred processes for the Crater Flat structural domain, with simple shear model given full weight (1.0). Superposed NW-SE dextral shear manifested as specific structures (tectonic models A, B, & C) (0.5) or not (tectonic model D) (0.5).	The source model incorporates various aspects of planar block fault , (preferred), detachment, lateral shear, and volcanic-tectonic models.	Alternative tectonic and structural models are considered primarily in the characterization of local faults: domino model (0.8) (planar fault); detachment (0.2) (includes hypothetical hidden strike-slip fault of either local or regional extent).	None of the tectonic models presented provides a unified explanation for all the seismic, geologic, and geophysical data. Alternative tectonic and structural models are considered primarily in the characterization of local faults. A coalescing fault model best fits the Yucca Mountain area.	Preferred model: oblique rift-planar faults. 3D strain accommodated on planar, strike-slip, normal, and oblique-slip faults. Rock Valley and Highway 95 faults act as accommodation zones in the rift.	Alternative tectonic and structural models are considered in the characterization of local faults. Preferred model for Crater Flat – Yucca Mountain is a half-graben formed within a larger rift that opens and deepens to the north. Deformation history and structure are associated with carapace effect, clockwise vertical axis rotation, basaltic volcanism, age and behavior of Bare Mountain fault.
Planar Block-Faulting Models	Regional faults are modeled as independent and linked (for selected faults) planar faults to maximum seismogenic depth. Local faults include linked and coalesced models; planar faults to maximum seismogenic depth, to depth of local detachment, or in some cases to a depth constrained by allowable aspect ratio or by intersection with a higher-order fault.	Regional faults are modeled as independent planar faults to maximum seismogenic depth. Local faults—the preferred model is that the faults are planar to a depth controlled by the brittle-ductile transition and the Bare Mountain fault; treated as independent and coalescing faults that merge at depth.	Regional faults are modeled as independent planar faults to maximum seismogenic depth. Local faults—include models of independent (0.95) and distributed (0.05) fault behavior; alternative structural models (domino-planar and detachment-listric) used to constrain downdip geometry and extent.	Bare Mountain and regional faults are modeled as independent planar faults to maximum seismogenic depth. Local faults—planar to listric (1 to 3 coalescing systems).	Regional faults are modeled as independent planar faults to maximum seismogenic depth. Local faults—Yucca Mountain faults are part of a half-graben, with Bare Mountain as the master fault, predominantly normal slip with a left-lateral component.	Regional faults are modeled as independent planar faults to maximum seismogenic depth. Local faults: half-graben model (1) end member—all Yucca Mountain faults are seismogenic, continuous planar faults to maximum seismogenic depth. (2) carapace effect—only major block-bounding faults are through-the-crust seismogenic faults; other intrablock faults are confined to the carapace (i.e., are aseismic) or link to faults having different attitudes and aspect ratios below the unconformity.

TABLE 4-1
SUMMARY OF SEISMIC SOURCE CHARACTERIZATION MODELS
Page 2 of 9

Issue	AAR Team	ASM Team	DFS Team	RYA Team	SBK Team	SDO Team
Shear Models (buried strike-slip faults or fault systems)	Included three alternatives: Model A – Throughgoing regional dextral shear zone (0.05); Model B - right-stepping dextral shear zone that produces a pull-apart basin WITHOUT an underlying cross-basin fault (0.6); and Model C - right-stepping dextral shear zone that produces a pull-apart basin WITH an underlying cross-basin fault (0.35).	Model 1 – Continuous, long (240-km) strike-slip fault zone as proposed by Schweikert considered. Regional (60-km-long) strike-slip fault given low weight. Model 2 – Shorter (25-km), more complex or segmented zone. Assessment of existence of buried strike-slip fault conditional (yes–0.2; no–0.05) on whether or not detachment exists; assessment of the seismogenic potential of the buried strike-slip fault is conditional on the depth of the detachment (shallow–0.8, moderate–0.6, deep–0.0).	Model allows for component of northwest-directed right-lateral strike-slip strain. Hypothetical hidden strike-slip fault source ($P_A = 0.05$) is included in detachment model. Two postulated strike-slip fault sources are included: regional strike-slip fault (0.5) local strike-slip fault (0.5)	None (possibility of local buried source covered by background source).	A buried regional shear zone model is given low weight (0.01); no evidence for a buried strike-slip fault trending northwest across Crater Flat that would result in a earthquake larger than the maximum assigned to the host source zone.	Three sources of dextral shear were evaluated to account for vertical axis rotation at Yucca Mountain: (1) distributed shear (restricted to Crater Flat basin; basin is a discrete domain controlled by local bounding faults); (2) external transcurrent strike-slip fault (passes through the basin, totally hidden); and (3) external strike-slip fault enters basin from southeast (manifested at Yucca Mountain by the N25°W striking "hingeline") and terminates in Crater Flat. Only (1) and (3) are credible modifications to the basic model.
Detachment Models	Regional detachment not viable (0.0), but hypothesized local detachments included, with weights dependent on the type of dextral shear structures assumed to be present. Local detachments not included as specific seismic sources; detachments affect only down-dip fault extent for local fault sources. Depths included for local detachments range from 3 km to the maximum thickness of the seismogenic crust, with 3 to 10 km preferred.	Detachment Model (0.15): Hypothesized detachment affects down-dip geometry and extent of local fault sources; seismogenic detachment is included as possible fault source with very low probability (see below).	Detachment Model (0.2): Hypothesized detachment chiefly affects down-dip geometry and extent of local fault sources; seismogenic detachment is included as possible fault source with very low probability (see below).	Detachments are not explicitly modeled. Possibility that local faults truncate down dip in a detachment or zone of decoupling is included in coalescing fault model.	Hypothesized detachment affects only the down-dip extent of local fault sources.	A seismogenic detachment (modeled as an independent source) was thoroughly considered but could not be substantiated by the available evidence.

TABLE 4-1
SUMMARY OF SEISMIC SOURCE CHARACTERIZATION MODELS
Page 3 of 9

Issue	AAR Team	ASM Team	DFS Team	RYA Team	SBK Team	SDO Team
Volcanic-Tectonic Models ("ash event")	The possibility of simultaneous rupture on subparallel Yucca Mountain faults as postulated for the "ash event" is included in coalesced fault models for local faults.	The possibility that some surface rupturing earthquakes in Crater Flat are accompanied by dike injection (e.g., the 70-ka "ash event") is included in simultaneous rupture models for local faults.	The possibility of simultaneous rupture on subparallel Yucca Mountain faults as postulated for the "ash event" is included in the distributed faulting model for local faults.	The coalescing fault model used to model local faults (see below) would explain the apparent sychroneity of faulting on Yucca Mountain faults (i.e., the 70 ka "ash event").	Explicitly models a simultaneous rupture event (triggered by volcanic event; see Local Fault Model)	Distributed fault models involve simultaneous rupture of local faults that are parallel to each other. Such models would account for volcanism and tectonic faulting as a coupled process.
Thickness of Seismogenic Crust	Dmax1 11 km (0.185) 15 km (0.63) 17 km (0.185) Dmax2 14 km (0.185) 18 km (0.63) 22 km (0.185)	12 (0.1) 15 (0.6) 17 (0.3)	12 (0.6) 14 (0.3) 16 (0.1)	12 km (0.2) 15 km (0.7) 20 km (0.1)	12 (0.3) 15 (0.6) 17 (0.1)	14 km (0.2) 17 km (0.7) 19 km (0.1)
SEISMIC SOURCES						
Seismic Source Zones	Four scenarios: Scenario I w/3 zones (0.3), Scenario II w/2 zones (0.3), Scenario III w/3 zones (0.3), and Scenario IV w/1 zone (0.1). For all scenarios, a host zone (within 20-km radius) is defined only for assigning a lower M_{max}—not for separate recurrence estimate.	Two source zones within 100-km radius of site. A local zone (within 50-km radius) is included that is defined solely for assigning a lower M_{max}.	Model A (0.2) One zone Model B (0.8) Three zones Both models include a local zone that is defined for constraining M_{max} in the area of the detailed site characterization studies.	Three primary source zones within 100 km of site; two alternative configurations to model Zone A (local Yucca Mountain region) and Zone B (the zone surrounding Zone A).	Model A (0.7) 3 zones Model B (0.3) 4 zones Both models include a local zone that is defined solely for assigning a lower M_{max}.	Eight source zones within a 300-km radius of the site were considered initially, but only 3 remained given a filter of radius <100 km.
Seismic Source Zones—Recurrence	Truncated exponential recurrence model (1.0)	Truncated exponential recurrence model (1.0)	Truncated exponential recurrence model (1.0)	Truncated exponential recurrence model (1.0)	Truncated exponential recurrence model (1.0)	Truncated exponential recurrence model (1.0)

TABLE 4-1
SUMMARY OF SEISMIC SOURCE CHARACTERIZATION MODELS
Page 4 of 9

Issue	AAR Team	ASM Team	DFS Team	RYA Team	SBK Team	SDO Team
Seismicity Catalog	300-km radius catalog Version 7 (1.0) Adjustment made for UNEs in relevant source zones.	300-km radius catalog Version 7 (0.7) Version 5 (0.3) Adjustment made for UNEs.	300-km radius catalog Version 7 (0.5) Version 5 (0.5)	100-km radius catalog Version 5 (0.5) Version 7 (0.5)	100-km radius catalog Version 7 (0.3 -0.6) Version 5 (0.4 -0.7) Weights vary depending on source zone. In relevant zones, adjustments made for UNEs weighted (0.4) versus no adjustment (0.6).	300-km radius catalog Version 5 (0.6) Version 7 (0.2) Version 8 (0.2)
Spatial Smoothing Model	For Scenarios I - III: Uniform (1.0). For Scenario IV: h = 5 km (0.25) h = 10 km (0.5) h = 20 km (0.25)	Uniform (1.0)	Model A: h = 10 km (0.25) h = 25 km (0.6) Uniform (0.15) Model B: h = 10 km (0.22) h = 25 km (0.53) Uniform (0.25)	Uniform (0.4); h = 5 km (0.4) h = 15 km (0.2)	Uniform (1.0)	Uniform (0.5) h = 10 km (0.25) h = 20 km (0.25)
Seismic Source Zones—M_{max}	Excluding Host Zone 6.6 (0.3) 6.9 (0.4) 7.3 (0.3) Host Zone (within 20 km) 6.0 (0.3) 6.3 (0.4) 6.6 (0.3)	Walker Lane 6.5 (0.185) 6.8 (0.63) 7.1 (0.185) Basin and Range 6.9 (0.185) 7.2 (0.63) 7.5 (0.185) Site Region (within 50 km) 6.0 (0.185) 6.3 (0.63) 6.6 (0.185)	Model A (not including site vicinity) 7.0 (0.2) 7.3 (0.6) 7.7 (0.2) Model B (not including site vicinity) SW Walker Lane 7.0 (0.2) 7.3 (0.6) 7.7 (0.2) NE Walker Lane and Basin and Range 7.0 (0.2) 7.25 (0.6) 7.5 (0.2) Site Vicinity 5.6 (0.2) 5.8 (0.6) 6.0 (0.2)	6.0 (0.185) 6.3 (0.63) 6.6 (0.185)	Excluding Local Zone: 6.2 (0.2) 6.3 (0.5) 6.4 (0.2) 6.6 (0.1) Local Zone 5.6 (0.2) 6.0 (0.6) 6.2 (0.2)	Within 100 km 6.4 ± 0.2 cumulative lognormal distribution 6.2 (0.03) 6.4 (0.5) 6.6 (0.97 Beyond 100 km: estimated from a correlation of fault length with magnitude for longest fault: in Zones 2 and 3 Ms 7.4 ± 0.2

TABLE 4-1
SUMMARY OF SEISMIC SOURCE CHARACTERIZATION MODELS

Issue	AAR Team	ASM Team	DFS Team	RYA Team	SBK Team	SDO Team
Regional Fault Sources	19 regional fault sources; includes faults with Pa of <1.0; includes two possibly linked fault systems: Death Valley with Furnace Creek (0.8), and Amargosa River with Pahrump (0.1); also includes five faults considered as segmented (max. rupture length < total fault length); included range of rupture lengths for each source. Preferred dips: normal 65° strike-slip 90°	24 regional faults (within 15 to 100 km of site); all fault sources active (1.0); considers alternative total lengths, generalized down-dip geometry (strike-slip 90°, normal 60°).	18 regional fault sources (within 100 km of site vicinity); all fault sources active (1.0); considered alternative total lengths, generalized down-dip geometry (strike-slip 90°, normal-60°).	11 regional fault sources (within 100 km of site); all fault sources active (1.0); includes possibility (0.1) of simultaneous rupture of Death Valley and Furnace Creek faults; includes alternative rupture lengths for 9 faults, generalized down-dip geometry (strike-slip 90°, normal 60°).	16 regional fault sources (within 100 km radius); includes faults with Pa < 1.0; includes range of rupture lengths for each source—for long faults ranges reflect probable rupture segment lengths, assigned dips based on fault type, with preferred values of: strike-slip 90°, normal 60°, and oblique 70°.	36 regional fault sources (24 faults (Pa 1.0), 12 faults (Pa < 1.0); two faults generally outside 100 km (Panamint Valley and Ash Hill fault zone) included; alternative total lengths, generalized down-dip geometry (strike-slip 90°, normal 60°).
Regional Faults—M_{max}	SRL (0.4) RA (0.2) SRL and S (0.4) M_{max} ± ¼ unit, M_{max} + ¼ = m°	SRL (1.0) M_{max} ± ¼ unit, M_{max} + ¼ = m°	SRL (1.0) Alternative rupture segments (SRL) are considered resulting in a range of M_{max} for each fault. M_{max} ± ¼ unit (with some exceptions)	SRL (0.35) RA (0.35) MD (0.3) Or RL (0.5) RA (0.5) depending on available data M_{max} ± 0.5 unit	SRL, RA, MD, AD, and moment approaches; weighted on a fault basis depending on available data. M_{max} ± ¼ unit, M_{max} + ¼ = m°	RL, MD, RL x MD, Slip rate +RL; weighted on a fault basis depending on available data. M_{max} ± ¼ unit, M_{max} + ¼ = m°
Regional Faults—Recurrence Approach	Slip Rate Approach (0.6); Recurrence Interval Approach (0.4) - where data are available. Characteristic (0.7) Modified exponential (0.3) DV–FC Characteristic (1.0) M_{max} + ¼ = m° b-value 0.80 (0.3), 1.00 (0.4), 1.20 (0.3)	Slip Rate Approach (0.5) Recurrence Interval (0.5) or Slip Rate (1.0) depending on available data. Characteristic (0.2) Maximum moment (0.8) b-value varies from fault to fault.	Slip Rate Approach (1.0) Characteristic (0.6) Maximum moment (0.3) Truncated exponential (0.1) b-value varies from fault to fault.	Slip Rate Approach (1.0) Characteristic (0.9) Truncated exponential(0.1) b-value 1.07 (0.185) 1.12 (0.63) 1.2 (0.185) M_{min} = 6.3	Slip Rate and Recurrence Interval Approaches; weights vary from fault to fault depending on available data. Characteristic and truncated exponential models used. Weights vary from fault to fault, with characteristic behavior favored for range-bounding faults, and exponential for zones with multiple distributed traces. b-value varies from fault to fault.	Moment rates (slip rates) Characteristic (0.7) Truncated exponential (0.3) b-value varies from fault to fault. M_{min} = 6.2

TABLE 4-1
SUMMARY OF SEISMIC SOURCE CHARACTERIZATION MODELS
Page 6 of 9

Issue	AAR Team	ASM Team	DFS Team	RYA Team	SBK Team	SDO Team
Local Fault Sources	20 individual faults included w/ P[s] 0.1 to 1.0 Synchronous Behavior Approach: (1) Faults rupture independently or are grouped in distributed systems by linkages along strike or coalescence down dip. (2) Likelihood of coalesced behavior is dependent on tectonic model (in general, coalesced behavior strongly favored over independent behavior). (3) Four coalesced models defined with from one to four fault systems. Assigned weights depend on tectonic models, but models having three to four systems are strongly favored. (4) For independent fault behavior, two cases of possibly linked faults are generally favored. Preferred dip 60°. Dominantly normal slip w/ left-lateral component.	Planar Fault Block Model-5 faults modeled as major block-bounding faults (seismogenic–1.0) 5 faults modeled as minor or secondary faults (probability of being seismogenic—fault, P_A ranges from 0.5 to 0.9). Simultaneous rupture models are based on the probability of linkage at depth (geometric constraints) and temporal overlap inferred from paleoseismic data.	Two Fault Behavioral Models: Distributed (0.05) 9 scenarios Independent (0.95) Two Structural Models: *Domino* model (0.8) (high-angle planar faults to seismogenic depth except where they intersect larger-throw fault); existence of H95 fault not dependent on domino model—considered as an independent source with low probability of being an active seismogenic structure. *Detachment* model (0.2) listric geometry detachment modeled at 6 km depth; includes hidden strike-slip fault sources.	Coalescing Fault Model (1.0) Bare Mountain fault, independent planar fault to seismogenic depths. Yucca Mountain faults are assumed to coalesce down dip at relatively shallow depth (2 to 5 km). Three faults (WW, SC, and PBC) are primary independent seismogenic faults in three-fault system. Coalescing Models: 12 km (0.2) and 15 km (0.7) seismogenic depth: 1-fault system (0.1) 2-fault system (0.5) 3-fault system (0.4) 20 km (0.1) seismogenic depth 1-fault system (0.3) 2-fault system (0.4) 3-fault system (0.3) Planar fault and detachment-decoupled model geometries are considered part of range of behavior for coalesced systems.	Within Crater Flat domain, included 11 individual faults (9 YM, BM, and Hwy 95); excluded 7 mapped faults ($P_A = 0$) based on no or low rates of Quaternary activity (including GD and SD). Model- local faults sole into detachment between 5 km and base of seismogenic zone (0.01). Model- block-bounding faults coalesce at depth either in one or two master faults (0.09) Model (end member) - 4 linked block-bounding faults (0.4) Model (end member) - faults behave independently (0.5) All of the above models include a simultaneous rupture scenario that acts as an additional source; weights on activity vary according to rupture model (0.1 on independent and linked; 0.5 on detachment and coalescing models).	Behavior models included: (1) single-fault (2) linked-fault (3) distributed-fault Single-fault scenarios - 6 major local faults 9 linked-fault scenarios 8 distributed fault scenarios
Local Faults—M_{max}	RLD (for buried structures) or SRL (all others) RA SRL + S Moment Equation	General weights SRL (0.3) SRL x D (0.3) MD (0.15) AD (0.15) RA (0.1)	RL (0.4) RA (0.6) ± 0.25 units	RL (0.5) RA (0.5) ± 0.5 units	SRL, RA, MD, AD, M_o inferred from stress drop; weights vary depending on available data.	RL (0.206) MD (0.104) RL x MD (0.207) RA (0.207) SRL + S (0.069) Seismic Moment (0.207)

TABLE 4-1
SUMMARY OF SEISMIC SOURCE CHARACTERIZATION MODELS
Page 7 of 9

Issue	AAR Team	ASM Team	DFS Team	RYA Team	SBK Team	SDO Team
	Different weights assigned depending on fault length (< or ≥ 25 km), tectonic model, and coalesced behavior model. M_{max} ± ¼ unit, M_{max} + ¼ = m^u	Modified on a fault basis depending on available data. M_{max} ± ¼ unit, M_{max} + ¼ = m^u			M_{max} ± ¼ unit, M_{max} + ¼ = m^u	M_{max} ± ¼ unit, M_{max} + ¼ = m^u
Local Faults—Recurrence	Slip-Rate Approach (0.6); Recurrence Interval Approach (0.4) - where data are available. Characteristic (0.7), Modified exponential (0.3) b-value 0.80 (0.3), 1.00 (0.4), 1.20 (0.3)	Slip-Rate Approach (0.5) Recurrence Interval Approach (0.5) Characteristic (0.7) Truncated Exponential (0.2) Maximum moment (0.1)	Slip-Rate Approach (1.0) Independent behavior- Characteristic (0.6) Maximum moment(0.3) Exponential (0.1) Distributed behavior- Characteristic (0.6) Maximum moment(0.2) Exponential (0.2)	Slip-Rate Approach (0.7) Recurrence Interval Approach (0.3) Characteristic and truncated exponential—weights vary depending on coalescing model used.	Slip-Rate Approach (0.7 to 1.0) Recurrence Interval Approach (used where data are available, but given lower weight, 0.2 to 0.3) Both characteristic and truncated exponential models used (weight varies depending on fault model)	Moment Rate (0.33) Average Recurrence Interval (0.33) Interseismic Recurrence Interval (0.33) Characteristic (0.7) Truncated exponential (0.3)
OTHER SOURCES						
Buried Regional Dextral Shear Zone	Included w/ P[s] = 1.0 for Tectonic Model A (0.05). Regional strike-slip fault 50 to 100 km in length Slip Rate 0.05 (0.3) 0.1 (0.4) 0.2 (0.3)	Yes; see above. M_{MAX} M_w 7.1 (0.3) 60-km rupture M_w .6.7 (0.7) 25-km rupture Slip Rate 0.1 mm/yr (0.6) 0.025 mm/yr (0.2) 0.24 mm/yr (0.2)	Includes a hypothetical strike-slip fault of regional or local extent, with low probability (0.05) that it is a seismogenic source. Local strike-slip fault (0.5) 30-km length. Regional strike-slip fault (0.5) 200-km length.	Not included as fault source; possible buried strike-slip fault judged incapable of producing earthquakes larger than the maximum background earthquake or any other source included in the source model.	Not included as fault source; possibility is covered by seismic source zone.	Yes; see above. Fault Length 20 km (minimum) 27 km (preferred) 120 km (maximum) Slip Rate 0.001 (minimum) 0.005 (preferred) 0.02 (maximum)

TABLE 4-1
SUMMARY OF SEISMIC SOURCE CHARACTERIZATION MODELS
Page 8 of 9

Issue	AAR Team	ASM Team	DFS Team	RYA Team	SBK Team	SDO Team
Seismogenic Detachment (modeled as independent source)	No (possibility is covered by areal source zone).	Detachment Model (0.15) Probability—seismogenic (0.01) Depth to detachment 6 km (0.25) (BD-6) / 2- 6 km (0.5) BD (0.25) BD=brittle-ductile transition Maximum magnitude 7.1 (0.15) 7.6 (0.7) 8.0 (0.15) Slip Rate 0.05 mm/yr (0.6) 0.013 mm/yr (0.2) 0.12 mm/yr (0.2) Mean Recurrence 25 kyr (0.15) 75 kyr (0.7) 200 kyr (0.15) Characteristic (1.0)	Yes (Paintbrush Canyon /Stagecoach fault in the detachment model (0.2) is modeled as a shallow-dipping, seismogenic source that extends beneath the Crater Flat Basin).	Possibility of a seismic detachment is excluded.	No (shallow and deeper detachments as active seismogenic structures are given no weight). Hypothesized detachments affect only down-dip fault extent of Yucca Mountain faults; depth is dependent on Bare Mountain fault.	A seismogenic detachment (modeled as an independent source) was thoroughly considered but could not be substantiated by the available evidence.
Volcanic Source Zone (basaltic)	No (possibility is covered by areal source zone).	No (maximum magnitudes for volcanic-related earthquakes are less than M_{max} for fault and background seismic zones, and recurrence rate for volcanic eruptive events is estimated to be insignificant compared to seismicity rates).	No (possibility is covered by seismic source zones).	Yes (0.7) Spatial location (basaltic cones in site vicinity). Preferred return periods 2×10^5 and 2×10^6 $M_{max} = 5.5$.	No (possibility is covered by seismic source zones).	Defines two volcanic sources with probabilities of 0.25 and 0.7. Recurrence—2 to 3 volcanic events per Ma Maximum magnitude distribution for volcanic events: 6.0 ± 0.2 (0.1) 5.8 ± 0.4 (0.6) 5.5 ± 0.3 (0.3)

TABLE 4-1
SUMMARY OF SEISMIC SOURCE CHARACTERIZATION MODELS
Page 9 of 9

Issue	AAR Team	ASM Team	DFS Team	RYA Team	SBK Team	SDO Team
Gravity Fault	Considered distinct from Ash Meadows fault, which is included as a regional fault; accounted for in assessment of M_{max} for background source zones >20 km from site.	Not discussed. Ash Meadows fault is included as regional fault source (probability of activity 1.0).	Amargosa/Gravity (Ash Meadows) fault is included as regional fault source (probability of activity 1.0).	Not discussed. Ash Meadows fault included as regional fault.	Included as potential northern extension of the Ash Meadows fault (0.1).	Characterized as a regional fault source, probability of activity (0.9).
Cross-Basin Fault	Included w/ P[s] = 1 in Tectonic Model C (0.35)	Includes local buried strike-slip fault with low probability (see above); preferred length (25-km) (0.7) based on down-on-east segments along the west side of Crater Flat.	A local hidden strike-slip fault is included with a low probability (P_A = 0.05) in the detachment model for local faults.	Not explicitly included in SSC model; see comment above regarding buried strike-slip faults.	Not included.	Based on evidence for distributed dextral faulting, the hingeline-Pahrump-Stewart Valley fault is characterized as a buried strike-slip fault.
Highway 95 or Carrara Fault	Included w/: P[s] = 0.5 for Tectonic Model A P[s] = 0.8 for Tectonic Models B & C.	Carrara fault characterized as active (P_A = 0.85) regional fault source.	Included with low probability (P_A = 0.1) as a hypothetical regional source.	Not included.	Included as independent fault source (P_A = 0.4).	Highway 95 fault assigned a probability of 0.2 (regional fault source).

TABLE 4-2
ACRONYMS FOR FAULT SOURCES

LOCAL FAULT SOURCES	
AW	Abandoned Wash Fault
BC	Black Cone Fault
BM	Bare Mountain Fault
BWR	Bow Ridge Fault
CF	Crater Flat Fault
CCF	Central Crater Flat Fault
CWW	Central Windy Wash Fault
E-SIDE (ES)	East Side Fault (PC+SR+BWR+MWV+GD+WD1+WD2+EB (Team AAR)
EB	East Busted Butte Fault
ELC	East Lathrop Cone Fault
FW	Fatigue Wash Fault
GD	Ghost Dance Fault
H95	Carrara (Highway 95) Fault
IR	Iron Ridge Fault
MWV	Midway Valley Fault
NCF	Northern Crater Flat Fault
NPC	Northern Paintbrush Canyon Fault
NWW	Northern Windy Wash Fault
PBC	Paintbrush Canyon Fault
SC	Solitario Canyon Fault
SCF	Southern Crater Flat Fault
SPC	Southern Paintbrush Canyon Fault
SR	Stagecoach Road Fault
SWW	Southern Windy Wash Fault
WD1	West Dune Wash Fault #1
WD2	West Dune Wash Fault #2
W-SIDE 1	West Side Fault #1 (SC+IR) (Team AAR)
W-SIDE 2	West Side Fault #2 (WW+FW+CF) (Team AAR)
WW	Windy Wash Fault
WSIDE	West Side Fault (Team RYA)

TABLE 4-2 (Continued)

REGIONAL FAULT SOURCES	
AH	Ash Hill Fault
AM	Ash Meadows Fault
AR	Amargosa River Fault
BH	Buried Hills Fault
BLR	Belted Range Fault
BM	Bare Mountain Fault
CB	Carpetbag Fault
CS	Cane Spring Fault
DV	Death Valley Fault
EDV	Eastern Death Valley Fault
EM	Emigrant Fault
EN	East Nopah Fault
EPR	East Pintwater Range Fault
ER	Eleana Range Fault
ESR	East Spector Range Fault
EVN	Emigrant Valley North Fault
EVS	Emigrant Valley South Fault
FC	Furnace Creek Fault
FLV	Fish Lake Valley Fault
GM	Grapevine Mountains Fault
GV	Grapevine Fault
H95	Cararra (Highway 95) Fault
HM	Hunter Mountains Fault
JFG	Jackass Flats Gravity Fault
KR	Kawich Range Fault
KW	Keane Wonder Fault
MDV	Middle Death Valley Fault
MM	Mine Mountain Fault
OAK	Oak Springs Fault
OSV	Oasis Valley Fault
PAN	Panamint Valley Fault
PC	Peace Camp Fault
PM1	Pahute Mesa Fault
PRP	Pahrump Fault
RV	Rock Valley Fault
RWBW	Rocket Wash-Beatty Wash Fault
SF	Sarcobatus Flat Fault
SPR	Spotted Range Fault
SPRP	South Pahrump Fault
SSC	South Silent Canyon Fault

TABLE 4-2 (Concluded)

REGIONAL FAULT SOURCES (Cont'd.)	
TOL	Tolicha Pass Fault
TP	Towne Pass Fault
WAH	Wahmonie Fault
WDV	Western Death Valley Fault
WPR	West Pintwater Range Fault
WSM	West Spring Mountains Fault
WSR	West Spector Range Fault
YB	Yucca Butte Fault
YC	Yucca Fault
YCL	Yucca Lake Fault

INFERRED STRIKE-SLIP FAULT SOURCES	
TI-BSS	Team ASM Buried Strike-Slip Fault
T2-HSS	Team DFS Hidden Strike-Slip Fault
T4-CB	Team AAR Cross Basin Fault
T4-PA2	Team AAR North-Bounding Strike-Slip Fault
T4-SS	Team AAR Regional Strike-Slip Fault
T6-SS	Team SDO Strike-Slip Fault

SUMMARY OF SSFD EXPERT TEAM FAULT DISPLACEMENT HAZARD CHARACTERIZATIONS

Page 1 of 6

Issue	AAR team	ASM team	DFS team	RYA team	SBK team	SDO team
PRINCIPAL FAULTING APPROACH	Displacement approach [0.67]; Earthquake approach [0.33]	Earthquake approach [1.0]	Displacement approach [1.0]	Displacement approach [1.0]	Displacement approach [0.85-0.9] Earthquake approach [0.1-0.15]	Earthquake approach [1.0]
Displacement Approach for Principal Faulting						
Probability That Principal Faulting Can Occur P(C)	Evaluate P(C) based on probability fault is seismogenic	NA	Evaluate P(C) based on probability fault being seismogenic	Evaluate P(C) based on probability fault is seismogenic	Evaluate P(C) based on probability fault being seismogenic	Evaluate P(C) based on probability fault being seismogenic
Frequency of Displacement Events	Slip rate, (*SR*) [1.0]	NA	$SR/\overline{D}_E$ [0.5]; Recurrence intervals (*RI*) [0.5]	Slip rate [0.2]; Recurrence intervals [0.8]	Slip rate [0.8]; Recurrence intervals [0.2]	NA
Slip Rate (*SR*)	Quaternary slip rates used in SSC model	NA	Paleoseismic data [0.7]; uniform post-Tiva Canyon [0.1]; uniform post-Rainier Mesa [0.1]; decreasing slip rate model [0.1]	Quaternary slip rates used in SSC model	Quaternary paleoseismic data point specific or interpolated	NA
Average Displacement Per Event, $\overline{D}_E$	$\overline{D}_E$ =0.83 MD^{max} MD^{max} from fault length [0.3]; D_{cum} [0.3]; paleoseismicity data [0.4]	NA	Paleoseismologic data [0.5]; $SR \times RI$ [0.5]	Paleoseismic data [1.0]	Paleoseismic data [0.8]; From *AD-RL* [0.1]; From *MD-RL* [0.1];	NA
Conditional Probability of Exceedance, *P(D>d)*	Distribution for D/MD^{max} [1.0]	NA	Distribution for *D/AD* [1.0]	Distribution for *D/AD* [0.5]; Distribution for D/MD^{max} [0.5]	D/AD_{paleo} $D/AD_{F(RL)}$ $D/MD_{F(RL)}$ correlated with $\overline{D}_E$	NA

Table 4-3
SUMMARY OF SSFD EXPERT TEAM FAULT DISPLACEMENT HAZARD CHARACTERIZATIONS

Issue	AAR team	ASM team	DFS team	RYA team	SBK team	SDO team
Earthquake Approach for Principal Faulting						
Probability That Principal Faulting Can Occur, *P*(C)	P(C) = P(S) from SSC model	P(C) = P(S) from SSC model	NA	NA	P(C) = P(S) from SSC model	P(C) = P(S) from SSC model
Frequency of Earthquakes on Principal Faulting Source	Earthquake frequency from SSC model	Earthquake frequency from SSC model	NA	NA	Earthquake frequency from SSC model	Earthquake frequency from SSC model
Probability of Surface Rupture	Randomization of rupture depth with rupture width based on *RL*/aspect ratio; *RL* specified by magnitude-*RL* [0.5]; magnitude-rupture area [0.5]	Empirical models 32 GB earthquakes [0.5]; 105 EC earthquakes [0.5]	NA	NA	Empirical model 32 GB earthquakes [1.0]	Empirical models 32 GB earthquakes [0.5]; 47 NB&R earthquakes [0.5]

SUMMARY OF SSFD EXPERT TEAM FAULT DISPLACEMENT HAZARD CHARACTERIZATIONS

Issue	AAR team	ASM team	DFS team	RYA team	SBK team	SDO team
Conditional Probability of Exceedance, *P(D>d)*	Maximum displacement per event, *MD*, from *SRL* [0.33]; M_w [0.33]; and *RLD* [0.34]; *D/MD* from Wheeler data [1.0]	*MD* from M_w [1.0] *D/MD* from Wheeler data [1.0]	NA	NA	*MD* from M_w [1.0] *D/MD* from Wheeler data [0.5]; fractal model [0.5]	*AD* and distribution for *D/AD* [0.5]; *AD* from* M_w [0.2]; *RL* [0.4]; and Paleoseismic data [0.4] *MD* and distribution for *D/MD* [0.5]; *MD* from* M_w [0.2]; *RL* [0.4]; and Paleoseismic data [0.4]; *D/MD* from Wheeler data [0.8], and fractal model [0.2] * for $m<m^U$-½ use only M_w Ramelli curve also was used for Solitario Canyon fault

Table 4-3
SUMMARY OF SSFD EXPERT TEAM FAULT DISPLACEMENT HAZARD CHARACTERIZATIONS
Page 4 of 6

Issue	AAR team	ASM team	DFS team	RYA team	SBK team	SDO team
DISTRIBUTED FAULTING APPROACH	Displacement approach [0.67]; Earthquake approach [0.33]	Earthquake approach [1.0]	Displacement approach [1.0]	Displacement approach [1.0]	Displacement approach [0.8]; Earthquake approach [0.2]	*On Principal Faults–* Earthquake approach [1.0]; *Other Sites–* Displacement approach [0.3, Earthquake approach [0.7]
Earthquake Approach for Distributed Faulting						
Probability of Occurrence P(C)	If capable of principal faulting P(C) = P(S) Otherwise, P(C) based on slip-tendency	Function of the category and orientation of feature, cos(strike azimuth)	NA	NA	P(C)=1.0	Slip tendency [1.0]
Frequency of Earthquakes on Seismic Sources	Earthquake frequency from SSC model	Earthquake frequency from SSC model	NA	NA	Earthquake frequency from SSC model	Earthquake frequency from SSC model
Probability of Slip Per Event, P_i(Slip|Event on j)	Logistic regression of historical faulting data [1.0]	Probability a function of r and hanging wall-footwall location; preferred model [0.6]; upper-bound model [0.4]	NA	NA	$P(\theta)\times F(event)$ $P(\theta)$ based on slip tendency [0.5]; Relative orientation [0.5] $F(event)$ based on logistic regression of historical surface faulting data [0.5], peak velocity [0.5]	$P(\theta)\times F(event)$ $P(\theta)$ based on relative orientation [1.0] $F(event)$ based on logistic regression of historical surface faulting data [1.0]

Table 4-3
SUMMARY OF SSFD EXPERT TEAM FAULT DISPLACEMENT HAZARD CHARACTERIZATIONS

Issue	AAR team	ASM team	DFS team	RYA team	SBK team	SDO team
Conditional Probability of Exceedance, $P(D>d)$	Distribution for D/MD^{max} [1.0]		Distribution for D/AD [1.0]	Distribution for D/AD [0.5] Distribution for D/MD^{max} [0.5] with $MD^{max} = AD/0.83$	Distribution for D/D_{cum} [1.0]	For AAR scaling distribution for D/MD^{max}, for SBK scaling distribution for D/D_{cum}

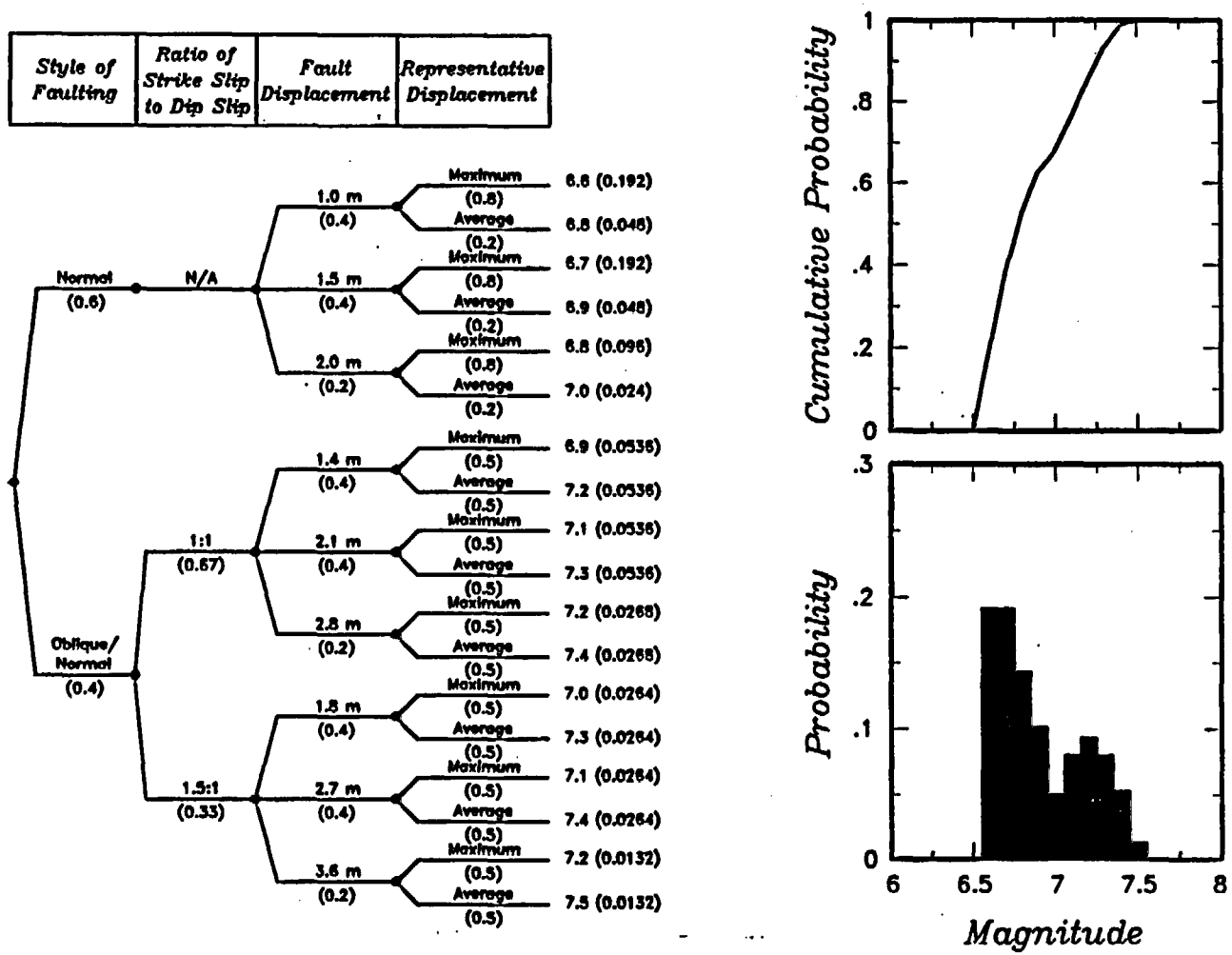

Figure 4-1 Example logic tree and resulting discrete probability distributions for assessing the magnitudes of paleoearthquakes

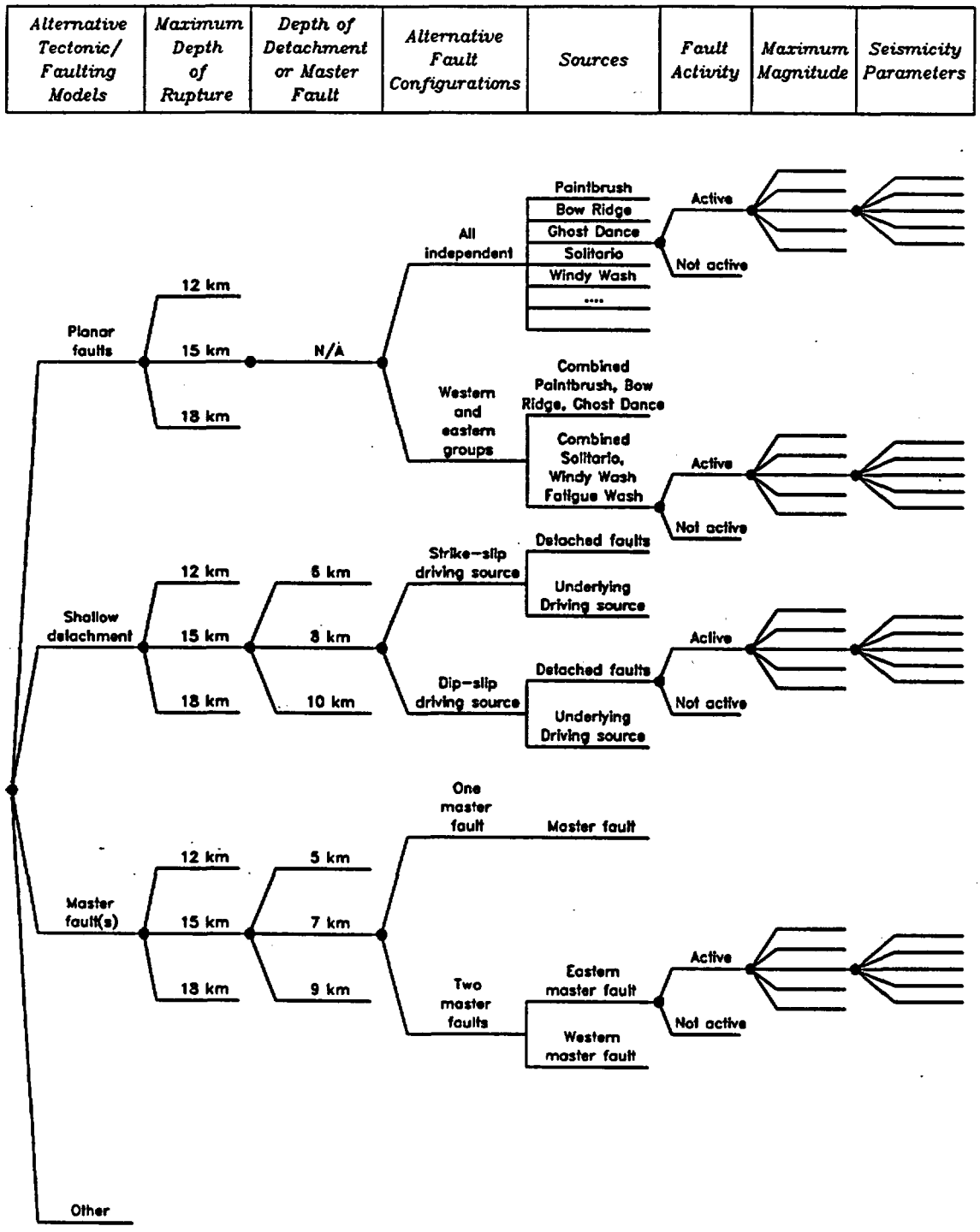

Figure 4-2 Example logic tree for expressing the uncertainty in characterizing local fault sources

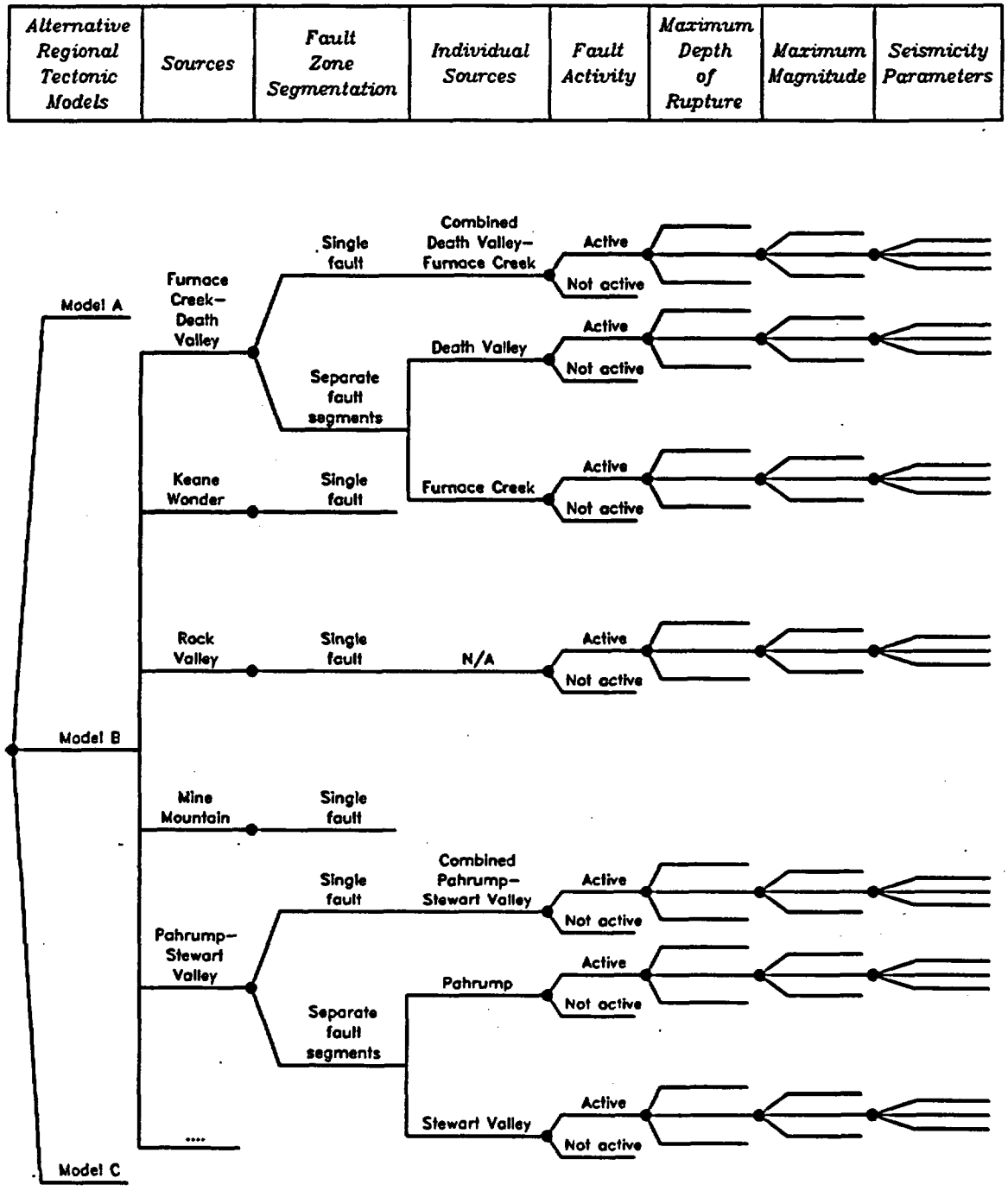

Figure 4-3 Example logic tree for expressing the uncertainty in characterizing regional fault sources

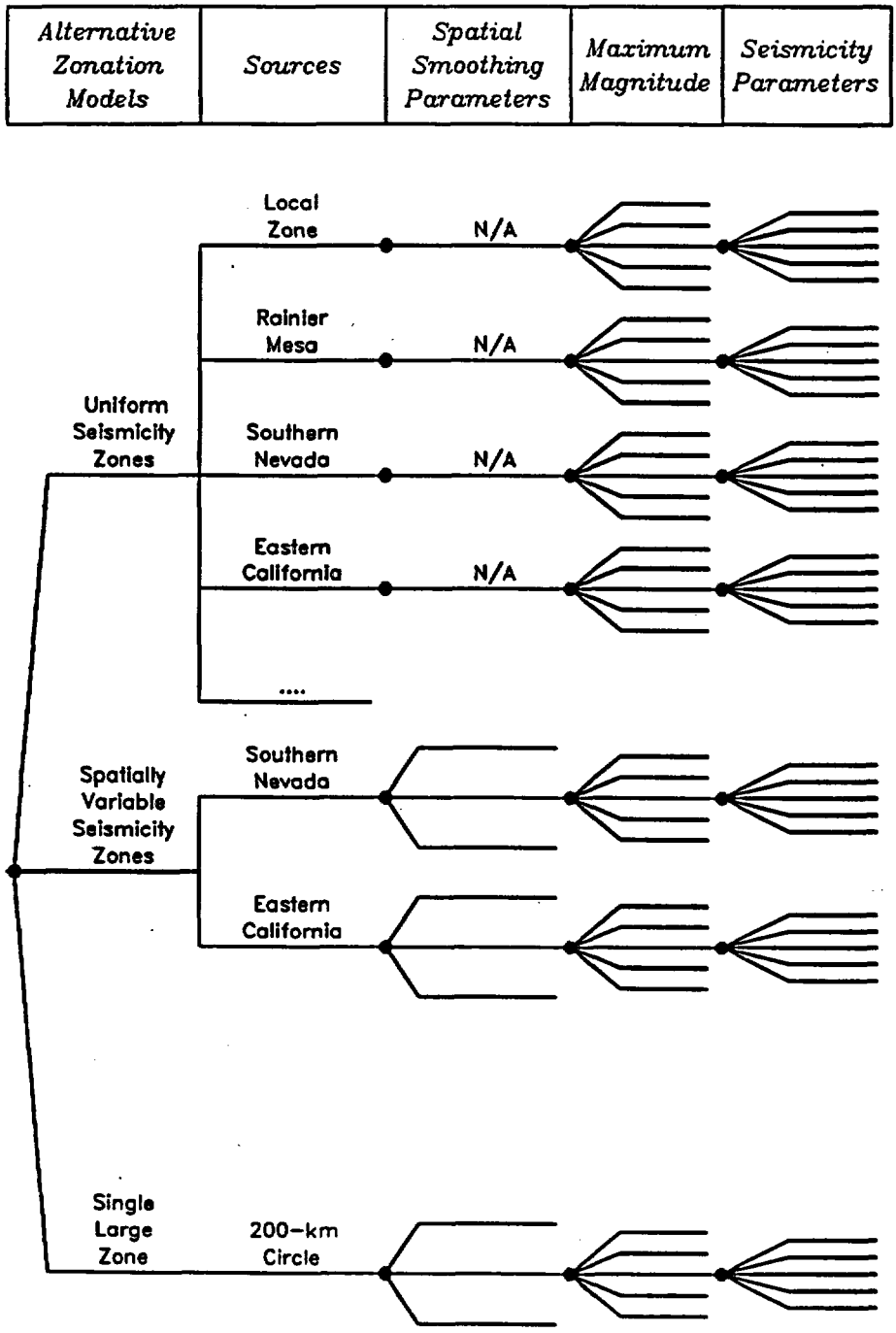

Figure 4-4 Example logic tree for expressing the uncertainty in characterizing regional areal source zones

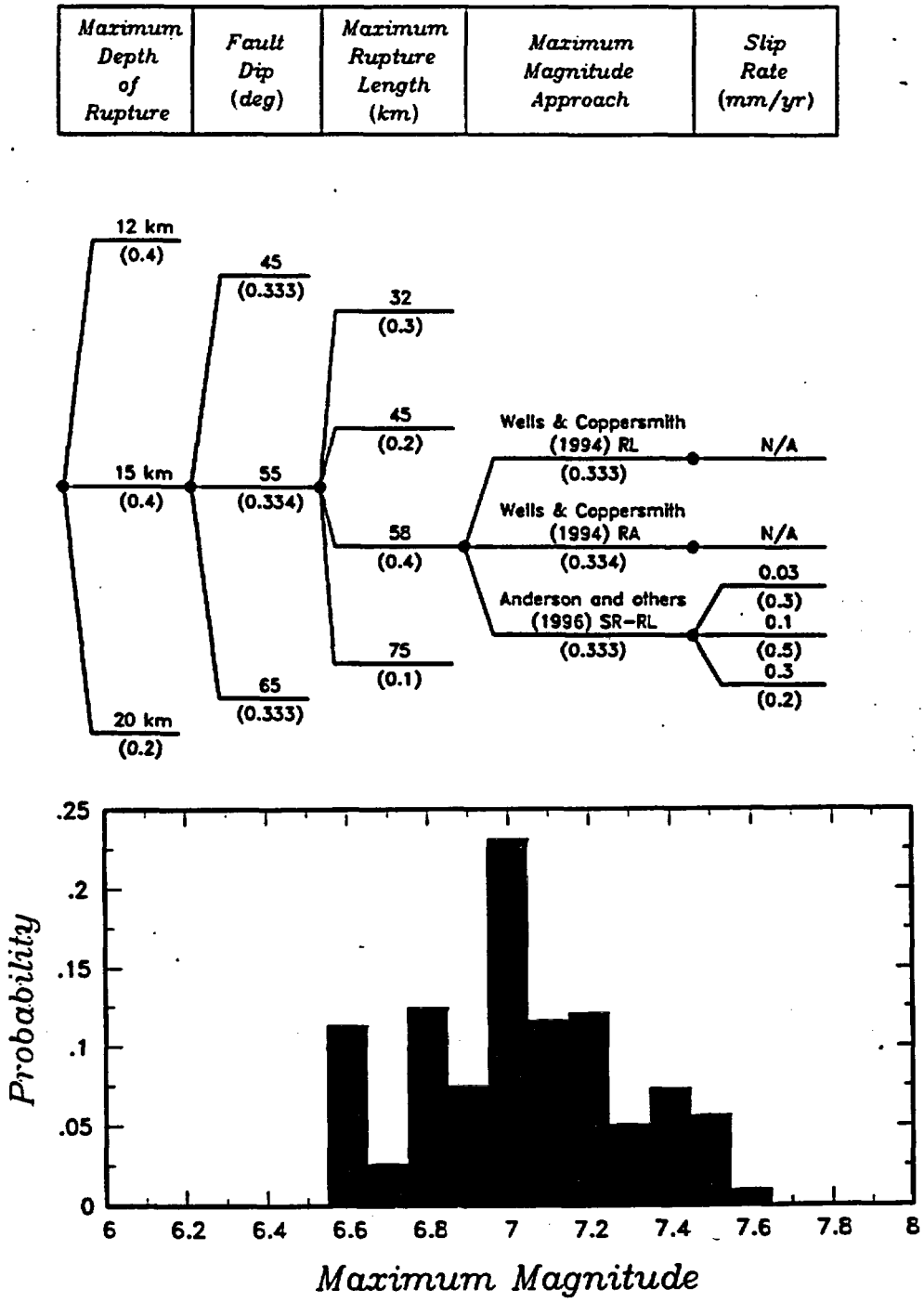

Figure 4-5 Example assessment of maximum magnitude for a fault source. Top, logic tree for uncertainty assessment. Bottom, resulting discrete distribution for maximum magnitude.

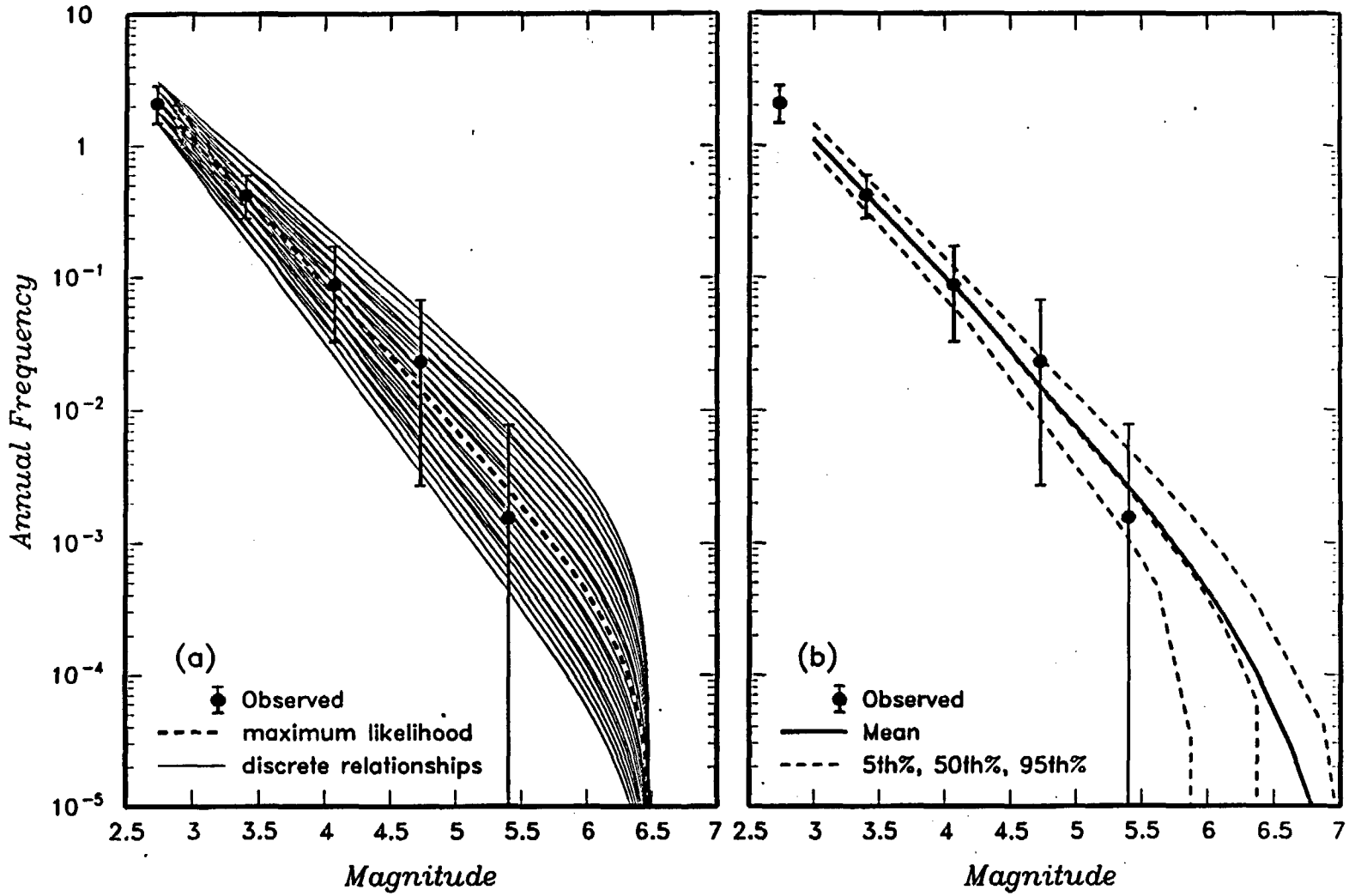

Figure 4-6 Example assessment of the recurrence relationships for an areal source zone. Left, 25 alternative recurrence relationships defined from maximum likelihood fit to observed seismicity. Right, resulting mean and percentile recurrence relationships for source zone.

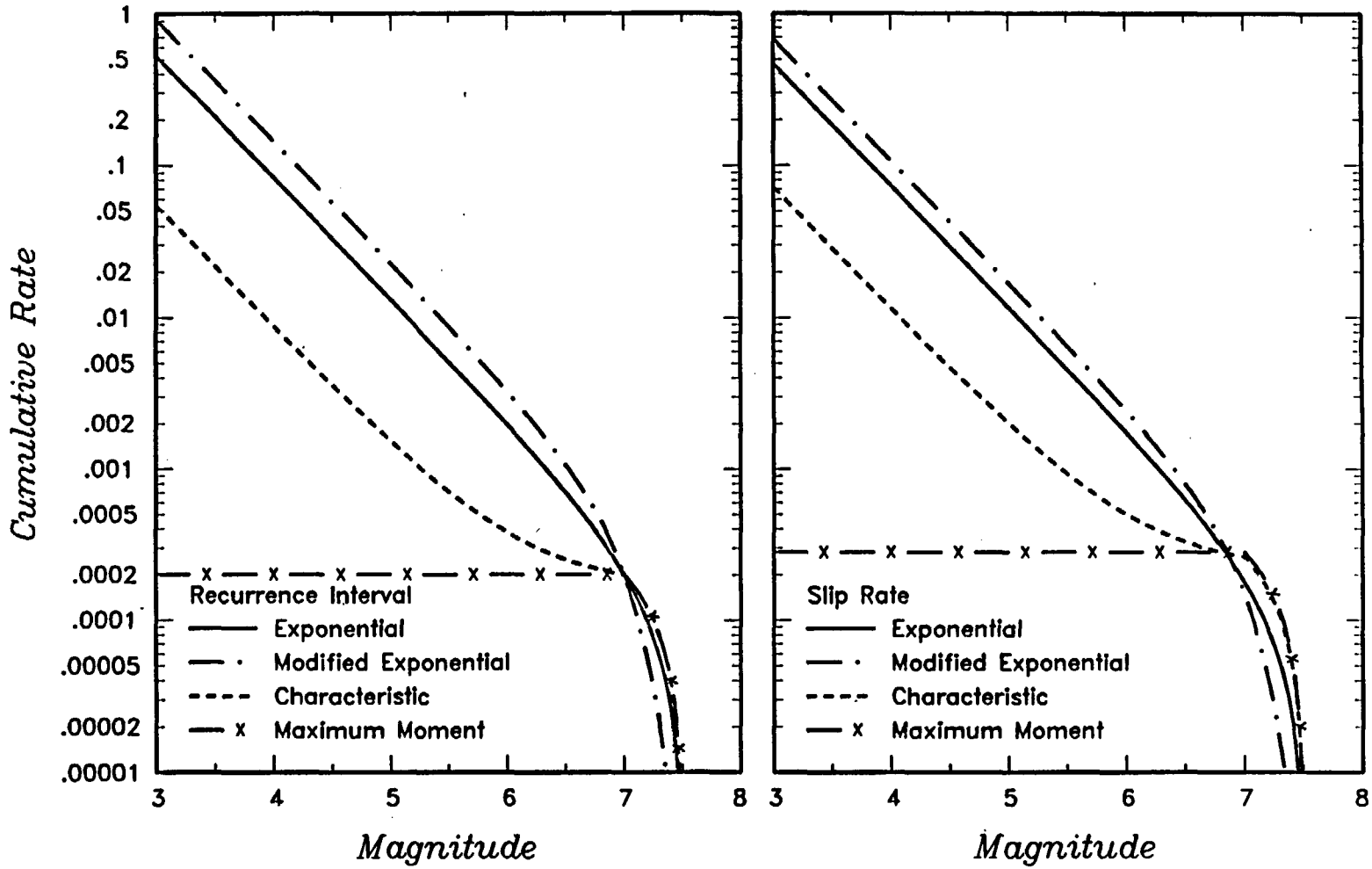

Figure 4-7 Alternative recurrence models constrained by either the recurrence interval for large events (left) or by fault slip rate converted to moment rate (right)

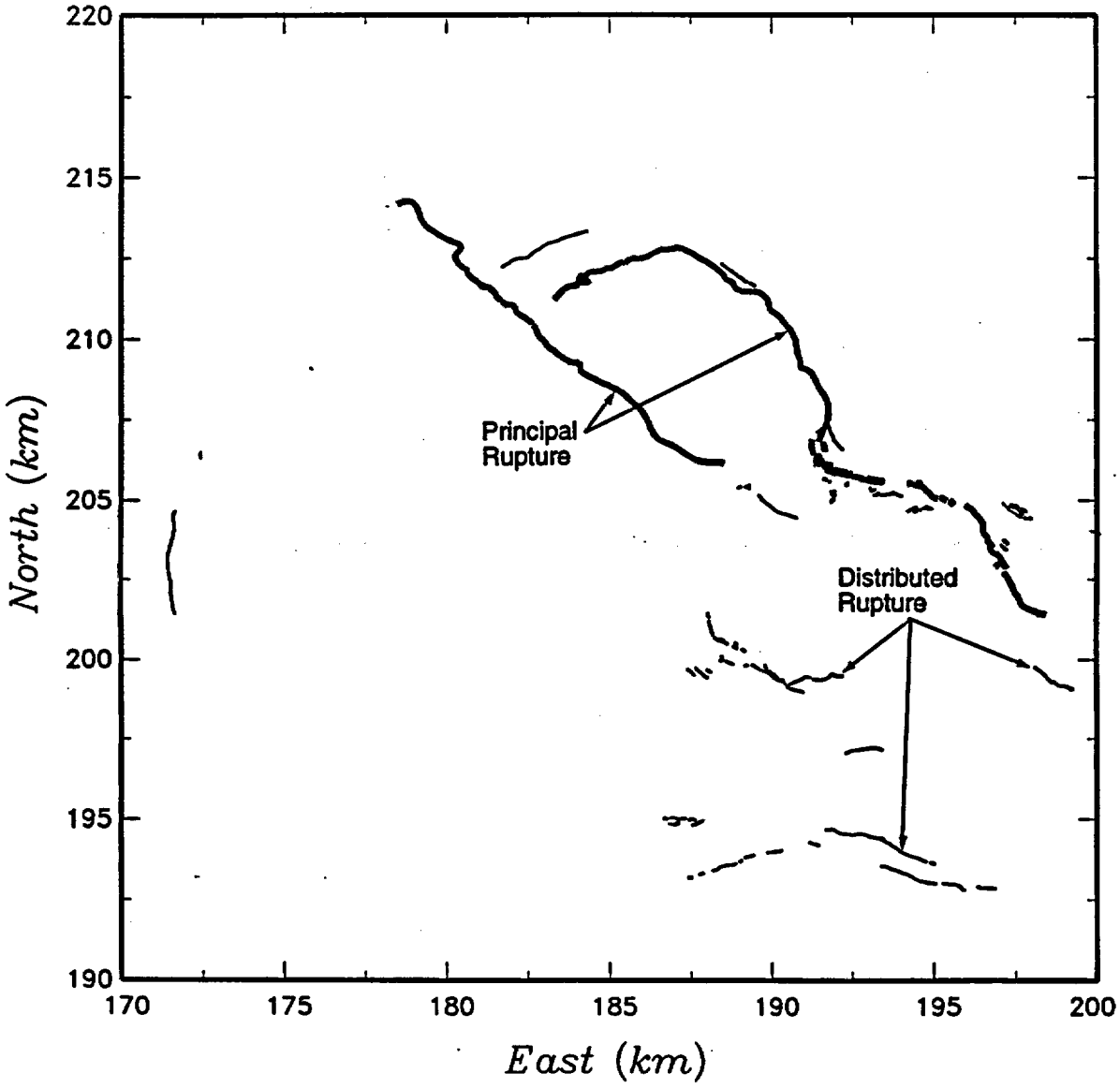

Figure 4-8 Examples of principal and distributed rupture in an earthquake

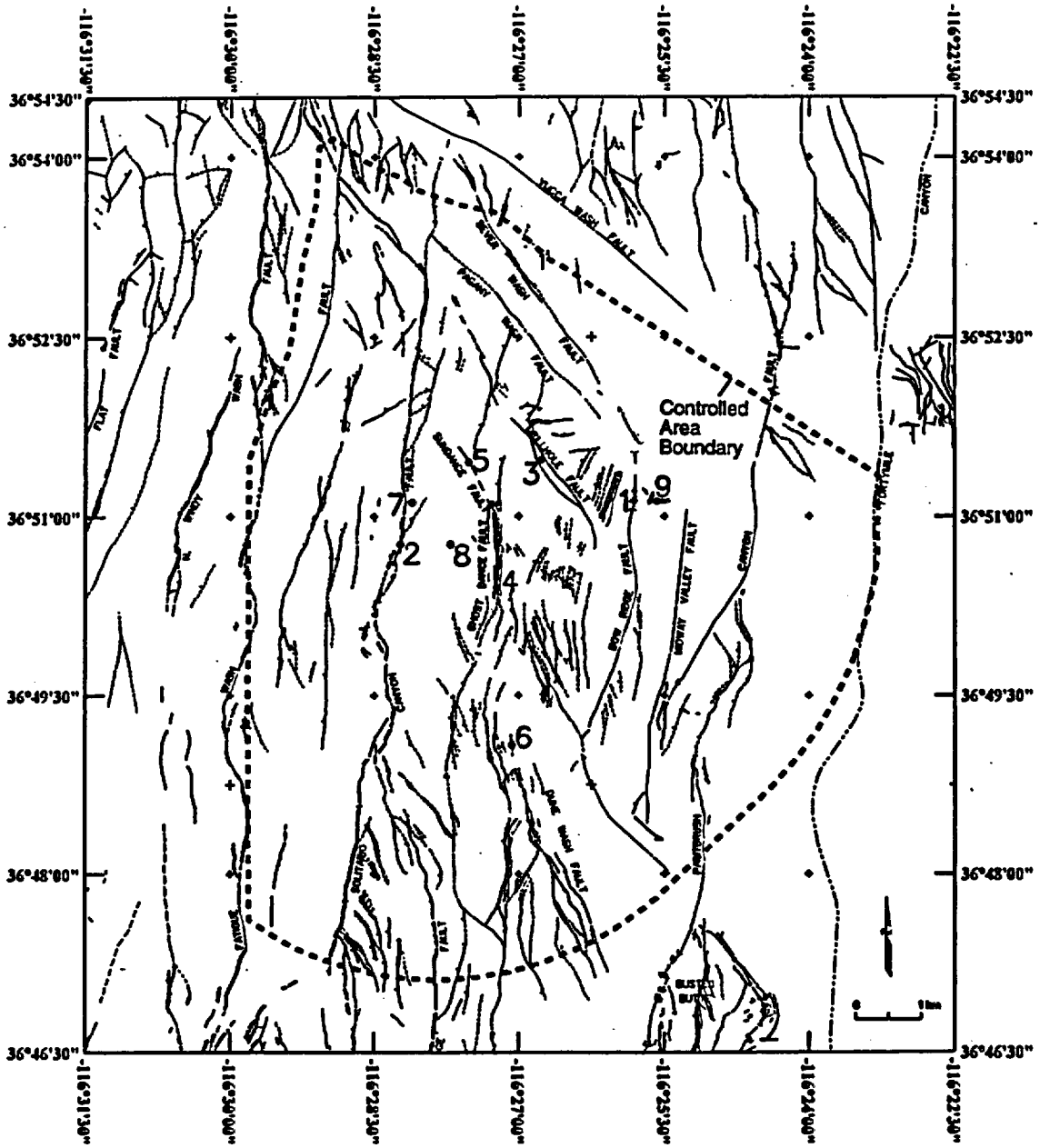

Figure 4-9 Location of nine points for demonstration of fault displacement hazard assessment

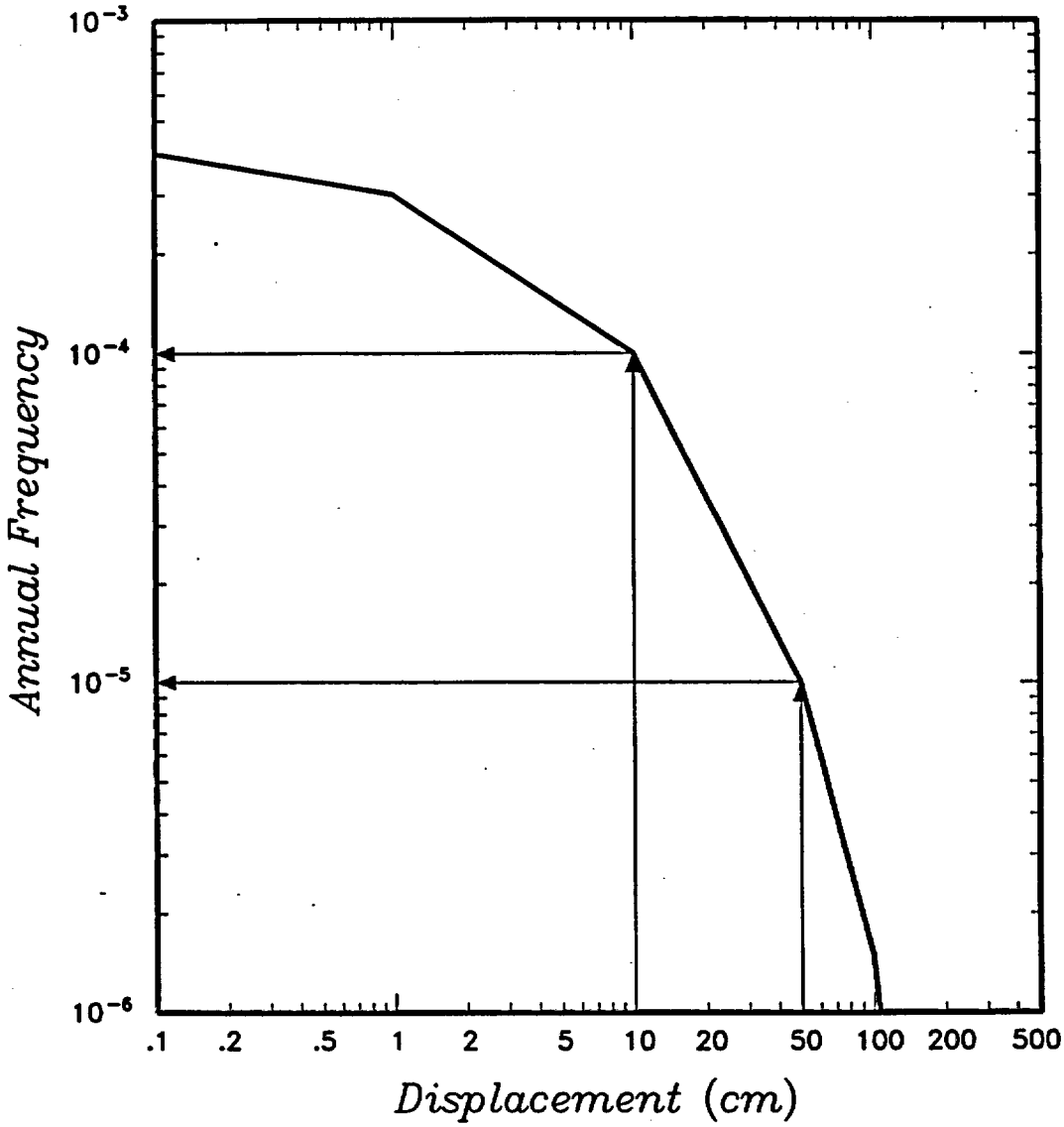

Figure 4-10 Example fault displacement hazard curve

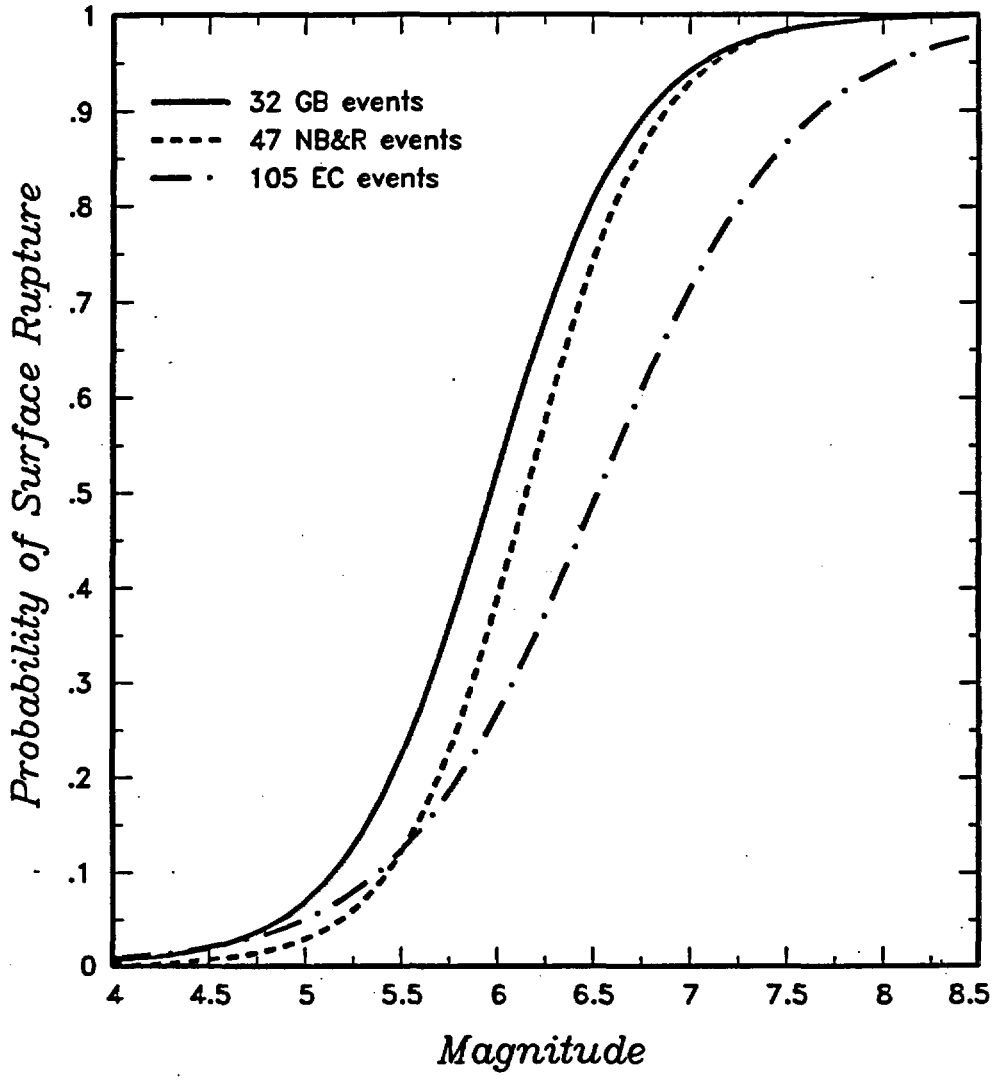

Figure 4-11 Probability of surface rupture as a function of earthquake magnitude computed from various data sets given in Pezzopane and Dawson (1996)

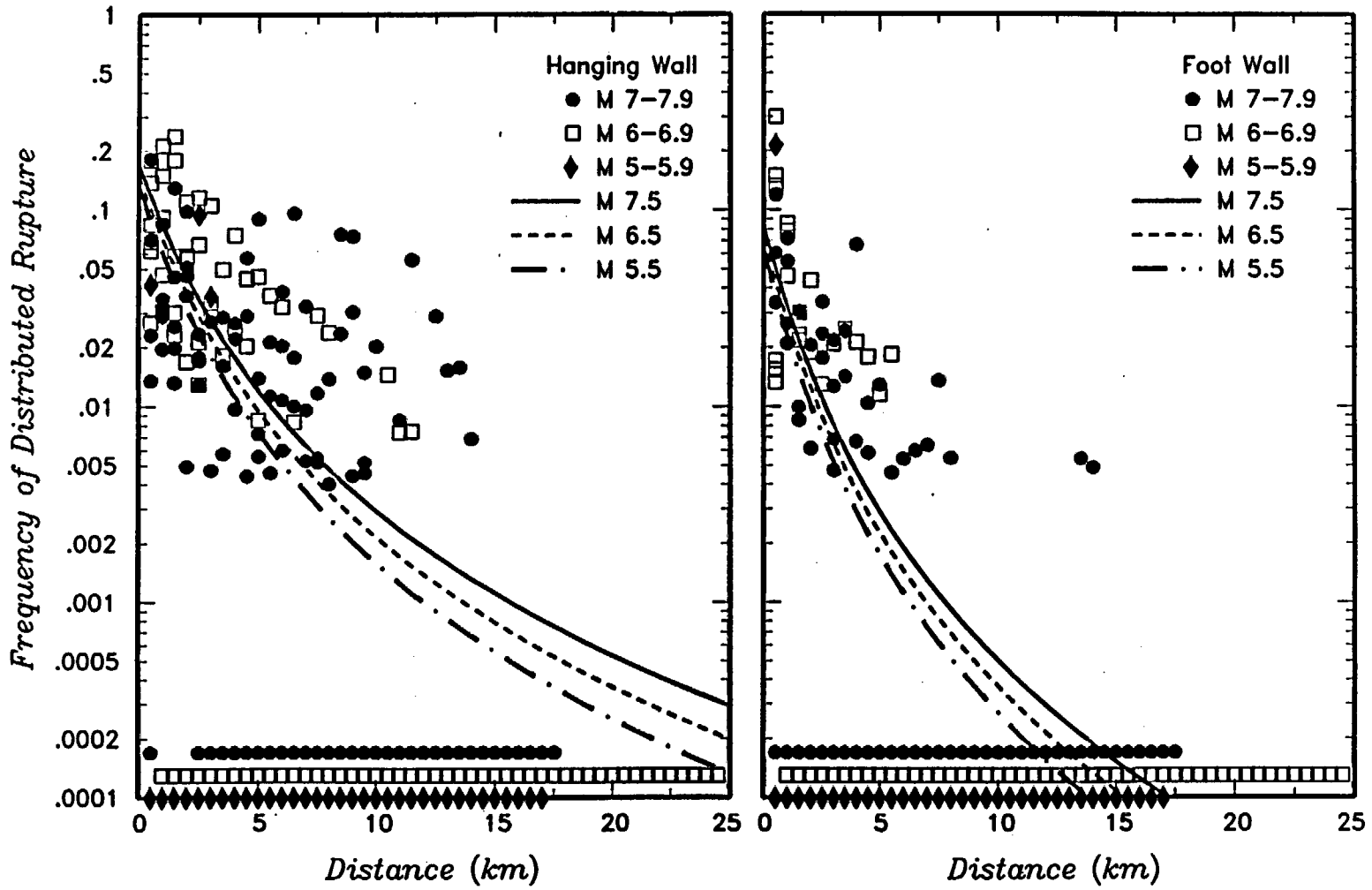

Figure 4-12 Probability of induced distributed slip as a function of distance from the rupture and hanging wall/footwall location computed from the data presented in Pezzopane and Dawson (1996). Curves show logistic regression fits to the data.

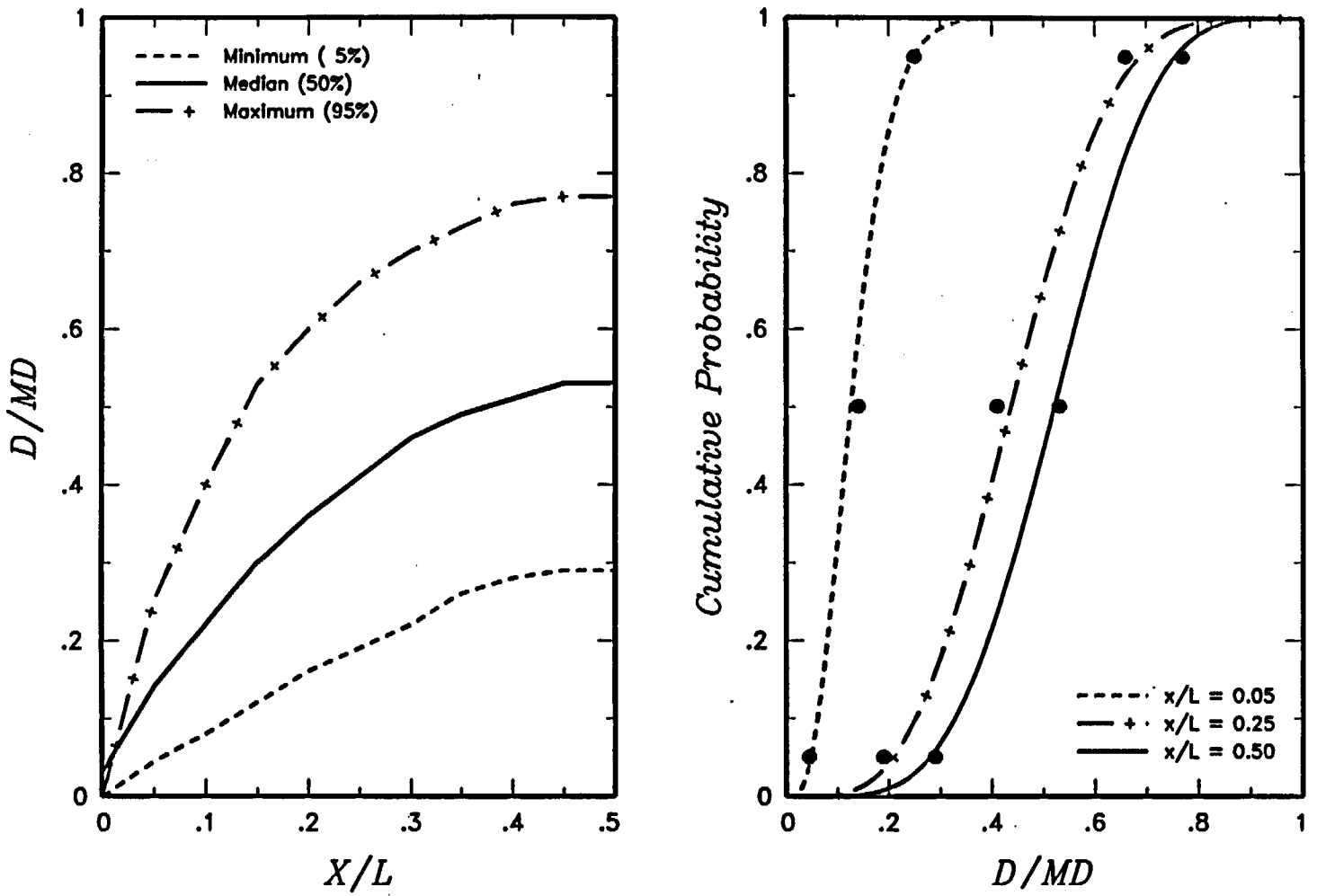

Figure 4-13 Probability distributions for D/MD as a function of location along a principal rupture. Left, smooth curves for minimum, median, and maximum values of D/MD developed by the ASM team from analysis of historical ruptures. Right, Beta distributions fit to the D/MD values at specific values of x/L.

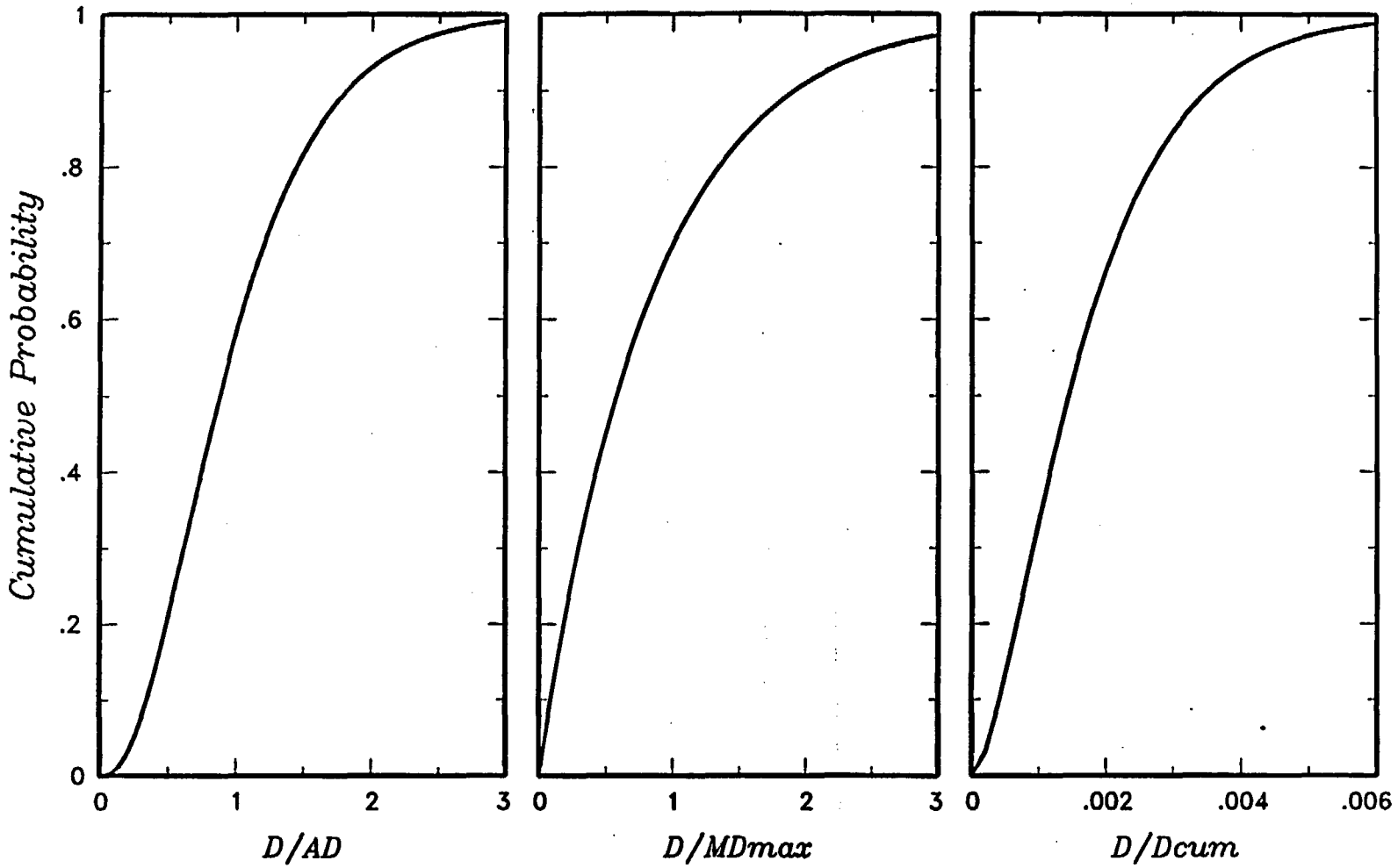

Figure 4-14 Example distributions for computing the conditional probability of exceeding a specific displacement, *d*

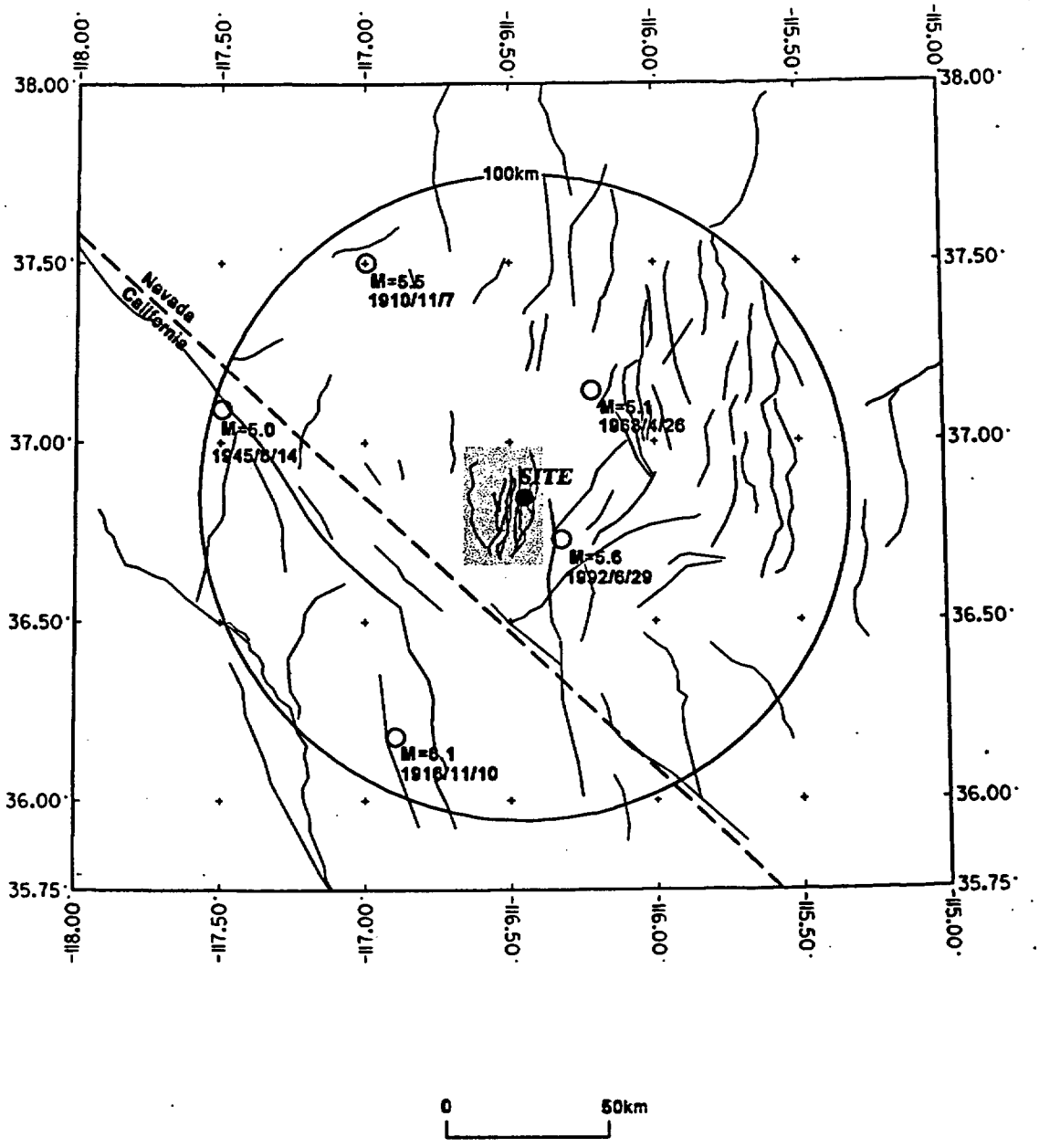

Figure 4-15 Region used for comparison of earthquake recurrence relationships developed from SSFD team models. Also shown are recorded earthquakes of magnitude M_W5 and greater.

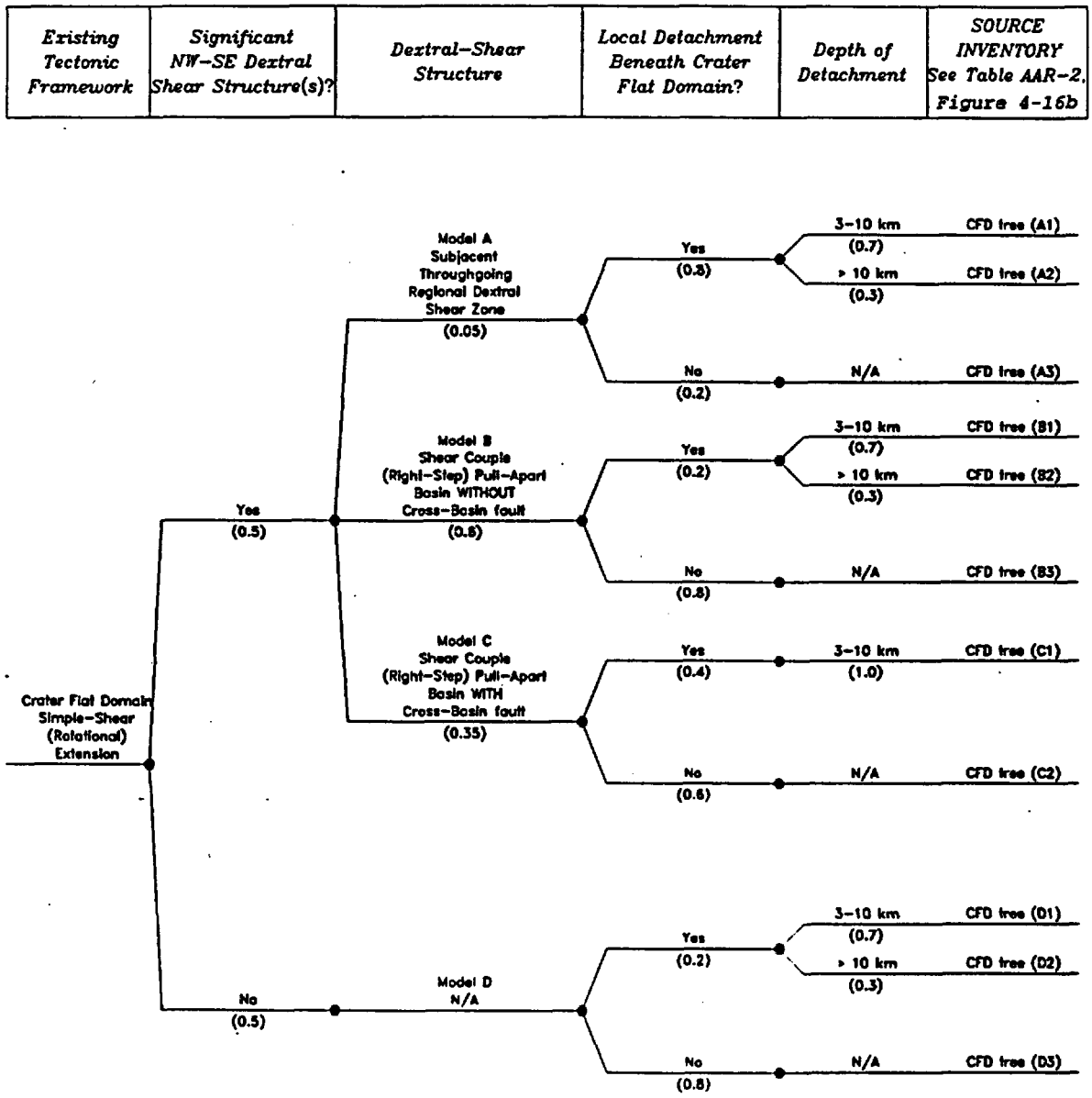

Figure 4-16a Logic tree for local fault source models developed by the AAR team

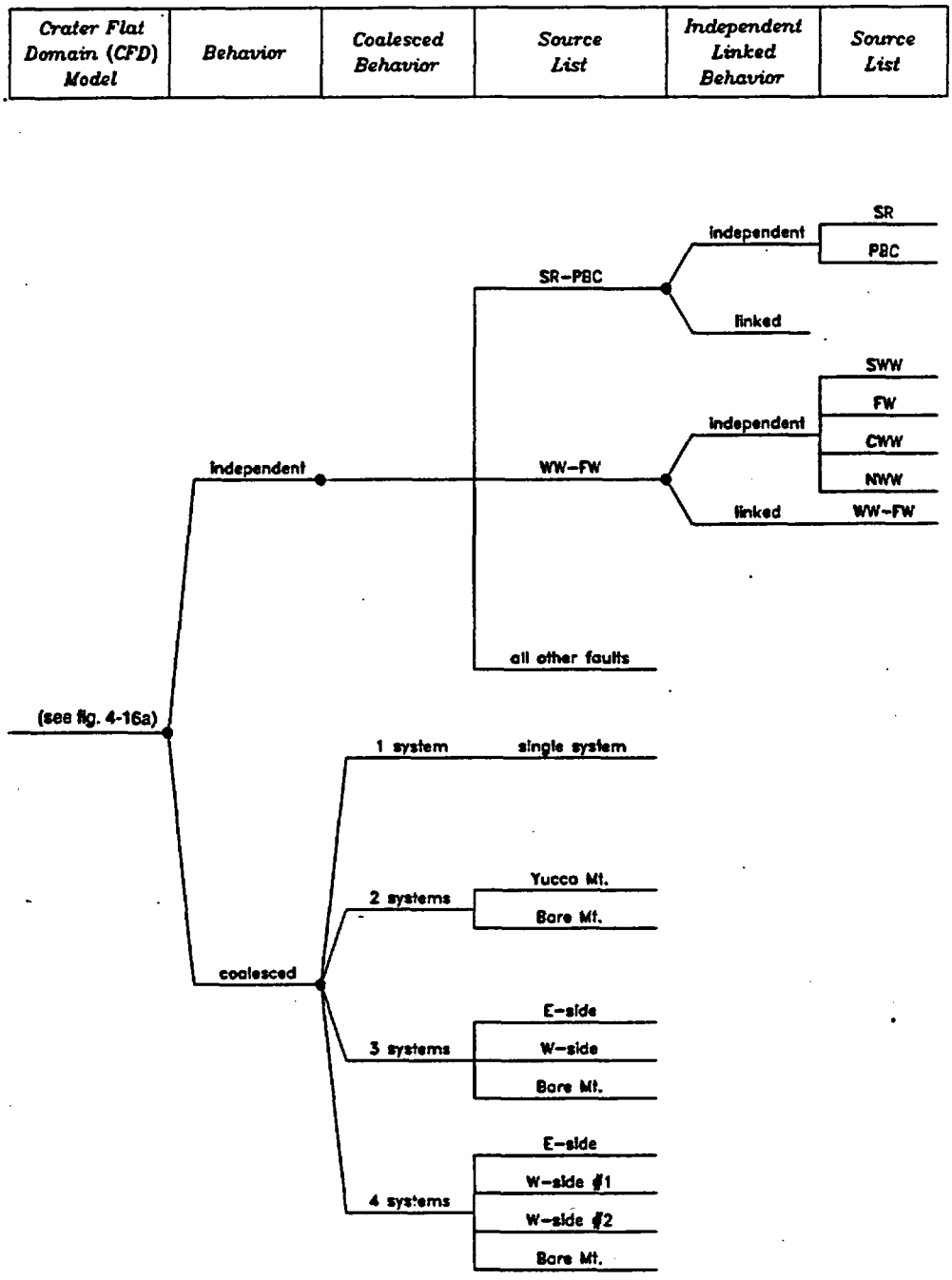

Figure 4-16b Logic tree for local fault source behavior developed by the AAR team

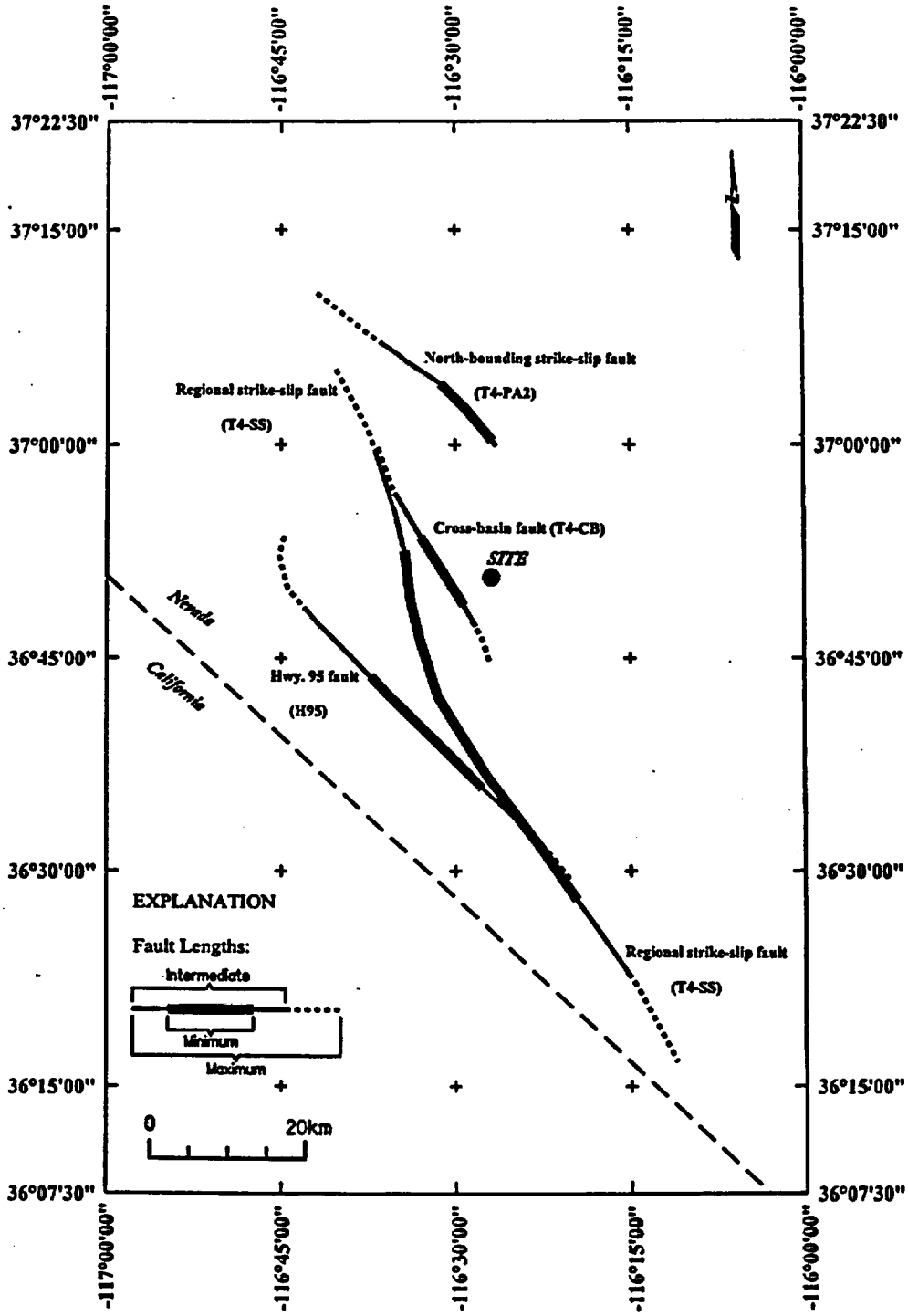

Figure 4-17 Location of AAR team's inferred local dextral shear sources

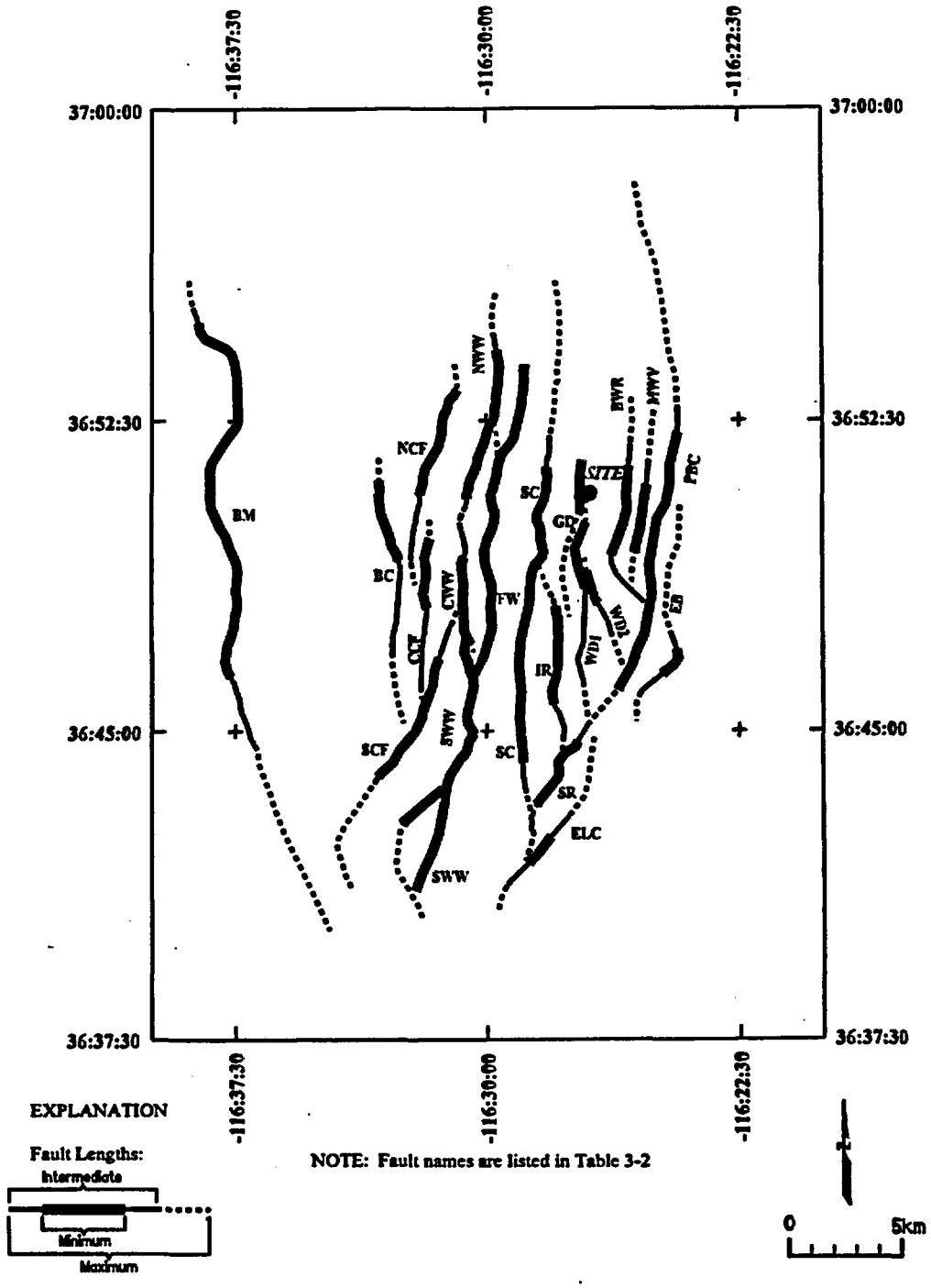

Figure 4-18 Location of local faults considered by the AAR team to be acting as independent sources

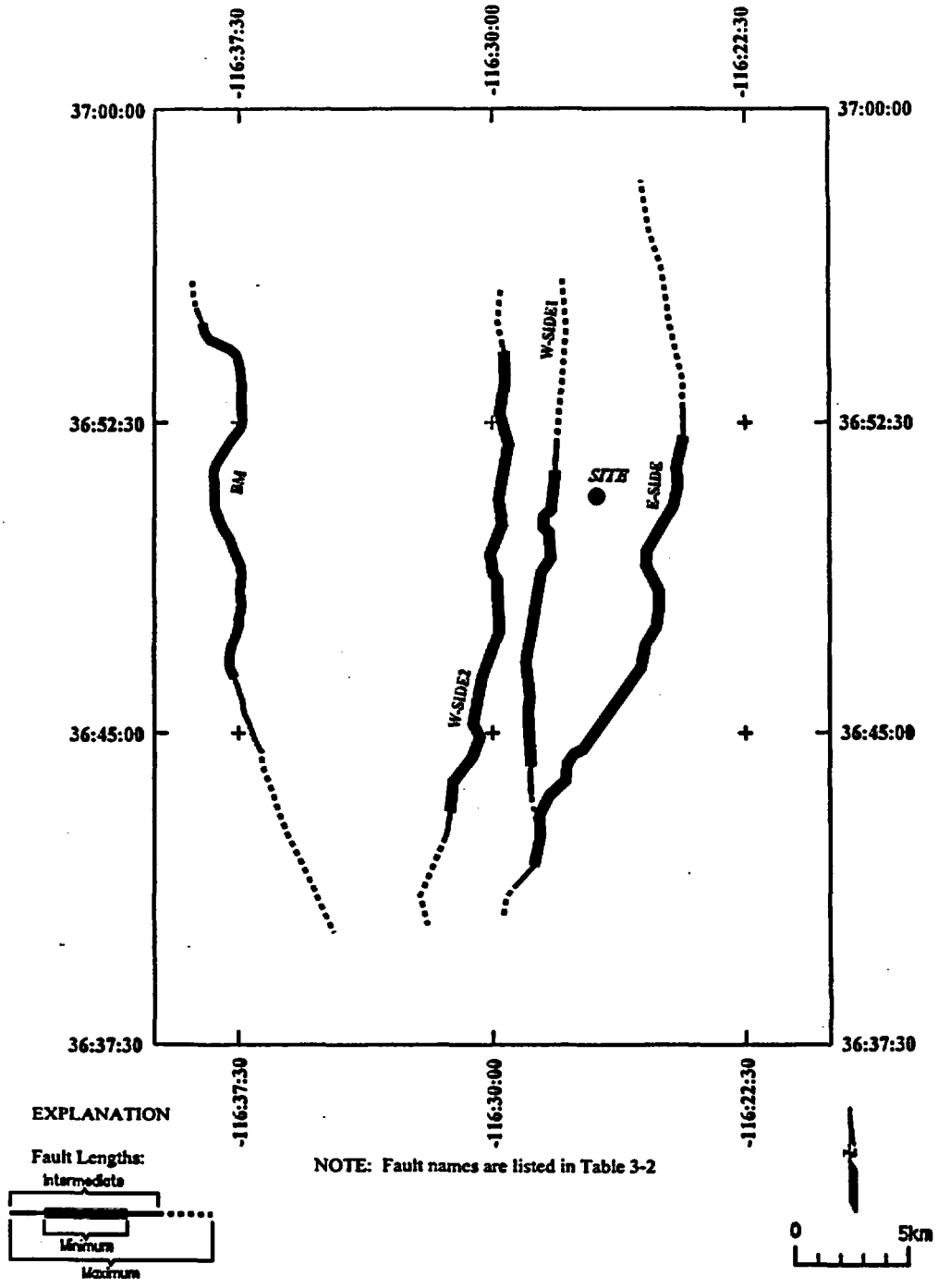

Figure 4-19 Location of coalesced faults considered by the AAR team

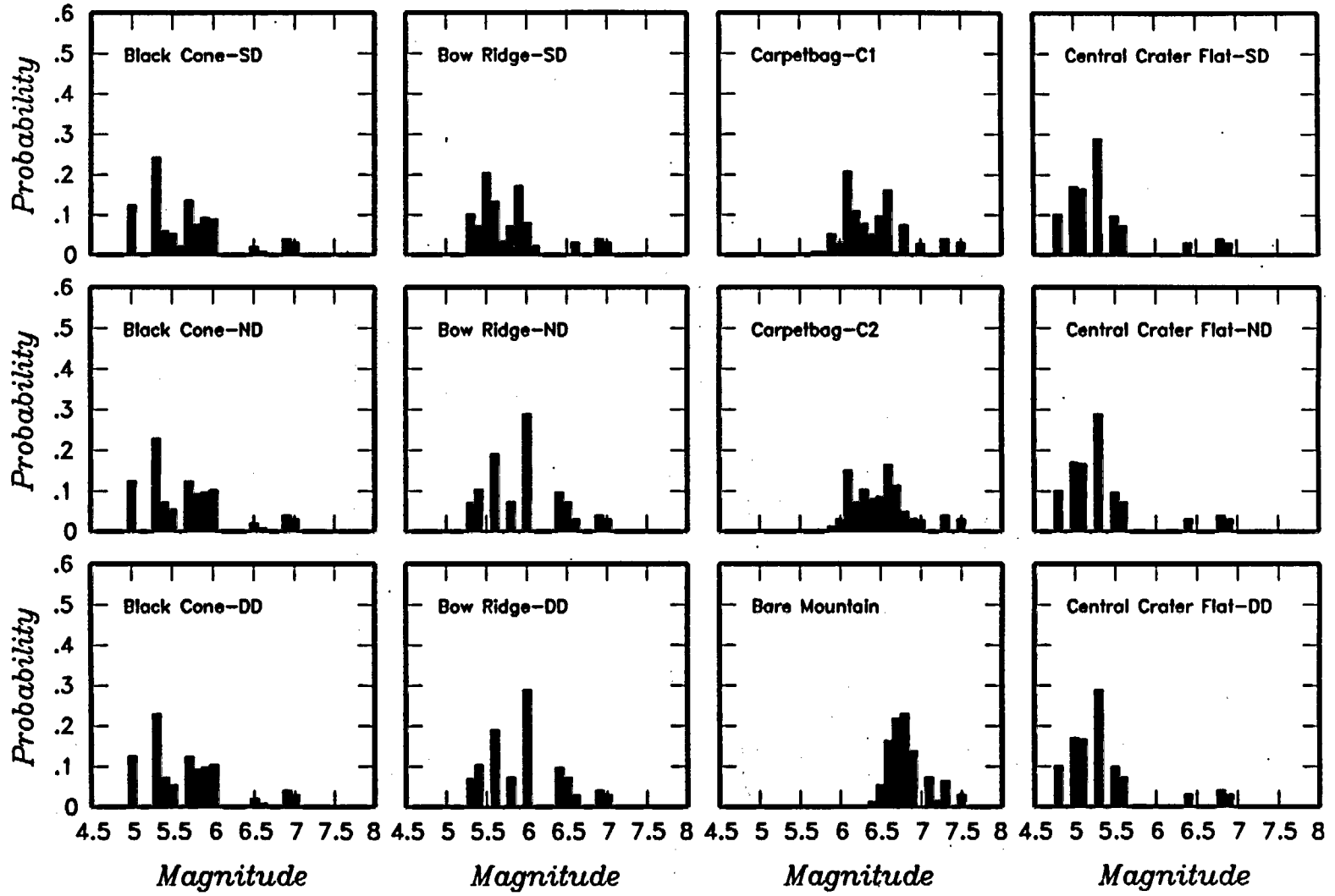

Figure 4-20 Maximum magnitude distributions for AAR team's local fault sources. A, B, and C and numbers refer to variations of tectonic models A, B, and C; DD–deep detachment, ND–no detachment, SD-shallow detachment, SINGLE–single rupture (BM and YM faults), Single west-side rupture of west-side faults (WS1+WS2), Single Yucca Mountain–coalesced single YM system.

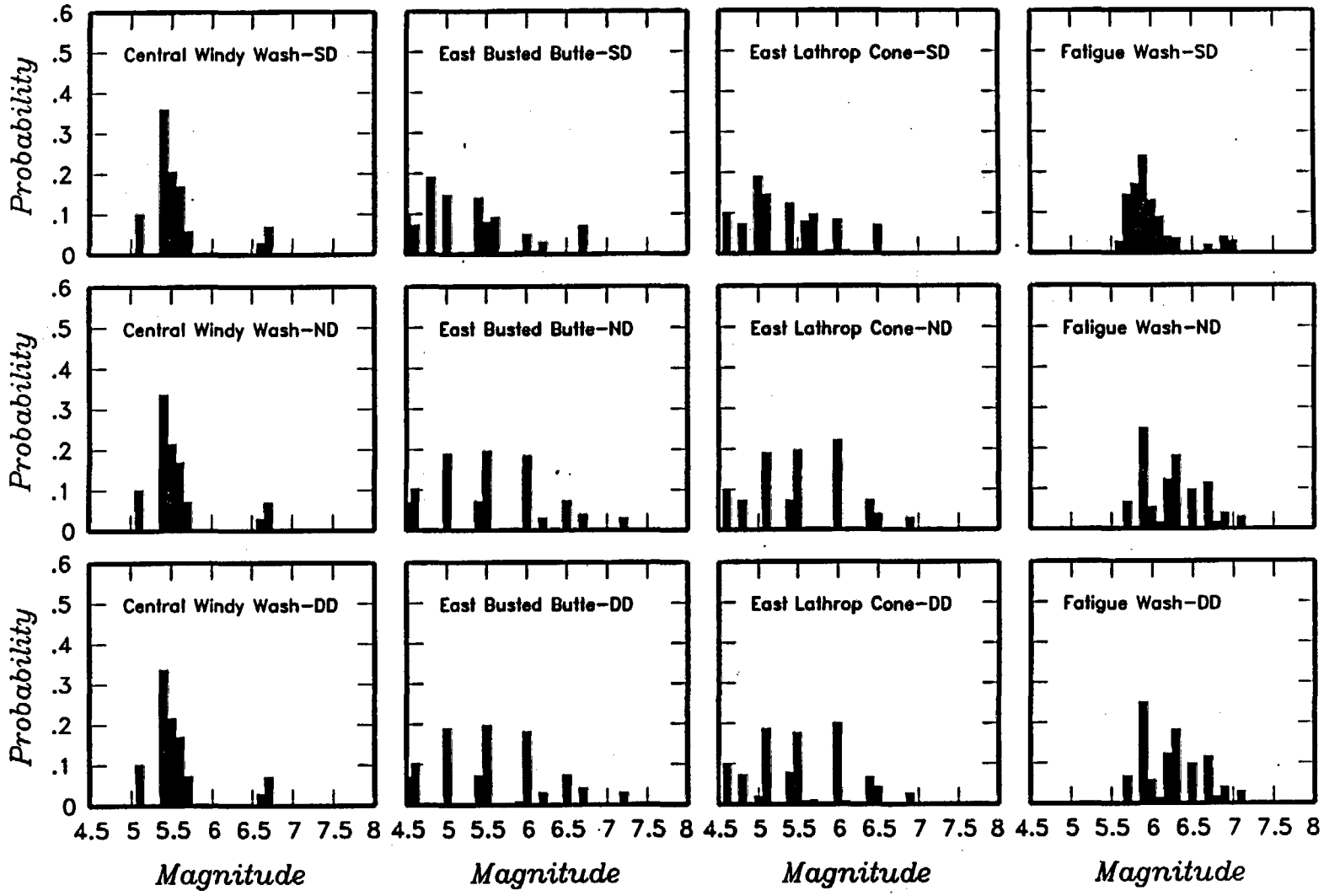

Figure 4-20 (Cont'd.) Maximum magnitude distributions for AAR team's local fault sources

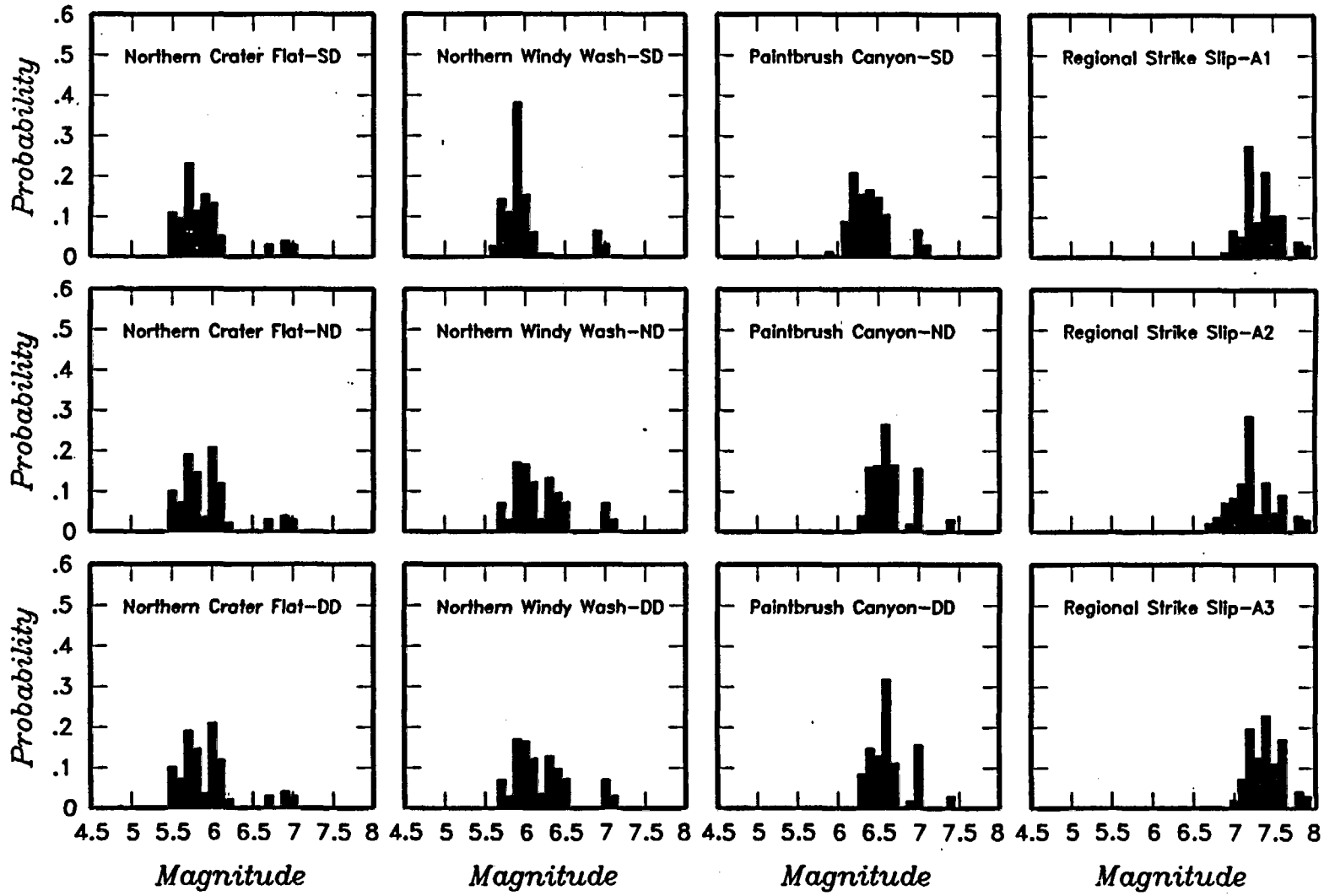

Figure 4-20 (Cont'd.) Maximum magnitude distributions for AAR team's local fault sources

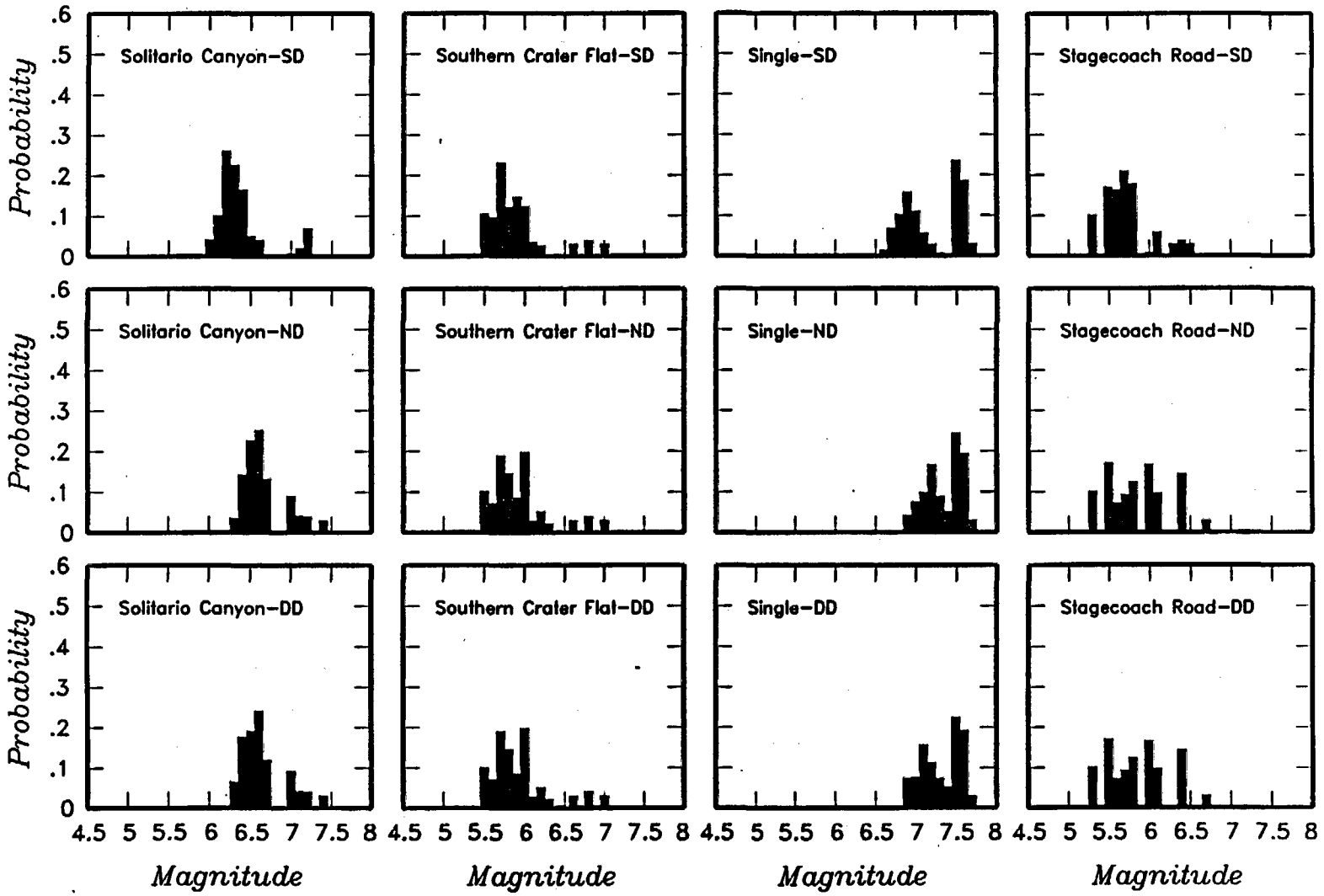

Figure 4-20 (Cont'd.) Maximum magnitude distributions for AAR team's local fault sources

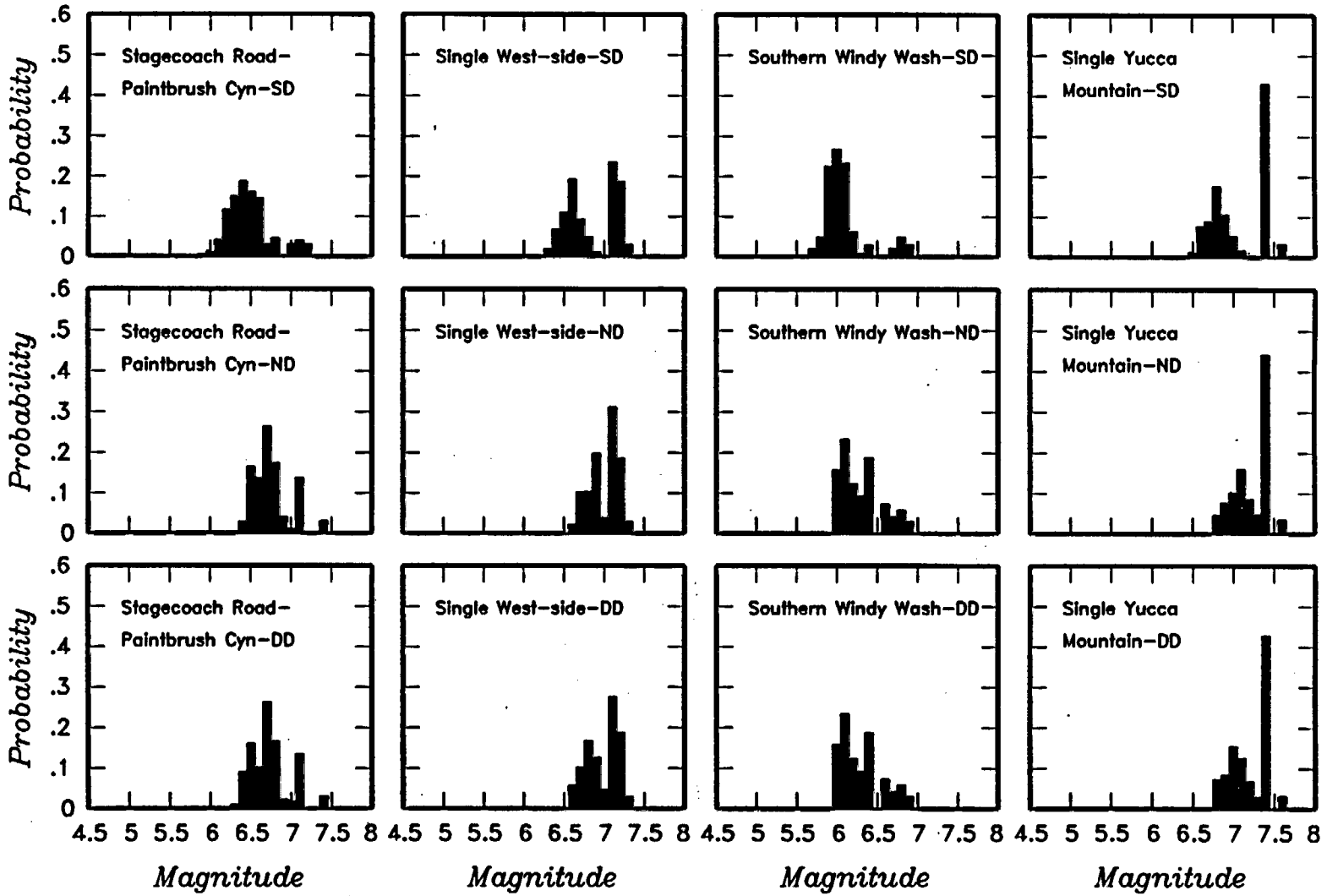

Figure 4-20 (Cont'd.) Maximum magnitude distributions for AAR team's local fault sources

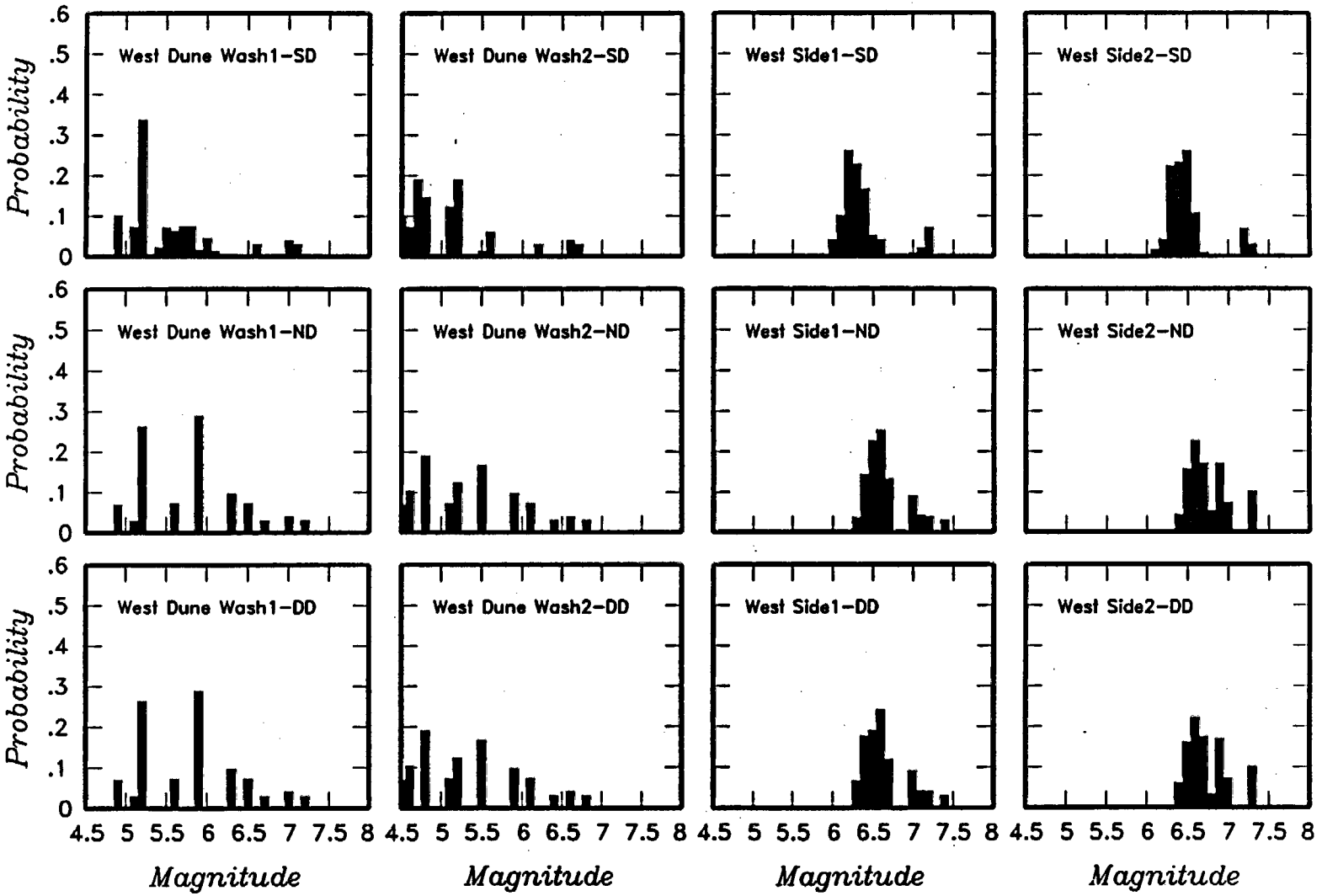

Figure 4-20 (Cont'd.) Maximum magnitude distributions for AAR team's local fault sources

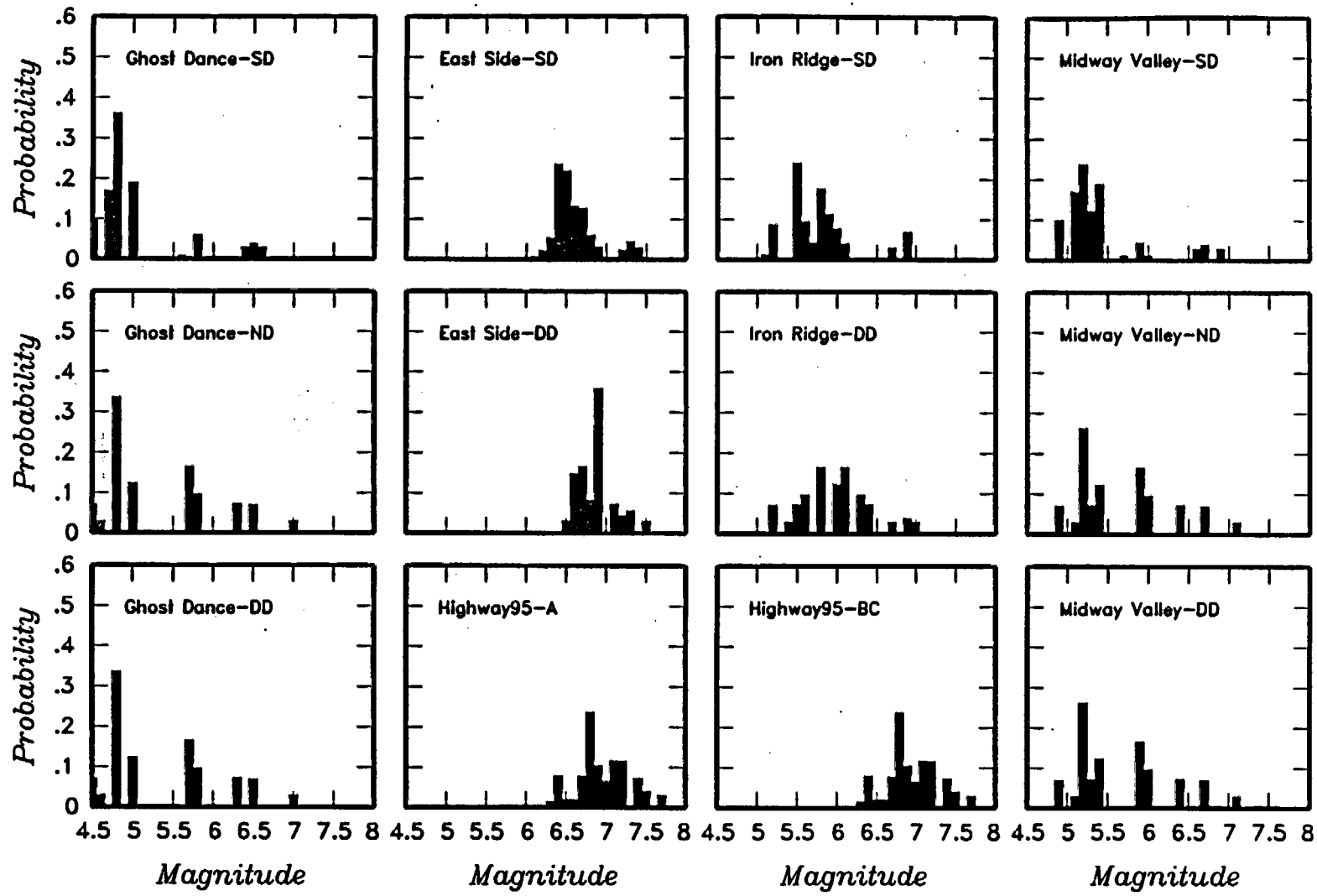

Figure 4-20 (Cont'd.) Maximum magnitude distributions for AAR team's local fault sources

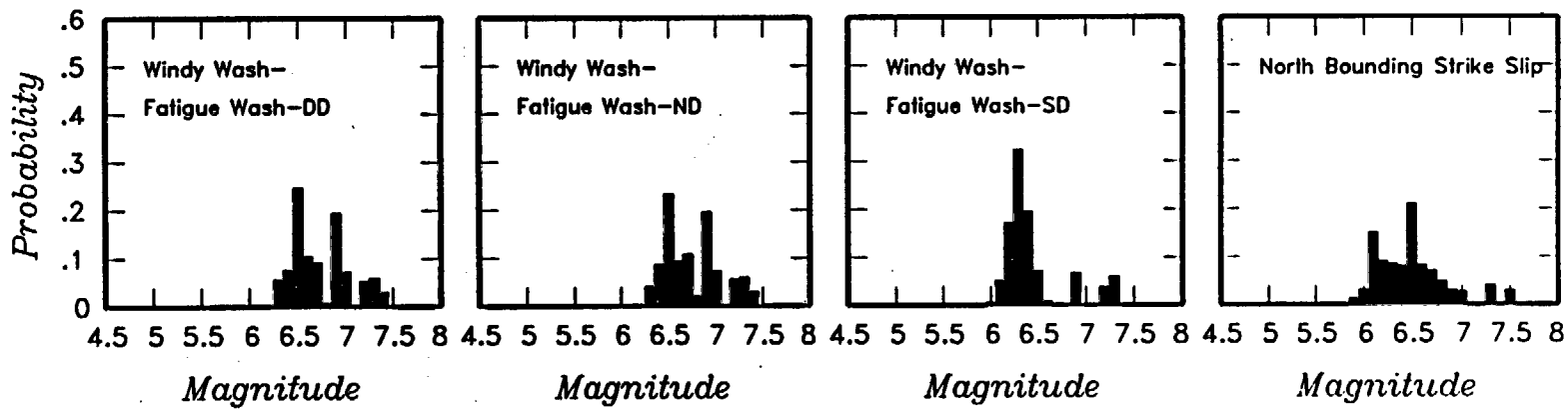

Figure 4-20 (Cont'd.) Maximum magnitude distributions for AAR team's local fault sources

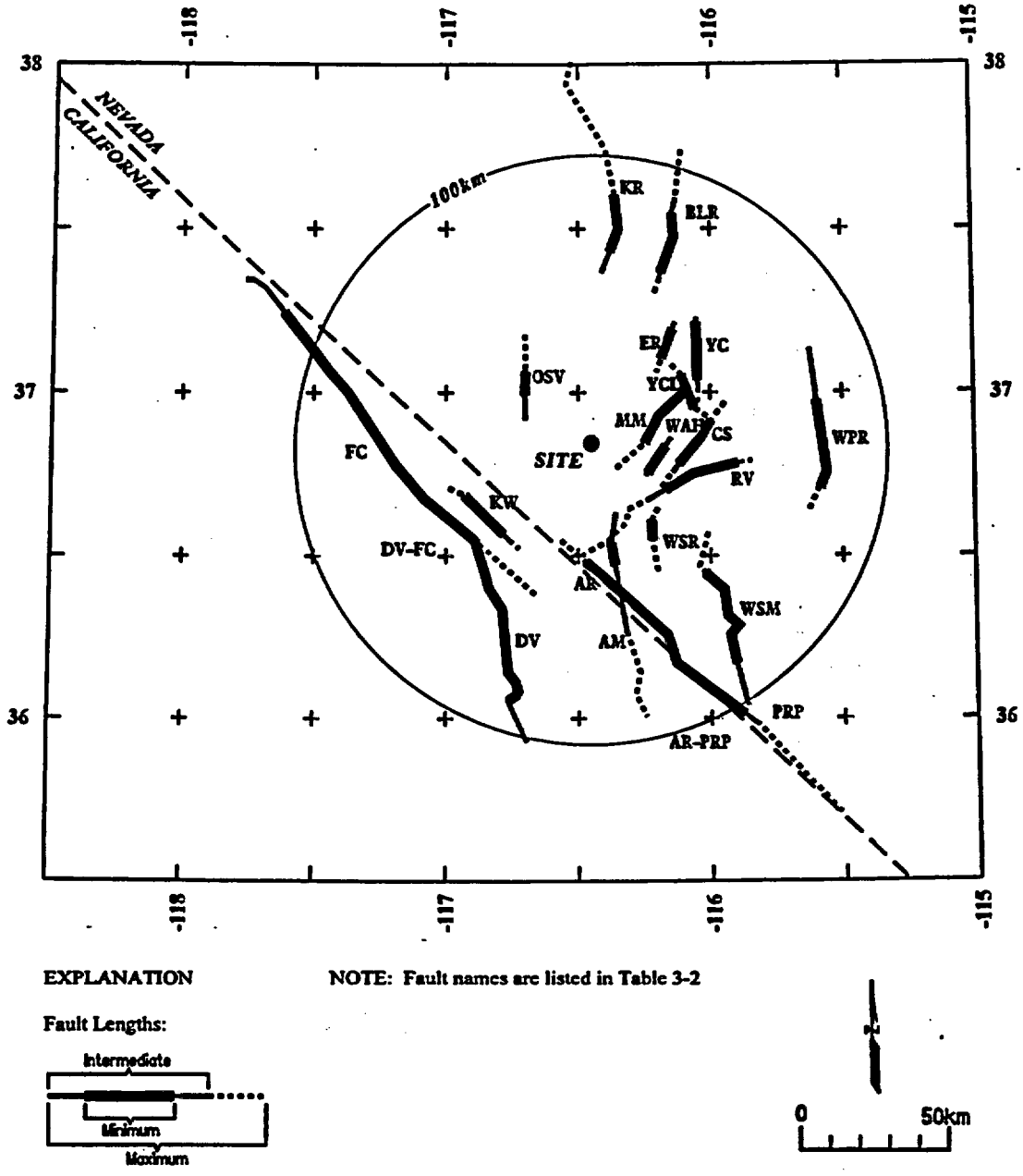

Figure 4-21 Regional fault sources considered by the AAR team

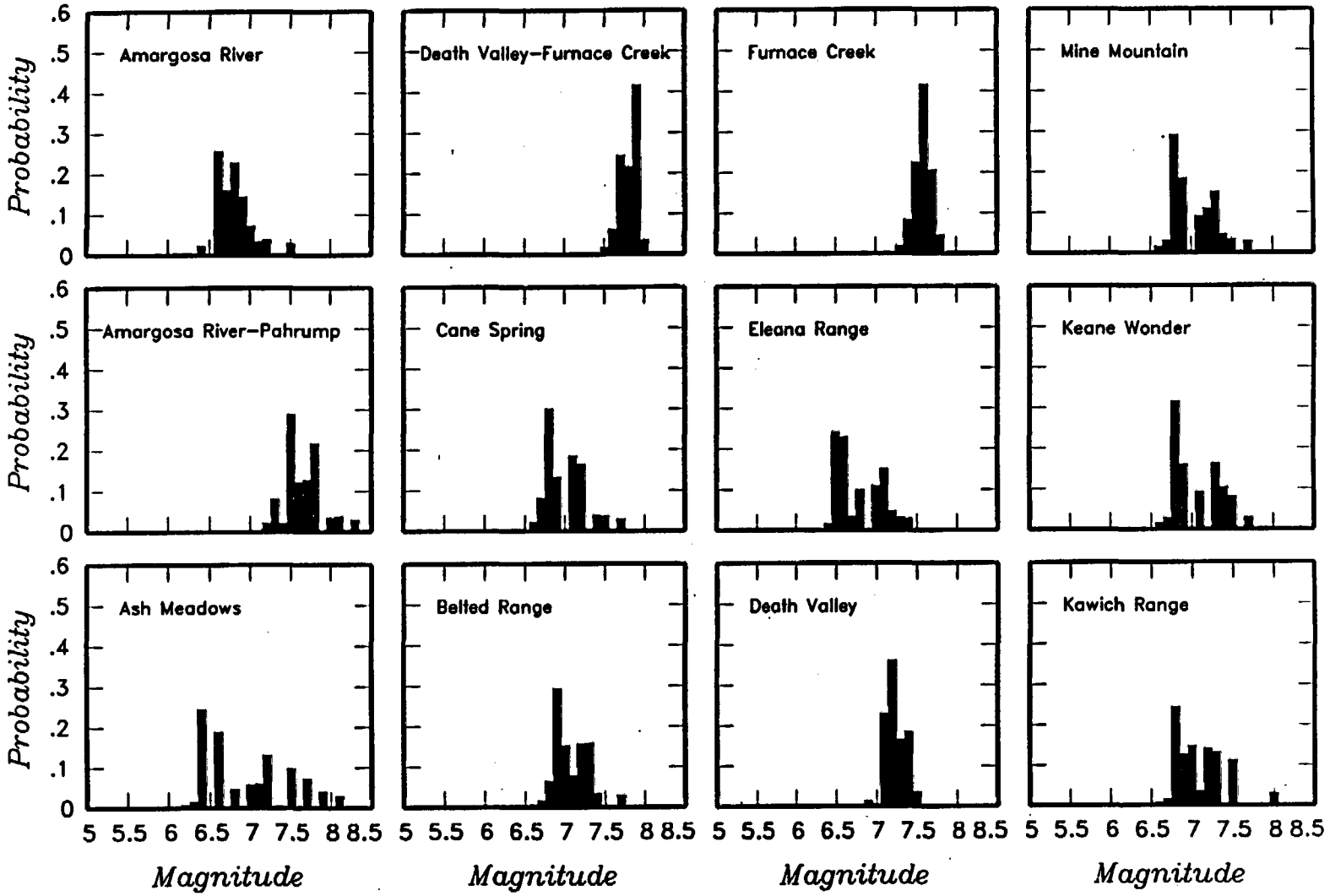

Figure 4-22 Maximum magnitude distributions for AAR team's regional fault sources

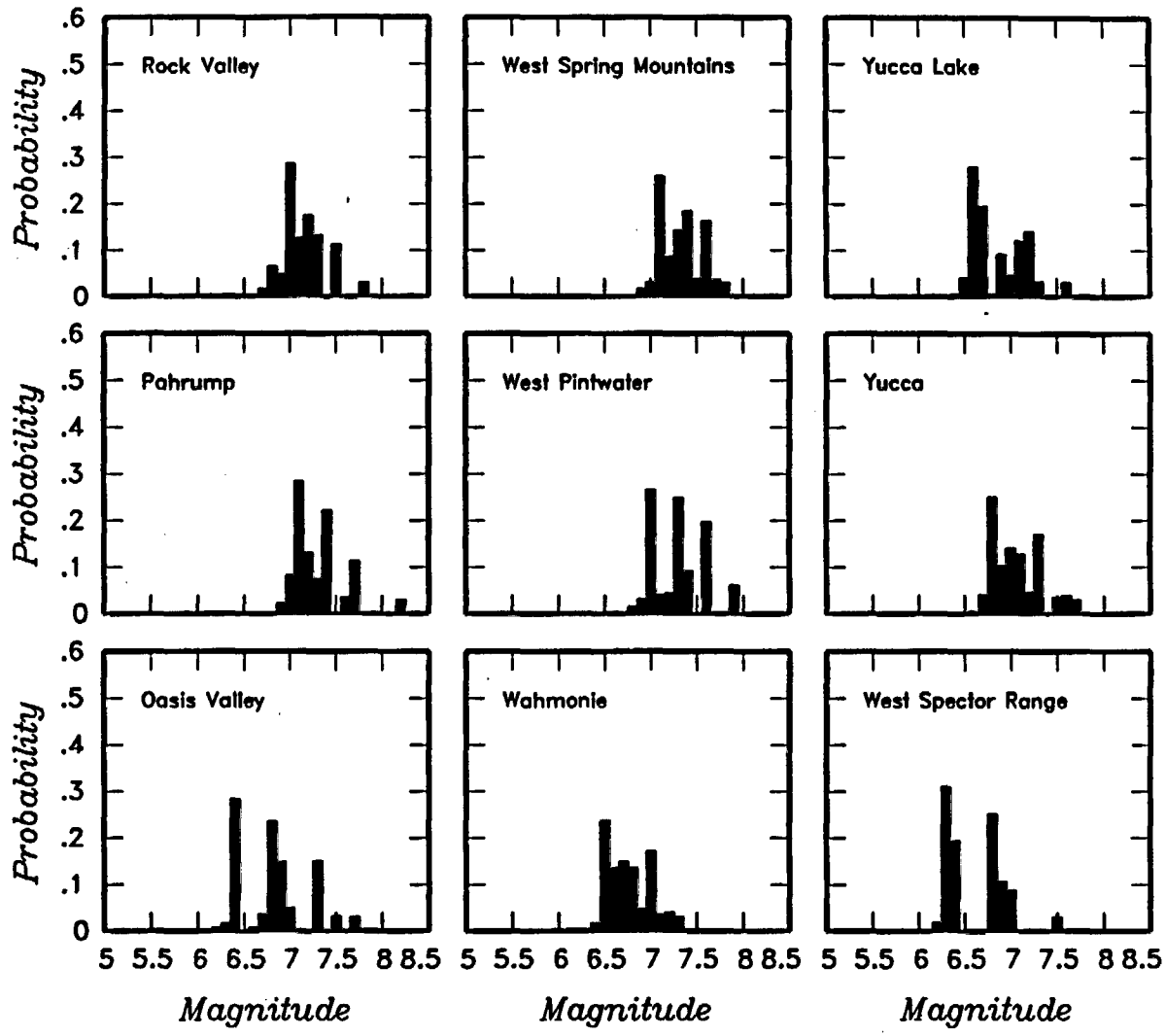

Figure 4-22 (Cont'd.) Maximum magnitude distributions for AAR team's regional fault sources

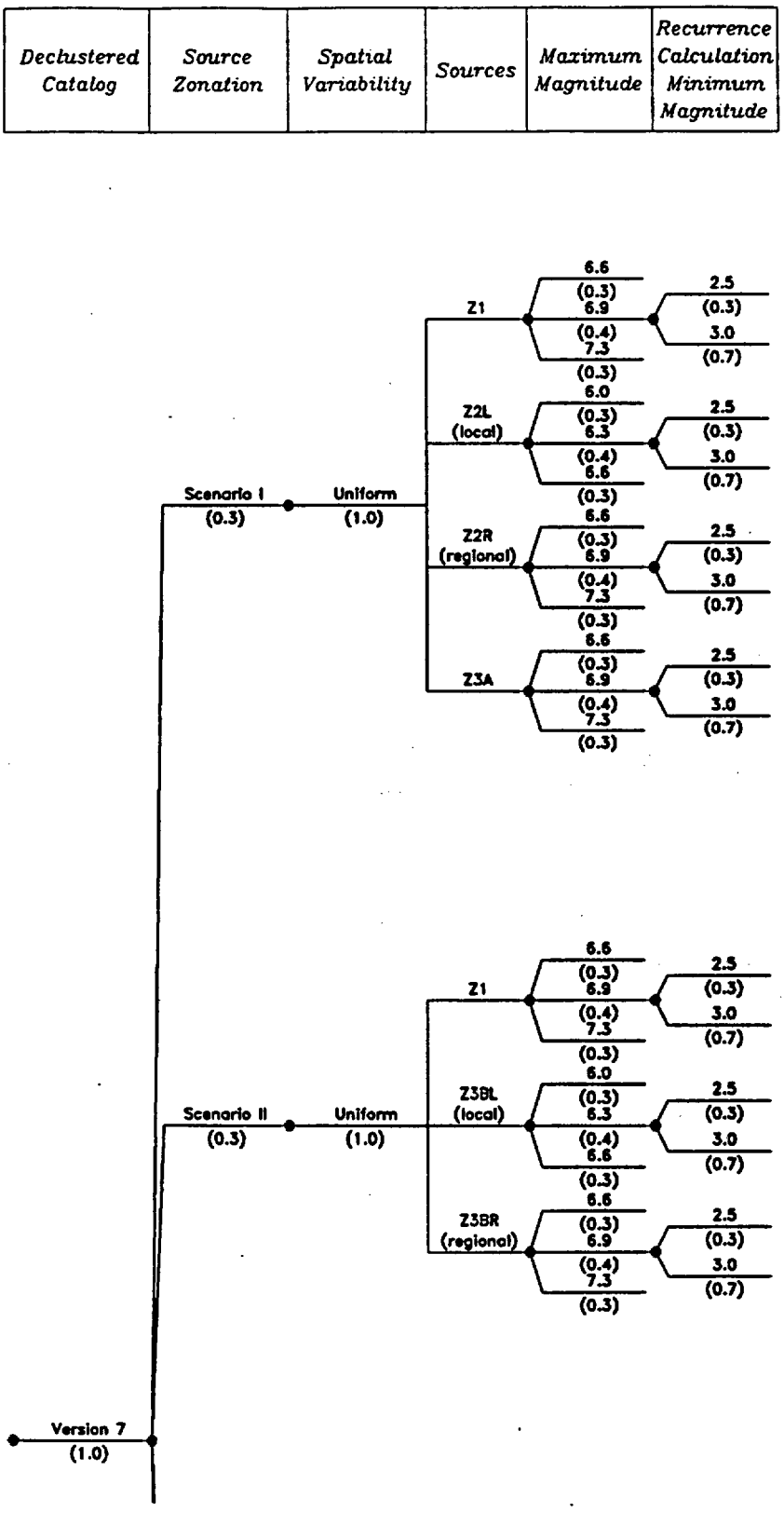

Figure 4-23 Logic tree for regional source zones developed by the AAR team

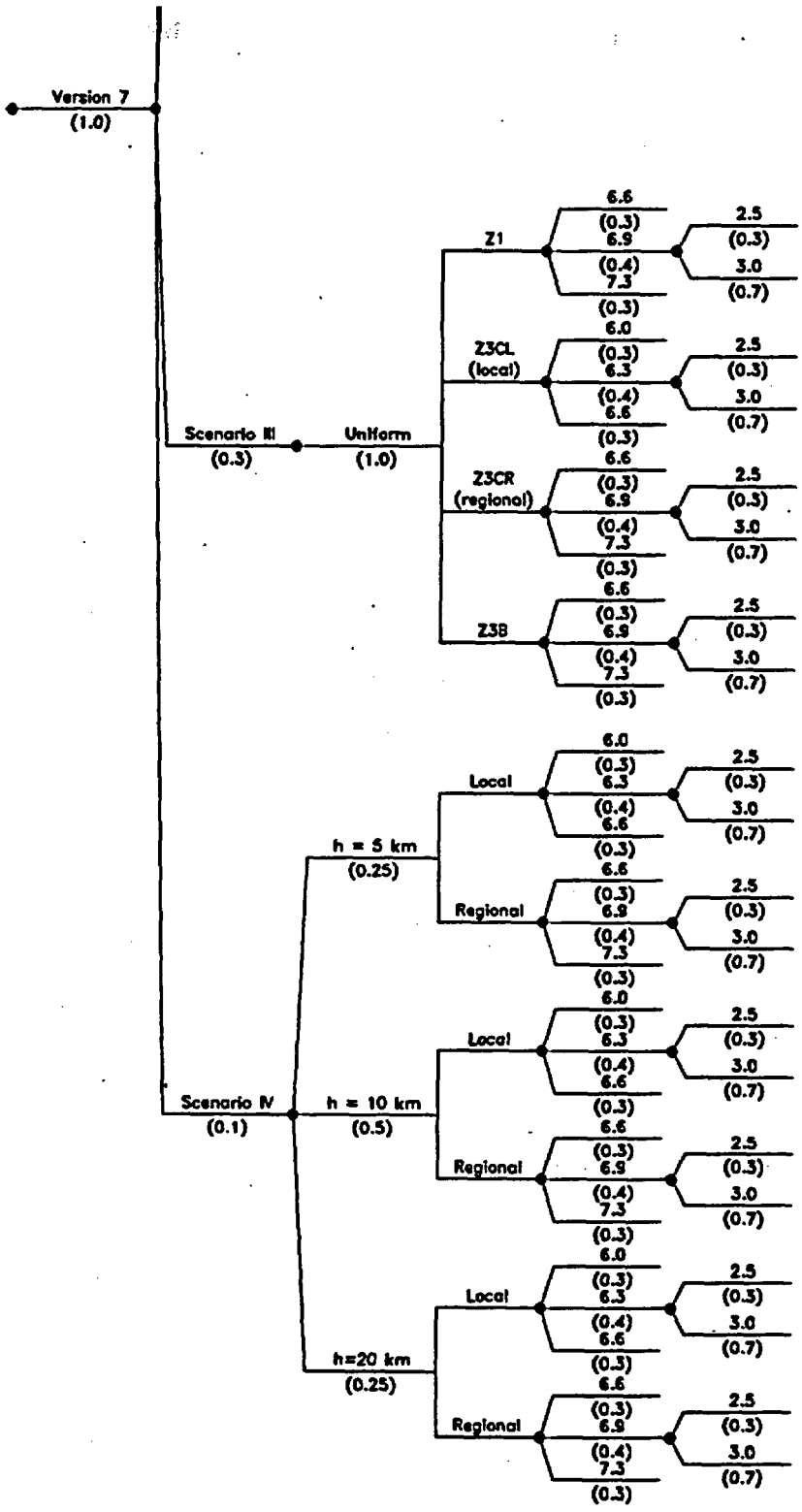

Figure 4-23 (Cont'd.) Logic tree for regional source zones developed by the AAR team

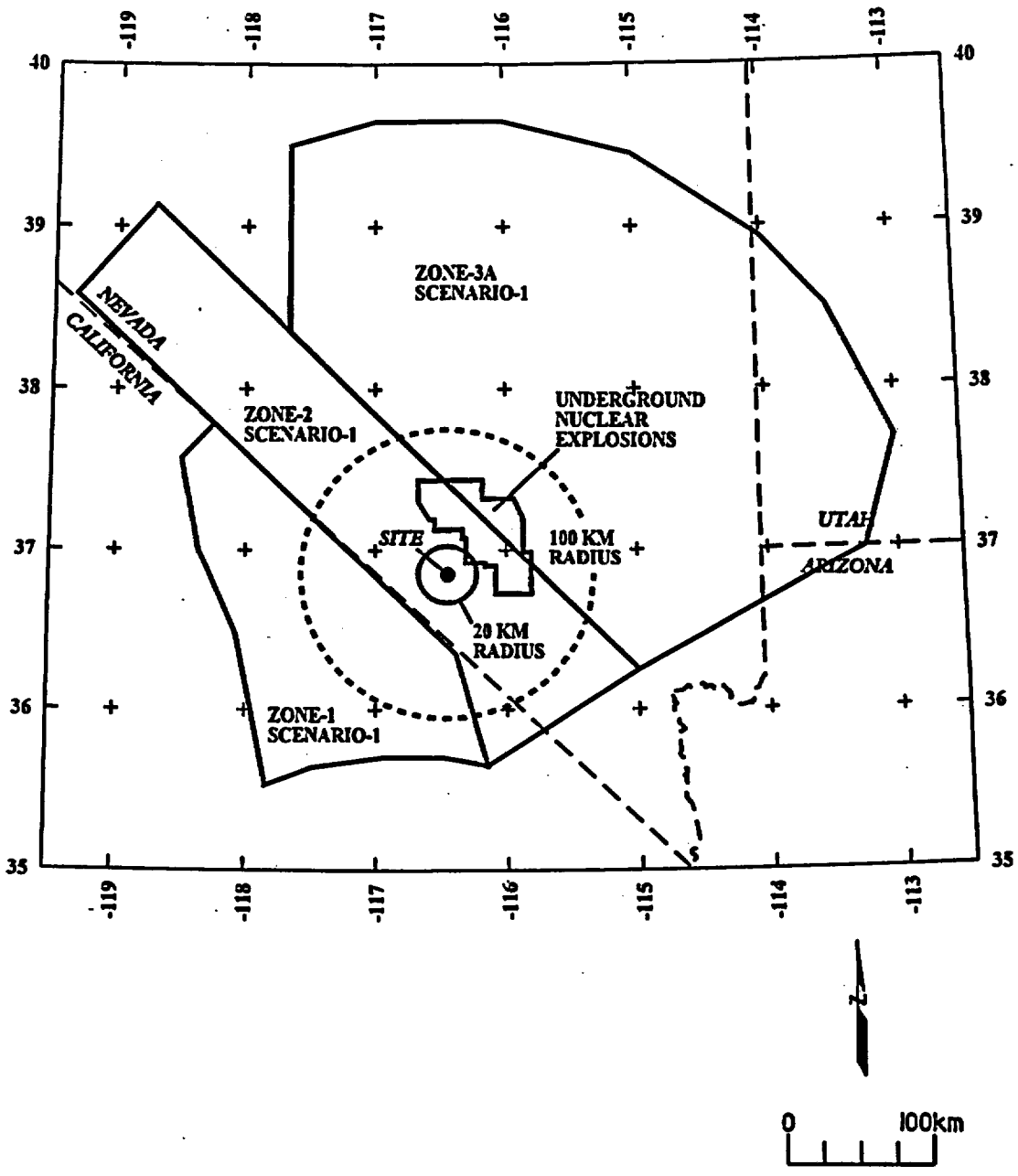

Figure 4-24 Alternative regional source zone models considered by the AAR team

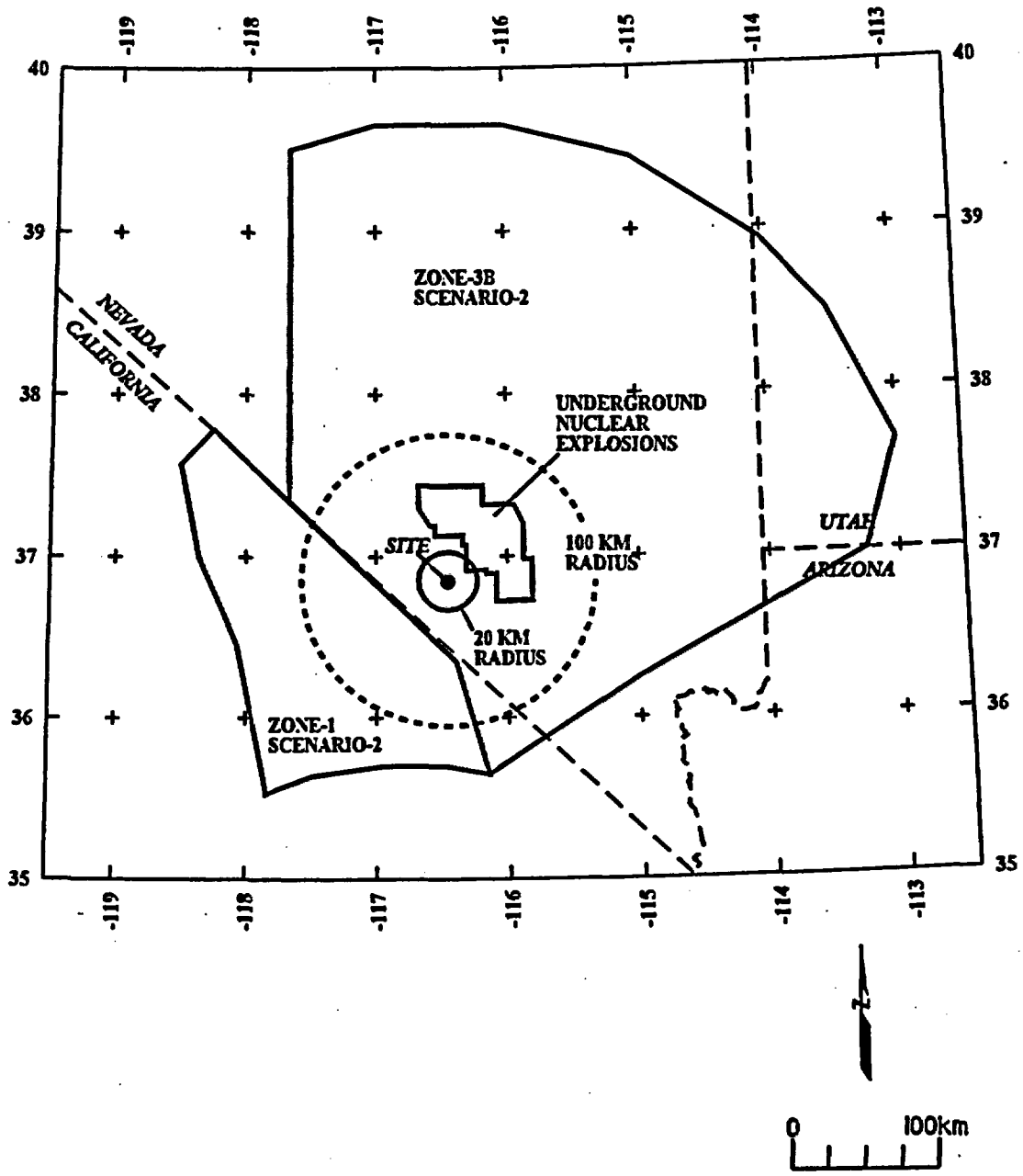

Figure 4-24 (Cont'd.) Alternative regional source zone models considered by the AAR team

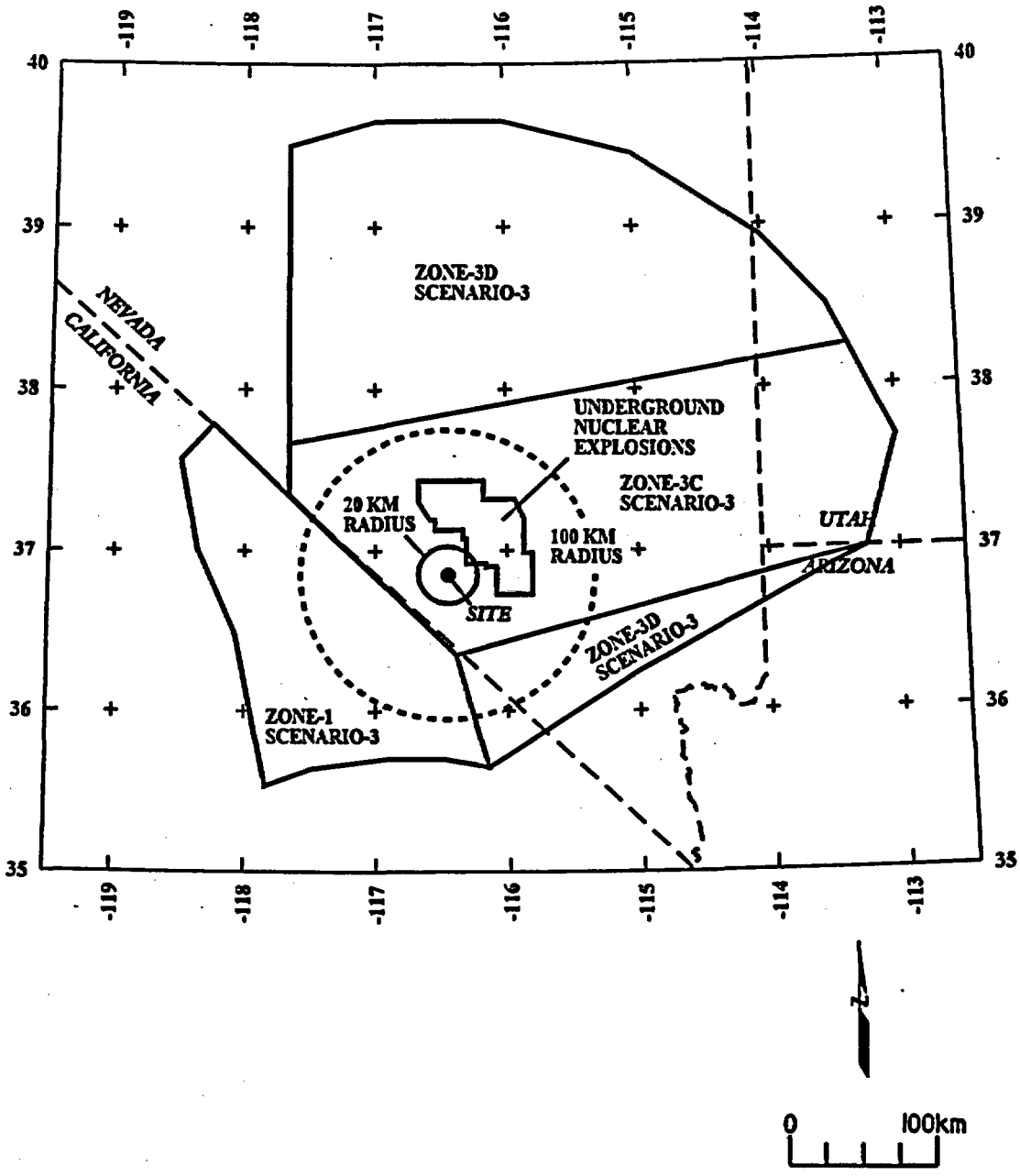

Figure 4-24 (Cont'd.) Alternative regional source zone models considered by the AAR team

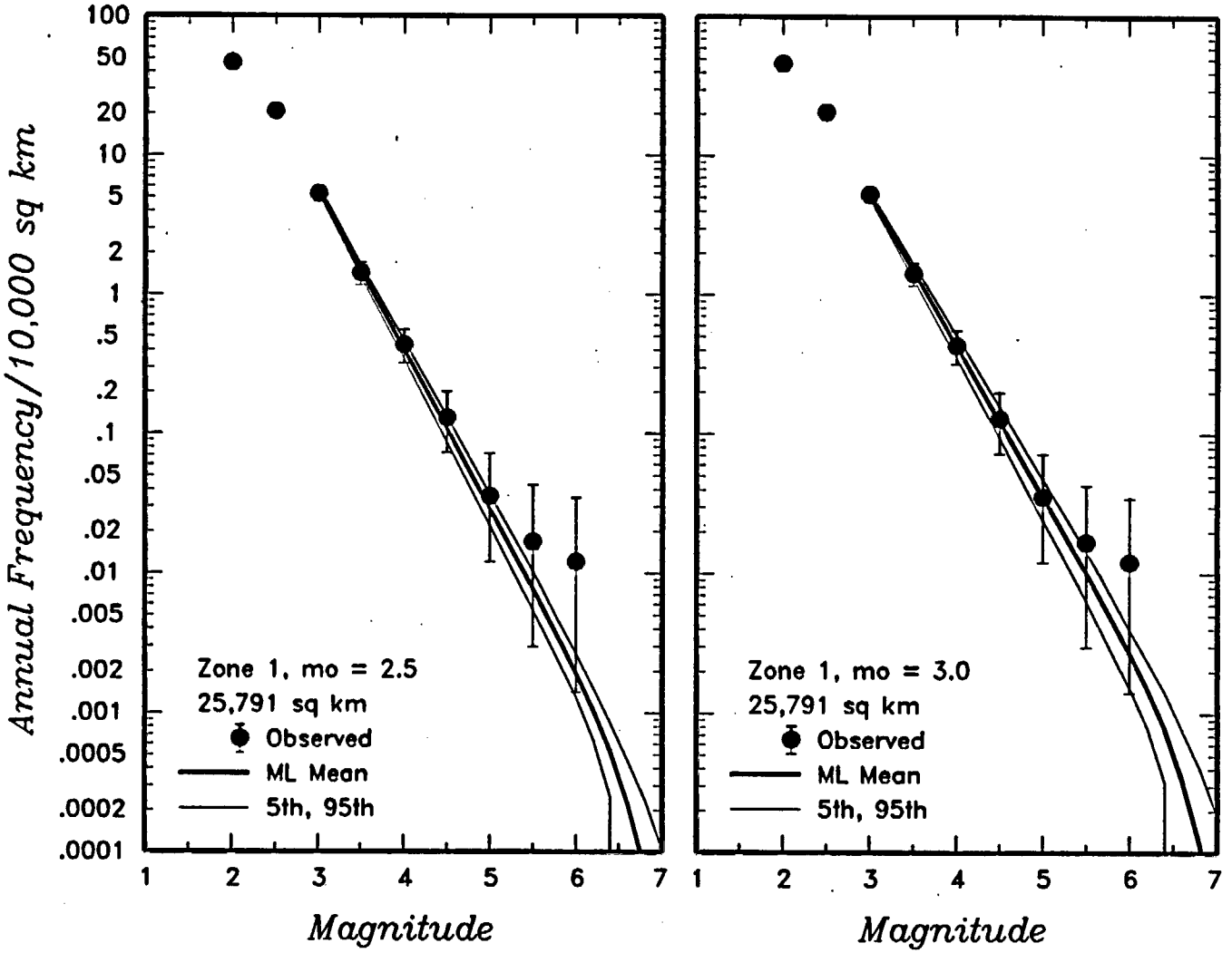

Figure 4-25 Earthquake recurrence relationships for the regional source zones defined by the AAR team. The solid dots with vertical error bars represent the observed data. The thick and thin solid curves are the mean, 5th, and 95th percentiles of the recurrence rates based on the uncertainty in recurrence parameters and maximum magnitude.

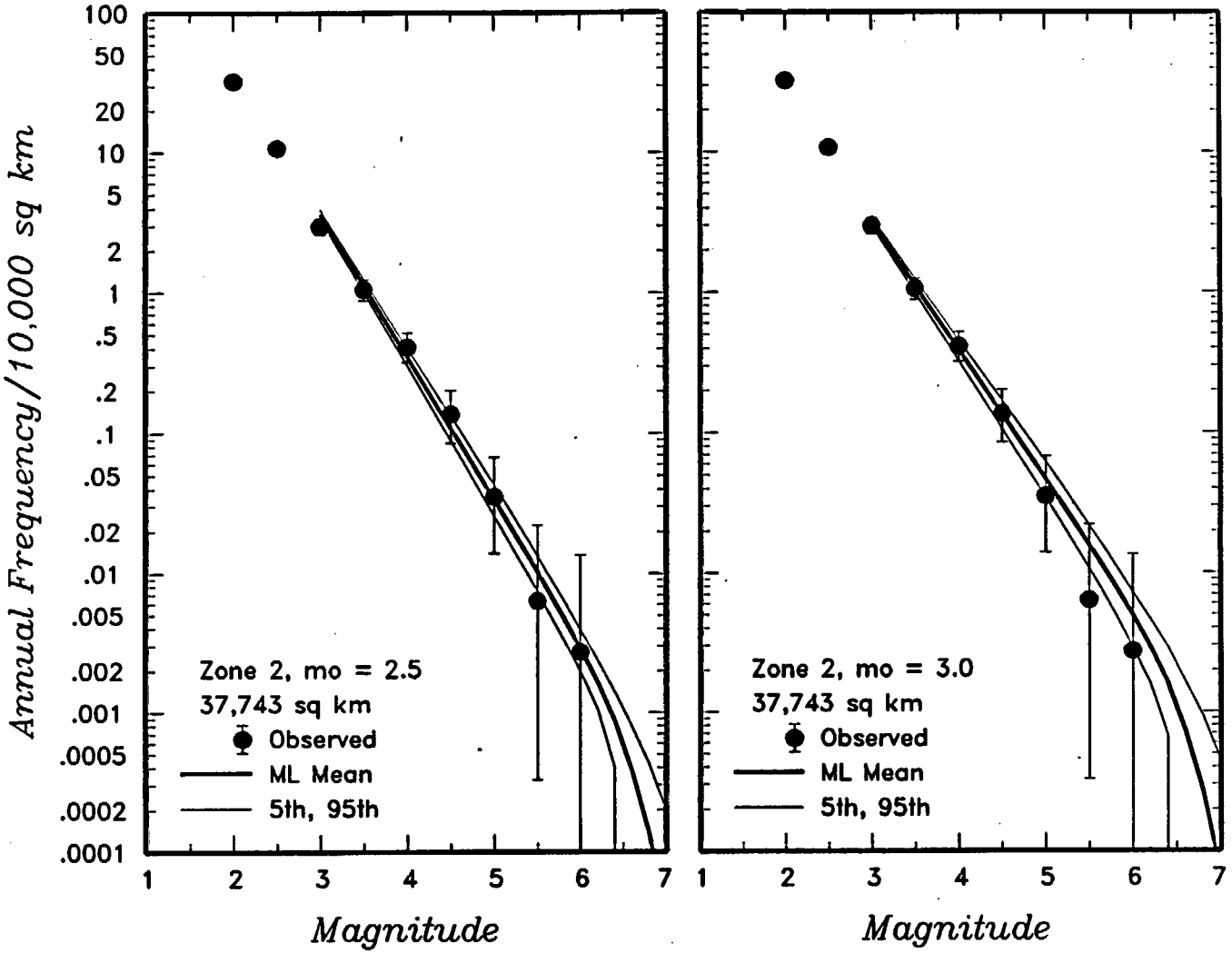

Figure 4-25 (Cont'd.) Earthquake recurrence relationships for the regional source zones defined by the AAR team

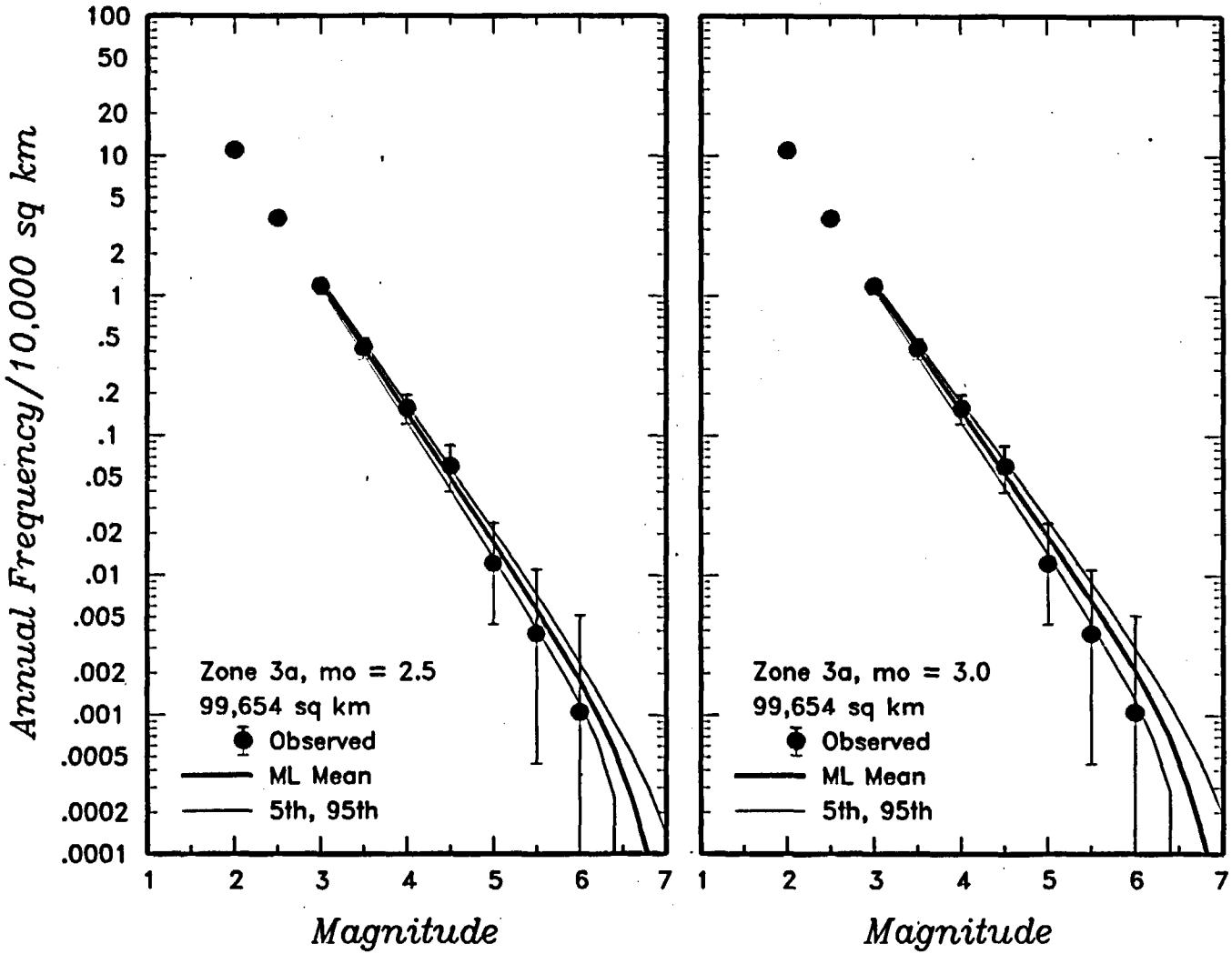

Figure 4-25 (Cont'd.) Earthquake recurrence relationships for the regional source zones defined by the AAR team

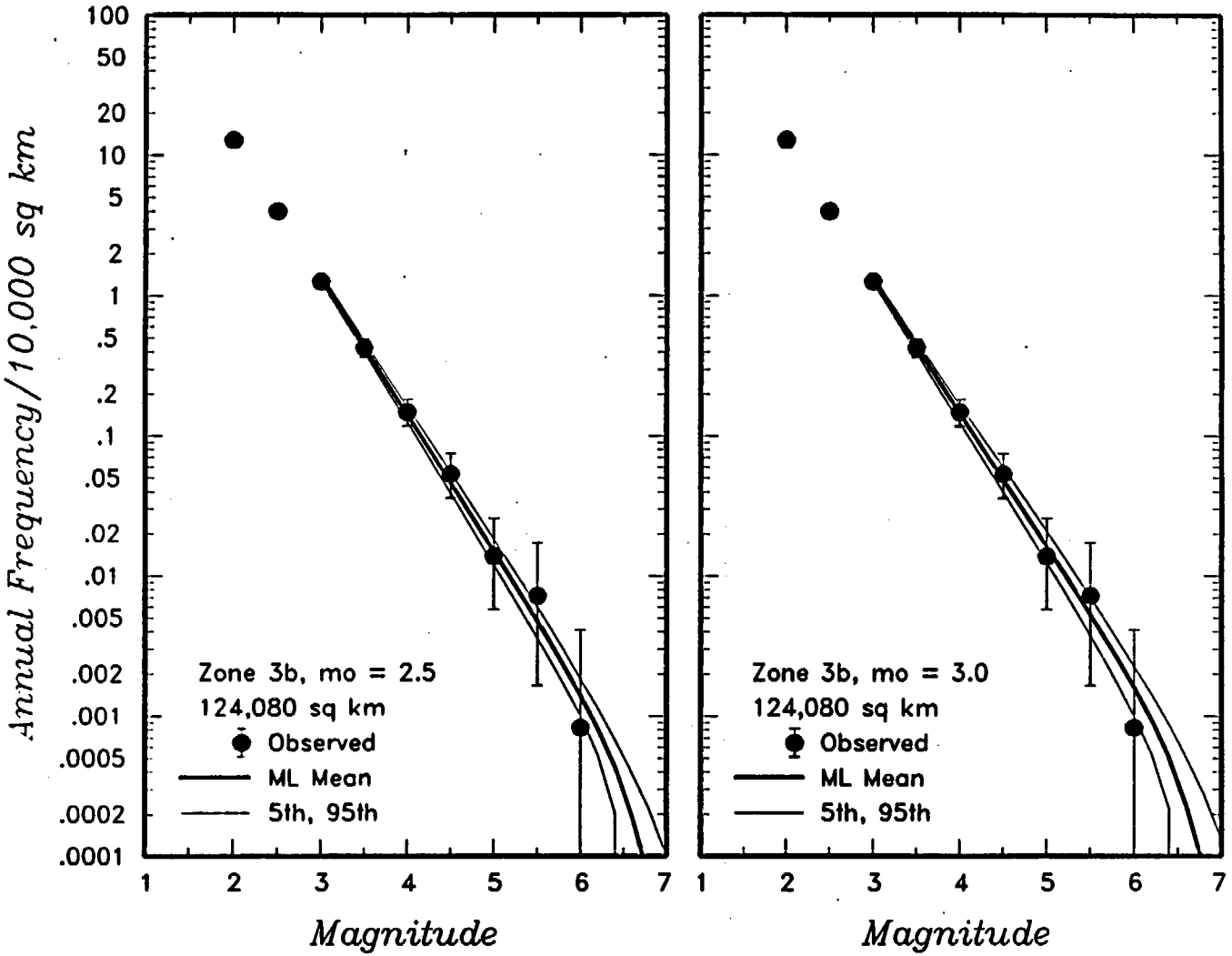

Figure 4-25 (Cont'd.) Earthquake recurrence relationships for the regional source zones defined by the AAR team

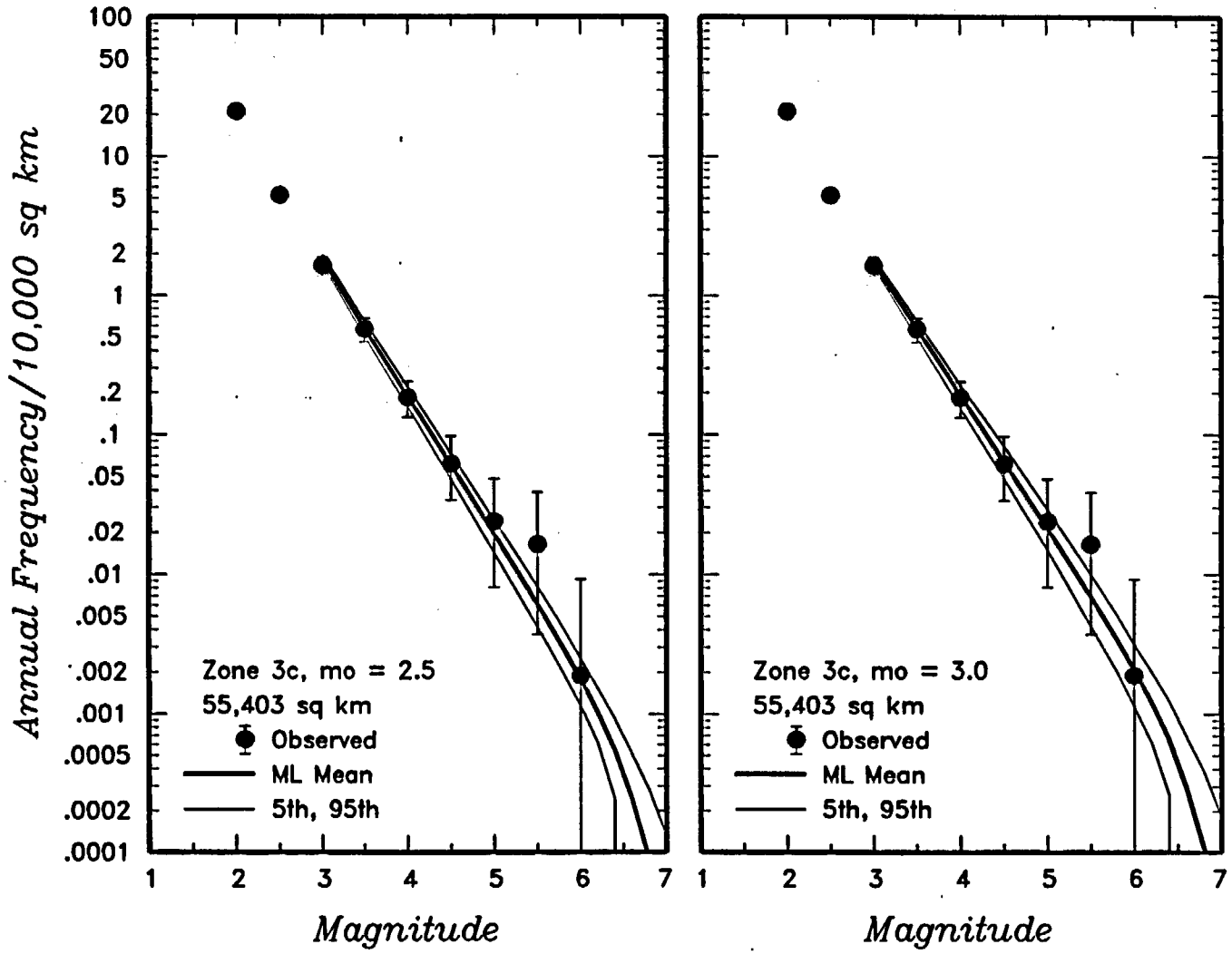

Figure 4-25 (Cont'd.) Earthquake recurrence relationships for the regional source zones defined by the AAR team

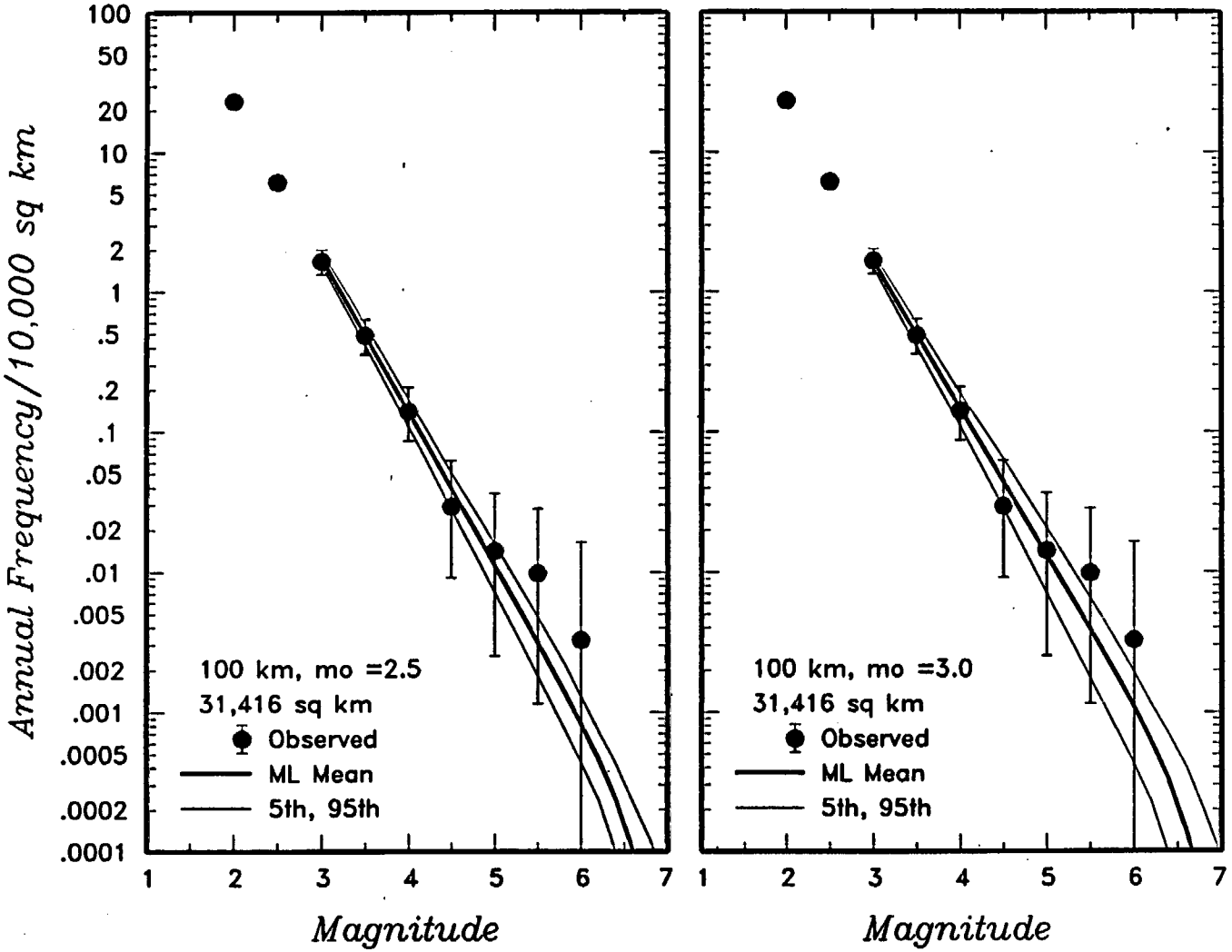

Figure 4-25 (Cont'd.) Earthquake recurrence relationships for the regional source zones defined by the AAR team

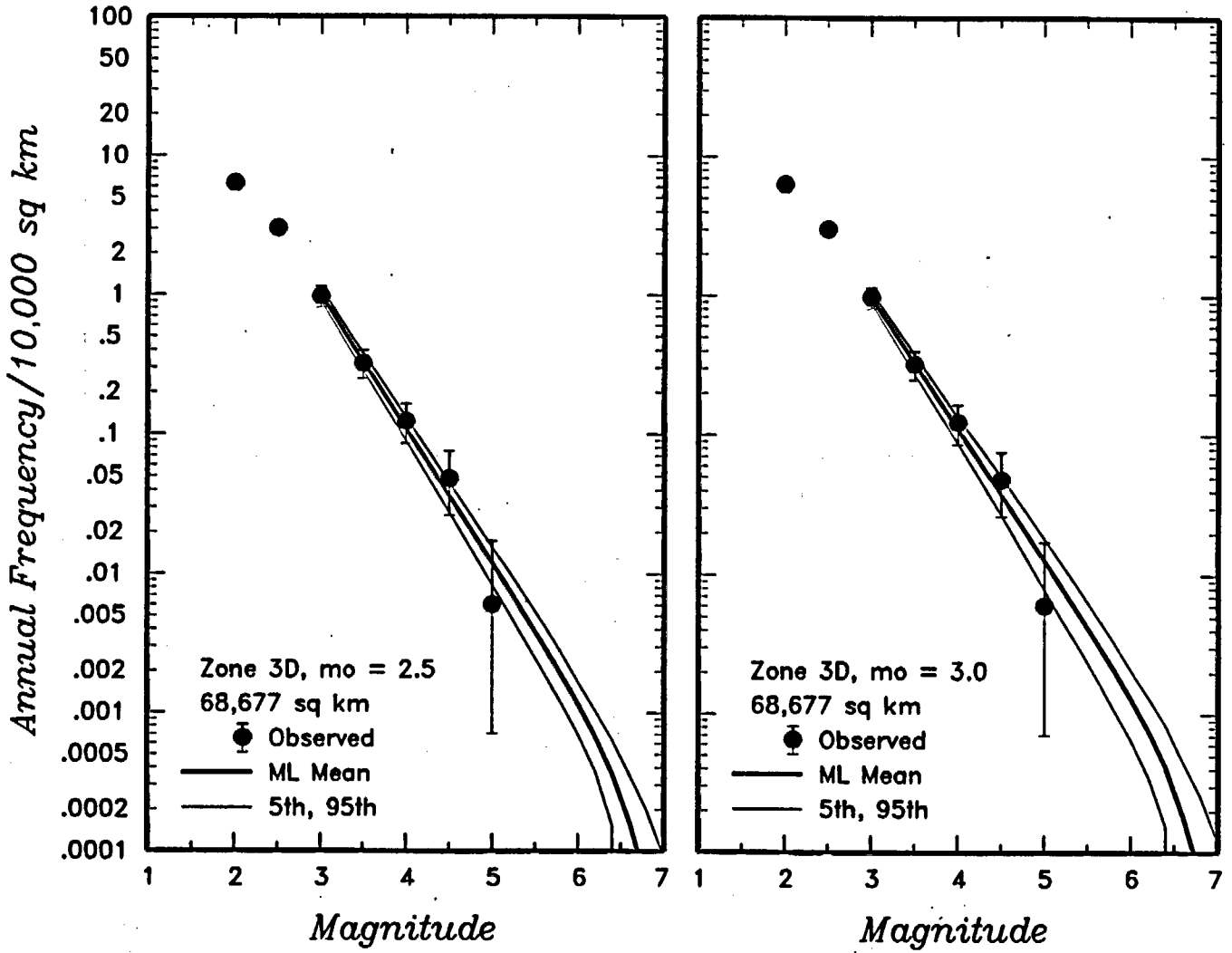

Figure 4-25 (Cont'd.) Earthquake recurrence relationships for the regional source zones defined by the AAR team

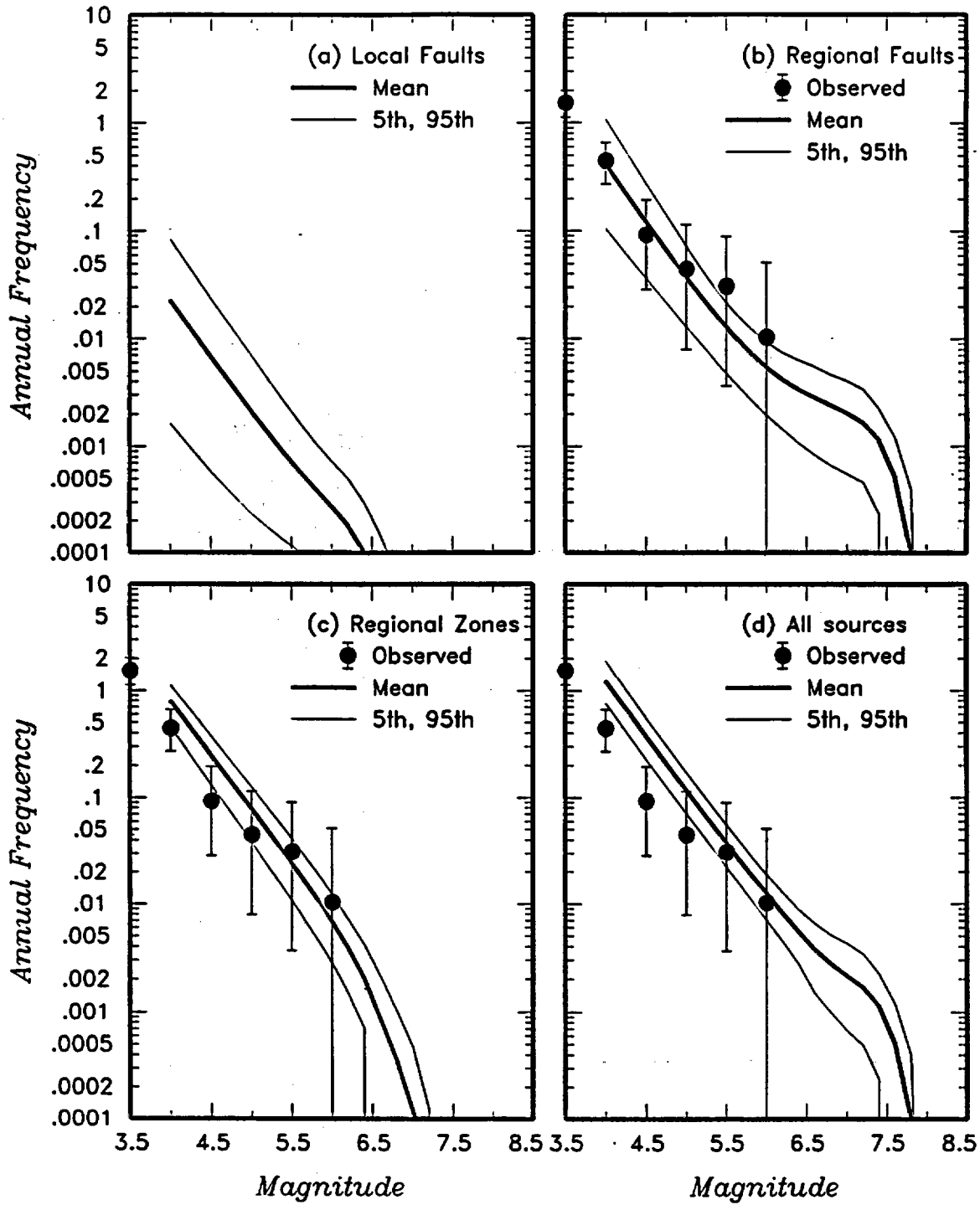

Figure 4-26 Predicted mean, 5th-, and 95th-percentile recurrence rates for (a) local fault sources, (b) regional fault sources, (c) regional source zones, and (d) all sources combined for the AAR team. The solid dots with vertical error bars show the observed frequency of earthquakes occurring within 100 km of the Yucca Mountain site.

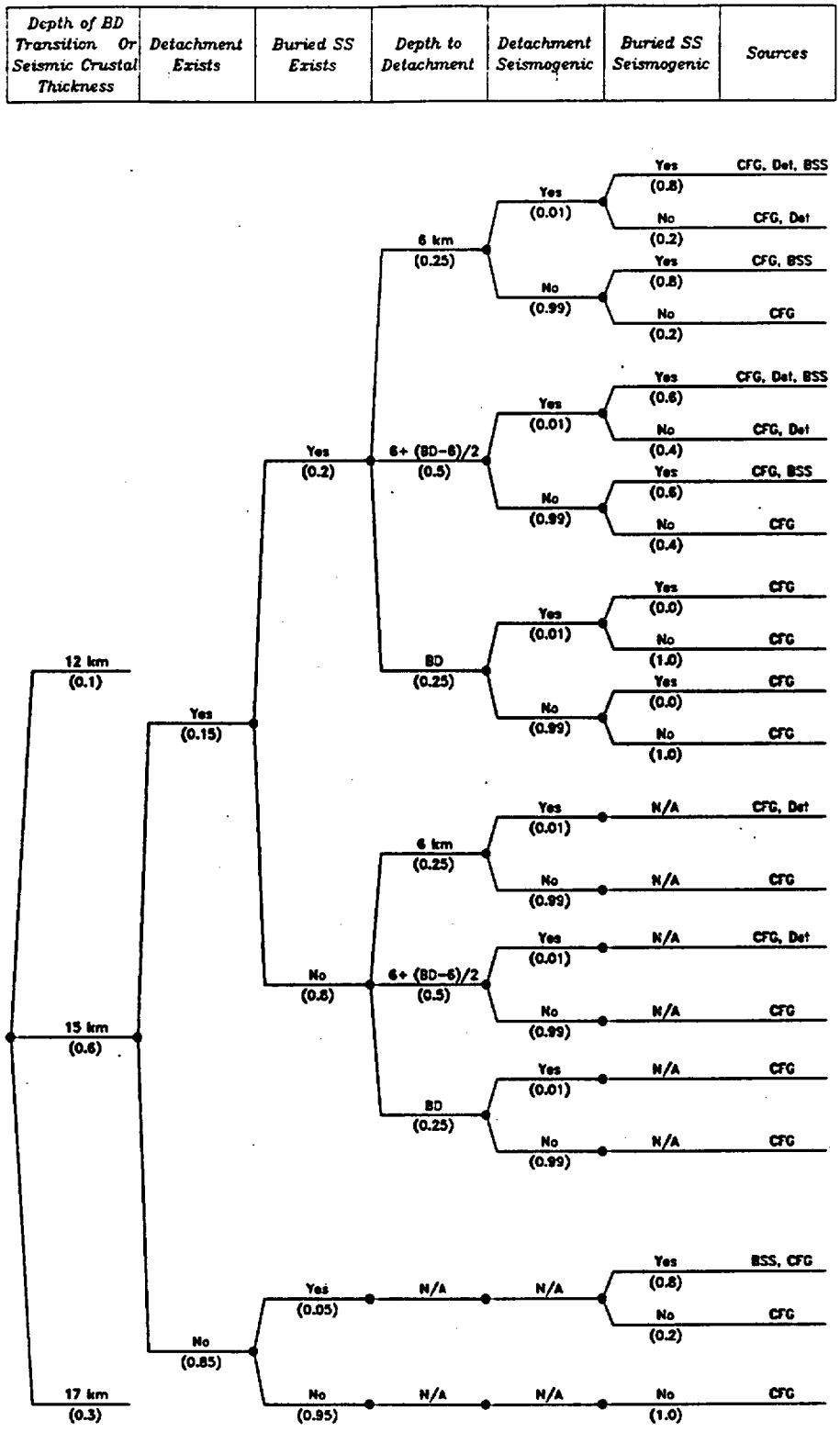

Figure 4-27a Logic tree for local fault sources developed by the ASM team

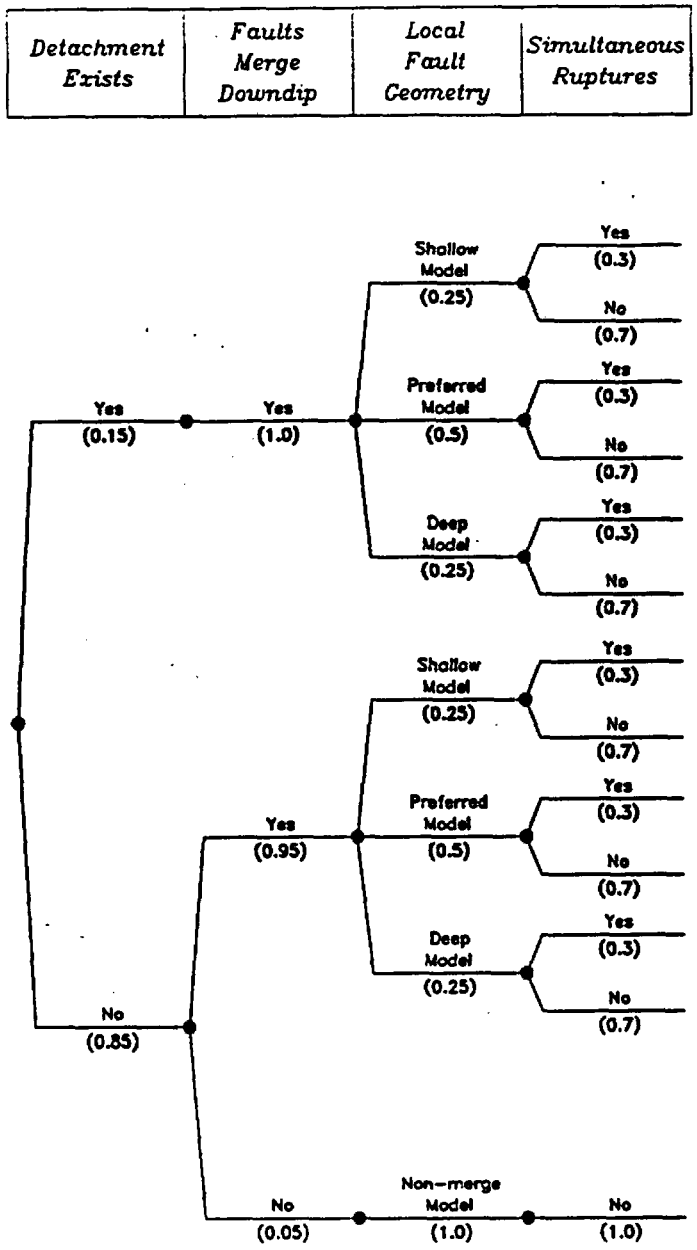

Figure 4-27b Logic tree for rupture behavior of Crater Flat group of faults

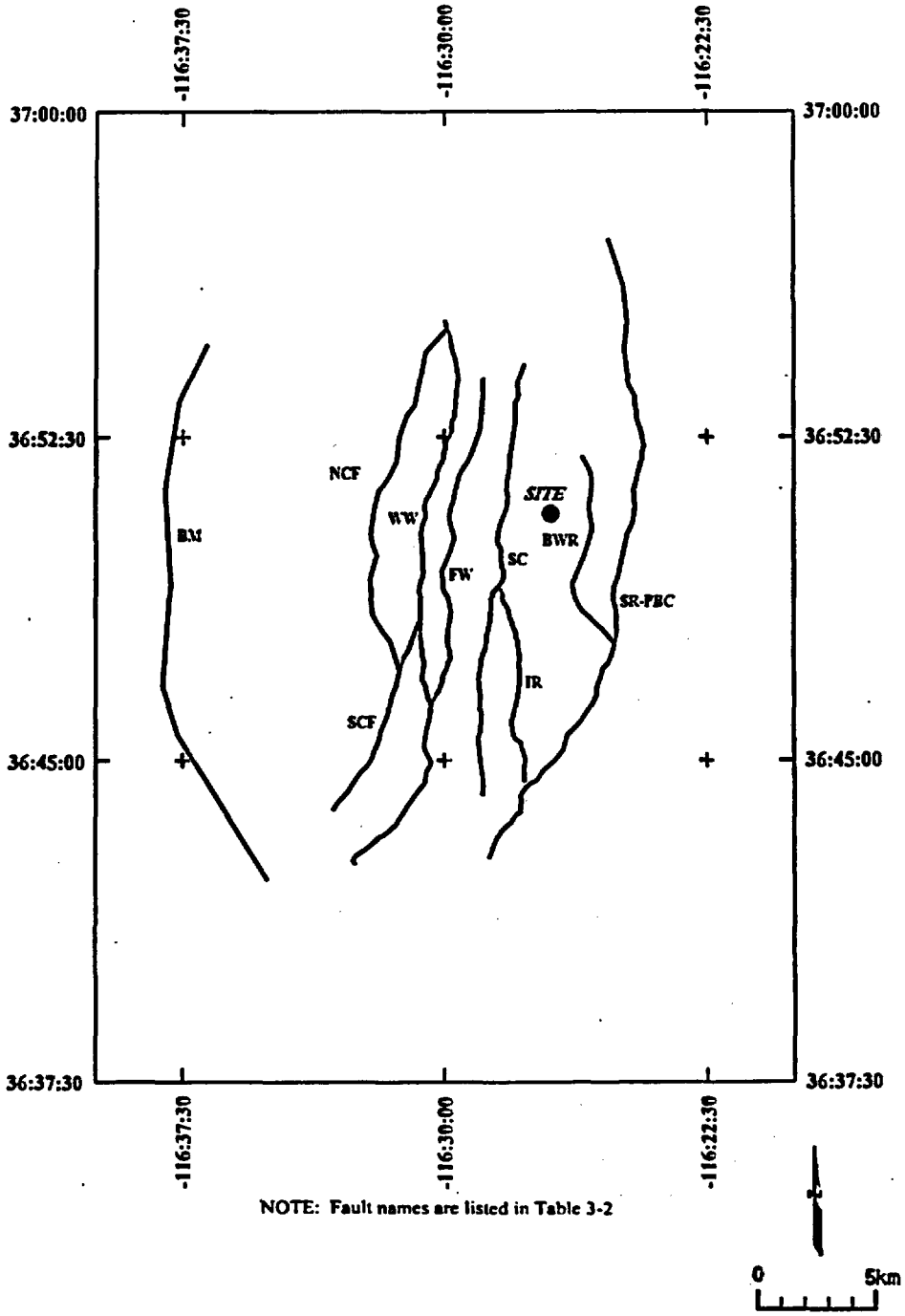

Figure 4-28 Location of fault sources considered by the ASM team

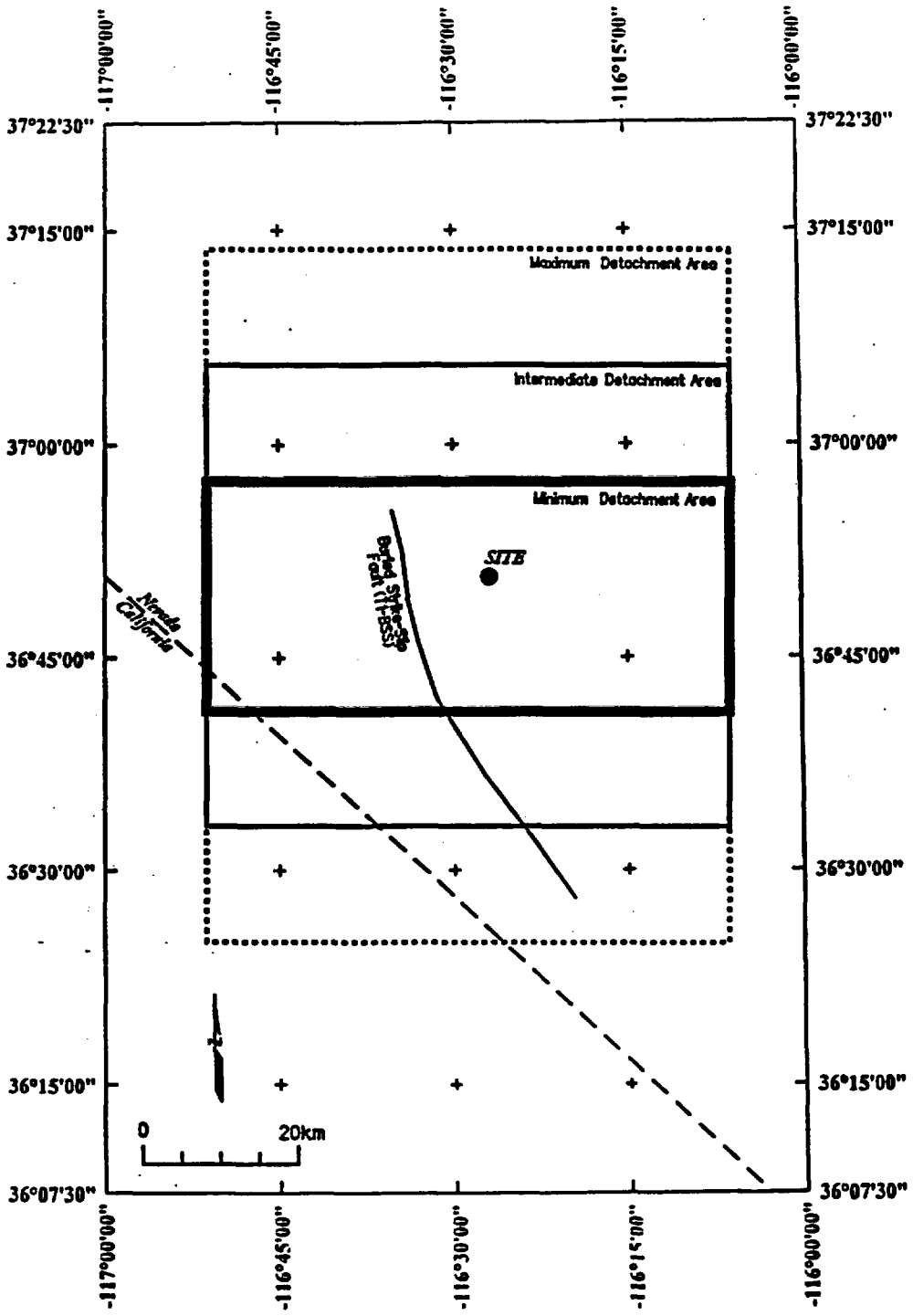

Figure 4-29 Location of hypothetical buried strike-slip and detachment faults in the vicinity of Yucca Mountain included in the ASM seismic source model

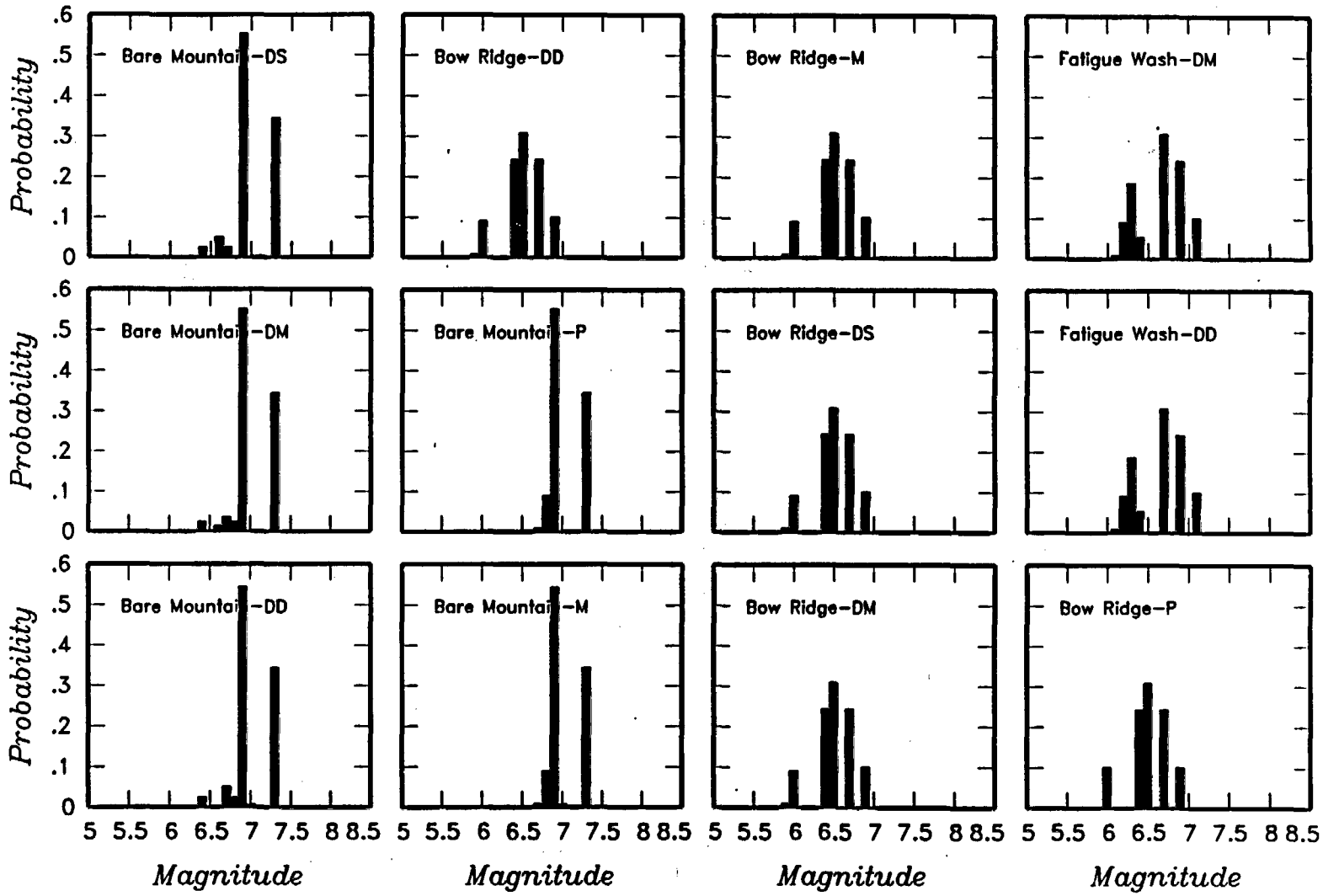

Figure 4-30 Maximum magnitude distributions for ASM team's local fault sources. DS–shallow detachment, DM–preferred detachment, DD–deep detachment; M–merging model, P–planar model; BM–Bare Mountain, W–Windy Wash, SRPBC–Stagecoach Road-Paintbrush Canyon.

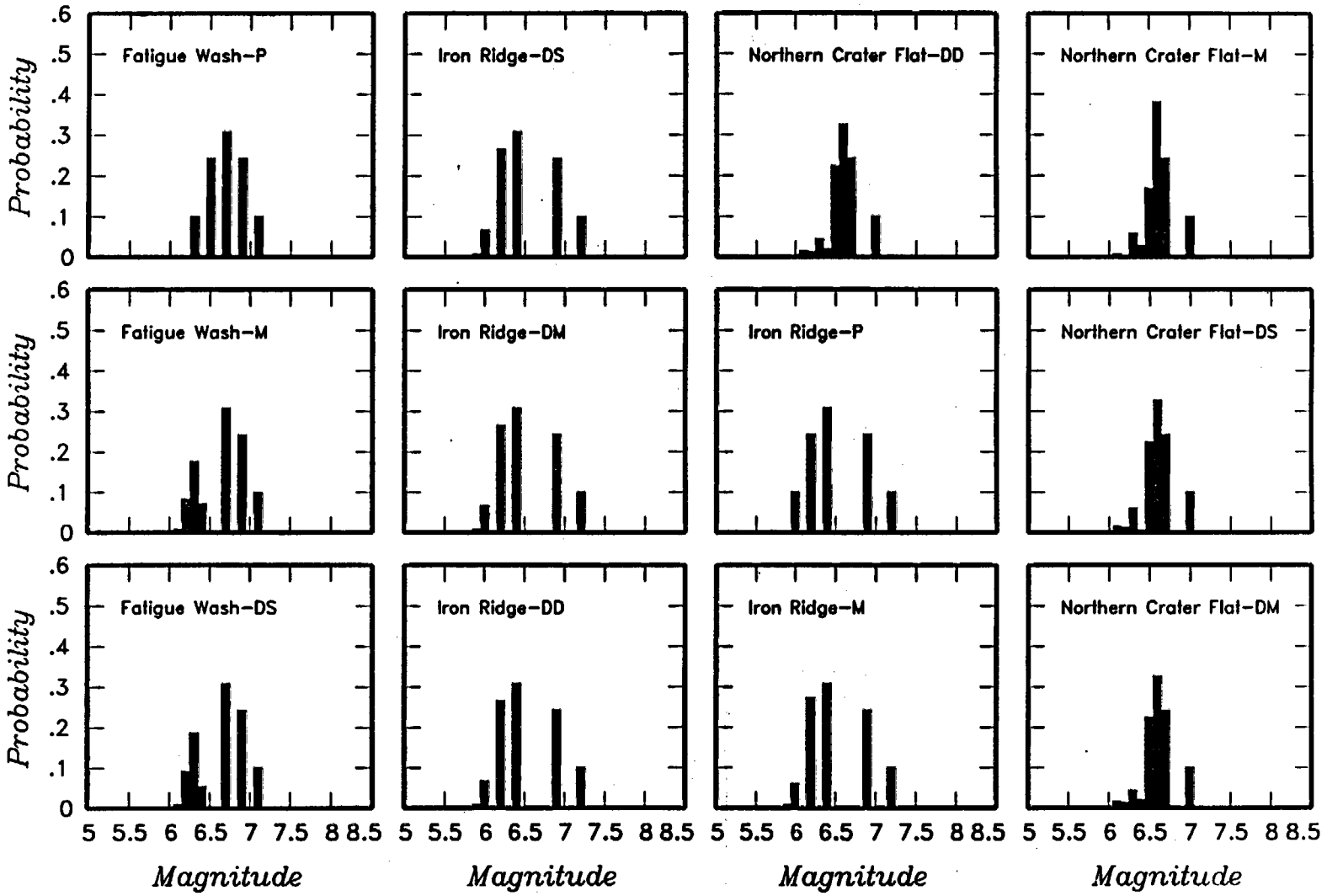

Figure 4-30 (Cont'd.) Maximum magnitude distributions for ASM team's local fault sources

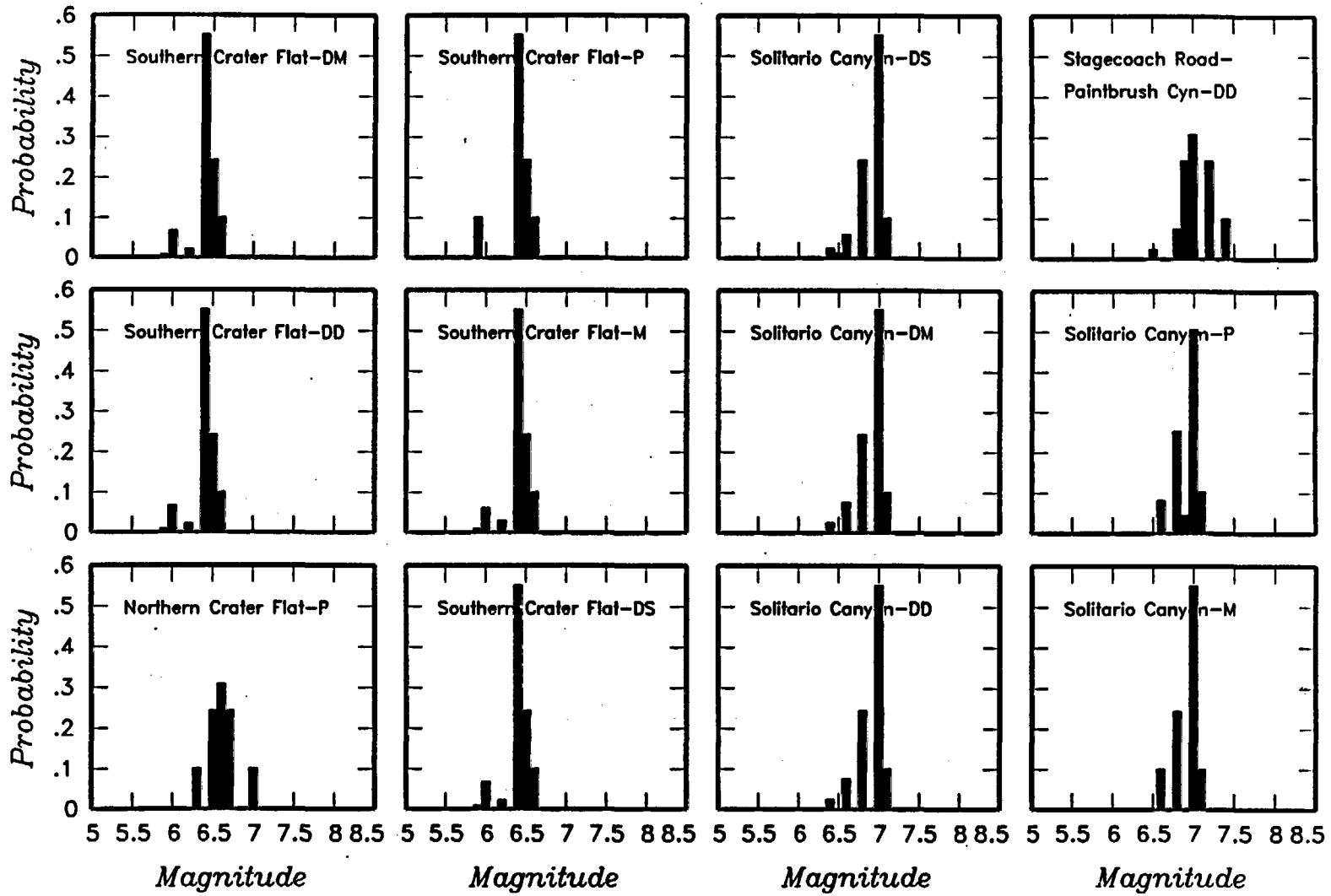

Figure 4-30 (Cont'd.) Maximum magnitude distributions for ASM team's local fault sources

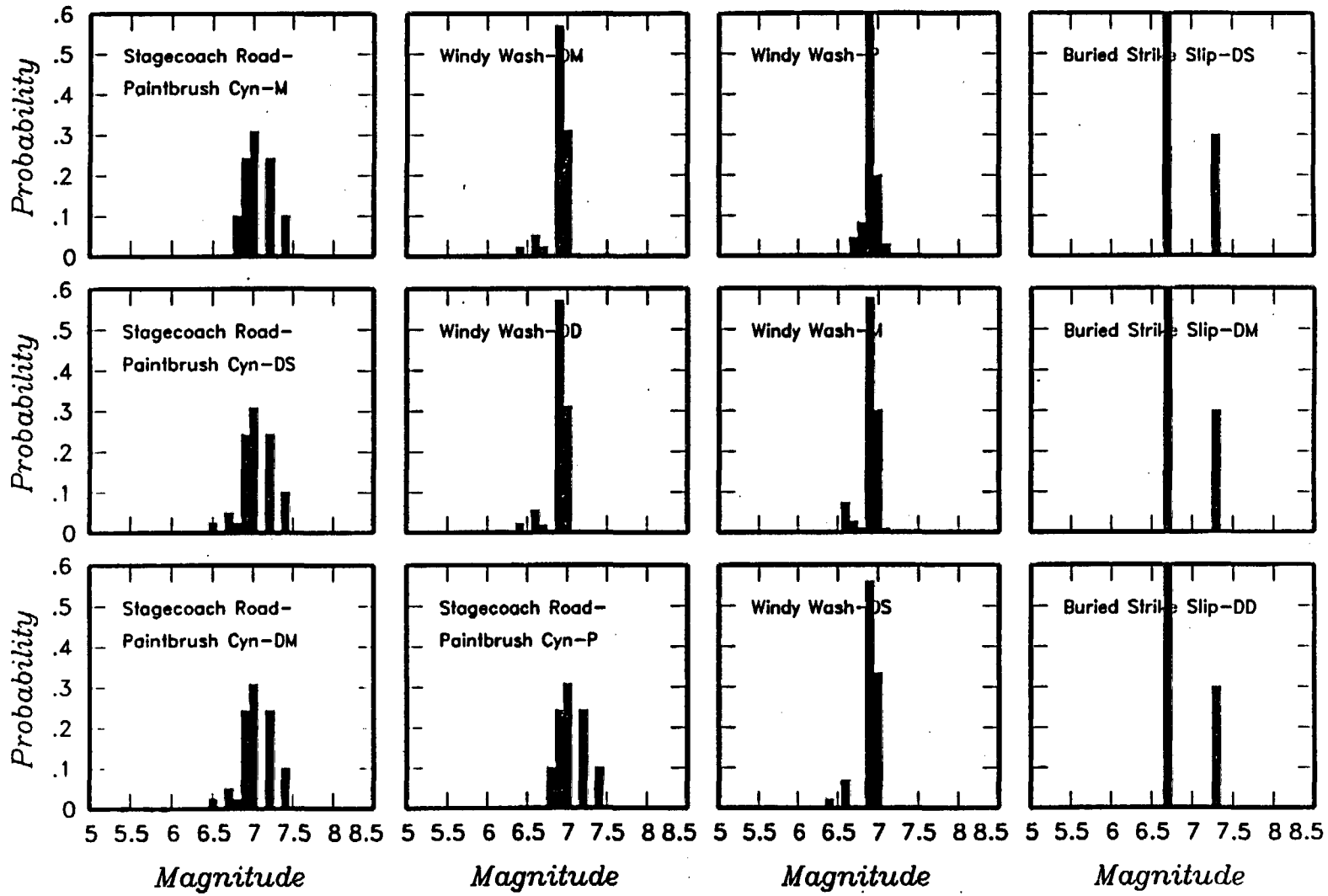

Figure 4-30 (Cont'd.) Maximum magnitude distributions for ASM team's local fault sources

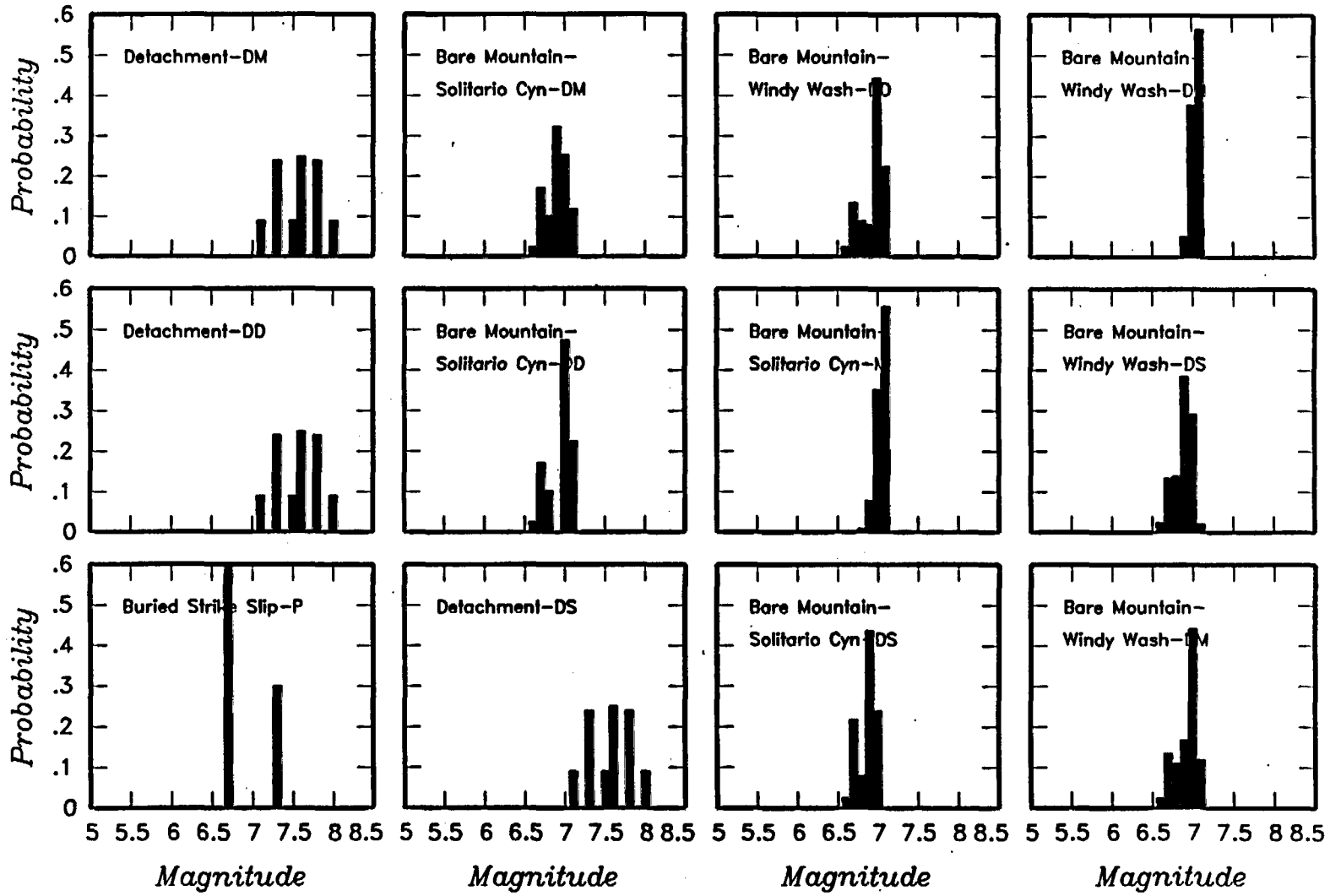

Figure 4-30 (Cont'd.) Maximum magnitude distributions for ASM team's local fault sources

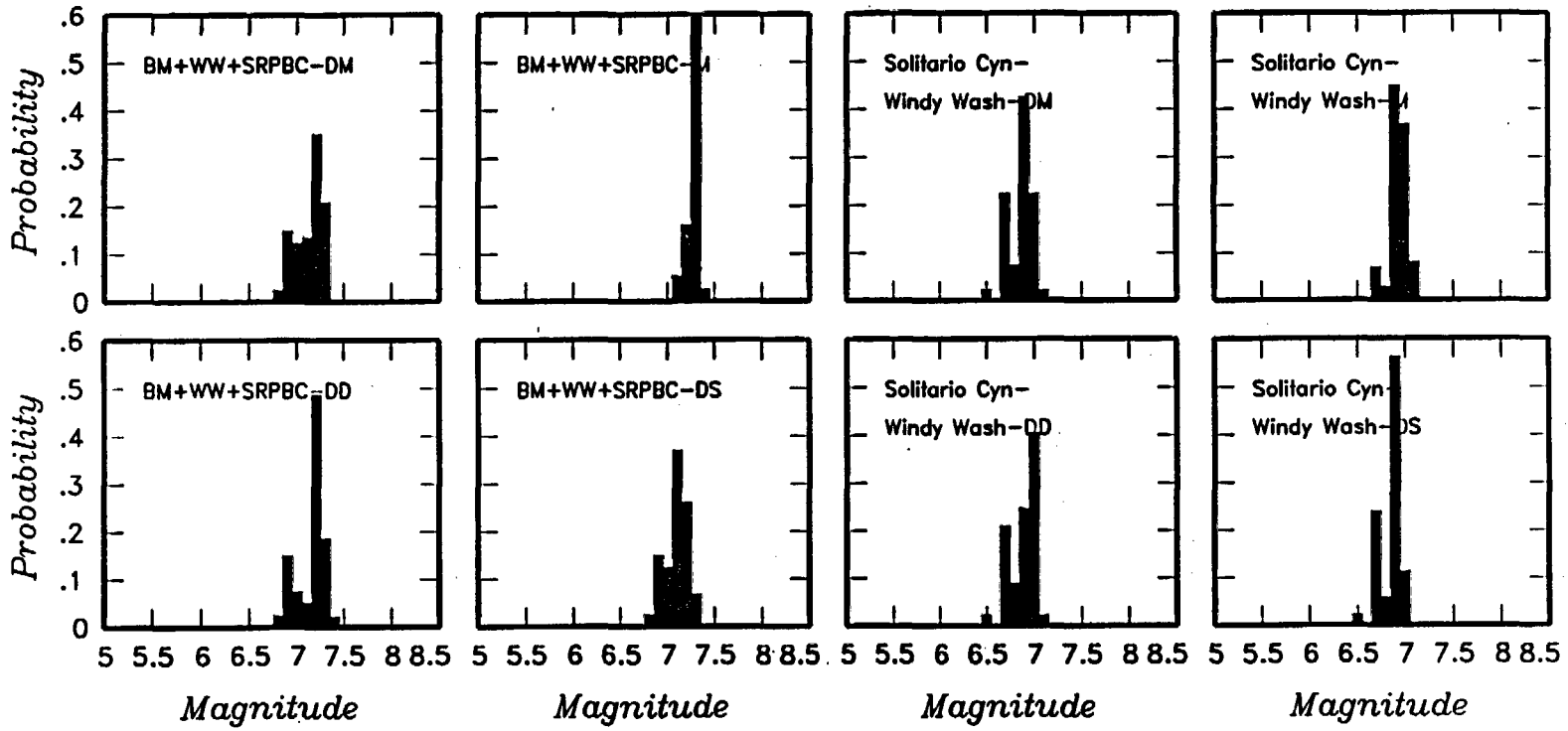

Figure 4-30 (Cont'd.) Maximum magnitude distributions for ASM team's local fault sources

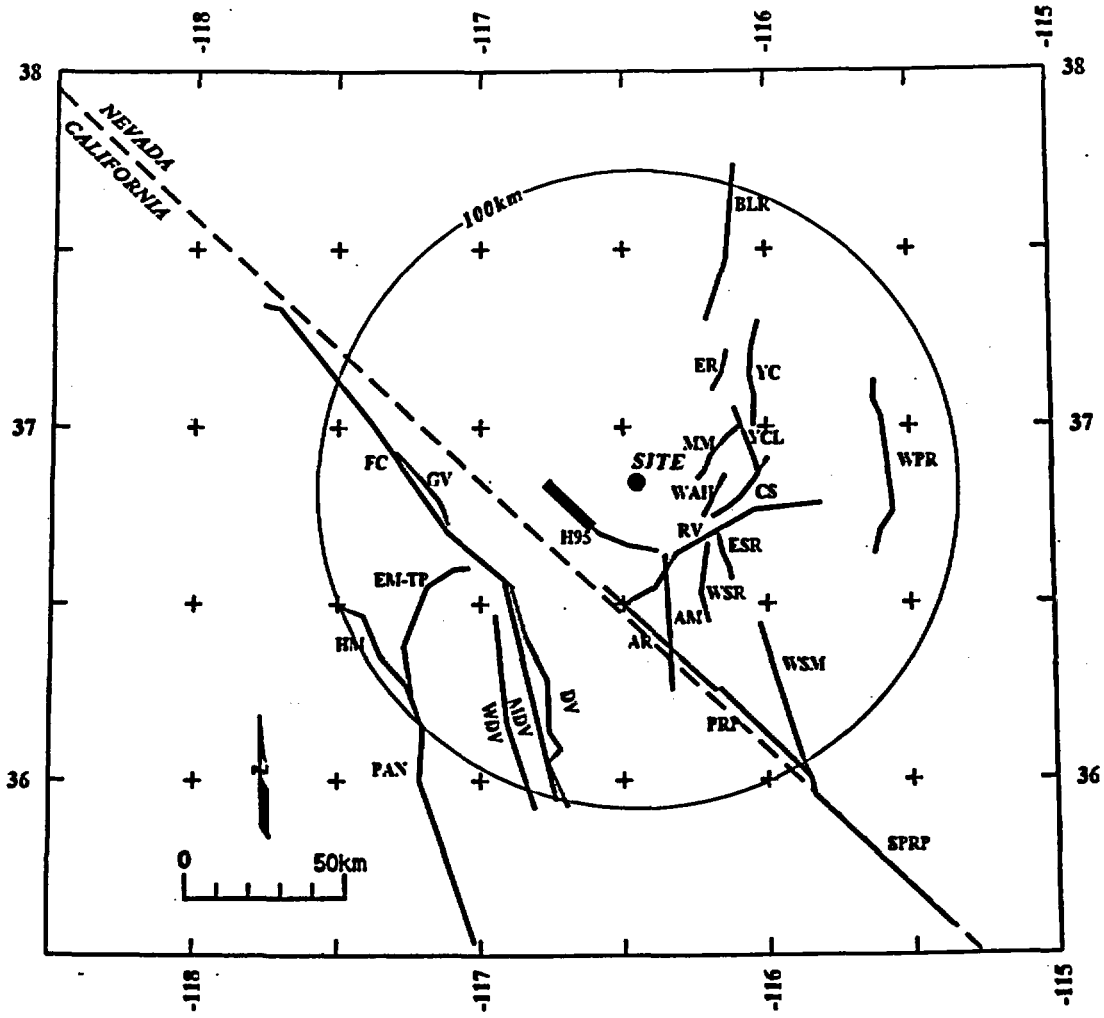

EXPLANATION

NOTE: Fault names are listed in Table 3-2

Fault Lengths:

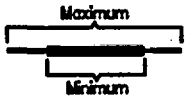

Figure 4-31 Reginal fault sources considered by the ASM team

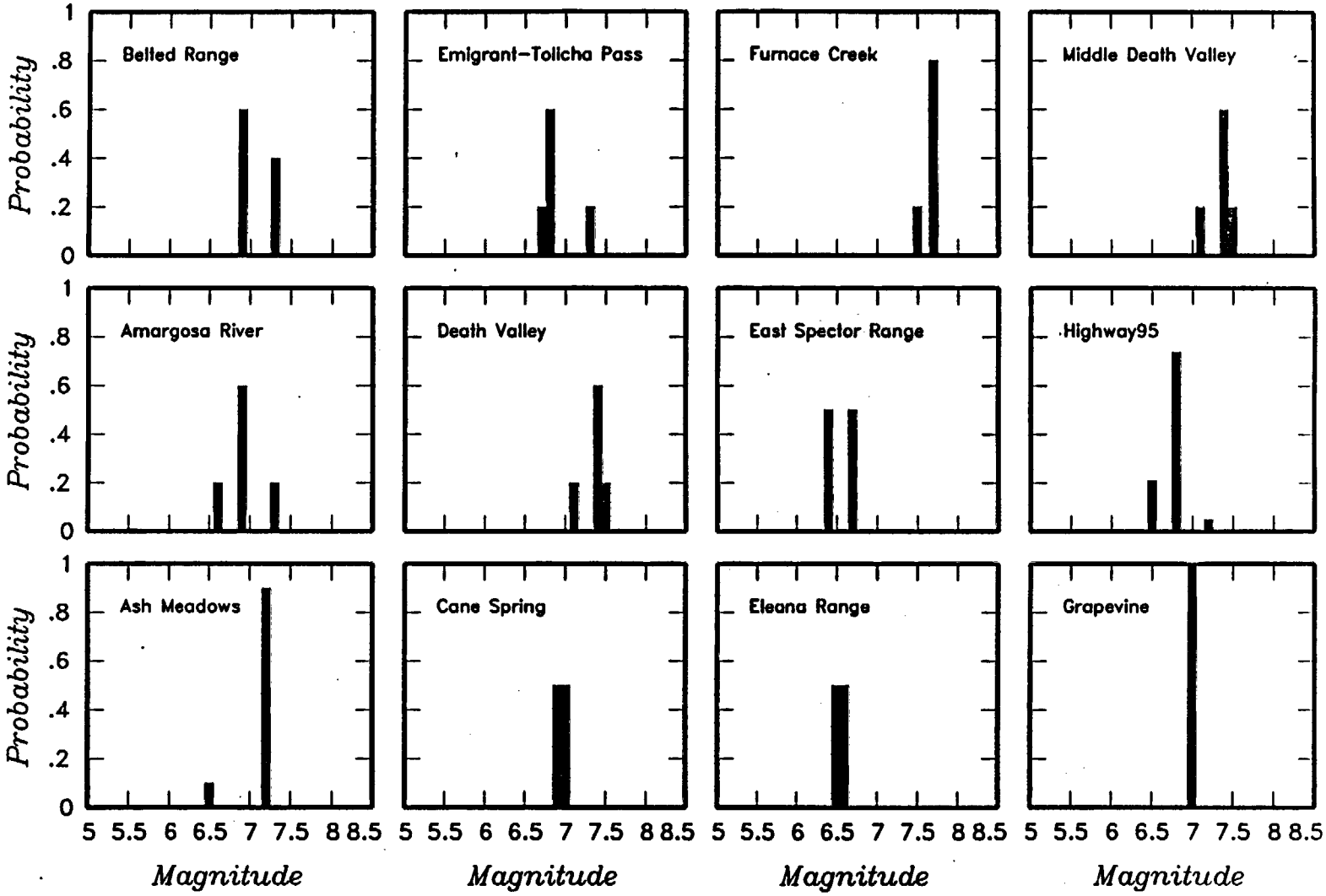

Figure 4-32 Maximum magnitude distributions for ASM team's regional fault sources

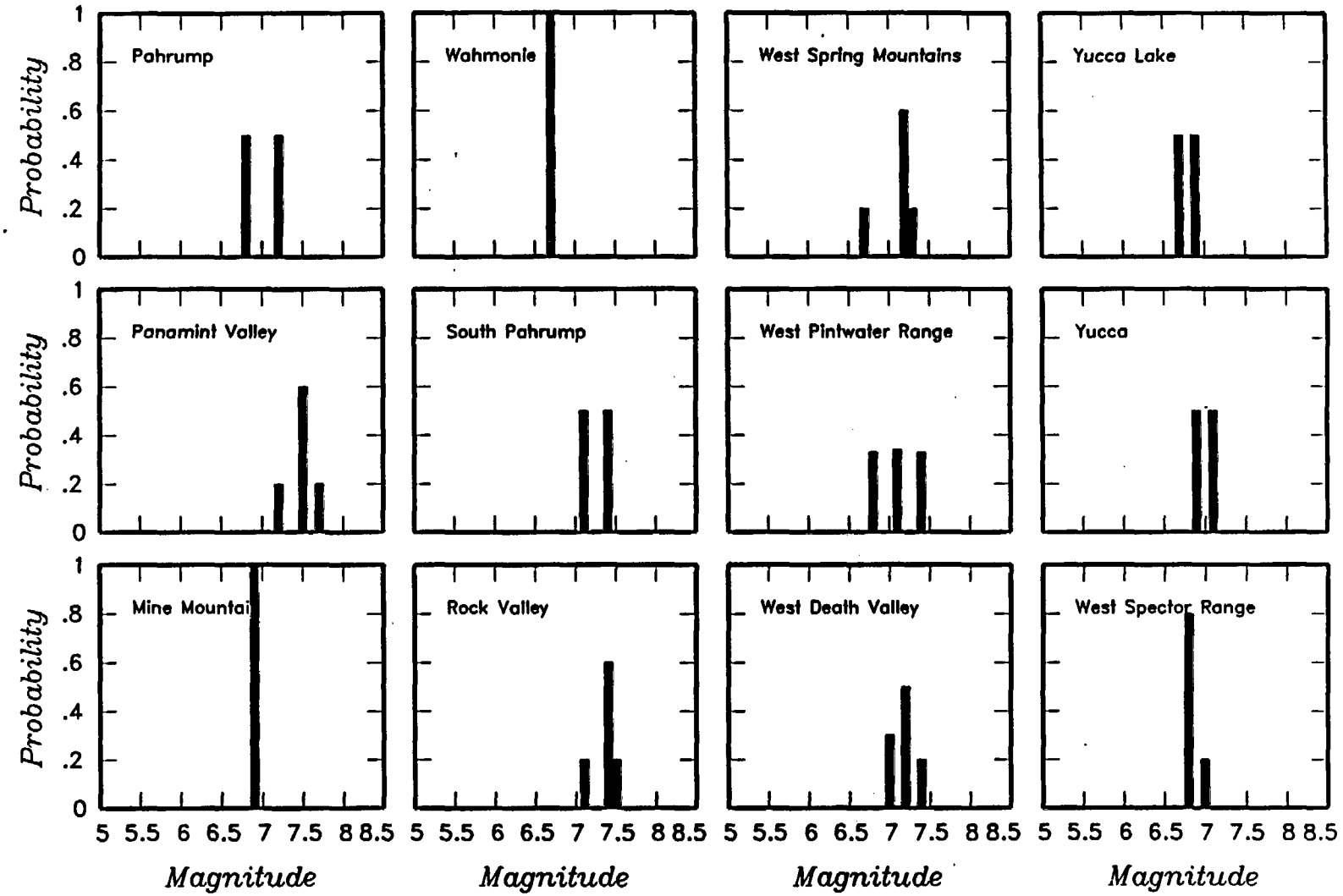

Figure 4-32 (Cont'd.) Maximum magnitude distributions for ASM team's regional fault sources

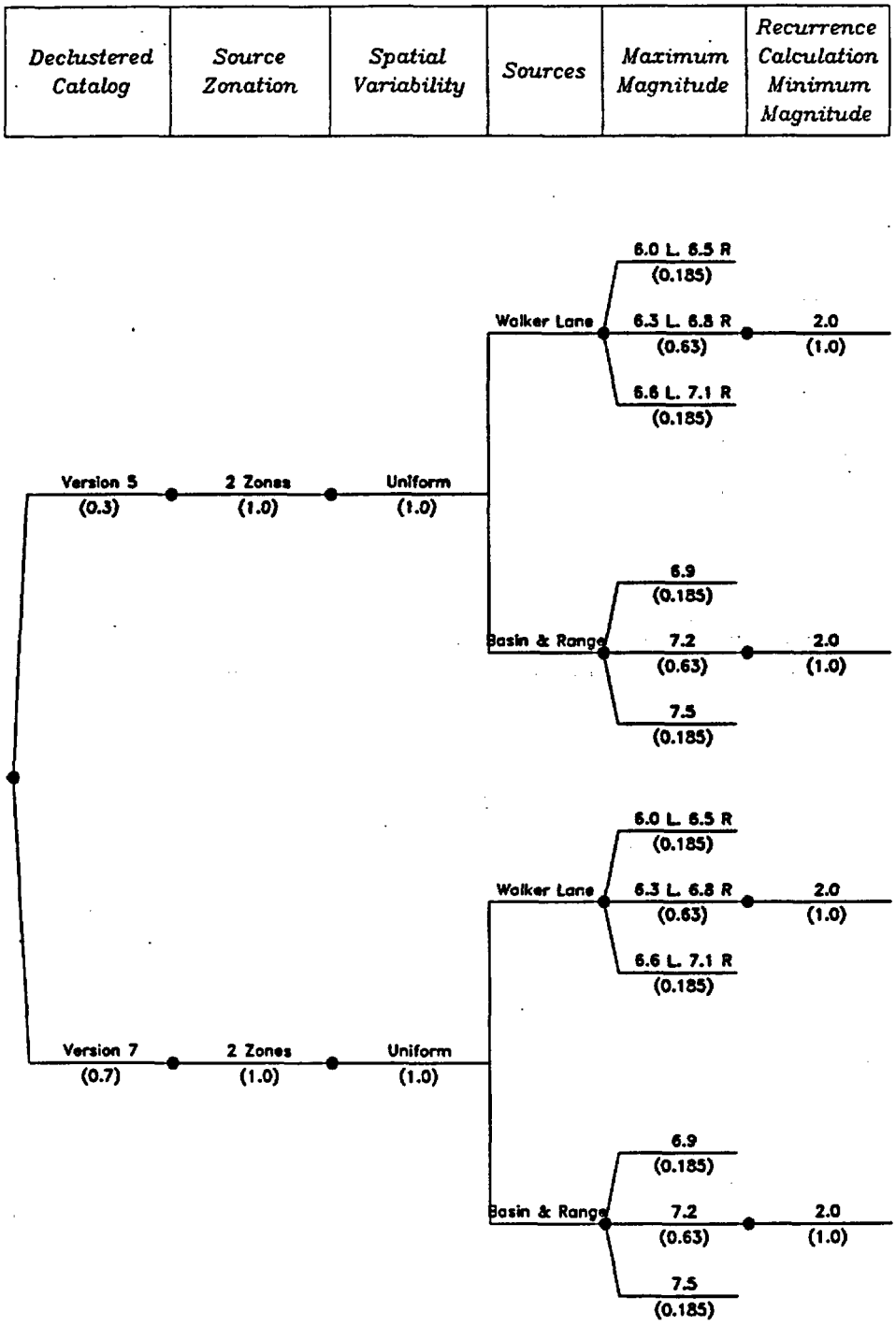

Figure 4-33 Logic tree for regional source zones developed by the ASM team

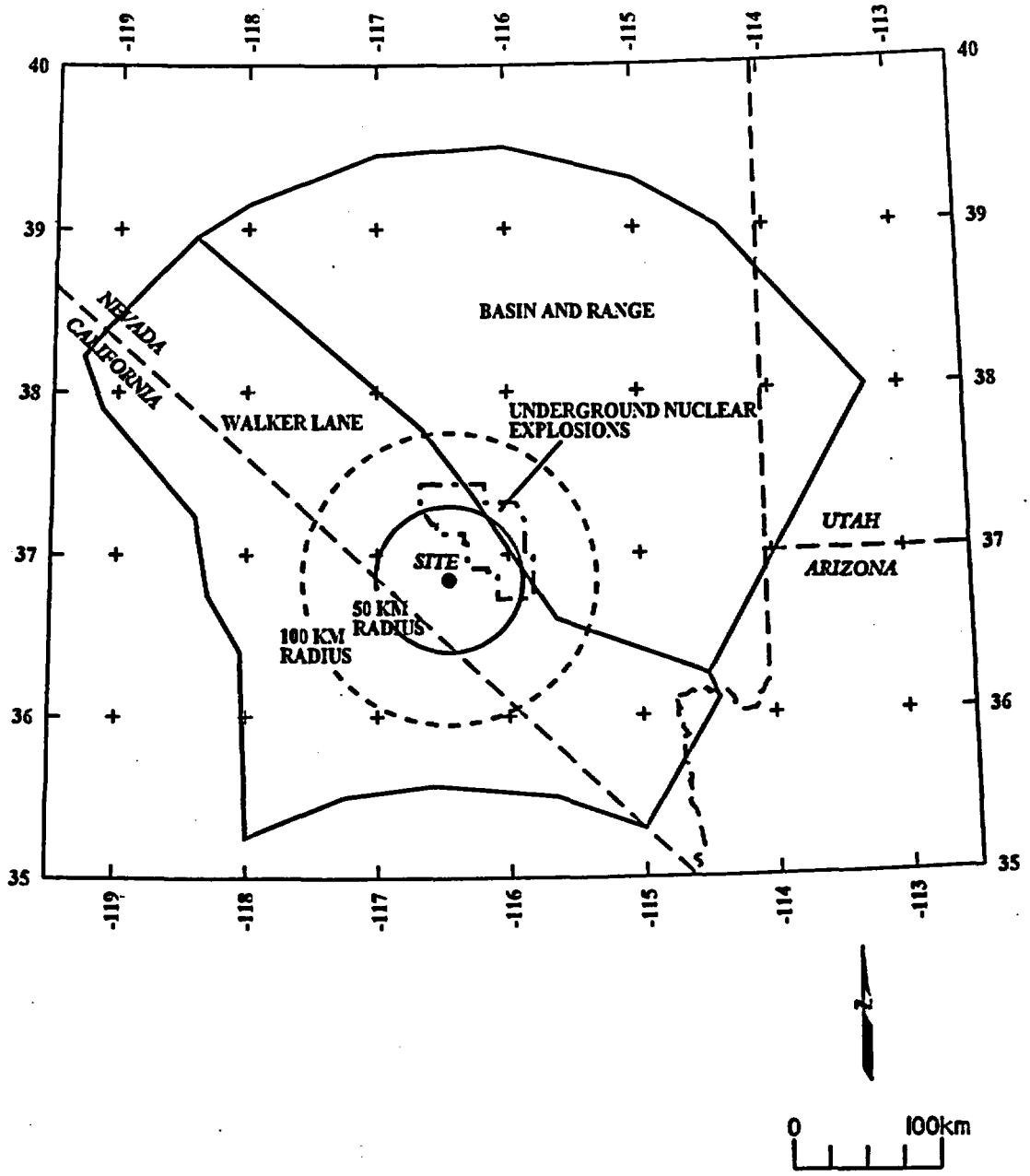

Figure 4-34 Regional source zones considered by the ASM team

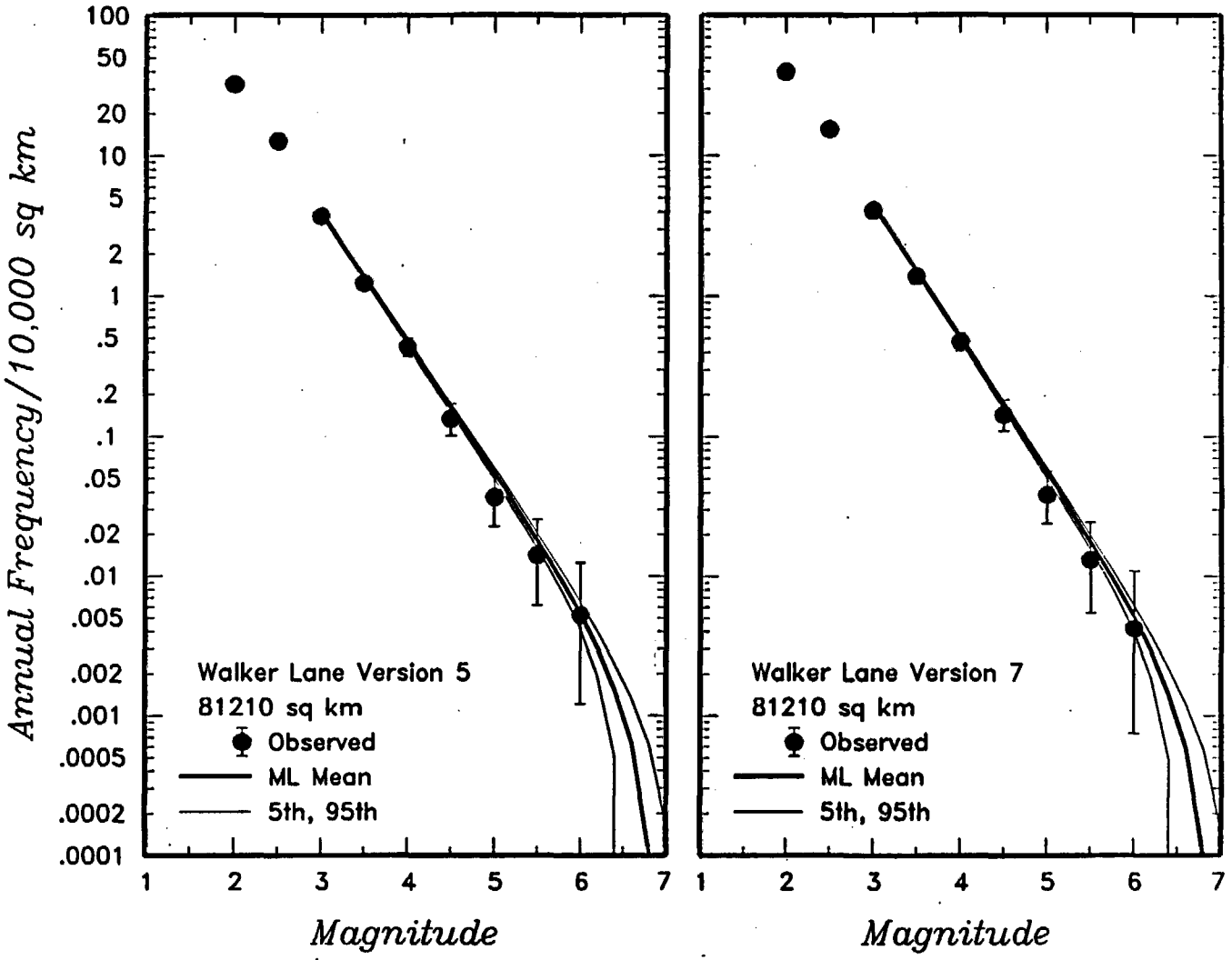

Figure 4-35 Earthquake recurrence relationships for the regional source zones defined by the ASM team. The solid dots with vertical error bars represent the observed data. The thick and thin solid curves are the mean, 5th, and 95th percentiles of the recurrence rates based on the uncertainty in recurrence parameters and maximum magnitude.

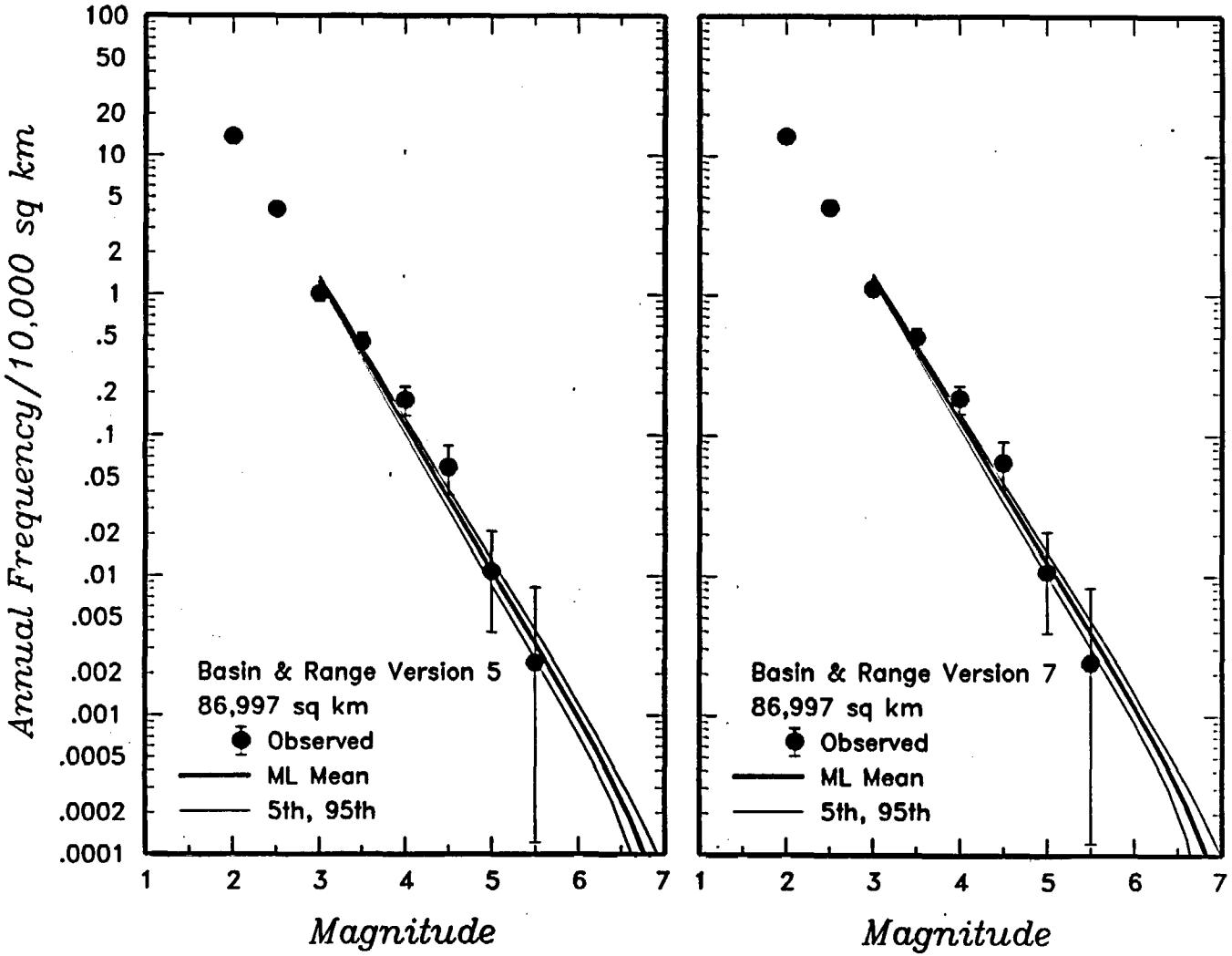

Figure 4-35 (Cont'd.) Earthquake recurrence relationships for the regional source zones defined by the ASM team

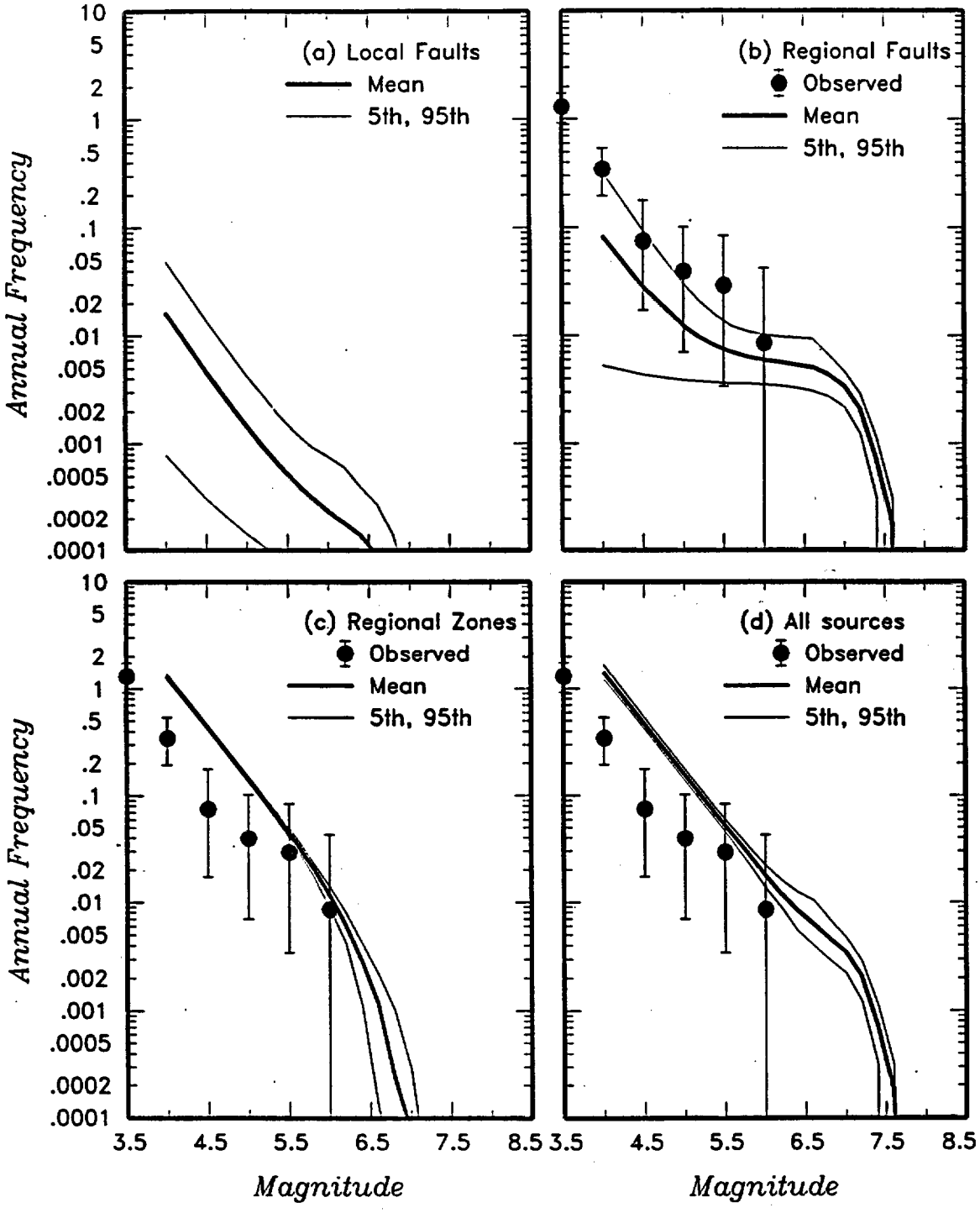

Figure 4-36 Predicted mean, 5th-, and 95th-percentile recurrence rates for (a) local fault sources, (b) regional fault sources, (c) regional source zones, and (d) all sources combined for the ASM team. The solid dots with vertical error bars indicate the observed frequency of earthquakes occurring within 100 km of the Yucca Mountain site.

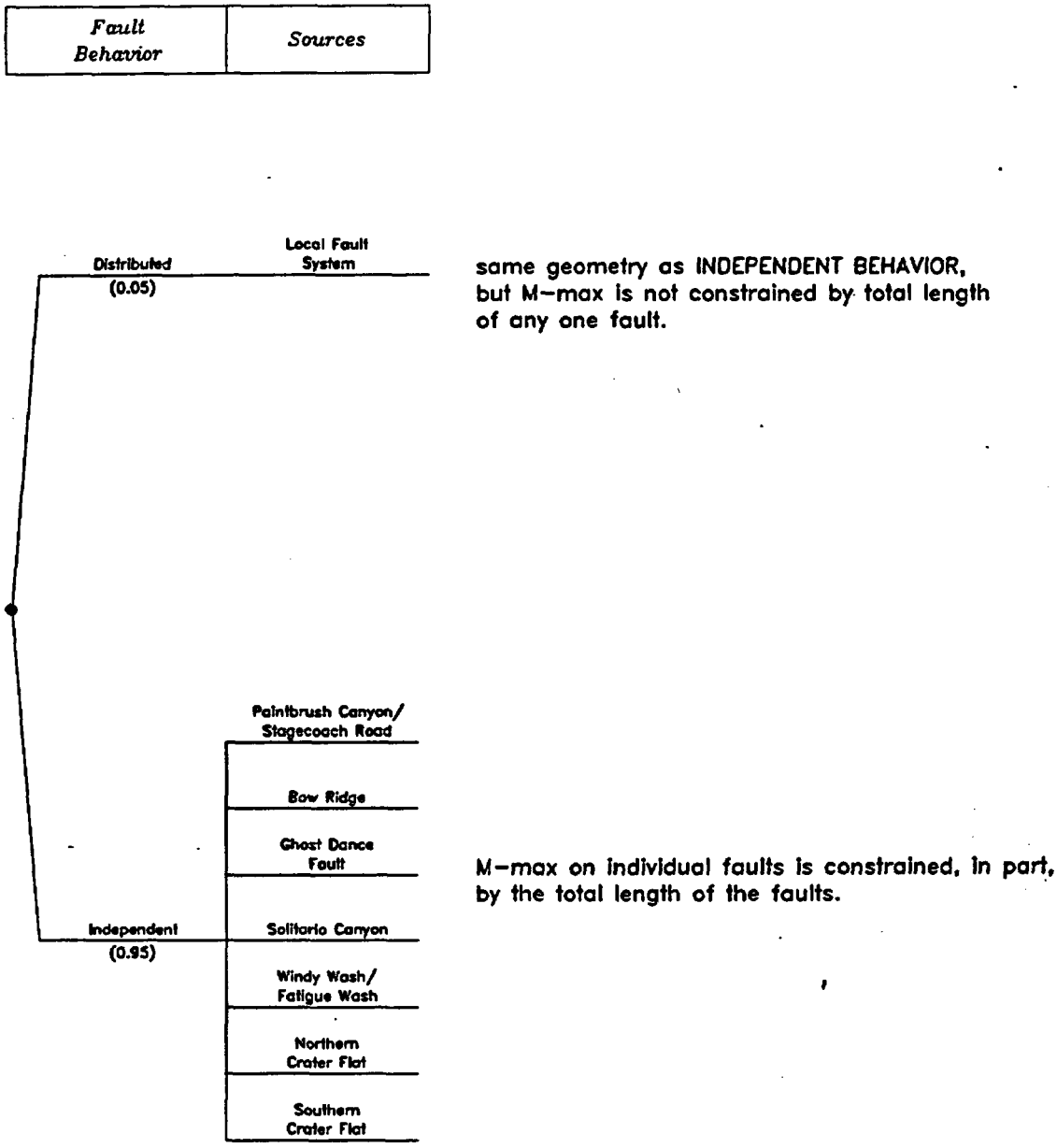

Figure 4-37a Logic tree for local fault sources developed by the DFS team

Seismic Source	*Total Fault Length Scenarios*	*Maximum Rupture Length*	*Structural Model*	*Dip/Width*	*Slip Rate (mm/yr)*	*Maximum Earthquake Method*	*Earthquake Recurrence Model*

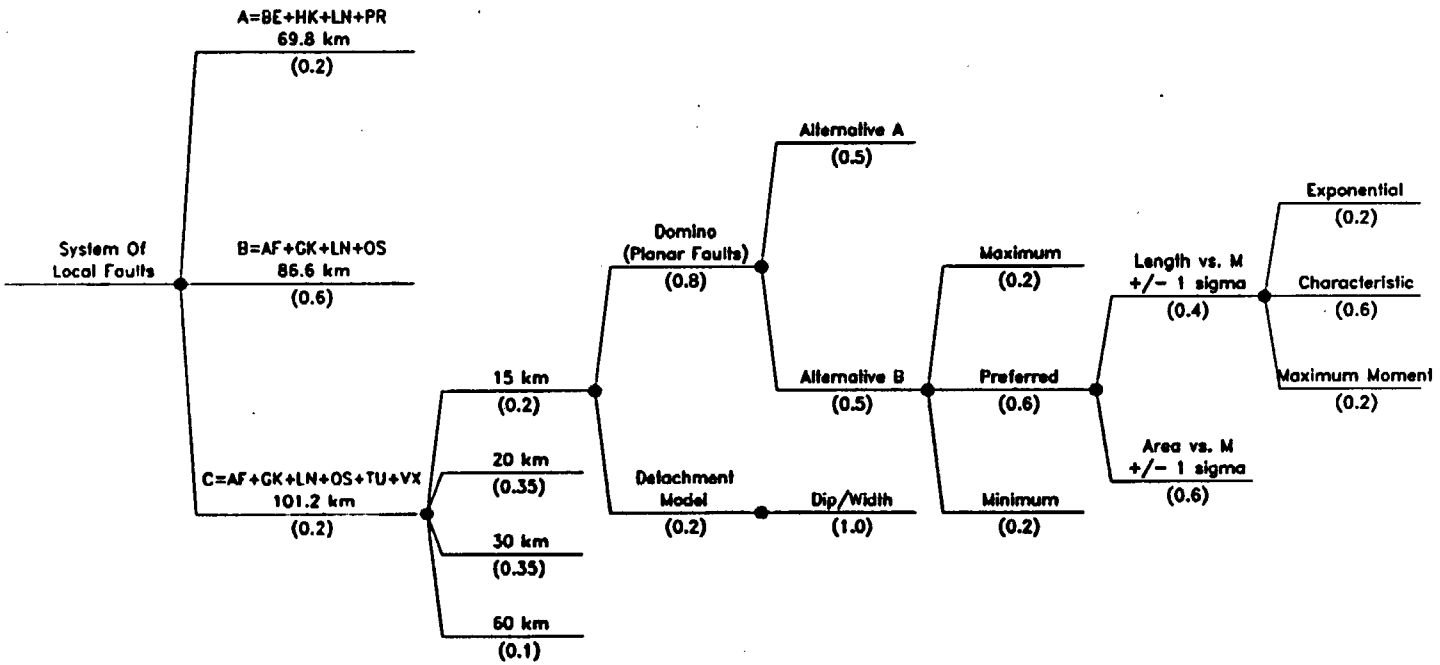

Figure 4-37b Logic tree for local fault source given distributed fault behavior

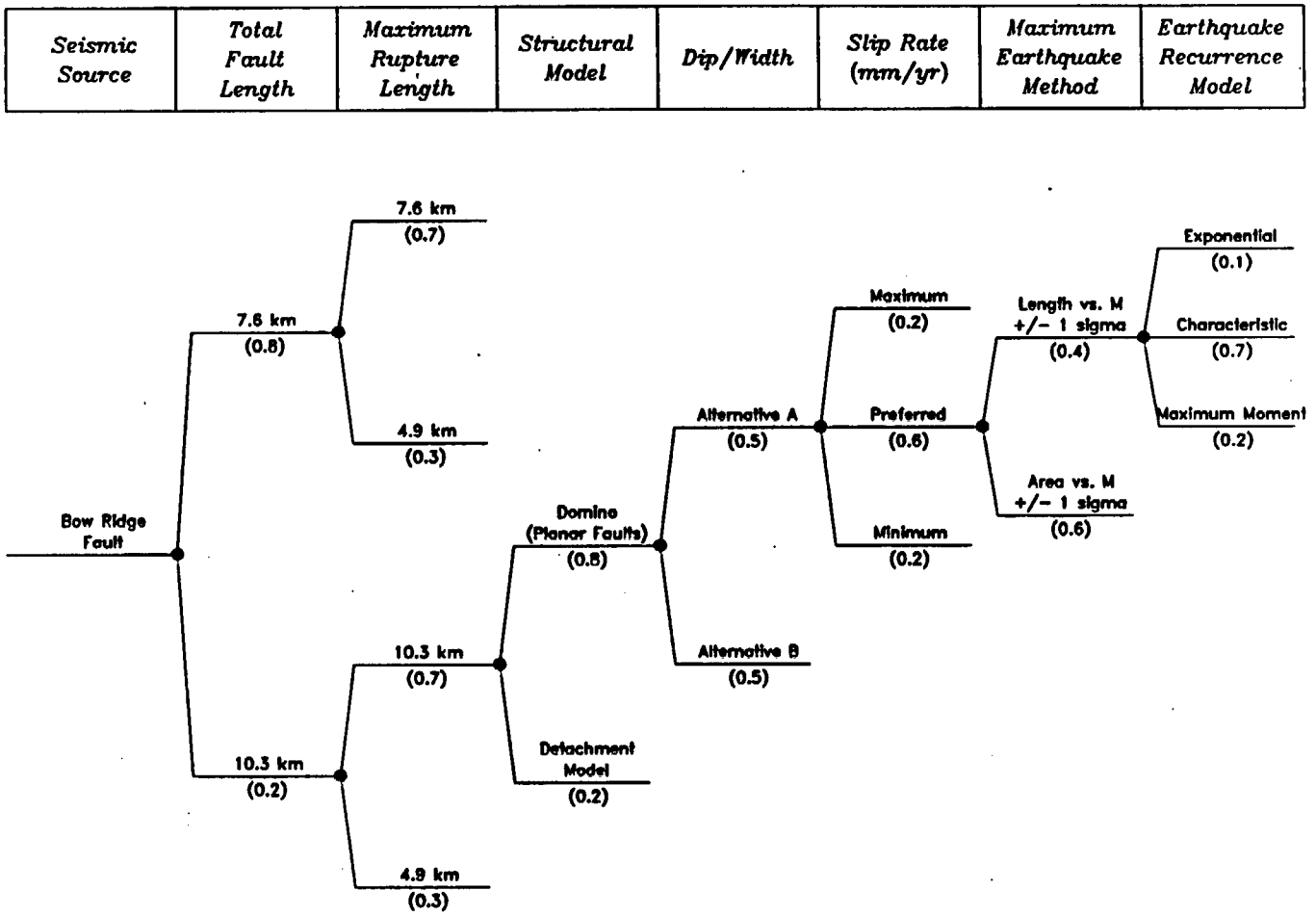

Figure 4-37c Example logic tree for local fault source given independent fault behavior

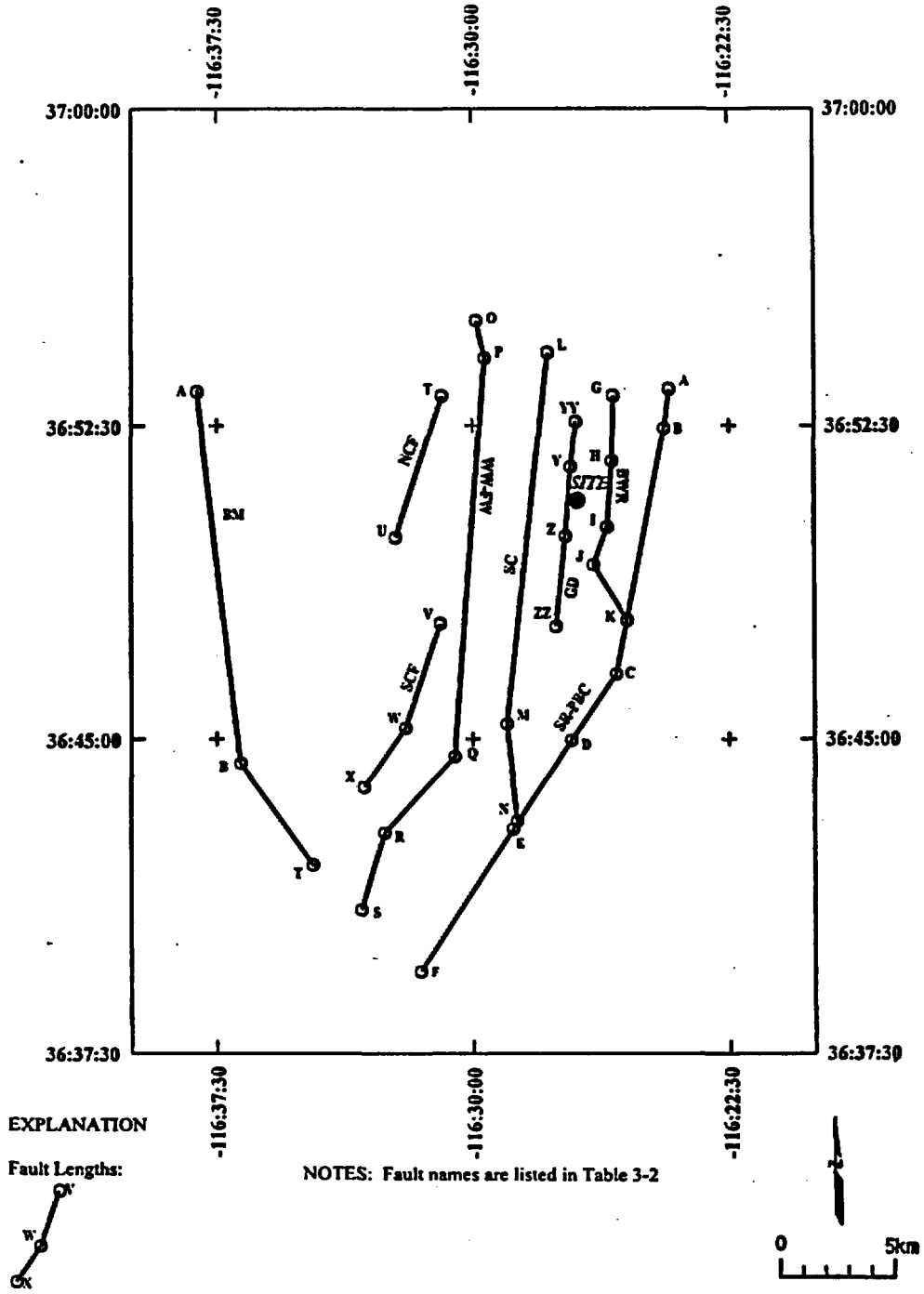

Figure 4-38 Location of local faults considered by the DFS team to be acting as independant sources

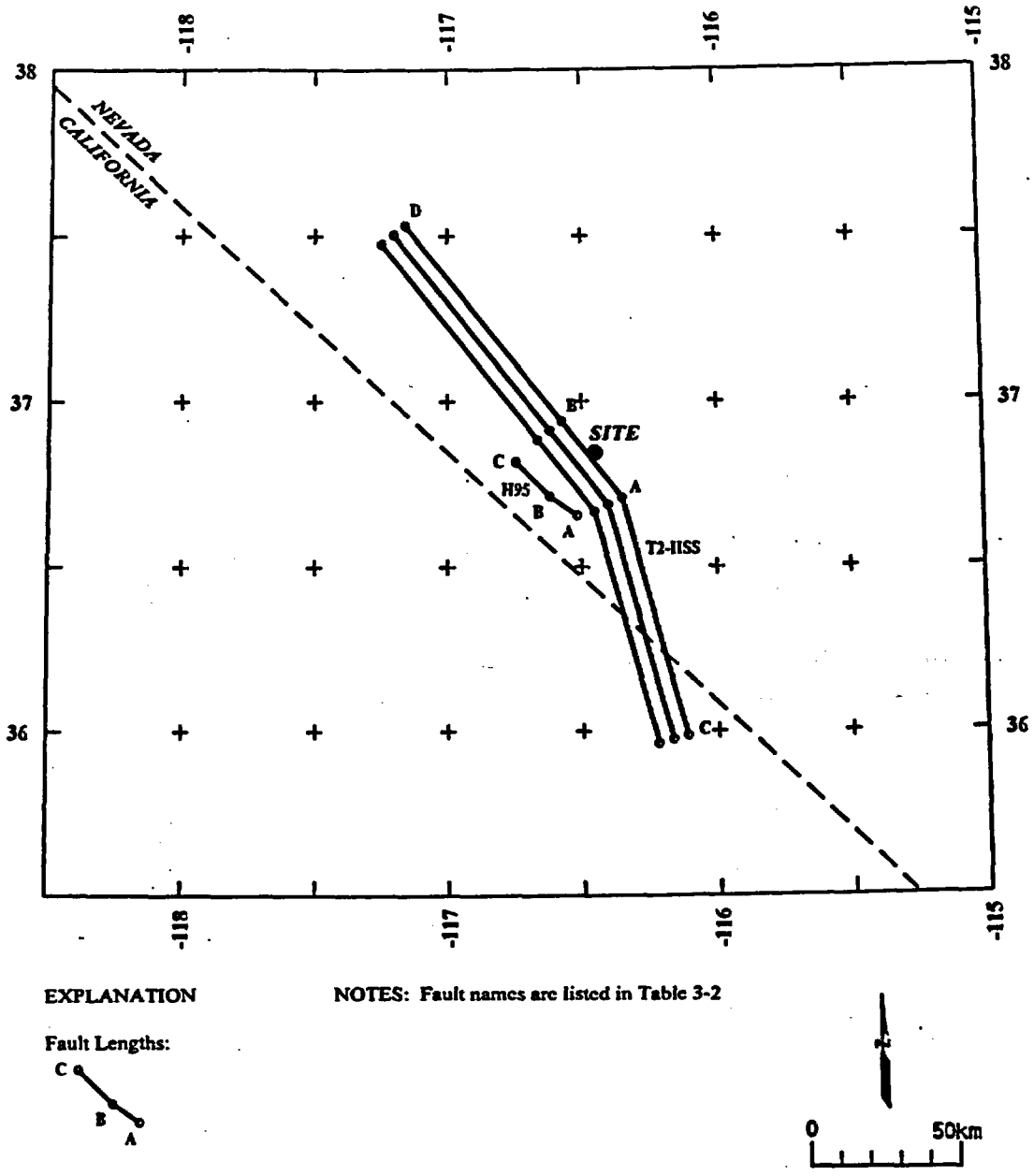

Figure 4-39 Potential locations of DFS team's inferred buried strike-slip sources

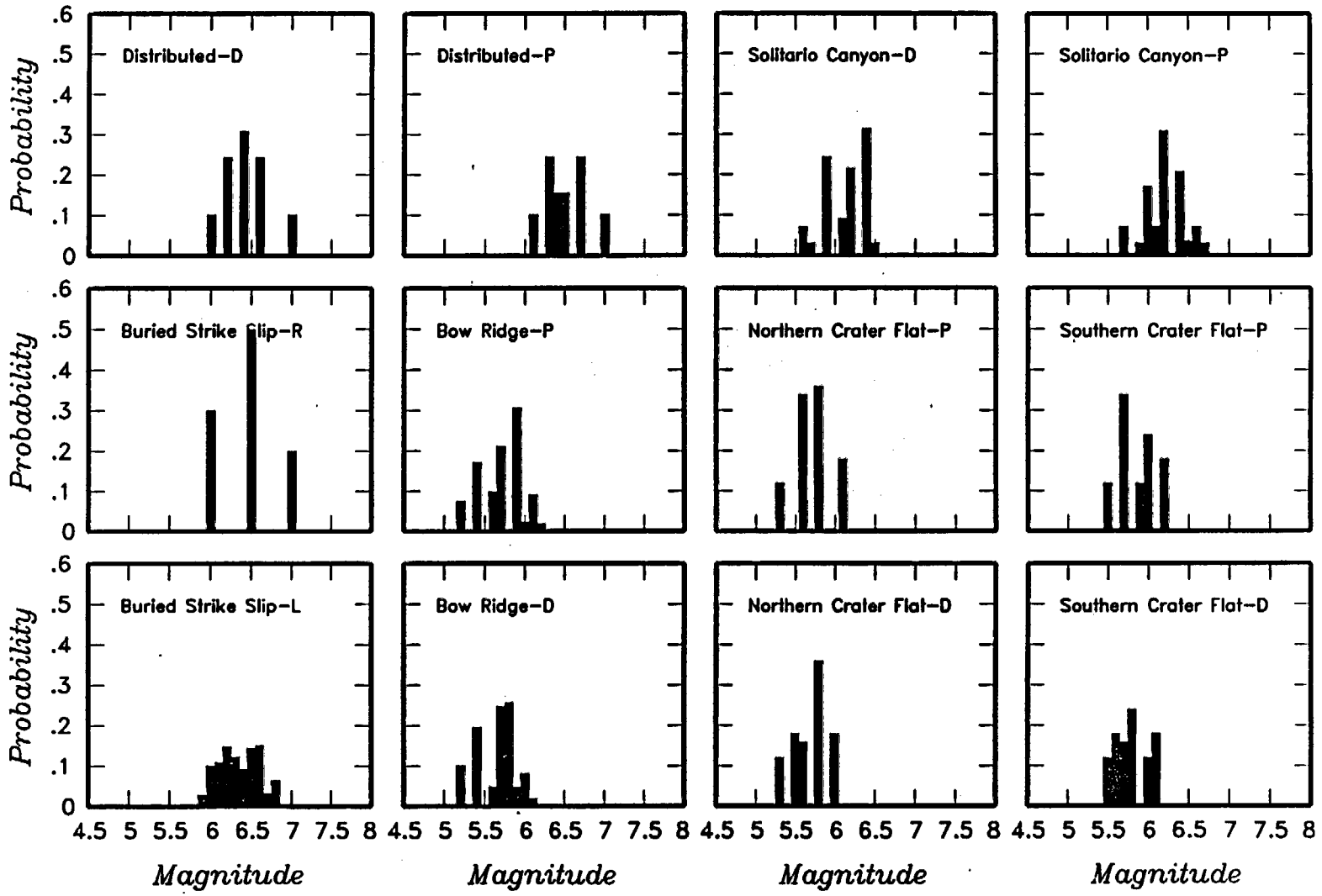

Figure 4-40 Maximum magnitude distributions for DFS team's local fault sources. D–detachment, L–local, R–regional, P–planar.

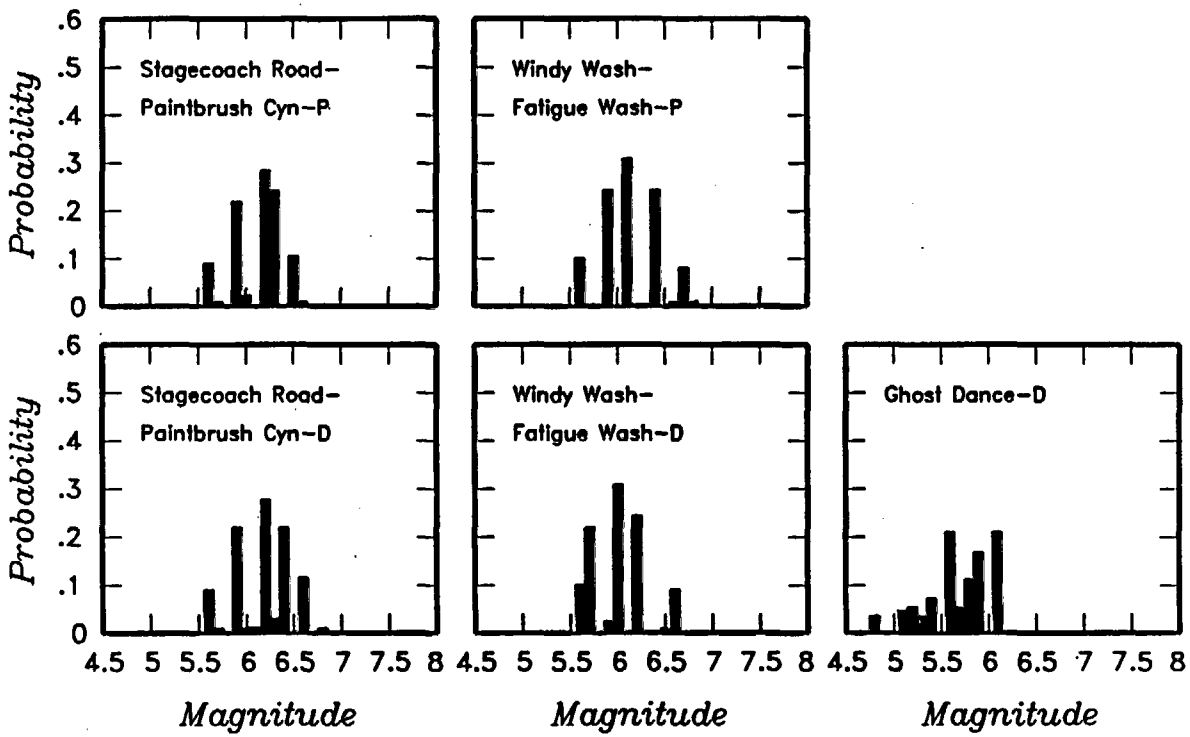

Figure 4-40 (Cont'd.) Maximum magnitude distributions for DFS team's local fault sources

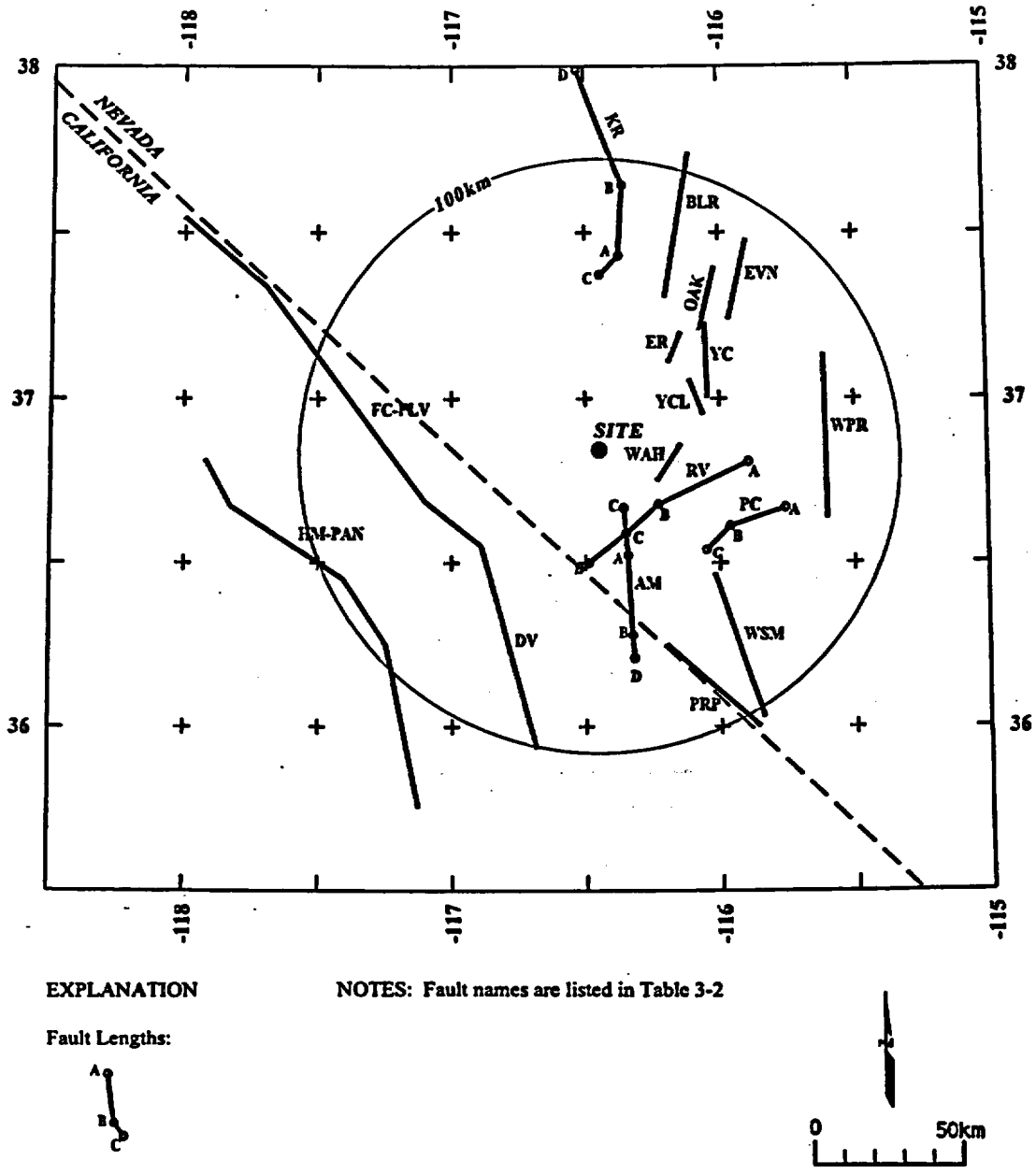

Figure 4-41 Regional fault sources considered by the DFS team

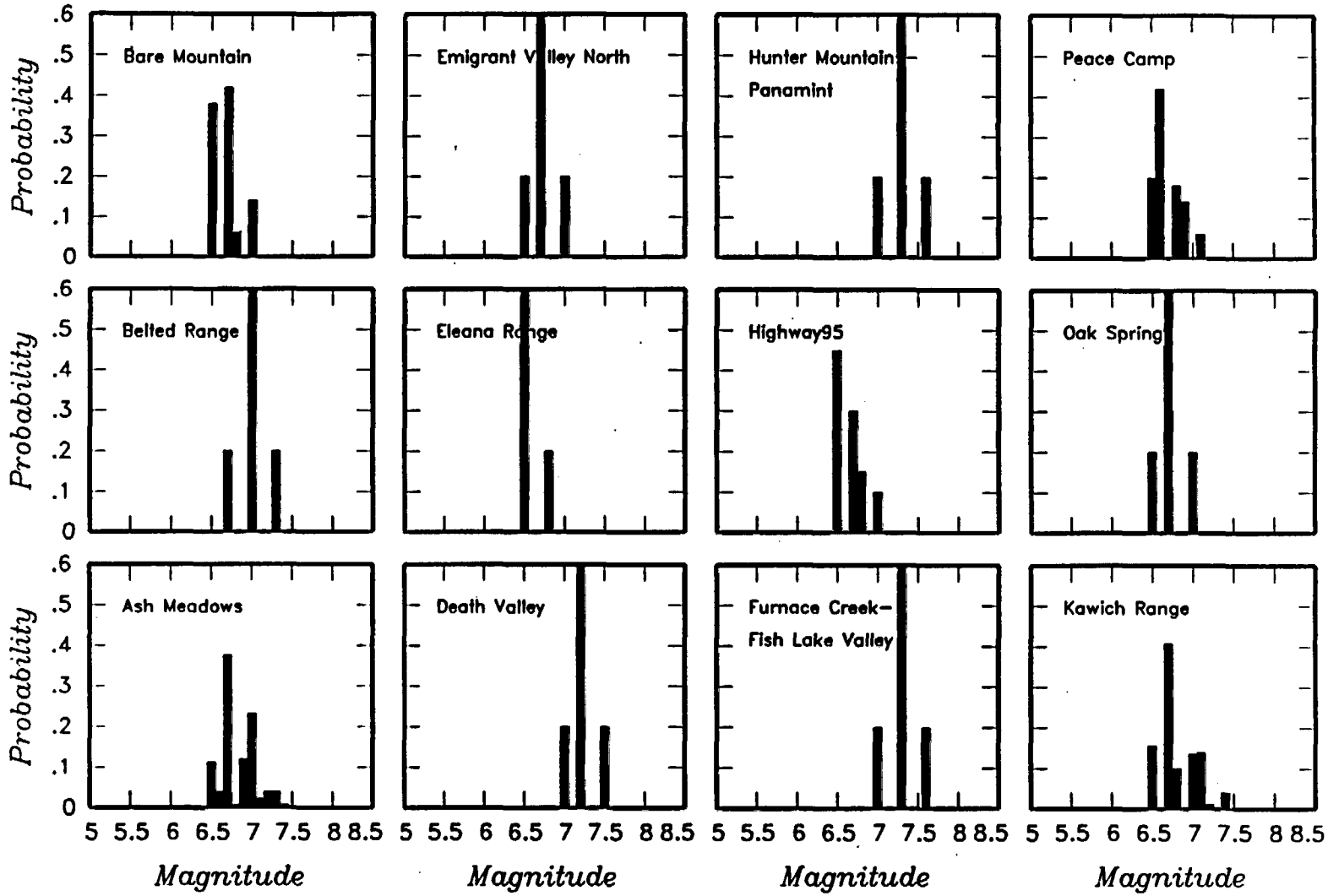

Figure 4-42 Maximum magnitude distributions for DFS team's regional fault sources

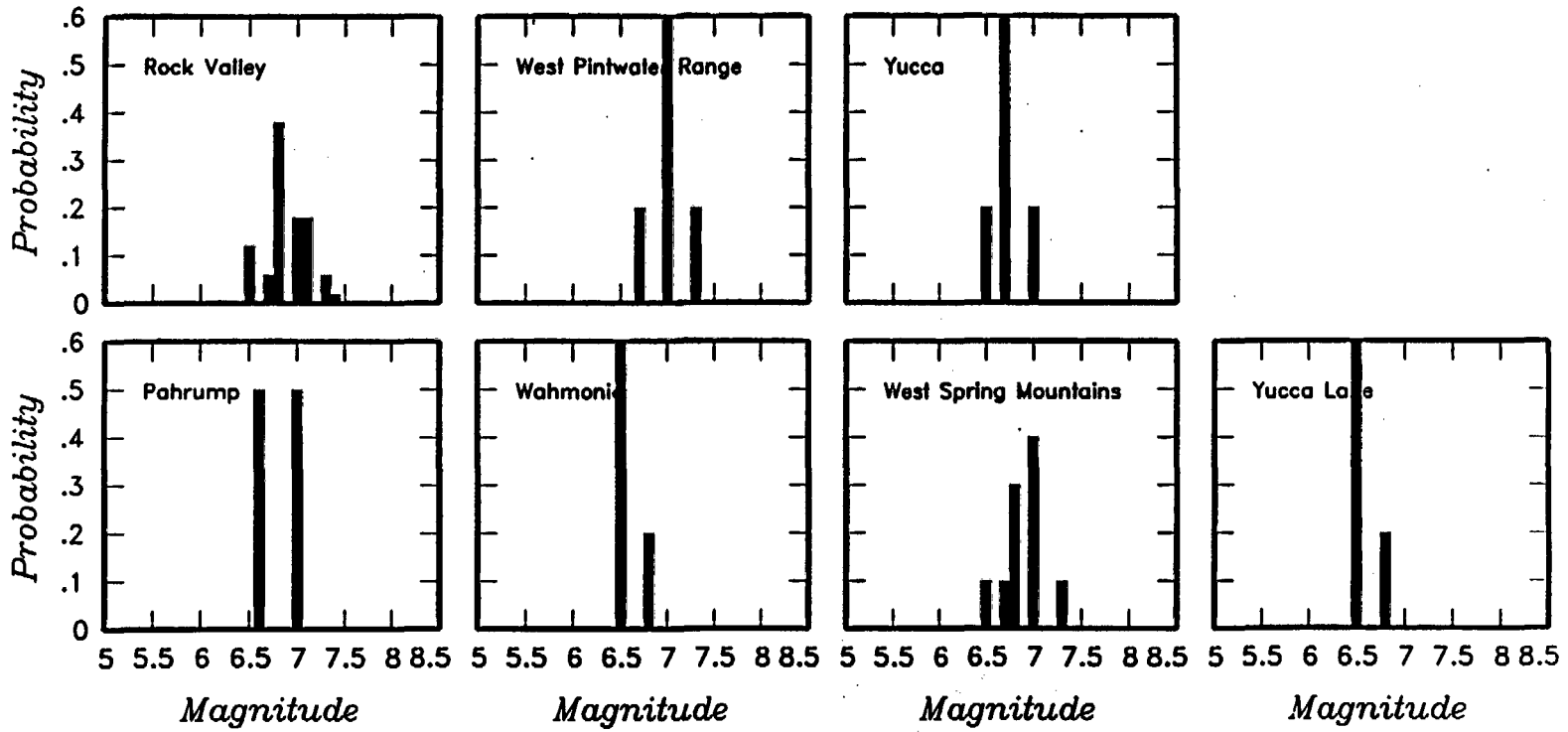

Figure 4-42 (Cont'd.) Maximum magnitude distributions for DFS team's regional fault sources

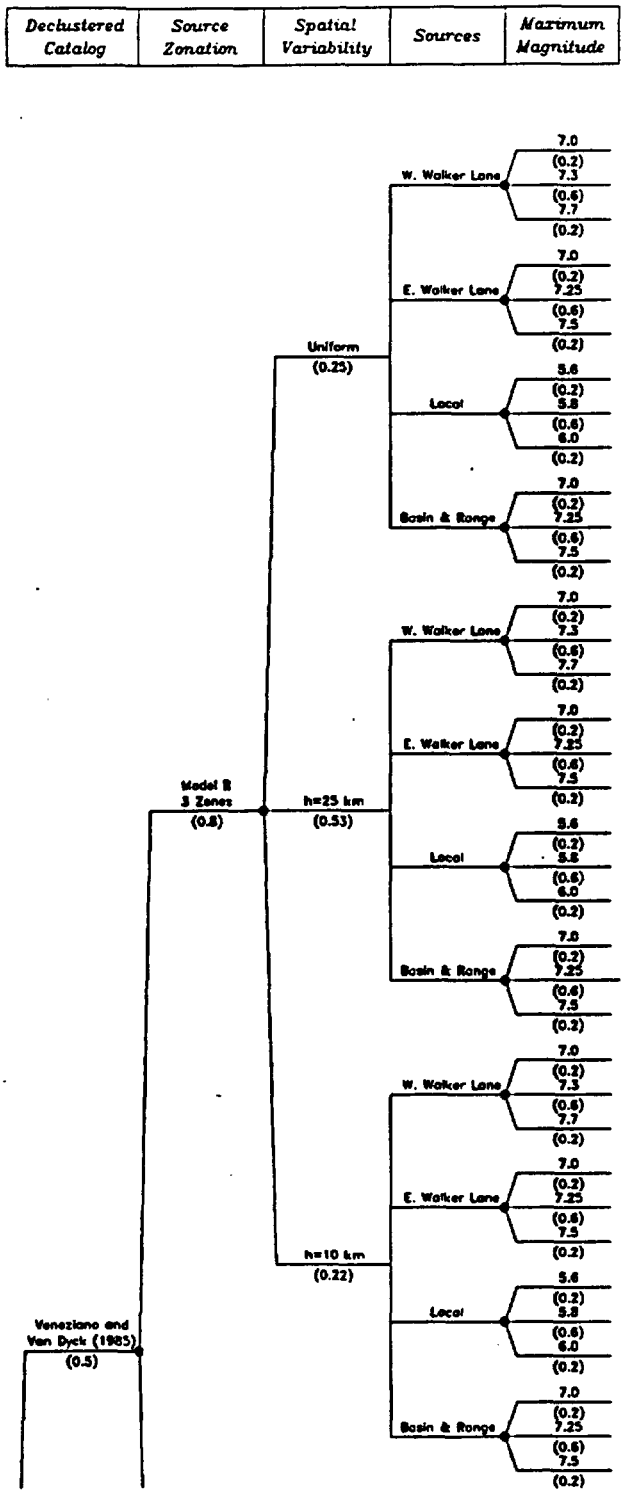

Figure 4-43 Logic tree for regional source zones developed by the DFS team

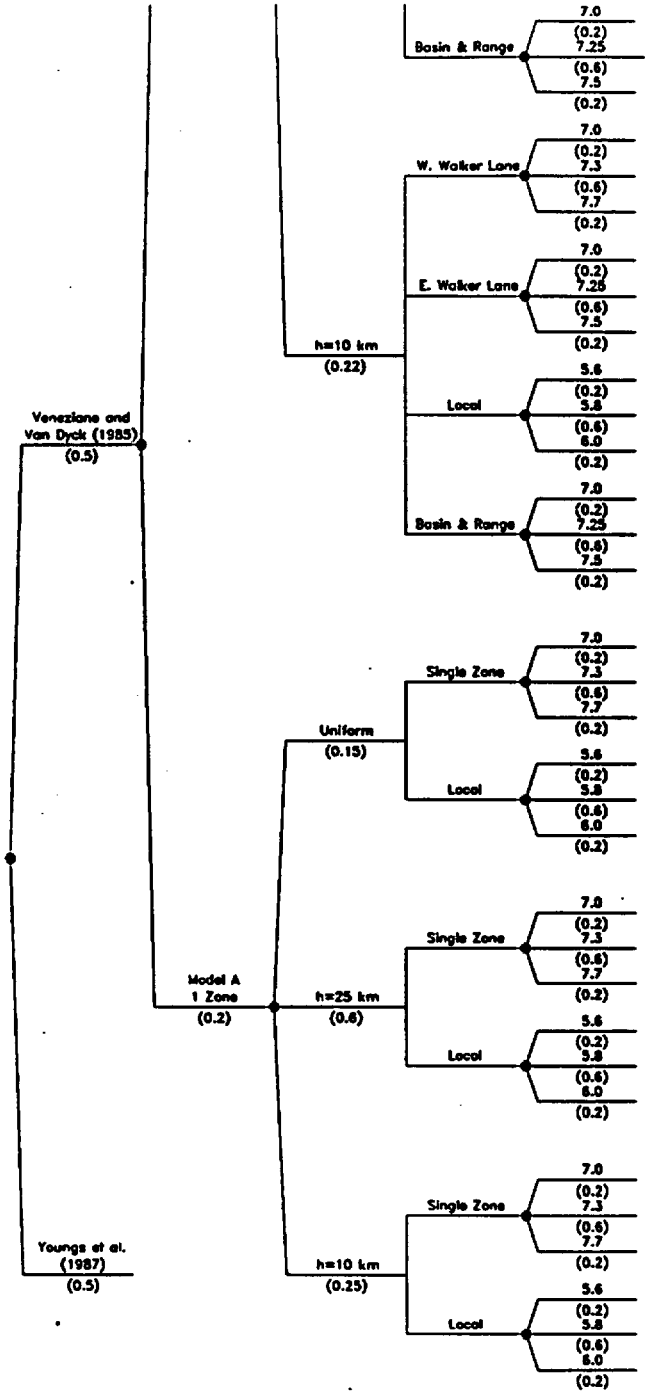

Figure 4-43 (Cont'd.) Logic tree for regional source zones developed by the DFS team

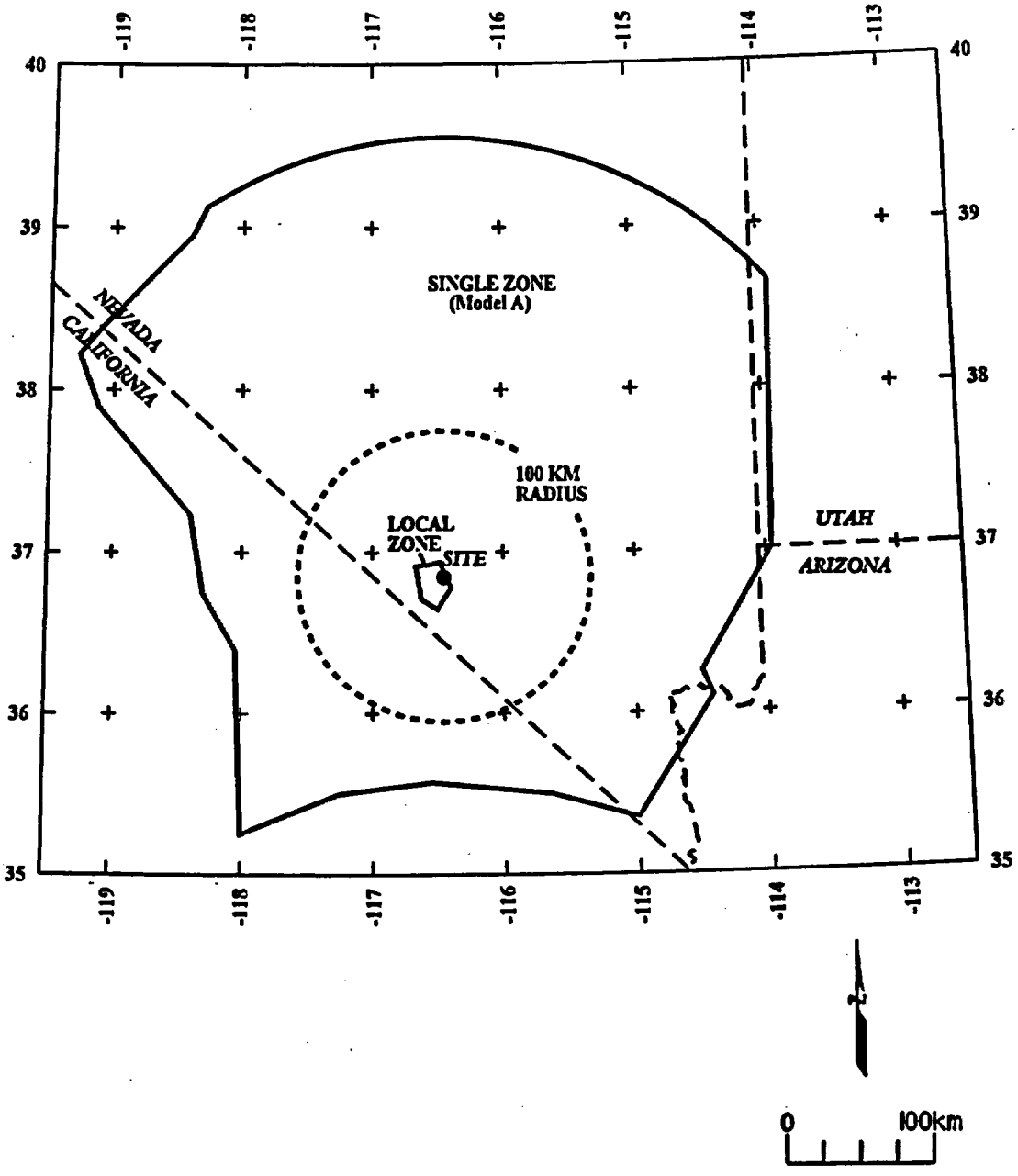

Figure 4-44 Alternative regional source zone models considered by the DFS team

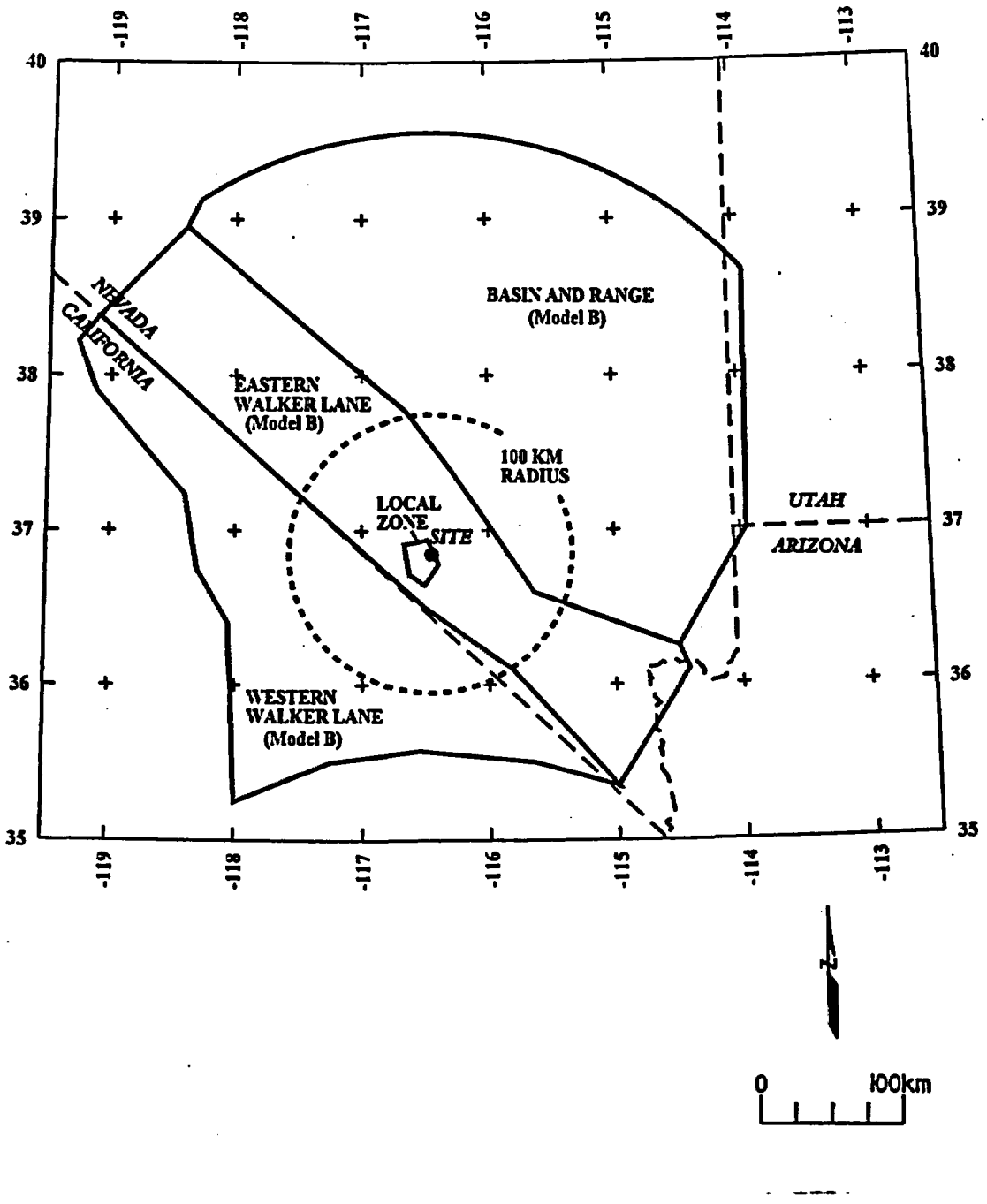

Figure 4-44 (Cont'd.) Alternative regional source zone models considered by the DFS team

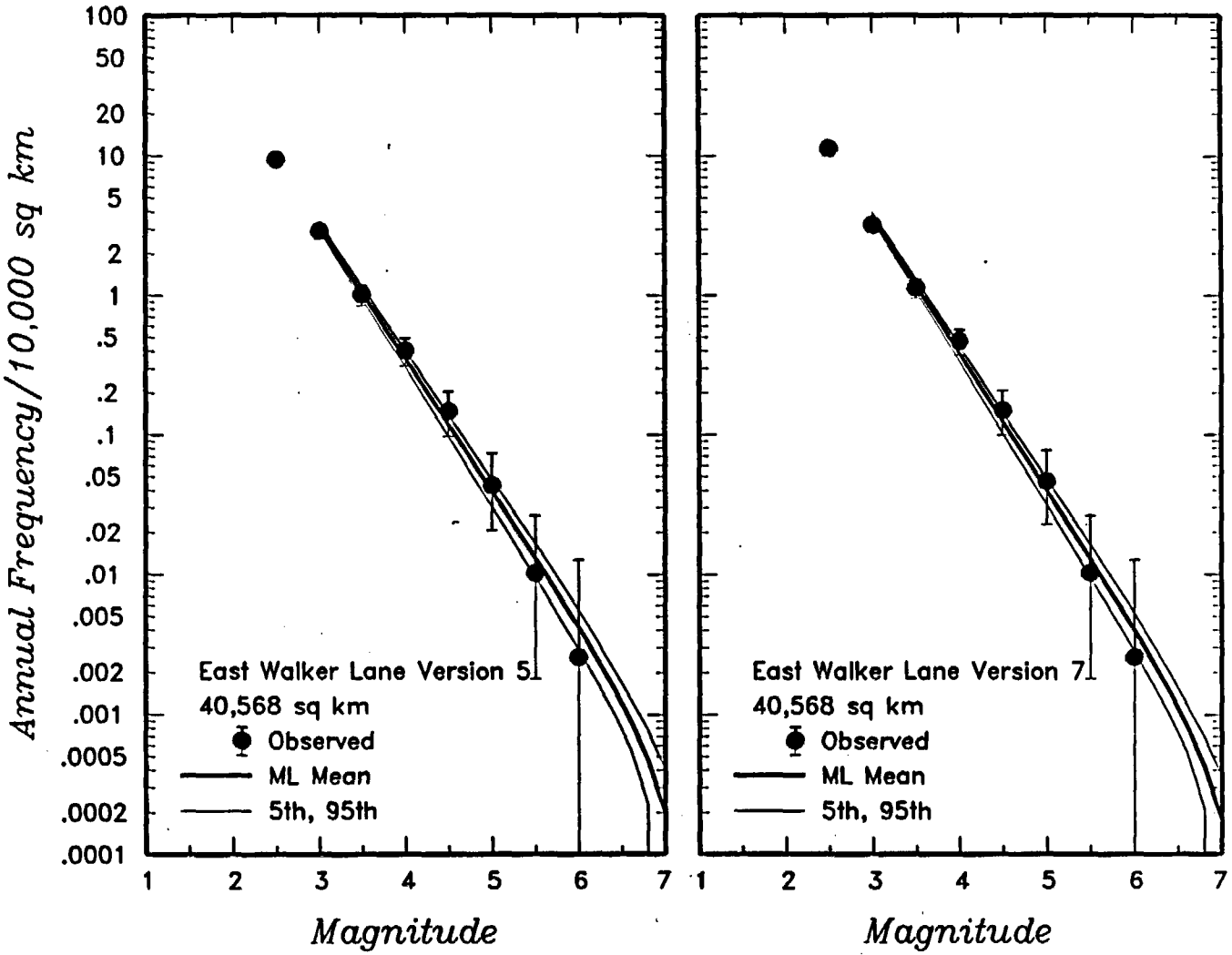

Figure 4-45 Earthquake recurrence relationships for the regional source zones defined by the DFS team. The solid dots with vertical error bars represent the observed data. The thick and thin solid curves are the mean, 5th, and 95th percentiles of the recurrence rates based on the uncertainty in recurrence parameters and maximum magnitude.

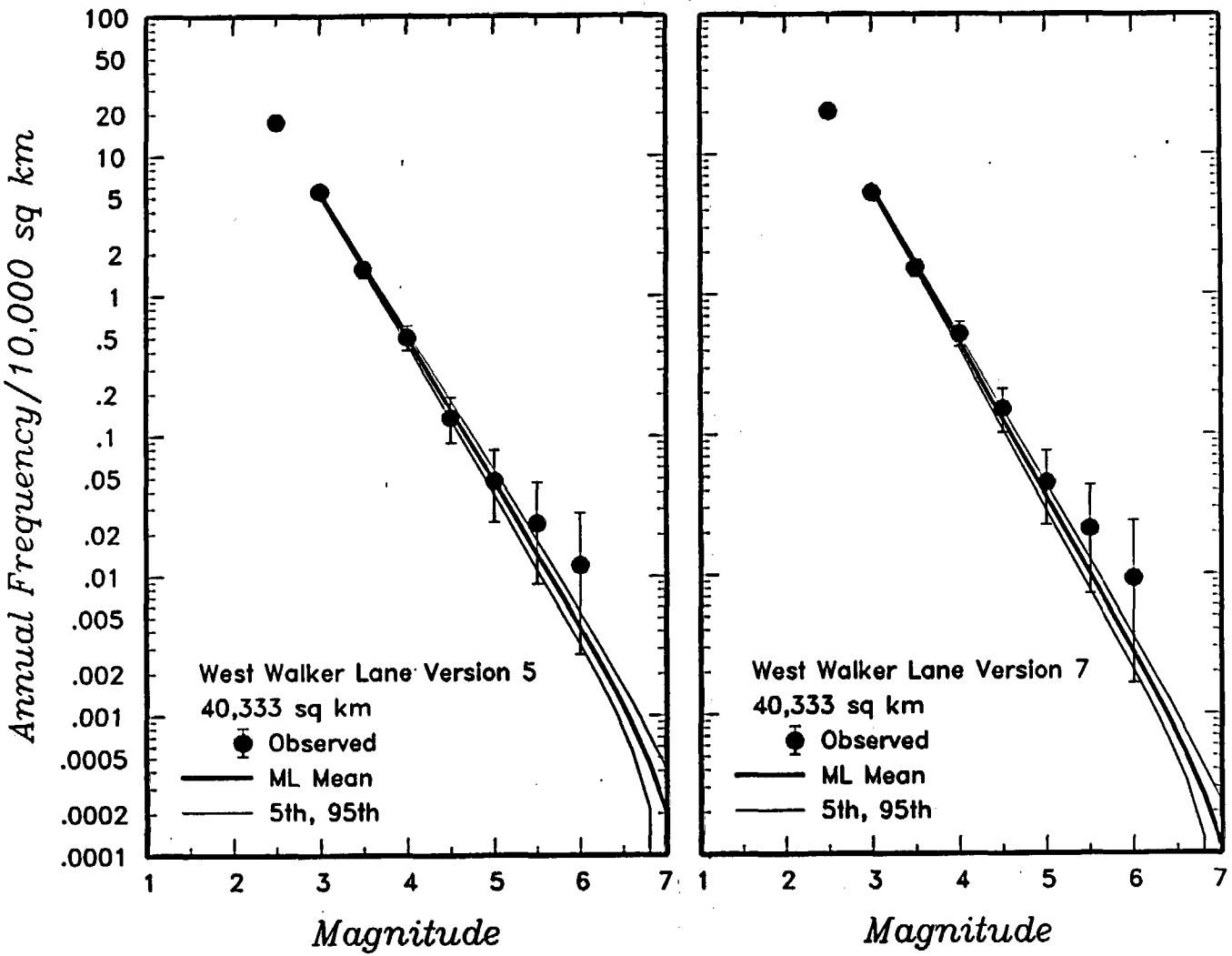

Figure 4-45 (Cont'd.) Earthquake recurrence relationships for the regional source zones defined by the DFS team

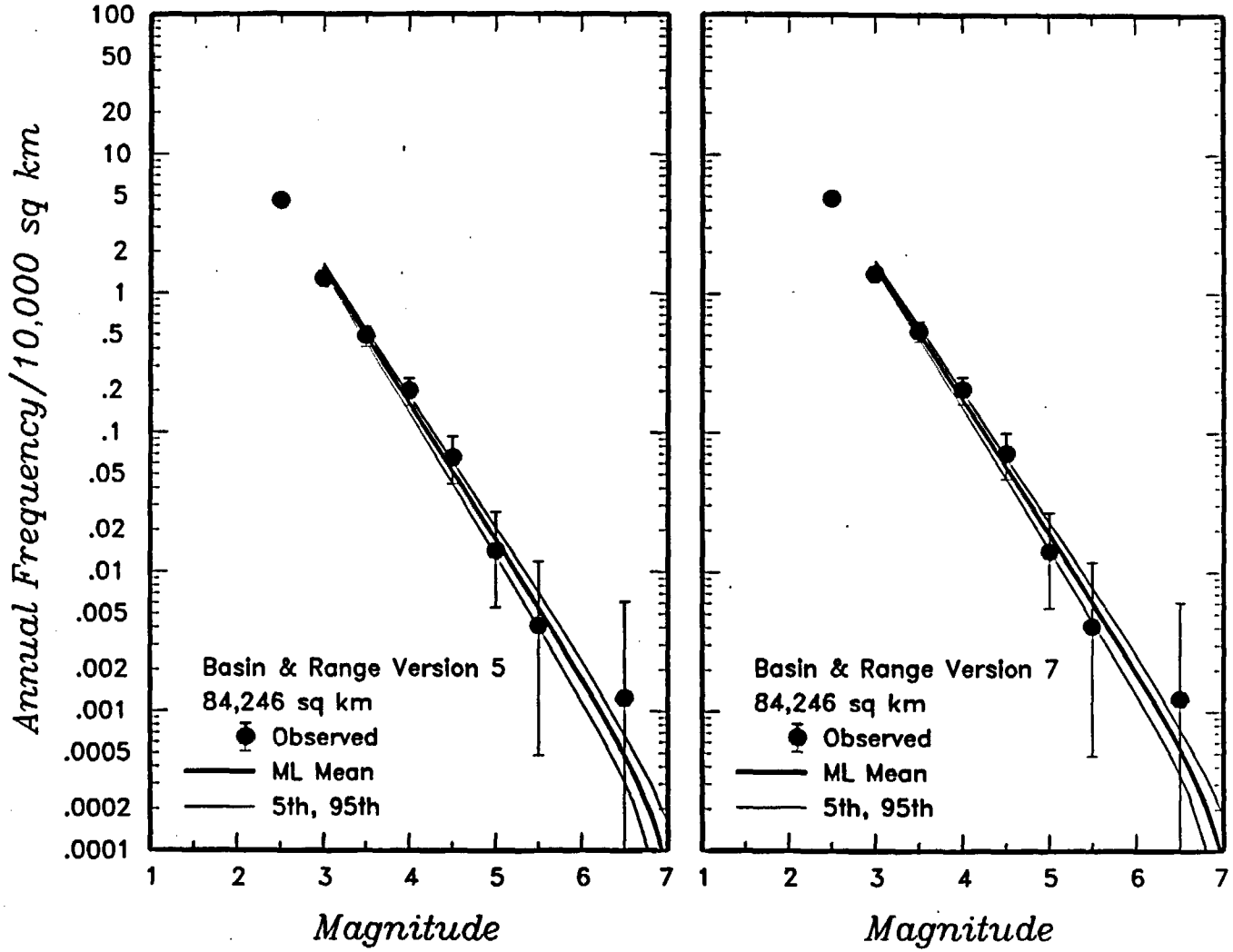

Figure 4-45 (Cont'd.) Earthquake recurrence relationships for the regional source zones defined by the DFS team

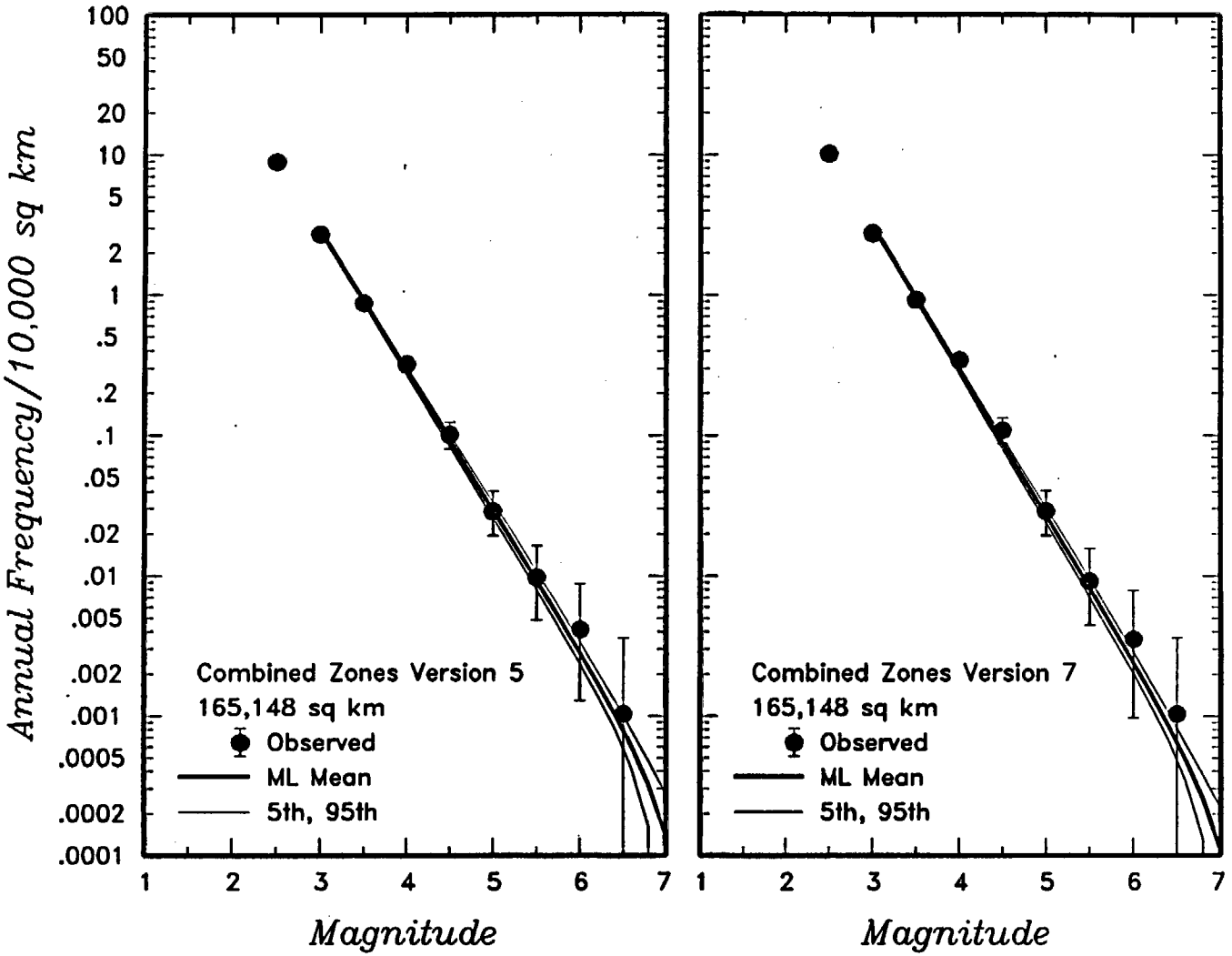

Figure 4-45 (Cont'd.) Earthquake recurrence relationships for the regional source zones defined by the DFS team

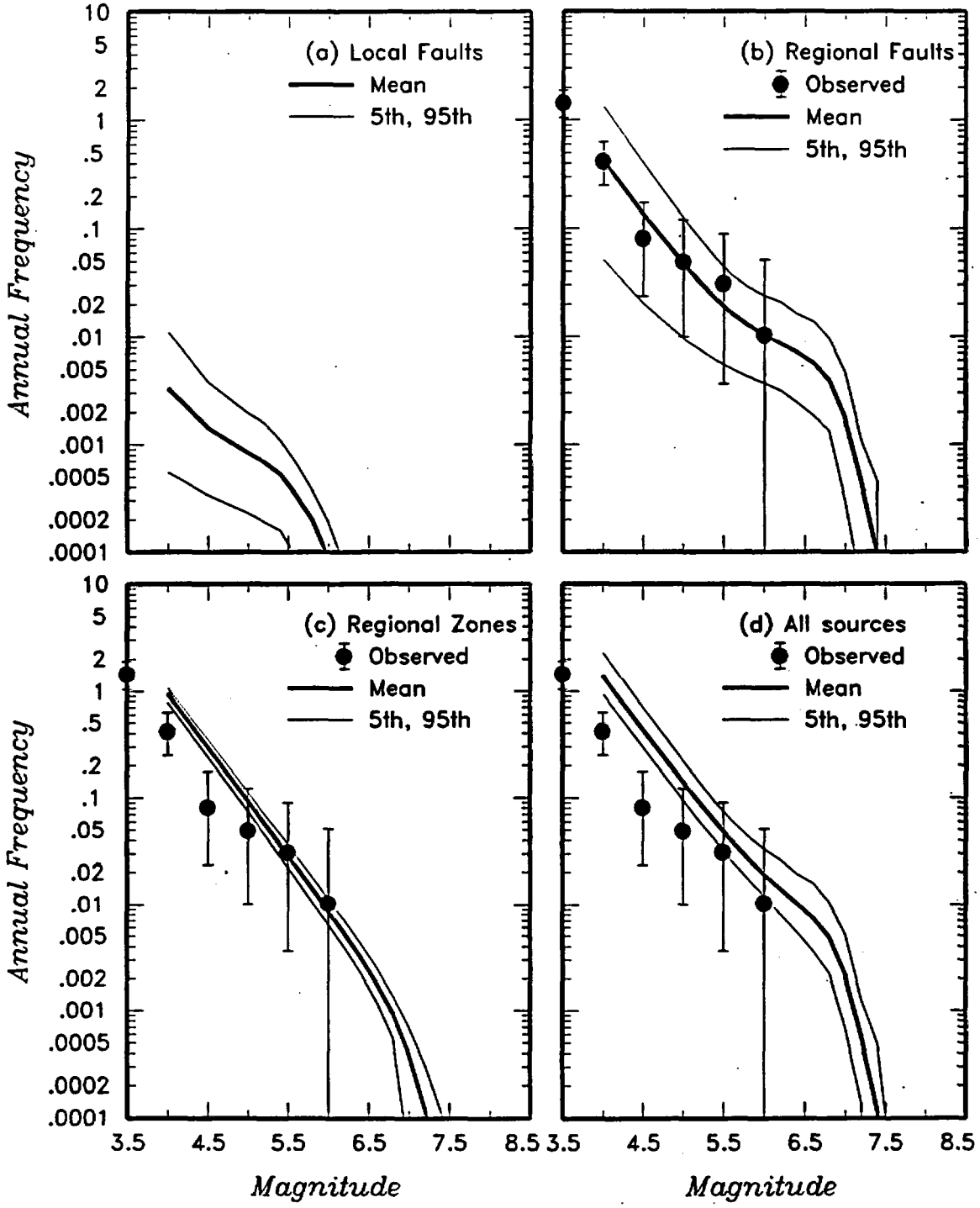

Figure 4-46 Predicted mean, 5th-, and 95th-percentile recurrence rates for (a) local fault sources, (b) regional fault sources, (c) regional source zones, and (d) all sources combined for the DFS team. The solid dots with vertical error bars indicate the observed frequency of earthquakes occurring within 100 km of the Yucca Mountain site.

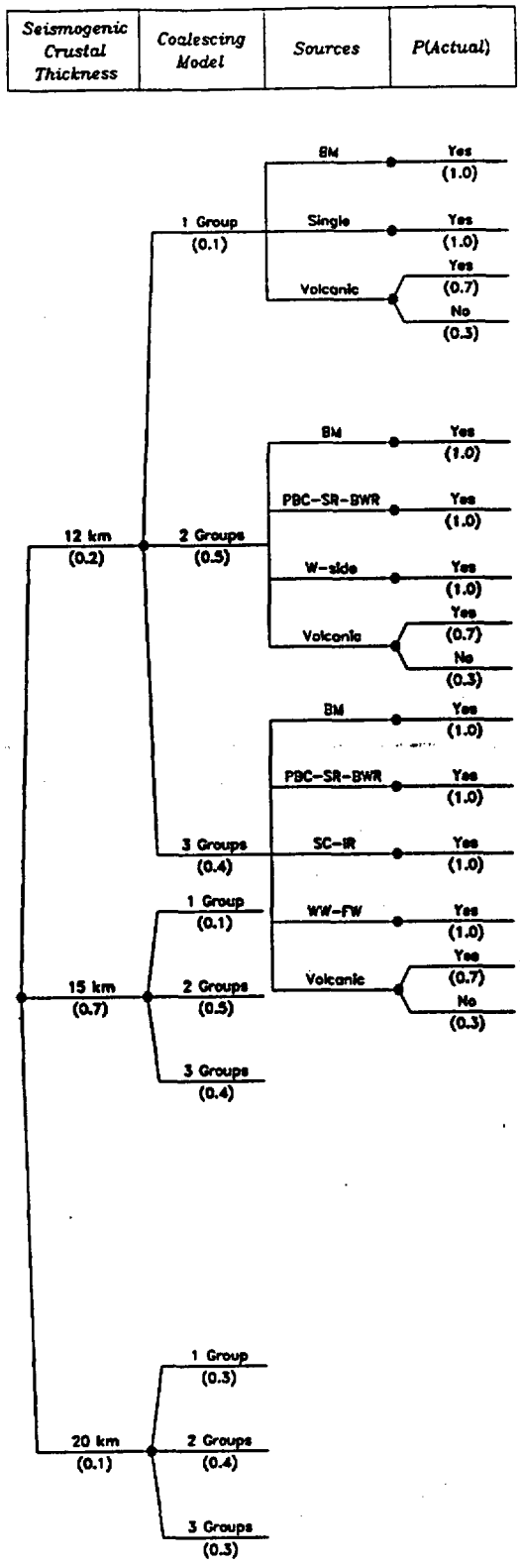

Figure 4-47 Logic tree for local fault sources developed by the RYA team

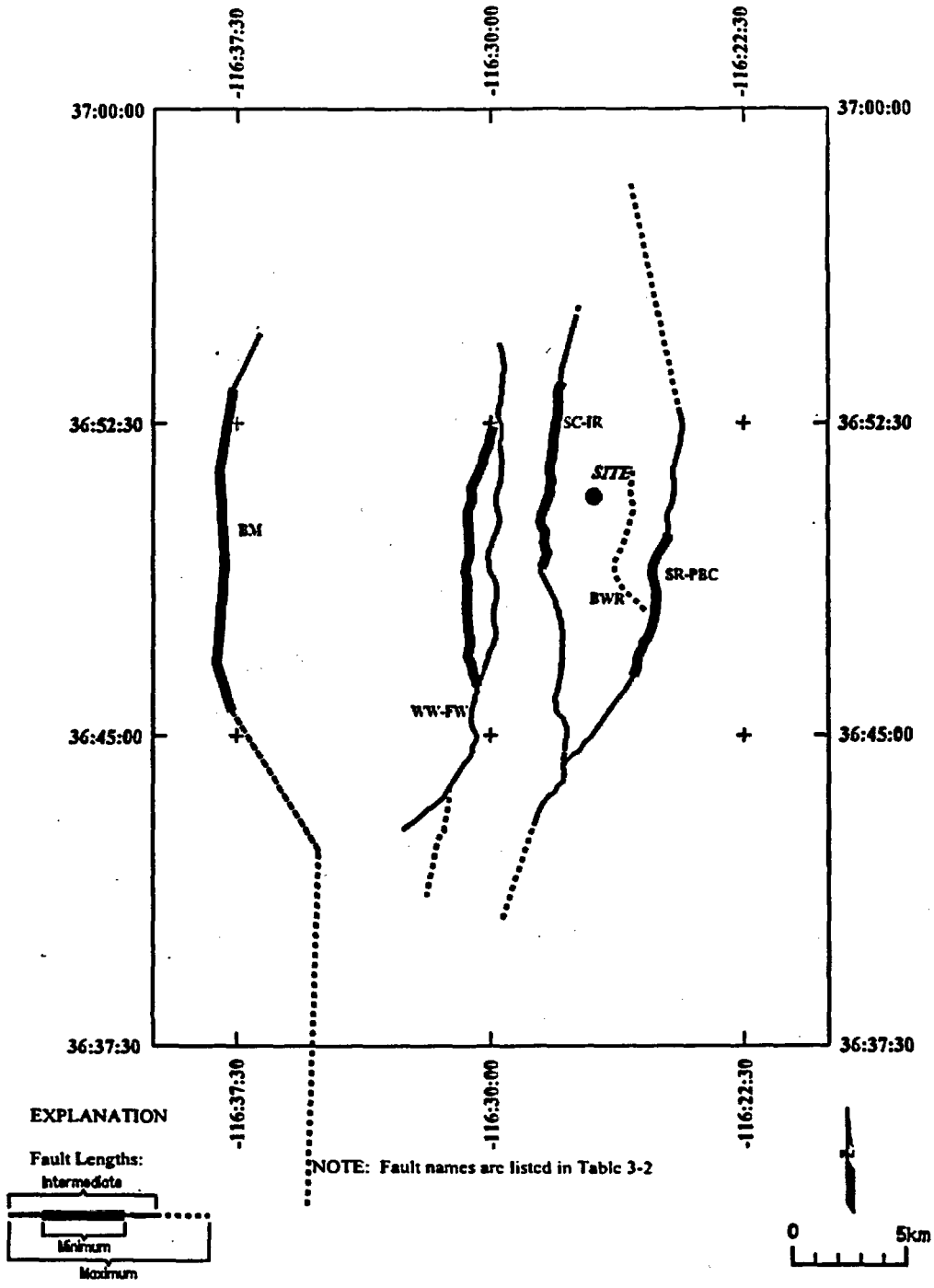

Figure 4-48 Location of local fault sources considered by the RYA team

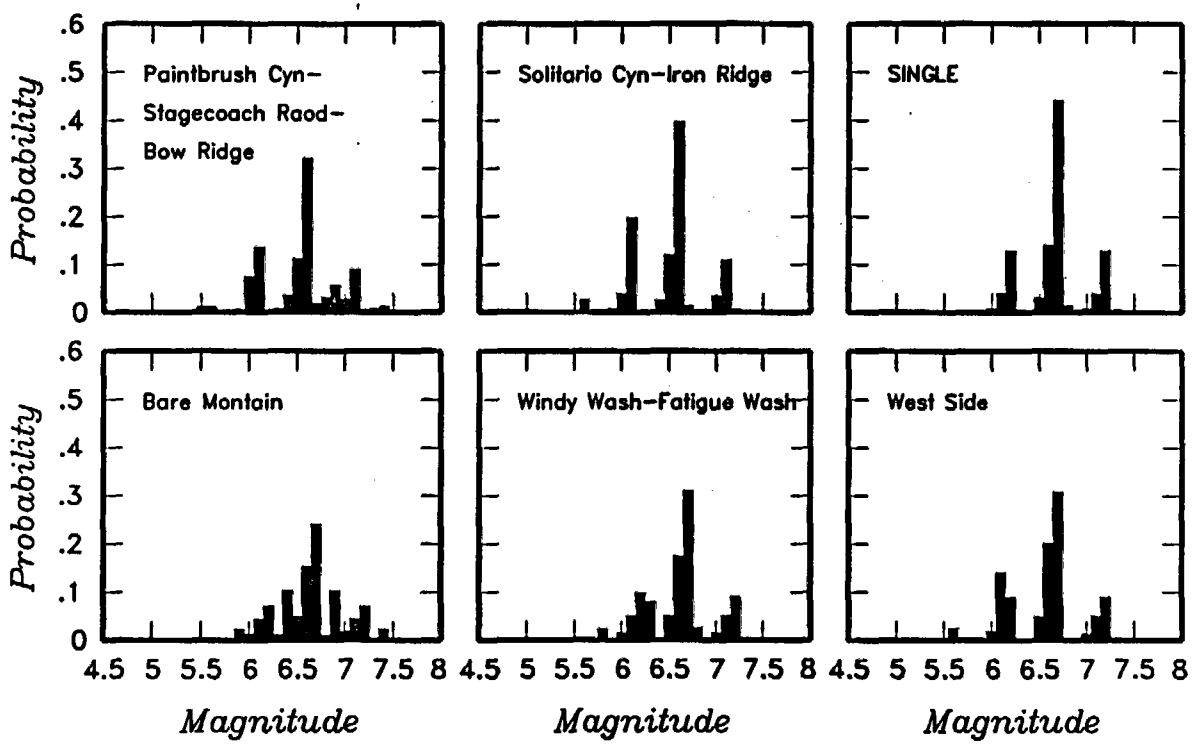

Figure 4-49 Maximum magnitude distributions for RYA team's local fault sources. SINGLE–coalescing source model with single fault system.

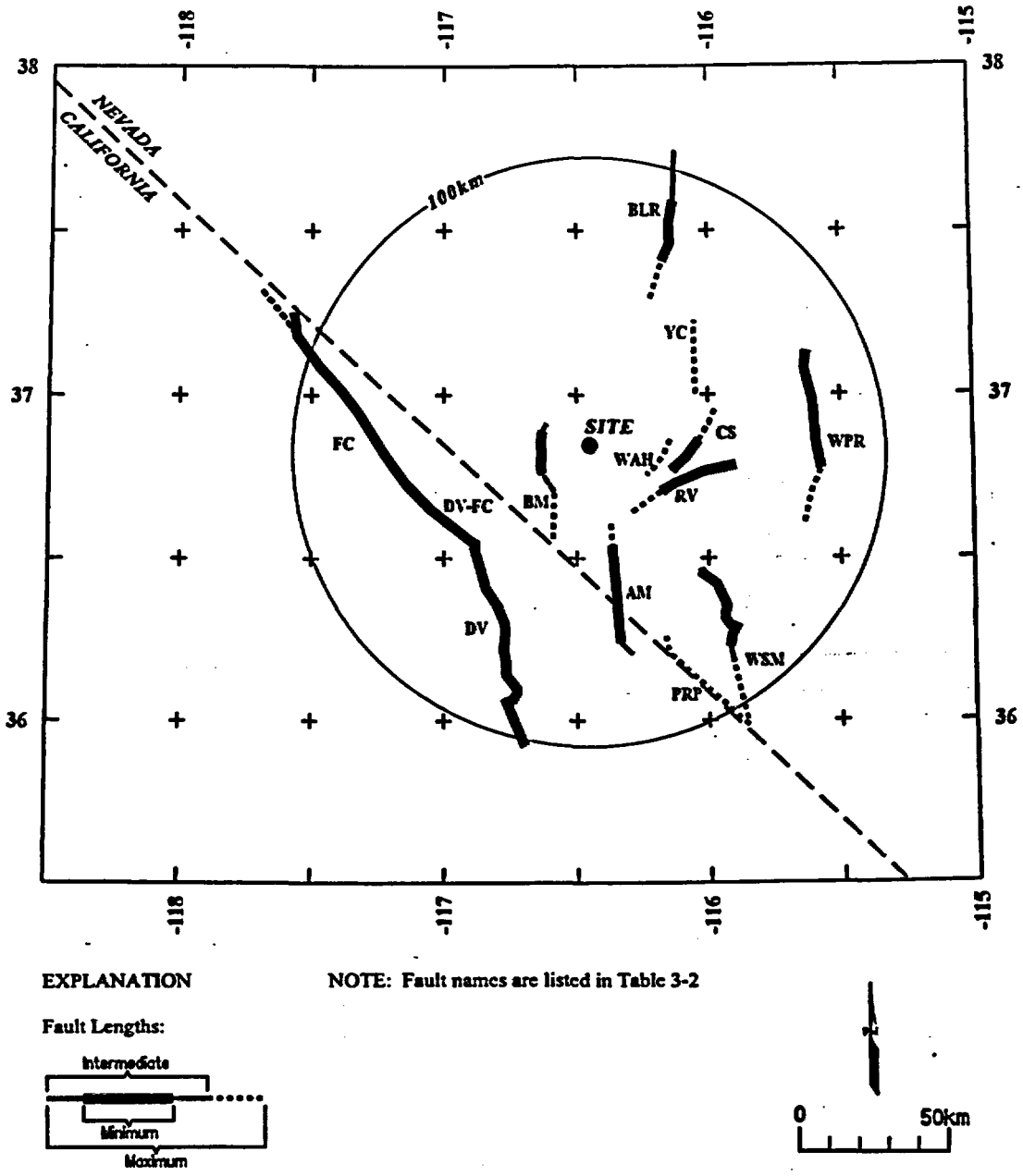

Figure 4-50 Regional fault sources considered by the RYA team

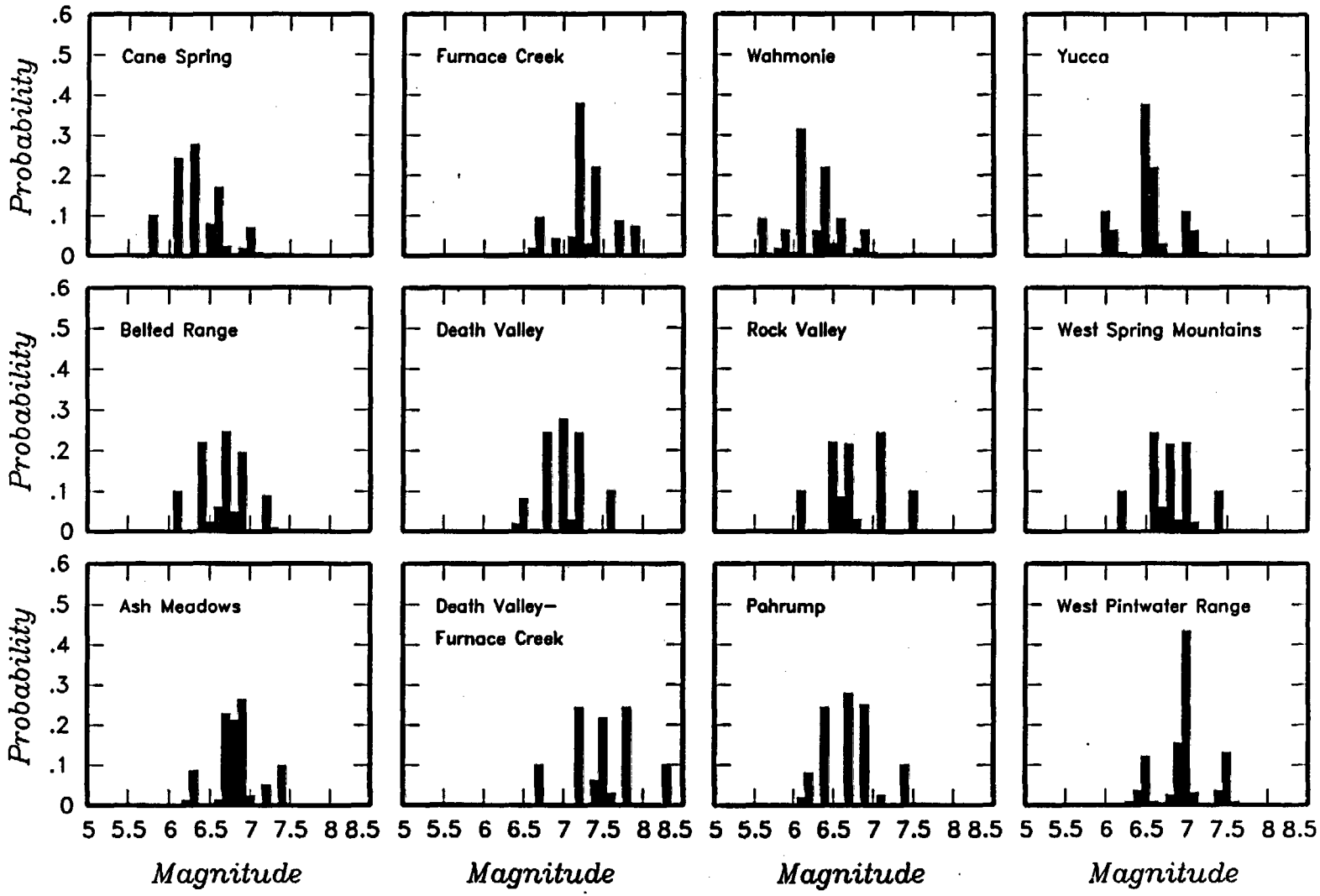

Figure 4-51 Maximum magnitude distributions for RYA team's regional fault sources

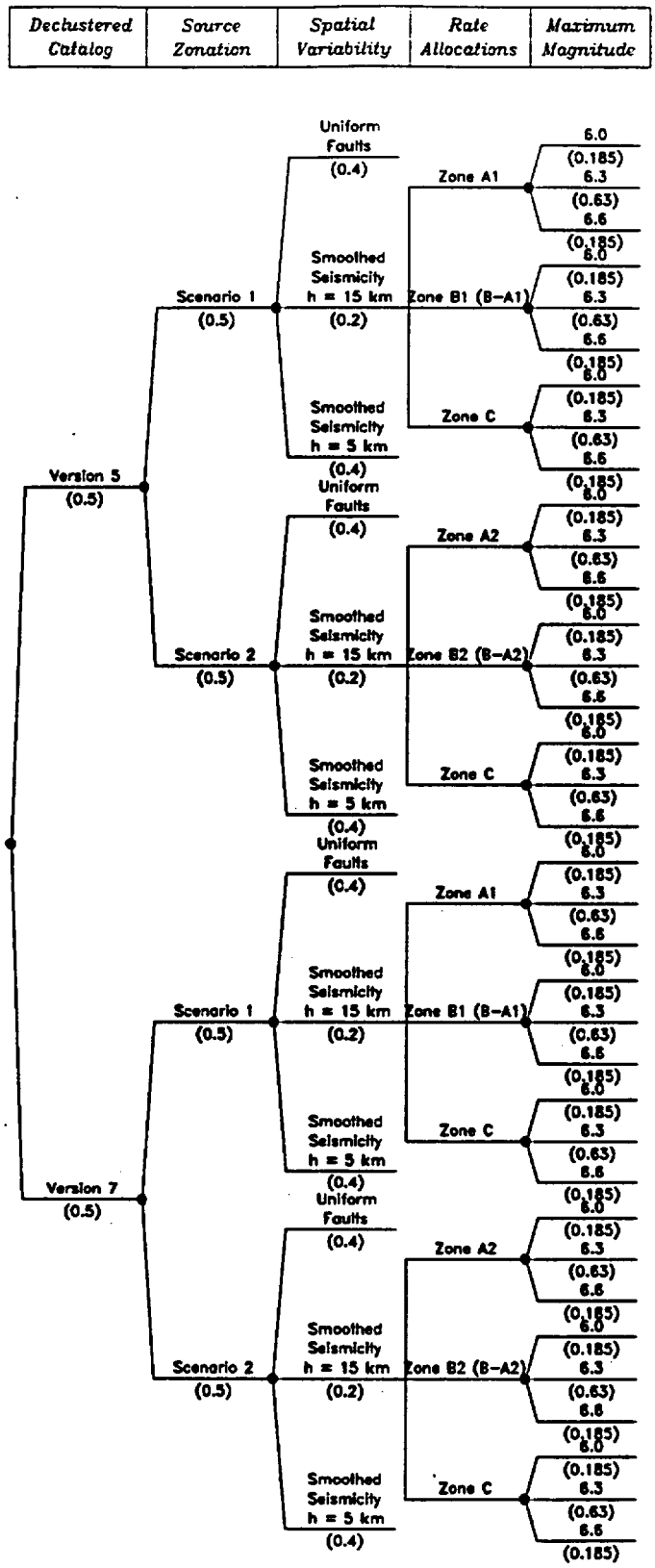

Figure 4-52 Logic tree for regional source zones developed by the RYA team

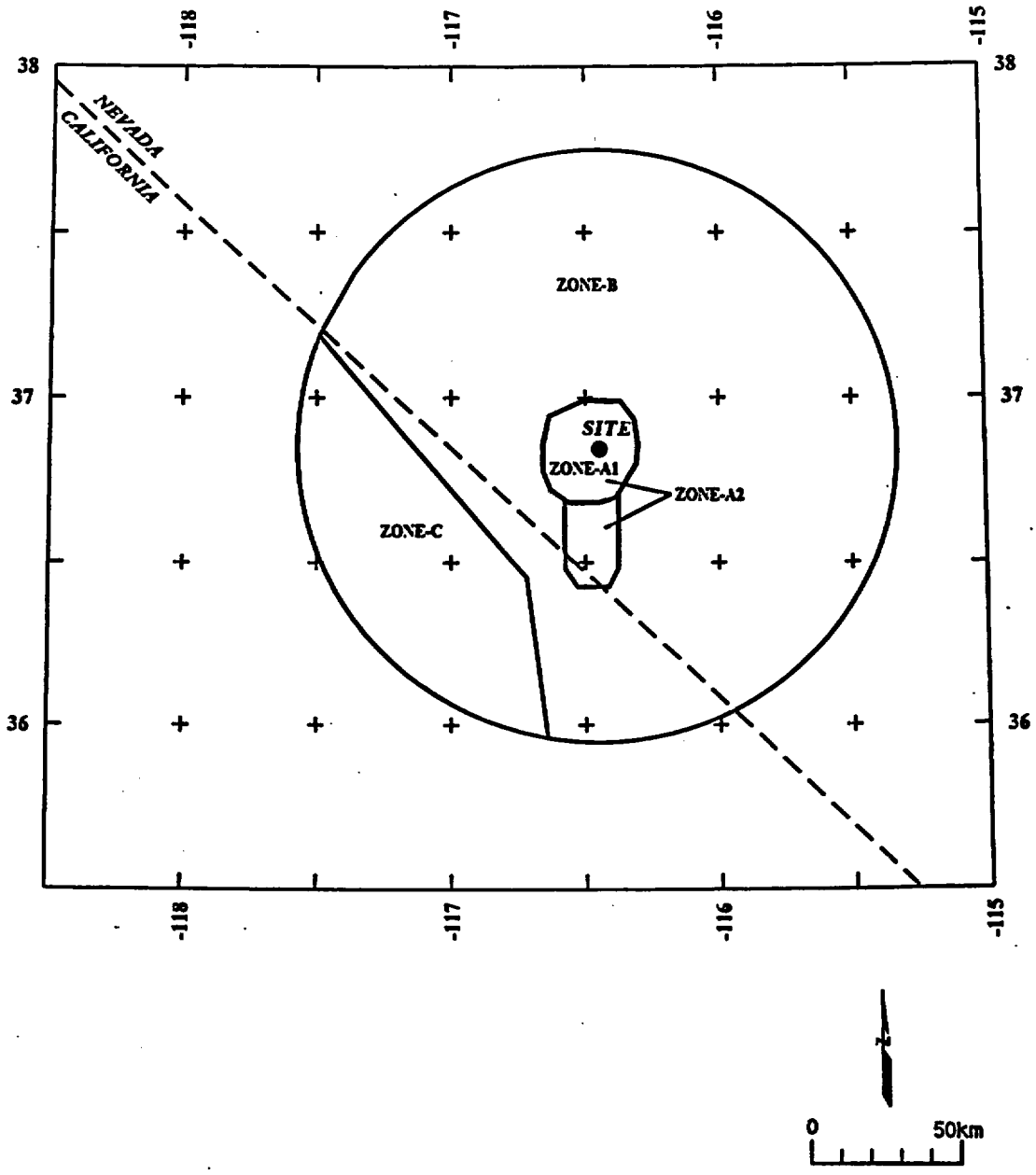

Figure 4-53 Alternative regional source zone models considered by the RYA team

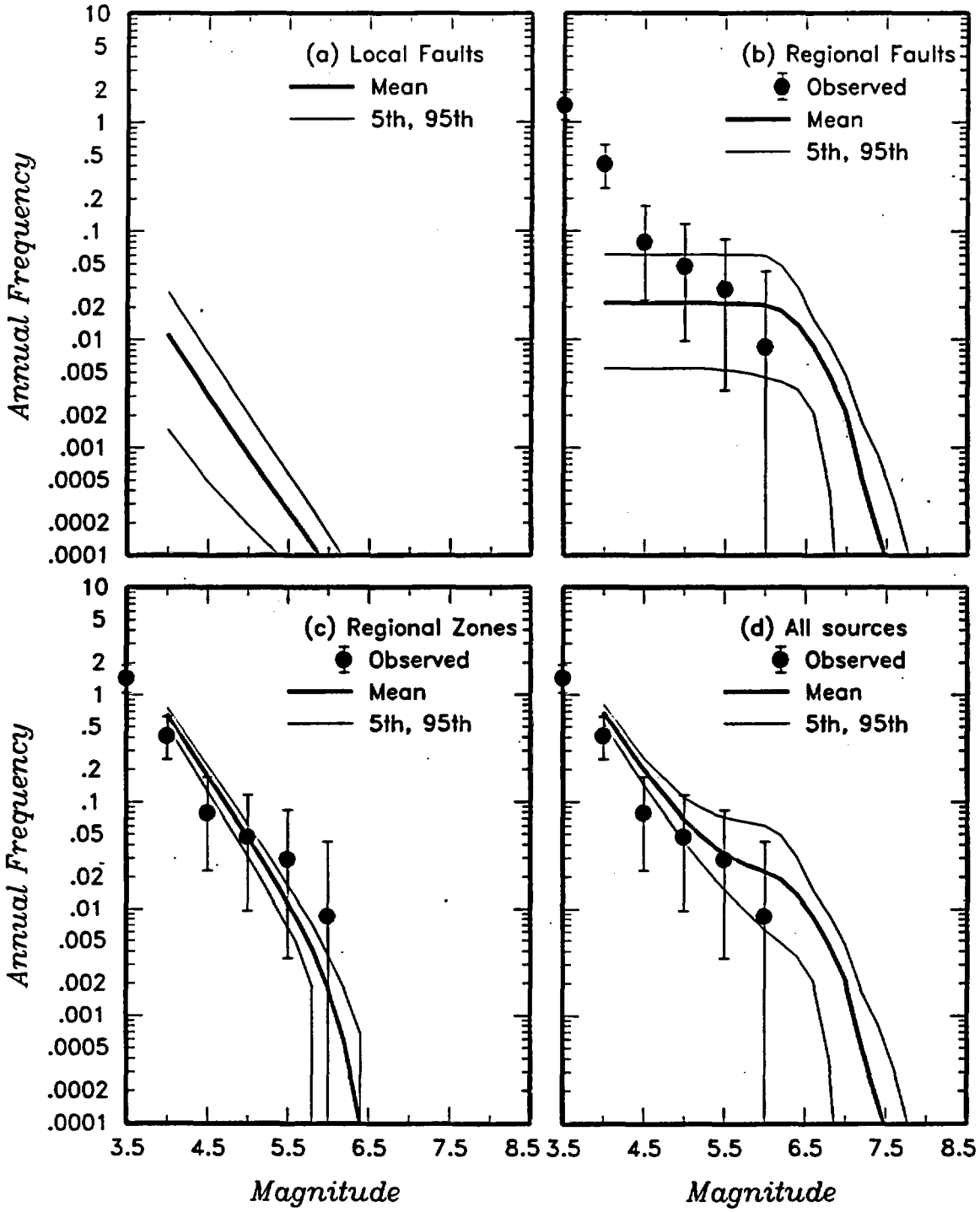

Figure 4-54 Predicted mean, 5th-, and 95th-percentile recurrence rates for (a) local fault sources, (b) regional fault sources, (c) regional source zones, and (d) all sources combined for the RYA team. The solid dots with vertical error bars indicate the observed frequency of earthquakes occurring within 100 km of the Yucca Mountain site.

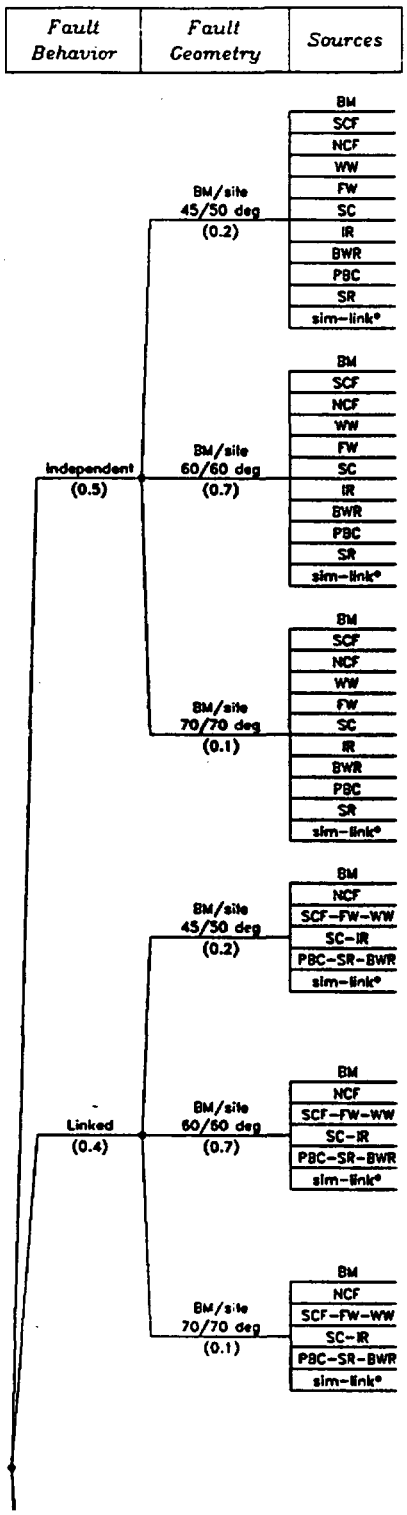

Figure 4-55 Logic tree for local fault sources developed by the SBK team

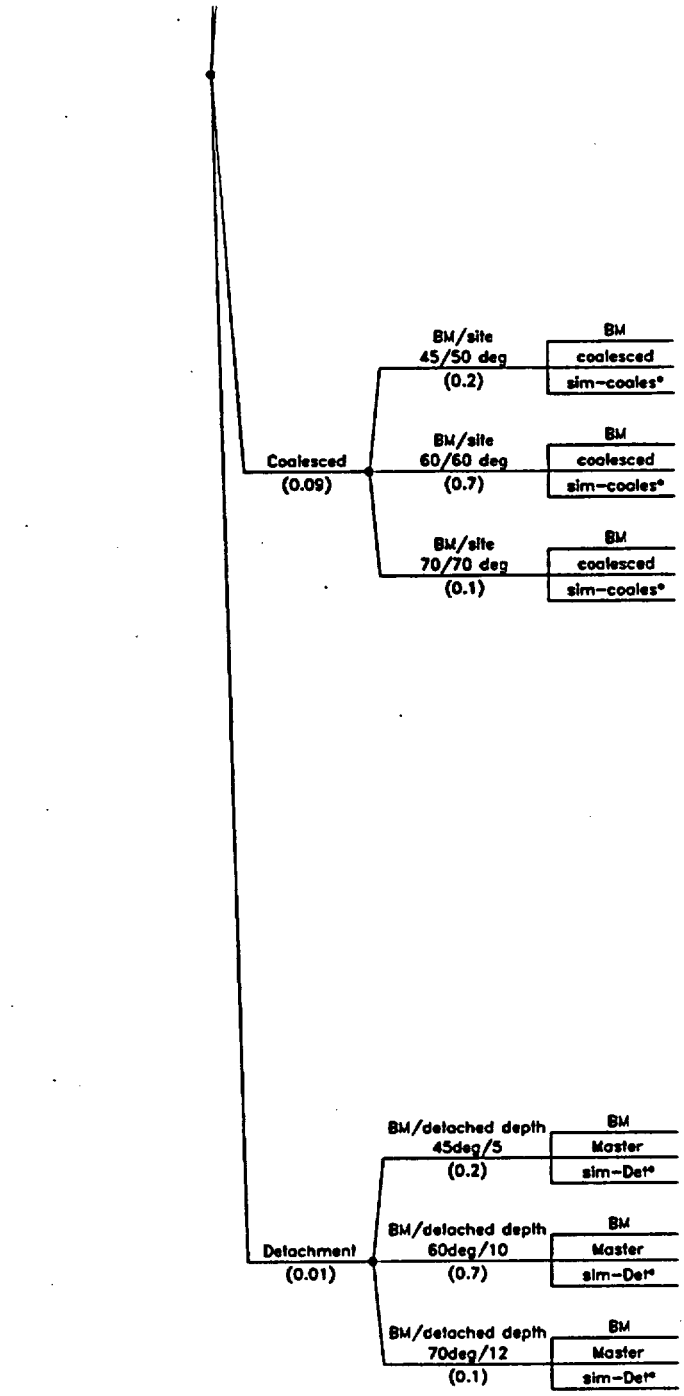

* sim-link, sim-coales and sim-det are synchronous rupture scenarios that act as additional sources of large events

Figure 4-55 (Cont'd.) Logic tree for local fault sources developed by the SBK team

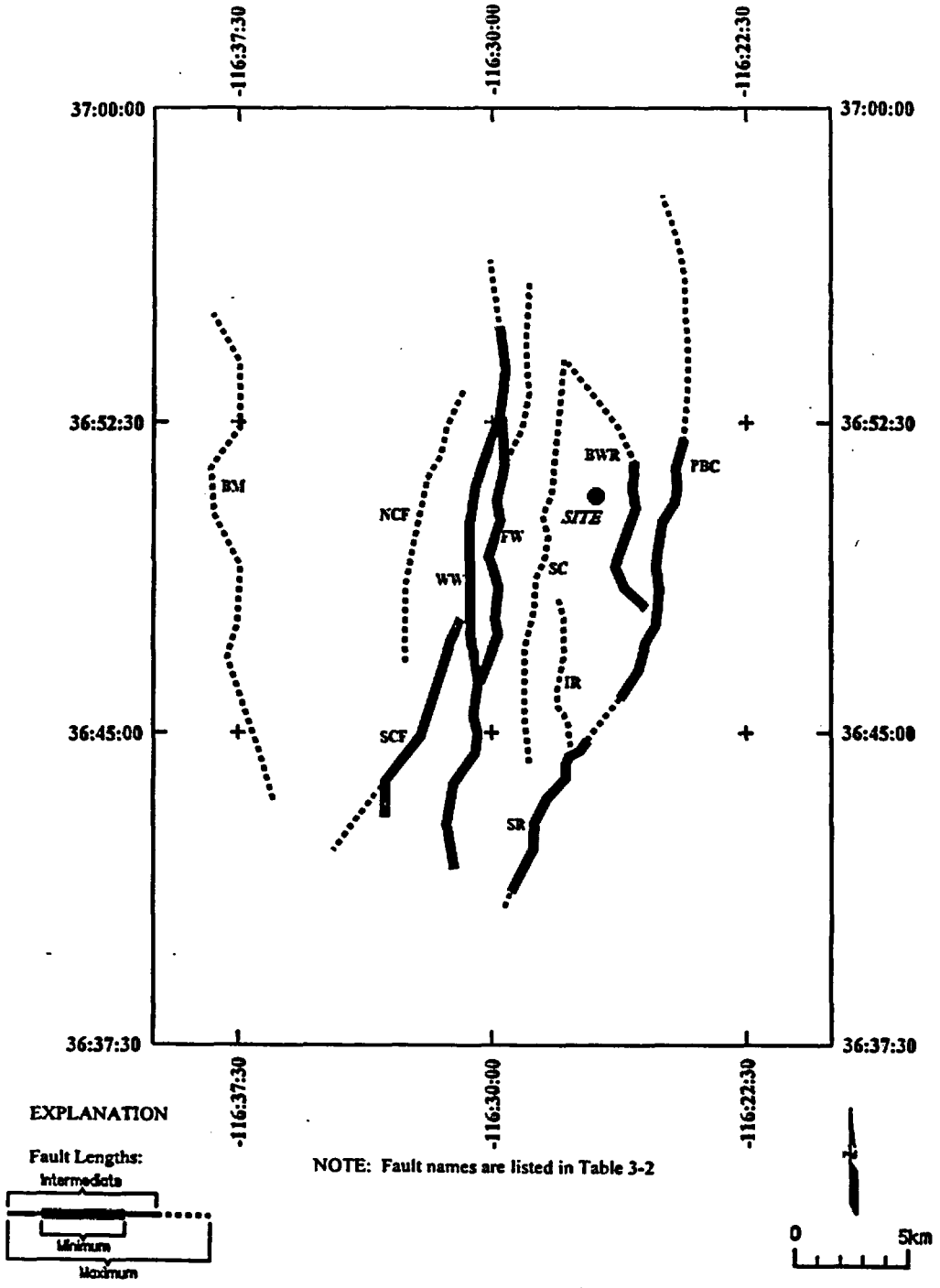

Figure 4-56 Location of local faults characterized by the SBK team

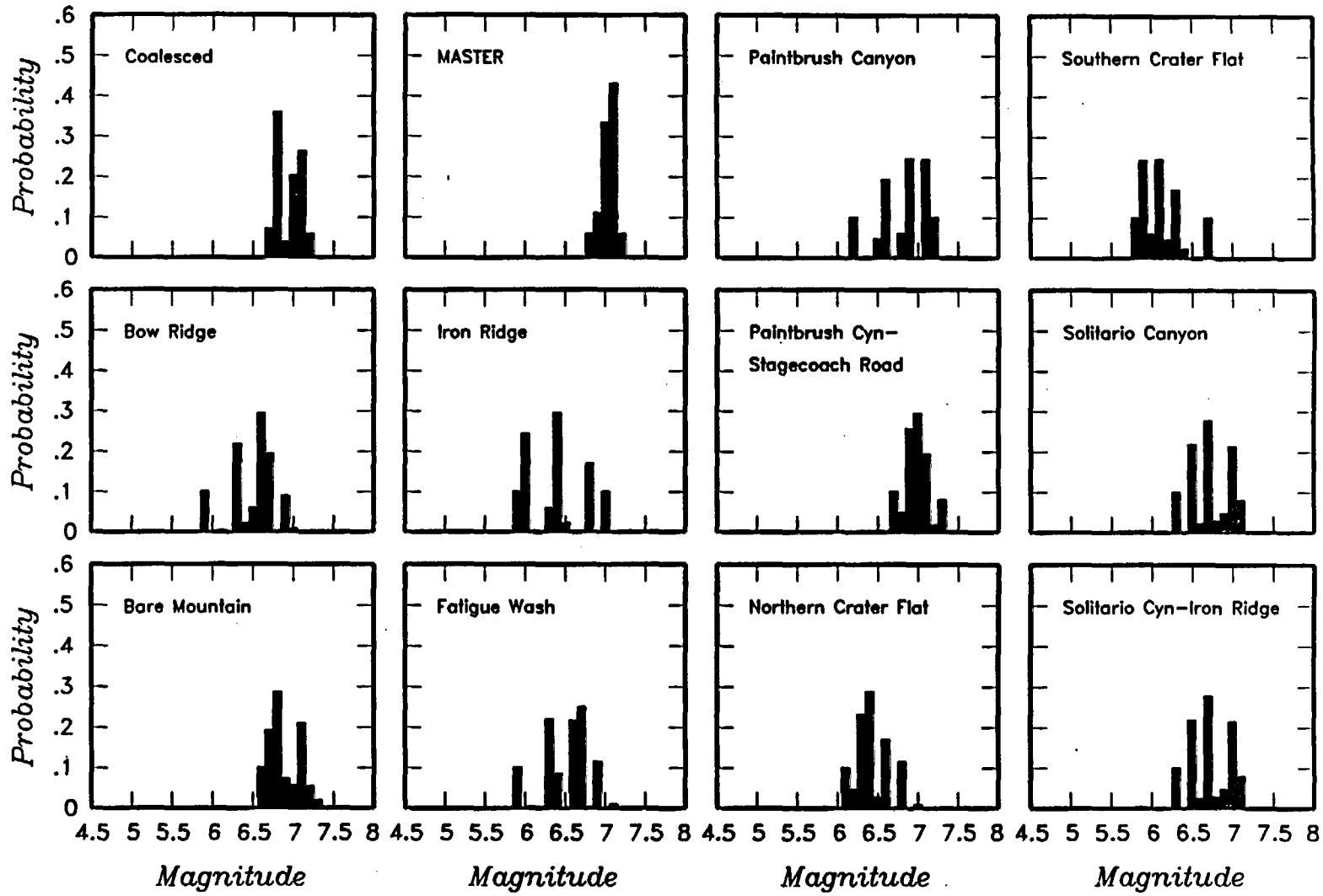

Figure 4-57 Maximum magnitude distributions for SBK team's local fault sources. MASTER–detachment with underlying master fault.

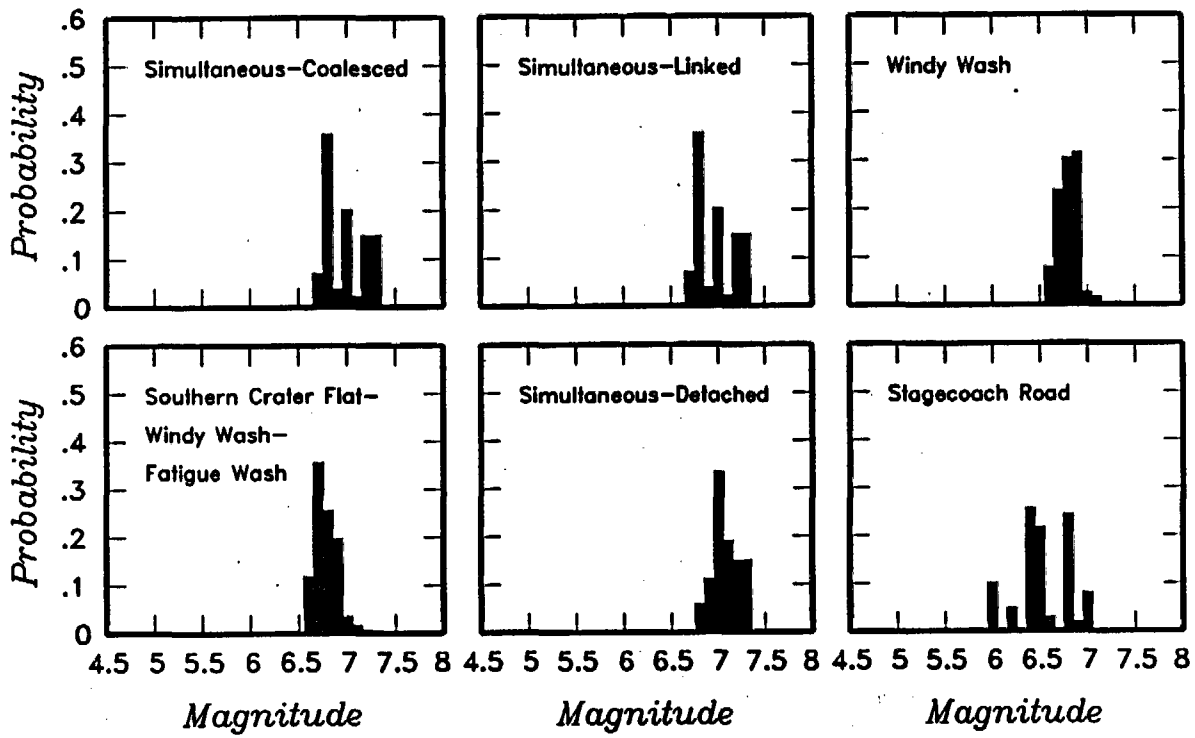

Figure 4-57 (Cont'd.) Maximum magnitude distributions for SBK team's local fault sources. MASTER–detachment with underlying master fault.

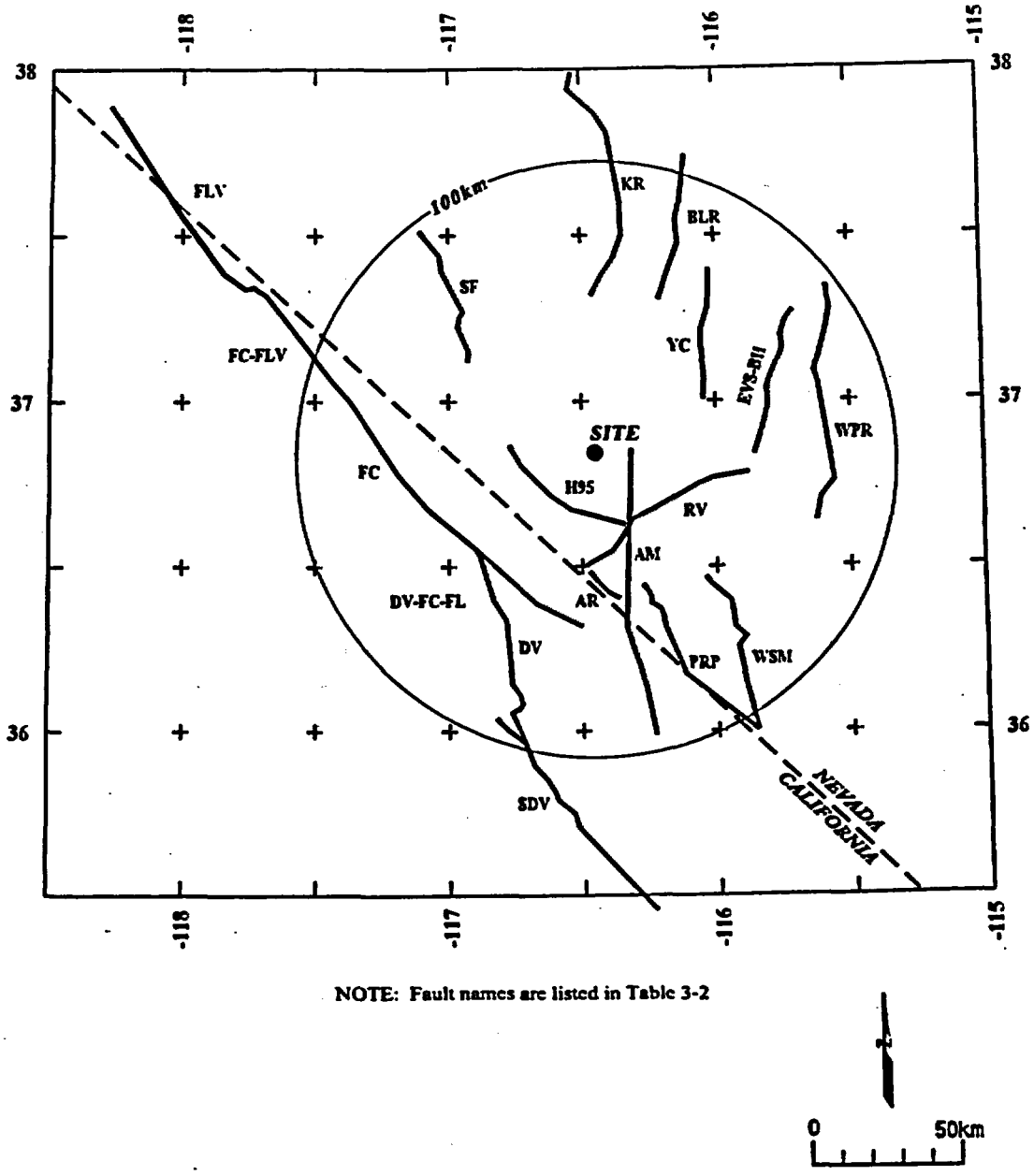

NOTE: Fault names are listed in Table 3-2

Figure 4-58 Regional fault sources characterized by the SBK team

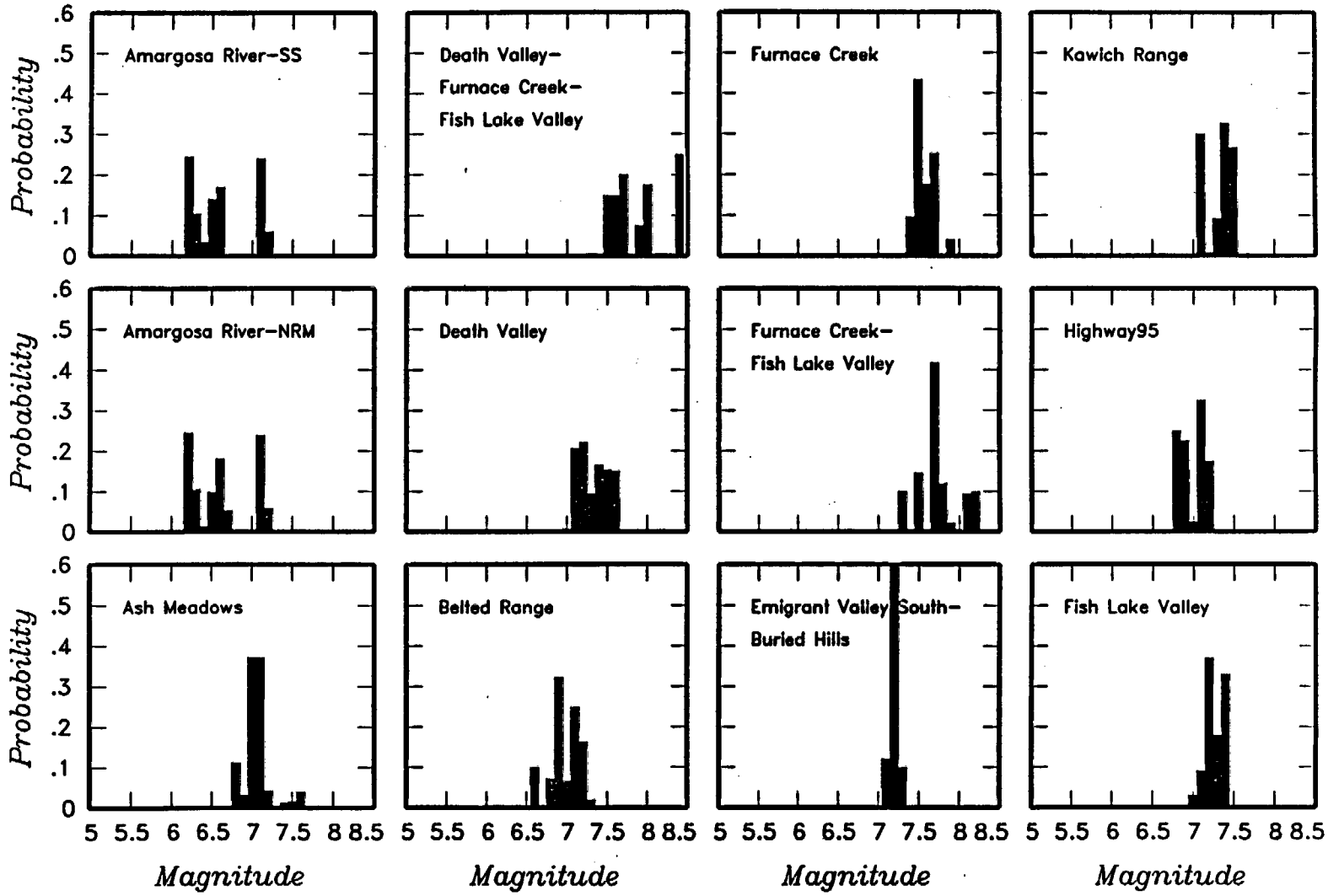

Figure 4-59 Maximum magnitude distributions for SBK team's regional fault sources. SS–strike slip; NRM–normal slip, OBL–oblique slip.

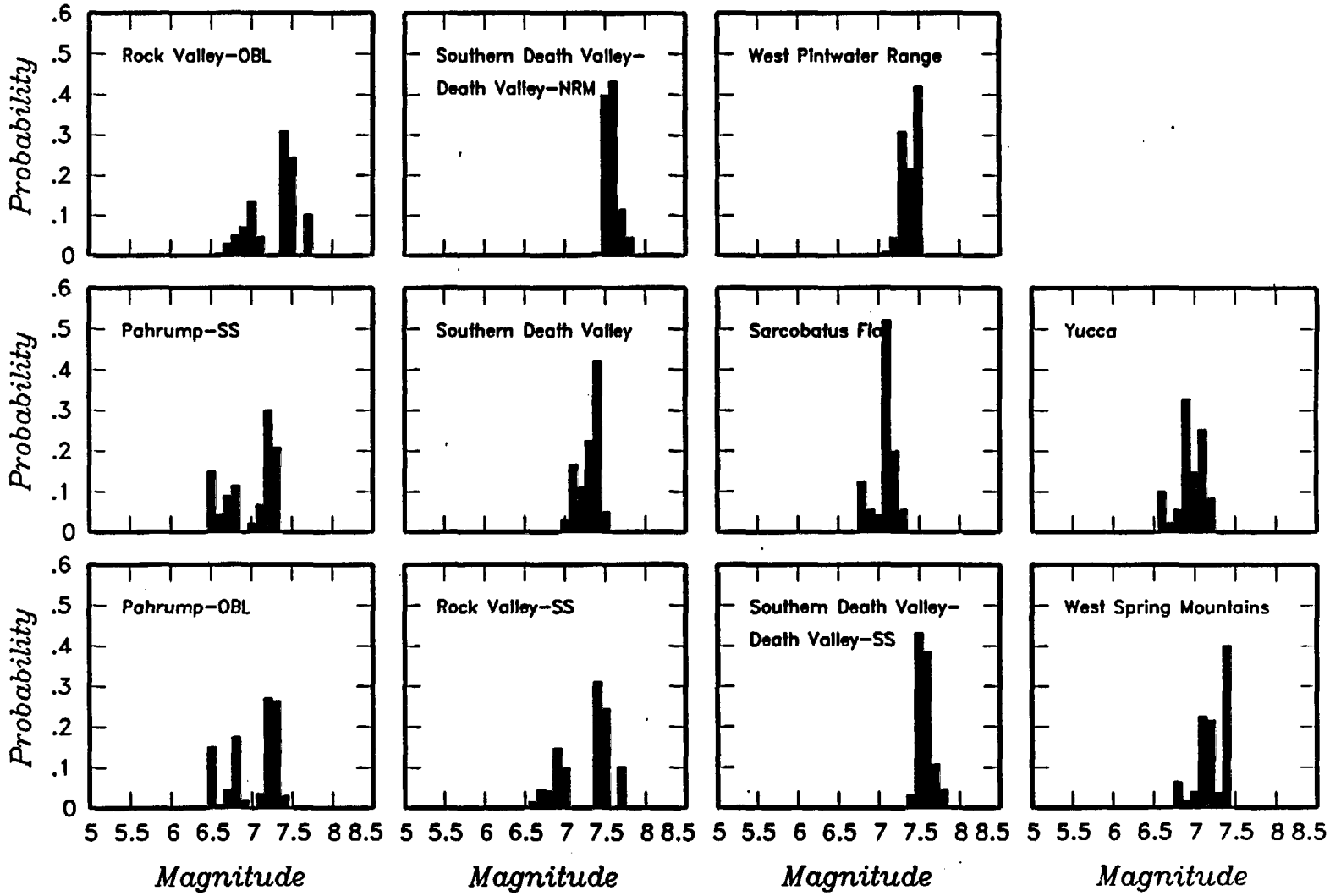

Figure 4-59 (Cont'd.) **Maximum magnitude distributions for SBK team's regional fault sources. SS–strike slip; NRM–normal slip, OBL–oblique slip.**

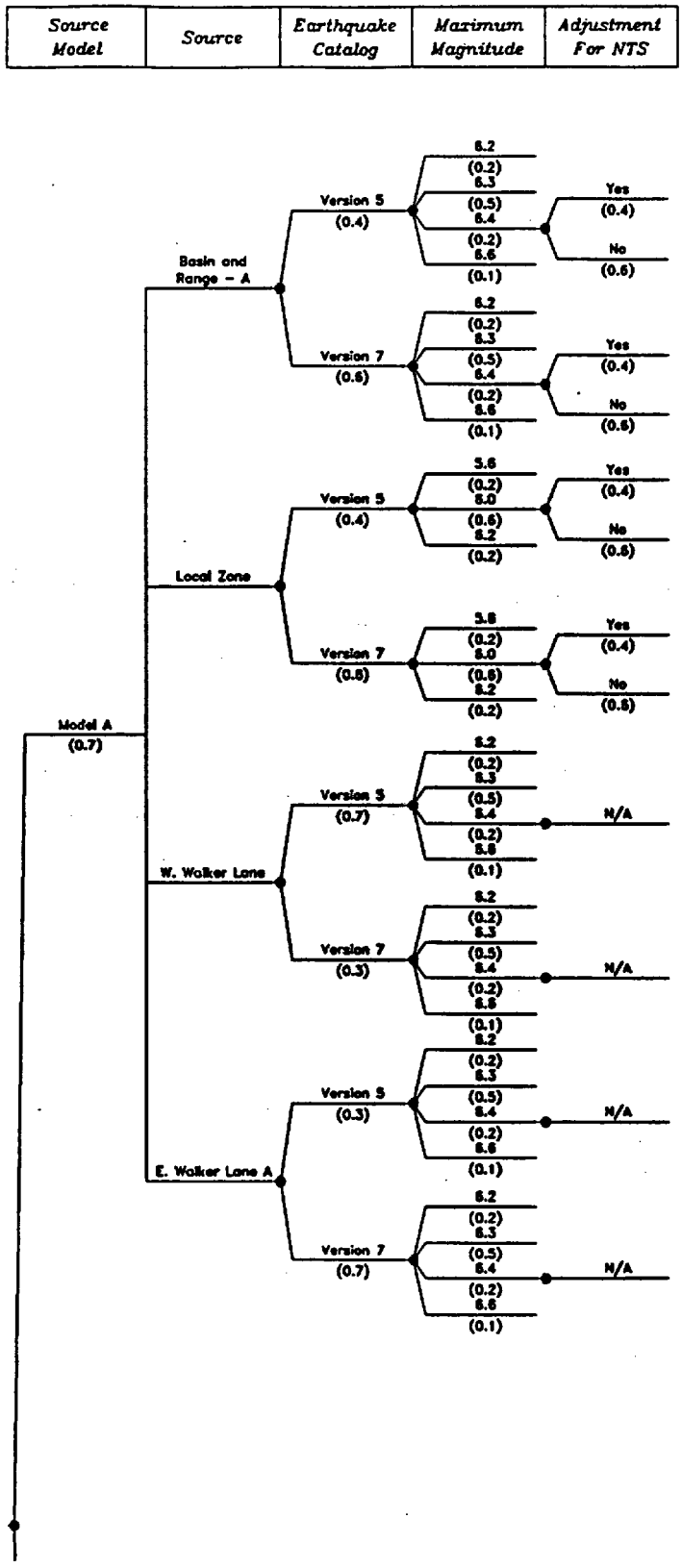

Figure 4-60 Logic tree for regional source zones developed by the SBK team

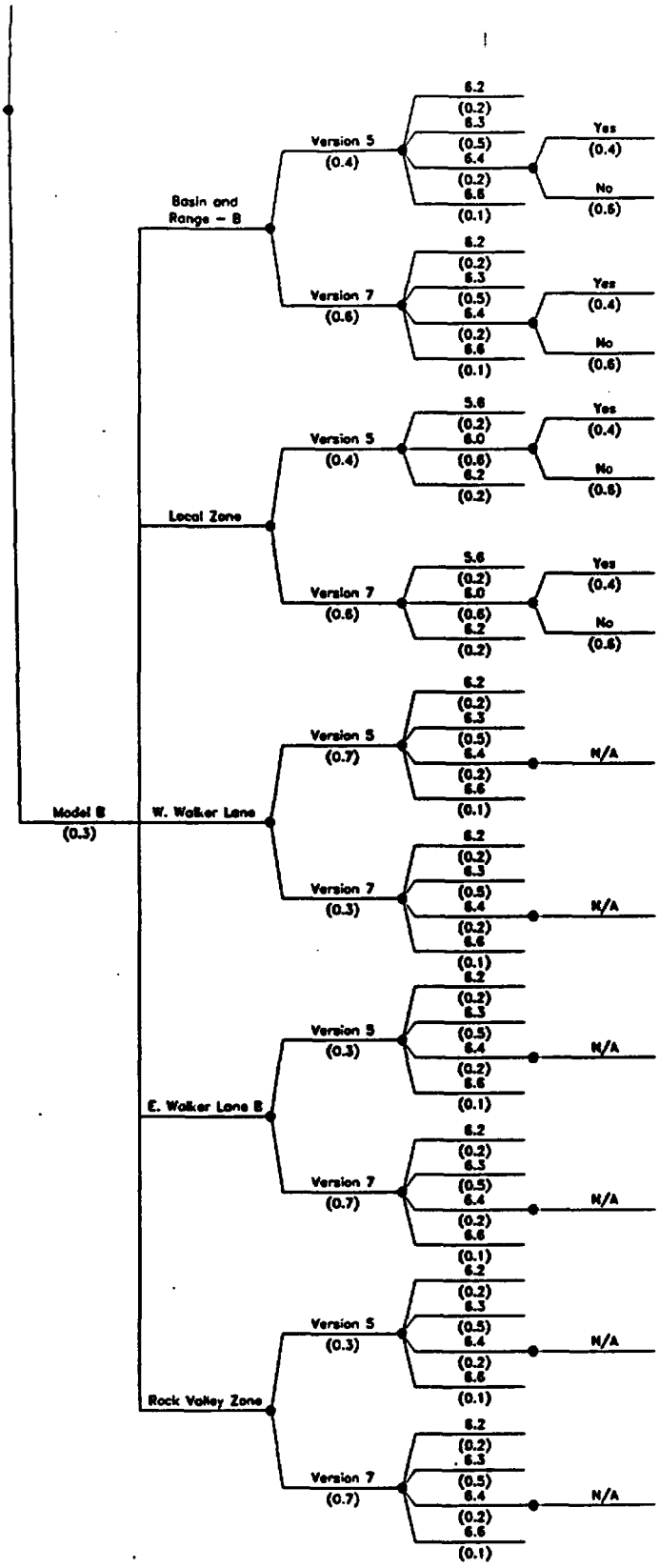

Figure 4-60 (Cont'd.) Logic tree for regional source zones developed by the SBK team

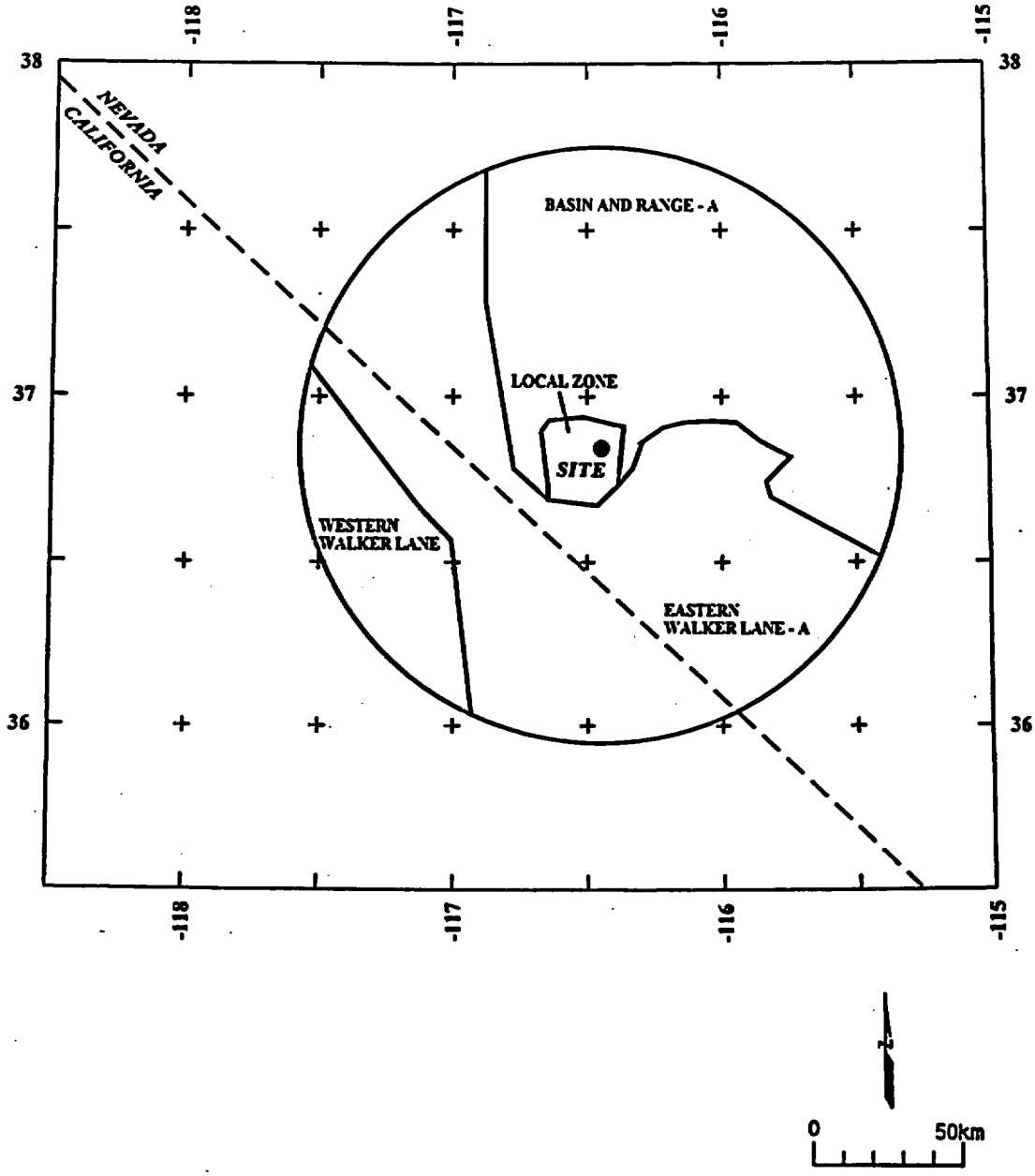

Figure 4-61 Alternative regional source zone models considered by the SBK team

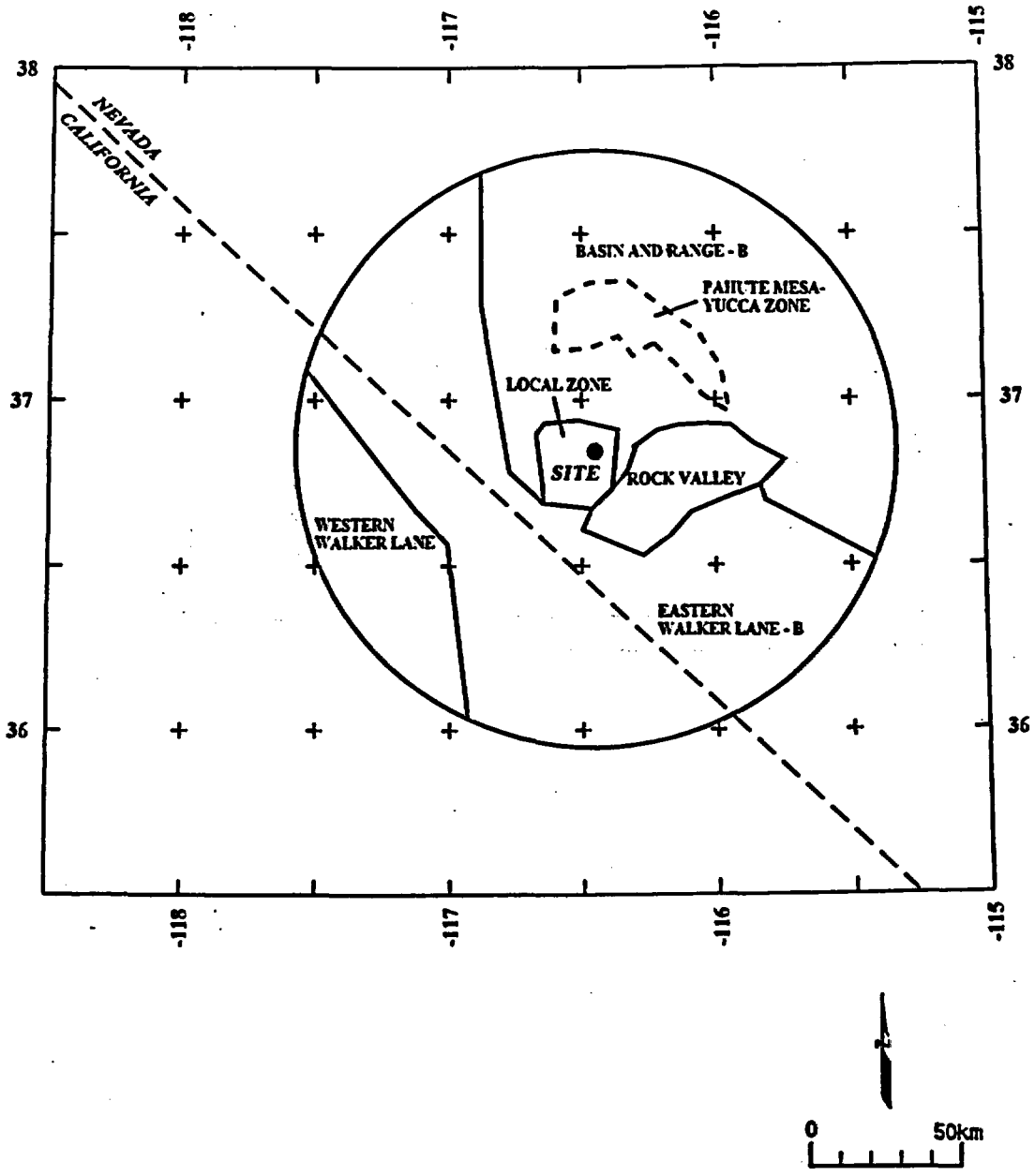

Figure 4-61 (Cont'd.) Alternative regional source zone models considered by the SBK team

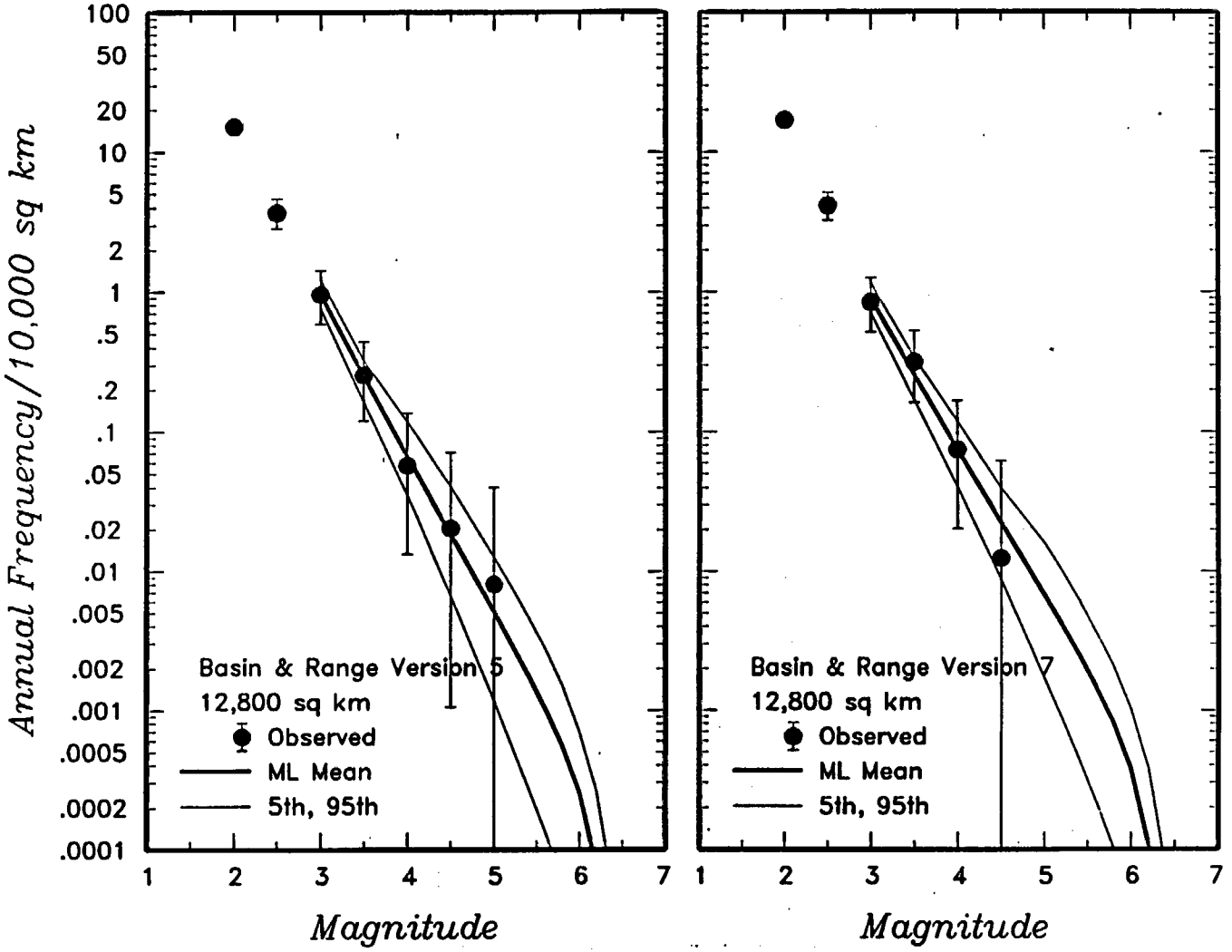

Figure 4-62 Earthquake recurrence relationships for the regional source zones defined by the SBK team. The solid dots with vertical error bars represent the observed data. The thick and thin solid curves are the mean, 5th, and 95th percentiles of the recurrence rates based on the uncertainty in recurrence parameters and maximum magnitude.

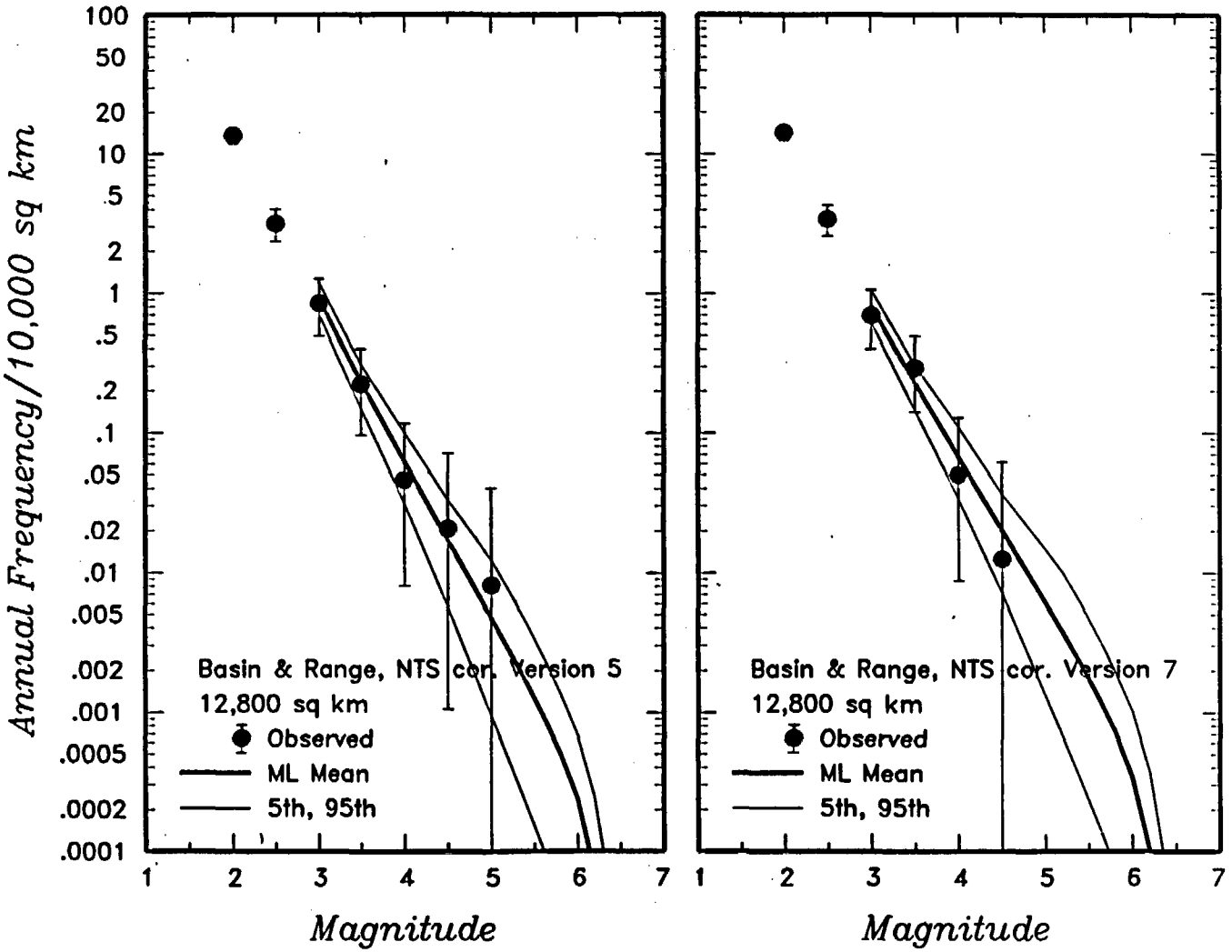

Figure 4-62 (Cont'd.) Earthquake recurrence relationships for the regional source zones defined by the SBK team.

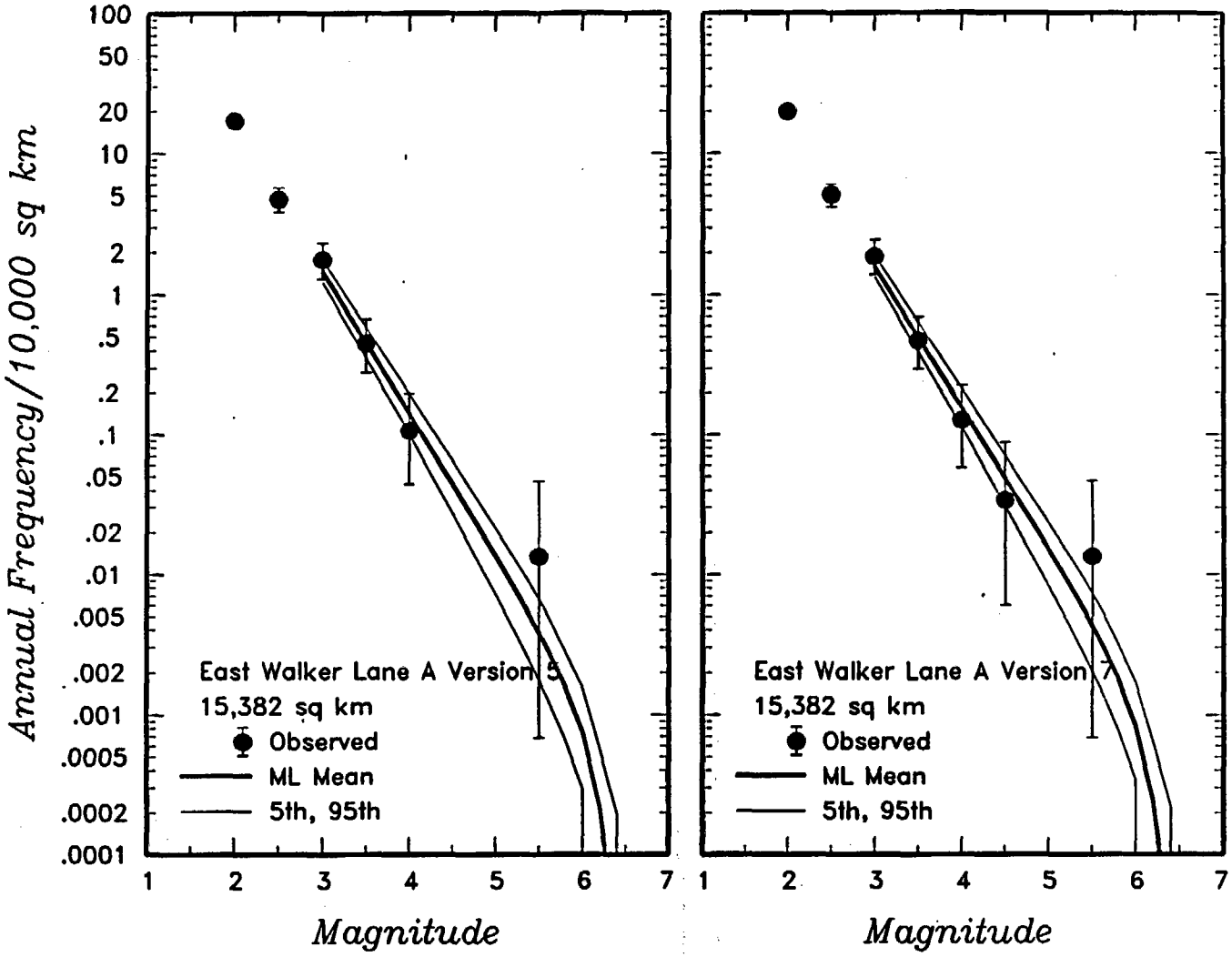

Figure 4-62 (Cont'd.) Earthquake recurrence relationships for the regional source zones defined by the SBK team.

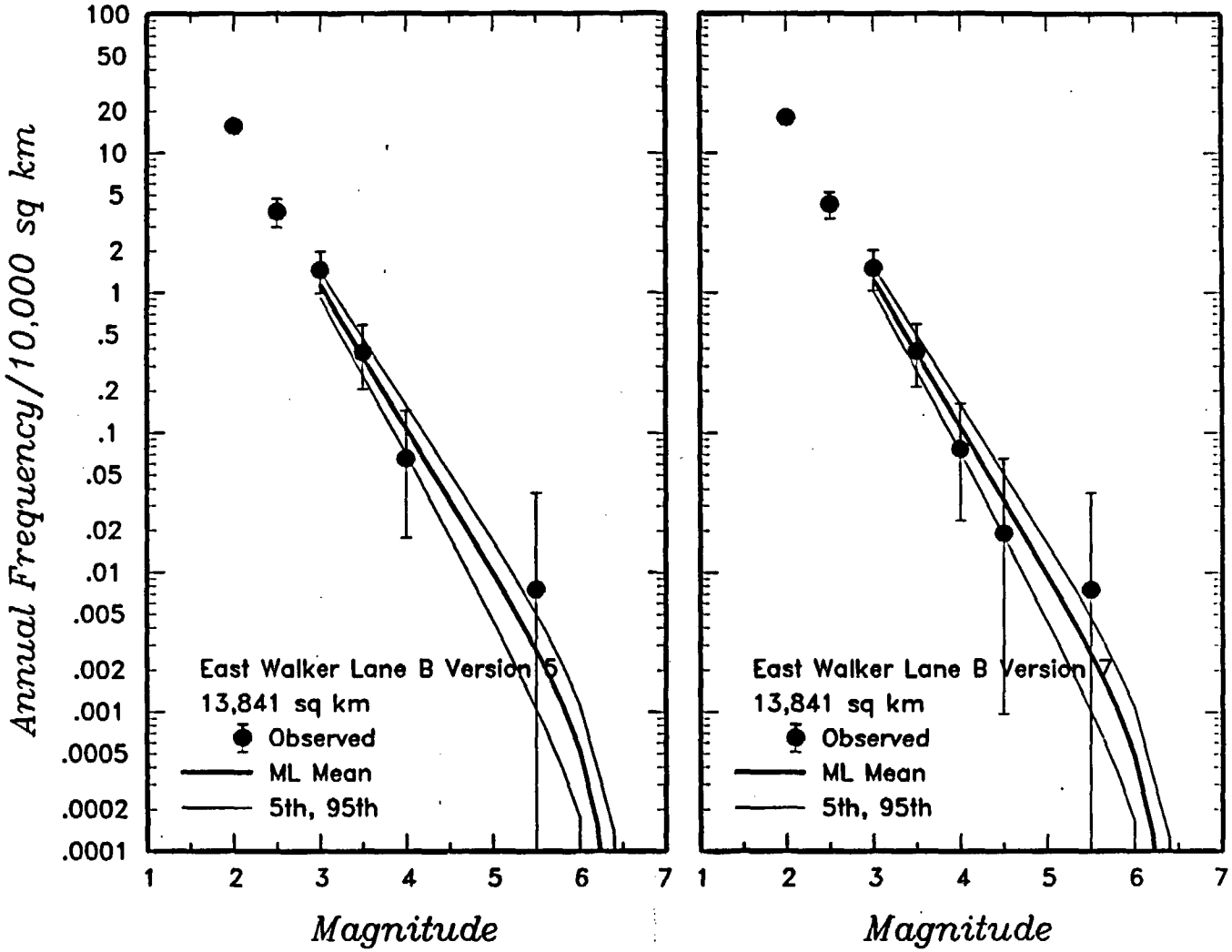

Figure 4-62 (Cont'd.) Earthquake recurrence relationships for the regional source zones defined by the SBK team.

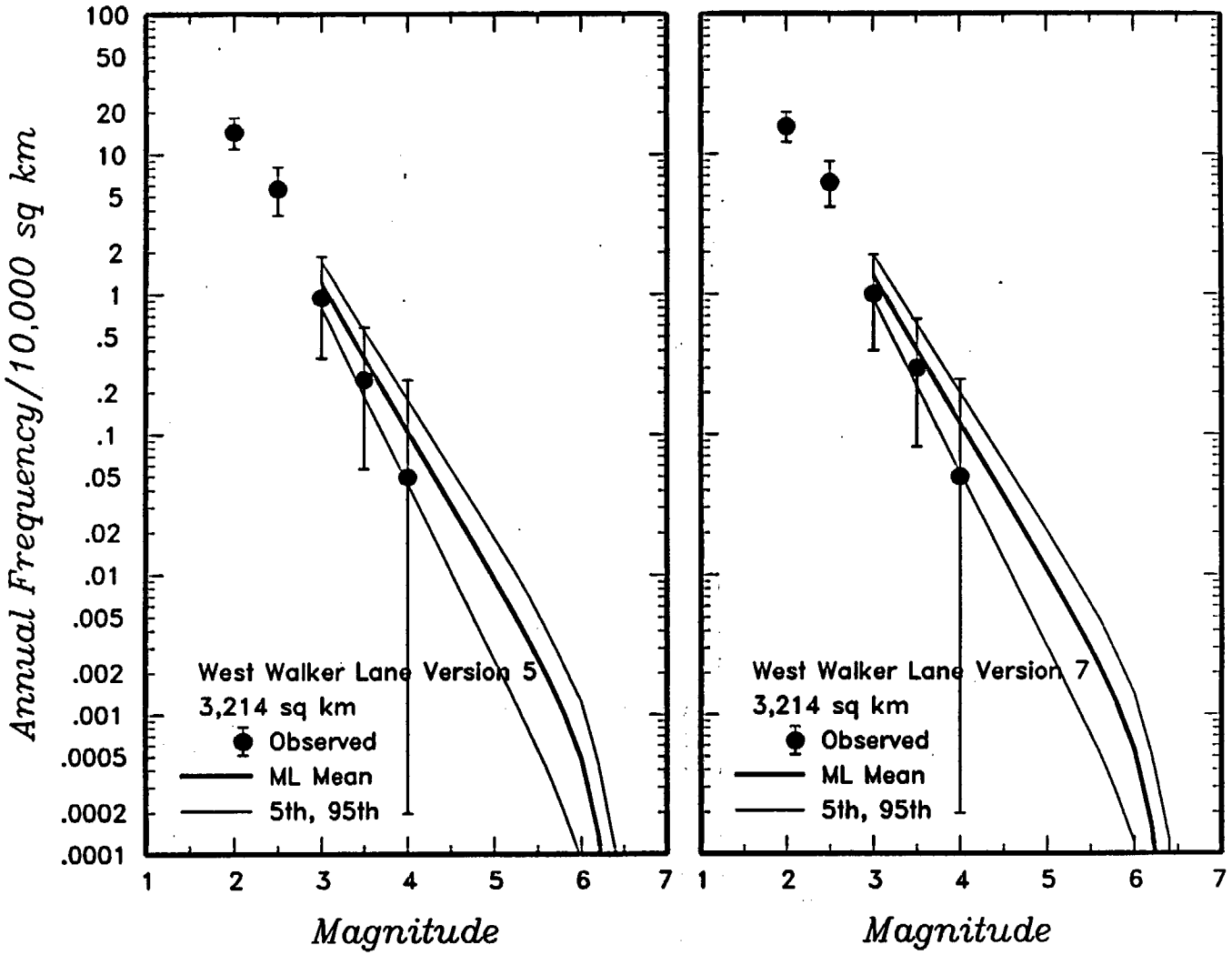

Figure 4-62 (Cont'd.) Earthquake recurrence relationships for the regional source zones defined by the SBK team.

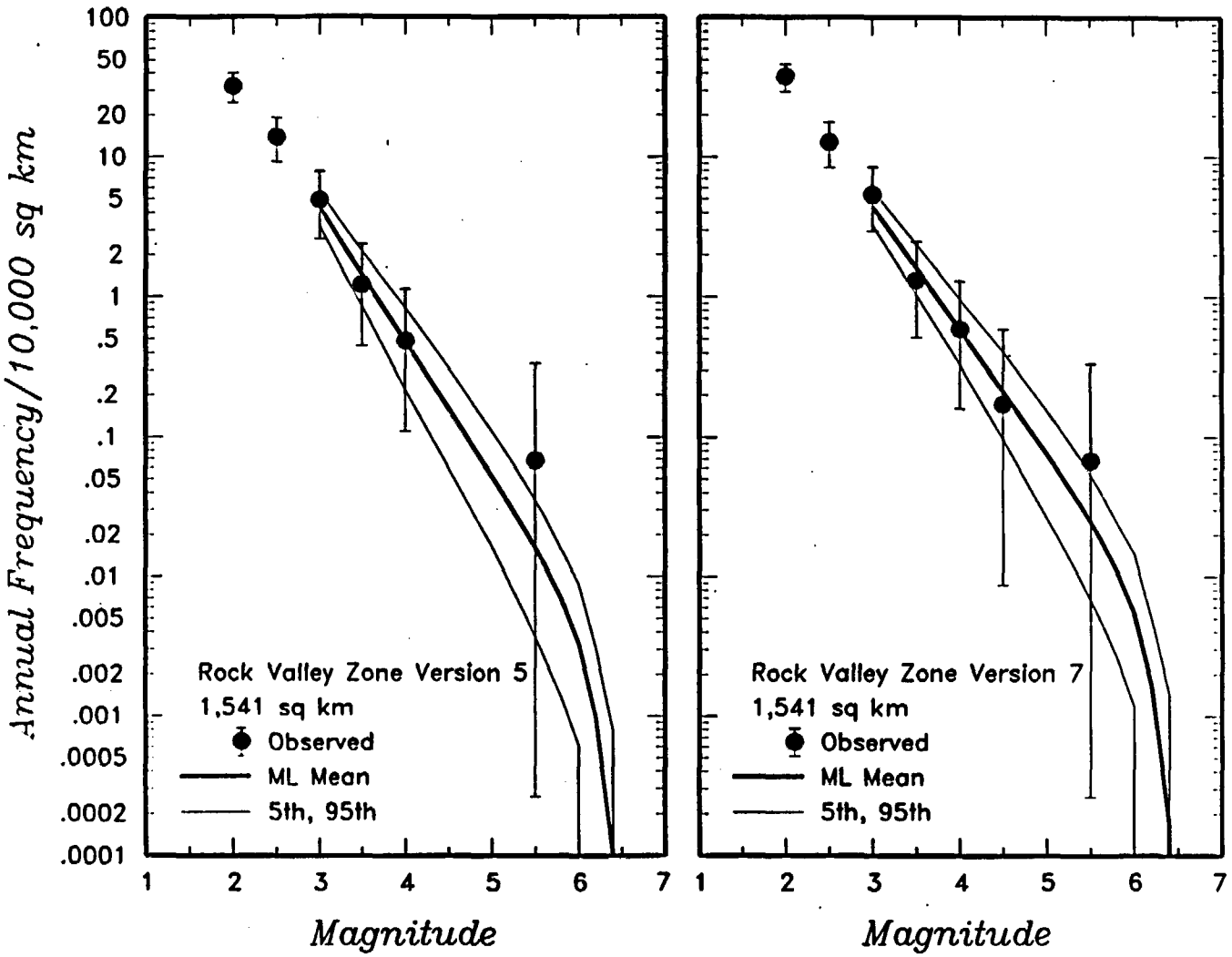

Figure 4-62 (Cont'd.) Earthquake recurrence relationships for the regional source zones defined by the SBK team.

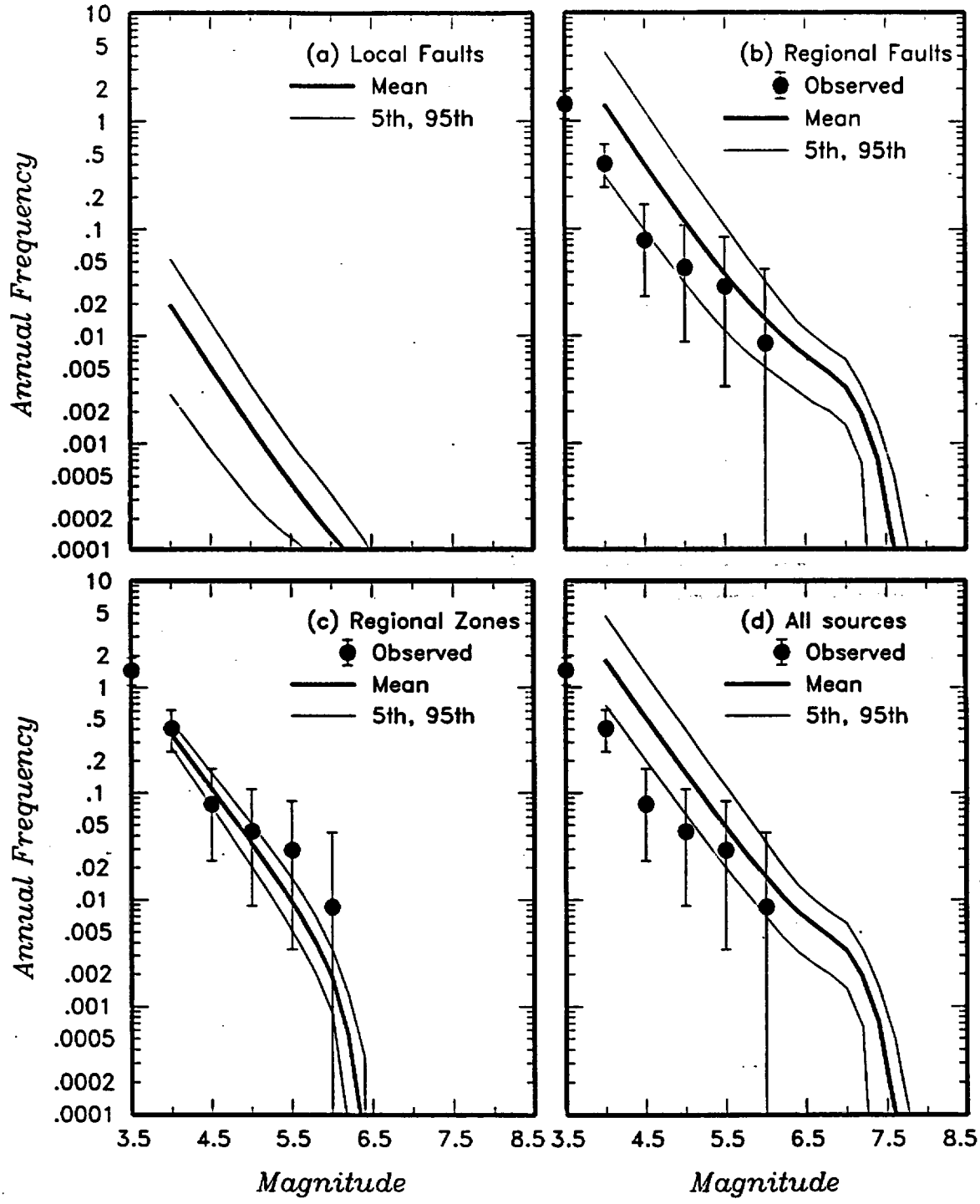

Figure 4-63 Predicted mean, 5th-, and 95th-percentile recurrence rates for (a) local fault sources, (b) regional fault sources, (c) regional source zones, and (d) all sources combined for the SBK team. The solid dots with vertical error bars represent the observed frequency of earthquakes occurring within 100 km of the Yucca Mountain site.

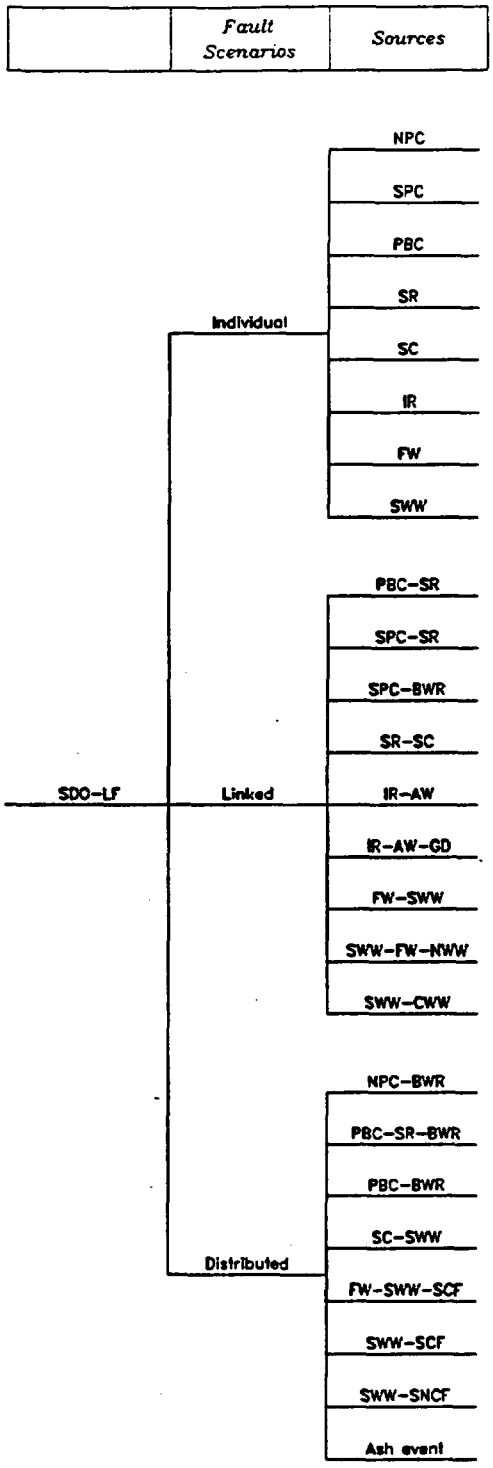

Figure 4-64 Logic tree for local fault sources developed by the SDO team

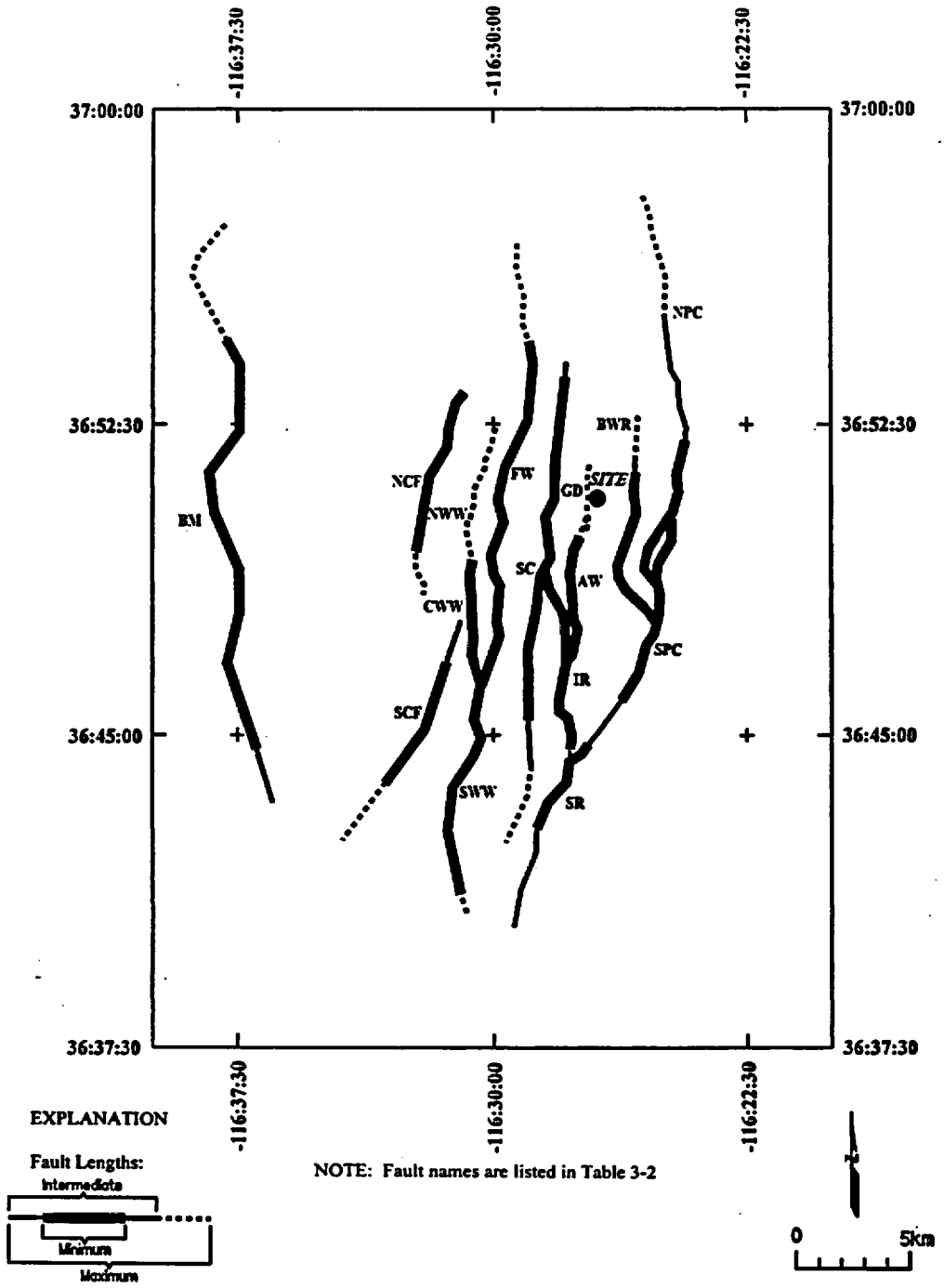

Figure 4-65 Location of local fault sources considered by the SDO team

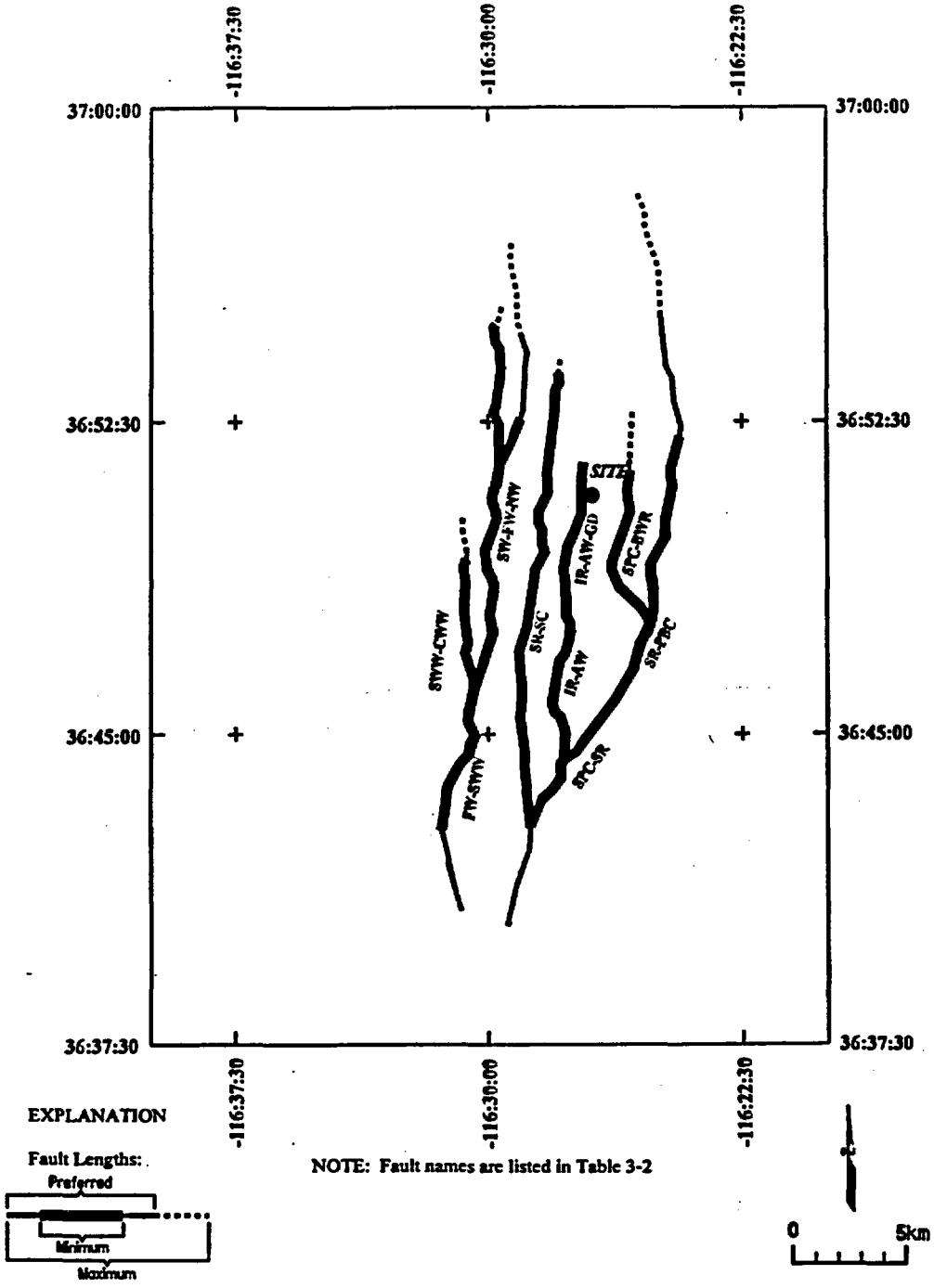

Figure 4-65 (Cont'd.) Location of local fault sources considered by the SDO team

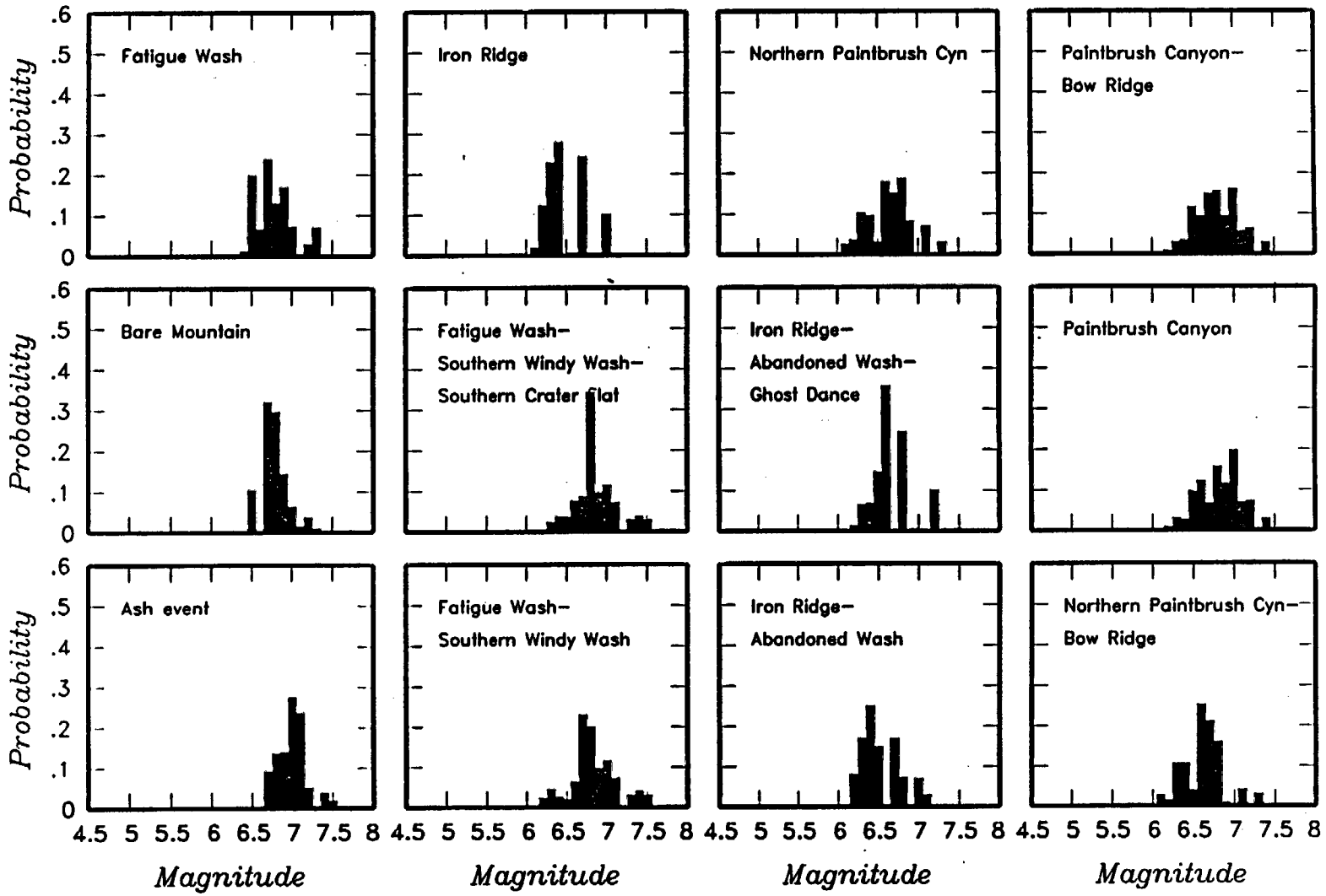

Figure 4-66 Maximum magnitude distributions for SDO team's local fault sources

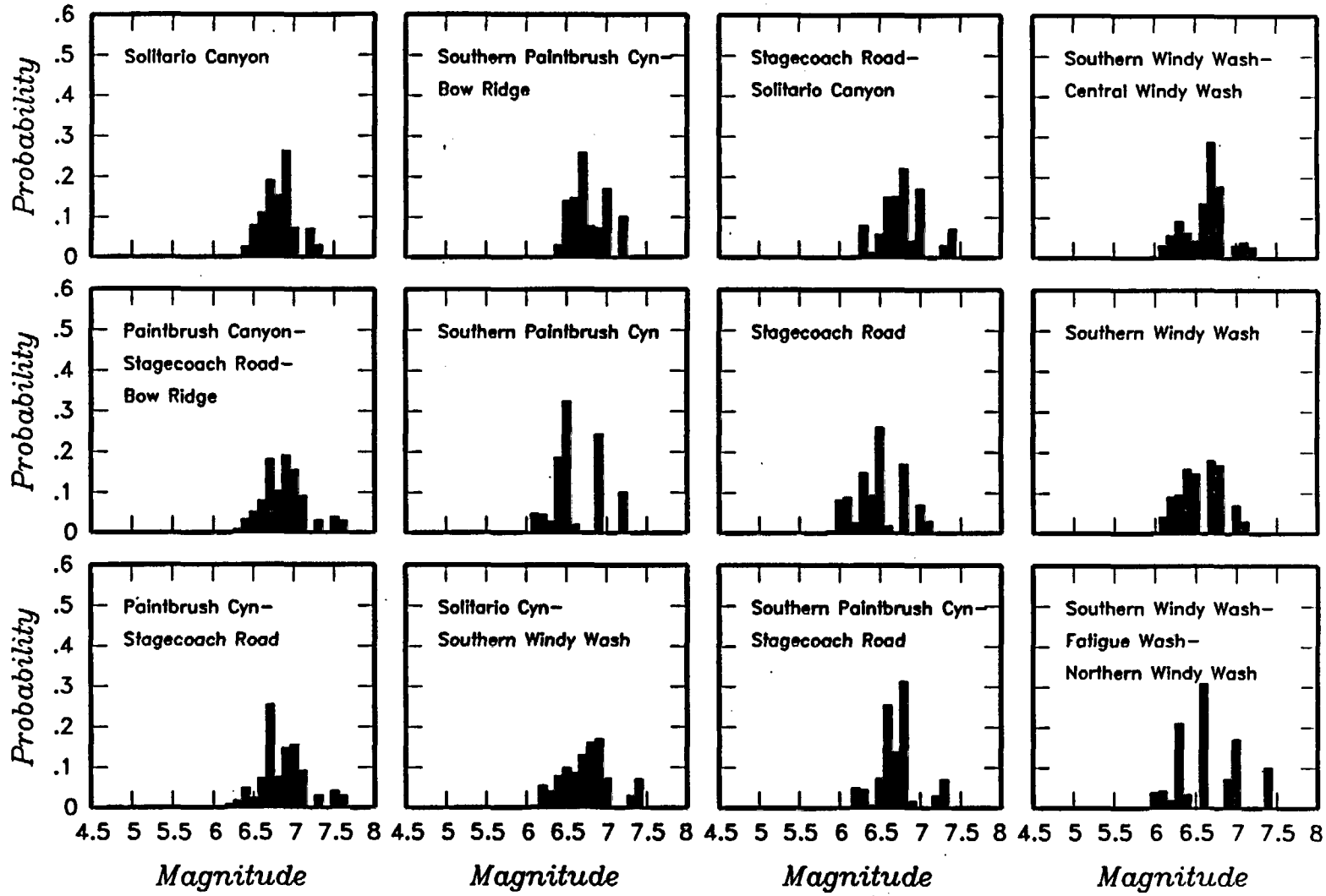

Figure 4-66 (Cont'd.) Maximum magnitude distributions for SDO team's local fault sources

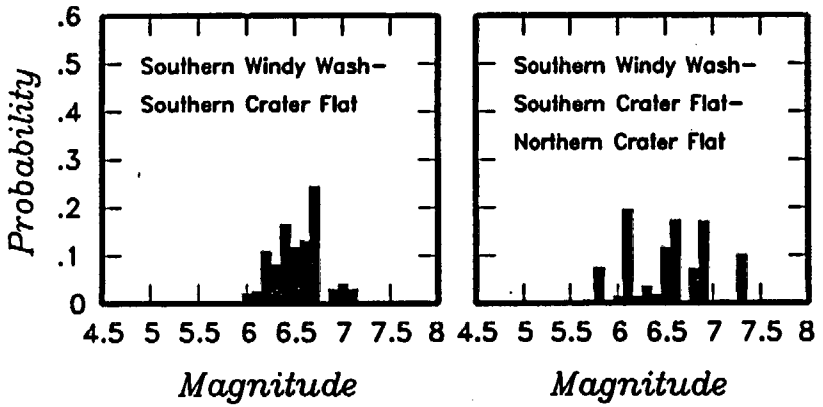

Figure 4-66 (Cont'd.) Maximum magnitude distributions for SDO team's local fault sources

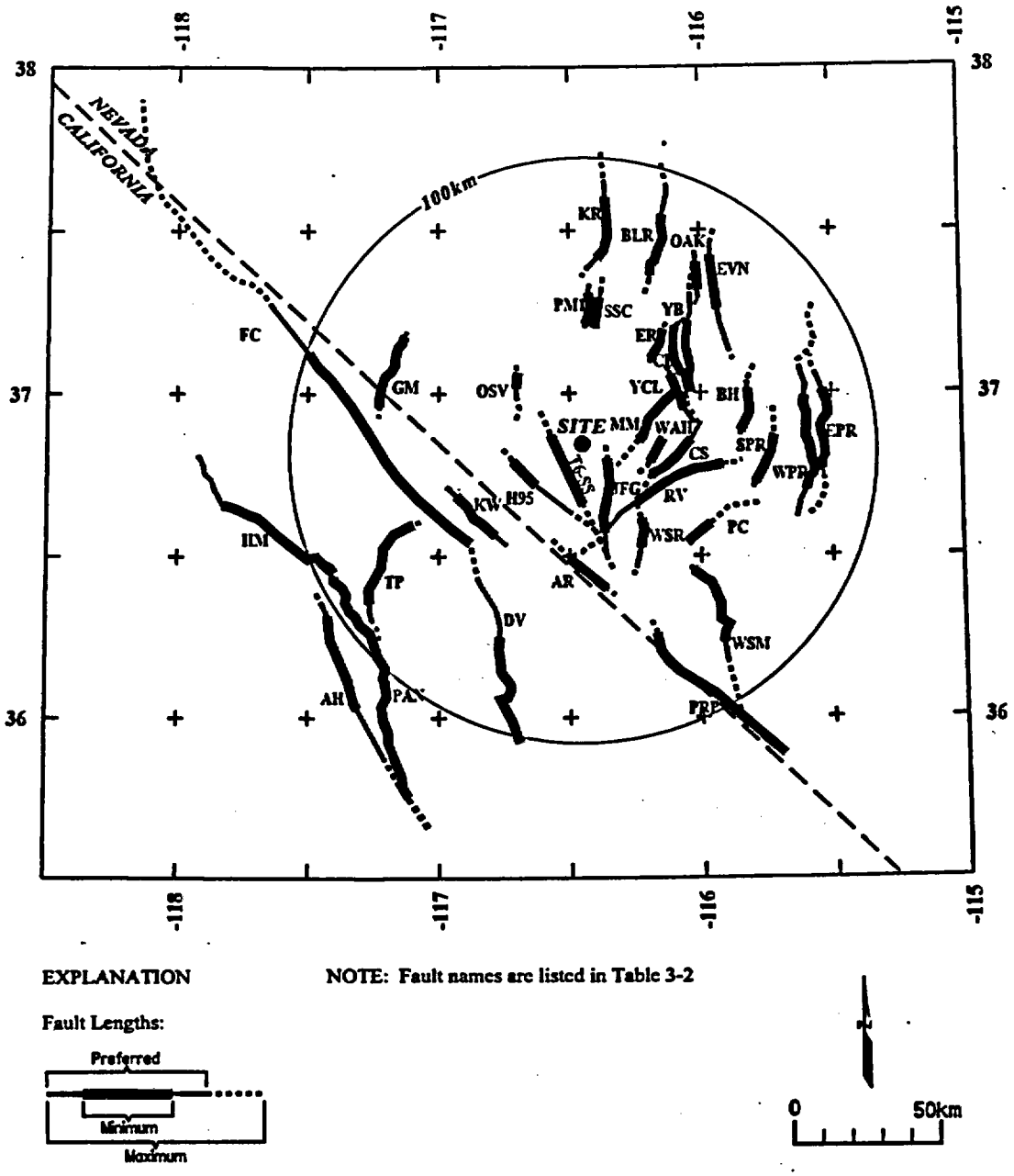

Figure 4-67 Regional fault sources considered by the SDO team

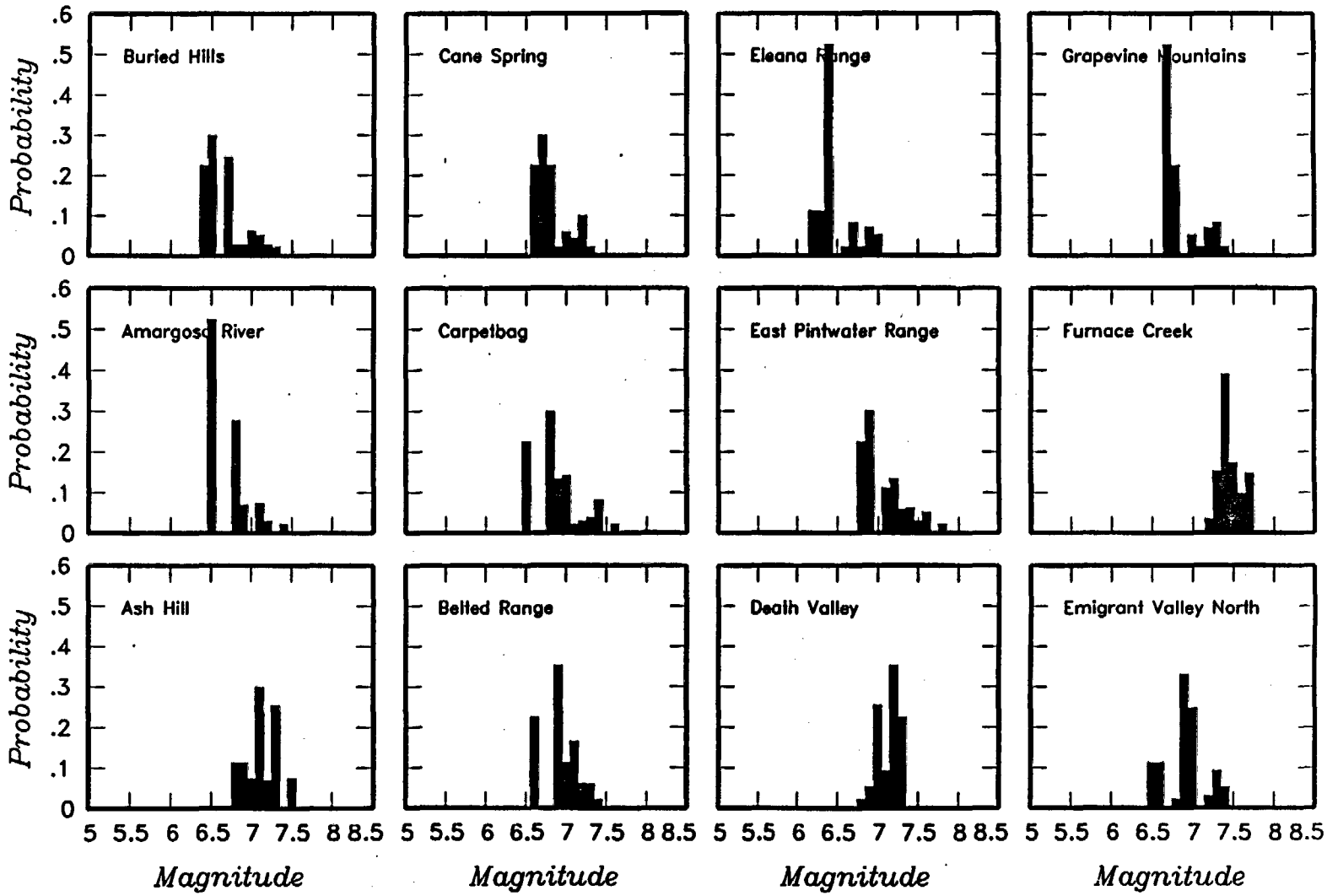

Figure 4-68 Maximum magnitude distributions for SDO team's regional fault sources

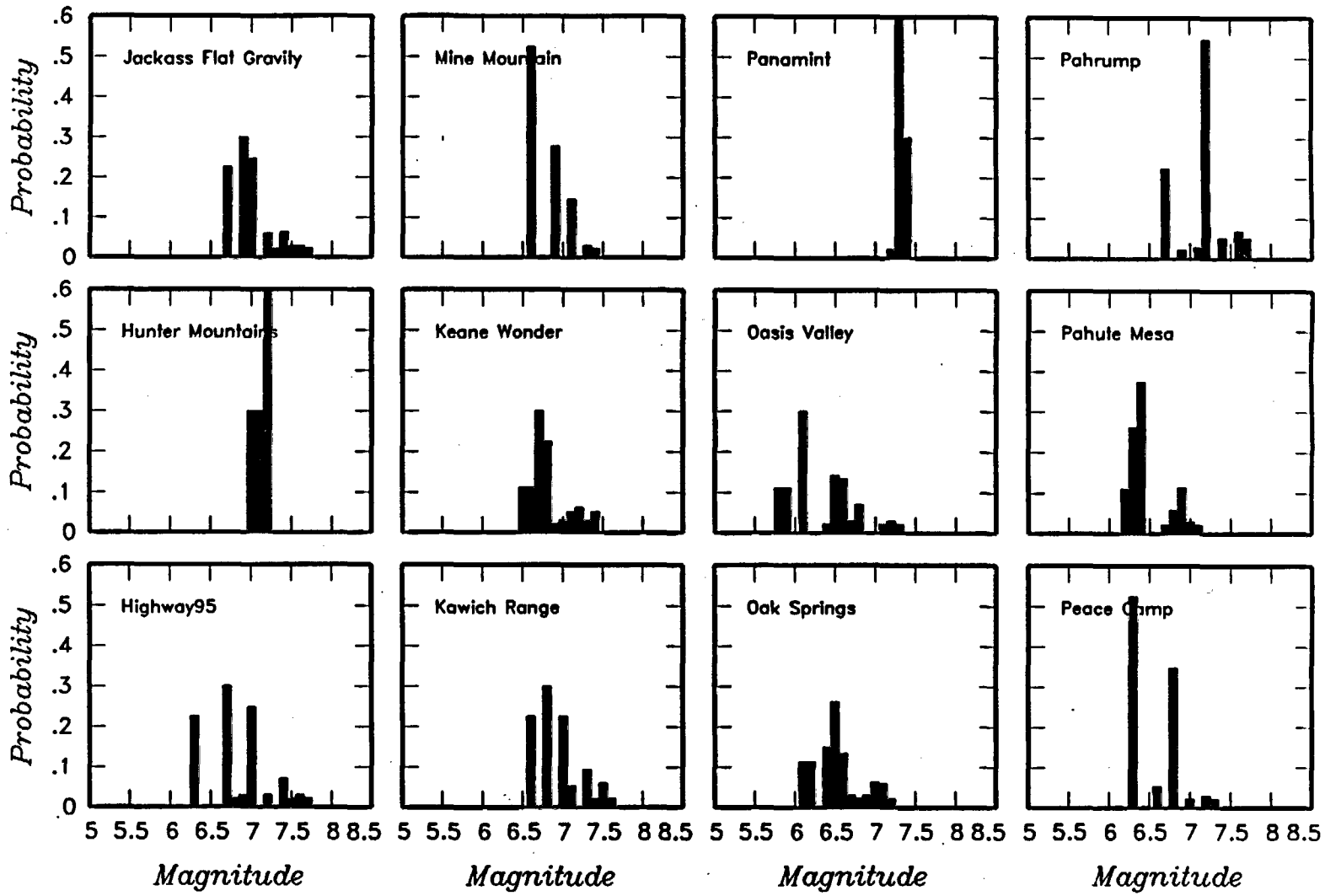

Figure 4-68 (Cont'd.) Maximum magnitude distributions for SDO team's regional fault sources

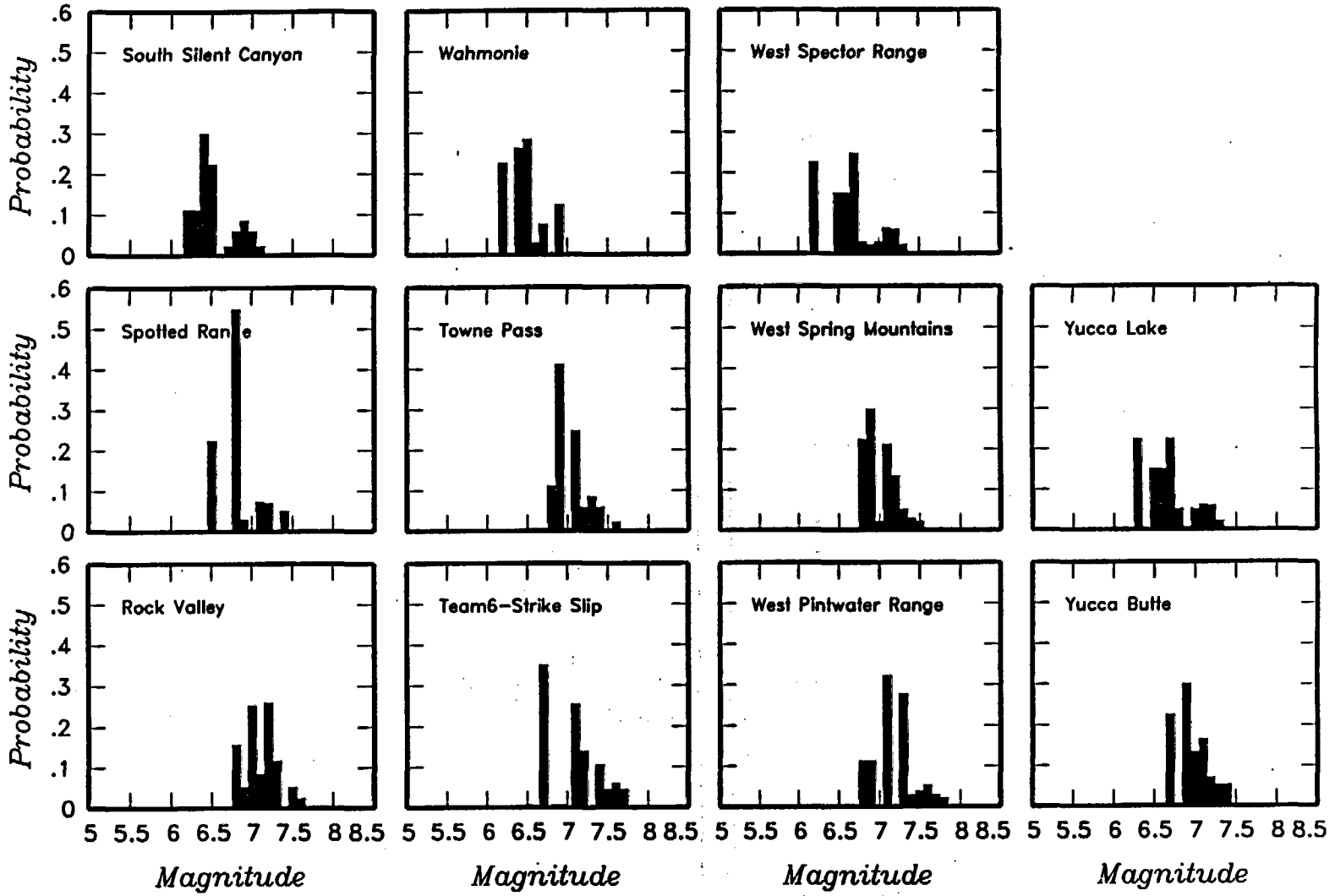

Figure 4-68 (Cont'd.) Maximum magnitude distributions for SDO team's regional fault sources

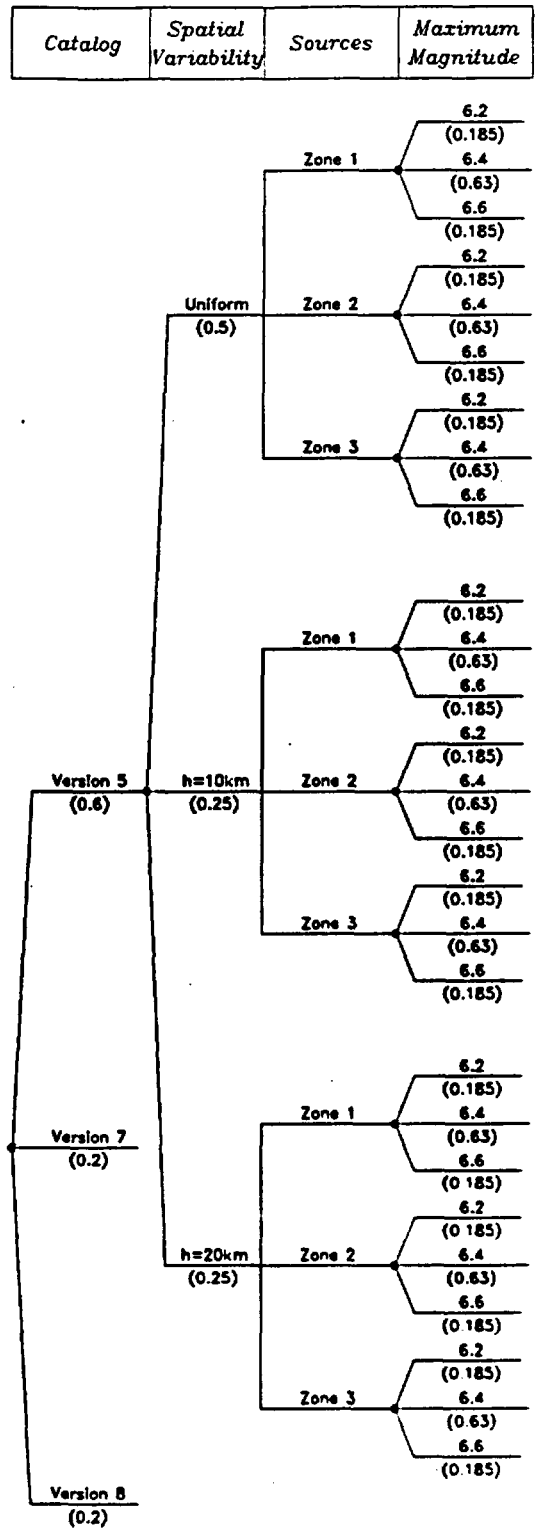

Figure 4-69 Logic tree for regional source zones developed by the SDO team

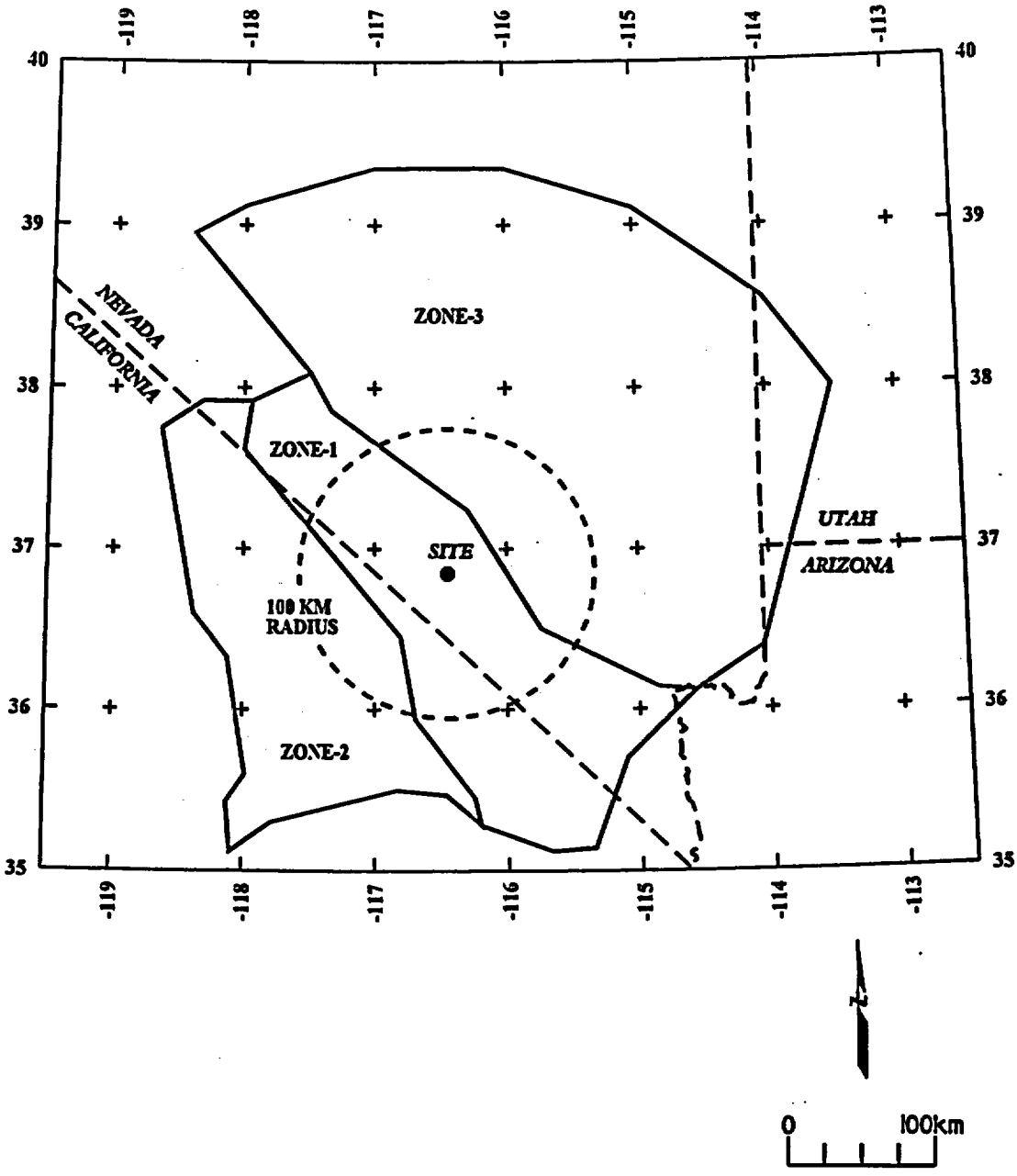

Figure 4-70 Alternative regional source zone models considered by the SDO team

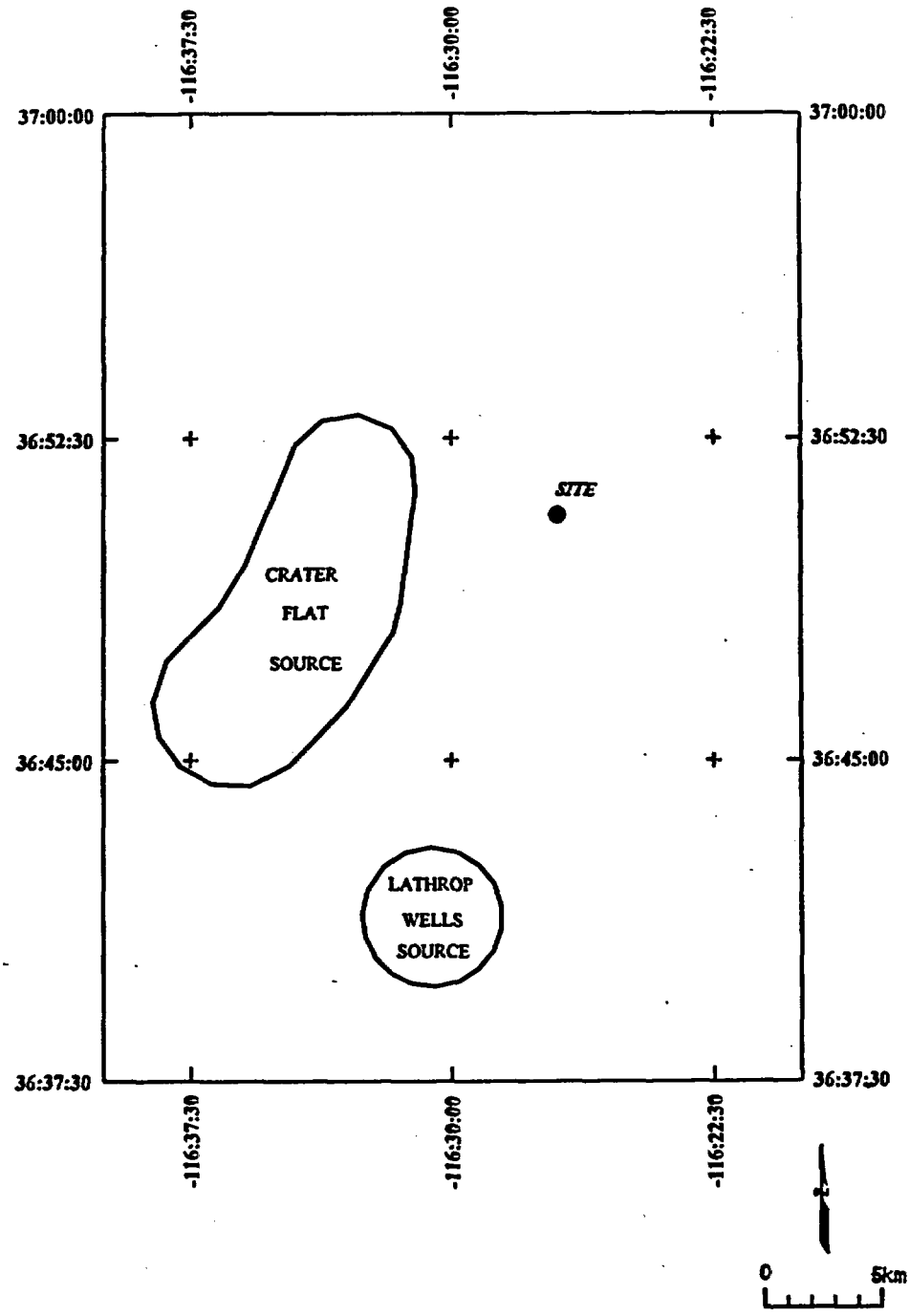

Figure 4-71 Volcanic source zones considered by the SDO team

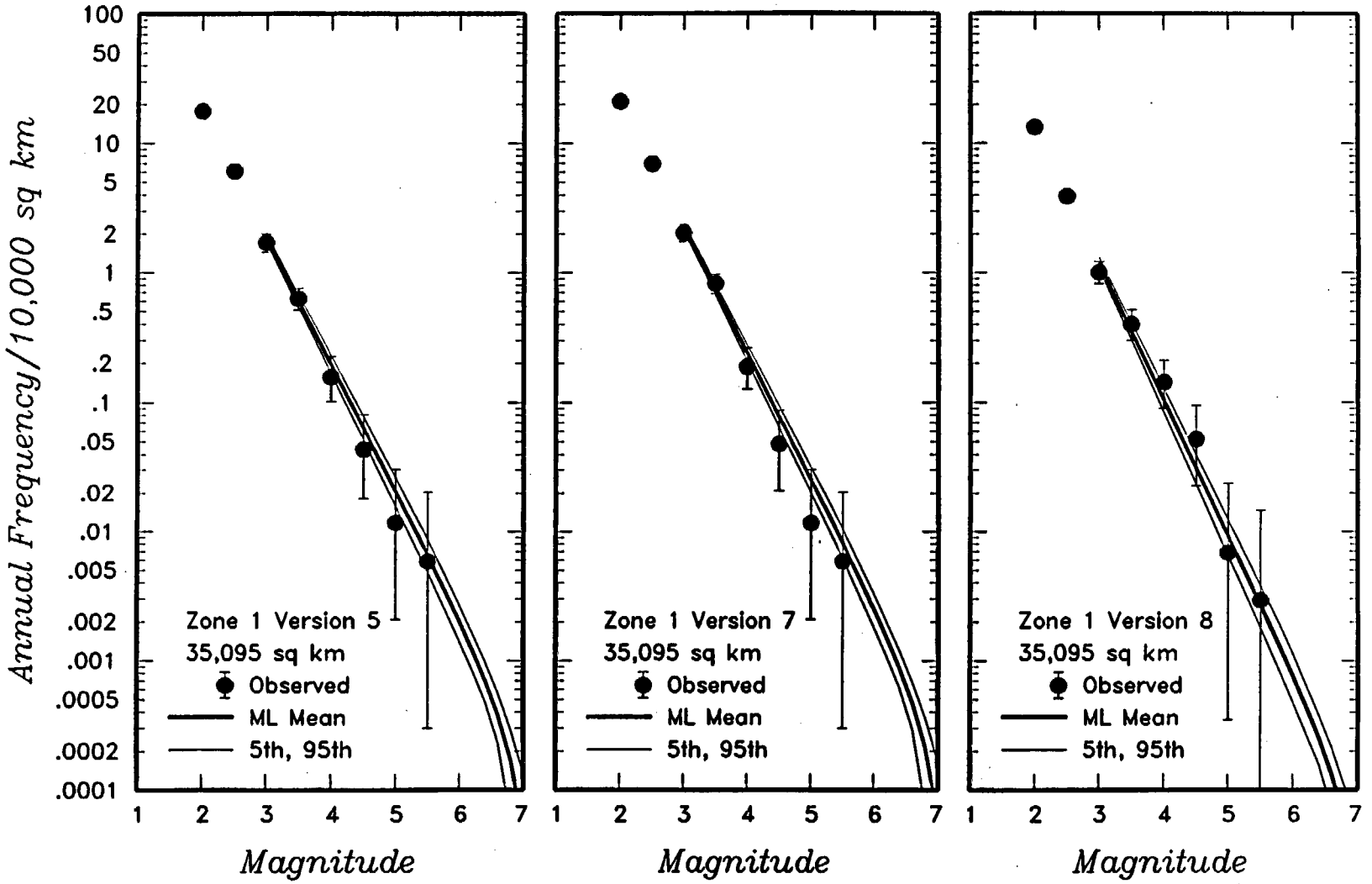

Figure 4-72 Earthquake recurrence relationships for the regional source zones defined by the SDO team. The solid dots with vertical error bars represent the observed data. The thick and thin solid curves are the mean, 5th, and 95th percentiles of the recurrence rates based on the uncertainty in recurrence parameters and maximum magnitude.

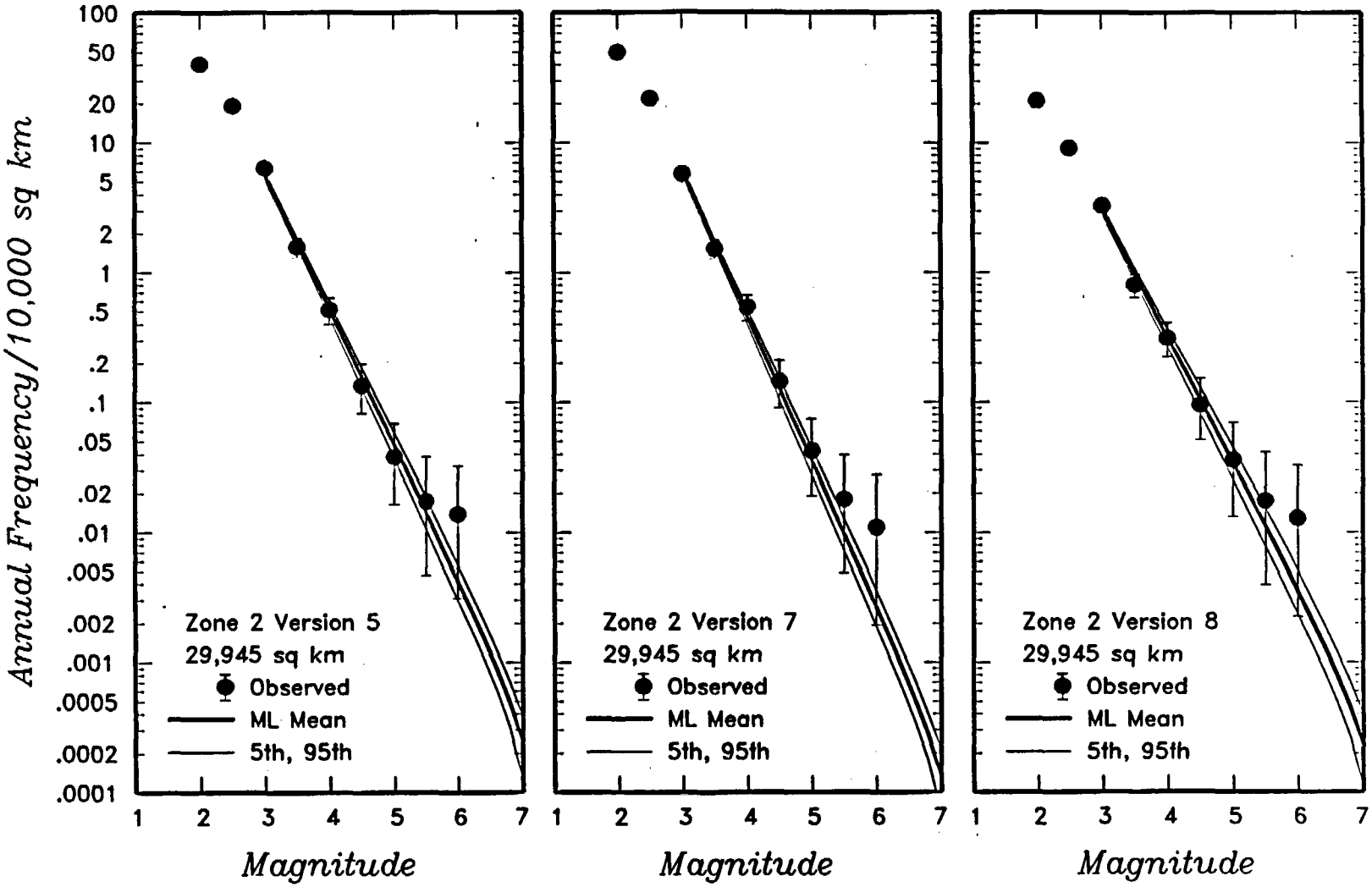

Figure 4-72 (Cont'd.) Earthquake recurrence relationships for the regional source zones defined by the SDO team.

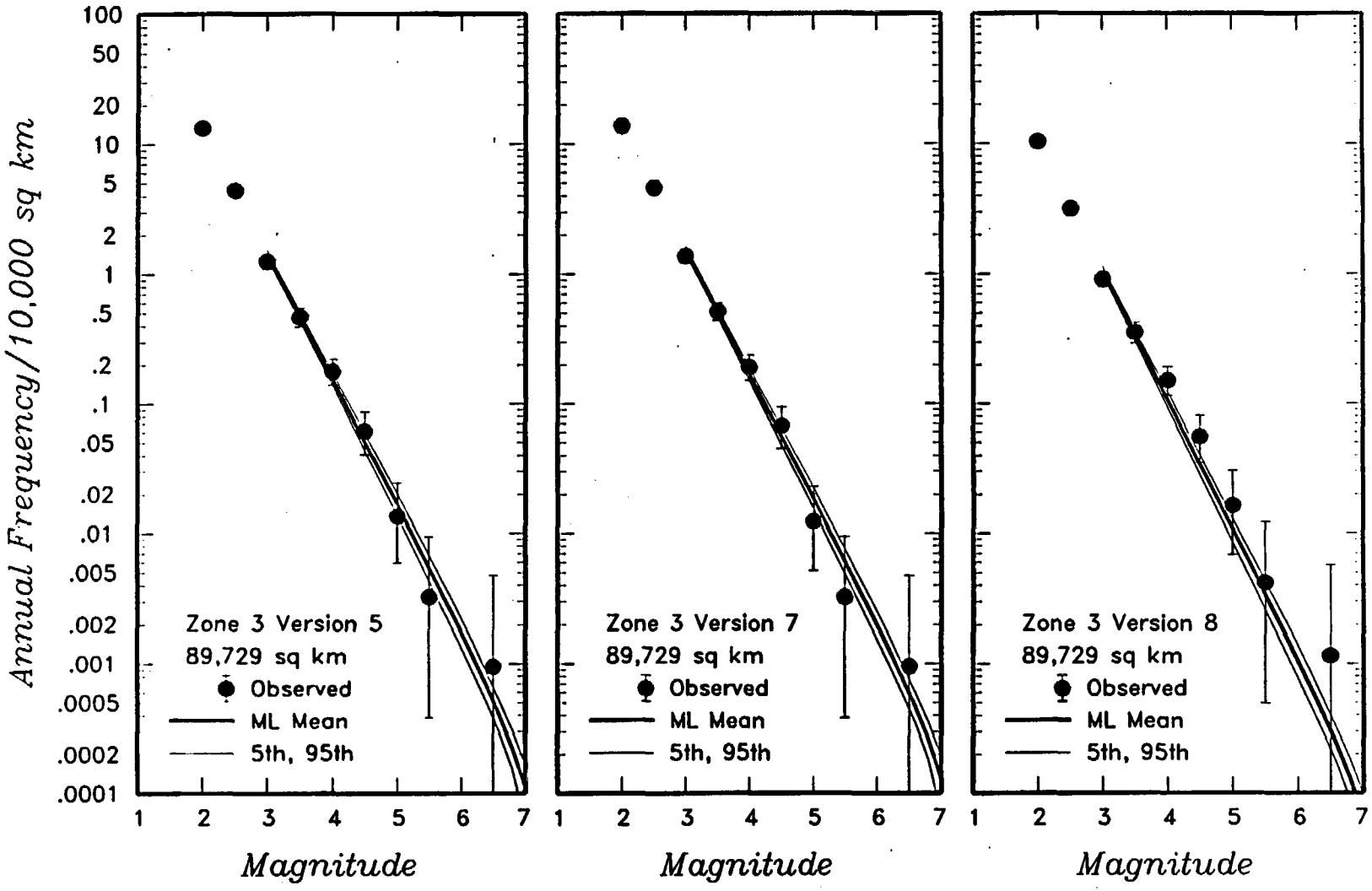

Figure 4-72 (Cont'd.) Earthquake recurrence relationships for the regional source zones defined by the SDO team.

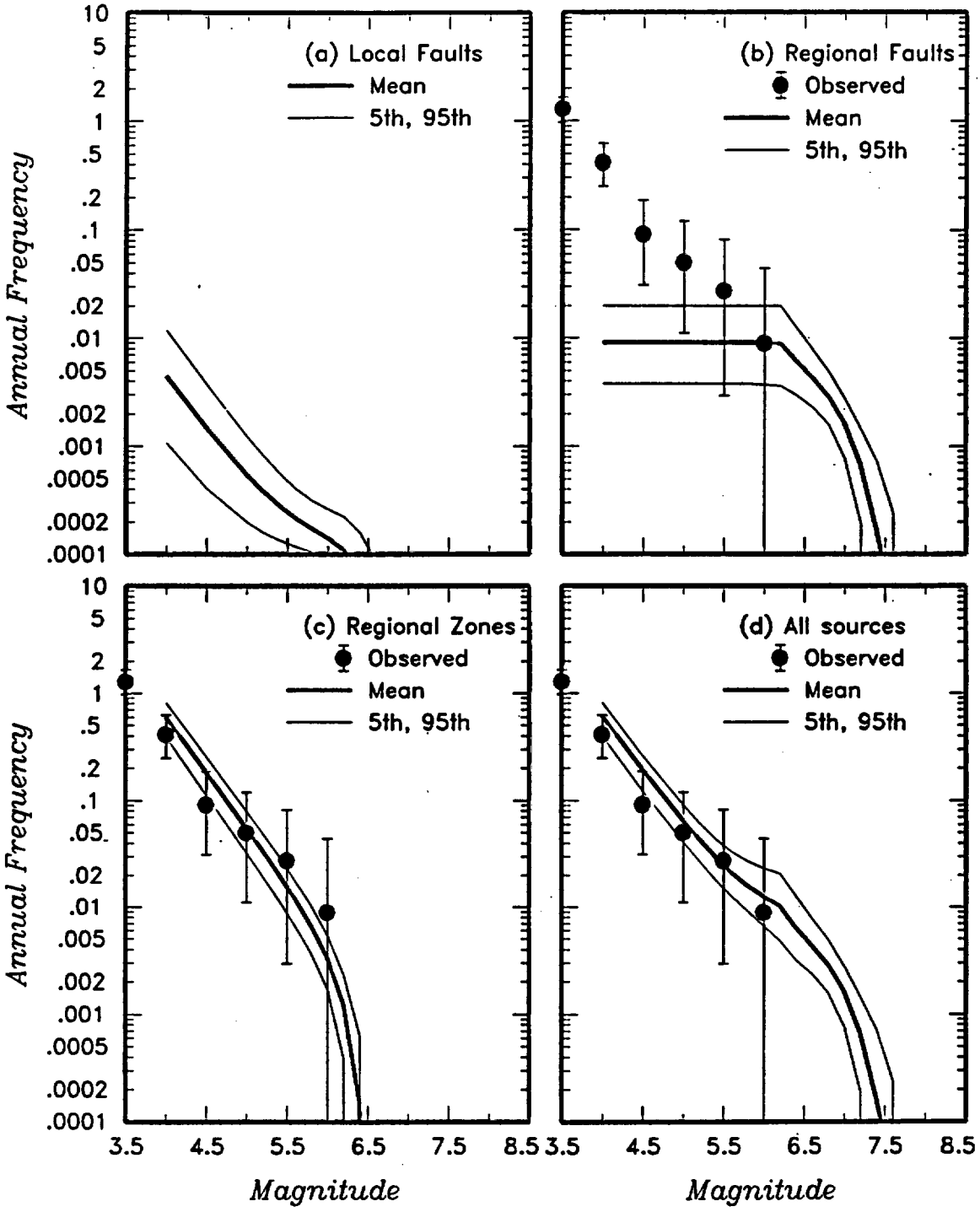

Figure 4-73 Predicted mean, 5th-, and 95th-percentile recurrence rates for (a) local fault sources, (b) regional fault sources, (c) regional source zones, and (d) all sources combined for the SDO team. The solid dots with vertical error bars represent the observed frequency of earthquakes occurring within 100 km of the Yucca Mountain site.

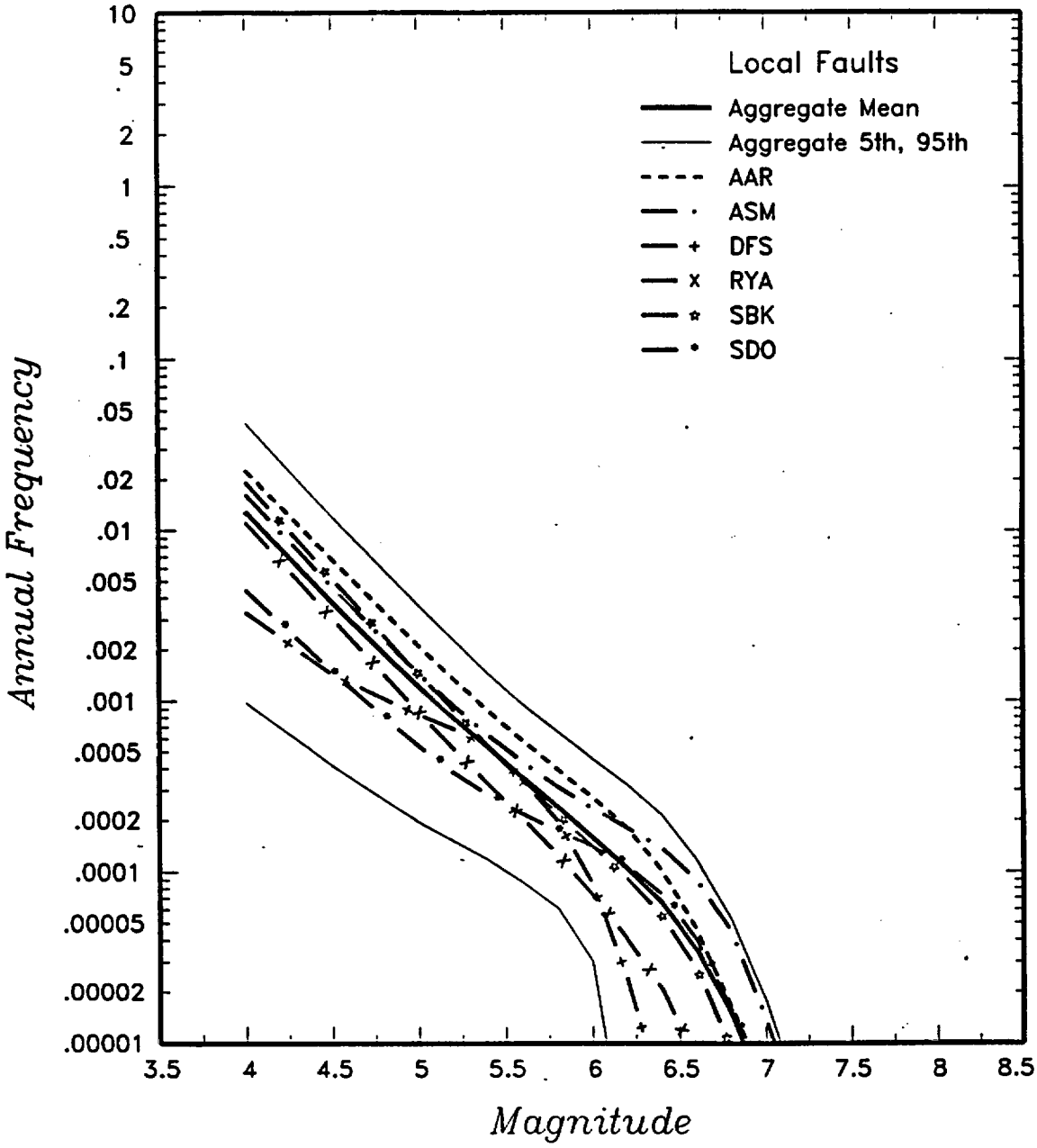

Figure 4-74 Predicted mean, 5th-, and 95th-percentile recurrence rates for local fault sources for all teams combined compared to mean recurrence estimates for individual team.

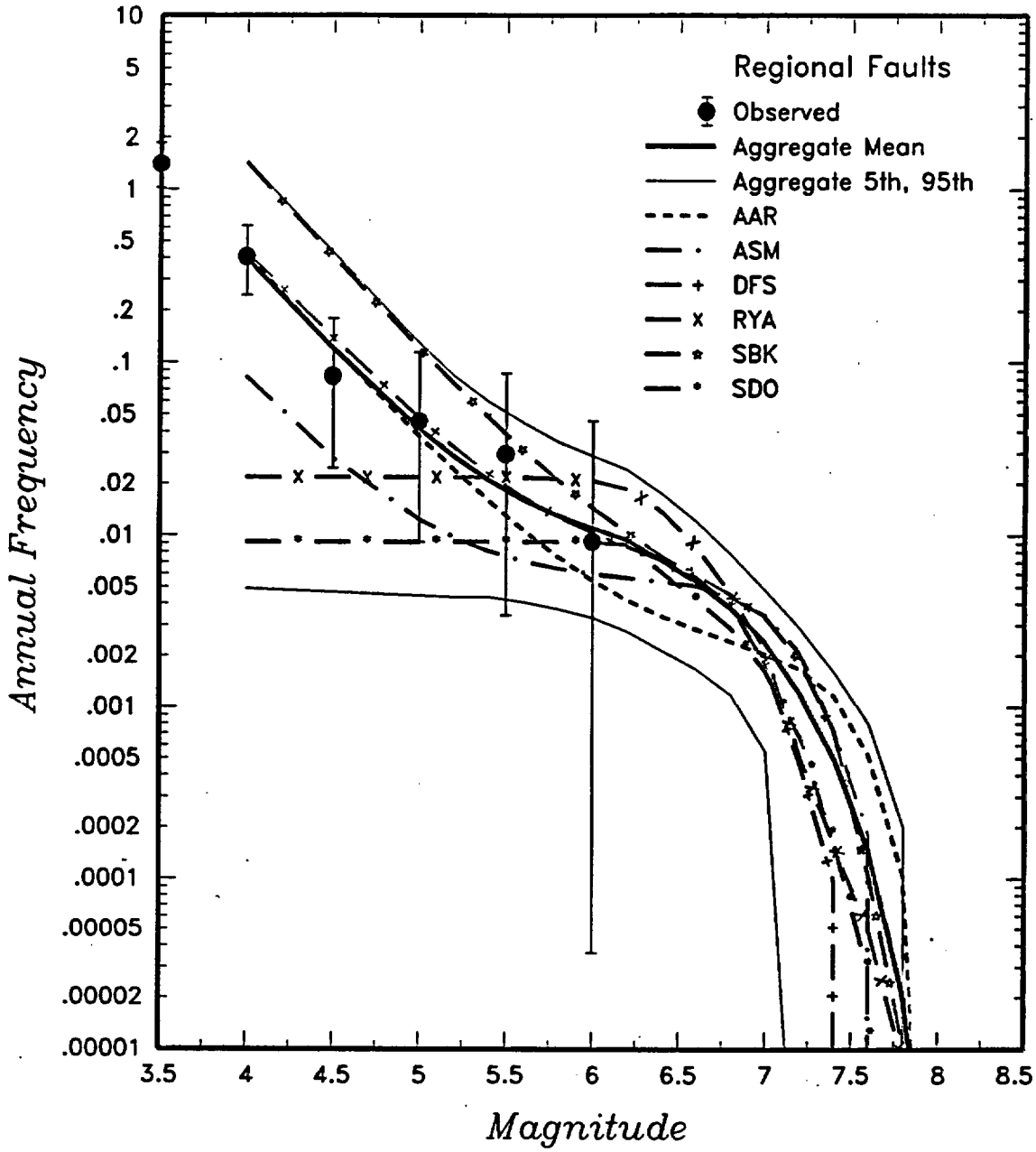

Figure 4-75 Predicted mean, 5th-, and 95th-percentile recurrence rates for regional fault sources for all teams combined compared to mean recurrence estimates for individual teams. The solid dots with vertical error bars represent the observed frequency of earthquakes occurring within 100 km of the Yucca Mountain site.

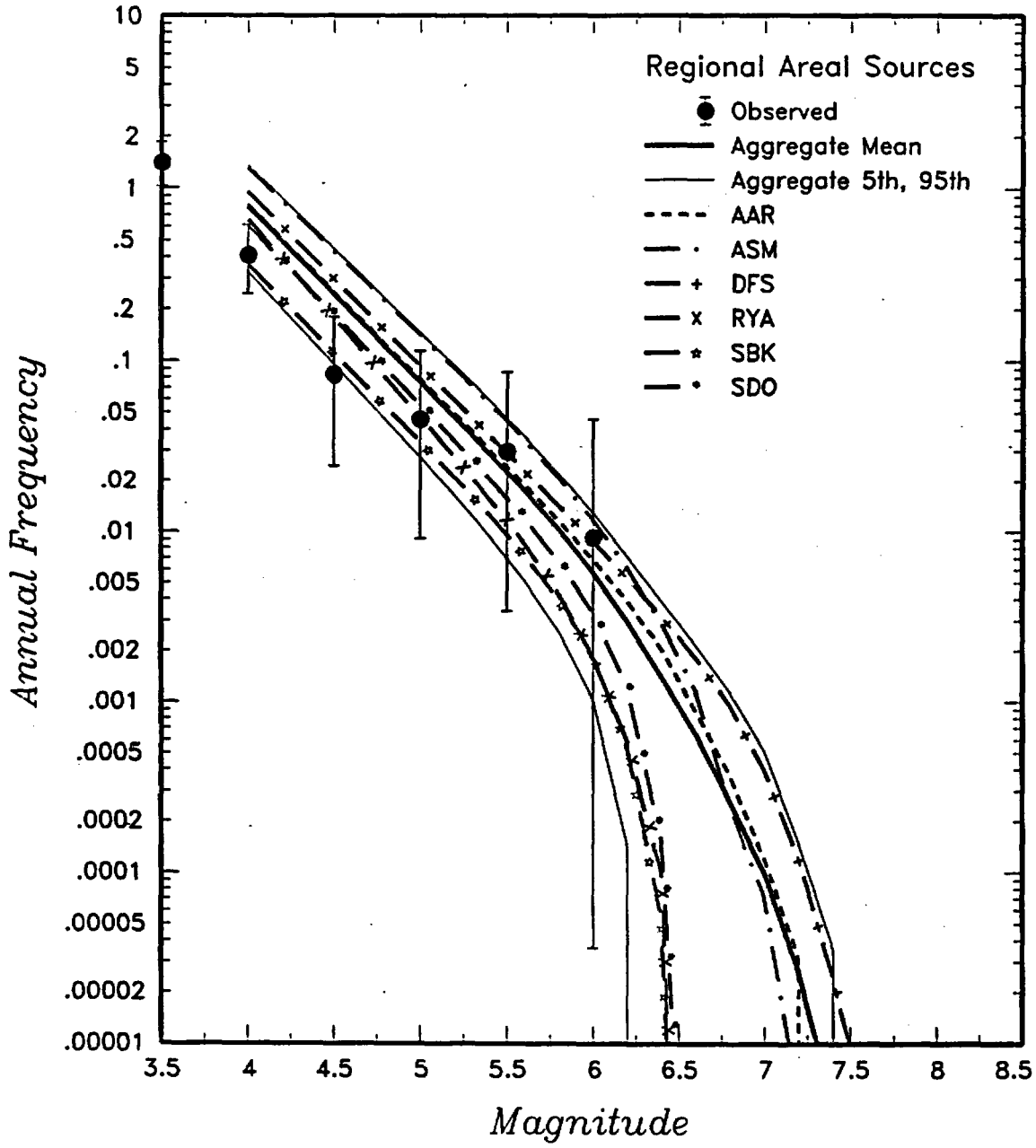

Figure 4-76 Predicted mean, 5th-, and 95th-percentile recurrence rates for regional source zones for all teams combined compared to mean recurrence estimates for individual team. The solid dots with vertical error bars represent the observed frequency of earthquakes occurring within 100 km of the Yucca Mountain site.

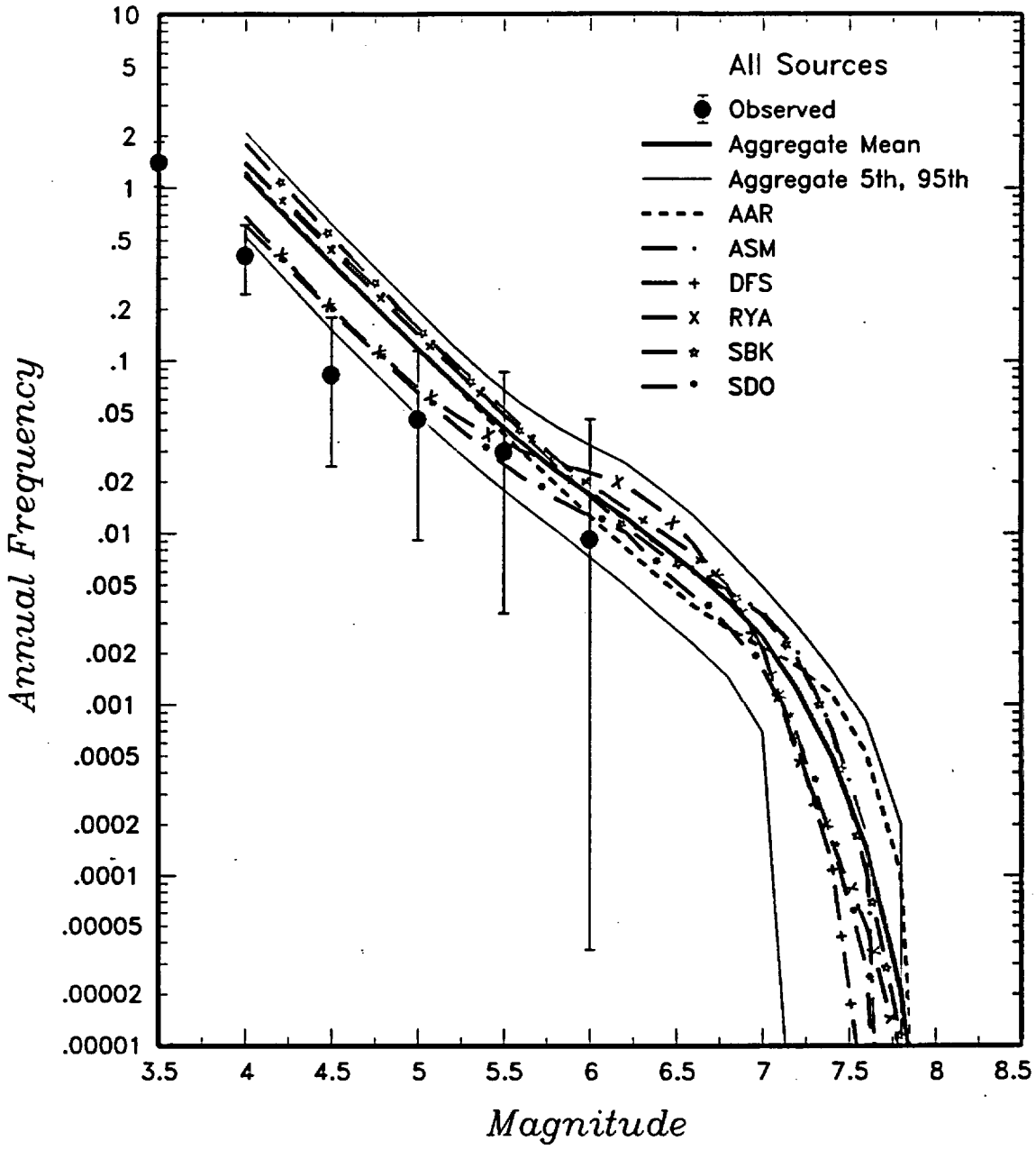

Figure 4-77 Predicted mean, 5th-, and 95th-percentile recurrence rates for all sources combined for all teams combined compared to mean recurrence estimates for individual team. The solid dots with vertical error bars represent the observed frequency of earthquakes occurring within 100 km of the Yucca Mountain site.

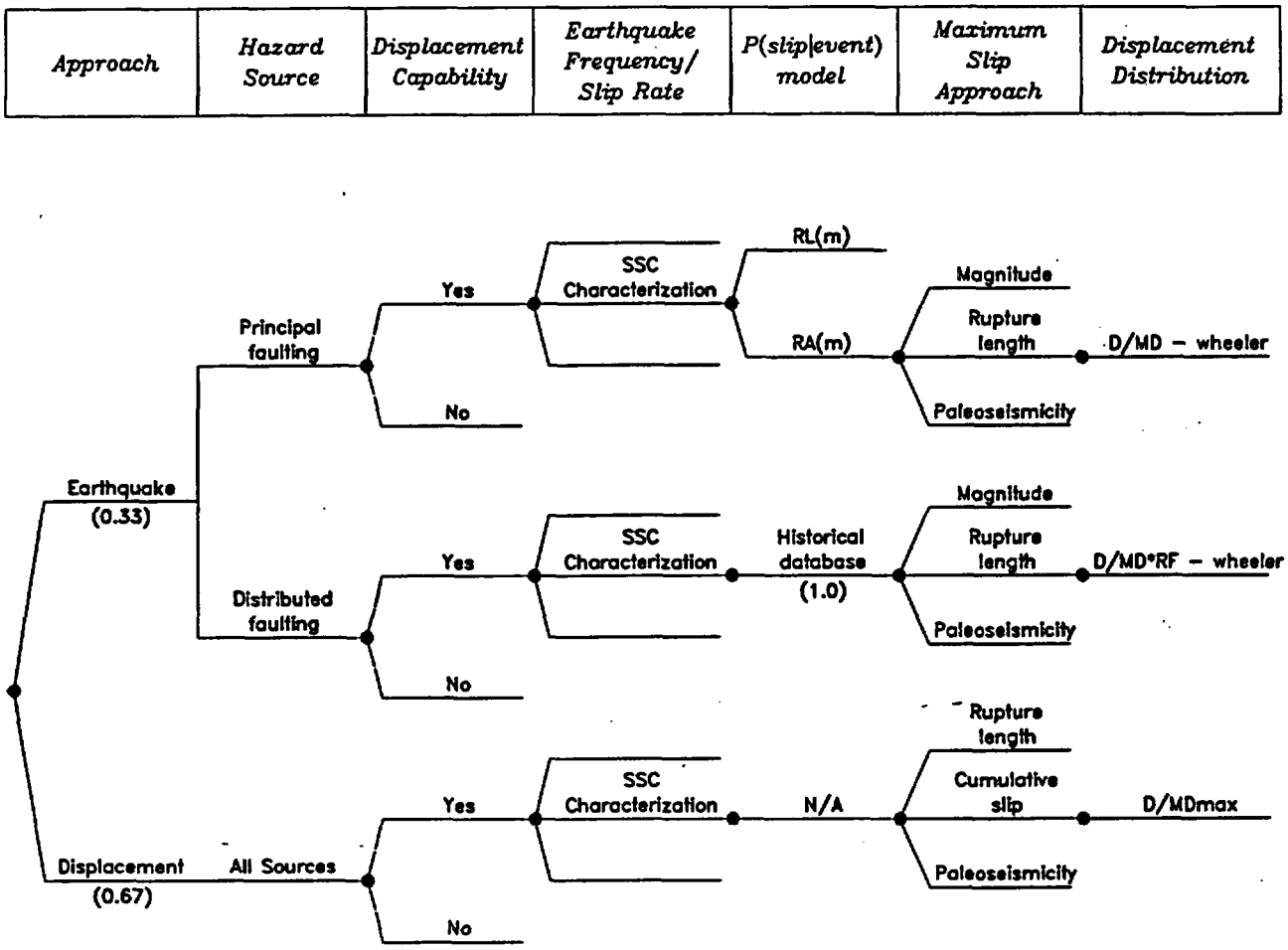

Figure 4-78 Logic tree defining the AAR team's characterization of displacement hazard at sites subject to principal faulting

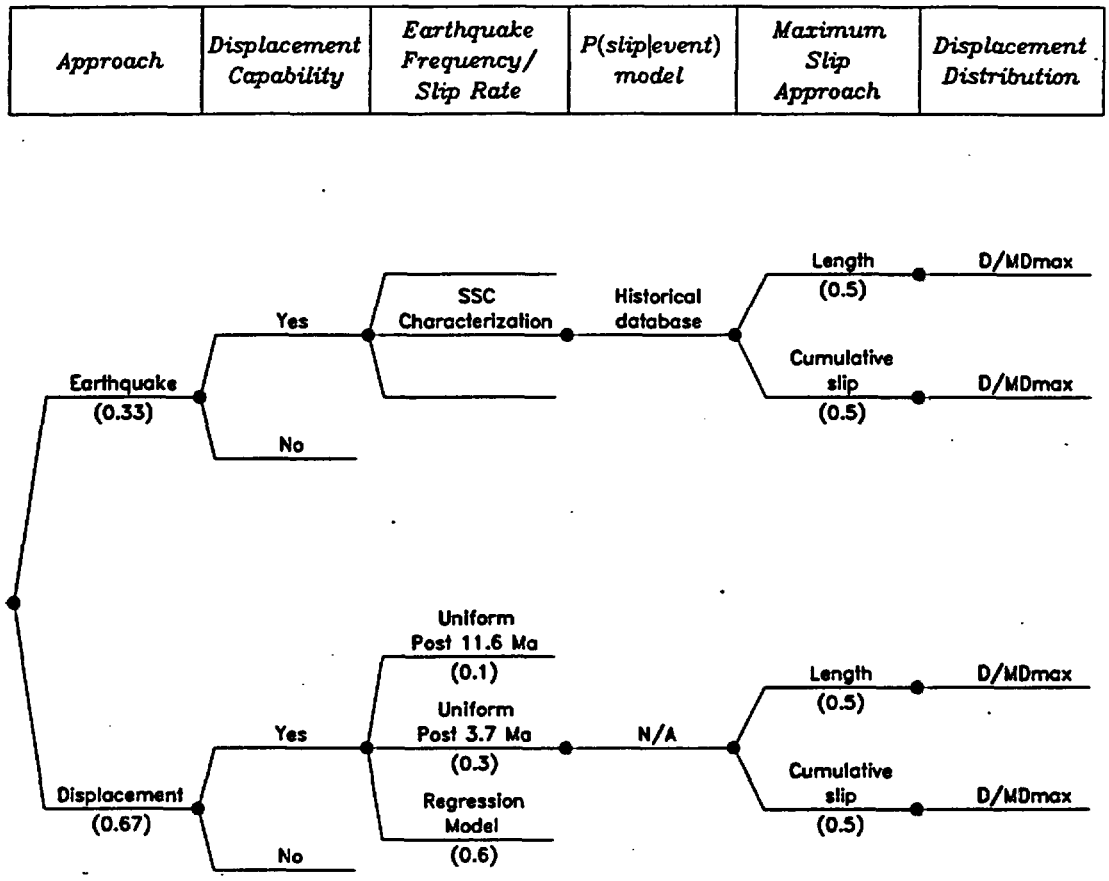

Figure 4-79 Logic tree defining the AAR team's characterization of displacement hazard at sites subject to distributed faulting

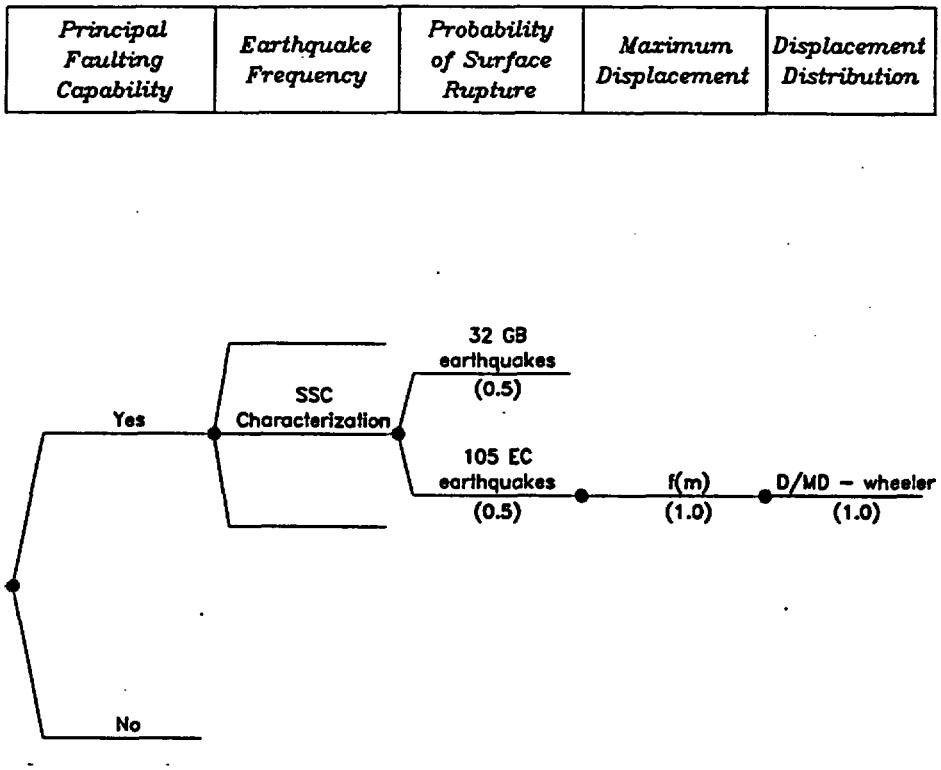

Figure 4-80 Logic tree defining the ASM team's characterization of principal faulting displacement hazard

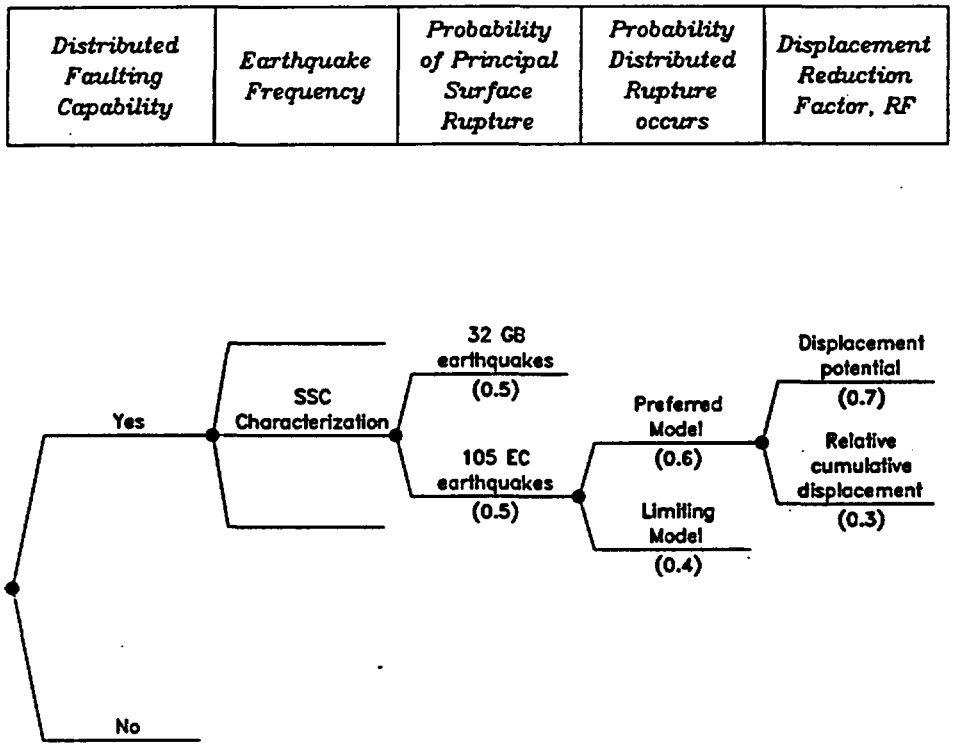

Figure 4-81 Logic tree defining the ASM team's characterization of distributed faulting displacement hazard

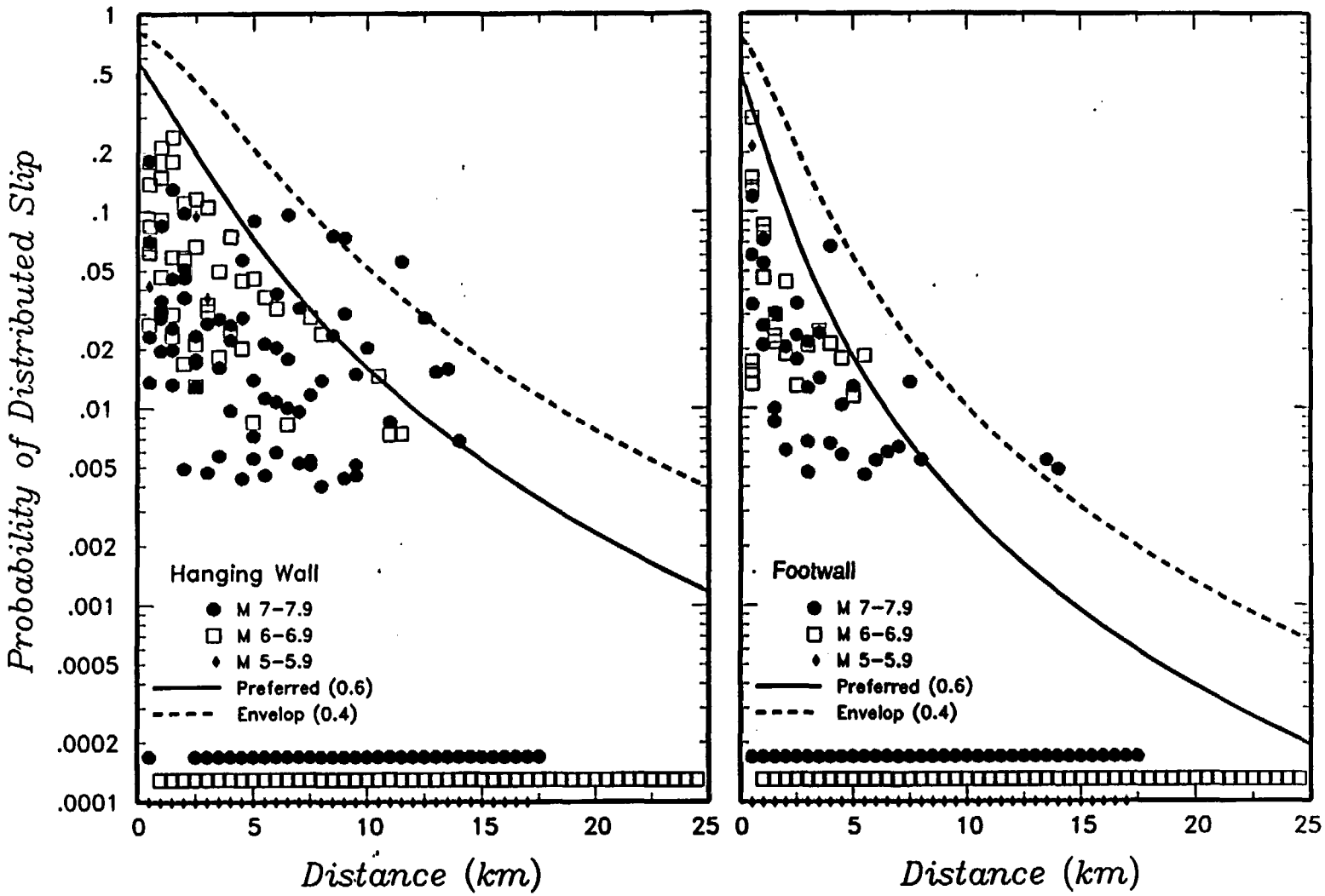

Figure 4-82 Probability of distributed rupture as a function of distance from the principal rupture defined by the ASM team. Data are the same as those presented on Figure H-13b

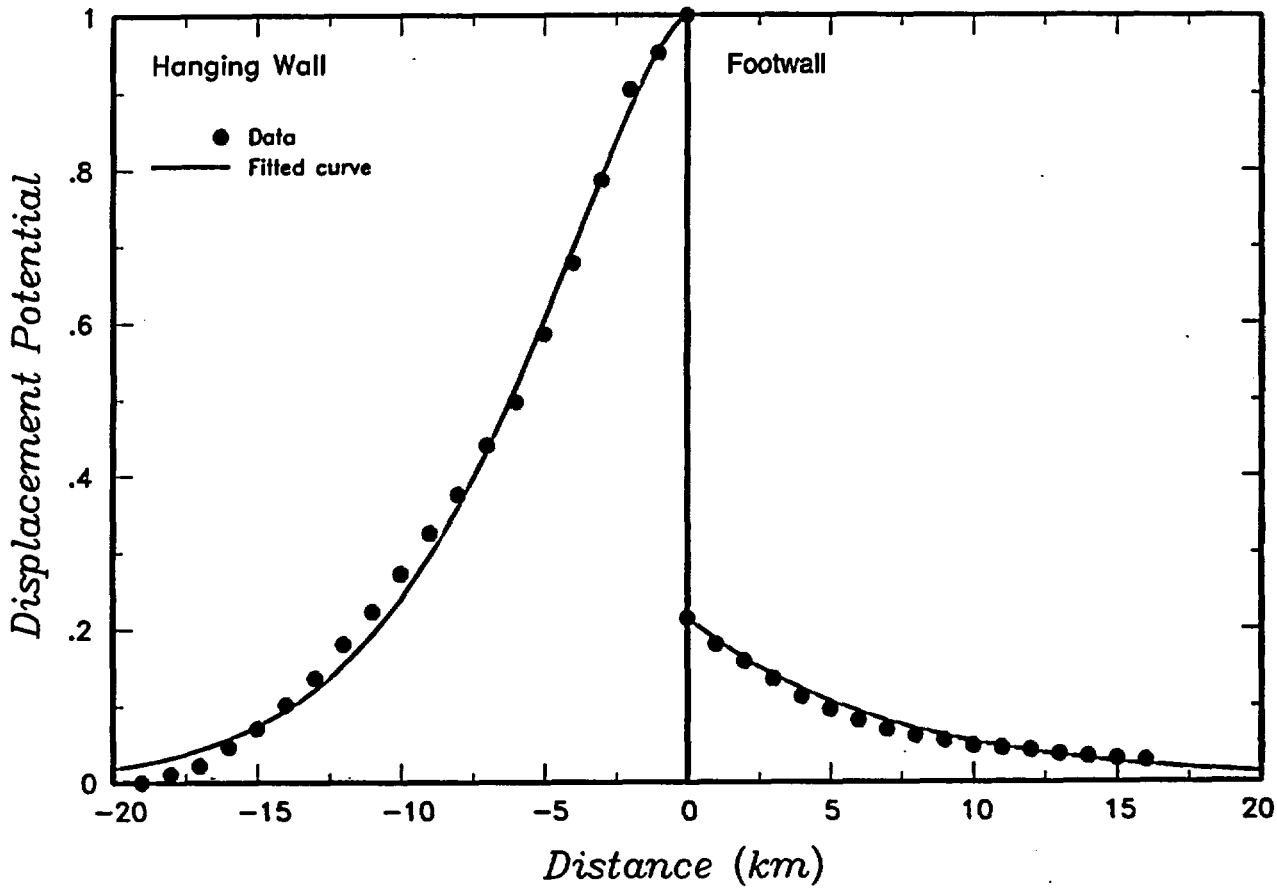

Figure 4-83 Normalized displacement profile for the 1983 Borah Peak, Idaho earthquake used by the ASM team to define the distributed faulting displacement potential

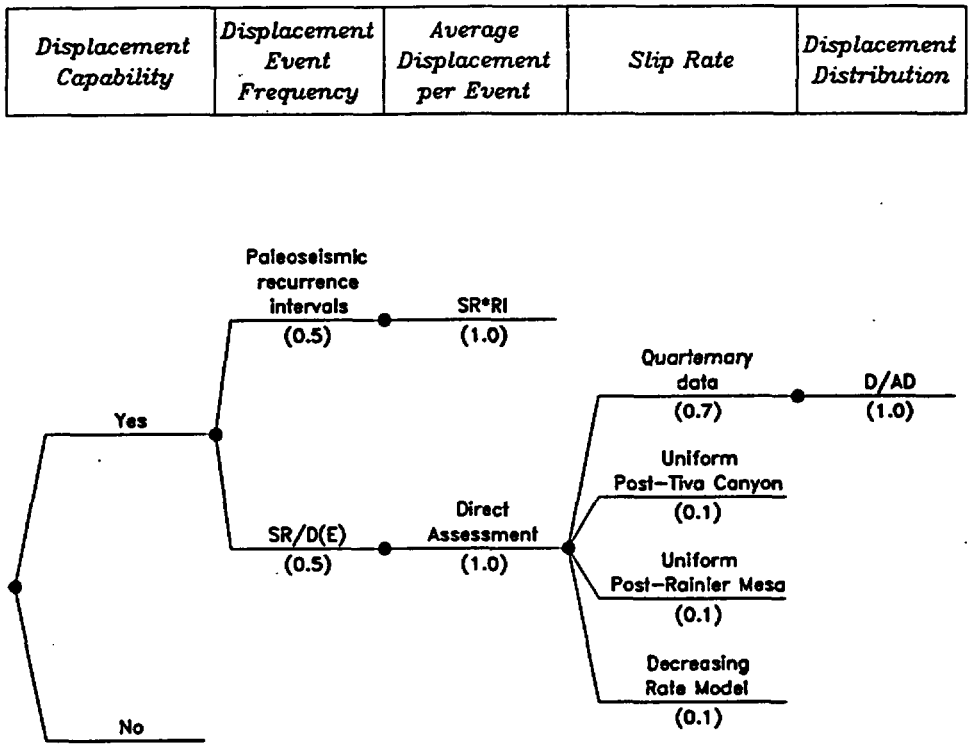

Figure 4-84 Logic tree defining the DFS team's characterization of displacement hazard

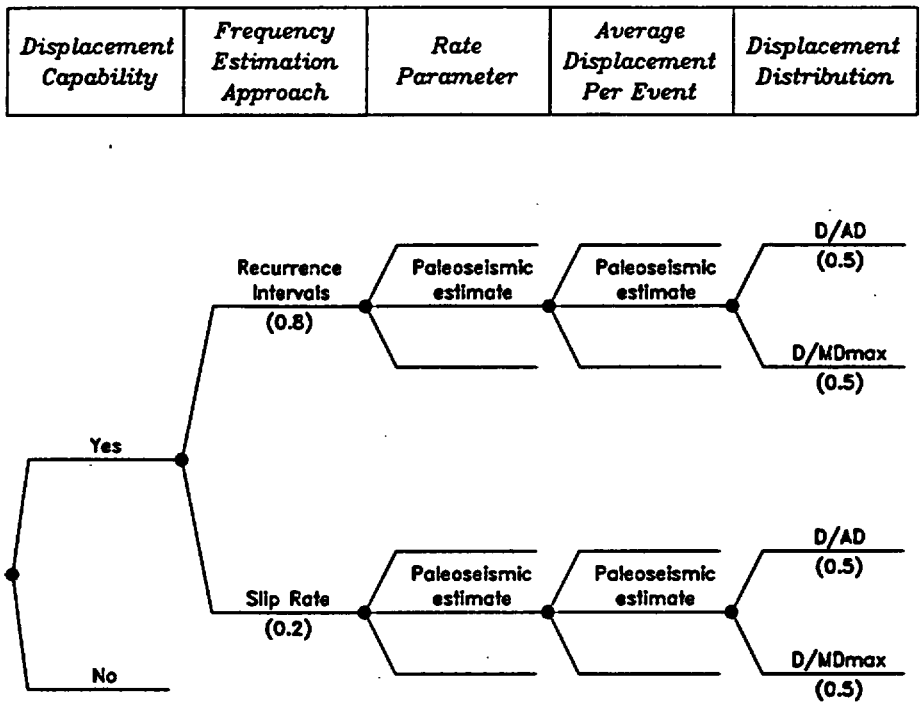

Figure 4-85 Logic tree defining the RYA team's characterization of displacement hazard at sites with Quaternary data for fault displacement

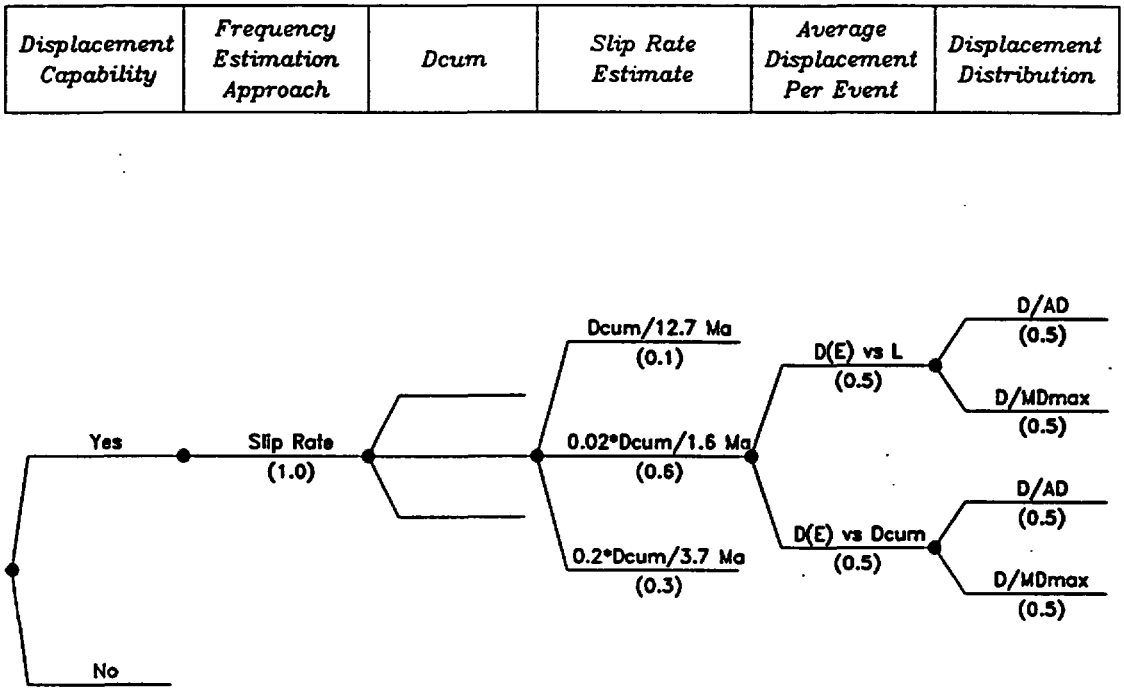

Figure 4-86 Logic tree defining the RYA team's characterization of displacement hazard at sites without Quaternary data for fault displacement

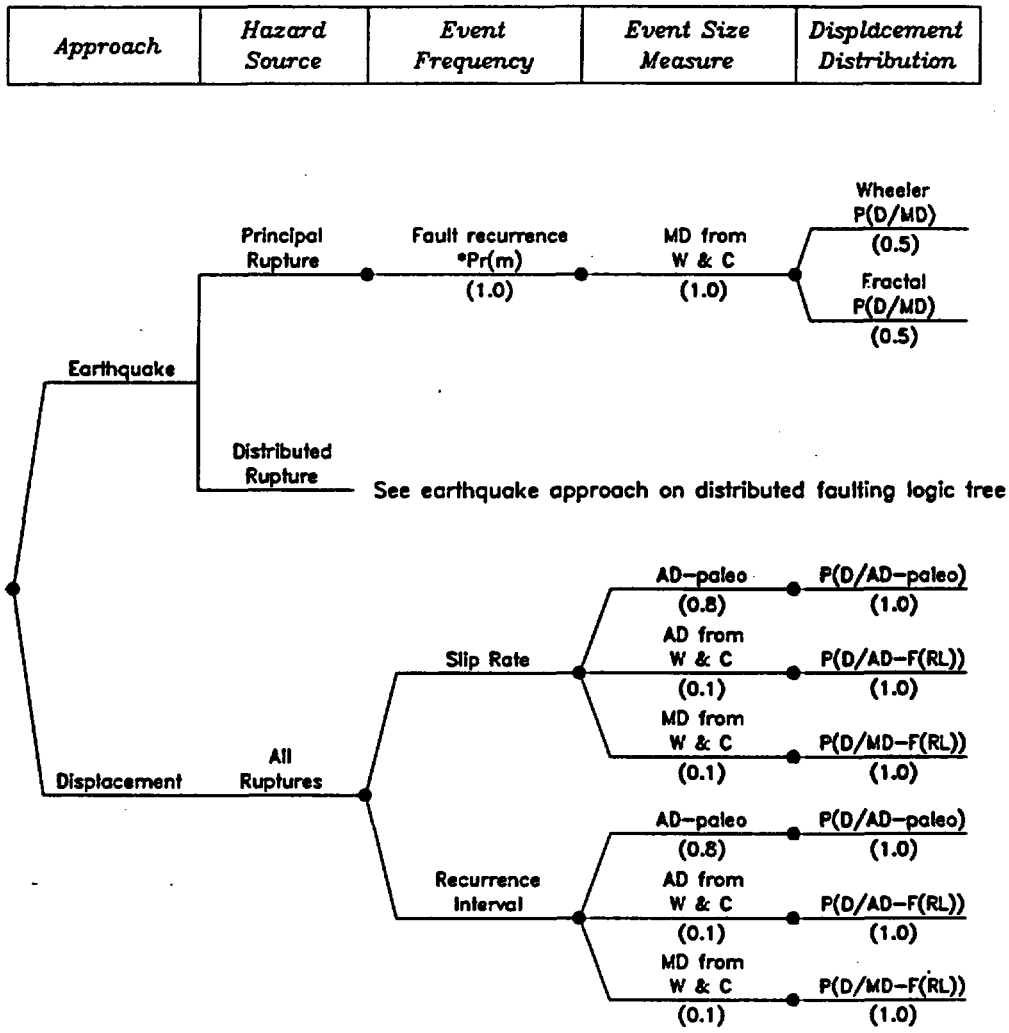

Figure 4-87 Logic tree defining the SBK team's characterization of principal faulting displacement hazard

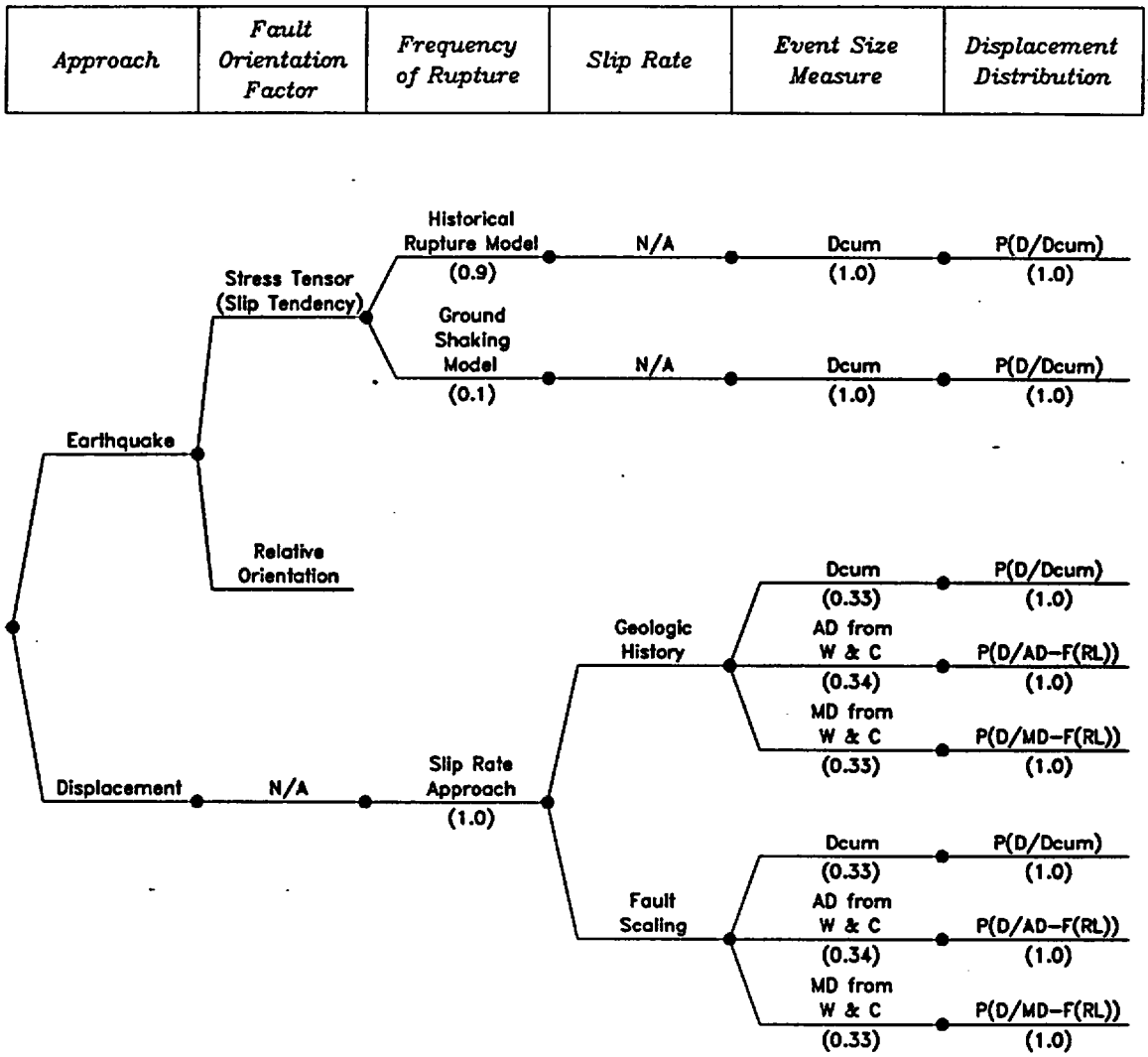

Figure 4-88 Logic tree defining the SBK team's characterization of distributed faulting displacement hazard

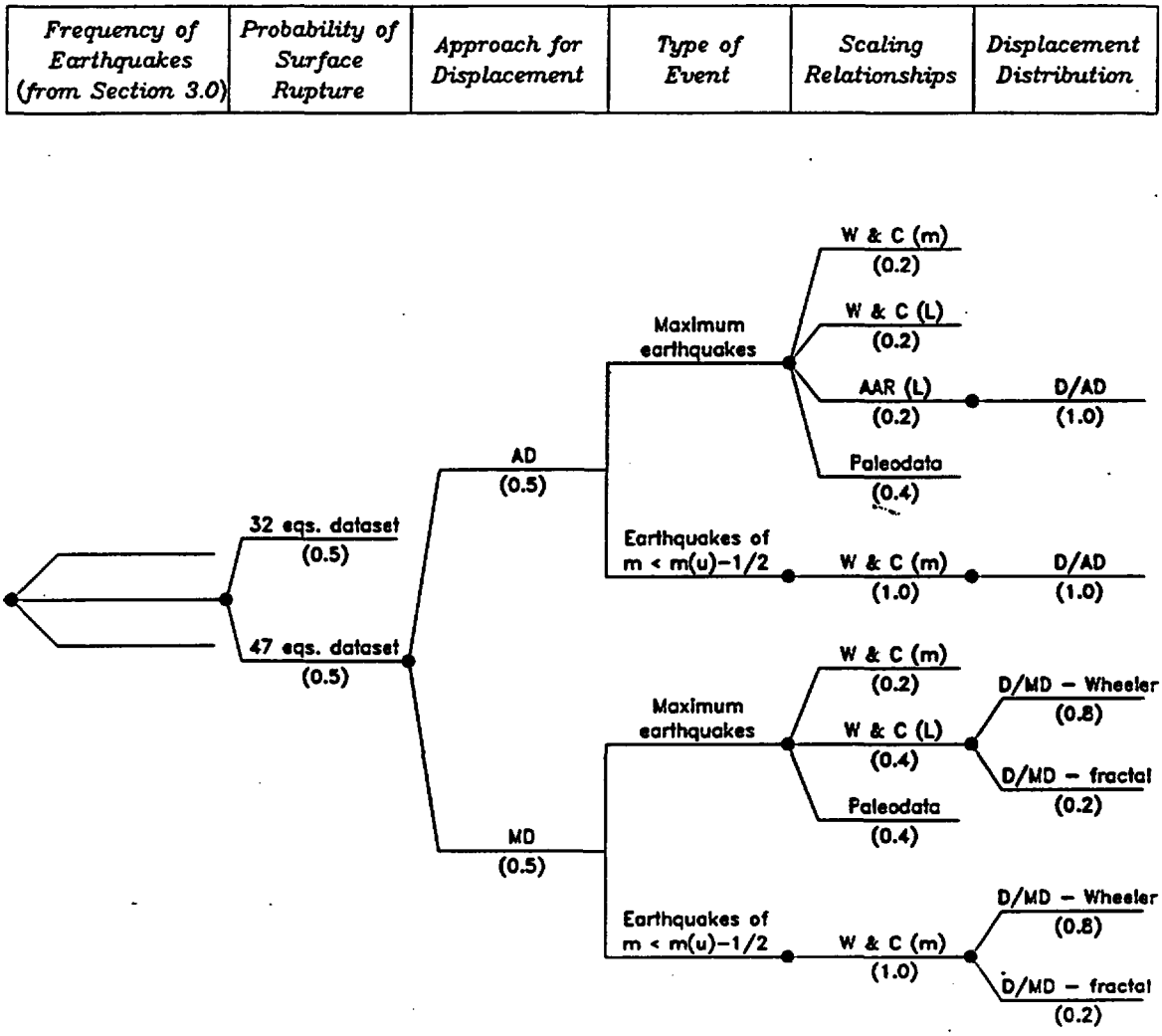

Figure 4-89 Logic tree defining the SDO team's characterization of principal faulting displacement hazard

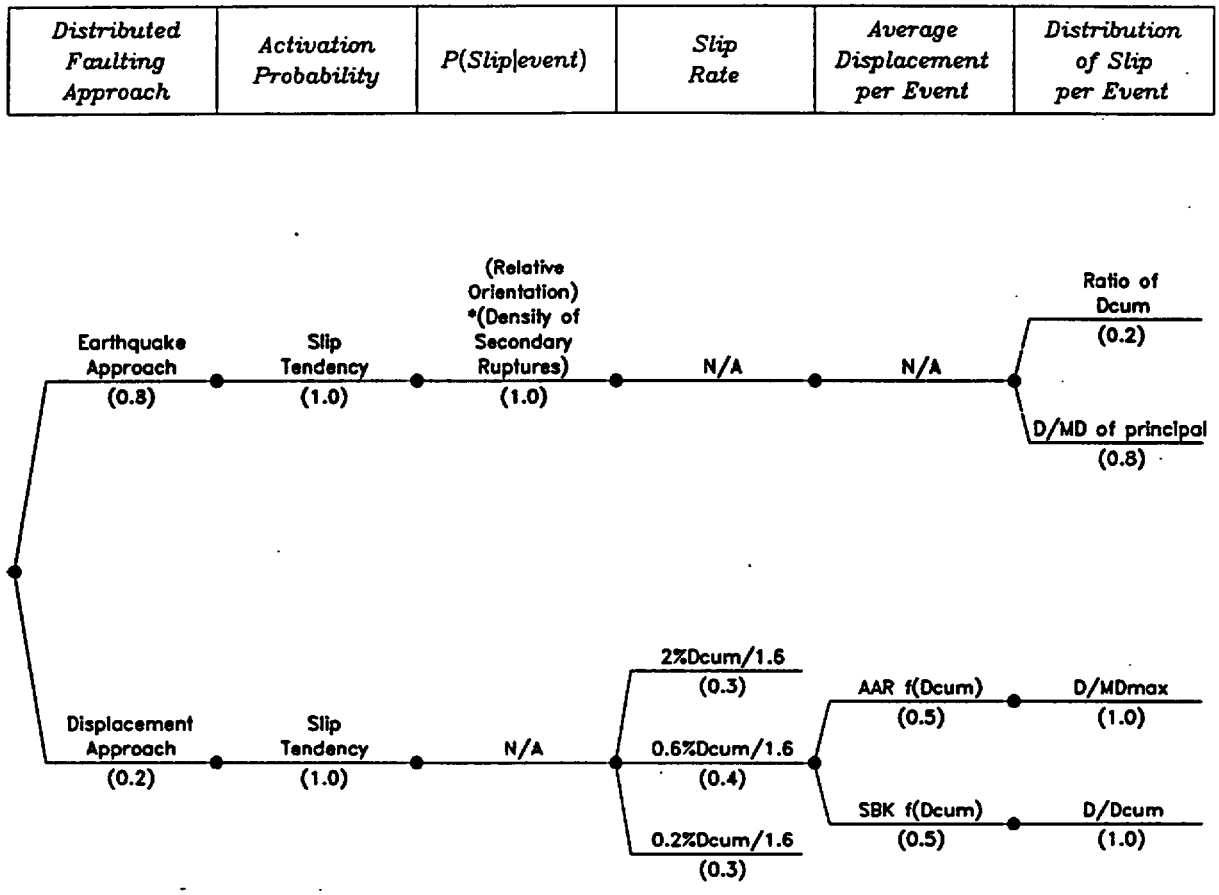

Figure 4-90 Logic tree defining the SDO team's characterization of distributed faulting displacement hazard

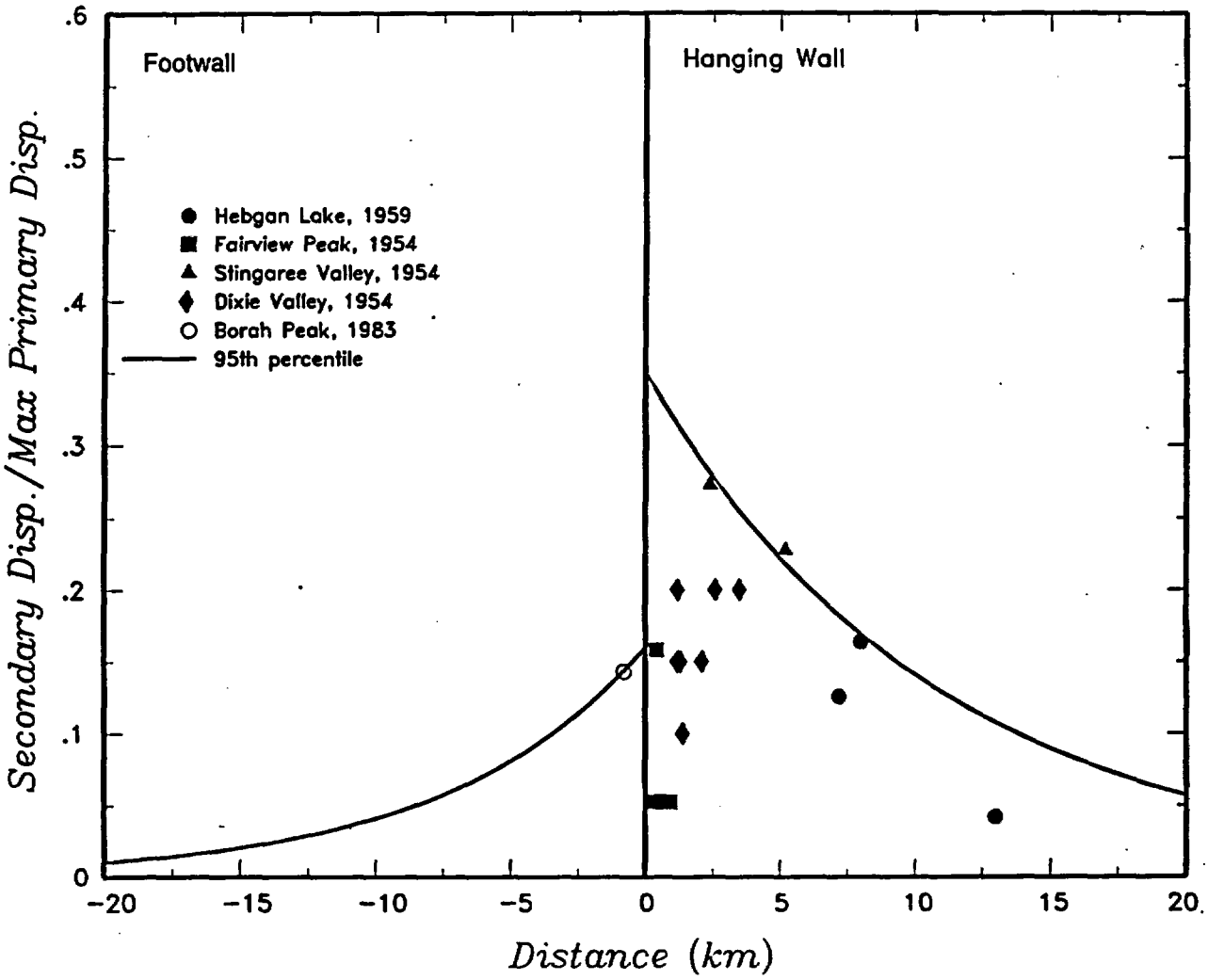

Figure 4-91 Curve defining the 95th percentile of the distribution for displacement on a distributed rupture developed by the SDO team

5.0
GROUND MOTION CHARACTERIZATION FACILITATION APPROACH

The goal of the ground motion characterization was to formulate vibratory ground motion models for input into the PSHA. The description of ground motion in this context consists of ground motion attenuation relations specific to the repository site. The ground motion study has been structured to incorporate the uncertainty in the science of ground motion estimation. A ground motion evaluation necessarily involves interpreting data, existing predictive models, and geologic and geophysical characteristics of Yucca Mountain. These data and the process by which they are synthesized into a predictive model have associated uncertainties. Therefore, fully evaluating uncertainty is an essential element of a comprehensive study. In this chapter, the approach utilized by the GM Facilitation Team to elicit interpretations from the GM experts as well as the experts' methodologies are described.

5.1 EXPERT ELICITATION PROCESS

Development of the expert interpretations was coordinated and facilitated in a series of three technical workshops. Each workshop was designed to accomplish a specific step in the overall process of developing the interpretations in order to ensure that all relevant data and credible interpretations were fully considered by each expert.

The ground motion characterization required coordination with the SSFD Facilitation Team and the PSHA Calculations Team. During the course of the project, the focus of the ground motion activity was tailored to take into account the range of seismic source descriptions identified in that activity. As first envisioned, the relevant sources included normal dip-slip faults and vertical strike-slip faults. Single ruptures of each source were assumed. However, the seismic source characterization activity identified the possibility of multiple ruptures on parallel dipping faults and a possible low-angle detachment surface underlying Yucca Mountain. Consequently, these types of seismic sources were also included in the suite of sources for which ground motion estimates were developed.

Using the various information and data discussed below, the GM experts each developed a series of estimates of ground motion for a defined suite of earthquake magnitudes and distances, fault geometries, and faulting styles. The estimates included the median ground motion and its (aleatory) variability, and the scientific (epistemic) uncertainty on both. These "point estimates" were fitted to yield attenuation equations as a function of all four parameters. The independent variables used in the regression were selected by the expert and the computations were performed by the facilitation team.

Each expert formed his or her interpretations using the information and data presented in three workshops. Additionally, the elicitation process included a formal interview, led by a normative expert, in which each expert presented and defended his or her preliminary point estimates. The facilitator challenged each expert to defend and, as necessary, clarify his or her thought process to ensure that all relevant data and information were evaluated.

As a computational aid, the GM Facilitation Team Leader provided the experts with summaries of proponent model estimates – computed ground motions from numerous empirical attenuation relations and numerical simulations the experts selected for study. All such derivative data are documented in a series of Ground Motion Data Packages, 12 volumes in all. The Data Package volumes are listed in Appendix B.

5.1.1 Compilation and Discussion of Data and Information

To ensure that all experts had equal access to data and information, a key element of the elicitation process was the dissemination of data. Two workshops were organized specifically to facilitate presentation and discussion of the data. Detailed agenda and workshop plans were provided to all participants in advance, copies of all presentation materials were made available during each meeting, and the proceedings were summarized by the GM Facilitation Team. Copies of the workshop summaries are contained in Appendix D.

Workshop #1 - Data Needs held in April 1995 identified the tectonic, geologic, seismologic, and ground motion issues to be evaluated and the primary data sets and derivative products needed to complete the evaluations. This workshop provided the experts a review of the seismologic setting of Yucca Mountain. It allowed the experts to debate the significance of

various technical issues and the data and information available to resolve them. As a result, several data needs identified by the experts were subsequently provided in the project.

Workshop #2 - Methods, Models, and Preliminary Interpretations held in January 1997 focused on methods of characterizing ground motion for the PSHA, new data and derivative analyses, and a review of the point estimate format required for the interpretations. Technical presentations centered on competing empirical attenuation models and results of synthetic modeling. Several of these proponent models were developed for other geographic regions. The experts discussed how to interpret ground motions from other regions and also discussed methods of developing adjustment factors that account for the differences between Yucca Mountain and these regions.

Although discussions of the data and other information were most focused among the experts during the workshops, throughout the project there was a continual informal dialog among the experts themselves and between the experts and the GM Facilitation Team Leader. During informal interaction among the experts, an expert was most often acting as a proponent to resolve questions regarding the application of his specific model. During informal interaction between the experts and the GM Facilitation Team, the experts raised issues that required general clarification by the GM Facilitation Team Leader.

In addition to the workshops, two working meetings were held to discuss the proponent models. These two working meetings addressed issues related to the proponent models and conversion factors that had not been resolved at the workshops. The meetings also provided additional feedback to the experts.

5.1.2 Elicitation Interviews

A formal elicitation interview between the GM Facilitation Team and each expert was held following Workshop #2. The interviews were conducted in accordance with guidelines developed by the SSHAC (1997). The elicitation team (Facilitation Team, Dr. Jean Savy, and Dr. Peter Morris) met prior to the first interview to establish a systematic approach to the questioning to ensure that the first expert would be asked the same questions as the last.

Dr. Abrahamson served as a generalist in all interviews. In the first interview (with Silva), Dr. Morris served as the normative expert. In the next four interviews (Walck, Campbell, Somerville, and Anderson), Jean Savy served as the normative expert. Dr. Morris was not available during the remaining interviews; based on guidance from Dr. Morris and their previous experience with elicitation interviews, Drs. Savy and Abrahamson conducted the remaining interviews. Dr. Becker documented the interviews.

The interviews were private and uninterrupted. Each expert provided written documentation of the proponent models he deemed relevant to the study and the means by which he formed point estimates from the proponent models. In the interview, each expert was asked to explain the procedures he adopted to obtain median estimates, aleatory uncertainties, and the epistemic uncertainties on both. Each defended his selection of 'relevant' proponent models and also explained on what basis other models were rejected.

The elicitation interview was an important source of feedback for the experts. Inconsistencies in the treatment of uncertainty and use of conversion factors were identified and later corrected by the experts. In advance of the interview, several experts had considered only a limited number of proponent models. They tended to expand the number of models considered following challenges in the elicitation to defend their initial selection. Most importantly, in preparation for the interview, all experts had used weighted averages of the proponent models to develop preliminary estimates. All had also used the concept of classes of models; the weights of the individual models were often selected so that a desired relative weight between the model classes was achieved. As a result of the interviews, a formal dual weighting scheme was adopted by each expert in which the weights were separated into weights for classes of models and weights for models within a class.

A major conclusion following the interviews was that the volume of point estimates ultimately requested could not be managed readily by the experts. The key issue was the effort needed for the computation of the weighted combinations of the proponent model estimates and appropriate adjustment factors on which the experts point estimates were based. To facilitate this effort, the GM Facilitation Team calculated the preliminary ground motion estimates for each expert using weights supplied by the expert. Consequently, a single computer program was developed by the GM Facilitation Team Leader for use by all

experts to weight proponent models as a step towards forming their point estimates. This computer program (WT_AVE) was used to compute weighted model values (used as preliminary point estimates) for each of the experts. This allowed the experts to simply develop weights for the models freeing them to concentrate on evaluating the resulting point estimates. The weighted values were used solely for preliminary computations: the experts were charged to evaluate the preliminary estimates to form their final point estimates.

5.1.3 Feedback and Revision

Feedback for the experts occurred at several different times in addition to the formal Feedback Workshop. At the working meetings, interaction among the experts was significant as they discussed the alternative approaches and proponent models. As mentioned above, the elicitation interviews resulted in significant feedback in terms of identifying inconsistencies and misconceptions by the experts. The experts were also encouraged to discuss the issues among themselves as needed in between the formal workshops and working meetings.

The Feedback Workshop informed the experts of the implications of their preliminary interpretations on the hazard computation. This workshop included a joint session with the SSFD expert teams to facilitate understanding of the technical issues and models each expert had developed. Preliminary hazard results were also presented and the sensitivity of the hazard to various input parameters was assessed. The workshop primarily consisted of discussions of the technical basis for each expert's point estimates and the attenuation equations developed from the expert's interpretations by the GM Facilitation Team. A few selected cases (magnitude, distance, and frequency combinations) were selected for in-depth discussions among the experts. The reasons for the differences in the point estimates for these cases were explored including discussions of the strengths and weaknesses of the proponent models for each case. As part of this discussion, a formal procedure for developing statistical estimates of the epistemic uncertainties was agreed upon. By the conclusion of the workshop, each participant was fully briefed on the technical basis for all other experts' estimates.

An additional working meeting, which provided additional feedback, was held shortly after the Feedback Workshop. This meeting included an exercise to focus the experts on the values of the point estimates and not on the weights given to the models.

Following the Feedback Workshop and working meeting, the experts revised their estimates. The GM Facilitation Team developed revised attenuation models based on the experts' revised estimates. The experts were then given the opportunity to revise their point estimates and/or the functional form of the regression equations. This process was repeated until the experts were satisfied that the regression models adequately characterized their estimates of the ground motion.

5.1.4 Documentation

Each expert documented the reasoning behind his development of the point estimates. This documentation is given in Appendix D. An outline of key sections was provided to each expert to ensure a standardized format was followed in the reports. The GM Facilitation Team first reviewed the documentation for internal consistency and completeness. The reports were then reviewed by the Project Management Team, and finally by the Review Panel.

5.2 REVIEW OF TECHNICAL ISSUES

Yucca Mountain lies within the Basin and Range Province, a regime primarily characterized by extensional crustal stresses. Known late Quaternary faulting within 20 km of the proposed repository is principally normal dip-slip, occurring both with and without an oblique component. Major strike-slip faults, which contribute to the potential ground shaking hazard at the site, have been identified at distances of 25 km and greater.

Ideally, ground motions recorded from earthquakes in the Yucca Mountain region, or at a minimum the Basin and Range Province, should be used to develop attenuation relations for Yucca Mountain; however, strong motion data from these environments are not sufficient to adequately constrain an empirical model. A key issue in characterizing ground motion attenuation at Yucca Mountain was the applicability of standard western U. S. attenuation models to the Basin and Range Province. Empirical attenuation relations commonly applied in the western U.S. are based primarily on recordings from California strike-slip and reverse earthquakes. For example, in the data base used by Sadigh *et al.* (1993), 15% of the earthquakes and less than 2% of the recordings used to develop their attenuation relations are

from normal or normal/oblique faulting events. This data distribution is similar for all other western U.S. attenuation models in common use. Due to the sparse amount of strong motion data recorded from normal faulting earthquakes, separate style-of-faulting factors typically have not been estimated for these types of events. Instead, the normal faulting event data are usually grouped with strike-slip faulting earthquakes because the few recorded normal event strong ground motions had not been found to be statistically different than those predicted for strike-slip events in previous evaluations (Westaway and Smith, 1989).

Further, significant differences may exist in the seismic source, regional crustal, and shallow site properties for Yucca Mountain as compared to the average source, path, and site properties represented in the western U.S. strong motion data set. An issue that the experts addressed was whether, or to what degree, these differences could affect median ground motions or variability in ground motions expected at Yucca Mountain compared to those predicted by those proponent models based primarily on California data.

5.3 GROUND MOTION WORKSHOPS AND MEETINGS

Three workshops and two working meetings on ground motion characterization were held and they are summarized below. The complete workshop summaries are contained in Appendix D.

5.3.1 Workshop #1 - Data Needs

The goal of Workshop #1 was to identify critical data needs requiring additional analyses and, secondarily, to provide site-specific information about ground motion attenuation at Yucca Mountain. The goals of the PSHA and the relevance of the ground motion characterization within the overall PSHA project were presented as background to the experts.

Because incorporation of scientific uncertainty was a key element of the study, the means by which uncertainty is characterized were discussed. Total uncertainty was decomposed as epistemic and aleatory, each of which is partitioned into parametric and modeling variability.

Various technical issues and available seismologic data were presented. Known and suspected Quaternary faults and their characteristics were described. Data on source parameters, crustal structure, attenuation parameter Q, and site effects were summarized and ranges of stress drops and Q values reported in various studies were noted. The effect of site conditions on spectra using empirical and theoretical data was illustrated. Using theoretical data, the potential influence of the uncertainty in the site properties as compared to the potential influence of the variability of source properties was examined in terms of the resulting variability of the ground motion. Key seismological data include records of the June 29, 1992 Little Skull Mountain main shock and aftershock sequence and the 1993 Rock Valley sequence. The experts were briefed on source focal mechanisms, event locations, and seismograms from this sequence. Estimated values of kappa and site amplification were provided corresponding to several stations in the Yucca Mountain region. Site response effects were examined using UNE data, which indicate strong azimuthal dependence. The data were evaluated for two-dimensional crustal structure to explain the amplification.

Two ongoing Yucca Mountain Project site characterization activities had direct relevance to the ground motion characterization activity. The first was to evaluate empirical vibratory ground motion models for extensional tectonic regimes. Spudich *et al.* (1996) had assembled a worldwide data set from normal and strike-slip faulting in these regions. Their goal was to first evaluate several empirical attenuation relations and, if they did not adequately describe the data, to develop correction factors for the relations or alternatively produce a new relation based on the extensional data (Spudich *et al.*, 1996). The second activity was the ground motion modeling of scenario earthquakes at Yucca Mountain. The activity was aimed at developing ground motion time histories and response spectra for realistic earthquake faulting scenarios (Schneider *et al.*, 1996). As part of this project, the modeling procedures were calibrated against the Little Skull Mountain records.

Ground motion estimation methods were reviewed including empirical attenuation relations, numerical simulations, and hybrid empirical-numerical schemes. The input required by each model was summarized as well as source parameters that were not well defined at the time at Yucca Mountain.

5.3.1.1 Issues from the Data Needs Workshop. Throughout Workshop #1, the GM Facilitation Team Leader and experts discussed the technical issues to be resolved and data required for a thorough assessment of ground motions. Six principal issues were identified for further study and were prioritized as to importance by the experts (Table 5-1). Most arose from a lack of detailed information or from a need to further evaluate an available data set.

Issue #1 Site Response. Site response issues were discussed in terms of measured nonlinear response of tuff samples obtained from Yucca Mountain. With the change of the reference site condition from the surface of the tuff to the "repository outcrop," the nonlinear properties of the tuff are not needed for the development of ground motions in this study. The results were used to define damping in the tuff in the upper 300 m, that is in the strata overlying the repository. The measured damping in the shallow tuff was used to adjust the measured surface kappa to the repository outcrop kappa (i.e., removing the effects of damping in the top 300 m). Very little damping was found in the upper 300 m; the kappa for the repository outcrop was reduced to 0.0186 sec from 0.02 sec observed at the surface. The nonlinear properties of the tuff will be used later to develop the ground motion for surface facilities as part of the Seismic Design Project.

Issue #2 Stress drops for Normal Faulting Earthquakes. Median stress drops were computed using the normal-faulting earthquakes in the Spudich *et al.* (1996) worldwide data set and were found to be consistently lower than those for California events, which comprise the majority of the strong ground motion data base used to develop empirical attenuation relations.

Issue #3 Shallow Slip. Based on foam rubber modeling, weak surficial layers were shown to significantly reduce the ground motion from near-surface slip due to increased rise time. This supports ground motion modeling experience, which consistently shows reduced high-frequency ground motions radiated from shallow slip. In addition, it was also shown that significant differences in near-fault ground motions for normal and reverse faults are observed in foam rubber models.

Issue #4 Numerical Simulations. Regarding the finite source numerical simulations, three preferred methodologies were identified by the experts from the six included in the Scenario

Earthquake Modeling Project. The selected procedures were Zeng and Anderson, Silva, and Somerville. These procedures were selected based on their perceived superior modeling ability as evidenced by comparisons included in the Scenario Earthquake Modeling Project (Schneider *et al.*, 1996).

Issue #5 Regional Q Models. Discrepancies in the literature regarding regional attenuation (Q) were identified; a consistent Q model was required for use by the experts.

Issue #6 2-D and 3-D Effects. Data recorded at Yucca Mountain from UNEs were shown to result in large surface waves. The surface waves are strongly affected by lateral variations in the shallow crust. However, confined shallow seismic sources such as blasts are unlike large earthquakes. The conclusion was that the variability in ground motions due to shallow lateral velocity variations in the crust developed from energy released at typical earthquake depths would be much less than that observed in the blast data.

5.3.1.2 Resolution of Data Needs Issues. The site response characteristics specific to Yucca Mountain (Issue 1), the range of source parameters (stress drops) for earthquakes in the region (Issue 2), and reported amplification of motion relative to other Nevada Test Site (NTS) sites (Issue 6) were to be resolved by evaluating new or existing data. The question of a seismic slip in the uppermost few kilometers of crust for earthquakes with rupture reaching the surface (Issue 3) originated in workshop discussions regarding numerical simulation procedures. However, none of the experts felt this issue was significant enough to account for in their point estimates. Yucca Mountain-specific ground motions predicted by numerical ground motion simulations (Issue 4) were requested, which was a furtherance of the Scenario Earthquake Modeling Project (Schneider *et al.*, 1996). Finally, the basis for the apparent discrepancies in regional attenuation (combined effect of Q and geometrical spreading) (Issue 5) was to be investigated and resolved.

5.3.2 Workshop #2 - Methods, Models, and Preliminary Interpretations

The second workshop was held after a 1-year project hiatus. The primary goals of this workshop were to refamiliarize the experts with the issues, present available models for characterizing ground motions (proponent models), and discuss ways in which elements inherent to the proponent models may differ from conditions at Yucca Mountain.

Secondarily, the technical issues raised in Workshop #1 were addressed. The experts also participated in a preliminary ground motion modeling exercise for a postulated earthquake. The exercise was intended to focus the workshop discussions on modeling techniques and highlight issues that were to be resolved in the workshop. Lastly, the range of the magnitude and distance modeling to be covered by the experts' interpretations was specified.

An important change from Workshop #1 was the reference site condition. In Workshop #1, the reference site condition was a site on the surface of the tuff. The reference site condition was redefined as a "reference rock outcrop" at the ground surface with properties equivalent to the existing conditions at repository level. The reference rock outcrop velocity profile is based on the Yucca Mountain velocity profile from the Scenario Earthquake Modeling Project (Schneider *et al*, 1996.) with the top 300 m removed. This velocity profile is listed in Table 5-2. This change in the reference site condition was made to facilitate estimation of the ground motion at the depth of the repository using procedures currently being developed for the NRC. Using reference rock outcrop ground motions is the best approach for computing the ground motions at any of the SSC locations (at depth or on the surface).

5.3.2.1 Proponent Models. The balance of Workshop #2 focused on proponent models. The point-source random vibration theory (RVT) model, the hybrid empirical model, models derived from nuclear blast data, the finite source numerical simulation models arising from the Scenario Earthquake Modeling Project, and available empirical models were all presented. During the workshop, the experts added to the list of proponent models they wished to consider in their deliberations. For example, McGarr's (1984) model relating peak ground motions with stress state and focal depth was included. All models ultimately evaluated by the experts are listed in Table 5-3.

The Spudich *et al.* (1996) data base of strong ground motion records in extensional tectonic regimes was presented and these ground motions were compared with existing empirical attenuation relations. The data set contains both strike-slip and normal faulting events from extensional regimes around the world. The study focused on calculating correction factors for empirical relations to better fit the extensional data and on developing a new predictive relation derived from the extensional data. The factors included a bias correction and a standard deviation correction, and many showed a frequency dependence. The new

attenuation relations were presented, and as they are based solely on extensional regime data, could be applied at Yucca Mountain without changes to the source.

Although the Yucca Mountain region has not experienced a major earthquake in historic times, the western boundary of the Basin and Range Province has, and clues to ground motion attenuation may be found in studies of the numerous precariously balanced rocks found regionwide. The distance of balanced rocks from historic ruptures, combined with the ground accelerations required to topple these rocks, provide physical evidence of the attenuation of ground motion from an historic earthquake. This information was collated to provide a constraint on ground motion attenuation in the region.

The GM experts presented trial estimates of median ground motion and uncertainties for two postulated M_w 6.5 earthquakes occurring at 10 km distance: one event as a result of strike-slip faulting and the other, normal faulting. The purpose of the exercises was to familiarize the experts with the process and the point estimate format. Several experts only used their own proponent models as their estimates rather than evaluating the suite of alternative credible models. (Consequently, the distinct roles of proponent expert and evaluator expert were again emphasized.) As a result, expert-to-expert variability in estimates was large; the estimates of the median peak ground acceleration varied by about a factor of two for the strike-slip case, up to three for the hanging wall of the normal faulting case, and over three for the footwall.

The experts were presented with the range of earthquake magnitudes, source distances, faulting styles, and fault geometries to be interpreted. They were to develop ground motions as a series of point estimates for 51 specified magnitudes and source - site geometries (Tables 5-4 and 5-5). Both strike-slip faulting on a vertical surface and normal slip on a moderately dipping fault were to be considered. Horizontal and vertical motions were to be estimated for peak ground acceleration, peak ground velocity, and spectral acceleration at frequencies of 0.33, 0.5, 1, 2, 5, 10, and 20 Hz. The experts were to provide the median motion, aleatory variability, and the epistemic uncertainties on both the median and the aleatory variability.

5.3.3 Working Meeting #1

Subsequent to Workshop #2, an interim working meeting was held for the experts at which they were provided with the first of several volumes of documentation of proponent models and the estimates derived from the proponent models. These "Ground Motion Data Packages" (Appendix B) were provided throughout the project as a tool to facilitate the experts' comparisons of their point estimates against the many proponent models and against the estimates of the other experts. Discussions at the working meeting were focused by the GM Facilitation Team Leader on the differences between estimates arising from the various classes of proponent models and also the differences between estimates arising from the various proponent models in each class. For convenience of comparison, classes of models were defined as empirical, finite source numerical, point source (RVT), and blast. These estimation methodologies had been presented previously in the workshops.

5.3.4 Elicitation Interview

In the formal elicitation interviews, each GM expert explained the procedures he/she adopted to obtain estimates of the median (μ), aleatory uncertainty (σ), and the epistemic uncertainties on both (σ_μ, σ_σ). As each expert explained the reasoning for the weights given to each model, it became apparent that all of the experts had included the concept of assigning weights to general classes of models and then assigning separate weights to the models within each class. The underlying logic was a dual weighting scheme with the weight for a model given by the product of the class weight and the model weight, although not all experts formally applied the approach. Once this dual weighting scheme was identified during the interviews, the experts all adopted a formal class/model weighting approach. With this common structure to the model weights, it became much easier to compare the weights used by the experts.

In general, each expert developed weighting schemes for the proponent models, applied the weights, and evaluated the resulting ground motions. In most cases, the weights were not the same for all magnitudes, distances, and frequencies as the experts considered the strengths and weaknesses of each of the classes of models and of the individual models within each class. Two experts included unique aspects in their approaches. Marianne Walck developed a method to identify outlier points among the proponent values and eliminated these from further consideration. John Anderson implemented two weighting schemes, which he then

combined to develop his estimates. In the first scheme, he accommodated all relevant proponent models and developed a uniform distribution between the maxima and minima of all of the empirical models. In the second scheme he selected preferred empirical and numerical simulation proponent models.

In all interviews, inconsistencies in the treatment of the aleatory uncertainty (σ) and epistemic uncertainty on the median estimates (σ_m) and on the aleatory uncertainty (σ_a) were identified. Therefore, the treatment of uncertainty was reviewed and each expert worked out how it should be applied in the context of his estimates.

In order to modify the empirical models to reflect Yucca Mountain repository-depth conditions, several proponent scaling and conversion factors had been provided earlier in the project. While the technical aspects of the development of the conversion factors were well understood, some inconsistencies in the details of their application were identified. Misconceptions were clarified by reviewing the sections in the Ground Motion Data Package that summarized the factors.

Substantial revisions in the experts' point estimates resulted from the interviews, largely the product of clarifying misconceptions, identifying inconsistencies, and formalizing the dual class/model weighting approach. Further, when challenged to defend their use or elimination of each model, in some instances experts identified previously unconscious bias in their approach. The tendency was to expand the number of models considered by each expert.

As a result of the elicitation interviews, many of the differences in the ground motion estimates were identified as not resulting from differences in scientific opinion, but rather from misconceptions or other inconsistencies. Removal of these unintended differences was one of the main goals of the expert elicitation process.

5.3.5 Workshop #3 - Feedback

To give the GM experts a better understanding of the technical issues of the overall PSHA, a joint session was held with the SSFD experts. In the joint session, preliminary models developed by the experts in the two groups were summarized. Although the SSFD expert teams developed models with numerous fault geometries, the GM experts developed ground

motion estimates for a few specified fault geometries. These geometries were taken as representations of 'average' geometries, and the fault geometry variation within a range was incorporated as aleatory uncertainty in the ground motion estimates. Seismic source characteristics that introduce additional uncertainty in the estimates include deviations from the specified geometry, multiple ruptures on parallel faults, and a subhorizontal detachment fault. The latter two cases deviate so far from the average models that special consideration was needed. These special cases were discussed subsequently during the workshop.

Preliminary hazard computations were presented, based on the preliminary models developed by the source characterization teams and the fits based on the preliminary ground motion point estimates. Large magnitude earthquakes on distant faults dominated the hazard at long period and the contribution from faults and areal sources more local to the site dominated at all other periods. Significant hazard arose from multiple ruptures. However, many of the multiple ruptures coalesce at shallow depths. Separate ground motions were not estimated for these cases using numerical simulations because the numerical proponent models consider shallow slip to be nearly aseismic, which is the consensus of expert opinion. However, there were some cases for rupture coalescing at depths of 5 km or more. These cases were evaluated using numerical simulations to develop scaling factors for multiple-rupture scenarios. In general, the preliminary results showed that the largest contribution to uncertainty in the hazard is uncertainty in the ground motion models, emphasizing the importance of proper treatment of uncertainty in the ground motion estimates.

Because the focus of Workshop #3 was feedback and discussion among the experts, all outlined their approach to developing their point estimates. Each of the experts employed a weighting scheme to compute their preliminary point estimates from the proponent models. Due to the large number of points to be estimated, using a weighted average of the proponent models was the only practical approach to developing the preliminary estimates; however, it was reiterated that the role of the experts is to develop point estimates of the ground motion and not weights for models. The weights are a means of getting preliminary results, but the need for the experts to focus on the resulting ground motions was emphasized.

Using the weights for the median ground motion and aleatory uncertainty was straightforward and well understood by all the experts, but the methodology for computing the epistemic

uncertainties (in both μ and σ) was not well understood. In particular, an issue that was raised was how the epistemic uncertainties from the individual proponent models should be combined with the epistemic uncertainties computed from the weighted proponent models. At the workshop, a procedure was agreed upon. This procedure is described in the documentation of the WT_AVE computer program (see Data Package Vol. 1b).

To facilitate comparisons between the individual experts' point estimates, a series of plots of these estimates and the proponent model estimates on which they were based was shown. For a given earthquake magnitude and distance, and at a given response frequency, the proponent model estimates had a bimodal distribution. Empirical estimates were generally tightly grouped separately from the numerical simulation estimates, which were less closely clustered. Because the experts weighted both empirical attenuation relations and numerical simulation proponent estimates, in general their point estimates lay between the two distributions. The experts discussed differences in the numerical proponent models at length to determine if differences in modeling methodology would require further adjustments in the point estimates. This discussion led to further checking of the numerical simulations subsequent to the workshop. These checks identified several errors in the inputs to the finite-fault numerical simulation proponent model calculations. Corrected proponent ground motions for these models were computed and these corrections were explained to the experts and discussed by them at Working Meeting #2, which was held shortly after the Feedback Workshop. After the corrections were made, the bimodal nature of the empirical estimates and the simulations was reduced. In most cases, the distributions overlapped significantly (see Data Package Vols. 2, 7, and 8).

Closure was reached on the study of precarious rocks. At four locations near large historic earthquakes, the motion required to topple the rocks was computed and compared to motions for a M_W 6.5 earthquake estimated by the experts. In general, the expert estimates significantly exceeded the toppling motions suggesting that the estimates were in turn larger than the motions that had actually occurred. However, because the study evaluated only rocks that had not toppled, and not those that had, and because the effects of motion duration, frequency content, and location in a possible shadow zone could not be quantified in the case of the precarious rocks, most of the experts believed that this information could not yet be incorporated in their estimates.

Two seismic sources had been defined by the SSFD expert teams that were significantly different than the strike-slip and normal faulting cases the GM experts had evaluated. The two rupture scenarios were (1) multiple ruptures on parallel faults, perhaps coalescing at depth, and (2) rupture on a low-angle detachment zone with multiple parallel faults near the surface. The multiple rupture scenario was shown to have a large contribution to the preliminary hazard computation for both shallow (3 km) and deeply (8 km) coalescing faults whereas the contribution from a low-angle rupture had little effect. The first scenario was investigated in numerical modeling studies. For the multiple rupture scenario, both the parallel faults and deep coalescing model results suggested that the rate of attenuation was approximately the same whether several faults ruptured or whether only the central fault ruptured. Issues that pertain to estimating these motions were identified as including moment partitioning among the rupture planes, the relative timing of the ruptures, and the distances of each plane to the site. Regarding rupture on a low-angle detachment fault, issues that affected ground motions included the stress drops of the events and the geometry. Because these issues cannot be determined *a priori*, the experts were to address any changes to their point estimates for these scenarios by incorporating additional uncertainty.

At the close of the workshop, experts briefly described potential changes to their weighting schemes applied to the proponent models based on the workshop presentations. None of the experts anticipated major modifications to their procedures, but rather refinements based on closer reevaluations of various proponent models.

5.3.6 Working Meeting #2

A second working meeting was held following the Feedback Workshop. Its first goal was to correct errors identified in checks of the finite source simulations. Inconsistencies in kappa and the crustal model had been uncovered that affected two of the models, and directivity effects were corrected in a third model. Discussions centered on the effect of these modifications on the numerical simulations. The second goal was a training exercise developed to focus the experts on their point estimates as opposed to model weights. They were shown a plot of proponent estimates (median, aleatory uncertainty, and epistemic uncertainties) and each visually formed a preferred composite estimate. This training was

effective in drawing their attention to the 'estimates' themselves and not the numerical weights given to the models.

5.4 PROPONENT MODELS

The GM Facilitation Team provided an initial list of candidate proponent models for the experts to consider. The experts added additional models that they wanted to evaluate. The proponent models were separated into classes: empirical attenuation relations, hybrid empirical, point source numerical simulation, finite-fault numerical simulations, and blast models. A complete list of the models is shown in Table 5-3.

The empirical attenuation models are results of regression analyses of empirical strong motion recordings. The models are primarily based on recordings from California earthquakes, but the hybrid model, developed by Campbell, incorporates the conversion factors discussed below directly into the model. The details of the development of this model are given in the Data Package Vol. 1.

The numerical simulations are computer-generated ground motions based on seismological models of the source, path, and site effects. There are two groups of numerical simulations: point source models and finite source models. The point source models are the simplest models with the smallest number of parameters. The point source model (with an omega-squared source) is well understood. The major source of uncertainty is in the selection of the median stress-drop, its aleatory variability, and the epistemic uncertainty in both the median and aleatory variability. To allow each expert freedom to set the stress-drops to the values that he/she preferred, the results of this proponent model were presented with median stress-drops, aleatory variability of stress-drops, and epistemic uncertainties in both as parameters to be set by each expert.

The finite-source numerical simulation models significantly differ in the model parameters required and in the procedures used to estimate ground motion. These differences can lead to significant variations in the predicted ground motions. Therefore, three different finite fault simulation procedures were used: Zeng and Anderson, Silva, and Somerville. The first two proponents additionally provided results for various alternative modeling cases. Zeng and

Anderson presented three alternative models (A, B, and C) for the ground motions from their model. Case A, their base model, used the specified source geometries. Case B used shorter fault rupture lengths for the M_W 7.5 and 8.0 events to reflect the geometric constraints on the fault length determined from faults in the region. Case C used the same fault dimensions as case B, but with nonlinear properties of the shallow tuff (top 12 km) applied to the "repository outcrop."

Silva presented two models. His base model (Case A) included the spatial variability of ground motion along the length of the fault. The variability was very large for long ruptures because the ground motion estimates off the ends of the fault were lower than elsewhere along the fault length. (This variability was not included in the other two proponent finite fault models.) In an alternative model (Case B) for the large-magnitude events, he computed the median and parametric aleatory variability for a single site located 1/3 of the rupture length from the end of the rupture (consistent with the approach used by the other two finite fault simulation methods). Case B resulted in higher median ground motion estimates and lower variability than Case A.

The blast models are based on empirical recordings from UNEs at NTS. The three blast models include alternative approaches to account for the differences in the source of earthquakes and sources of explosions.

5.4.1 Conversion Models

The ground motions developed in this study are intended to characterize surface shaking at a hypothetical site with properties the same as those encountered at a depth of 300 m at Yucca Mountain ("YM300"). The faulting styles considered are normal and strike-slip. These conditions are different than those represented by events comprising the data sets used to develop the WUS empirical relations.

A fundamental question that the experts were to address is whether ground motions at Yucca Mountain differ significantly from the motions represented by the data set that forms the basis for empirical models and, if they differ, by how much. Differences could be caused by source effects (extensional versus compressional regimes and normal versus strike-skip faulting), path effects (differences in the regional crustal structure), or site effects (differences

in the shallow site properties). The region-and site-specific aspects of the ground motion can be directly incorporated as input for the numerical simulations, but for the empirically based models, proponent conversion factors were developed to account for these differences.
Suites of conversion factors were computed to address the experts' needs. They were developed specifically in this project using the results of (1) numeric finite-fault simulations, (2) stochastic point source simulations, and (3) empirical attenuation relations. Complete summaries of the conversion factors are presented in Data Package Vol. 1. The conversion factors included corrections for

- Source - western U.S. sources to Yucca Mountain extensional sources (values ranging between about 0.35 to 0.9),
- Crust - western U.S. crust to Yucca Mountain crust (ranging between about 0.9 and 1.2),
- Site - Repository outcrop to Yucca Mountain surface (ranging between about 1.1 and 2.2).

The proponent conversion models for source and crust/site effects considered by the experts are listed in Tables 5-6a and b, respectively. For each proponent model estimate, the experts selected whichever source and crust/site conversions they wished to be applied. If a model did not require a correction term, "no correction" was selected. For example, the numerical simulations were computed for Yucca Mountain repository outcrop conditions so no crust/site correction was needed and none was applied.

An additional issue was that many of the empirical models did not cover the full range of ground motion parameters required in this study. In particular, not all of the empirical models included 20 Hz spectral acceleration, peak velocity, horizontal component-to-component variability, or vertical component ground motions. Therefore scaling rules to estimate these ground motion parameters were also required. These models are listed in Table 5-7a, b, c, and d. Again, the experts selected the appropriate scaling factors for each model. For example, the Boore *et al.* (1994) empirical model does not include 20 Hz estimates. To use this model at 20 Hz, rules for computing it must be specified (e.g., log-log interpolation). If no correction is selected for a model that does not include the desired parameter, then that model is not used in a weighted average (e.g., zero weight).

In Workshops #1 and #2, the experts had requested that the numerical simulations developed in the Scenario Earthquake Project (Schneider *et al.*, 1996) be reevaluated to encompass the suite of magnitudes and distances needed to characterize attenuation and also to reflect repository outcrop (YM300) conditions. They identified three finite fault simulation methods for this additional study (Table 5-4) and the requested computations were made. Results are summarized in Data Package Vols. 1, 1B, and 2. Further, they requested that the stochastic point source/RVT model also be used to develop motions and, consequently, an attenuation model. Synthetics from this model are presented in Data Package Vols. 1 and 2.

5.5 WEIGHTING PROCEDURE

Due to the large volume of estimates required, the experts used numerical weighting of proponent model estimates to develop their initial estimates. The weighting procedure applied two levels of weights. The models were first separated into classes and weights were assigned to each class based on the expert's judgment as to the applicability of each class. Then for each range of magnitude, distance, and fault type, weights were assigned to the models within each class based on the expert's judgment as to the strengths and weaknesses of each model in terms of its applicability to Yucca Mountain. In general, each expert varied the class and model weights on a case-by-case basis to reflect his or her assessment of the applicability of each model. For example, an expert may have downweighted or eliminated an empirical model outside the magnitude range represented by the data on which the empirical model was based. The weighting procedure produced initial estimates of the median ground motion, aleatory uncertainty, and the epistemic uncertainties on the median and aleatory uncertainty. The proponent models and conversion factors that each expert included in his analysis are summarized in Tables 5-8 and 5-9a through 5-9f.

Plots of the estimates of the ground motion resulting from the weighting procedure were provided to the experts. They reviewed the plots and revised their estimates on a case-by-case basis by either adjusting the weights, setting bounds, or by setting the values of the point estimates themselves. This process was repeated until the experts were satisfied with their estimates. Some experts revised their point estimates only once whereas others made up to five revisions.

5.6 EXPERTS POINT ESTIMATES

The experts estimated median ground motion, aleatory uncertainty, and associated epistemic uncertainties for a matrix of event magnitudes, distances, and faulting styles and at a suite of spectral frequencies. The experts' documentation of their evaluations is included as Appendix F. The information on which these estimates were based includes the many proponent models and combinations of conversion factors. The matrix of point estimates consisted of 51 combinations of parameters, which was judged to adequately define attenuation for the seismic sources considered in the PSHA. The matrix (Tables 5-4, 5-5, and Data Package Vol. 1) covers a range of M_w 5.0 to 8.0, distances from 1 to 160 km, strike-slip and normal faulting, and both hanging wall and footwall for the latter style. These magnitude-distance pairs were selected to provide adequate constraints on the attenuation without burdening the experts. The frequencies were selected to cover the range of interest for all facilities. The range was defined as 0.3 to 20 Hz. As with the magnitude-distance pairs, a minimum number of frequencies needed to adequately describe the spectral shape was used. The frequencies were selected to vary by approximately a factor of two between each frequency. The selected frequencies are: 20, 10, 5, 2, 1, 0.5, and 0.3 Hz plus peak ground acceleration and peak ground velocity.

All proponent data are summarized in Data Package Vols. 1, 1B, and 2. The experts' initial and revised point estimates are contained in a series of Data Package volumes. The proponent data are plotted together with the Revision 1 expert estimates in Data Package Vol. 3 (horizontal) and Vol. 4 (vertical). The experts' Revision 1 estimates are compared in Vol. 5. The proponent data are plotted together with the Revision 2 expert estimates in Data Package Vol. 7 (horizontal) and Vol. 8 (vertical). The experts' Revision 2 estimates are compared in Vol. 9. The final estimates (Revision 3) are compared in Vol. 12.

All point estimates for the 51 cases are plotted in Data Package Vol. 9. Median response spectral values (μ), aleatory variability (σ), epistemic uncertainty on the median (σ_μ), and epistemic uncertainty on the aleatory variability (σ_σ) are plotted for three cases on Figures 5-1 through 5-12. Shown are estimates for a smaller event (M_w 5.8) at moderate distance (20 km) and for a moderate event (M_w 6.5) at close distance (5 km), corresponding to hanging wall

sites in normal faulting (Figures 5-1 through 5-8). Estimates for a larger (M_w 7.5), relatively distant (50 km), strike-slip event are also included (Figures 5-9 through 5-12).

The two special faulting scenarios (on parallel multiple faults and on a deep, shallow-dipping detachment surface) were not envisioned when the matrix of cases was developed. In lieu of expanding the case definitions following the Feedback Workshop, the experts evaluated the adjustments to their point estimates needed to model the two scenarios. The adjustments consisted of modifications to the median estimates (μ) and the aleatory uncertainty (σ). Their documentation and the adjustments are also included in Appendix F.

TABLE 5-1
KEY ISSUES IDENTIFIED AT THE DATA NEEDS WORKSHOP

Issue 1	What are the site response characteristics specific to Yucca Mountain?
Issue 2	What is the range of values of source parameters for earthquakes in this region of the Basin and Range?
Issue 3	What is the explanation for the apparent aseismic slip in the uppermost few kilometers of crust for earthquakes with rupture that reaches the surface?
Issue 4	What is the Yucca Mountain specific ground motion attenuation predicted by various numerical simulation procedures?
Issue 5	What is the basis for apparent discrepancies in the literature regarding regional attenuation (combined effect of Q and geometrical spreading?
Issue 6	What is the explanation for the reported large amplification of motions at Yucca Mountain compared to other NTS sites?

TABLE 5-2
YUCCA MOUNTAIN VELOCITY AND Q PROFILES

LAYER	DEPTH TO TOP (m)	V_S (km/sec)	V_P (km/sec)	DENSITY (g/cm^3)	Q_S	Q_P
1	0	0.6	1.8	1.7	25	80
2	40	1.2	2.5	2.0	40	120
3	80	1.5	2.9	2.3	40	120
4	220	1.9	3.2	2.4	70	150
5	1000	2.1	3.6	2.4	100	200

Source: Schneider *et al.* (1996)

TABLE 5-3
MODEL CLASSES AND PROPONENT MODELS

MODEL CLASS	PROPONENT MODELS IN CLASS	USED FOR FINAL ESTIMATES?
Empirical	Abrahamson and Silva (1997)	Yes
	Boore *et al.* (1997) (Vs model)	Yes
	Boore *et al.* (1994) (Class A)	No
	Boore *et al.* (1994) (Class B)	No
	Campbell (1997) (Soft Rock)	Yes
	Campbell (1997) (Hard Rock)	No
	Campbell (1993, 1994)* (Hard Rock)	No
	Campbell (1990, 1994) (Soft Rock)	No
	Campbell (1990) (Soil, Soft Rock)	No
	Idriss (1993) (Rock, Stiff Soil)	No
	Idriss (written comm. 1997) (Rock, Stiff Soil)	Yes
	Joyner and Boore (1988) (Rock)	Yes
	Sadigh *et al.* (1997) (Rock)	Yes
	Sabetta and Pugliese (1996) (Rock)	Yes
	Spudich *et al.* (1996) (Rock)	Yes
	McGarr (1984) (Rock)	Yes
Hybrid Empirical	Campbell (This Study)	Yes
Finite Fault Simulation	Silva (This Study)	Yes
	Somerville (This Study)	Yes
	Zeng and Anderson (This Study)	Yes
Point Source RVT	Silva (This Study)	Yes
Blast	Bennett Model 1 (1995 Scenario Study)	No
	Bennett Model 2 (1995 Scenario Study)	Yes
	Bennett Model 3 (1995 Scenario Study)	No

*Campbell 1994 is Campbell and Borzognia (1994)

TABLE 5-4
POINT ESTIMATE MATRIX

DISTANCE[1]	DEEP FOCUS[2]		SHALLOW FOCUS[2]					
(KM)	M 5.0	5.8	5.0	5.8	6.5	7.0	7.5	8.0
1	SS[3]		SS, HW[3]	SS	SS, HW, FW[3]	SS	SS	
5	SS, HW	HW, FW		HW, FW	SS, HW, FW			
10		SS	SS, HW	SS, HW, FW	SS, HW, FW	SS, HW, FW	SS, HW	
20		HW			SS, HW, FW			
50			SS, HW	SS, HW	SS, HW	SS, HW	SS, HW	SS
100					SS			
160			SS		SS			SS

[1] Horizontal distance from surface expression of fault (up-dip extension)

[2] Shallow focus is centered at 5 km depth; bottom of deep focus rupture is at 14 km depth. See Data Package Vol. 1 for full definitions.

[3] HW refers to hanging wall location in normal faulting, FW to footwall location in normal faulting, and SS to strike-slip faulting.

TABLE 5-5
51 CASE DEFINITIONS FOR POINT ESTIMATES

CASE NO.	MAGNITUDE (M_W)	DEPTH[1]	X-DISTANCE[2] (km)	FAULTING STYLE[3]	R_{RUPT}[4] (km)	R_{JB}[4] (km)	R_{SEIS}[4] (km)
1	5.0	Shallow	1	SS	3.2	1.0	3.2
2	5.0	Shallow	1	HW	3.4	0.9	3.4
3	5.0	Deep	5	SS	11.3	5.0	11.3
4	5.0	Deep	5	HW	10.7	1.1	10.7
5	5.8	Deep	10	SS	12.2	10.0	12.2
6	5.8	Deep	20	HW	17.3	11.9	17.3
7	6.5	Shallow	1	SS	1.0	1.0	3.2
8	6.5	Shallow	1	HW	0.9	0.0	3.1
9	6.5	Shallow	-1	FW	1.0	1.0	4.1
10	6.5	Shallow	5	HW	4.3	0.0	4.4
11	6.5	Shallow	-5	FW	5.0	5.0	7.4
12	6.5	Shallow	50	SS	50.0	50.0	50.1
13	6.5	Shallow	50	HW	44.1	45.3	45.3
14	7.0	Shallow	10	SS	10.0	10.0	10.4
15	7.5	Shallow	50	SS	50.0	50.0	50.1
16	7.5	Shallow	50	HW	44.2	41.9	44.2
17	5.0	Deep	1	SS	10.2	1.0	10.2
18	5.8	Deep	5	HW	7.9	0.0	7.9
19	5.8	Deep	-5	FW	12.4	9.6	12.4
20	5.0	Shallow	10	SS	10.5	10.0	10.5
21	5.0	Shallow	10	HW	8.7	6.1	8.7
22	5.0	Shallow	50	SS	50.1	50.0	50.1
23	5.0	Shallow	50	HW	46.6	46.1	46.6
24	5.0	Shallow	160	SS	160.0	160.0	160.0
25	5.8	Shallow	1	SS	1.8	1.0	3.2
26	5.8	Shallow	5	HW	4.3	0.4	4.4
27	5.8	Shallow	-5	FW	6.4	6.1	7.4
28	5.8	Shallow	10	SS	10.1	10.0	10.4
29	5.8	Shallow	10	HW	8.7	5.4	8.7
30	5.8	Shallow	-10	FW	11.3	11.1	12.1
31	5.8	Shallow	50	SS	50.0	50.0	50.1
32	5.8	Shallow	50	HW	46.1	45.4	46.1
33	6.5	Shallow	5	SS	5.0	5.0	5.8
34	6.5	Shallow	10	SS	10.0	10.0	10.4
35	6.5	Shallow	10	HW	8.7	4.1	8.7
36	6.5	Shallow	-10	FW	10.0	10.0	12.1

TABLE 5-5 (Continued)

CASE NO.	MAGNITUDE (M_W)	DEPTH[1]	X-DISTANCE[2] (km)	FAULTING STYLE[3]	R_{RUPT}[4] (km)	R_{JB}[4] (km)	R_{SEIS}[4] (km)
37	6.5	Shallow	20	SS	20.0	20.0	20.2
38	6.5	Shallow	20	HW	17.3	14.1	17.3
39	6.5	Shallow	-20	FW	20.0	20.0	21.9
40	6.5	Shallow	100	SS	100.0	100.0	100.0
41	6.5	Shallow	160	SS	160.0	160.0	160.0
42	7.0	Shallow	1	SS	1.0	1.0	3.2
43	7.0	Shallow	10	HW	8.7	1.9	8.7
44	7.0	Shallow	-10	FW	10.0	10.0	12.1
45	7.0	Shallow	50	SS	50.0	50.0	50.1
46	7.0	Shallow	50	HW	44.2	41.9	44.2
47	7.5	Shallow	1	SS	1.0	1.0	3.2
48	7.5	Shallow	10	SS	10.0	10.0	10.4
49	7.5	Shallow	10	HW	8.7	1.9	8.7
50	8.0	Shallow	50	SS	50.0	50.0	50.1
51	8.0	Shallow	160	SS	160.0	160.0	160.0

[1] Shallow depth indicates rupture is centered at a depth of 5 km; deep depth indicates the bottom edge of rupture occurs at 14 km depth.

[2] X-distance is the horizontal distance from the surface "trace" of the fault.

[3] HW refers to hanging wall location in normal faulting, FW to footwall location in normal faulting, and SS to strike-slip faulting.

[4] R_{Rupt} is rupture distance, the closest distance from the site to the fault rupture surface; R_{JB} is the Joyner-Boore distance, the closest distance to the surface projection of the rupture surface; R_{Seis} is seismogenic distance, the closest distance to the assumed seismogenic part of the rupture surface, here used as the part of the rupture surface that lies at least 3 km below the ground surface.

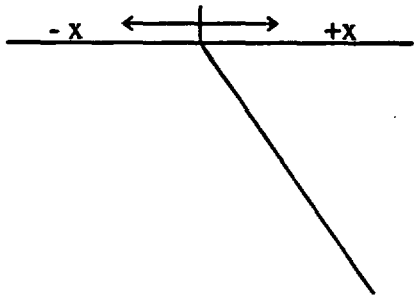

TABLE 5-6a
PROPONENT SOURCE CONVERSION FACTORS

Model #	Model
1	No correction for source
2	Spudich *et al.* (1996) extensional regime scale factors (d<20 km)[1]
3	Spudich *et al.* (1996) extensional regime scale factors (all distances)[1]
4	Campbell point source RVT (this study)[2]
5	Silva point source RVT (this study)[2]
6	Abrahamson and Silva (this study) normal faulting factors (horizontal comp)[3]
7	Abrahamson and Silva (this study) normal faulting factors (vertical comp)[3]
8	1/2 Abrahamson and Silva (this study) normal faulting factors (horizontal comp)[3]
9	1/2 Abrahamson and Silva (this study) normal faulting factors (vertical comp)[3]

[1] Based on the mean residuals of empirical attenuation relations
[2] Based on differences in $\Delta\sigma$ between California and Yucca Mountain (YM)
[3] Based on mean residuals for the Abrahamson and Silva (1997) empirical attenuation relation

TABLE 5-6b
PROPONENT CRUST/SITE CONVERSION FACTORS

Model #	Model
1	No correction for crust/site
2	Campbell point source RVT (this study): CA -> YM Repository outcrop[1]
3	Silva point source RVT (this study): CA -> YM Repository outcrop[1]
4	Silva point source RVT (this study): YM Surface-> YM Repository outcrop[2]
5	Silva finite fault (this study): YM Surface -> YM Repository outcrop[2]

[1] Based on differences in Q, kappa, and velocity profile from California to YM repository outcrop
[2] Based on differences in velocity profile and kappa from YM surface to YM repository outcrop

Note: Conversion factors are completely documented in Data Package Vol. 1.

TABLE 5-7a
PROPONENT VERTICAL/HORIZONTAL RATIO MODELS

Model #	Model
1	No correction
2	Campbell (1997) empirical attenuation
3	Silva (YM point source, this study)
4	Abrahamson & Silva (1997) empirical attenuation
5	Spudich *et al.* (1997) empirical attenuation
6	Sabetta & Pugliese (1996) empirical attenuation
7	Zeng and Anderson finite fault simulation (this study)
8	Somerville finite fault simulation (this study)

TABLE 5-7b
PROPONENT PEAK VELOCITY/SA(F) RATIO MODELS

Model #	Model
1	No correction
2	pgv/pga Campbell (1997) empirical attenuation
3	pgv/pga Silva (YM point source this study)
4	pgv/pga Joyner and Boore (1988) empirical attenuation
5	pgv/pga Sabetta & Pugliese (1996) empirical attenuation
6	pgv/pga Zeng and Anderson finite fault simulation (this study)
7	pgv/pga Somerville finite fault simulation (this study)
8	pgv/ pga Silva finite fault simulation (this study)
9	pgv/Sa(f=1 Hz) Campbell (1997) empirical attenuation
10	pgv/Sa(f=1 Hz) Silva (YM point source this study)
11	pgv/Sa(f=1 Hz) Joyner and Boore (1988) empirical attenuation
12	pgv/Sa(f=1 Hz) Sabetta & Pugliese (1996) empirical attenuation
13	pgv/Sa(f=1 Hz) Zeng and Anderson finite fault (this study)
14	pgv/Sa(f=1 Hz) Somerville finite fault simulation (this study)
15	pgv/Sa(f=1 Hz) Silva finite fault simulation (this study)

Note: Models are completely documented in Data Package Vol. 1.

TABLE 5-7c
PROPONENT HORIZONTAL COMPONENT-TO-COMPONENT VARIABILITY MODELS

Model #	Model
1	No correction
2	Boore *et al.* (1997) empirical attenuation
3	Spudich *et al.* (1996) empirical attenuation

TABLE 5-7d
PROPONENT 20 HZ SPECTRAL ACCELERATION INTERPOLATION MODELS

Model #	Model
1	No correction
2	Average coefficients for pga and 10 Hz
3	log-log interpolation between 33 Hz (pga) and 10 Hz
4	Boore scaling (this study)

Note: Models are completely documented in Data Package Vol. 1.

TABLE 5-8
PROPONENT MODELS USED BY EACH EXPERT

Model Class	Proponent Models In Class	Anderson	Boore	Campbell	McGarr	Silva	Somerville	Walck
Empirical	Abrahamson and Silva (1997)	Yes	Yes	Yes[1]	Yes	Yes	Yes	Yes
	Boore *et al.* (1997) (Vs model)	Yes	Yes	Yes[1]	Yes	Yes	No	Yes
	Campbell (1997) (Soft Rock)	Yes	Yes	Yes[1]	Yes	Yes	Yes	Yes
	Idriss (1997) (Rock, Stiff Soil)	Yes	Yes	Yes[1]	Yes	No	Yes	Yes
	Joyner and Boore (1988) (Rock)	No	Yes	Yes[1]	Yes	Yes	Yes	Yes
	McGarr (1984) (Rock)	No	Yes	No	Yes	No	No	Yes
	Sadigh *et al.* (1997) (Rock)	Yes	Yes	Yes[1]	Yes	Yes	Yes	Yes
	Sabetta and Pugliese (1996) (Rock)	Yes	No	No	No	No	No	Yes
	Spudich *et al.* (1996) (Rock)	Yes	Yes	Yes[1]	Yes	No	Yes	Yes
Hybrid Empirical	Campbell (This Study)	No	No	Yes	No	No	No	No
Finite Fault Simulation	Silva Case A (This Study)	Yes	Yes	Yes	Yes	Yes	Yes	Yes
	Silva Case B (This Study)	No	No	No	No	No	No	No
	Somerville (This Study)	Yes	Yes	Yes	Yes	Yes	Yes	Yes
	Zeng and Anderson Case A (This Study)	Yes	Yes	Yes	Yes	Yes	Yes	Yes
	Zeng and Anderson Case B (This Study)	Yes	No	No	No	No	No	No
	Zeng and Anderson Case C (This Study)	Yes	No	No	No	No	No	No
Point Source RVT	Silva (This Study)	Yes	Yes	Yes	Yes	Yes	Yes	Yes
Blast	Bennett Model 2 (1995 Scenario Study)	No	No	No	No	No	Yes	Yes

[1]These empirical models are incorporated in the Hybrid Empirical model.

TABLE 5-9a
SOURCE CONVERSION FACTORS USED BY EACH EXPERT

Conversion Factor	Anderson	Boore	Campbell	McGarr	Silva	Somerville	Walck
Spudich (d < 20 km)	No	No	No	No	No	No	No
Spudich (all distances)	No	No	No	No	No	No	No
Campbell (point source RVT)	No	No	Yes	No	No	No	Yes
Silva (point source RVT)	No	Yes	No	Yes	No	No	Yes
Abrahamson & Silva (horizontal)	No	No	No	No	No	Yes	No
Abrahamson & Silva (vertical)	No	No	No	No	No	No	No
1/2 Abrahamson & Silva (horizontal)	No	No	No	No	Yes	No	No
1/2 Abrahamson & Silva (vertical)	No	No	No	No	Yes	No	No

TABLE 5-9b
CRUST/SITE CONVERSION FACTORS USED BY EACH EXPERT

Conversion Factor	Anderson	Boore	Campbell	McGarr	Silva	Somerville	Walck
Campbell (point source) CA -> YM outcrop	Yes	Yes	Yes	Yes	Yes	Yes	Yes
Silva (point source) CA -> YM outcrop	Yes	No	No	No	No	No	No
Silva (point source) YM surface -> YM outcrop	Yes	No	No	No	No	No	No
Silva (finite fault) YM surface -> YM outcrop	Yes	No	No	No	No	No	No

TABLE 5-9c
VERTICAL/HORIZONTAL RATIO MODELS USED BY EACH EXPERT

RATIO MODEL	ANDERSON	BOORE	CAMPBELL	MCGARR	SILVA	SOMERVILLE	WALCK
Campbell (1997) empirical	No	No	No	No	No	No	Yes
Silva (YM point source)	No	No	Yes	Yes	Yes	No	Yes
Abrahamson and Silva (1997) empirical	No	No	No	No	No	No	No
Spudich *et al.* (1997) empirical	No	No	No	No	No	No	No
Sabetta and Pugliese (1996) empirical	No	No	No	No	No	No	No
Zeng and Anderson finite fault	No	No	No	No	No	No	No
Somerville finite fault	No	No	No	No	No	No	No

TABLE 5-9d
PEAK VELOCITY/SA(F) RATIO MODELS USED BY EACH EXPERT

RATIO MODEL	ANDERSON	BOORE	CAMPBELL	MCGARR	SILVA	SOMERVILLE	WALCK
pgv/pga Campbell (1997) empirical	No	No	No	No	No	No	No
pgv/pga Silva (YM point source)	No	No	No	No	Yes	No	No
pgv/pga Joyner and Boore (1988) empirical	No	No	No	No	No	No	No
pgv/pga Sabetta and Pugliese (1996) empirical	No	No	No	No	No	No	No
pgv/pga Zeng and Anderson finite fault	No	No	No	No	No	No	No
pgv/pga Somerville finite fault	No	No	No	No	No	No	No
pgv/pga Silva finite fault	No	No	No	No	No	No	No
pgv/Sa (f=1Hz) Campbell (1997) empirical	No	No	No	No	No	No	No
pgv/Sa (f=1Hz) Silva (YM point source)	No	Yes	No	No	No	No	No
pgv/Sa (f=1Hz) Joyner and Boore (1988) empirical	No	No	No	No	No	No	No
pgv/Sa (f=1Hz) Sabetta and Pugliese (1996) empirical	No	No	No	No	No	No	No
pgv/Sa (f=1Hz) Zeng and Anderson finite fault	No	No	No	No	No	No	No
pgv/Sa (f=1Hz) Somerville finite fault	No	No	No	No	No	No	No
pgv/Sa (f=1Hz) Silva finite fault	No	No	No	No	No	No	No

TABLE 5-9e
HORIZONTAL COMPONENT-TO-COMPONENT VARIABILITY MODELS USED BY EACH EXPERT

VARIABILITY MODEL	ANDERSON	BOORE	CAMPBELL	MCGARR	SILVA	SOMERVILLE	WALCK
Boore *et al.* (1997) empirical	Yes	Yes	Yes	Yes	Yes	Yes	Yes
Spudich *et al.* (1996) empirical	No	No	No	No	No	No	No

TABLE 5-9f
20 HZ SPECTRAL ACCELERATION INTERPOLATION MODELS USED BY EACH EXPERT

INTERPOLATION MODEL	ANDERSON	BOORE	CAMPBELL	MCGARR	SILVA	SOMERVILLE	WALCK
Average coefficients for pga and 10 Hz	Yes	No	No	Yes	No	No	No
log-log interpolation between 33 Hz (pga) and 10 Hz	No	No	Yes	No	No	No	Yes
Boore scaling (Appendix F)	No	Yes	No	No	Yes	No	Yes

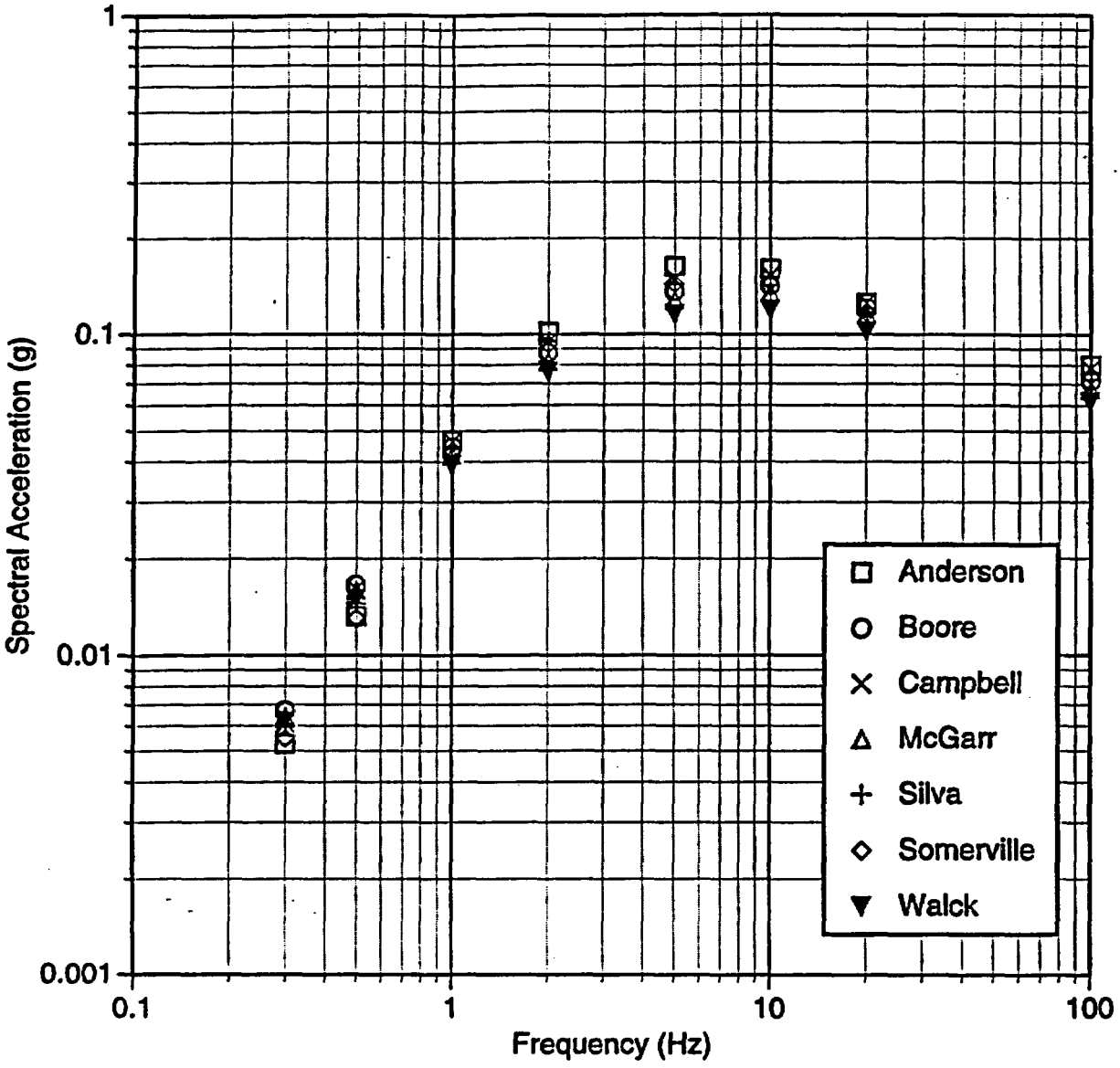

Figure 5-1 Median horizontal ground motion estimates for a M_W 5.8 earthquake at 17 km (rupture distance), normal faulting, hanging wall (Case 6)

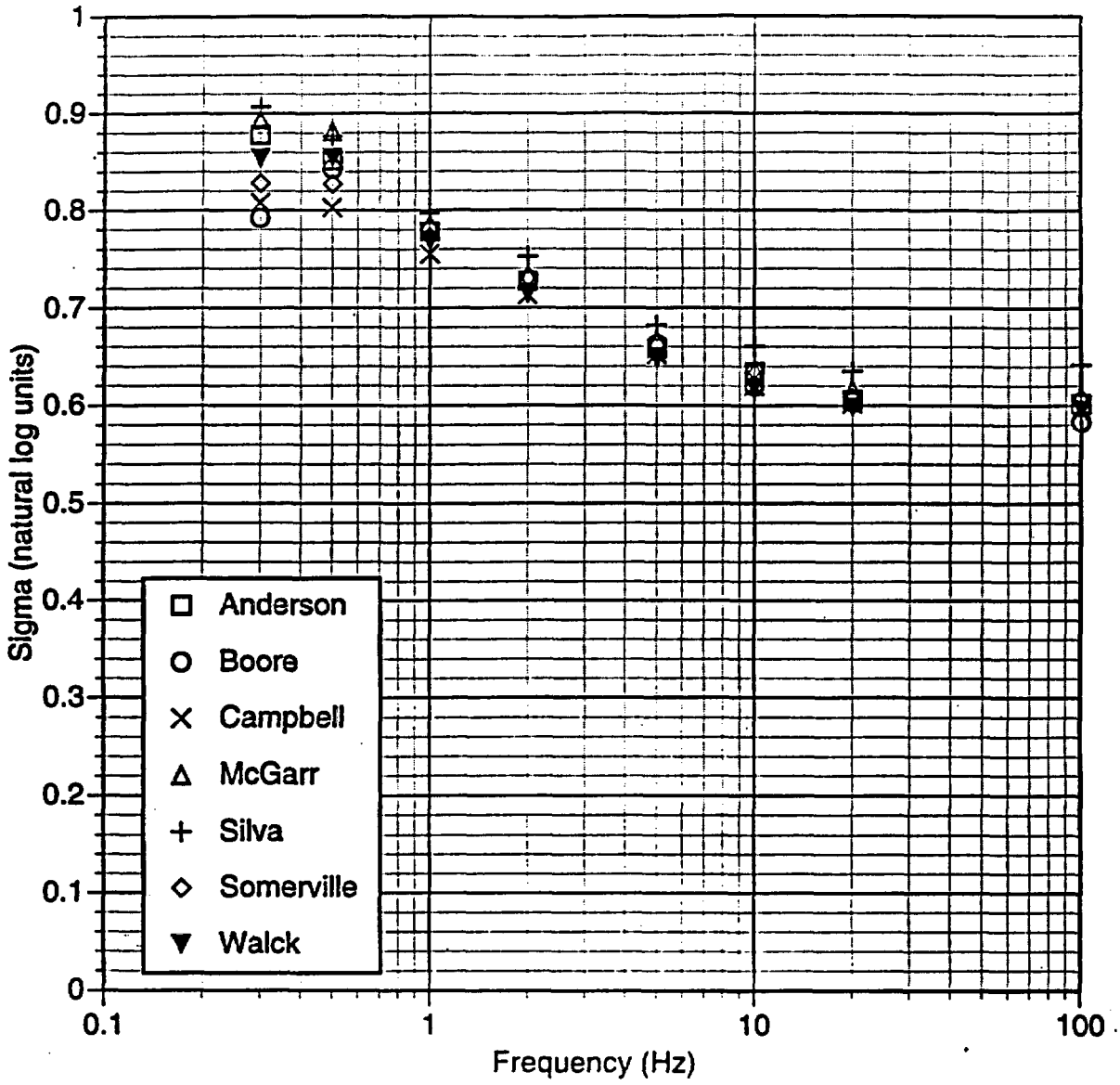

Figure 5-2 Aleatory variability in horizontal ground motion estimates for a Mw 5.8 earthquake at 17 km (rupture distance), normal faulting, hanging wall (Case 6)

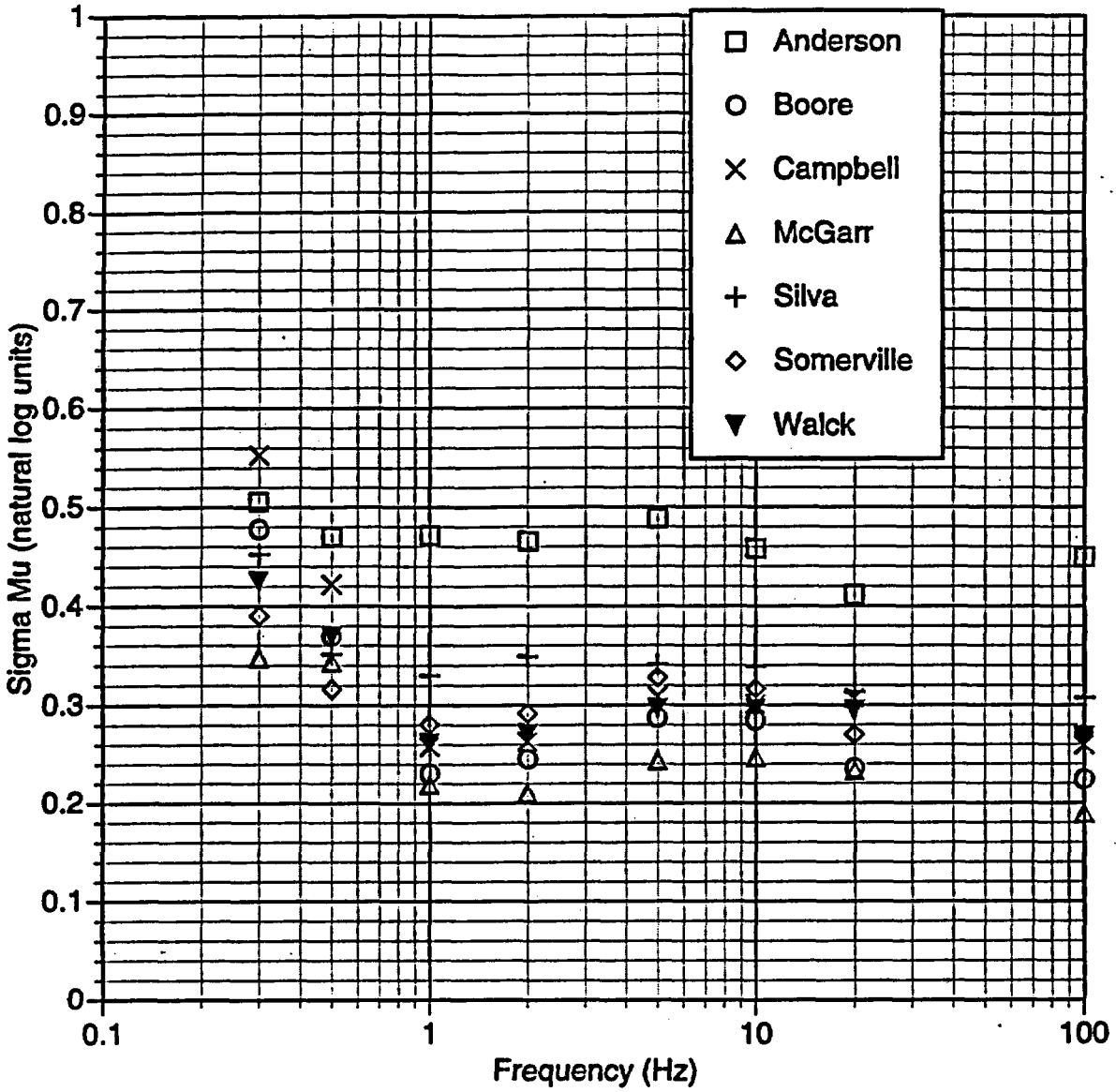

Figure 5-3 Epistemic uncertainty on the median horizontal ground motion estimates for a Mw 5.8 earthquake at 17 km (rupture distance), normal faulting, hanging wall (Case 6)

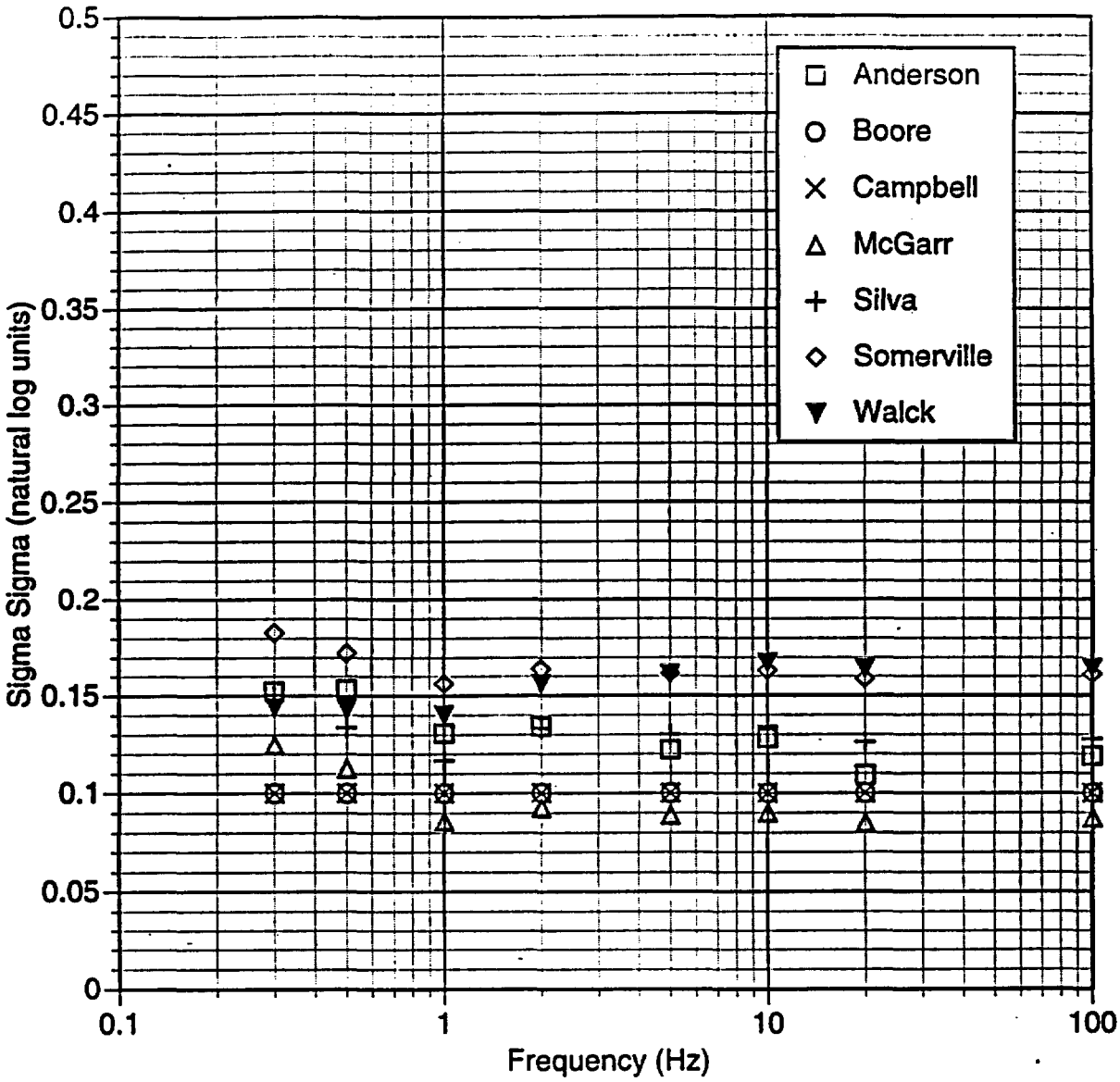

Figure 5-4 Epistemic uncertainty on the aleatory variability of horizontal ground motion estimates for a M_W 5.8 earthquake at 17 km (rupture distance), normal faulting, hanging wall (Case 6)

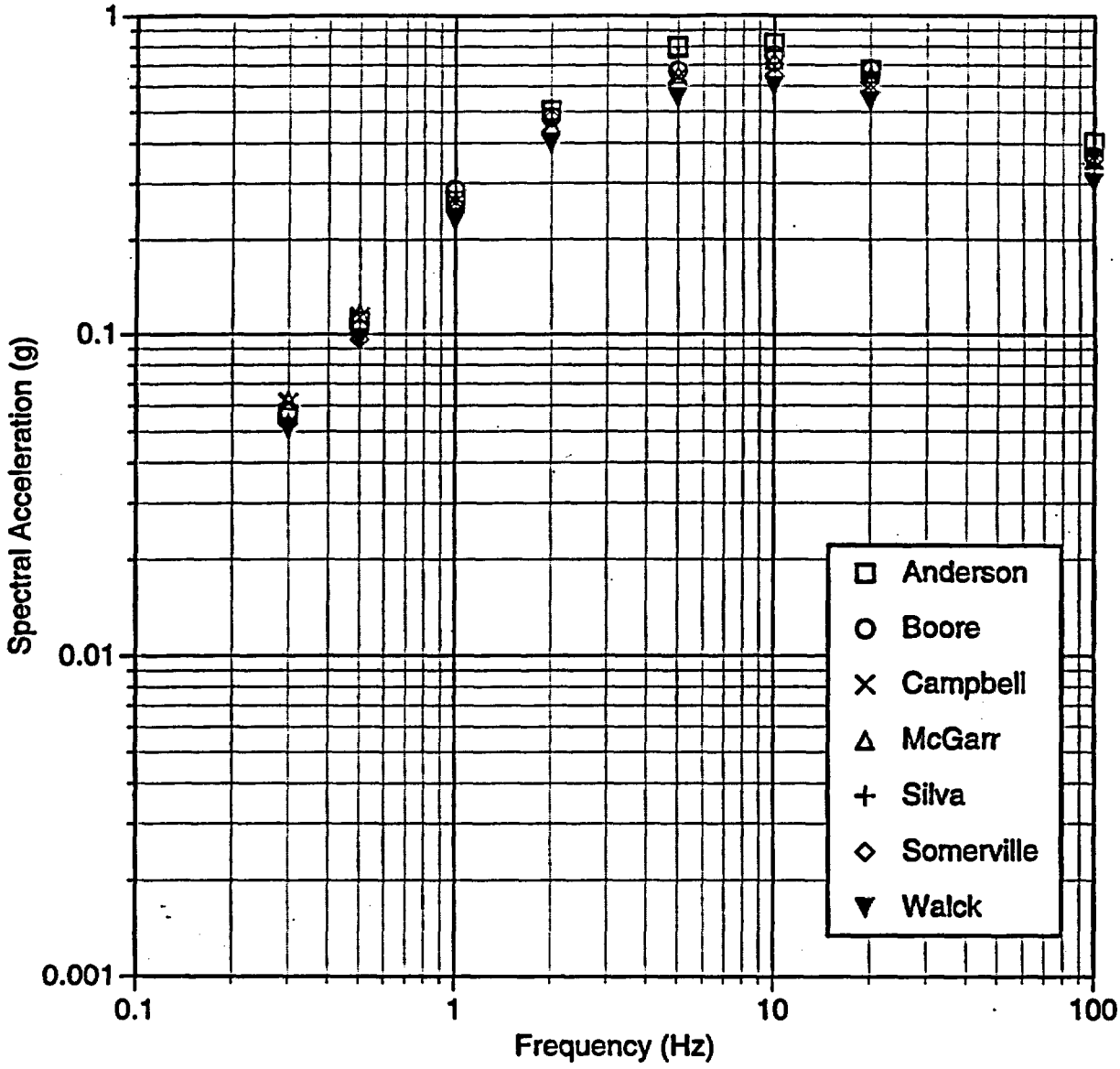

Figure 5-5 Median horizontal ground motion estimates for a Mw 6.5 earthquake at 4 km (rupture distance), normal faulting, hanging wall (Case 10)

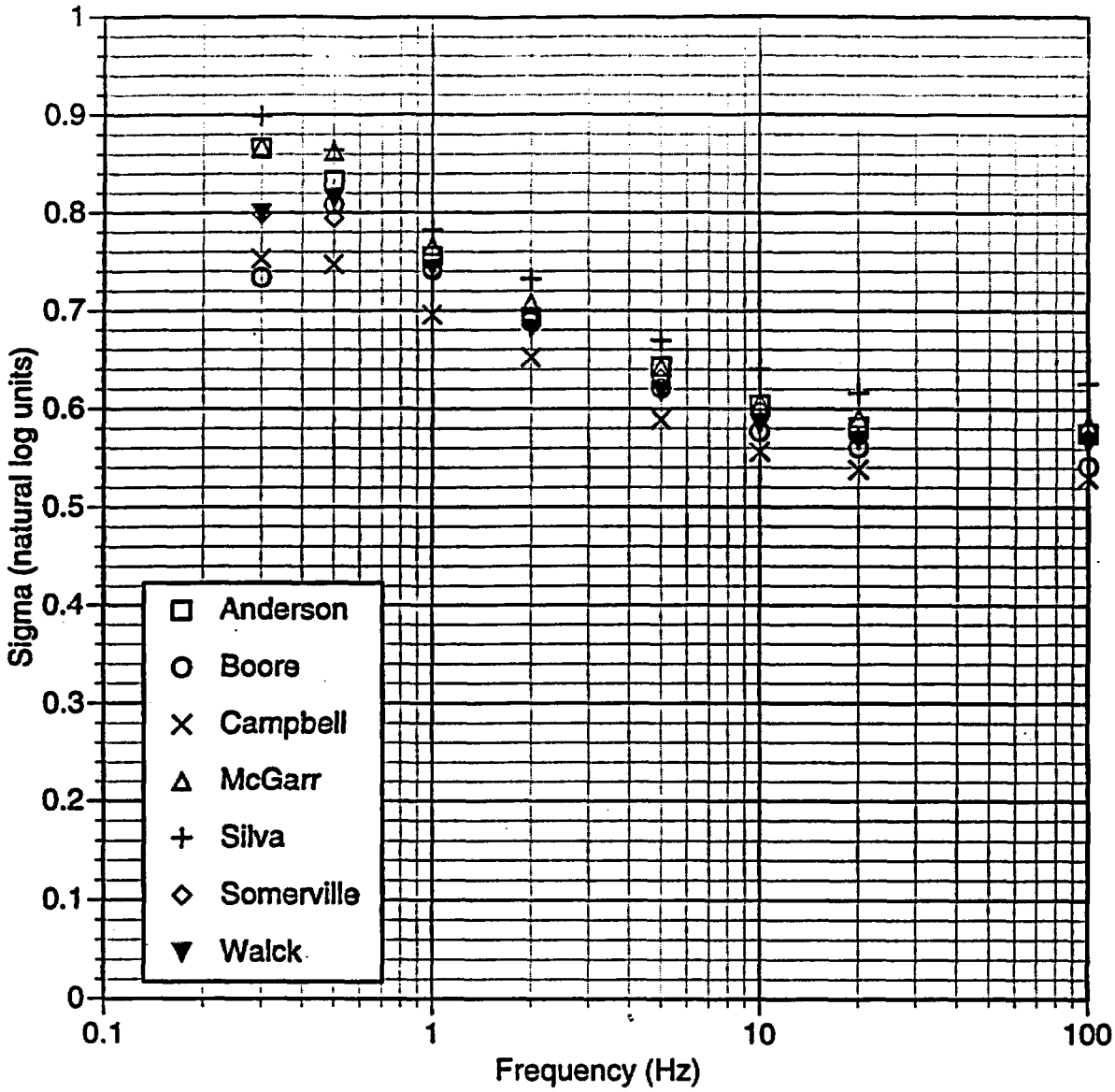

Figure 5-6 Aleatory variability in horizontal ground motion estimates for a M_W 6.5 earthquake at 4 km (rupture distance), normal faulting, hanging wall (Case 10)

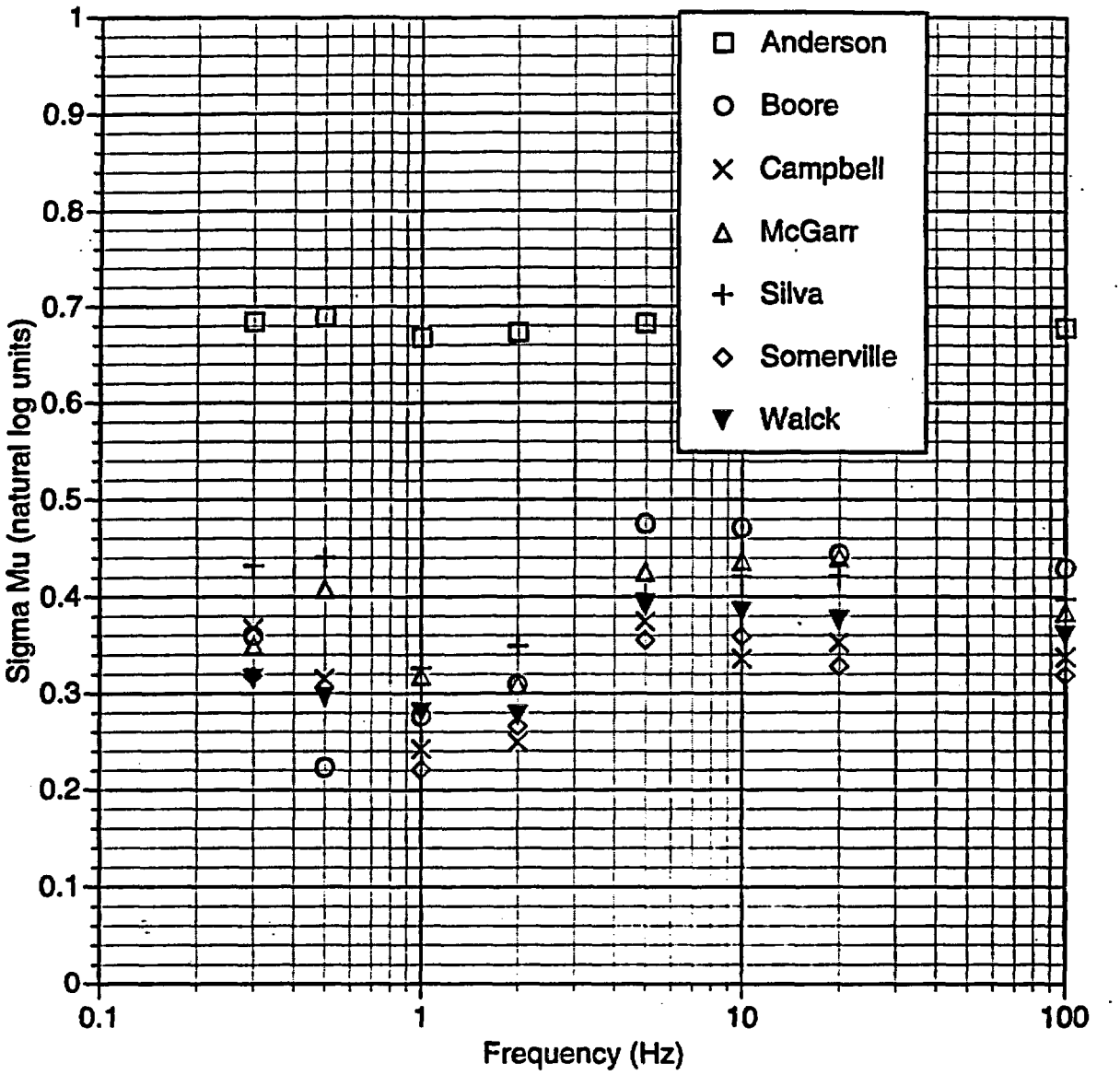

Figure 5-7 Epistemic uncertainty on the median horizontal ground motion estimates for a Mw 6.5 earthquake at 4 km (rupture distance), normal faulting, hanging wall (Case 10)

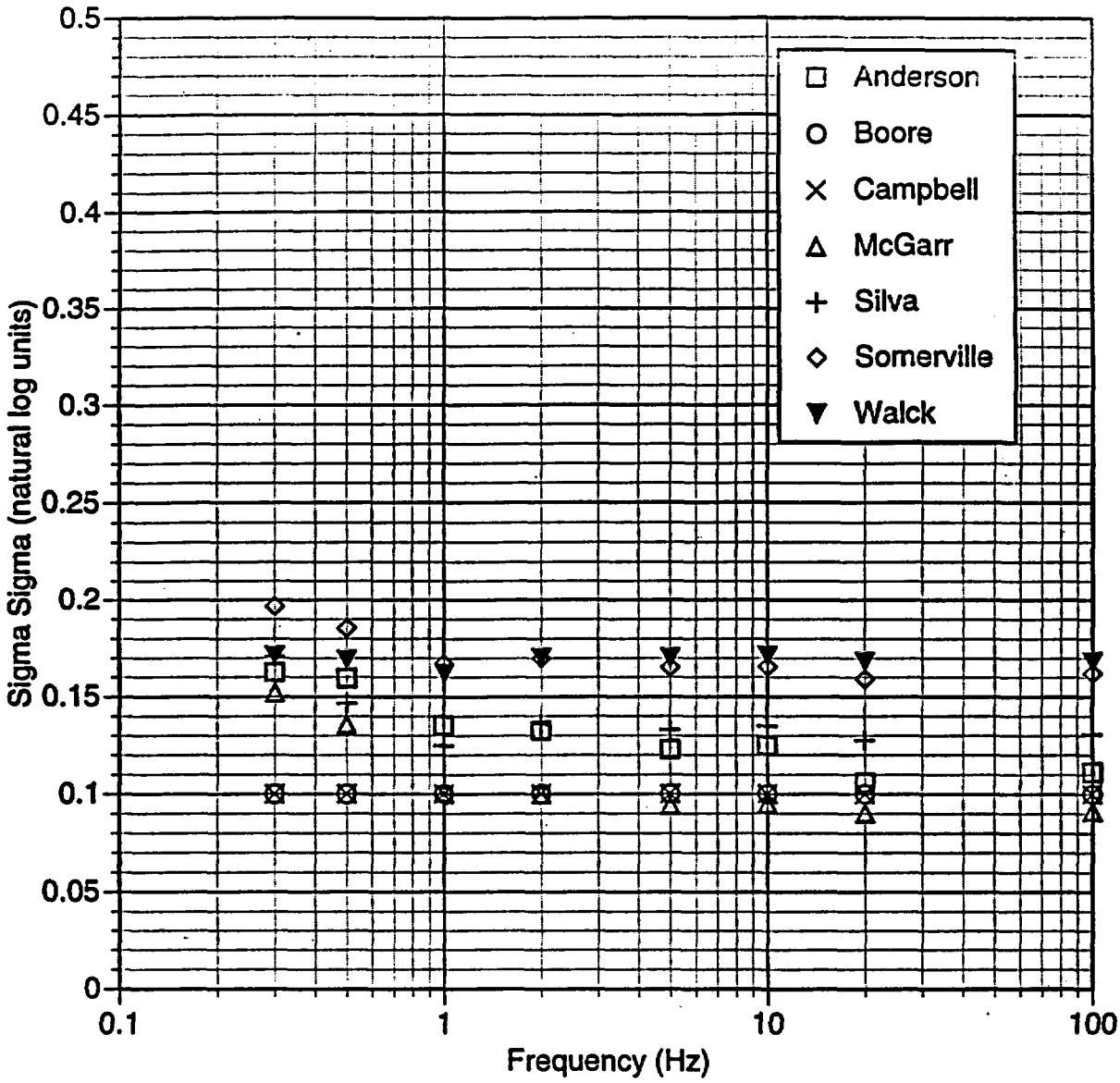

Figure 5-8 Epistemic uncertainty on the aleatory variability of horizontal ground motion estimates for a Mw 6.5 earthquake at 4 km (rupture distance), normal faulting, hanging wall (Case 10)

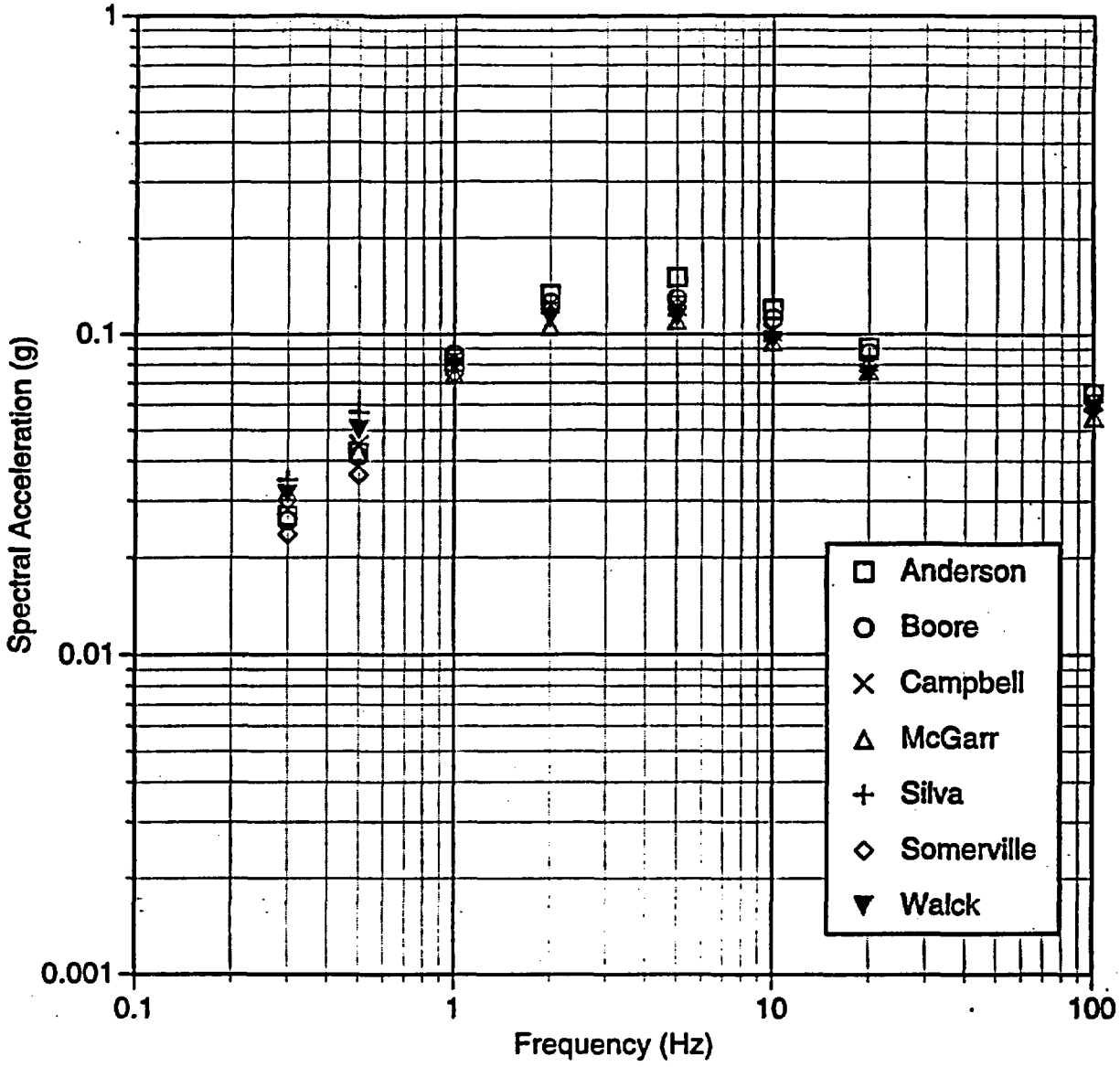

Figure 5-9 Median horizontal ground motion estimates for a Mw 7.5 earthquake at 50 km (rupture distance) strike-slip faulting (Case 15)

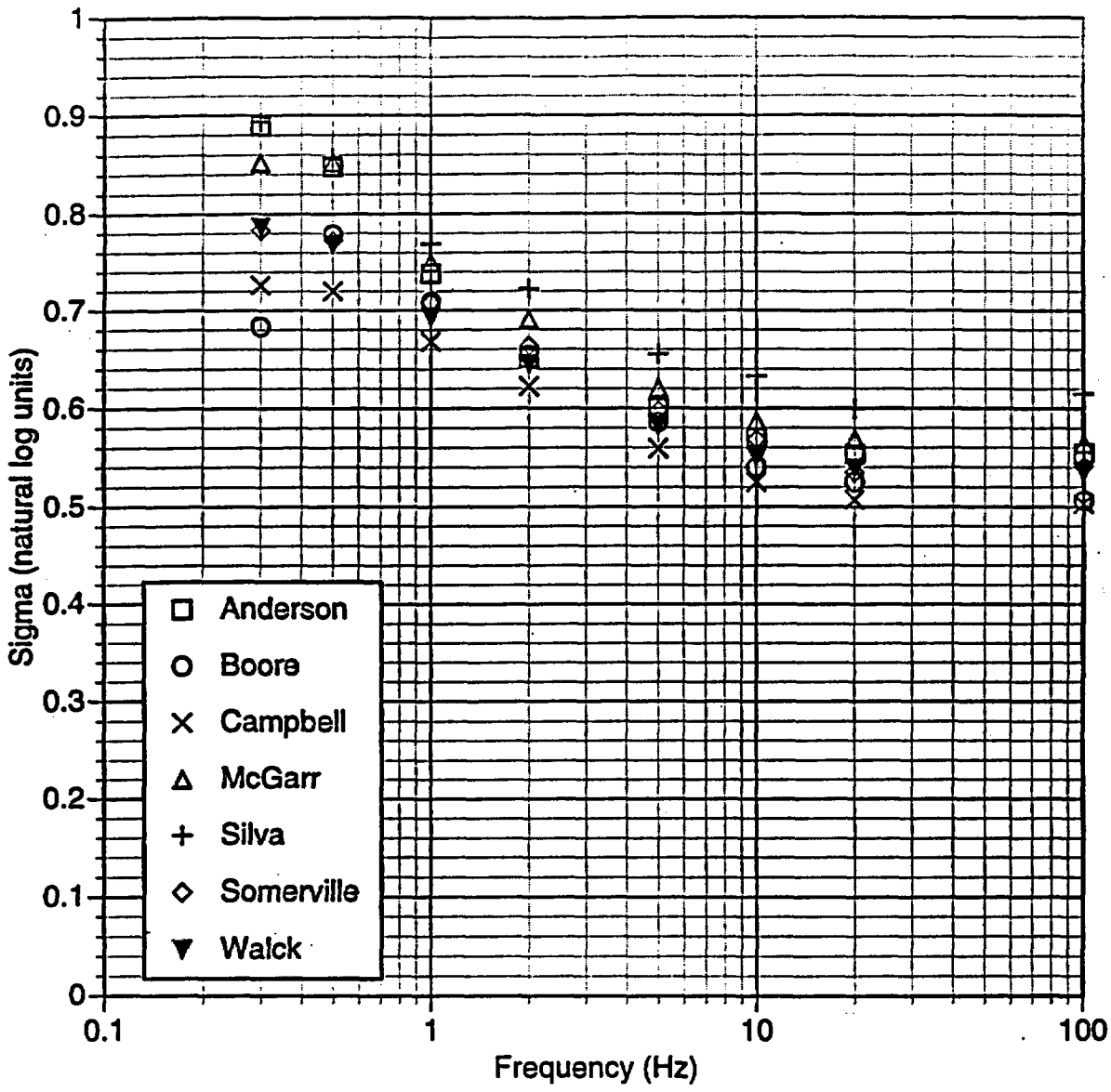

Figure 5-10 Aleatory variability in horizontal ground motion estimates for a Mw 7.5 earthquake at 50 km (rupture distance), strike-slip faulting (Case 15)

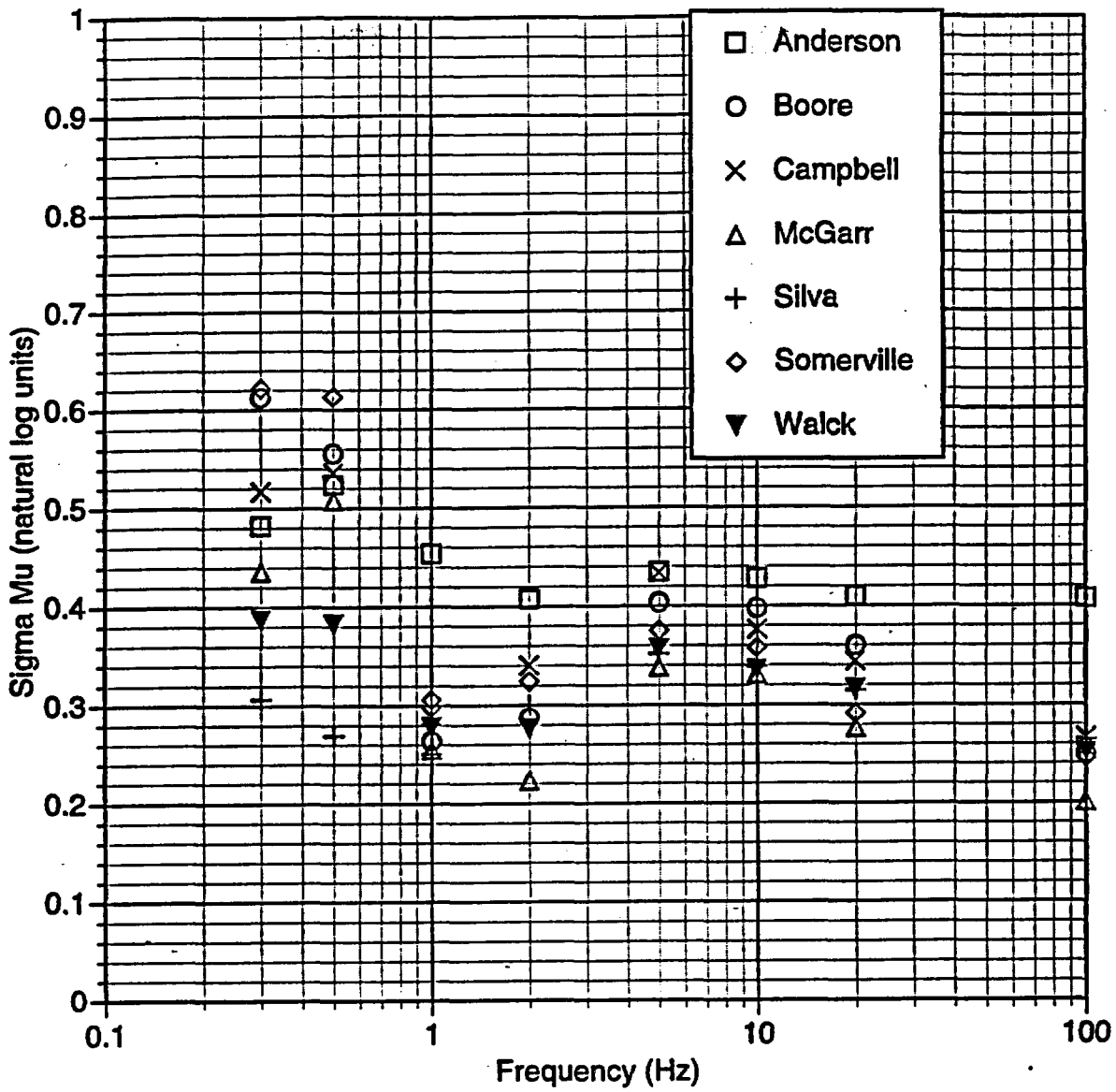

Figure 5-11 Epistemic uncertainty on the median horizontal ground motion estimates for a Mw 7.5 earthquake at 50 km (rupture distance), strike-slip faulting (Case 15)

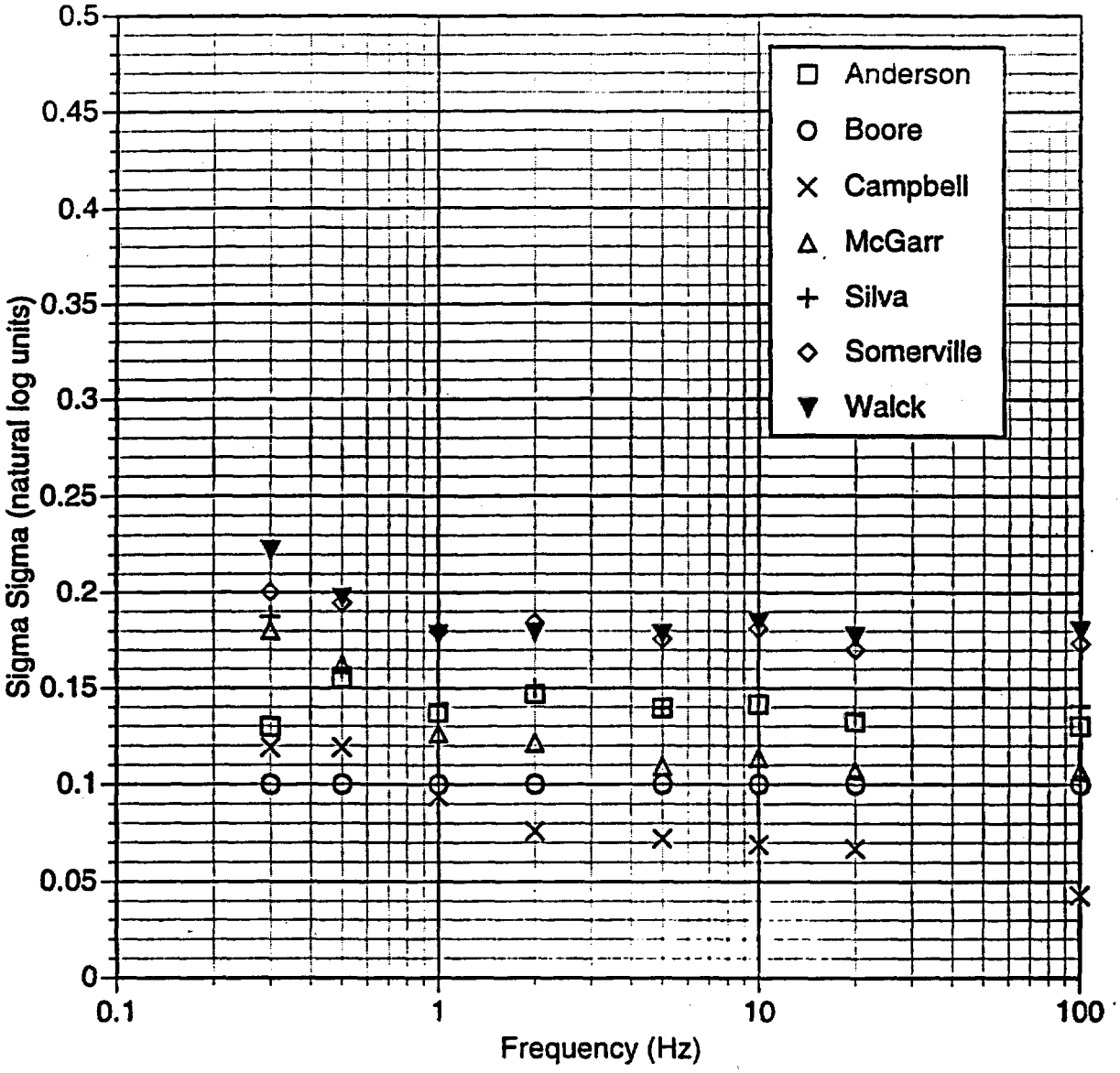

Figure 5-12 Epistemic uncertainty on the aleatory variability of horizontal ground motion estimates for a Mw 7.5 earthquake at 50 km (rupture distance), strike-slip faulting (Case 15)

6.0
GROUND MOTION ATTENUATION RELATIONS

To facilitate the use of the ground motion models in the hazard calculation, the experts' point estimates were parameterized by attenuation relations. The regression analysis to develop the attenuation relations was performed by the GM Facilitation Team. Each expert selected the distance measure used in the regression analyses for his/her point estimates. They chose whether the footwall and hanging wall point estimates were regressed together, resulting in a single normal faulting attenuation equation, or separately, yielding separate models for sites on the hanging wall and footwall. In addition, the experts could constrain the degree of magnitude saturation at close distances.

The experts reviewed the resulting regression models and either approved the models or made revisions to their point estimates or to the functional form used in the regression. This process was repeated until each expert was satisfied with the resulting models and is documented in Data Package Vols. 3 through 12. The final regression results are presented in this chapter.

6.1 REGRESSION MODEL FORM

Based on an examination of the experts' point estimates and with feedback from the experts, general functional forms were selected. Different functional forms were used for the median estimates, the aleatory variability, and the epistemic uncertainties.

The independent variables used in all regressions correspond to:

- M_w Moment magnitude
- R Distance (experts' selected distance measure in km)
- F Mechanism flag (0=strike-slip, 1 = normal)
- W_H Hanging wall flag (1=hanging wall, 0 = not hanging wall)
- W_F Footwall flag (1=footwall, 0=not footwall)

The predicted values for μ are in natural logarithm of g for spectral acceleration and natural logarithm of cm/sec for peak velocity. The σ_{al}, σ_{μ}, and σ_{σ} are all in natural log units. All of

the experts except for Campbell selected "rupture distance," defined as the closest distance from the site to the fault rupture as the distance metric. Campbell selected "seismogenic distance," the closest distance from the site to the assumed seismogenic part of the rupture (herein used as the part of the rupture that is at a depth of least 3 km)

The adopted general forms for the regression model are given below. As noted above, in some instances the experts added constraints to these general forms. These constraints are summarized in Table 6-1.

Median (μ):

For $M < m_1$,

$$\mu = a_1 + a_2(M - m_1) + a_6(8.5 - M)^2 + \left[a_3 + a_5(M - m_1)\right] \cdot \ln\sqrt{R^2 + a_8^2} + a_7 F + a_9 W_H f_1(M,R) + a_{10} W_F f_1(M,R) \quad \text{(6-1a)}$$

For $M \geq m_1$,

$$\mu = a_1 + a_4(M - m_1) + a_6(8.5 - M)^2 + \left[a_3 + a_5(M - m_1)\right] \cdot \ln\sqrt{R^2 + a_8^2} + a_7 F + a_9 W_H f_1(M,R) + a_{10} W_F f_1(M,R) \quad \text{(6-1b)}$$

in which

$$f_1(M,R) = \begin{cases} 0 & \text{for } R \leq x_1 \\ \dfrac{R - x_1}{x_2 - x_1} & x_1 < R < x_2 \\ 1 & x_2 \leq R \leq x_3 \\ \dfrac{x_4 - R}{x_4 - x_3} & x_3 < R < x_4 \\ 0 & \text{for } R \geq x_4 \end{cases} \cdot \begin{cases} 0 & \text{for } M < a_{11} \\ \dfrac{M - a_{11}}{a_{12} - a_{11}} & \text{for } a_{11} \leq M \leq a_{12} \\ 1 & \text{for } M > a_{12} \end{cases} \quad \text{(6-2)}$$

Aleatory Variability (σ_{al}):

For $M < b_4$,

$$\sigma_{al} = b_1 + b_2(M - b_4) \quad \text{(6-3a)}$$

For $M \geq b_4$,

$$\sigma_{al} = b_1 \tag{6-3b}$$

Epistemic Uncertainty in the Median (σ_μ):

$$\sigma_\mu = c_1 + c_2(M - c_6) + c_3 \ln(R+1) + c_4[\ln(R+1)]^2 + c_5 F \tag{6-4}$$

Epistemic Uncertainty in the Aleatory Variability (σ_σ):

For $M < d_4$, $$\sigma_\sigma = d_1 + d_2(M - d_4) \tag{6-5a}$$

For $M \geq d_4$, $$\sigma_\sigma = d_1 \tag{6-5b}$$

6.2 REGRESSION RESULTS

The following values are used for all models and for all periods:

$x_1 = 3$
$x_2 = 8$
$x_3 = 20$
$x_4 = 30$
$m_1 = 6.25$

Coefficients a_i, b_i, c_i, and d_i are listed in Appendix I. The process of fitting the experts' point estimates with a smooth equation leads to additional aleatory variability due to the misfit between the equation and the point estimates. To account for this additional variability, the total aleatory variability is given by the combination of the experts' estimate of the aleatory variability (parameterized by the regression equation as σ_{al}) and the standard deviation of the fit to the median ground motion (listed as Sigma Fit in the Appendix I tables). The total aleatory variability is given by

$$\sigma_{total} = \sqrt{\sigma_{fit}^2 + \sigma_{al}^2} \tag{6-6}$$

Comparisons of the regression model fits and the experts' point estimates are contained in Data Package Vols. 11A through 11G. Examples of the resulting attenuation relations for the

seven experts are compared for peak ground acceleration and for 1 Hz spectral acceleration for two faulting cases: a M_w 6.5 normal earthquake on the hanging wall and a M_w 7.5 strike-slip earthquake. The models for the horizontal component median ground motions are compared on Figures 6-1 through 6-4. These figures show that the range in the median ground motions from these models is generally less than a factor of 1.5. The models for the horizontal component aleatory variability are compared on Figures 6-5 and 6-6 for peak acceleration and spectral acceleration at a period of 1.0 sec. The range in the aleatory variability in the models is generally less than 0.1 natural log unit. The epistemic variability in the median horizontal ground motion is compared on Figures 6-7 to 6-10. The range of the models is generally less than 0.1 natural log units except for Anderson's model, which has much larger values due to his larger estimates of the epistemic uncertainty for the proponent model median estimates. Finally, the epistemic uncertainty in the aleatory variability is shown on Figures 6-11 to 6-12. The range of these models is generally less than 0.1 natural log unit.

A corresponding set of plots of the models for the vertical component are shown on Figures 613 through 6-24. The vertical median ground motion models tend to be more variable between experts than the horizontal models. This larger variability is due to having fewer vertical proponent models available and much less validation for the numerical simulations. The experts individual estimates of the epistemic uncertainty also tend to be larger for the vertical component than for the horizontal component.

6.3 HYPOCENTRAL-BASED MODELS

The seismic source characterization also includes areal source zones, which are treated as point sources in the hazard calculation. Since the GM expert point estimates and the attenuation relations were developed for closest distance, a conversion factor is needed to make the model applicable to hypocentral distance, which is the relevant distance for areal sources.

The use of hypocentral distance rather than closest distance affects both the median ground motion and the aleatory variability since for a given hypocentral distance, there is a range of possible closest distances. Rather than developing independent attenuation models based on

hypocentral distance, the GM Facilitation Team evaluated the relation between hypocentral distance and rupture distance based on an assumed distribution of hypocenters on the fault plane. Note that this distribution is not the same as the distribution of hypocenters with depth in an earthquake catalog, but rather the distribution of the hypocenters on the rupture plane for a specific rupture dimension. With this relation between hypocentral distance and rupture distance, the uncertainty of the ground motion due to uncertainty in the closest-distance can be directly propagated using standard methods for propagation of errors (see Appendix J).

The adjustments using hypocentral distance are presented as a mapping of the mean rupture distance (as a function of the hypocentral distance and magnitude) and additional aleatory variability. The additional epistemic uncertainty in the median ground motion and aleatory variability due to the uncertainty in the distribution of hypocenters on the rupture plane are also estimated, but they are negligible. The development of these correction factors is given in Appendix J. Here, just the final models are presented.

For a given hypocentral distance H (in km) and magnitude M, the mean rupture distance R (in km) is given by

$$R = \begin{cases} H(1 + e_1 + e_2(M-5)) + H^2(e_3 + e_4(M-5)) & \text{for } H \le 30 \text{ km} \\ H + 30(e_1 + e_2(M-5)) + 900(e_3 + e_4(M-5)) & \text{for } H > 30 \text{ km} \end{cases} \quad (6\text{-}7)$$

in which the estimated coefficients are listed in Table 6-2.

The aleatory variability of the rupture distance as a function of the hypocentral distance and M is given by:

$$\sigma_R(H,M) = \sqrt{\left[(e_5 + e_6(M-5))\tanh\left\{H(e_7 + e_8(M-5))\right\}\right]^2 + 1.2^2} \quad (6\text{-}8)$$

with the coefficients listed in Table 6-2.

The additional aleatory variability in ground motion due to the use of hypocentral distance is given by

$$\sigma_{Hypo} = \left|\frac{\partial Y}{\partial R}\right| \sigma_R(H,M) \quad (6\text{-}9)$$

in which Y is the natural log of the ground motion parameter of interest. Ignoring hanging wall and footwall effects, then

$$\frac{\partial Y}{\partial R} = \left(a_3 + a_5(M - 6.25)\right)\frac{R(H,M)}{R^2(H,M) + a_8^2} \tag{6-10}$$

in which a_3, a_5, and a_8 are coefficients in the regression equations for each expert (Appendix I tables). This additional aleatory variability is combined with the total aleatory variability for the experts' models (Equation 6-6) to give the total aleatory variability of ground motion for the hypocentral model:

$$\sigma_{total}^{hypo} = \sqrt{\sigma_{hypo}^2 + \sigma_{total}^2} \tag{6-11}$$

The additional epistemic uncertainties in ground motion for a hypocentral distance model are computed in Appendix J. They are small enough to be neglected.

6.4 SPECIAL CASES

The experts developed scaling rules to apply their ground motion models to the two special cases discussed in Chapter 5.0: rupture of multiple (parallel) faults, and a shallow detachment fault.

6.4.1 Multiple Rupture Case

In the hazard calculation, the multiple rupture case is simplified and approximated by summing the moment of all of the ruptures and using the closest distance of any of the ruptures to the site. The resulting ground motion estimates must be adjusted, however, because using the total moment at the closest distance is not conservative compared to the case of multiple faults rupturing near the site. Multiple ruptures with small magnitude events can produce constructive interference that will result in larger ground motion than would be predicted for a single larger-magnitude event. Therefore, the GM Facilitation Team developed scale factors for the calculated ground motions, based on rules given by each of the experts.

Most of the experts used the concept of random vibration theory to predict the effect of multiple ruptures on ground motion. The main issue is whether the ground motions from the

multiple ruptures are correlated or are independent. In general, the experts considered the ground motions to be independent.

The scale factors for multiple ruptures are the ratios of ground motion as predicted by the experts' rules to the ground motion predicted from the experts' attenuation relations, using the full moment at the closest distance. Each expert's rules for developing the multiple rupture scale factors are given in the experts' documentation in Appendix F.

The scale factors are presented for cases of 2, 3, 4, and 5 faults rupturing simultaneously. The faults are assumed to be separated by 2 to 3 km (between any two faults). The ground motion was evaluated for several locations within 5 km of any of the faults. The average adjustment factors for the median, the aleatory uncertainty, and epistemic uncertainties are listed in Tables 6-3 to 6-9. The experts provided their adjustment factors for the uncertainties in either of two ways: as a scale factor or as an addition (in a square root of the sum of the squares method) to the total.

6.4.2 Detachment Fault Case

The second special case is a low-angle detachment fault with a dip of about 30 degrees. At Workshop #2, this case was presented as a combination of a low-angle detachment and multiple parallel faults that splayed off from the detachment fault. Six of the seven experts addressed the low-angle detachment separately from the multiple parallel faults; Somerville addressed the combined case. The adjustment factors for this case are listed in Tables 6-10 and 6-11. These factors should be applied to the computed ground motions based on the experts' attenuation relations.

TABLE 6-1
CONSTRAINTS ON THE REGRESSION

EXPERT	MEDIAN: INCREASE SATURATION AT SHORT DISTANCES?	MEDIAN: INCLUDE FOOTWALL AND HANGING WALL DIFFERENCES?	σ_μ: MAGNITUDE DEPENDENCE?	σ_μ: DISTANCE DEPENDENCE?
Anderson	Yes	Yes	No	Yes
Boore	No	Yes	Yes	Yes
Campbell	Yes	No	No	Yes
McGarr	Yes	No	No	Yes
Silva	Yes	Yes	No	No
Somerville	No	Yes	Yes	Yes
Walck	Yes	Yes	No	Yes

TABLE 6-2
REGRESSION MODEL COEFFICIENTS FOR THE HYPOCENTRAL-BASED MODELS

COEFFICIENT	ESTIMATE
e_1	-0.207
e_2	-0.323
e_3	0.0058
e_4	0.0059
e_5	1.894
e_6	3.854
e_7	0.0116
e_8	0.0094
e_9	-0.177
e_{10}	0.0055
e_{11}	0.0111

TABLE 6-3
J. G. ANDERSON: MULTIPLE RUPTURE SCENARIO
FACTORS APPLIED TO MEDIAN ESTIMATES

COMPONENT	FREQUENCY (HZ)	MEDIAN 2 FAULTS	MEDIAN 3 FAULTS	MEDIAN 4 FAULTS	MEDIAN 5 FAULTS	FACTOR SIGMA	FACTOR SIGMA-MU	ADDITIONAL SIGMA (SRSS)	ADDITIONAL SIGMA-MU (SRSS)
Horizontal	PGA	1.20	1.31	1.40	1.47	1.0	1.0	-	-
	20.	1.21	1.33	1.42	1.50	1.0	1.0	-	-
	10.	1.20	1.31	1.41	1.48	1.0	1.0	-	-
	5.	1.19	1.30	1.39	1.45	1.0	1.0	-	-
	2.	1.16	1.24	1.31	1.36	1.0	1.0	-	-
	1.	1.13	1.21	1.27	1.32	1.0	1.0	-	-
	0.5	1.09	1.13	1.17	1.21	1.0	1.0	-	-
	0.3	1.05	1.05	1.07	1.08	1.0	1.0	-	-
	PGV	1.13	1.20	1.25	1.29	1.0	1.0	-	-
Vertical	PGA	1.11	1.17	1.21	1.24	1.0	1.0	-	-
	20.	1.11	1.17	1.21	1.24	1.0	1.0	-	-
	10.	1.17	1.27	1.35	1.41	1.0	1.0	-	-
	5.	1.18	1.30	1.39	1.45	1.0	1.0	-	-
	2.	1.14	1.22	1.29	1.35	1.0	1.0	-	-
	1.	1.12	1.18	1.24	1.29	1.0	1.0	-	-
	0.5	1.04	1.04	1.06	1.07	1.0	1.0	-	-
	0.3	1.00	0.98	0.98	0.98	1.0	1.0	-	-
	PGV	1.11	1.16	1.20	1.24	1.0	1.0	-	-

TABLE 6-4
D. M. BOORE: MULTIPLE RUPTURE SCENARIO
FACTORS APPLIED TO MEDIAN ESTIMATES

COMPONENT	FREQUENCY (HZ)	MEDIAN 2 FAULTS	MEDIAN 3 FAULTS	MEDIAN 4 FAULTS	MEDIAN 5 FAULTS	FACTOR SIGMA	FACTOR SIGMA-MU	ADDITIONAL SIGMA (SRSS)	ADDITIONAL SIGMA-MU (SRSS)
Horizontal	PGA	1.25	1.38	1.48	1.55	1.0	1.0	-	-
	20.	1.26	1.38	1.48	1.55	1.0	1.0	-	-
	10.	1.25	1.37	1.47	1.53	1.0	1.0	-	-
	5.	1.24	1.37	1.46	1.53	1.0	1.0	-	-
	2.	1.21	1.31	1.39	1.45	1.0	1.0	-	-
	1.	1.18	1.26	1.33	1.37	1.0	1.0	-	-
	0.5	1.17	1.25	1.31	1.36	1.0	1.0	-	-
	0.3	1.10	1.13	1.16	1.18	1.0	1.0	-	-
	PGV	1.15	1.22	1.26	1.30	1.0	1.0	-	-
Vertical	PGA	1.22	1.33	1.41	1.46	1.0	1.0	-	-
	20.	1.22	1.32	1.4	1.45	1.0	1.0	-	-
	10.	1.22	1.32	1.39	1.44	1.0	1.0	-	-
	5.	1.21	1.31	1.39	1.44	1.0	1.0	-	-
	2.	1.19	1.28	1.35	1.39	1.0	1.0	-	-
	1.	1.17	1.24	1.3	1.34	1.0	1.0	-	-
	0.5	1.13	1.18	1.22	1.25	1.0	1.0	-	-
	0.3	1.09	1.11	1.14	1.16	1.0	1.0	-	-
	PGV	1.15	1.20	1.24	1.27	1.0	1.0	-	-

TABLE 6-5
K. W CAMPBELL: MULTIPLE RUPTURE SCENARIO
FACTORS APPLIED TO MEDIAN ESTIMATES

COMPONENT	FREQUENCY (HZ)	MEDIAN 2 FAULTS	MEDIAN 3 FAULTS	MEDIAN 4 FAULTS	MEDIAN 5 FAULTS	FACTOR SIGMA	FACTOR SIGMA-MU	ADDITIONAL SIGMA (SRSS)	ADDITIONAL SIGMA-MU (SRSS)
Horizontal	PGA	1.0	1.0	1.0	1.0	1.2	1.0	-	-
	20.	1.0	1.0	1.0	1.0	1.2	1.0	-	-
	10.	1.0	1.0	1.0	1.0	1.2	1.0	-	-
	5.	1.0	1.0	1.0	1.0	1.2	1.0	-	-
	2.	1.0	1.0	1.0	1.0	1.2	1.0	-	-
	1.	1.0	1.0	1.0	1.0	1.2	1.0	-	-
	0.5	1.0	1.0	1.0	1.0	1.2	1.0	-	-
	0.3	1.0	1.0	1.0	1.0	1.2	1.0	-	-
	PGV	1.0	1.0	1.0	1.0	1.2	1.0	-	-
Vertical	PGA	1.0	1.0	1.0	1.0	1.2	1.0	-	-
	20.	1.0	1.0	1.0	1.0	1.2	1.0	-	-
	10.	1.0	1.0	1.0	1.0	1.2	1.0	-	-
	5.	1.0	1.0	1.0	1.0	1.2	1.0	-	-
	2.	1.0	1.0	1.0	1.0	1.2	1.0	-	-
	1.	1.0	1.0	1.0	1.0	1.2	1.0	-	-
	0.5	1.0	1.0	1.0	1.0	1.2	1.0	-	-
	0.3	1.0	1.0	1.0	1.0	1.2	1.0	-	-
	PGV	1.0	1.0	1.0	1.0	1.2	1.0	-	-

TABLE 6-6
A. MCGARR MULTIPLE RUPTURE SCENARIO
FACTORS APPLIED TO MEDIAN ESTIMATES

COMPONENT	FREQUENCY (HZ)	MEDIAN 2 FAULTS	MEDIAN 3 FAULTS	MEDIAN 4 FAULTS	MEDIAN 5 FAULTS	FACTOR SIGMA	FACTOR SIGMA-MU	ADDITIONAL SIGMA (SRSS)	ADDITIONAL SIGMA-MU (SRSS)
Horizontal	PGA	1.0	1.0	1.0	1.0	1.2	1.0	-	-
	20.	1.0	1.0	1.0	1.0	1.2	1.0	-	-
	10.	1.0	1.0	1.0	1.0	1.2	1.0	-	-
	5.	1.0	1.0	1.0	1.0	1.2	1.0	-	-
	2.	1.0	1.0	1.0	1.0	1.2	1.0	-	-
	1.	1.0	1.0	1.0	1.0	1.2	1.0	-	-
	0.5	1.0	1.0	1.0	1.0	1.2	1.0	-	-
	0.3	1.0	1.0	1.0	1.0	1.2	1.0	-	-
	PGV	1.0	1.0	1.0	1.0	1.2	1.0	-	-
Vertical	PGA	1.0	1.0	1.0	1.0	1.2	1.0	-	-
	20.	1.0	1.0	1.0	1.0	1.2	1.0	-	-
	10.	1.0	1.0	1.0	1.0	1.2	1.0	-	-
	5.	1.0	1.0	1.0	1.0	1.2	1.0	-	-
	2.	1.0	1.0	1.0	1.0	1.2	1.0	-	-
	1.	1.0	1.0	1.0	1.0	1.2	1.0	-	-
	0.5	1.0	1.0	1.0	1.0	1.2	1.0	-	-
	0.3	1.0	1.0	1.0	1.0	1.2	1.0	-	-
	PGV	1.0	1.0	1.0	1.0	1.2	1.0	-	-

TABLE 6-7
W. J. SILVA: MULTIPLE RUPTURE SCENARIO
FACTORS APPLIED TO MEDIAN ESTIMATES

COMPONENT	FREQUENCY (HZ)	MEDIAN 2 FAULTS	MEDIAN 3 FAULTS	MEDIAN 4 FAULTS	MEDIAN 5 FAULTS	FACTOR SIGMA	FACTOR SIGMA-MU	ADDITIONAL SIGMA (SRSS)	ADDITIONAL SIGMA-MU (SRSS)
Horizontal	PGA	1.29	1.44	1.56	1.66	1.0	1.0	-	-
	20.	1.30	1.46	1.58	1.68	1.0	1.0	-	-
	10.	1.29	1.45	1.57	1.66	1.0	1.0	-	-
	5.	1.29	1.44	1.56	1.65	1.0	1.0	-	-
	2.	1.25	1.39	1.49	1.57	1.0	1.0	-	-
	1.	1.22	1.34	1.43	1.50	1.0	1.0	-	-
	0.5	1.46	1.56	1.64	1.70	1.0	1.0	-	-
	0.3	1.40	1.45	1.50	1.54	1.0	1.0	-	-
	PGV	1.21	1.32	1.40	1.46	1.0	1.0	-	-
Vertical	PGA	1.29	1.45	1.57	1.66	1.0	1.0	-	-
	20.	1.30	1.46	1.58	1.67	1.0	1.0	-	-
	10.	1.29	1.43	1.55	1.63	1.0	1.0	-	-
	5.	1.28	1.43	1.54	1.63	1.0	1.0	-	-
	2.	1.25	1.38	1.48	1.55	1.0	1.0	-	-
	1.	1.22	1.34	1.42	1.49	1.0	1.0	-	-
	0.5	1.45	1.55	1.62	1.69	1.0	1.0	-	-
	0.3	1.39	1.45	1.49	1.51	1.0	1.0	-	-
	PGV	1.22	1.33	1.42	1.48	1.0	1.0	-	-

TABLE 6-8
P. G. SOMERVILLE: MULTIPLE RUPTURE SCENARIO
FACTORS APPLIED TO MEDIAN ESTIMATES

COMPONENT	FREQUENCY (HZ)	MEDIAN 2 FAULTS	MEDIAN 3 FAULTS	MEDIAN 4 FAULTS	MEDIAN 5 FAULTS	FACTOR SIGMA	FACTOR SIGMA-MU	ADDITIONAL SIGMA (SRSS)	ADDITIONAL SIGMA-MU (SRSS)
Horizontal	PGA	1.63	1.63	1.63	1.63	-	-	0.3	0.2
	20.	1.63	1.63	1.63	1.63	-	-	0.3	0.2
	10.	1.63	1.63	1.63	1.63	-	-	0.3	0.2
	5.	1.63	1.63	1.63	1.63	-	-	0.3	0.2
	2.	1.58	1.58	1.58	1.58	-	-	0.3	0.2
	1.	1.5	1.5	1.5	1.5	-	-	0.3	0.2
	0.5	1.5	1.5	1.5	1.5	-	-	0.3	0.2
	0.3	1.5	1.5	1.5	1.5	-	-	0.3	0.2
	PGV	1.5	1.5	1.5	1.5	-	-	0.3	0.2
Vertical	PGA	1.63	1.63	1.63	1.63	-	-	0.3	0.2
	20.	1.63	1.63	1.63	1.63	-	-	0.3	0.2
	10.	1.63	1.63	1.63	1.63	-	-	0.3	0.2
	5.	1.63	1.63	1.63	1.63	-	-	0.3	0.2
	2.	1.58	1.58	1.58	1.58	-	-	0.3	0.2
	1.	1.5	1.5	1.5	1.5	-	-	0.3	0.2
	0.5	1.5	1.5	1.5	1.5	-	-	0.3	0.2
	0.3	1.5	1.5	1.5	1.5	-	-	0.3	0.2
	PGV	1.5	1.5	1.5	1.5	-	-	0.3	0.2

TABLE 6-9
M. C. WALCK: MULTIPLE RUPTURE SCENARIO
FACTORS APPLIED TO MEDIAN ESTIMATES

COMPONENT	FREQUENCY (HZ)	MEDIAN 2 FAULTS	MEDIAN 3 FAULTS	MEDIAN 4 FAULTS	MEDIAN 5 FAULTS	FACTOR SIGMA	FACTOR SIGMA-MU	ADDITIONAL SIGMA (SRSS)	ADDITIONAL SIGMA-MU (SRSS)
Horizontal	PGA	1.28	1.42	1.53	1.61	-	-	0.0	0.1
	20.	1.30	1.45	1.58	1.67	-	-	0.0	0.1
	10.	1.29	1.43	1.55	1.63	-	-	0.0	0.1
	5.	1.27	1.42	1.53	1.61	-	-	0.0	0.1
	2.	1.23	1.35	1.45	1.52	-	-	0.0	0.1
	1.	1.20	1.30	1.38	1.43	-	-	0.0	0.1
	0.5	1.17	1.25	1.31	1.36	-	-	0.0	0.2
	0.3	1.13	1.17	1.22	1.25	-	-	0.0	0.2
	PGV	1.21	1.32	1.40	1.46	-	-	0.0	0.1
Vertical	PGA	1.25	1.37	1.46	1.53	-	-	0.0	0.1
	20.	1.26	1.39	1.48	1.55	-	-	0.0	0.1
	10.	1.26	1.39	1.49	1.56	-	-	0.0	0.1
	5.	1.25	1.38	1.47	1.54	-	-	0.0	0.1
	2.	1.20	1.30	1.38	1.43	-	-	0.0	0.1
	1.	1.18	1.26	1.33	1.37	-	-	0.0	0.1
	0.5	1.14	1.19	1.23	1.26	-	-	0.0	0.2
	0.3	1.09	1.11	1.13	1.14	-	-	0.0	0.2
	PGV	1.20	1.28	1.35	1.40	-	-	0.0	0.1

TABLE 6-10
LOW-ANGLE DETACHMENT FAULT SCENARIO
SCALE FACTORS

EXPERT	MEDIAN SCALE FACTOR	SIGMA-MU SCALE FACTOR	SIGMA SCALE FACTOR	ADDITIONAL SIGMA-MU (SRSS[1])	ADDITIONAL SIGMA (SRSS[1])
Anderson	1.0	1.0	1.0	-	-
Boore	1.0	1.0	1.0	-	-
Campbell (D = depth to bottom of rupture)	1.0 for D < 8 1.0+0.2*(D-8)/7 + 1 for 8<D<15 1.2 for D > 15	1.2	1.2	-	-
McGarr	1.0	1.3	1.0	-	-
Silva	1.0	1.0	1.0	-	-
Somerville[2]	See Table 4-17	-	-	0.3	0.2
Walck	1.0	-	-	0.25	0.0

[1] Square root of the sum of the squares method.

[2] Somerville addressed the case of a low-angle detachment fault combined with multiple parallel faults splaying off of the detachment (as requested). All of the other experts addressed the detachment fault by itself.

TABLE 6-11
ADJUSTMENT FACTORS FOR SIMULTANEOUS RUPTURES ON PARALLEL FAULTS AND A DEEP DETACHMENT SURFACE (SOMERVILLE)

FREQUENCY (HZ)	MEDIAN SCALE FACTOR	ADDITIONAL SIGMA (SRSS[1])	ADDITIONAL SIGMA-MU (SRSS[1])
PGA	1.0	0.3	0.2
20	1.0	0.3	0.2
10	1.0	0.3	0.2
5	1.0	0.3	0.2
2	1.2	0.3	0.2
1	2.2	0.3	0.2
0.5	2.2	0.3	0.2
0.3	1.7	0.3	0.2
PGV	2.2	0.3	0.2

[1] Square root of the sum of the squares method.

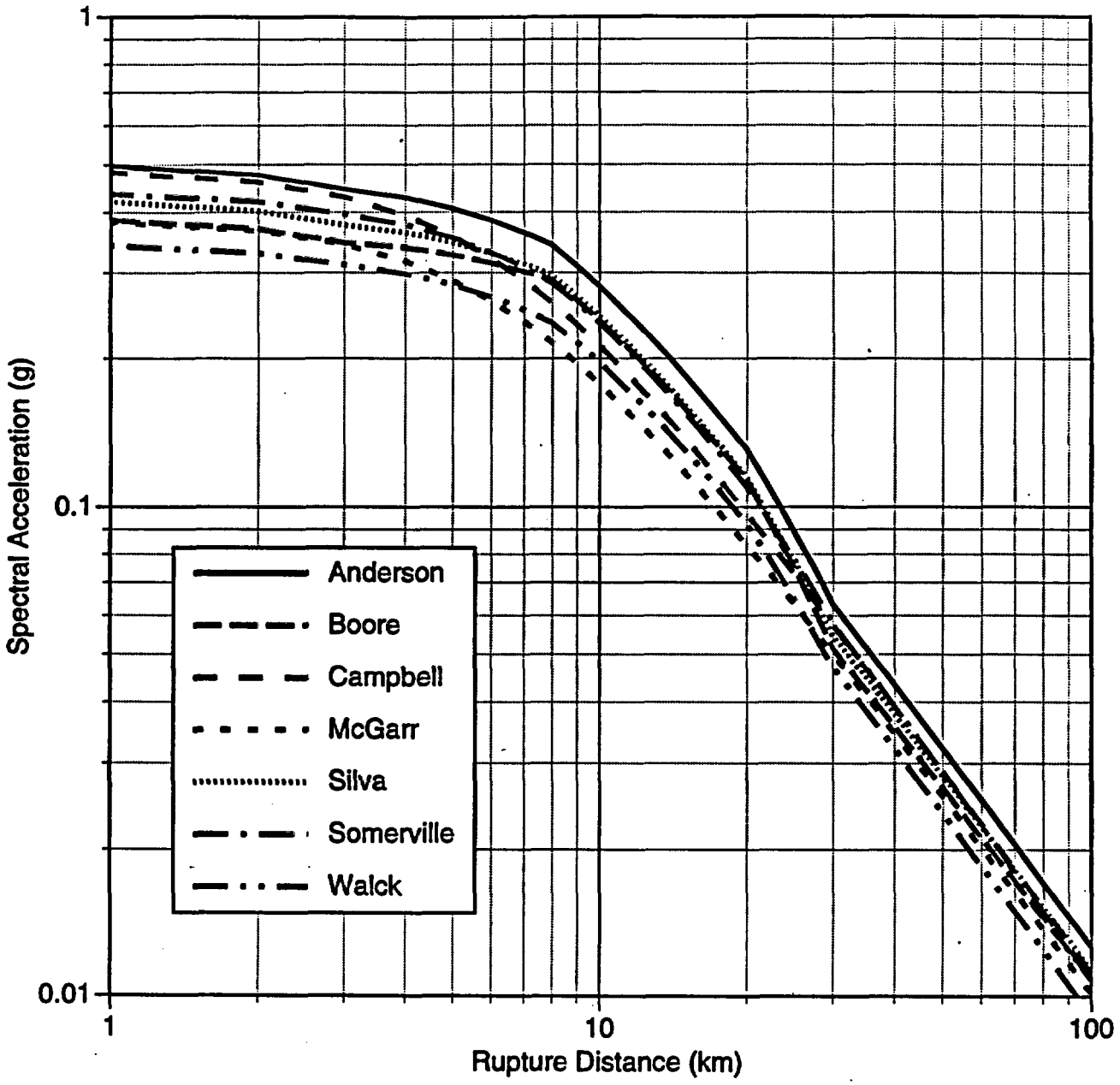

Figure 6-1 Comparison of median attenuation of horizontal PGA for M_W 6.5, normal faulting, hanging wall

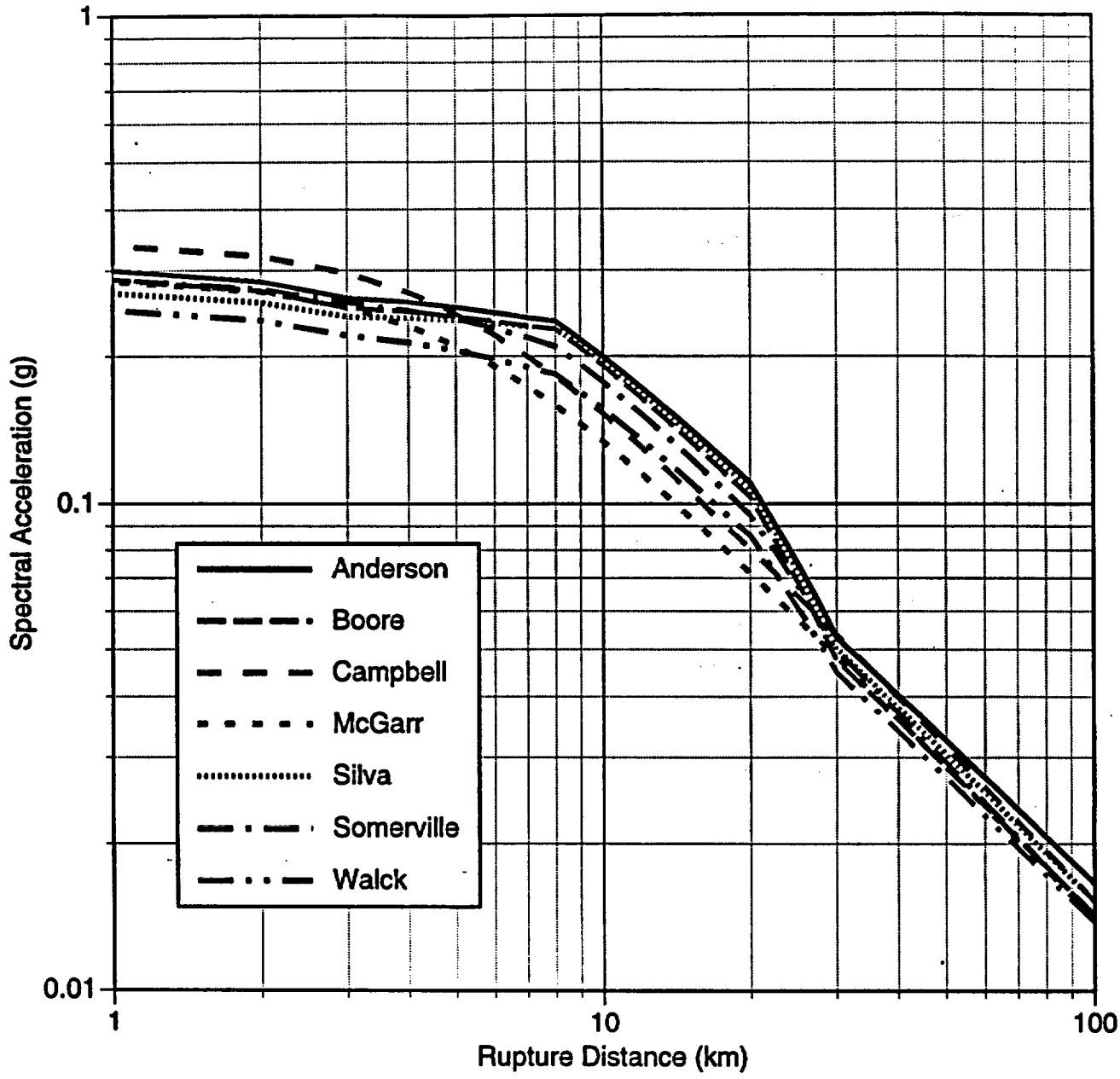

Figure 6-2 Comparison of median attenuation of horizontal spectral acceleration (T = 1.0 sec, 5% damping) for M_W 6.5, normal faulting, hanging wall

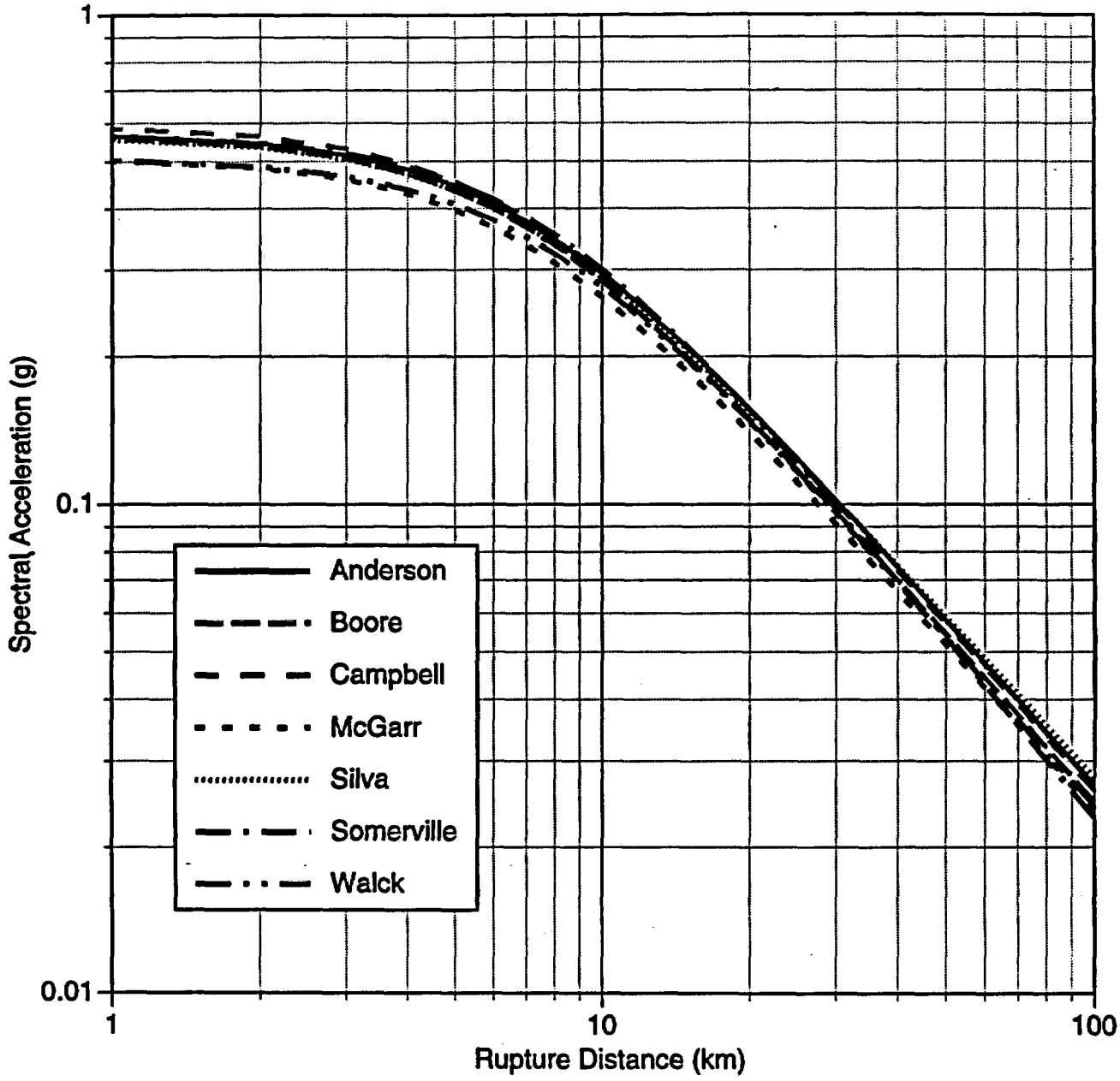

Figure 6-3 Comparison of median attenuation of horizontal PGA for M_W 7.5, strike-slip faulting

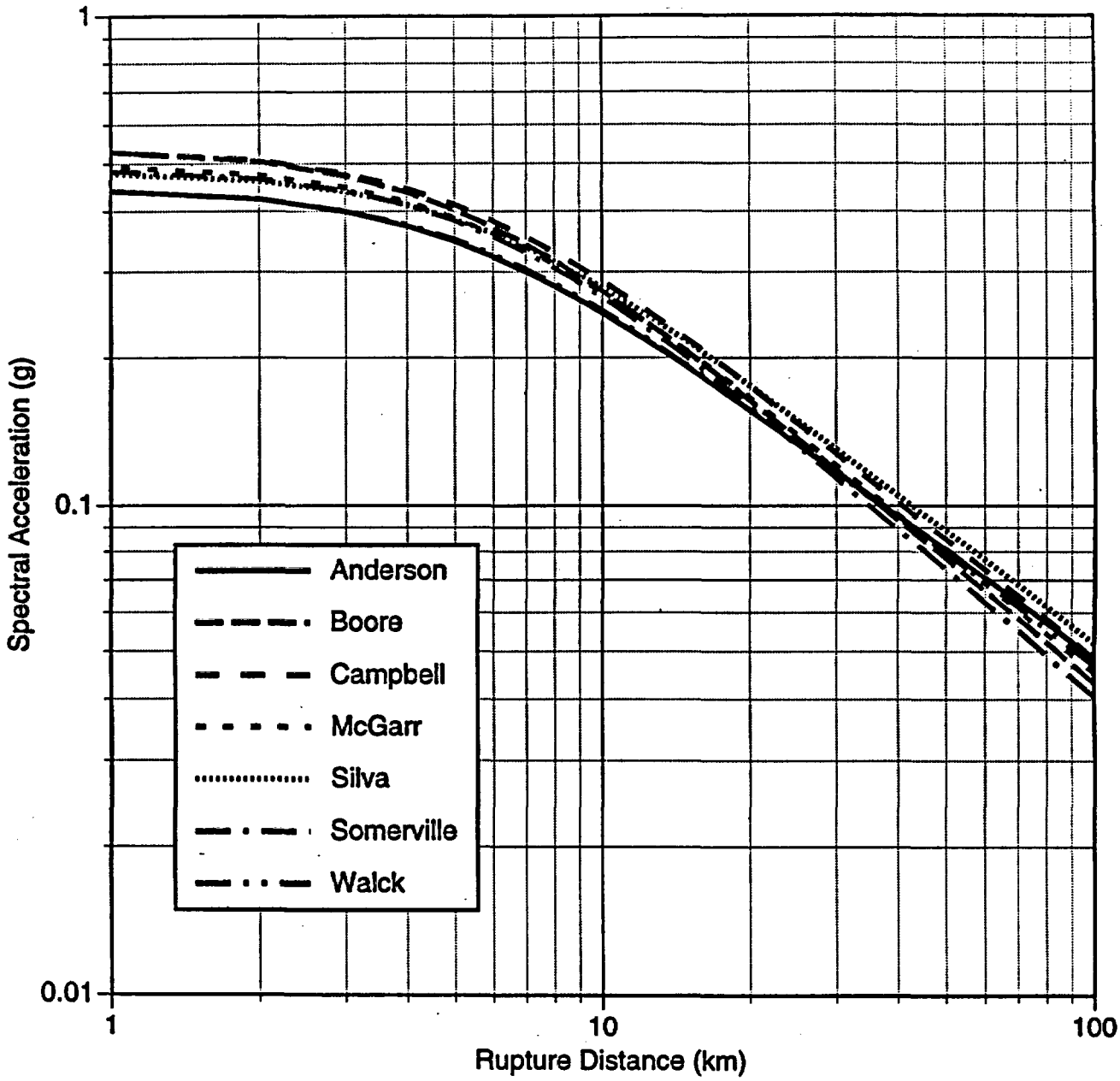

Figure 6-4 Comparison of median attenuation of horizontal spectral acceleration (T = 1.0 sec, 5% damping) for M_W 7.5, strike-slip faulting

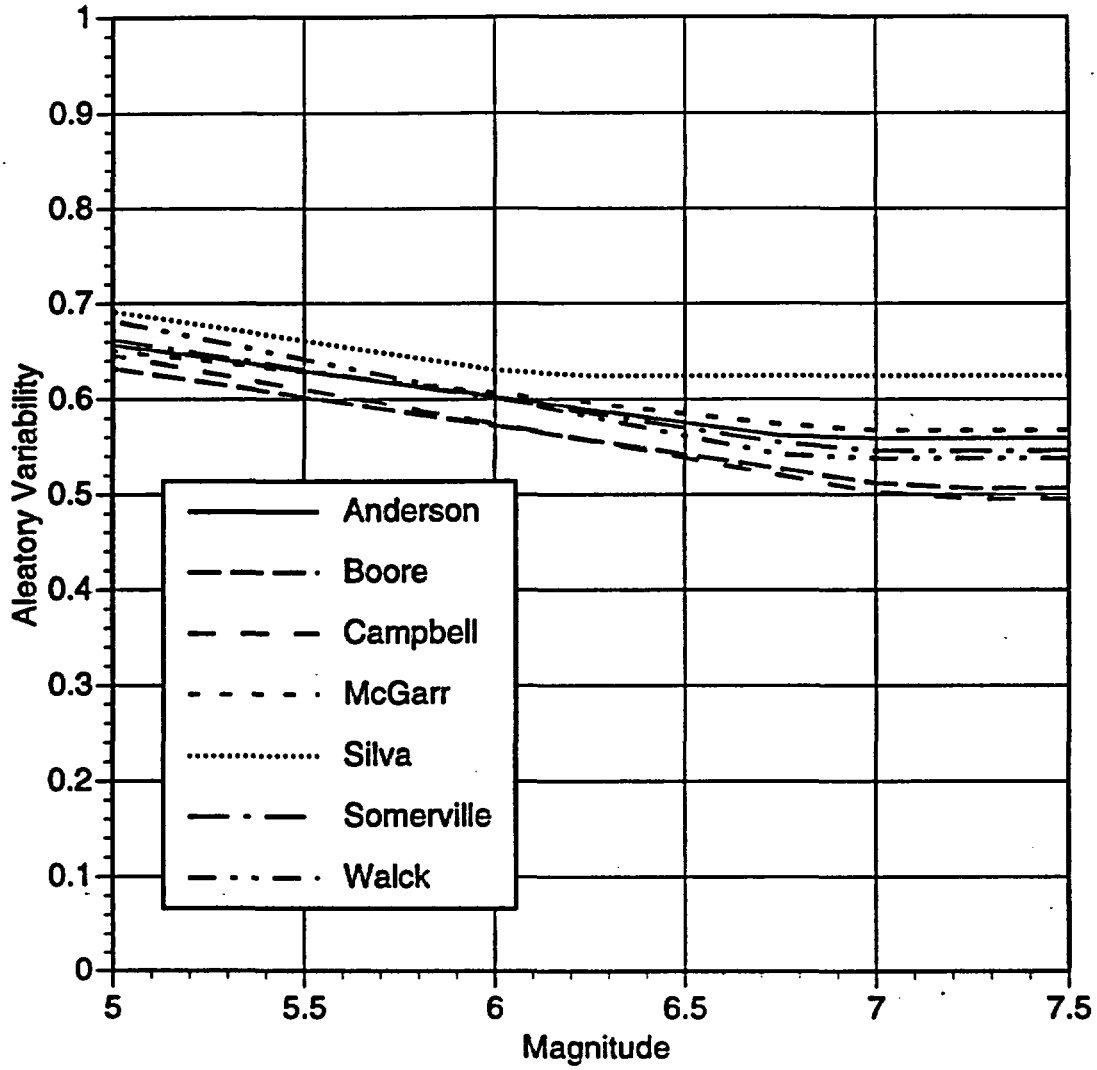

Figure 6-5 Comparison of aleatory variability of horizontal PGA

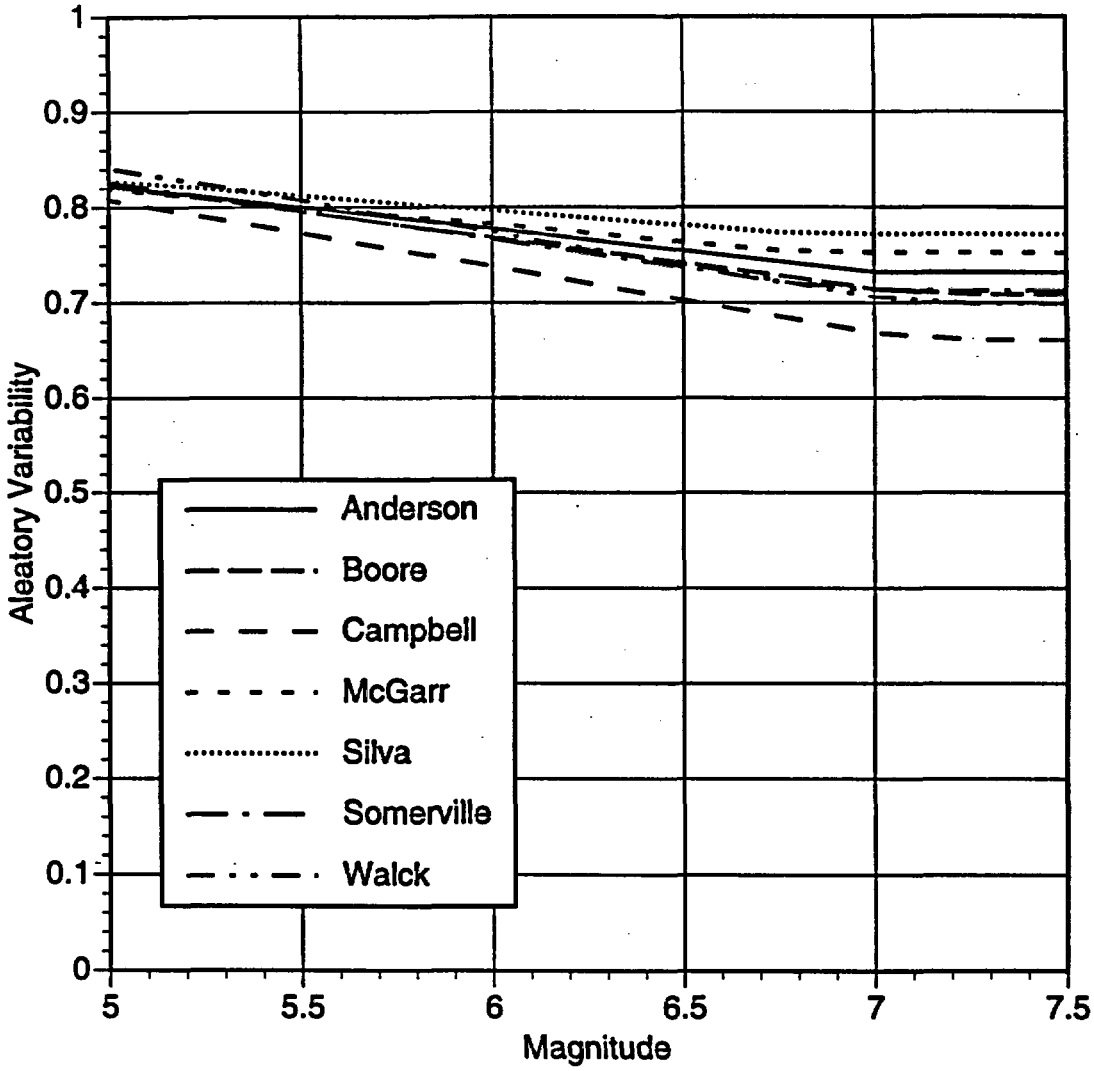

Figure 6-6 Comparison of aleatory variability of 1.0 sec horizontal spectral acceleration (at 5% damping)

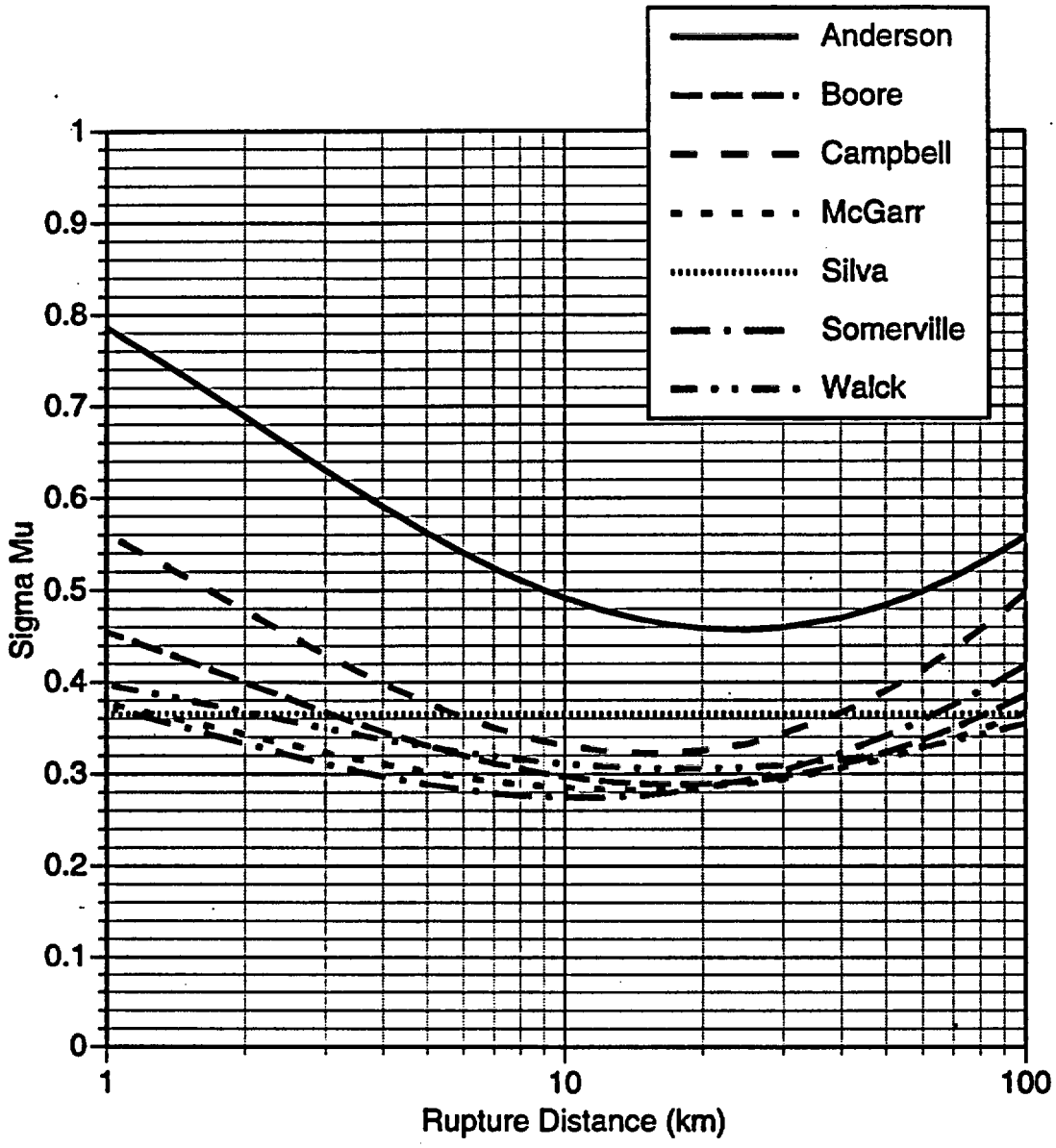

Figure 6-7 Comparison of epistemic uncertainty in the median horizontal PGA for M_W 6.5, normal faulting

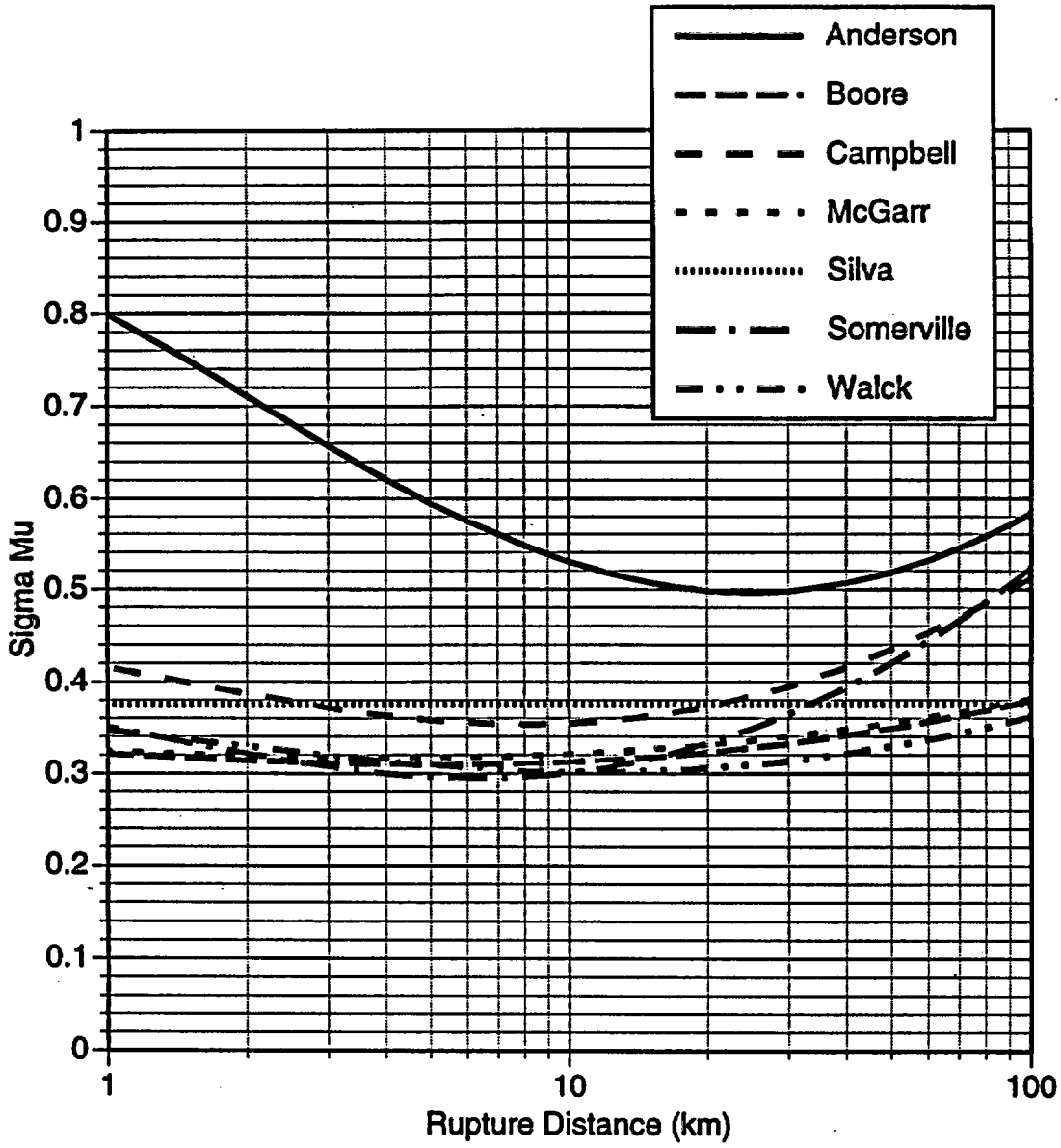

Figure 6-8 Comparison of epistemic uncertainty in the median 1.0 sec horizontal spectral acceleration (at 5% damping) for M_W 6.5, normal faulting

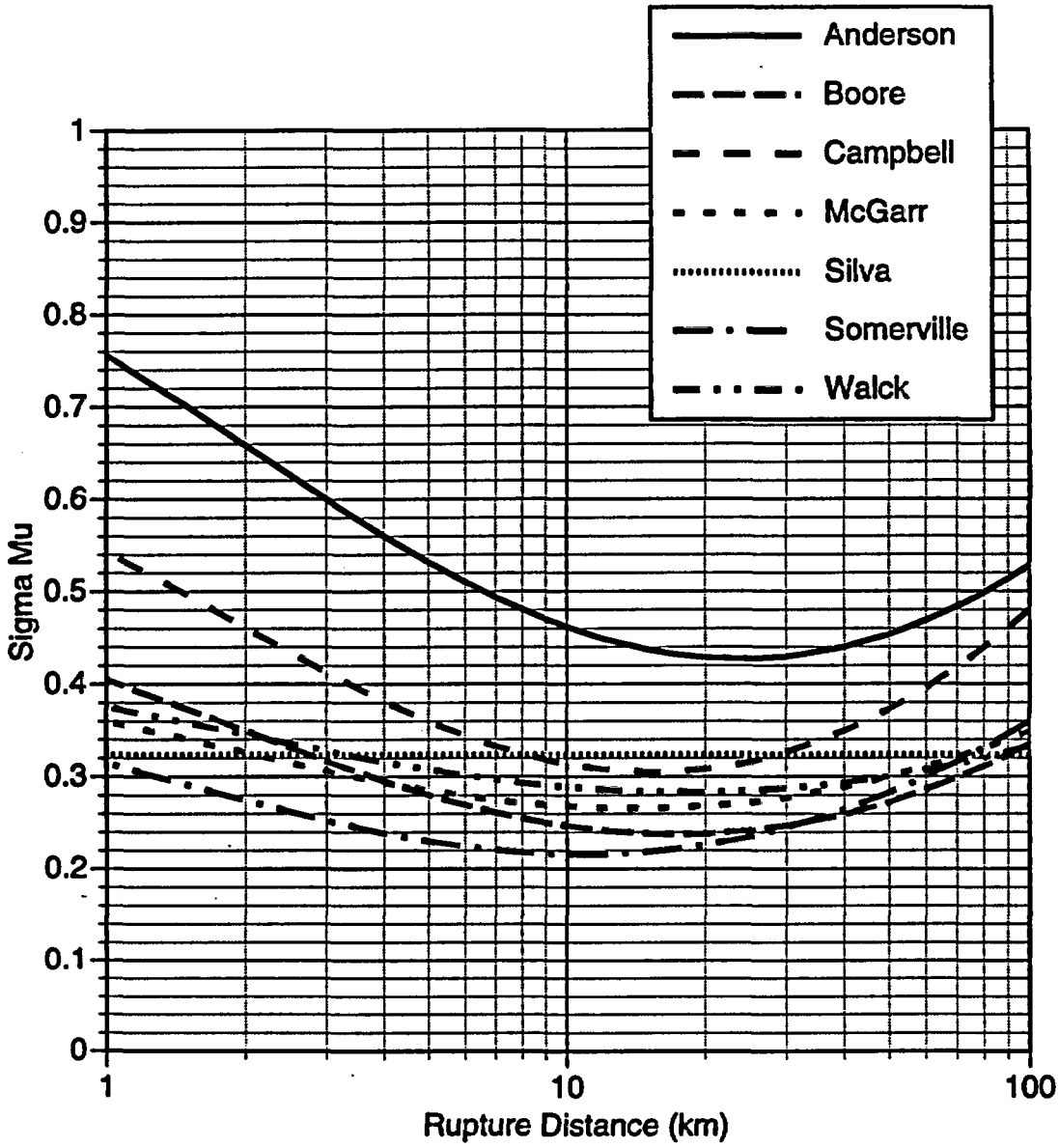

Figure 6-9 Comparison of epistemic uncertainty in the median horizontal PGA for M_W 7.5, normal faulting

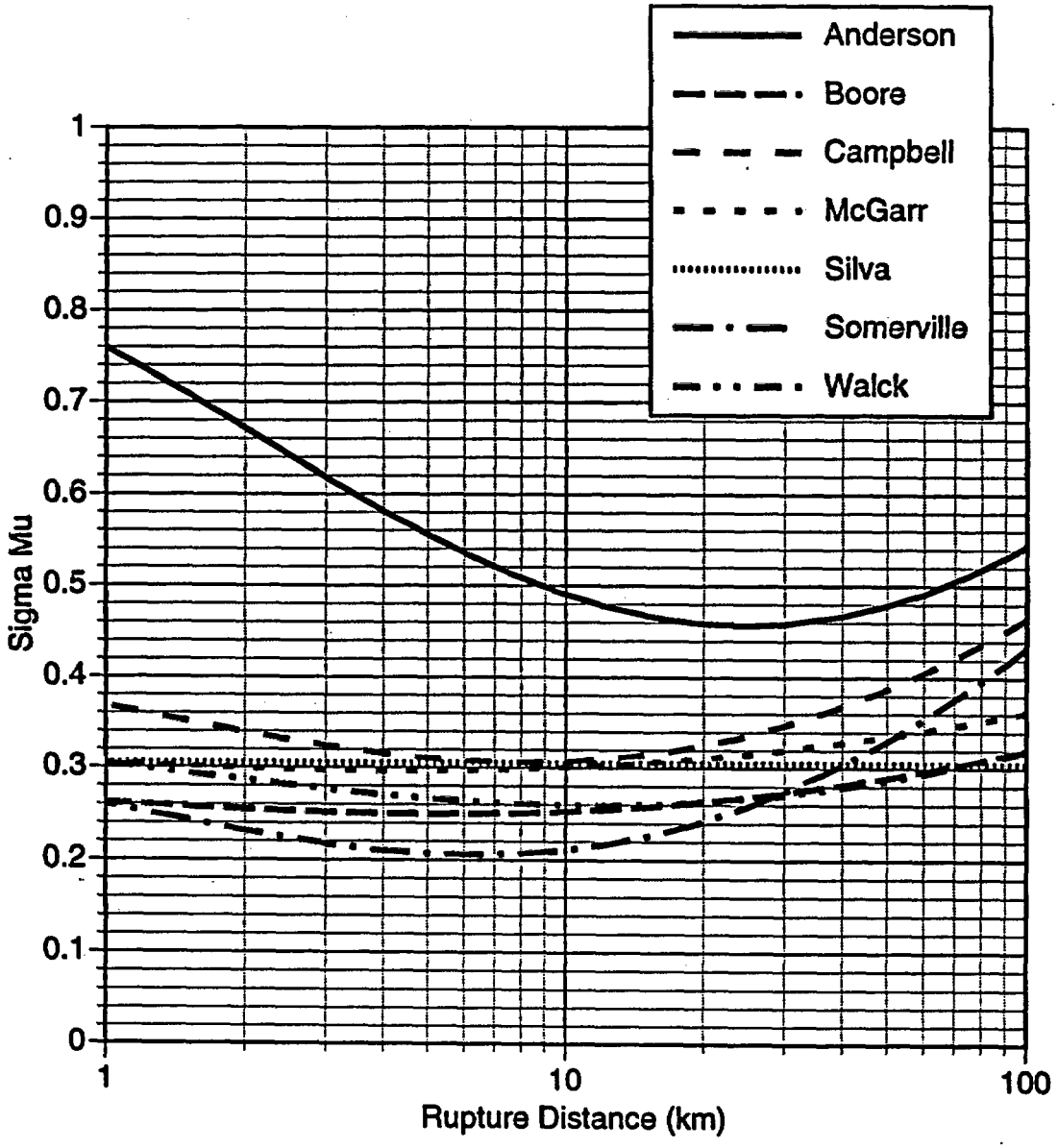

Figure 6-10 Comparison of epistemic uncertainty in the median 1.0 sec horizontal spectral acceleration (at 5% damping) for M_W 7.5, normal faulting

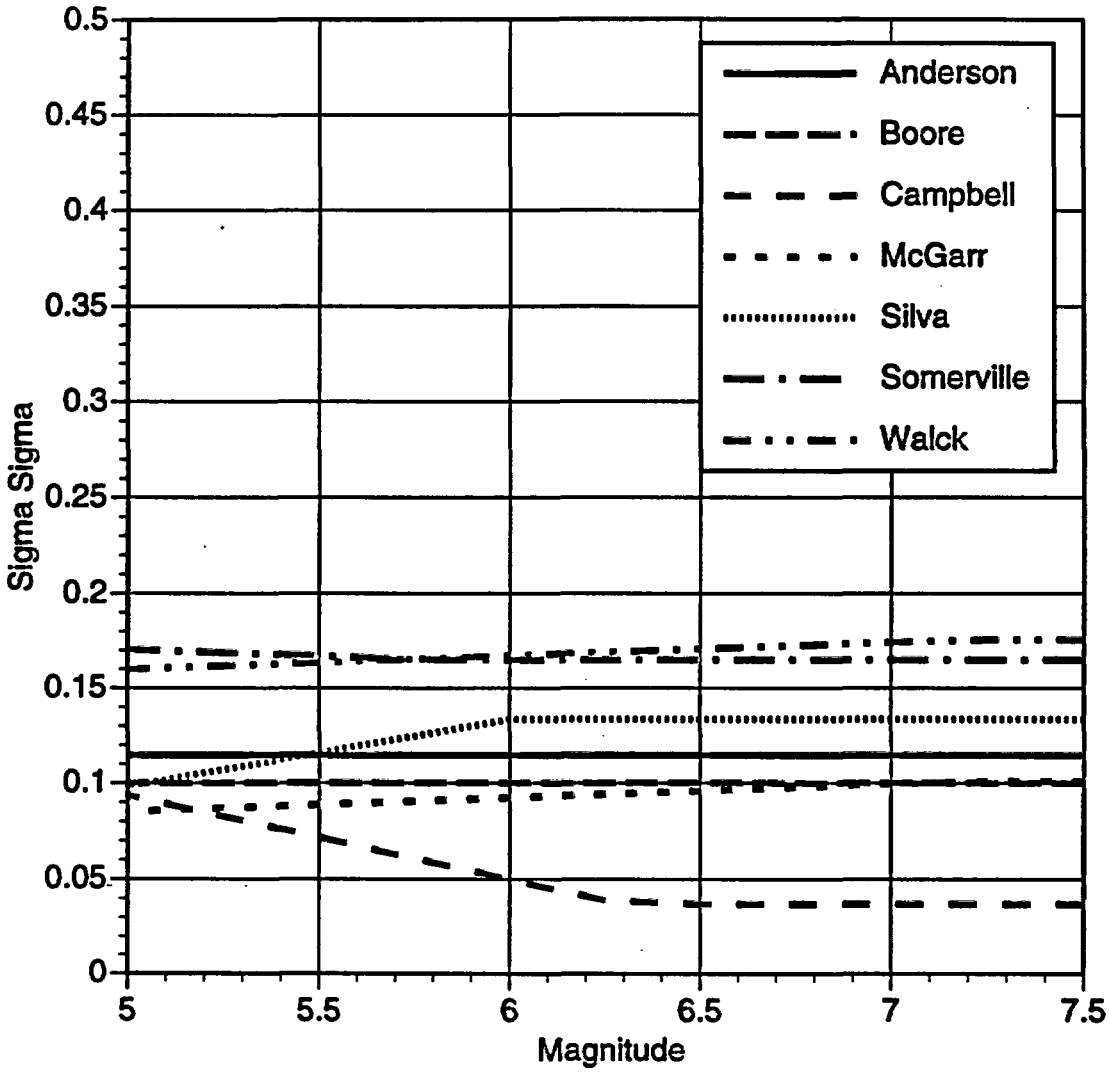

Figure 6-11 Comparison of epistemic uncertainty in the aleatory variability of horizontal PGA

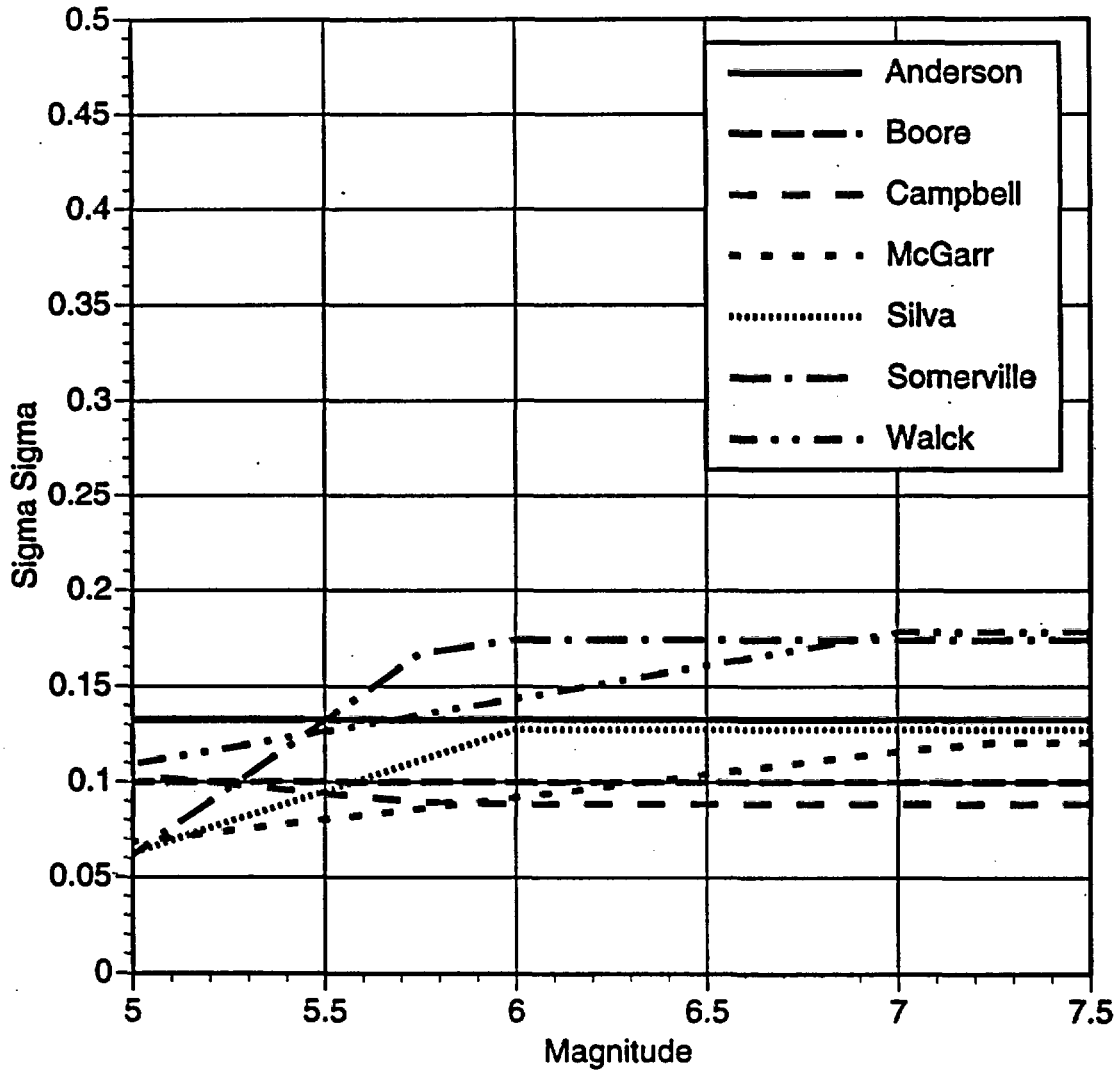

Figure 6-12 Comparison of epistemic uncertainty in the aleatory variability of 1.0 sec horizontal spectral acceleration (at 5% damping)

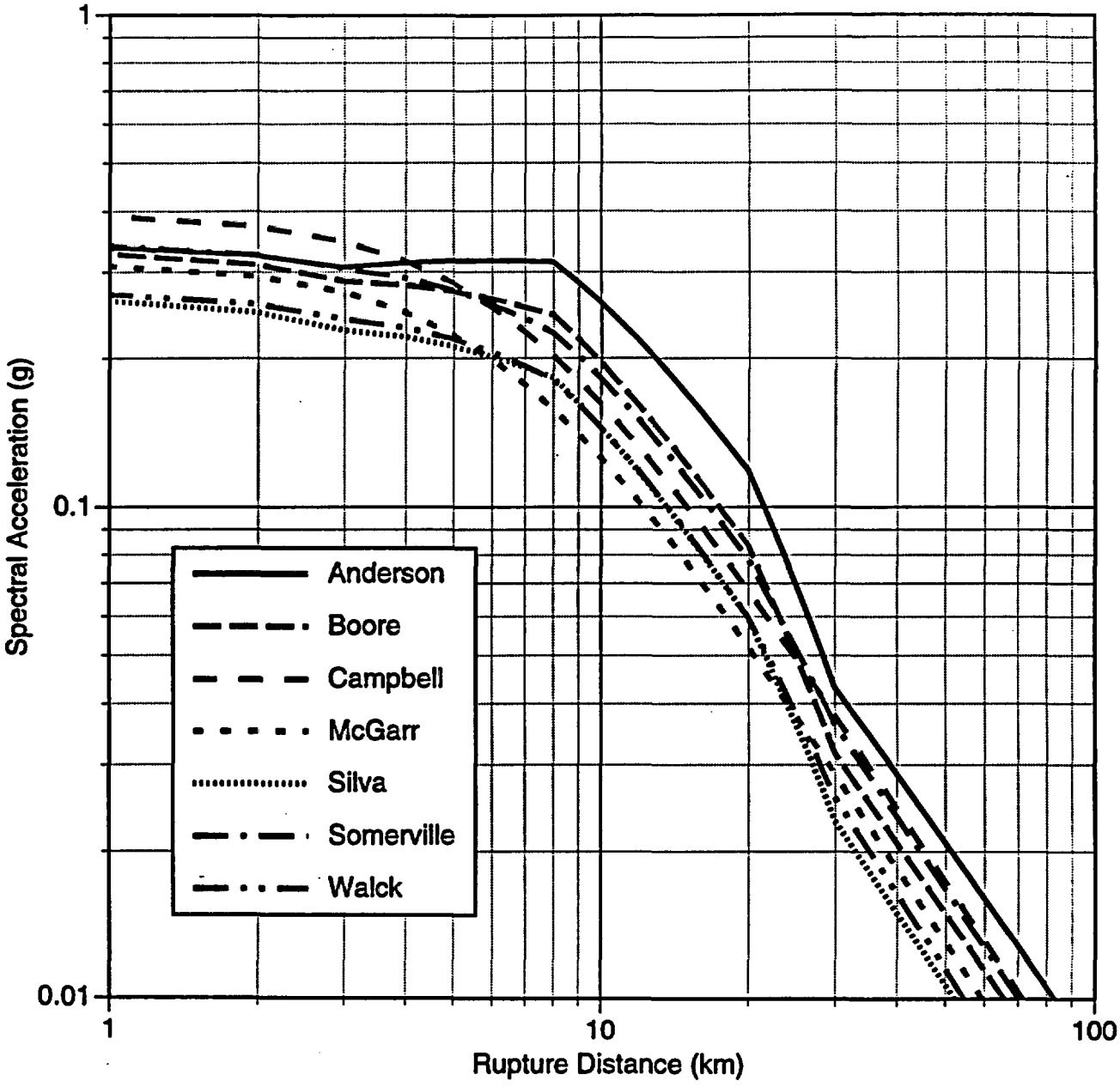

Figure 6-13 Comparison of median attenuation of vertical PGA for M_W 6.5, normal faulting, hanging wall

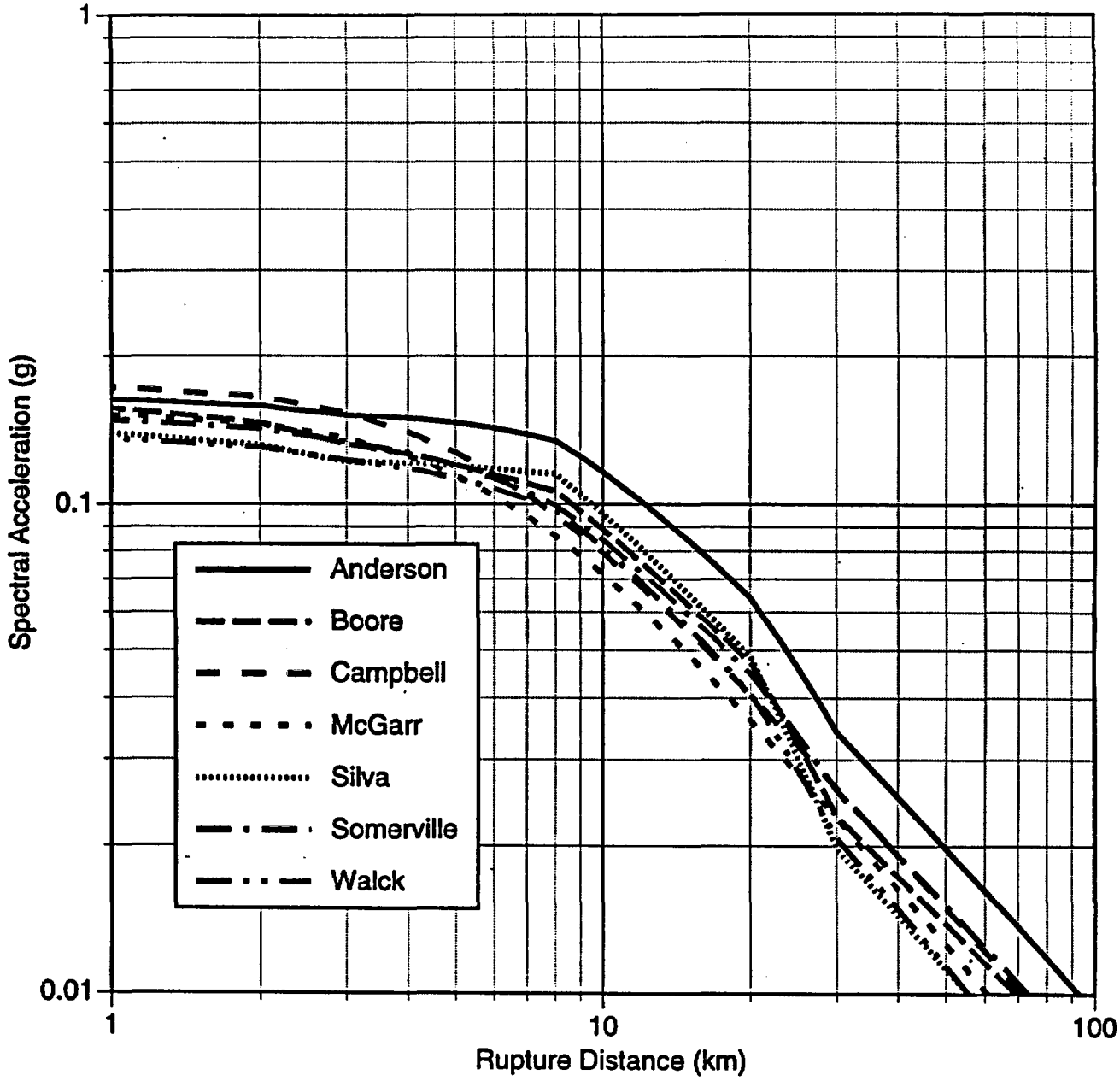

Figure 6-14 Comparison of median attenuation of vertical spectral acceleration (T= 1.0 sec, 5% damping) for M_W 6.5, normal faulting, hanging wall

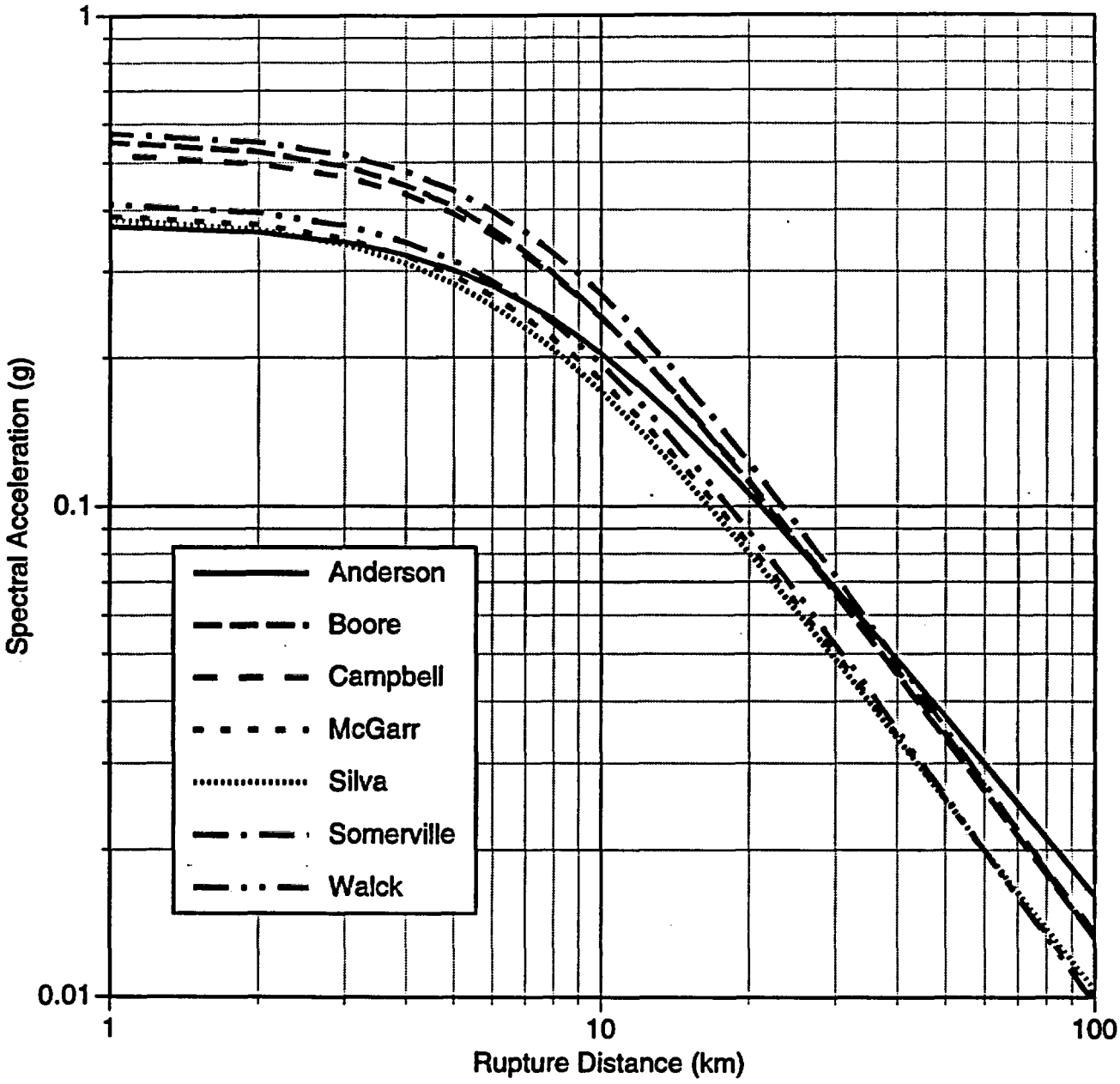

Figure 6-15 Comparison of median attenuation of vertical PGA for M_W 7.5, strike-slip faulting

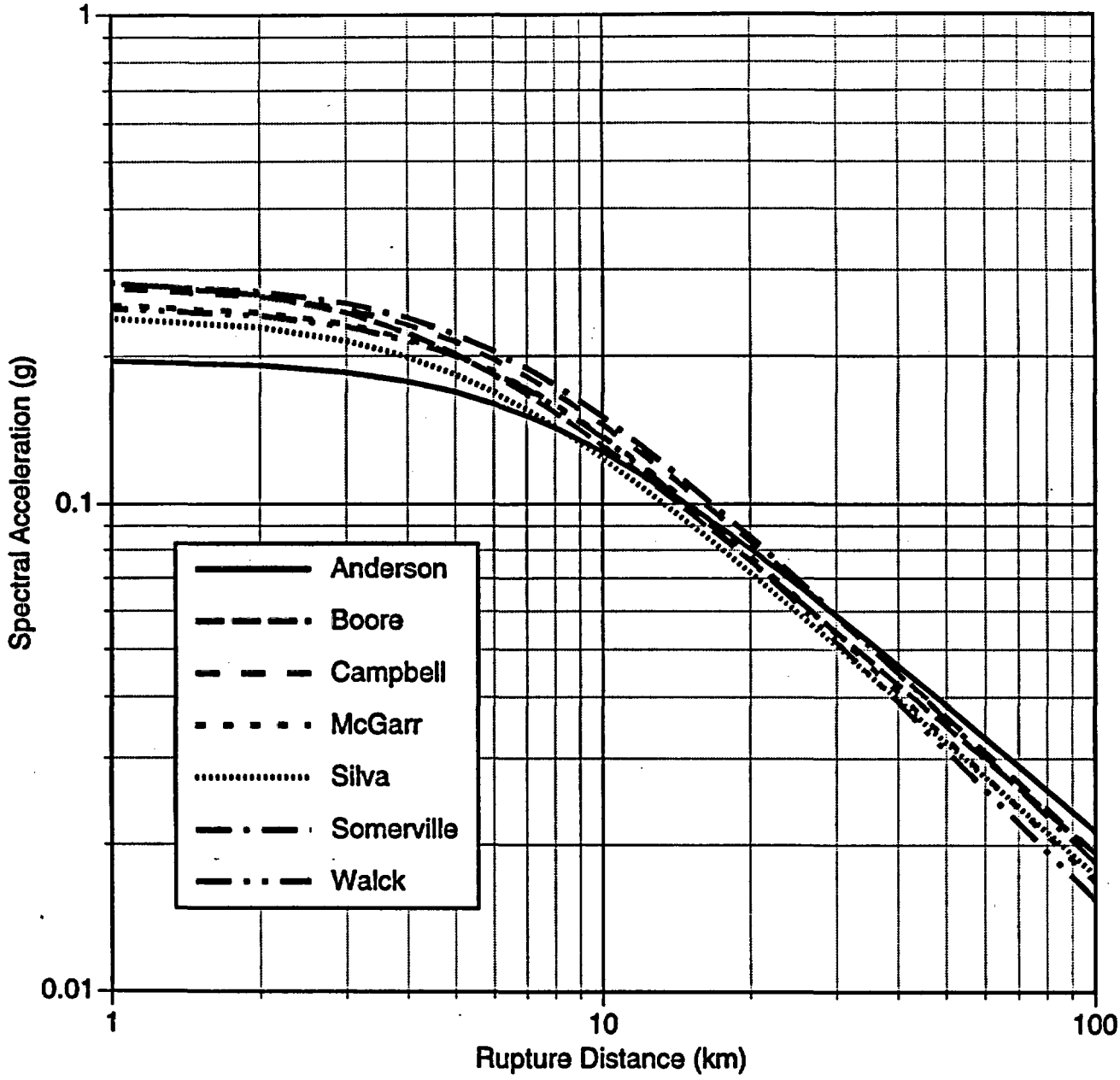

Figure 6-16 Comparison of median attenuation of vertical spectral acceleration (T= 1.0 sec, 5% damping) for Mw 7.5, strike-slip faulting

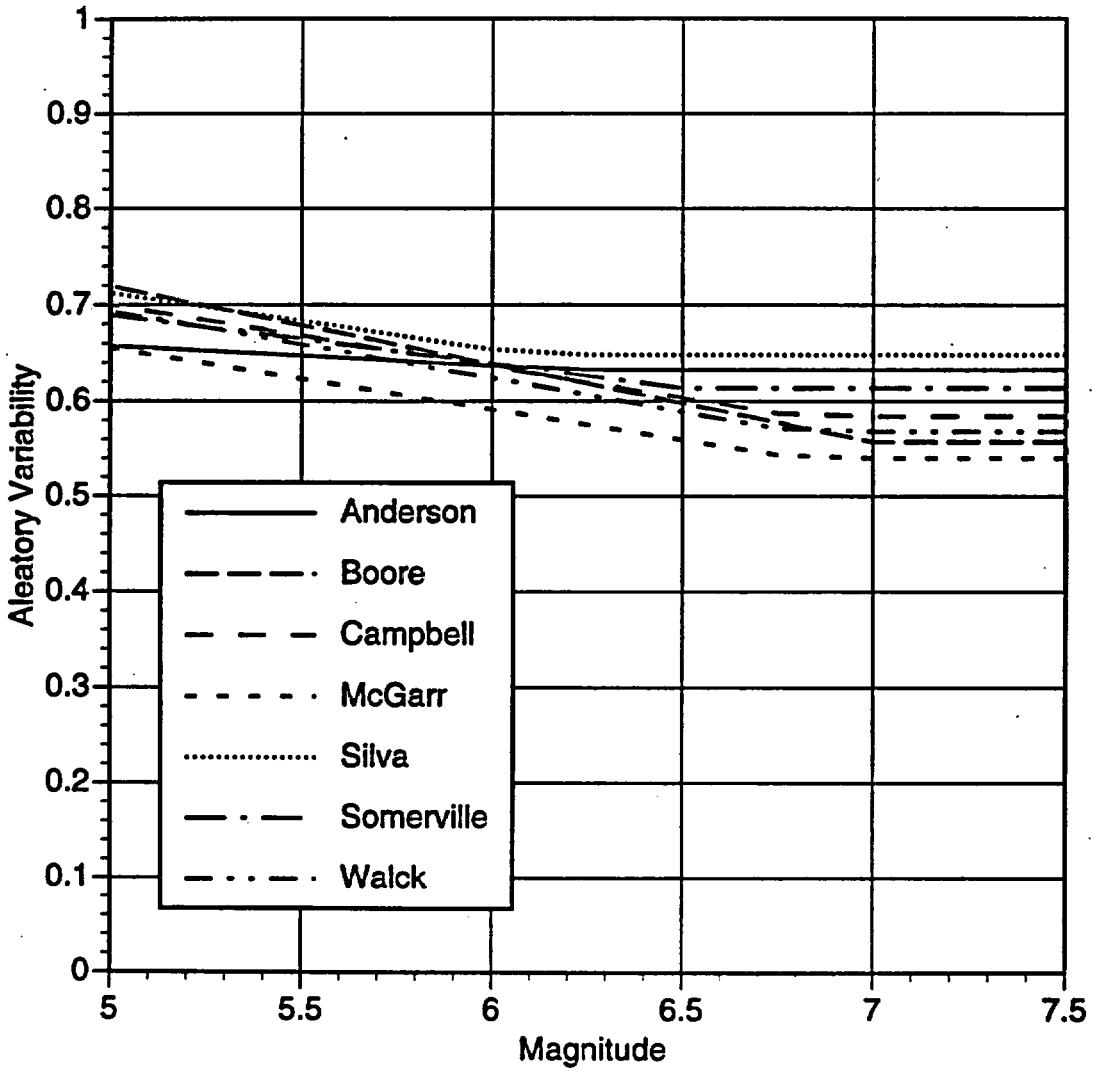

Figure 6-17 Comparison of aleatory variability of vertical PGA

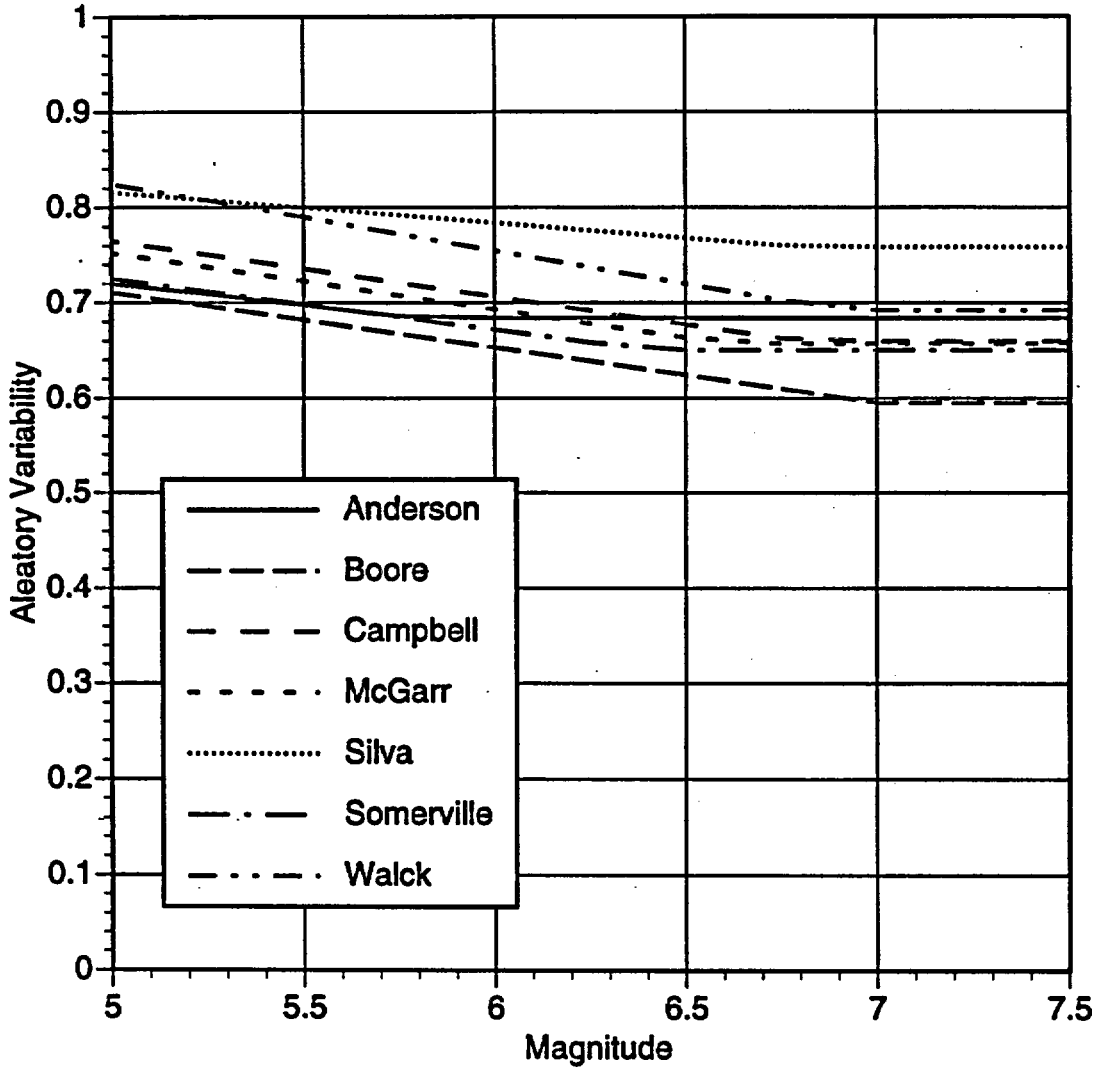

Figure 6-18 Comparison of aleatory variability of 1.0 sec vertical spectral acceleration (at 5% damping)

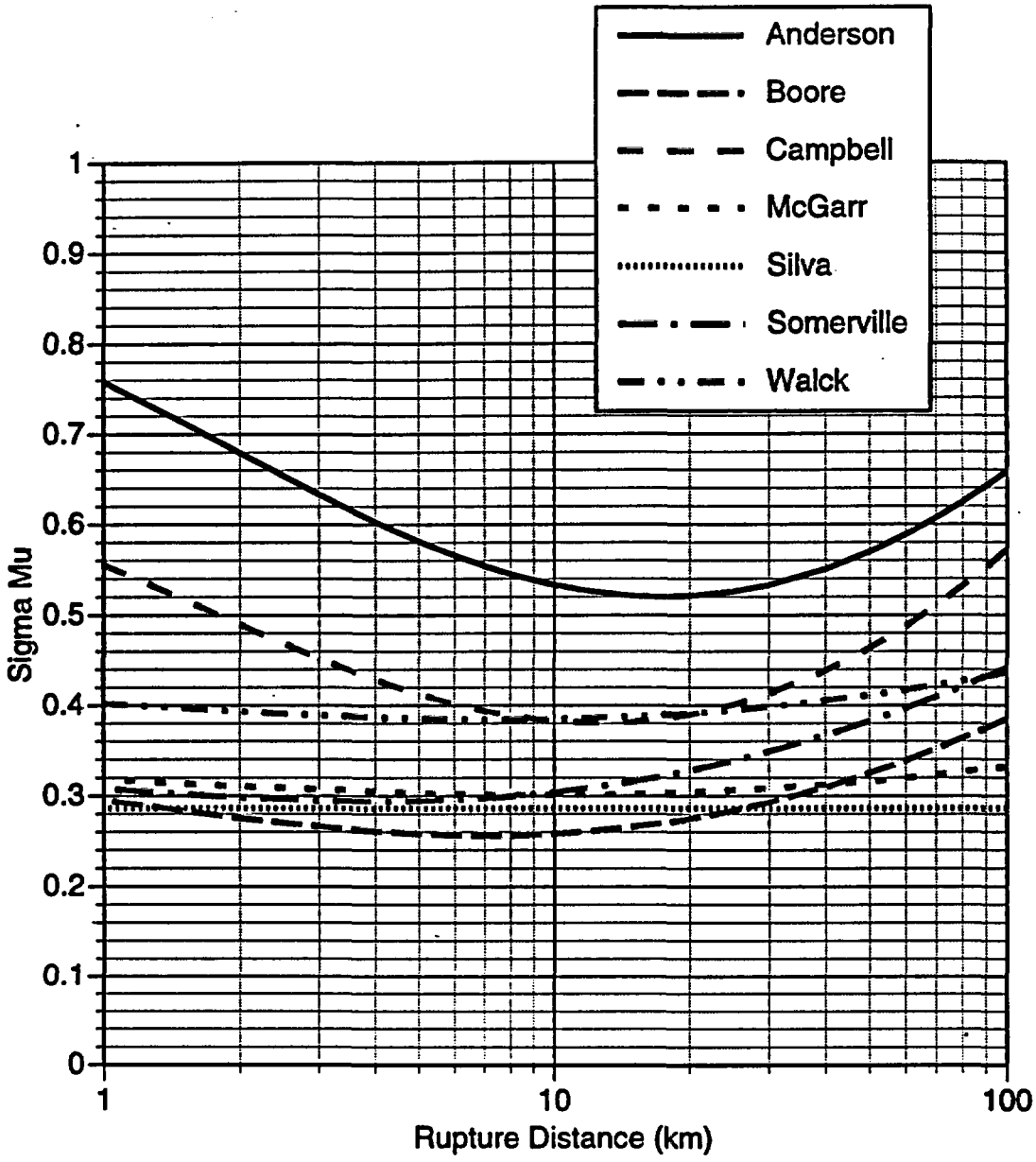

Figure 6-19 Comparison of epistemic uncertainty in the median vertical PGA for M_W 6.5, normal faulting

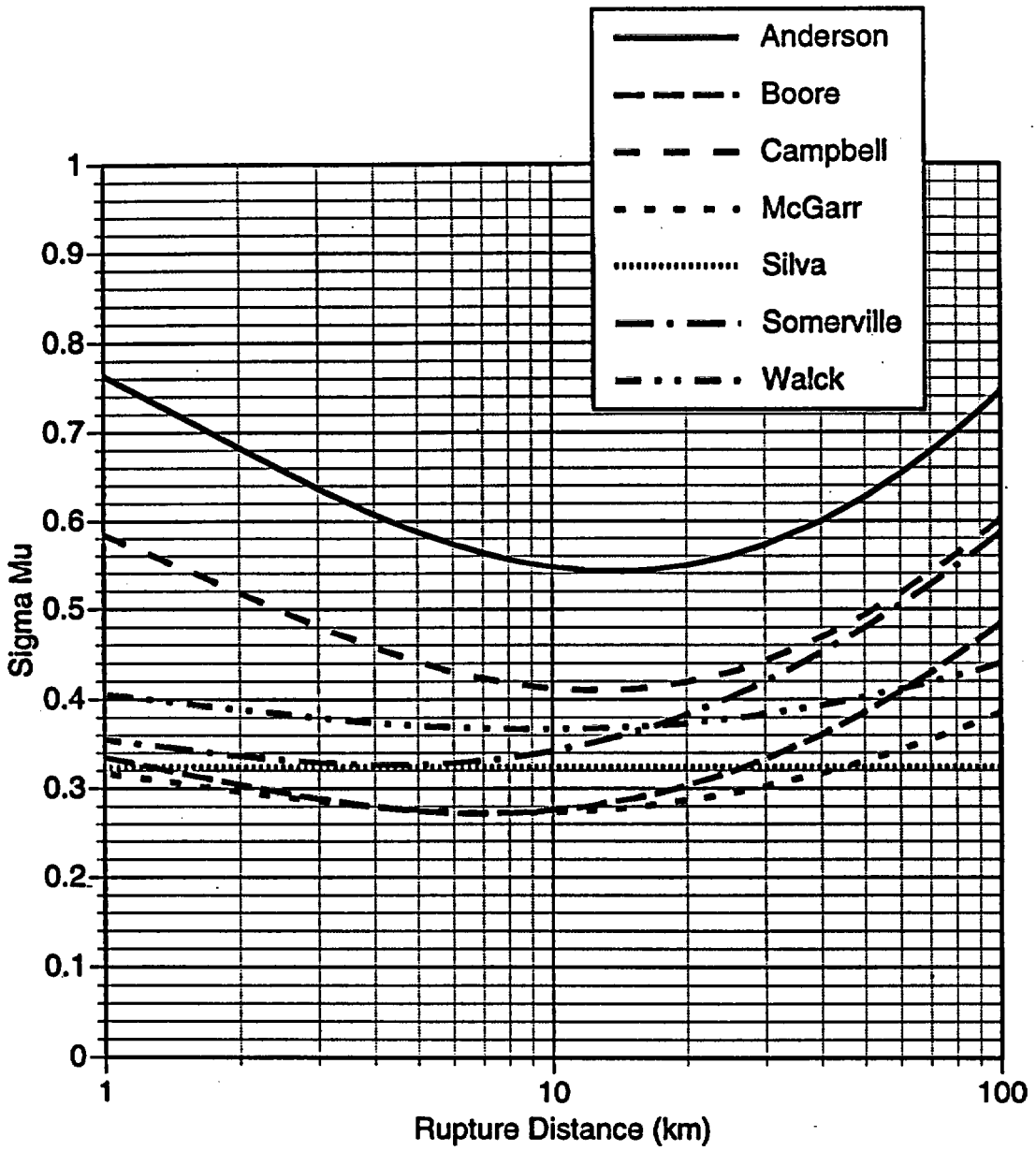

Figure 6-20 Comparison of epistemic uncertainty in the median 1.0 sec vertical spectral acceleration (at 5% damping) for M_W 6.5, normal faulting

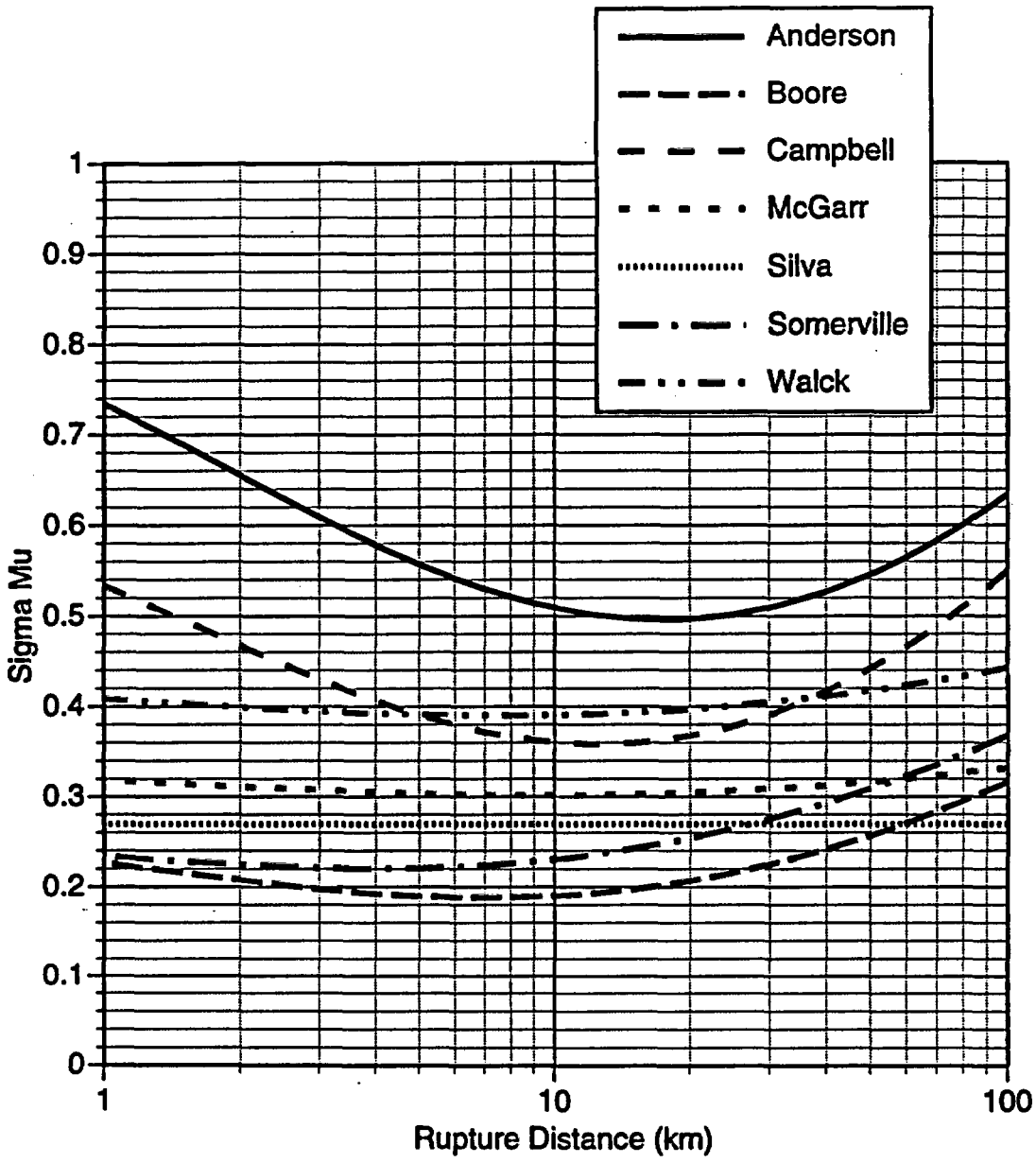

Figure 6-21 Comparison of epistemic uncertainty in the median vertical PGA for M_W 7.5, normal faulting

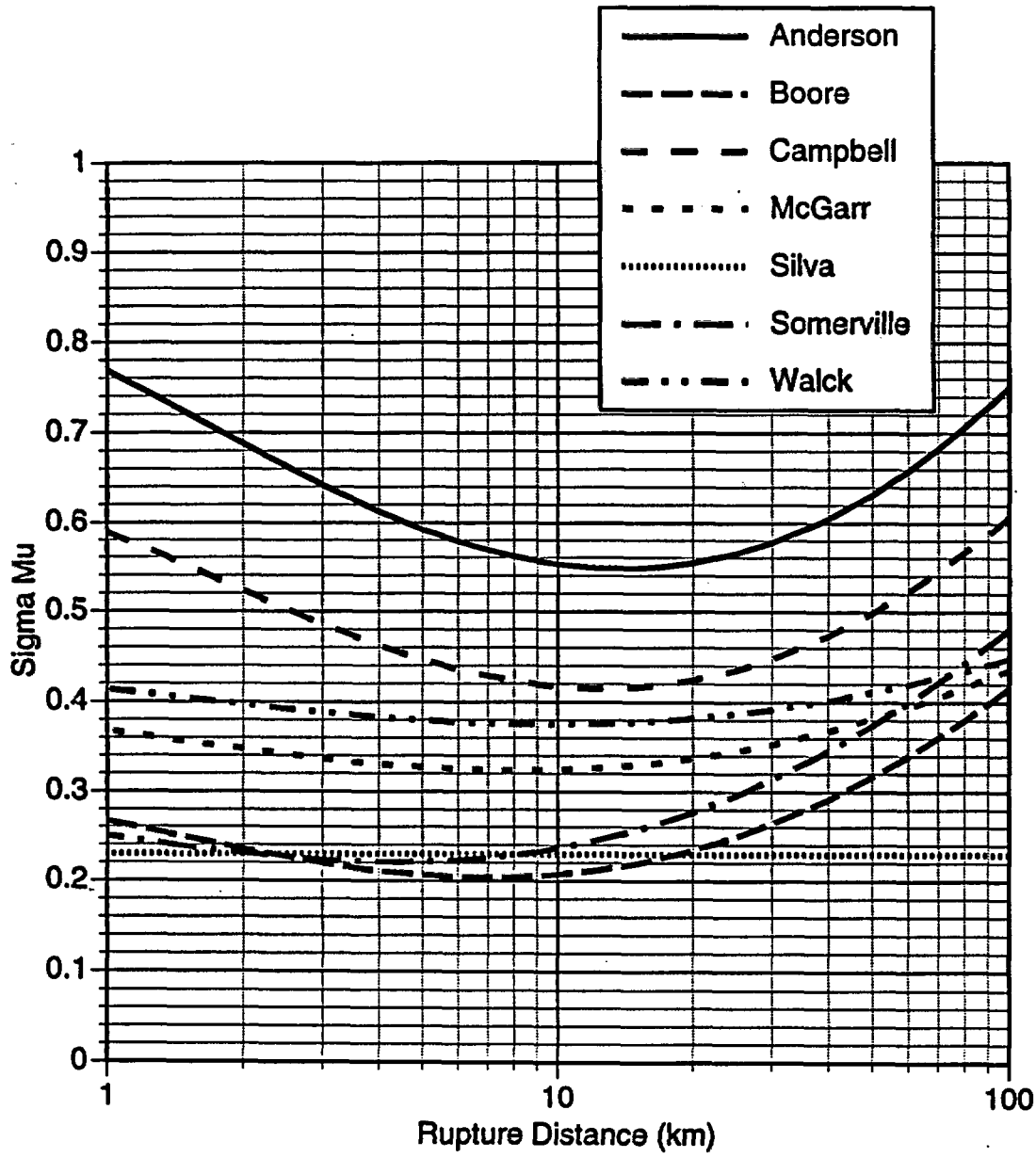

Figure 6-22 Comparison of epistemic uncertainty in the median 1.0 sec vertical spectral acceleration (at 5% damping) for M_w 7.5, normal faulting

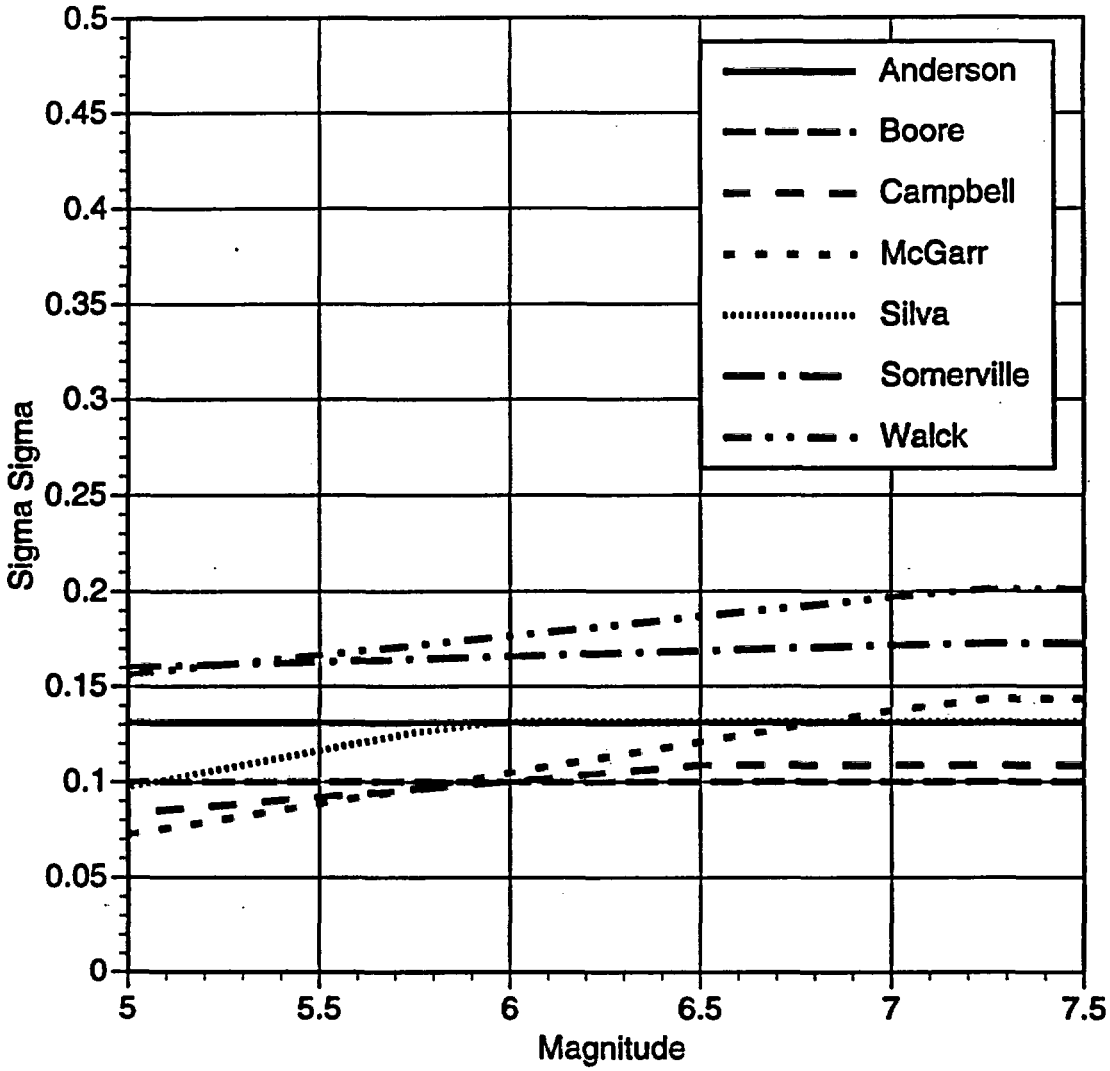

Figure 6-23 Comparison of epistemic uncertainty in the aleatory variability of vertical PGA

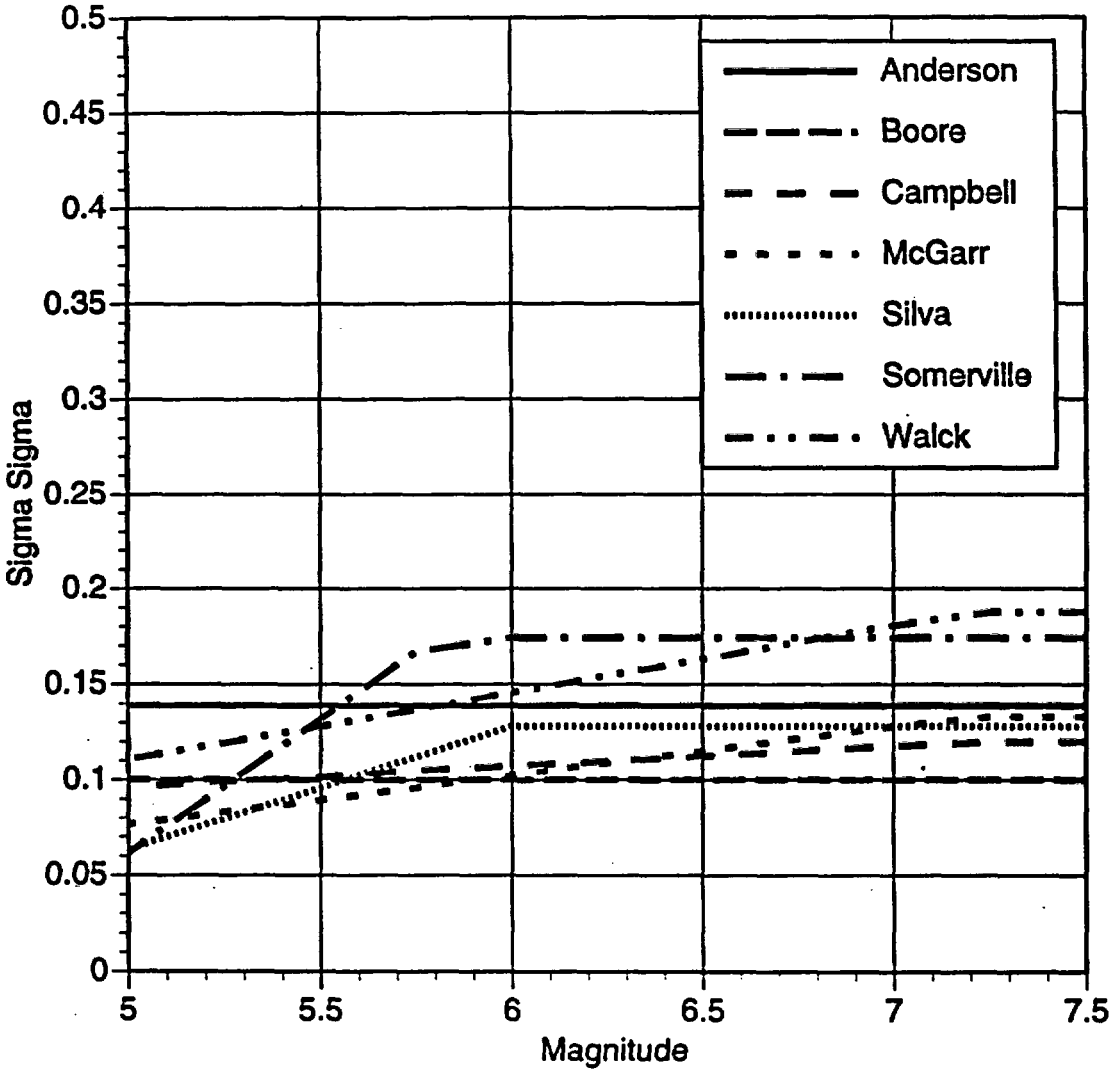

Figure 6-24 Comparison of epistemic uncertainty in the aleatory variability of 1.0 sec vertical spectral acceleration (at 5% damping)

7.0
PSHA METHODOLOGY AND RESULTS FOR GROUND MOTION HAZARD ANALYSIS

This chapter describes the methodology used to perform the PSHA for vibratory ground motion and the resulting calculations for the Yucca Mountain site. Section 7.1 provides an overview of the PSHA approach and introduces some key terms. Section 7.2 provides details about the implementation of the PSHA methodology specifically for the Yucca Mountain site. Section 7.3 presents the seismic hazard results, integrated over all SSFD expert teams and GM experts. Section 7.4 presents sensitivity results divided into three parts: Section 7.4.1, a comparison of hazard results across SSFD expert teams; Section 7.4.2, sensitivity to the alternative models formulated by each SSFD expert team; and Section 7.4.3, sensitivity to GM experts.

The hazard was calculated for reference rock outcrop (Figure 1-1) at the center of the potential repository block between the Solitario Canyon and Ghost Dance faults. The site coordinates are UTM 547.953 km easting, 4077.750 km northing.

7.1 BASIC PSHA MODEL

The methodology to calculate the probabilistic ground motion hazard at a site is well established in the literature (Cornell, 1968, 1971; McGuire, 1976, 1978). Calculation of the hazard requires specification of the following three inputs:

- The geometry of a seismic source (e.g., source i) relative to the site, and a relationship between rupture size and magnitude determine the conditional probability distribution of distance r from the earthquake rupture to the site (given magnitude): $f_{R(i)M(i)}(r,m)$. The types of sources are faults and areal source zones.

- The mean annual rate of occurrence ν_i and magnitude distribution $f_{M(i)}(m)$ of earthquakes occurring on each source i. This characterization includes the M_{max} that a seismic source can produce. The M_w scale is used in all the final hazard calculations.

- An attenuation relation for the estimation of ground motion amplitude (e.g., peak ground acceleration [PGA] or spectral acceleration) at the site as a function of earthquake magnitude and distance. This characterization includes both an equation for the median amplitude and a standard deviation s that describes the site-to-site and event-to-event scatter in ground motion amplitude observations for the same magnitude and distance.

These inputs are illustrated on Figure 7-1, Parts a through c. Figure 7-1a shows the geometry of a seismic source and the distance distribution for a given value of magnitude. The distribution of magnitude $f_{M(i)}(m)$ for an areal source is typically specified as the doubly truncated exponential distribution. Seismicity for a source with the exponential magnitude distribution is completely specified by the minimum magnitude m_o and parameters a and b. Parameter a is a measure of seismic activity, b is a measure of relative frequency of large versus small events, and $\log[\nu_i f_{M(i)}(m)]$ is proportional to bm for $m \leq m_{max}$. Except for truncation effects near M_{max}, this is the well-known Gutenberg-Richter relation. The distribution of magnitude $f_{M(i)}(m)$ for a fault is specified by an exponential distribution, a characteristic distribution (Youngs and Coppersmith, 1985, as illustrated on Figure 2-1b), or a maximum-moment distribution (Wesnousky *et al.*, 1983). The rate information for these three distribution shapes may be specified, respectively, as the rate ν_i, the rate of large earthquakes (magnitude greater than M_{max} - ½), or the slip rate (for faults only).

The ground motion is modeled by an attenuation function, as illustrated on Figure 7-1c. Attenuation functions are usually of the form $ln[A] = f(M,R) + \varepsilon$, where A is ground motion amplitude, M is magnitude, R is distance, and ε is a random variable (with mean zero and standard deviation σ) that represents scatter in $ln[A]$ for the same magnitude and distance. The attenuation function is used to calculate $G_{A|m,r}(a^*) = P[A > a^*|m,r]$: the probability that the ground motion amplitude A is larger than a^*, for a given M and R. The seismic hazard over all sources is calculated as a summation:

$$\nu(a^*) = \sum_i \nu_i \int_r \int_m G_{A|m,r}(a^*)\, f_{M(i)}(m) f_{R(i)/m(i)}\, dm\, dr \qquad (7\text{-}1)$$

in which $\nu(a^*)$ is the annual rate of earthquakes that produce amplitudes $A > a^*$ at the site, and the summation is performed over all seismic sources i. The integration on magnitude in Equation 7-1 considers only earthquakes with magnitudes greater than a minimum magnitude m_o, typically taken as M_w 5. Smaller earthquakes are assumed to produce no damage to engineered structures, regardless of the ground motion amplitudes they generate. Thus, both n_i and $f_{M(i)}(m)$ are only specified for magnitudes greater than m_o, although smaller magnitudes are considered in the determination of the rate and magnitude distribution.

Equation 7-1 is formulated using the assumption that earthquakes (most particularly, successive earthquakes) are independent in size and location. In all seismic hazard applications, primary interest is focused on computing probabilities for the occurrence of high (rare) ground motions (as a result, the probability of two exceedances in 1 year is negligible). Thus, the quantity on the right side of Equation 7-1, which is the annual rate of earthquakes with amplitude $A > a^*$, is a very good approximation to the probability of exceeding amplitude a^* in one year.

The calculation of hazard from all sources is performed for multiple values of a^*. The result is a hazard curve, which gives the annual probability of exceedance as a function of a^*. This calculation is performed for multiple measures of ground motion amplitude (i.e., PGA and spectral acceleration at multiple frequencies).

7.1.1 Treatment of Uncertainty

The most recent PSHA studies distinguish between two types of uncertainty, namely epistemic and aleatory. Aleatory uncertainty (sometimes called randomness) is probabilistic variability that results from natural physical processes. The size, location, and time of the next earthquake on a fault and the details of the ground motion are examples of quantities considered aleatory. In current practice, these quantities cannot be predicted, even with the collection of additional data. Thus, the aleatory component of uncertainty is irreducible. The second category of uncertainty is epistemic (sometimes called simply uncertainty), which results from imperfect knowledge about earthquakes and their effects. An example of epistemic uncertainty is the shape of the magnitude distribution for a given seismic source. In principle, this uncertainty can be reduced with advances in knowledge and the collection of additional data.

These two types of uncertainty are treated differently in advanced PSHA studies. Integration is carried out over aleatory uncertainties to get a single hazard curve (see Equation 7-1), whereas epistemic uncertainties are expressed by incorporating multiple assumptions, hypotheses, models, or parameter values. These multiple interpretations are propagated through the analysis, resulting in a suite of hazard curves and their associated weights. Results are presented as curves showing statistical summaries (e.g., mean, median, fractiles) of the exceedance probability for each ground motion amplitude. The mean and median hazard curves convey the central tendency of the calculated exceedance probabilities. The separation among fractile curves conveys the net effect of epistemic uncertainty about the source characteristics and ground motion prediction on the calculated exceedance probability.

Epistemic uncertainties are associated with each of the three inputs to the seismic-hazard evaluation. The seismogenic potential of faults and other geologic features is uncertain, as a result of (1) uncertainty about the tectonic regime operating in the region and (2) incomplete knowledge of these geological features. The geometry of these geologic features is also uncertain. Uncertainty in the rate of seismicity is generally divided into uncertainty in M_{max}, uncertainty in the type of magnitude distribution, uncertainty in the rate parameter (i.e., activity rate, rate of large events, or slip rate), and uncertainty in b or other shape parameters of the magnitude distribution $f_{M(I)}(m)$. Finally, the attenuation functions are uncertain, which arises from uncertainty about the dynamic characteristics (source, path, and site effects) of earthquake ground motions in the vicinity of Yucca Mountain. This uncertainty is large because few strong motions have been recorded in the region. Uncertainties in seismic source characterization and ground motion attenuation relations were quantified by considering inputs from six SSFD expert teams and seven GM experts, and by each team's and expert's own assessment of uncertainty.

That is, each SSFD expert team formulated multiple alternative interpretations about the seismogenic characteristics of potential seismic sources, and assigned weights to these hypotheses according to their credibility given the current state of knowledge and the degree to which they are supported by data. Each GM expert applied a similar procedure to alternative interpretations about the source, path, and site characteristics affecting ground motions. The development of these seismic source and ground motion interpretations was described previously in Chapters 4.0, 5.0, and 6.0.

7.2 IMPLEMENTATION OF METHODOLOGY IN THIS STUDY

This section describes the PSHA calculation methodology in more detail, with emphasis on methodological developments that were introduced to represent the specific conditions at Yucca Mountain.

7.2.1 Fault Sources

Fault sources were modeled as planar features and their geometry was represented in three dimensions by a fault trace, a dip angle, and minimum and maximum depths. Earthquakes occurring on these faults are treated as having finite, magnitude-dependent length and width, which are calculated using the Wells and Coppersmith (1994) relationship for subsurface rupture length (all fault types).

Due to the presence of closely spaced parallel local faults, all of the SSFD expert teams included scenarios in which ruptures occur simultaneously on two or more of these faults. The teams specified these seismic sources by indicating the associated faults, their occurrence or slip rates, and their magnitude distributions.

The ASM, RYA, SBK, and SDO expert teams specified the multiple-rupture scenarios as having magnitudes comparable to their M_{max} (i.e., these scenarios have maximum-moment magnitude distributions) and always rupturing all the faults involved. Smaller events on these faults are only considered as part of the respective individual sources, which are not mutually exclusive from the multiple-rupture sources.

The AAR and DFS expert teams specified the multiple-rupture sources as having exponential or characteristic magnitude distributions and being capable of single- as well as multiple-rupture events, depending on their magnitude. Each team specified the range of magnitudes associated with ruptures on one fault, two faults, three faults, etc., for each multiple-rupture scenario. These multiple-rupture sources are therefore mutually exclusive from the corresponding single-rupture fault sources.

For events with multiple ruptures, the rupture length and width on each fault are calculated as $L\,n^{-1/5}$ and $Wn^{-1/5}$, respectively, where L is the single-rupture length and W is the single-rupture width given by Wells and Coppersmith (1994), and n is the number of simultaneous ruptures. This equation arises from the assumption that the seismic moment of the multiple-rupture event is divided equally among the various faults and that the stress drop is constant across ruptures and is the same for single-rupture and multiple-rupture events.

The SSFD expert teams specified which simultaneous-rupture sources should be treated as multiple ruptures for the purposes of ground motion evaluation (see below), and which should be treated as single rupture plane events.

The GM experts parameterized ground motion amplitude from multiple-rupture events as a function of the total magnitude of the event, the distance to the closest rupture, and the number of faults that rupture simultaneously. According to some of their interpretations, multiple ruptures affect not only the median amplitude, but also the aleatory and/or the epistemic standard deviations (Section 6.4.1).

7.2.2 Areal Source Zones

Areal source zones are defined by a polygon in latitude-longitude space. In most PSHA studies, areal zones are assumed to have uniform activity rate per unit area (EPRI, 1986; USGS, 1996, constitute notable exceptions). This study allowed for both uniform and variable rates per unit area. Each SSFD expert team specified the approach to use for each areal zone. If they specified variable seismicity, they also specified the degree of smoothing. The teams could also specify that an areal zone could have both uniform and variable seismicity, or multiple degrees of smoothing, by means of alternative branches in the logic tree. The methodology to calculate variable seismicity utilizes the spatial pattern of historical seismicity within the source, as described in Section 4.1.4.1.

Hypocentral depth is considered explicitly in the hazard integration (as part of the calculation of $f_{R(i)M(i)}(r;m)$ in Equation 7-1). The SSFD expert teams specified the distribution of hypocentral depth, as well as optional values for the minimum and maximum depths. All distributions specified are well represented by normal distributions.

The depth distributions specified by the SSFD expert teams are assumed to apply to small events (with negligible source dimensions) and are modified for the effect of magnitude-dependent rupture dimensions. The approach followed is described in Appendix J and is summarized below.

The down-dip rupture width for a given magnitude is calculated using the corresponding relationship by Wells and Coppersmith (1994) and projected into a vertical width using a typical dip angle of 70 degrees. The vertical location of the hypocenter is taken as uniformly distributed over the lower 75% of the vertical width. Using this distribution, we calculate the probability that a certain hypocentral depth is realizable, for a given magnitude. This is simply the probability that the top of the rupture is below ground, given hypocentral depth and rupture width. Viewed as a function of depth, this probability has the shape of a ramp. The resulting magnitude-dependent depth distribution is obtained by multiplying the small-event magnitude distribution by the magnitude-dependent probability that each depth is realizable, and then normalizing so that the distribution integrates to unity. The resulting distribution forces the hypocenters of larger events to greater depths. Figure 7-2 illustrates this calculation. This distribution is consistent with the depths on Figure 9-11 of Pezzopane and Dawson (1996), which shows focal depths as a function of magnitude for events in the Basin and Range Province.

Because the attenuation equations predict amplitude as a function of magnitude and distance to the rupture, a relationship between hypocentral and rupture distance is required. This relationship takes the form of equations for the conditional mean and standard deviation of rupture distance given magnitude and hypocentral distance (Appendix J). The effect of the conditional standard deviation in rupture distance is to make the aleatory uncertainty given hypocentral distance larger than the aleatory uncertainty given rupture distance, as has been observed in the development of empirical attenuation equations (e.g., Campbell, 1981).

7.2.3 Ground Motion Attenuation

Each GM expert characterized epistemic uncertainty in the median amplitude and the ground motion scatter by means of standard deviations σ_μ and σ_σ, respectively. For the purposes of the PSHA calculations, it is necessary to represent these uncertainties as discrete values of the associated "epistemic" variables ε_μ and ε_σ. Following EPRI (1993) and Toro *et al.* (1997),

ε_μ was discretized into four points at locations $\pm 0.74\sigma_\mu$ (weight 0.454) and $\pm 2.33\sigma_\mu$ (weight 0.0454) (Figure 7-3). The variable ε_σ was discretized conditionally on σ_μ, as follows. For $\varepsilon_\mu = \pm 0.74\sigma_\mu$, ε_σ was discretized into three points at 0 (weight 2/3) and $\pm 1.73\ \sigma_\sigma$ (weight 1/6 each). For $\varepsilon_\mu = \pm 2.33\sigma_\mu$, ε_σ was discretized into two points at $\pm 1\sigma_\sigma$ (weight 0.5 each). Each combination of ε_μ and ε_σ is treated as one attenuation equation in the PSHA calculations. The resulting total number of attenuation equations for all seven experts is 70.

7.2.4 Calculations

Hazard calculations for vibratory ground motions for a single SSFD expert team proceeded in two steps, as follows:

1. Calculation of seismic hazard from each individual source: This calculation was performed for each combination of attenuation equation and seismic source parameters resulting in one hazard curve and one weight for each combination.

2. Calculation of total hazard (i.e., the hazard from all seismic sources) and its epistemic uncertainty. For the calculation of quantities other than the mean hazard, this calculation takes into account the probabilistic dependence introduced by hypotheses in the logic tree that affect more than one source. This calculation considers each possible branch of the overall logic tree (which includes attenuation equations as well as seismic source characteristics). The hazard associated with one branch of the logic tree includes only those sources that are active given that branch and only those source parameters that are consistent with that branch. The result of this calculation is a set of mean and fractile hazard curves. (We compute 11 fractiles in order to carry distribution-shape information into the integration step below.)

Calculation of the integrated hazard (across all SSFD expert teams) was performed by combining the expert teams' mean and fractile hazard curves, giving each team equal weight. The result is a set of integrated mean and fractile hazard curves.

In addition to these main results, deaggregation results calculate and display the contributions of various magnitude-distance-ε combinations to the mean hazard. This information is required

for the selection of the magnitude-distance-ε combinations to use in seismic design. Furthermore, sensitivity results provide insights into the effect of various parameters and assumptions on the calculated seismic hazard and its uncertainty.

7.3 INTEGRATED RESULTS

The integrated results provide a representation of seismic hazard and its uncertainty at the site, based on the interpretations and parameters developed by the six SSFD expert teams and seven GM experts. Separate results are obtained for PGA and spectral accelerations at 0.3, 0.5, 1, 2, 5, 10, and 20 Hz. The results for each ground motion measure are in the form of summary hazard curves. Figures 7-4 through 7-6 show the mean and fractile hazard curves for PGA and for 10- and 1-Hz spectral acceleration. The mean and median hazard curves convey the central tendency of the calculated exceedance probabilities. The separation between the 15th and 85th percentile curves conveys the effect of epistemic uncertainty on the calculated exceedance probability. A large portion of this epistemic uncertainty results from epistemic uncertainty in ground motions, as will be shown in Section 7.4.3. Figure 7-7 shows the uniform hazard spectrum (UHS) for 10^{-4} annual exceedance probability, which is calculated from the spectral acceleration hazard curves (PGA is treated as 100-Hz spectral acceleration for these plots).

Figures 7-8 through 7-11 show analogous hazard curves and spectrum for the vertical component of ground motion. Figure 7-12 shows the horizontal and vertical mean UHS for 10^{-4} annual exceedance probability in a tripartite scale. This scale shows the spectrum in terms of spectral acceleration, spectral velocity, and spectral displacement. Table 7-1 lists the mean UHS values for 10^{-3} and 10^{-4} annual exceedance probability, and for both horizontal and vertical motions.

Figures 7-13 and 7-14 show the deaggregation of the mean hazard (for 10^{-4} annual exceedance probability) into magnitude-distance-ε bins, where ε is the difference between the logarithm of the ground motion amplitude and the mean logarithm of ground motion (for that M and R) measured in units of the standard deviation σ of log (ground motion). Figure 7-13 indicates that the 5 to 10-Hz ground motions (and other high-frequency motions as well) are dominated by events of less than M_w 6.5 at distances less than 15 km. In contrast, ground motions at 1 to 2 Hz (and other low-frequency motions as well) contain a sizable contribution from M_w 7 and

greater events at distances beyond 50 km. Results in Section 7.4 will show this contribution is primarily from the Death Valley, Furnace Creek, and Fish Lake Valley faults, which have higher M_{max} and much higher activity rates than the local faults.

7.4 SENSITIVITY RESULTS

Sensitivity results provide insights into the effect of various interpretations and parameters on the calculated seismic hazard and its uncertainty. These results provide insight into the PSHA process. They also provide a consistency check for the experts and analysts.

7.4.1 Comparisons Across SSFD Expert Teams

Figures 7-15 through 7-18 compare the mean hazard curves obtained by the six SSFD expert teams, for PGAs and spectral accelerations at 10, 1, and 0.3 Hz. These results show a reasonable degree of consistency among the mean estimates of the expert teams, with less than a factor of three (in annual exceedance probability) between the lowest and the highest teams. This consistency among experts is likely the result of using a large common information base and of having an elicitation and feedback format that minimizes differences in knowledge or understanding among experts.

7.4.2 Sensitivity Results for Each SSFD Expert Team's Interpretations

Several types of sensitivity results are presented in this section for each SSFD expert team. (AAR, Figures 7-19 through 7-50; ASM, Figures 7-51 through 7-78; DFS, Figures 7-79 through 7-102; RYA, Figures 7-103 through 7-130; SBK, Figures 131 through 156; and SDO, Figures 7-157 through 7-175). Table 7-2 provides a "road map" for these figures, whereas the following text first describes the results generally, then discusses results specifically for each team. The number and type of figures shown vary somewhat between teams, as each team defined different logic trees and different sources.

The most straightforward type of sensitivity results are obtained by deaggregating the calculated mean hazard into contributions by source group, by individual source, or by magnitude-distance-ε bins. Six figures of this type are first presented for each SSFD expert team (three for 10-Hz and three for 1 Hz), as follows:

1. Mean seismic hazard by source type (i.e., local faults, local areal zones, and regional faults). The local fault type is subdivided into single-rupture and multiple-rupture fault sources. This subdivision is based on whether the single-rupture or multiple-rupture attenuation equations apply to a fault or faults, as specified by the SSFD expert team. (Recall that the expert teams specified that the multiple-rupture attenuation equations are applicable to some, but not all, the multiple-rupture fault sources.)

2. Dominant seismic sources, based on their contribution to seismic hazard at 1.1g (for 10 Hz) and at 0.5g (for 1 Hz). Each source is labeled to indicate its type.

3. Magnitude-distance-ε deaggregation of the mean hazard for each source type.

Note two important considerations when examining the figures showing dominant sources. First, the contributions shown on these figures are mean contributions. Thus, the contribution of a source may be written as

P [Source is Active] x Mean Hazard given that the Source is Active

Therefore, a source that can produce a high hazard (if active), but with a low probability of activity, will not necessarily show as having a high contribution to the mean hazard. The importance of this source may be seen in the sensitivity to the logic tree branch that controls whether the source is active. Second, the definition of a "source" for the purposes of this and other figures has some limitations. Consider the Solitario Canyon fault as an example and assume that the SSFD expert team is certain that the fault is active. The Solitario Canyon fault may appear by itself in some branches of the logic tree and also as part of a multiple-rupture source in other branches. These and other figures show separate contributions from Solitario Canyon fault (alone) and from the multiple-rupture source.

Next, sensitivity results with respect to interpretations or parameters are presented separately for a variety of seismic sources. They show the effect of each interpretation or parameter on the calculated seismic hazard from that type of source. Results for the local faults and areal source zones are shown for 10 Hz; results for the regional faults are shown for 1 Hz because these faults are important only at low frequencies. Sensitivities to all global interpretations and

parameters (i.e., those that affect more than one seismic source) were calculated and examined; all important sensitivities are shown here. Sensitivities to source parameters were calculated and examined for the two or three most important sources in each type. Typically, only the results for the most important source in each type are shown here. Results for other sources have smaller contributions to the total uncertainty and are not shown.

Sensitivity results with respect to global interpretations are calculated by computing the mean hazard for each interpretation and then comparing the results obtained with the various interpretations. The weights assigned to the various interpretations or branches of the logic tree are also an important element of these comparisons and are shown (in parentheses) on all figures.

Sensitivity results with respect to source parameters are calculated in a different manner. For instance, to investigate the sensitivity to the M_{max} of the Solitario Canyon fault, the following steps are implemented:

1. Compute the combined hazard from all local faults, for all combinations of global and fault parameters.

2. Group these hazard curves into bins defined so that the parameters of all hazard curves in one bin differ only in the M_{max} for the Solitario Canyon fault (i.e., all other parameters used to compute these hazard curves are the same).

3. For each bin, calculate the mean and standard deviation of hazard and create mean $\pm \sigma$ hazard curves.

4. Compute the average of the mean + σ curves over all bins. Do the same for the mean - σ curves. The resulting difference between the mean - σ and mean + σ curves indicates the sensitivity of the results to uncertainty in the M_{max} of the Solitario Canyon fault. If the fault does not appear in all branches of the logic tree, an additional curve (labeled NA) is also shown, corresponding to the mean hazard from those branches of the logic tree where the fault does not appear. (Recall that the Solitario Canyon fault by itself may not appear in all branches of the logic tree, even if the SSFD expert team considers this fault to be active with certainty.)

This approach is more convenient because source parameters may have distributions that vary as a function of the values of other variables in the logic tree. For instance, the distribution of M_{max} has a range of number of magnitudes, a range of values, and different weights, depending on fault length. Other source parameters, such as the recurrence of areal source zones, have up to 25 different (rate,b) pairs. These factors make it difficult to display and interpret these results in the same manner as the global sensitivity results. It is important to emphasize that this approach shows the mean $\pm$ σ effect *on hazard* of the uncertain parameter, not simply the results associated with the mean - σ and mean + σ values of the parameter.

The following discusses sensitivity results specifically by team. This discussion focuses on the amplitudes associated with 10^{-4} annual exceedance probability (1.1 g for 10 Hz, 0.5 g for 1 Hz). When necessary, the discussion includes a brief description of some elements of a team's seismic source characterization.

7.4.2.1 AAR Team

Figures 7-19 and 7-20 show the contributions of the various source types to the mean hazard. For 10 Hz, both the individual local faults and the areal sources are the major contributors to the hazard. For 1 Hz, the individual local faults, the areal zones, and the regional faults contribute similarly to the hazard.

Figures 7-21 and 7-22 show the contributions of the most important individual seismic sources from all source types. The most important local faults are two coalesced fault systems, namely the East-side (all local faults east of Yucca Mountain; active with a probability of 75%), and West-side #2 (all local faults west of Yucca Mountain except the Solitario Canyon and Iron

Ridge faults, active with a probability of 60%. Both of these fault systems involve simultaneous ruptures on multiple faults. The AAR team associated these fault systems with the single-rupture attenuation equations because most of the seismic moment release is postulated to occur on a single-rupture plane. The most important areal zone is Zone 2, which includes the Nevada Walker Lane, the host areal source zone for Scenario 1 (see Section 4.3.1.1). The most important regional fault is the Death Valley-Furnace Creek fault system, which is also the most important contributor to hazard at 1 Hz.

The 10-Hz deaggregation results (Figure 7-23) show that most of the hazard comes from events of M_w 5 to 6.5 at short distances (<15 km occurring on local faults and generally within areal zones). The 1-Hz results (Figure 7-24) show a shift to higher magnitudes for the local faults and areal sources, and a large contribution from regional faults in the 45 to 60 km distance range and magnitudes greater than M_w 7 (associated with the Death Valley-Furnace Creek fault system).

Figures 7-25 through 7-39 show sensitivity results of the AAR local faults for 10-Hz horizontal spectral acceleration. The major nodes in the AAR global logic tree for local faults represent the existence of NW-SE dextral structures, the type of dextral structure, and the existence of a detachment. Additional branches consider detachment depth, the possibility of coalescence, coalescence pattern (i.e., which groups of faults rupture simultaneously), and seismogenic crustal thickness. The probability of coalesced behavior depends on preceding branches of the logic tree, with a high marginal probability of coalescence. The existence and pattern of coalescence are the only nodes to show significant sensitivity. Other branches of the local fault global logic tree show negligible sensitivity. Of the source parameters for the East-side fault system, recurrence model and recurrence (given the recurrence model and recurrence approach) show moderate sensitivity; b-value, rupture length, M_{max}, and recurrence approach show low sensitivity. Similar trends are observed in the sensitivity to the parameters of the West-side fault system (only results for recurrence model are shown here).

Figures 7-40 through 7-44 show sensitivity results for the AAR areal zones and 10-Hz horizontal spectral acceleration. The major nodes in the AAR global logic tree for areal zones represent three scenarios with differing areal zone configurations, and a fourth scenario containing only one areal zone. The first three scenarios use uniform seismicity; the fourth

scenario uses variable seismicity, with four alternative degrees of smoothing. In all scenarios, a portion of the host areal source zone (20-km radius around the site), is assigned a lower M_{max} by the AAR team due to more detailed knowledge of local fault sources. Sensitivity to scenario and to spatial variability is important. Sensitivity to minimum magnitude used in the recurrence calculations, M_{max}, and recurrence is low.

Figures 7-45 through 7-50 show sensitivity results for the AAR regional faults and 1-Hz spectral acceleration. The only regional faults that make any significant contribution to the hazard are Death Valley and Furnace Creek faults, which may be linked (i.e., rupture together, probability 80%) or independent (i.e., rupture separately, probability 20%). Sensitivity to the recurrence of the Death Valley-Furnace Creek fault system is moderate; sensitivity is low for other global and source parameters (i.e., linked vs. independent, fault lengths, sense of slip, recurrence used, dip angles, b-values, and M_{max}).

7.4.2.2 ASM Team

Figures 7-51 and 7-52 show the contributions of the various source types to the mean hazard. For 10 Hz, both the areal source zones and the single-rupture local faults are the major contributors to the hazard. For 1 Hz, the single-rupture local faults, the areal zones, and the regional faults contribute significantly to the hazard.

Figures 7-53 and 7-54 show the contributions of the most important individual seismic sources from all types of sources. The Walker Lane areal source is dominant, both at 10 Hz and 1 Hz, and its contribution is a factor of two or three larger than that of the next source. Important local faults include Stagecoach Road-Paintbrush Canyon and Solitario Canyon faults. Important regional faults include the Furnace Creek and Death Valley faults.

The 10-Hz deaggregation results (Figure 7-55) show that most of the hazard comes from short distances (<15 km), either M_w 5 to 6.5 events from the areal zones or M_w 5 to 7 events on the local faults. The 1-Hz results (Figure 7-56) show a shift to higher magnitudes for the local faults and areal zones, and a large contribution from regional faults in the 45 to 60 km distance range and magnitudes greater than M_w 7 to 7.5 associated with the Furnace Creek and Death Valley faults.

Figures 7-57 through 7-69 show sensitivity results of the ASM local faults for 10-Hz horizontal spectral acceleration. The major nodes in the ASM global logic tree for local faults consider the existence of a detachment and whether the detachment is seismogenic, the existence of a buried strike-slip fault and whether it is seismogenic, whether the faults merge at depth, the occurrence of simultaneous ruptures, the recurrence approach used, and dip angles. The type of recurrence approach (slip rates versus recurrence intervals) and the occurrence of simultaneous ruptures are the only nodes that show significant sensitivity. Of the source parameters of the Stagecoach Road-Paintbrush Canyon fault system, the recurrence model and recurrence (given the recurrence model and recurrence approach) show significant sensitivity.

Figures 7-70 through 7-73 show sensitivity results of the ASM areal zones for 10-Hz horizontal spectral acceleration. The only node in the ASM global logic tree for areal zones corresponds to the choice of alternative seismicity catalogs. The two areal zones (Walker Lane and Basin and Range) use uniform seismicity. Sensitivity to the catalog used is very low. Sensitivity to source parameters of the Walker Lane source (i.e., recurrence and M_{max}) is low. Figure 7-73 shows the sensitivity to the M_{max} of the Walker Lane source for 1-Hz horizontal spectral acceleration. This sensitivity is also low, although somewhat higher than the one for 10 Hz shown on Figure 7-71.

Figures 7-74 through 7-78 show sensitivity results for the ASM regional faults and 1-Hz horizontal spectral acceleration. The only regional faults that make any significant contribution to the hazard are the Furnace Creek and middle Death Valley faults. The global logic tree for regional faults has nodes to represent recurrence model, recurrence approach, b-value, and maximum depth. Sensitivity to all these nodes is low. Sensitivity to recurrence and M_{max} is also low.

7.4.2.3 DFS Team

Figures 7-79 and 7-80 show the contributions of the various source types to the mean hazard. For 10 Hz, both the individual local faults and the areal zones are the major contributors to the hazard. For 1 Hz, the individual local faults and areal zones contribute equally to the hazard; the regional faults contribute slightly less.

Figures 7-81 and 7-82 show the contributions of the most important individual seismic sources from all source types. The most important local faults are the Stagecoach Road-Paintbrush Canyon fault system and the Solitario Canyon fault. The most important areal zone for both 10-Hz and 1-Hz motions is the East Walker Lane for their Model B, which includes a local host areal zone. The most important regional fault is the Death Valley-Furnace Creek fault system, which is a moderate contributor to hazard at 1 Hz.

The 10-Hz deaggregation results (Figure 7-83) show that most of the hazard comes from short distances (<15 km), and M_w 5 to 6.5 events for local faults or M_w 5 to 7 events for areal sources. The 1-Hz results (Figure 7-84) show a shift to higher magnitudes for the local faults and areal zones (with a shift to longer distances in the latter), and a moderate contribution from regional faults in the 45 to 60 km range and M_w 6.5 to 7.5 associated with the Death Valley, Furnace Creek, and Fish Lake Valley faults.

Figures 7-85 through 7-92 show sensitivity results of the DFS local faults for 10-Hz horizontal spectral acceleration. The major nodes in the DFS global logic tree for local faults consider the presence of independent versus multiple-fault ruptures, the subsurface geometry (planar versus detached, with two planar-fault scenarios) and multiple-fault rupture scenarios, the recurrence model, and the b-value. Sensitivity to the presence of multiple-fault ruptures versus independent faulting is important although the multiple branch has low weight, so that the resulting uncertainty is low. Sensitivity to other nodes in the global logic tree is low. Sensitivity to M_{max} and the recurrence of the Stagecoach Road-Paintbrush Canyon fault system is also low.

Figures 7-93 through 7-97 show sensitivity results of the DFS areal zones for 10-Hz horizontal spectral acceleration. The major nodes in the DFS global logic tree for areal zones represent the catalog used, zonation (one model with three source zones, the other with a single zone), and spatial variability and smoothing of seismicity within a source. The host zones included in both models contain a small local portion with a lower M_{max}. The sensitivity to spatial smoothing is low to moderate; all other sensitivities to global parameters are low. Sensitivities to M_{max} and the recurrence are also low.

Figures 7-98 through 7-102 show sensitivity results for the DFS regional faults and 1-Hz horizontal spectral acceleration. The major nodes in the DFS global logic tree for regional faults represent recurrence model, maximum depth, and b-value. Sensitivity to these three quantities is low. Sensitivity to the slip rate of the Death Valley fault is moderate, but the sensitivity to the corresponding M_{max} is low.

7.4.2.4 RYA Team

Figures 7-103 and 7-104 show the contributions of the various source types to the mean hazard. For 10 Hz, the single- and multiple-rupture local faults, together with the areal zones, are the major contributors to the hazard. For 1 Hz, the regional faults contribute the most, but the other source types also have important contributions to seismic hazard.

Figures 7-105 and 7-106 show the contributions of the most important individual seismic sources from all source types. The most important local faults are the Paintbrush Canyon-Stagecoach Road-Bow Ridge and the West-side coalesced fault systems. The latter involves the Solitario Canyon, Iron Ridge, Windy Wash, and Fatigue Wash faults, and is associated with the multiple-rupture attenuation equations. The most important areal source zones are A2 and A1: two alternative geometries for a small host source. The most important regional faults are the Furnace Creek and Death Valley, which are also the two most important contributors to hazard at 1 Hz.

The 10-Hz deaggregation results (Figures 7-107) show that most of the hazard comes from short distances (<15 km) and M_w 5 to 6.5 events for areal sources and M_w 5 to 7.0 events for local faults. The 1-Hz results (Figure 7-108) show a large contribution from regional faults in the 45 to 75 km range and M_w 6.5 to 7.5 associated with the Death Valley and Furnace Creek faults.

Figures 7-109 through 7-119 show sensitivity results of the RYA local faults for 10-Hz horizontal spectral acceleration. The major nodes in the RYA global logic tree for local faults represent maximum fault depth, coalescence model, b-values, fault lengths, and recurrence approach. Sensitivity is significant only for recurrence approach, and moderate for fault lengths. Other sensitivity branches are low. Sensitivity to the source parameters (recurrence model, M_{max}, and recurrence) of the East-side faults, the Paintbrush Canyon-Stagecoach Road-

Bow Ridge fault system is low to moderate. Sensitivity to the M_{max} and recurrence of the West-side fault system is moderate.

Figures 7-120 through 7-124 show sensitivity results of the RYA areal zones for 10-Hz horizontal spectral acceleration. The major nodes in the RYA global logic tree for areal zones represent choice of catalog used, zonation, and spatial smoothing of seismicity (in all but the host source). Sensitivity to all these branches is low. Sensitivity to the M_{max} and the recurrence of A2 zone is also low.

Figures 7-125 through 7-130 show sensitivity results of the RYA regional faults for 1-Hz horizontal spectral acceleration. The major nodes in the RYA global logic tree for regional faults are the configuration of the Death Valley-Furnace Creek fault system (linked or separate), the recurrence model, the maximum fault depth, and the b-value. Sensitivity to all of these branches is low. Sensitivity to the M_{max} and recurrence of the Furnace Creek fault is also low.

7.4.2.5 SBK Team

Figures 7-131 and 7-132 show the contributions of the various source types to the mean hazard. For 10 Hz, the single-rupture local faults are the major contributors to the hazard. For 1 Hz, the regional faults and the single-rupture local faults are the major contributors.

Figures 7-133 and 7-134 show the contributions of the most important individual seismic sources from all source types. The most important local faults are the Paintbrush Canyon-Stagecoach Road and Solitario Canyon faults. The most important areal zone is the Basin and Range zone, which is the host source zone. The most important regional fault is the Furnace Creek fault, which is also the most important contributor to hazard at 1 Hz.

The 10-Hz deaggregation results (Figure 7-135) show that most of the hazard comes from individual local faults; events at short distances (<15 km) and M_w 5 to 7. The 1-Hz results (Figure 7-136) show a large contribution from regional faults in the 45 to 60 km range and M_w 7 to 7.5 (associated with the Death Valley-Furnace Creek-Fish Lake Valley fault system).

Figures 7-137 through 7-144 show sensitivity results of the SBK local faults for 10-Hz horizontal spectral acceleration. The major nodes in the SBK global logic tree for local faults

represent fault behavior (independent, linked, coalesced, or detachment), fault dip, maximum depth, and b-value. Sensitivity to all of these nodes is low. Sensitivity to recurrence approach and recurrence model of the Paintbrush Canyon-Stagecoach Road fault system is moderate to low; sensitivity to other source parameters (M_{max} and recurrence) is low.

Figures 7-145 through 7-149 show sensitivity results of the SBK areal sources for 10-Hz spectral acceleration. The major nodes in the SBK global logic tree for areal zones represent zonation, choice of catalog (treated as independent across source zones), and adjustment for NTS events. Sensitivity to these nodes is low. Sensitivity to source parameters of the Basin and Range zone is moderate for recurrence and low for M_{max}.

Figures 7-150 through 7-156 show sensitivity results for the SBK regional faults and 1-Hz horizontal spectral acceleration. The major nodes in the SBK global logic tree for regional faults represent the rupture behavior of the Death Valley-Furnace Creek-Fish Lake Valley fault system, sense of slip of the Death Valley fault, maximum depth, dip angles, and b-values. Sensitivity is high for the scenario in which all faults in the Death Valley-Furnace Creek-Fish Lake Valley fault system are linked. The resulting contribution to uncertainty is low, however, because the branch associated with this scenario has a very low probability. Sensitivity to other global branches is low. Sensitivity is low for source characteristics of the Furnace Creek fault (i.e., recurrence approach, recurrence model, M_{max}, and recurrence).

7.4.2.6 SDO Team

Figures 7-157 and 7-158 show the contributions of the various source types to the mean hazard. For 10 Hz, both the single-rupture local faults and the areal source zones are the major contributors to the hazard. For 1 Hz, the single-rupture local faults, the areal zones, and the regional faults contribute equally to the hazard.

Figures 7-159 and 7-160 show the contributions of the most important individual seismic sources from all source types. The most important local fault is Solitario Canyon fault. The most important areal zone is Zone 1, the host zone, which represents the Walker Lane. Zone 1 is also the largest contributor to hazard at both 10 Hz and 1 Hz. The most important regional fault is the Furnace Creek fault.

The 10-Hz deaggregation results (Figure 7-161) show that most of the hazard comes from short distances (<15 km) and M_w 5 to 6.5 events for areal zones or M_w 5 to 7 events for local faults. The 1-Hz results (Figure 7-162) show a large contribution from regional faults, with a peak in the 45 to 60 km distance range and M_w 7 to 7.5 associated with the Death Valley and Furnace Creek faults. In addition, regional faults at other distances significantly contribute.

Figures 7-163 through 7-167 show sensitivity results of the SDO local faults for 10-Hz horizontal spectral acceleration. The SDO global logic tree for local faults considers only the b-value. Multiple-rupture scenarios are treated as part of the aleatory model (e.g., over time, some events involve multiple simultaneous ruptures, others involve single ruptures). Sensitivity to b-values is very low. Source parameters for the local faults include maximum depth, recurrence model, M_{max}, and recurrence. Sensitivity to these parameters is shown for the Solitario Canyon fault, and found to be low.

Figures 7-168 through 7-171 show sensitivity results of the SDO areal zones for 10-Hz spectral acceleration. The major nodes in the SDO global logic tree for areal zones represent choice of catalog and spatial variability and smoothing of seismicity within an areal zone. Sensitivity to choice of catalogs is moderate, with Version 8 giving a hazard that is roughly half the hazard from either of the other two catalogs. Sensitivity to spatial variability is low. Sensitivity to the parameters of Zone 1 (i.e., M_{max} and recurrence) is also low.

Figures 7-172 through 7-175 show sensitivity results for the SDO regional faults and 1-Hz horizontal spectral acceleration. The major nodes in the SDO global logic tree for regional faults represent maximum depth, recurrence model, and b-value. Sensitivity to these nodes is low. Source parameters include fault length, M_{max}, and activity rates. Sensitivity to these parameters for the Furnace Creek fault is low.

7.4.2.7 Overall Trends

The sensitivity results for all SSFD expert teams indicate the following general trends:

- Seismic source parameters with a direct effect on activity rates (e.g., recurrence approach [either slip rates or recurrence intervals], and recurrence model [characteristic, exponential, or maximum moment] are the parameters that contribute the most to uncertainty in seismic hazard, for the exceedance probabilities of interest in this study.

- M_{max} has a small effect on uncertainty for the exceedance probabilities of interest in this study, especially for 10 Hz, because a large fraction of the hazard comes from more frequent moderate-magnitude events.

- Geometric fault parameters (e.g., rupture lengths, dips, maximum depths) are minor contributions to uncertainty. These parameters have a moderate effect on the locations of earthquakes and an effect on M_{max}, but do not affect earthquake frequency. (Fault geometry affects occurrence rates when activity is specified by slip rates. However, the increased activity that results from increased length of a fault that comes near the site [and whose closest approach to the site is the perpendicular distance] will occur away from the site and will have little effect on the hazard)

- Although expert teams vary somewhat, the dominant sources for seismic hazard at 10 Hz are the Paintbrush Canyon-Iron Ridge faults, the Solitario Canyon fault (or coalesced fault systems including these two faults), and the host areal zone (not necessarily in that order). At 1 Hz, the dominant sources are the Death Valley-Furnace Creek fault system and the same three sources mentioned above.

- Multiple-rupture scenarios of the type with comparable seismic moment release on more than one fault (i.e., those requiring modification of the attenuation equations) make a small contribution to the total hazard for five of the six expert teams.

- All expert teams considered the existence of buried strike-slip faults and seismogenic detachments. Several of them explicitly included these sources in their models. The contribution of these sources to the total seismic hazard is negligible primarily because the corresponding branches in the logic tree have low probabilities. This is also true for volcanic sources of seismicity, which were explicitly considered by only two expert teams.

7.4.3 Sensitivity to Ground Motion Experts and Parameters

Figures 7-176 through 7-185 show the sensitivity of the total hazard to the GM experts and their interpretations. These comparisons all use the seismic source interpretations by the ASM team

as an example. Results are shown for 10 Hz, 1 Hz, and 0.3 Hz. Three types of figures are shown, as follows:

1. Mean hazard calculated using the interpretations by each GM expert.

2. Mean hazard curves for all values of $\varepsilon_{\mu,}$, the parameter that scales each expert's median prediction to represent the expert's assessment of epistemic uncertainty in the median ground motion. These figures show the contribution of σ_μ to uncertainty in the hazard. σ_μ also has an effect on the mean hazard, because of the skewness of the lognormal distribution of ε_μ.

3. Mean $\pm$ σ curves showing the effect of σ_σ (each expert's assessment of epistemic uncertainty in σ) on the uncertainty in the calculated hazard (see the discussion of this type of sensitivity results in Section 3.3.2). σ_σ also affects the mean hazard, because the calculated seismic hazard is a nonlinear function of σ (with a positive second derivative).

In general, the most important ground motion contributors to uncertainty in the hazard are σ_μ and σ_σ (i.e., within-expert uncertainties), rather than expert-to-expert uncertainties. The moderate expert-to-expert variation is likely the result of using a common information base and of having an elicitation and feedback format that minimizes differences in knowledge and understanding among experts.

Other sensitivity results (not included in this report) indicate that the effect of σ_μ is higher for Anderson, and to a lesser extent for Boore, than for the other GM experts. This is one of the factors that make Anderson's results higher. The effect of σ_σ is more uniform across GM experts.

The importance of σ_σ increases as frequency decreases. This is consistent with the magnitude-distance-ε distributions on Figures 7-13 and 7-14, which show that the contribution from events with $\varepsilon > 2$ is more important for 1 Hz than for 10 Hz.

The total uncertainty due to ground motion issues (i.e., the combined expert-to-expert and within-expert uncertainties) is larger than the uncertainty due to seismic source-characterization issues. This conclusion may be qualitatively confirmed by comparing Figures 7-5 and 7-177. This is a common situation in multiple-expert PSHA studies.

In summary, the major contributor to epistemic uncertainty in seismic hazard is the uncertainty in ground motion amplitude that was expressed by each individual GM expert (within-expert epistemic uncertainty). Additional contributions to epistemic uncertainty arise from moderate differences among the SSFD expert teams and among the GM experts, as well as from the uncertainties expressed by the seismic source logic trees.

TABLE 7-1
MEAN UNIFORM HAZARD SPECTRAL VALUES (g)
FOR REFERENCE ROCK OUTCROP

Freq. (Hz)	Horizontal		Vertical	
	10^{-3}	10^{-4}	10^{-3}	10^{-4}
0.3	0.051	0.168	0.029	0.105
0.5	0.091	0.278	0.046	0.159
1	0.162	0.471	0.073	0.222
2	0.263	0.782	0.130	0.406
5	0.346	1.083	0.200	0.660
10	0.355	1.160	0.250	0.906
20	0.284	0.951	0.225	0.853
PGA	0.169	0.534	0.112	0.391

TABLE 7-2
GUIDE TO WITHIN-TEAM SENSITIVITY RESULTS

Figure Numbers	Team	Description
7-19 through 7-20	AAR	Mean hazard by source group
7-21 through 7-22	AAR	Dominant seismic sources
7-23 through 7-24	AAR	M-R- deaggregation by source group
7-25 through 7-32	AAR	Local faults, sens. to global parameters
7-33 through 7-39	AAR	Local faults, sens. to source parameters
7-40 through 7-41	AAR	Area sources, sens. to global parameters
7-42 through 7-44	AAR	Area sources, sens. to source parameters
7-45 through 7-46	AAR	Regional faults, sens. to global parameters
7-47 through 7-50	AAR	Regional faults, sens. to source parameters
7-51 through 7-52	ASM	Mean hazard by source group
7-53 through 7-54	ASM	Dominant seismic sources
7-55 through 7-56	ASM	M-R- deaggregation by source group
7-57 through 7-65	ASM	Local faults, sens. to global parameters
7-66 through 7-69	ASM	Local faults, sens. to source parameters
7-70	ASM	Area sources, sens. to global parameters
7-71 through 7-73	ASM	Area sources, sens. to source parameters
7-74 through 7-76	ASM	Regional faults, sens. to global parameters
7-77 through 7-78	ASM	Regional faults, sens. to source parameters
7-79 through 7-80	DFS	Mean hazard by source group
7-81 through 7-82	DFS	Dominant seismic sources
7-83 through 7-84	DFS	M-R- deaggregation by source group
7-85 through 7-90	DFS	Local faults, sens. to global parameters
7-91 through 7-92	DFS	Local faults, sens. to source parameters
7-93 through 7-95	DFS	Area sources, sens. to global parameters
7-96 through 7-97	DFS	Area sources, sens. to source parameters
7-98 through 7-100	DFS	Regional faults, sens. to global parameters
7-101 through 7-102	DFS	Regional faults, sens. to source parameters

TABLE 7-2 (continued)

Figure Numbers	Team	Description
7-103 through 7-104	RYA	Mean hazard by source group
7-105 through 7-106	RYA	Dominant seismic sources
7-107 through 7-108	RYA	M-R- deaggregation by source group
7-109 through 7-113	RYA	Local faults, sens. to global parameters
7-114 through 7-119	RYA	Local faults, sens. to source parameters
7-120 through 7-122	RYA	Area sources, sens. to global parameters
7-123 through 7-124	RYA	Area sources, sens. to source parameters
7-125 through 7-128	RYA	Regional faults, sens. to global parameters
7-129 through 7-130	RYA	Regional faults, sens. to source parameters
7-131 through 7-132	SBK	Mean hazard by source group
7-133 through 7-134	SBK	Dominant seismic sources
7-135 through 7-136	SBK	M-R- deaggregation by source group
7-137 through 7-140	SBK	Local faults, sens. to global parameters
7-141 through 7-144	SBK	Local faults, sens. to source parameters
7-145 through 7-147	SBK	Area sources, sens. to global parameters
7-148 through 7-149	SBK	Area sources, sens. to source parameters
7-150 through 7-152	SBK	Regional faults, sens. to global parameters
7-153 through 7-156	SBK	Regional faults, sens. to source parameters
7-157 through 7-158	SDO	Mean hazard by source group
7-159 through 7-160	SDO	Dominant seismic sources
7-161 through 7-162	SDO	M-R- deaggregation by source group
7-163	SDO	Local faults, sens. to global parameters
7-164 through 7-167	SDO	Local faults, sens. to source parameters
7-168 through 7-169	SDO	Area sources, sens. to global parameters
7-170 through 7-171	SDO	Area sources, sens. to source parameters
7-172	SDO	Regional faults, sens. to global parameters
7-173 through 7-175	SDO	Regional faults, sens. to source parameters

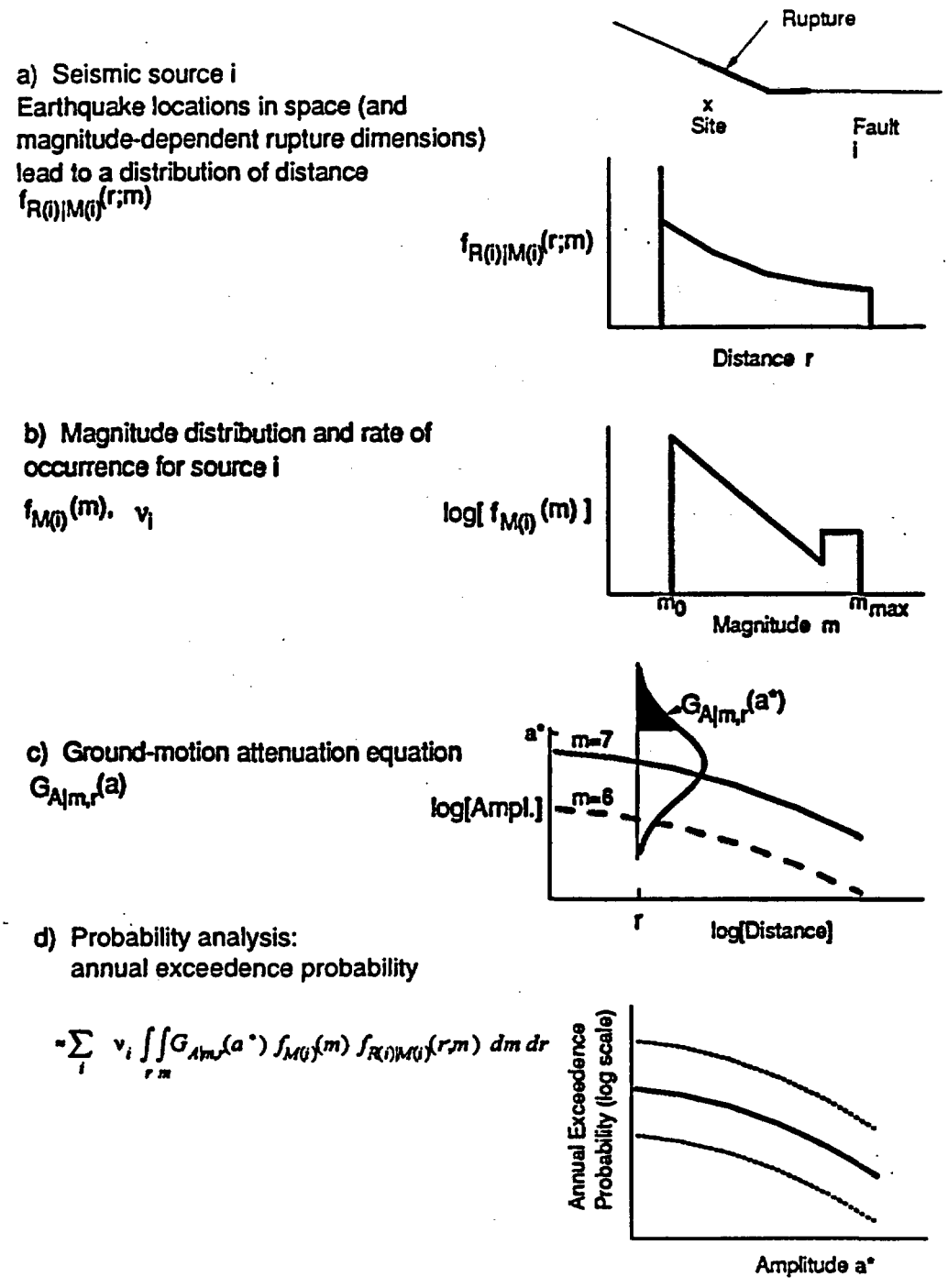

Figure 7-1 Seismic hazard computational model (modified from McGuire and Arabasz, 1990)

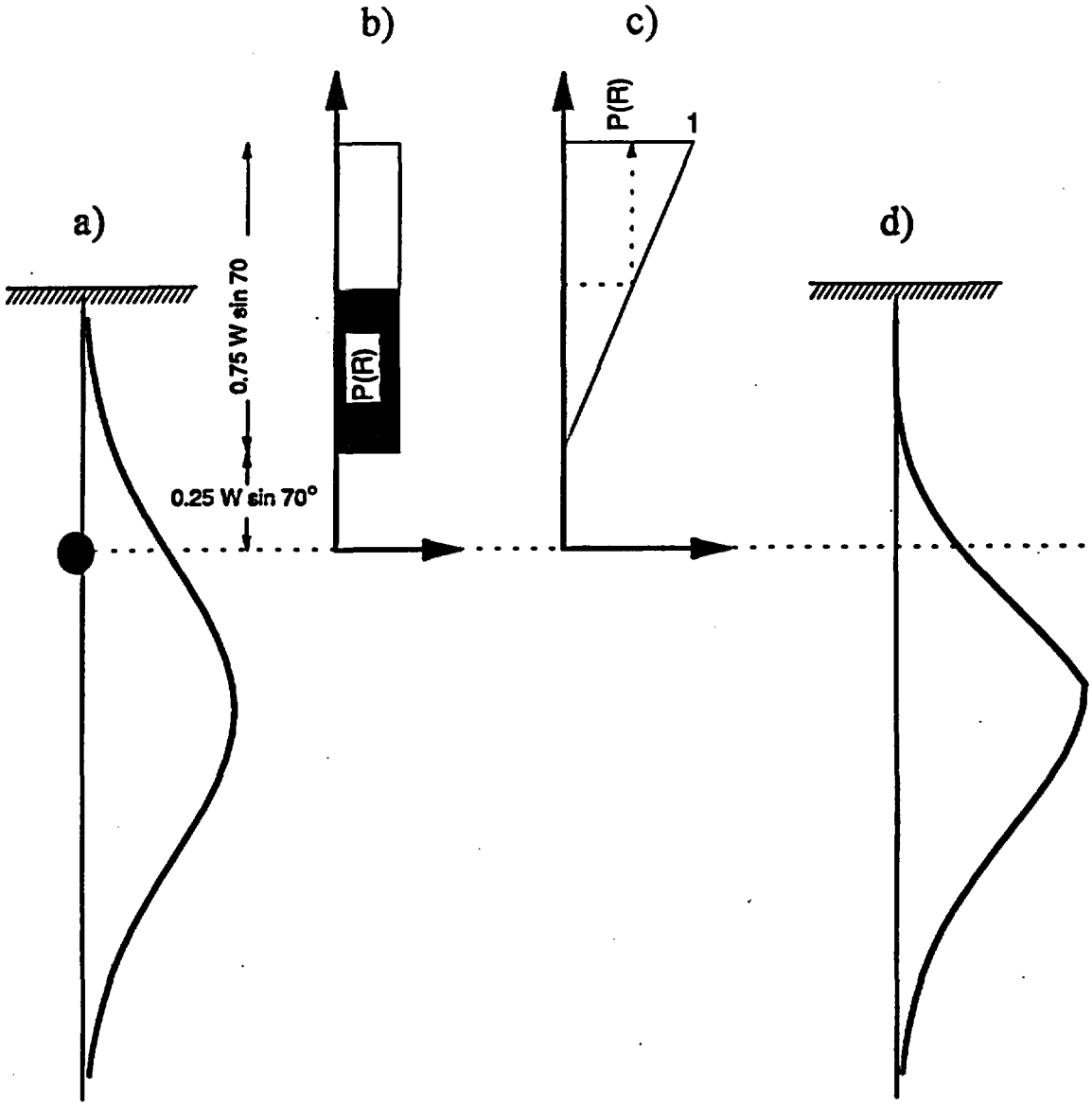

Figure 7-2 Calculation of hypocentral depth distribution for area sources considering the dimensions of the rupture. a) Normal distribution of depth for small events; the solid ellipse indicates a hypothetical hypocentral location. b) probability density function for the location of the top of the rupture. W is the magnitude-dependent rupture width. The probability P(R) that the event is realizable is the probability that the top of the rupture is below the ground surface (the shaded area). c) cumulative distribution function for the location of the top of the rupture, showing P(R). d) Distribution of depth for event with finite width W. This distribution is obtained by multiplying the distribution in (a) by P(R) and normalizing to an area of 1.

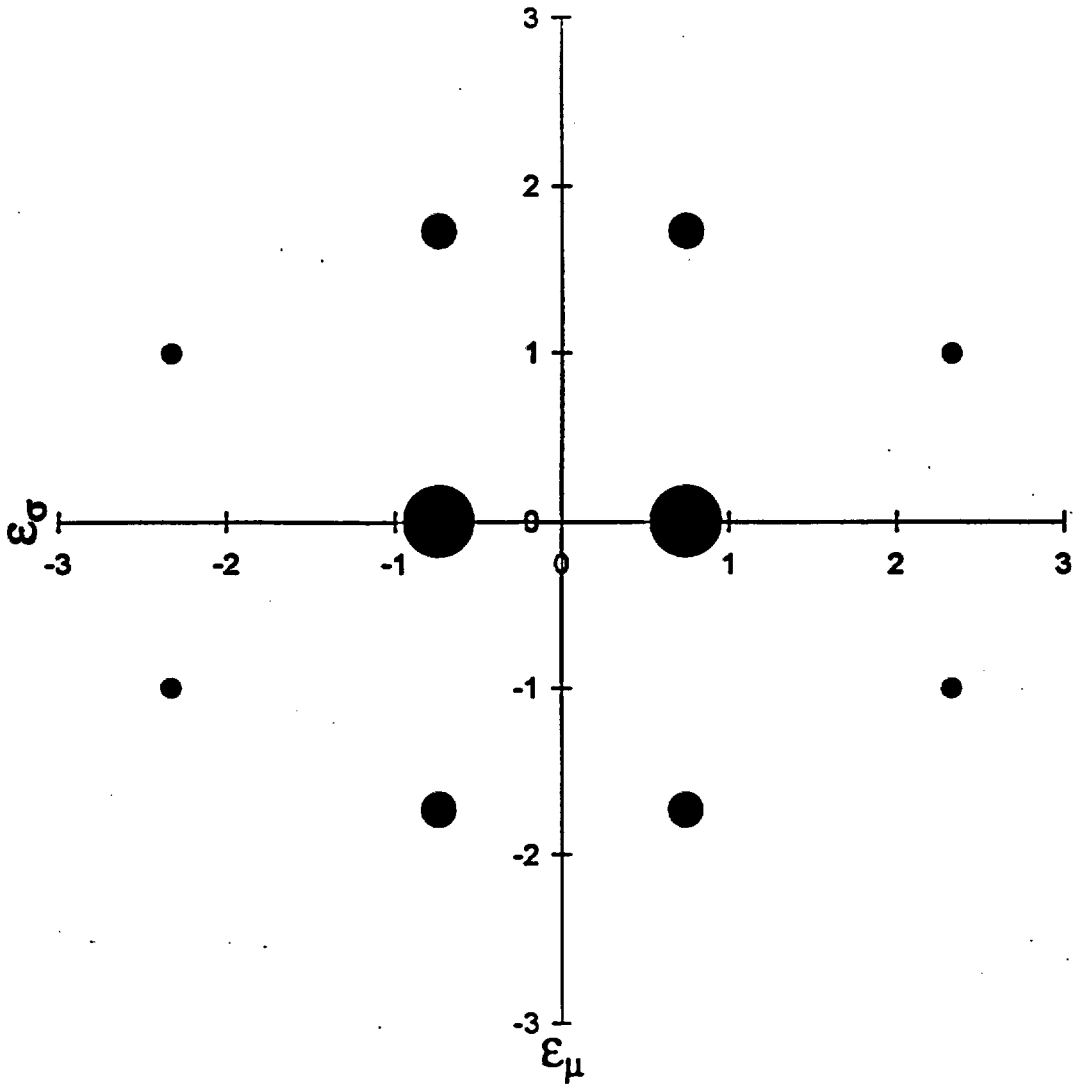

Figure 7-3 Discretization of the joint distribution of ε_μ (horizontal axis) and ε_σ (vertical axis) used to represent within-expert epistemic uncertainty in ground motions. The areas of the circles are proportional to the weights for the corresponding points.

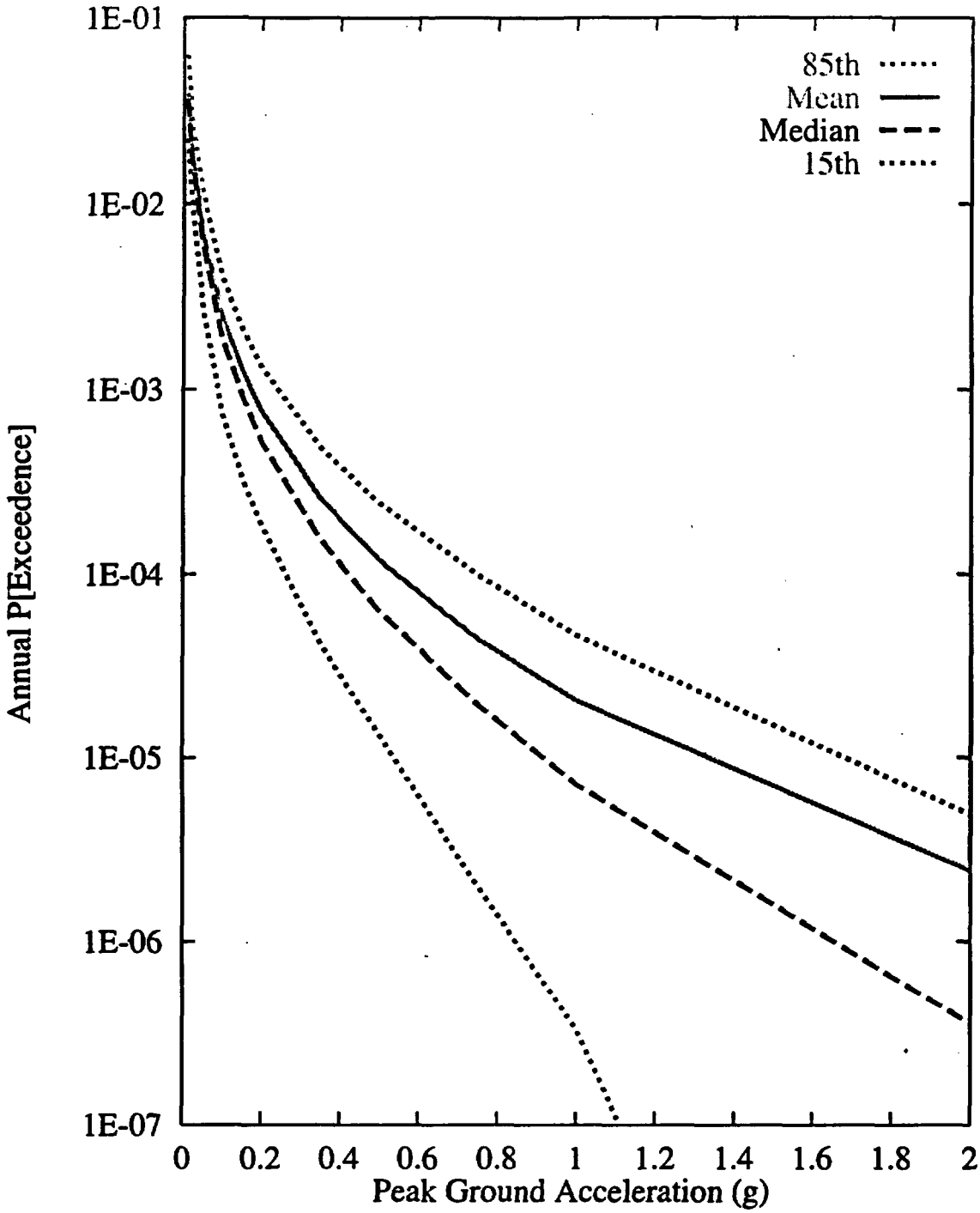

Figure 7-4 Integrated seismic hazard results: summary hazard curves for horizontal PGA

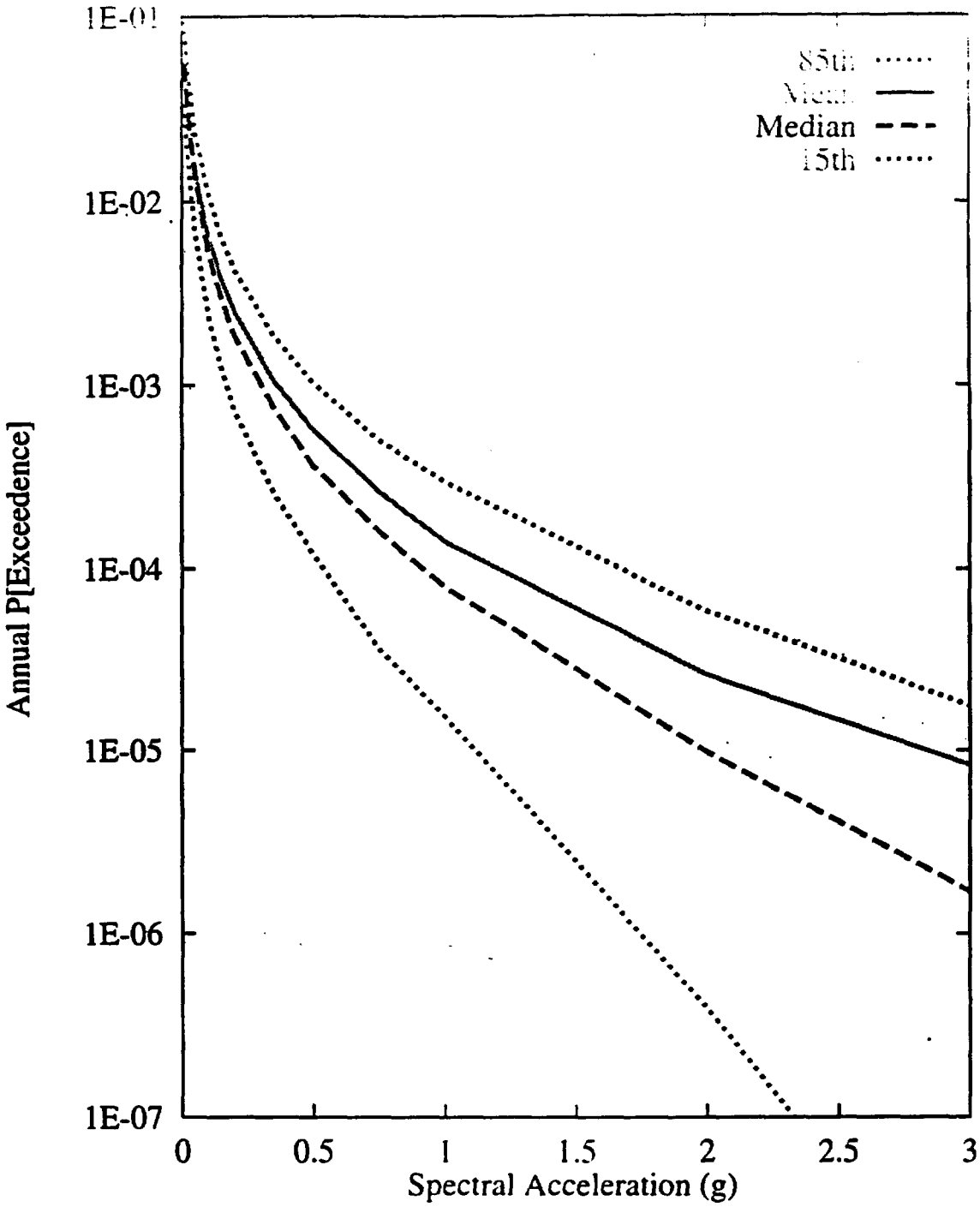

Figure 7-5 Integrated seismic hazard results: summary hazard curves for 10-Hz horizontal spectral acceleration

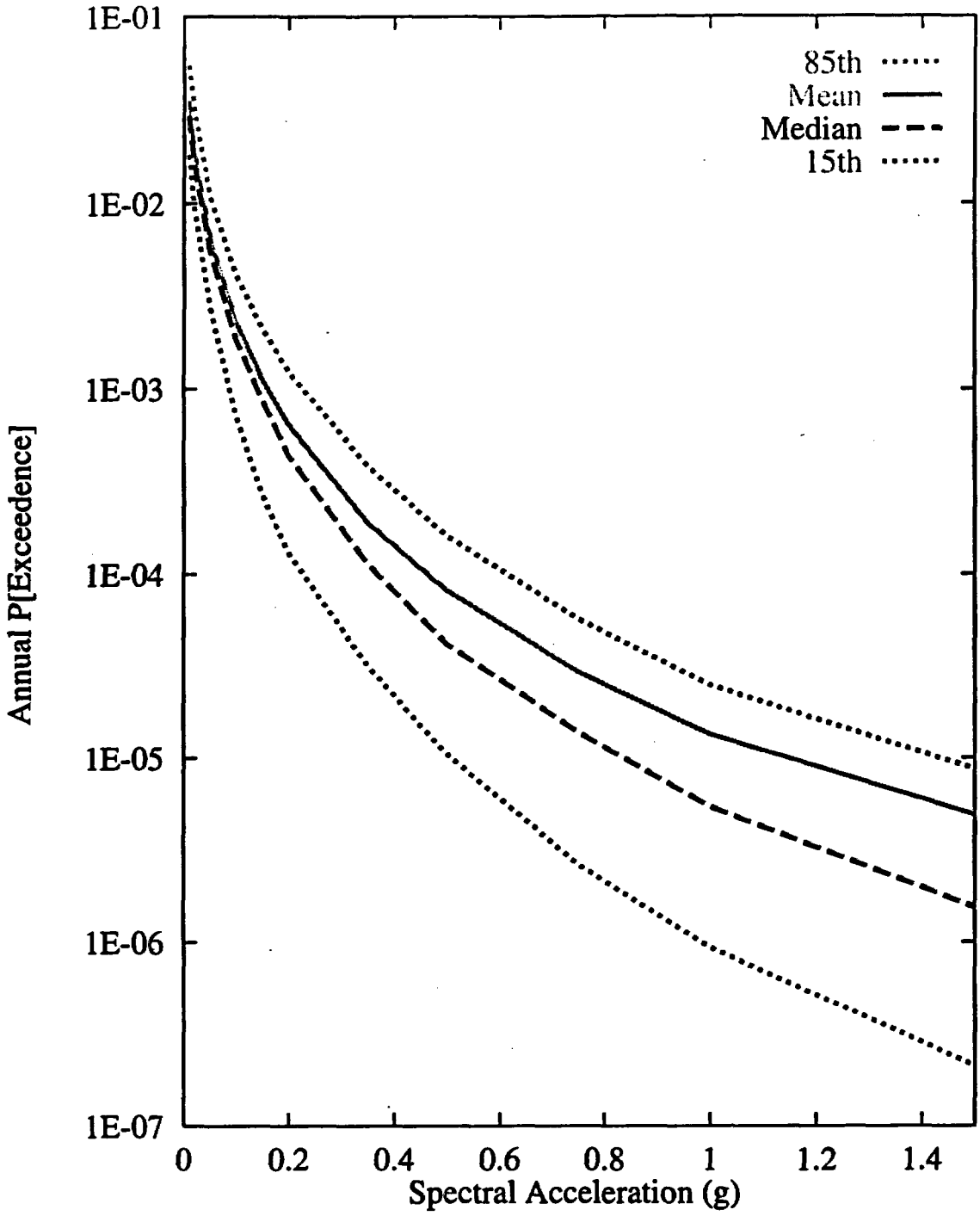

Figure 7-6 Integrated seismic hazard results: summary hazard curves for 1-Hz horizontal spectral acceleration

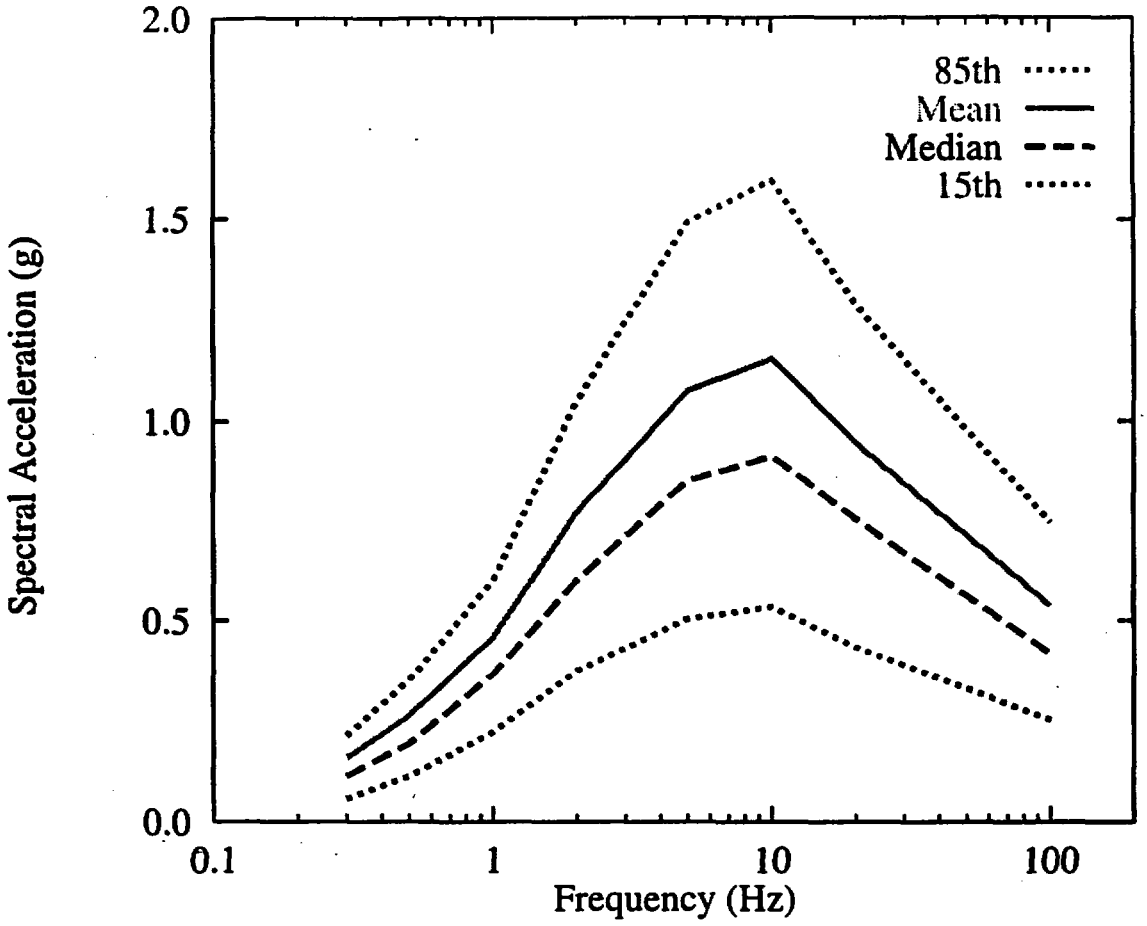

Figure 7-7 Integrated seismic hazard results: horizontal uniform hazard spectrum (UHS) for 10^{-4} exceedence probability

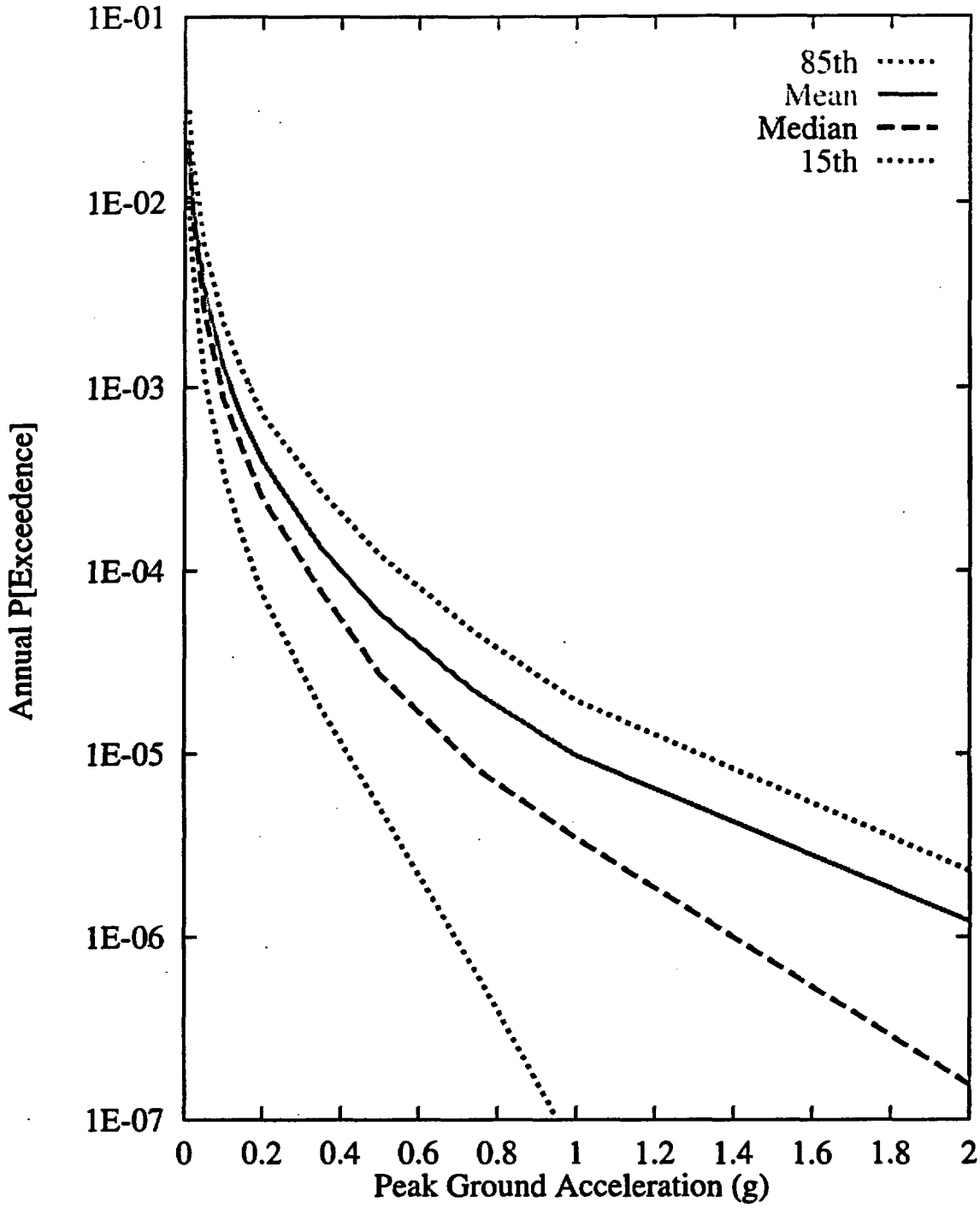

Figure 7-8 Integrated seismic hazard results: summary hazard curves for vertical PGA

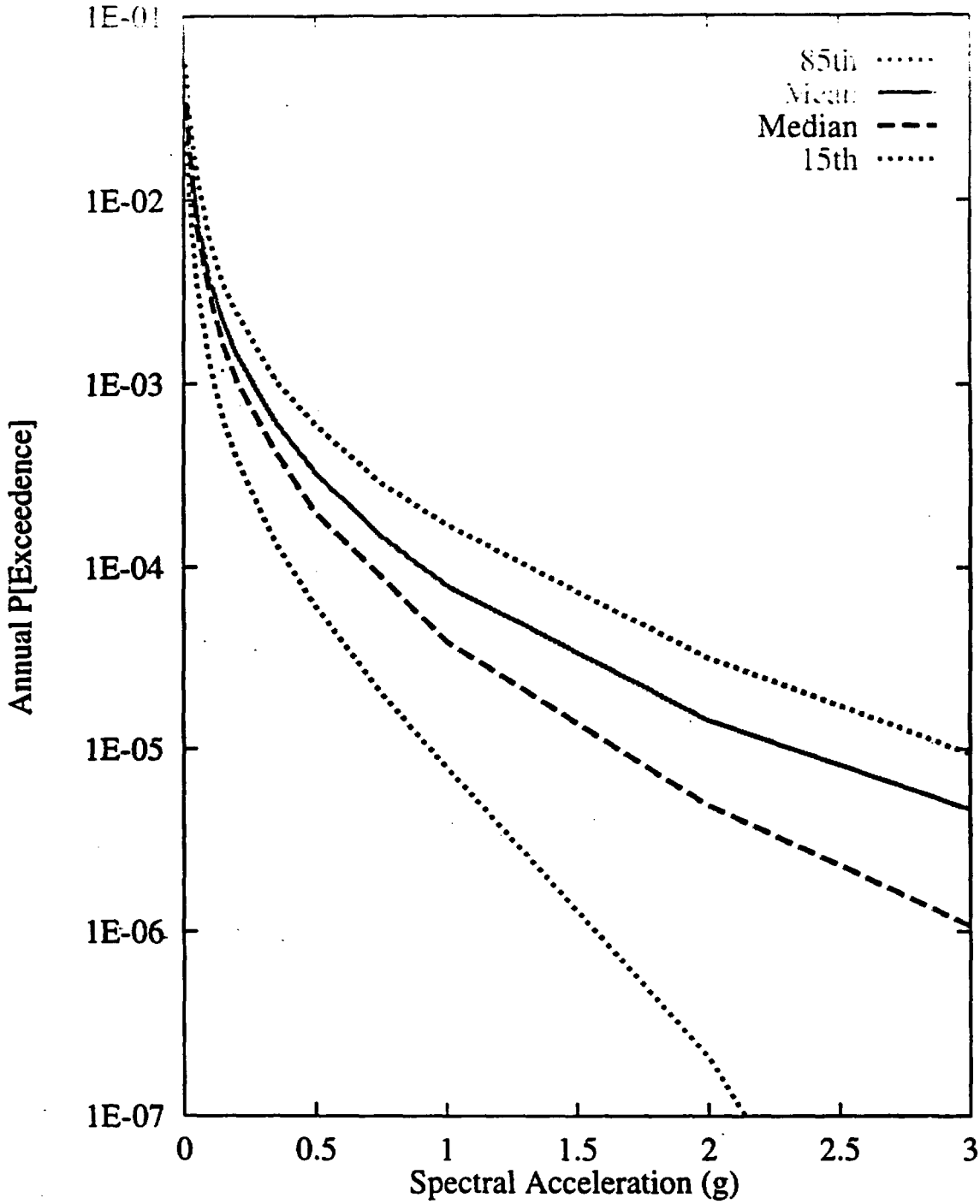

Figure 7-9 Integrated seismic hazard results: summary hazard curves for 10-Hz vertical spectral acceleration

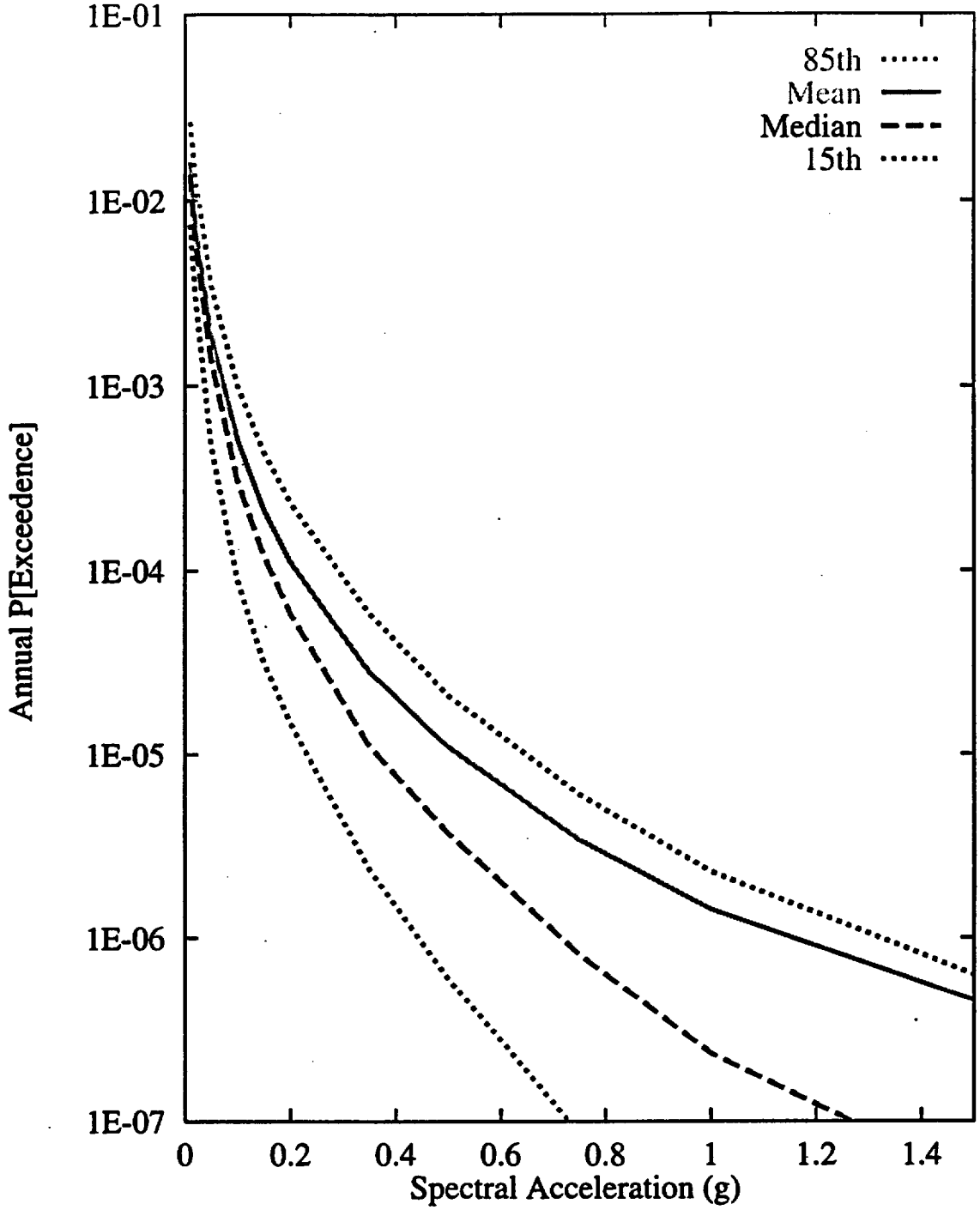

Figure 7-10 Integrated seismic hazard results: summary hazard curves for 1-Hz vertical spectral acceleration

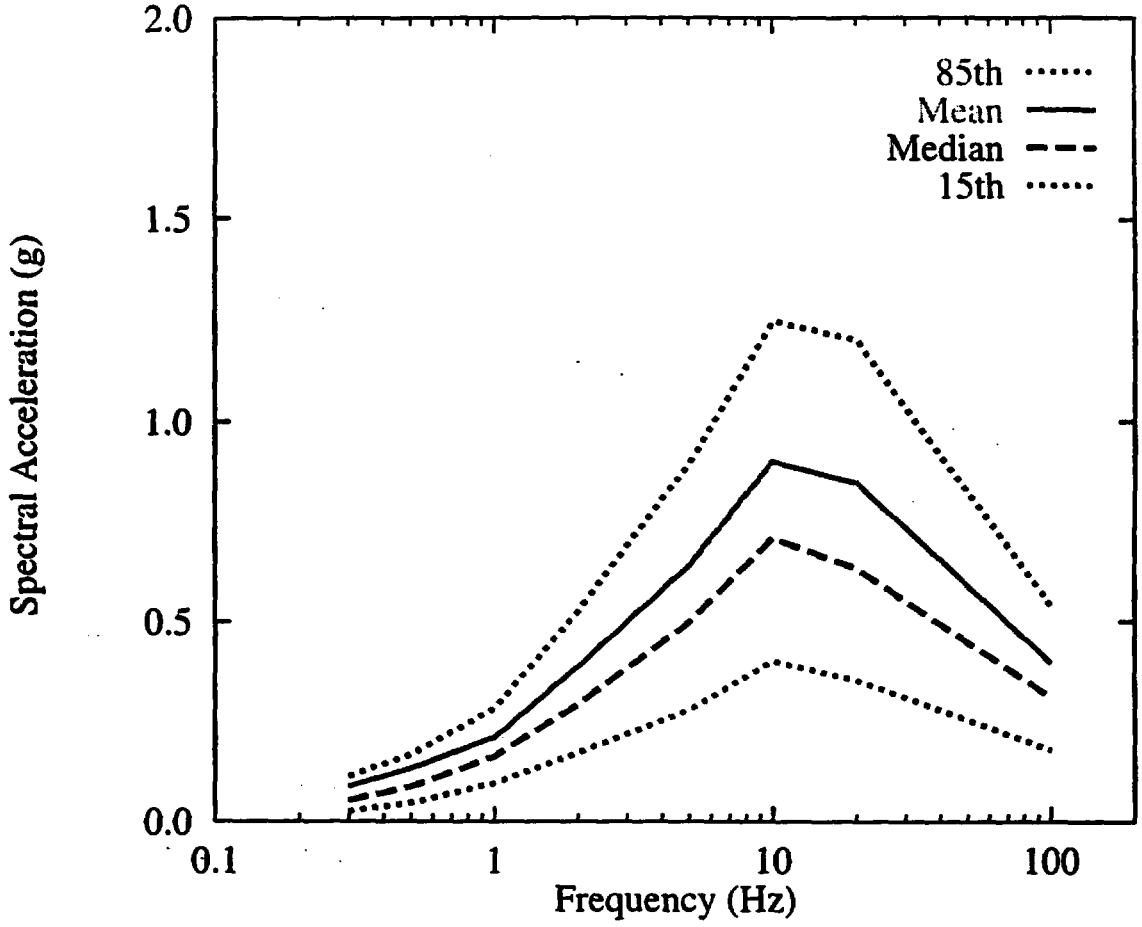

Figure 7-11 Integrated seismic hazard results: vertical uniform hazard spectrum (UHS) for 10^{-4} exceedence probability

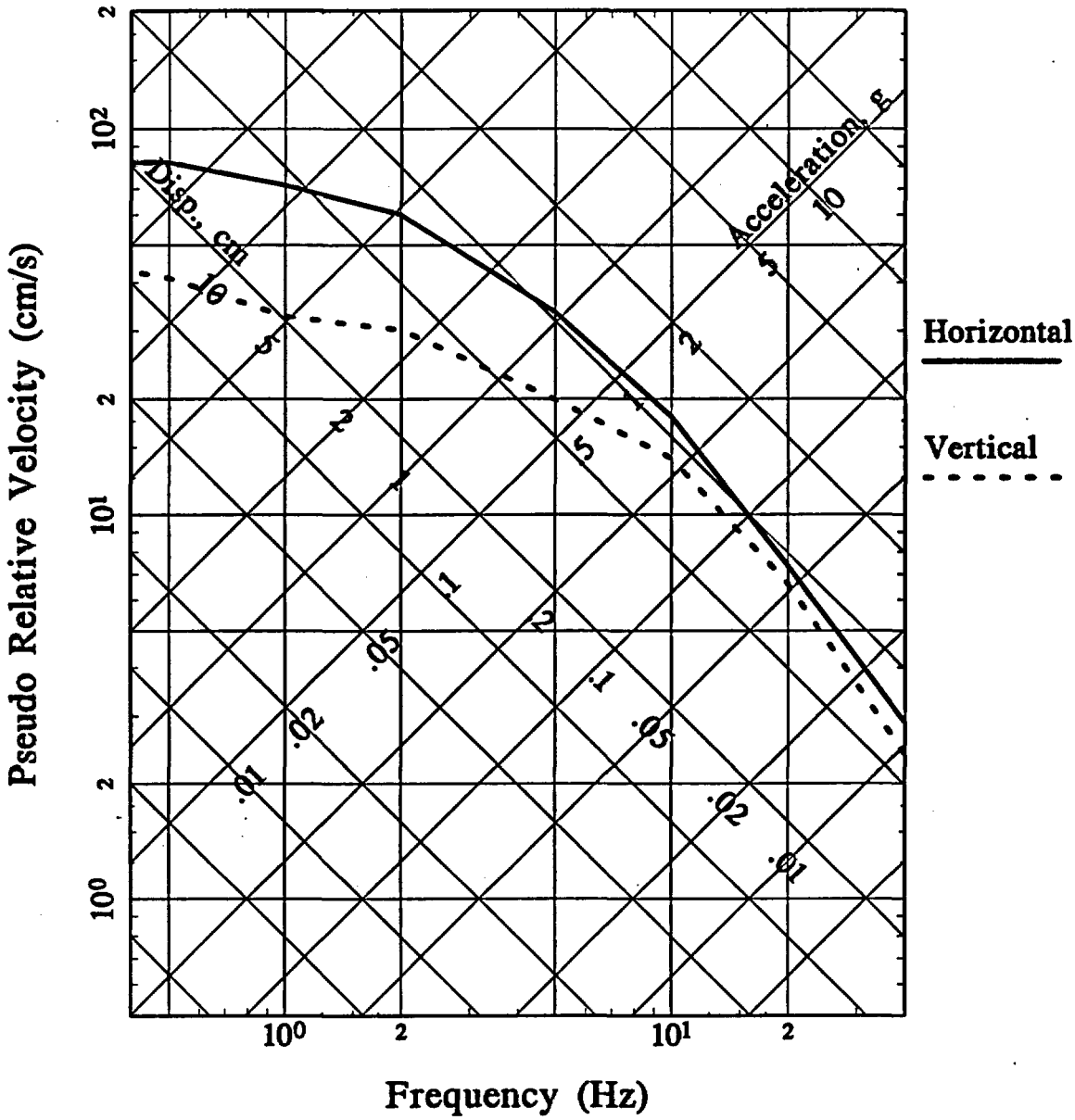

Figure 7-12 Integrated seismic hazard results: uniform hazard spectra for 10^{-4} exceedence probability shown in tripartite scale

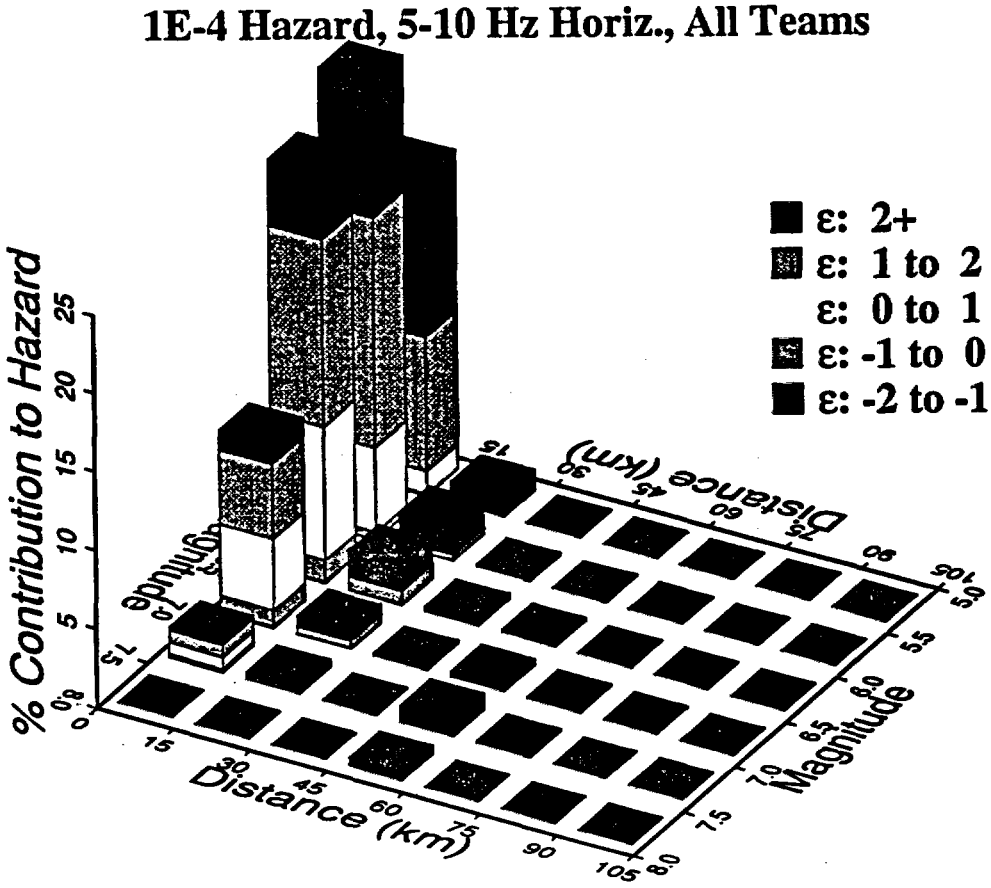

Figure 7-13 Magnitude-distance-epsilon deaggregation of integrated seismic hazard for 5- and 10-Hz horizontal spectral acceleration at 10^{-4} exceedence probability

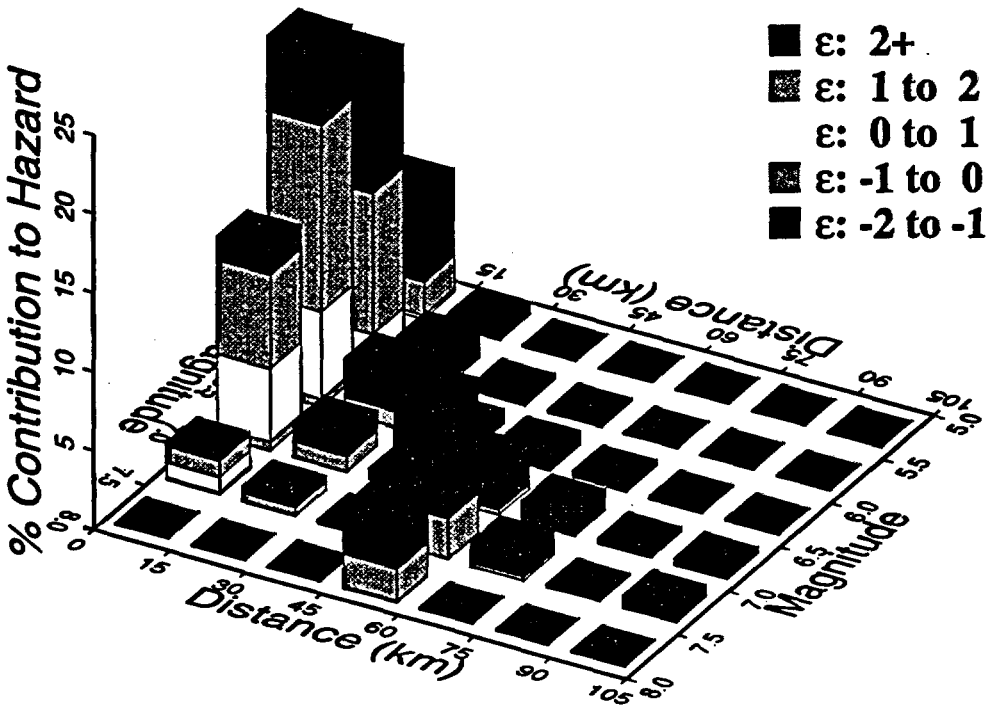

Figure 7-14 Magnitude-distance-epsilon deaggregation of integrated seismic hazard for 1- and 2-Hz horizontal spectral acceleration at 10^{-4} exceedence probability

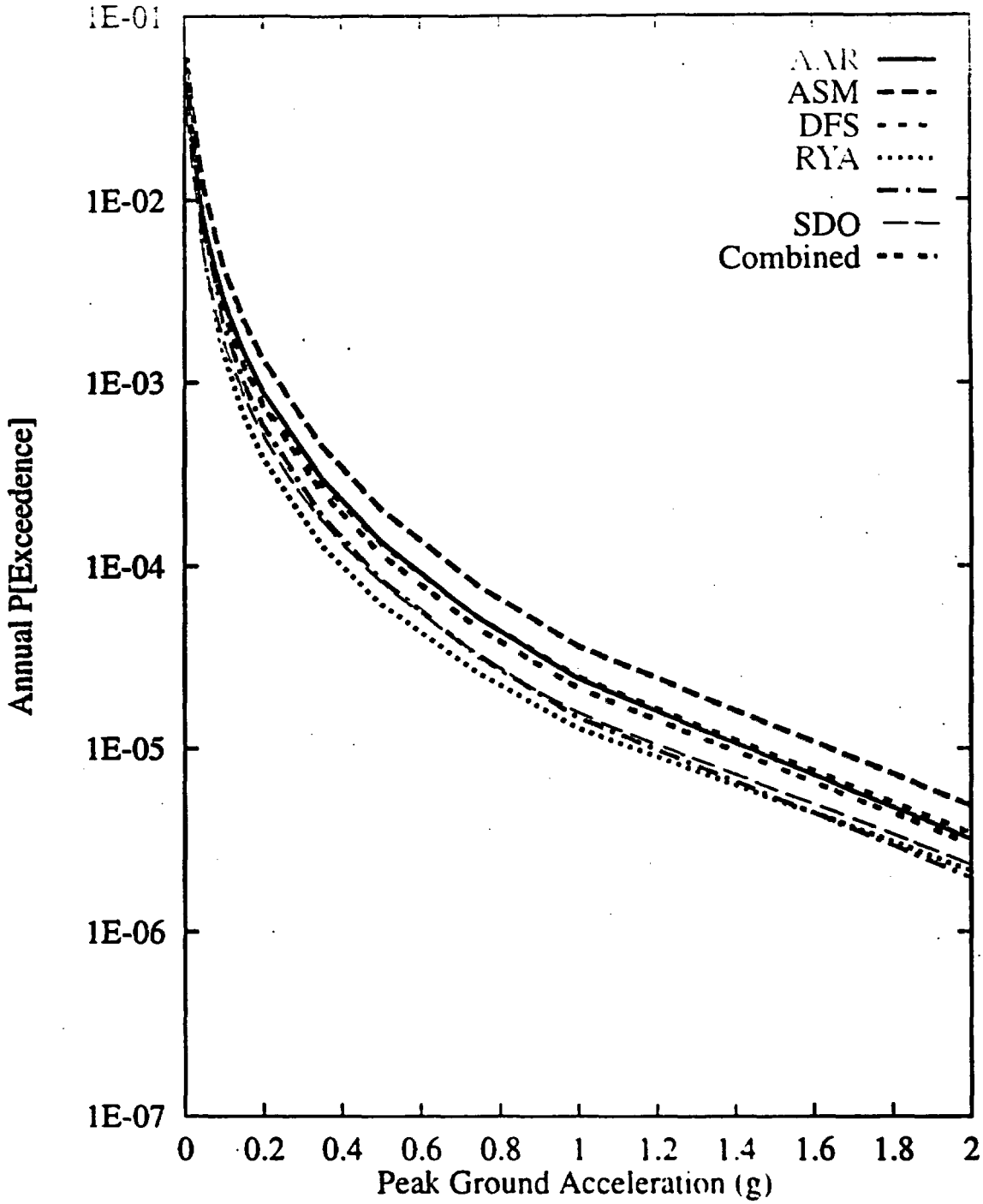

Figure 7-15 Mean hazard by team for horizontal PGA

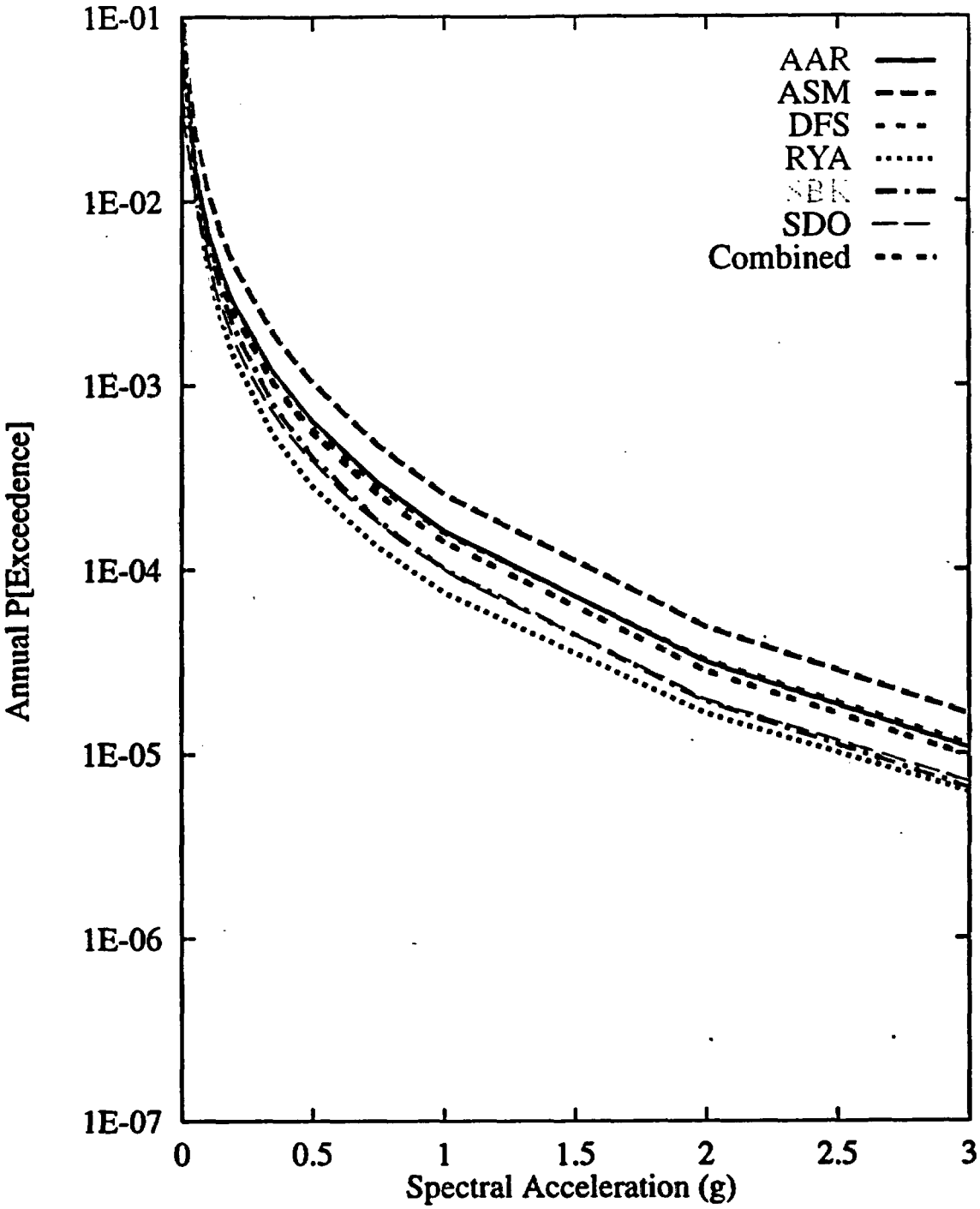

Figure 7-16 Mean hazard by team for 10-Hz horizontal spectral acceleration

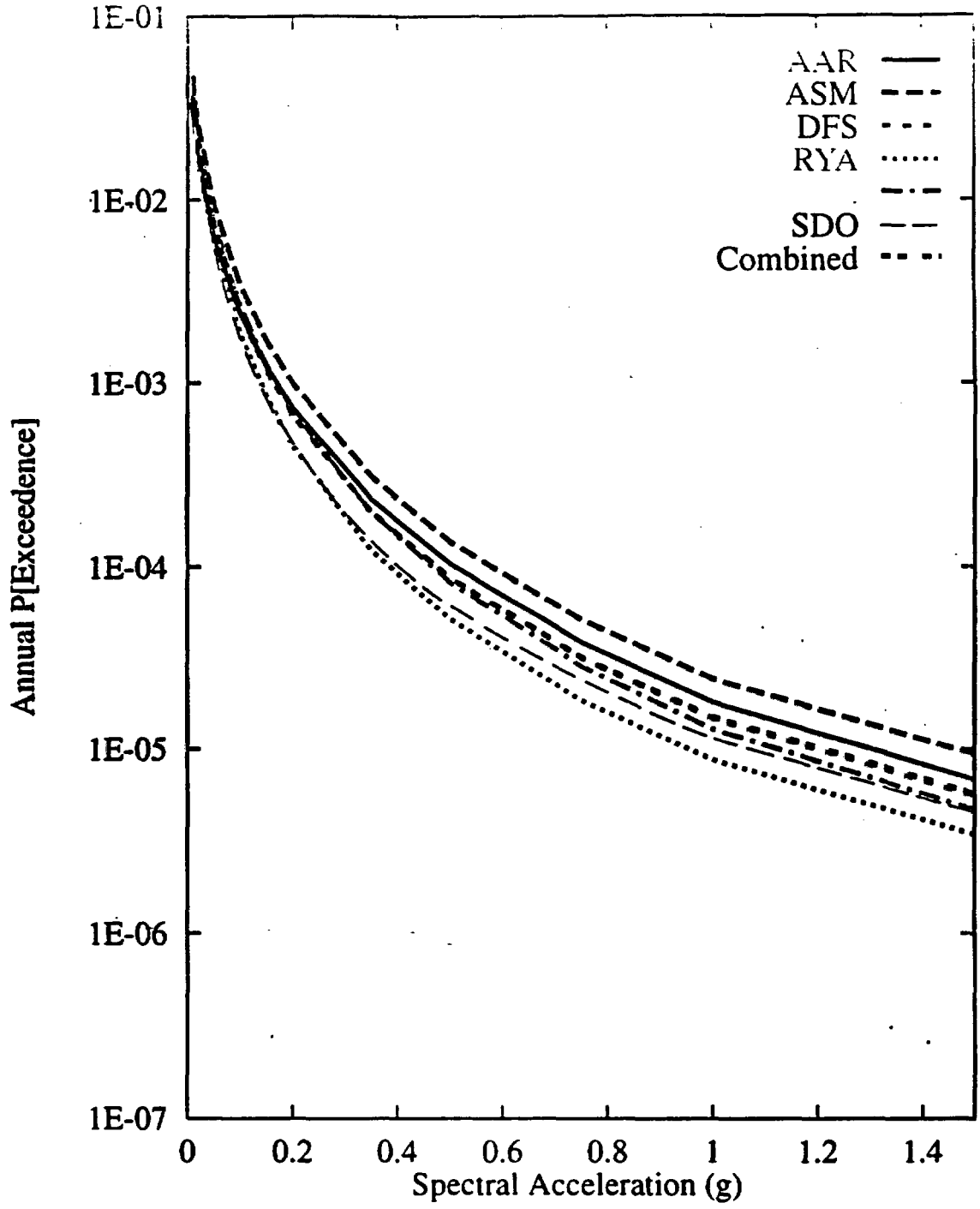

Figure 7-17 Mean hazard by team for 1-Hz horizontal spectral acceleration

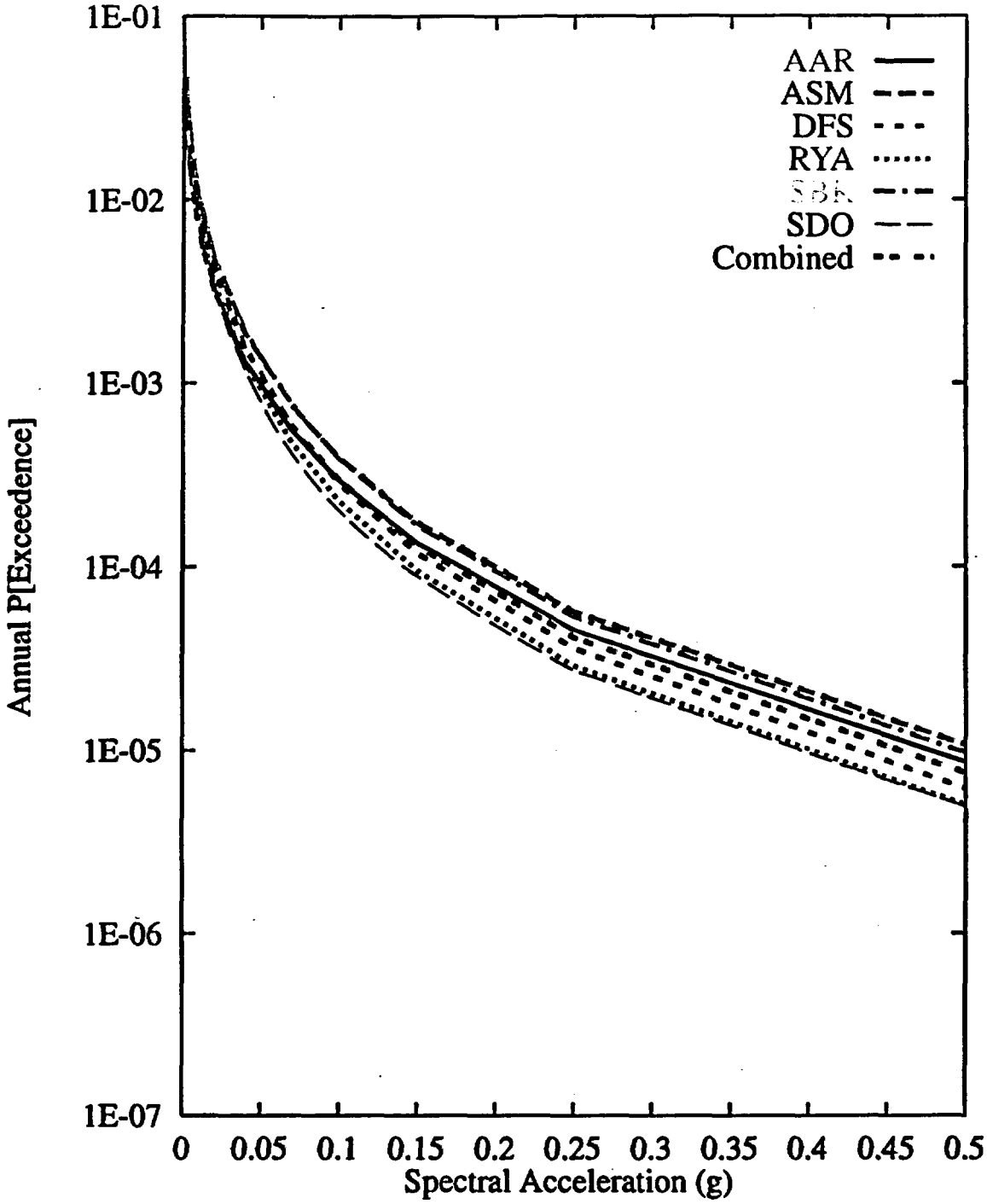

Figure 7-18 Mean hazard by team for 0.3-Hz horizontal spectral acceleration

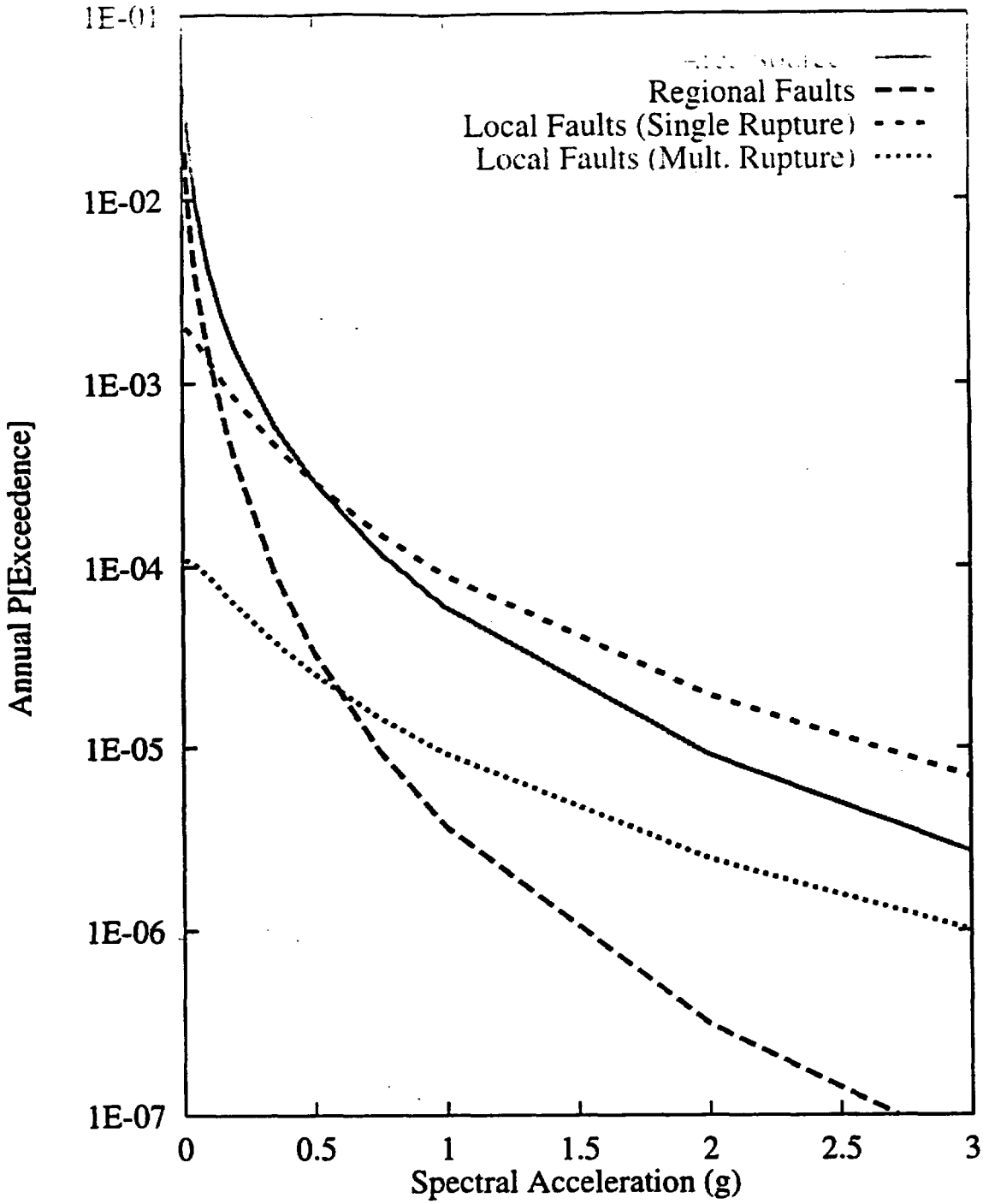

Figure 7-19 Contributions of source type to the mean hazard: AAR team, 10-Hz horizontal spectral acceleration

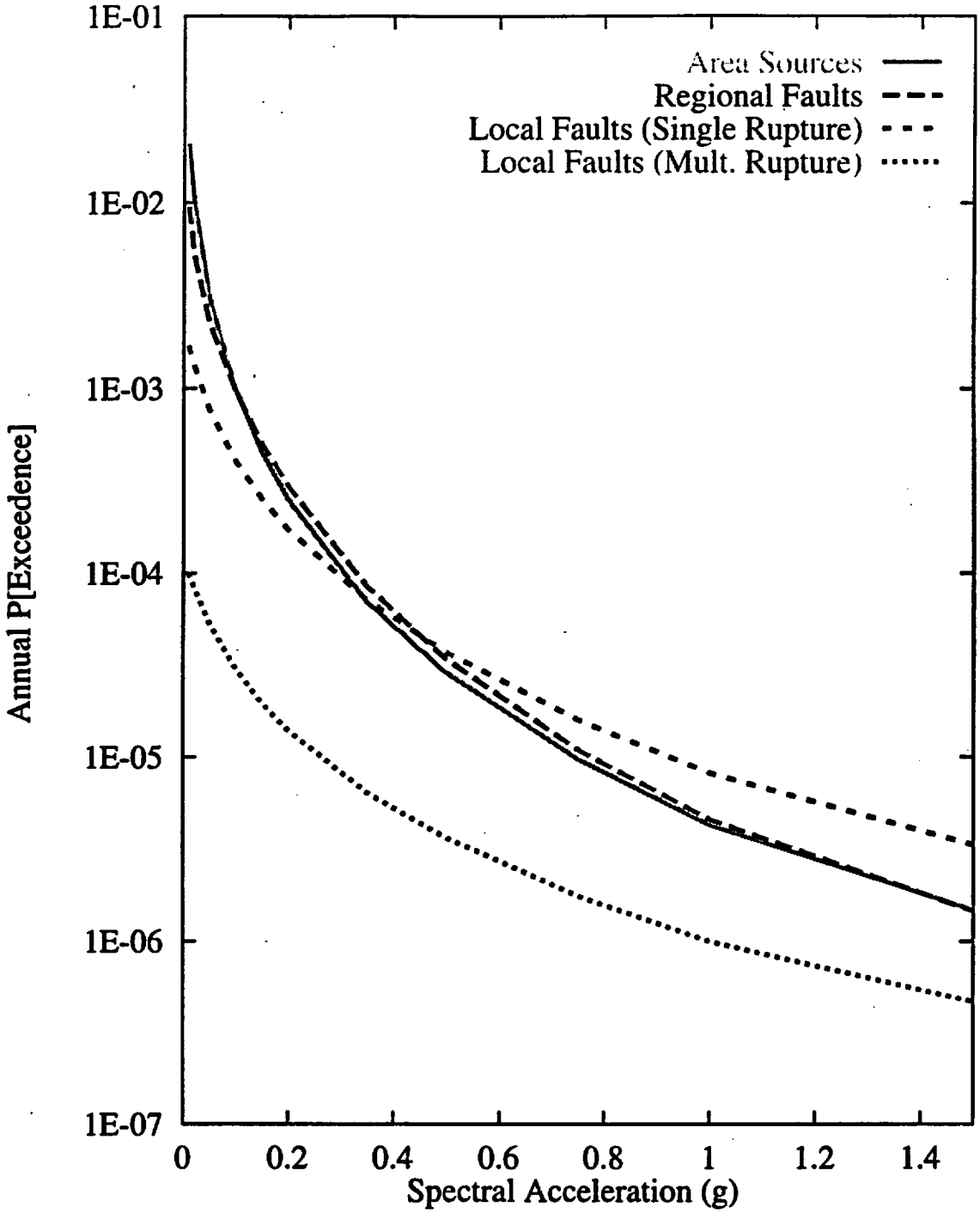

Figure 7-20 Contributions of source type to the mean hazard: AAR team, 1-Hz horizontal spectral acceleration

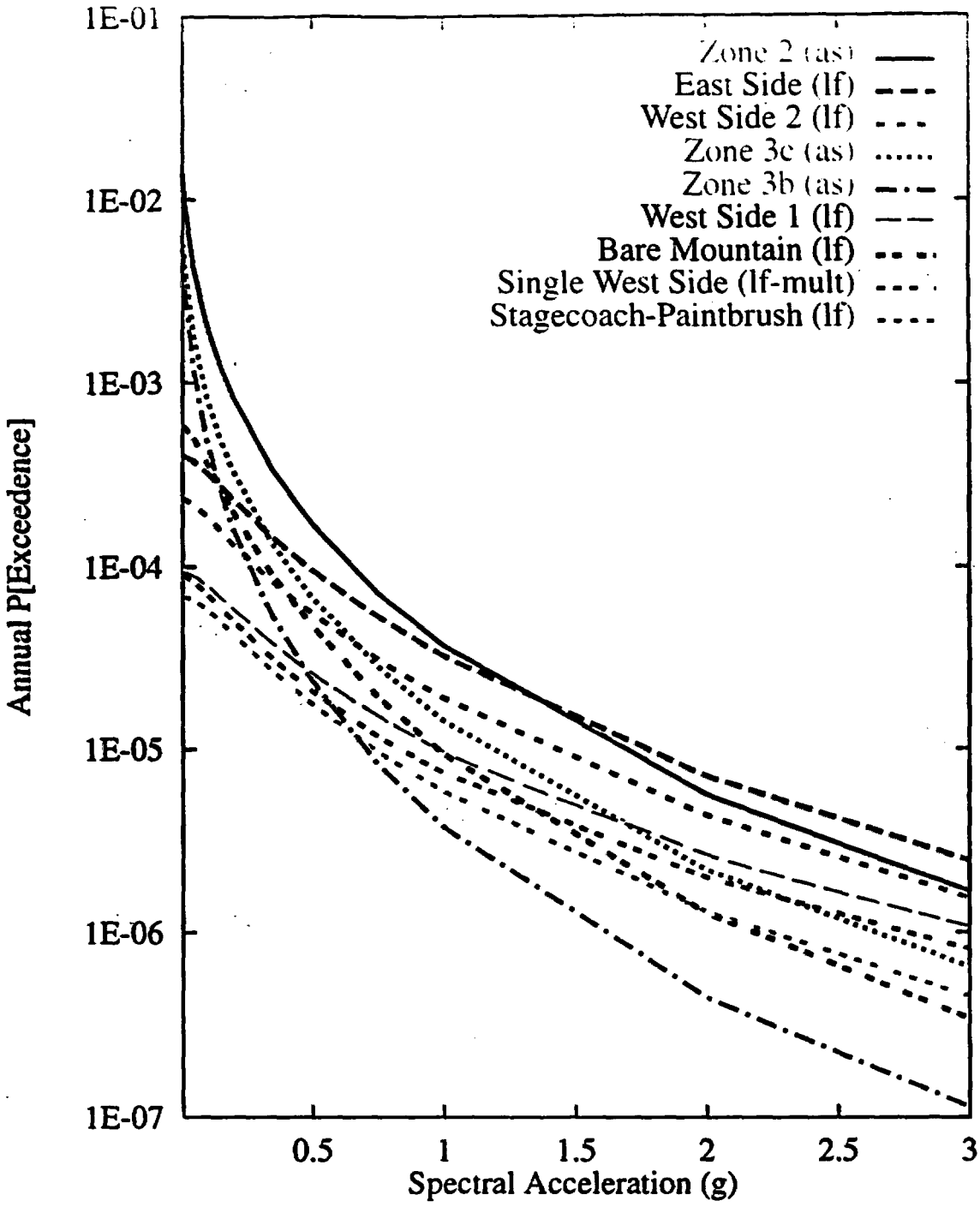

Figure 7-21 Mean seismic hazard from dominant seismic sources: AAR team, 10-Hz horizontal spectral acceleration. Acronyms in parentheses refer to source types: as-area source zone; lf-local fault; and mult-multiple fault rupture.

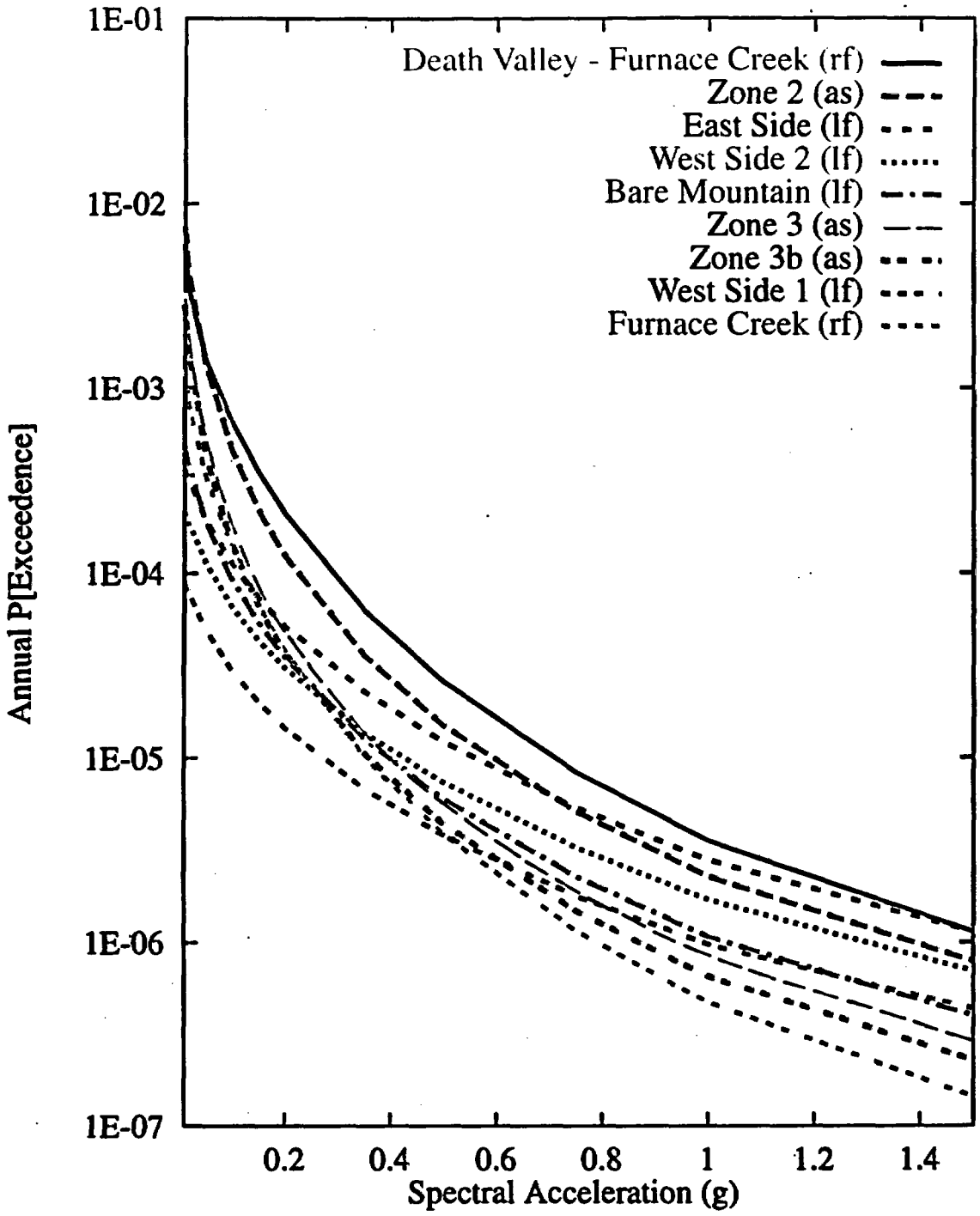

Figure 7-22 Mean seismic hazard from dominant seismic sources: AAR team, 1-Hz horizontal spectral acceleration. Acronyms in parentheses refer to source types: as-area source zone; rf-regional fault; and lf-local fault.

10 Hz, AAR Area Sources

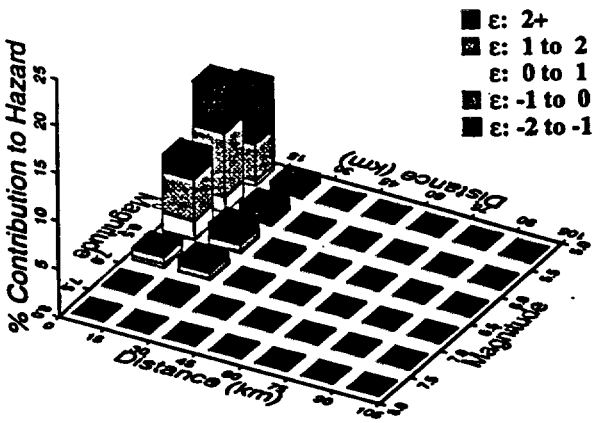

10 Hz, AAR Regional Faults

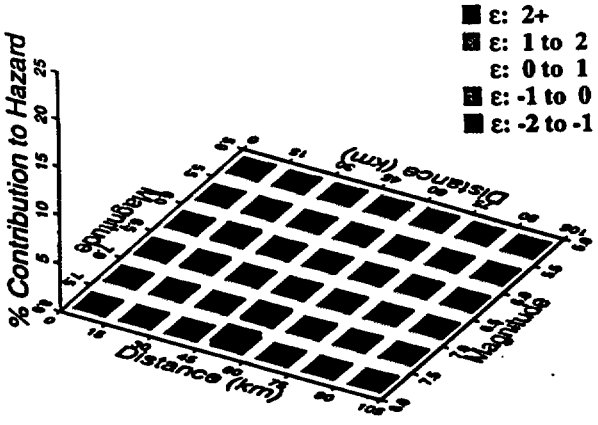

10 Hz, AAR Local Faults (Single)

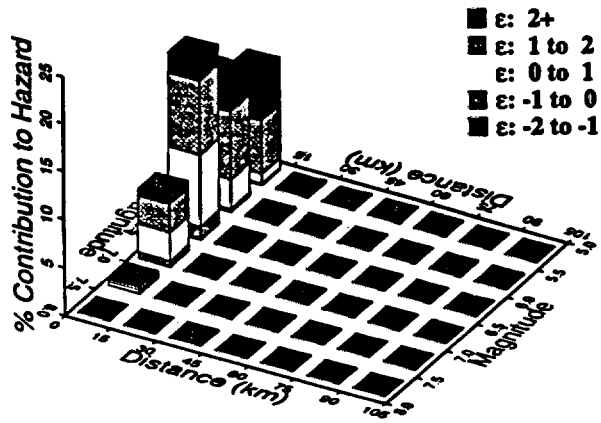

10 Hz, AAR Local Faults (Mult.)

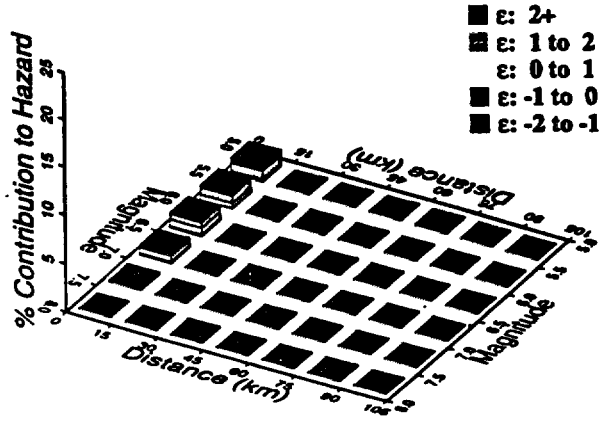

Figure 7-23 Magnitude-distance-epsilon distributions for the four source types: AAR team, 10-Hz horizontal spectral acceleration at 10^{-4} exceedance probability

1 Hz, AAR Area Sources

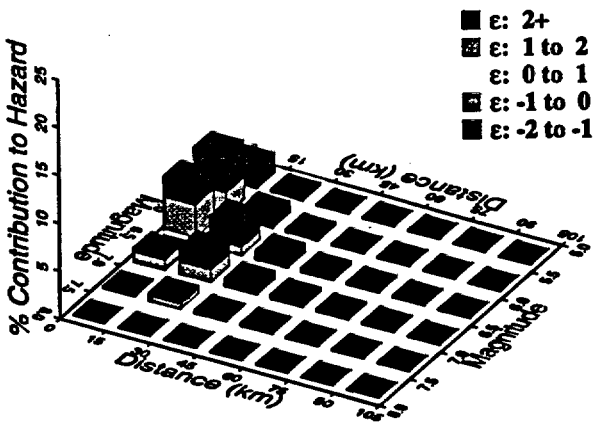

1 Hz, AAR Regional Faults

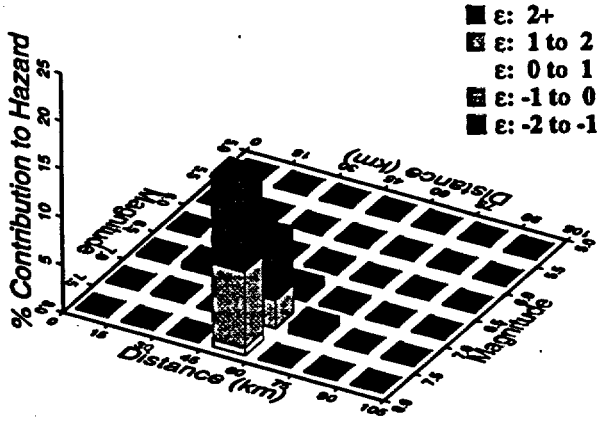

1 Hz, ARR Local Faults (Single)

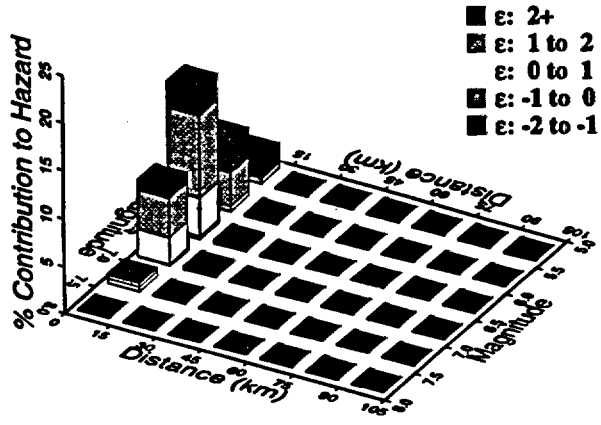

1 Hz, AAR Local Faults (Mult.)

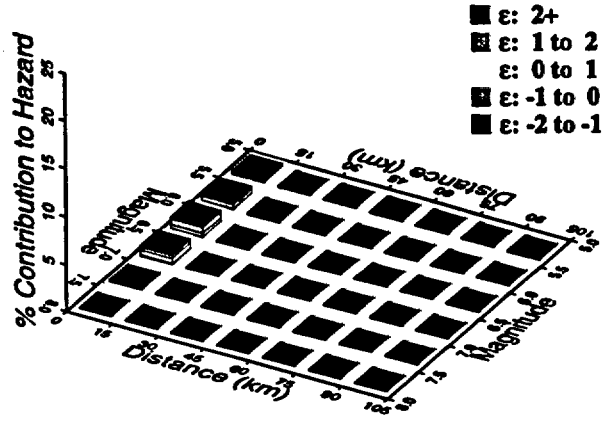

Figure 7-24 Magnitude-distance-epsilon distributions for the four source types: AAR team, 1-Hz horizontal spectral acceleration at 10^{-4} exceedance probability

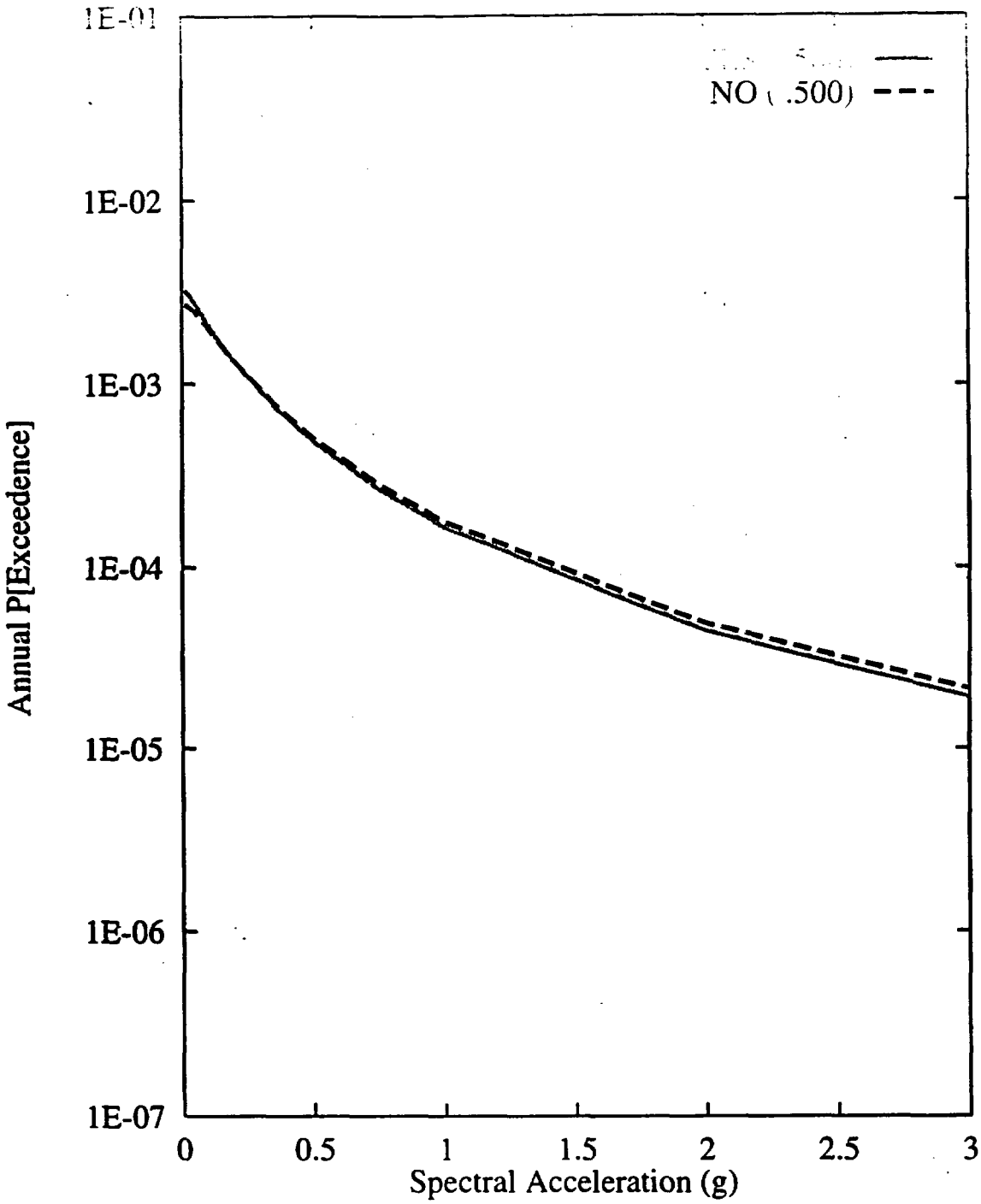

Figure 7-25 Sensitivity of seismic hazard from local faults to presence of dextral shear: AAR team, 10-Hz horizontal spectral acceleration

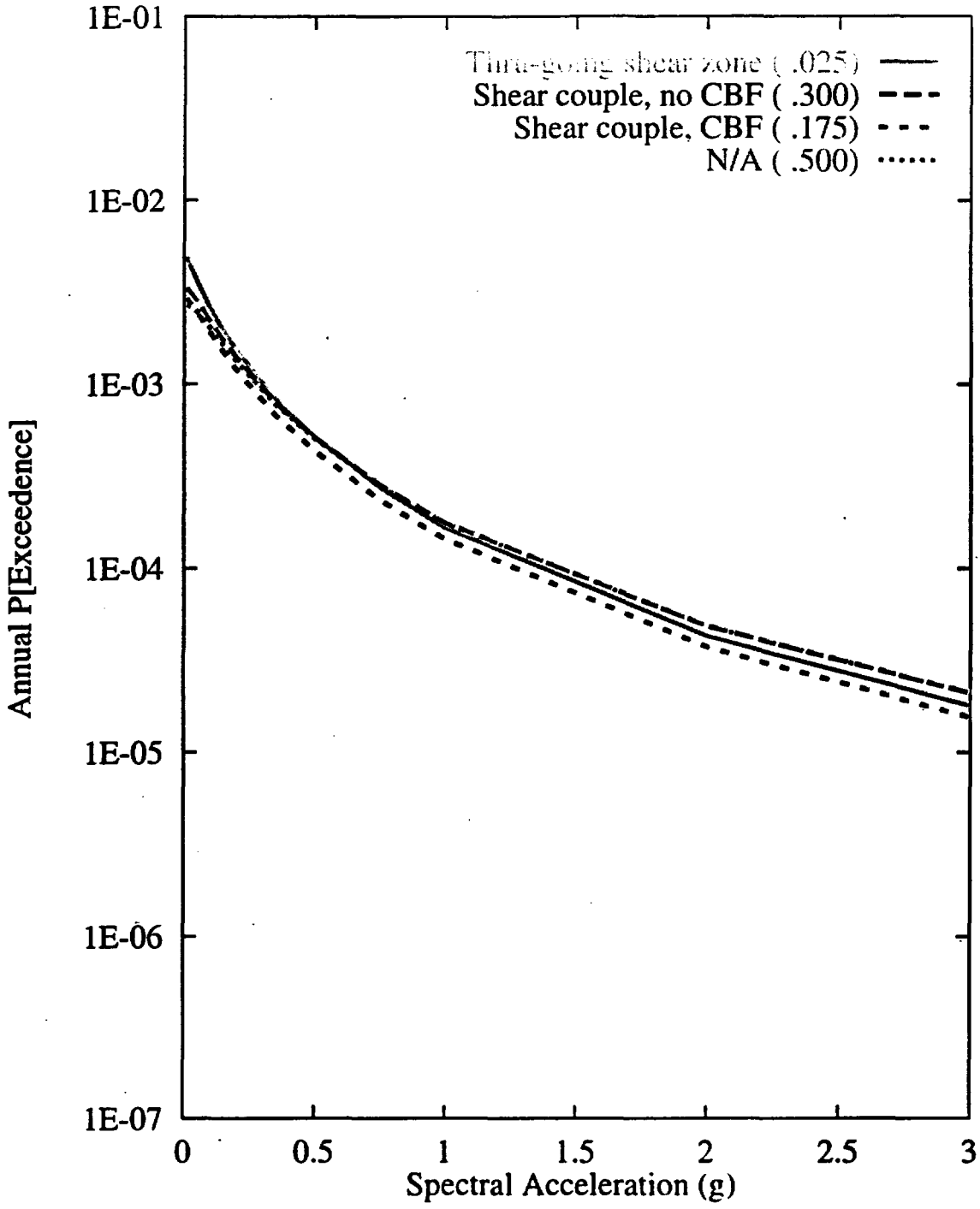

Figure 7-26 Sensitivity of seismic hazard from local faults to type of dextral shear structure: AAR team, 10-Hz horizontal spectral acceleration

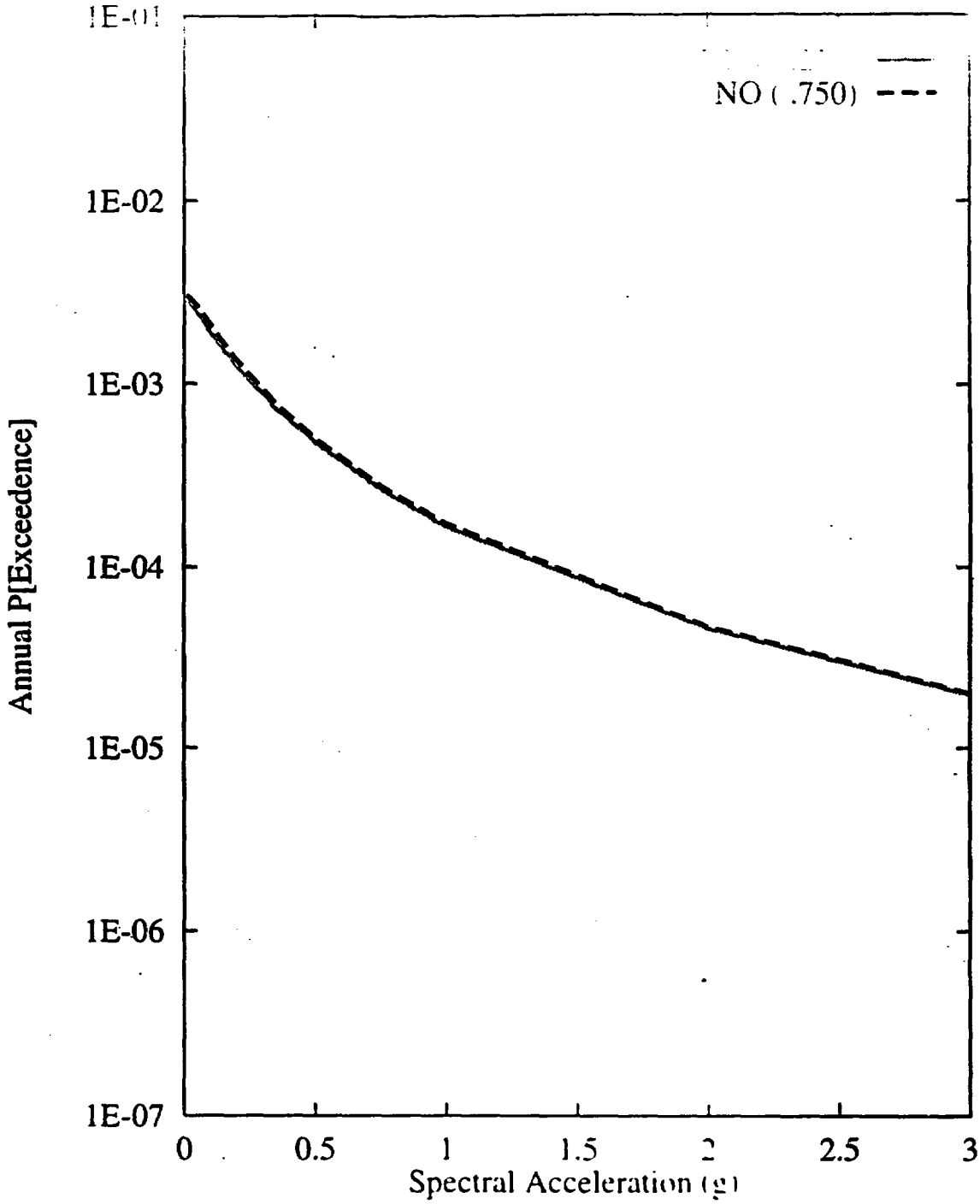

Figure 7-27 Sensitivity of seismic hazard from local fault to existence of local detachment AAR team, 10-Hz horizontal spectral acceleration

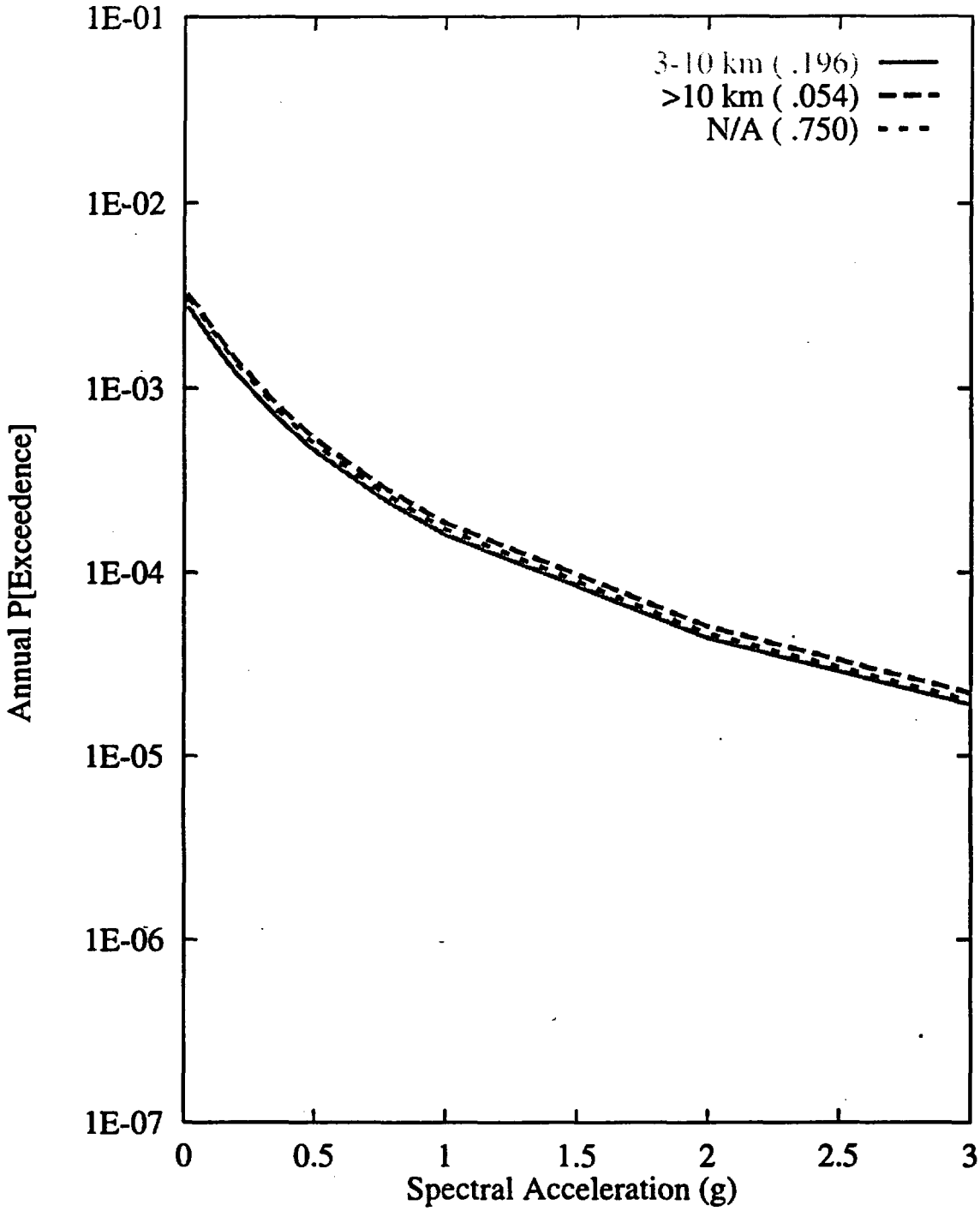

Figure 7-28 Sensitivity of seismic hazard from local faults to detachment depth: AAR team, 10-Hz horizontal spectral acceleration

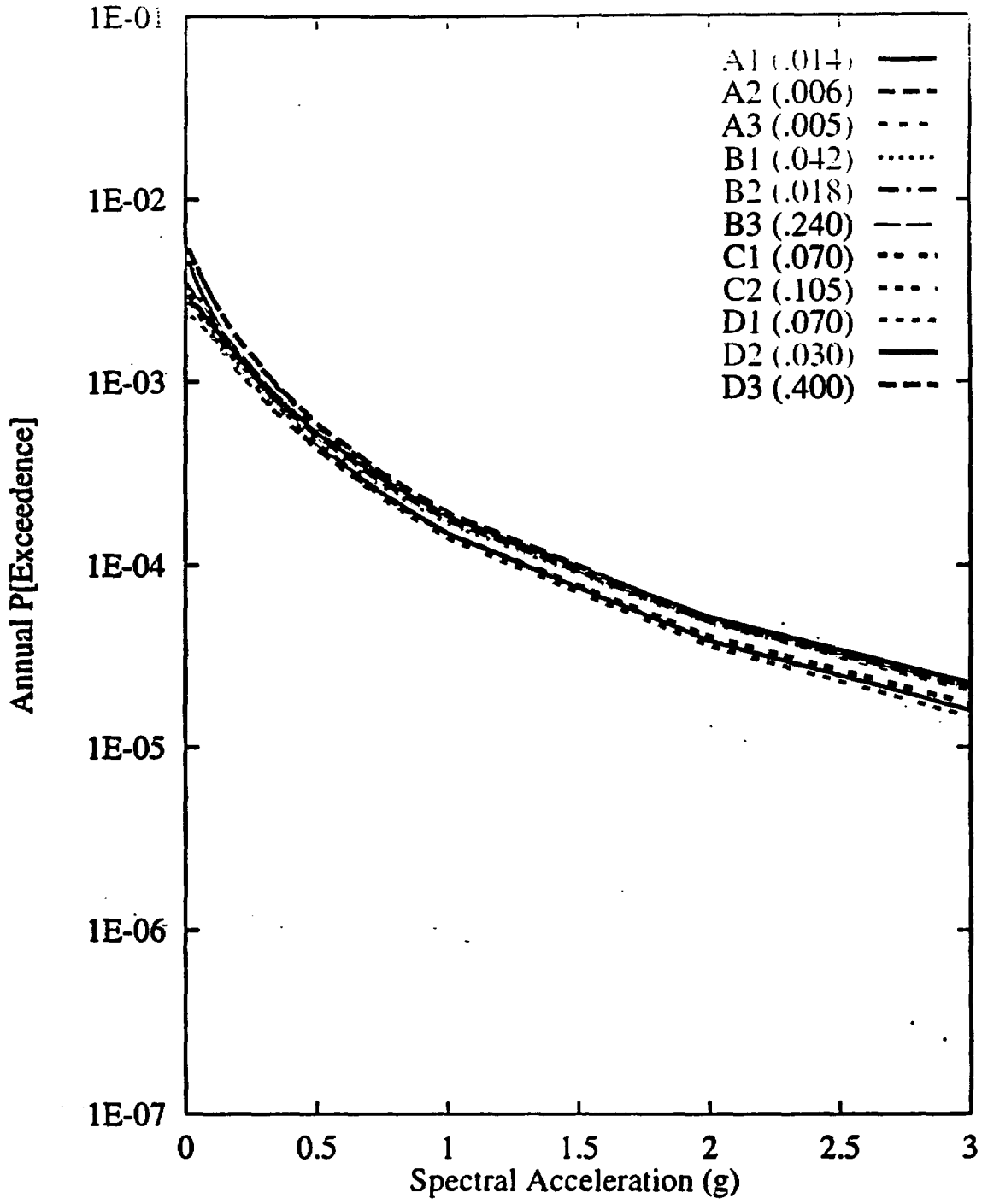

Figure 7-29 Sensitivity of seismic hazard from local faults to local fault scenarios: AAR team, 10-Hz horizontal spectral acceleration

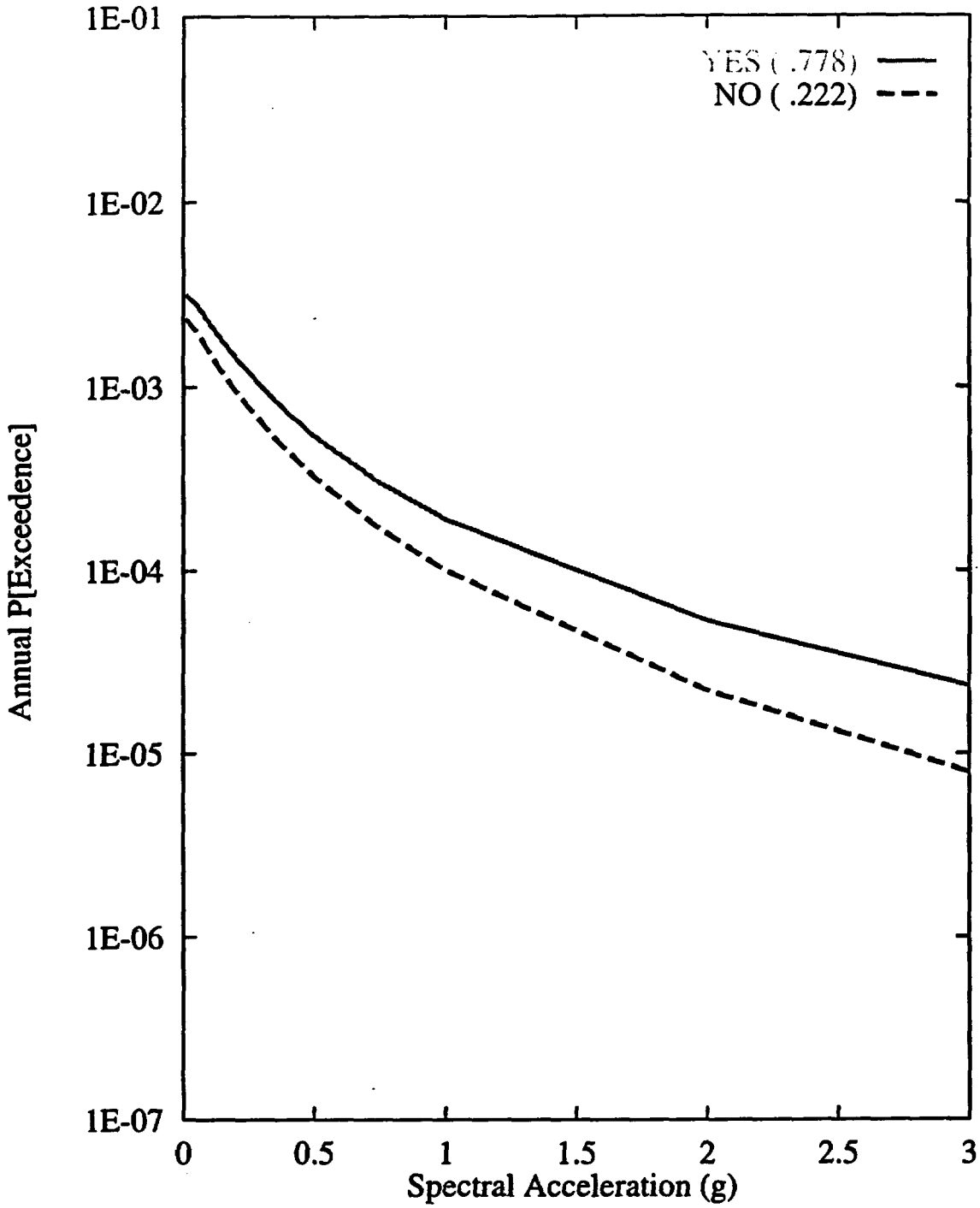

Figure 7-30 Sensitivity of seismic hazard from local faults to presence of coalescence: AAR team, 10-Hz horizontal spectral acceleration

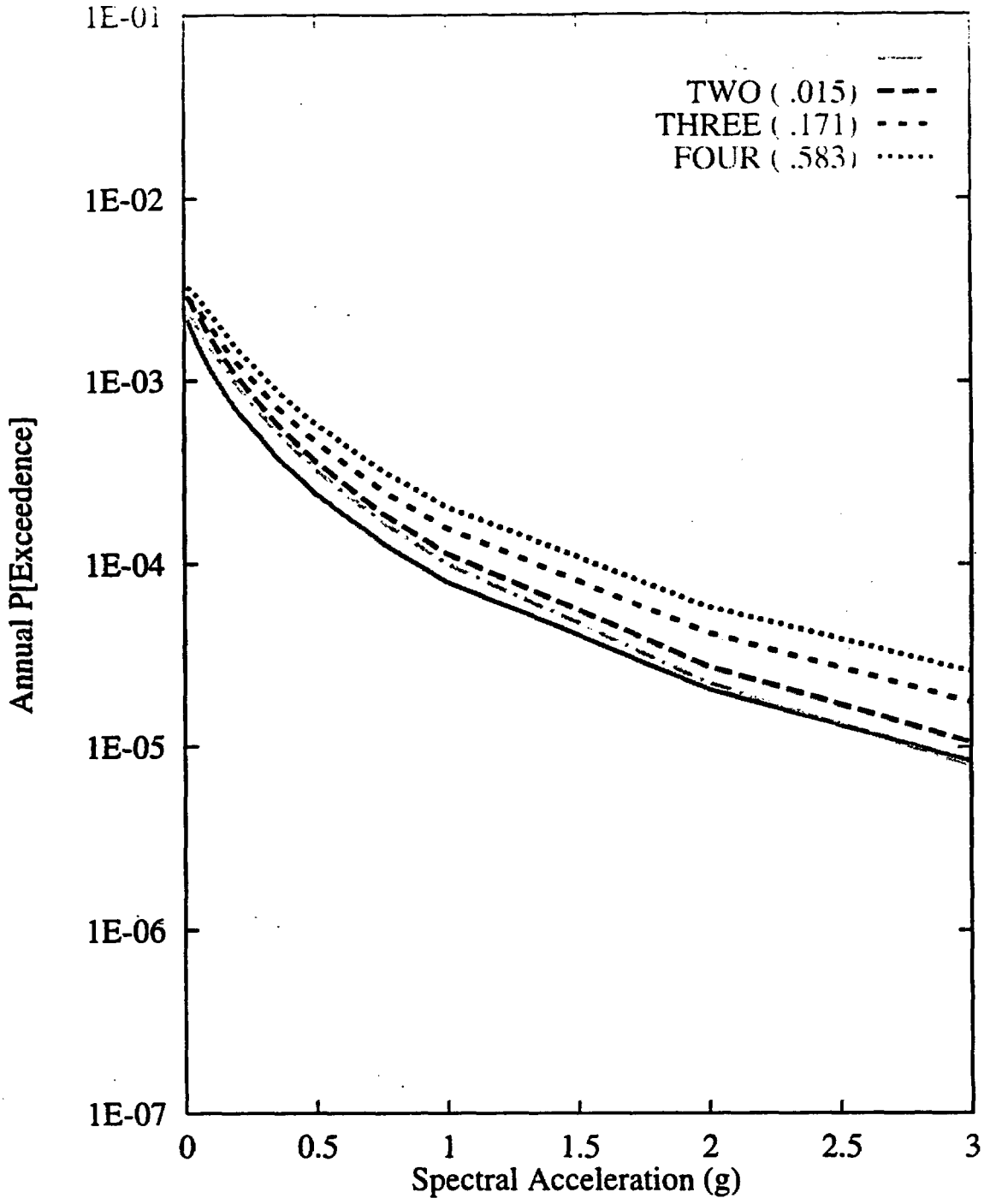

Figure 7-31 Sensitivity of seismic hazard from local faults to type of coalesced behavior: AAR team, 10-Hz horizontal spectral acceleration

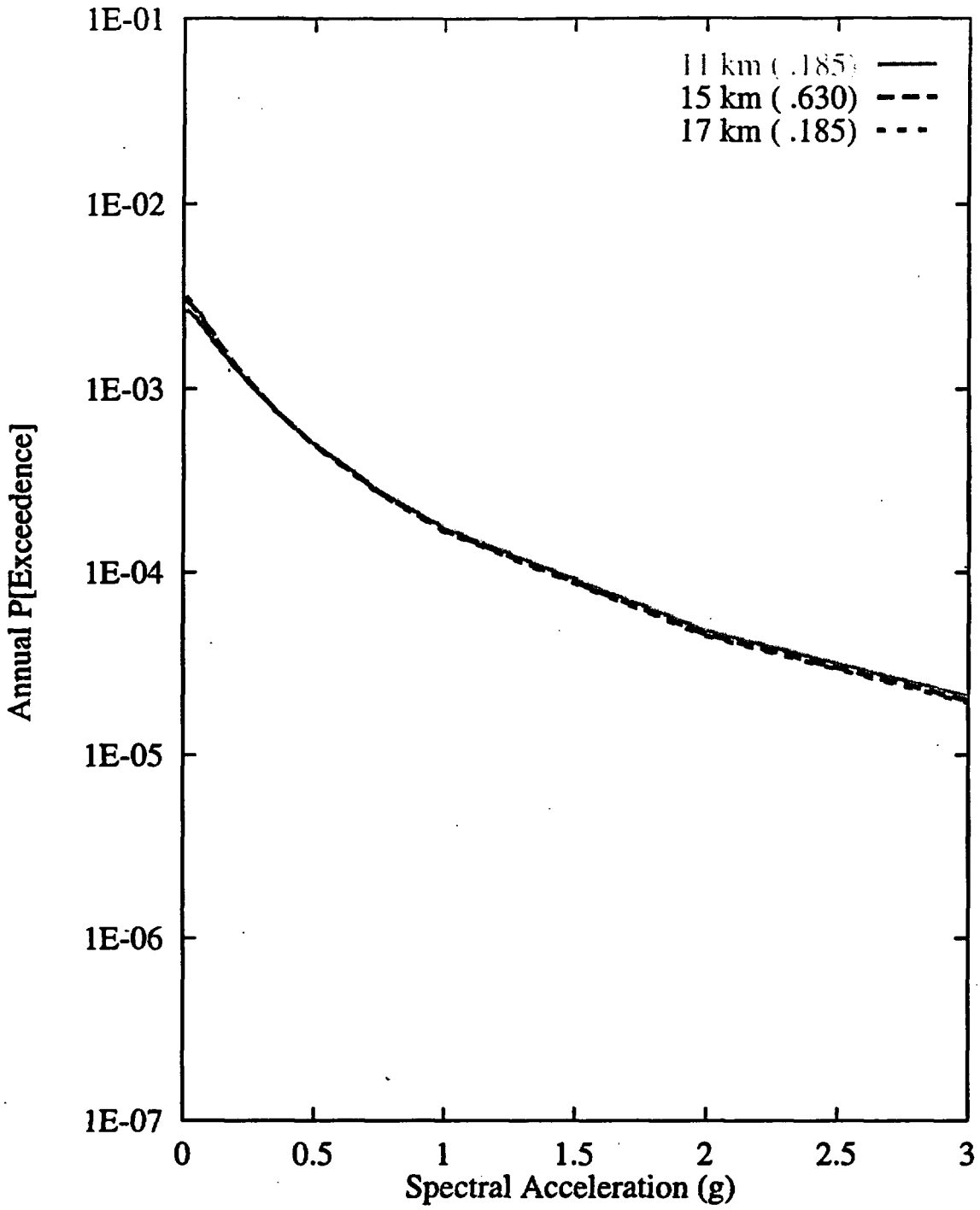

Figure 7-32 Sensitivity of seismic hazard from local faults to maximum fault depth: AAR team, 10-Hz horizontal spectral acceleration

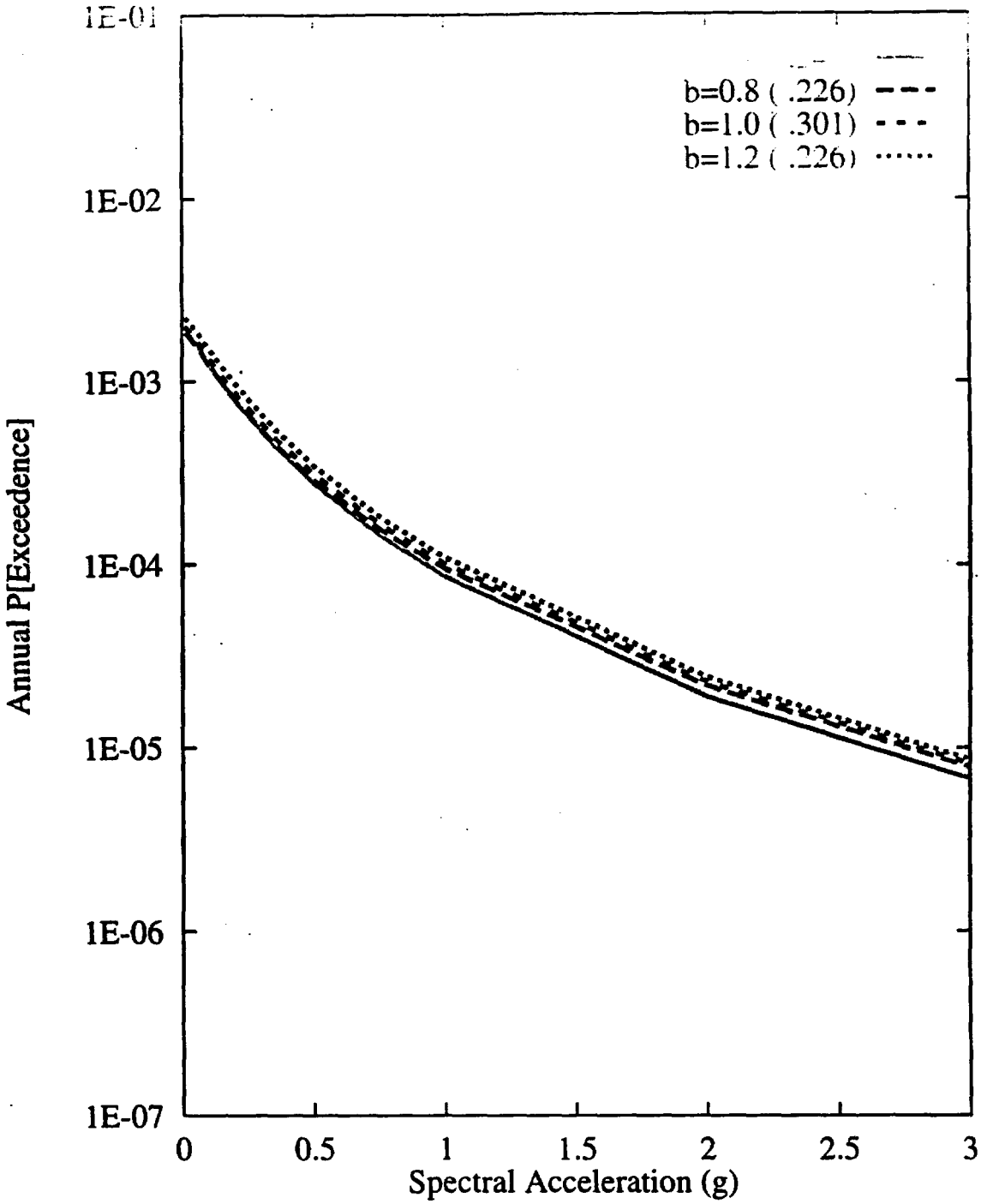

Figure 7-33 Sensitivity of seismic hazard from local faults to b-value of East-side fault system: AAR team, 10-Hz horizontal spectral acceleration

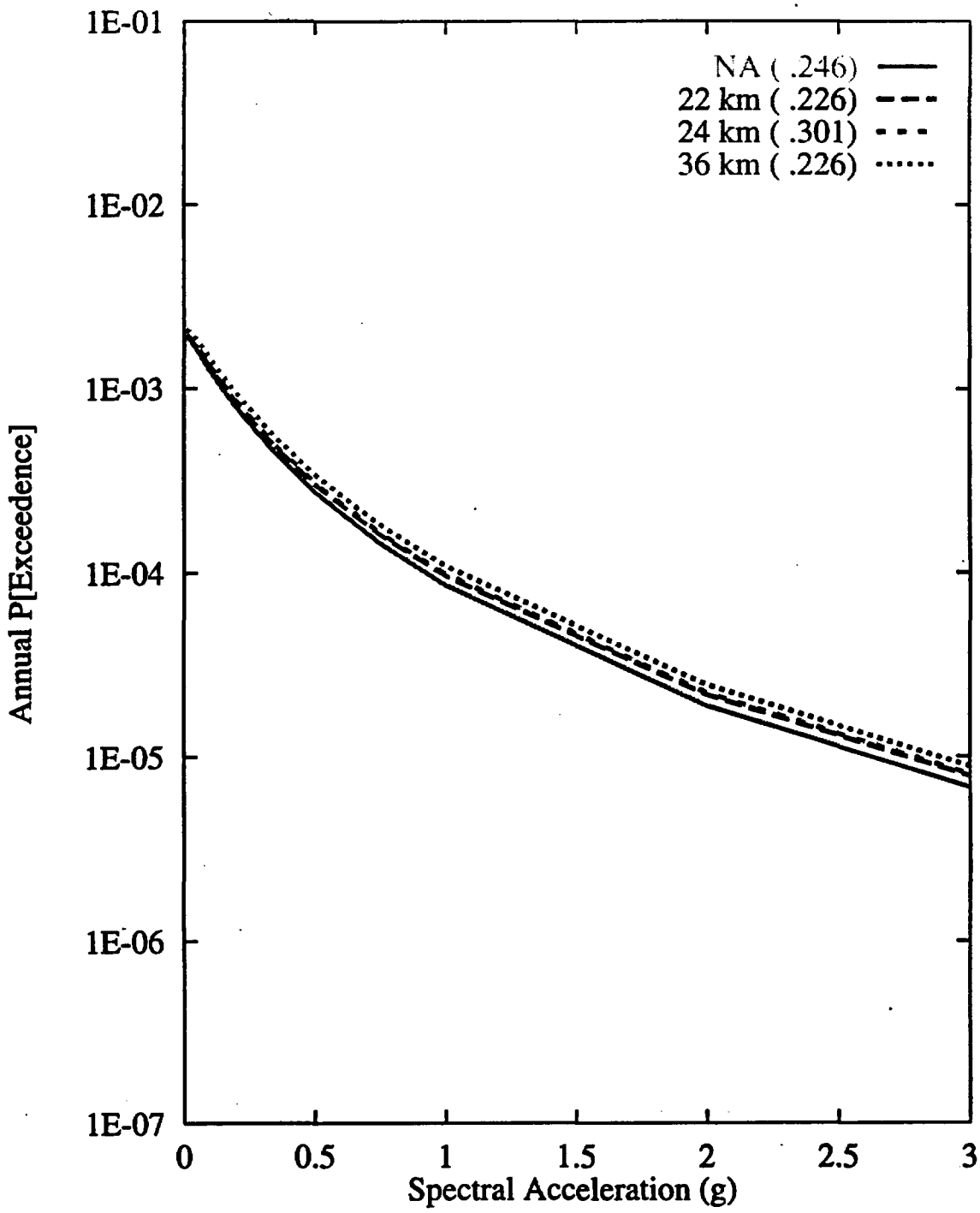

Figure 7-34 Sensitivity of seismic hazard from local faults to length of East-side fault system: AAR team, 10-Hz horizontal spectral acceleration

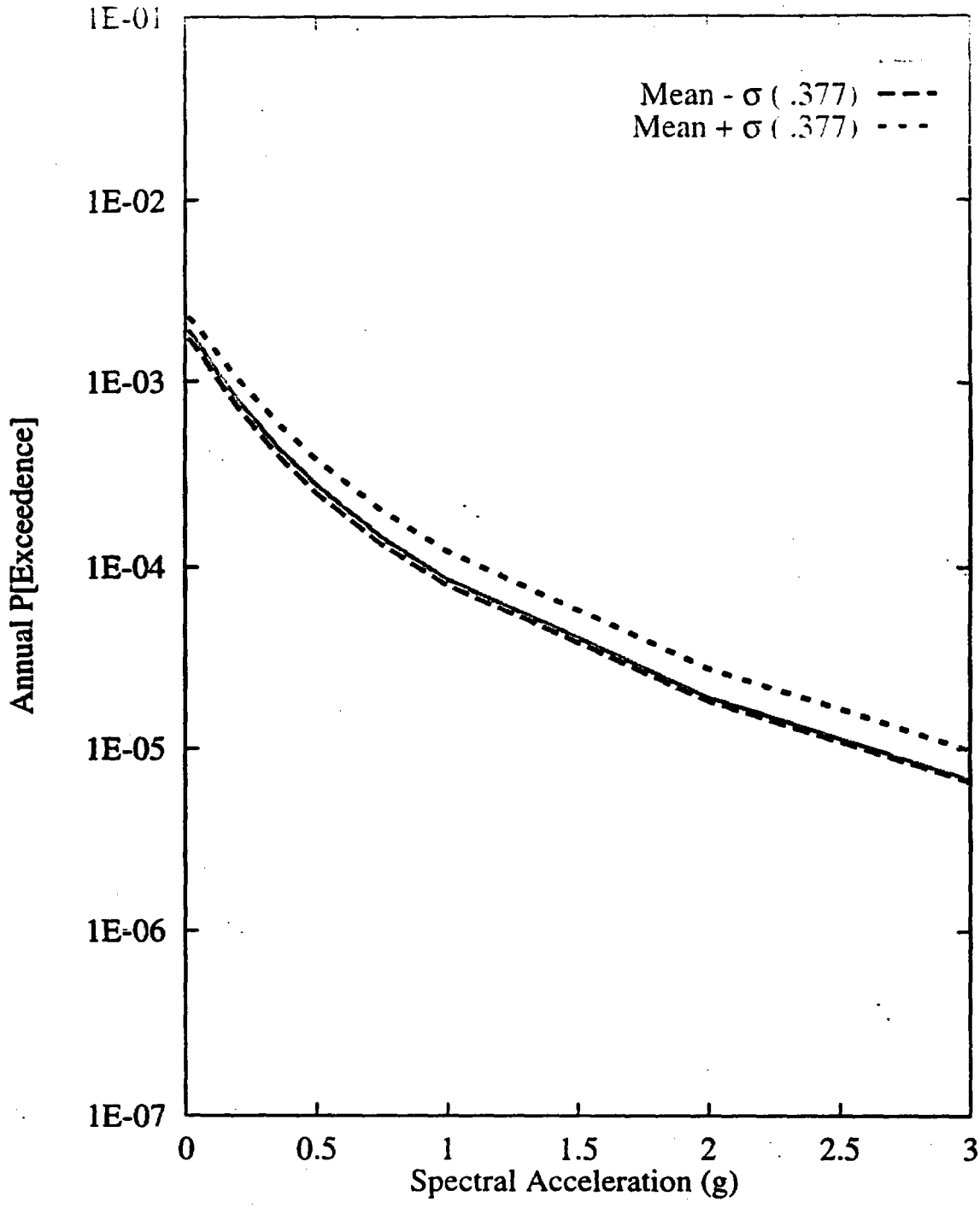

Figure 7-35 Sensitivity of seismic hazard from local faults to Mmax for the East-side fault system: AAR team, 10-Hz horizontal spectral acceleration

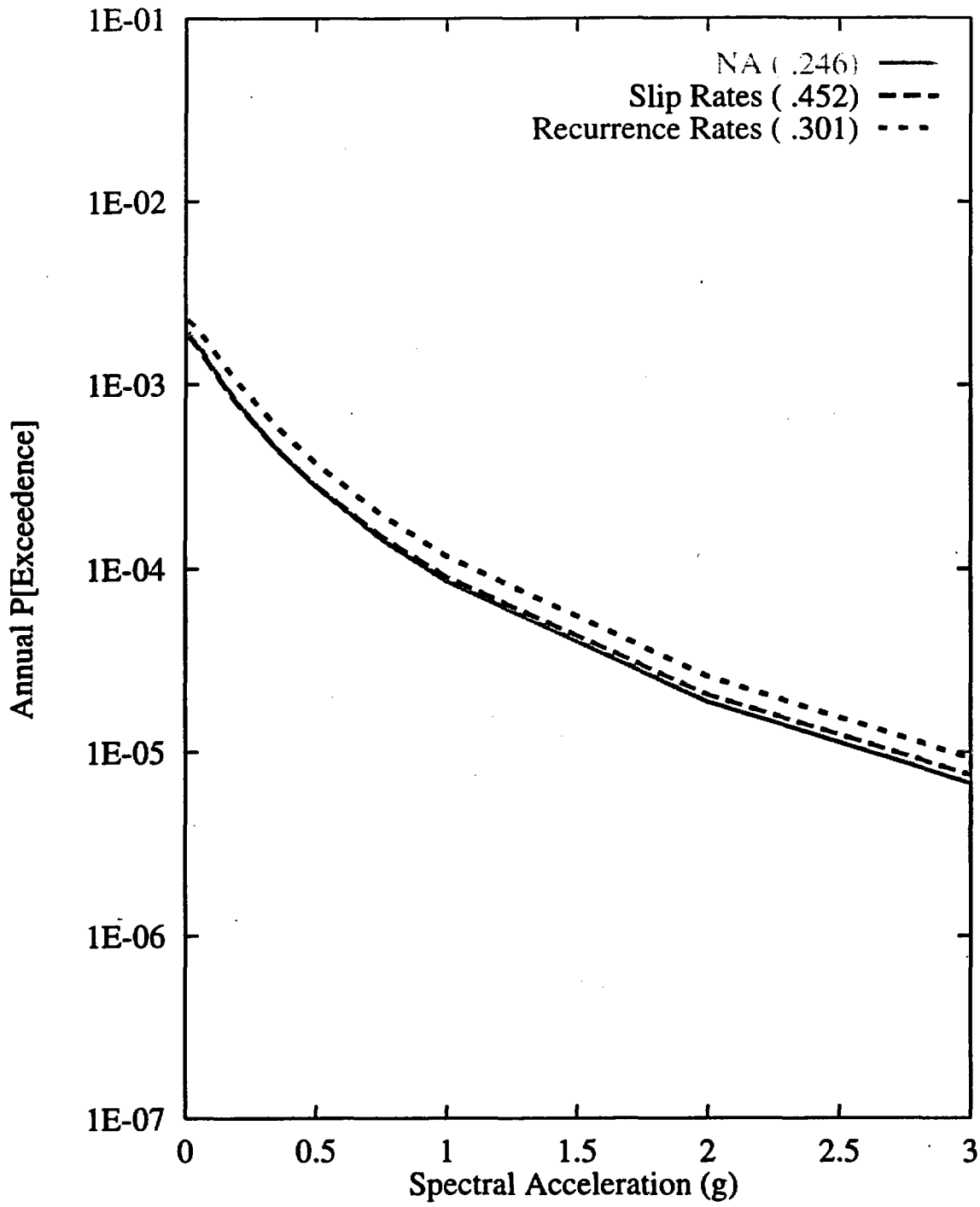

Figure 7-36 Sensitivity of seismic hazard from local faults to recurrence approach for the East-side fault system: AAR team, 10-Hz horizontal spectral acceleration

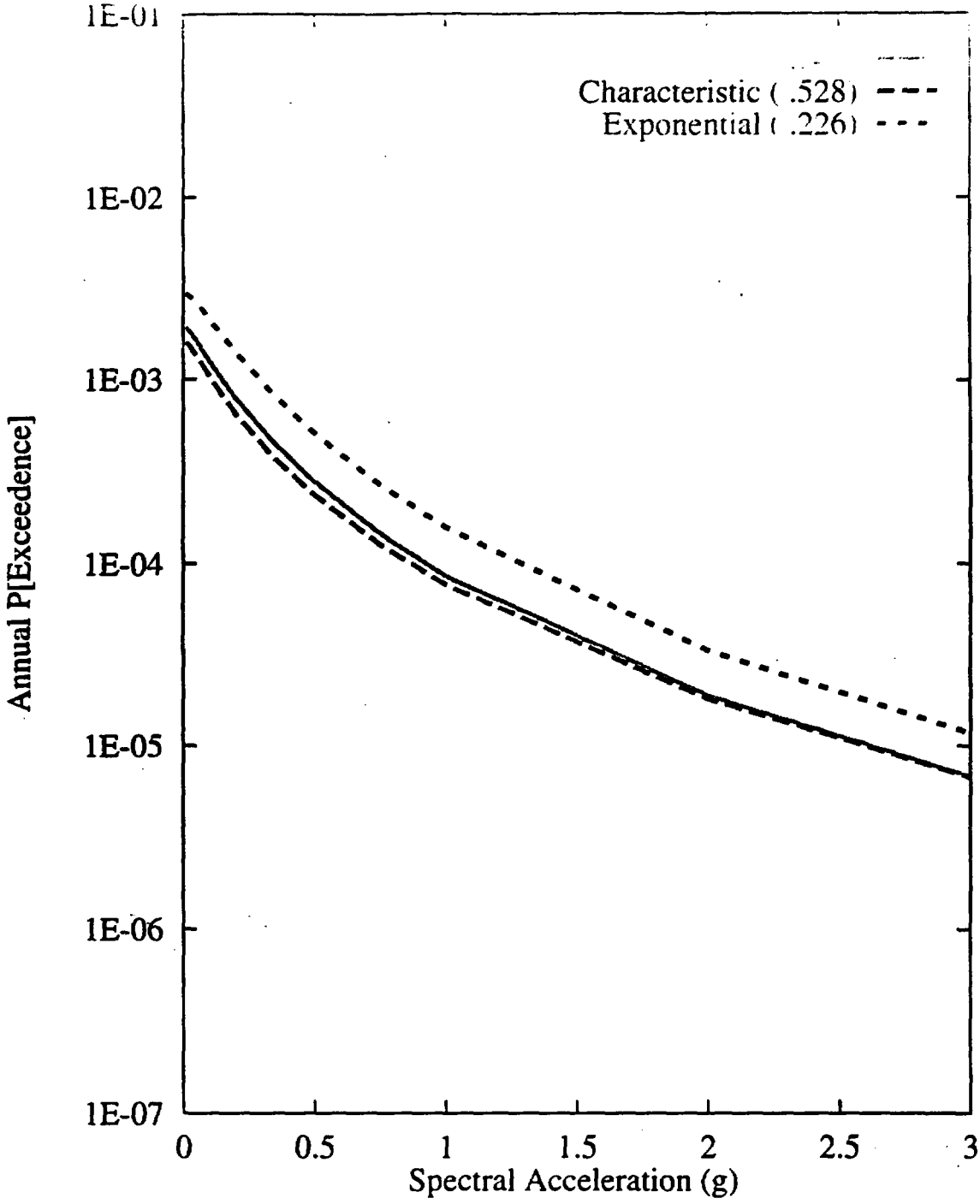

Figure 7-37 Sensitivity of seismic hazard from local faults to recurrence model for the East-side fault system: AAR team, 10-Hz horizontal spectral acceleration

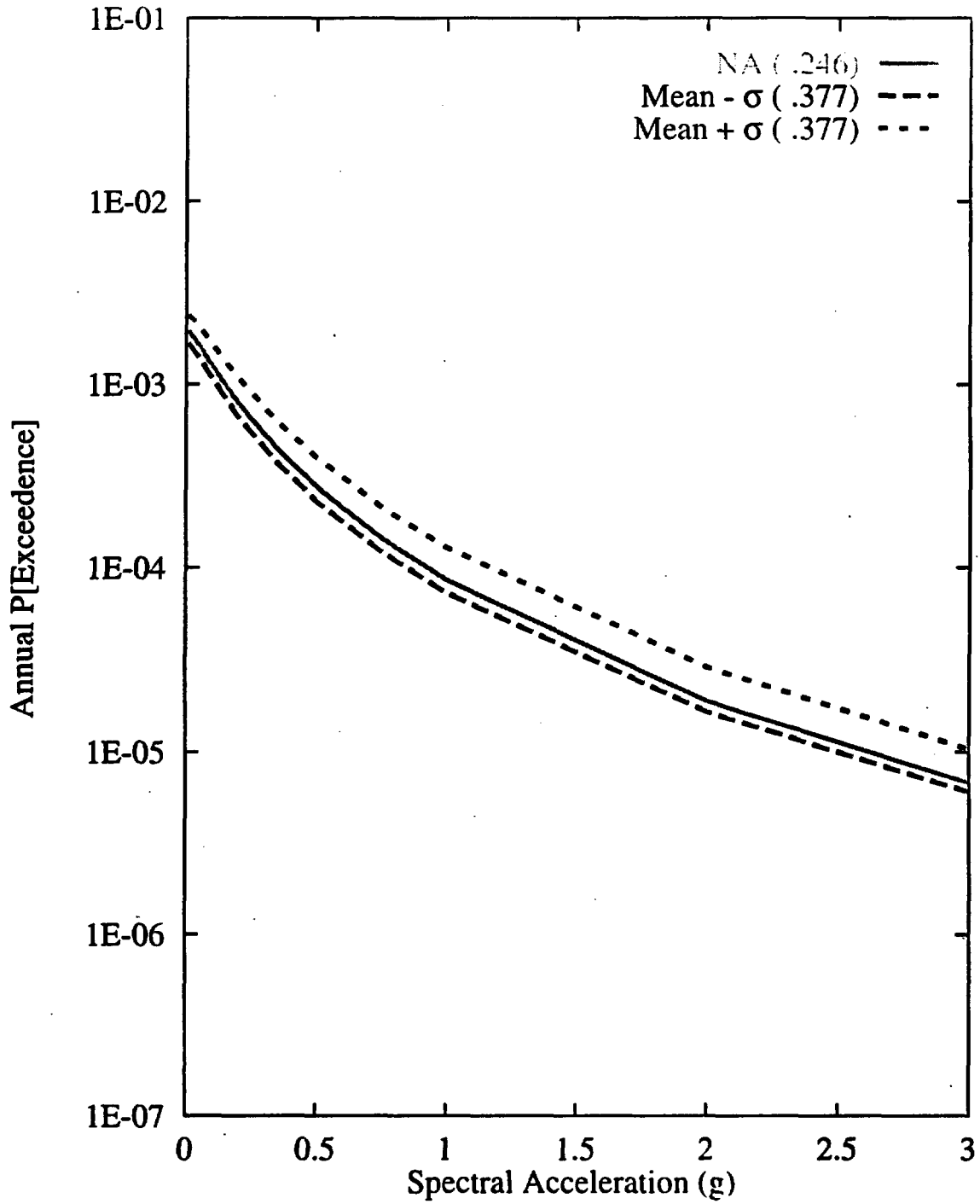

Figure 7-38 Sensitivity of seismic hazard from local faults to recurrence of the East-side fault system: AAR team, 10-Hz horizontal spectral acceleration

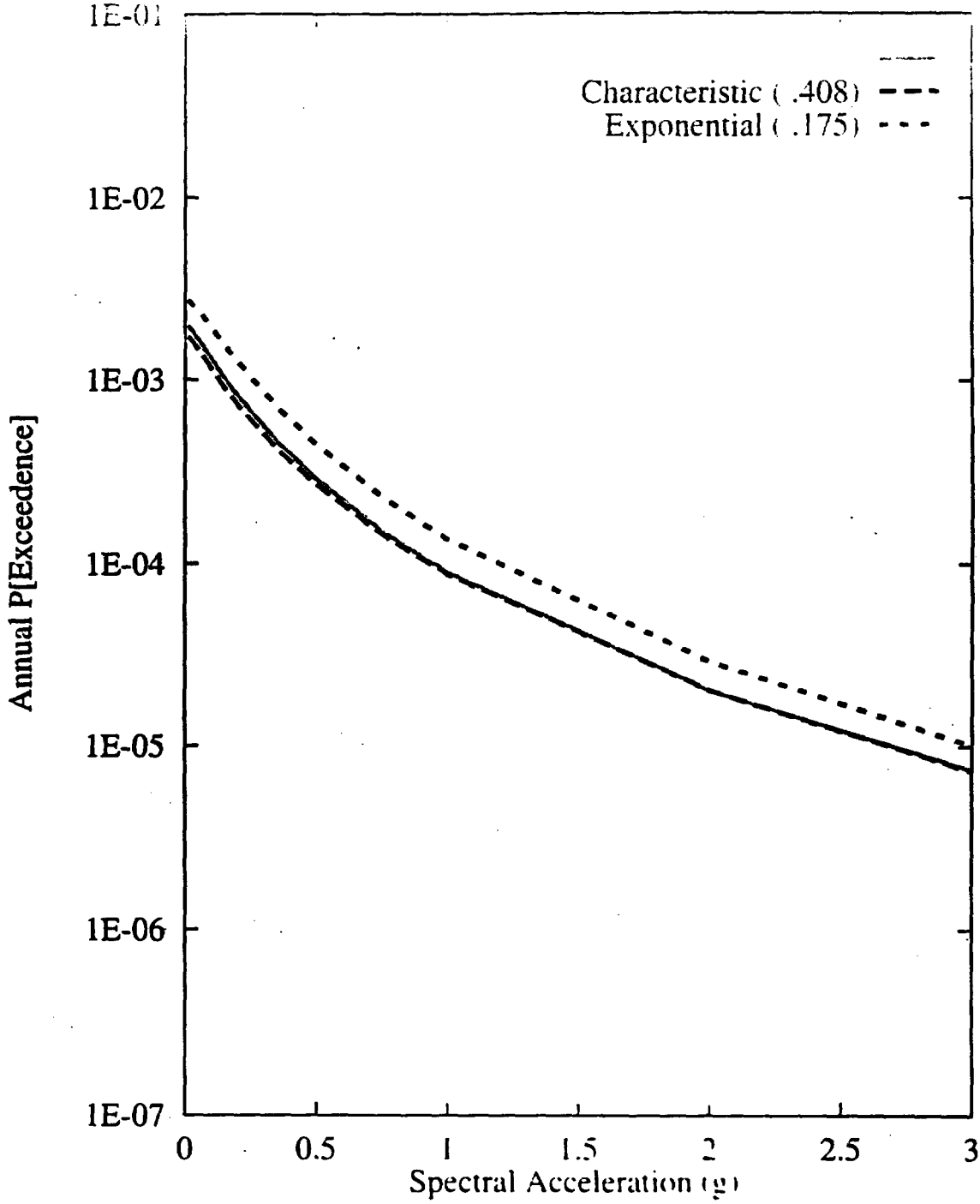

Figure 7-39 Sensitivity of seismic hazard from local faults to recurrence model of the West-side fault system. AAR team. 10-Hz horizontal spectral acceleration

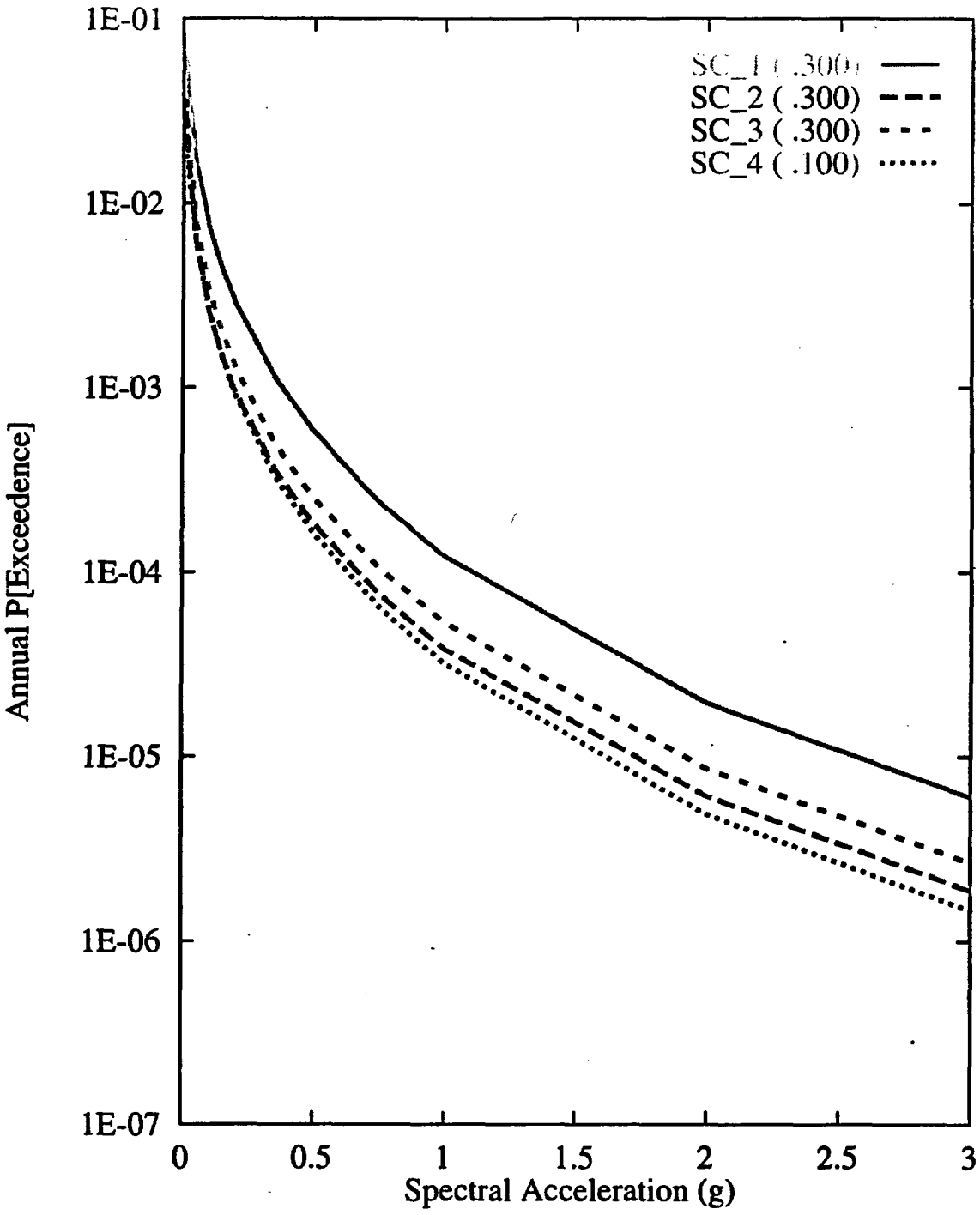

Figure 7-40 Sensitivity of seismic hazard from area source zones to various scenarios (SC) for zonation: AAR team, 10-Hz horizontal spectral acceleration

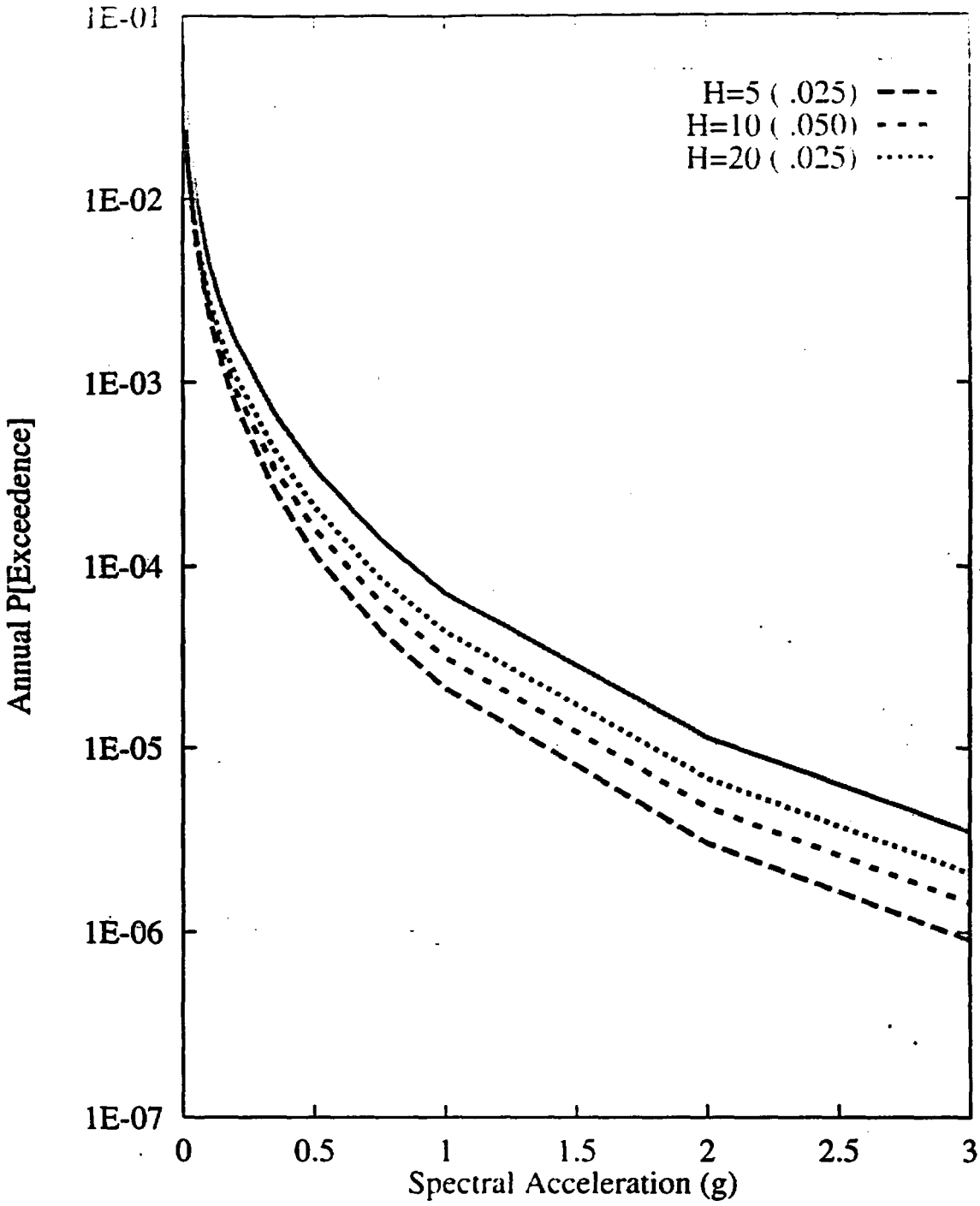

Figure 7-41 Sensitivity of seismic hazard from area source zones to spatial variability and smoothing (H): AAR team, 10-Hz horizontal spectral acceleration

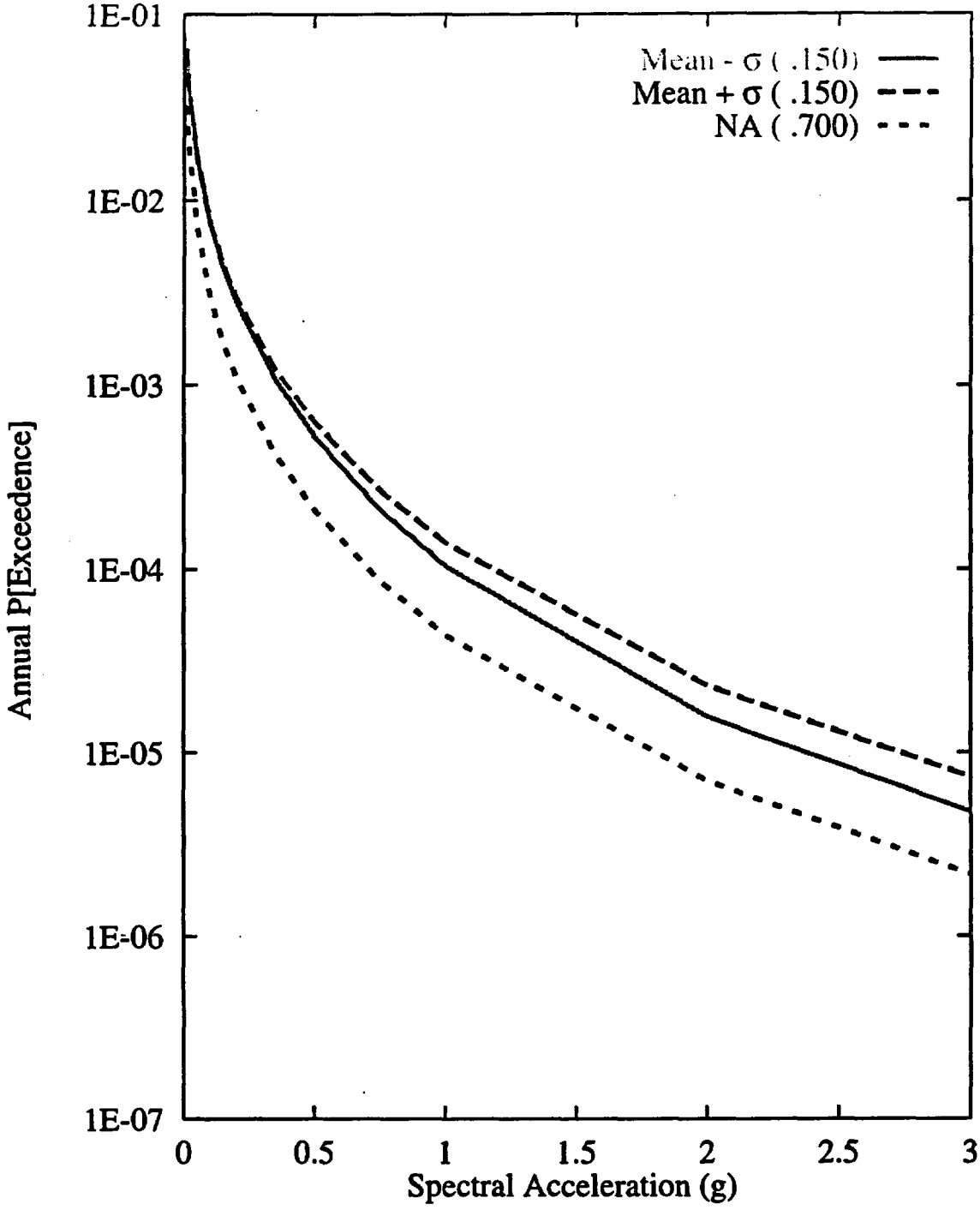

Figure 7-42 Sensitivity of seismic hazard from area source zones to Mmax for the Z2 area source: AAR team, 10-Hz horizontal spectral acceleration

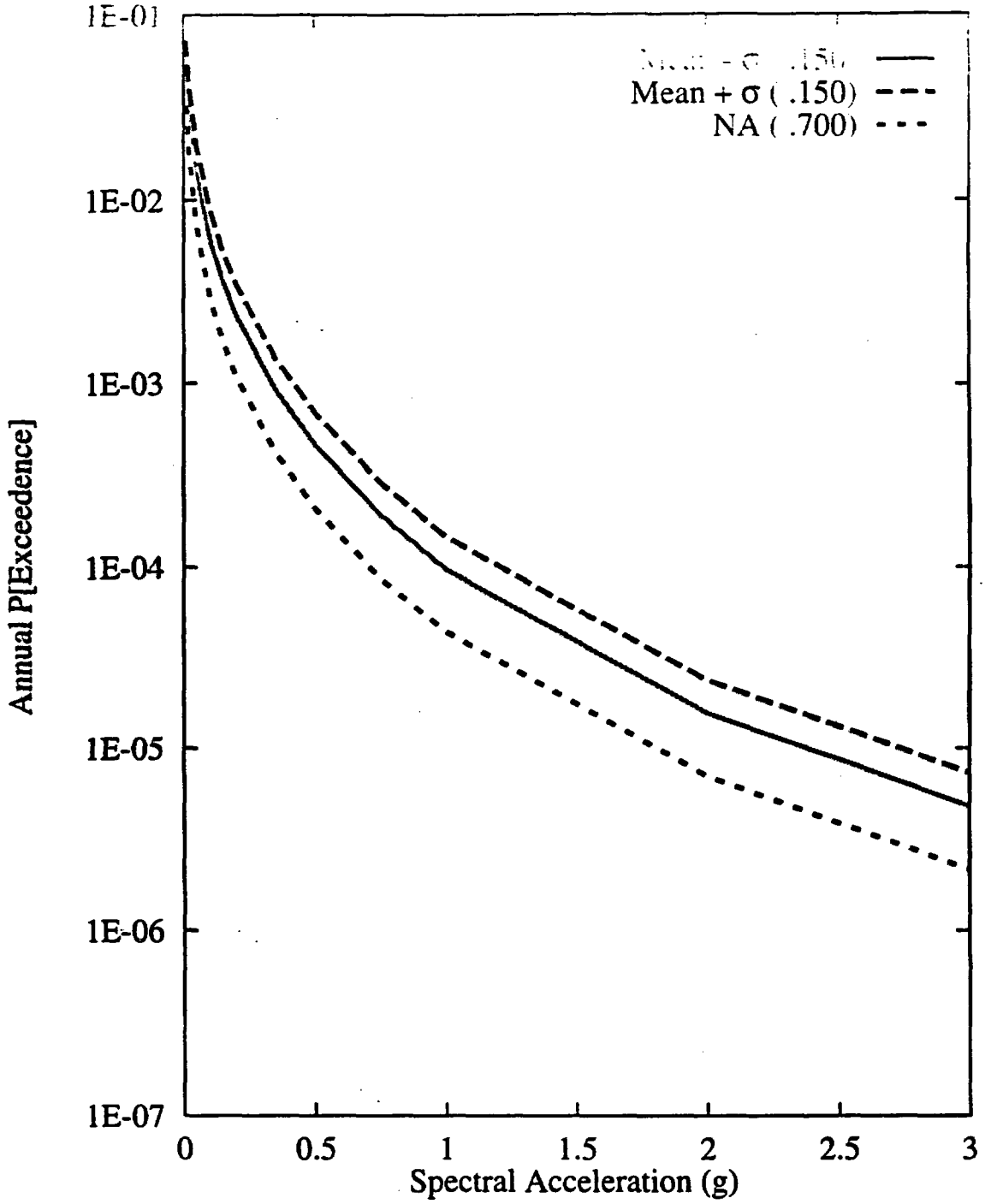

Figure 7-43 Sensitivity of seismic hazard from area source zone to recurrence of the Z2 source zone: AAR team, 10-Hz horizontal spectral acceleration

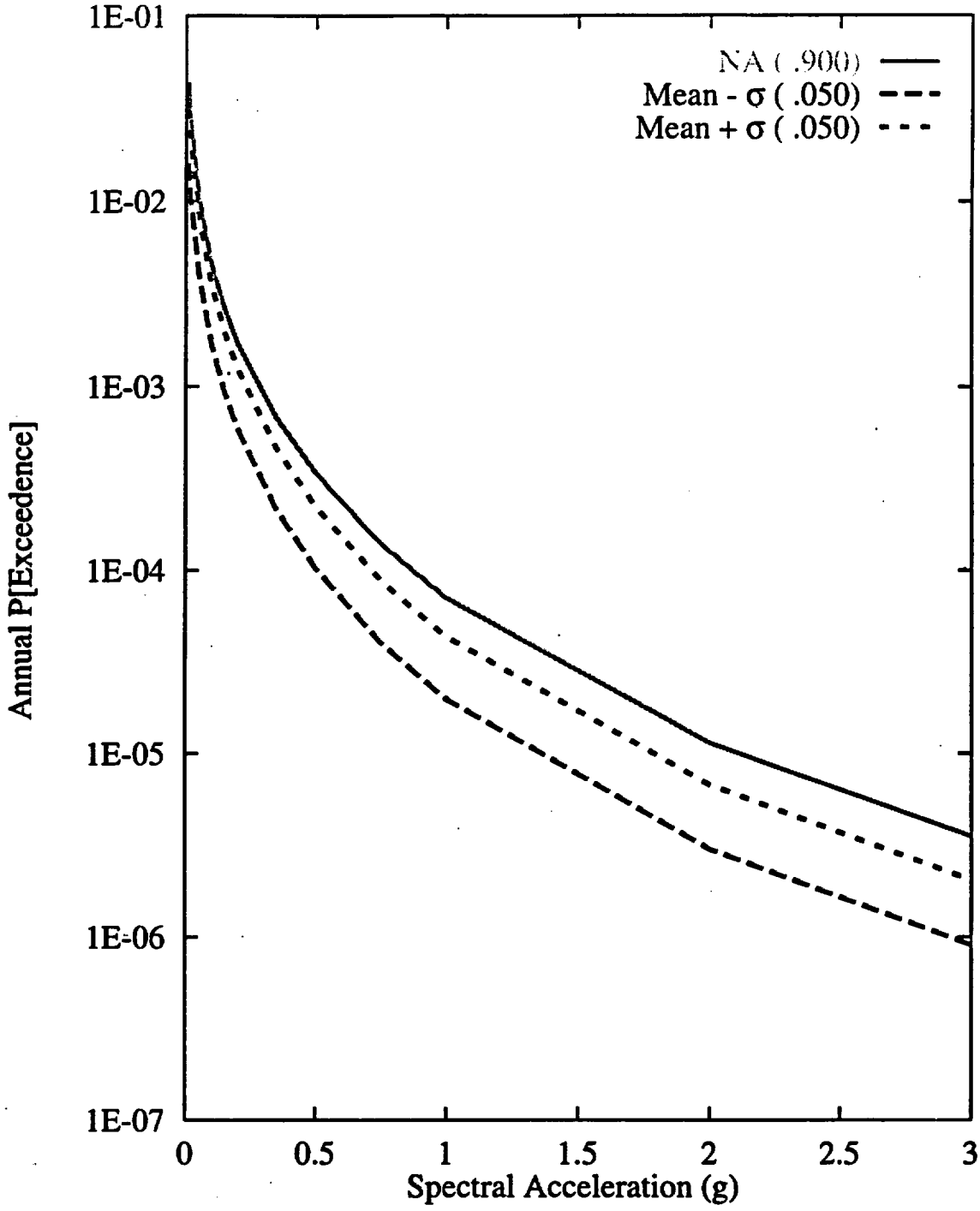

Figure 7-44 Sensitivity of seismic hazard from area source zone to recurrence of the 100-km background zone: AAR team, 10-Hz horizontal spectral acceleration

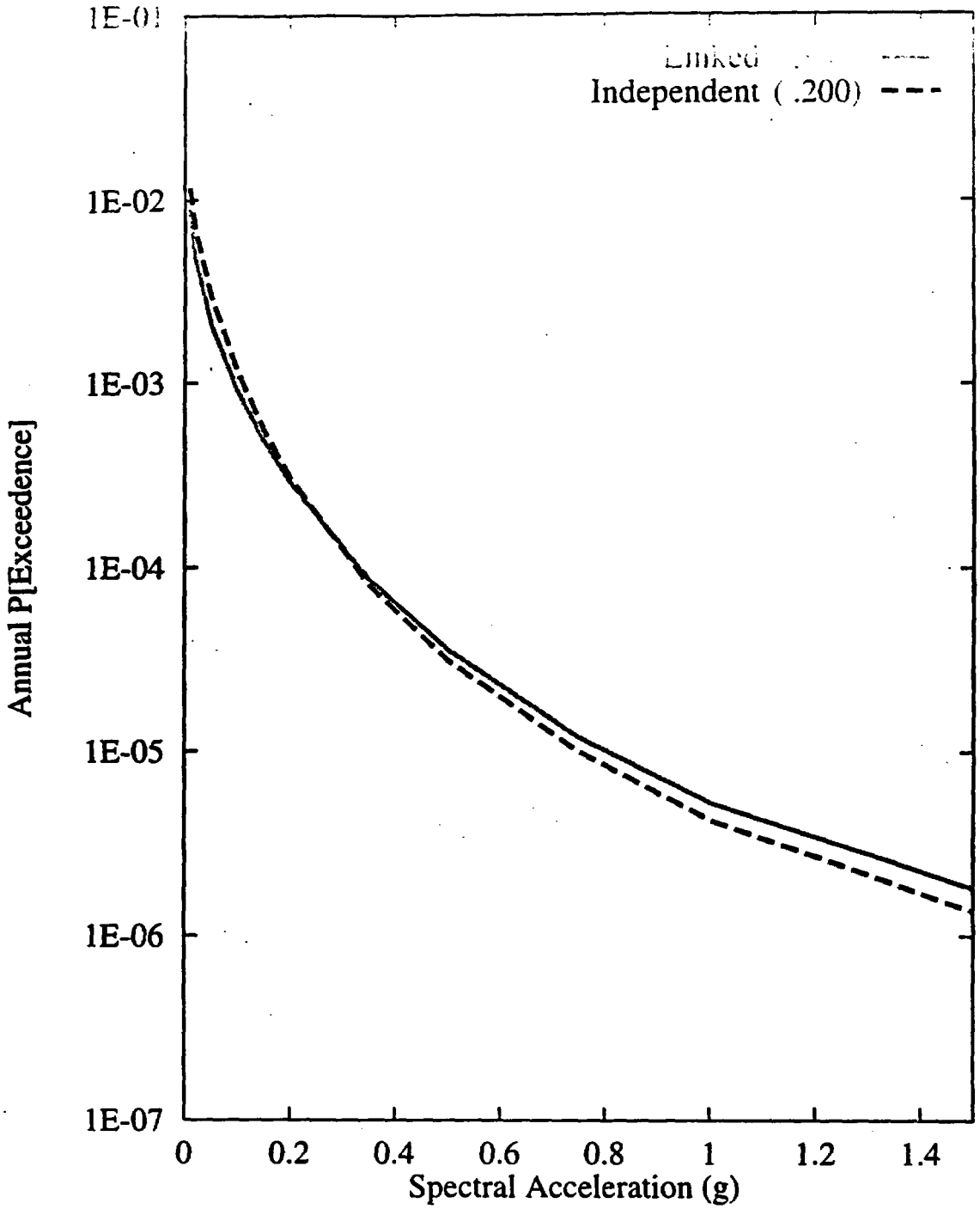

Figure 7-45 Sensitivity of seismic hazard from regional faults to configuration of the Death Valley-Furnace Creek fault system: AAR team, 1-Hz horizontal spectral acceleration

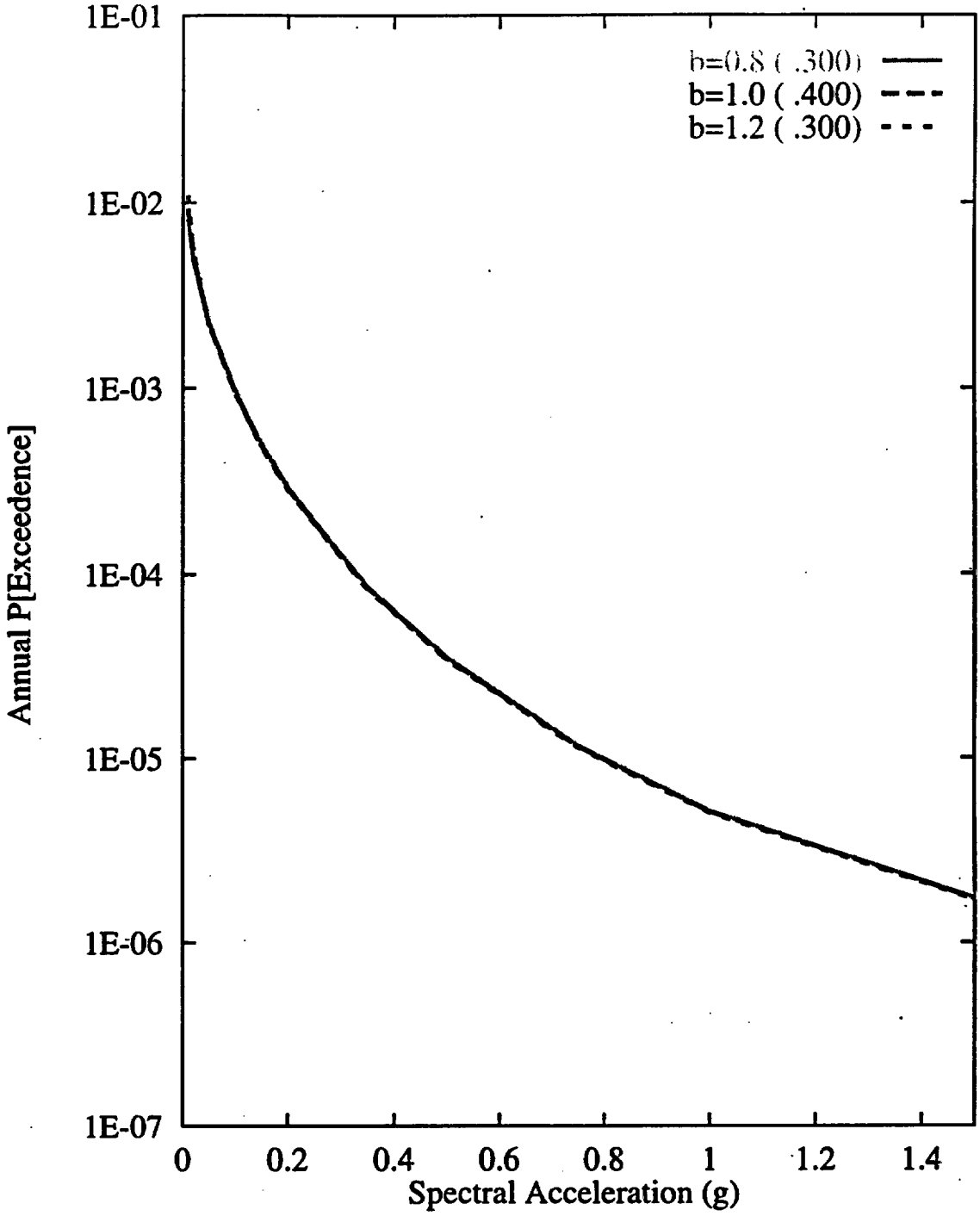

Figure 7-46 Sensitivity of seismic hazard from regional faults to b-values: AAR team, 1-Hz horizontal spectral acceleration

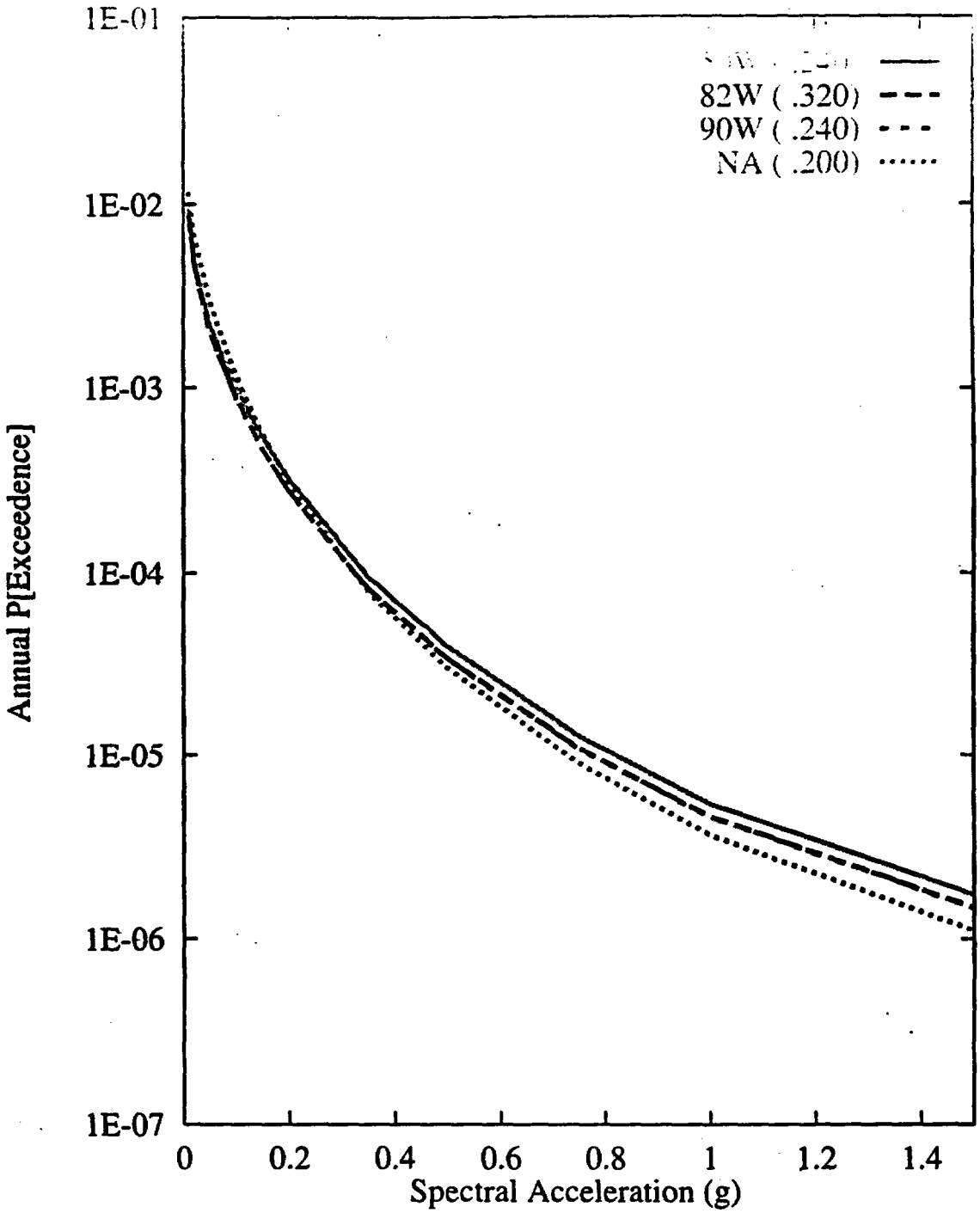

Figure 7-47 Sensitivity of seismic hazard from regional faults to the Death Valley-Furnace Creek fault system: AAR team, 1-Hz horizontal spectral acceleration

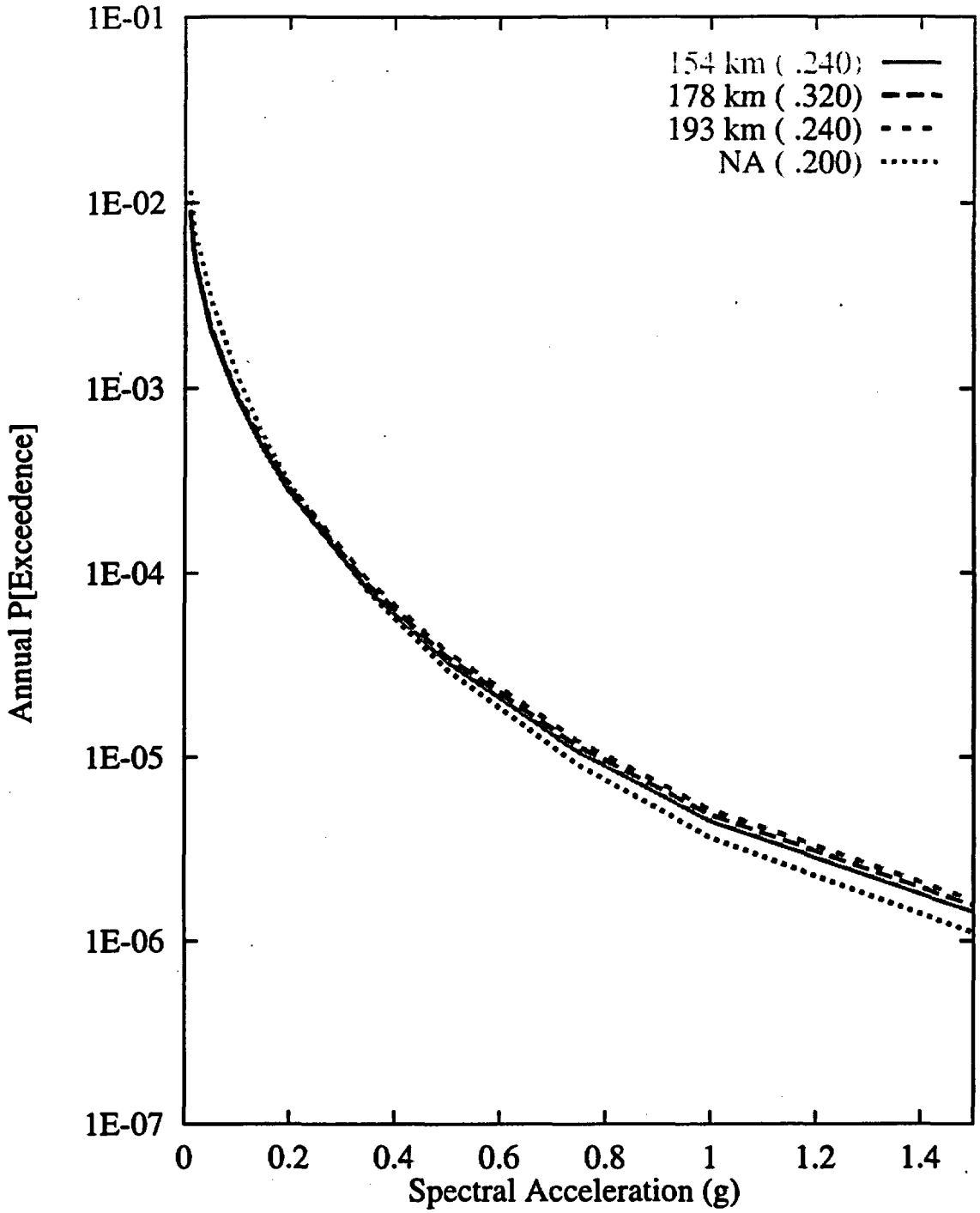

Figure 7-48 Sensitivity of seismic hazard from regional faults to length of the Death Valley-Furnace Creek fault system: AAR team, 1-Hz horizontal spectral acceleration

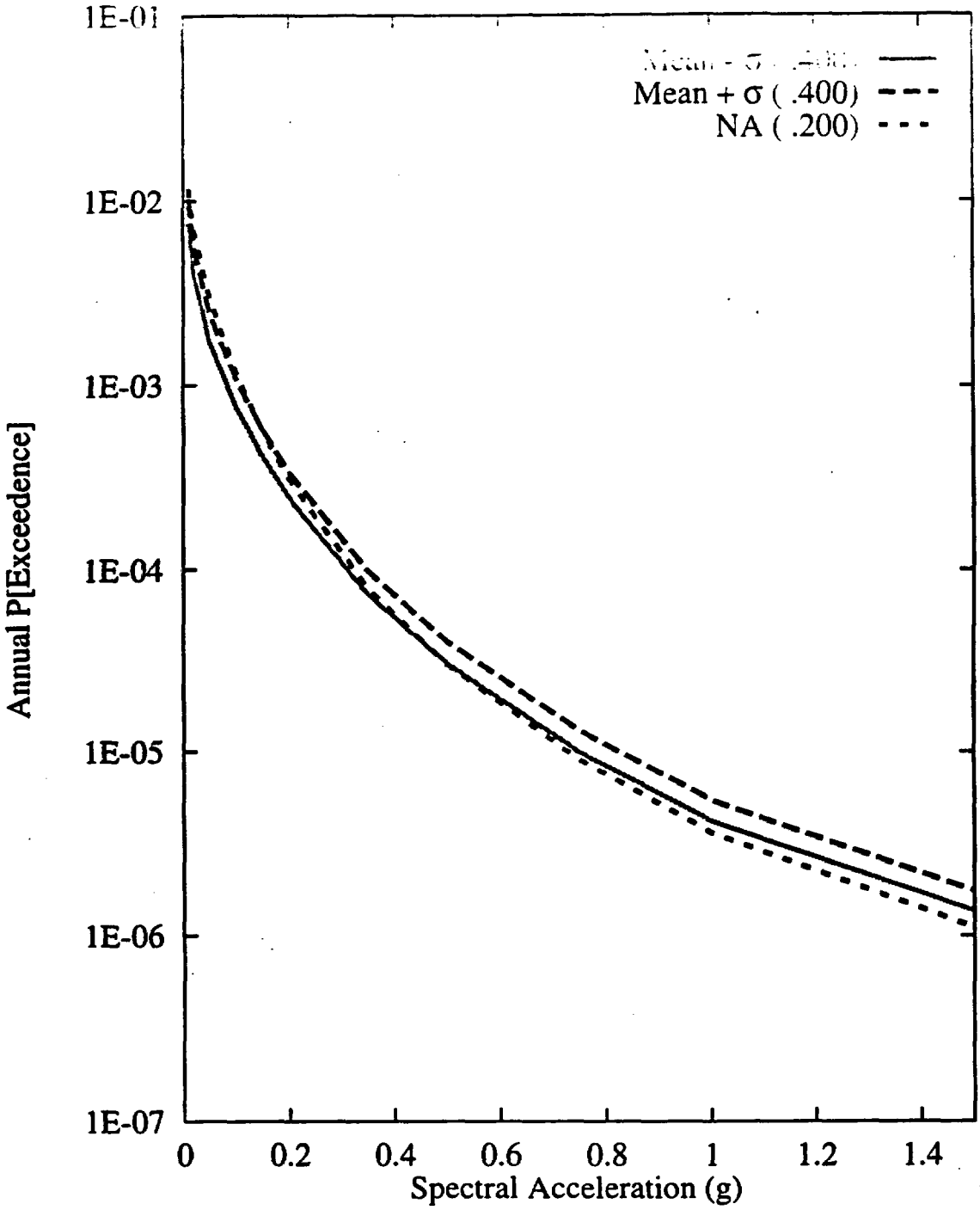

Figure 7-49 Sensitivity of seismic hazard from regional faults to Mmax of the Death Valley-Furnace Creek fault system: AAR team, 1-Hz horizontal spectral acceleration

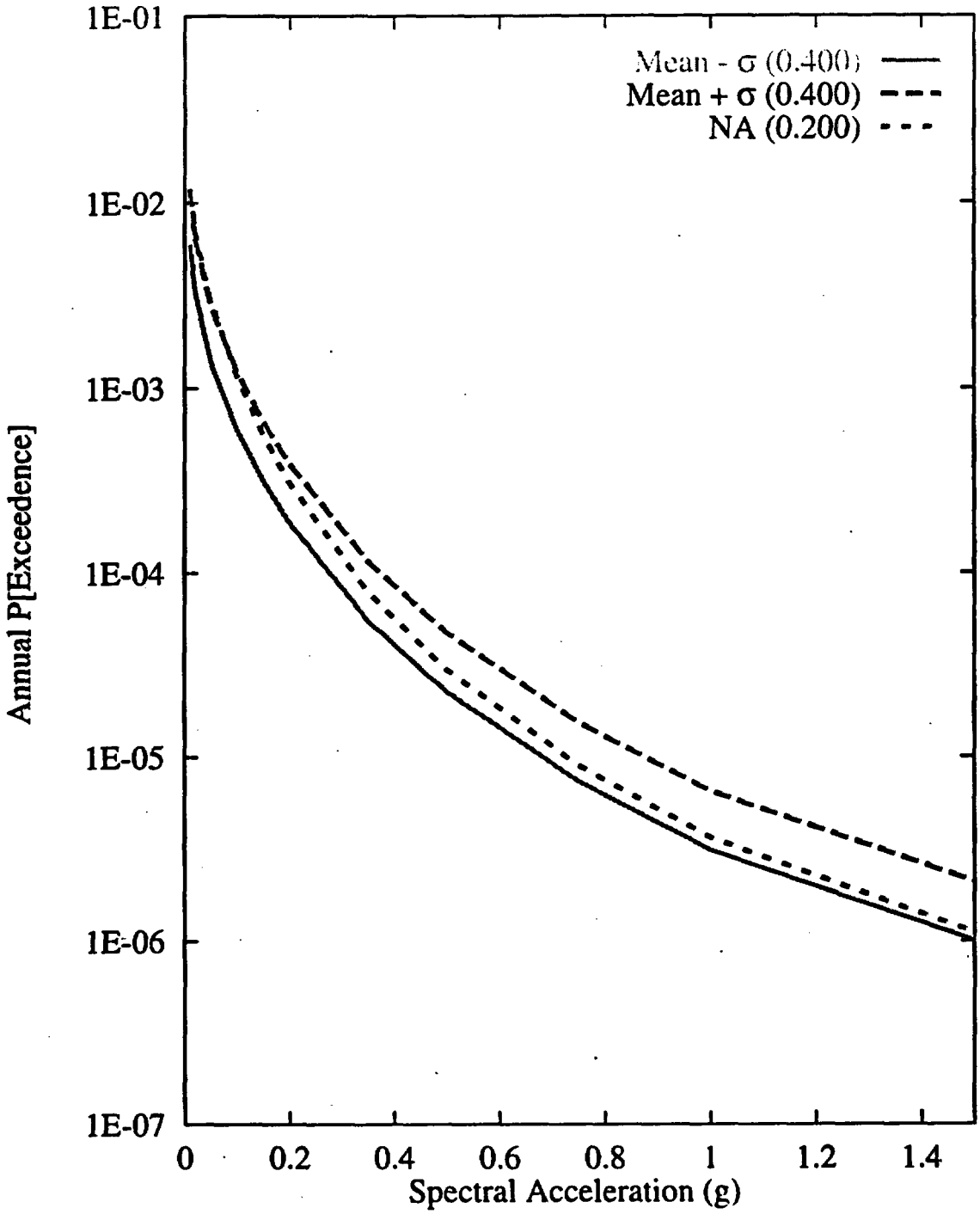

Figure 7-50 Sensitivity of seismic hazard from regional faults to recurrence of the Death Valley-Furnace Creek fault system: AAR team, 1-Hz horizontal spectral acceleration

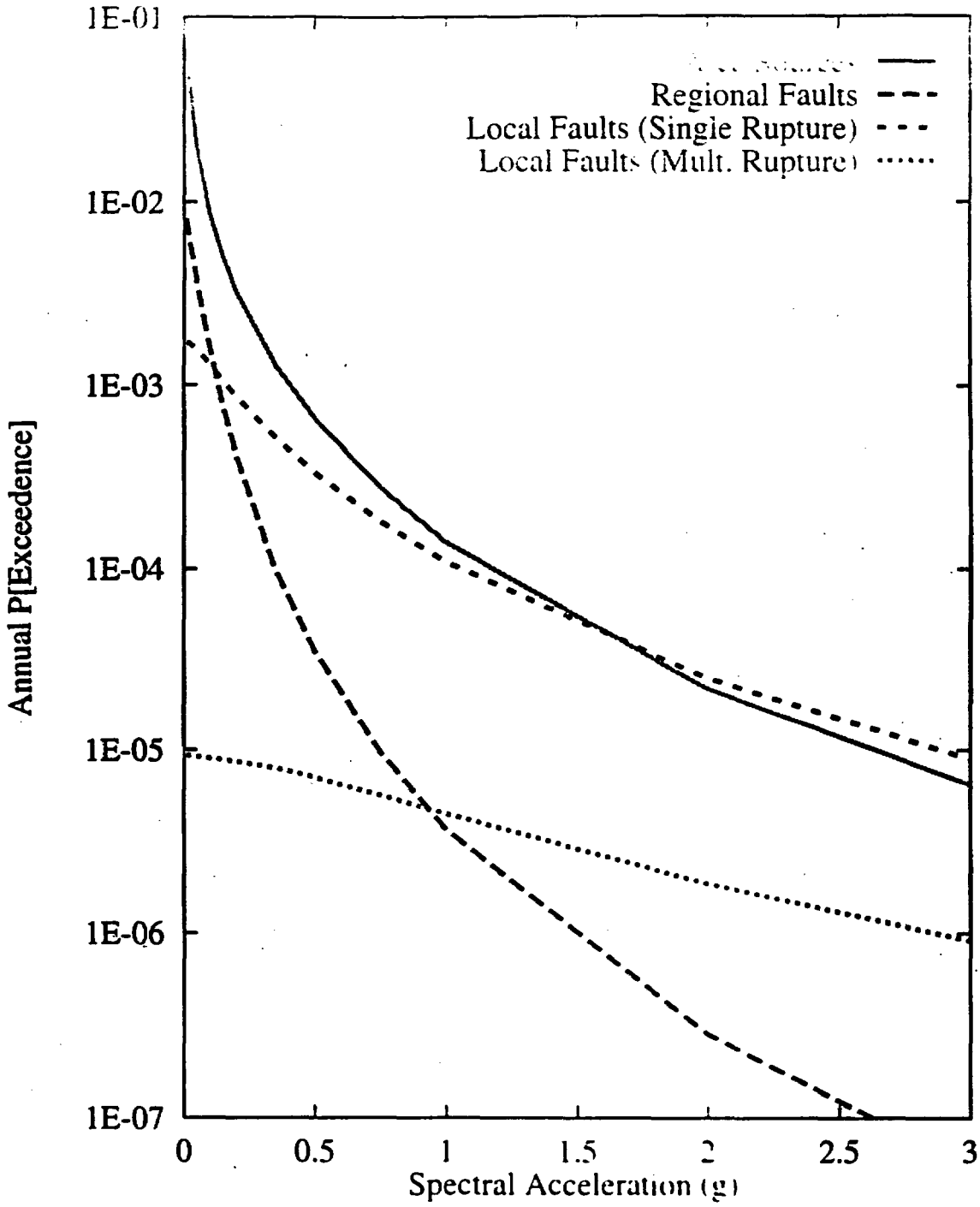

Figure 7-51 Contribution of source type to the mean hazard: ASM team, 10-Hz horizontal spectral acceleration.

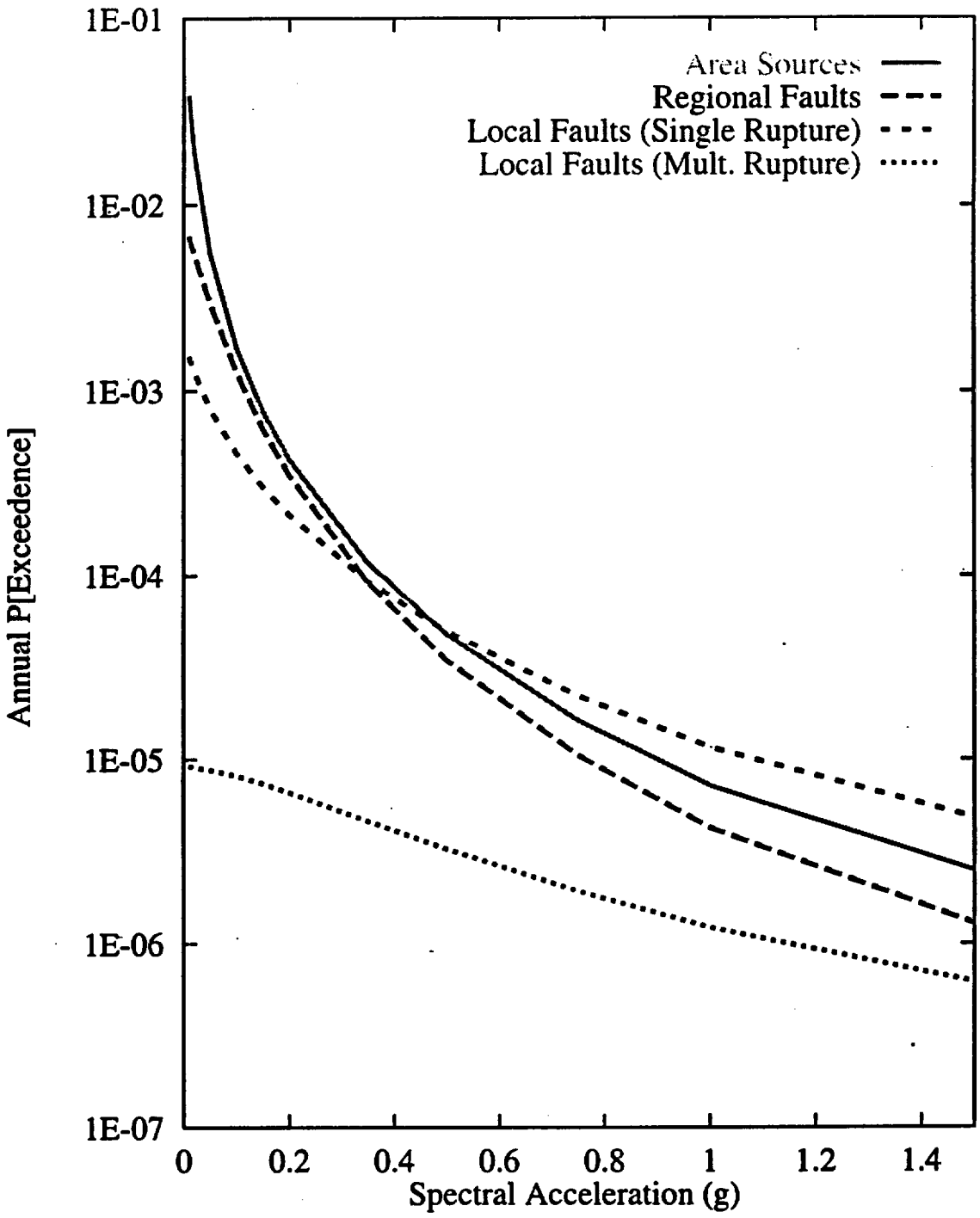

Figure 7-52 Contribution of source type to the mean hazard: ASM team, 1-Hz horizontal spectral acceleration

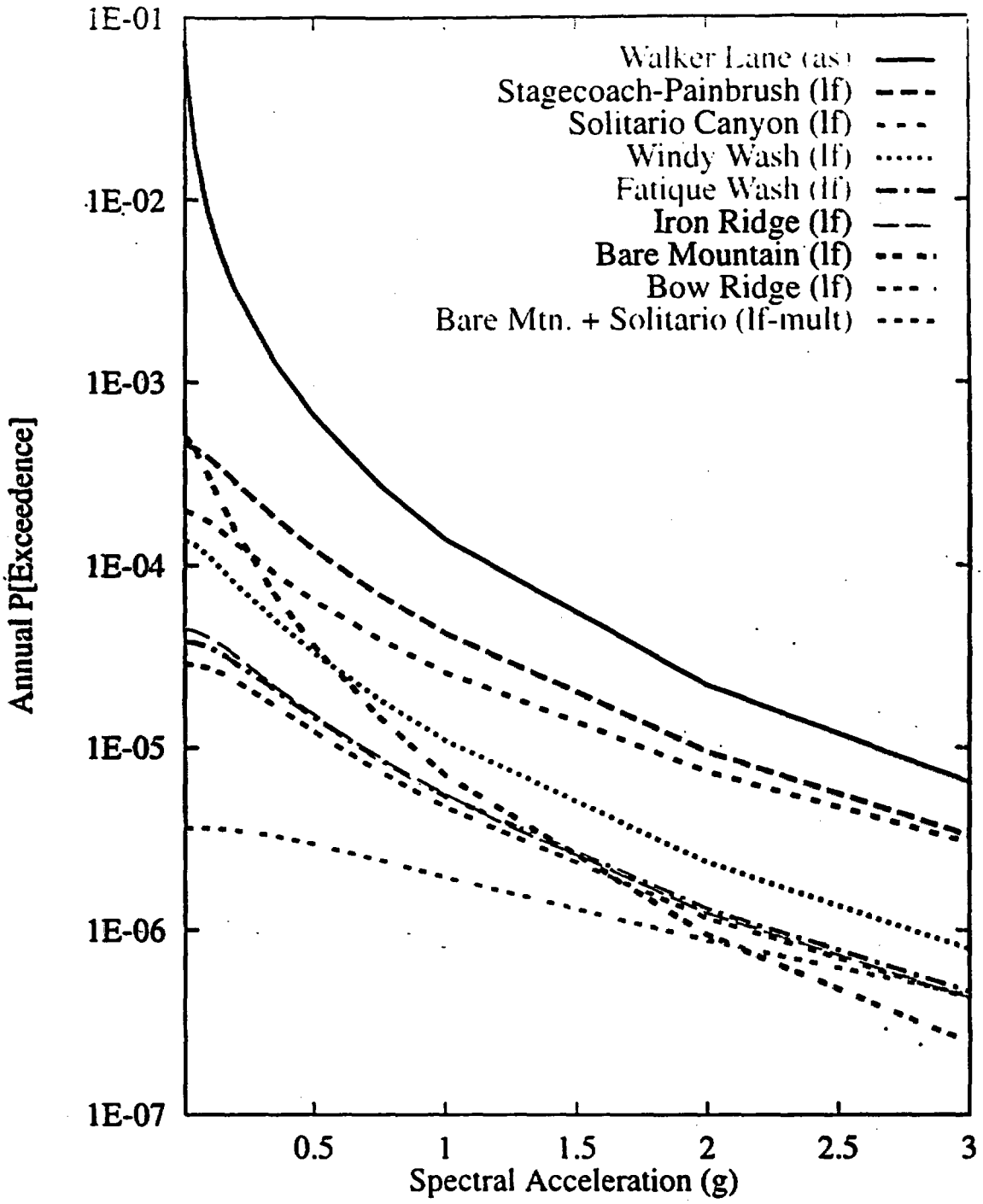

Figure 7-53 Mean seismic hazard from dominant seismic sources: ASM team, 10-Hz horizontal spectral acceleration. Acronyms in parentheses refer to source types: as-area source zone; lf-local fault; and mult-multiple fault rupture.

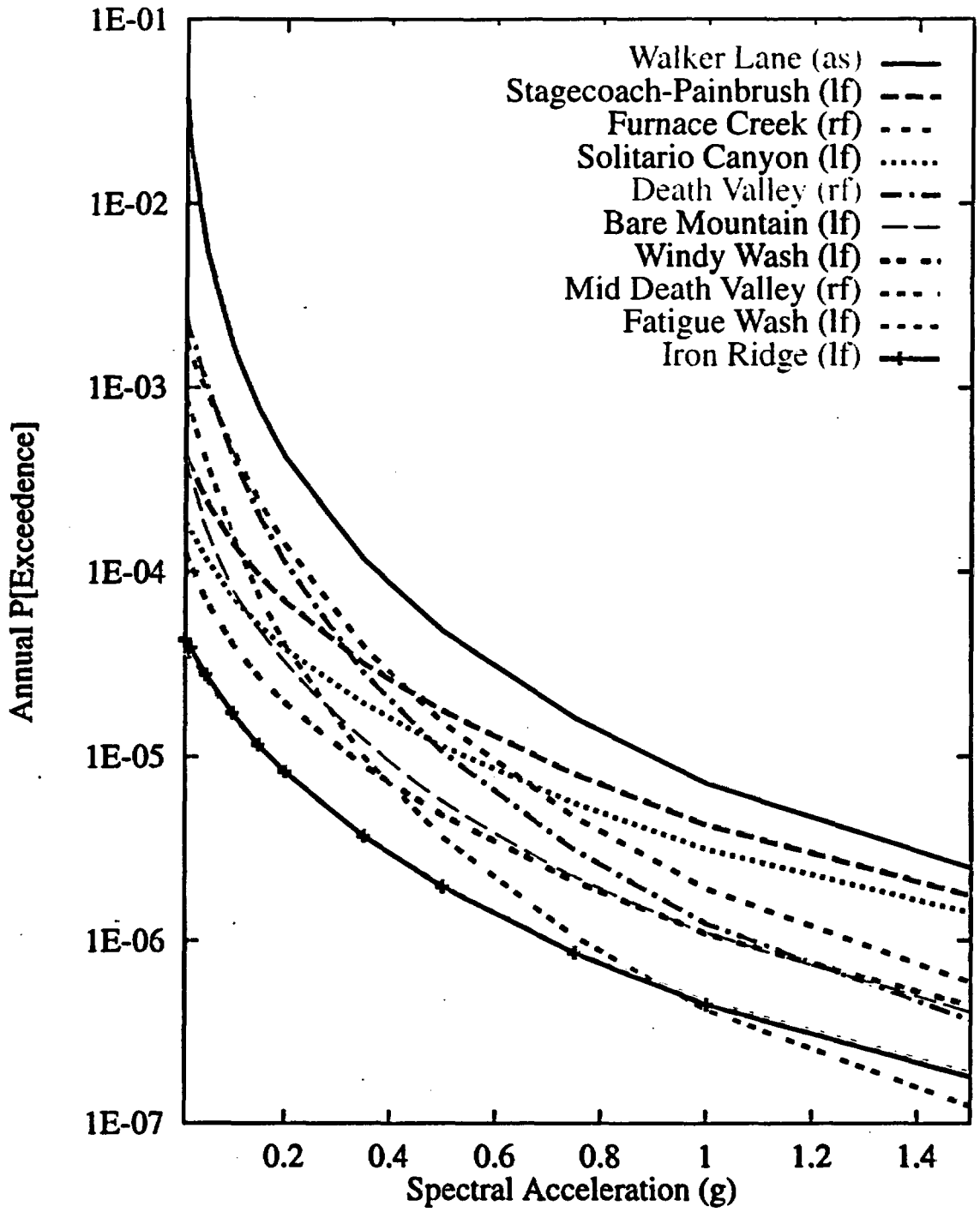

Figure 7-54 Mean seismic hazard from dominant seismic sources: ASM team, 1-Hz horizontal spectral acceleration. Acronyms in parentheses refer to source types: as-area source zone; lf-local fault; and rf-regional fault.

10 Hz, ASM Area Sources

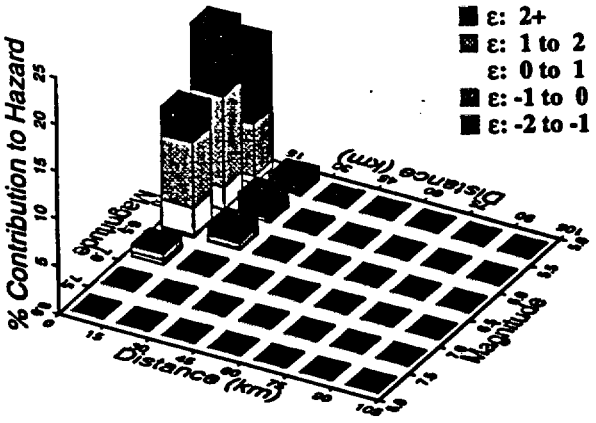

10 Hz, ASM Regional Faults

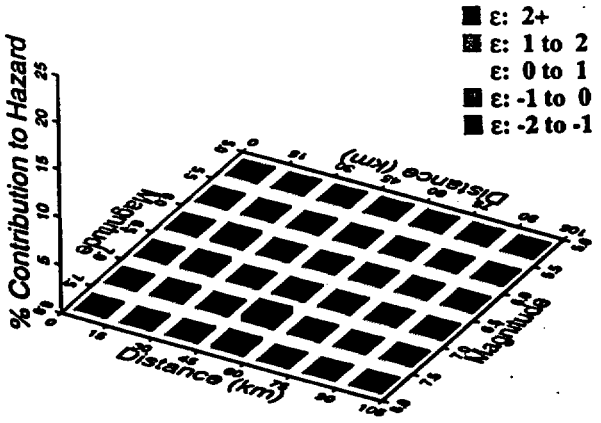

10 Hz, ASM Local Faults (Single)

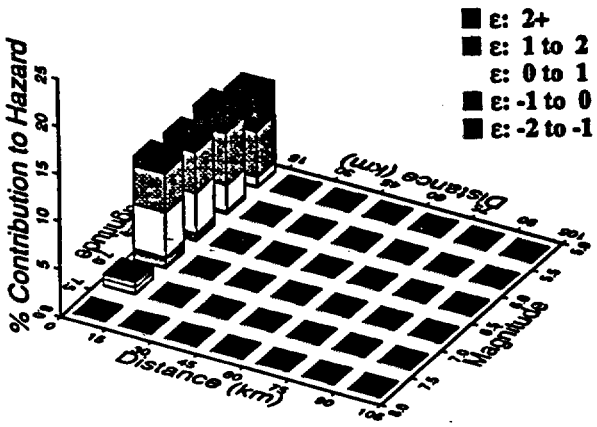

10 Hz, ASM Local Faults (Mult.)

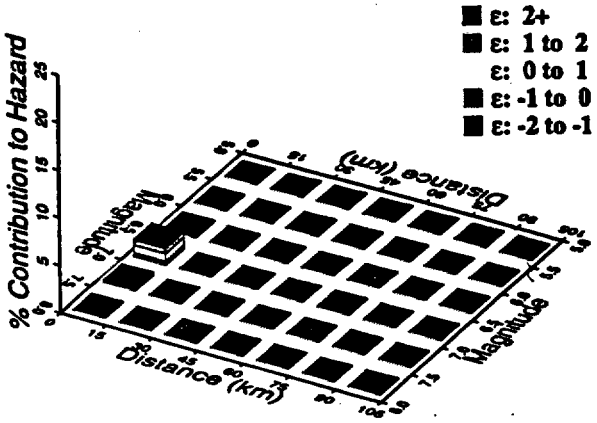

Figure 7-55 Magnitude-distance-epsilon distributions for the four source types: ASM team, 10-Hz horizontal spectral acceleration at 10^{-4} exceedance probability

1 Hz, ASM Area Sources

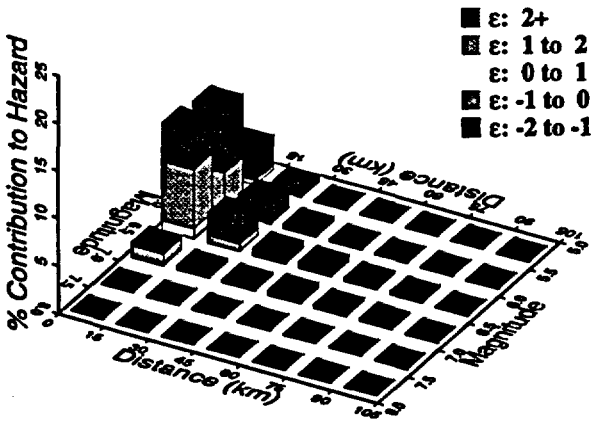

1 Hz, ASM Regional Faults

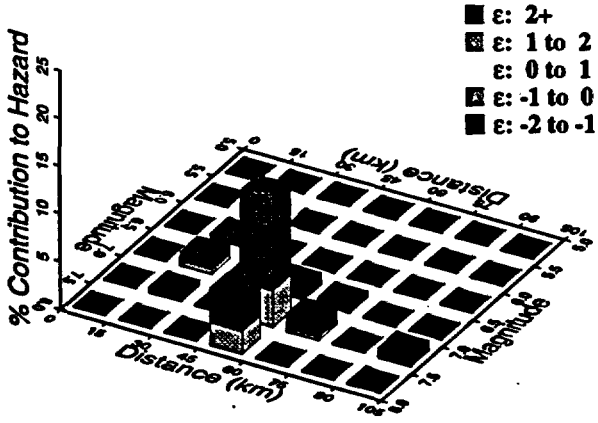

1 Hz, ASM Local Faults (Single)

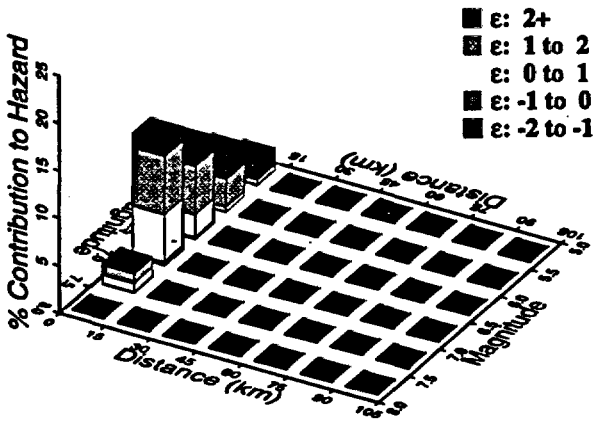

1 Hz, ASM Local Faults (Mult.)

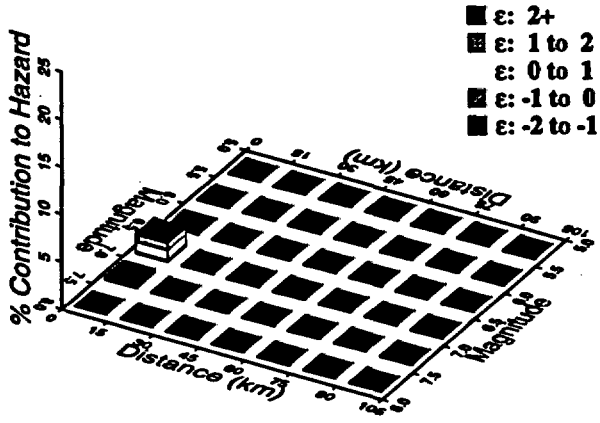

Figure 7-56 Magnitude-distance-epsilon distributions for the four source types: ASM team, 1-Hz horizontal spectral acceleration at 10^{-4} exceedance probability

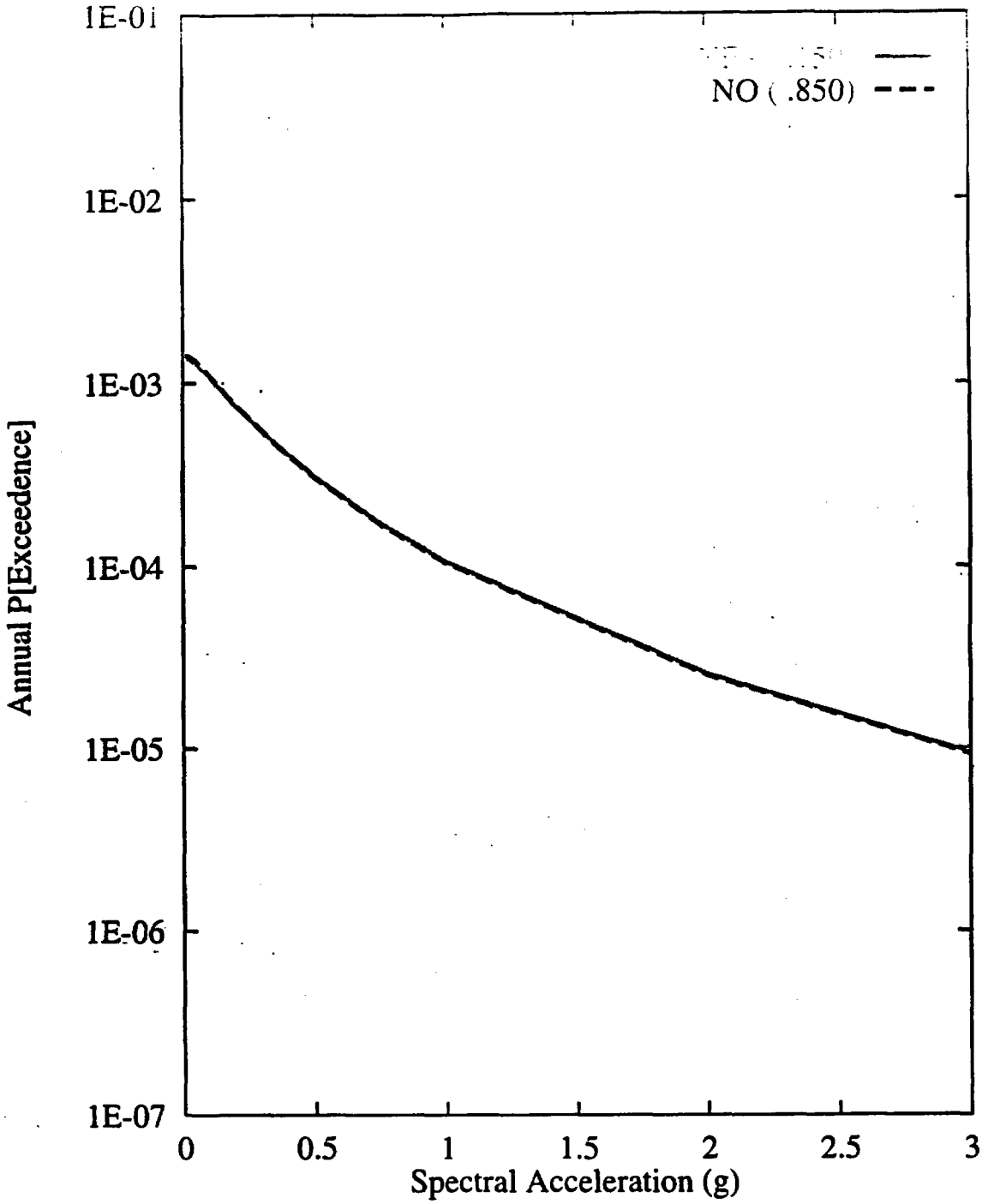

Figure 7-57 Sensitivity of seismic hazard from local faults to existence of detachment: ASM team, 10-Hz horizontal spectral acceleration

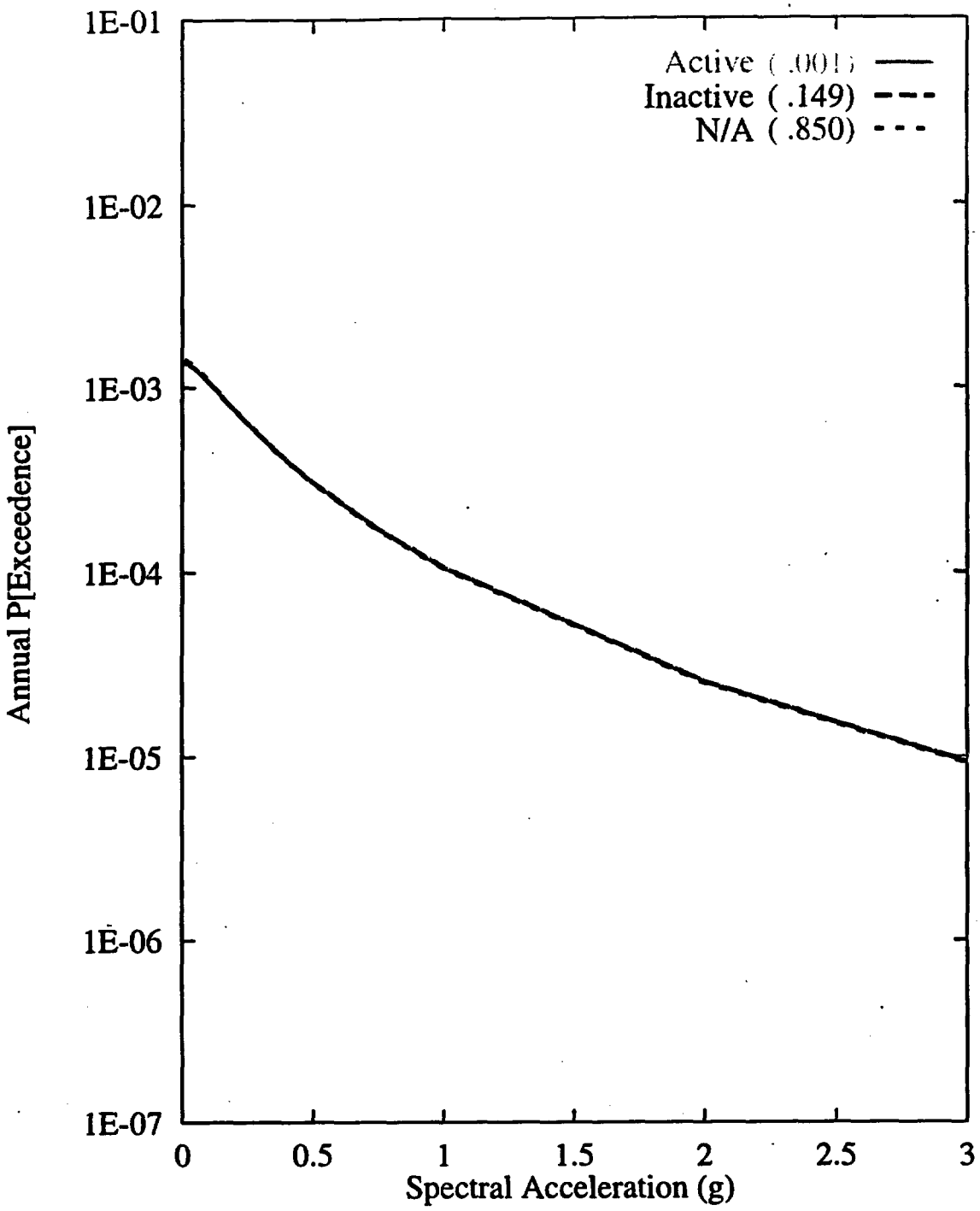

Figure 7-58 Sensitivity of seismic hazard from local faults to activity of datachment: ASM team, 10-Hz horizontal spectral acceleration

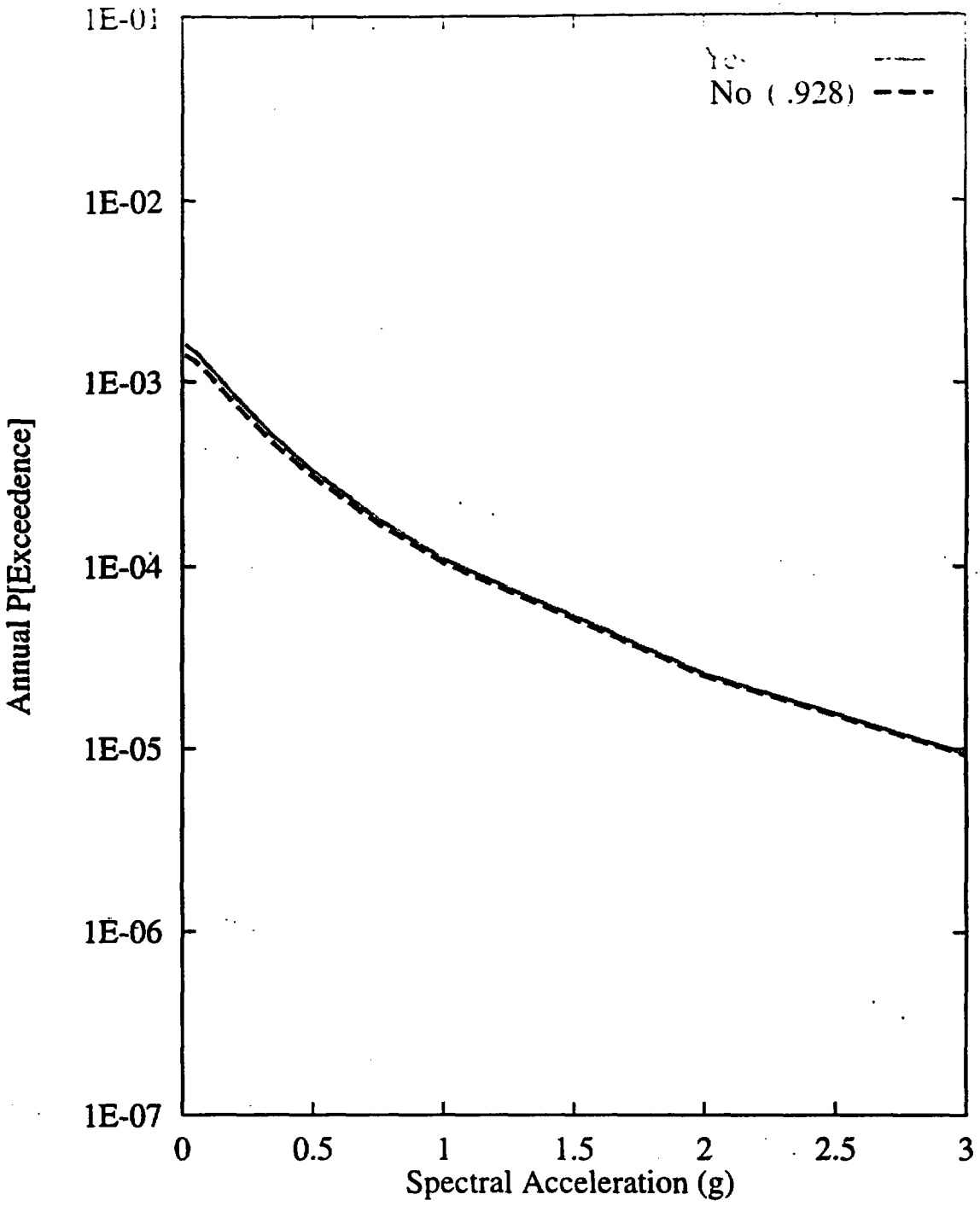

Figure 7-59 Sensitivity of seismic hazard from local faults to existence of buried strike-slip fault: ASM team, 10-Hz horizontal spectral acceleration

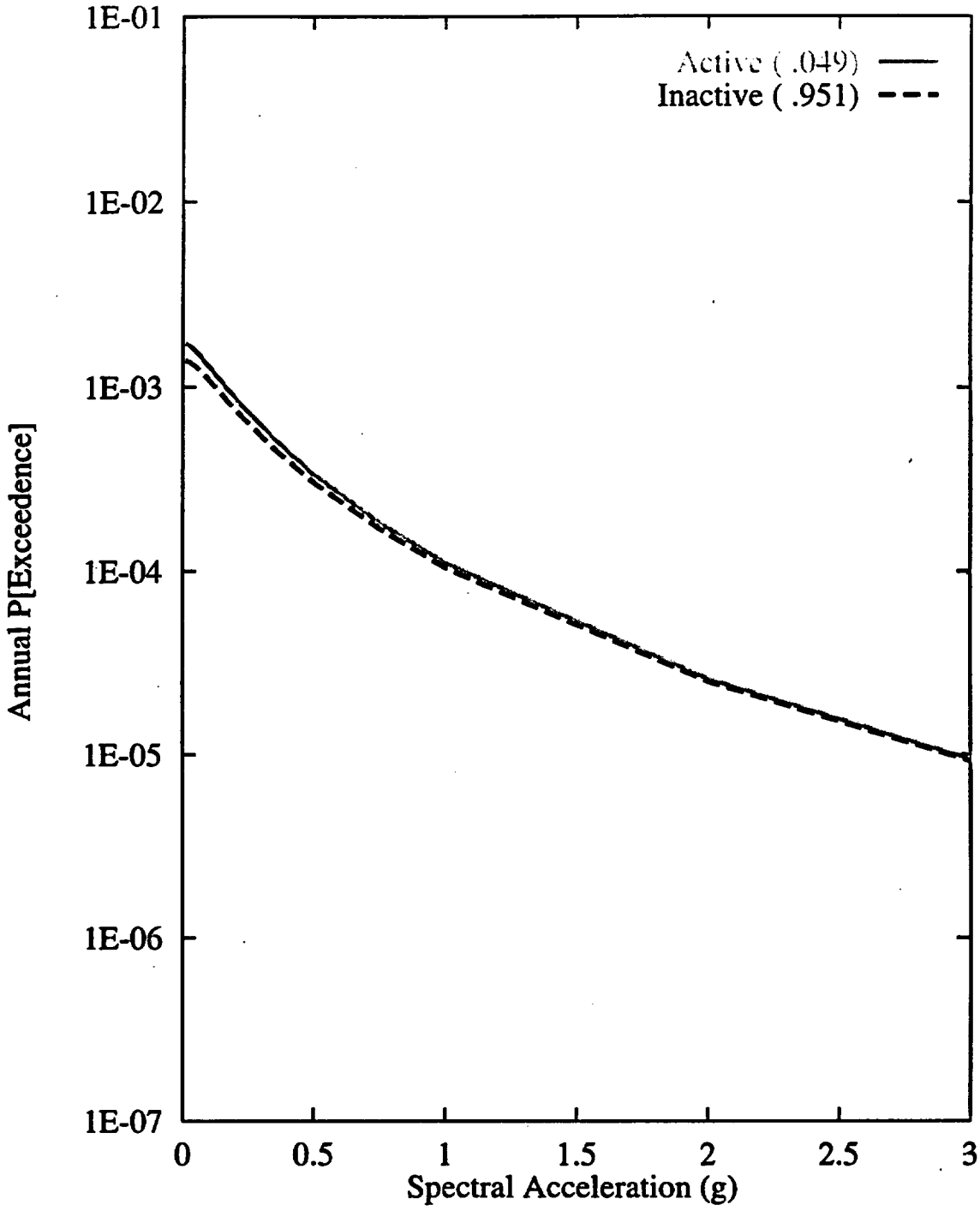

Figure 7-60 Sensitivity of seismic hazard from local faults to activity of buried-strike-slip fault: ASM team, 10-Hz horizontal spectral acceleration

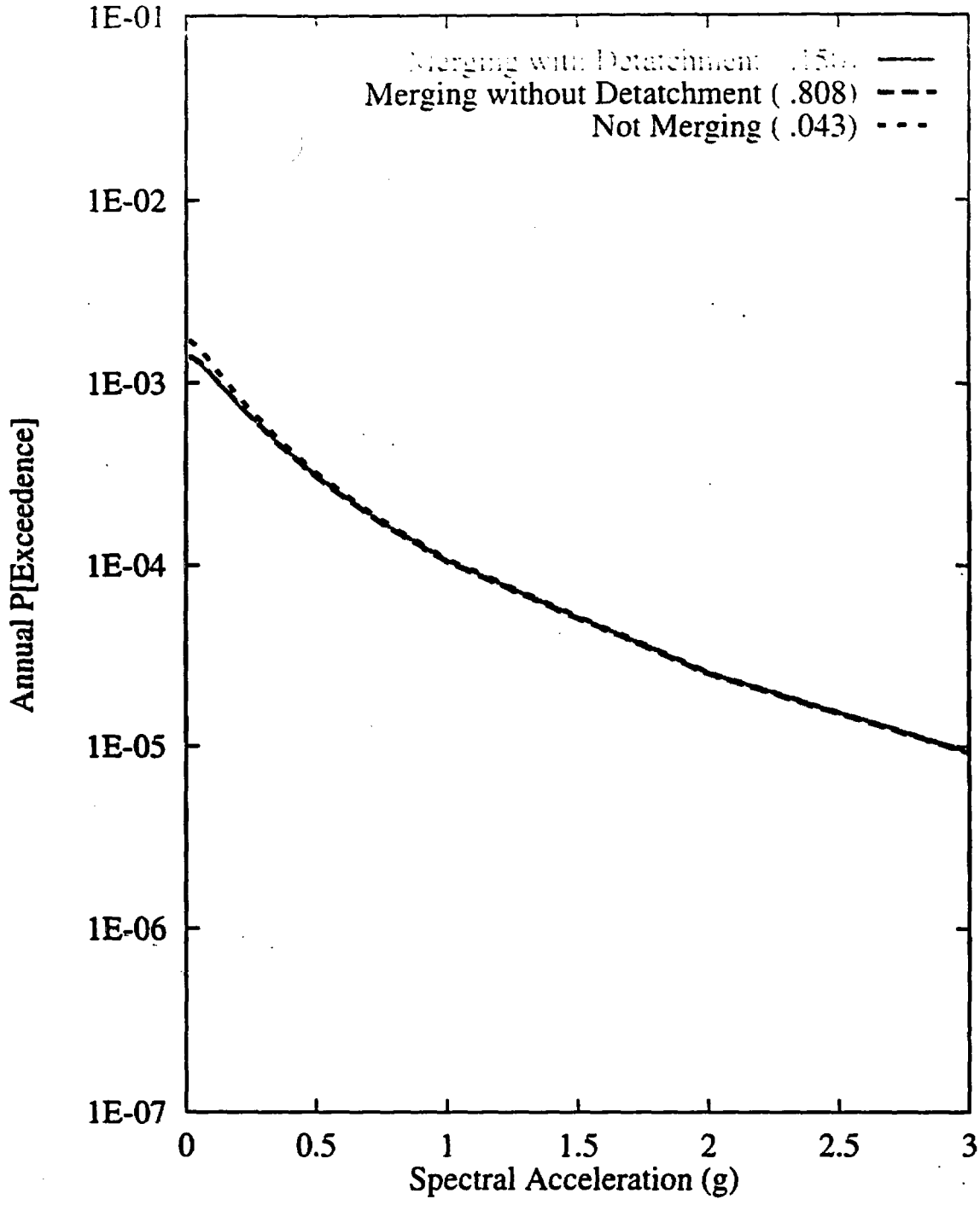

Figure 7-61 Sensitivity of seismic hazard from local faults to down-dip geometry: ASM team, 10-Hz horizontal spectral acceleration

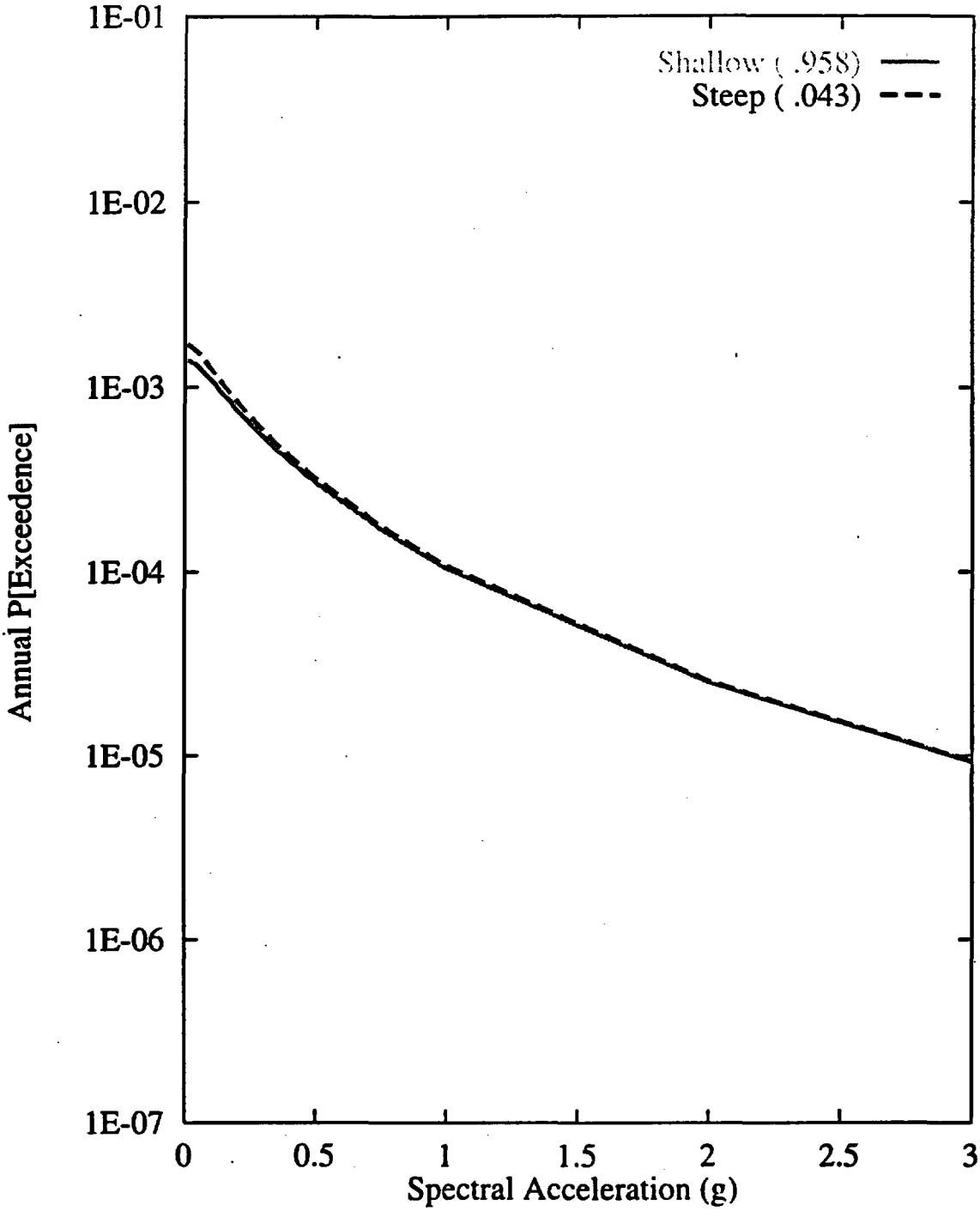

Figure 7-62 Sensitivity of seismic hazard from local faults to fault dip: ASM team, 10-Hz horizontal spectral acceleration

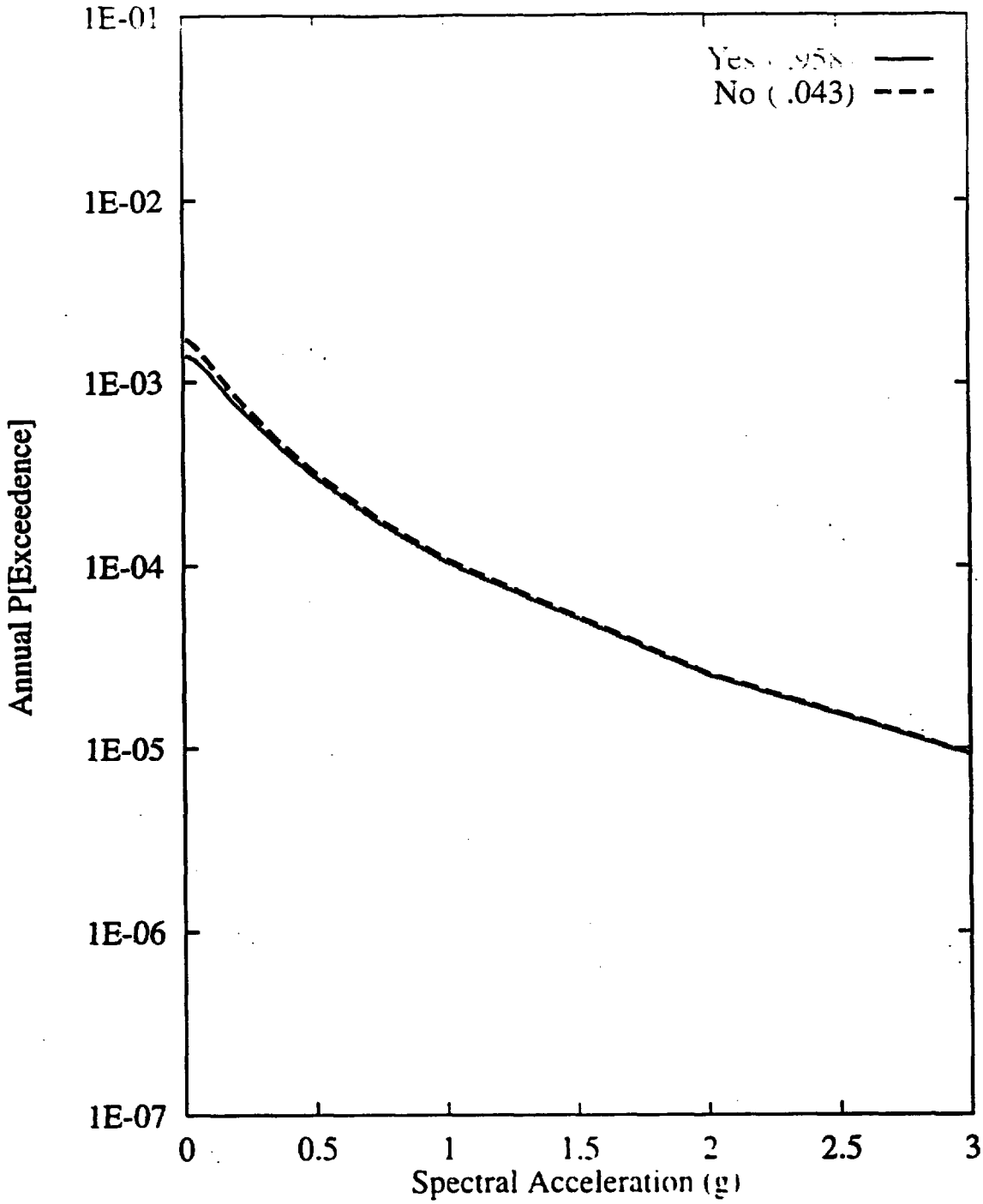

Figure 7-63 Sensitivity of seismic hazard from local faults to fault merging: ASM team, 10-Hz horizontal spectral acceleration

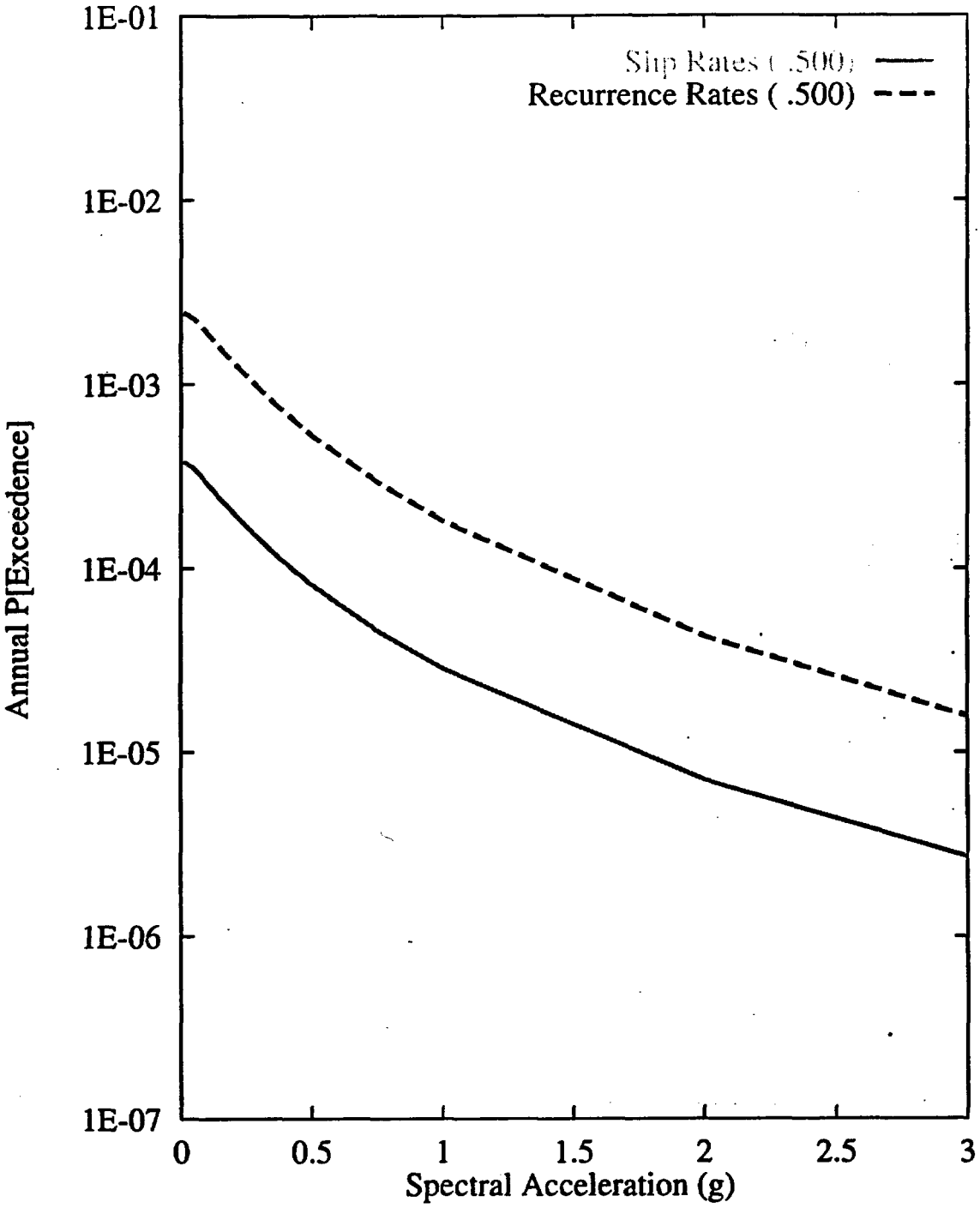

Figure 7-64 Sensitivity of seismic hazard from local faults to recurrence approach: ASM team, 10-Hz horizontal spectral acceleration

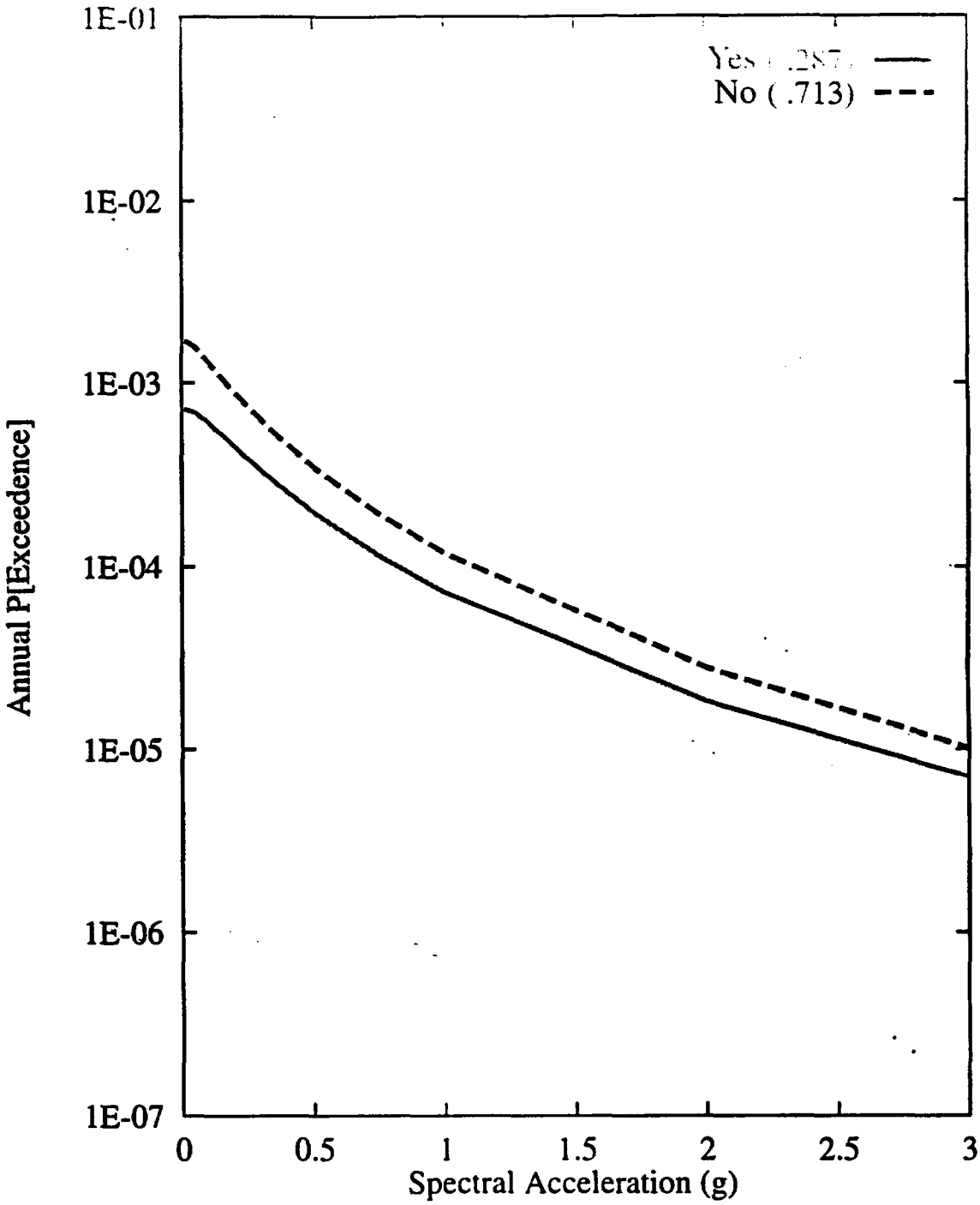

Figure 7-65 Sensitivity of seismic hazard from local faults to simultaneous ruptures: ASM team, 10-Hz horizontal spectral acceleration

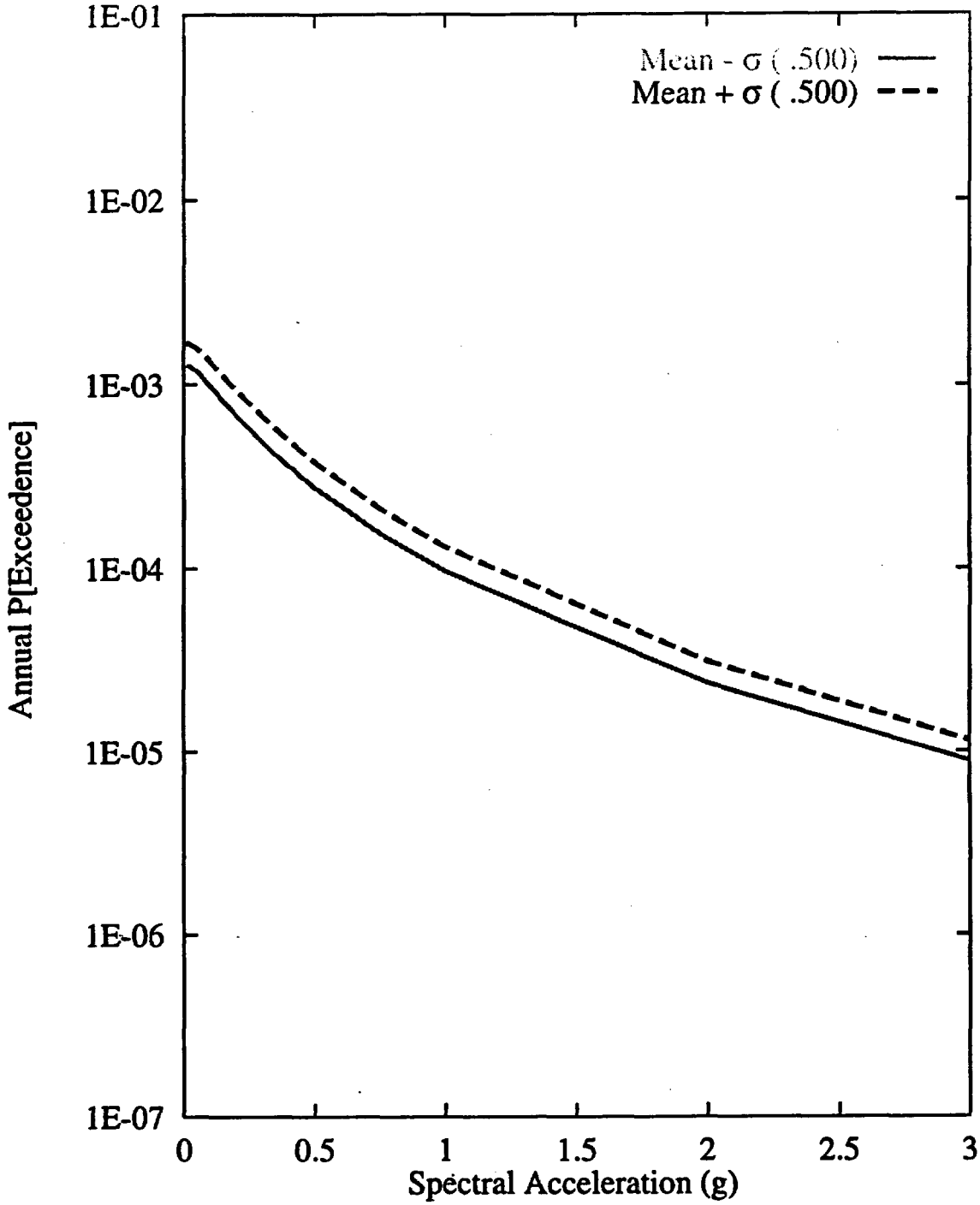

Figure 7-66 Sensitivity of seismic hazard from local faults to M_{max}, Stagecoach Road-Paintbrush Canyon faults: ASM team, 10-Hz horizontal spectral acceleration

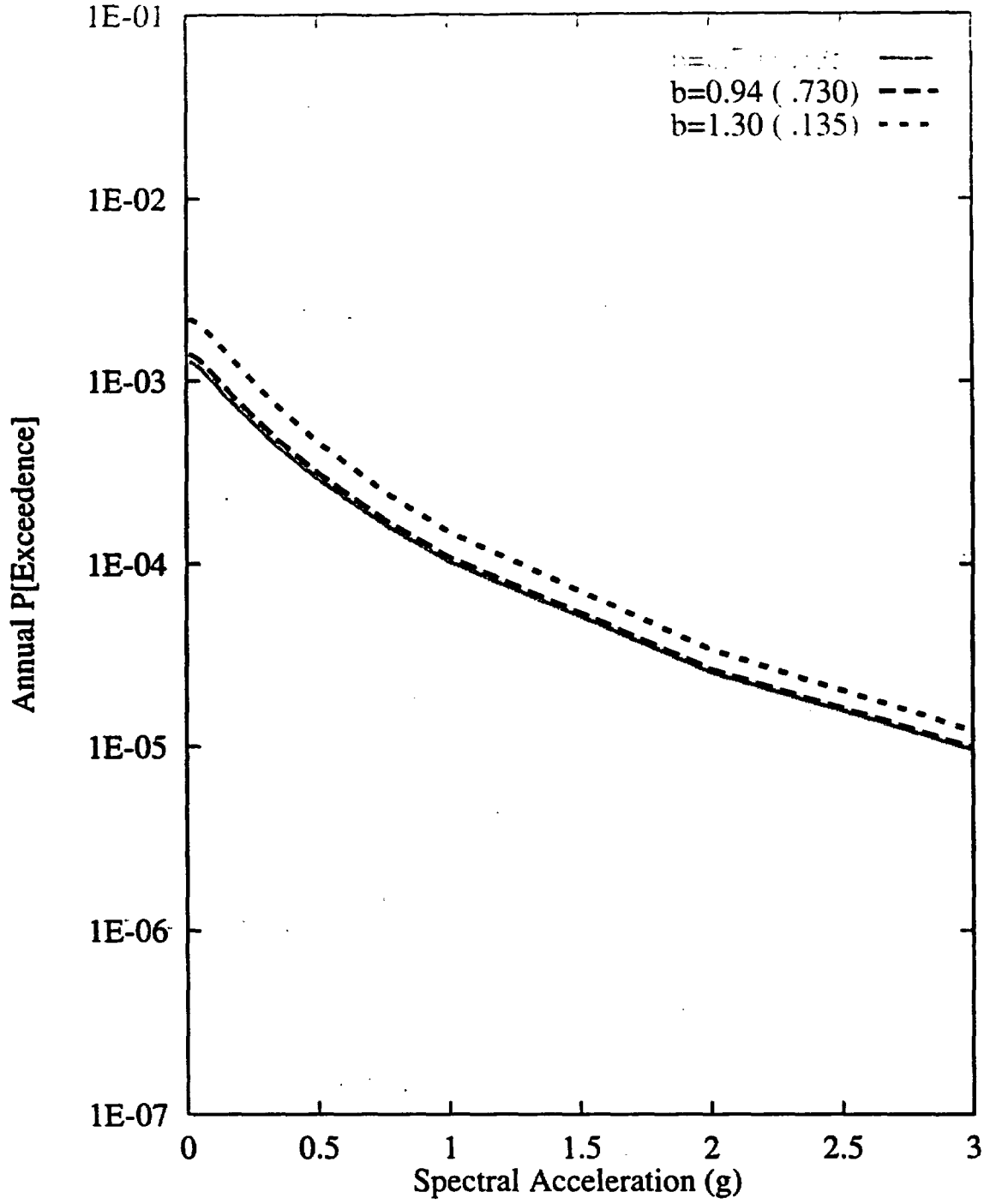

Figure 7-67 Sensitivity of seismic hazard from local faults to b-value, Stagecoach Road-Paintbrush Canyon fault system: ASM team, 10-Hz horizontal spectral acceleration

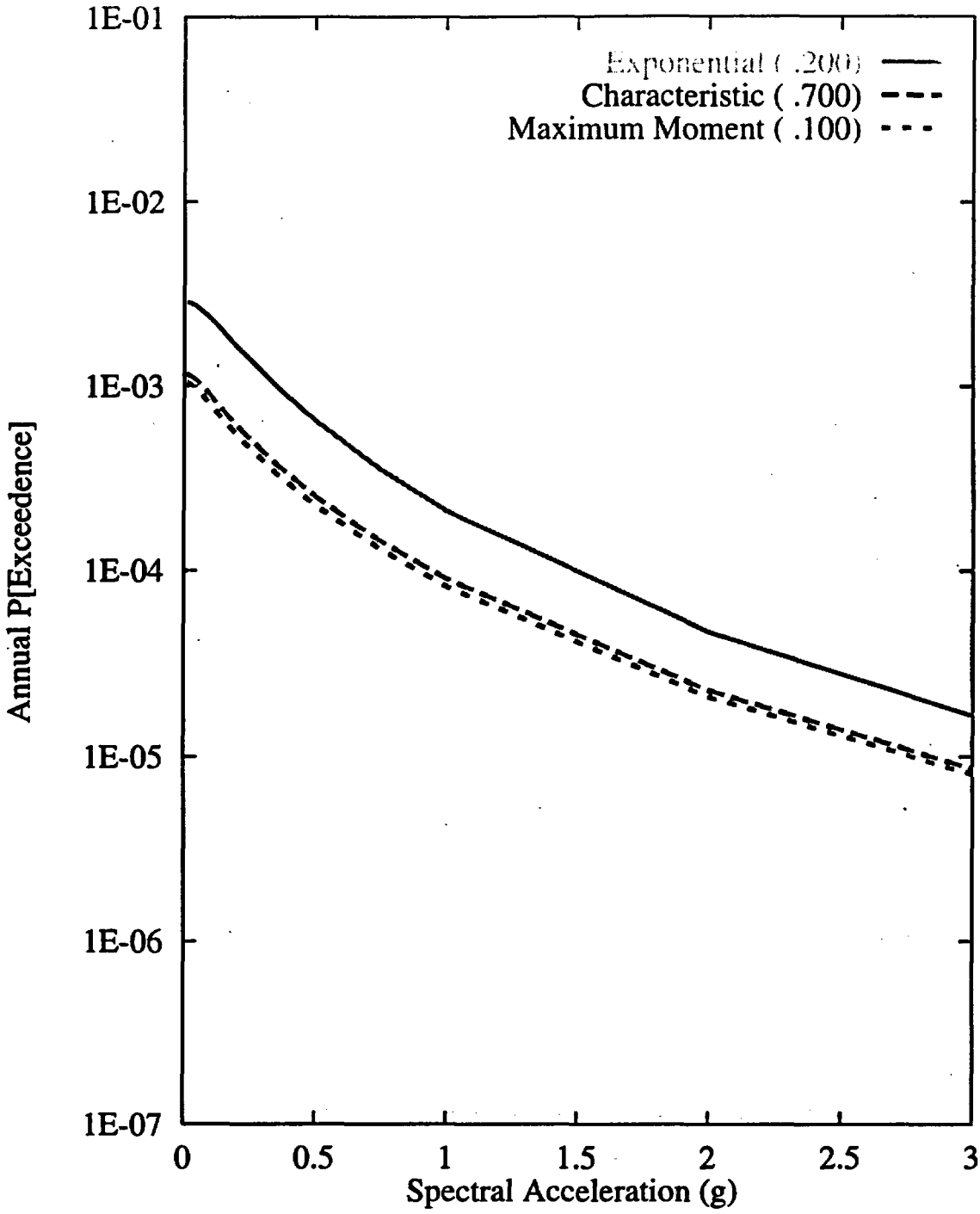

Figure 7-68 Sensitivity of seismic hazard from local faults to recurrence model, Stagecoach Road-Paintbrush Canyon fault system: ASM team, 10-Hz horizontal spectral acceleration

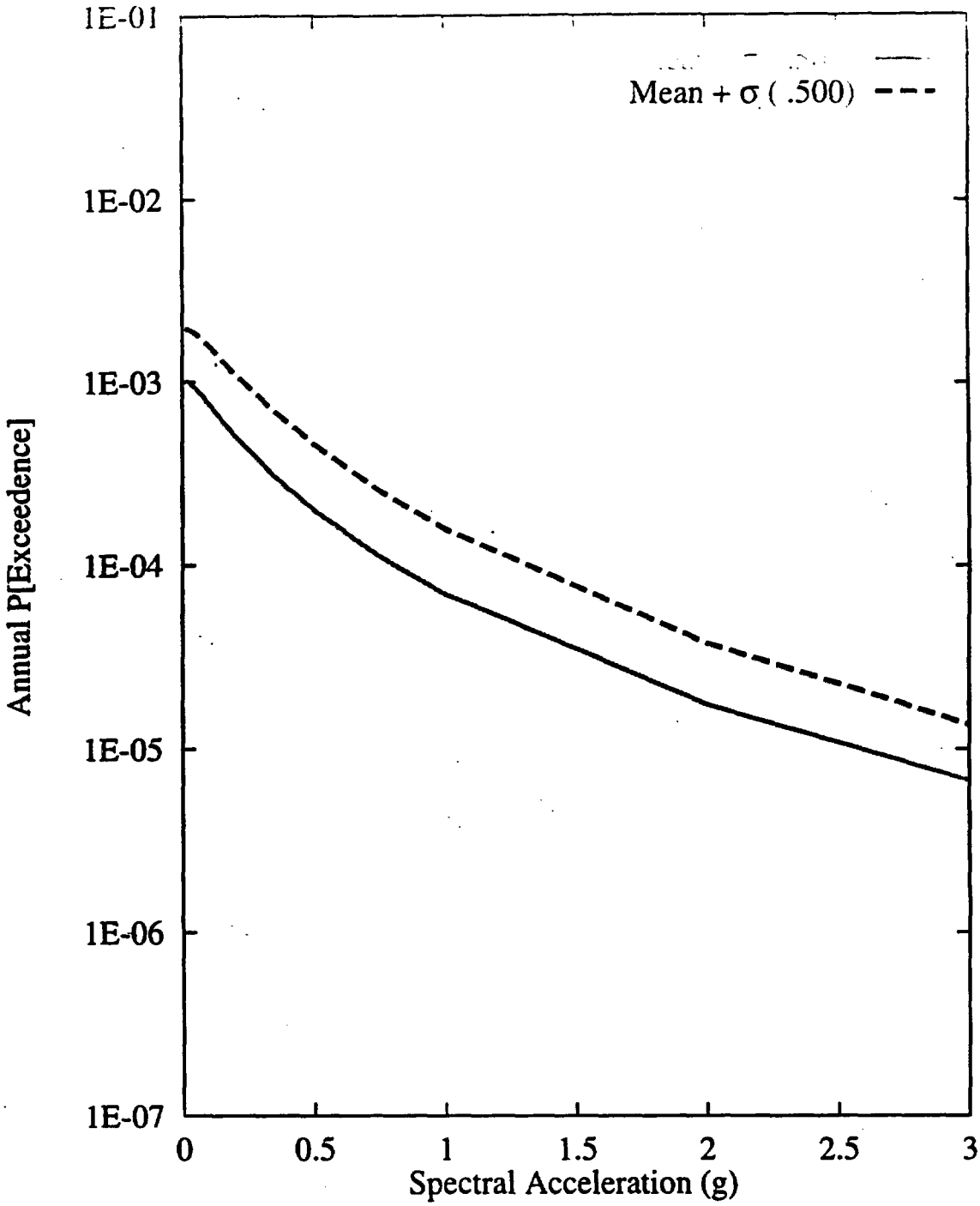

Figure 7-69 Sensitivity of seismic hazard from local faults to recurrence, Stagecoach Road- Paintbrush Canyon fault system: ASM team, 10-Hz horizontal spectral acceleration

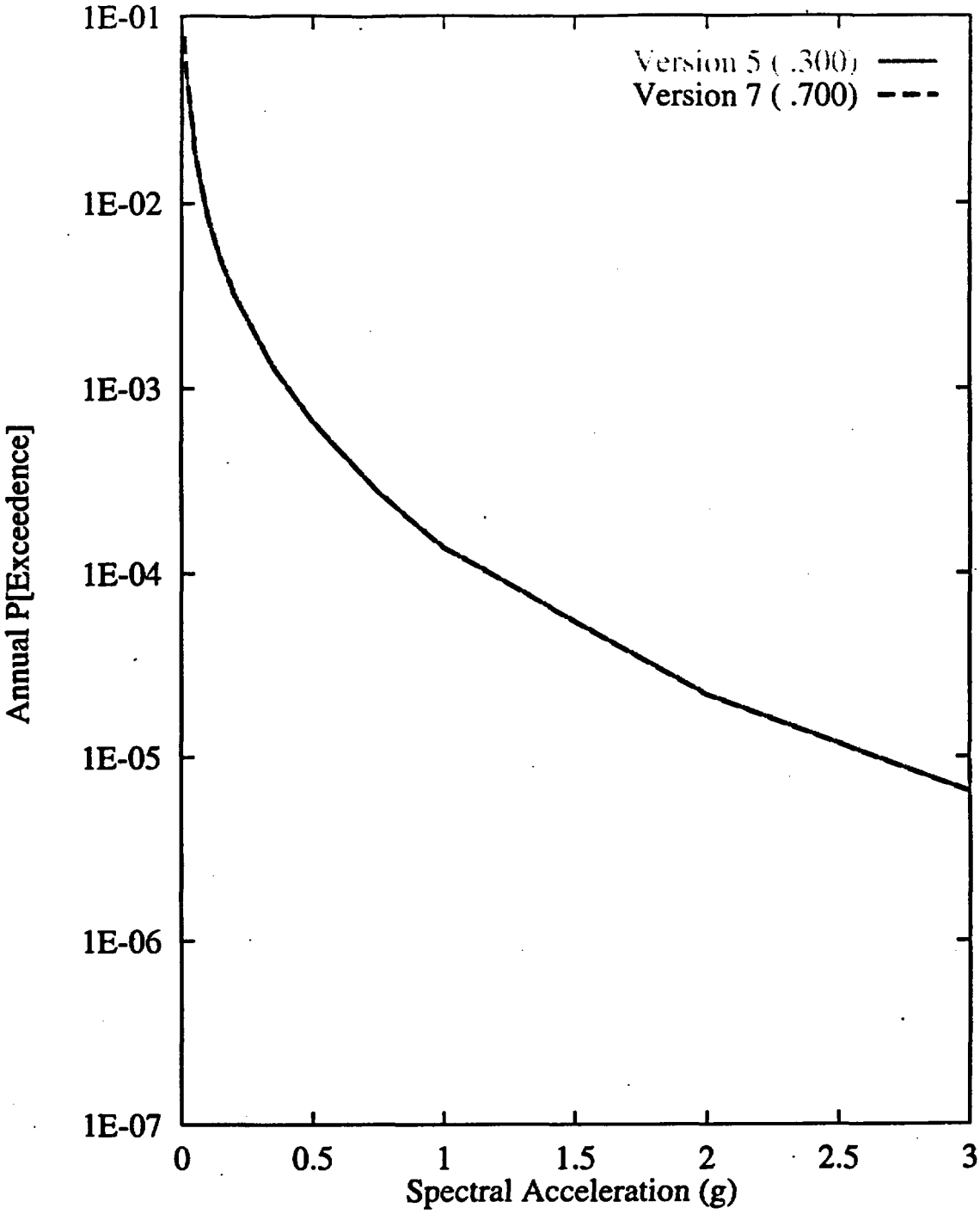

Figure 7-70 Sensitivity of seismic hazard from area zones to choice of seismicity catalog: ASM team, 10-Hz horizontal spectral acceleration

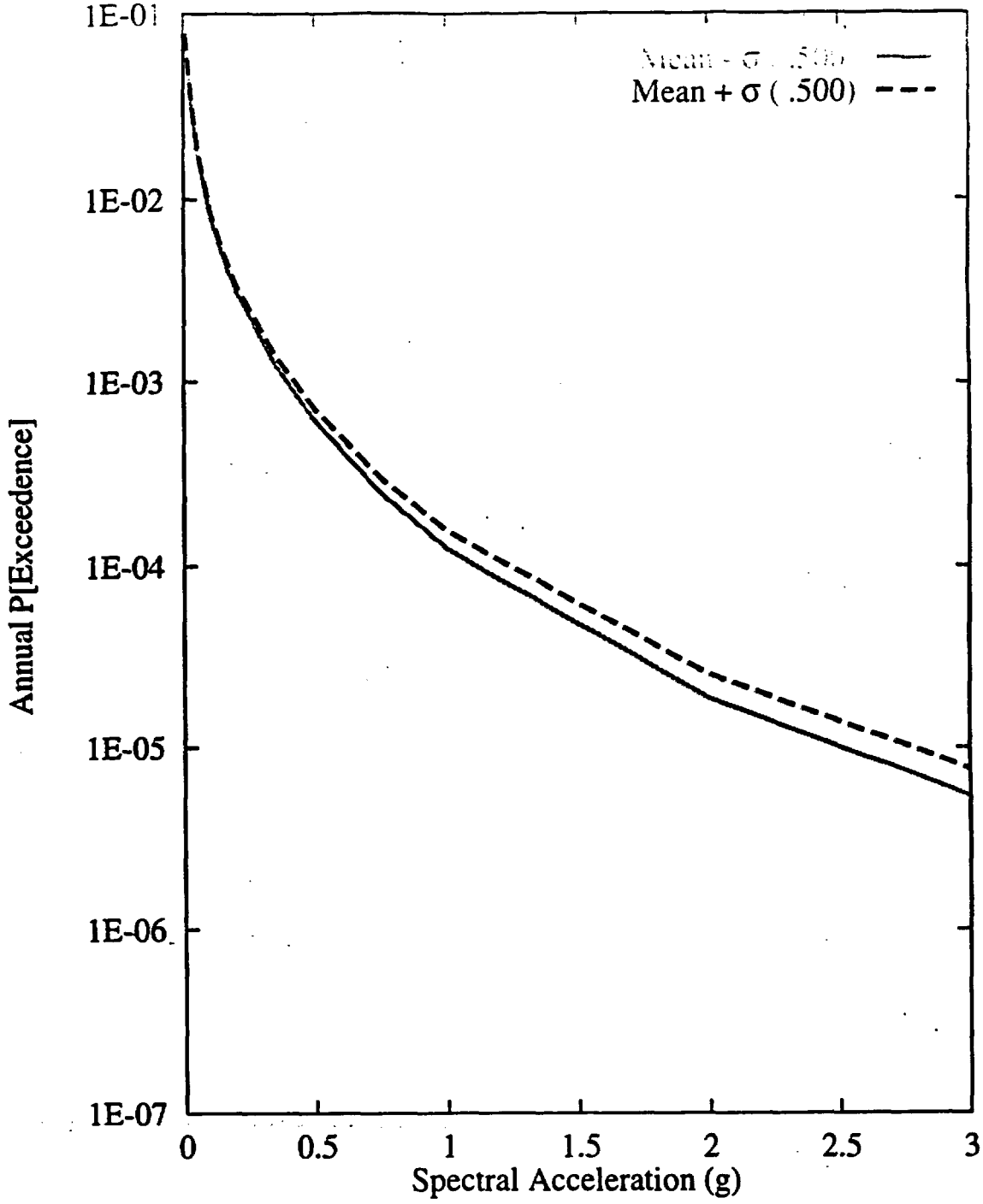

Figure 7-71 Sensitivity of seismic hazard from area zones to Mmax of the Walker Lane local source: ASM team, 10-Hz horizontal spectral acceleration

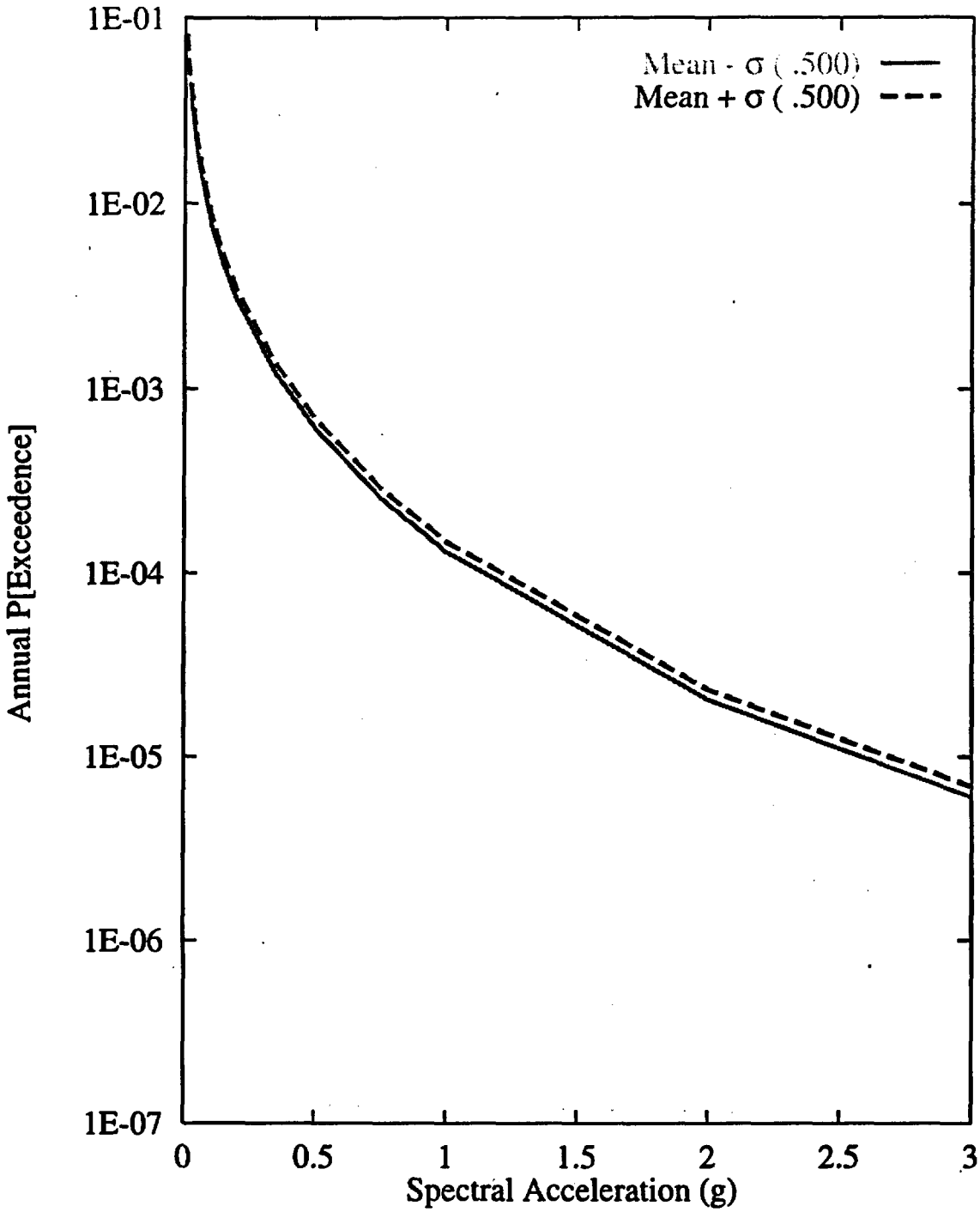

Figure 7-72 Sensitivity of seismic hazard from area zones to recurrence of the Walker Lane local source: ASM team, 10-Hz horizontal spectral acceleration

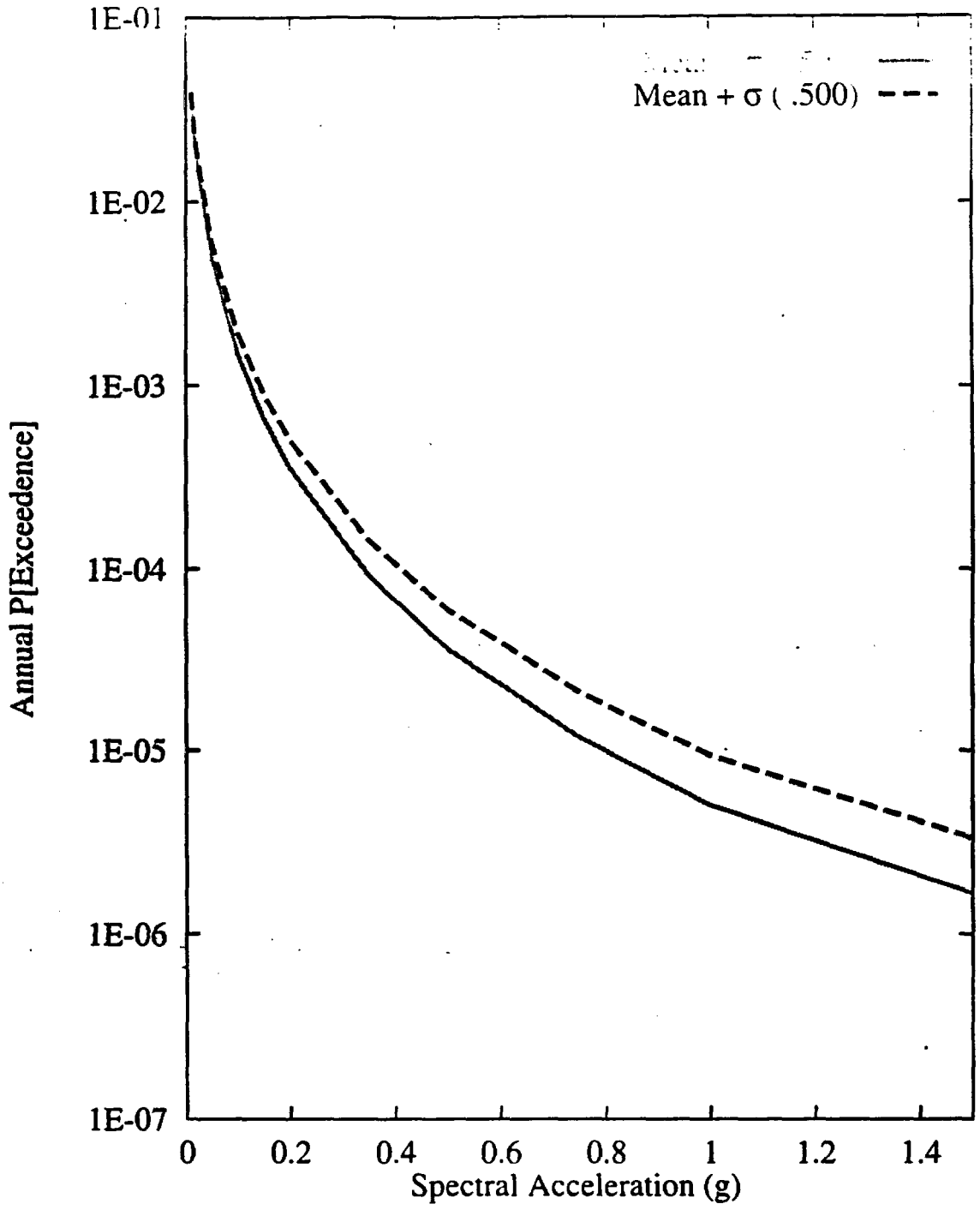

Figure 7-73 Sensitivity of seismic hazard from area zones to Mmax of the Walker Lane local source: ASM team, 1-Hz horizontal spectral acceleration

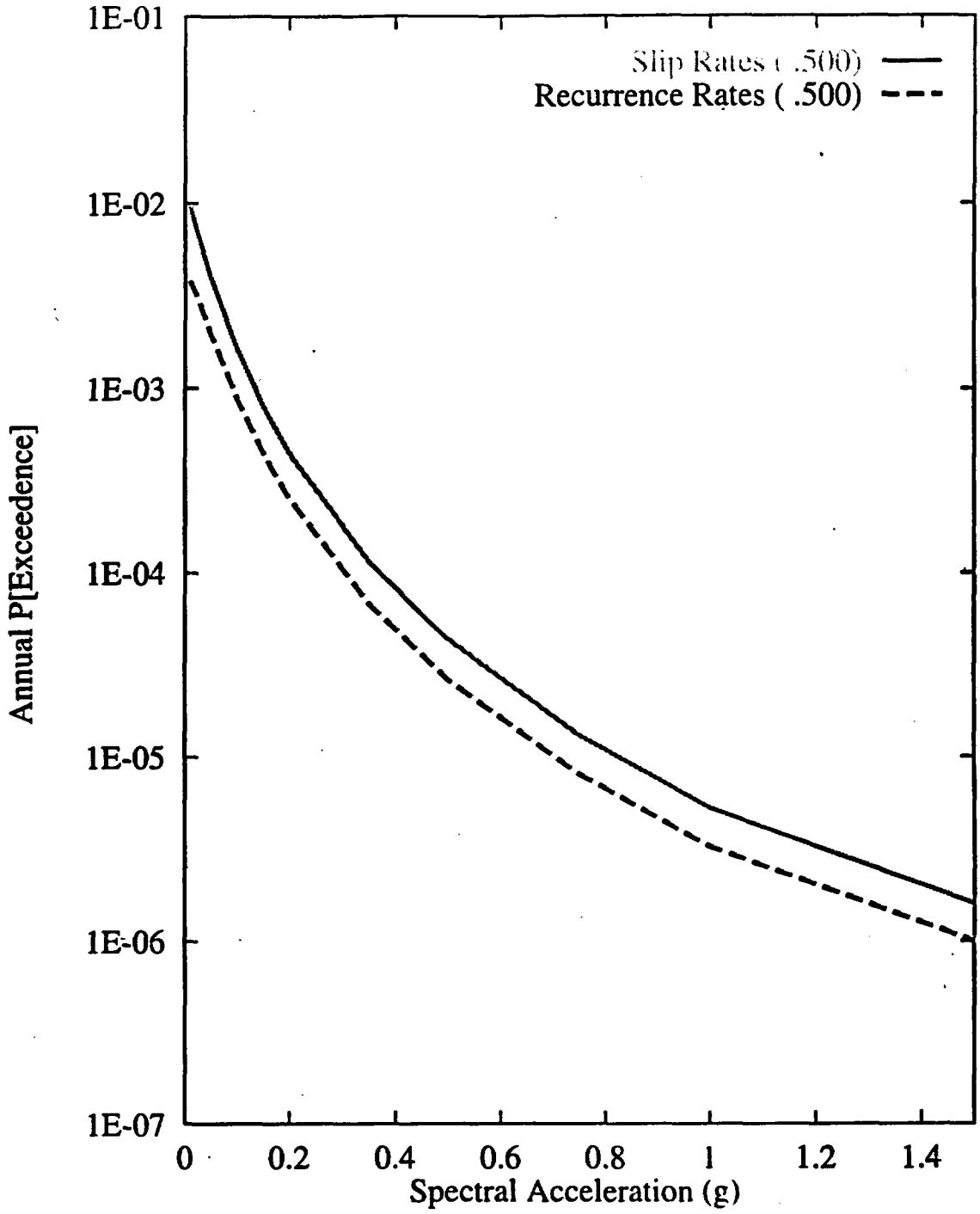

Figure 7-74 Sensitivity of seismic hazard from regional faults to recurrence approach used: ASM team, 1-Hz horizontal spectral acceleration

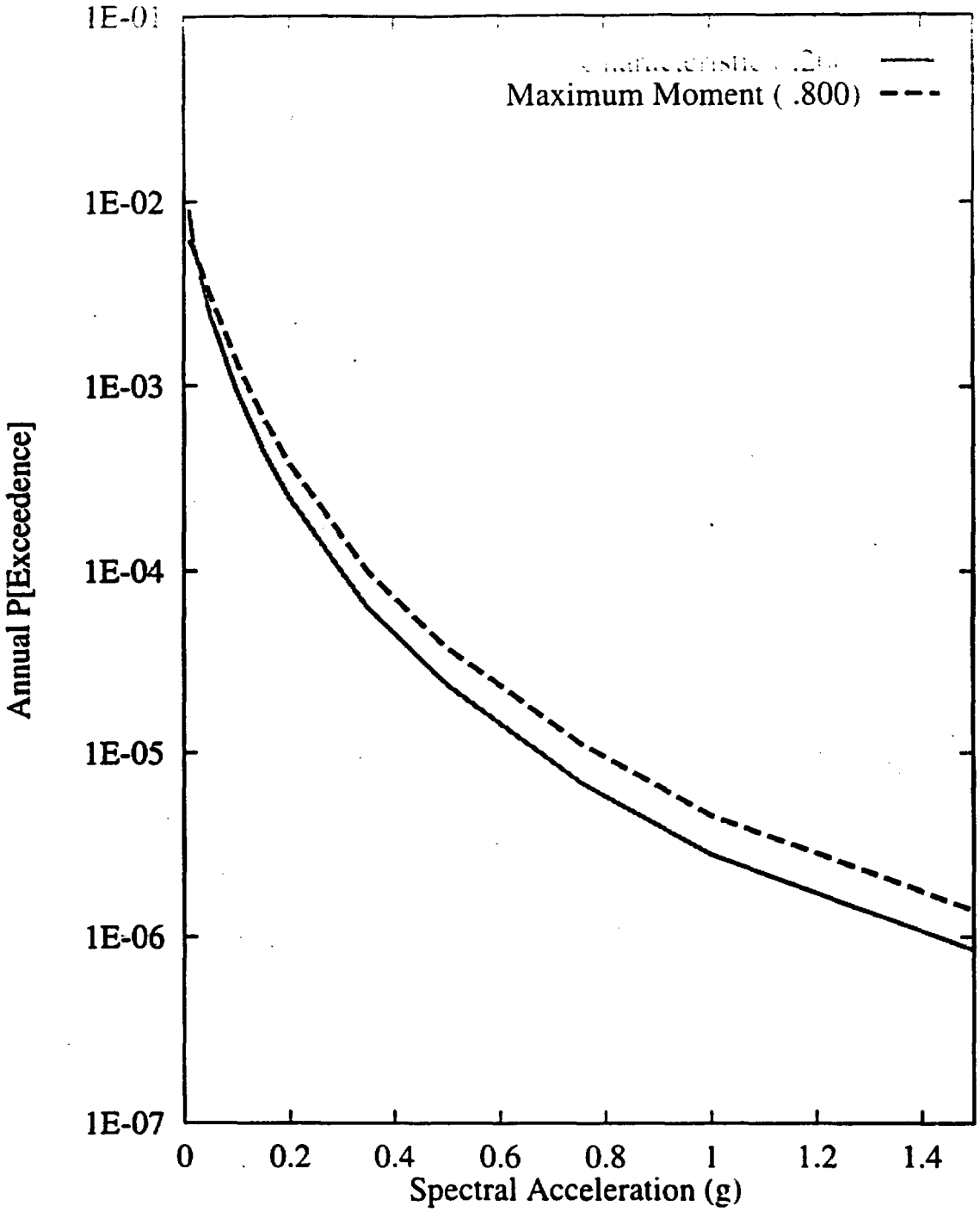

Figure 7-75 Sensitivity of seismic hazard from regional faults to recurrence model: ASM team, 1-Hz horizontal spectral acceleration

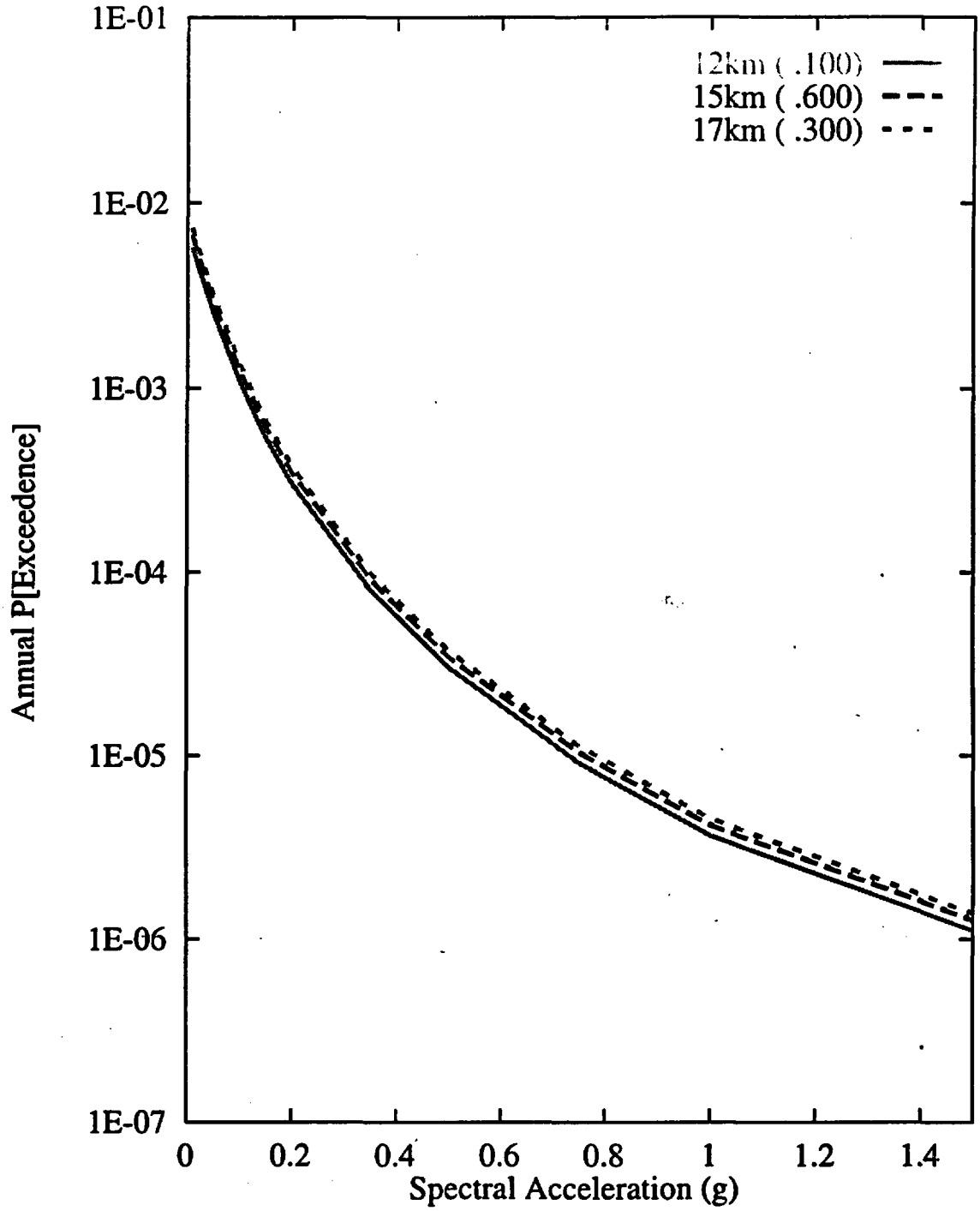

Figure 7-76 Sensitivity of seismic hazard from regional faults to maximum fault depth: ASM team, 1-Hz horizontal spectral acceleration

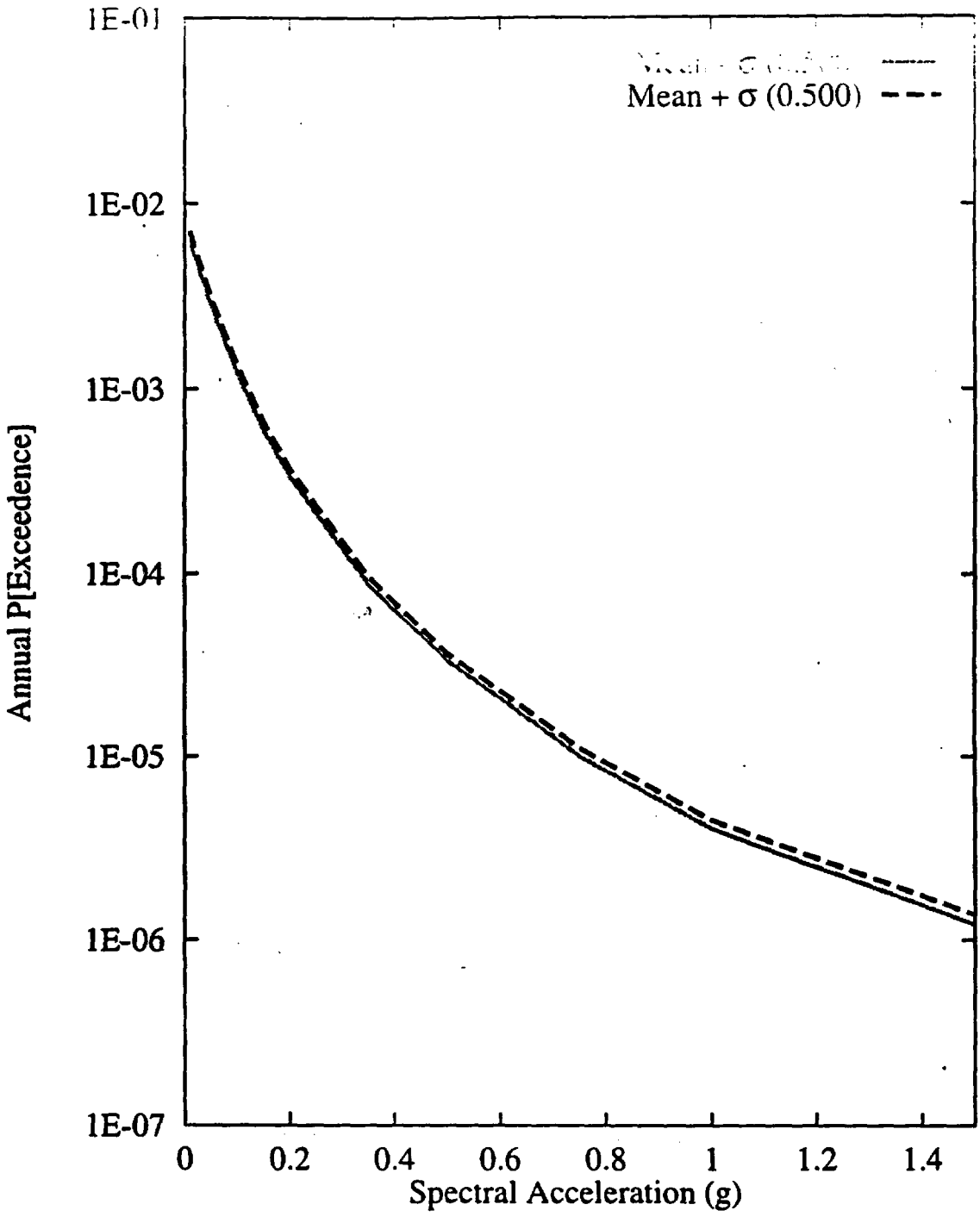

Figure 7-77 Sensitivity of seismic hazard from regional faults to Mmax on the Furnace Creek fault: ASM team, 1-Hz horizontal spectral acceleration

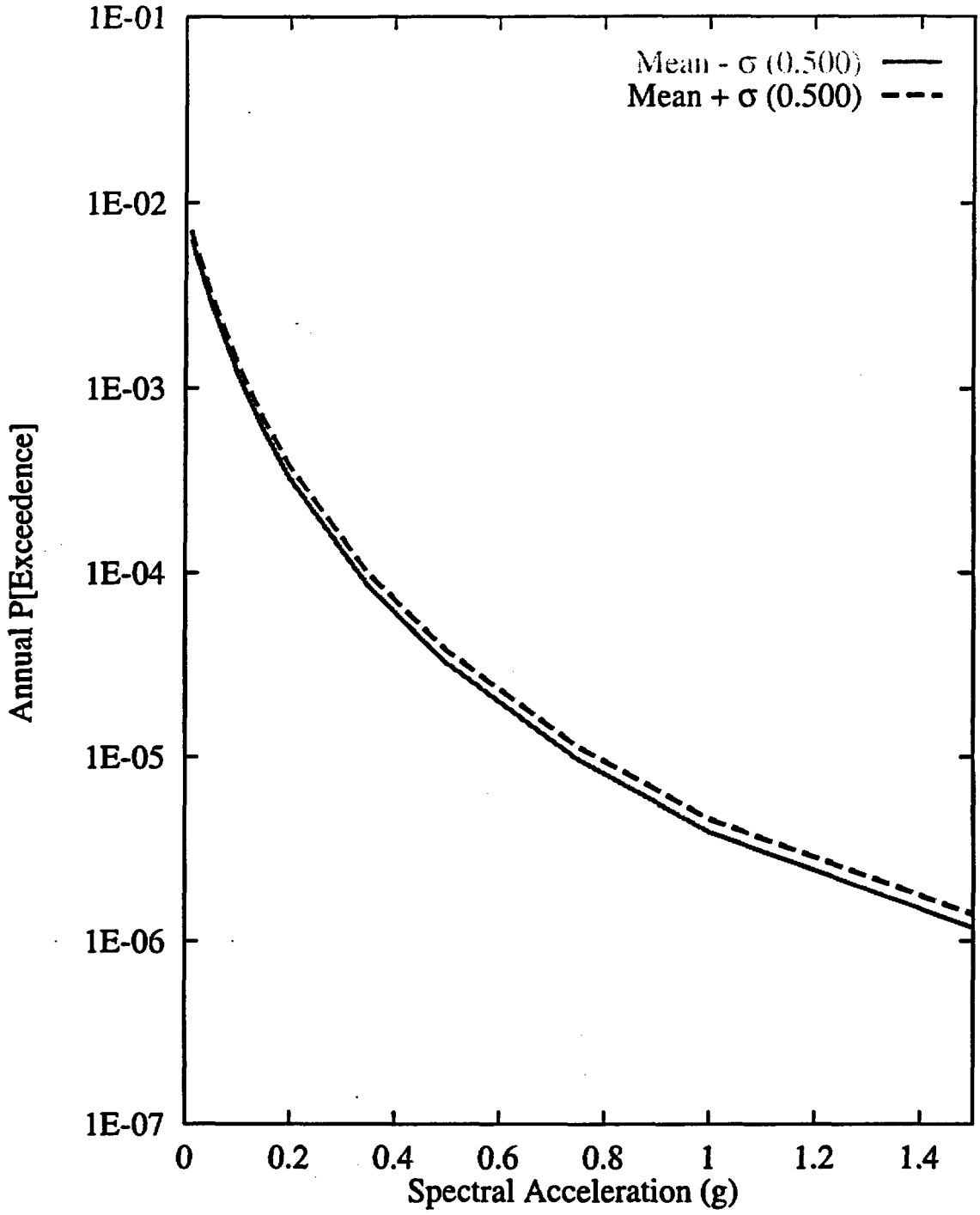

Figure 7-78 Sensitivity of seismic hazard from regional faults to recurrence, Furnace Creek fault: ASM team, 1-Hz horizontal spectral acceleration

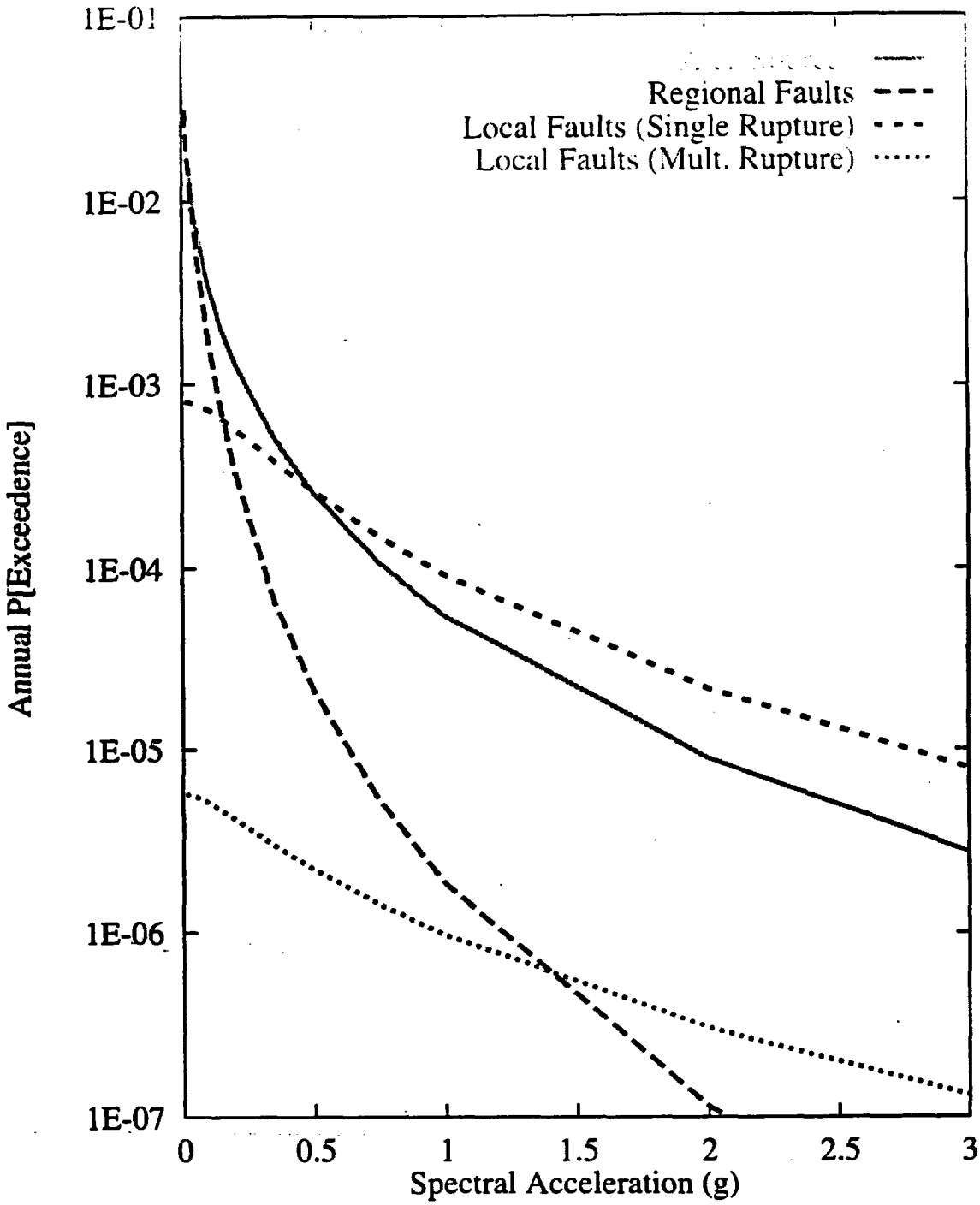

Figure 7-79 Contributions of source types to the mean hazard: DFS team, 10-Hz horizontal spectral acceleration

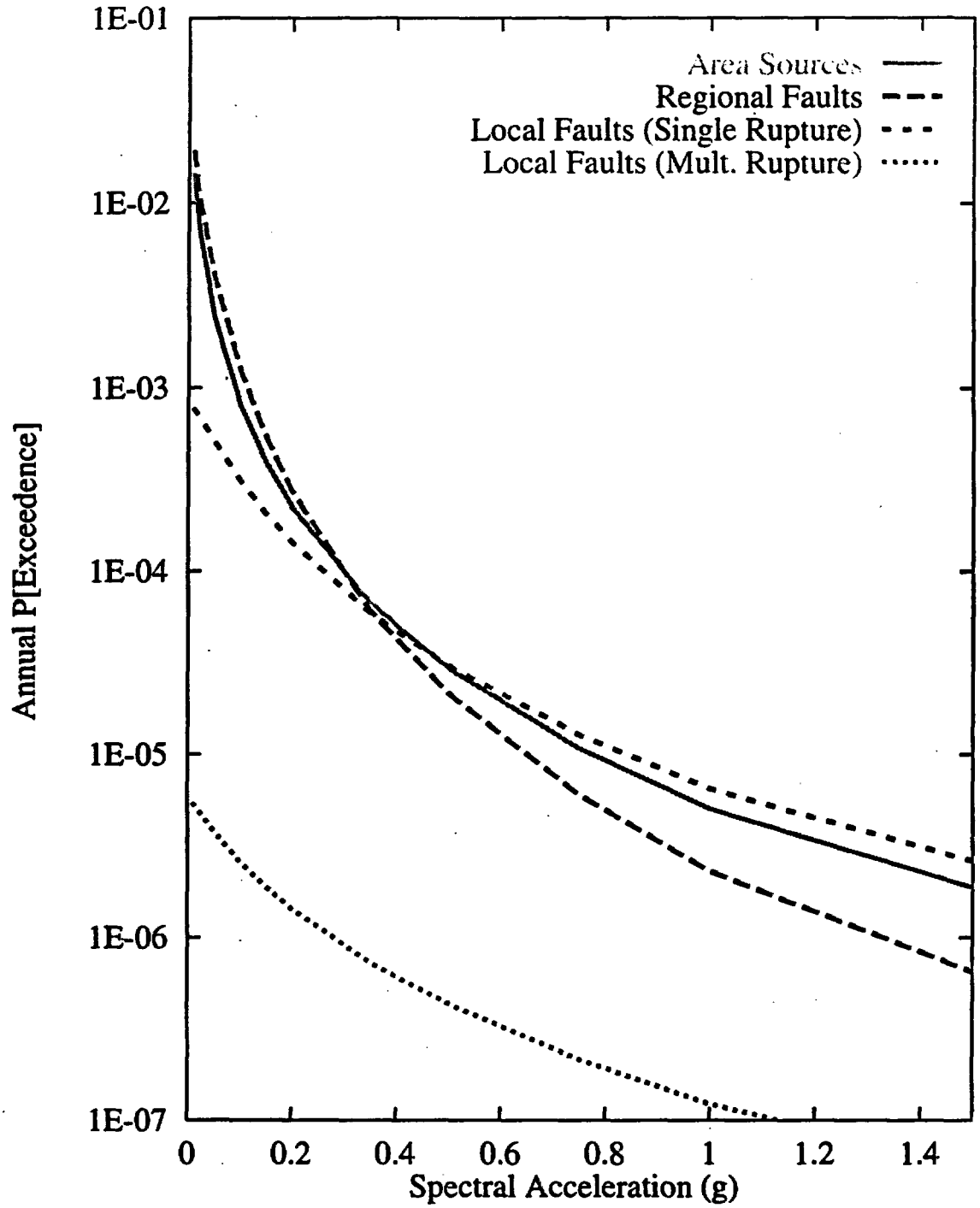

Figure 7-80 Contributions of source types to the mean hazard: DFS team, 1-Hz horizontal spectral acceleration

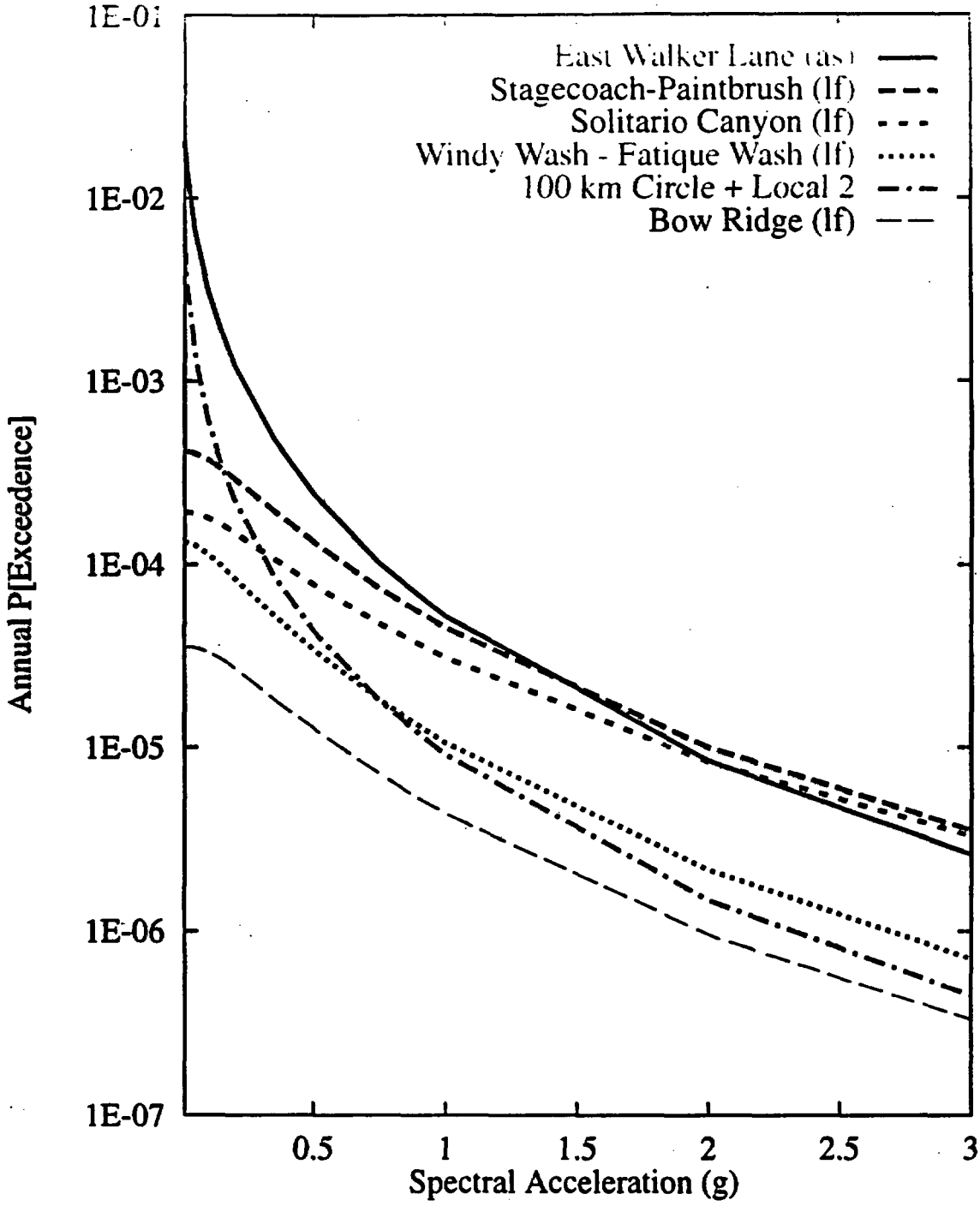

Figure 7-81 Mean seismic hazard from dominant seismic sources: DFS team, 10-Hz horizontal spectral acceleration. Acronyms in parentheses refer to source types: as-area source zone; and lf-local fault.

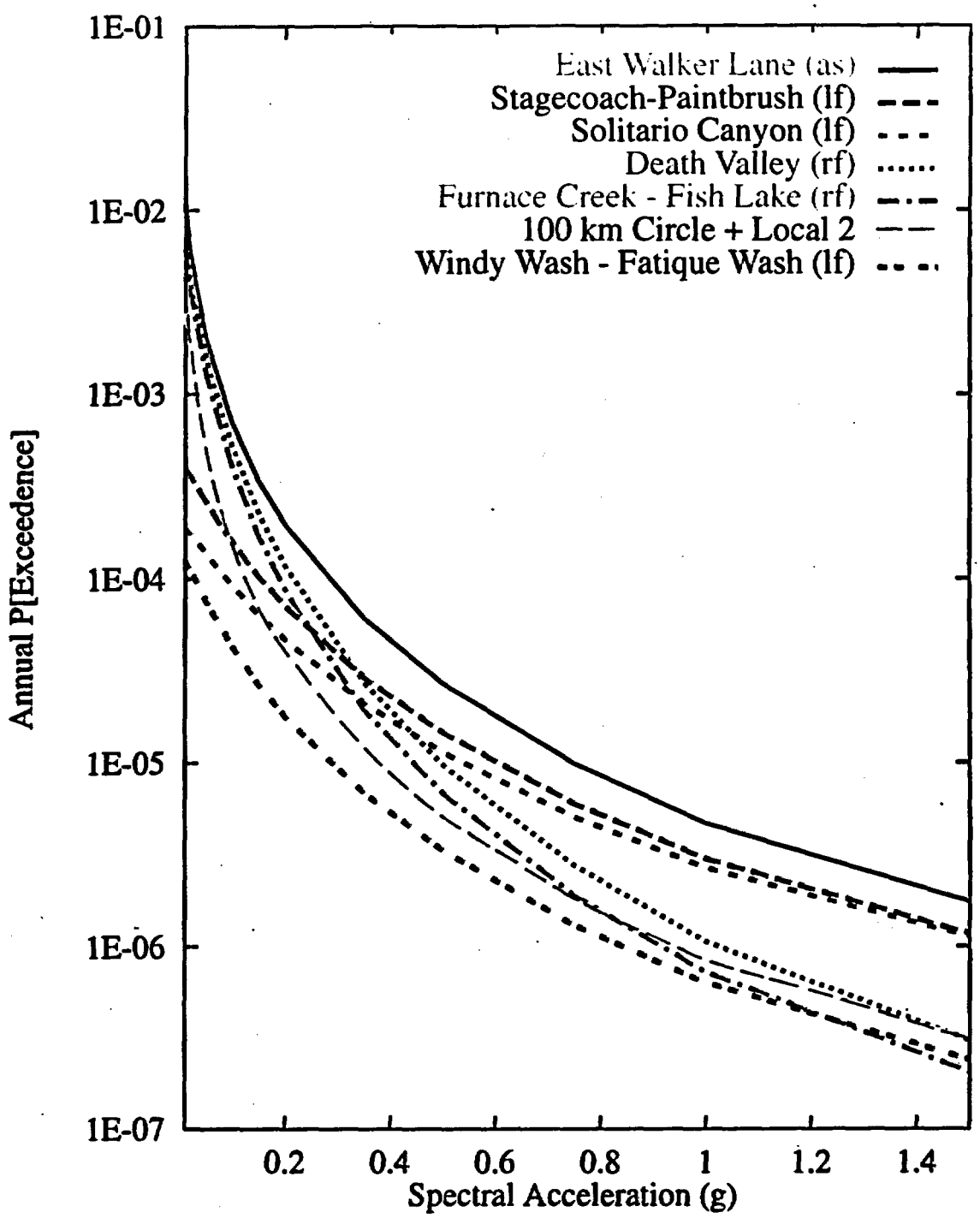

Figure 7-82 Mean seismic hazard from dominant seismic sources: DFS team, 1-Hz horizontal spectral acceleration. Acronyms in parentheses refer to source types: as-area source zone; lf-local fault; and rf-regional fault.

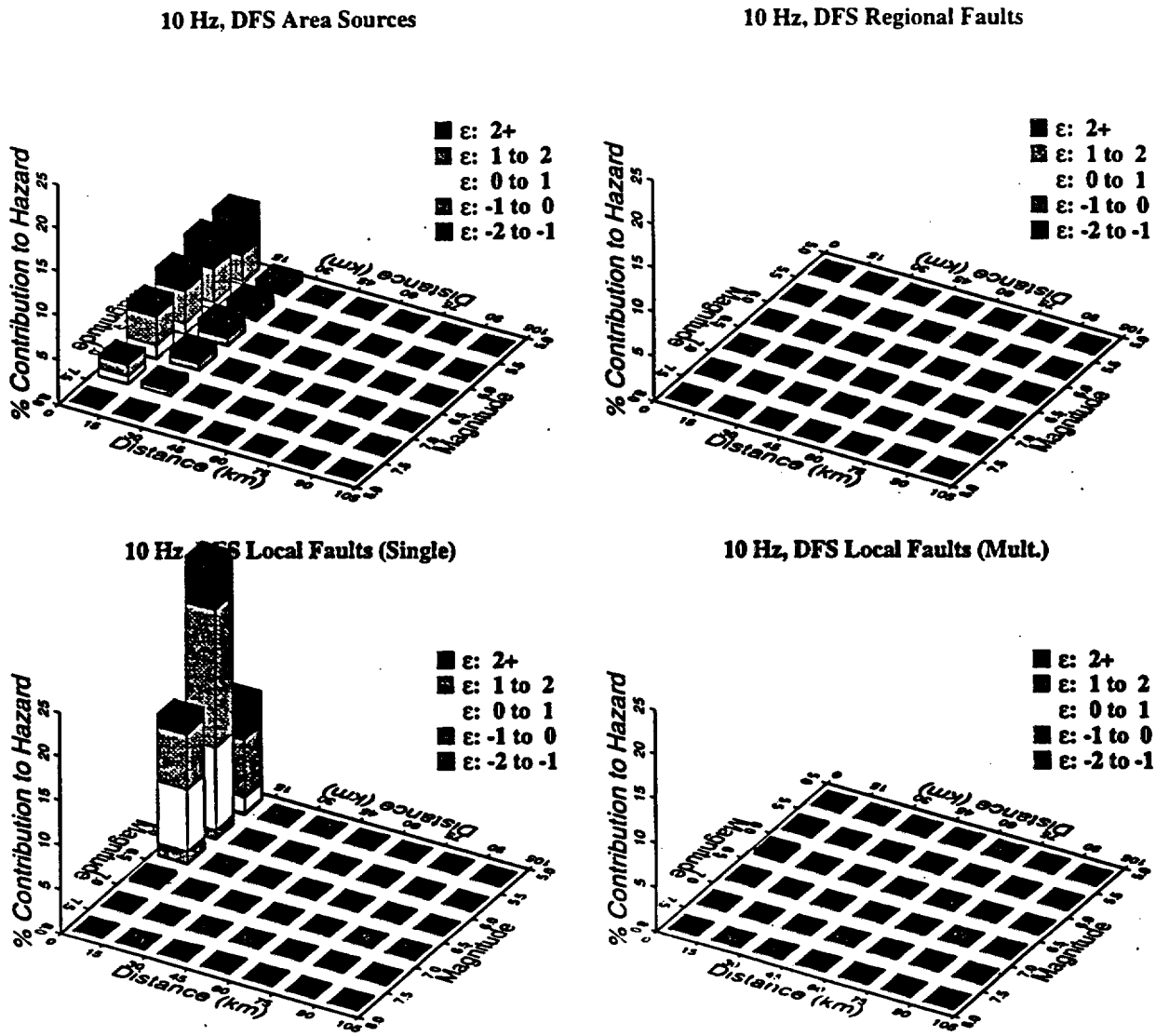

Figure 7-83 Magnitude-distance-epsilon distributions for the four source types: DFS team, 10-Hz horizontal spectral acceleration at 10^{-4} exceedance probability

1 Hz, DFS Area Sources

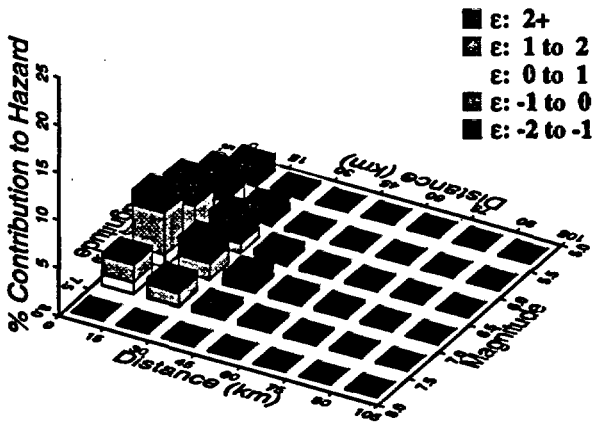

1 Hz, DFS Regional Faults

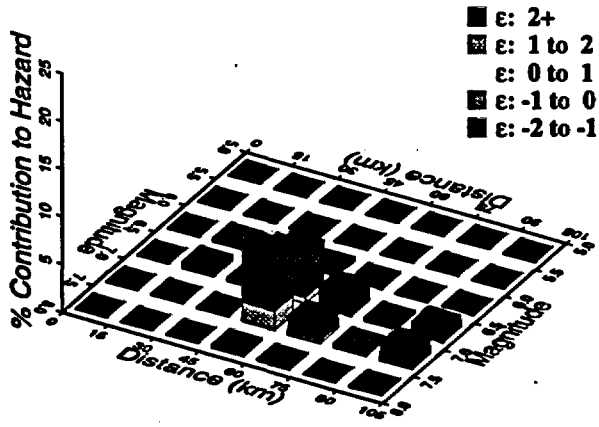

1 Hz, DFS Local Faults (Single)

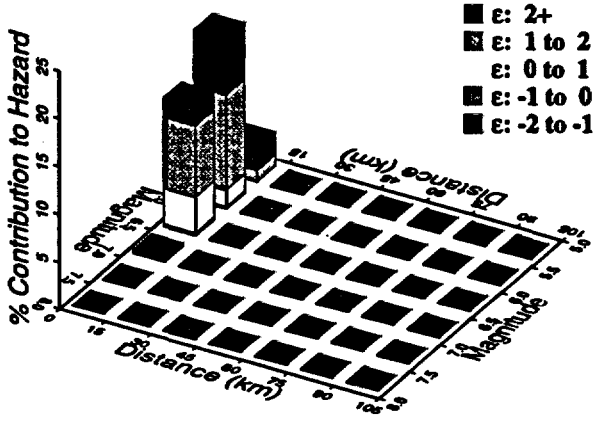

1 Hz, DFS Local Faults (Mult.)

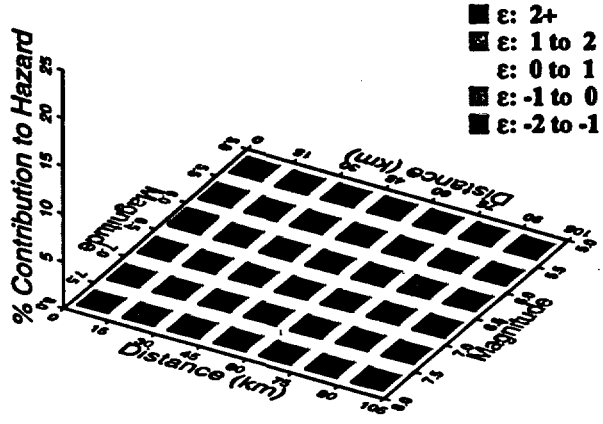

Figure 7-84 Magnitude-distance-epsilon distributions for the four source types: DFS team, 1-Hz horizontal spectral acceleration at 10^{-4} exceedance probability

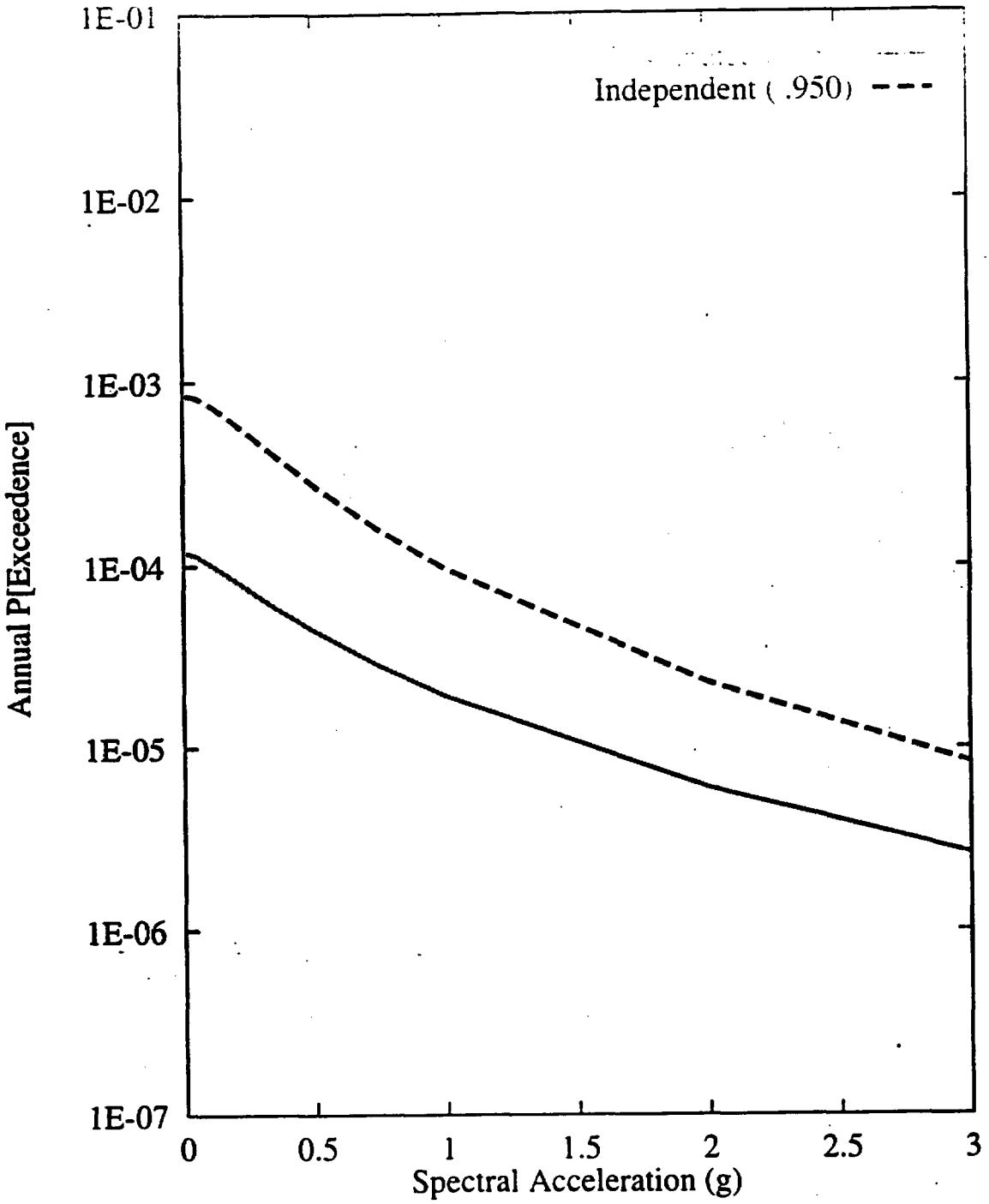

Figure 7-85 Sensitivity of seismic hazard from local faults to presence of distributed versus independent faults: DFS team, 10-Hz horizontal spectral acceleration

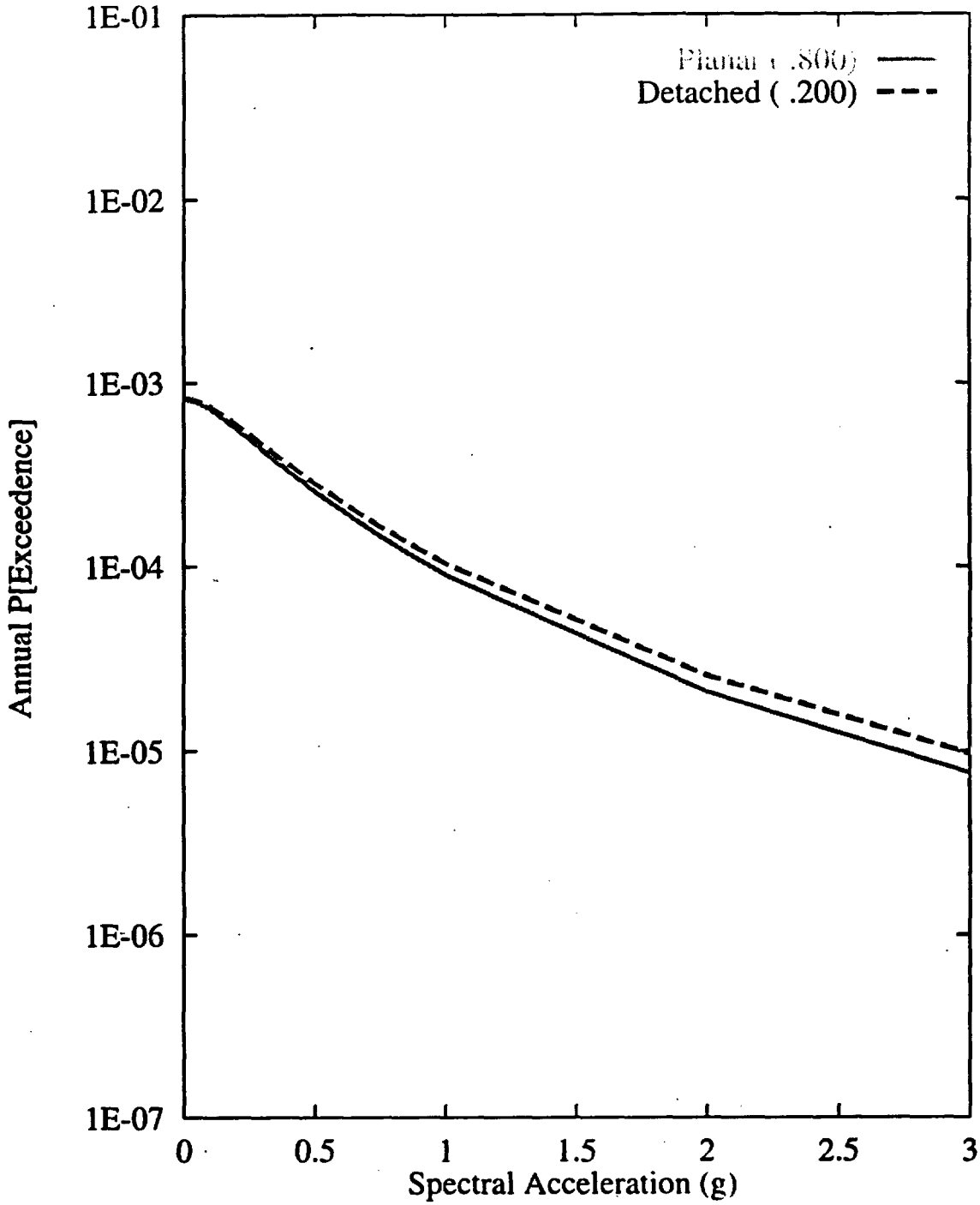

Figure 7-86 Sensitivity of seismic hazard from local faults to subsurface geometry: DFS team, 10-Hz horizontal spectral acceleration

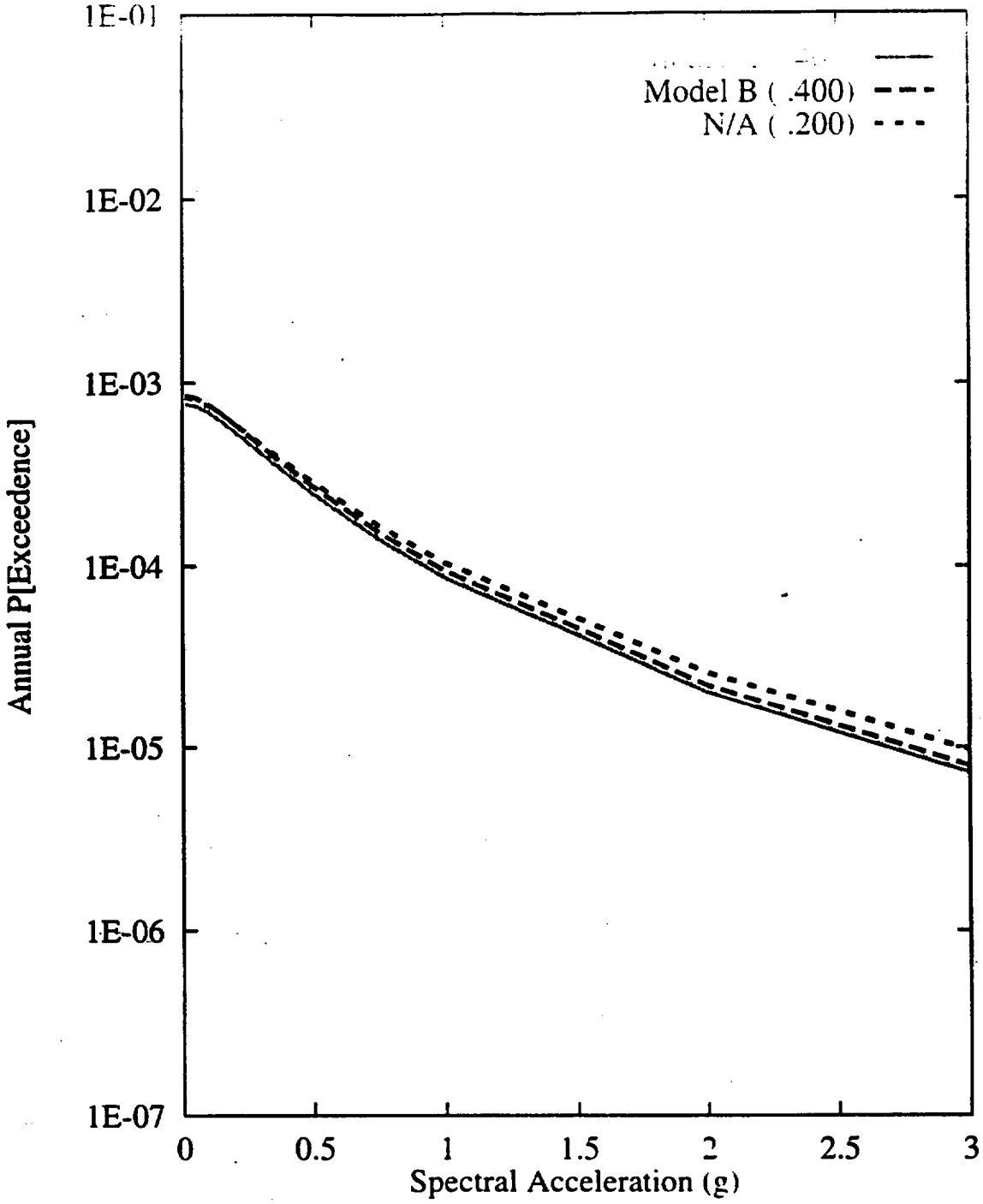

Figure 7-87 Sensitivity of seismic hazard from local faults to fault subsurface geometry for planar faults: DFS team, 10-Hz horizontal spectral acceleration

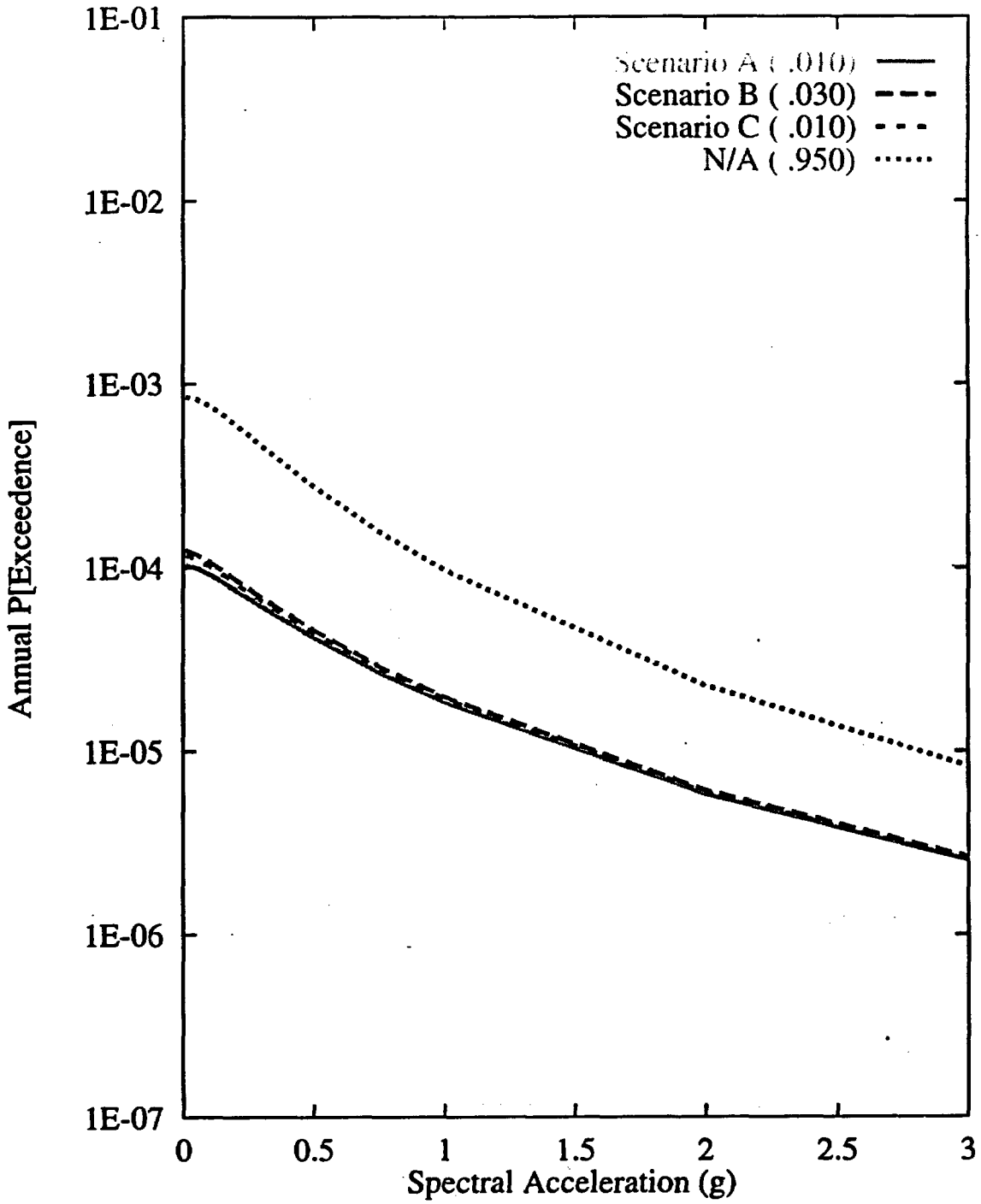

Figure 7-88 Sensitivity of seismic hazard from local faults to multiple-fault rupture scenarios: DFS team, 10-Hz horizontal spectral acceleration

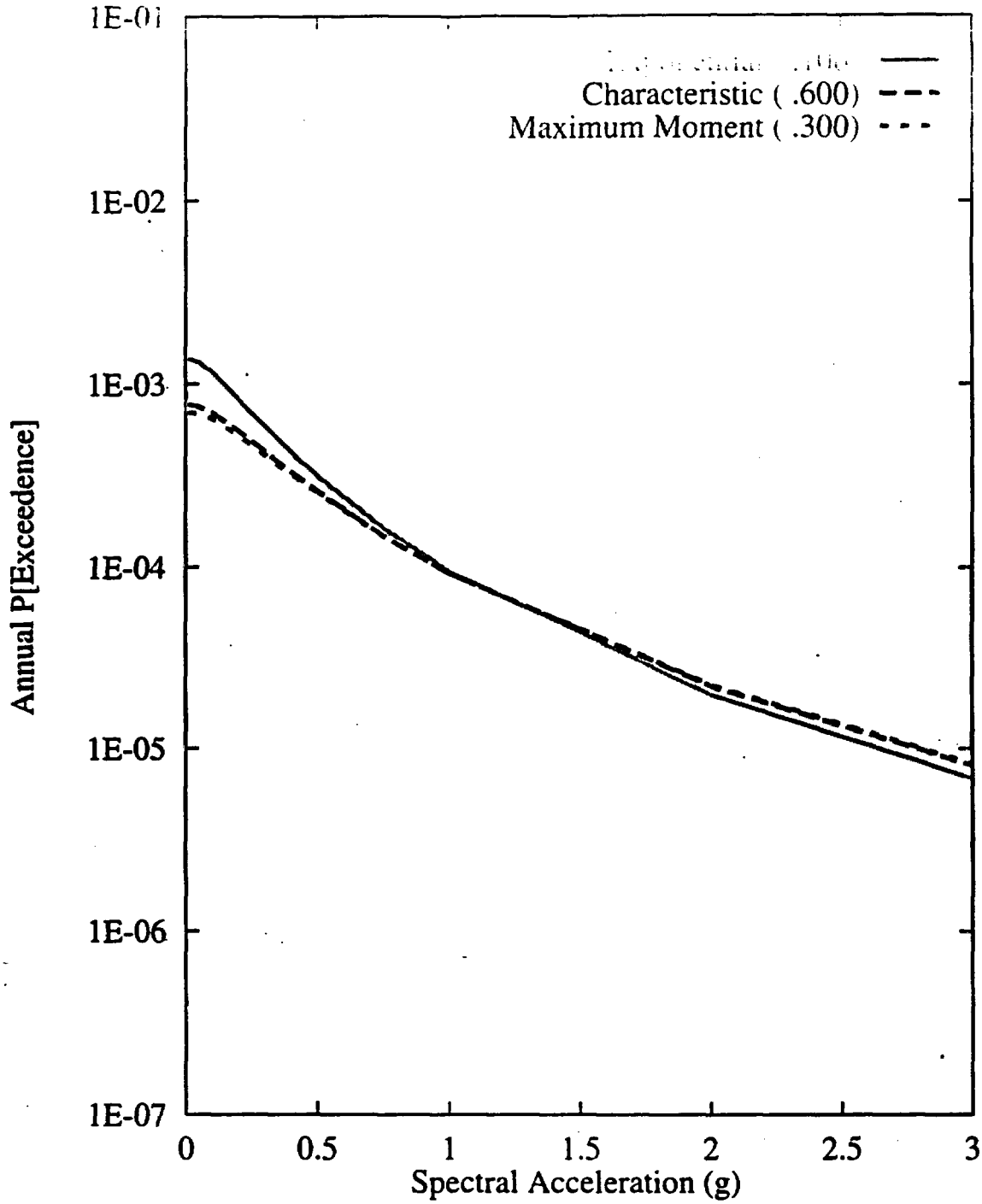

Figure 7-89 Sensitivity of seismic hazard from local faults to recurrence model: DFS team, 10-Hz horizontal spectral acceleration

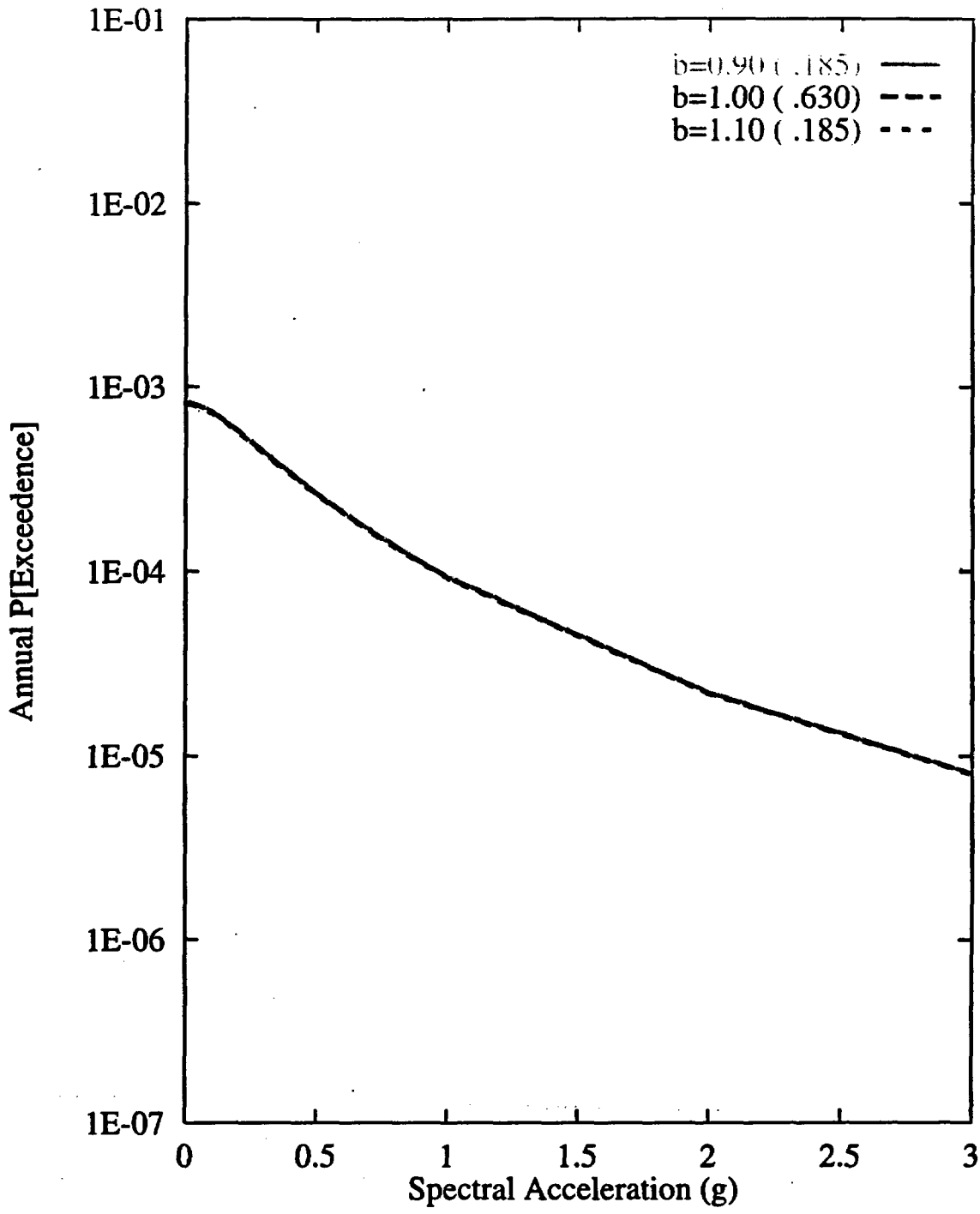

Figure 7-90 Sensitivity of seismic hazard from local faults to b-value: DFS team, 10-Hz horizontal spectral acceleration

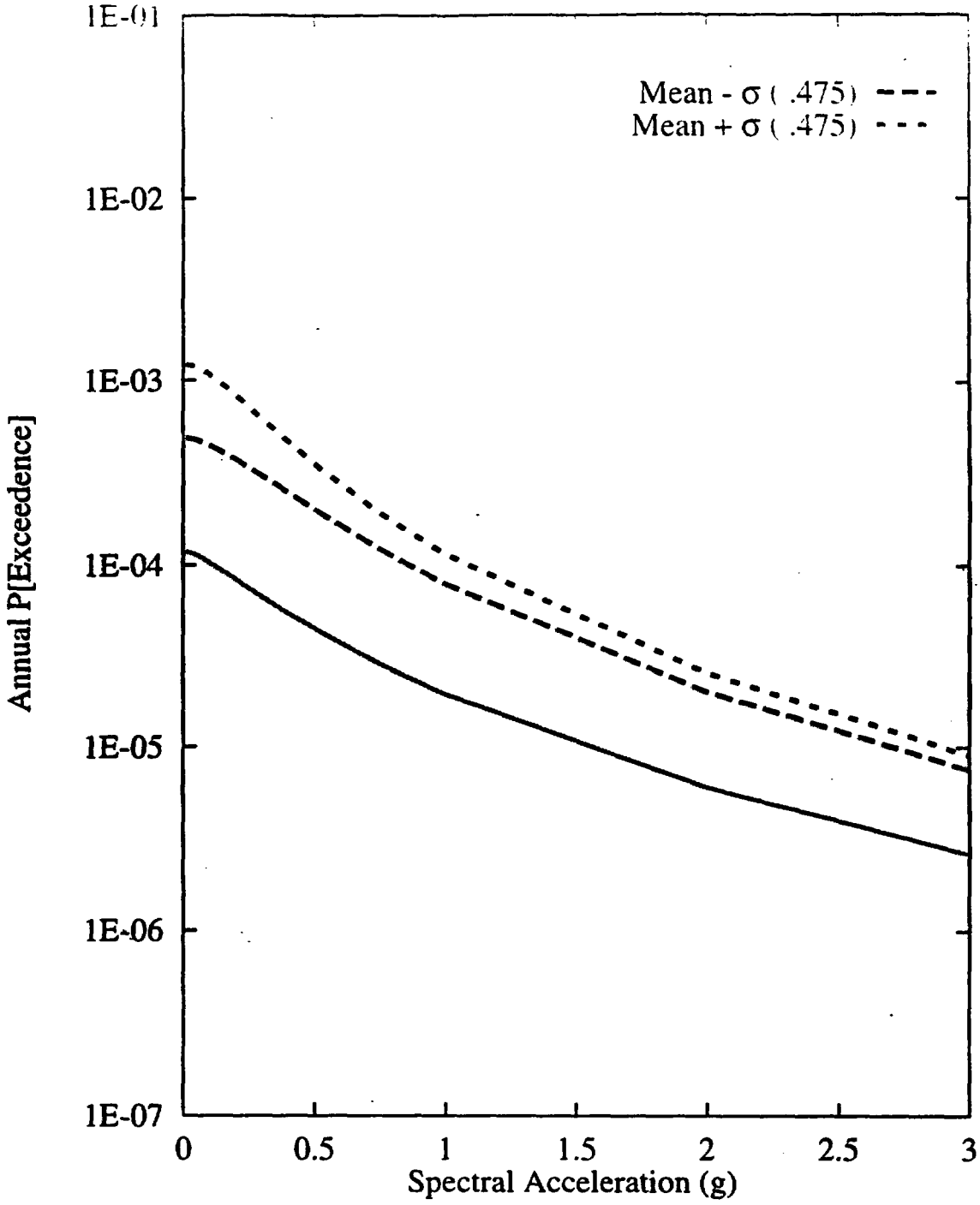

Figure 7-91 Sensitivity of seismic hazard from local faults to M_{max} on Stagecoach Road-Paintbrush Canyon fault system: DFS team, 10-Hz horizontal spectral acceleration

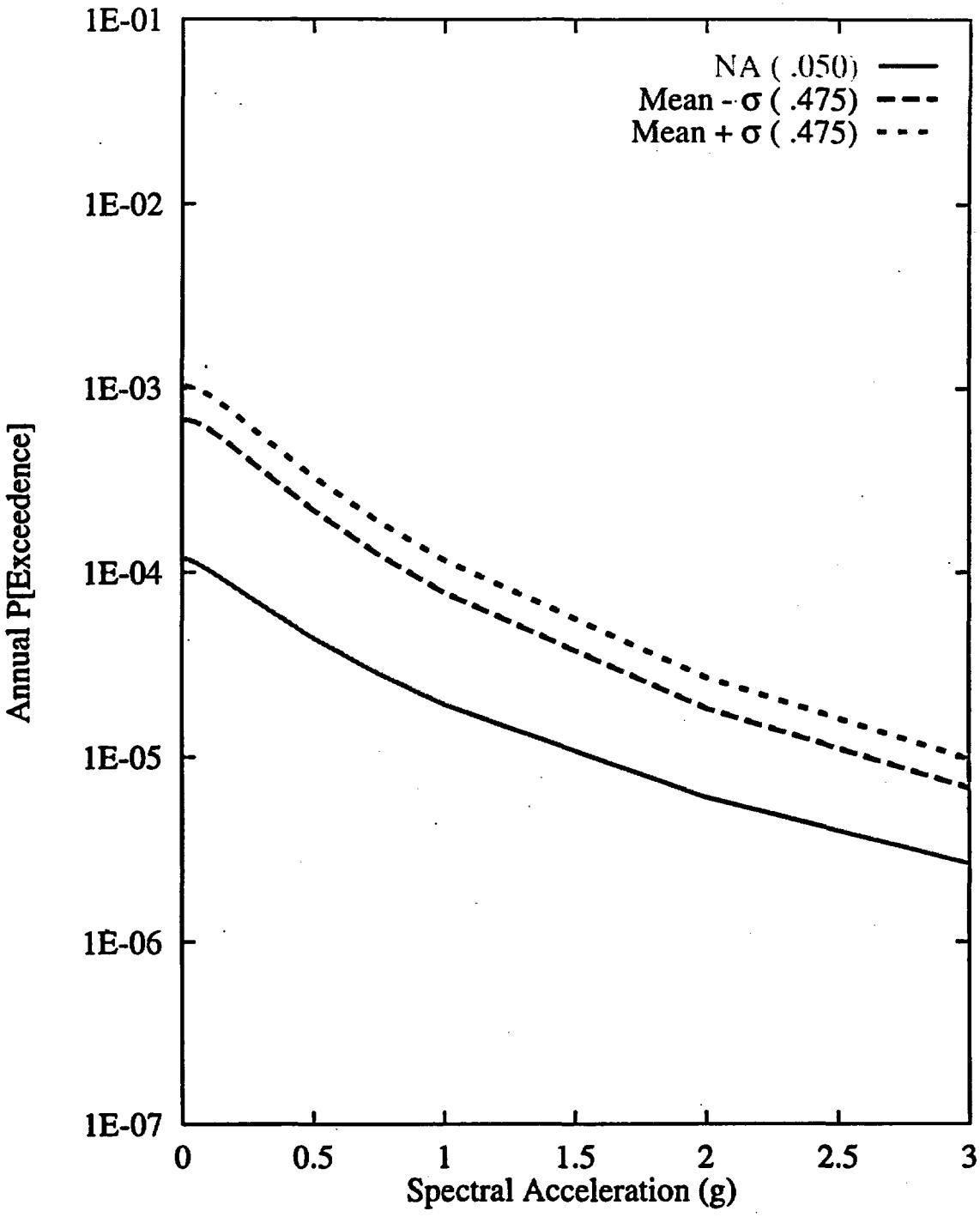

Figure 7-92 Sensitivity of seismic hazard from local faults to recurrence of Stagecoach Road-Paintbrush Canyon fault system: DFS team, 10-Hz horizontal spectral acceleration

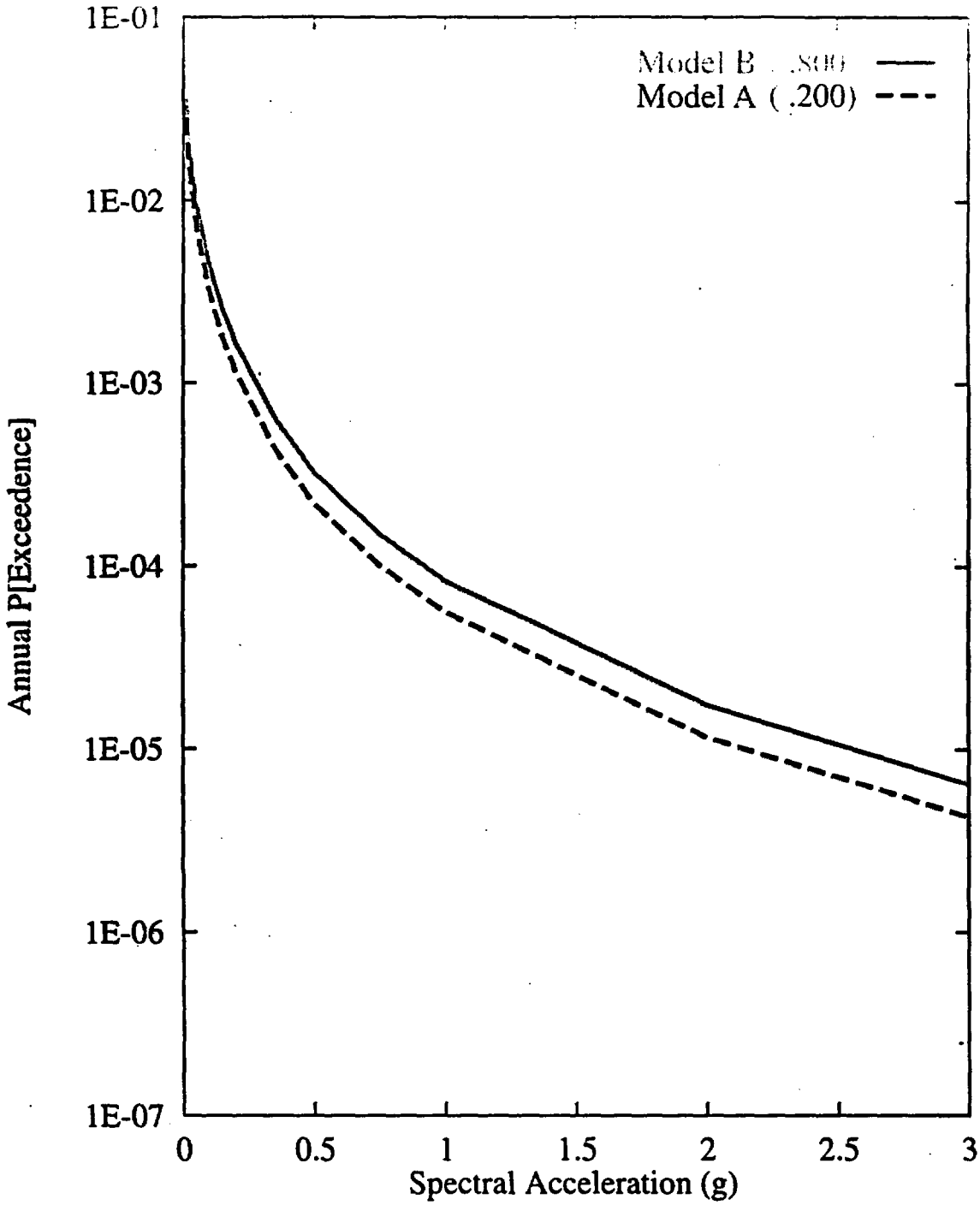

Figure 7-93 Sensitivity of seismic hazard from area zones to zonation: DFS team, 10-Hz horizontal spectral acceleration

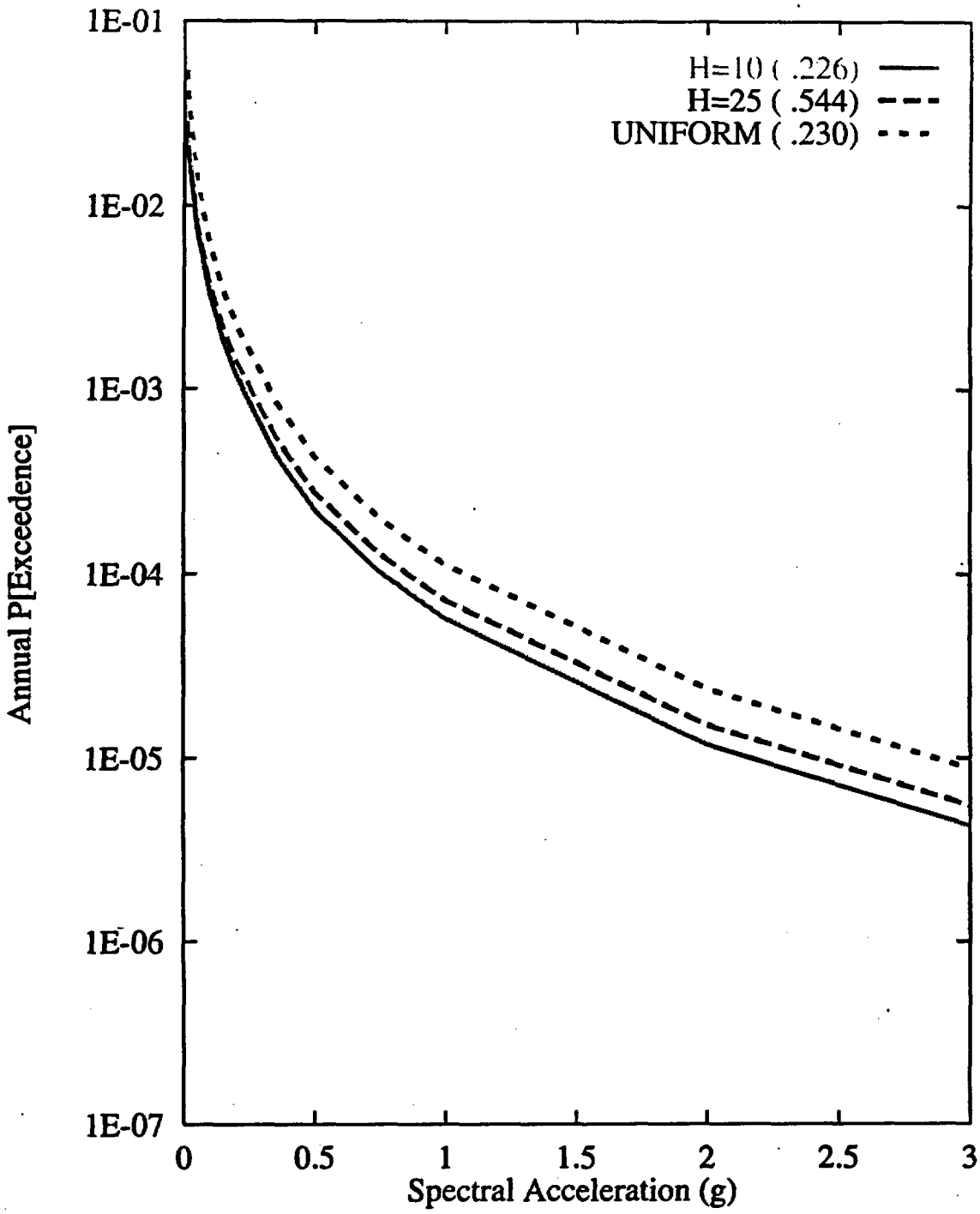

Figure 7-94 Sensitivity of seismic hazard from area zones to spatial variability and smoothing (H) of seismicity: DFS team, 10-Hz horizontal spectral acceleration

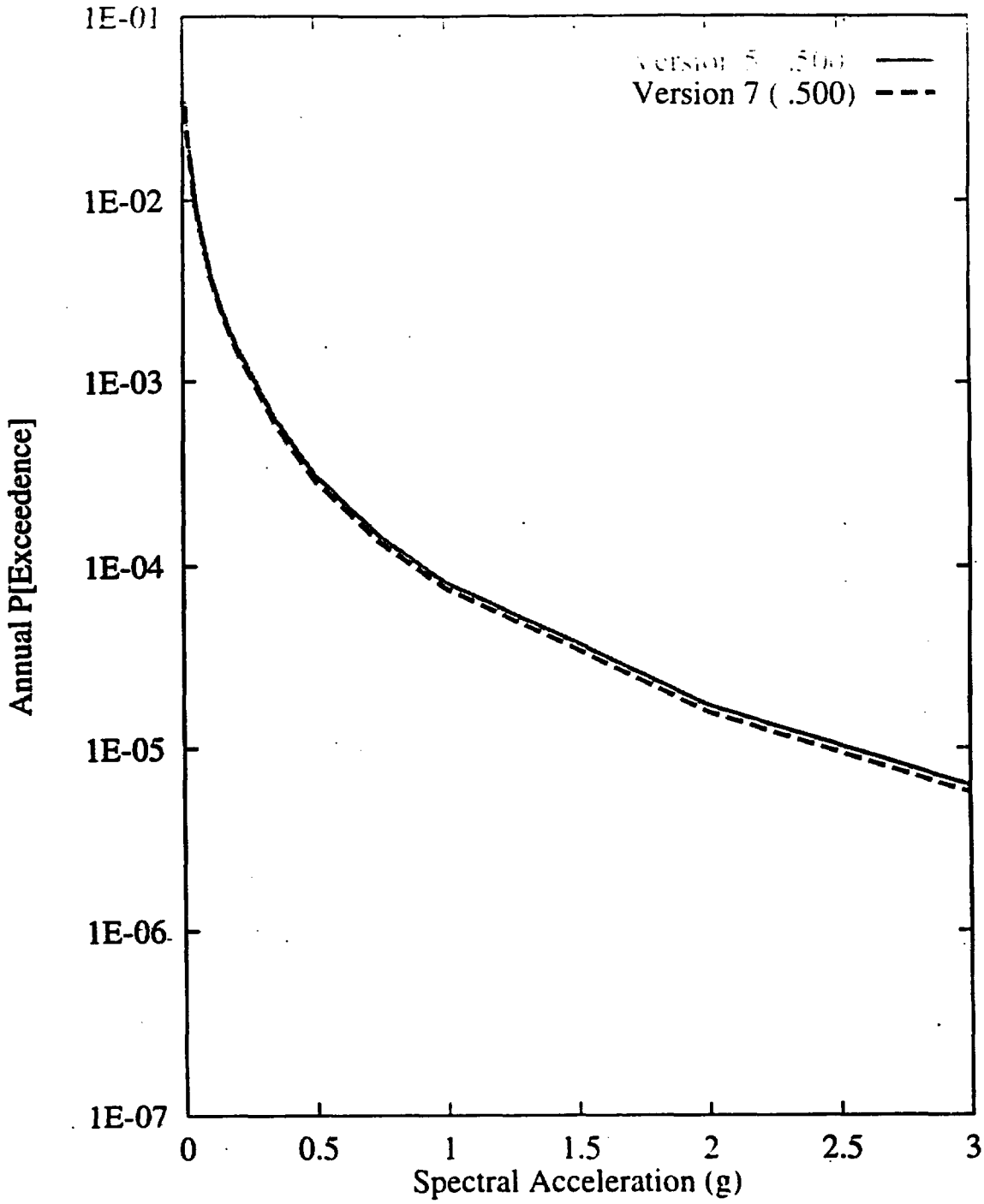

Figure 7-95 Sensitivity of seismic hazard from area zones to choice of seismicity catalog: DFS team, 10-Hz horizontal spectral acceleration

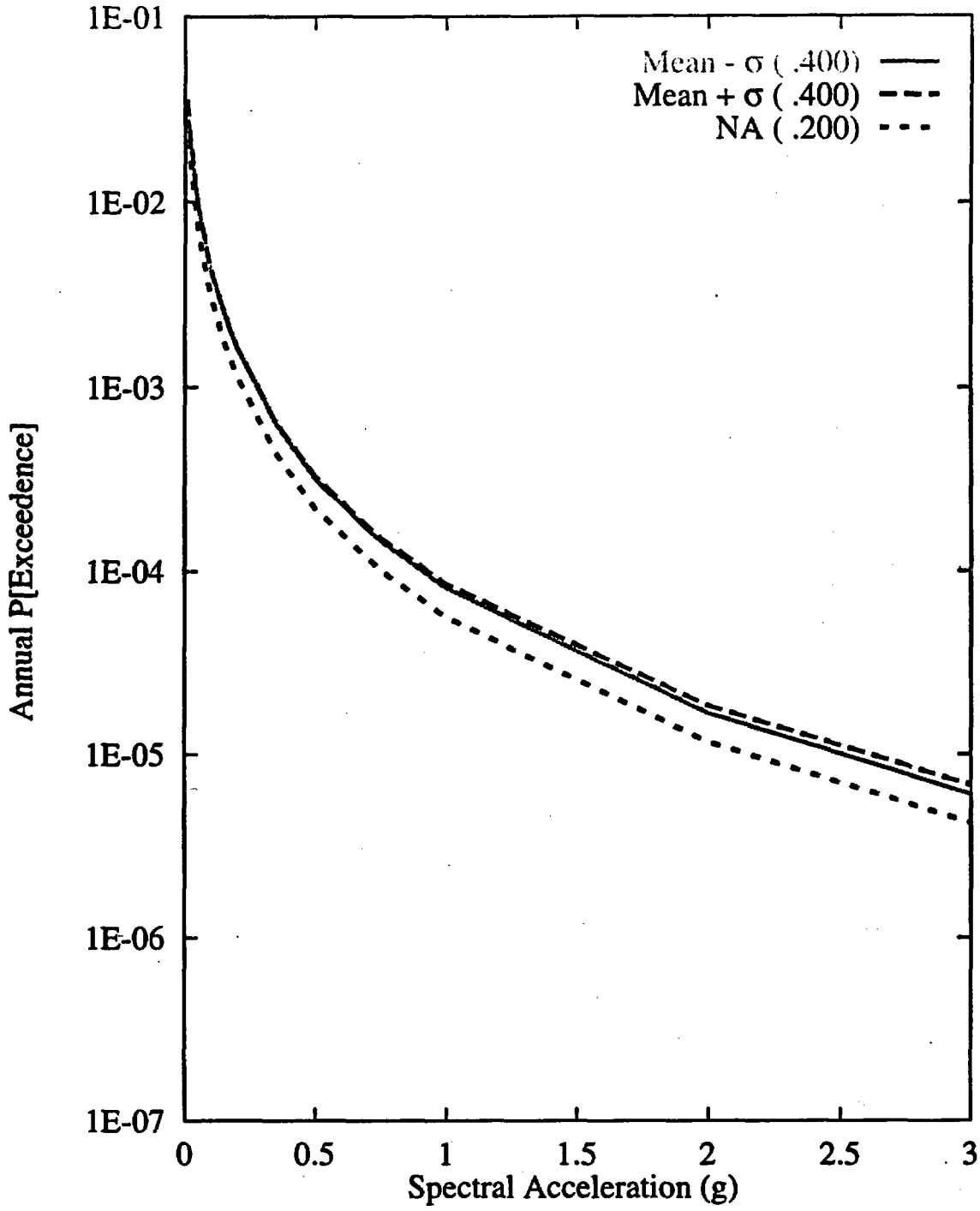

Figure 7-96 Sensitivity of seismic hazard from area zones to Mmax on the East Walker Lane+local seismic source: DFS team, 10-Hz horizontal spectral acceleration

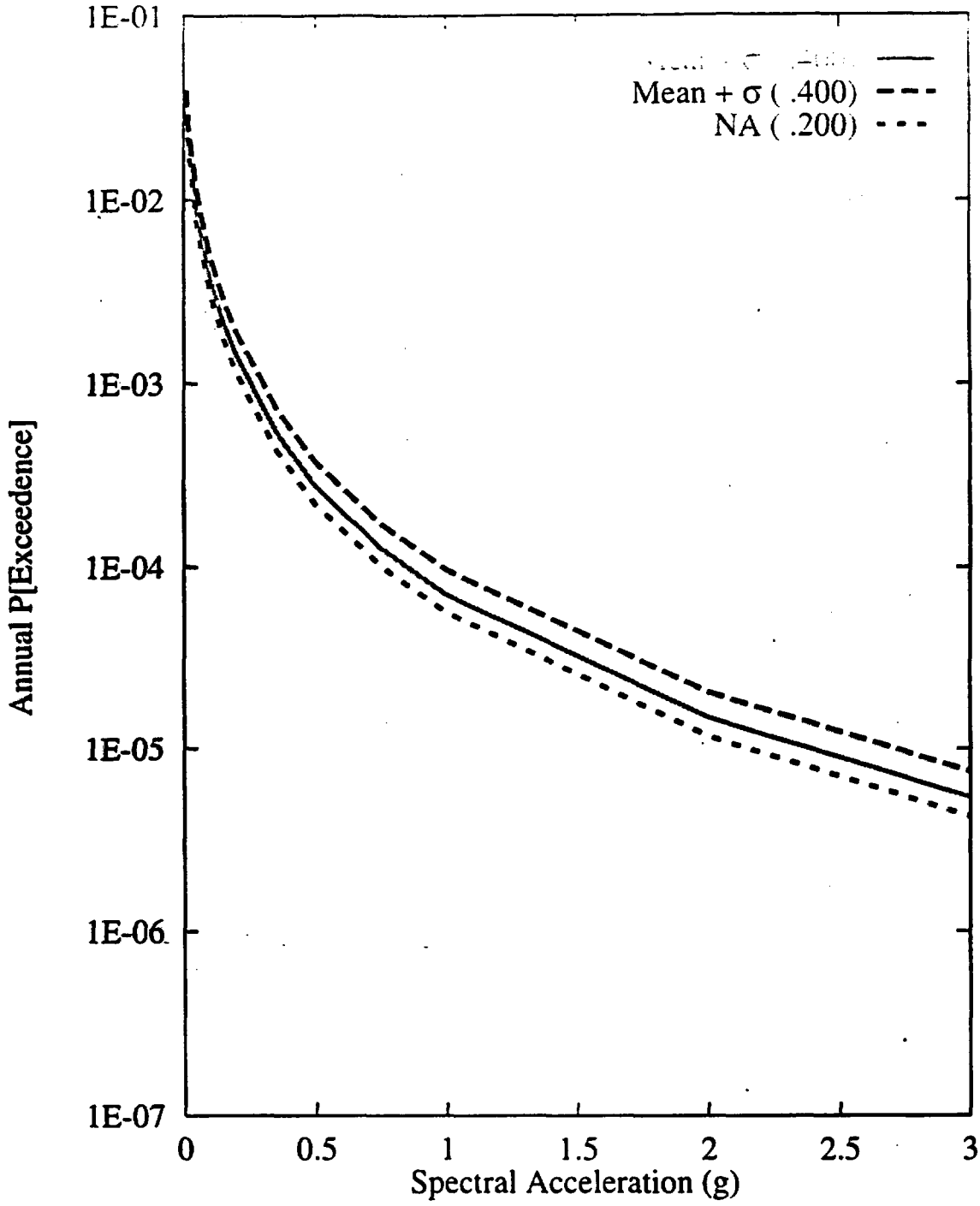

Figure 7-97 Sensitivity of seismic hazard from area zones to recurrence of the East Walker Lane+local seismic source: DFS team, 10-Hz horizontal spectral acceleration

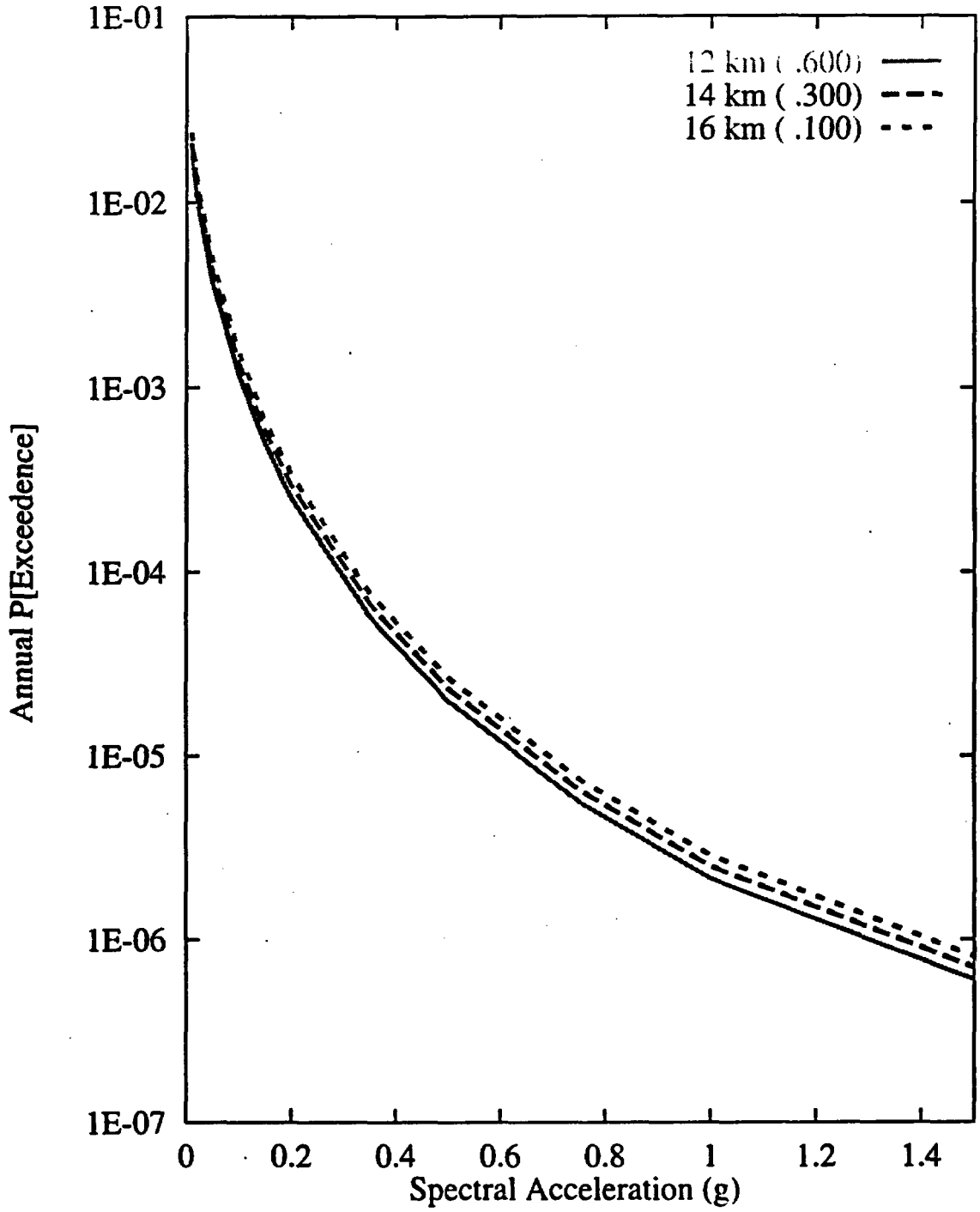

Figure 7-98 Sensitivity of seismic hazard from regional faults to maximum fault depth: DFS team, 1-Hz horizontal spectral acceleration

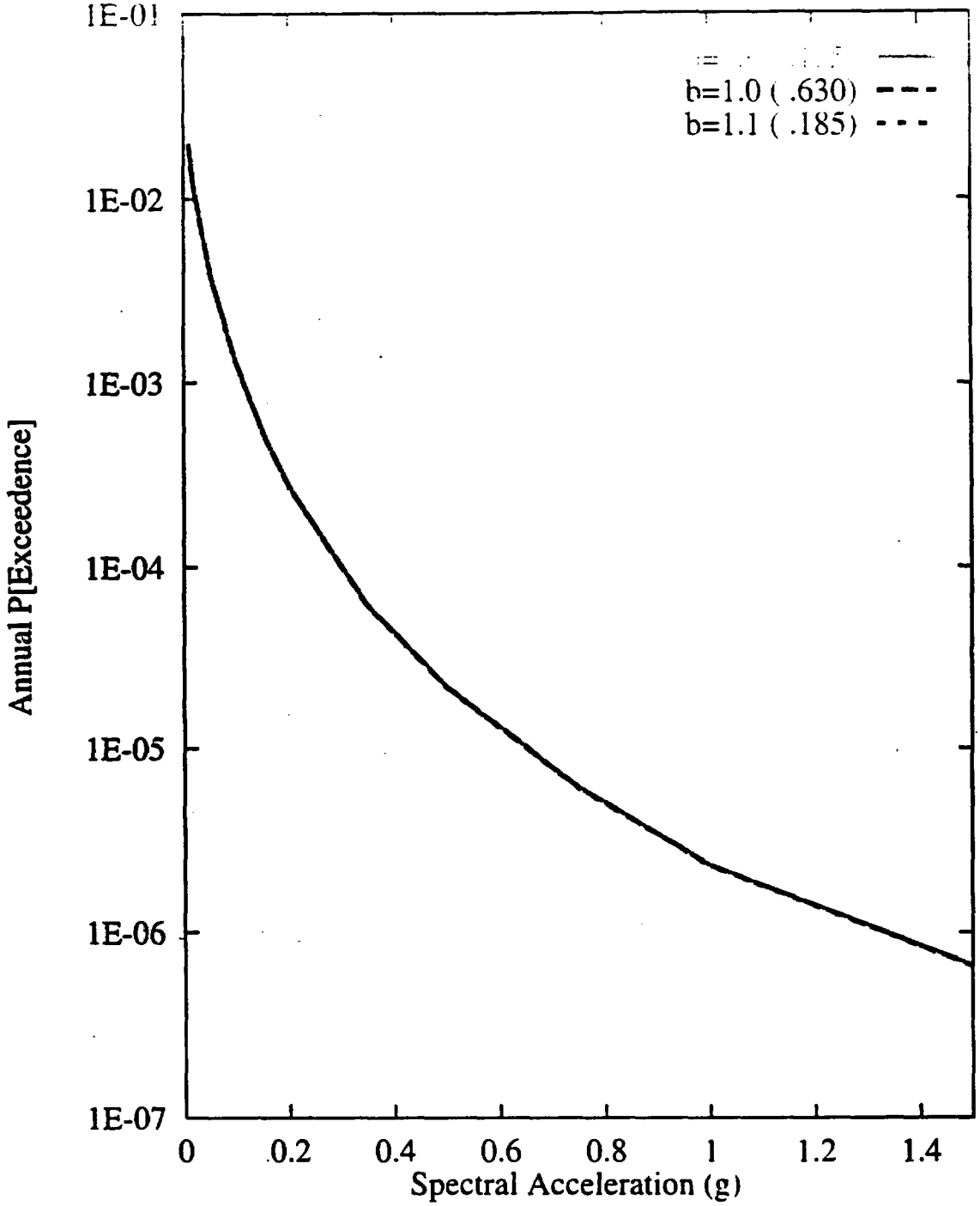

Figure 7-99 Sensitivity of seismic hazard from regional faults to b-values: DFS team, 1-Hz horizontal spectral acceleration

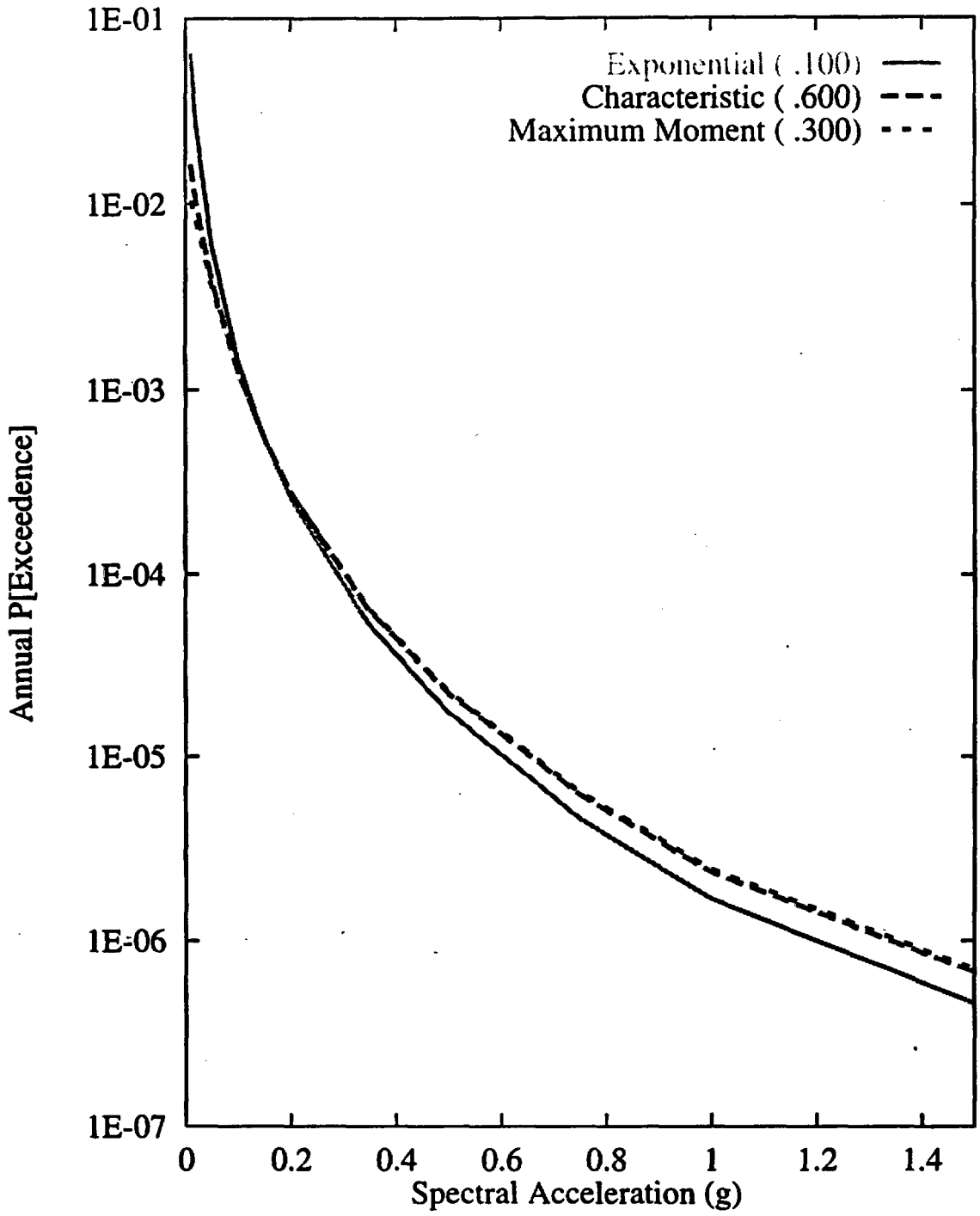

Figure 7-100 Sensitivity of seismic hazard from regional faults to recurrence model: DFS team, 1-Hz horizontal spectral acceleration

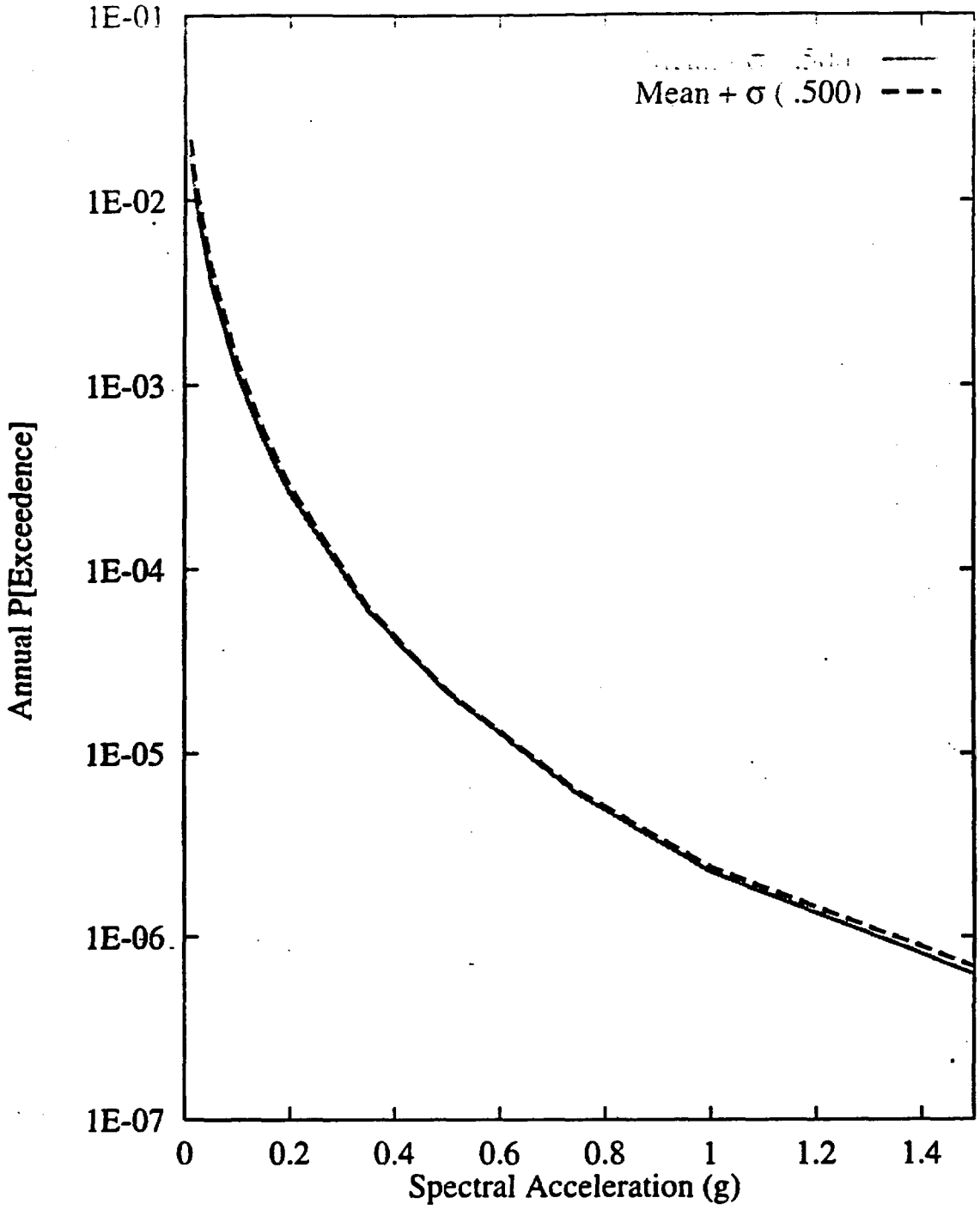

Figure 7-101 Sensitivity of seismic hazard from regional faults to M_{max} on the Death Valley fault: DFS team, 1-Hz horizontal spectral acceleration

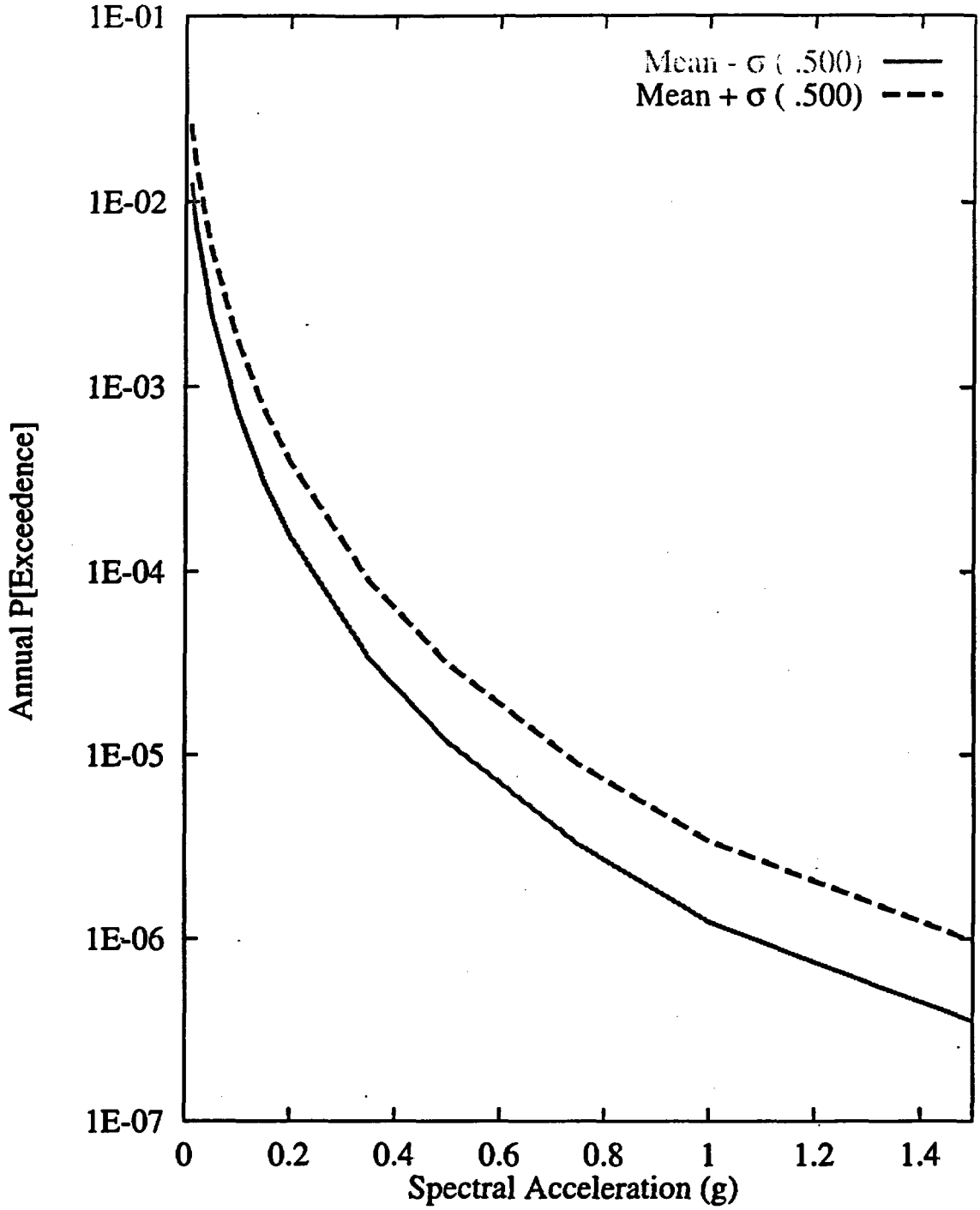

Figure 7-102 Sensitivity of seismic hazard from regional faults to slip rate of the Death Valley fault: DFS team, 1-Hz horizontal spectral acceleration

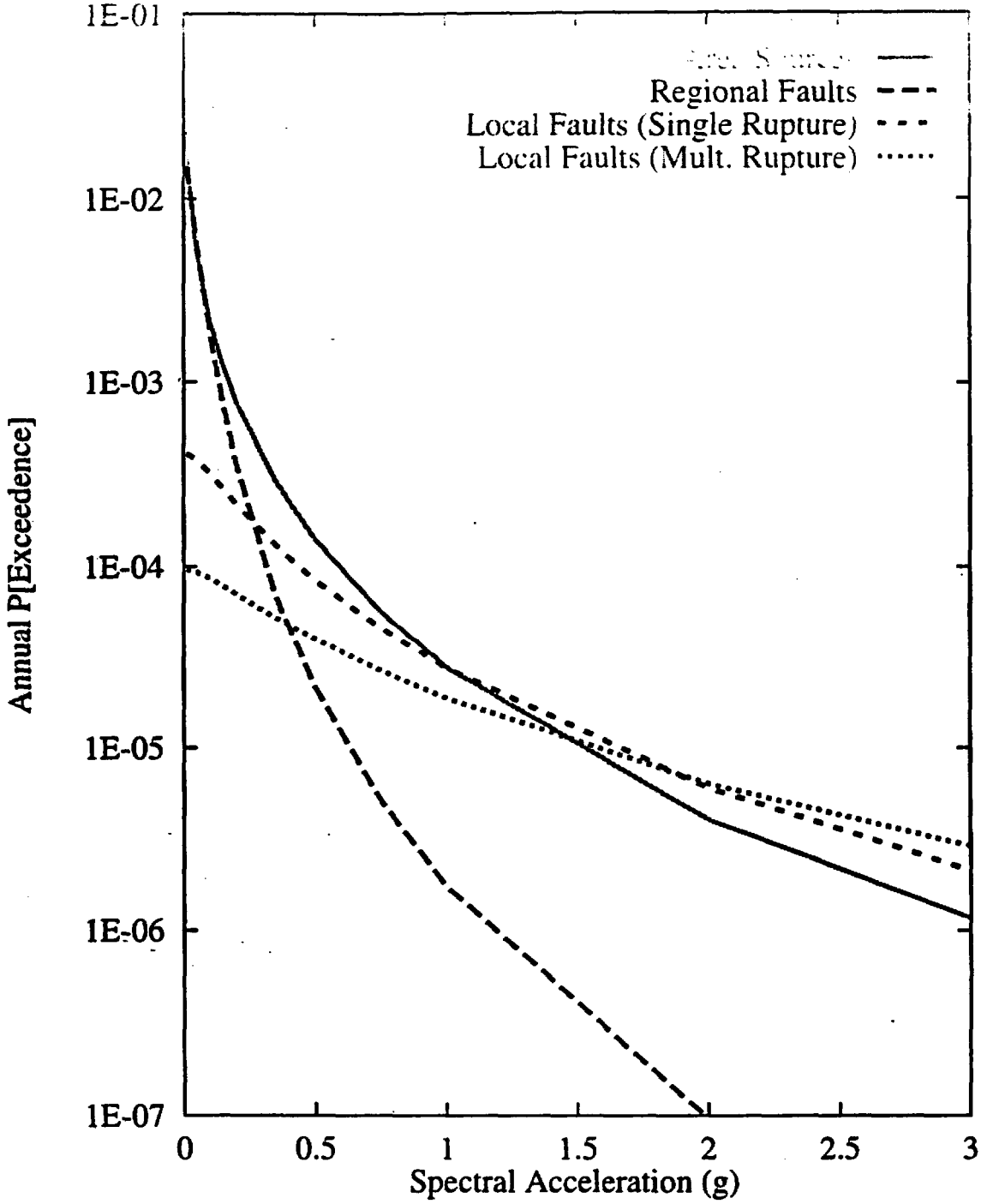

Figure 7-103 Contributions of source types to the mean hazard: RYA team, 10-Hz horizontal spectral acceleration

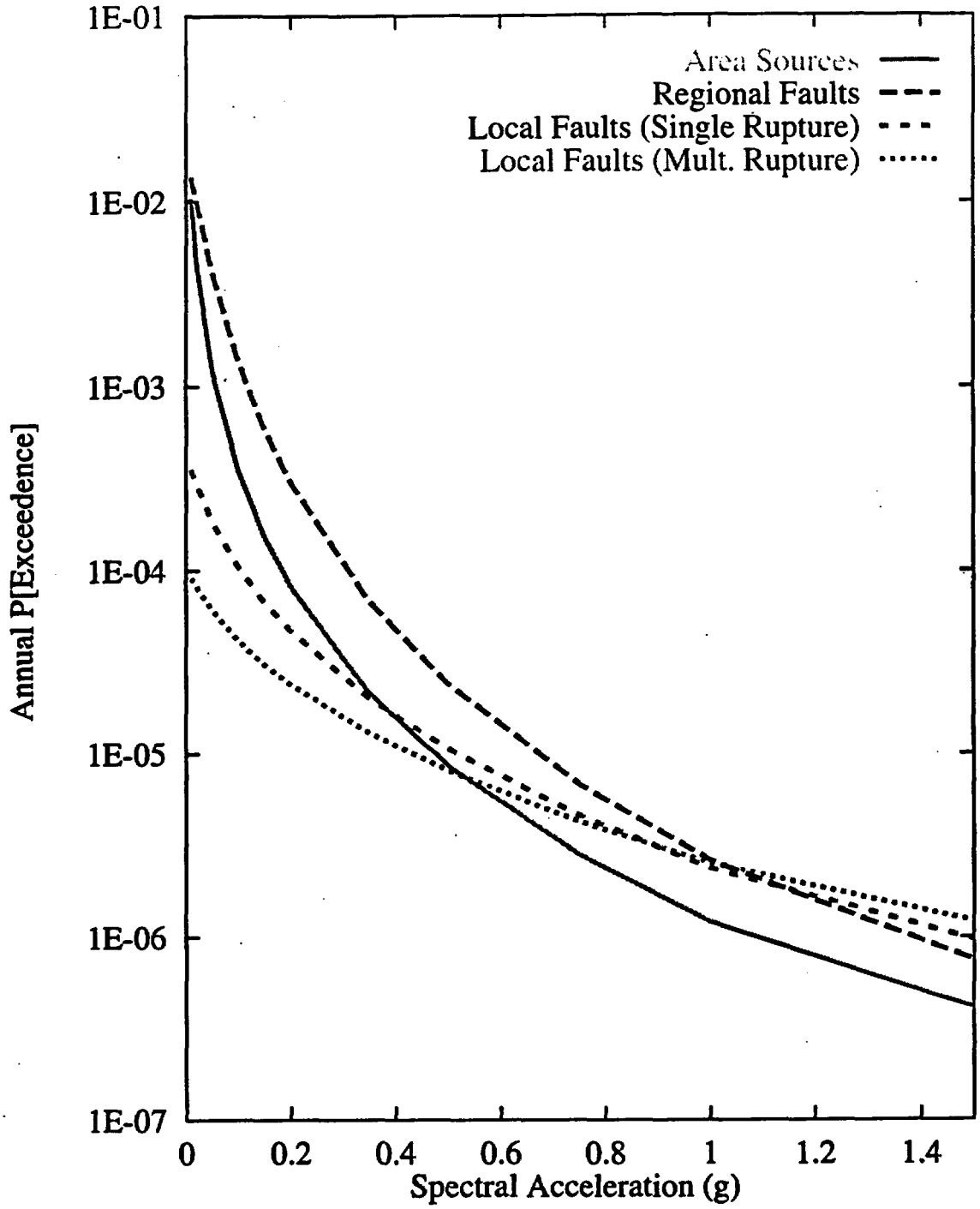

Figure 7-104 Contributions of source types to the mean hazard: RYA team, 1-Hz horizontal spectral acceleration

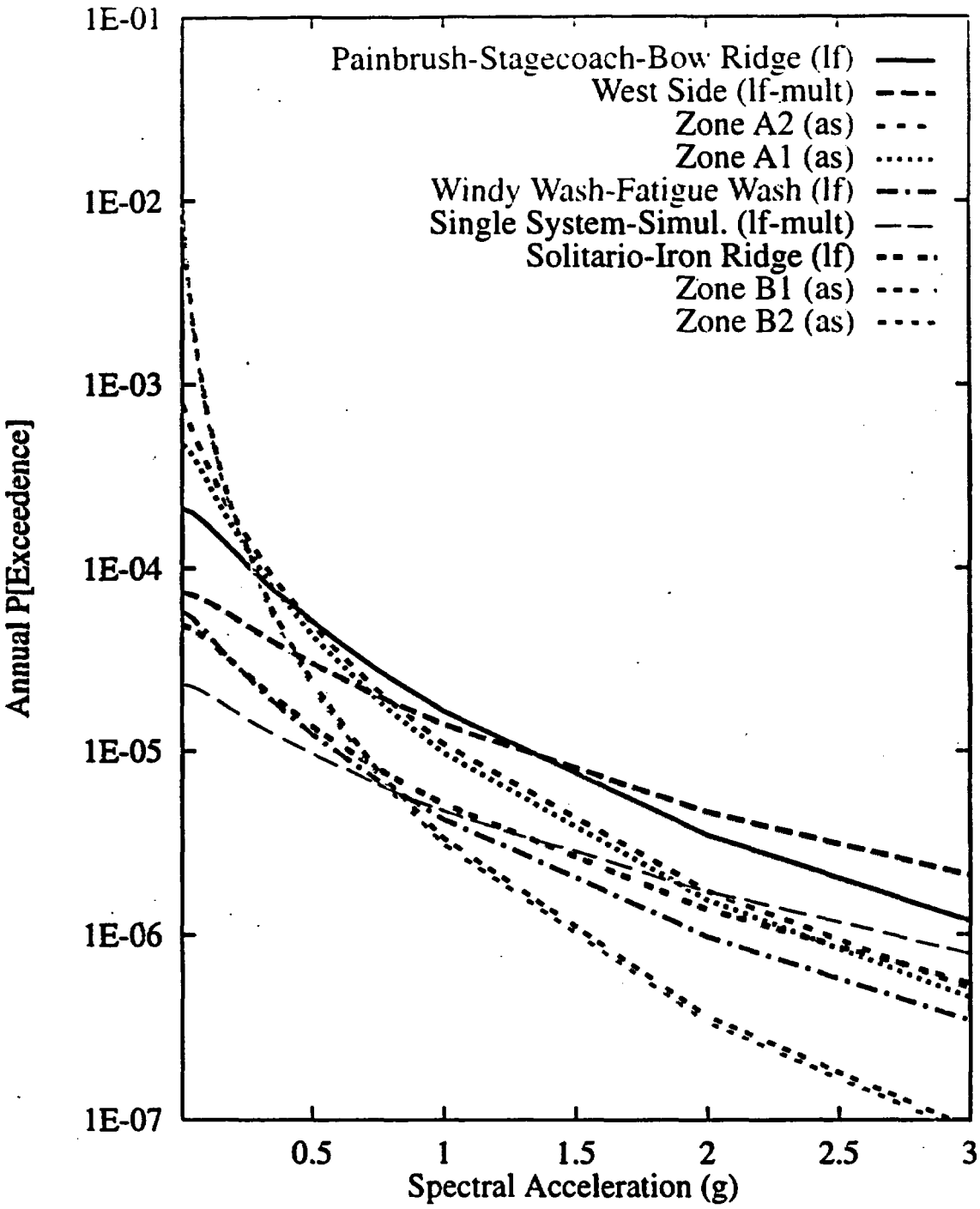

Figure 7-105 Mean seismic hazard from dominant seismic sources: RYA team, 10-Hz horizontal spectral acceleration. Acronyms in parentheses refer to source types: as-area source zone; lf-local fault; and mult-multiple fault.

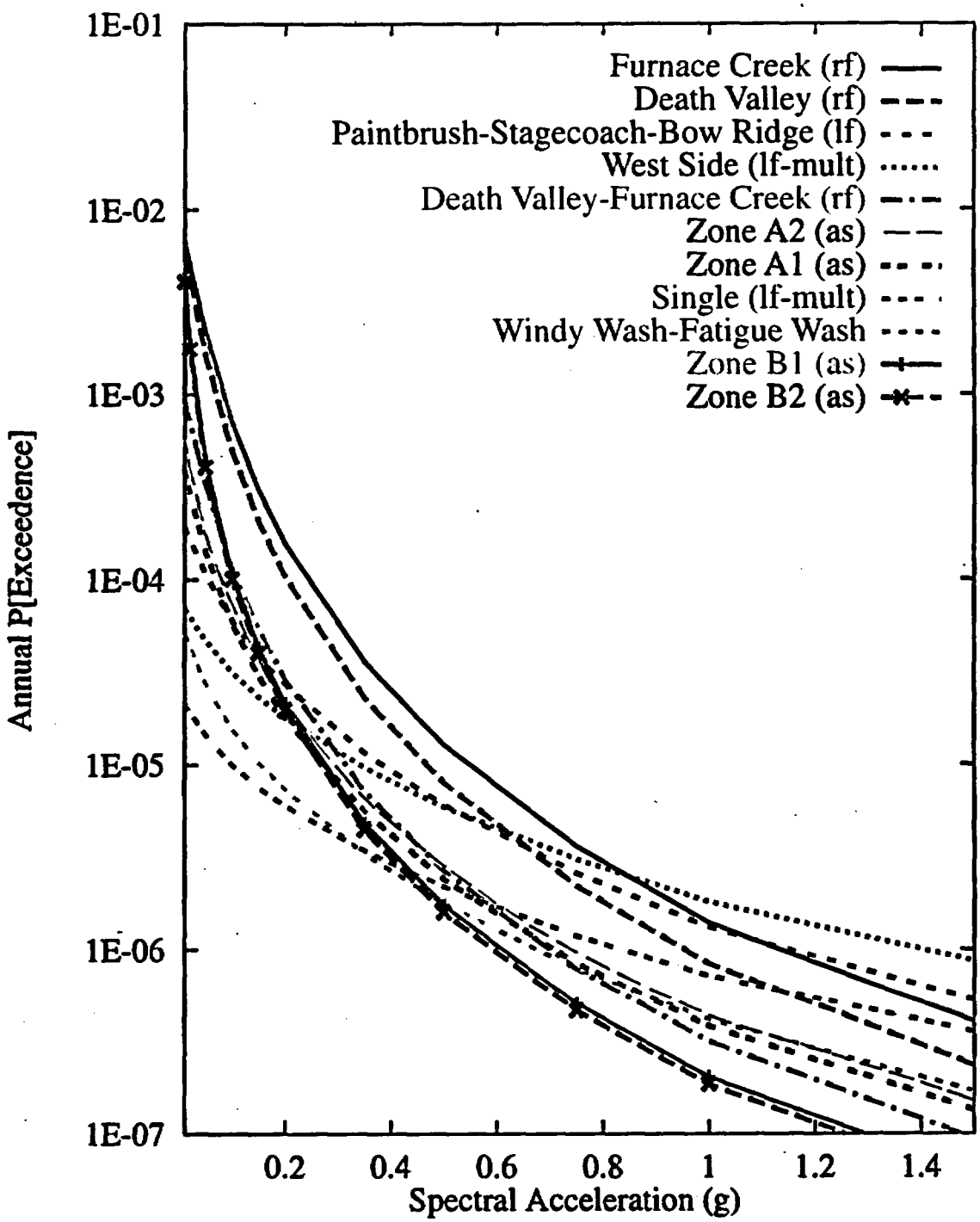

Figure 7-106 Mean seismic hazard from dominant seismic sources: RYA team, 1-Hz horizontal spectral acceleration. Acronyms in parentheses refer to source types: as-area source zone; rf-regional fault; lf-local fault; and mult-multiple fault.

10 Hz, RYA Area Sources

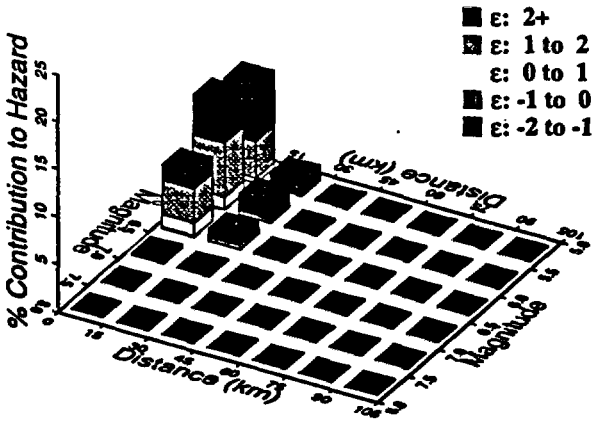

10 Hz, RYA Regional Faults

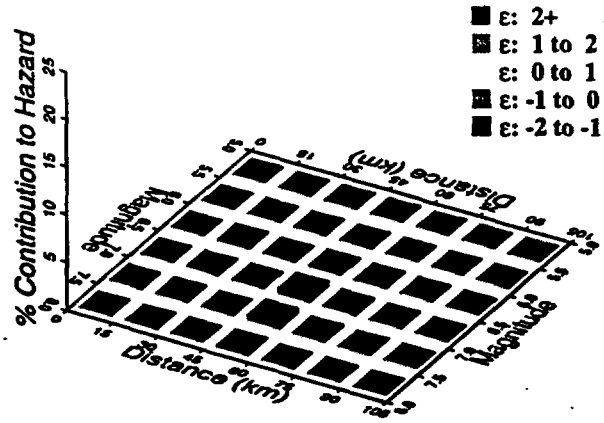

10 Hz, RYA Local Faults (Single)

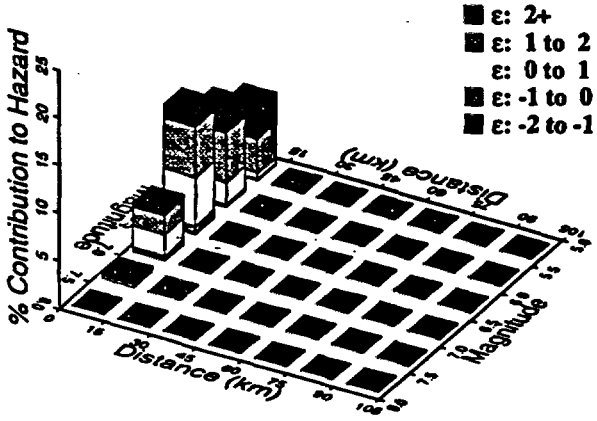

10 Hz, RYA Local Faults (Mult.)

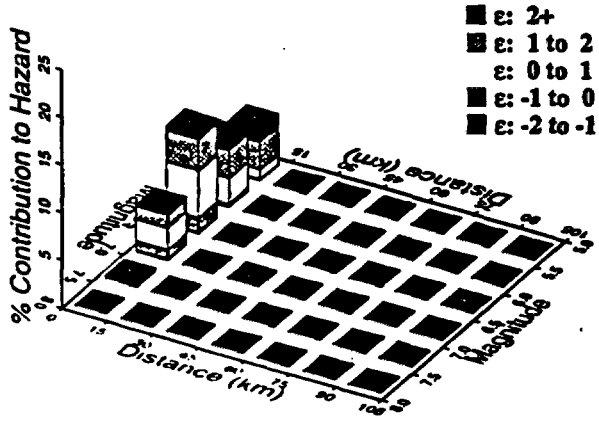

Figure 7-107 Magnitude-distance-epsilon distributions for the four source types: RYA team, 10-Hz horizontal spectral acceleration at 10^{-4} exceedance probability

1 Hz, RYA Area Sources

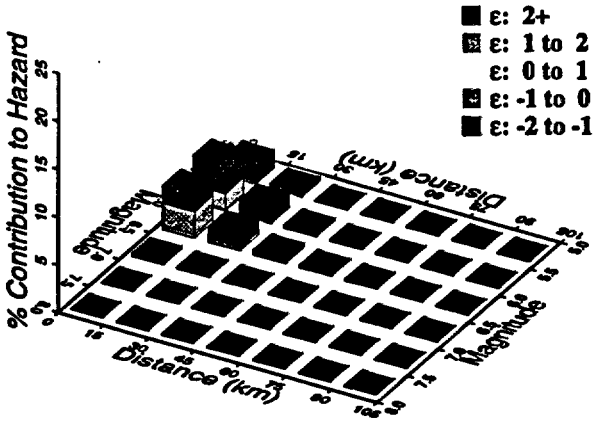

1 Hz, RYA Regional Faults

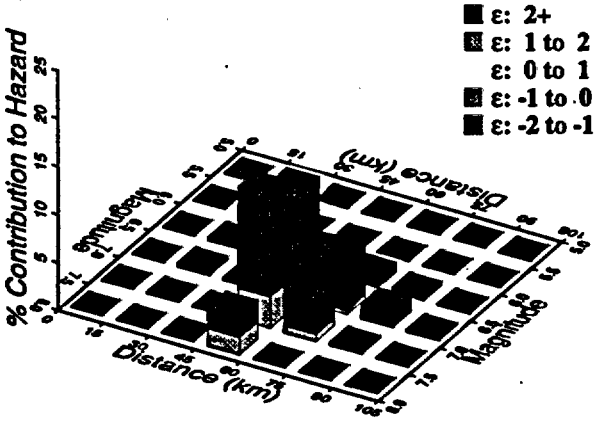

1 Hz, RYA Local Faults (Single)

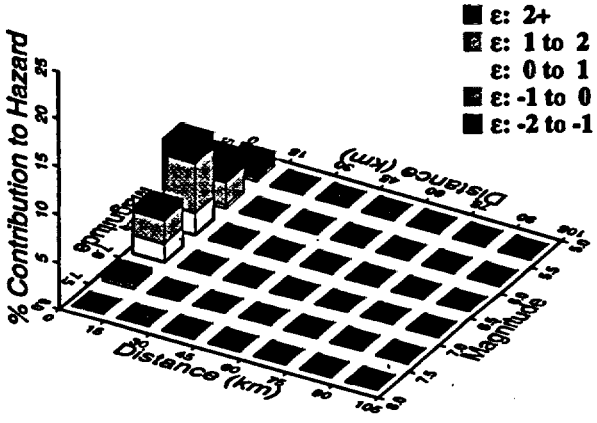

1 Hz, RYA Local Faults (Mult.)

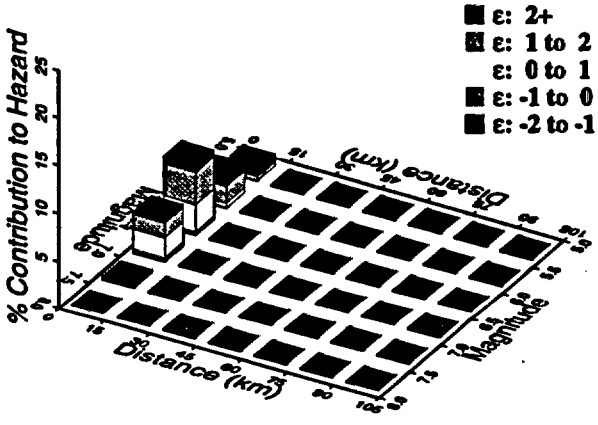

Figure 7-108 Magnitude-distance-epsilon distributions for the four source types: RYA team, 1-Hz horizontal spectral acceleration at 10^{-4} exceedance probability

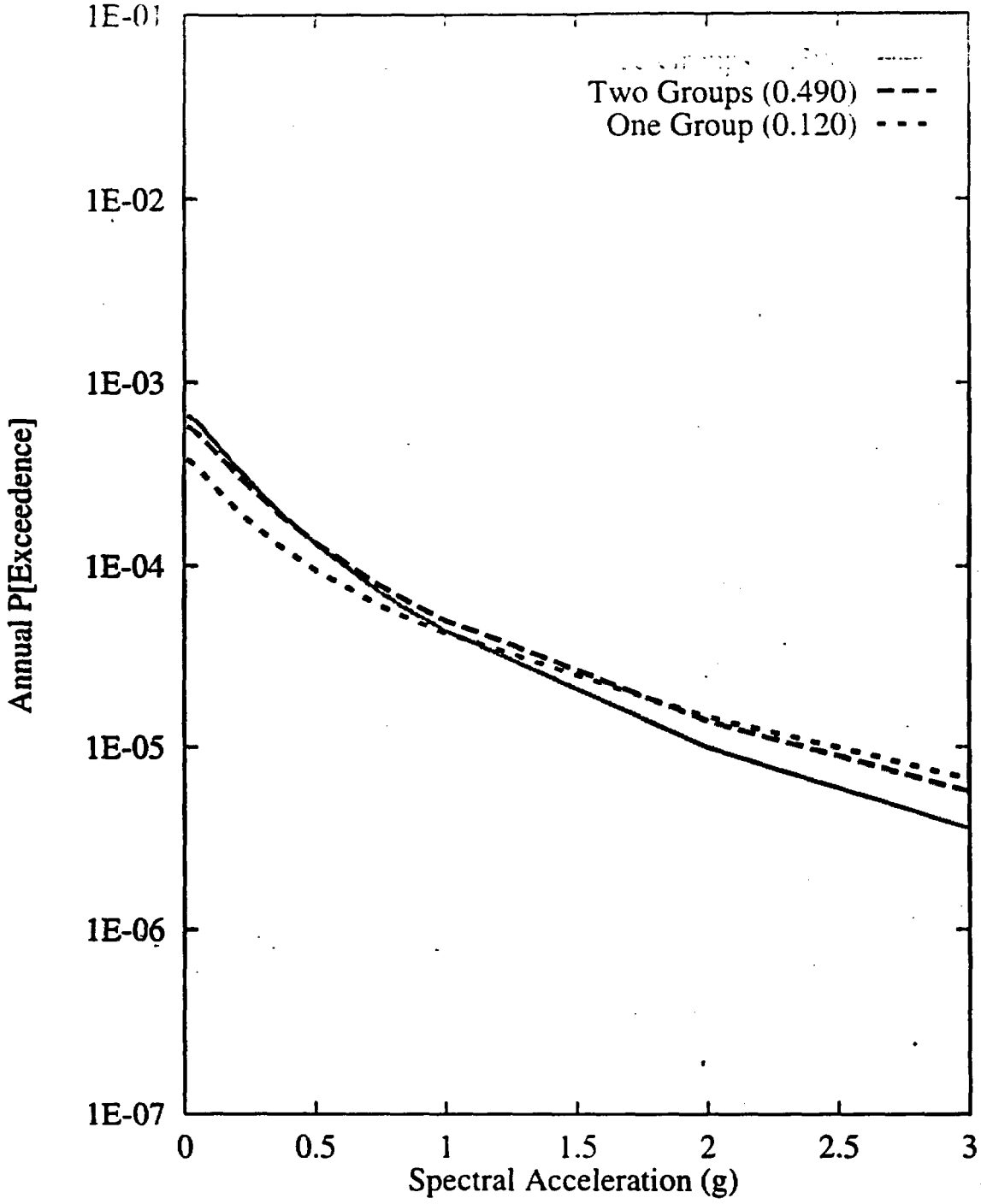

Figure 7-109 Sensitivity of seismic hazard from local faults to coalescence model: RYA team, 10-Hz horizontal spectral acceleration

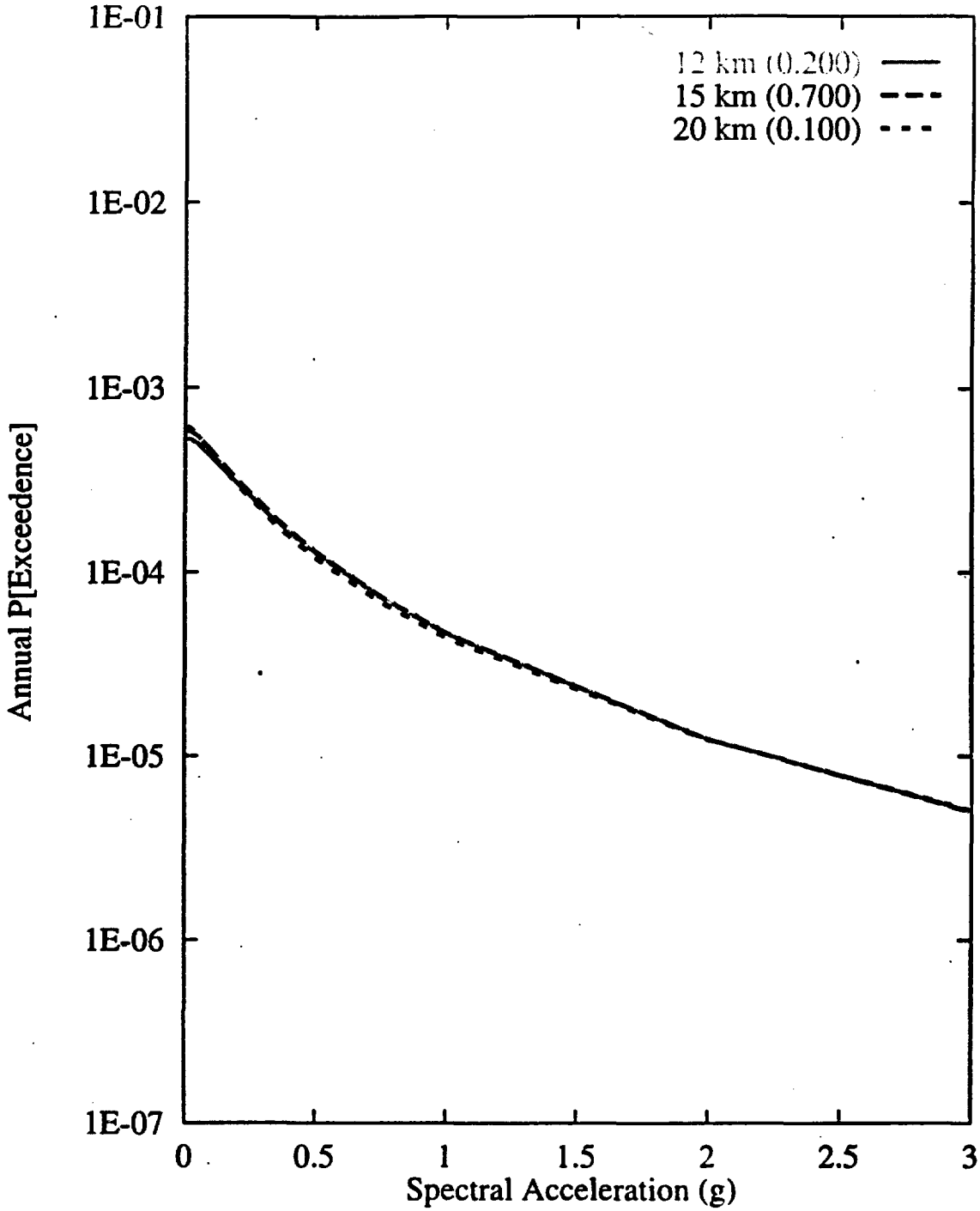

Figure 7-110 Sensitivity of seismic hazard from local faults to maximum fault depth: RYA team, 10-Hz horizontal spectral acceleration

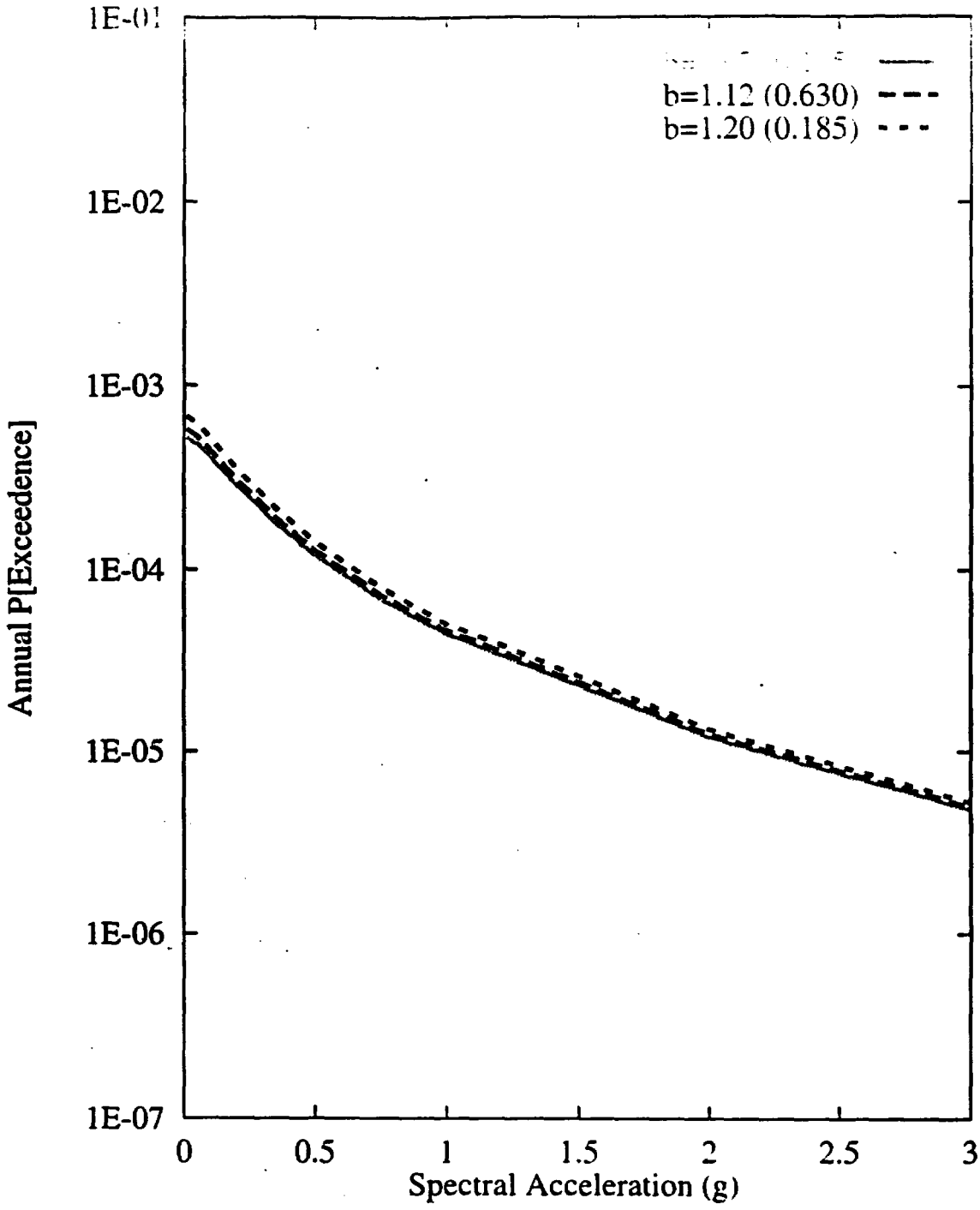

Figure 7-111 Sensitivity of seismic hazard from local faults to b-value: RYA team, 10-Hz horizontal spectral acceleration

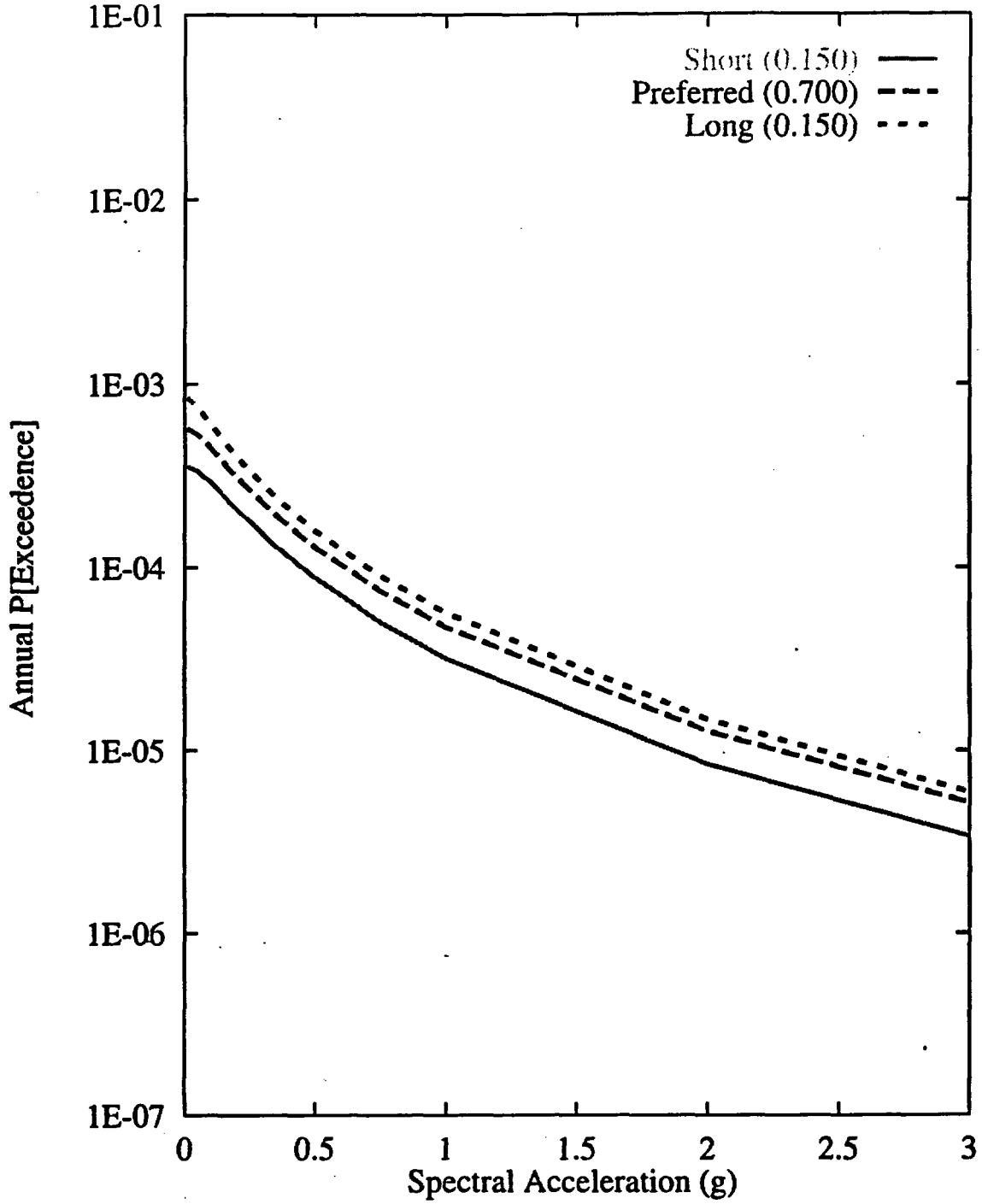

Figure 7-112 Sensitivity of seismic hazard from local faults to fault lengths: RYA team, 10-Hz horizontal spectral acceleration

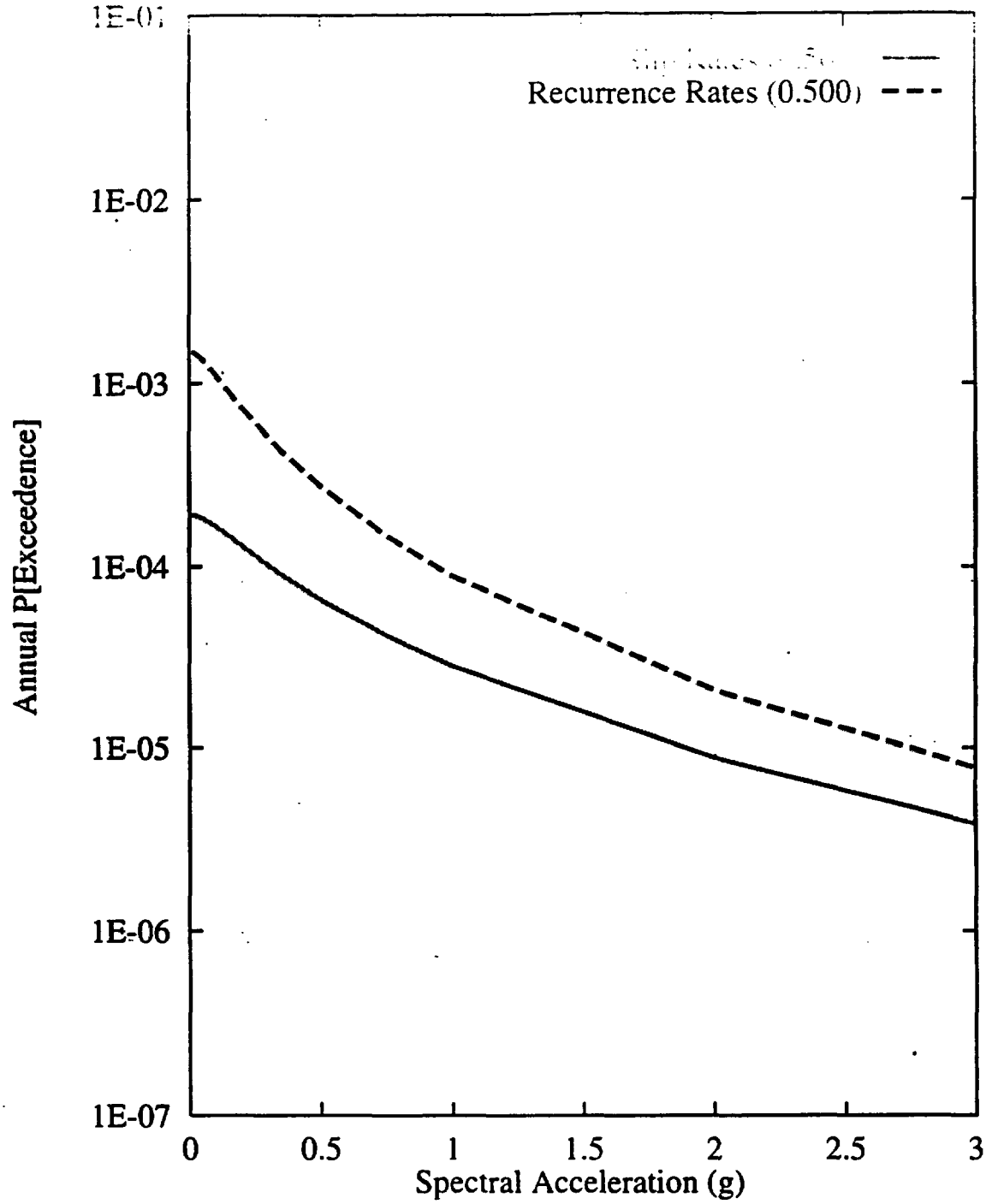

Figure 7-113 Sensitivity of seismic hazard from local faults to recurrence approach used: RYA team, 10-Hz horizontal spectral acceleration

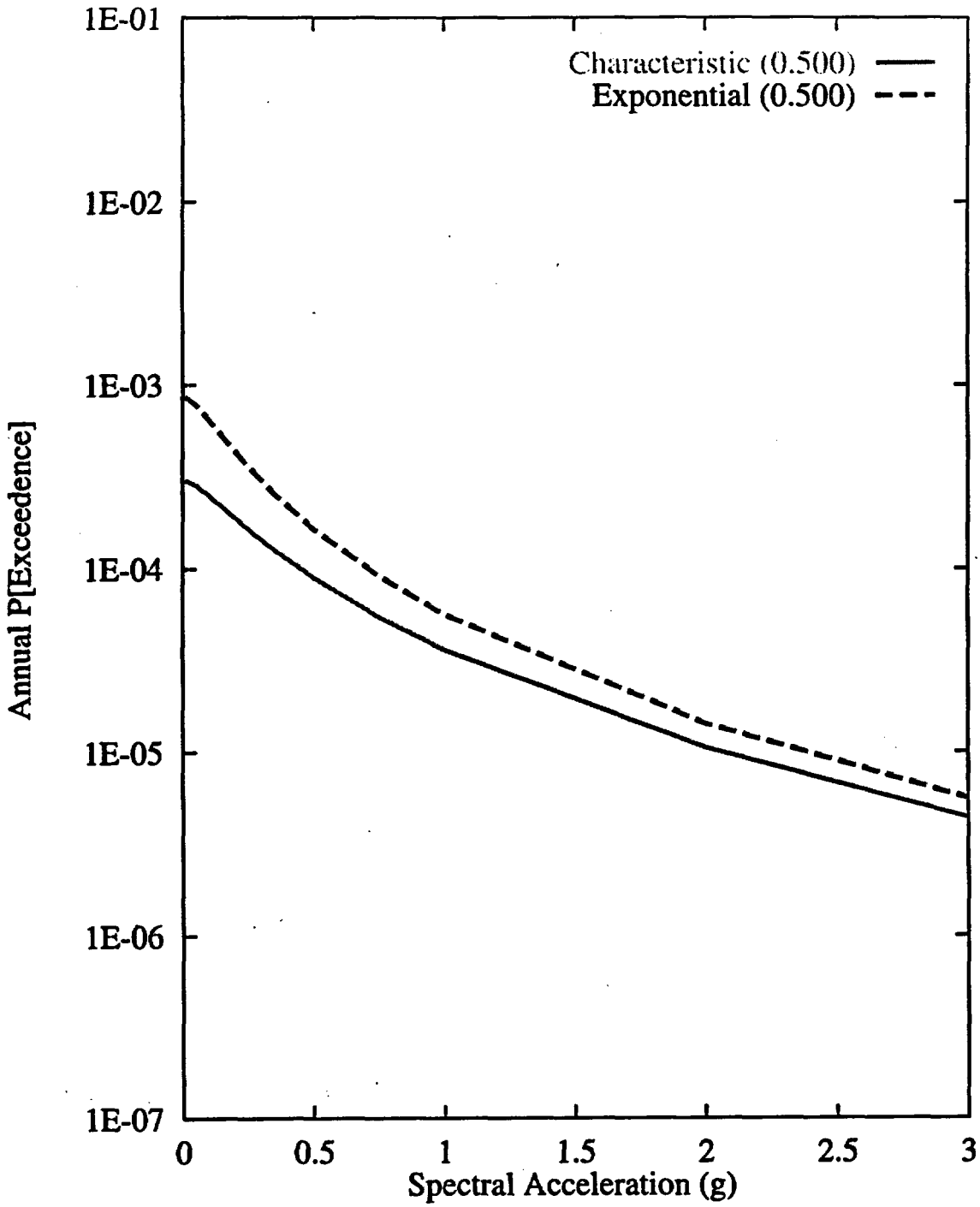

Figure 7-114 Sensitivity of seismic hazard from local faults to recurrence model for the Paintbrush Canyon-Stagecoach Road-Bow Ridge fault system: RYA team, 10-Hz horizontal spectral acceleration

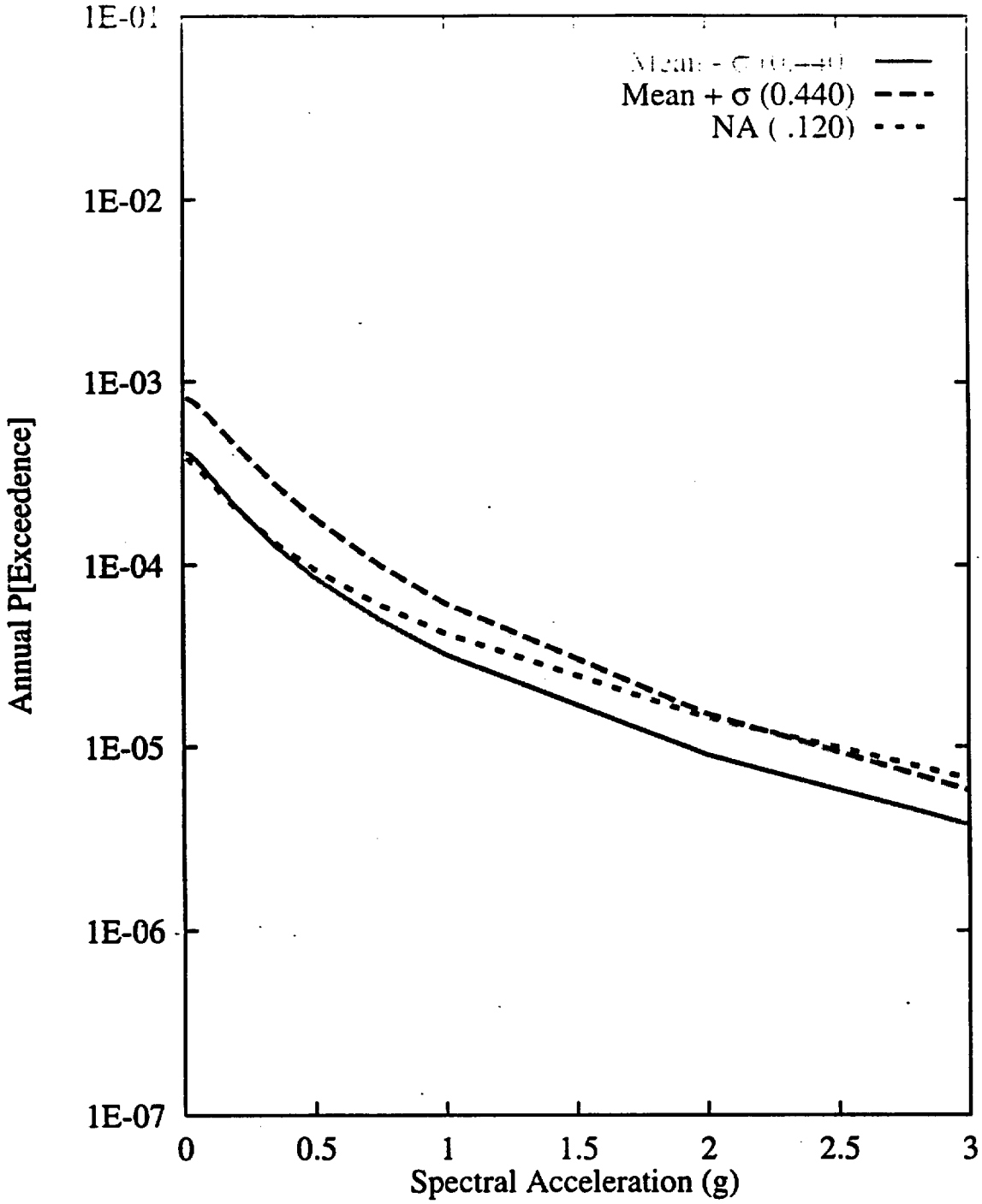

Figure 7-115 Sensitivity of seismic hazard from local faults to Mmax on the Paintbrush Canyon-Stagecoach Road-Bow Ridge fault system: RYA team, 10-Hz horizontal spectral acceleration

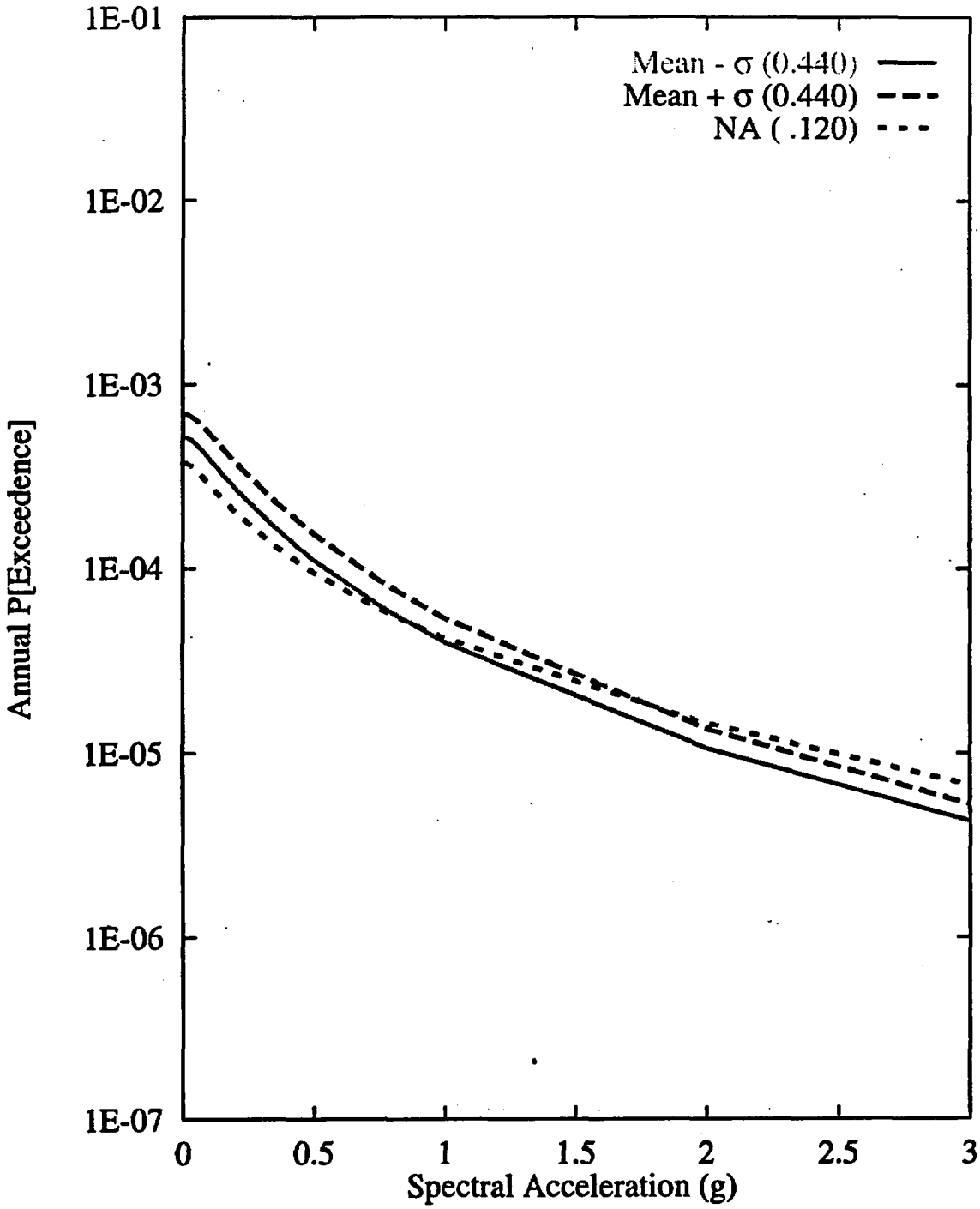

Figure 7-116 Sensitivity of seismic hazard from local faults to recurrence of the Paintbrush Canyon-Stagecoach Road-Bow Ridge fault system: RYA team, 10-Hz horizontal spectral acceleration

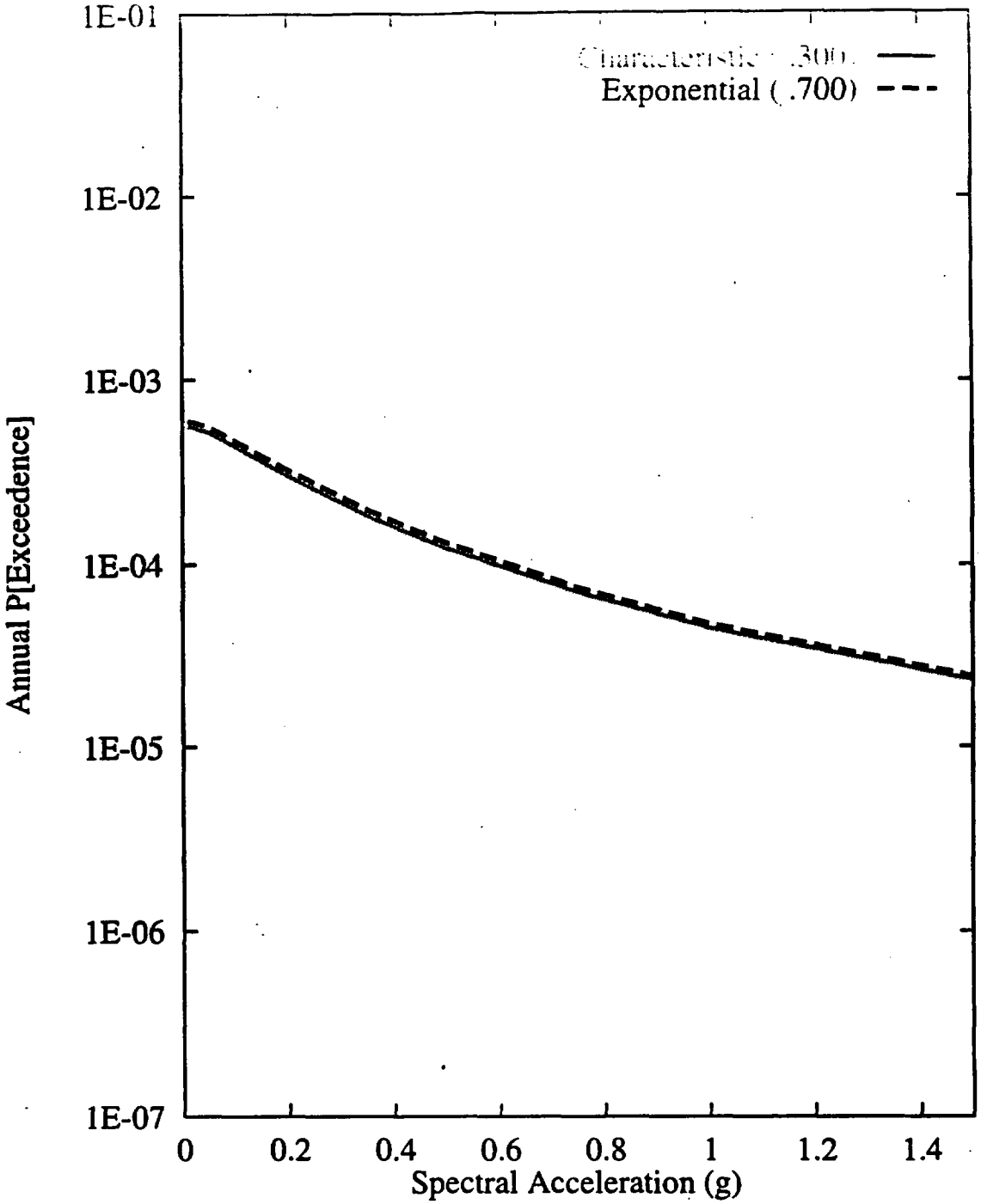

Figure 7-117 Sensitivity of seismic hazard from local faults to recurrence model for the West-side fault system: RYA team, 10-Hz horizontal spectral acceleration

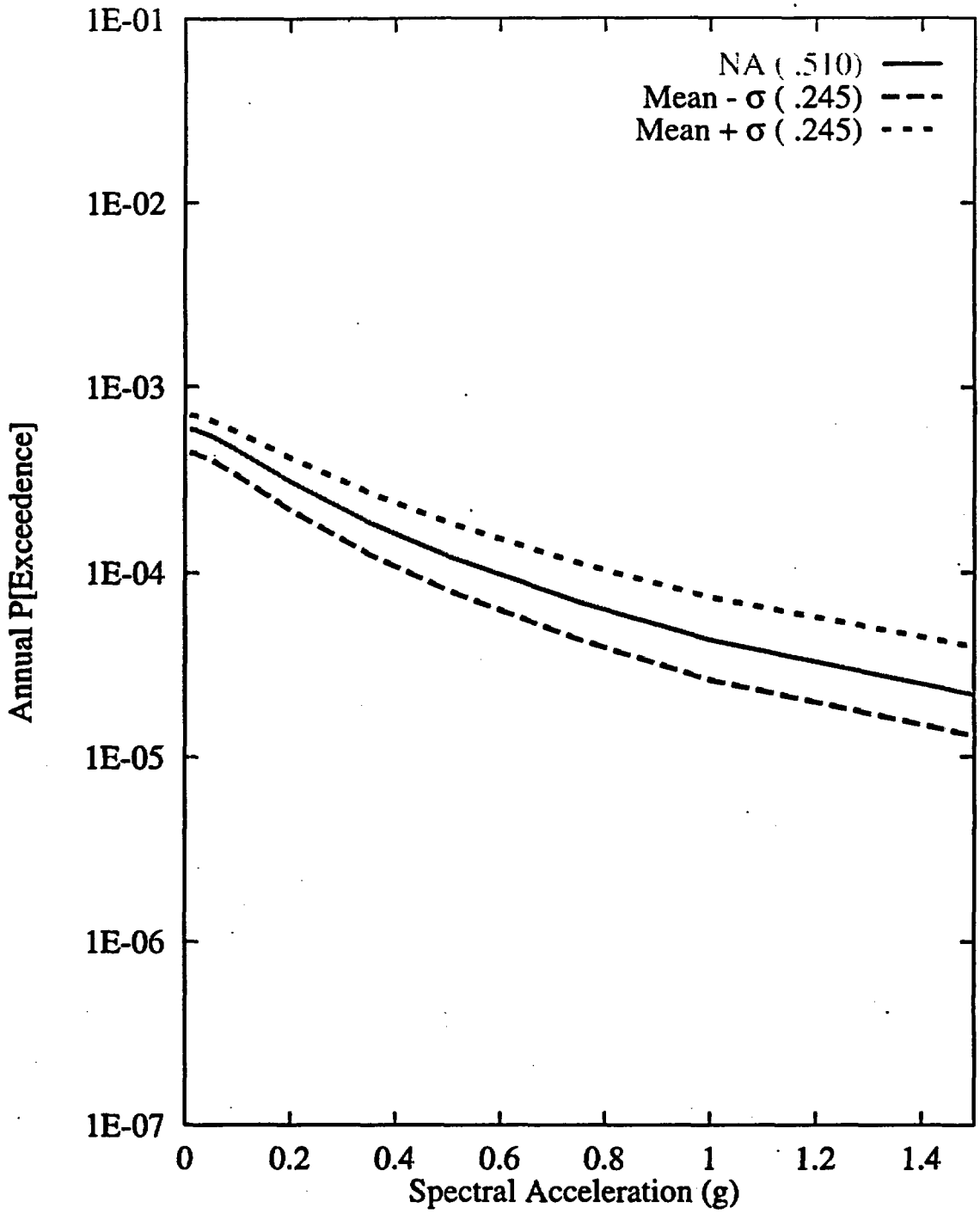

Figure 7-118 Sensitivity of seismic hazard from local faults to M_{max} on the West-side fault system: RYA team, 10-Hz horizontal spectral acceleration

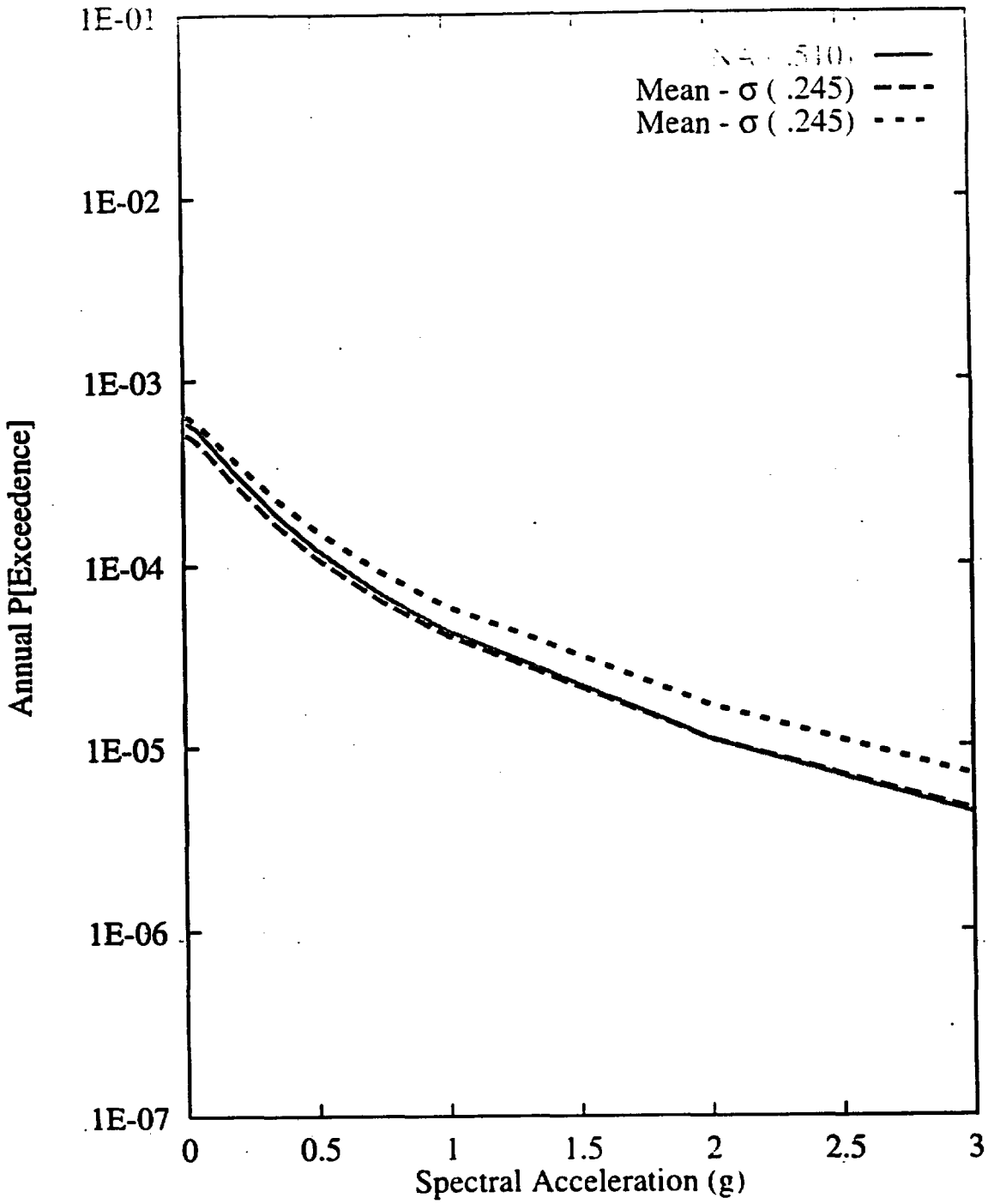

Figure 7-119 Sensitivity of seismic hazard from local faults to recurrence of the West-side fault system: RYA team, 10-Hz horizontal spectral acceleration

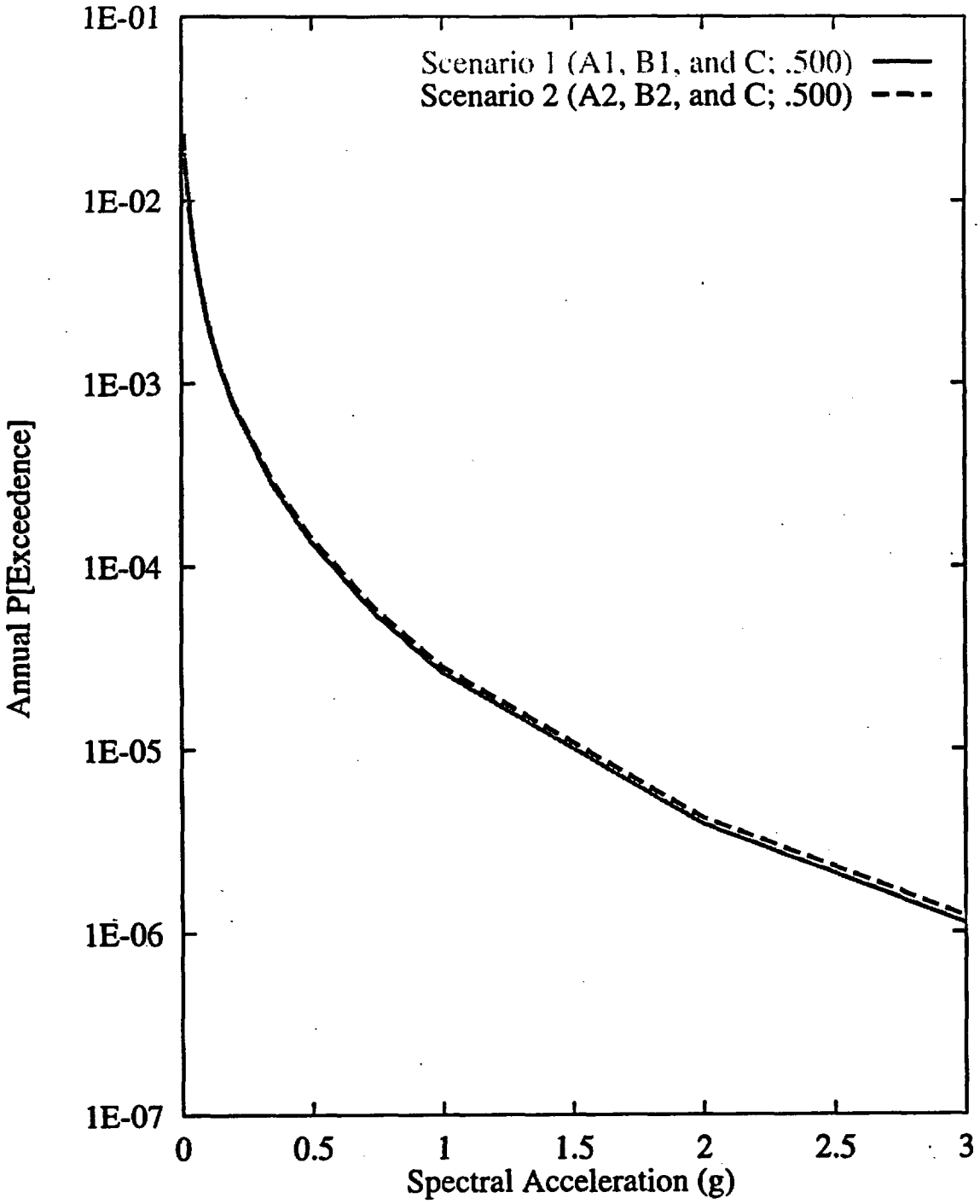

Figure 7-120 Sensitivity of seismic hazard from area zones to alternative zonation scenarios: RYA team, 10-Hz horizontal spectral acceleration

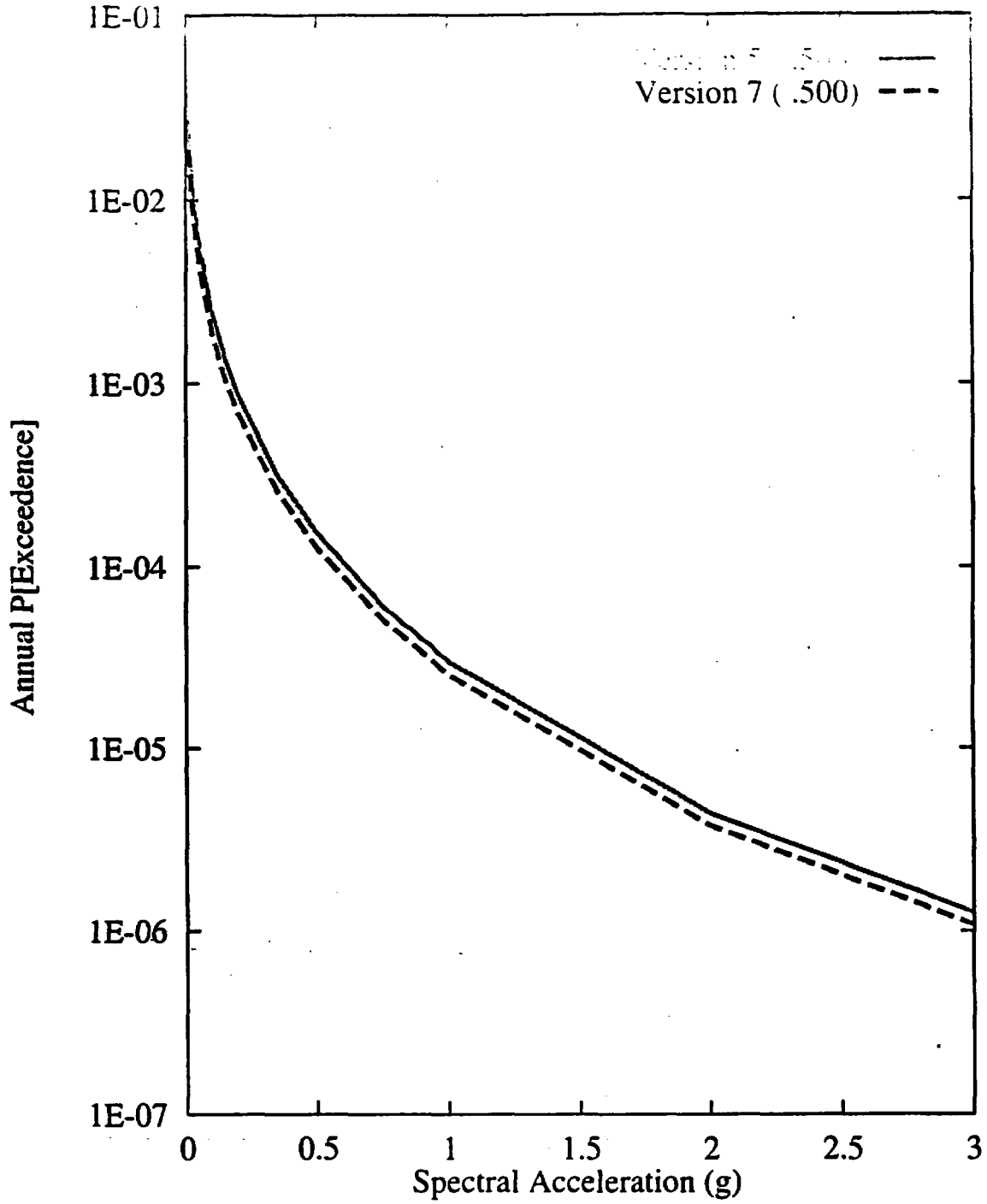

Figure 7-121 Sensitivity of seismic hazard from area zones to choice of seismicity catalog: RYA team, 10-Hz horizontal spectral acceleration

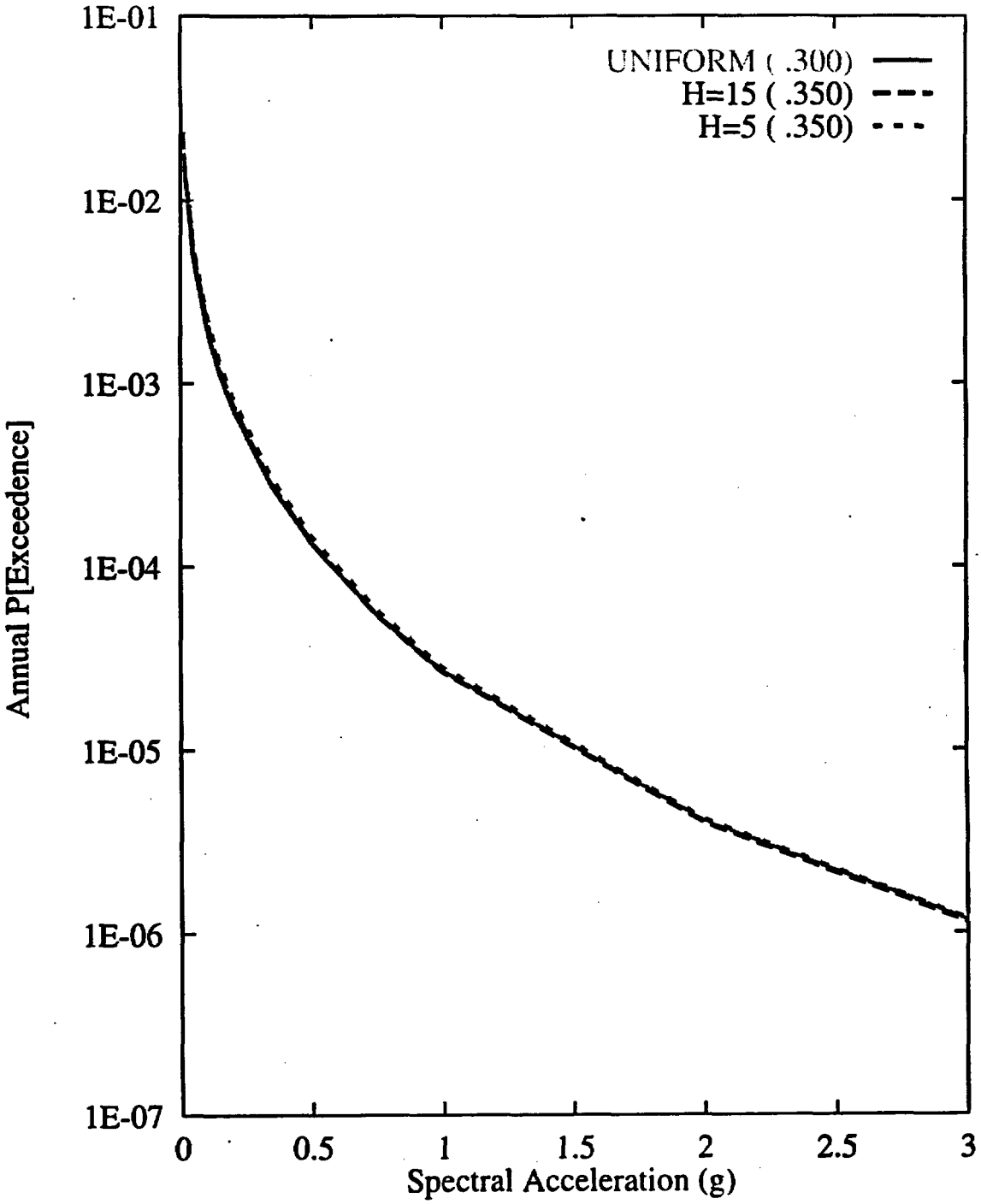

Figure 7-122 Sensitivity of seismic hazard from area zones to spatial variability and smoothing (H): RYA team, 10-Hz horizontal spectral acceleration

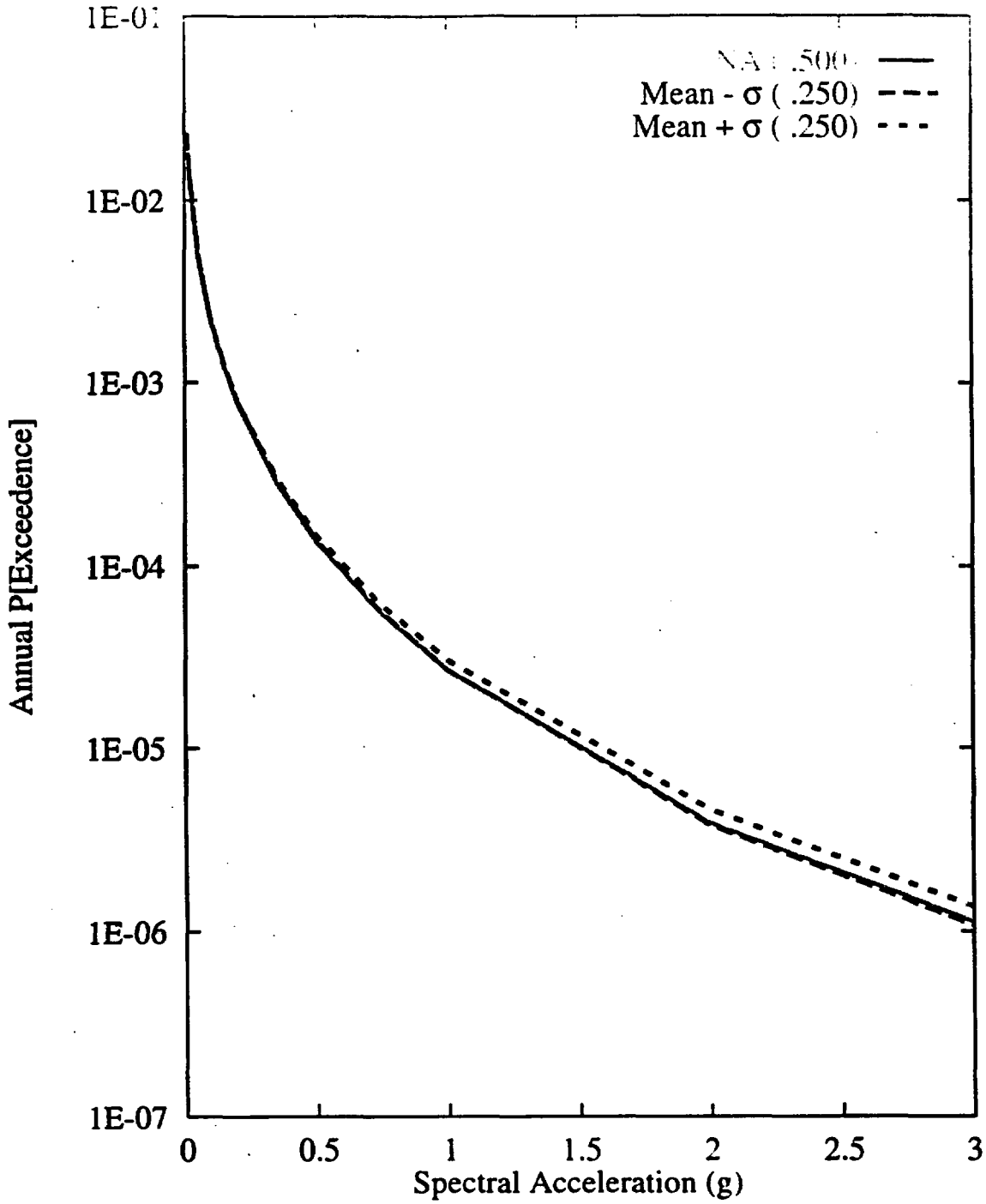

Figure 7-123 Sensitivity of seismic hazard from area zones to Mmax on source zone A2: RYA team, 10-Hz horizontal spectral acceleration

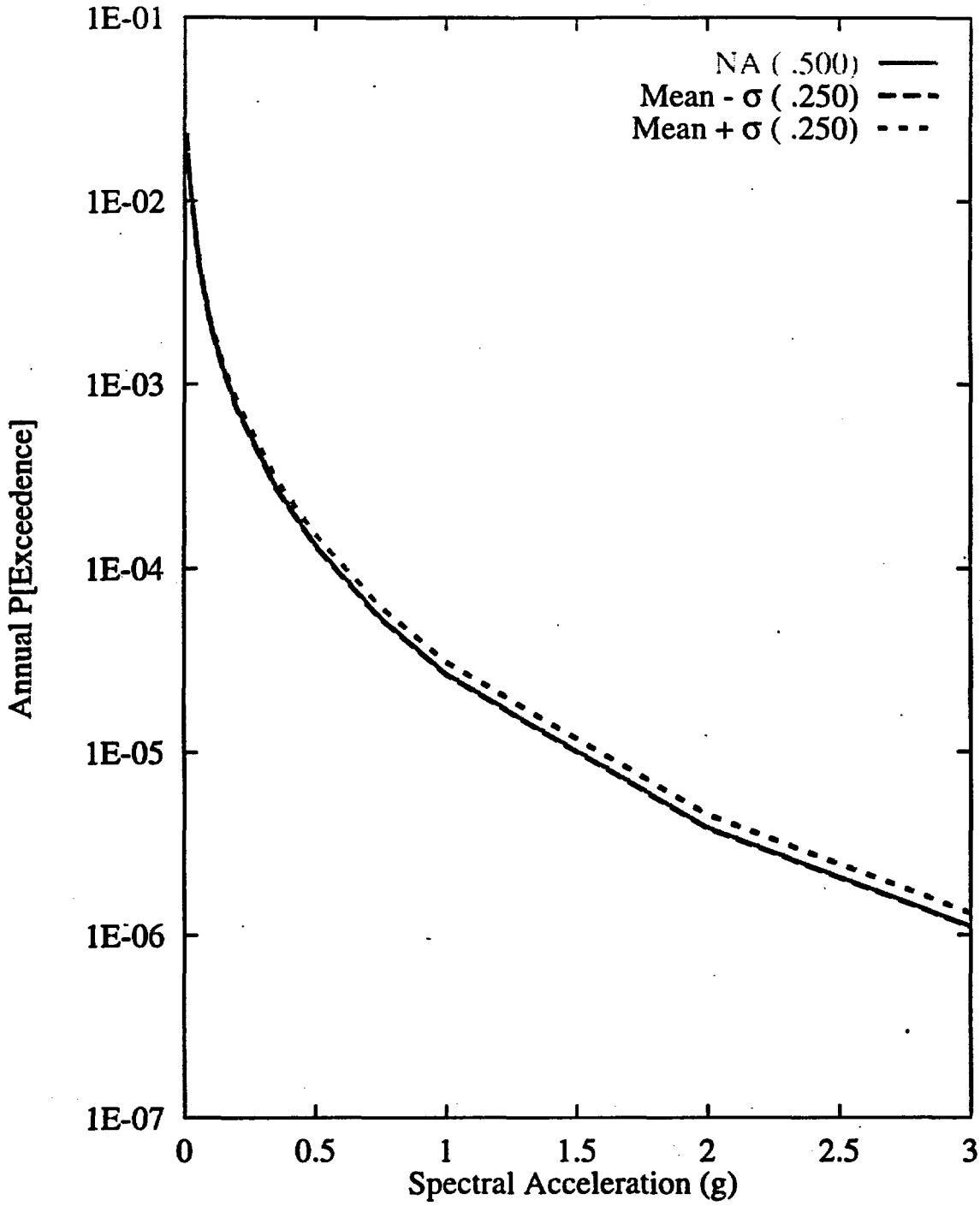

Figure 7-124 Sensitivity of seismic hazard from area zones to recurrence of source zone A2: RYA team, 10-Hz horizontal spectral acceleration

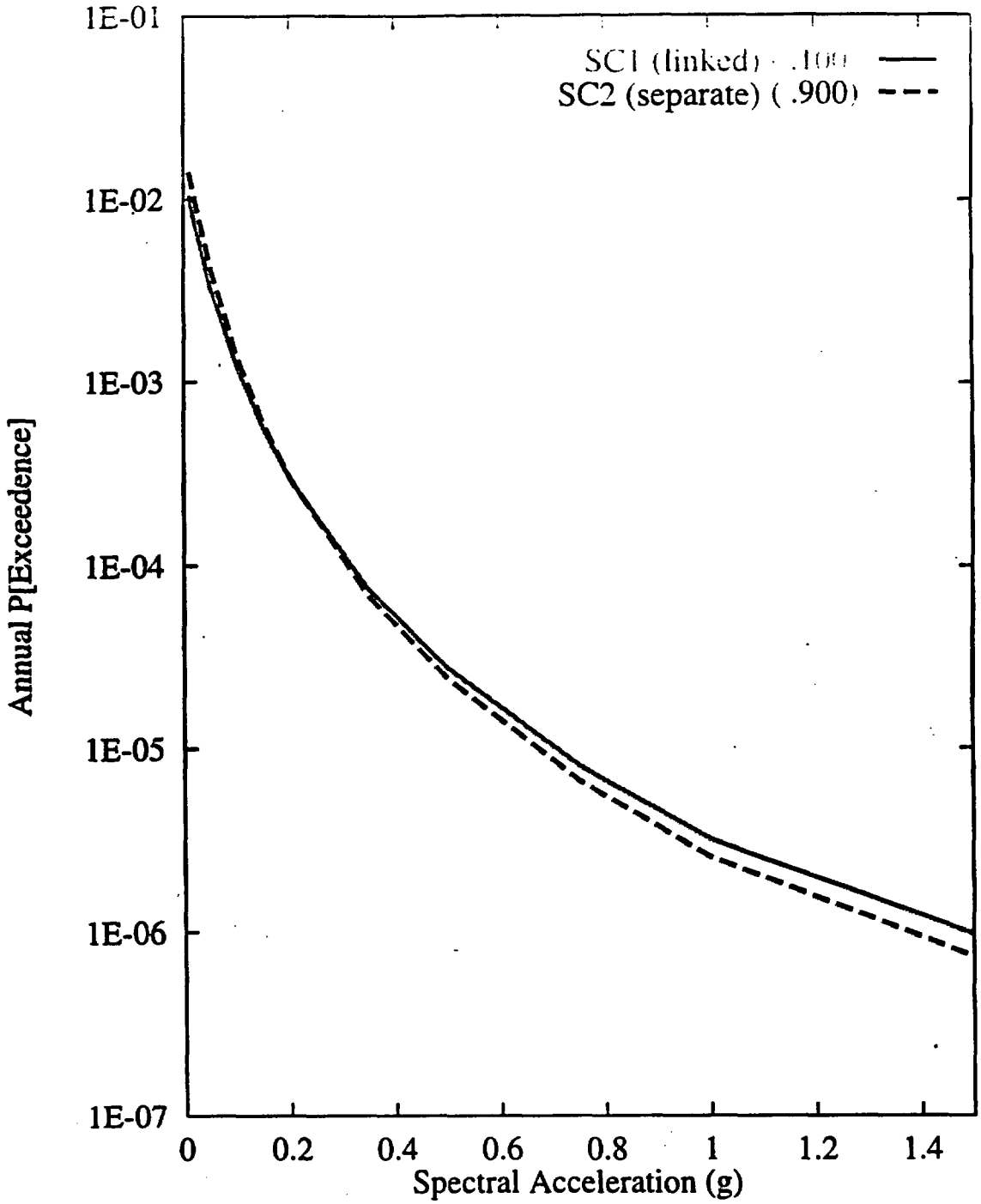

Figure 7-125 Sensitivity of seismic hazard from regional faults to Death Valley-Furnace Creek fault system behavior scenarios: RYA team, 1-Hz horizontal spectral acceleration

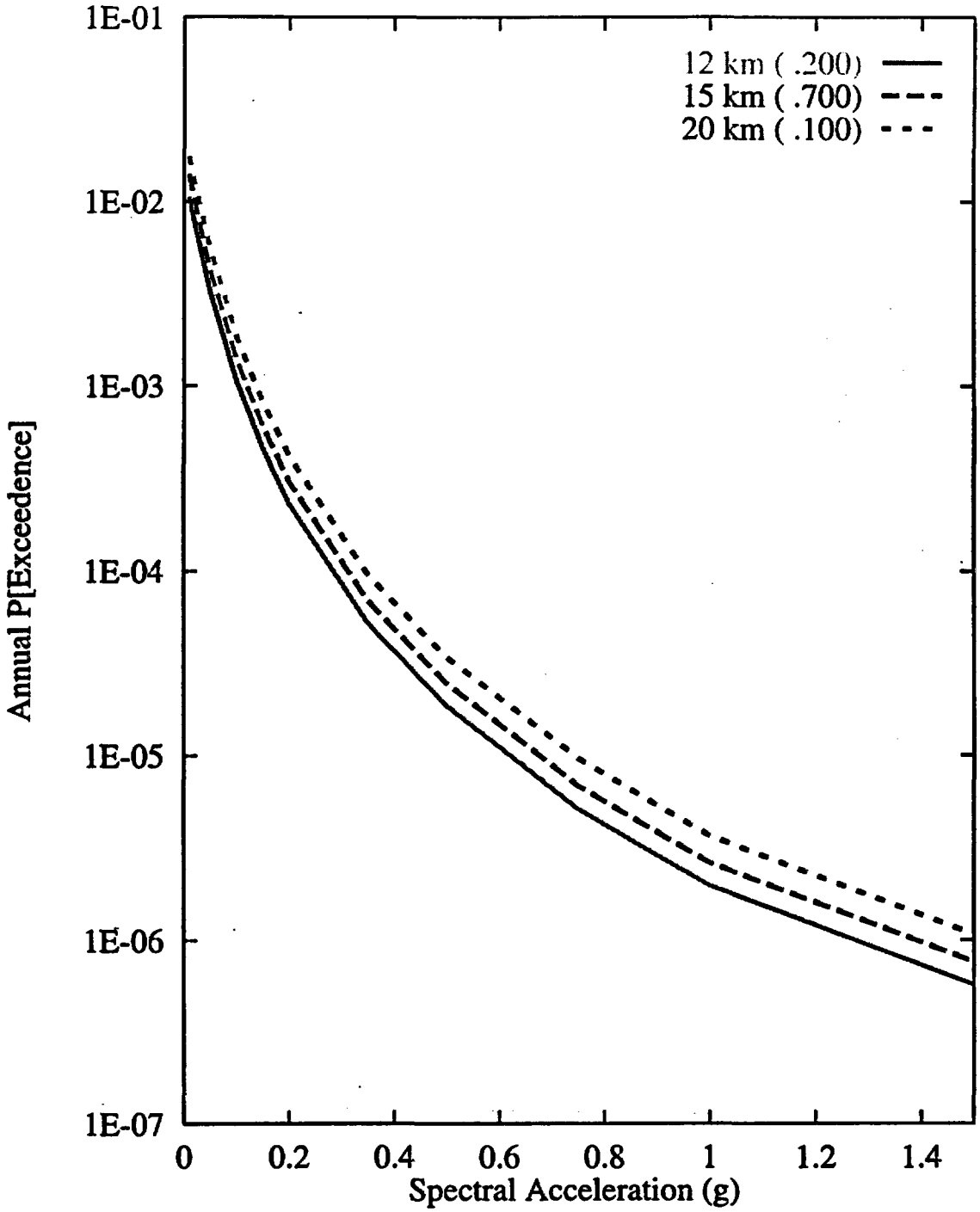

Figure 7-126 Sensitivity of seismic hazard from regional faults to maximum fault depth: RYA team, 1-Hz horizontal spectral acceleration

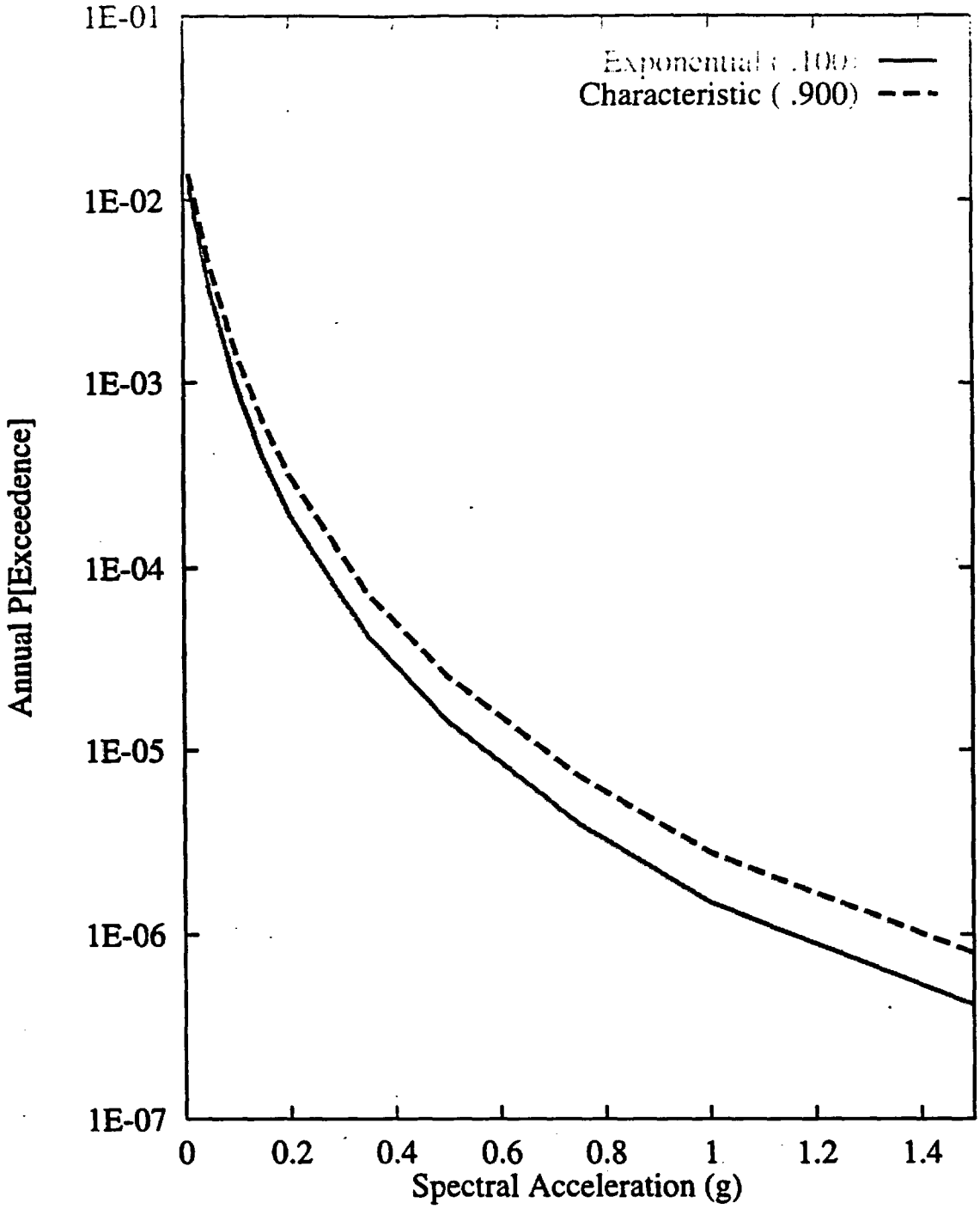

Figure 7-127 Sensitivity of seismic hazard from regional faults to recurrence model: RYA team, 1-Hz horizontal spectral acceleration

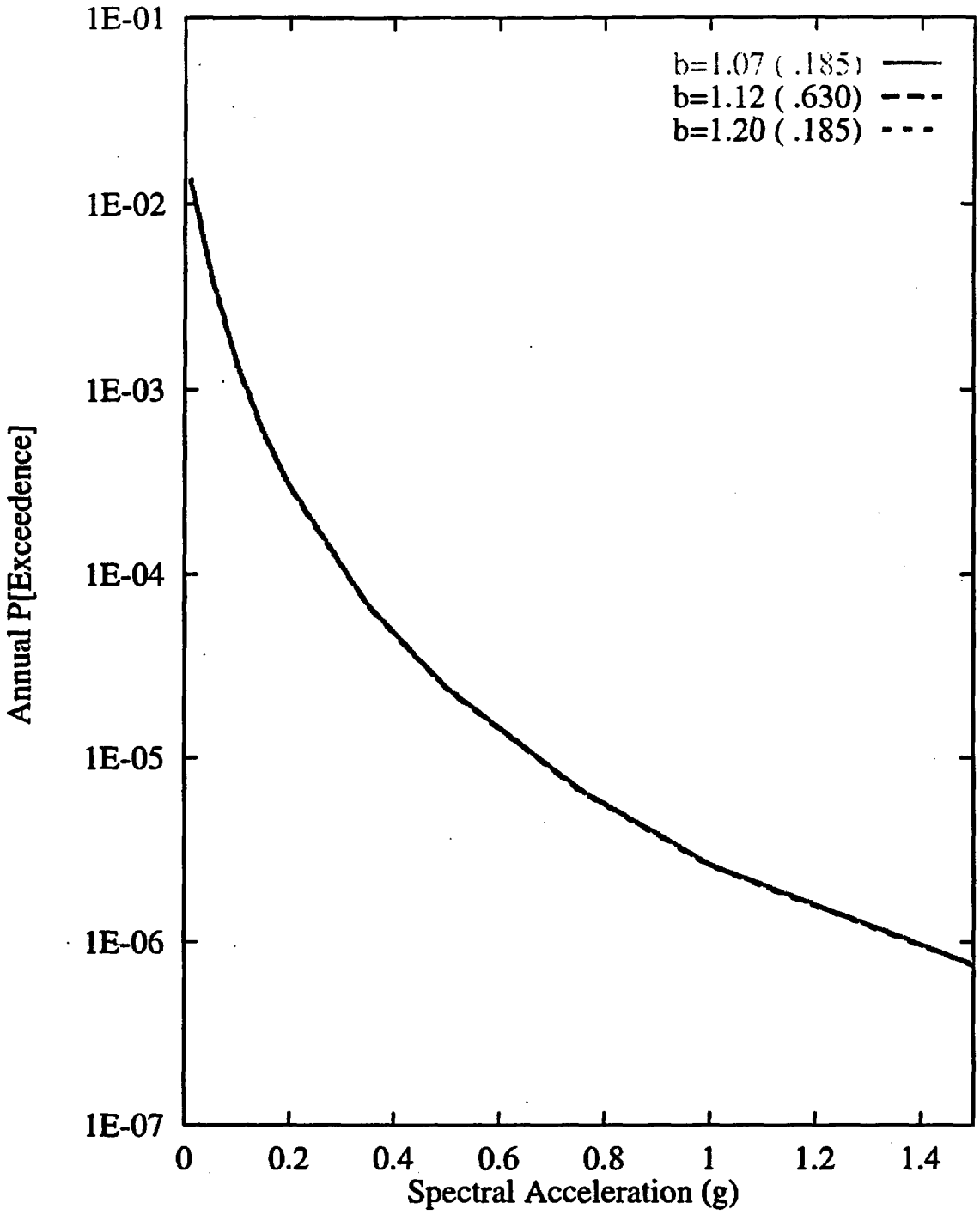

Figure 7-128 Sensitivity of seismic hazard from regional faults to b-value: RYA team, 1-Hz horizontal spectral acceleration

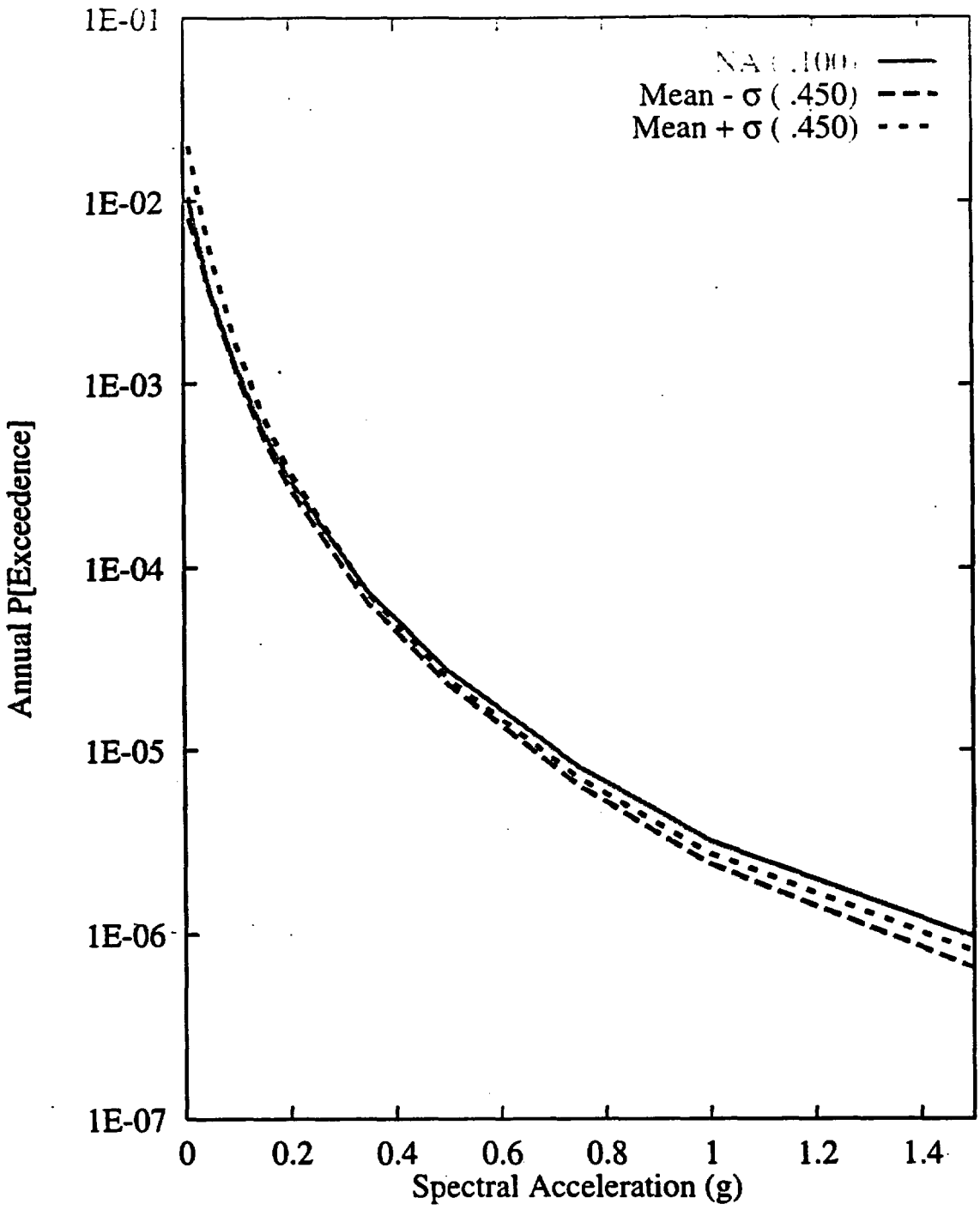

Figure 7-129 Sensitivity of seismic hazard from regional faults to Mmax on the Furnace Creek fault: RYA team, 1-Hz horizontal spectral acceleration

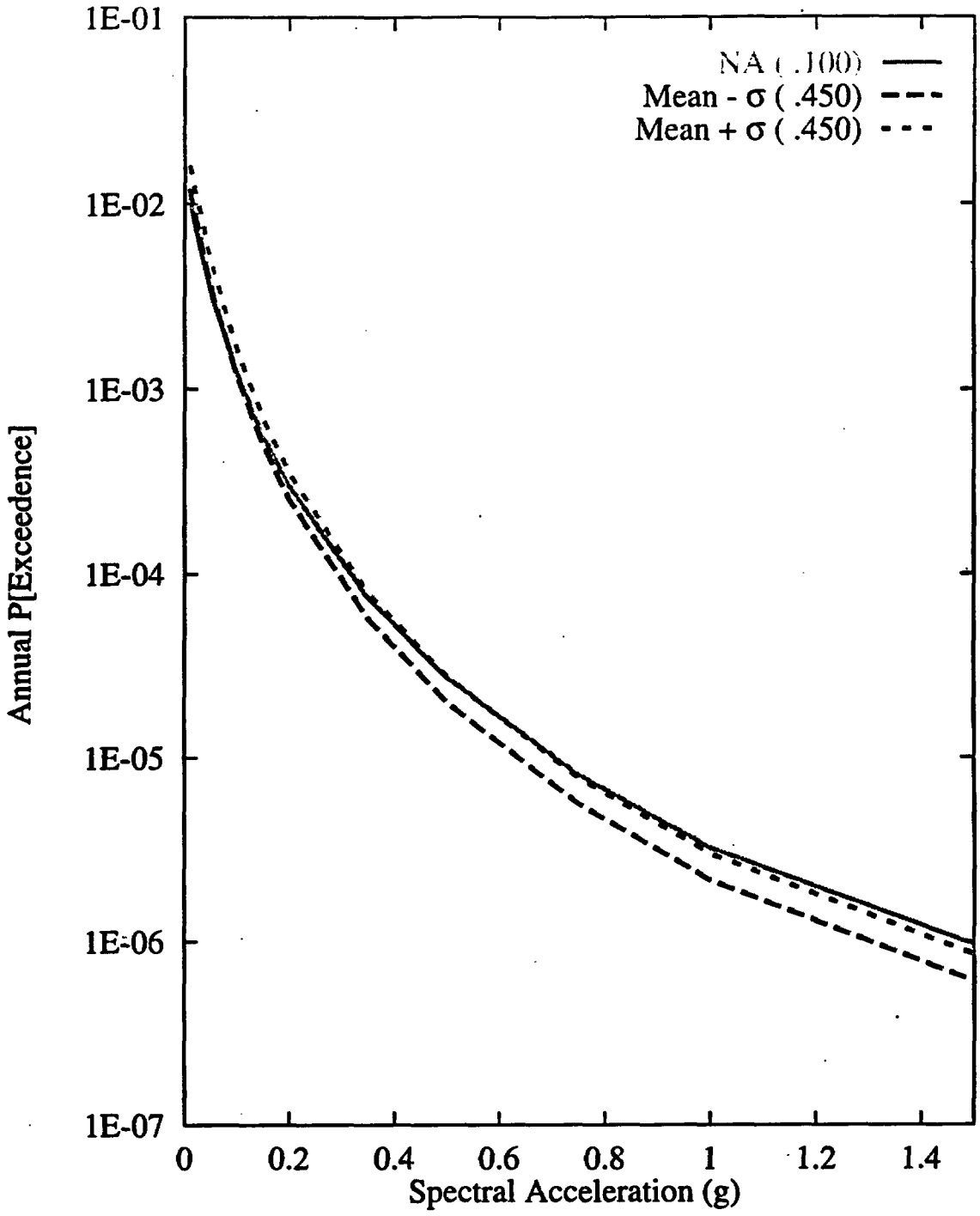

Figure 7-130 Sensitivity of seismic hazard from regional faults to recurrence of Furnace Creek fault: RYA team, 1-Hz horizontal spectral acceleration

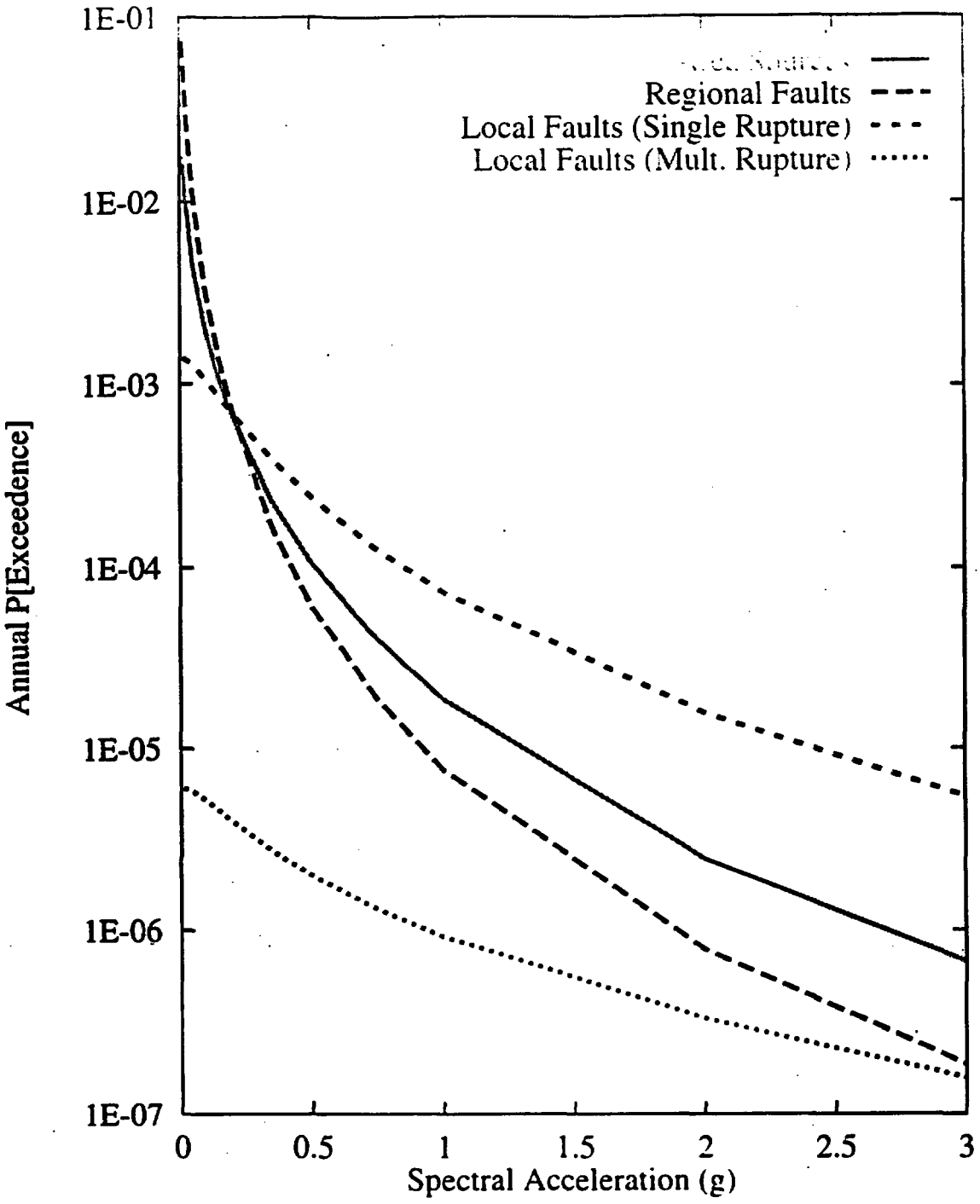

Figure 7-131 Contributions of source types to the mean hazard: SBK team, 10-Hz horizontal spectral acceleration

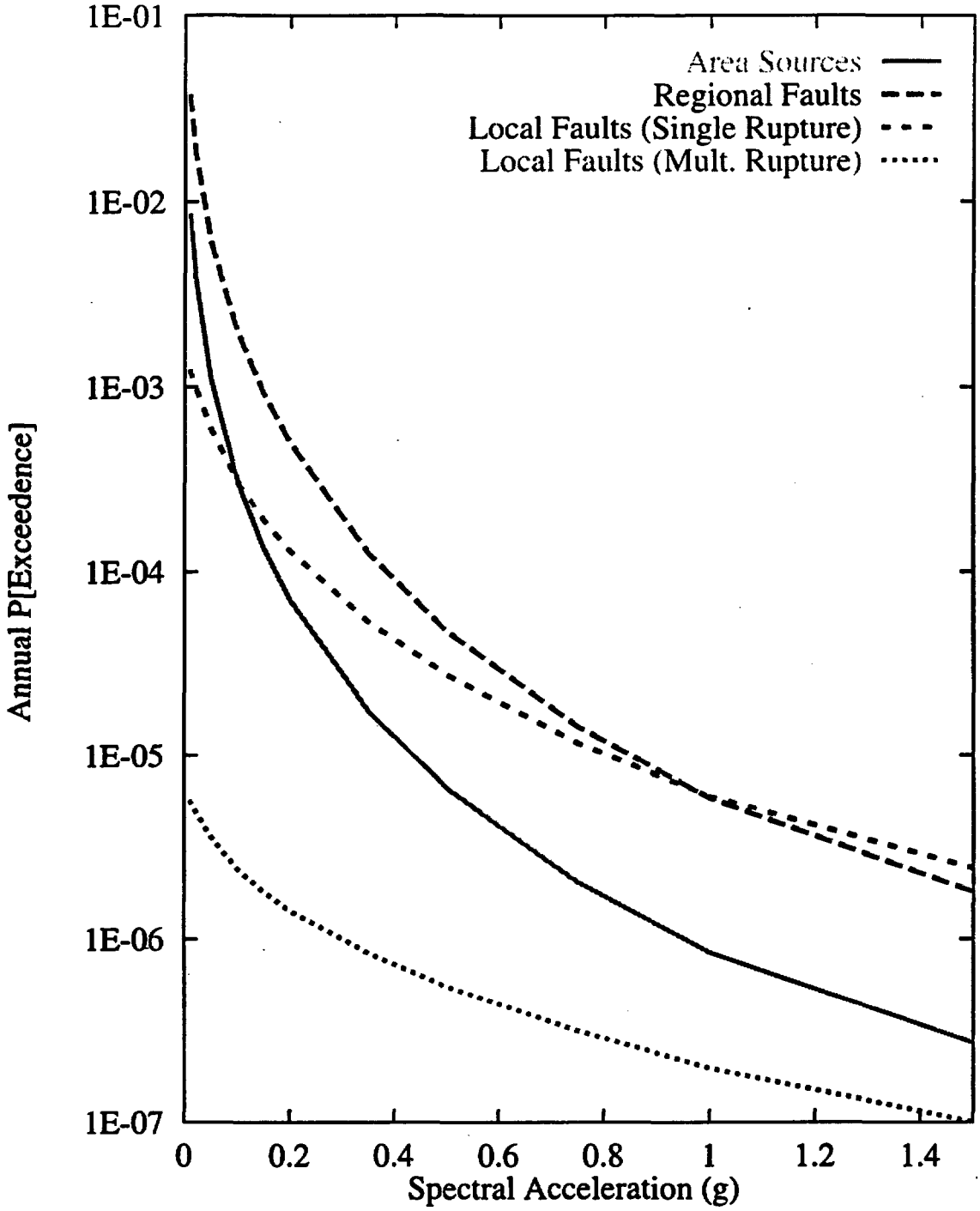

Figure 7-132 Contributions of source types to the mean hazard: SBK team, 1-Hz horizontal spectral acceleration

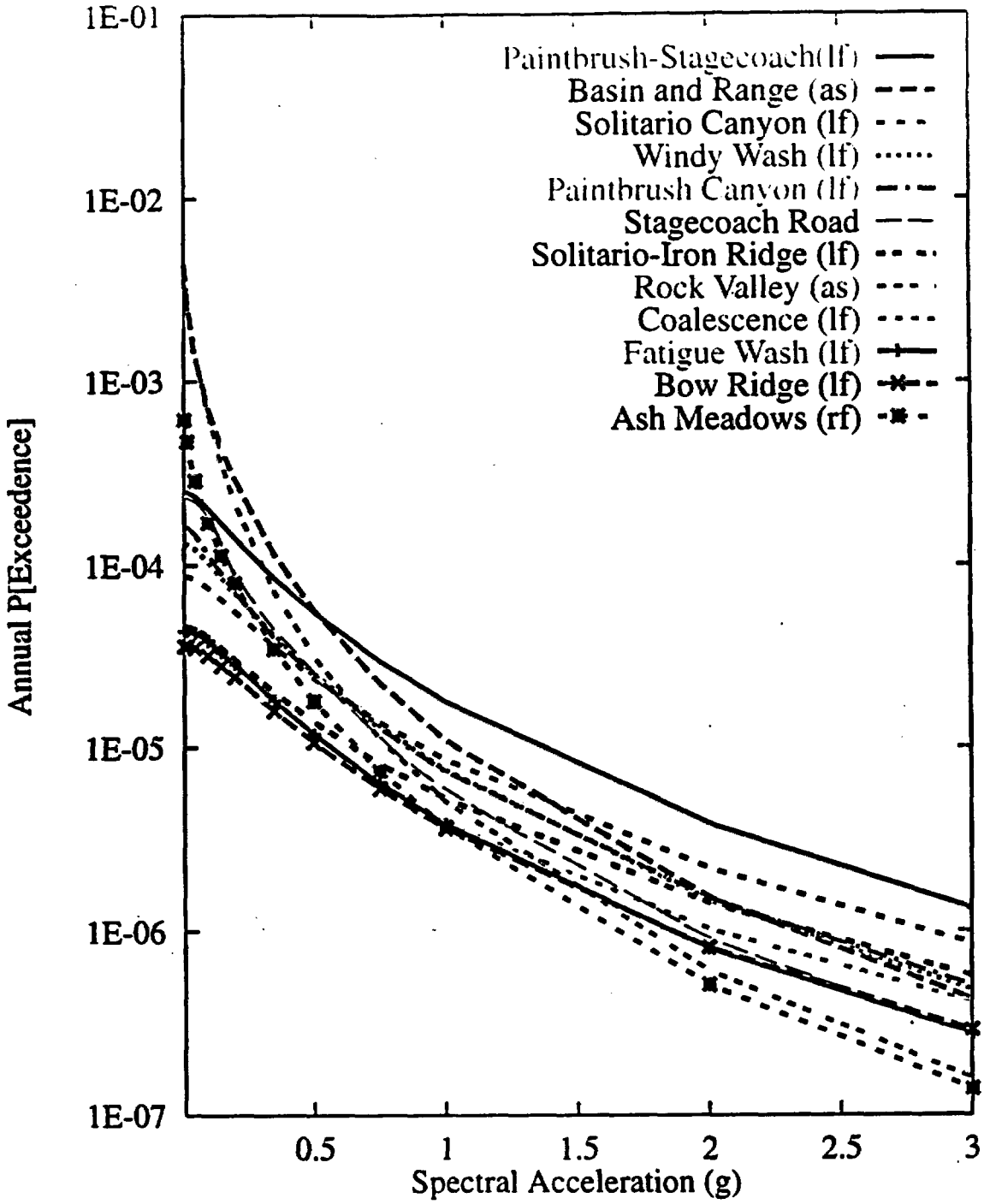

Figure 7-133 Mean seismic hazard from dominant seismic sources: SBK team, 10-Hz horizontal spectral acceleration

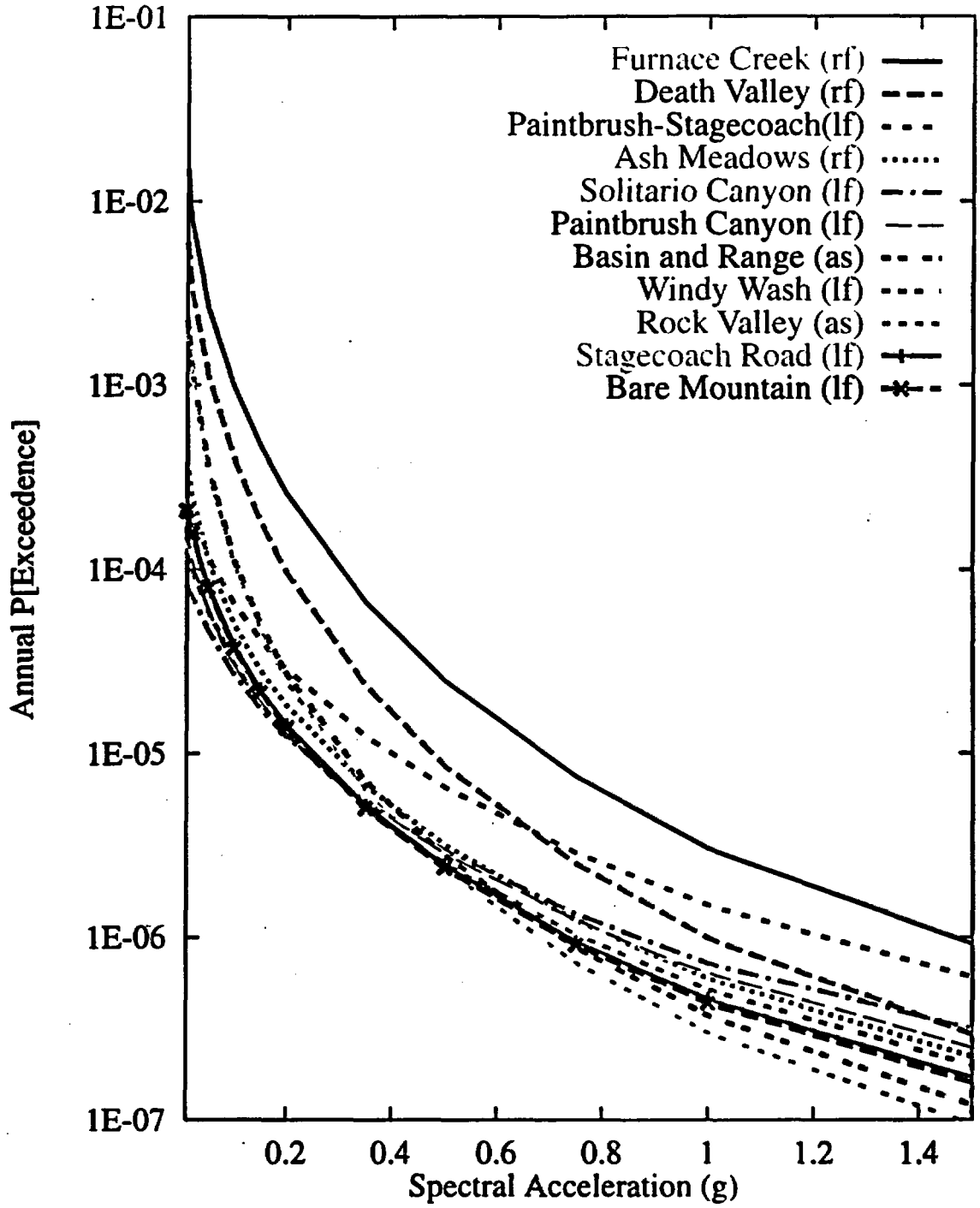

Figure 7-134 Mean seismic hazard from dominant seismic sources: SBK team, 1-Hz horizontal spectral acceleration

10 Hz, SBK Area Sources

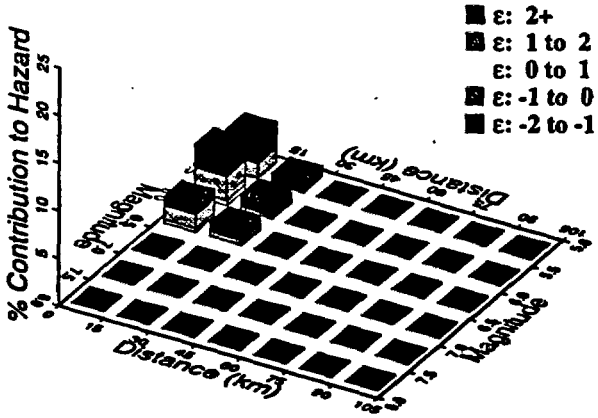

10 Hz, SBK Regional Faults

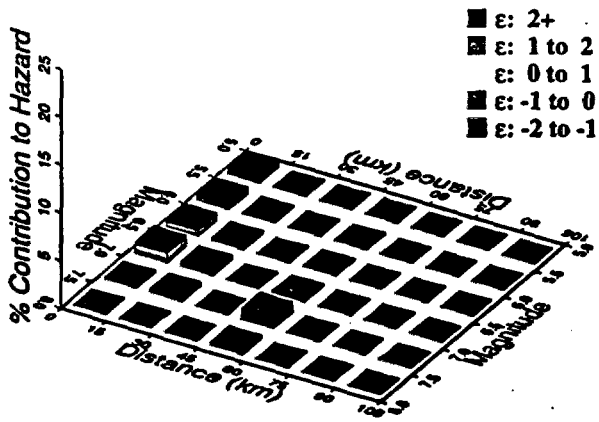

10 Hz, SBK Local Faults (Single)

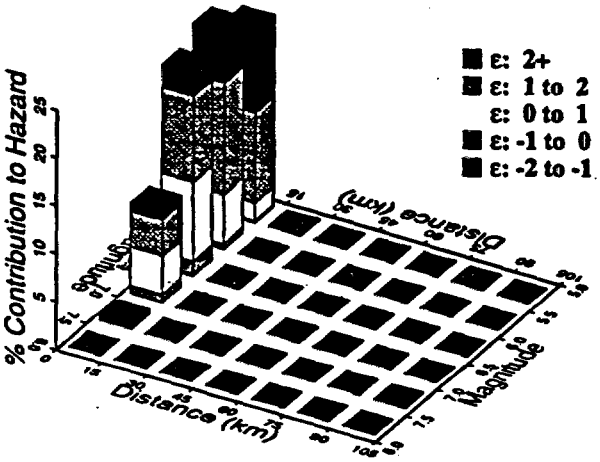

10 Hz, SBK Local Faults (Mult.)

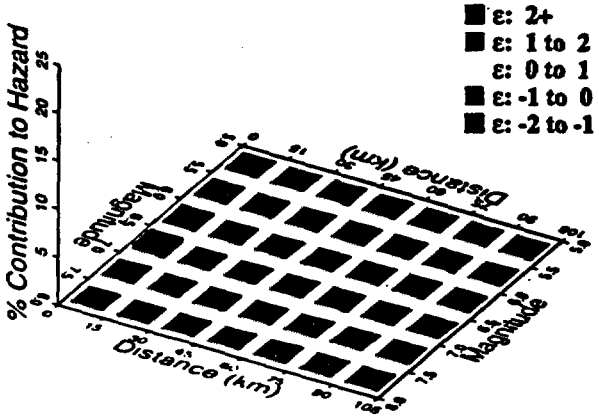

Figure 7-135 Magnitude-distance-epsilon distributions for the four source types: SBK team, 10-Hz horizontal spectral acceleration at 10-4 exceedance probability

1 Hz, SBK Area Sources

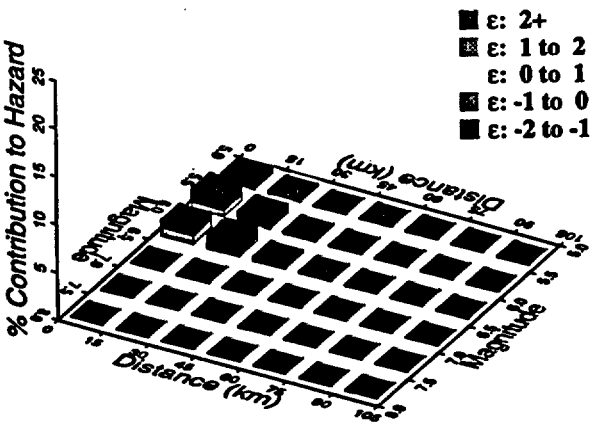

1 Hz, SBK Regional Faults

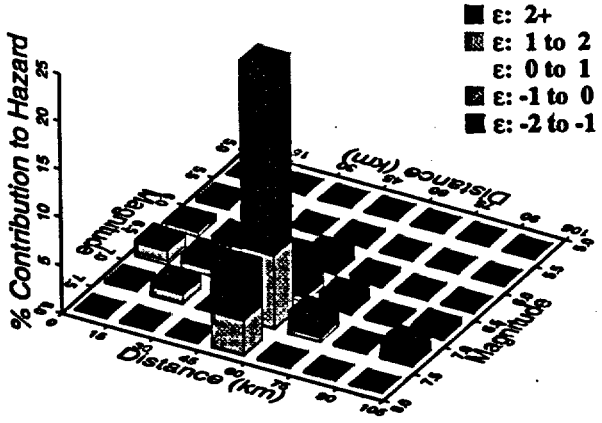

1 Hz, SBK Local Faults (Single)

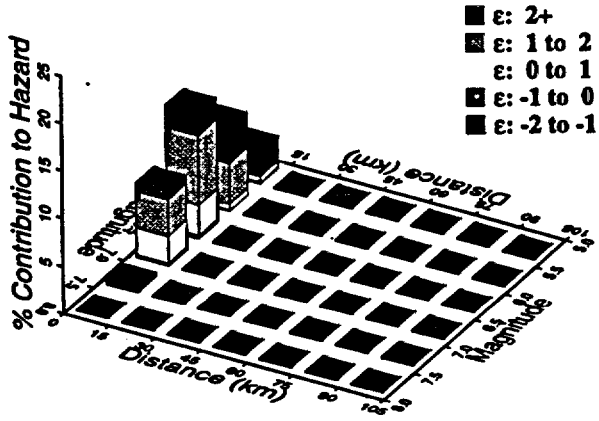

1 Hz, SBK Local Faults (Mult.)

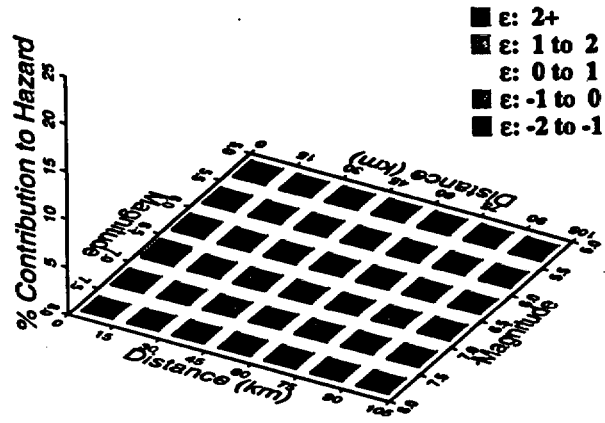

Figure 7-136 Magnitude-distance-epsilon distributions for the four source types: SBK team, 1-Hz horizontal spectral acceleration at 10^{-4} exceedance probability

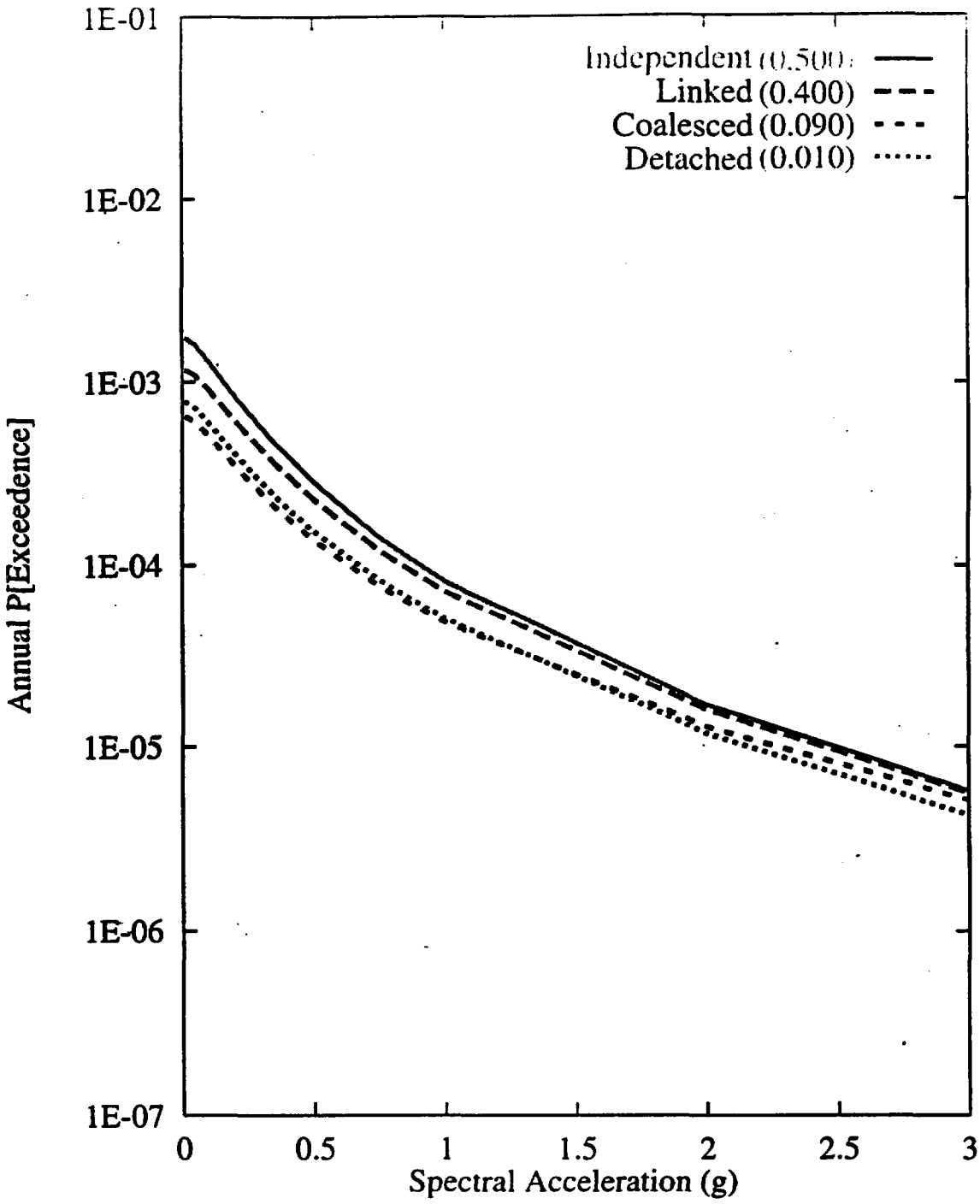

Figure 7-137 Sensitivity of seismic hazard from local faults to behavior of local faults: SBK team, 10-Hz horizontal spectral acceleration

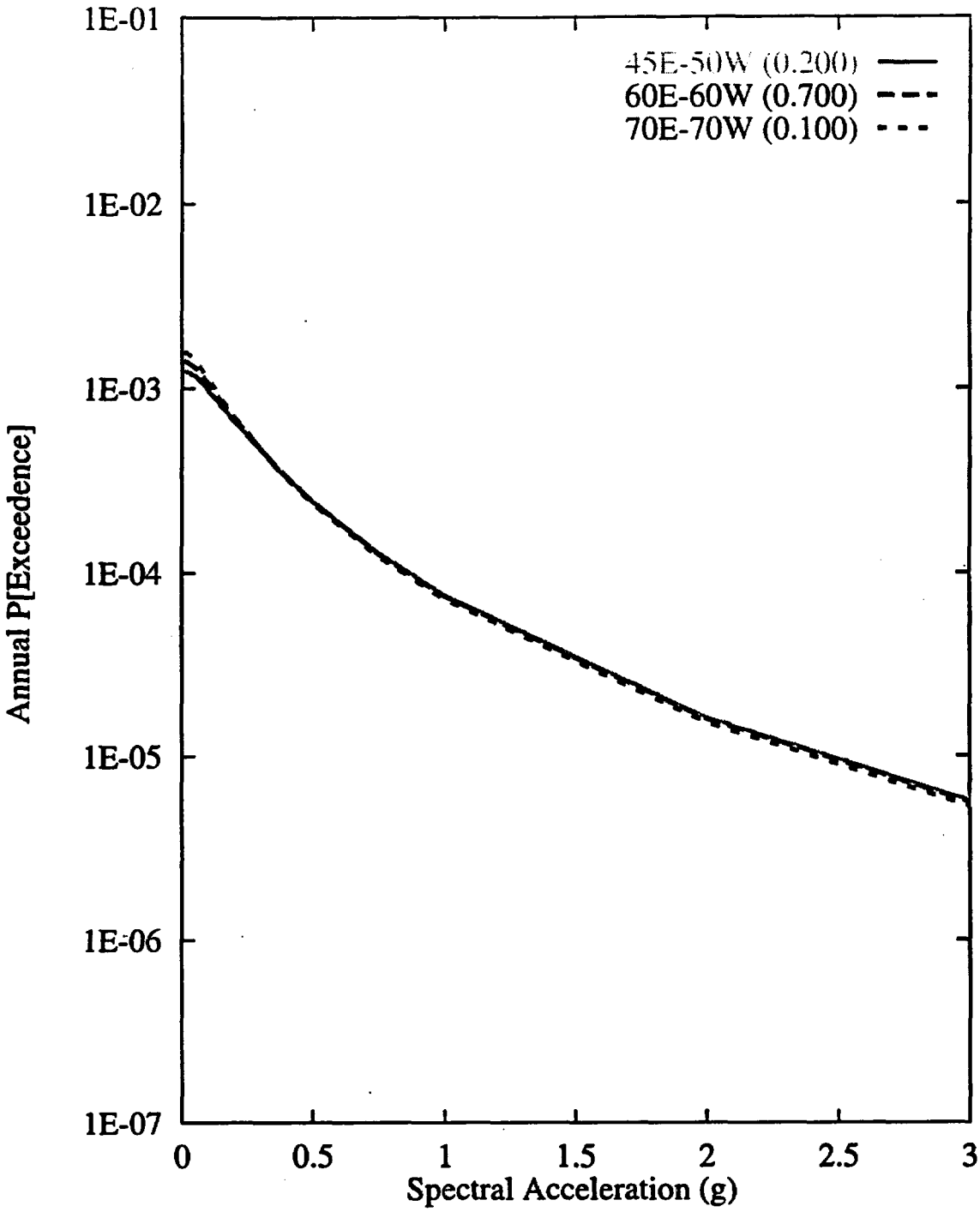

Figure 7-138 Sensitivity of seismic hazard from local faults to fault dip: SBK team, 10-Hz horizontal spectral acceleration

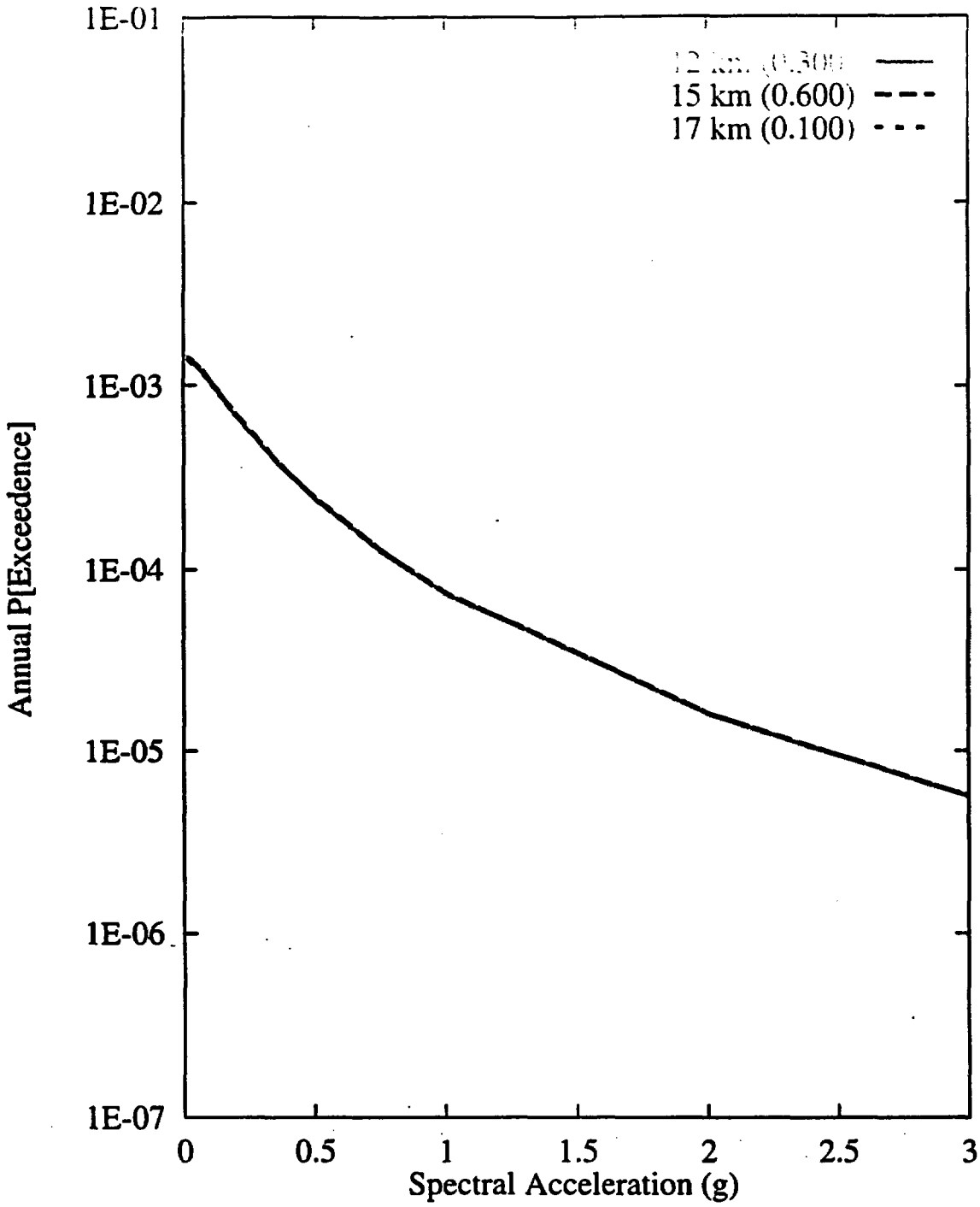

Figure 7-139 Sensitivity of seismic hazard from local faults to maximum fault depth: SBK team, 10-Hz horizontal spectral acceleration

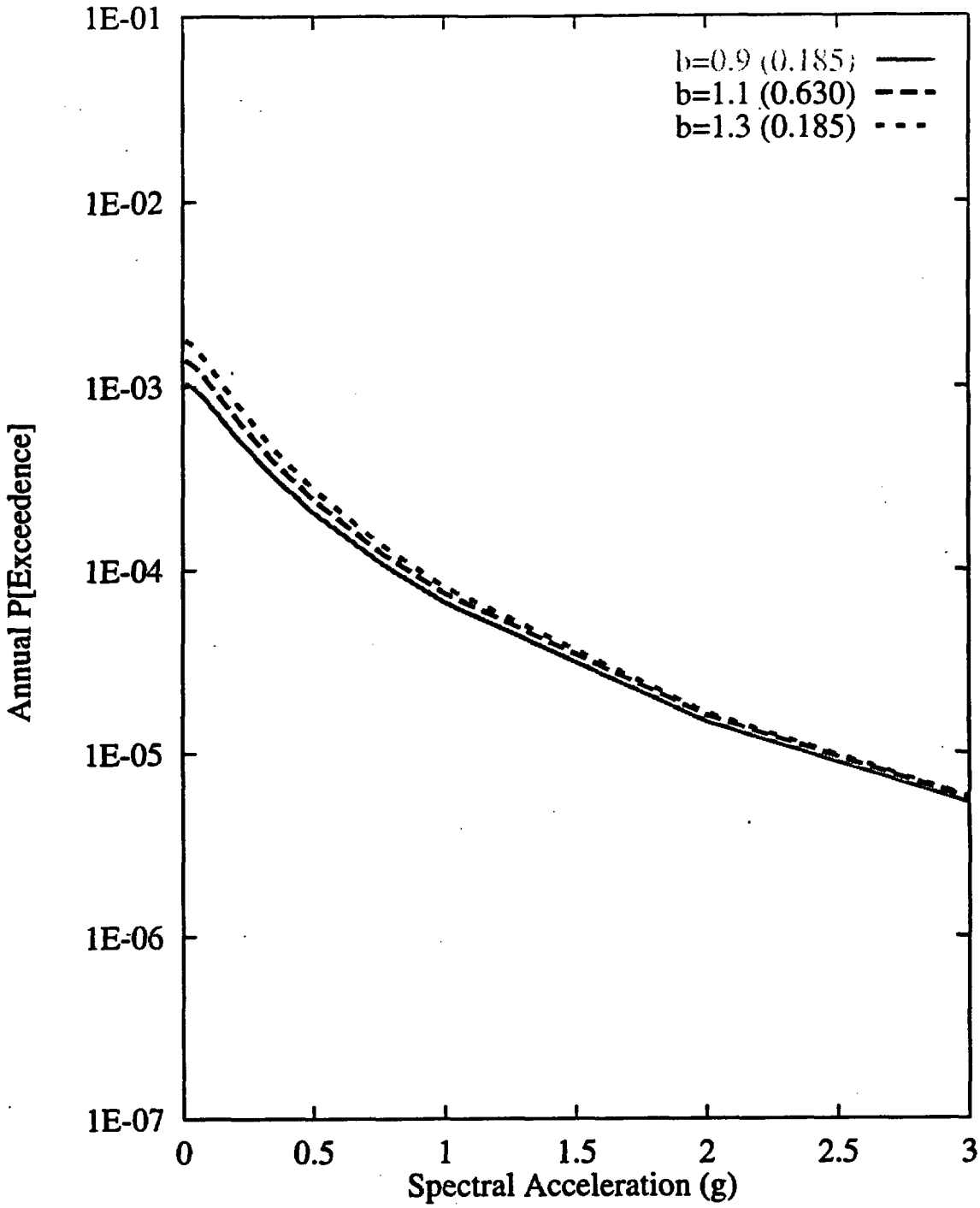

Figure 7-140 Sensitivity of seismic hazard from local faults to b-value: SBK team, 10-Hz horizontal spectral acceleration

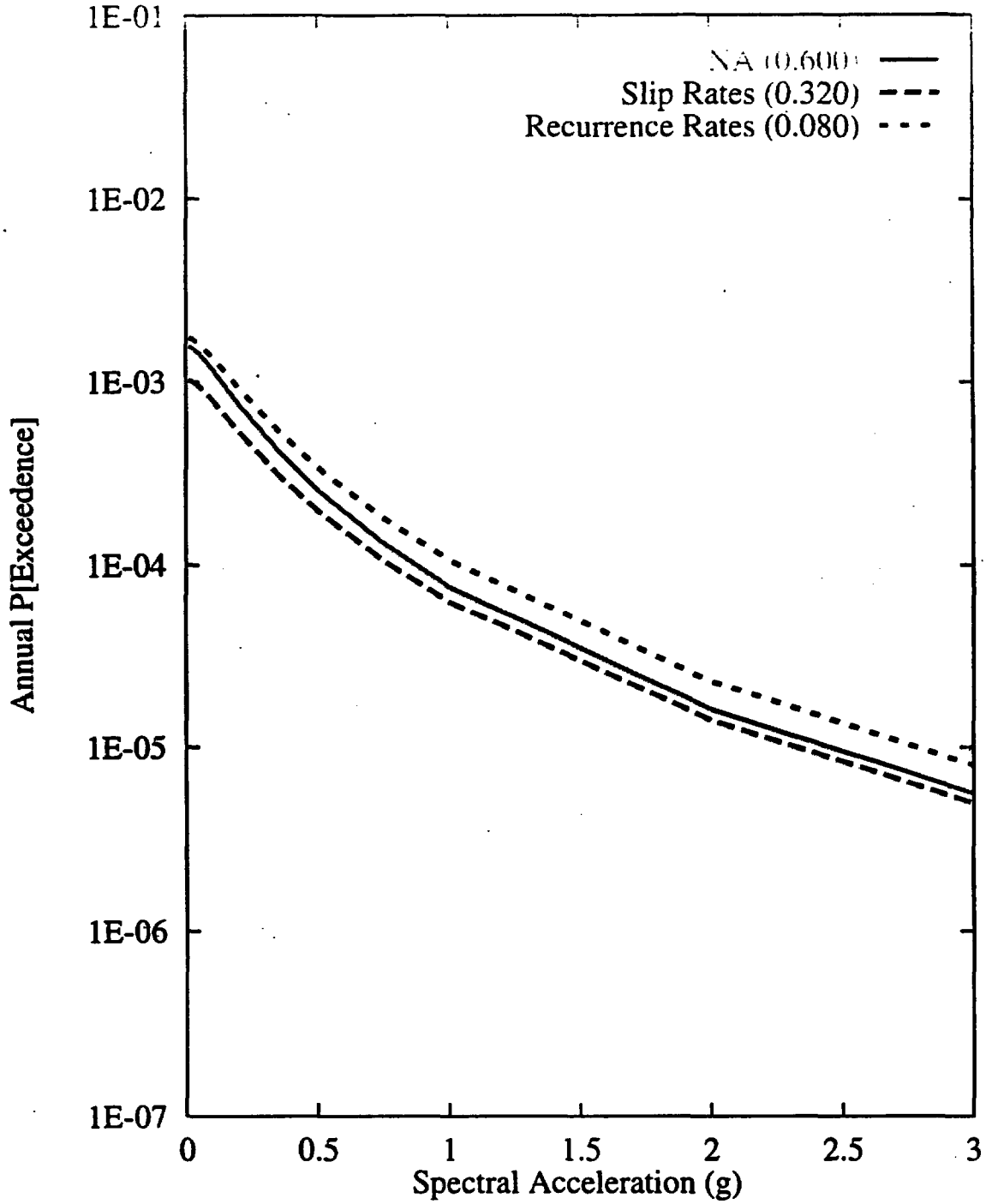

Figure 7-141 Sensitivity of seismic hazard from local faults to recurrence approach for the Paintbrush Canyon-Stagecoach Road fault system: SBK team, 10-Hz horizontal spectral acceleration

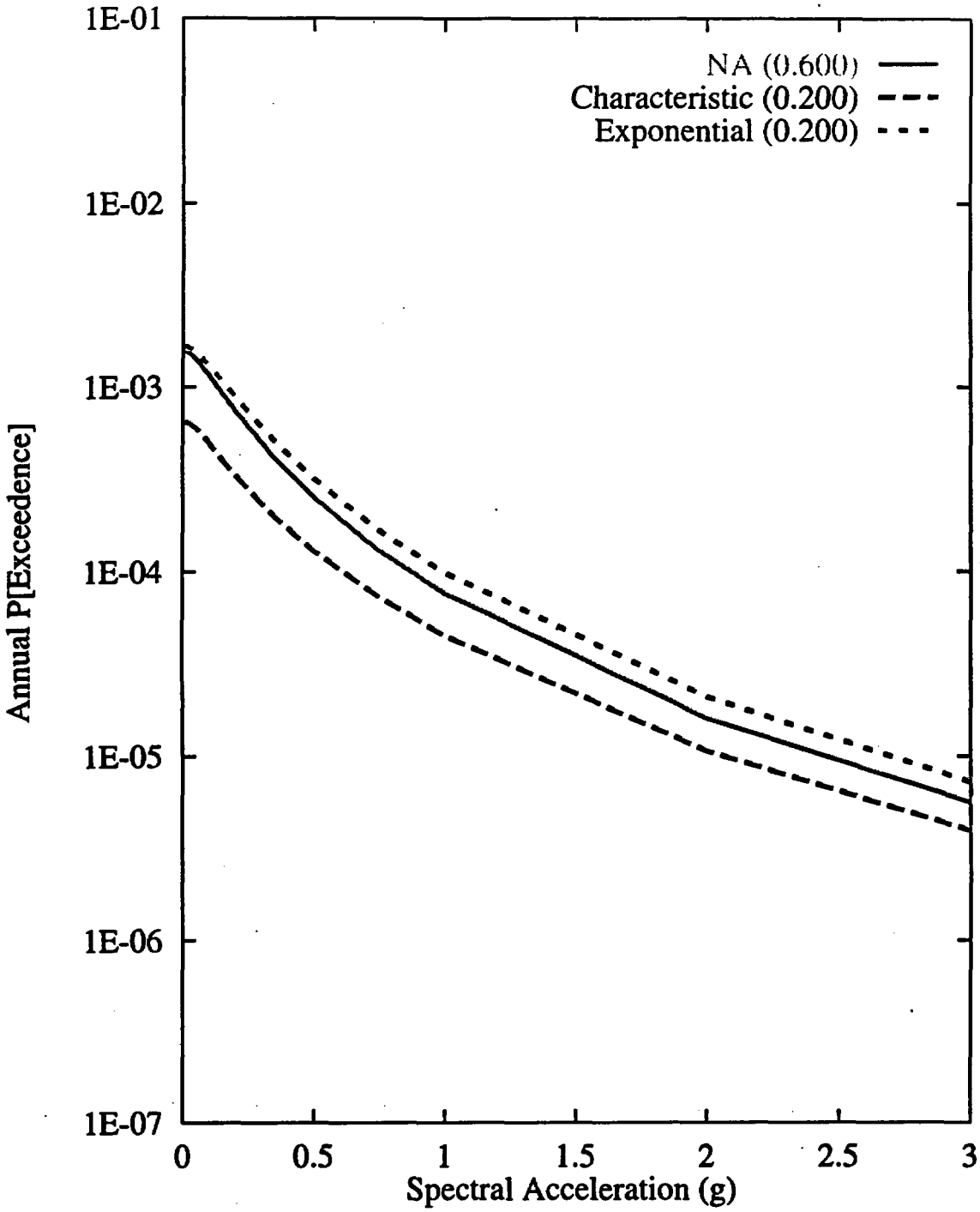

Figure 7-142 Sensitivity of seismic hazard from local faults to recurrence model for the Paintbrush Canyon-Stagecoach Road fault system: SBK team, 10-Hz horizontal spectral acceleration

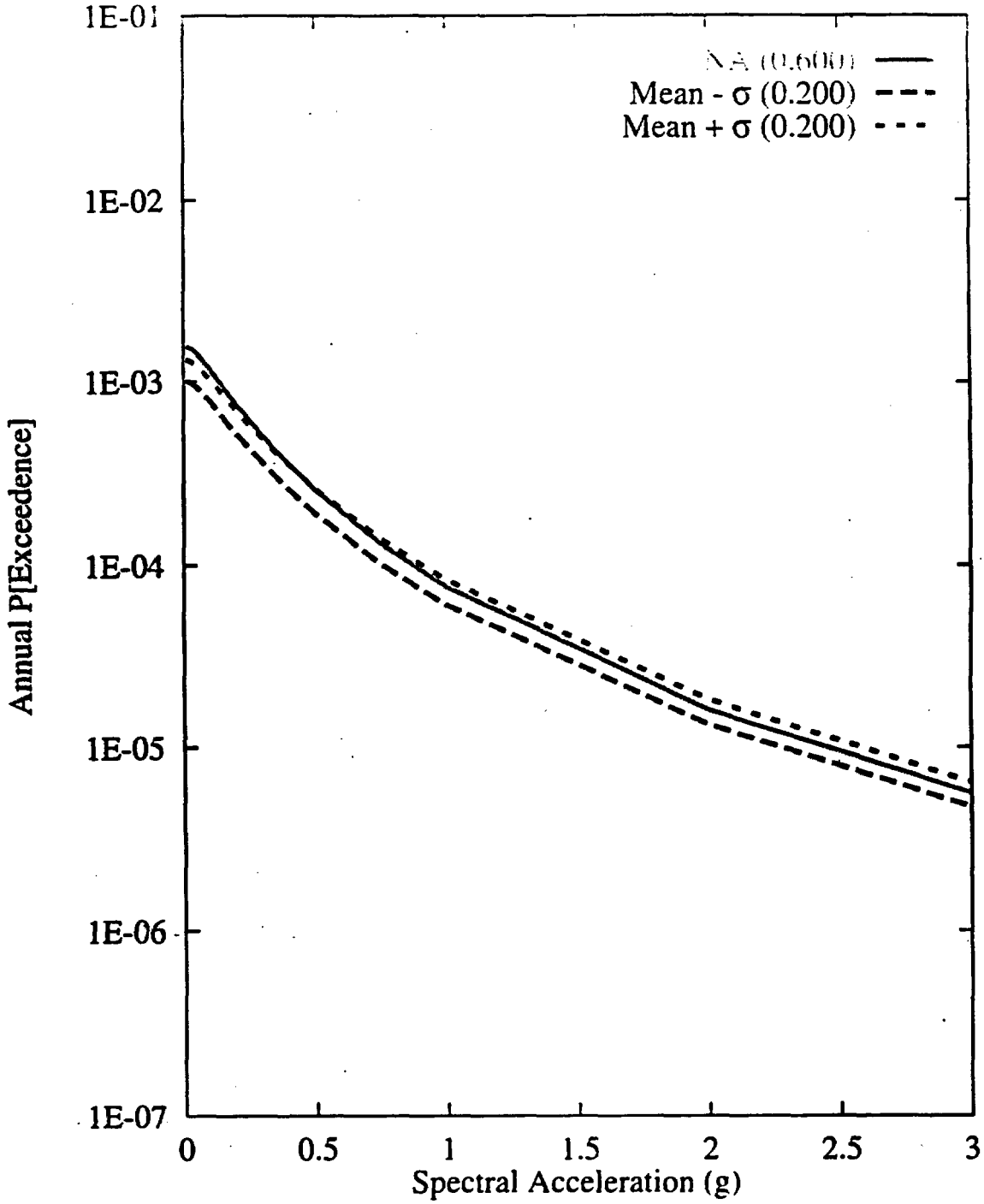

Figure 7-143 Sensitivity of seismic hazard from local faults to Mmax on the Paintbrush Canyon-Stagecoach Road fault system: SBK team, 10-Hz horizontal spectral acceleration

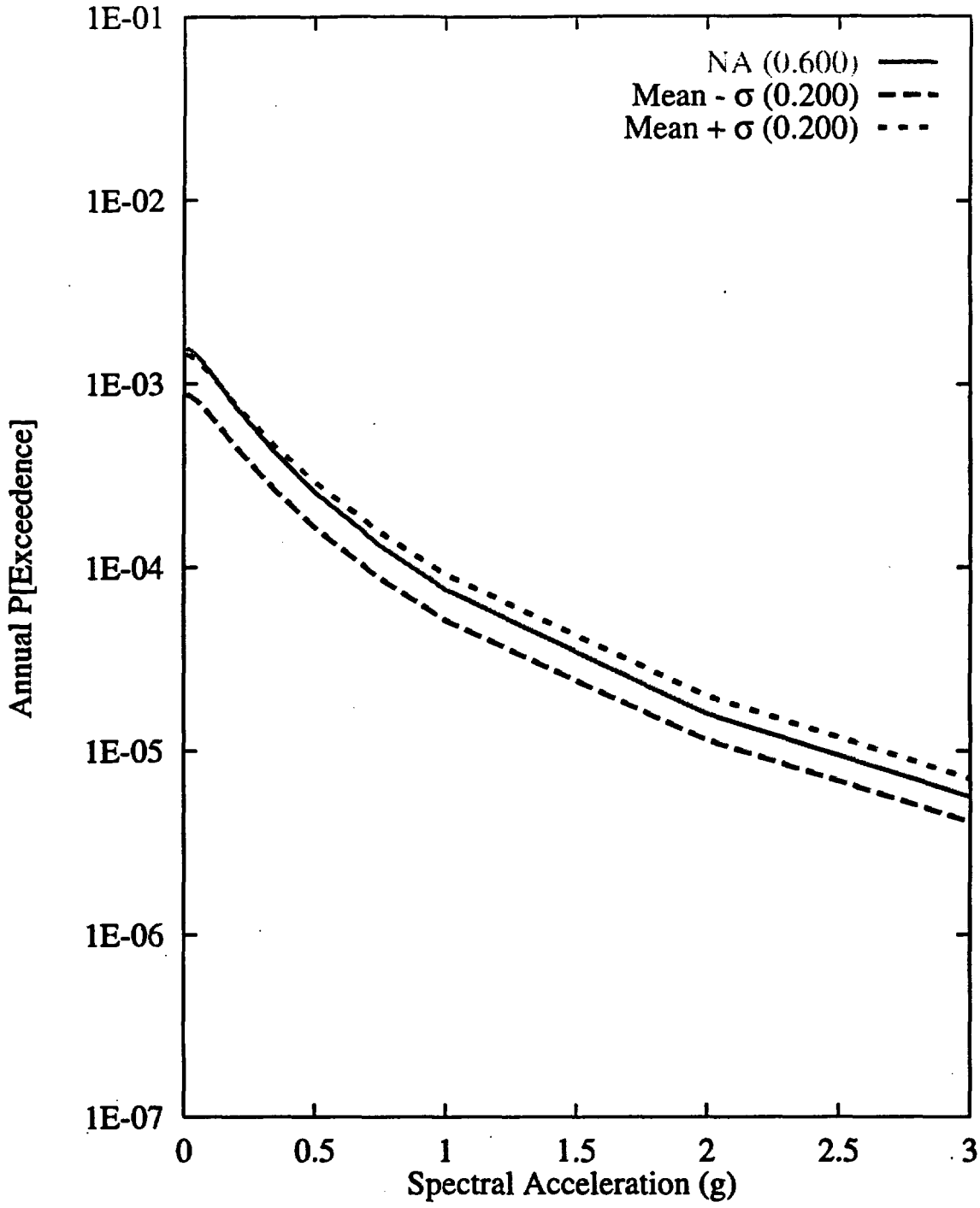

Figure 7-144 Sensitivity of seismic hazard from local faults to recurrence of the Paintbrush Canyon-Stagecoach Road fault system: SBK team, 10-Hz horizontal spectral acceleration

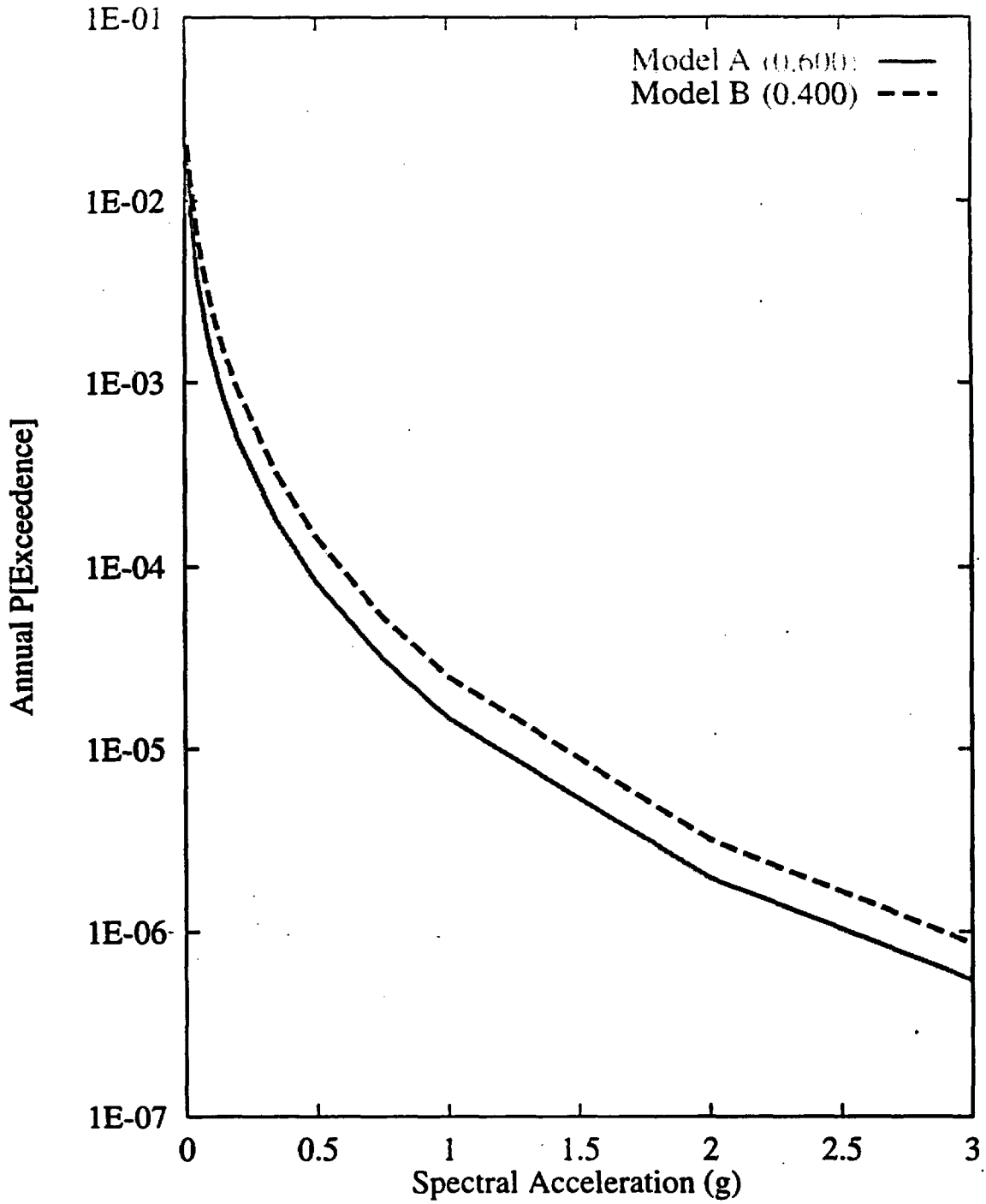

Figure 7-145 Sensitivity of seismic hazard from area zones to zonation: SBK team, 10-Hz horizontal spectral acceleration

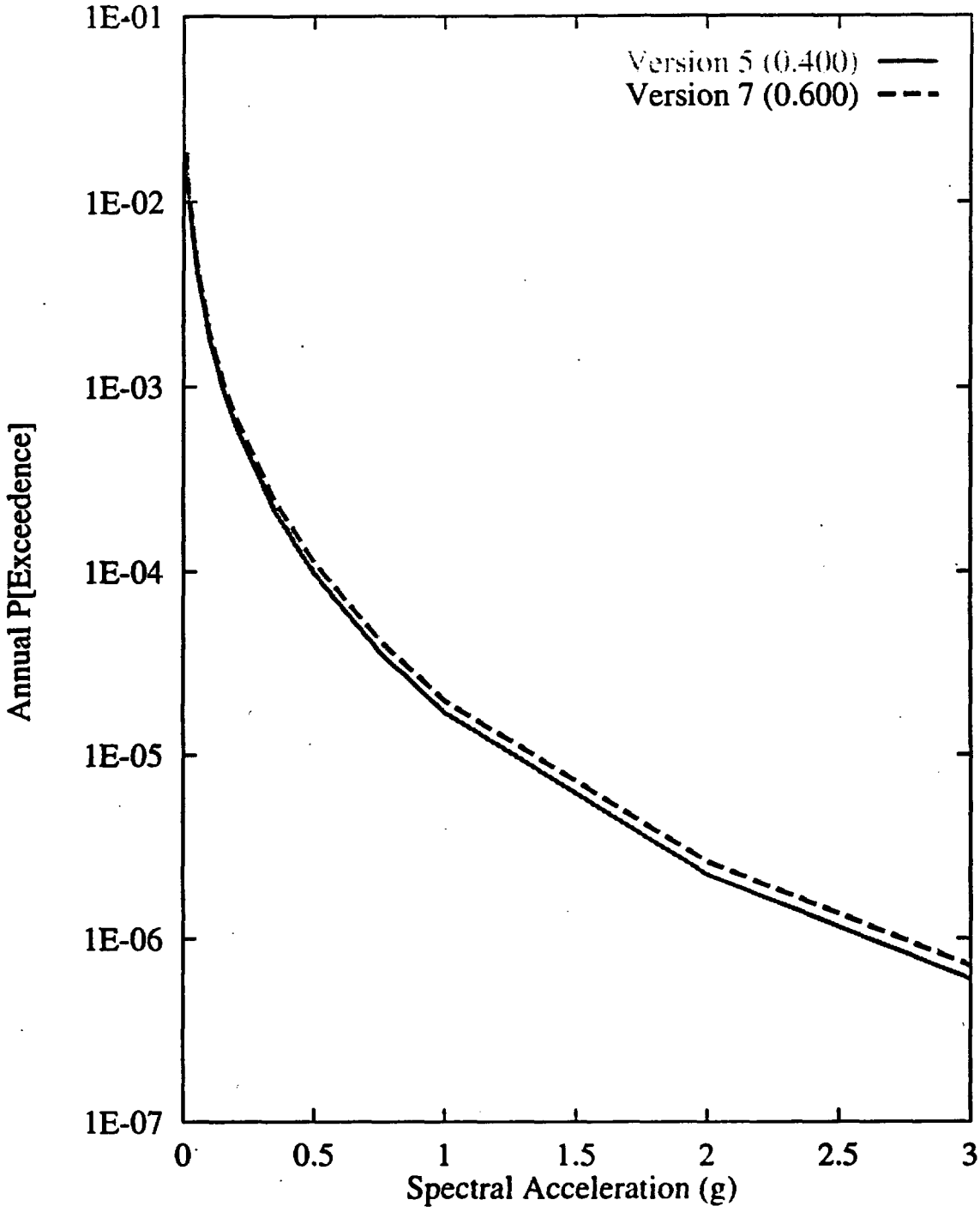

Figure 7-146 *Sensitivity of seismic hazard from area zones to choice of seismicity catalog for the* Basin and Range zone: SBK team, 10-Hz horizontal spectral acceleration

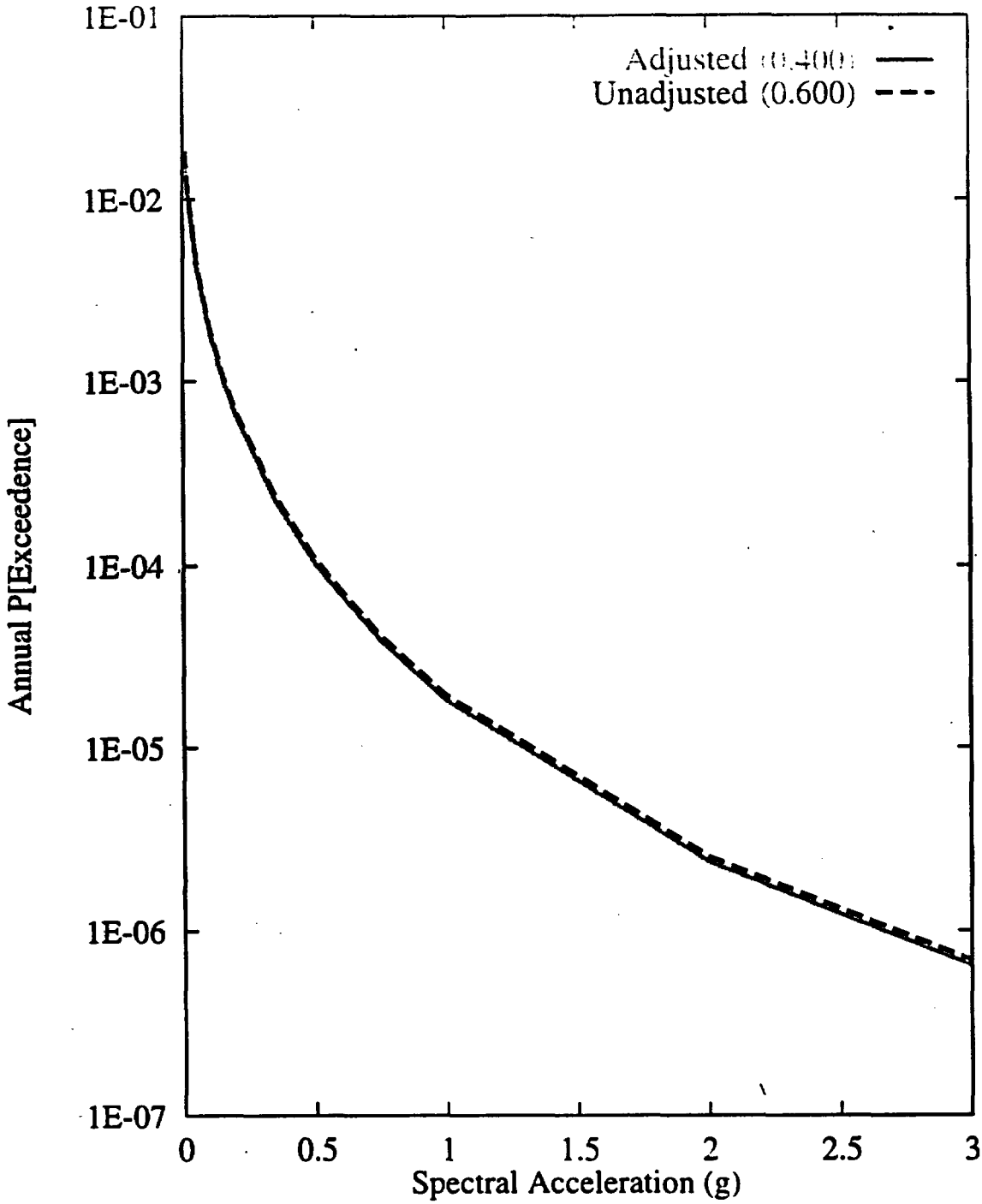

Figure 7-147 Sensitivity of seismic hazard from area zones to adjustment for NTS events: SBK team, 10-Hz horizontal spectral acceleration

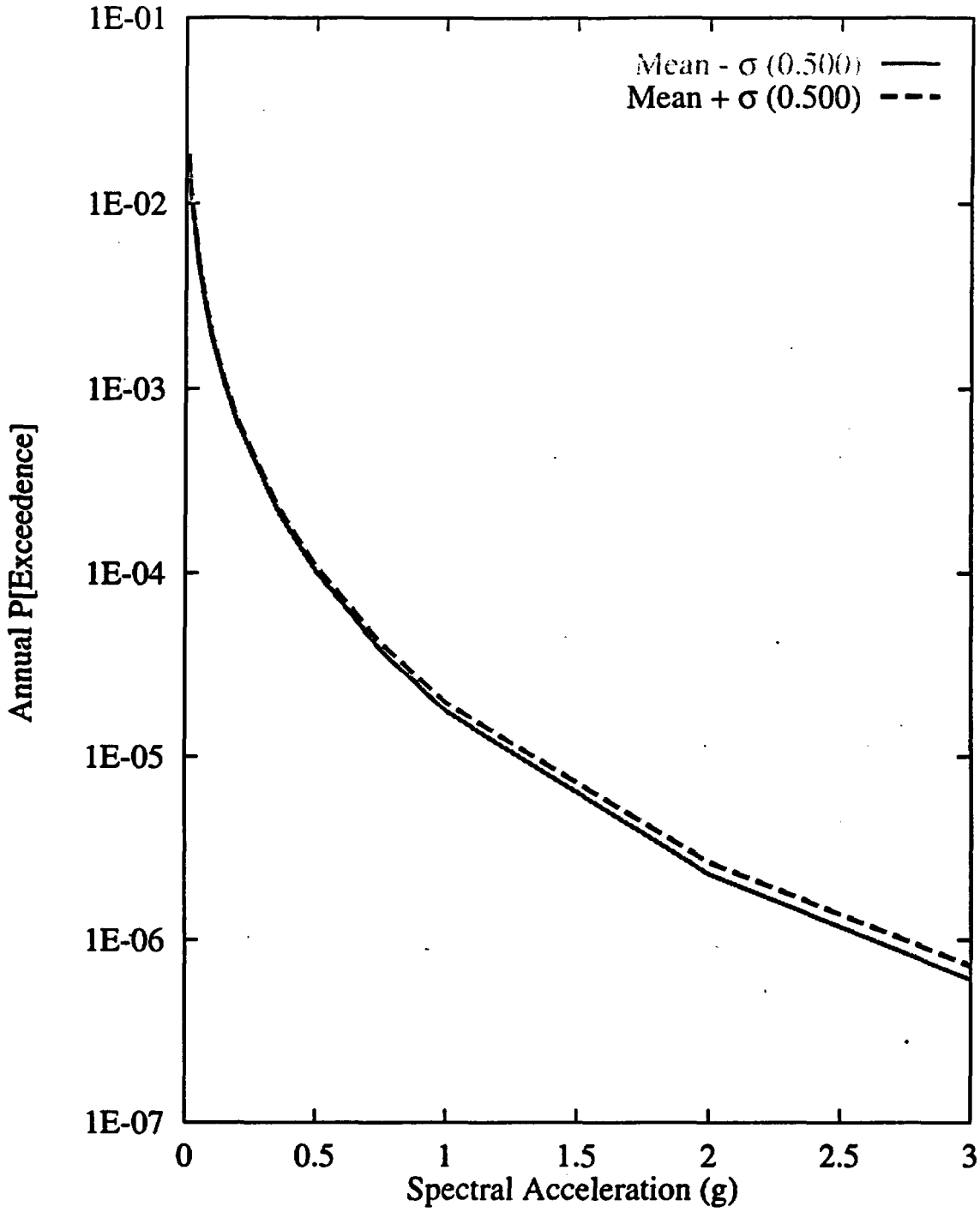

Figure 7-148 Sensitivity of seismic hazard from area zones to Mmax of the Basin and Range zone: SBK team, 10-Hz horizontal spectral acceleration

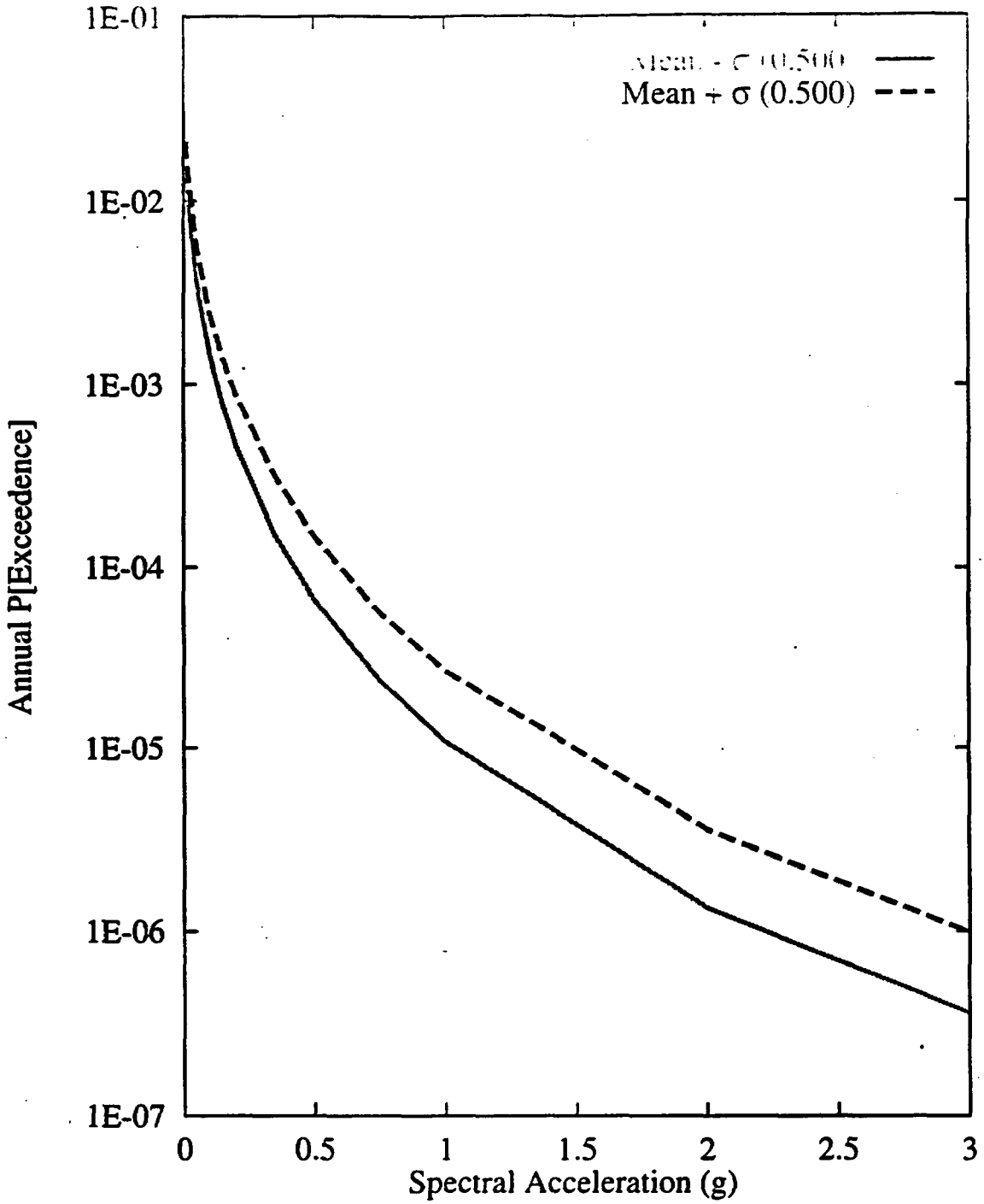

Figure 7-149 Sensitivity of seismic hazard from area zones to recurrence of the Basin and Range zone: SBK team. 10-Hz horizontal spectral acceleration

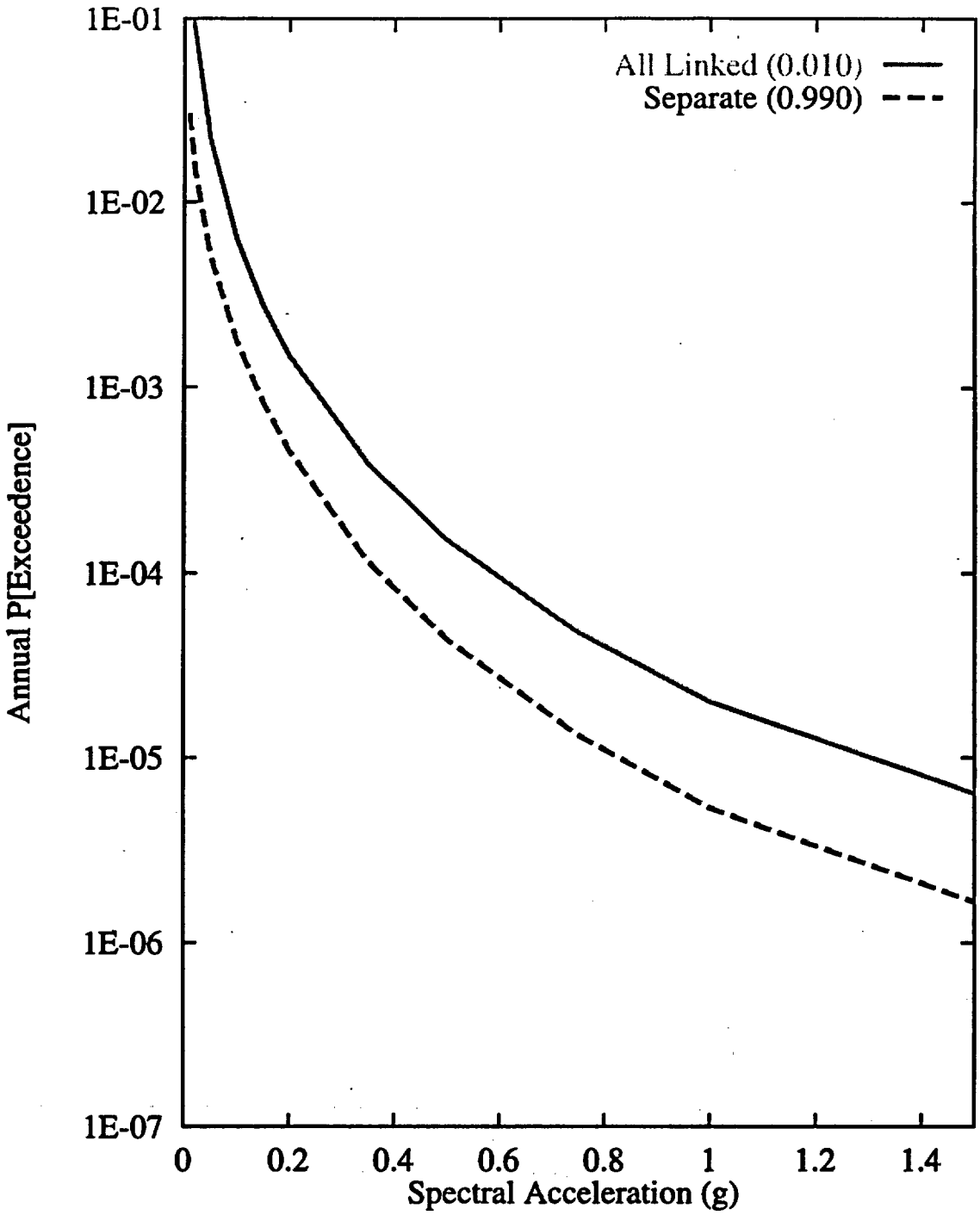

Figure 7-150 Sensitivity of seismic hazard from regional faults to rupture behavior of the Death Valley-Furnace Creek-Fish Lake Valley fault system: SBK team, 1-Hz horizontal spectral acceleration

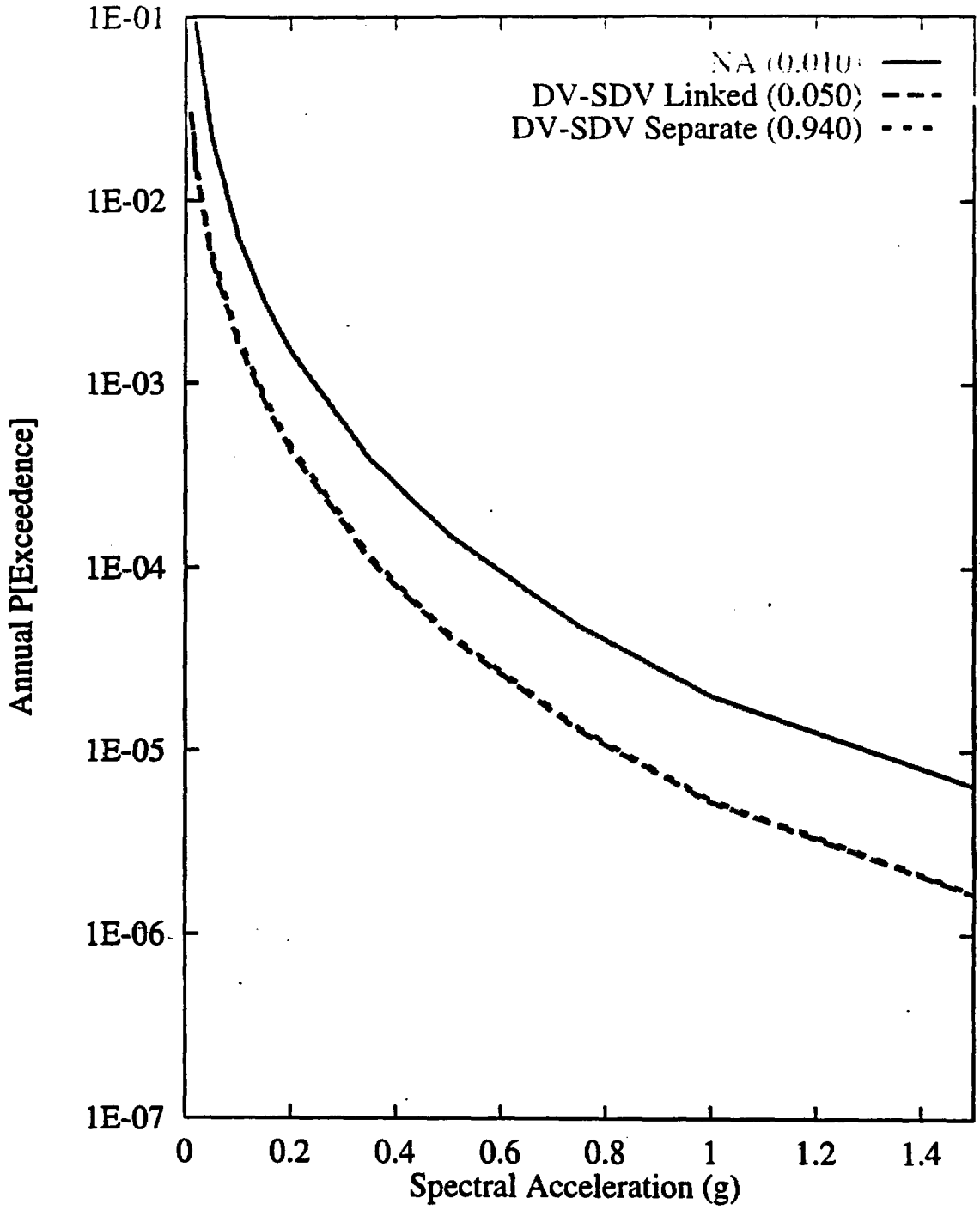

Figure 7-151 Sensitivity of seismic hazard from regional faults to rupture behavior of the Death Valley-southern Death Valley fault system: SBK team, 1-Hz horizontal spectral acceleration

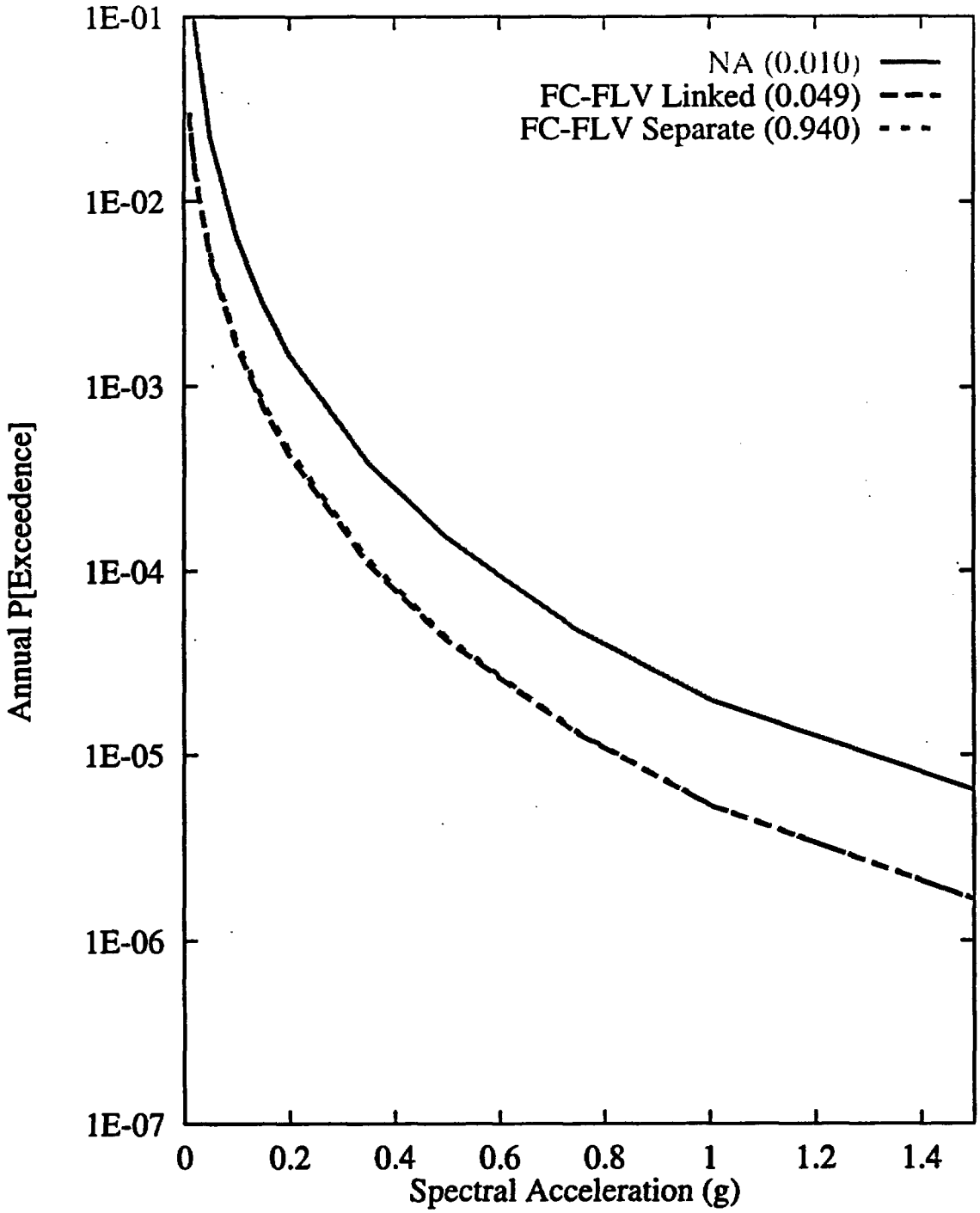

Figure 7-152 Sensitivity of seismic hazard from regional faults to rupture behavior of the Furnace Creek-Fish Lake Valley fault system: SBK team, 1-Hz horizontal spectral acceleration

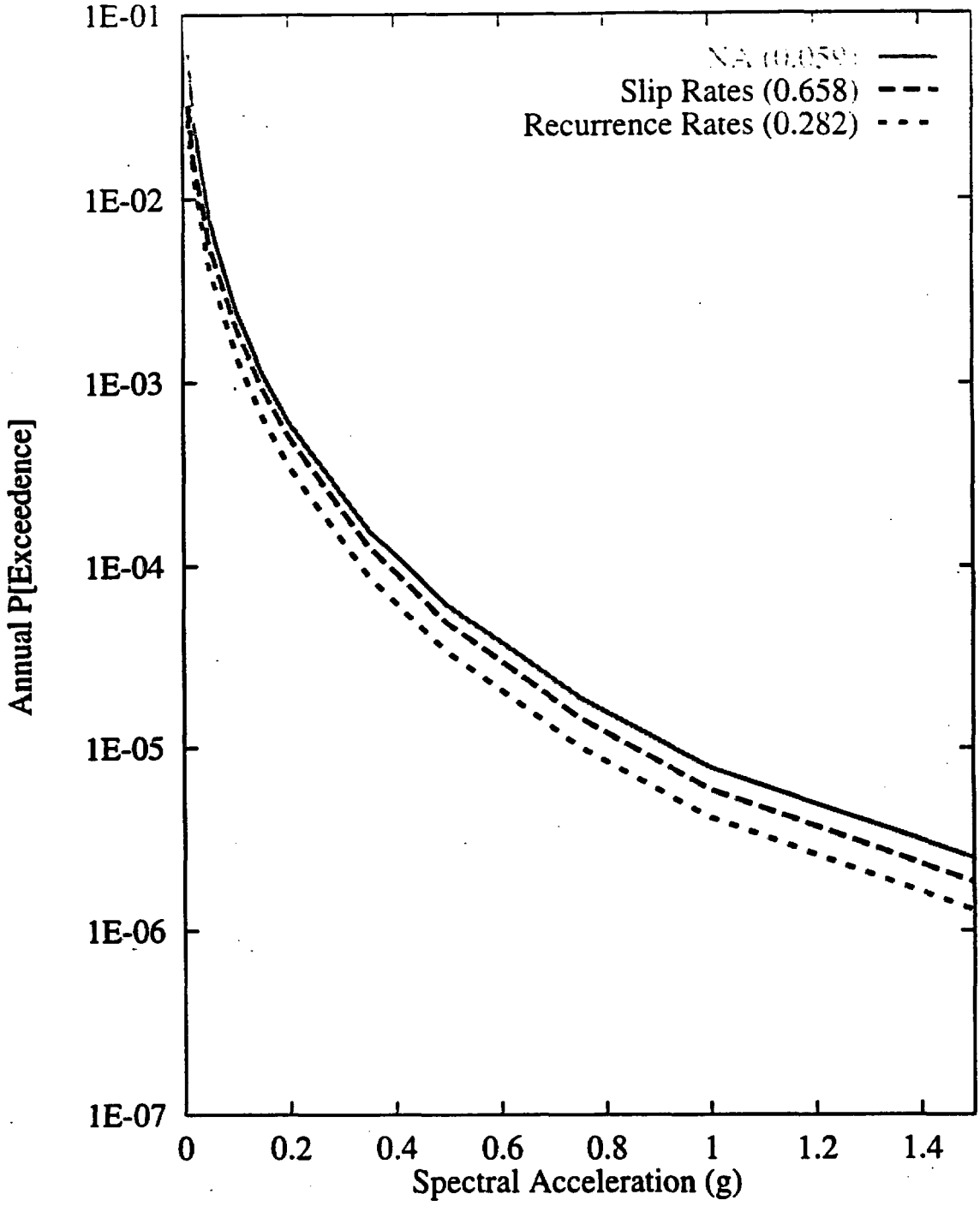

Figure 7-153 Sensitivity of seismic hazard from regional faults to recurrence of the Furnace Creek fault: SBK team, 1-Hz horizontal spectral acceleration

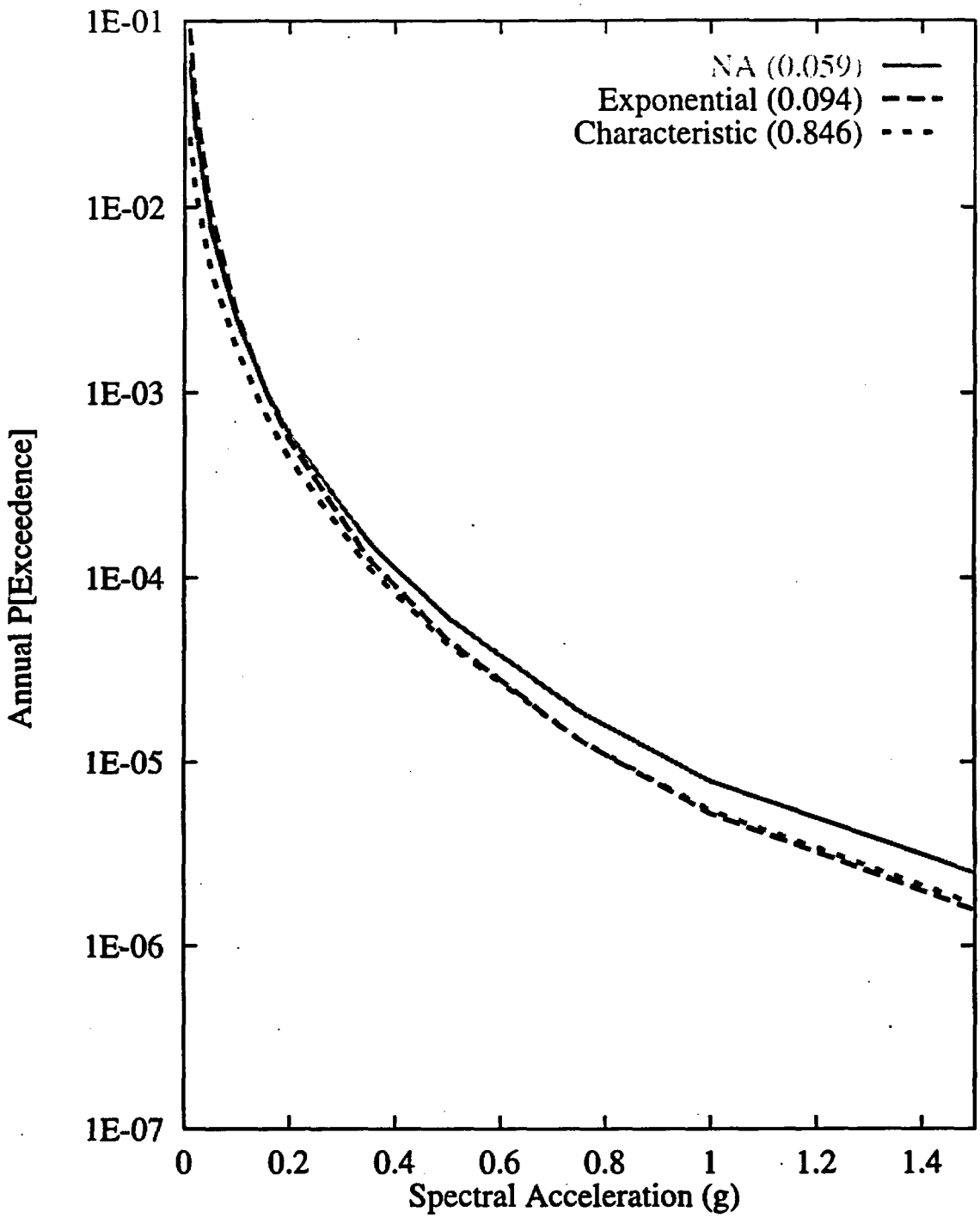

Figure 7-154 Sensitivity of seismic hazard from regional faults to recurrence model of the Furnace Creek fault: SBK team, 1-Hz horizontal spectral acceleration

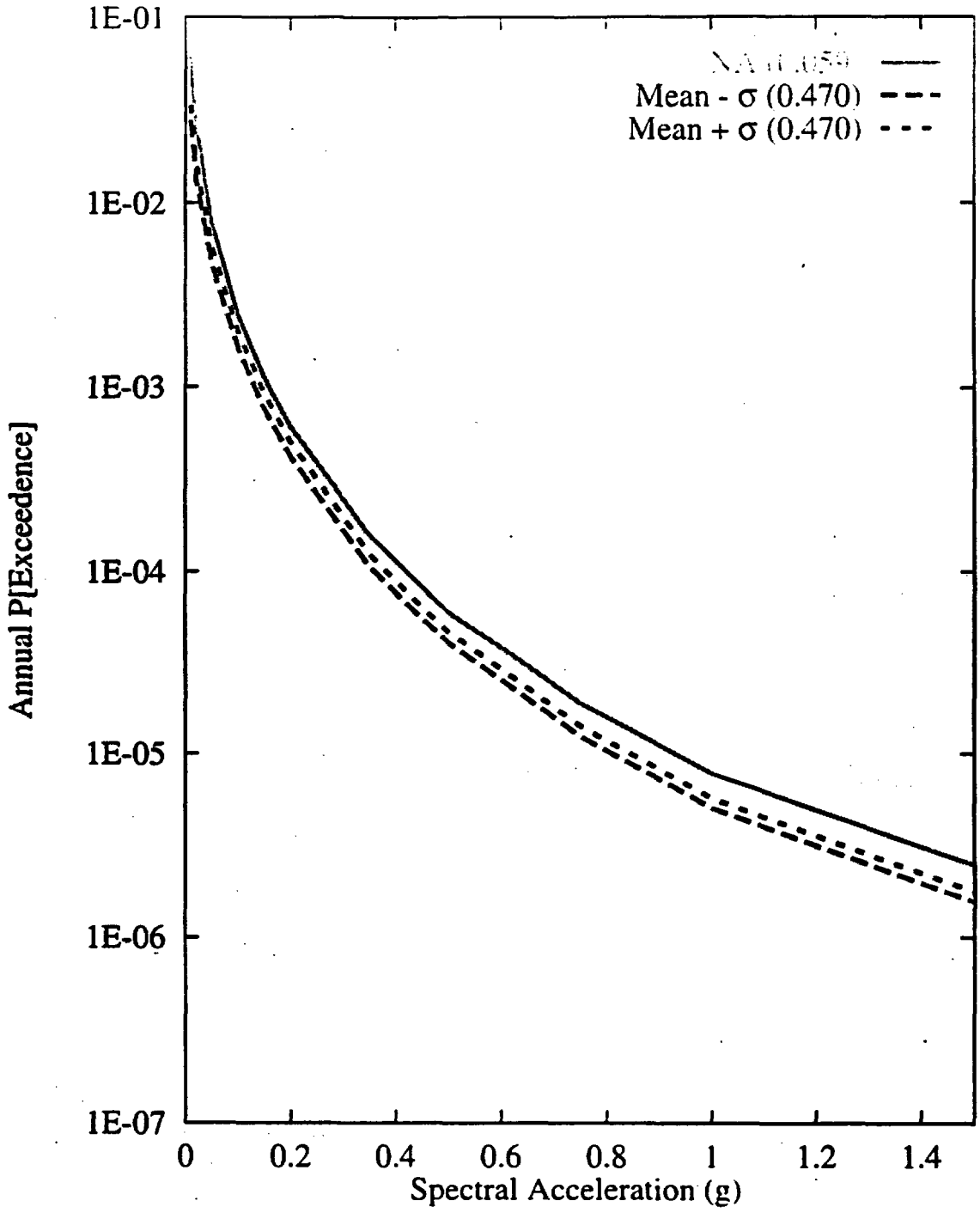

Figure 7-155 Sensitivity of seismic hazard from regional faults to Mmax on the Furnace Creek fault: SBK team, 1-Hz horizontal spectral acceleration

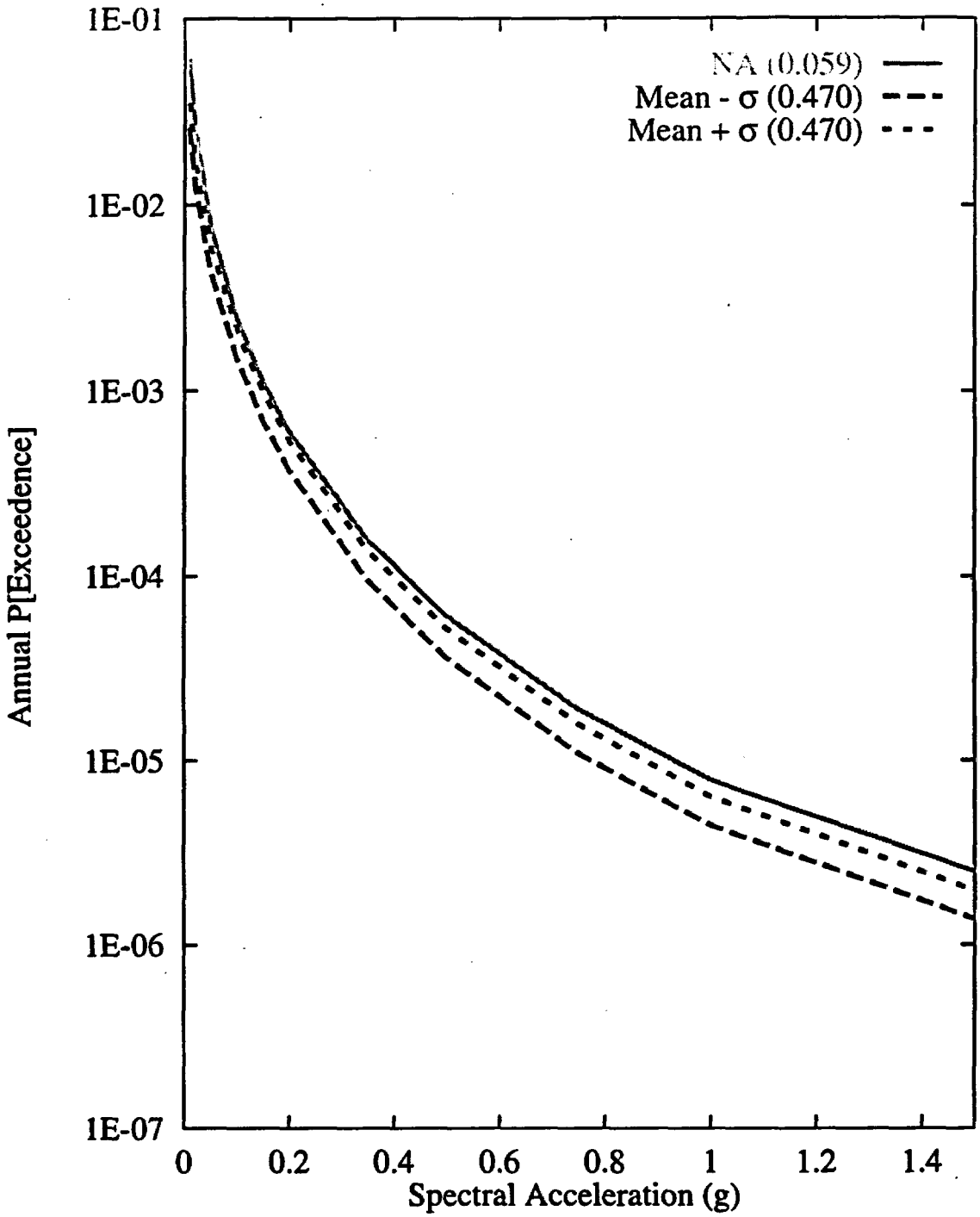

Figure 7-156 Sensitivity of seismic hazard from regional faults to recurrence of the Furnace Creek fault: SBK team, 1-Hz horizontal spectral acceleration

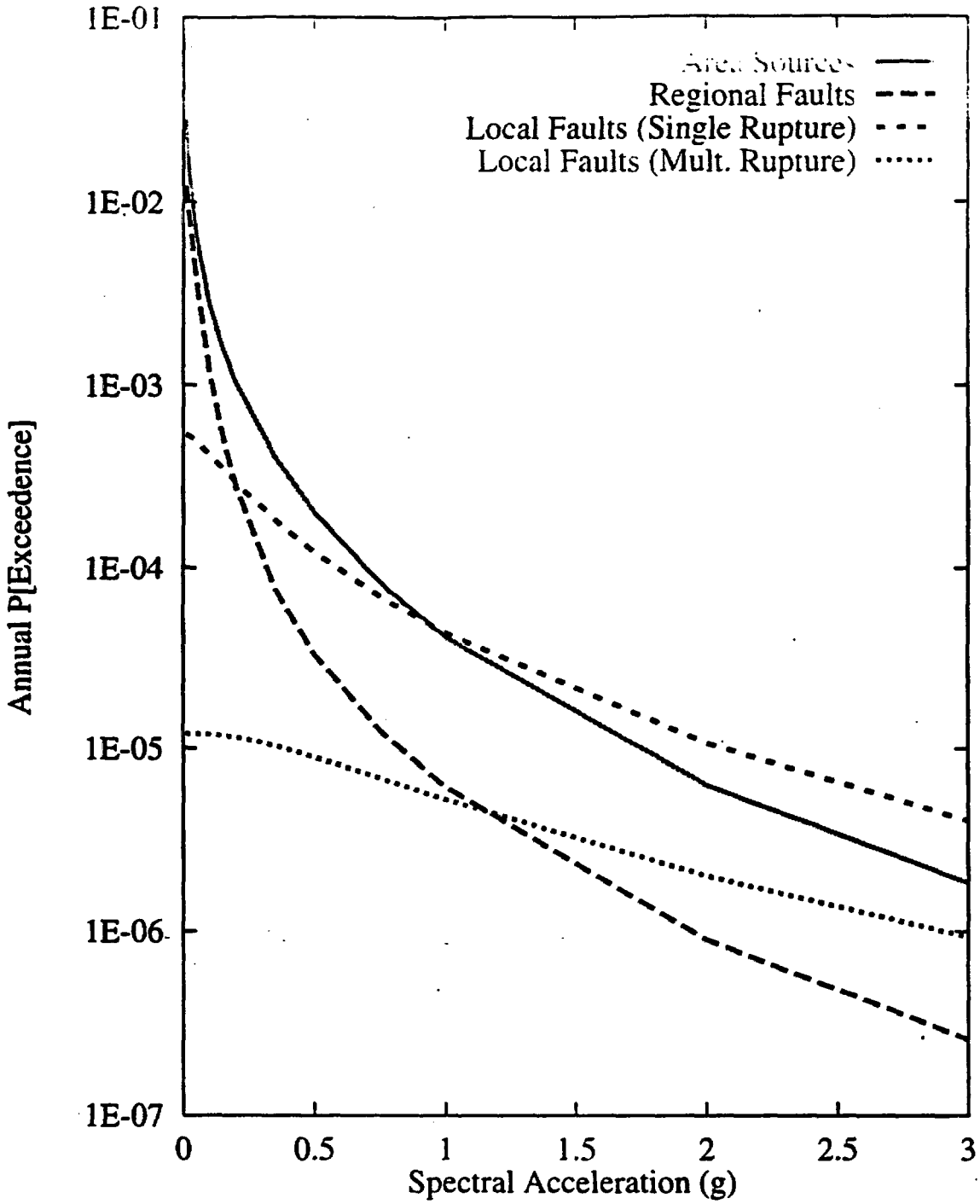

Figure 7-157 Contributions of source types to the mean hazard: SDO team, 10-Hz horizontal spectral acceleration

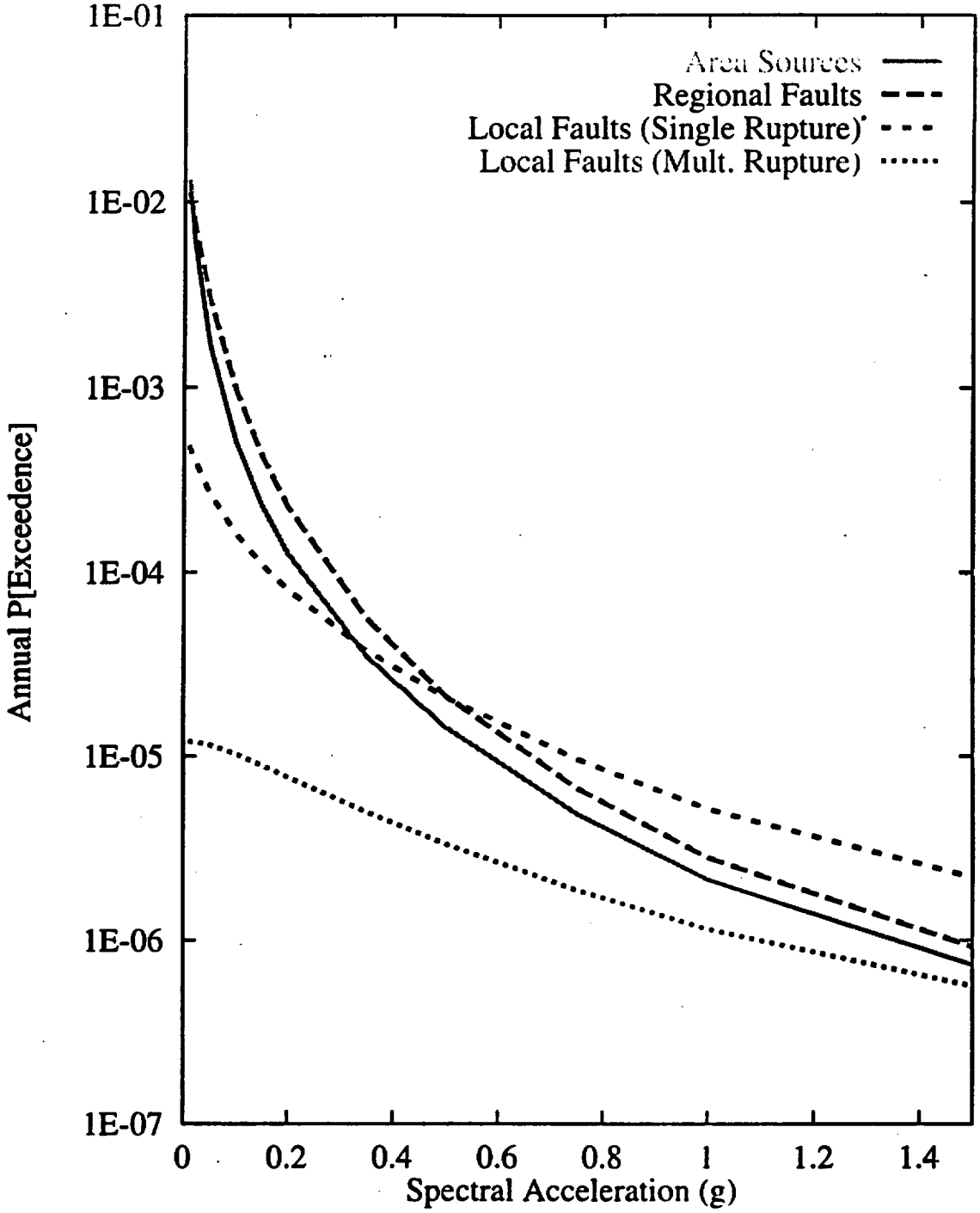

Figure 7-158 Contributions of source types to the mean hazard: SDO team, 1-Hz horizontal spectral acceleration

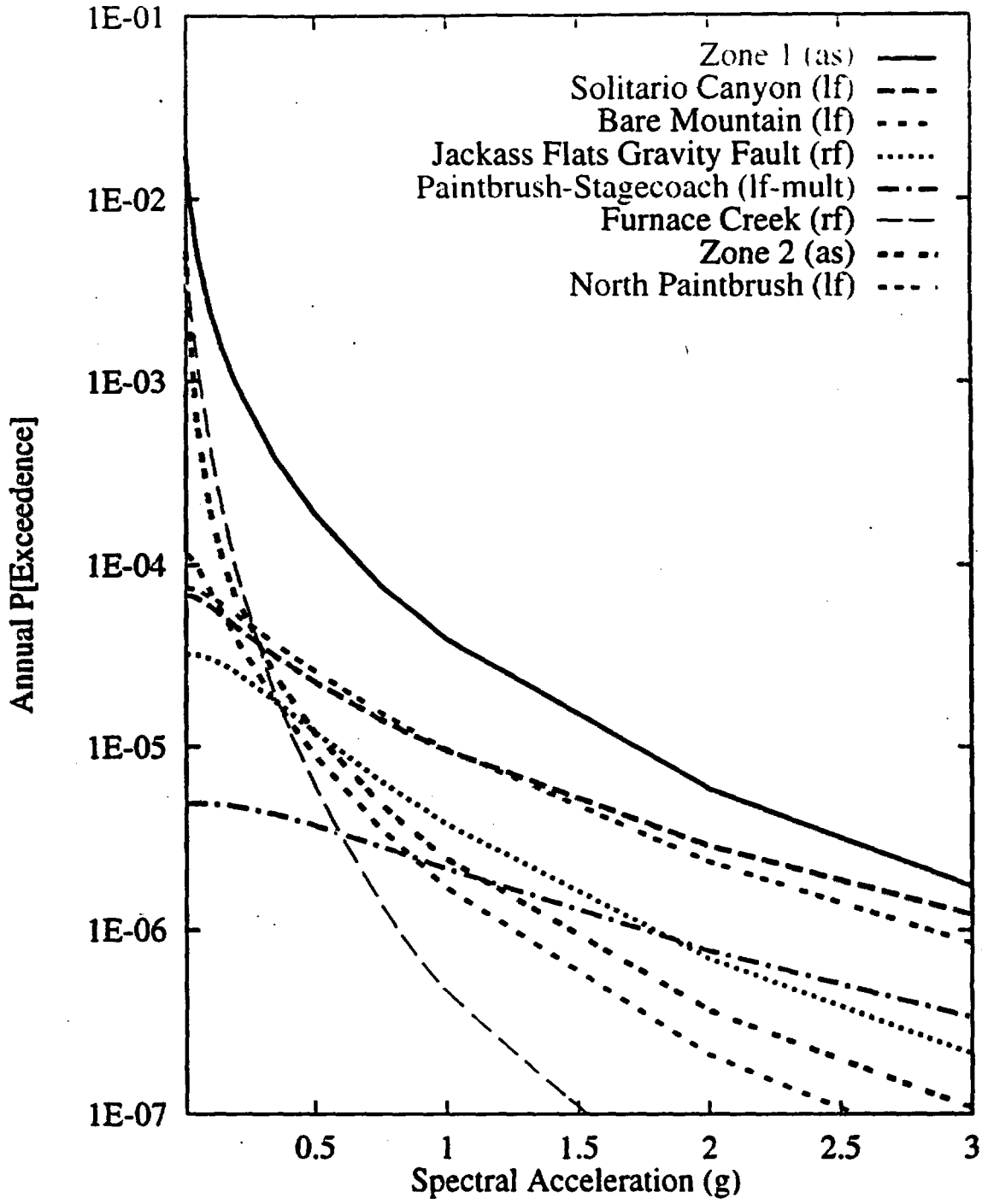

Figure 7-159 Mean seismic hazard from dominant seismic sources: SDO team, 10-Hz horizontal spectral acceleration. Acronyms in parentheses refer to source types: as-area source zone; lf-local fault; rf-regional fault; and mult-multiple fault.

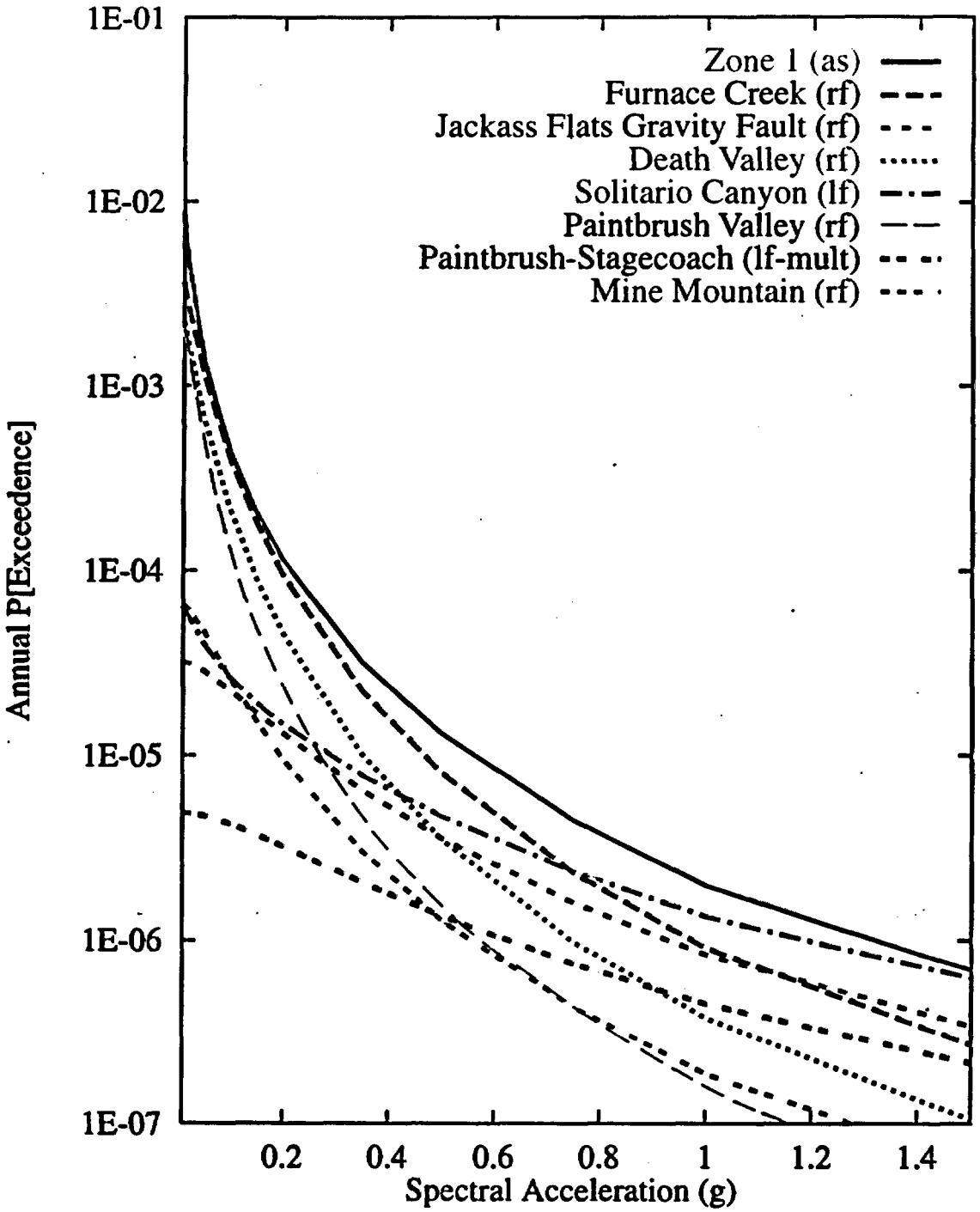

Figure 7-160 Mean seismic hazard from dominant seismic sources: SDO team, 1-Hz horizontal spectral acceleration. Acronyms in parentheses refer to source types: as-area source zone; rf-regional fault; lf-local fault; and mult-multiple fault.

10 Hz, SDO Area Sources

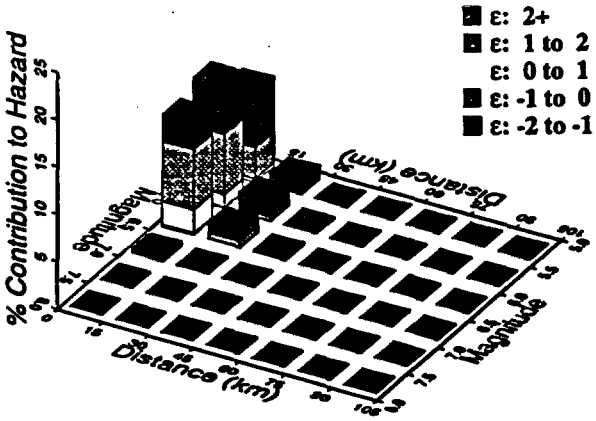

10 Hz, SDO Regional Faults

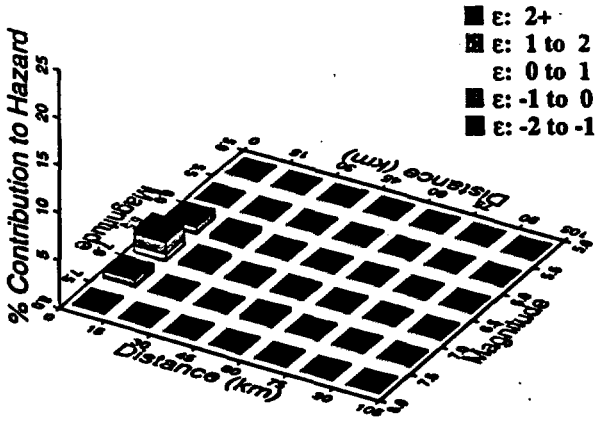

10 Hz, SDO Local Faults (Single)

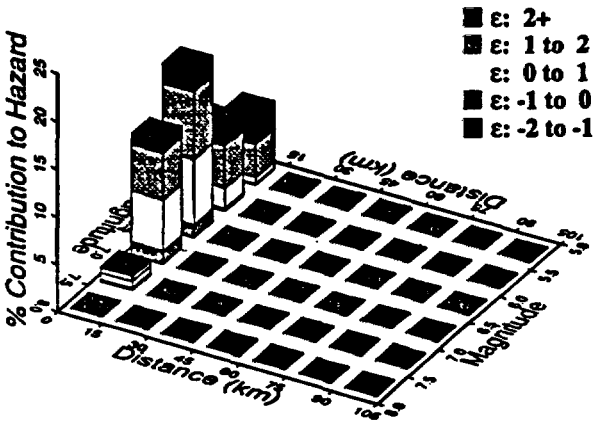

10 Hz, SDO Local Faults (Mult.)

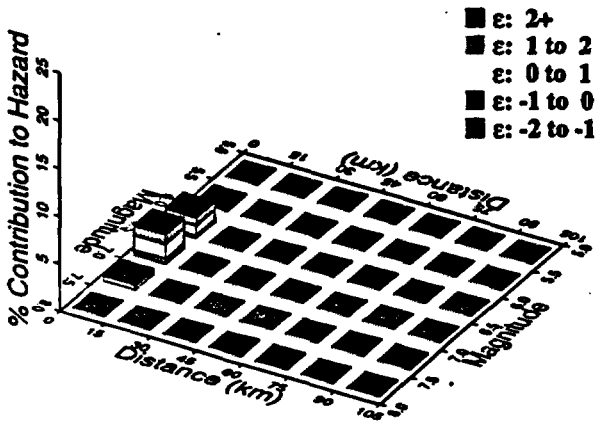

Figure 7-161 Magnitude-distance-epsilon distributions for the four source types: SDO team, 10-Hz horizontal spectral acceleration at 10^{-4} exceedance probability

1 Hz, SDO Area Sources

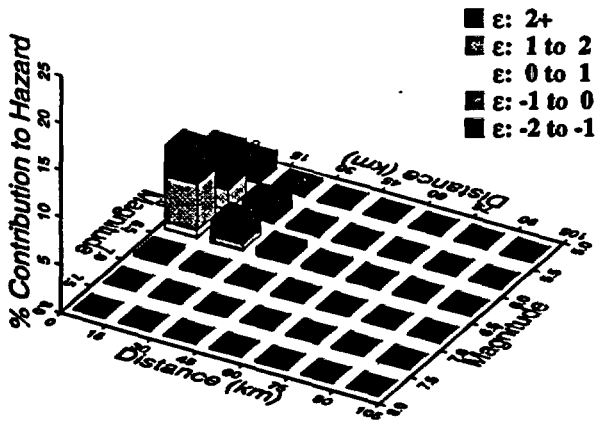

1 Hz, SDO Regional Faults

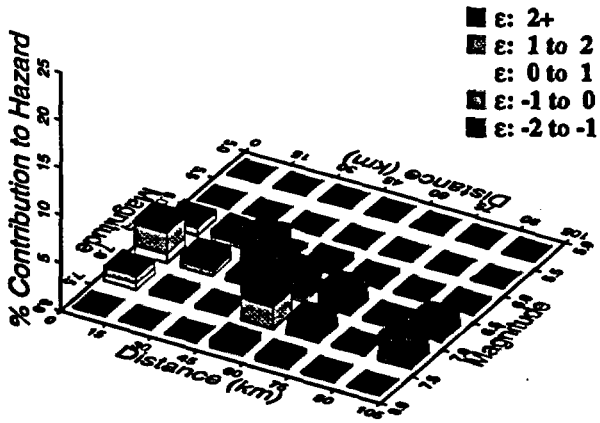

1 Hz, SDO Local Faults (Single)

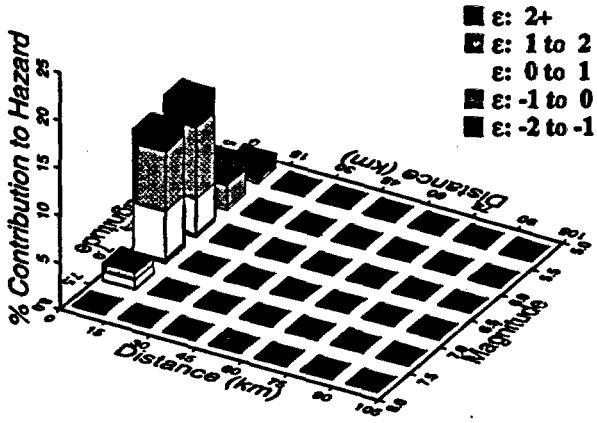

1 Hz, SDO Local Faults (Mult.)

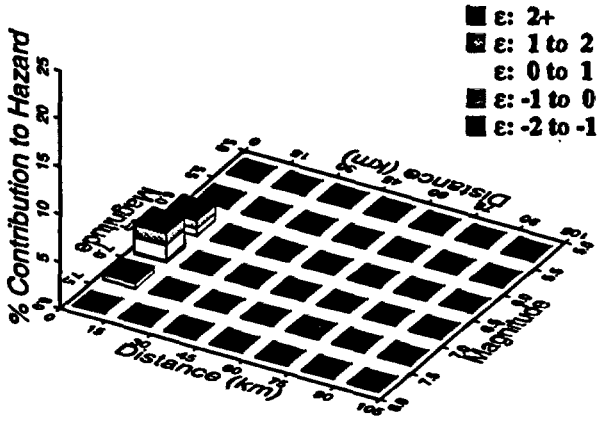

Figure 7-162 Magnitude-distance-epsilon distributions for the four source types: SDO team, 1-Hz horizontal spectral acceleration at 10^{-4} exceedance probability

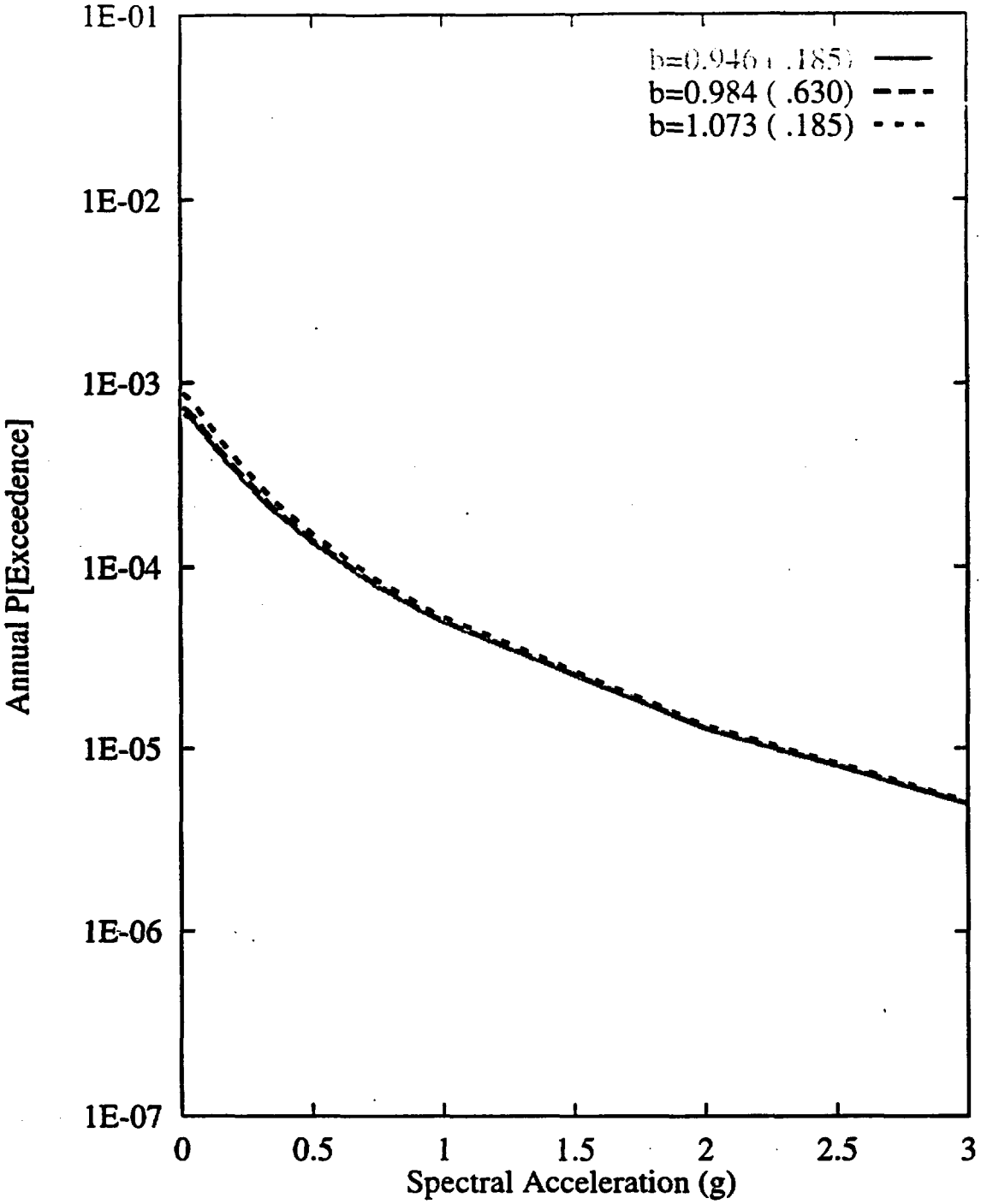

Figure 7-163 Sensitivity of seismic hazard from local faults to b-value: SDO team, 10-Hz horizontal spectral acceleration

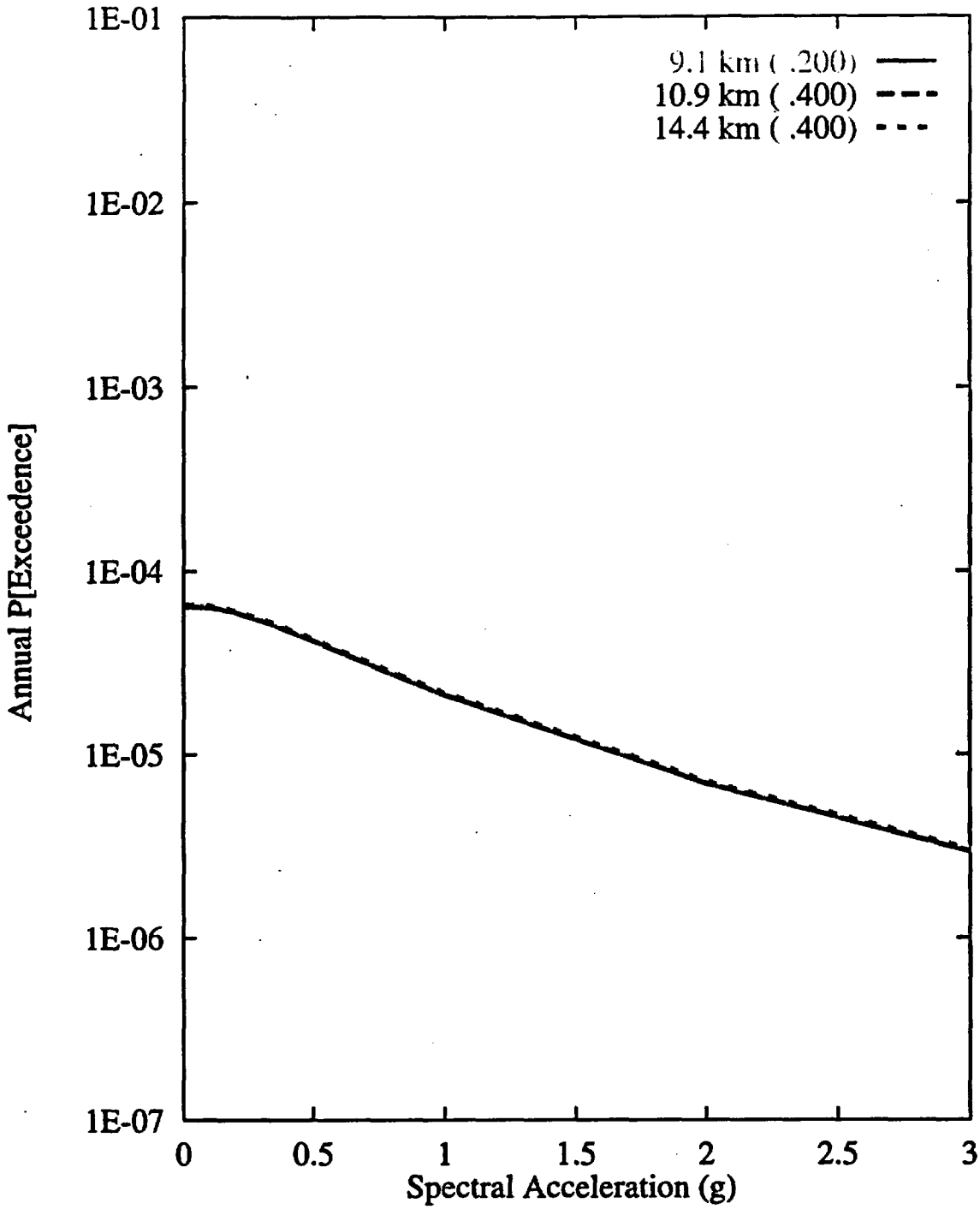

Figure 7-164 Sensitivity of seismic hazard from local faults to maximum depth of the Solitario Canyon fault: SDO team, 10-Hz horizontal spectral acceleration

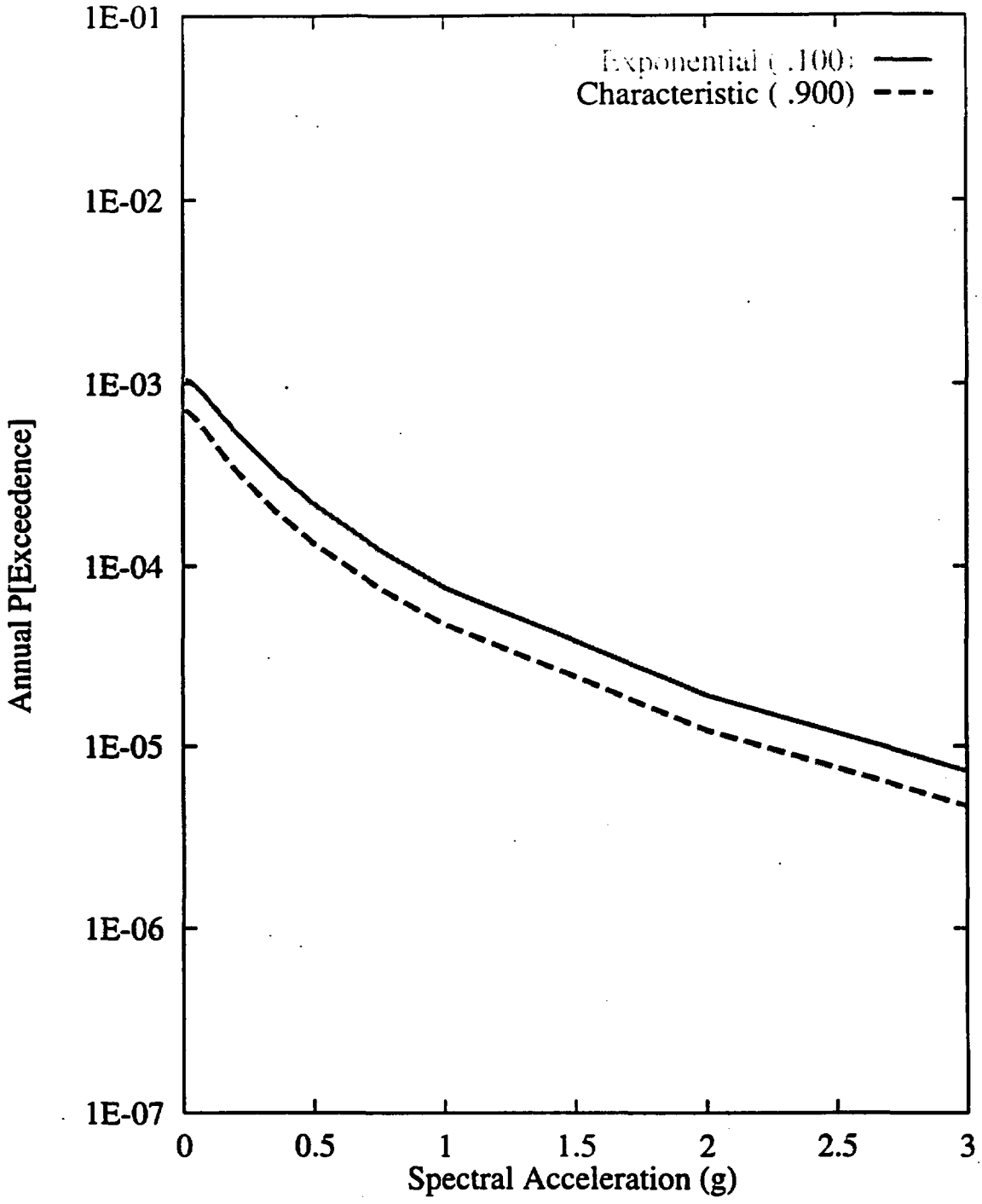

Figure 7-165 Sensitivity of seismic hazard from local faults to recurrence model of the Solitario Canyon fault: SDO team, 10-Hz horizontal spectral acceleration

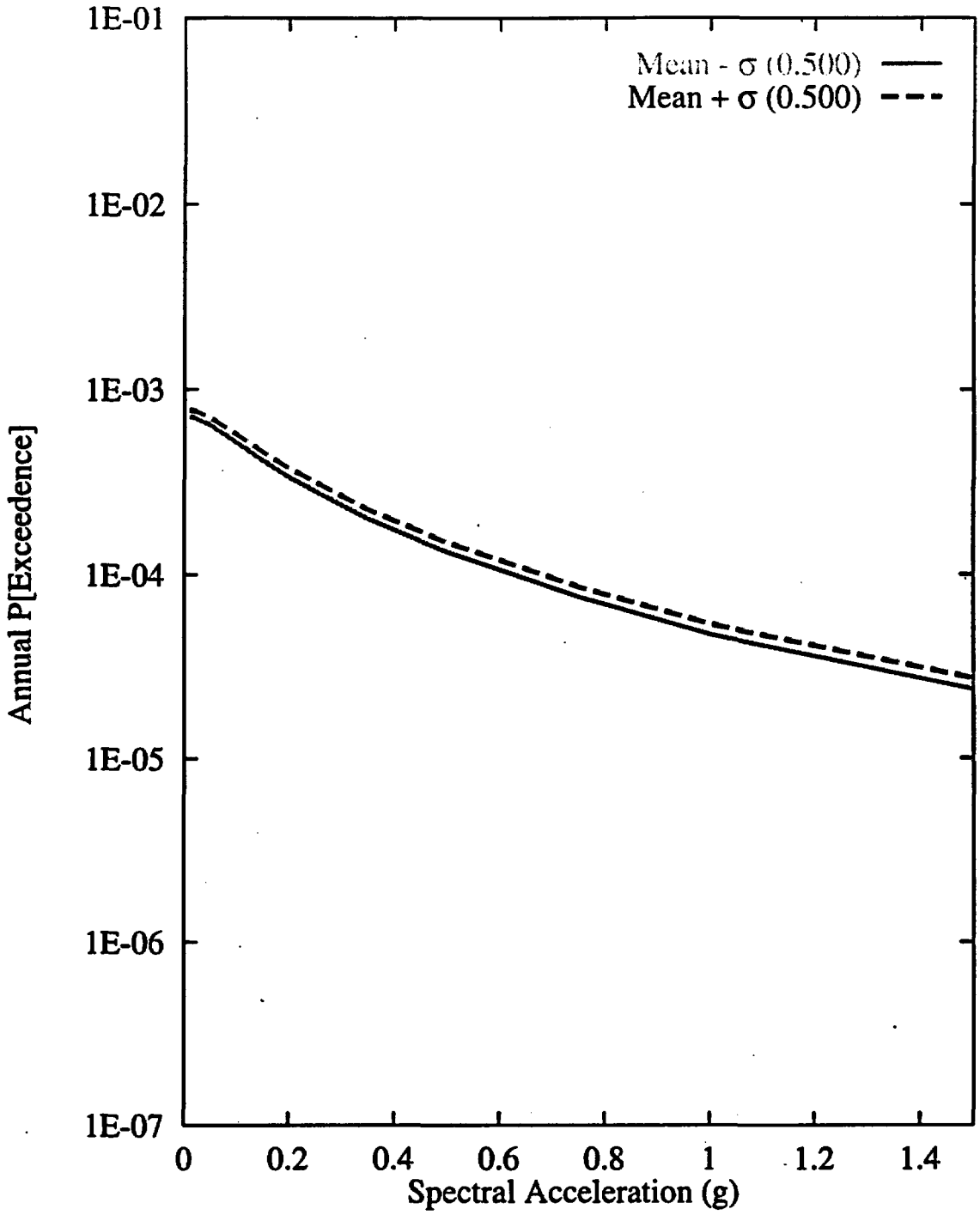

Figure 7-166 Sensitivity of seismic hazard from local faults to Mmax for the Solitario Canyon fault: SDO team, 10-Hz horizontal spectral acceleration

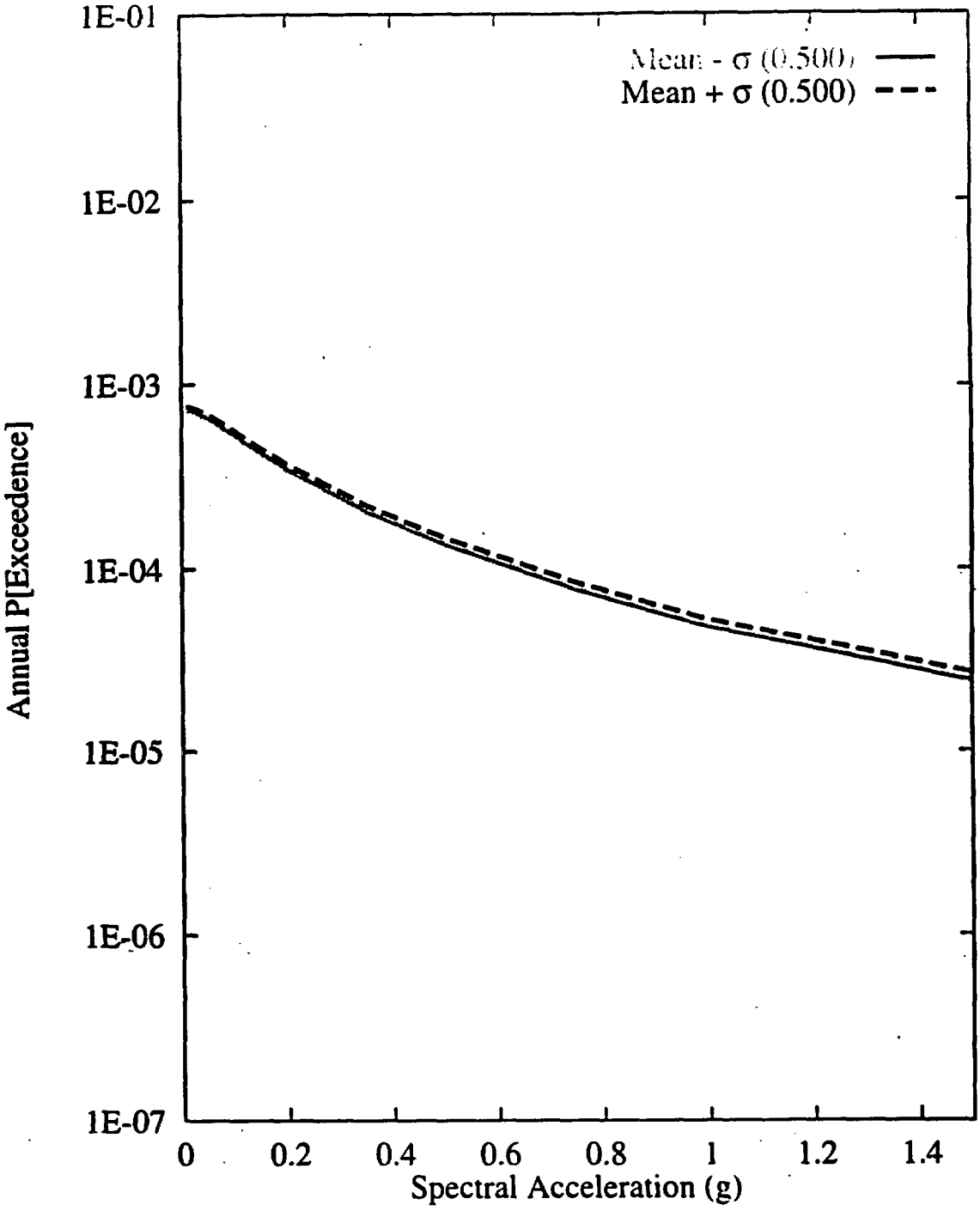

Figure 7-167 Sensitivity of seismic hazard from local faults to recurrence of the Solitario Canyon fault: SDO team, 10-Hz horizontal spectral acceleration

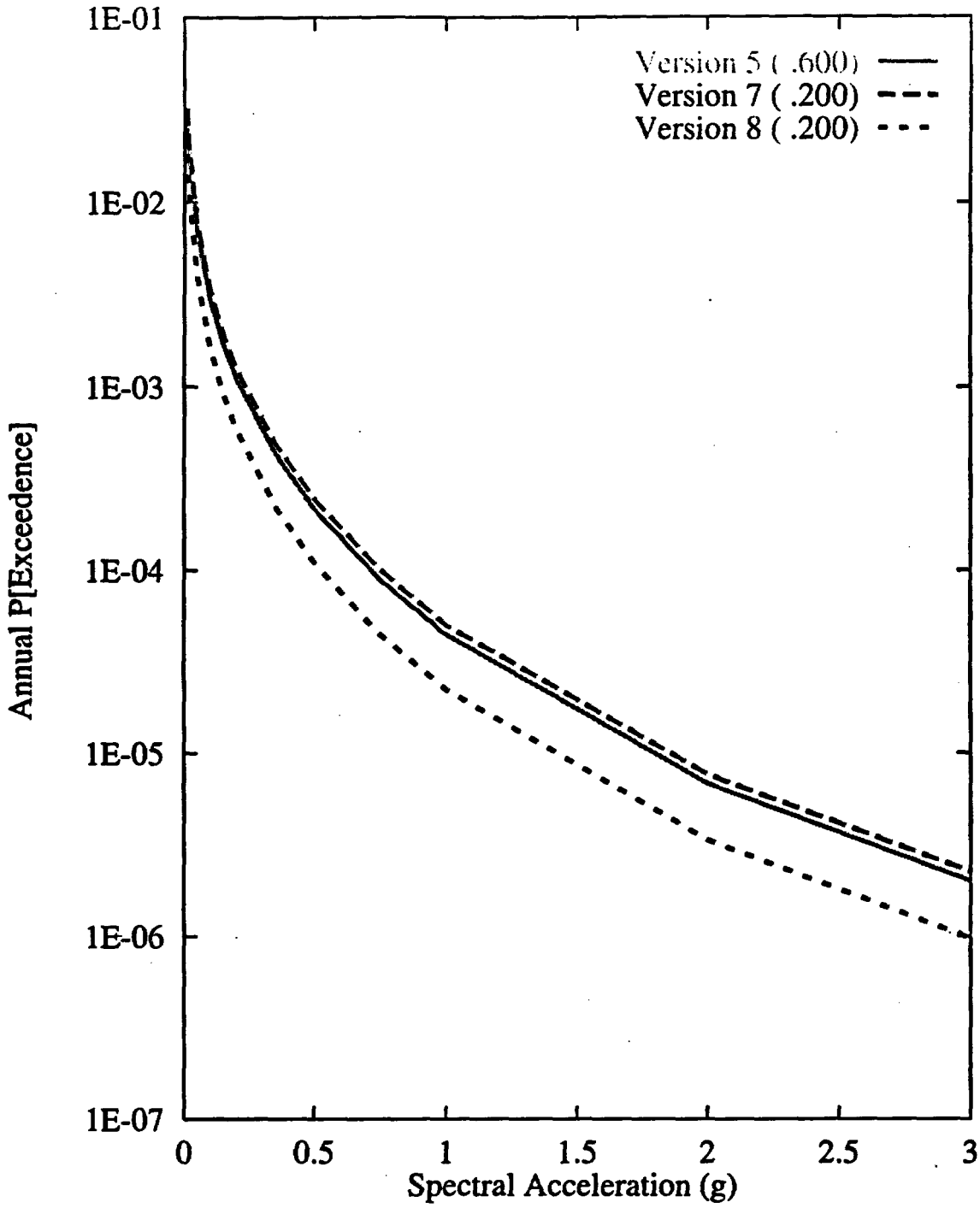

Figure 7-168 Sensitivity of seismic hazard from area zones to choice of seismicity catalog: SDO team, 10-Hz horizontal spectral acceleration

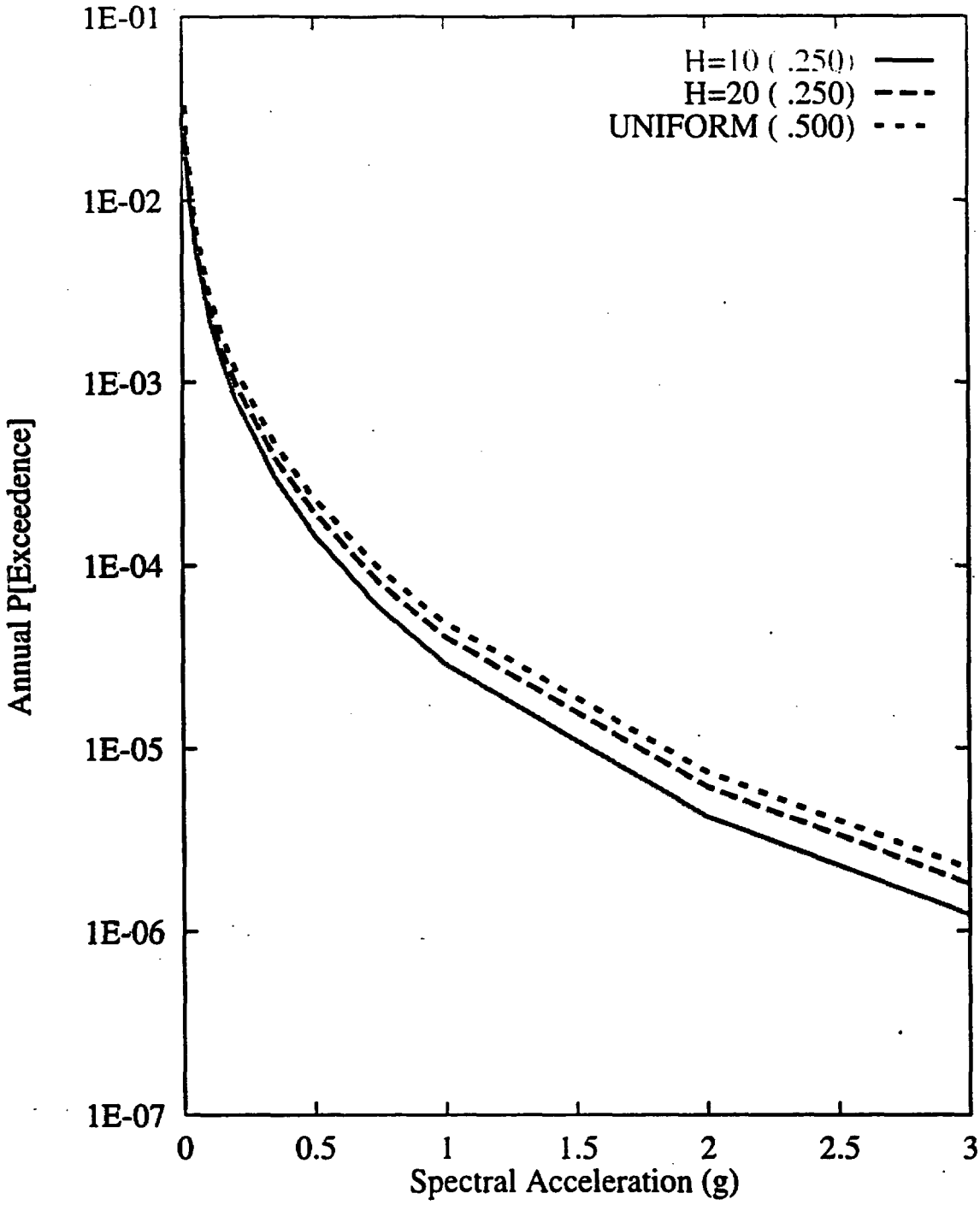

Figure 7-169 Sensitivity of seismic hazard from area zones to spatial variability and smoothing (H) of seismicity: SDO team, 10-Hz horizontal spectral acceleration

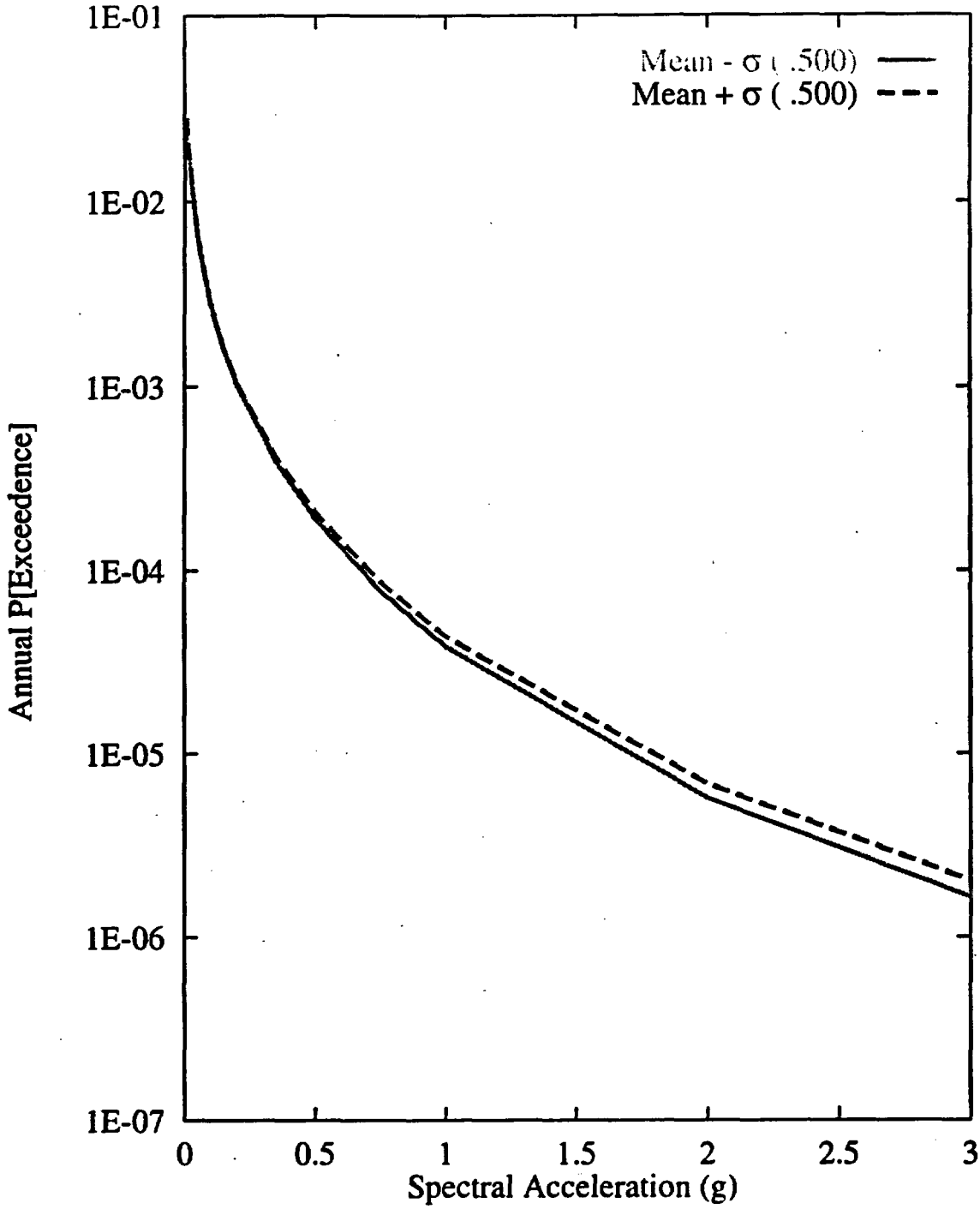

Figure 7-170 Sensitivity of seismic hazard from area zones to Mmax of the Z1 area zone: SDO team, 10-Hz horizontal spectral acceleration

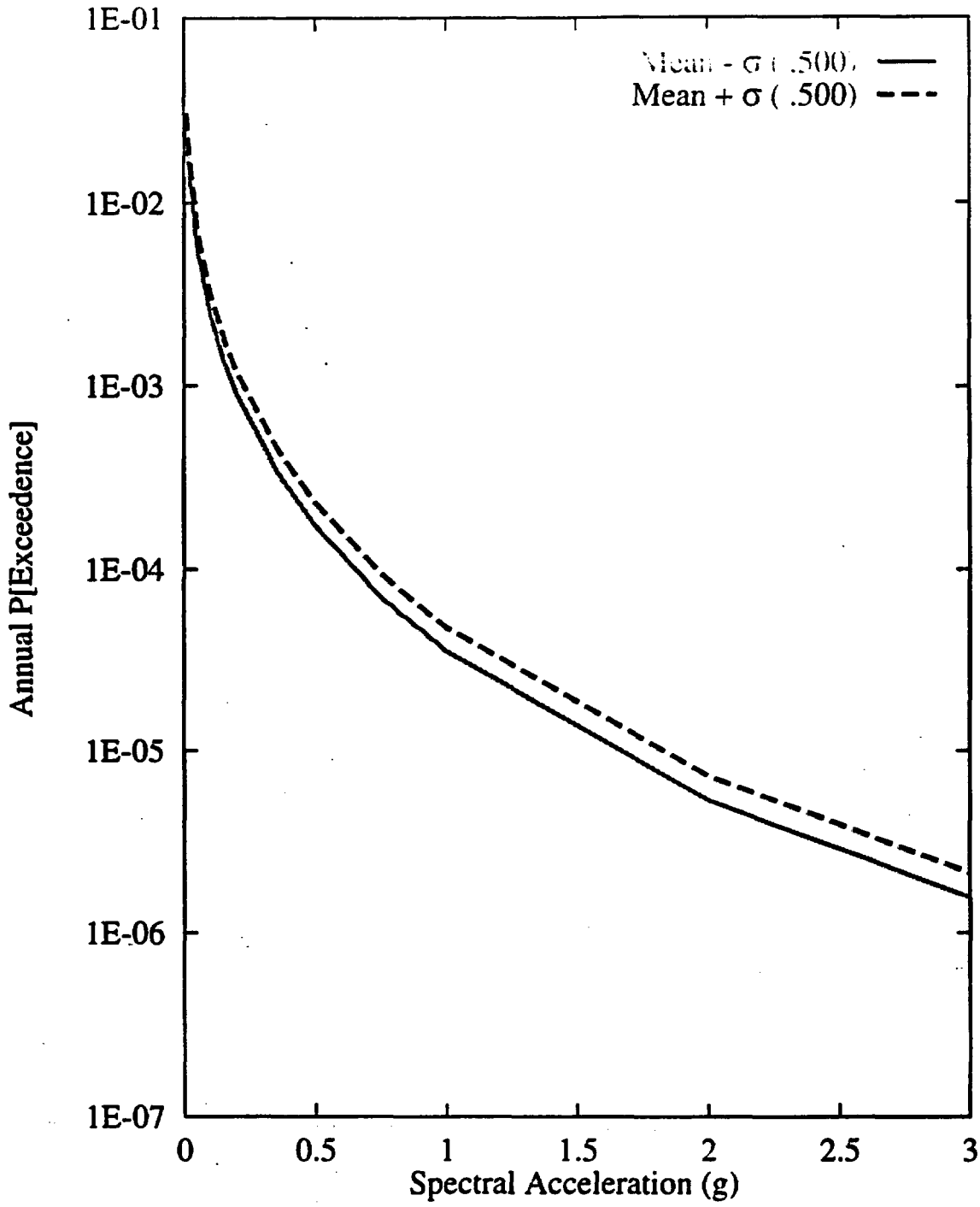

Figure 7-171 Sensitivity of seismic hazard from area zones to recurrence of the Z1 area zone: SDO team, 10-Hz horizontal spectral acceleration

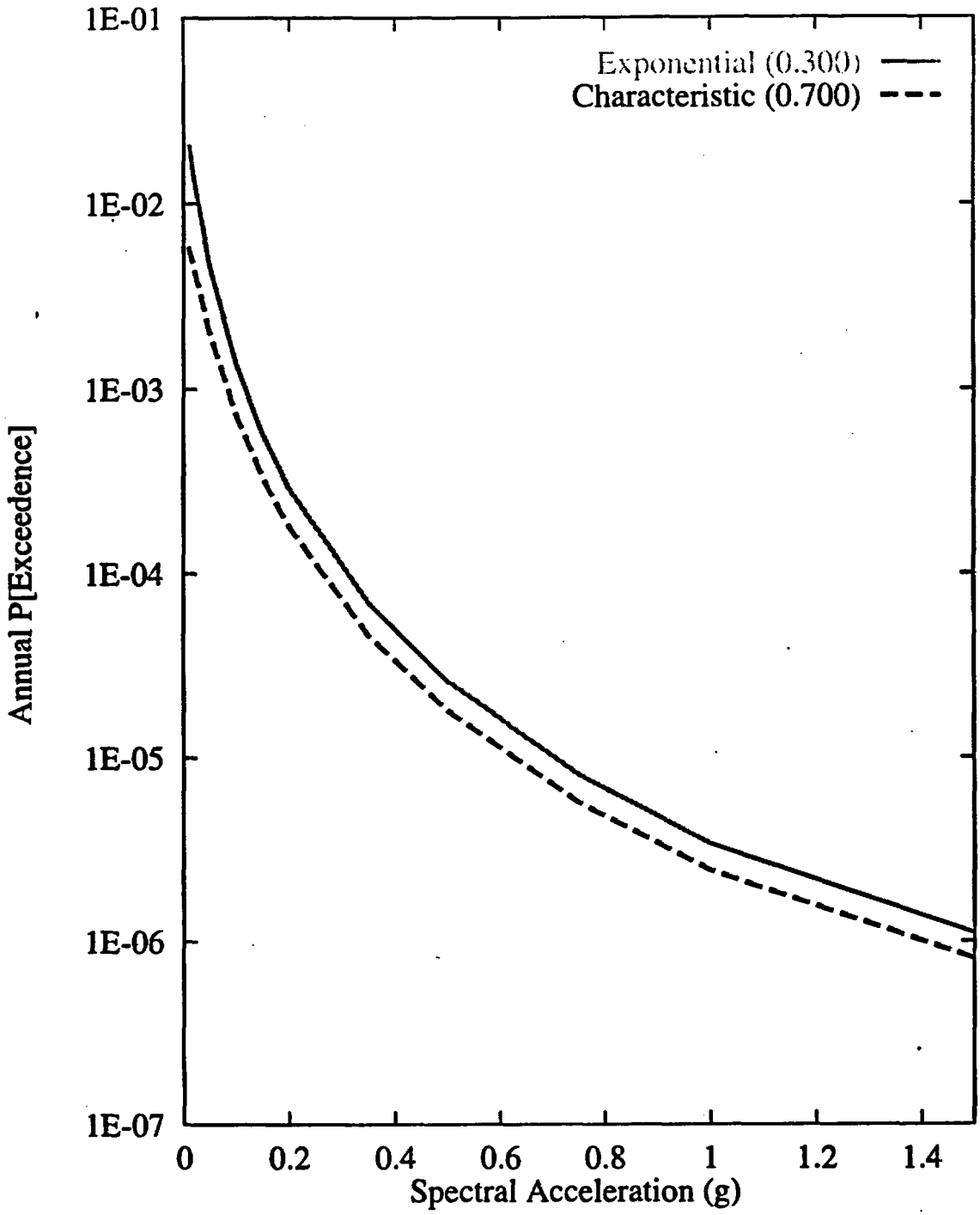

Figure 7-172 Sensitivity of seismic hazard from regional faults to recurrence model: SDO team, 1-Hz horizontal spectral acceleration

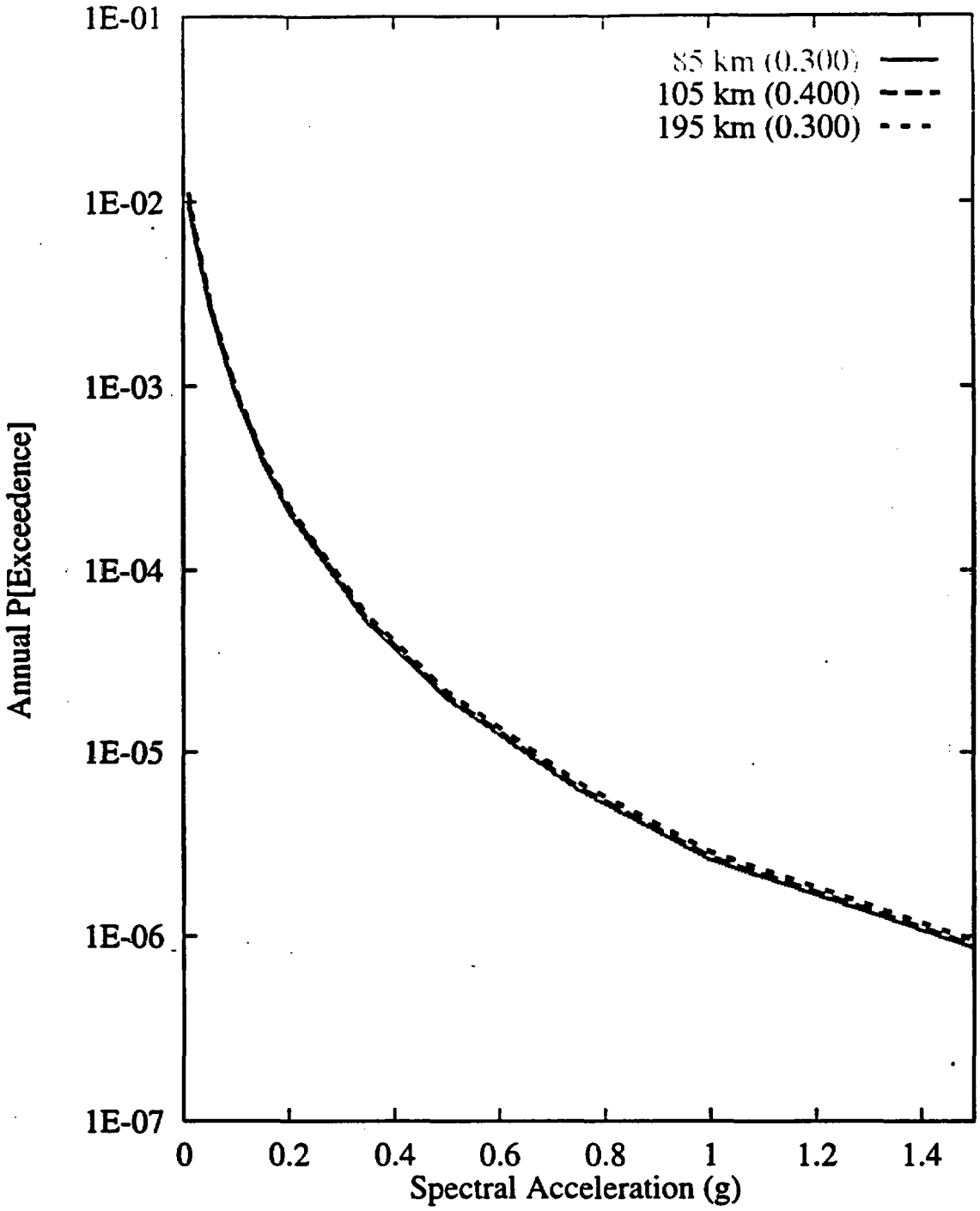

Figure 7-173 Sensitivity of seismic hazard from regional faults to length of the Furnace Creek fault: SDO team, 1-Hz horizontal spectral acceleration

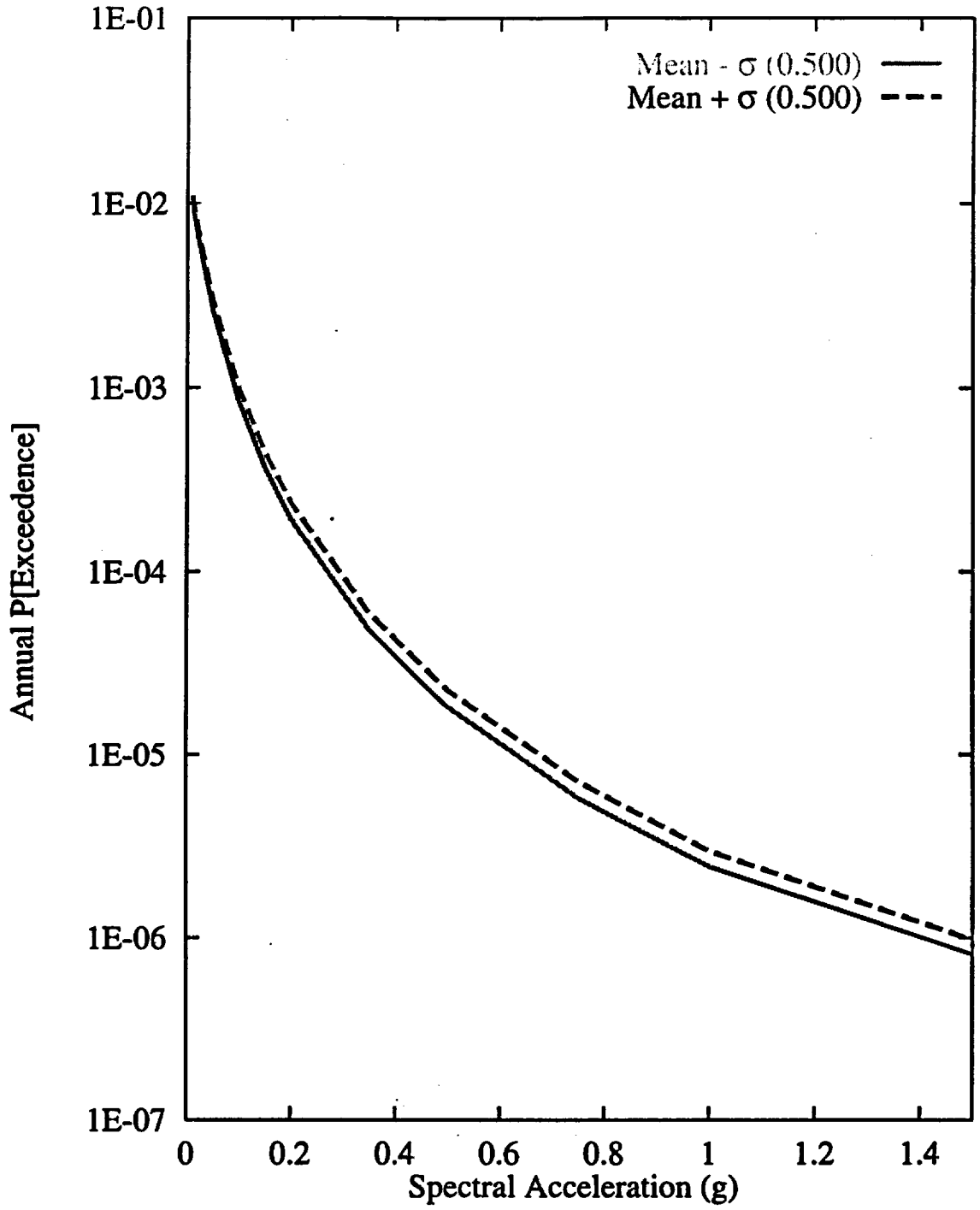

Figure 7-174 Sensitivity of seismic hazard from regional faults to M_{max} for the Furnace Creek fault: SDO team, 1-Hz horizontal spectral acceleration

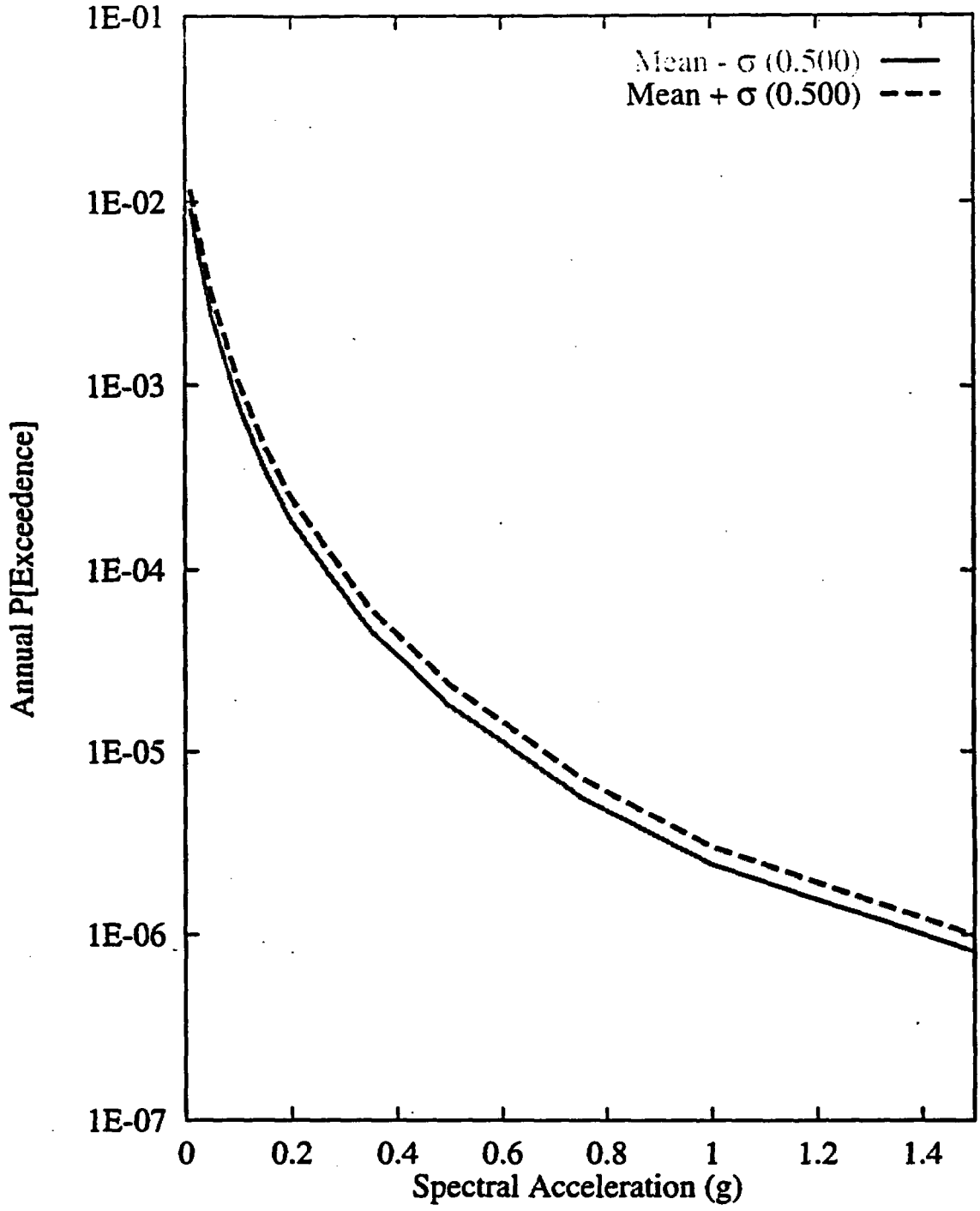

Figure 7-175 Sensitivity of seismic hazard from regional faults to recurrence of the Furnace Creek fault: SDO team, 1-Hz horizontal spectral acceleration

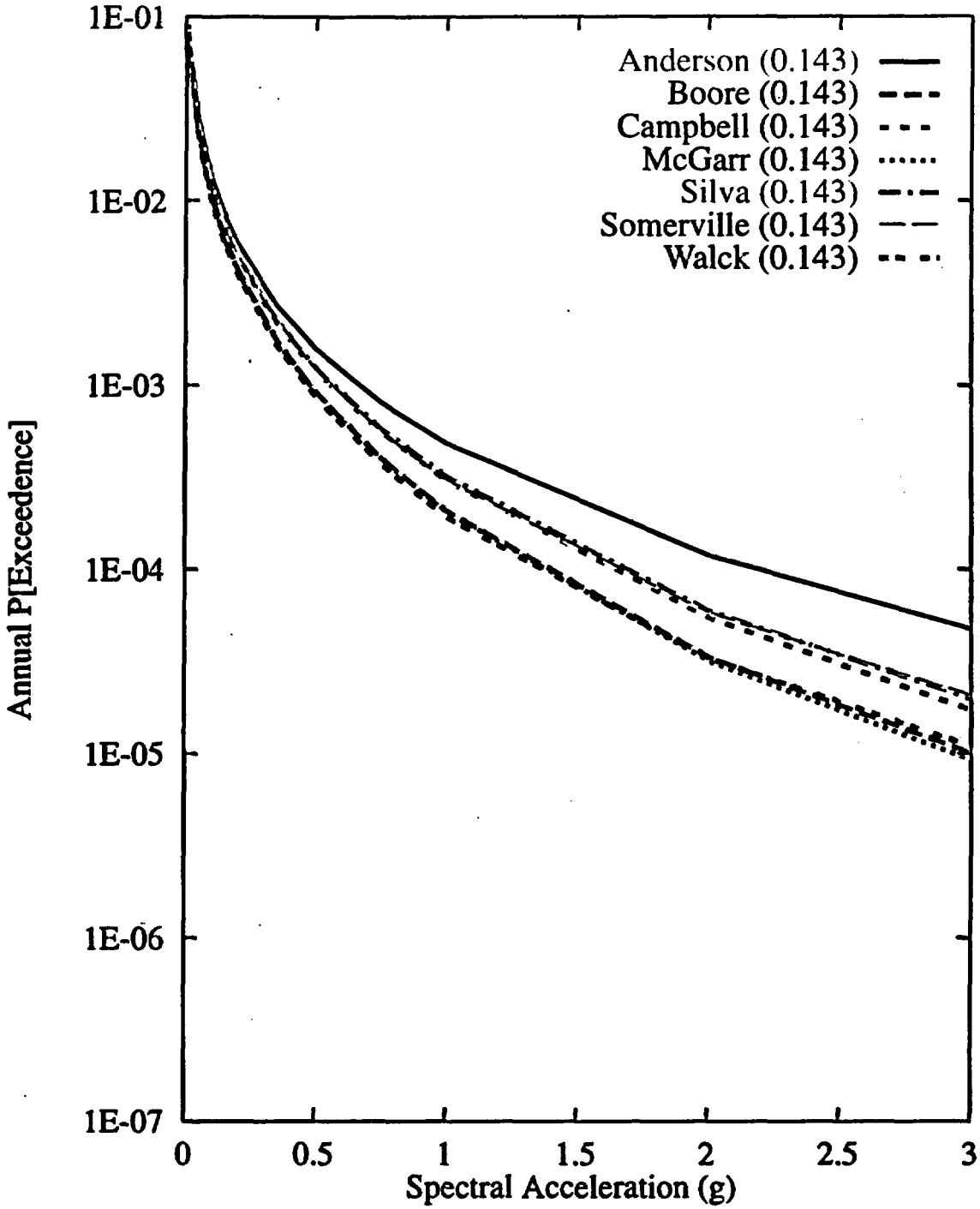

Figure 7-176 Sensitivity of seismic hazard to GM experts:
ASM team, 10-Hz horizontal spectral acceleration

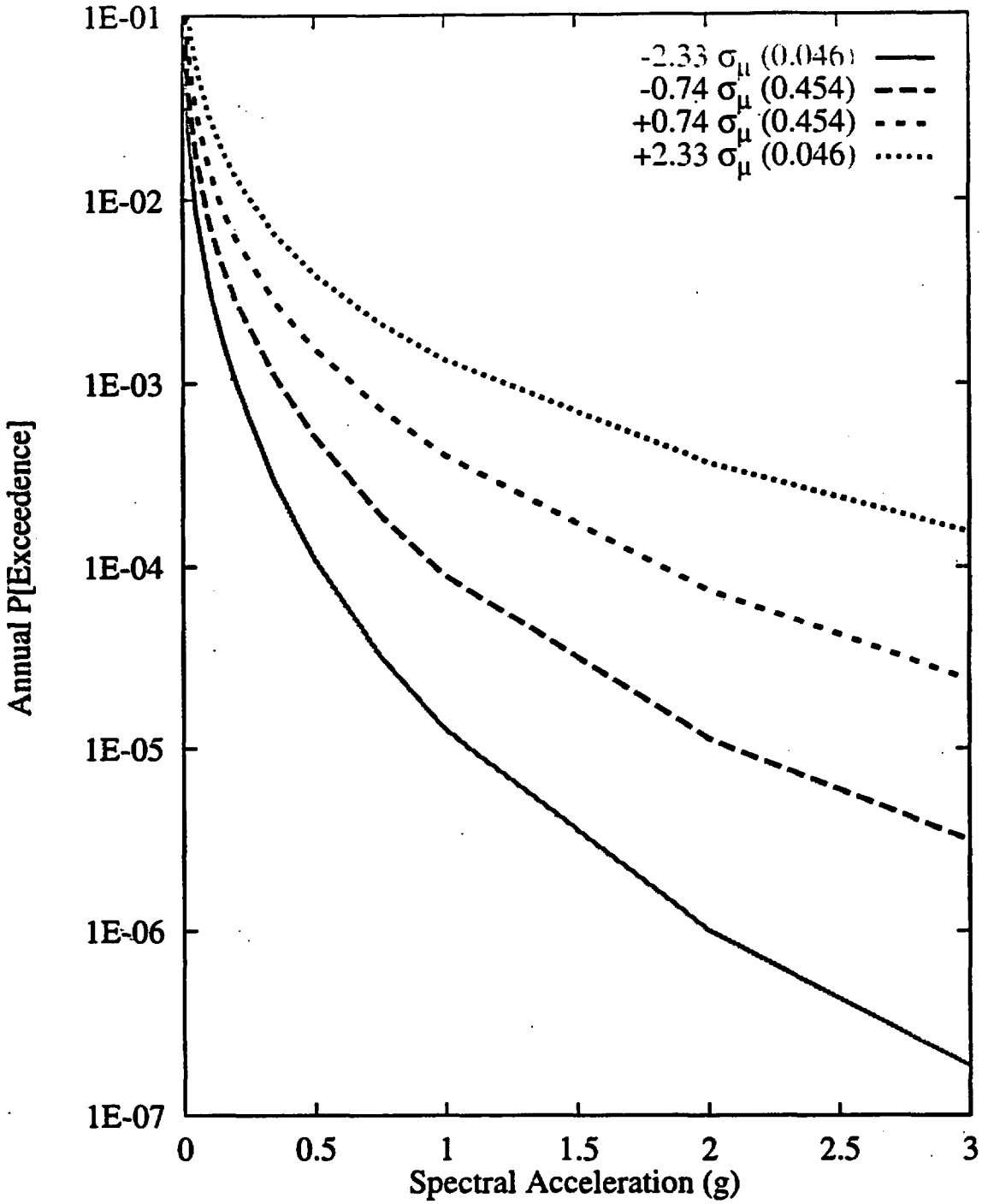

Figure 7-177 Sensitivity of seismic hazard to within-expert epistemic uncertainty in the median ground motion amplitude: ASM team, 10-Hz horizontal spectral acceleration

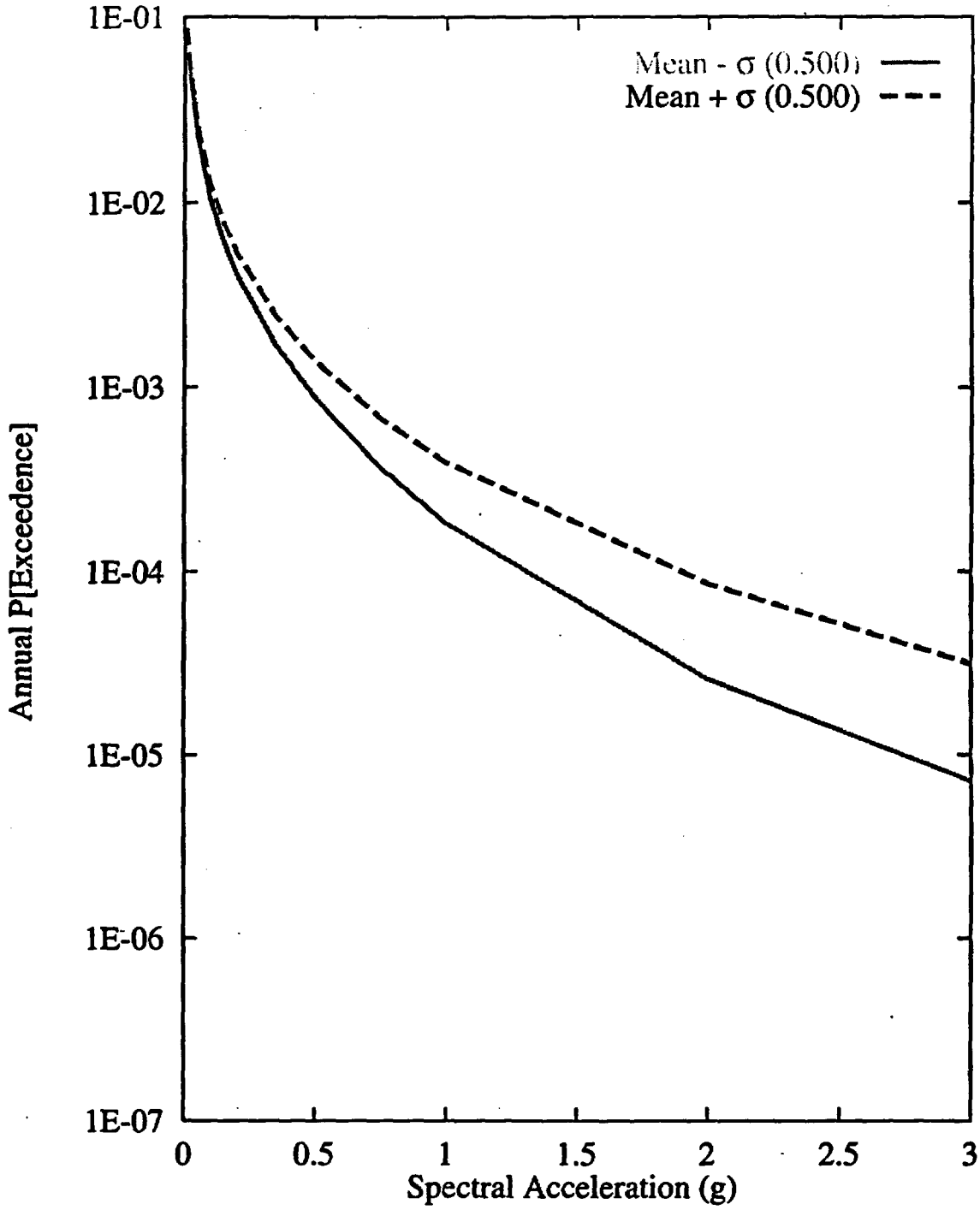

Figure 7-178 Sensitivity of seismic hazard to within-expert epistemic uncertainty in the standard deviation (sigma) of ground motion amplitude: ASM team, 10-Hz horizontal spectral acceleration

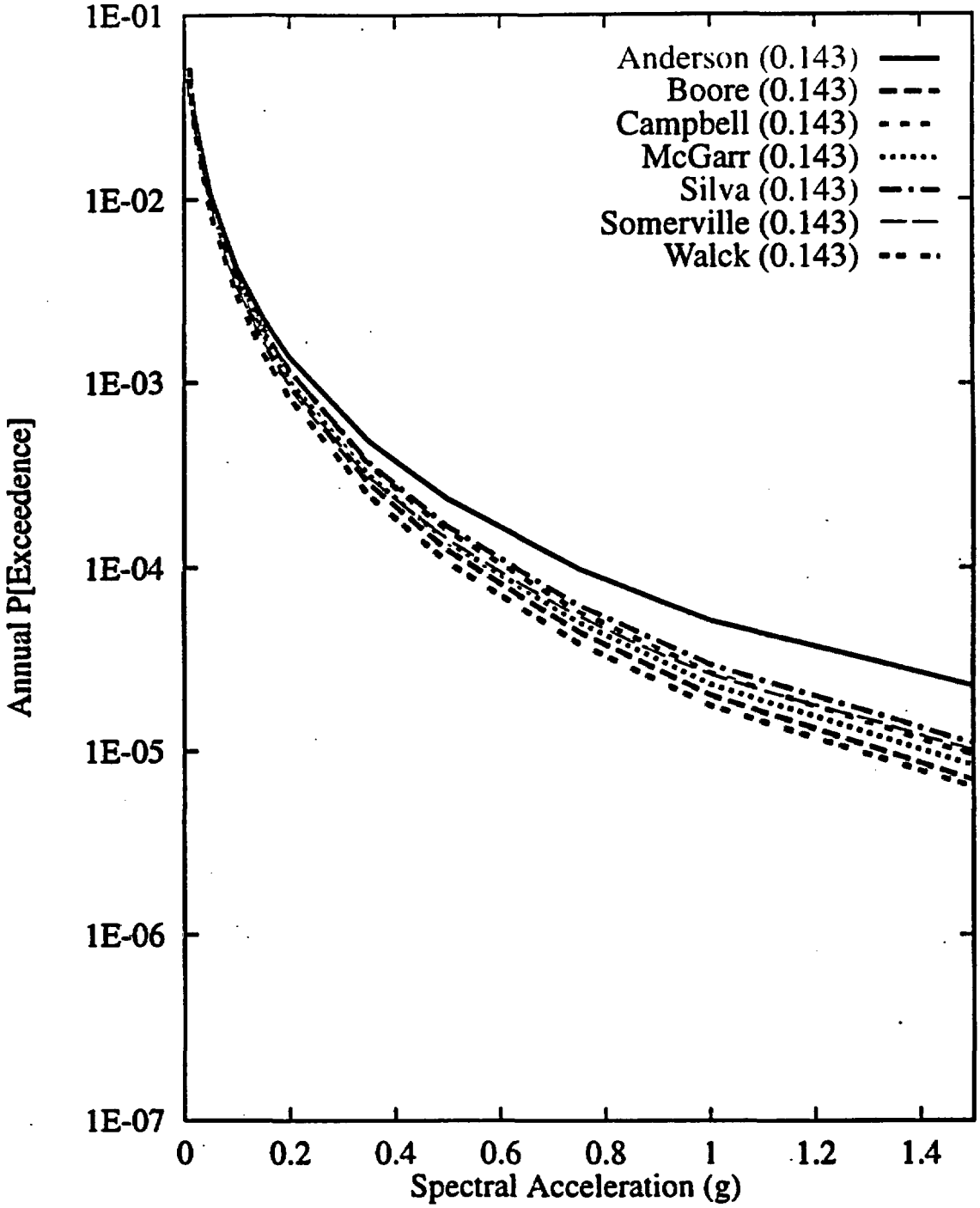

Figure 7-179 Sensitivity of seismic hazard to GM experts: ASM team, 1-Hz horizontal spectral acceleration

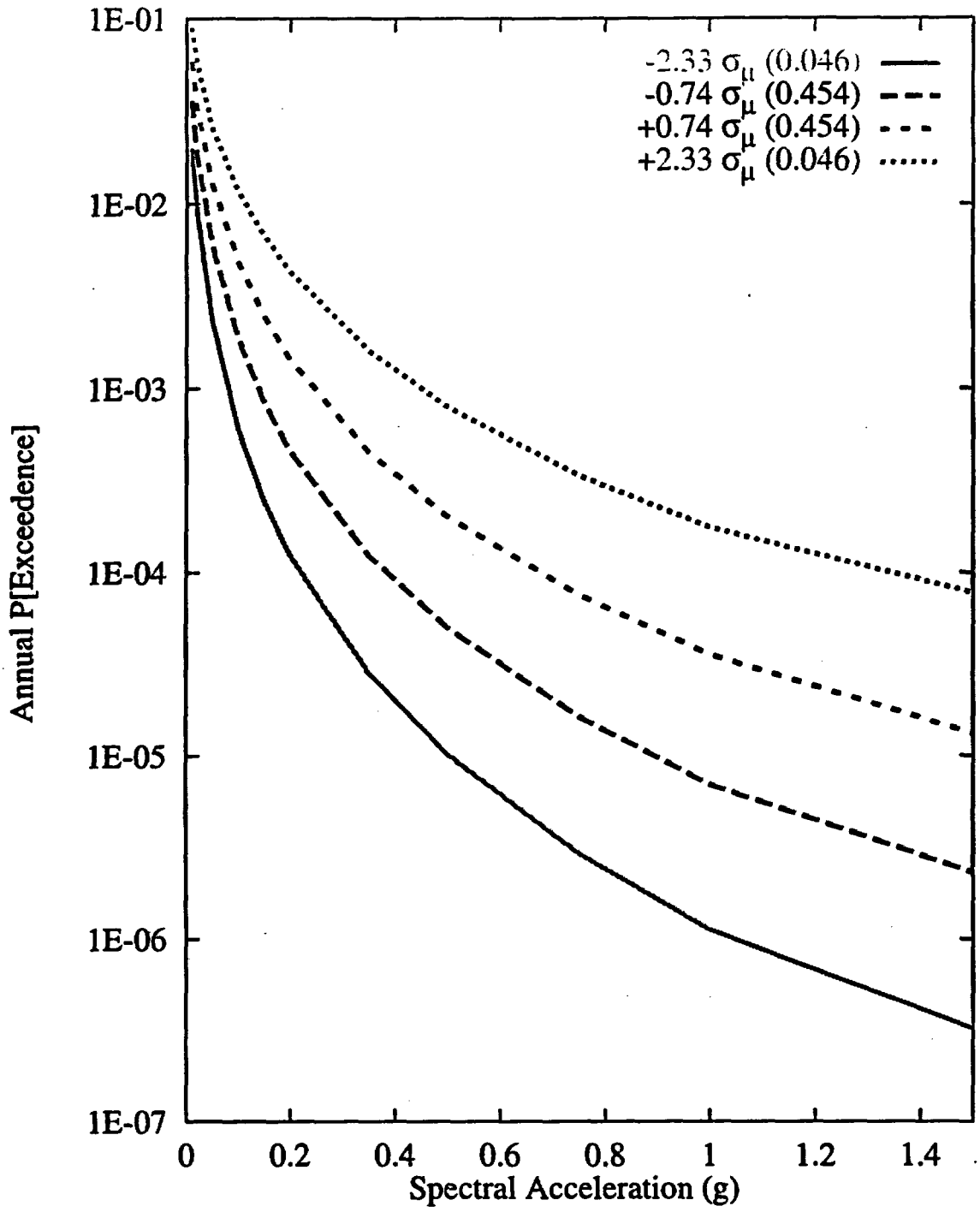

Figure 7-180 Sensitivity of seismic hazard to within-expert epistemic uncertainty in the median ground motion amplitude: ASM team, 1-Hz horizontal spectral acceleration

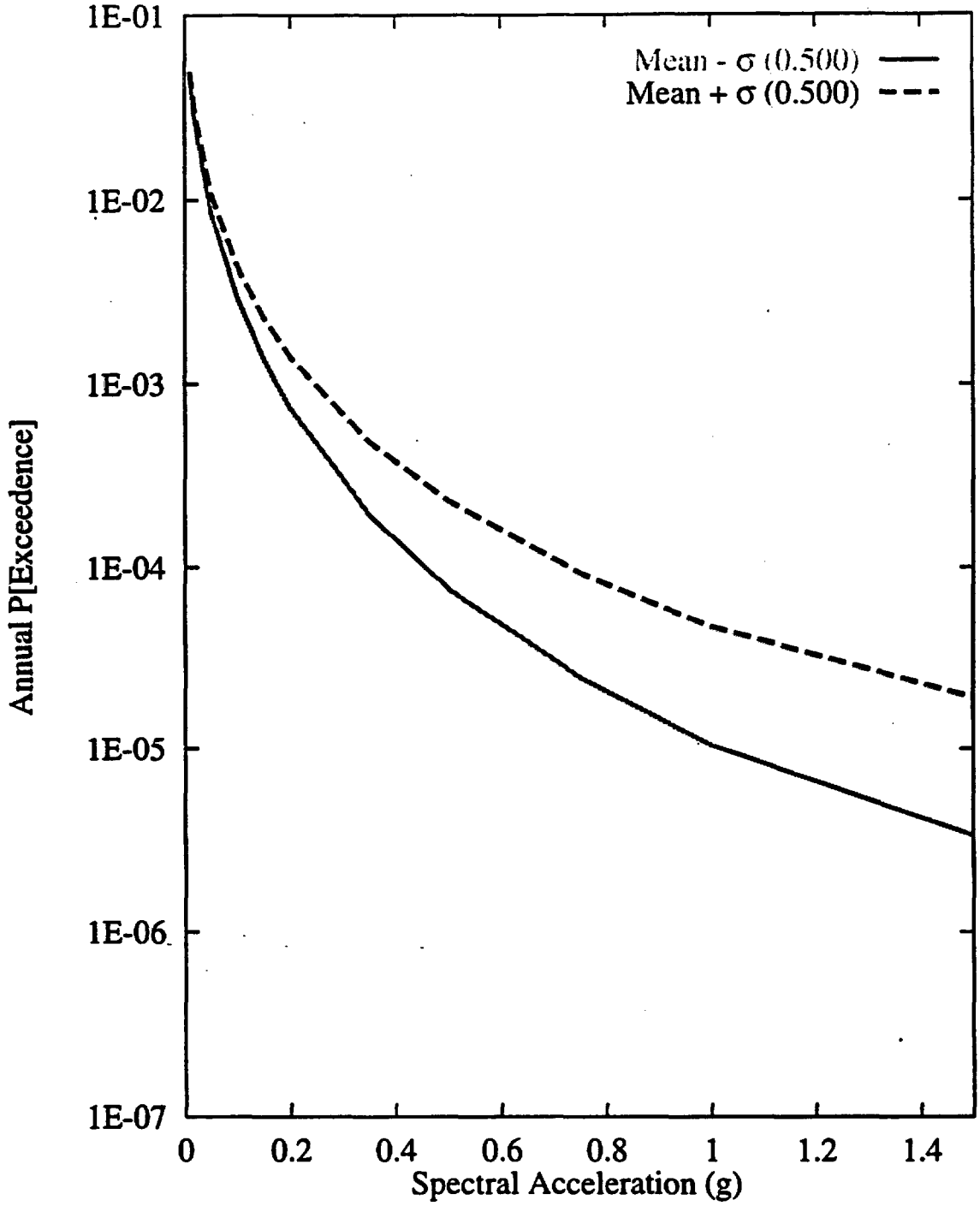

Figure 7-181 Sensitivity of seismic hazard to within-expert epistemic uncertainty in the standard deviation (sigma) of ground motion amplitude: ASM team, 1-Hz horizontal spectral acceleration

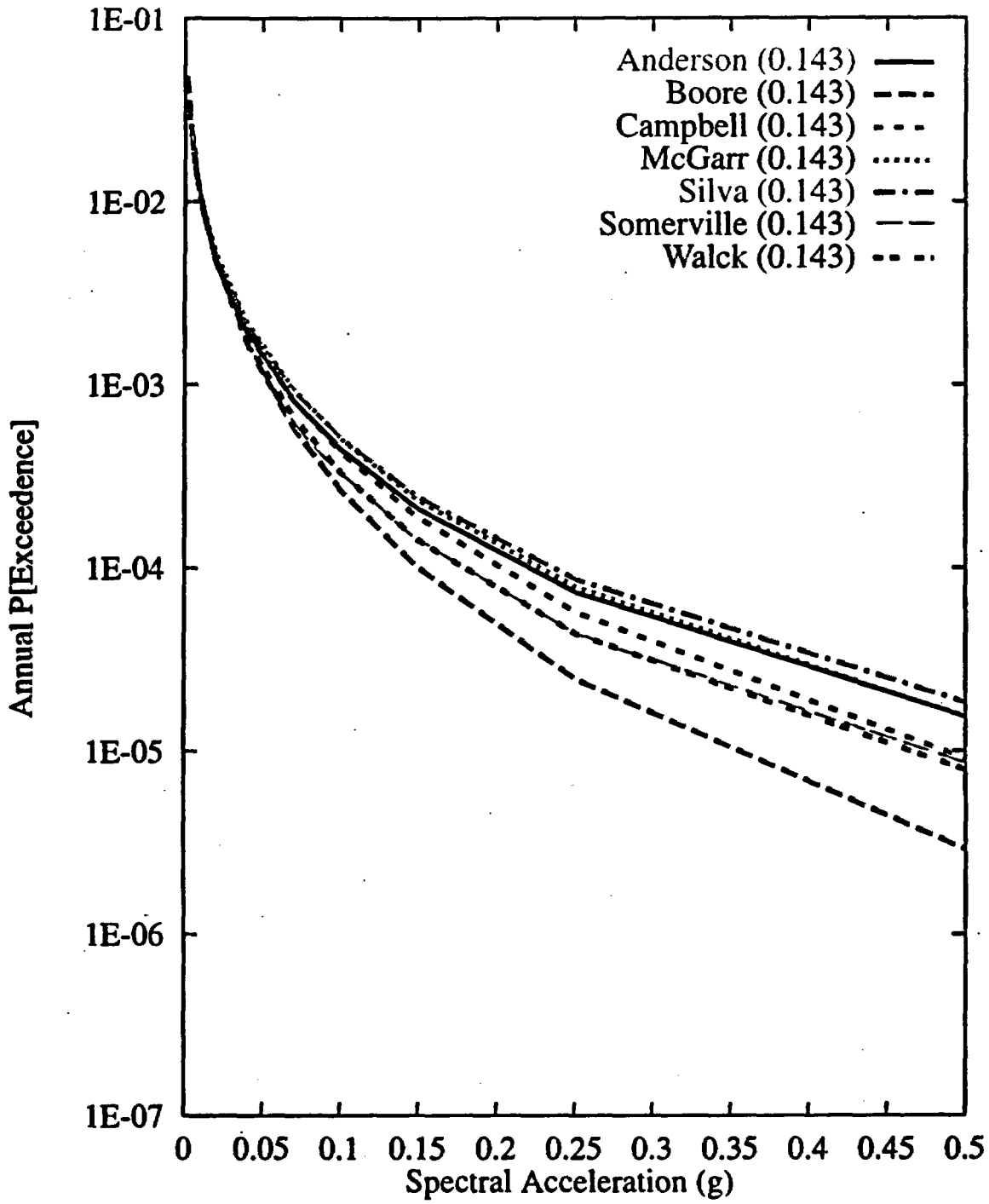

Figure 7-182 Sensitivity of seismic hazard to GM experts:
ASM team, 0.3-Hz horizontal spectral acceleration

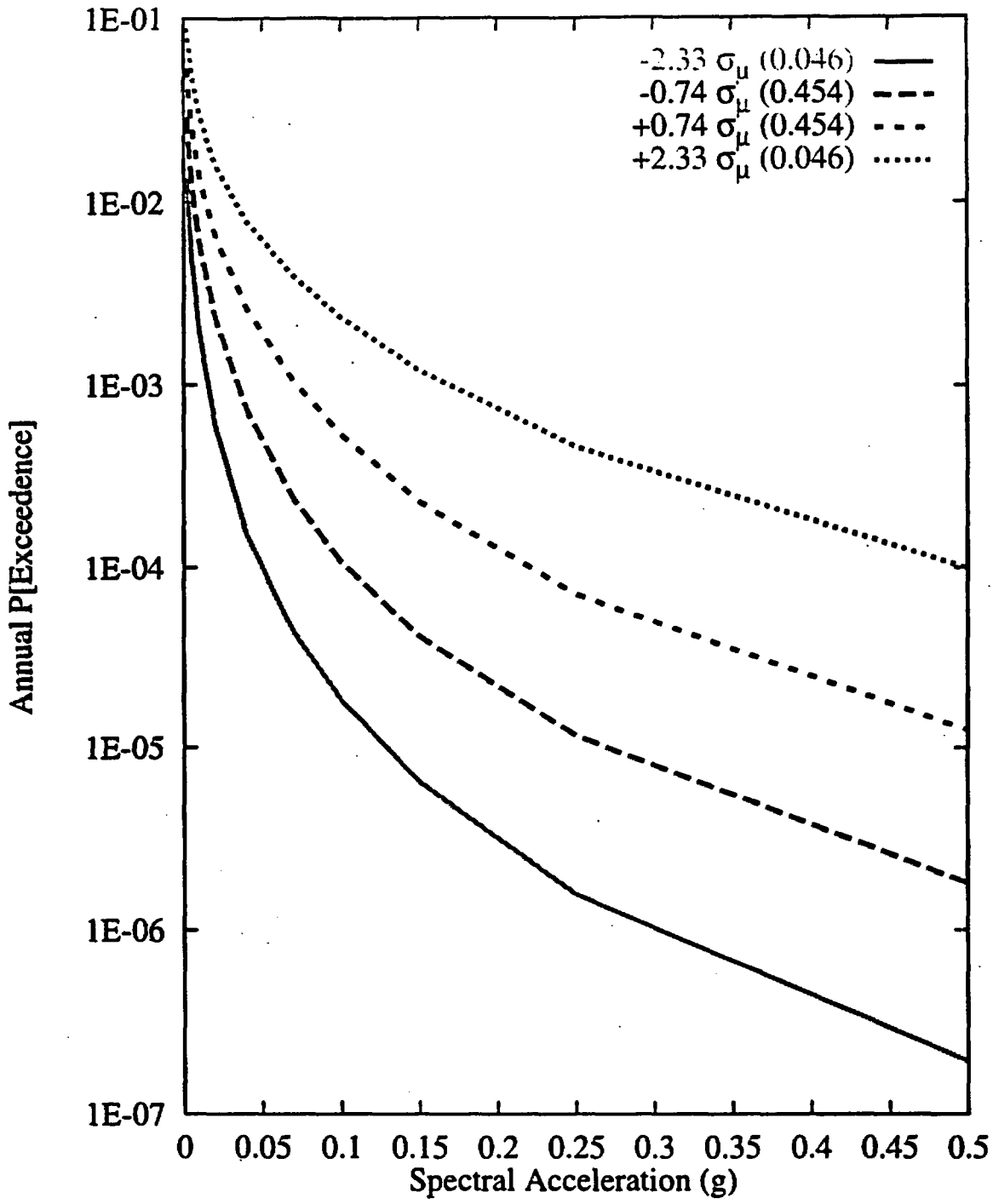

Figure 7-183 Sensitivity of seismic hazard to within-expert epistemic uncertainty in the median ground motion amplitude: ASM team, 0.3-Hz horizontal spectral acceleration

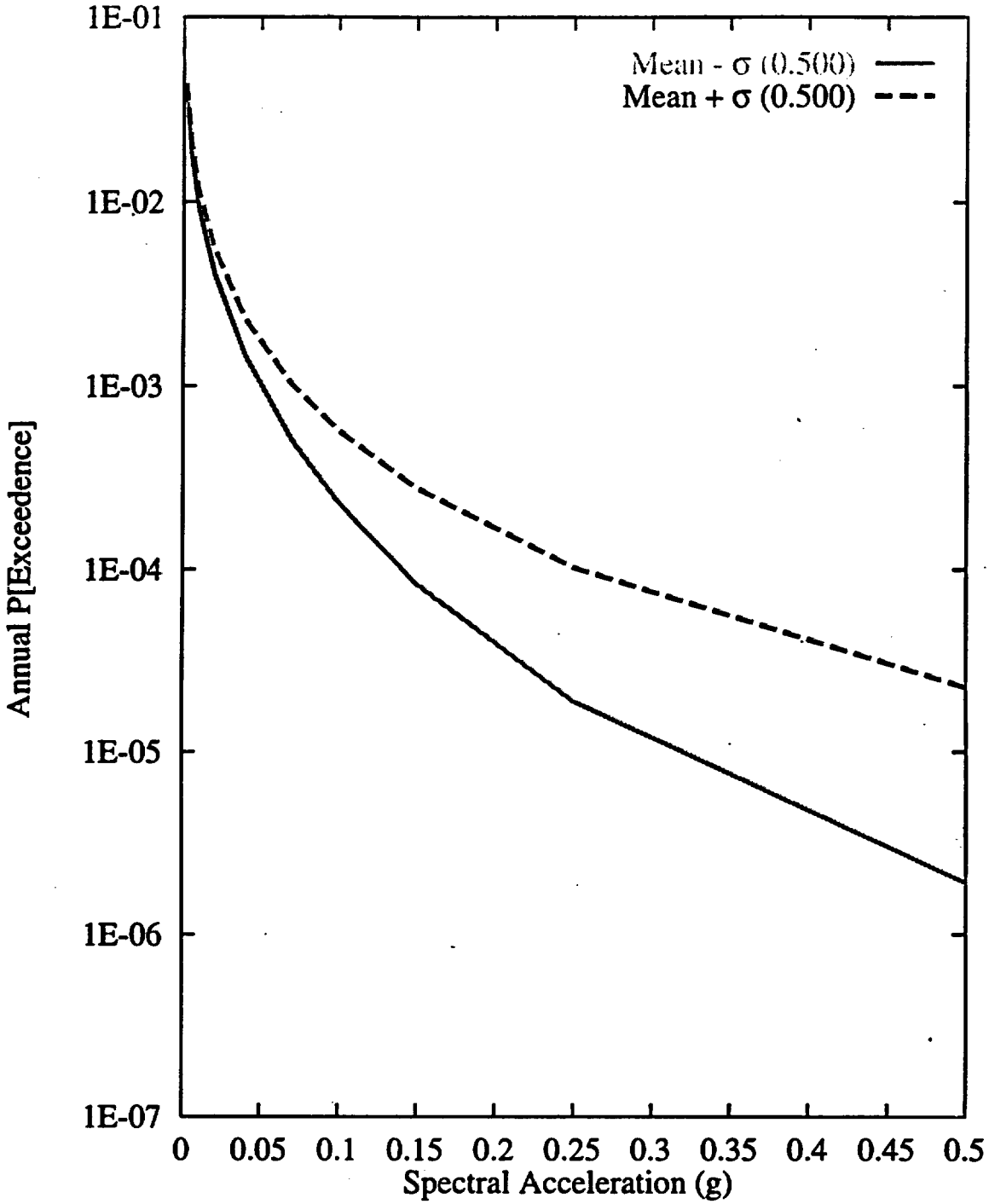

Figure 7-184 Sensitivity of seismic hazard to within-expert epistemic uncertainty in the standard deviation (sigma) of ground motion amplitude: ASM team, 0.3-Hz horizontal spectral acceleration

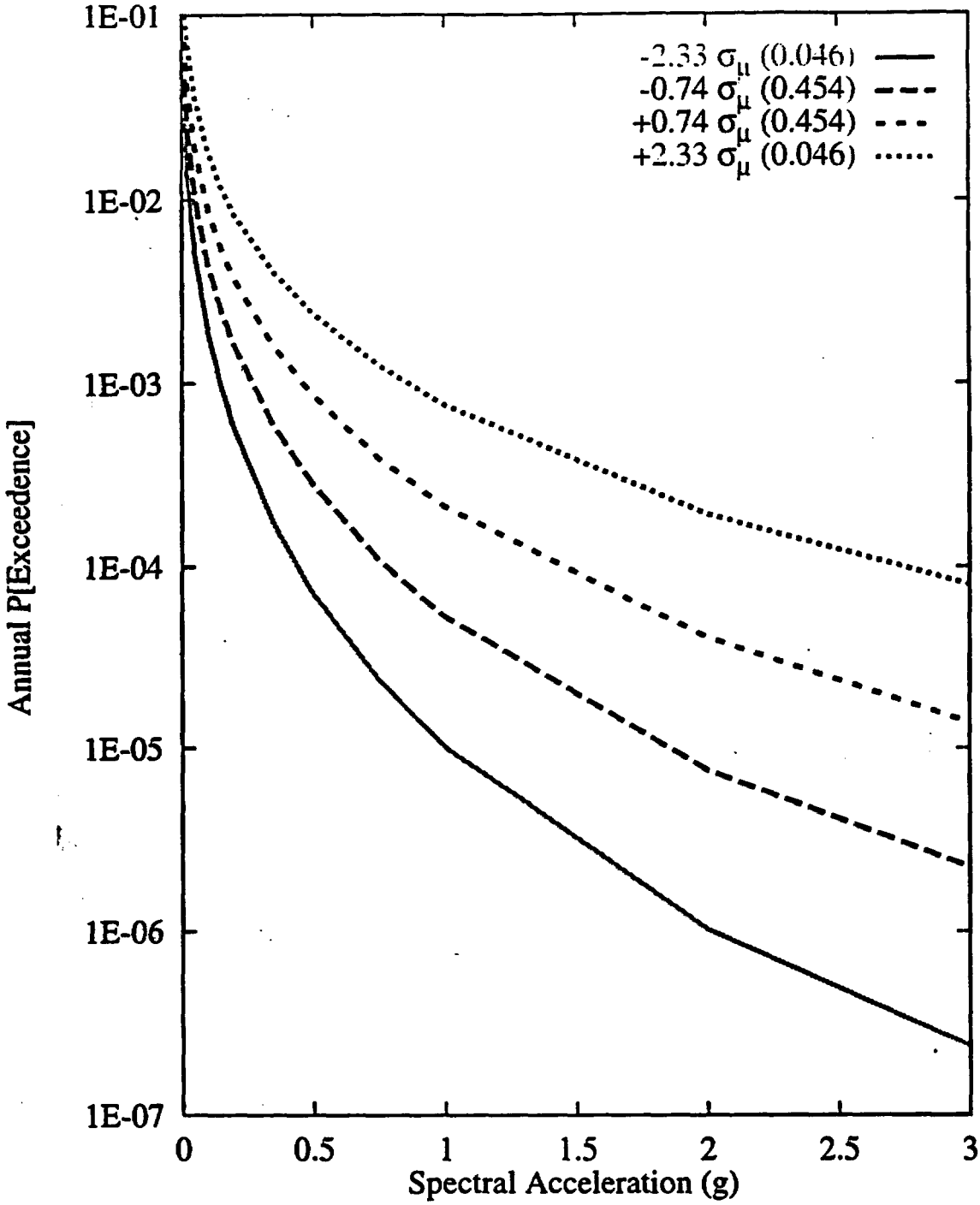

Figure 7-185 Sensitivity of seismic hazard to within-expert epistemic uncertainty in the median ground motion amplitude: ASM team, 10-Hz vertical spectral acceleration

8.0
PSHA METHODOLOGY AND RESULTS FOR FAULT DISPLACEMENT HAZARD

This section describes the methodology used to perform the probabilistic seismic hazard calculations for fault displacement at the Yucca Mountain site and the application of this methodology to nine points (referred to as "sites" in this chapter) within the Controlled Area. Section 8.1 introduces the PSHA methodology for assessing fault displacement hazard. This presentation uses many of the elements and concepts from the ground motion PSHA, which were introduced and described in Chapter 7.0. Section 8.2 presents the results for all nine demonstration sites, including sensitivity analyses.

8.1 PSHA METHODOLOGY FOR FAULT DISPLACEMENT

Fault displacement PSHA results in the probability that the tectonically induced fault displacement at a given site will exceed any value. The site of interest may or may not be on an active fault. Results are in the form of fault displacement hazard curves, which show annual exceedence probability for values of the displacement.

Of the two approaches for fault displacement PSHA described in Section 4.2, the earthquake approach calculates the principal and distributed faulting separately, using different attenuation equations, and then adds them to obtain a total displacement hazard curve. The displacement approach, on the other hand, considers both principal and distributed faulting but does not distinguish between them.

8.1.1 Earthquake Approach

The earthquake approach explicitly considers earthquake magnitudes and locations as intermediate variables in the calculation of fault displacement and uses the same seismic source models (i.e., source geometries and magnitude-recurrence models, and their associated uncertainties) that are used in the ground motion PSHA. The only substantive difference between the earthquake approach for fault displacement PSHA and the ground motion

analysis described in Section 7.0 relates to the attenuation equations. These differences fall into the following two categories:

1. Because both principal and distributed faulting are non-uniformly distributed, there is a probability of no displacement at the site under consideration, given the occurrence of an earthquake in the vicinity of the site. Thus, the attenuation equation is written as the product of two terms: (1) the probability of nonzero displacement given the occurrence of an earthquake of certain characteristics at a given location and (2) the probability that the displacement at the site will exceed a value d*, given non-zero displacement.

2. Both the probability of nonzero displacement and the conditional probability on the amount of displacement depend on a number of quantities besides magnitude and distance. These quantities may be grouped into three categories: (1) geometry of the site relative to the rupture (particularly the along-rupture location x/L defined in Figure 8-1), (2) characteristics of the principal fault (e.g., total length, cumulative displacement), and (3) characteristics of the feature where the site is located (e.g., total length, cumulative displacement).

The resulting attenuation equations for fault displacement are of the form

$$G_D\left(d^* \middle| M, \underline{R}, \underline{X}_{principal}, \underline{X}_{site}\right) = \lambda\left(M, \underline{R}, \underline{X}_{principal}, \underline{X}_{site}\right) \times P\left[D > d^* \middle| D > M, \underline{R}, \underline{X}_{principal}, \underline{X}_{site}\right] \quad (8\text{-}1)$$

where $\underline{R}$ represents the location of the rupture relative to the site (not just distance), and $\underline{X}_{principal}$ and $\underline{X}_{site}$ represent characteristics of the principal fault and site (all quantities in $\underline{X}_{principal}$ and $\underline{X}_{site}$ will be represented by $\underline{X}$ for the sake of brevity). Separate attenuation equations are developed for principal and distributed faulting. The attenuation equation for principal faulting is used only in conjunction with the fault where the site is located, if that fault is active. The attenuation equation for distributed faulting is used for all other faults and for the areal source zone containing the site

The calculation of fault displacement hazard, considering all seismic sources and all earthquake magnitudes, is performed using a modified version of Equation 7-1, namely

$$v(d^*) = \sum_i \nu_i \iint_{\underline{r}\, m} G_D(d^* | m, \underline{r}, \underline{X}) f_{M(i)}(m) f_{\underline{R}(i)|M(i)|}(\underline{r}; m)\, dm\, d\underline{r} \qquad (8\text{-}2)$$

where i indicates source number, ν_i is the rate of earthquakes on source i, $f_{M(i)}(m)$ is the probability density function of magnitude, and $f_{\underline{R}(i)|M(i)|}(\underline{r}; m)$ is the probability density function of earthquake location (given magnitude). The calculation of fault displacement hazard given by the equation above is performed for multiple values of d^*. The result is a hazard curve, which gives the annual probability of exceedance as a function of d^*.

As in the case of ground motions, the primary interest is focused on computing probabilities for large but rare displacements. As a result, the probability of two or more events with $D > d^*$ in one year is negligible. Thus, the quantity on the right side of Equation 8-2, which is the annual rate of earthquakes with displacement $D > d^*$ is a very good approximation to the probability of exceeding displacement d^* in one year. If the quantity of interest is the maximum single-event fault displacement during a long time period T, one can use the equation $P[D_{max}(T) > d^*] = 1 - \exp[-\nu(d^*)T]$. It should be emphasized that these hazard results are applicable to single events. If the quantity of interest is the cumulative displacement from one or more earthquakes over a long time period, which is not the intent in this study, it is necessary to use the theory of compound Poisson processes (Parzen, 1962).

8.1.2 Displacement Approach

The displacement approach uses a direct characterization of the occurrence rate of displacement events at the site and the probability distribution of displacement per event, without using earthquake magnitude and location as intermediate variables. The occurrence rate information may be provided as direct values of the rate λ or in the form of a slip rate SR. Specification of the probability distribution of displacement per event $P[D > d^* | \text{event}]$ is in

the form of a scale parameter (such as the average displacement per event $\overline{D}$, maximum displacement D_{max}, or cumulative displacement D_{cum}) and information about the shape and spread of the distribution.

Calculation of the fault displacement hazard curve for the displacement approach (under the assumption of rare events discussed above) is straightforward, namely:

$$v(d^*) = \lambda \, P[D > d^* | event] \tag{8-3}$$

8.1.3 Treatment of Uncertainty

As with the ground motion PSHA methodology (discussed in Section 7.1), the formulations given above for the earthquake and displacement approaches for the fault displacement PSHA represent the aleatory uncertainty in the natural phenomena of tectonically-induced fault displacement. Mathematically, aleatory uncertainty is represented by the rates and probability distributions in Equations 8-1, 8-2, and 8-3. Epistemic uncertainty is associated with imperfect knowledge about these phenomena. In the earthquake approach, epistemic uncertainty is in the seismic source characterization, the attenuation equations, and the characteristics of the site that affect fault displacement. In the displacement approach, epistemic uncertainty is in the two elements of the model, namely the rate information and the parameters of the displacement per event distribution, as well as in the characteristics of the site that affect fault displacement.

Epistemic uncertainties in seismic source characterization and fault displacement attenuation equations are quantified by considering inputs from the six SSFD expert teams, and by each team's own assessment of epistemic uncertainty. Each expert team selects an approach for fault displacement PSHA (earthquake, displacement, or a weighted combination of both), and then formulates multiple alternative interpretations for the fault displacement attenuation equations (if using the earthquake approach) or for the rate and the distribution of displacement per event (if using the displacement approach). Calculations for the earthquake approach consider each expert team's fault displacement attenuation equations in conjunction with that team's source characterization.

Further details on the fault displacement models developed by the six SSFD expert teams are provided in Sections 4.2 and 4.3.2 and in the expert summaries(Appendix E).

8.1.4 Implementation of Methodology for Fault-Displacement PSHA

In the following, the earthquake and displacement approaches are discussed in the context of the implementation of the PSHA methodology.

8.1.4.1 Earthquake Approach. Calculations for the earthquake approach consider all local faults, as well as the host area source zone(s). The regional faults do not contribute to distributed fault displacement because the distributed displacement attenuation equations decay rapidly with distance, given the models formulated by the SSFD expert teams.

The rate portion of the attenuation equations for principal displacement (i.e., the first term in Equation 8-1) consists of a portion that depends on x/L (i.e., unity for x/L in the interval [0,1], zero otherwise), and a magnitude-dependent portion. The magnitude-dependent portion is a logistic function of magnitude, except for one team that considers the probability distribution of hypocentral depth, the magnitude-dependent rupture width, and the down-dip geometry of the fault. The rate portion of the attenuation equations for fault displacement is a logistic function of magnitude and distance, or peak ground velocity at the site. The rate portion for distributed faulting also includes the probability P[C] that the site is capable of fault displacement. This probability represents epistemic uncertainty (unless it is exactly zero or unity).

The distribution portion of the attenuation equations for principal and distributed displacement (i.e., the second term in Equation 8-1) is specified as an expression for the scale parameter of the distribution (e.g., mean displacement given magnitude, x/L, etc.), and information about the shape and spread of the distribution. For several teams, this expression consists of a product of several random terms. For instance, several teams calculate the principal displacement as the product of the maximum displacement, MD (taken as lognormal, with a median value that depends on magnitude) times a random shape function (which, for a given x/L, takes the form of a beta distribution with parameters that depend on x/L). In all these instances, these products are approximated using lognormal probability

distributions, with medians and coefficients of variation computed using the well-known approximations for products of random variables. The accuracy of all these approximations was tested by comparing the exact and approximate distribution shapes.

There are also situations in which the distribution portion of the attenuation equation for distributed displacement is not a function of the earthquake magnitude or distance, and depends only on some characteristic of the site. This approach constitutes a hybrid between the earthquake and displacement method, where the occurrence portion of the model considers earthquakes, but the distance-distribution portion depends only on the characteristics of the site.

8.1.4.2 Displacement Approach. Although calculation of the hazard curve for this approach does not require integration over magnitudes and distances or summation over seismic sources, a logic tree analysis is required because the expert teams specified multiple alternatives for the various elements of the model and for the characteristics of the site.

8.1.4.3 Models Selected by the SSFD Expert Teams. Each team had the option of using the earthquake approach (chosen by one team), the displacement approach (two teams), and a weighted combination of the two approaches (three teams). The details on each team's approaches are described in Section 4.3.2 and their expert summaries (Appendix E).

8.2 PSHA RESULTS FOR FAULT DISPLACEMENT

The following describes the probabilistic fault displacement hazard calculated at the nine demonstration sites described in Section 4.3.2 and shown in Figure 4-9. Two of the sites have four hypothetical conditions representative of the features encountered within the ESF.

8.2.1 Integrated Results

The integrated results provide a representation of fault displacement hazard and its uncertainty at the nine demonstration sites, based on the interpretations and parameters developed by the six SSFD expert teams. Separate results are obtained for each site in the form of summary hazard curves, which are shown on Figures 8-2 through 8-14. No results

are shown for Sites 7d and 8d because all summary curves for these sites are below an annual exceedance probability of 10^{-8}. Table 8-1 summarizes the mean displacement hazard results for the two annual exceedance probabilities of interest, 10^{-4} and 10^{-5}, at the nine demonstration sites.

With the exception of the block-bounding Bow Ridge and Solitario Canyon faults at 10^{-5} annual exceedance probability, the mean displacements are all less than 0.1 cm. At 10^{-5} probability, the mean displacements are 7.8 and 32 cm, respectively for the two faults (Table 8-1). Thus sites not located on the block-bounding faults such as sites on the intrablock faults, small faults, shear fractures, and intact rock are estimated to undergo displacements of significantly less than 0.1 cm for periods up to 100,000 years.

The mean and median hazard curves indicate the central tendency of the calculated exceedence probabilities. The separation between the 15th- and 85th-percentile curves conveys the effect of epistemic uncertainty on the calculated exceedance probability (note that for some sites the 15th percentile hazard curve, and sometimes the median hazard curve, does not appear on the figure because the entire curve is below 10^{-8} annual exceedance probability). This epistemic uncertainty includes team-to-team, as well as within-team epistemic uncertainty in both the fault displacement models and the source and site characterizations.

The epistemic uncertainty (measured by the distance between the 15^{th} and 85^{th} percentile curves), is higher for sites with no principal faulting, especially for those with the lowest cumulative displacements. Larger epistemic uncertainty at low hazard sites compared to high hazard sites is a common observation when comparing ground motion hazard PSHAs.

In some instances, the mean hazard curve is higher than the 85th percentile hazard curve. This is an indication that the mean hazard is being controlled by an interpretation that has a low weight, but predicts much higher hazard than the majority of the interpretations.

Some of the hazard curves also have a nearly flat portion for low displacements. For instance, Figure 8-3 is nearly flat between 0.1 and 10 cm. This implies that, if there is a

displacement event on Solitario Canyon fault, it is likely to cause a displacement greater than 10 cm.

8.2.2 Comparisons Across Teams

Figures 8-15 through 8-27 show the mean hazard by each team, for all sites except 7d and 8d. Two mean curves are shown for those teams that used two approaches. For Sites 7b, 7c, 8b, and 8c, some teams specified *P[C]*=0, which implies that the hazard is zero. Although these curves are not shown on the figures, they are considered in the calculation of the summary statistics for the site.

Figures 8-15 through 8-27 indicate that variation among the SSFD expert teams is a significant contributor to total uncertainty. Recalling that the differences among the seismic source characterizations by the expert teams were small contributors to uncertainty in the ground motion hazard (Section 7.4.3), we can infer that the large differences among teams seen here are due to differences in the fault displacement models.

8.2.3 Sensitivity Results for Each SSFD Expert Team's Interpretations

Sensitivity results provide insights into the effect of various interpretations and parameters on the calculated seismic hazard and its uncertainty. These results provide insight into the PSHA process. They also provide a consistency check for the experts and analysts.

Sensitivity results are shown for Sites 1 (subject to both principal and distributed faulting) and 7a (subject to distributed faulting only). Several types of results are presented here for each combination of SSFD expert team and approach (earthquake versus fault displacement):

1. Summary hazard curves for that team's approach combination

2. Dominant seismic sources (for the earthquake approach only)

3. Sensitivity to important parameters of the fault displacement attenuation equations (earthquake approach) or to important parameters of the displacement model (displacement approach).

The procedure to generate the sensitivity results is described in Section 7.3.2.

8.2.3.1 AAR Team's Earthquake Approach. Figures 8-28 through 8-31 show the summary hazard curves and dominant seismic sources for Sites 1 and 7a. The most important contributors to hazard at Site 1 are the East-side coalesced system and Areal Source 2 (both contributors to distributed faulting), and the Bow Ridge fault (principal). The most important contributors to hazard at Site 7a are the East-side coalesced system and Areal Source 2.

For Site 1, the alternative displacement attenuation functions have small contributions to epistemic uncertainty. Most of the uncertainty at Site 1 is due to source characterization parameters (not shown), particularly the recurrence parameters for the dominant sources. For Site 7a, parameter beta, which controls the ratio of maximum displacement at the site to maximum displacement on the principal fault, is an important contributor to epistemic uncertainty (Figure 8-32). The AAR earthquake approach for distributed faulting is an example of the hybrid earthquake-displacement approach mentioned earlier. Because the shape of the attenuation equations does not depend on magnitude or distance, the mean hazard curves from all sources have the same shape.

AAR Team's Displacement Approach. Figures 8-33 and 8-34 show the summary hazard curves for Sites 1 and 7a. The hazard curves for the latter site shows a much more rapid drop-off and a slightly higher uncertainty. For Site 1, the most important contributors to uncertainty in the hazard are the cumulative displacement and the slip rate (Figures 8-36 and 8-37). For Site 7a, the most important contributor to uncertainty is parameter beta, which controls the ratio of maximum displacement at the site to maximum displacement on the principal fault (Figure 8-37).

8.2.3.2 ASM Team's Earthquake Approach. Figures 8-38 through 8-41 show the summary hazard curves and dominant seismic sources for Sites 1 and 7a. (The contributions by source on these figures are those obtained using the Borah-Peak reduction factor [70% weight] (Section 4.3.2.1), not the actual mean contributions.) The results for Site 7a show

the effect of truncation at D_{sum}=2 m (Section 4.3.2.1). The most important contributors to hazard at Site 1 are the Stagecoach Road-Paintbrush Canyon (distributed) and Bow Ridge (principal) faults. The most important contributors to hazard at Site 7a are the Solitario Canyon and Stagecoach Road-Paintbrush Canyon faults.

For Site 1, the alternative displacement attenuation functions have small contributions to epistemic uncertainty. Most of the uncertainty at Site 1 is due to source-characterization parameters (not shown), particularly the recurrence parameters for the dominant sources. For Site 7a, the only important uncertainty in the displacement attenuation equations is the model used to scale displacement on the principal fault to distributed displacement at the site (Figure 8-42).

8.2.3.3 DFS Team's Displacement Approach. Figures 8-43 and 8-44 show the summary hazard curves for Sites 1 and 7a. For Site 1, the most important contributors to uncertainty in the hazard are the choice to use the recurrence interval or the average displacement per event $\overline{D}_E$ (both derived from paleoseismic observations; Figure 8-45), the value of $\overline{D}_E$ (Figure 8-46), and the value of the recurrence interval (Figure 8-47). For Site 7a, the most important contributors to uncertainty in the hazard are the capability for fault displacement at the site (Figure 8-48), the value of $\overline{D}_E$ (Figure 8-49), and the value of the recurrence interval (Figure 8-50).

8.2.3.4 RYA Team's Displacement Approach. Figures 8-51 and 8-52 show the summary hazard curves for Sites 1 and 7a. For Site 1, the most important contributors to uncertainty in the hazard are the recurrence interval (Figure 8-53) and the distribution shape (Figure 8-54). For Site 7a, the most important contributors to uncertainty in the hazard are parameter beta (discussed above for AAR and ASM; Figure 8-55), and the expression used in the calculation of slip rates from cumulative displacements (Figure 8-56).

8.2.3.5 SBK Team's Earthquake Approach. Figures 8-57 through 8-60 show the summary hazard curves and dominant seismic sources for Sites 1 and 7a. The most important contributors to hazard at Site 1 are the Stagecoach Road-Paintbrush Canyon fault and the Basin and Range source zone (both distributed) and the Bow Ridge fault (principal). The

most important contributors to hazard at Site 7a are the Basin and Range source zone and the Stagecoach Road-Paintbrush Canyon and Solitario Canyon faults.

For both Sites 1 and 7a, the alternative displacement attenuation functions have small contributions to epistemic uncertainty. The most important among these is the model for the probability of displacement given an event (not shown), for which SBK uses two models. The first model is a logistic function in terms of magnitude and distance. The second model is a logistic function in terms of the peak ground velocity predicted by the ground motion models. Although the latter model predicts higher hazard, its contribution to epistemic uncertainty is small because it has a weight of only 10%.

SBK Team's Displacement Approach. Figures 8-61 through 8-62 show the summary hazard curves for Sites 1 and 7a. For Site 1, the most important contributors to uncertainty in the hazard are the average displacement per event (Figure 8-63) and the recurrence interval (Figure 8-64). Site 7a has no important contributors to uncertainty in the hazard, as indicated by the tight clustering of the fractile hazard curves on Figure 8-62.

8.2.3.6 SDO Team's Earthquake Approach. Figures 8-65 through 8-68 show the summary hazard curves and dominant seismic sources for Sites 1 and 7a. For both Sites 1 and 7a, the alternative displacement attenuation functions have small contributions to epistemic uncertainty. Source characteristics also have a small contribution to epistemic uncertainty, as indicated by the tight clustering of the fractile hazard curves on Figures 8-65 and 8-66.

SDO Team's Displacement Approach. Figure 8-69 shows the summary hazard curves for Site 7a (no results are shown for Site 1 because SDO does not apply the displacement approach to sites with principal faulting). The most important contributors to uncertainty in the hazard are the ratio beta (Figure 8-70), the procedure to calculate the average displacement per event (Figure 8-71; SDO uses the procedures formulated by the AAR and SBK teams), and the procedure to calculate slip rate from cumulative displacement (Figure 8-72).

8.3 SUMMARY

The results shown here illustrate the wide diversity in approaches used to evaluate fault displacement hazard (Section 4.3.2.1). This diversity is indicative of the state of practice in PSHA for fault displacement, which is less mature than PSHA for ground motions. Nonetheless, the results obtained here are considered robust by virtue of the extensive efforts at expert elicitation and feedback, as well as the methodological developments, that were undertaken as part of this study. In addition, much of the experience in ground motion PSHA can be transferred into fault displacement PSHA. Sites with the highest fault displacement hazard show uncertainties comparable to those obtained in ground motion PSHA. Sites with low hazard show much higher uncertainties.

There is also an interesting, but not unexpected, correlation between the amount of geologic data available at a site and the uncertainty in the calculated hazard at that site. For Sites 1 and 2, where there are significant geologic data, and even for Site 4 where there are some geologic constraints, the scatter among teams is less than one order of magnitude. For Sites 3, 5, 6, 7a, 7b, 8a, and 8b, the individual team curves span three orders of magnitude. These are the sites for which there are little or no data. The calculated hazard for these sites is driven largely by models.

Regarding the latter group of sites, it is important to note that most of the uncertainty relates to the lower portion of the epistemic distribution, as one can verify by noting that the mean and 85th percentile curves are relatively close to each other, whereas the 15th percentile curve is often much lower, if not lower than 10^{-8} (e.g., Figures 8-8 and 8-9). This implies that the experts agree that the hazard at these sites is low or very low, but they do not agree on how low it is.

TABLE 8-1
MEAN DISPLACEMENT HAZARD AT NINE DEMONSTRATION SITES

Site	Location	Mean Displacement (cm) Annual Exceedance Probability 10^{-4}	10^{-5}
1	Bow Ridge fault	<0.1	7.8
2	Solitario Canyon fault	<0.1	32
3	Drill Hole Wash fault	<0.1	<0.1
4	Ghost Dance fault	<0.1	<0.1
5	Sundance fault	<0.1	<0.1
6	Unnamed fault west of Dune Wash	<0.1	<0.1
7	100 m east of Solitario Canyon fault		
7a	2-m small fault	<0.1	<0.1
7b	10-cm shear	<0.1	<0.1
7c	fracture	<0.1	<0.1
7d	intact rock	<0.1	<0.1
8	Between Solitario Canyon and Ghost Dance faults		
8a	2-m small fault	<0.1	<0.1
8b	10-cm shear	<0.1	<0.1
8c	fracture	<0.1	<0.1
8d	intact rock	<0.1	<0.1
9	Midway Valley	<0.1	0.1

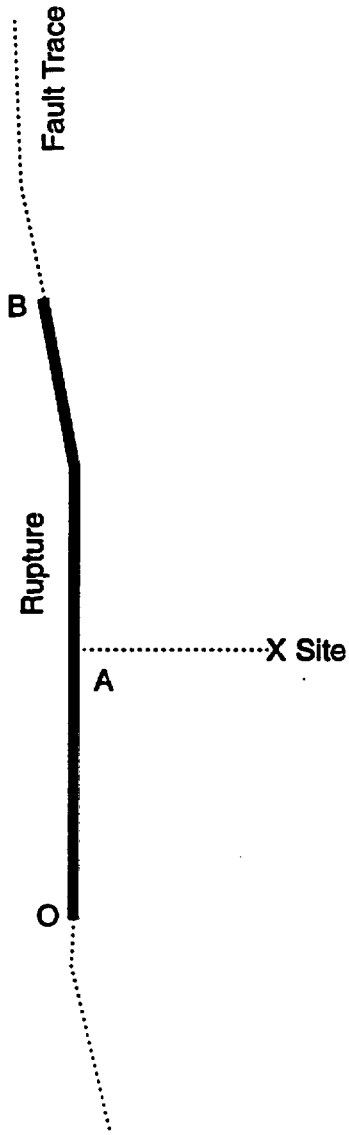

Figure 8-1 Definition of the along-strike location x/L (plane view). OX is the shortest distance from the site to the rupture. x/L is defined as OA/OB or AB/OB, whichever is smallest.

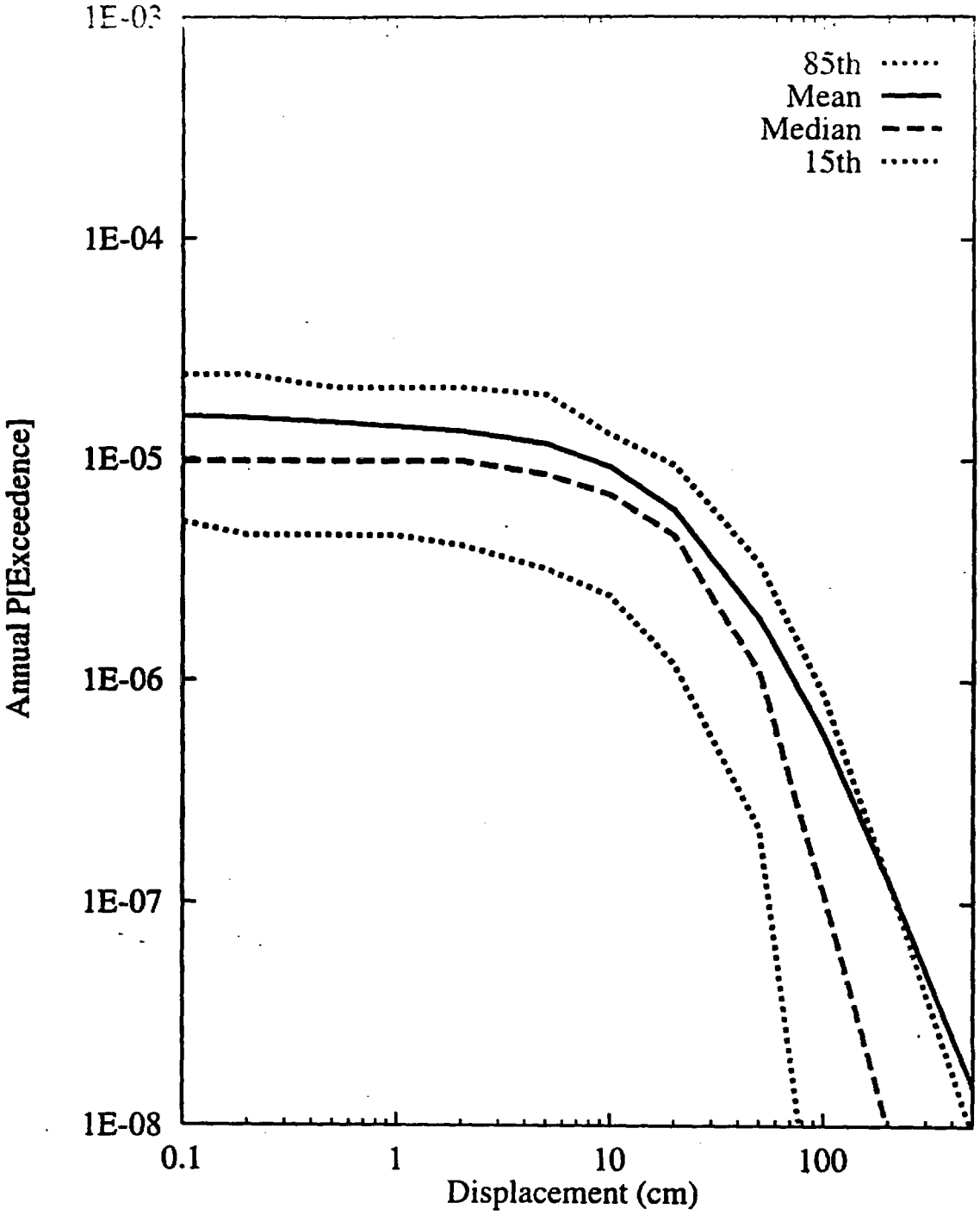

Figure 8-2 Integrated seismic hazard results: summary hazard curves for Site 1, Bow Ridge fault

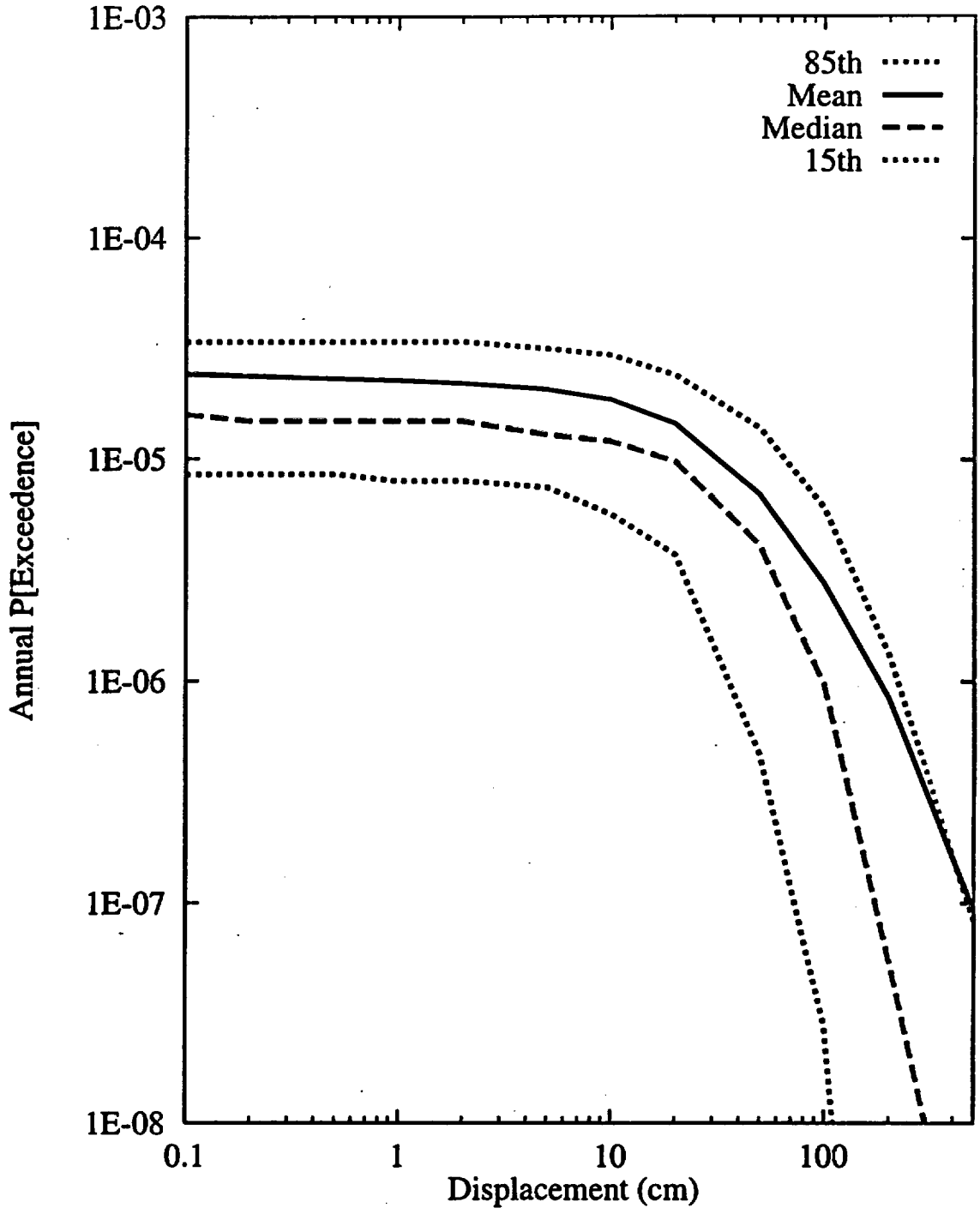

Figure 8-3 Integrated seismic hazard results: summary hazard curves for Site 2, Solitario Canyon fault

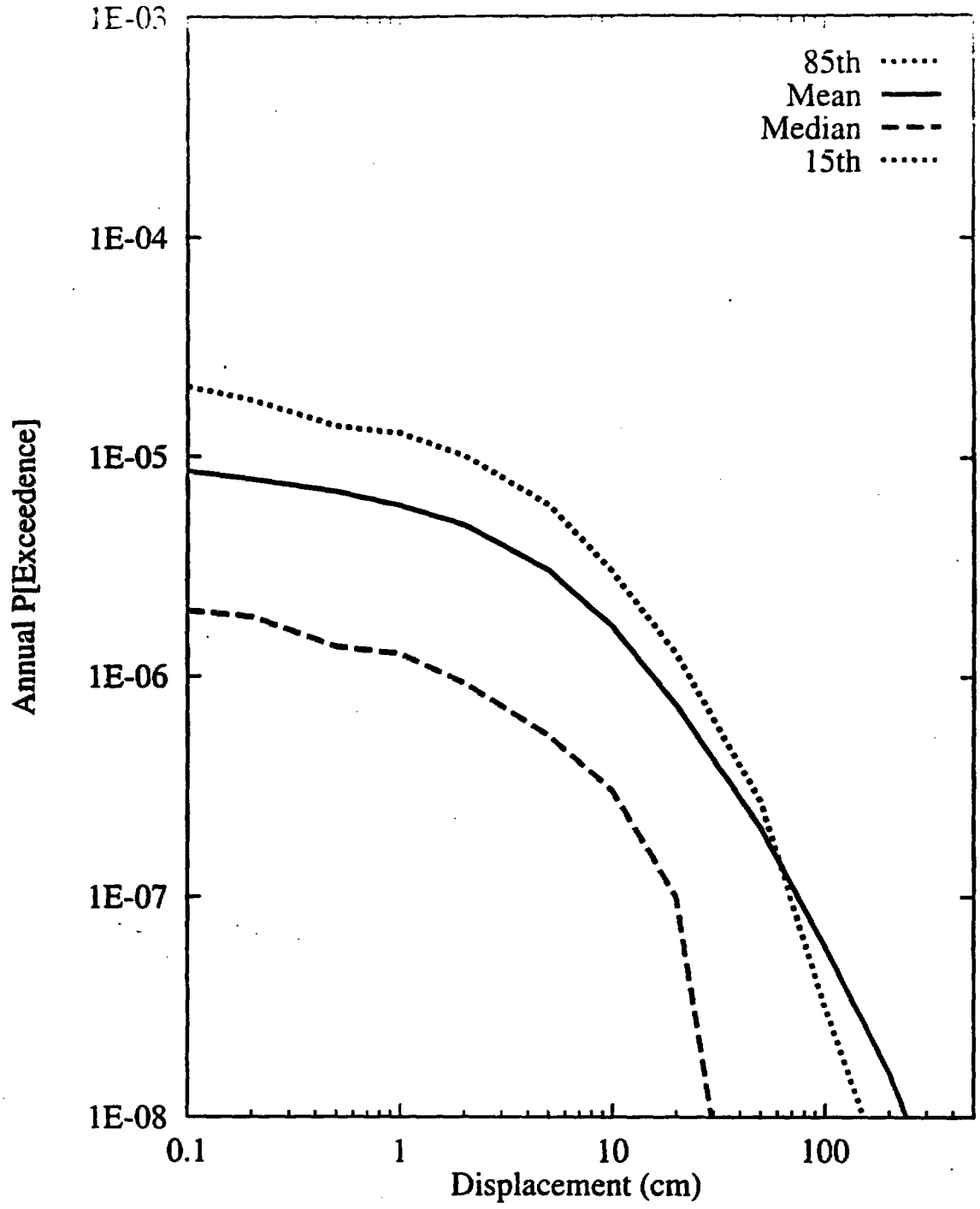

Figure 8-4 Integrated seismic hazard results: summary hazard curves for Site 3, Drill Hole Wash fault

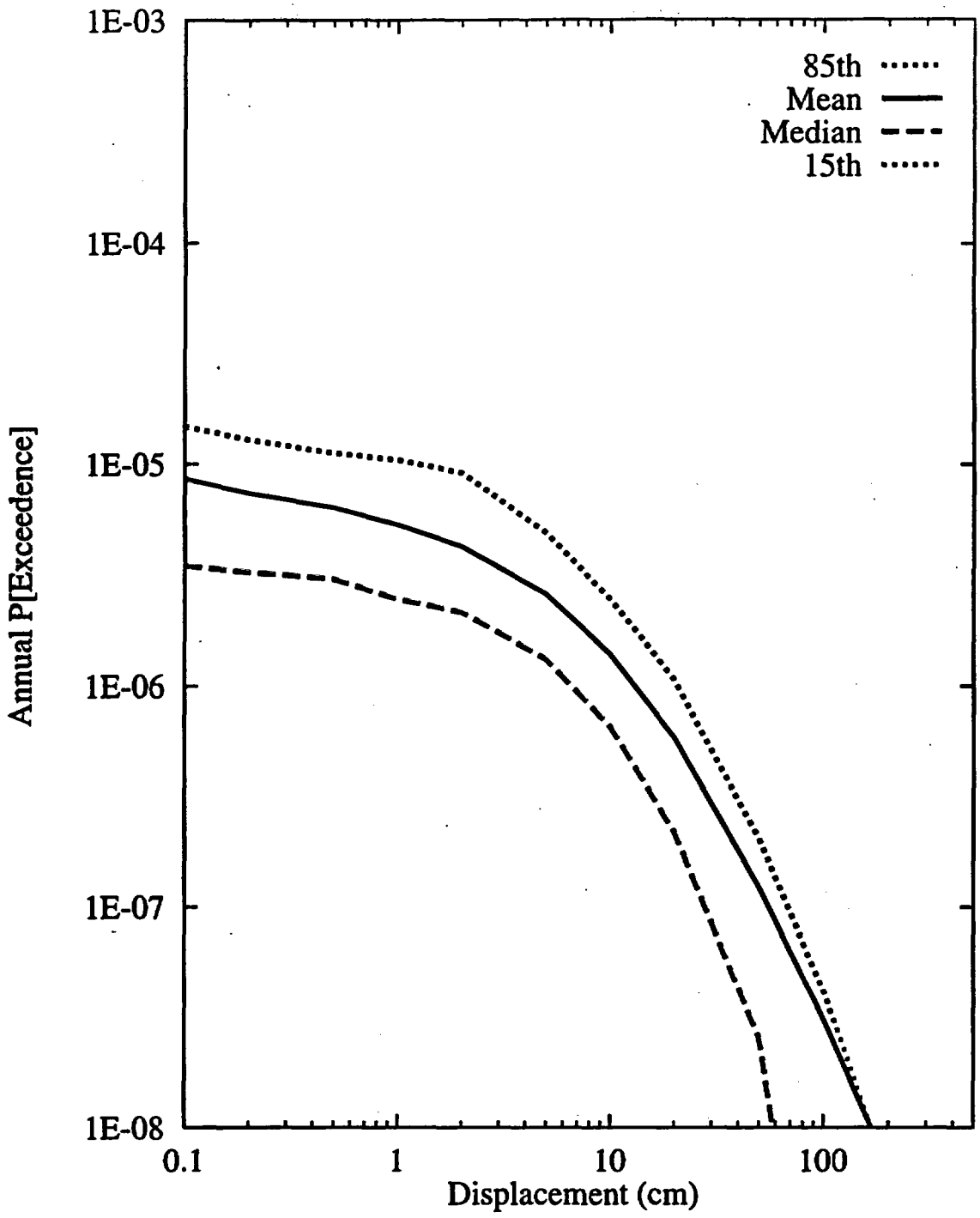

Figure 8-5 Integrated seismic hazard results: summary hazard curves for Site 4, Ghost Dance fault

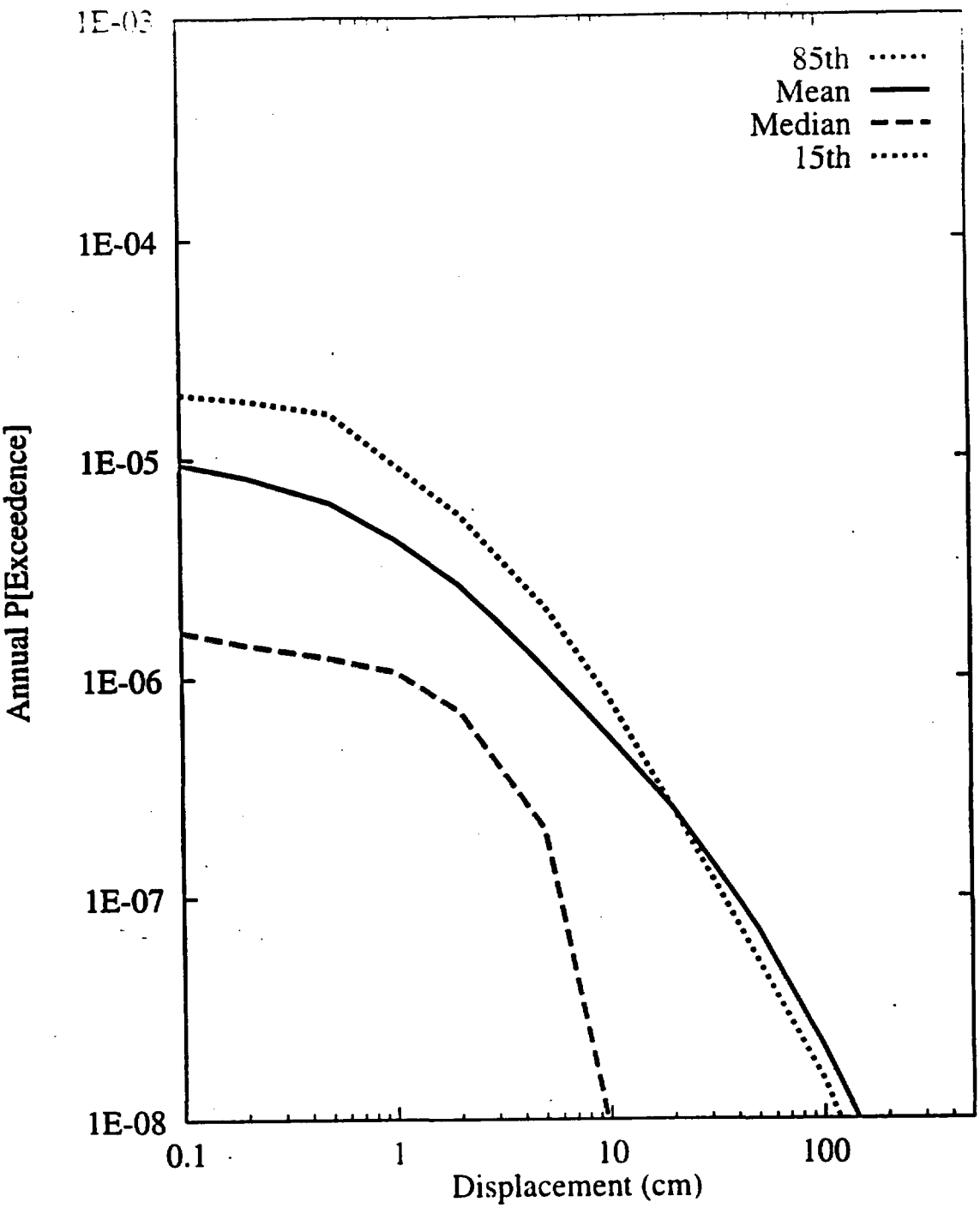

Figure 8-6 Integrated seismic hazard results: summary hazard curves for Site 5, Sundance fault

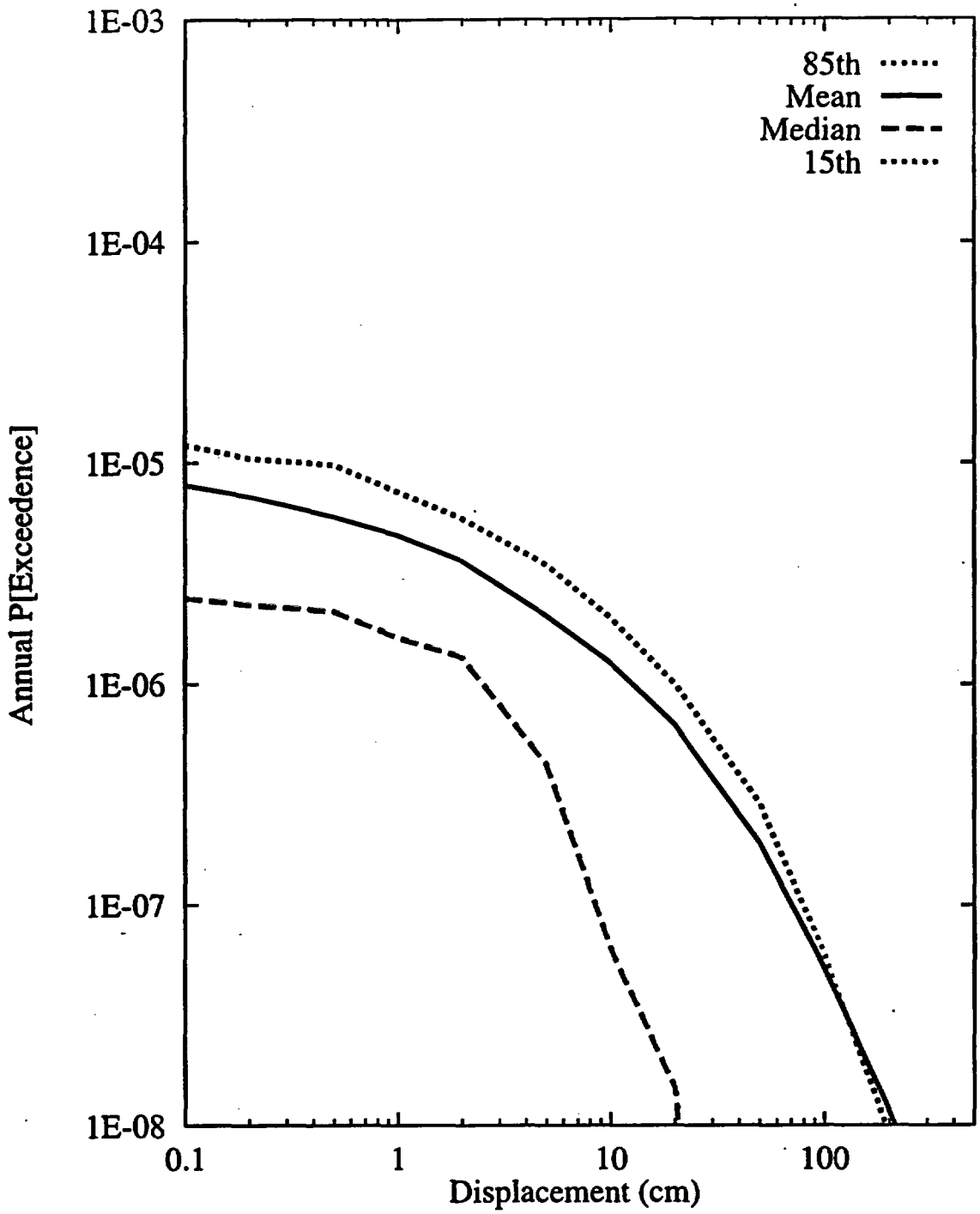

figure 8-7 Integrated seismic hazard results: summary hazard curves for Site 6, unnamed fault west of Dune Wash

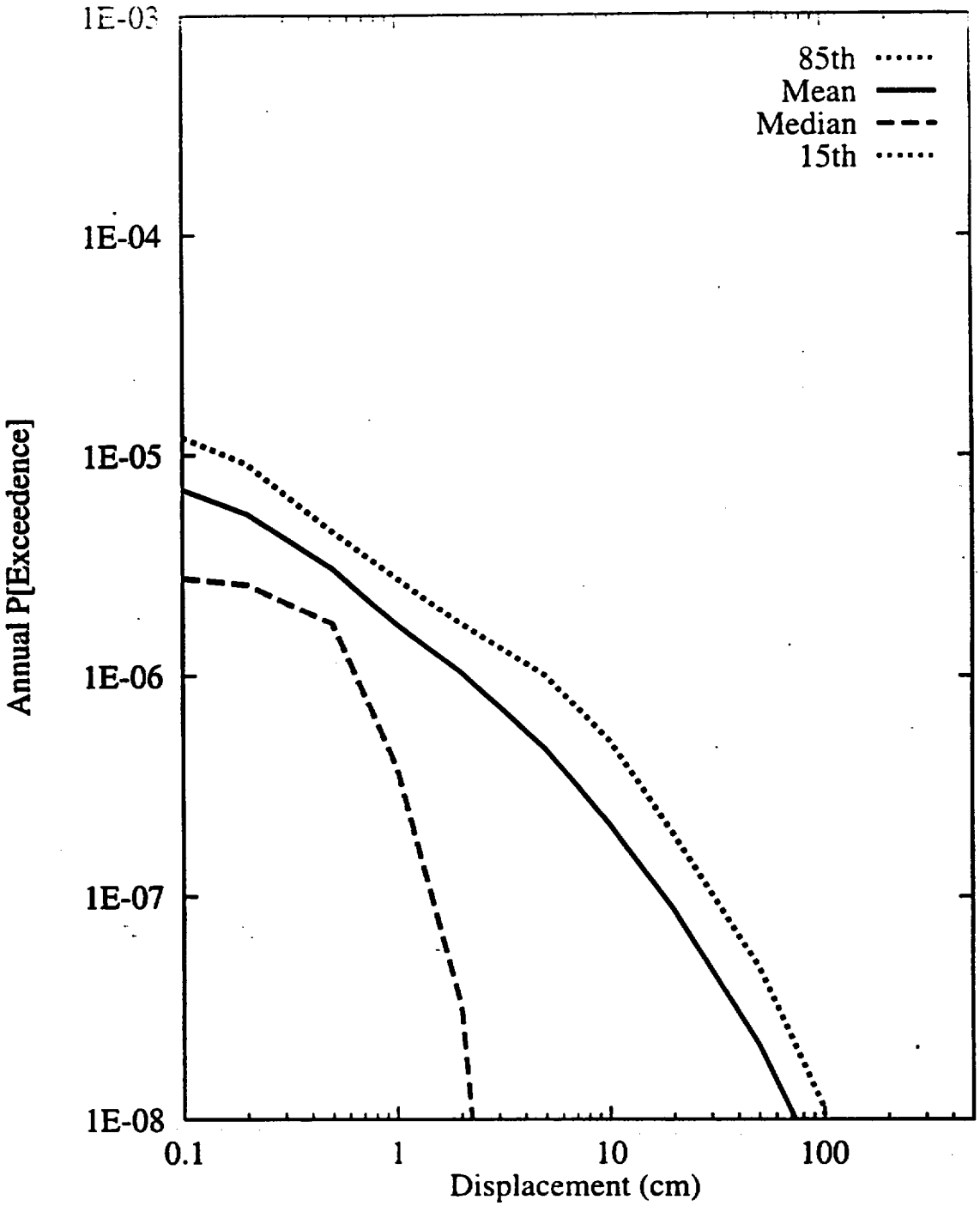

Figure 8-8 Integrated seismic hazard results: summary hazard curves for Site 7a, 100m east of Solitario Canyon fault (2m cumulative displacement)

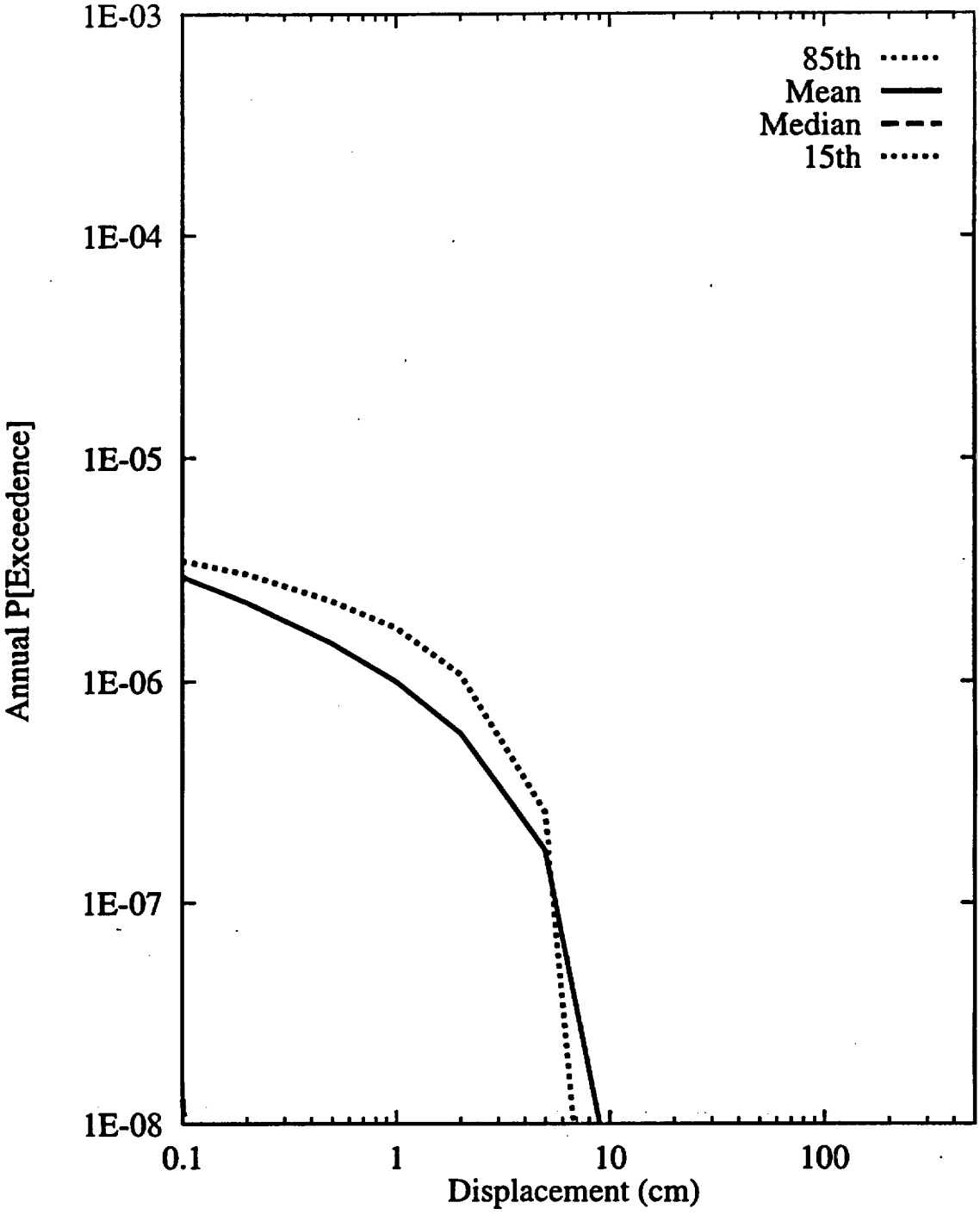

Figure 8-9 Integrated seismic hazard results: summary hazard curves for Site 7b, 100m east of Solitario Canyon fault (10cm cumulative displacement)

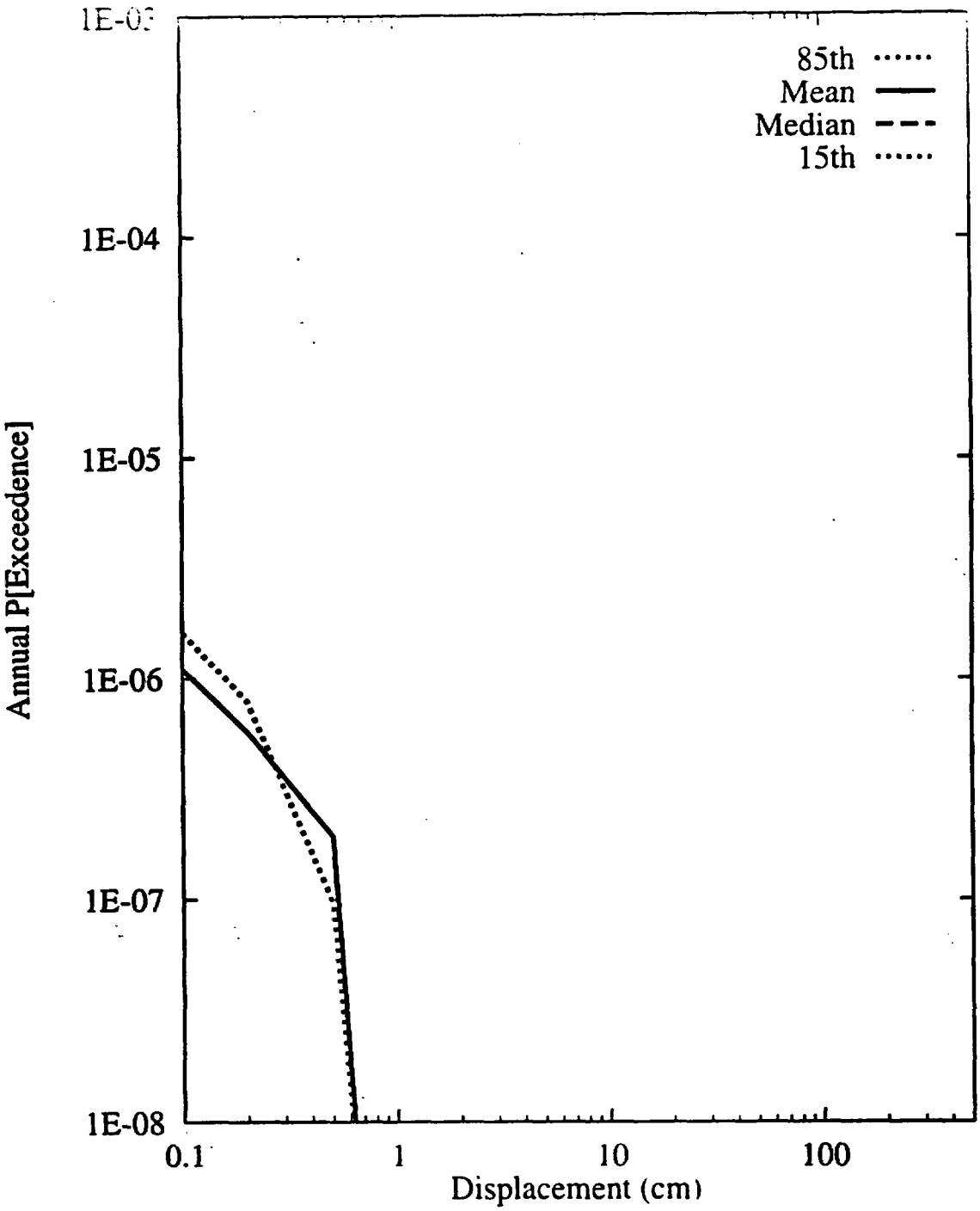

Figure 8-10 Integrated seismic hazard results: summary hazard curves for Site 7c, 100m east of Solitario Canyon fault (no measurable cumulative displacement)

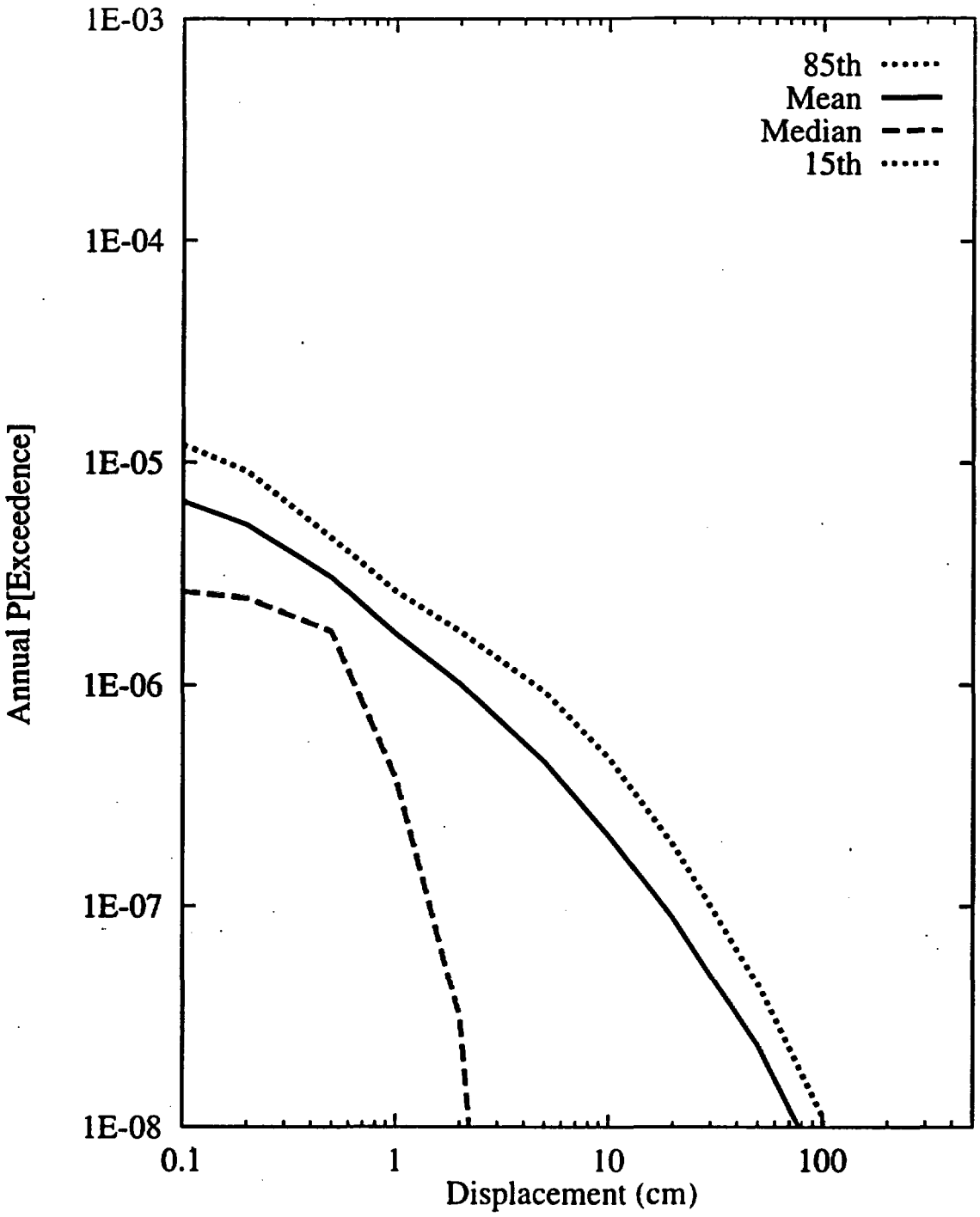

Figure 8-11 Integrated seismic hazard results: summary hazard curves for Site 8a, midway between the Ghost Dance and Solitario Canyon faults (2m cumulative displacement)

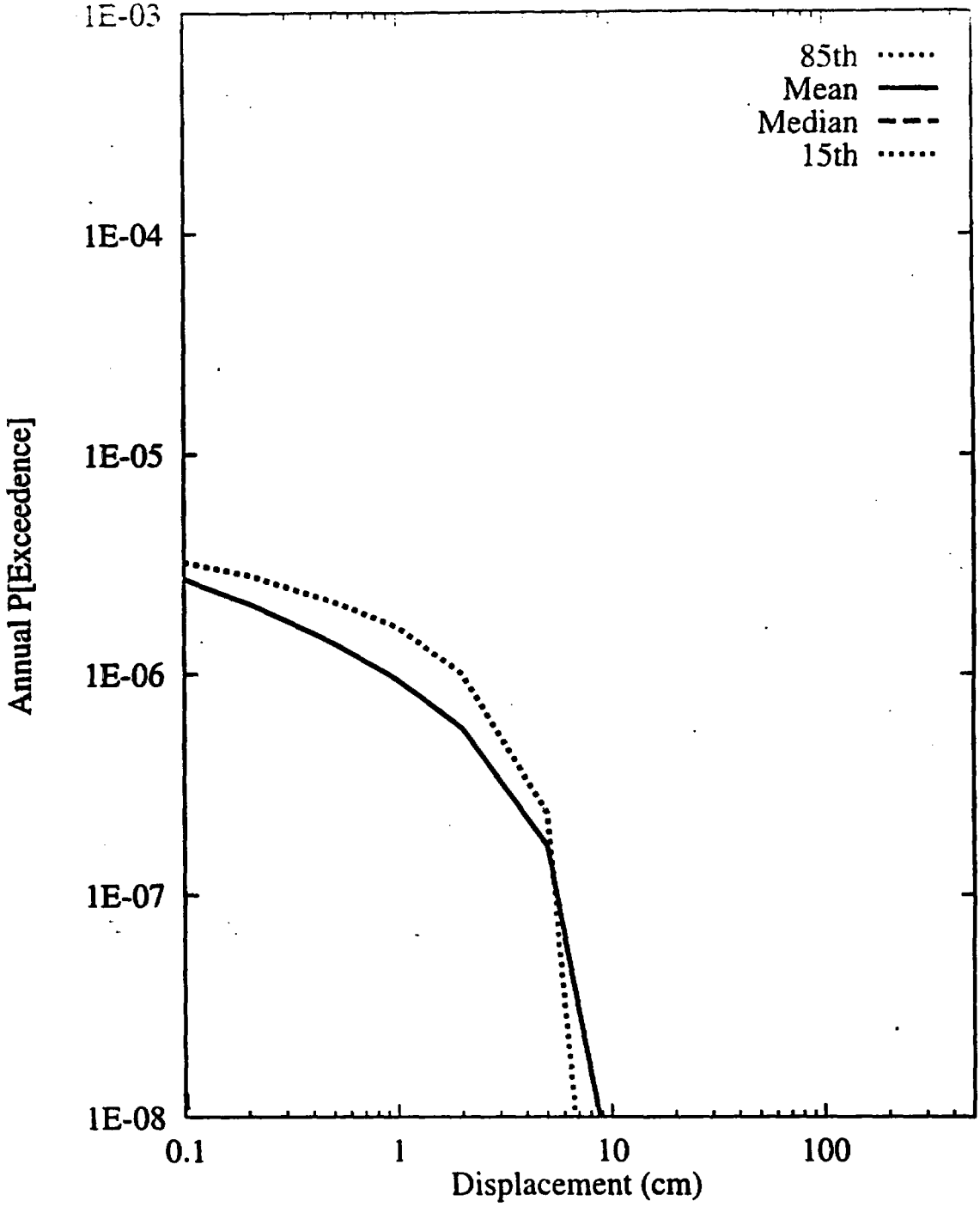

Figure 8-12 Integrated seismic hazard results: summary hazard curves for Site 8b, midway between the Ghost Dance and Solitario Canyon faults (10cm cumulative displacement)

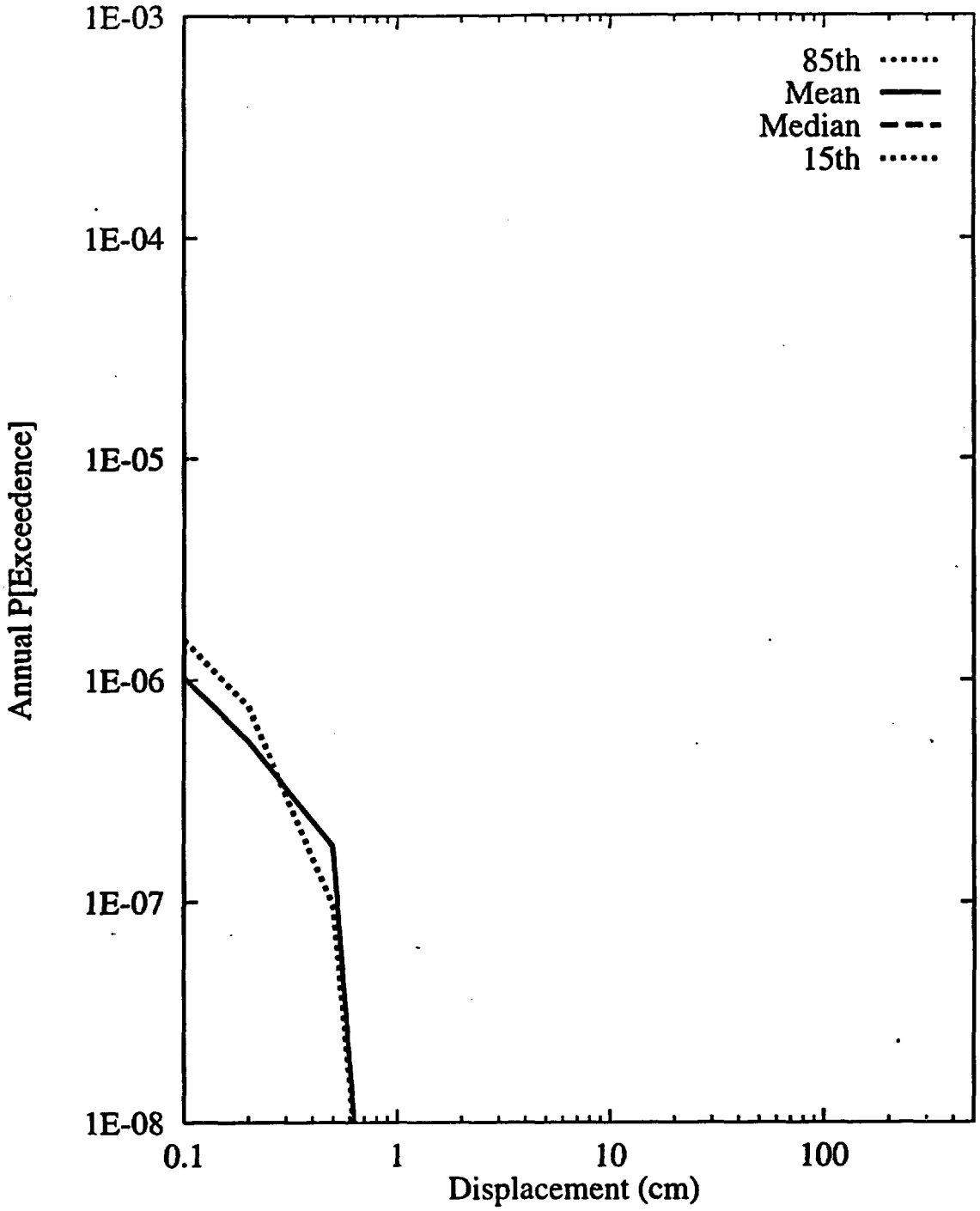

Figure 8-13 Integrated seismic hazard results: summary hazard curves for Site 8c, midway between the Ghost Dance and Solitario Canyon faults (no measurable cumulative displacement)

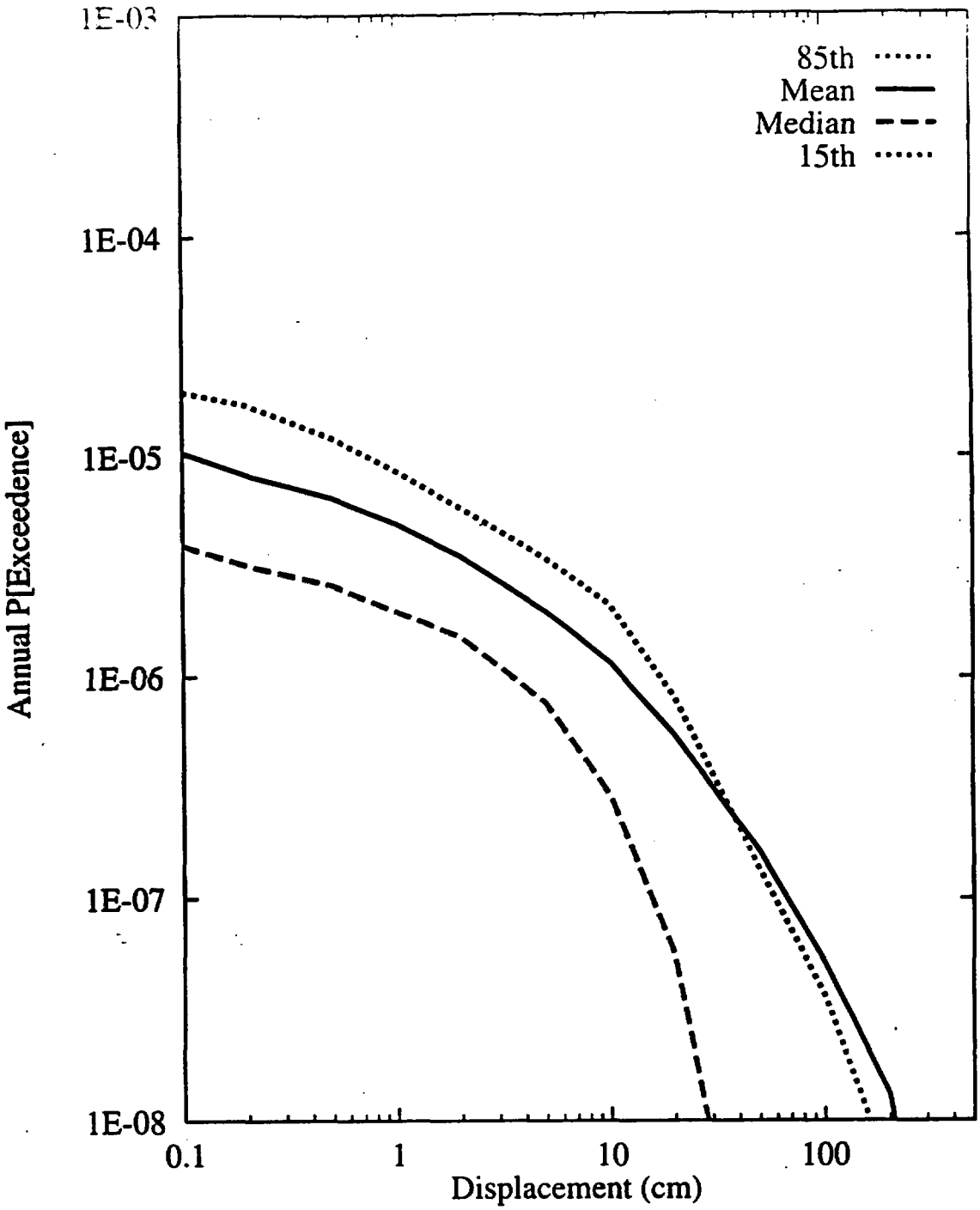

Figure 8-14 Integrated seismic hazard results: summary hazard curves for Site 9, Midway Valley

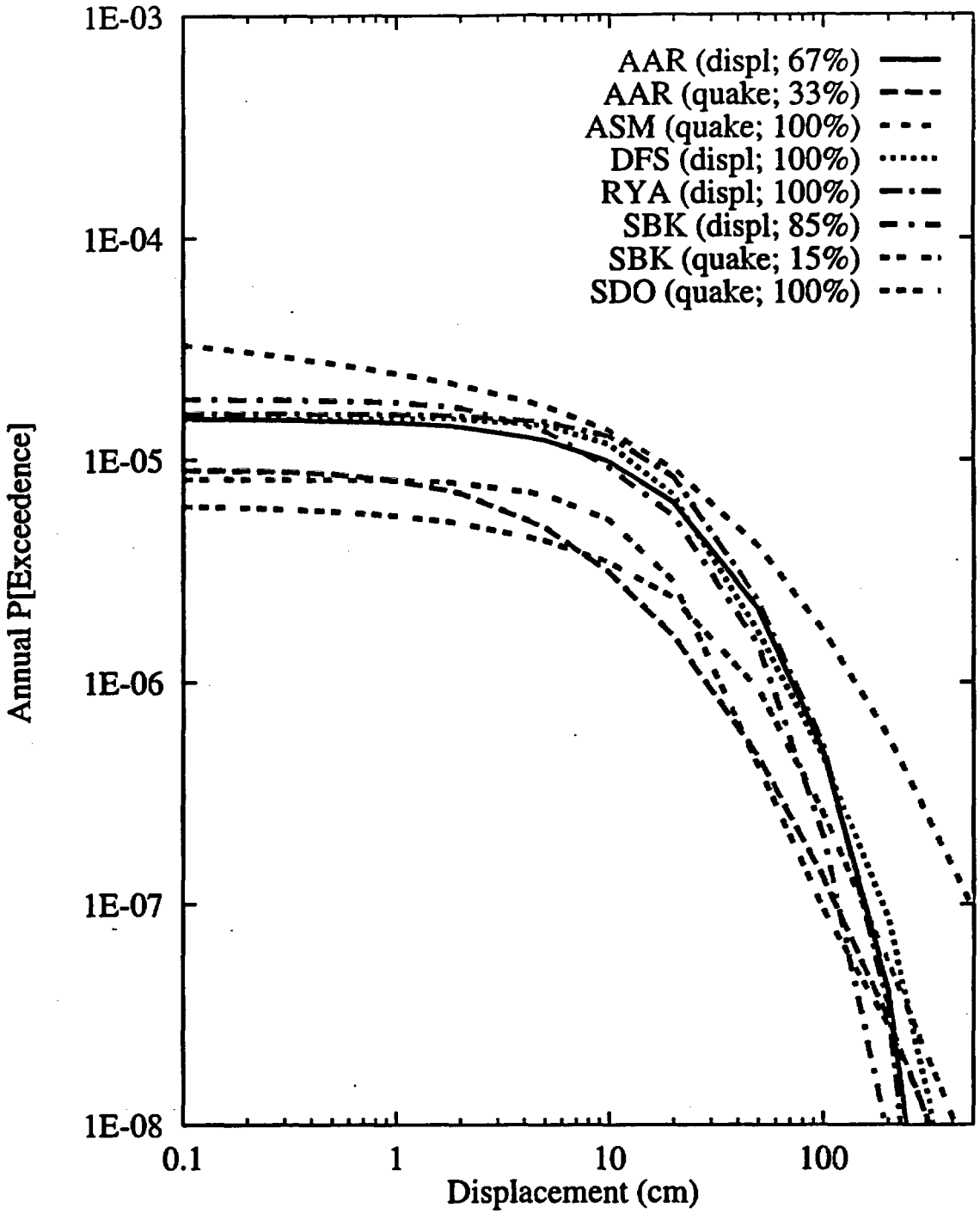

Figure 8-15 Mean hazard by teams and approaches for Site 1, Bow Ridge fault

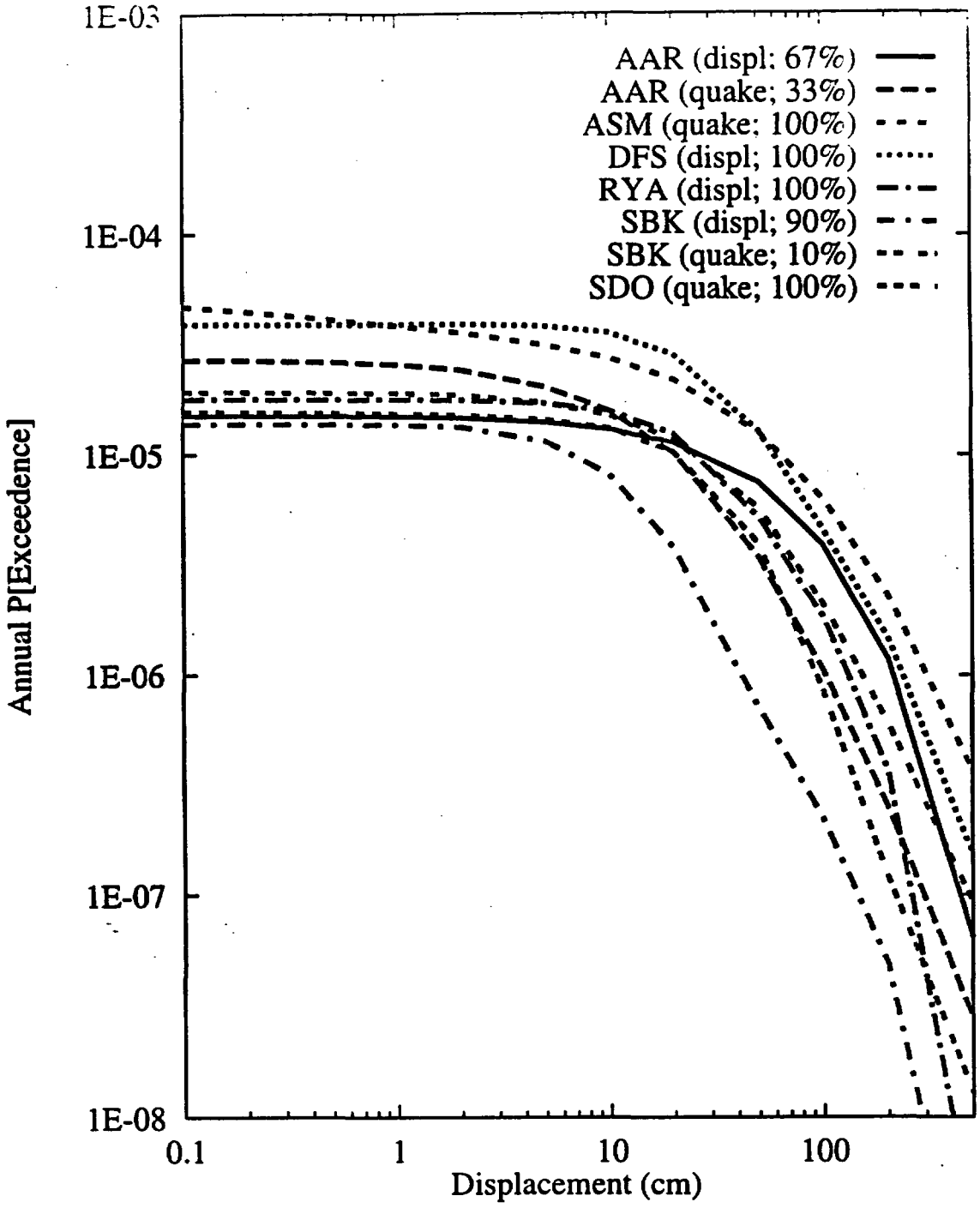

Figure 8-16 Mean hazard by teams and approaches for Site 2, Solitario Canyon fault

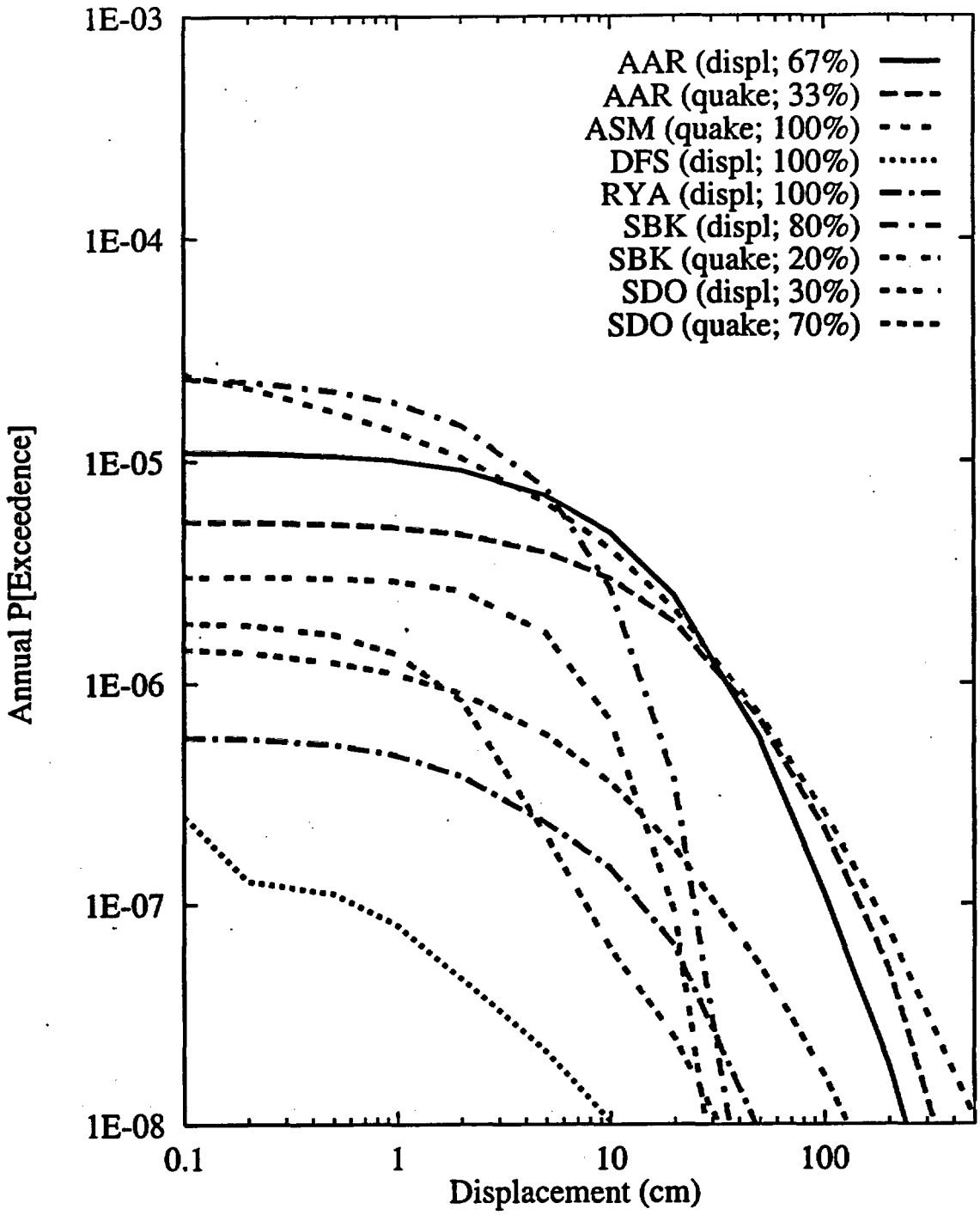

Figure 8-17 Mean hazard by teams and approaches for Site 3, Drill Hole Wash fault

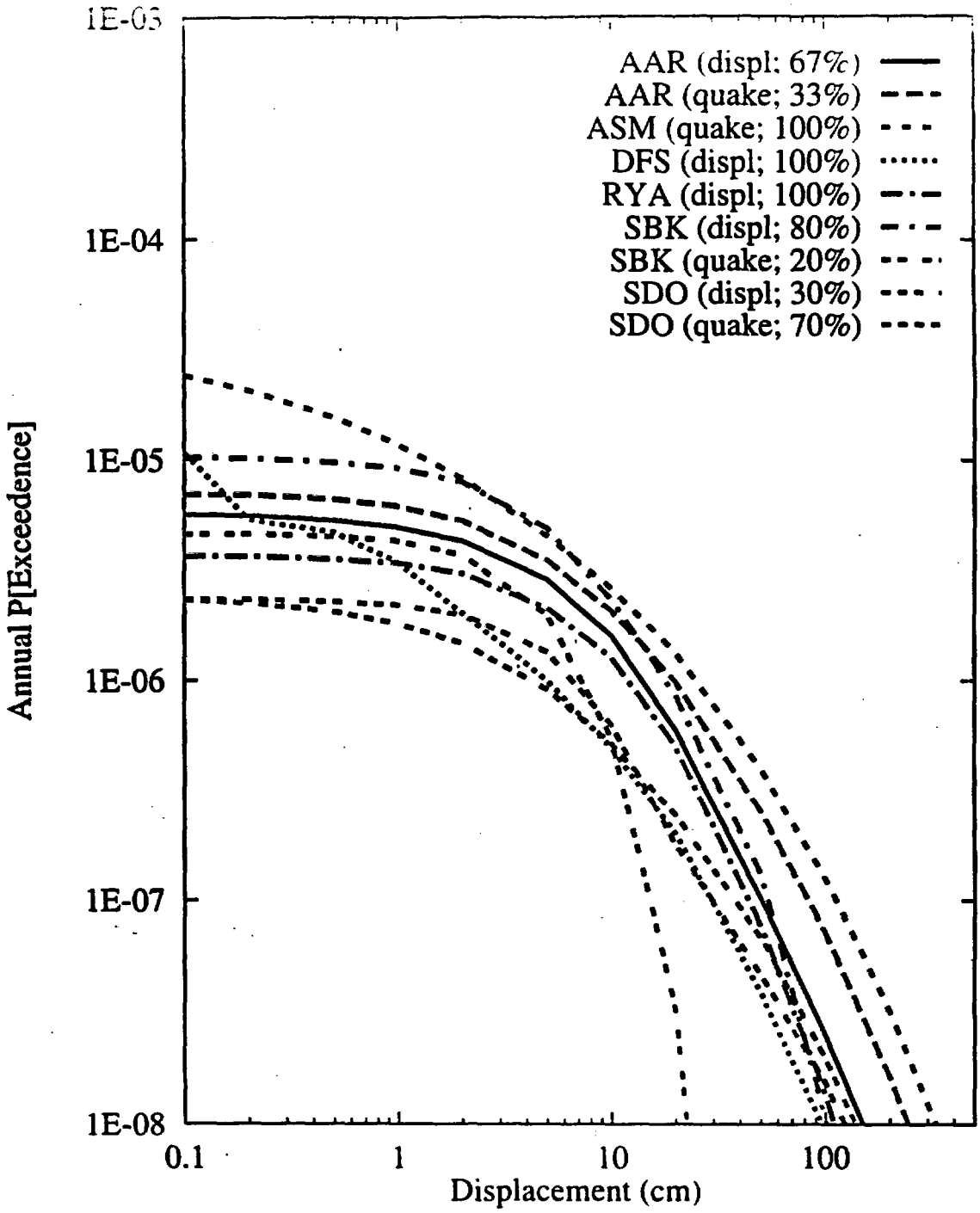

Figure 8-18 Mean hazard by teams and approaches for Site 4, Ghost Dance fault

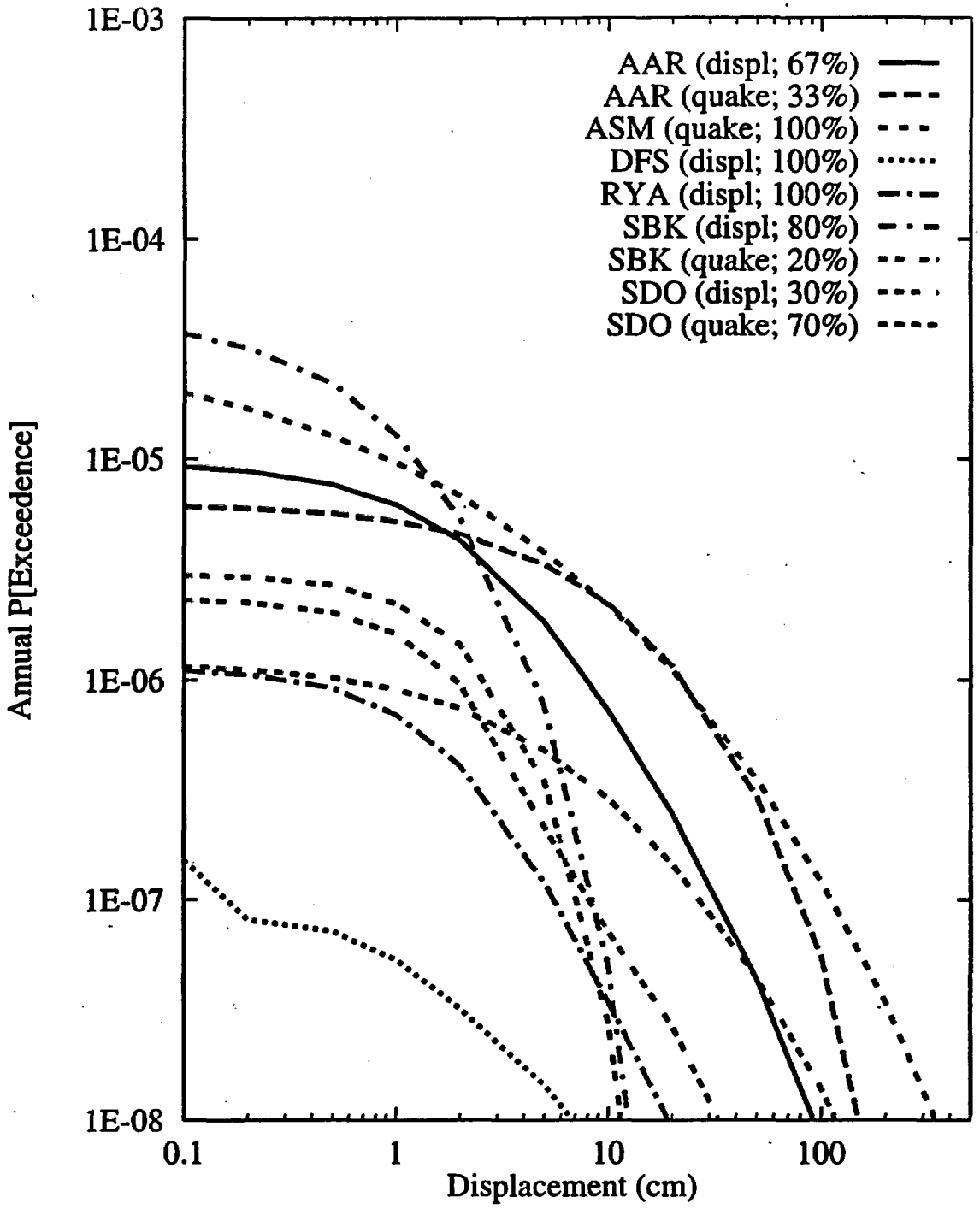

Figure 8-19 Mean hazard by teams and approaches for Site 5, Sundance fault

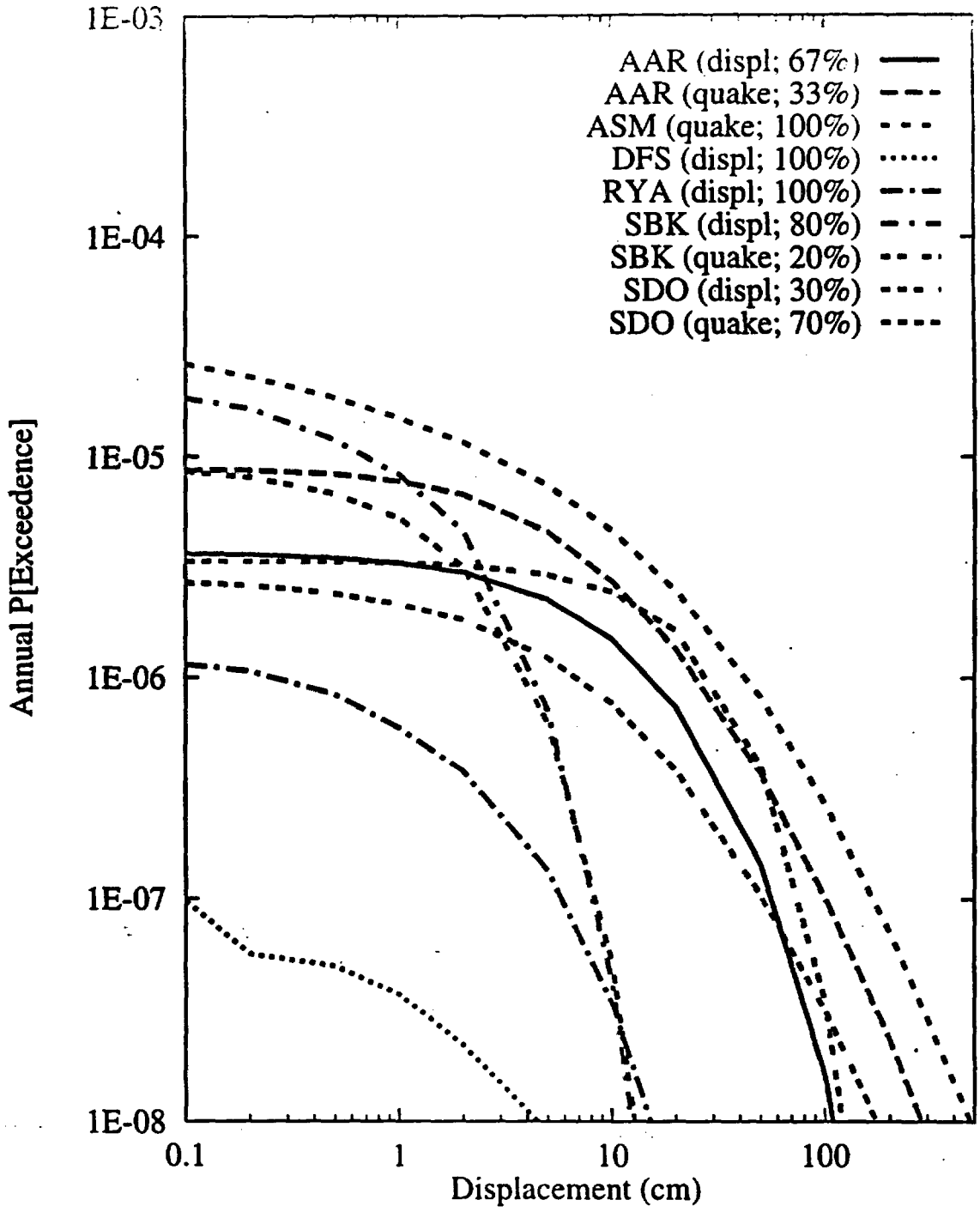

Figure 8-20 Mean hazard by teams and approaches for Site 6, unnamed fault west of Dune Wash fault

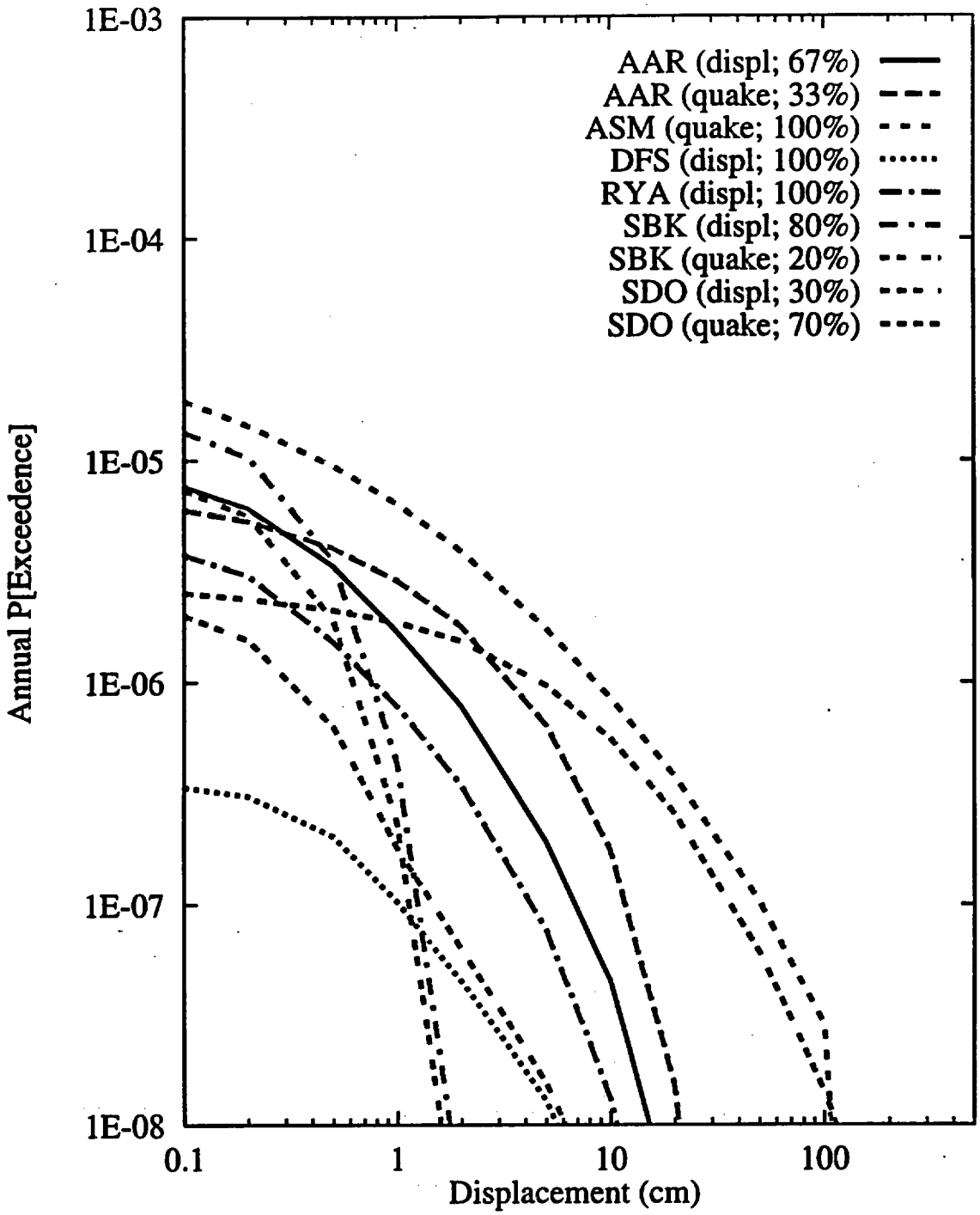

Figure 8-21 Mean hazard by teams and approaches for Site 7a, 100m east of Solitario Canyon fault (2m cumulative displacement)

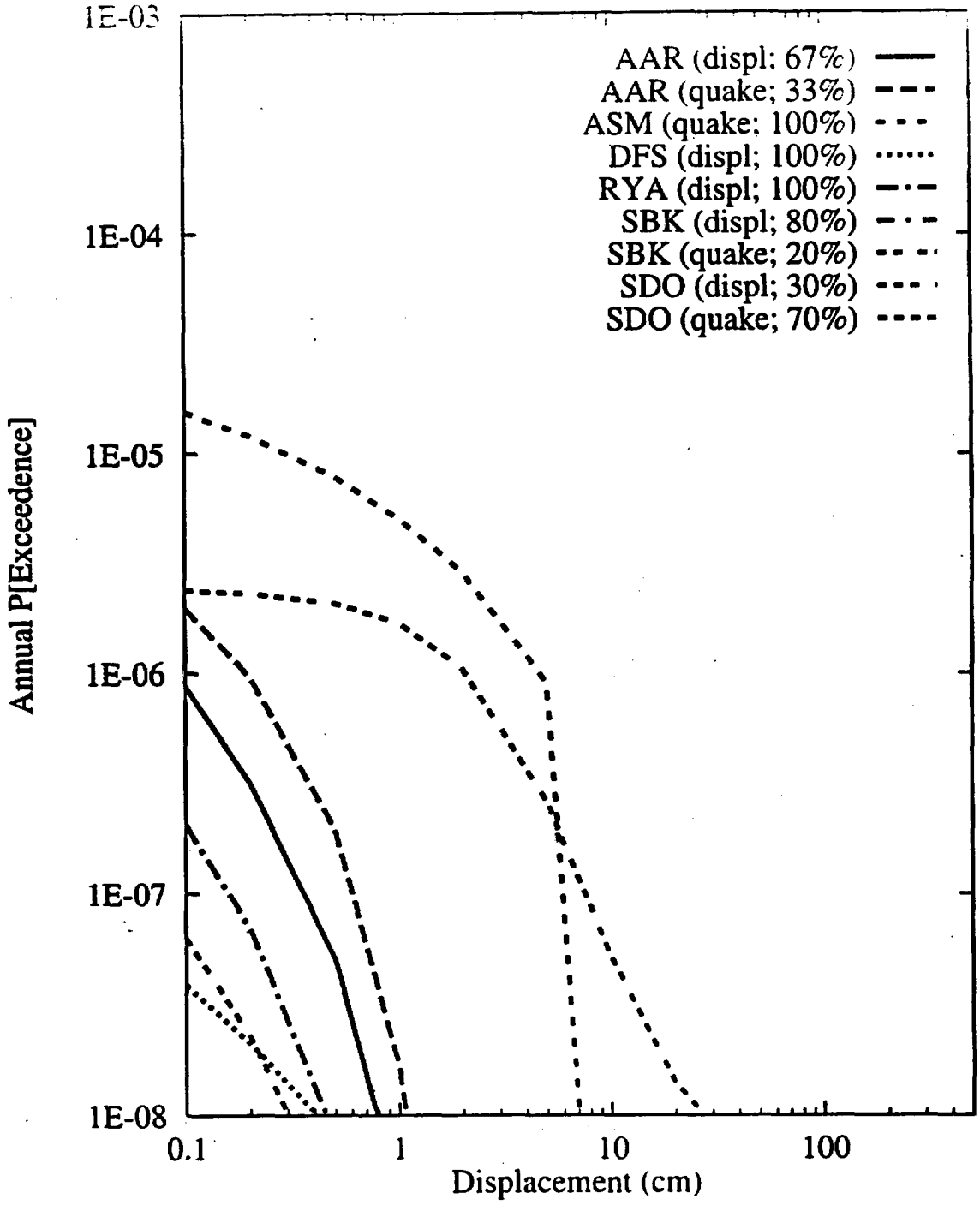

Figure 8-22 Mean hazard by teams and approaches for Site 7b, 100m east of Solitario Canyon fault (10cm cumulative displacement)

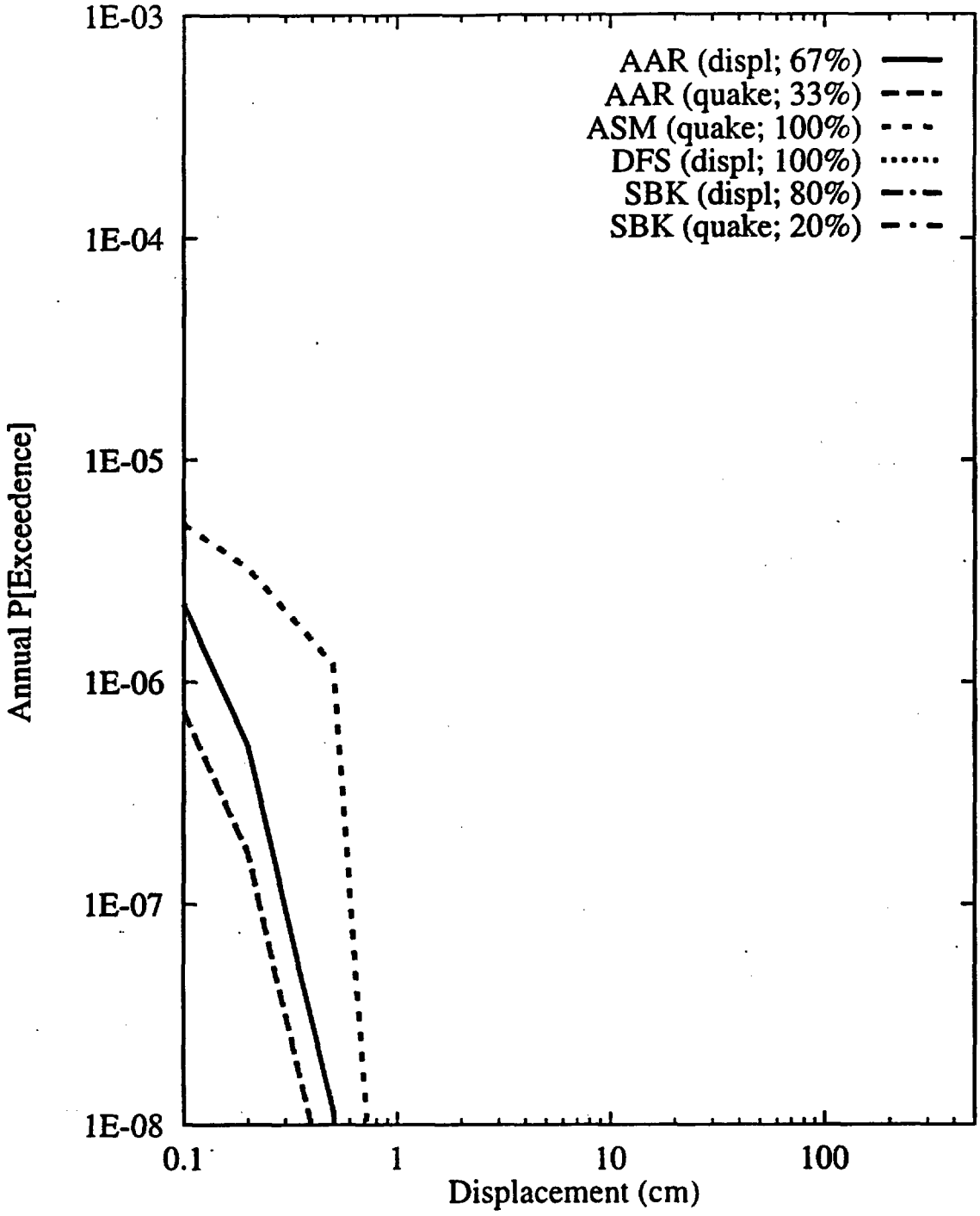

Figure 8-23 Mean hazard by teams and approaches for Site 7c, 100m east of Solitario Canyon fault (no measurable cumulative displacement)

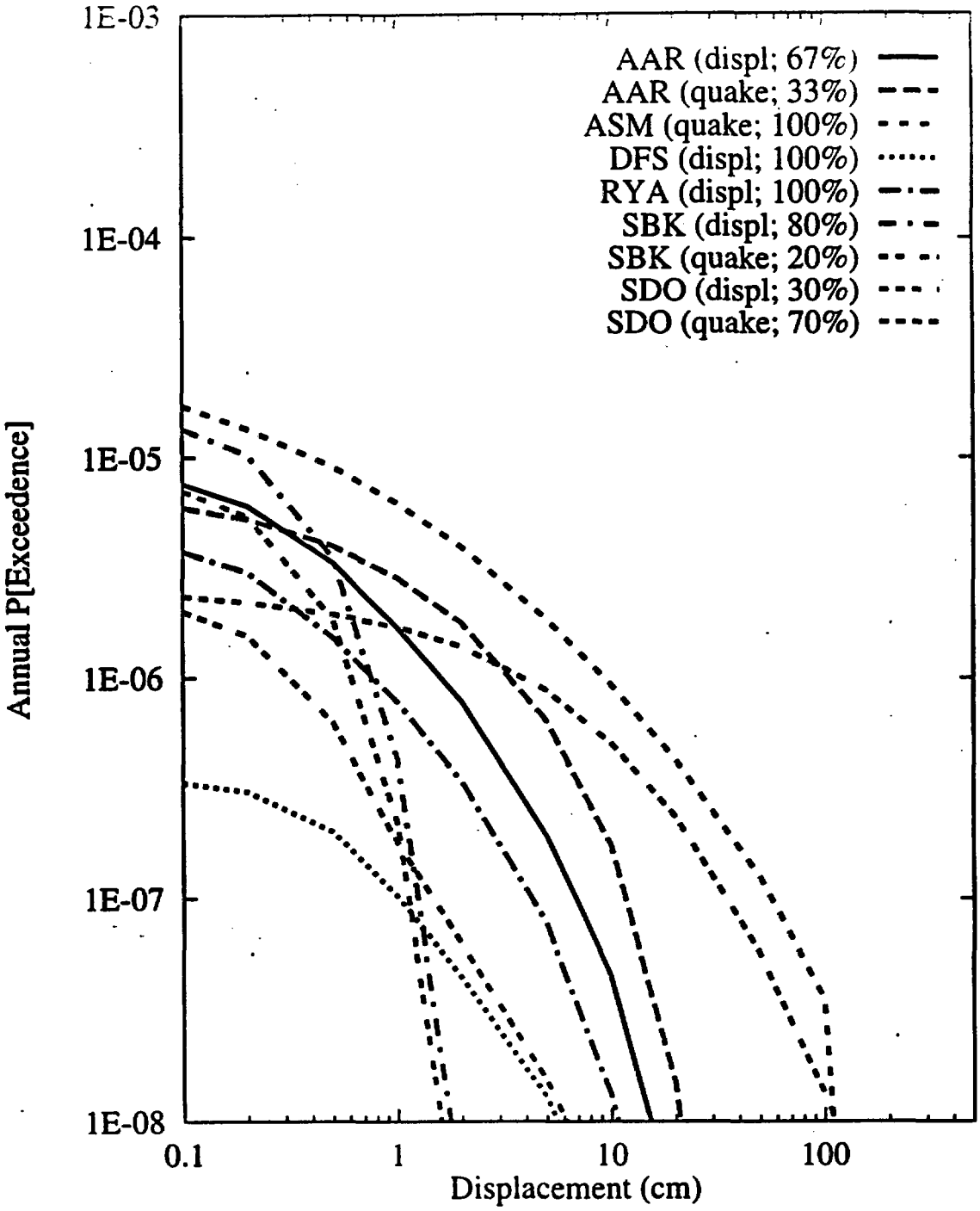

Figure 8-24 Mean hazard by teams and approaches for Site 8a, midway between the Ghost Dance and Solitario Canyon faults (2m cumulative displacement)

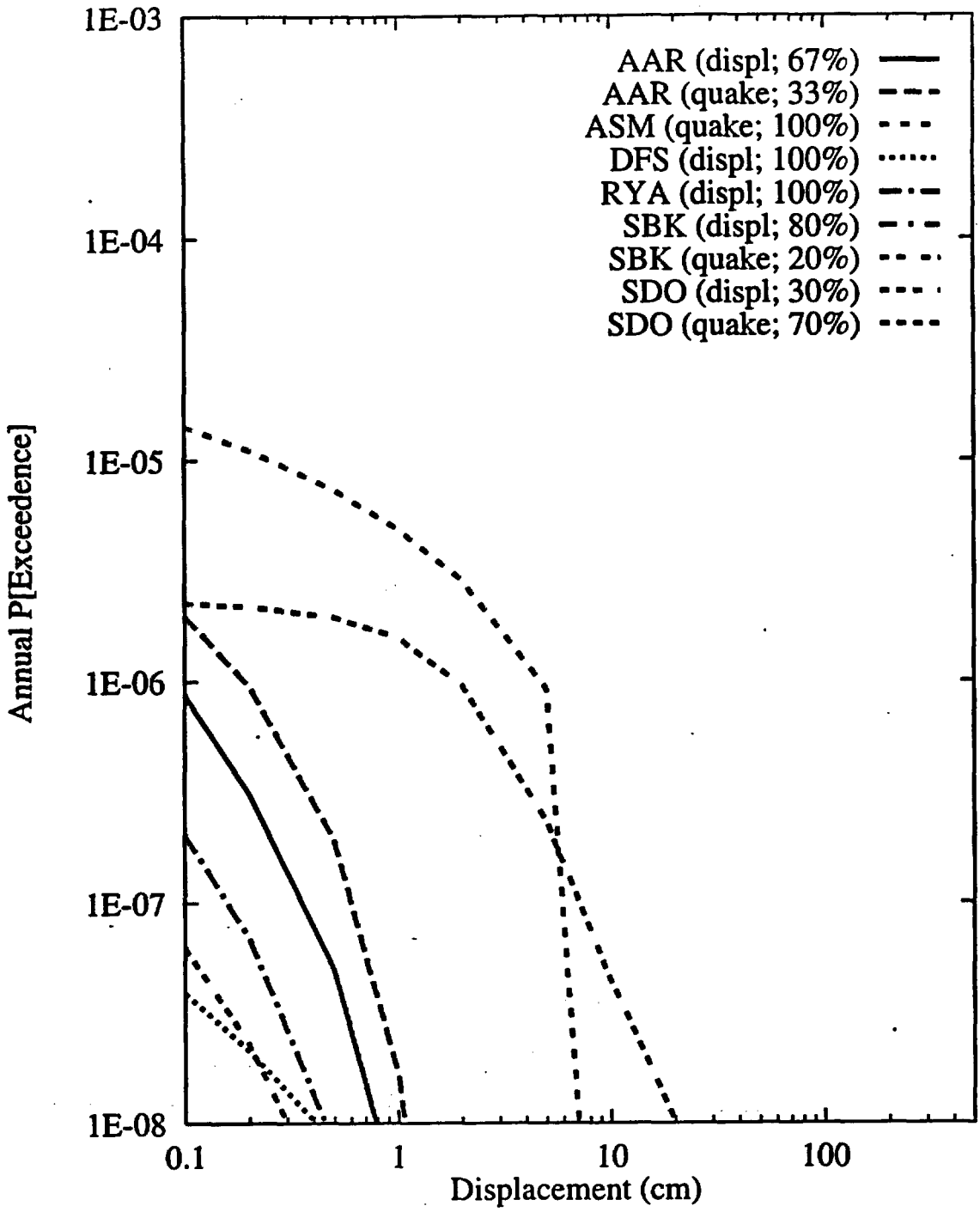

Figure 8-25 Mean hazard by teams and approaches for Site 8b, midway between the Ghost Dance and Solitario Canyon faults (10cm cumulative displacement)

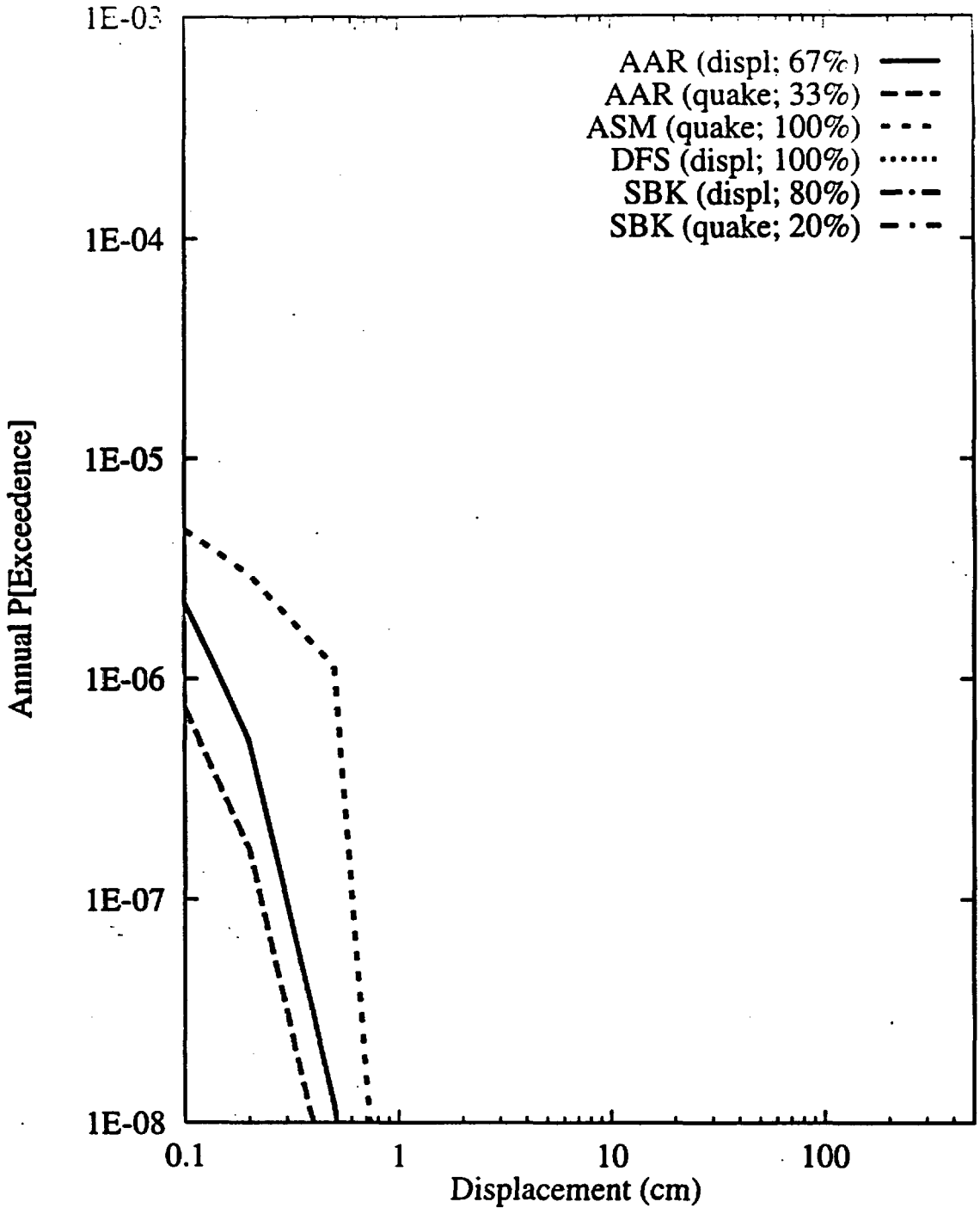

Figure 8-26 Mean hazard by teams and approaches for Site 8c, midway between the Ghost Dance and Solitario Canyon faults (no measurable cumulative displacement)

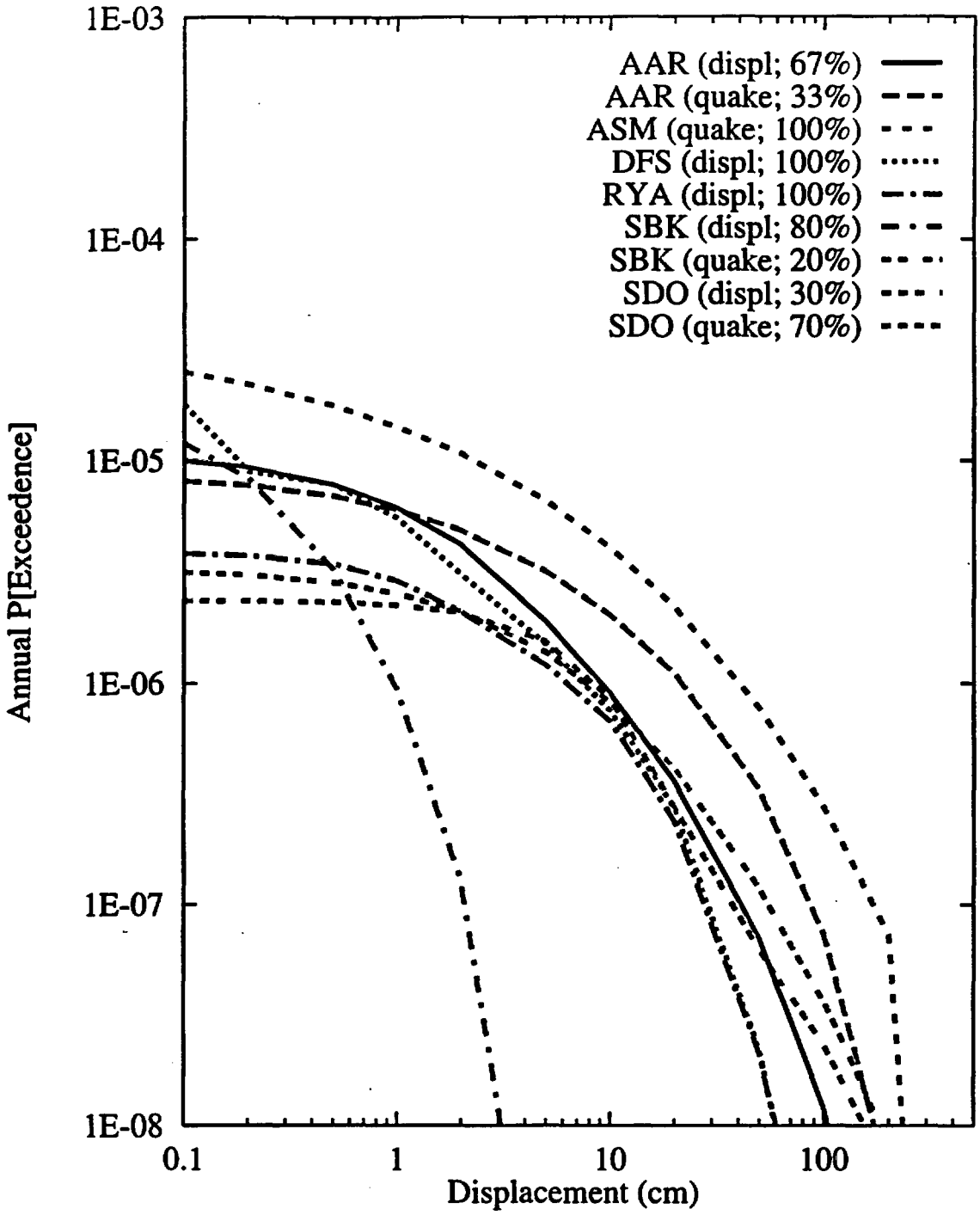

Figure 8-27 Mean hazard by teams and approaches for Site 9, Midway Valley

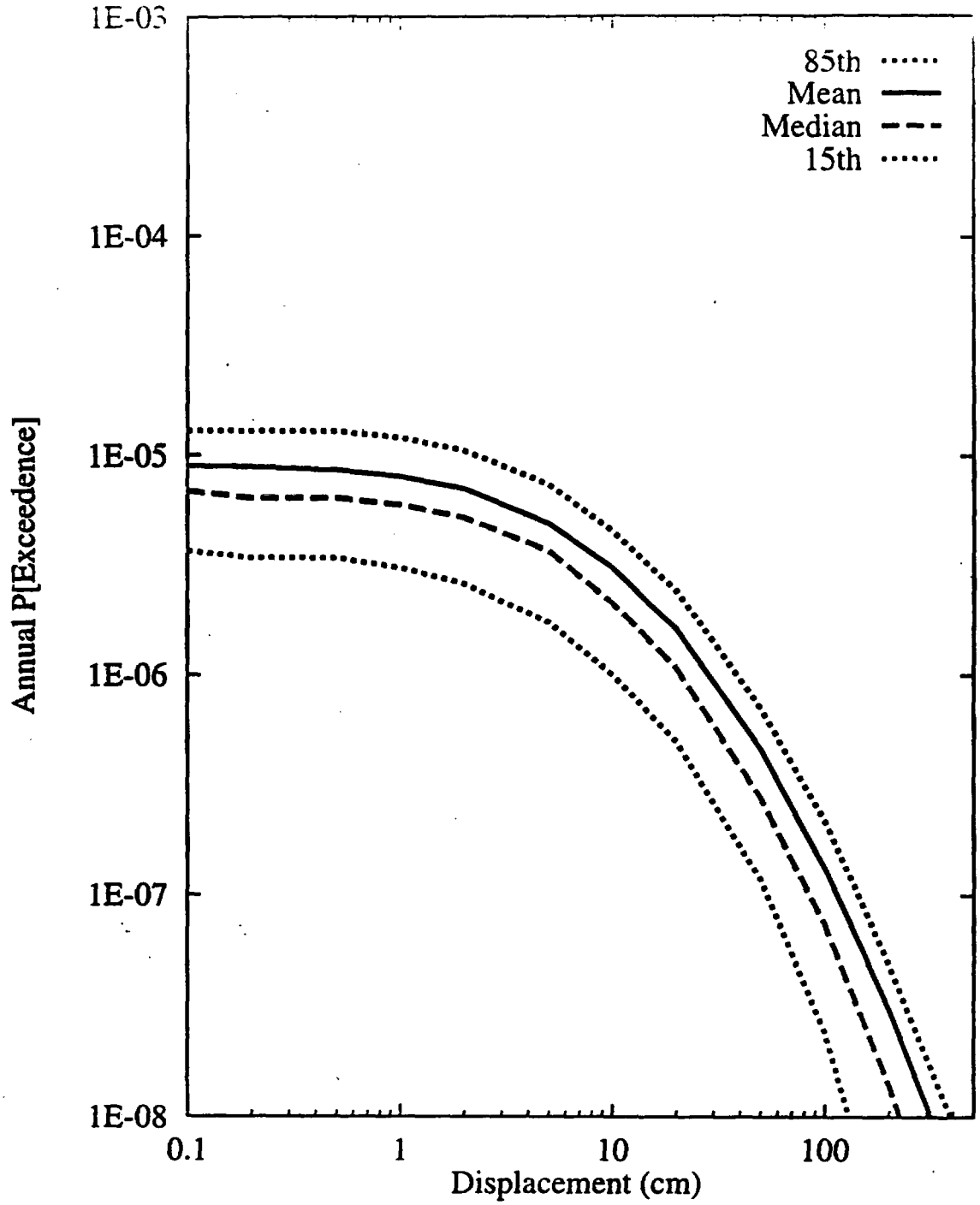

Figure 8-28 Summary hazard curves for Site 1: AAR team, earthquake approach

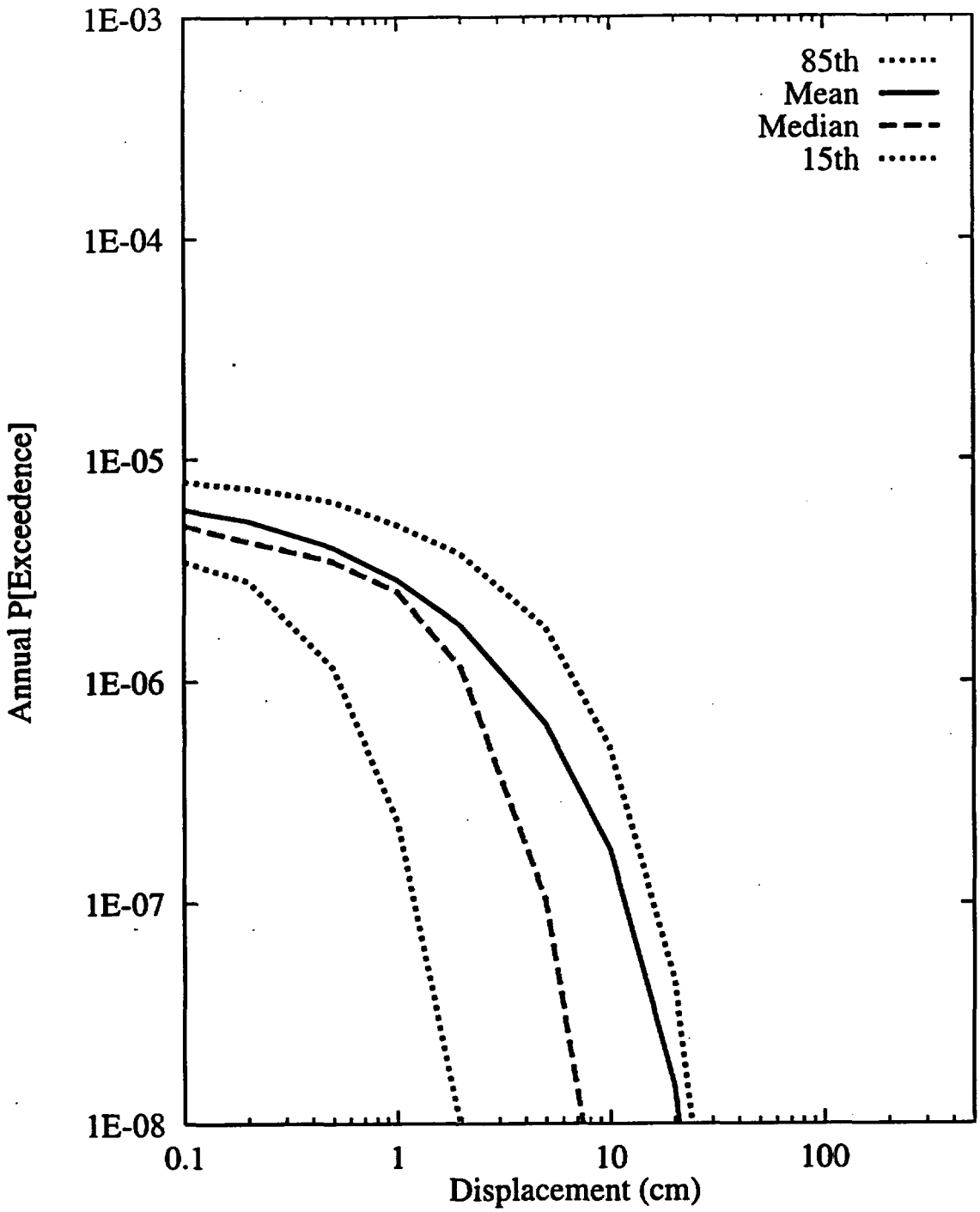

Figure 8-29 Summary hazard curves for Site 7a: AAR team, earthquake approach

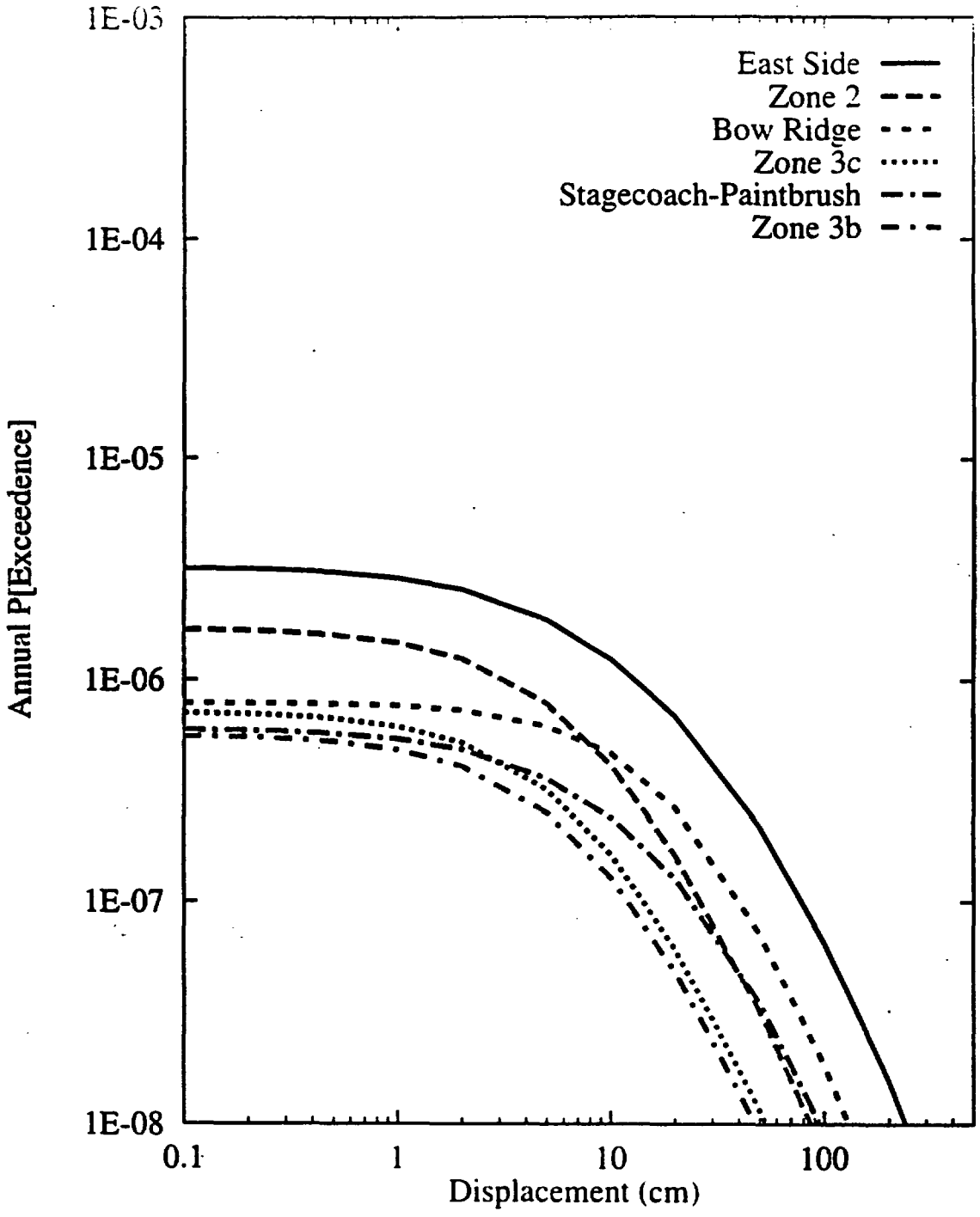

Figure 8-30 Mean hazard curves by source for Site 1 - AAR team, earthquake approach

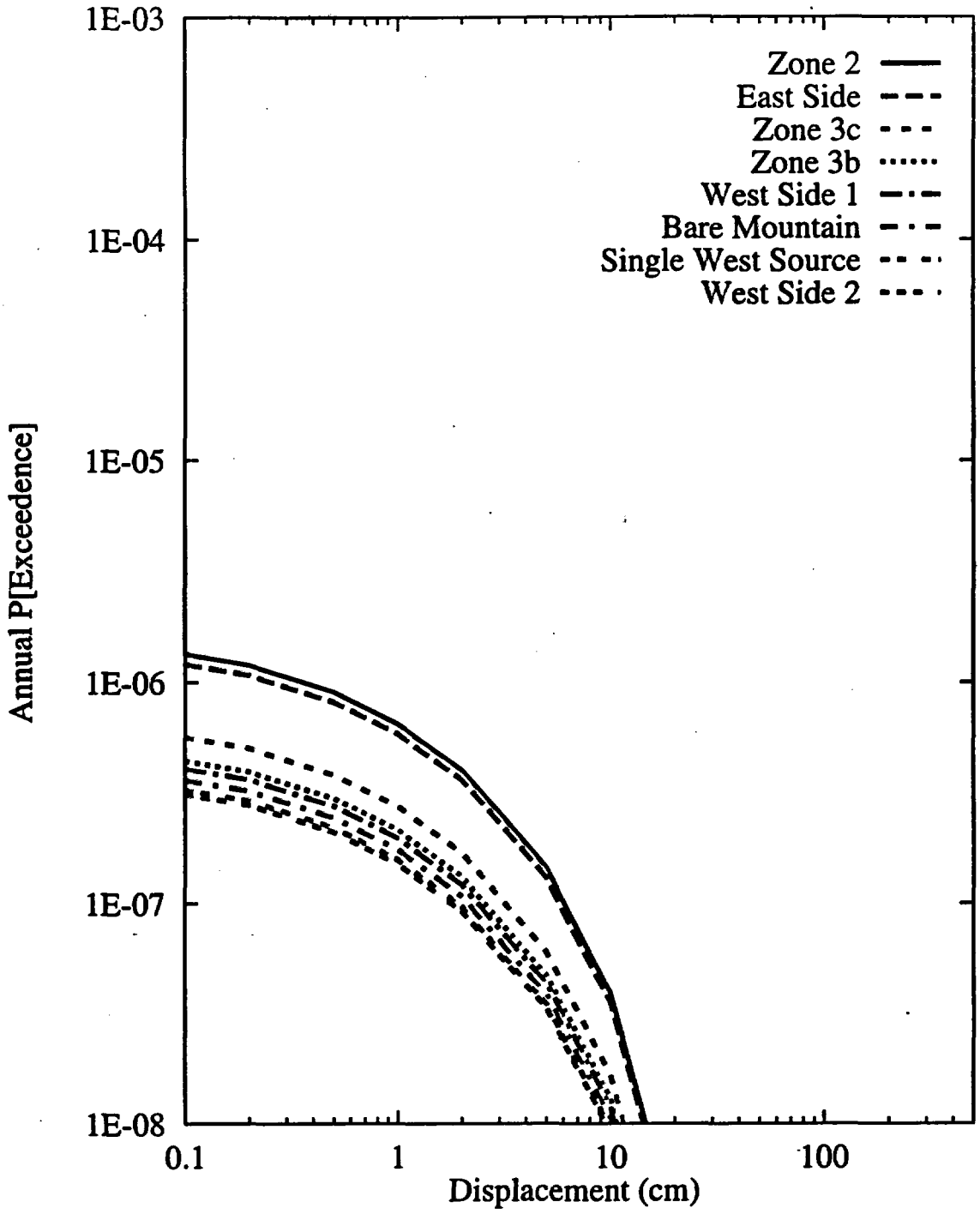

Figure 8-31 Mean hazard curves by source for Site 7a: AAR team, earthquake approach

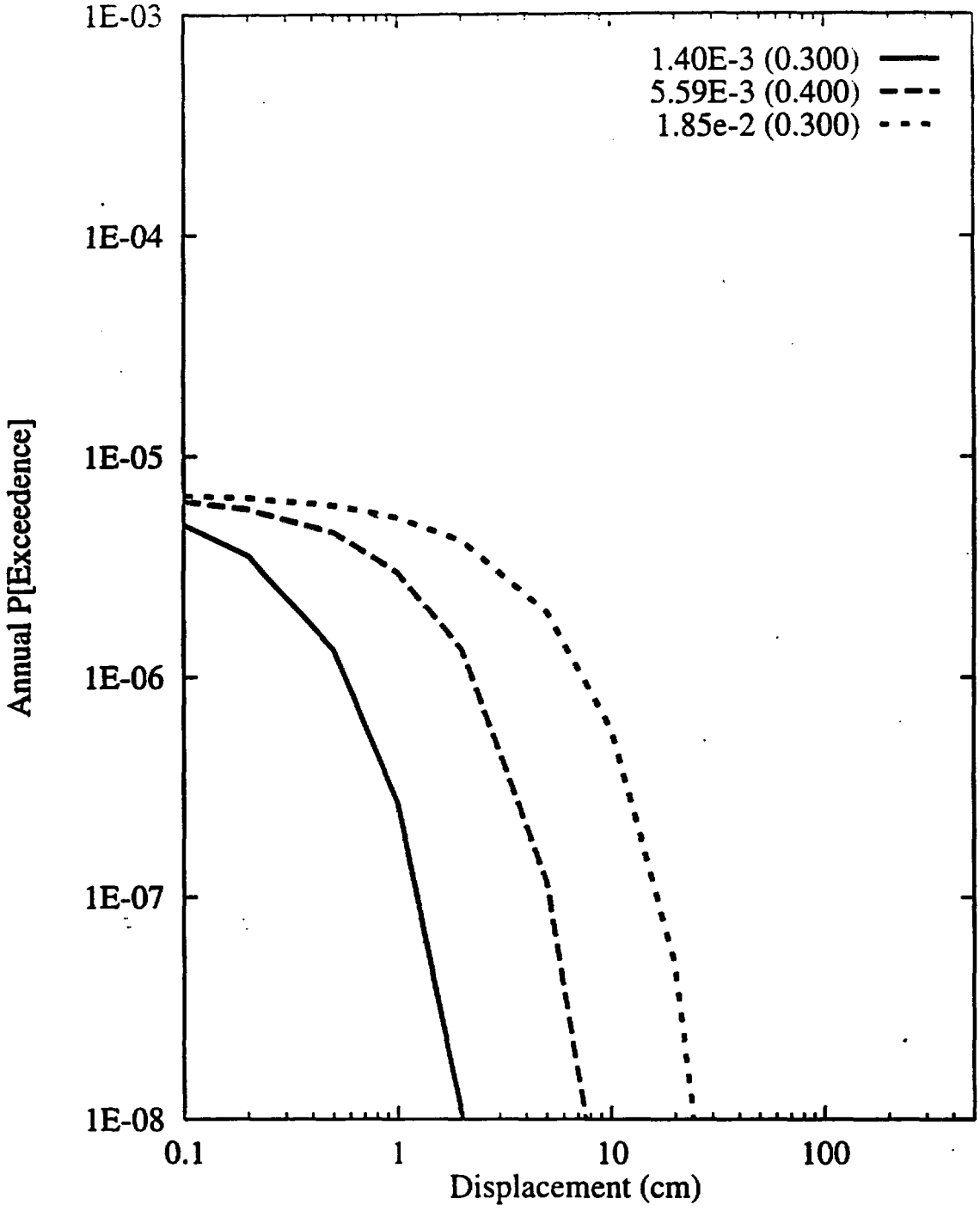

Figure 8-32 Sensitivity of displacement hazard for Site 1 to parameter beta: AAR team, earthquake approach

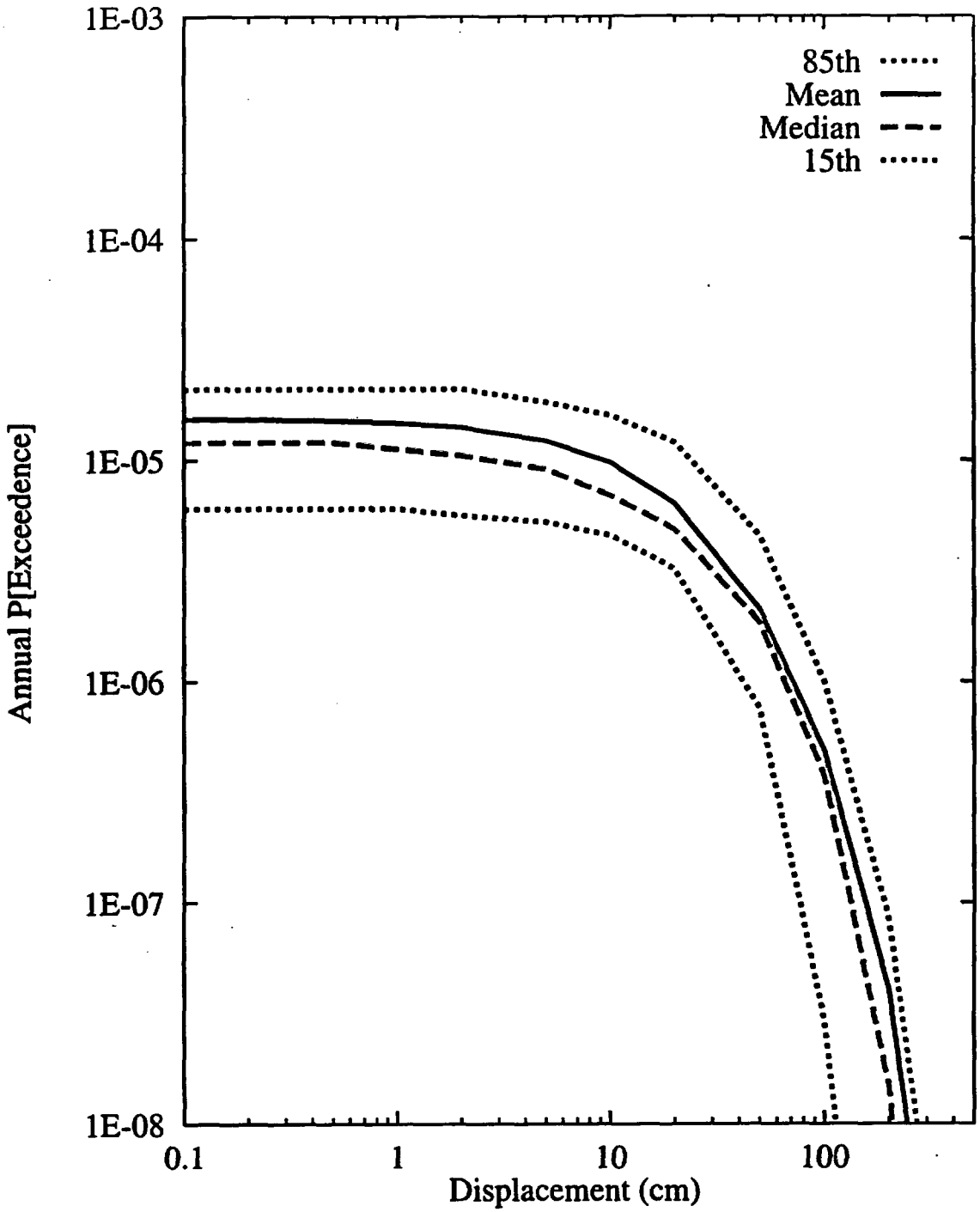

Figure 8-33 Summary hazard curves for Site 1: AAR team, displacement approach

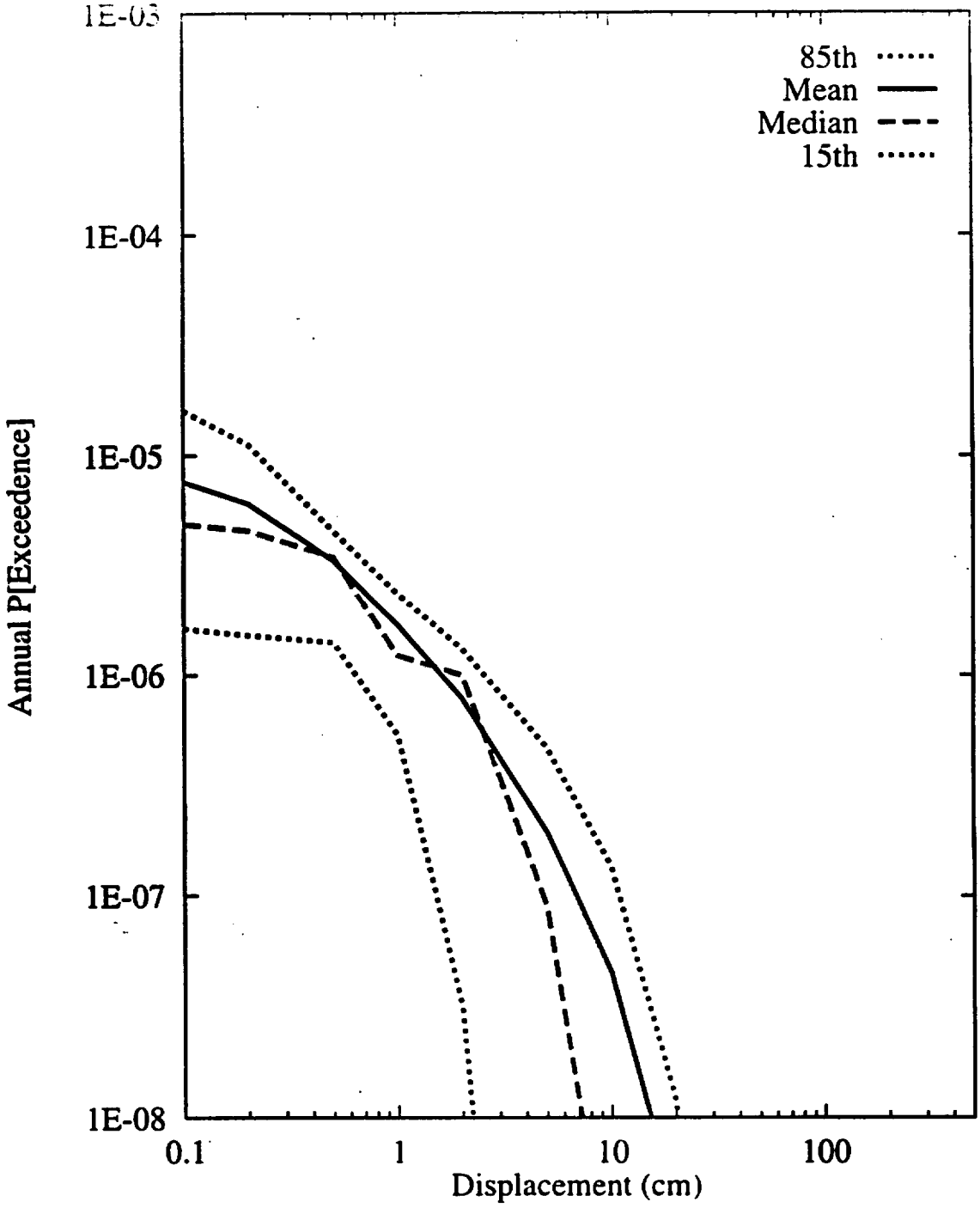

Figure 8-34 Summary hazard curves for Site 7a: AAR team, displacement approach

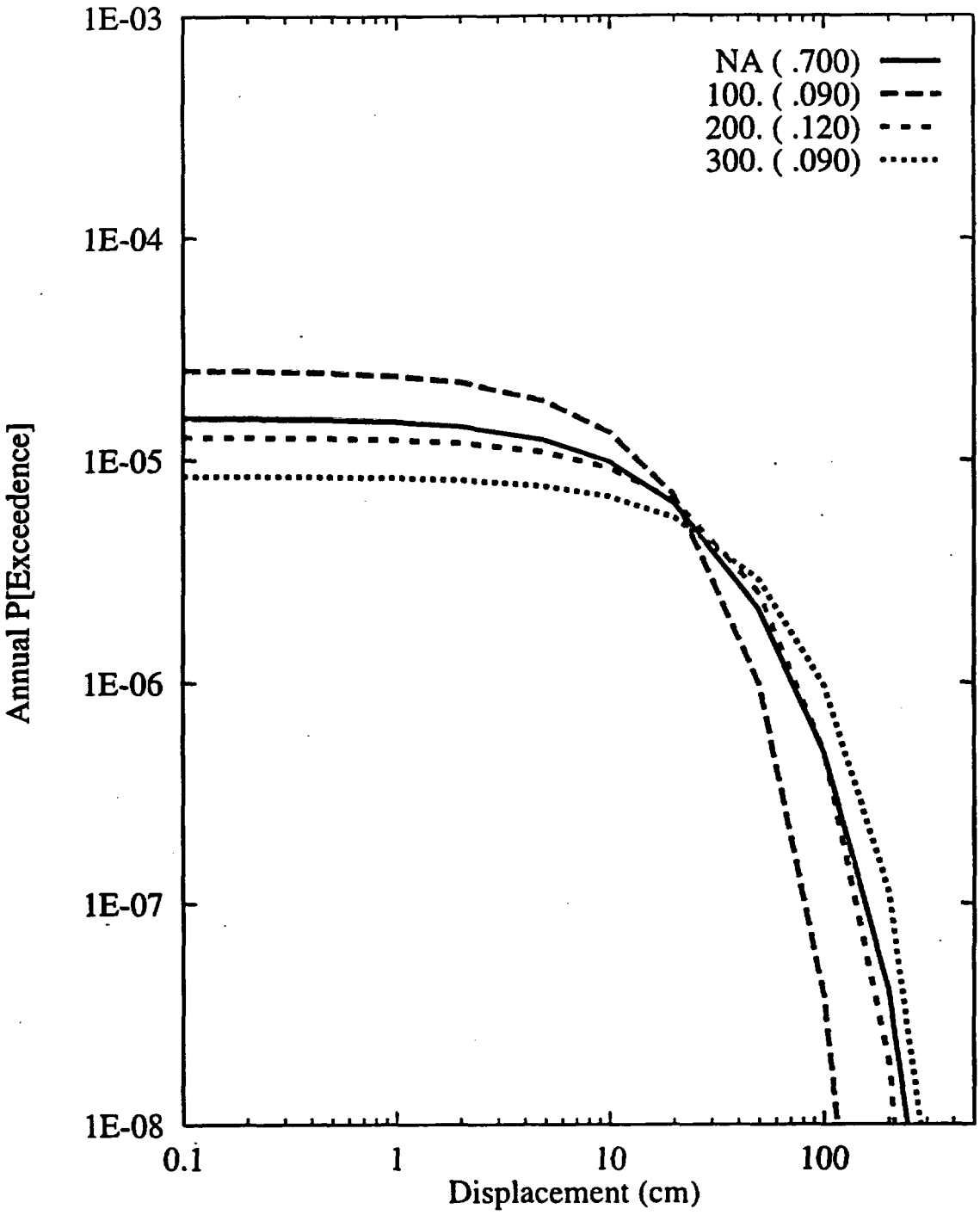

Figure 8-35 Sensitivity of displacement hazard for Site 1 to cumulative displacement: AAR team, displacement approach

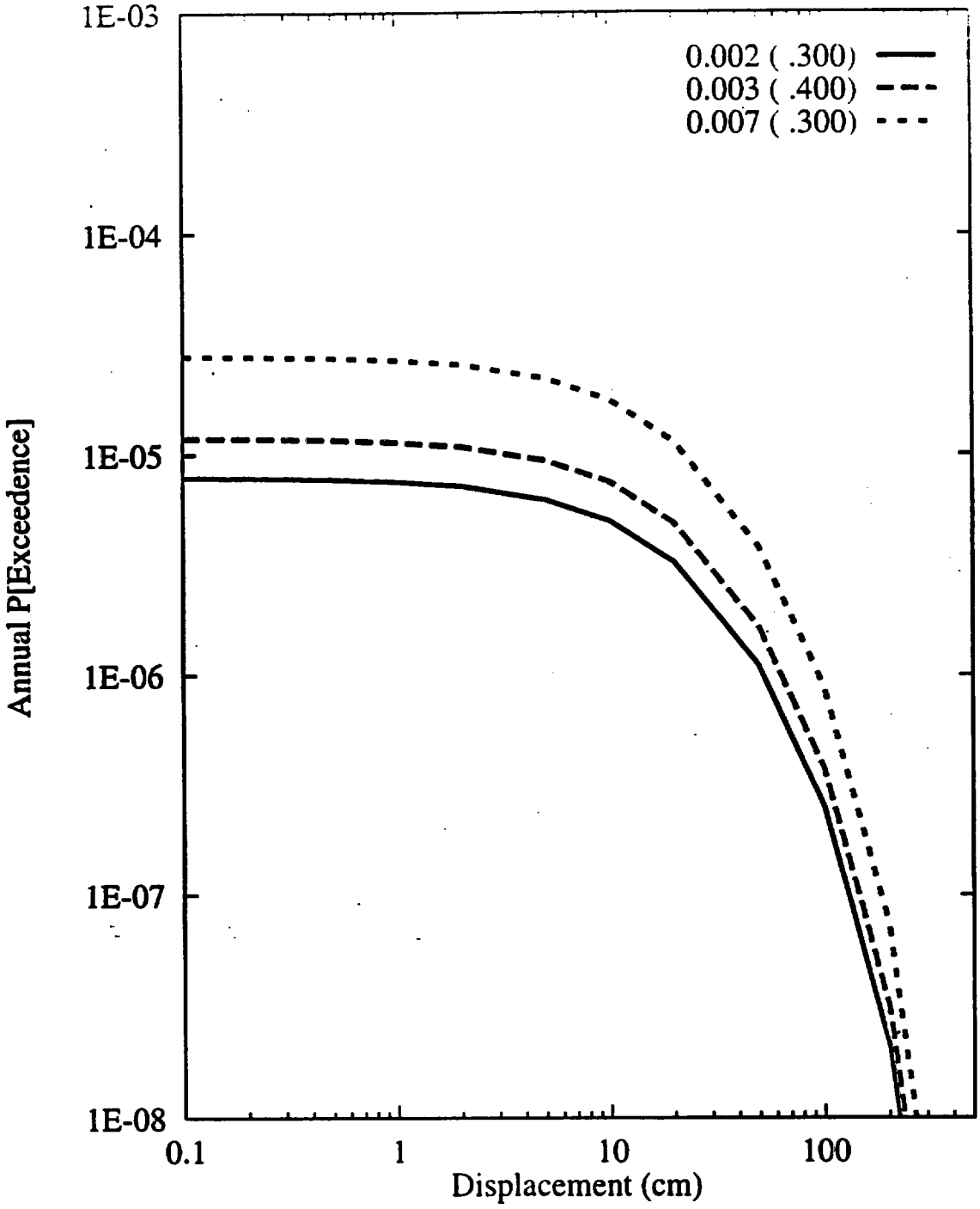

Figure 8-36 Sensitivity of displacement hazard for Site 1 to slip rate: AAR team, displacement approach

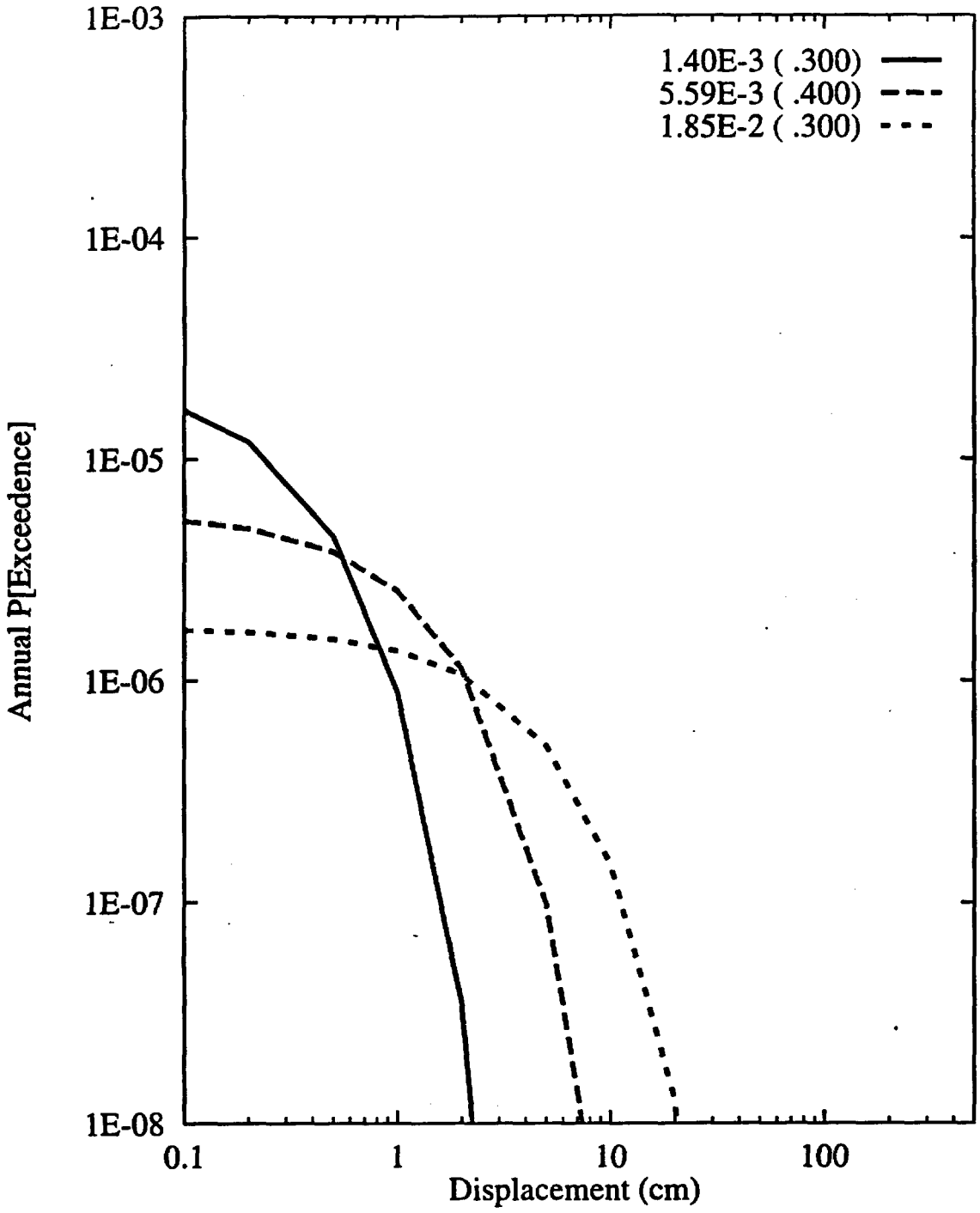

Figure 8-37 Sensitivity of displacement hazard for Site 7a to parameter beta: AAR team, displacement approach

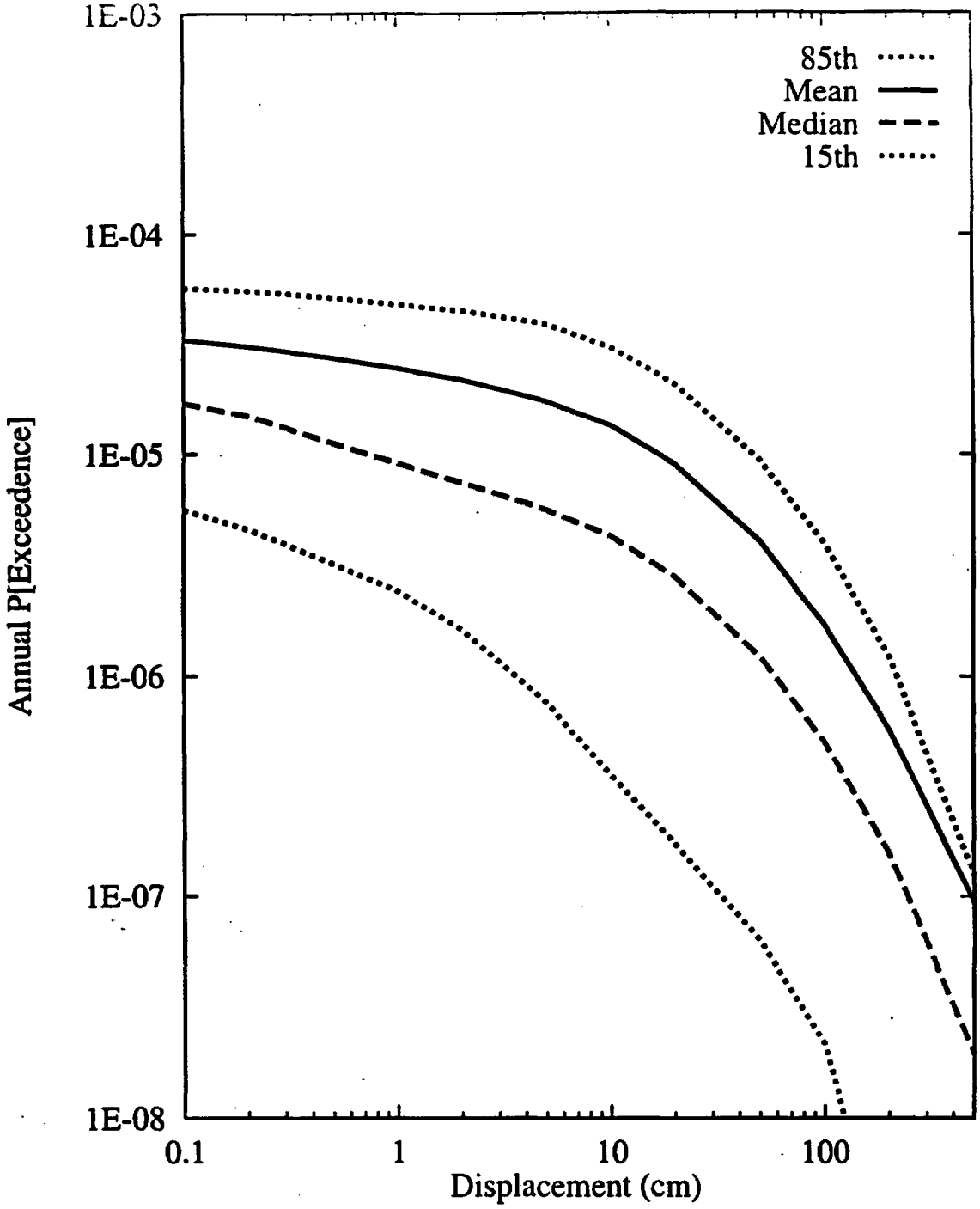

Figure 8-38 Summary hazard curves for Site 1: ASM team, earthquake approach

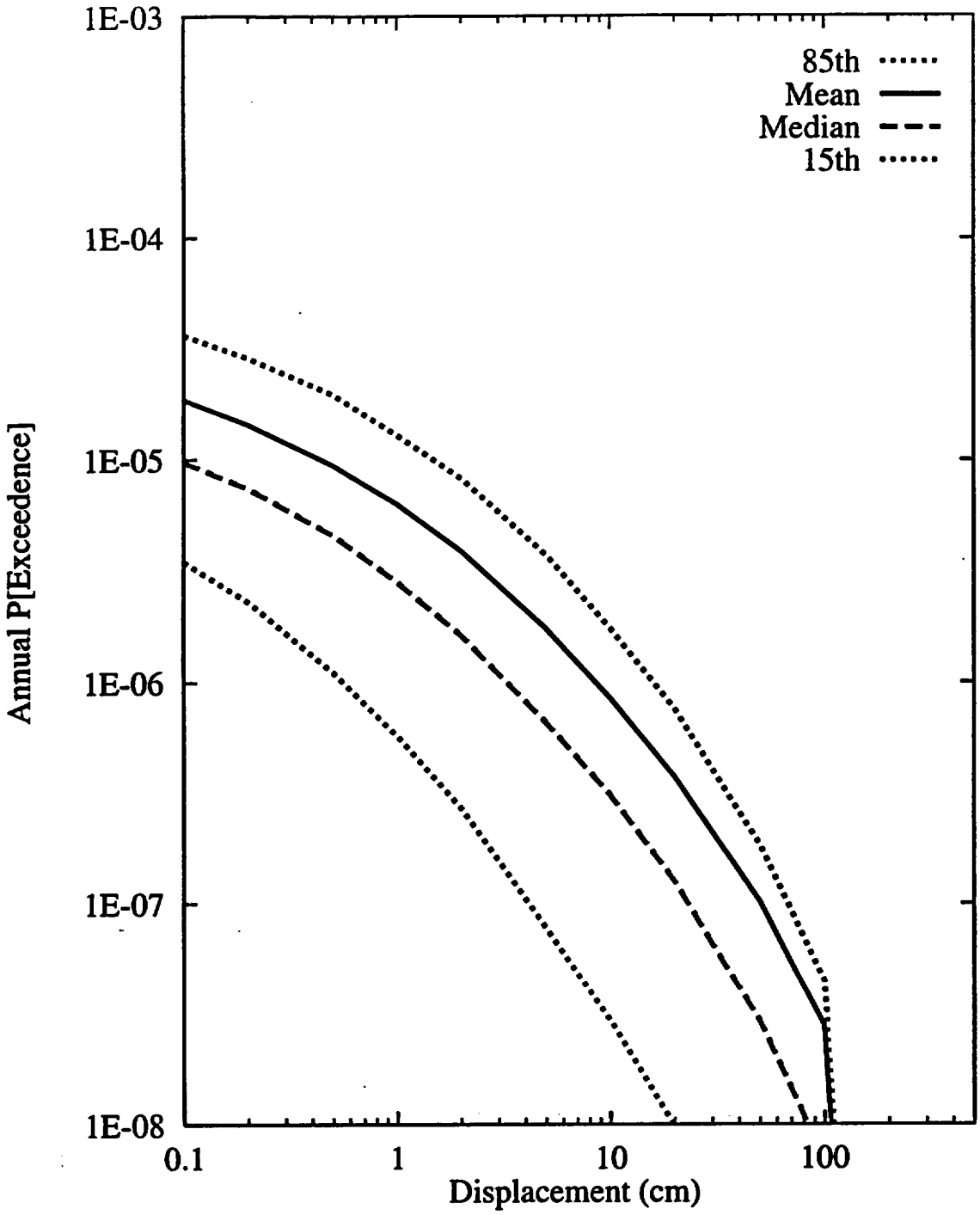

Figure 8-39 Summary hazard curves for Site 7a: ASM team, earthquake approach

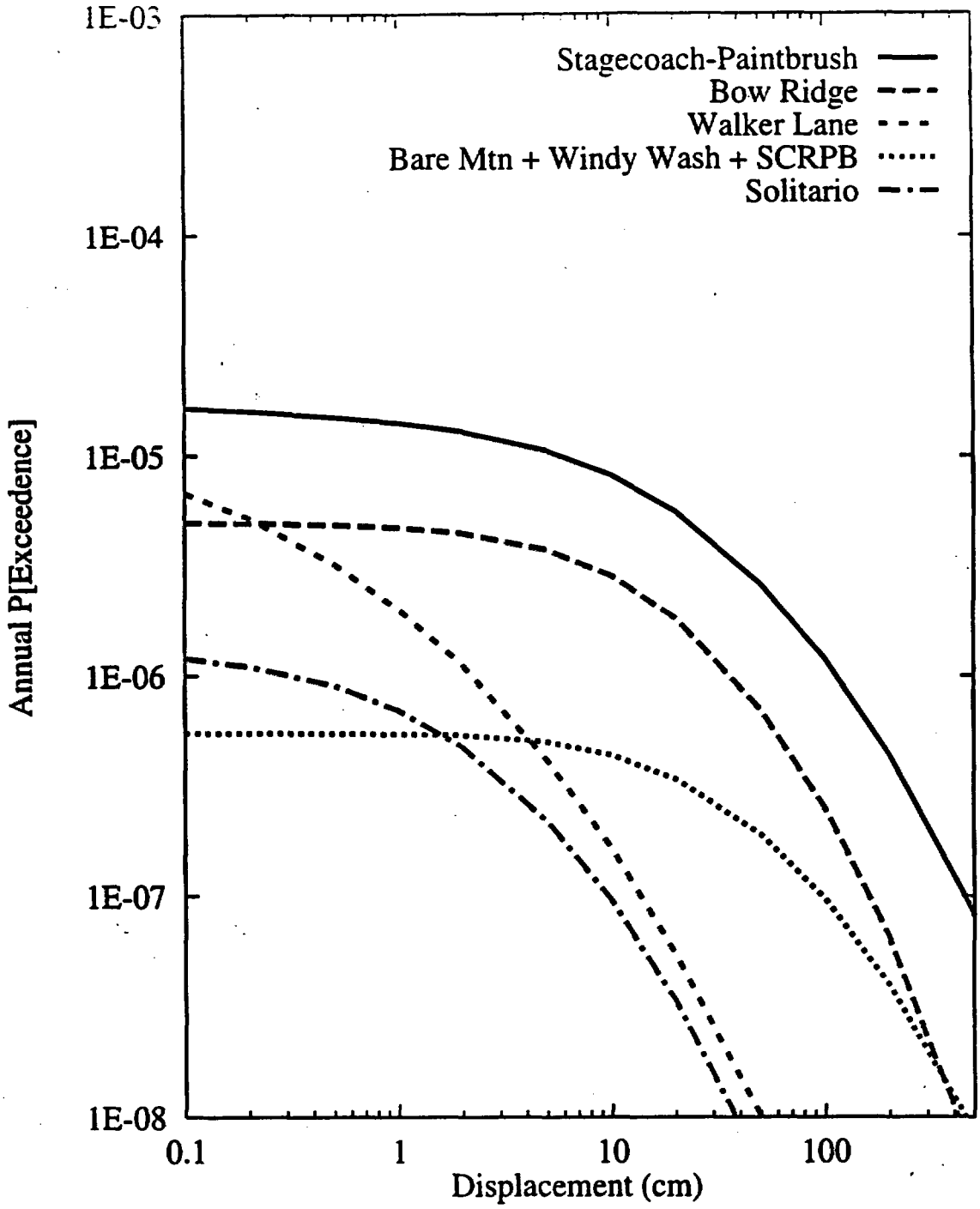

Figure 8-40 Mean hazard curves by source for Site 1: ASM team, earthquake approach

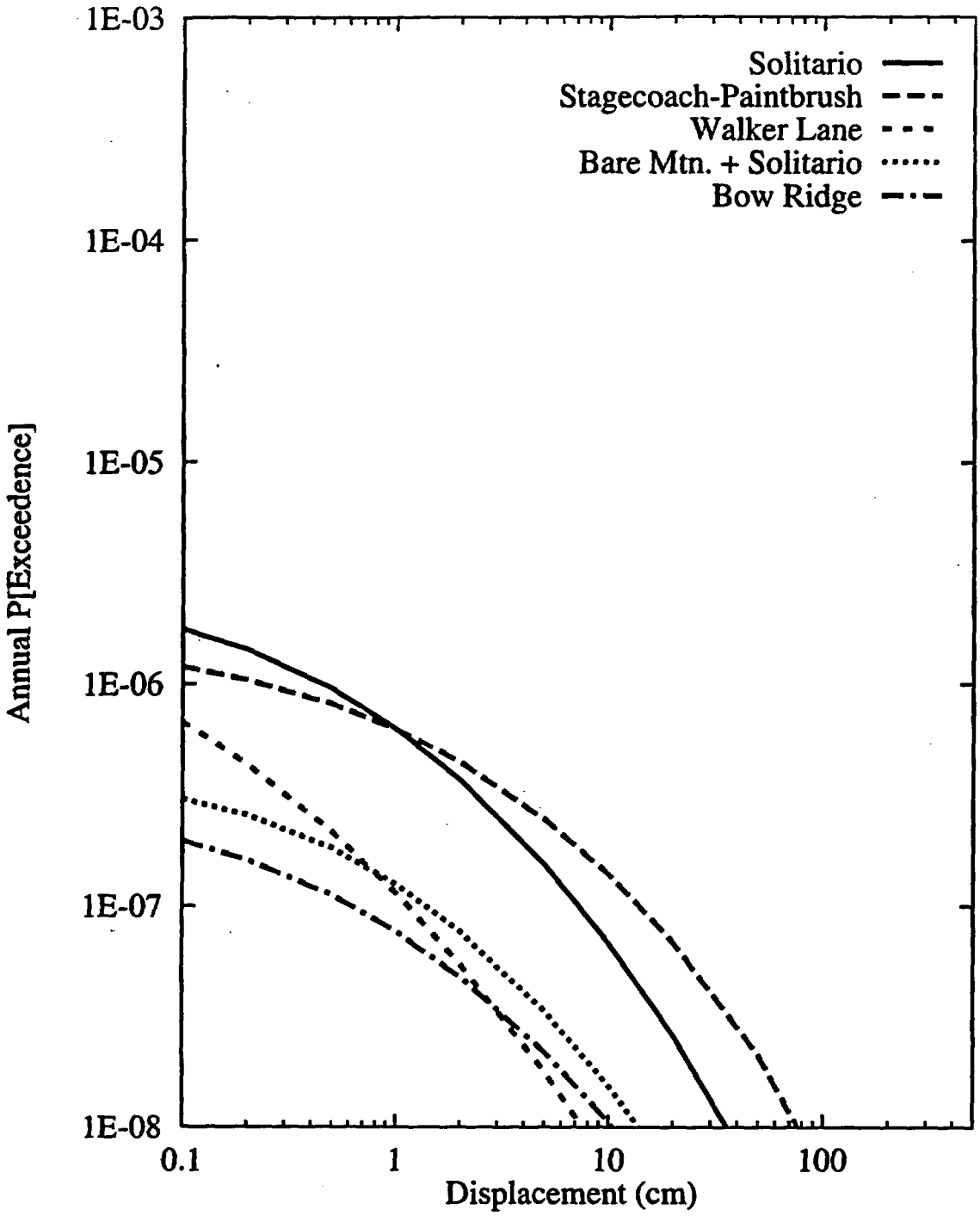

Figure 8-41 Mean hazard curves by source for Site 7a: ASM team, earthquake approach

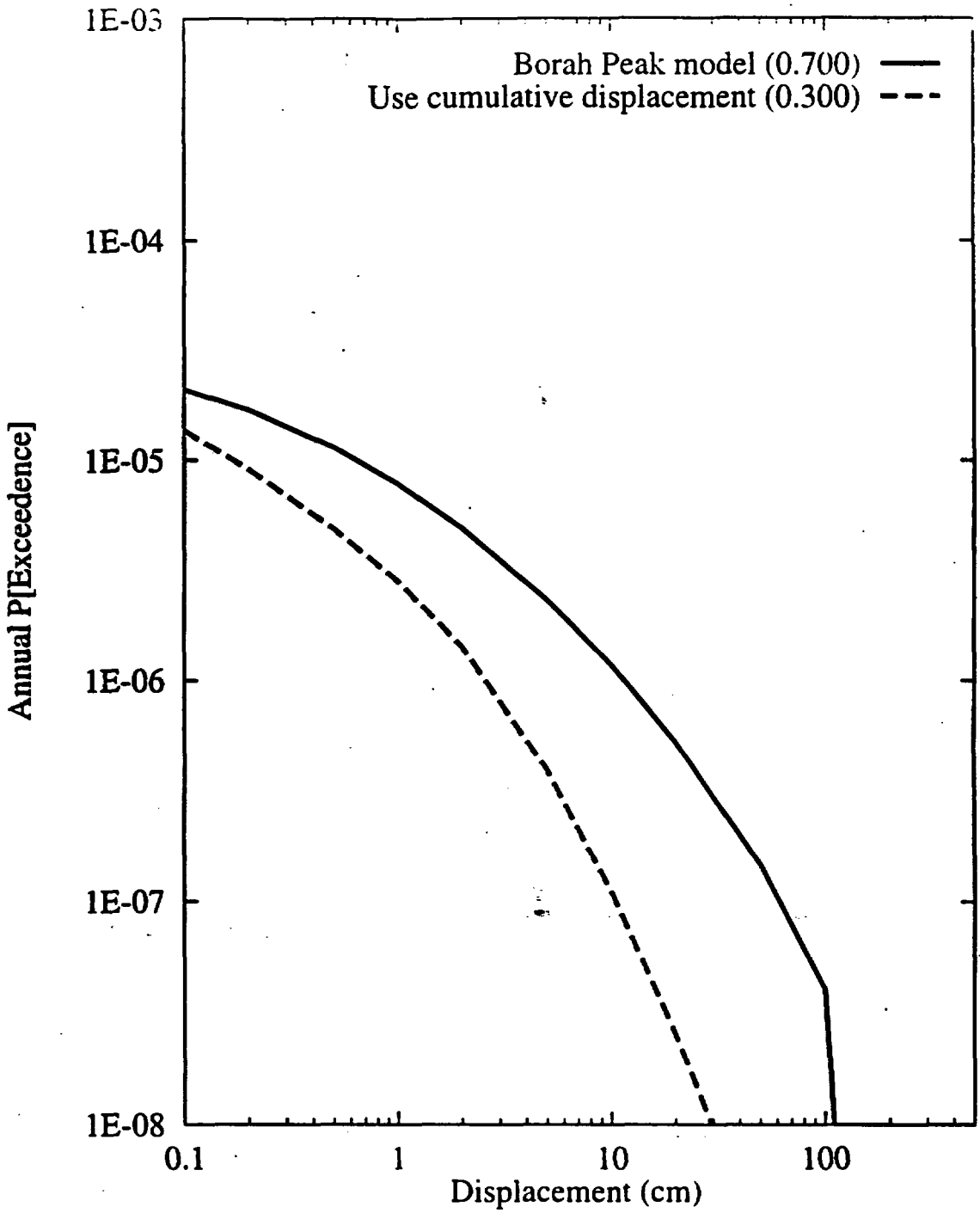

Figure 8-42 Sensitivity of displacement hazard for Site 7a to scaling of principal to distributed faulting: ASM team, earthquake approach

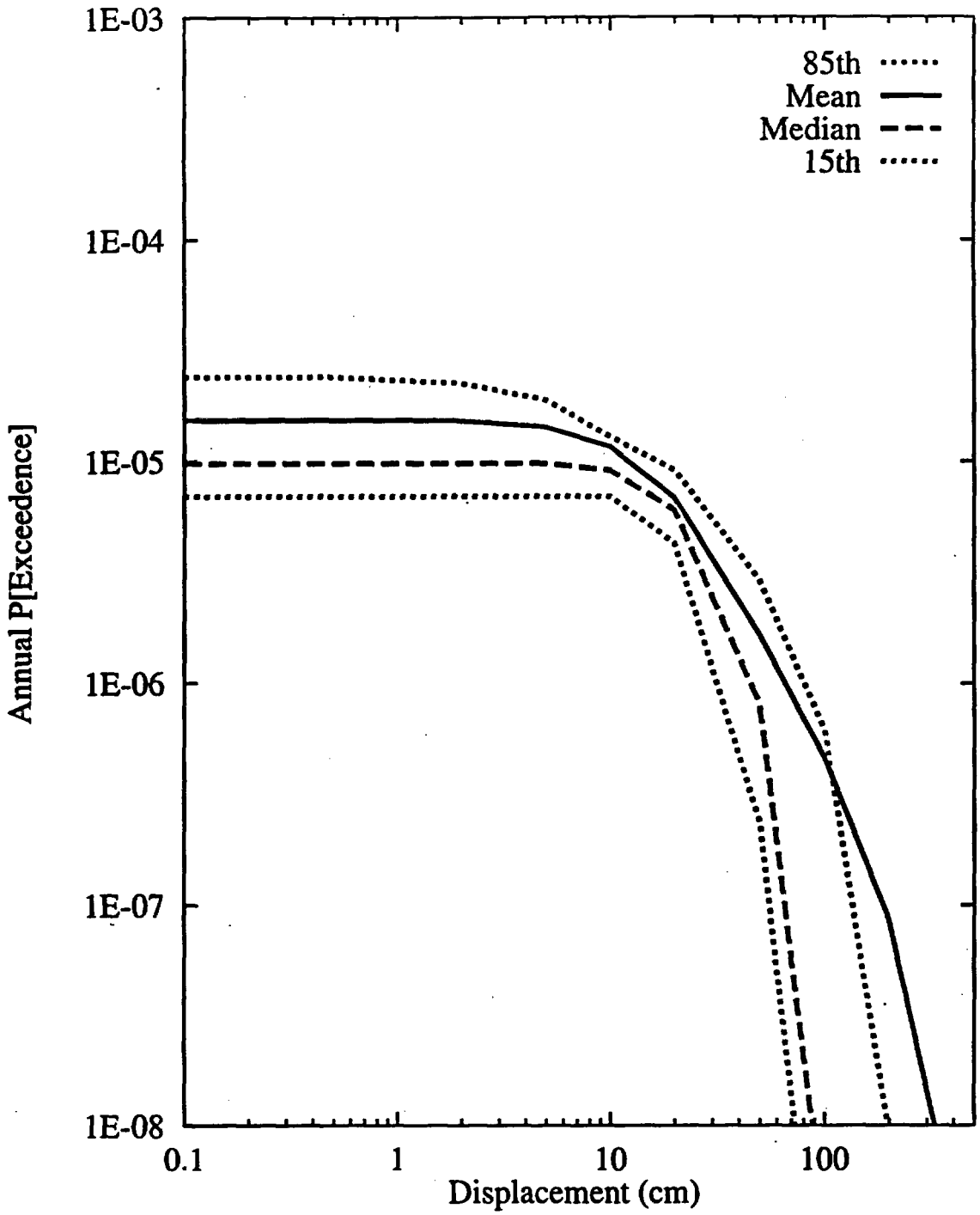

Figure 8-43 Summary hazard curves for Site 1: DFS team, displacement approach

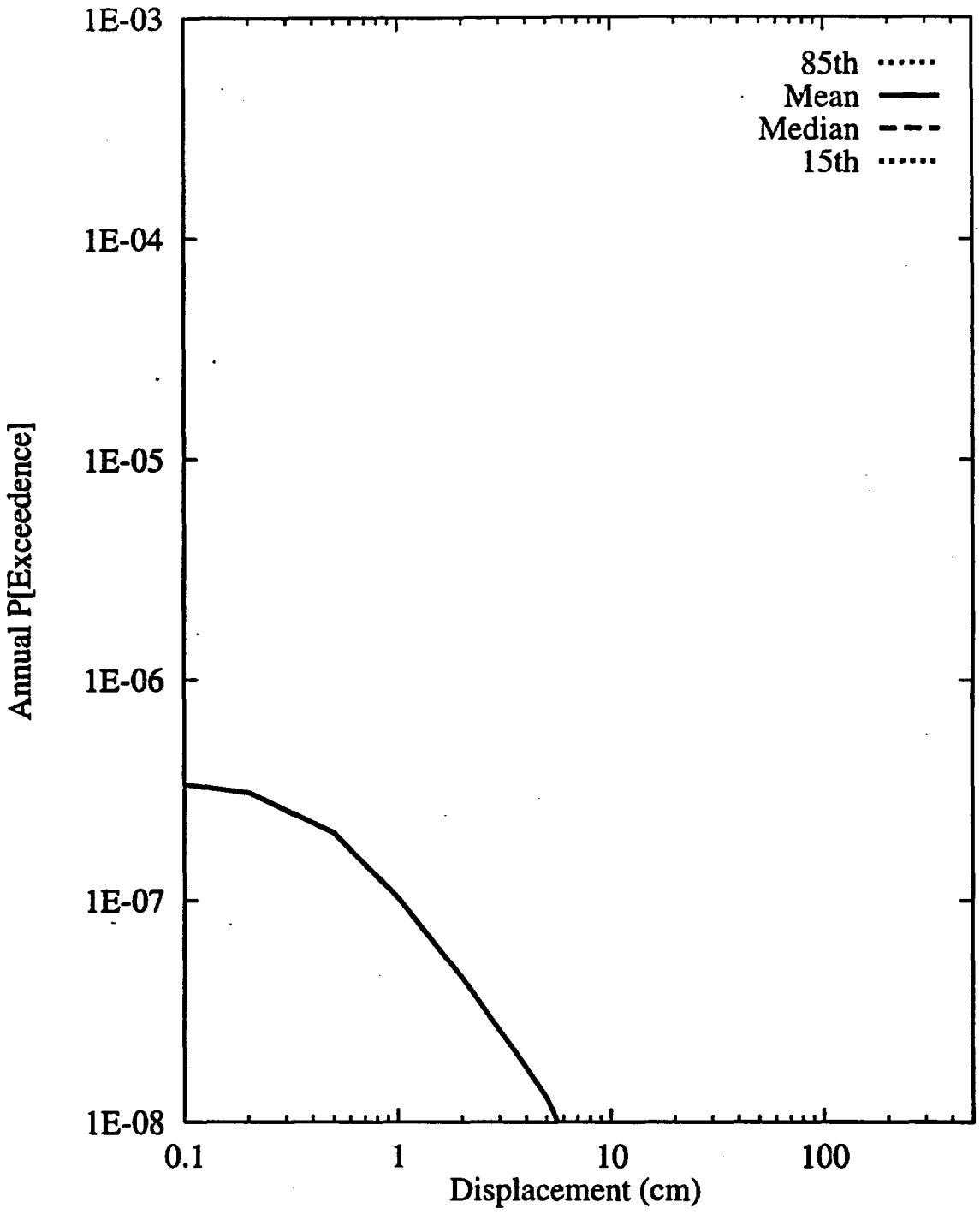

Figure 8-44 Summary hazard curves for Site 7a: DFS team, displacement approach

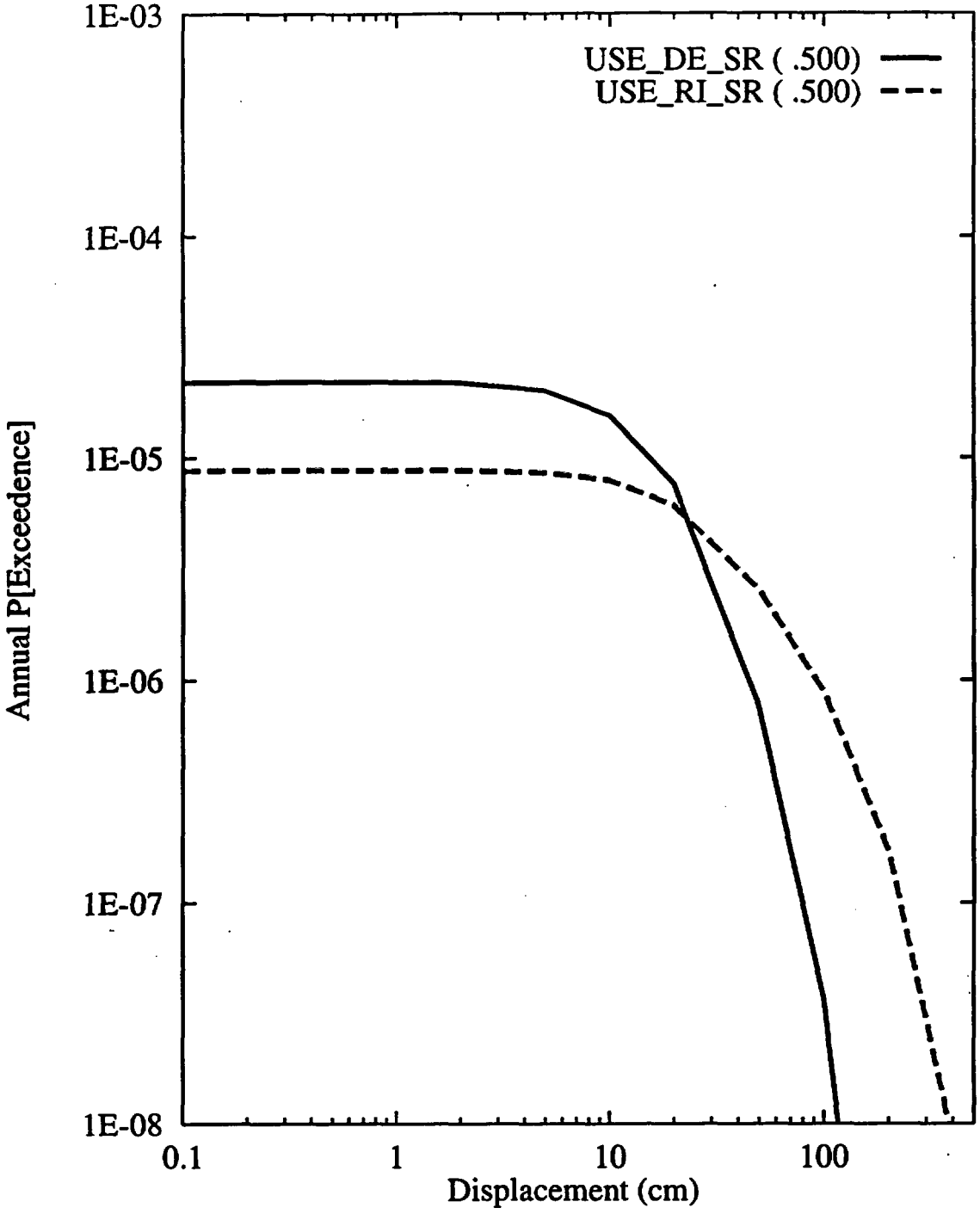

Figure 8-45 Sensitivity of displacement hazard for Site 1 to calculation option: DFS team, displacement approach

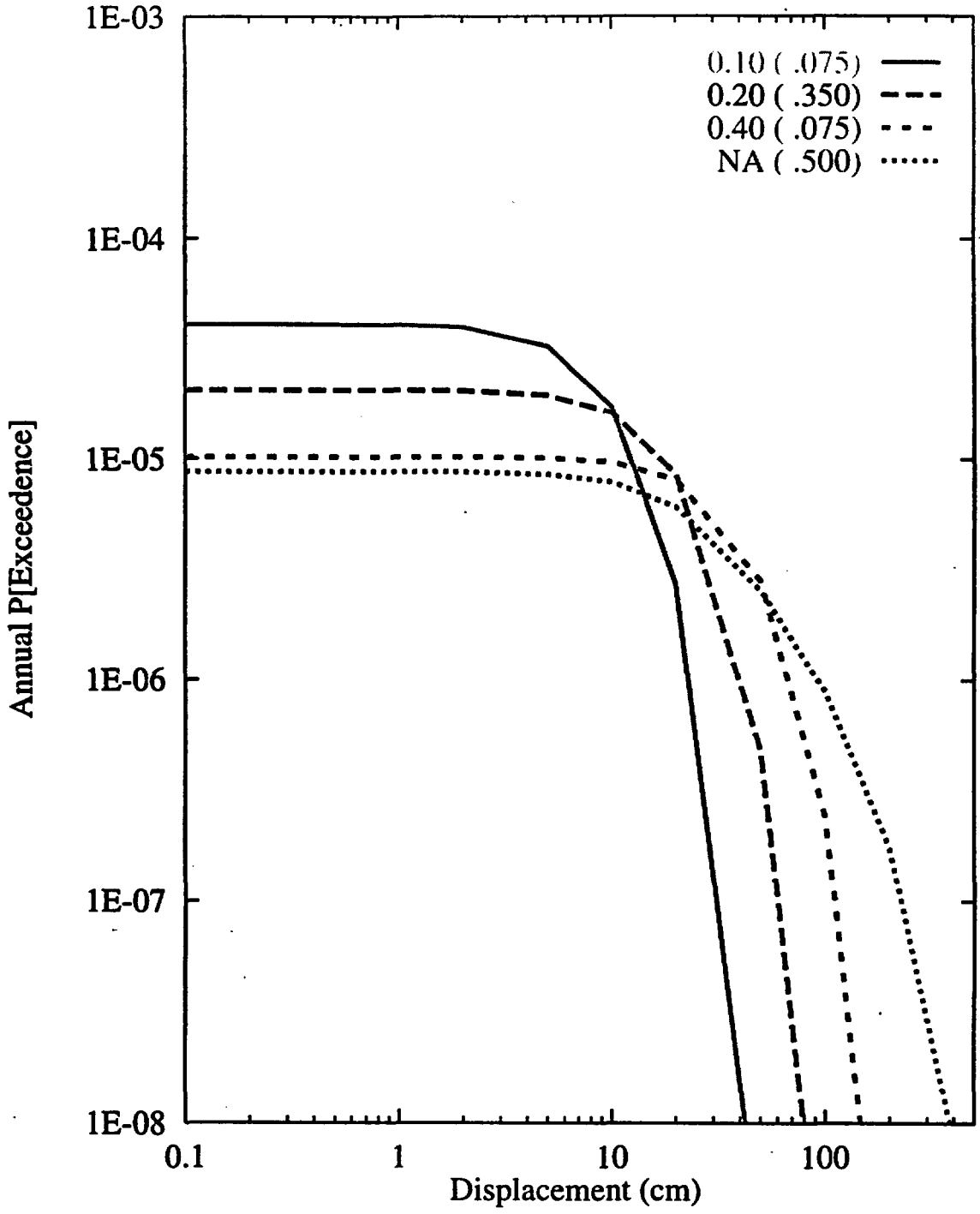

Figure 8-46 Sensitivity of displacement hazard for Site 1 to average displacement per event (m): DFS team, displacement approach

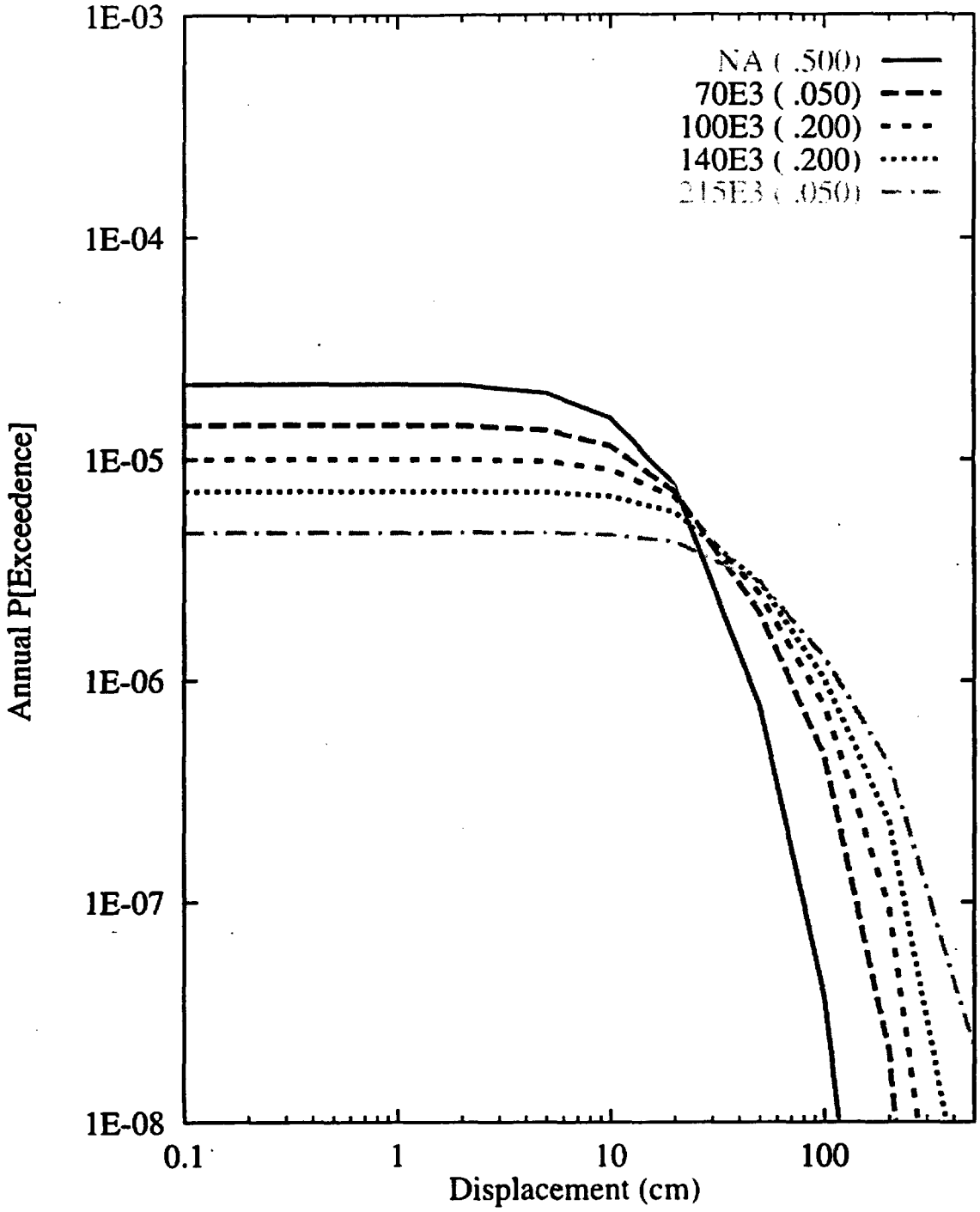

Figure 8-47 Sensitivity of displacement hazard for Site 1 to recurrence interval: DFS team, displacement approach

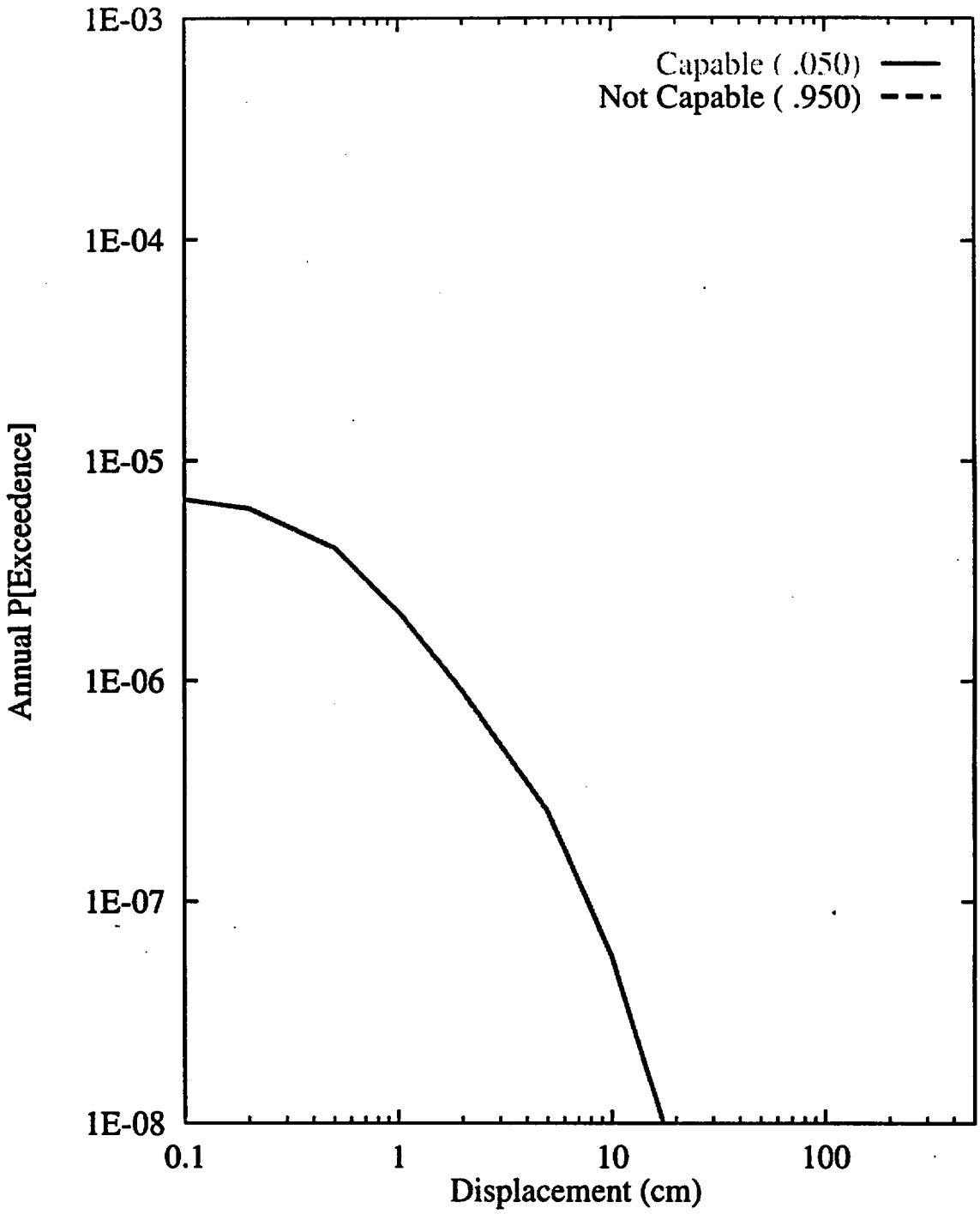

Figure 8-48 Sensitivity of displacement hazard for Site 7a to capability for fault displacement: DFS team, displacement approach

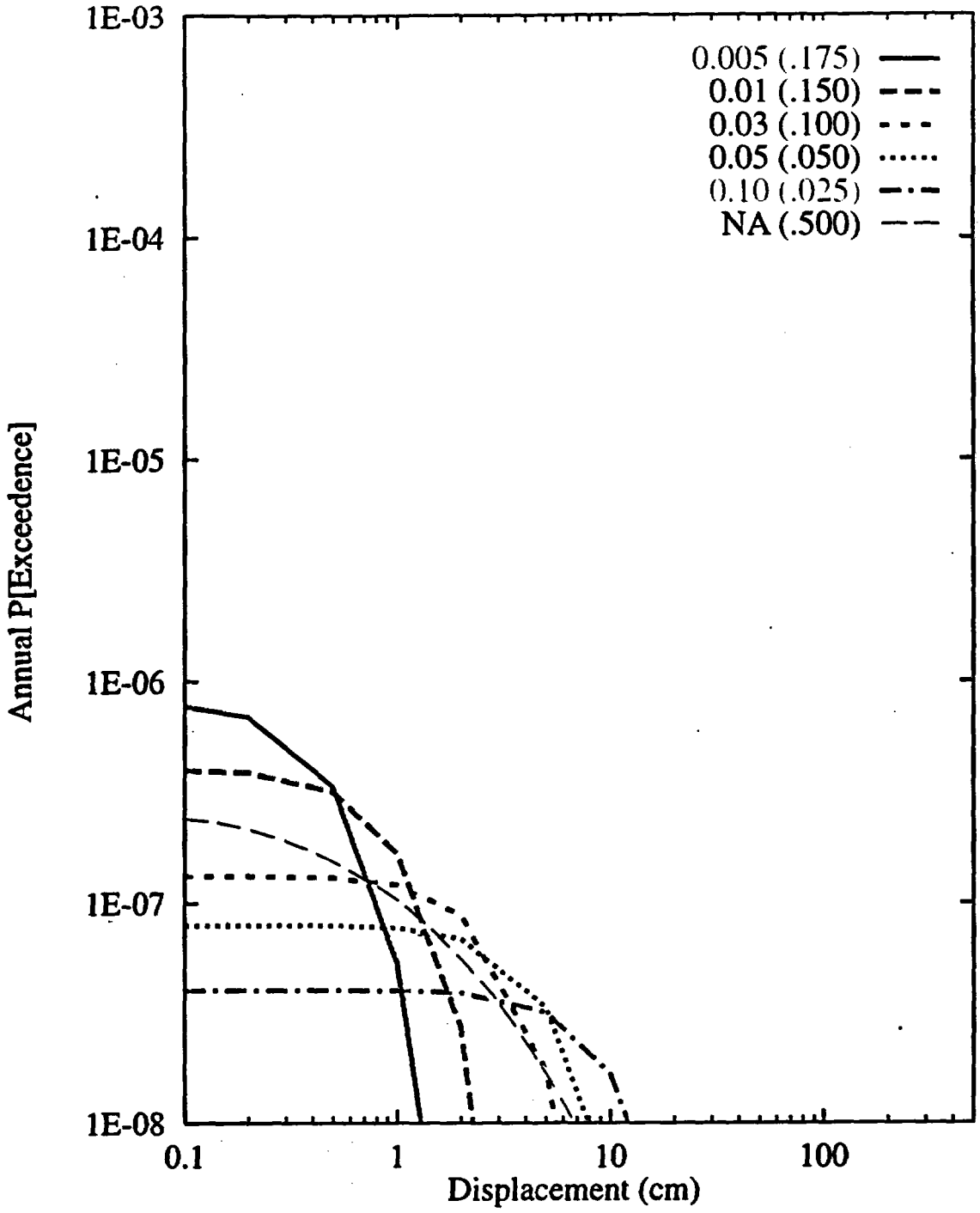

Figure 8-49 Sensitivity of displacement hazard for Site 7a to average displacement per event (m): DFS team, desplacement approach

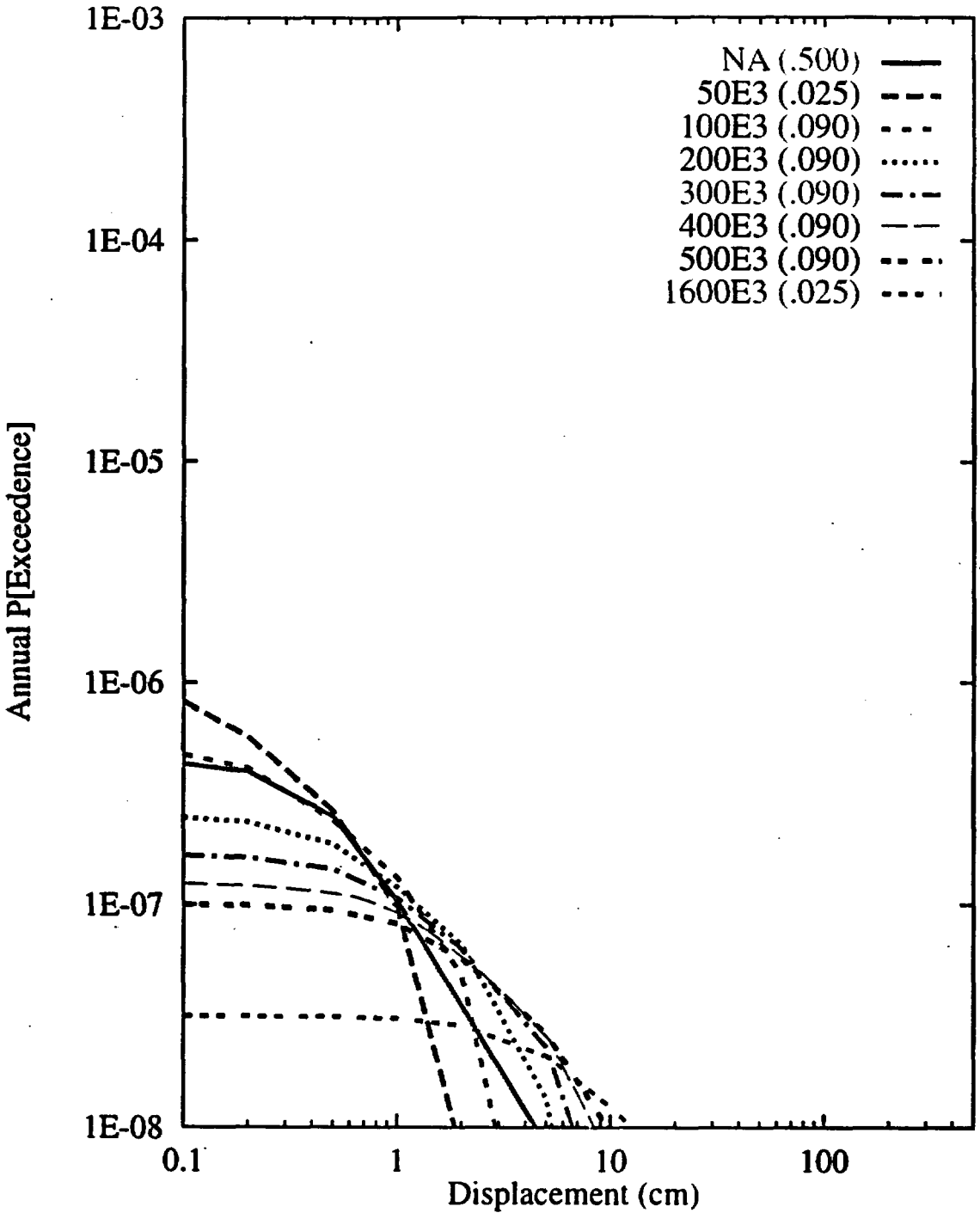

Figure 8-50 Sensitivity of displacement hazard for Site 7a to recurrence interval: DFS team, displacement approach

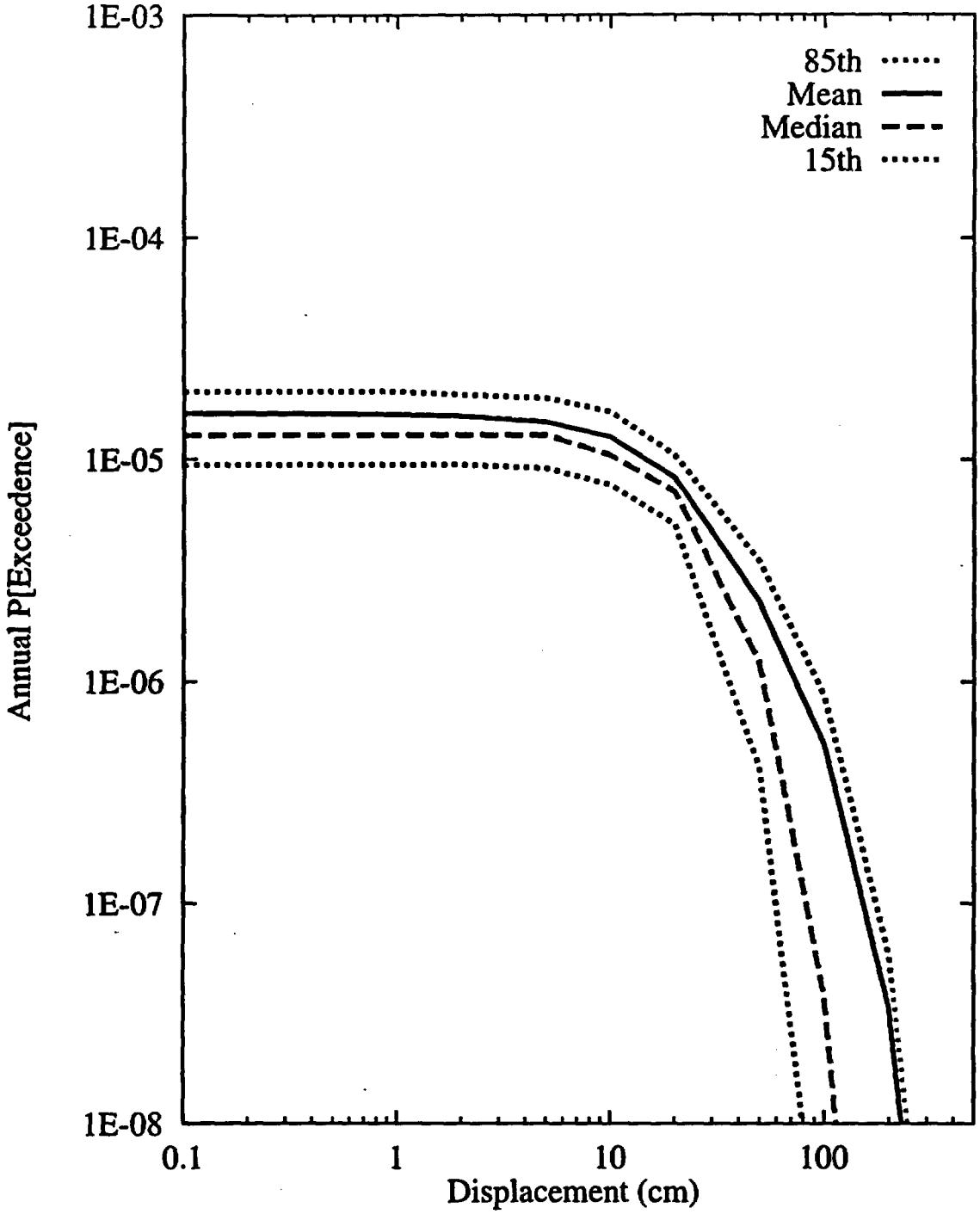

Figure 8-51 Summary hazard curves for Site 1: RYA team, displacement approach

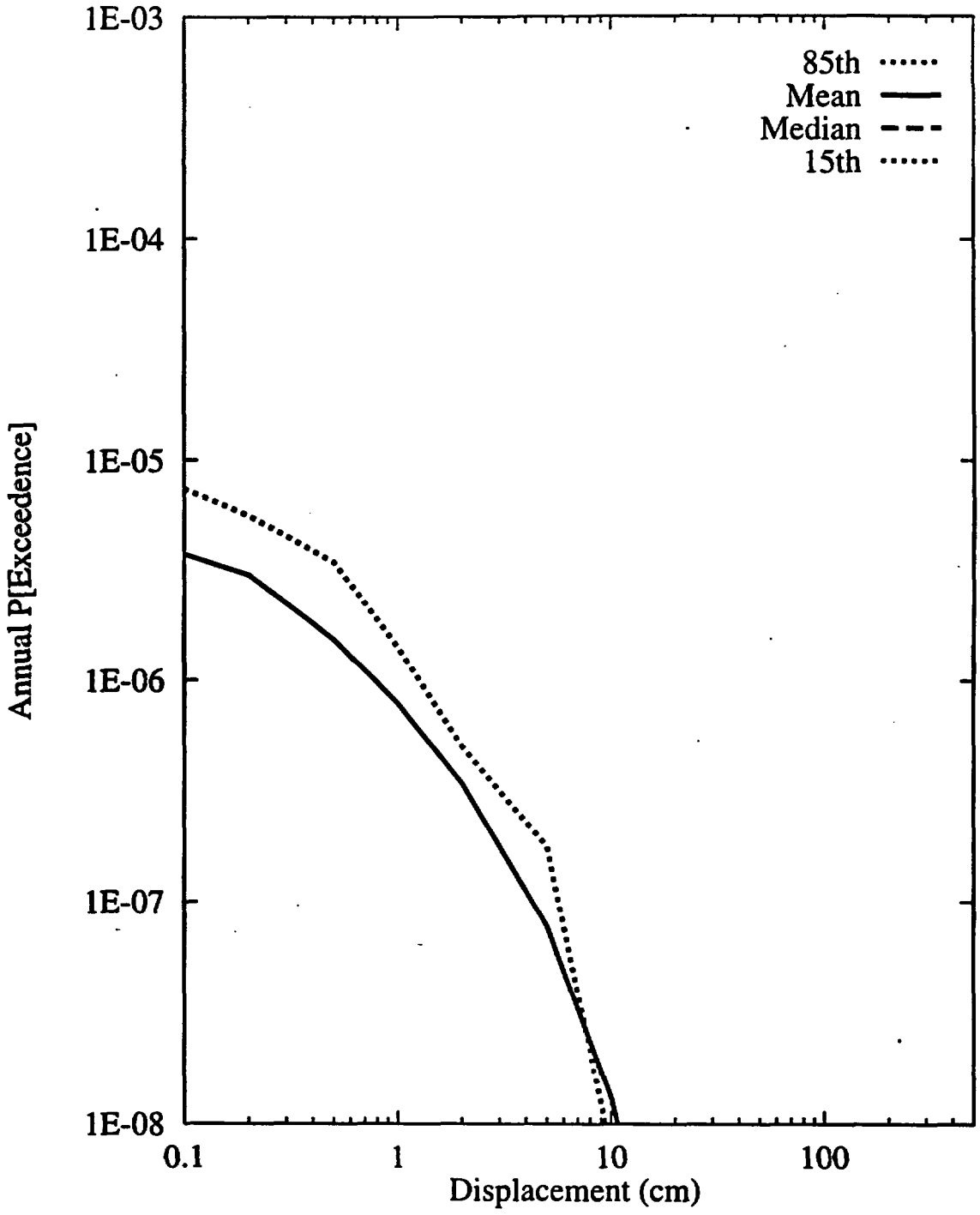

Figure 8-52 Summary hazard curves for Site 7a: RYA team, displacement approach

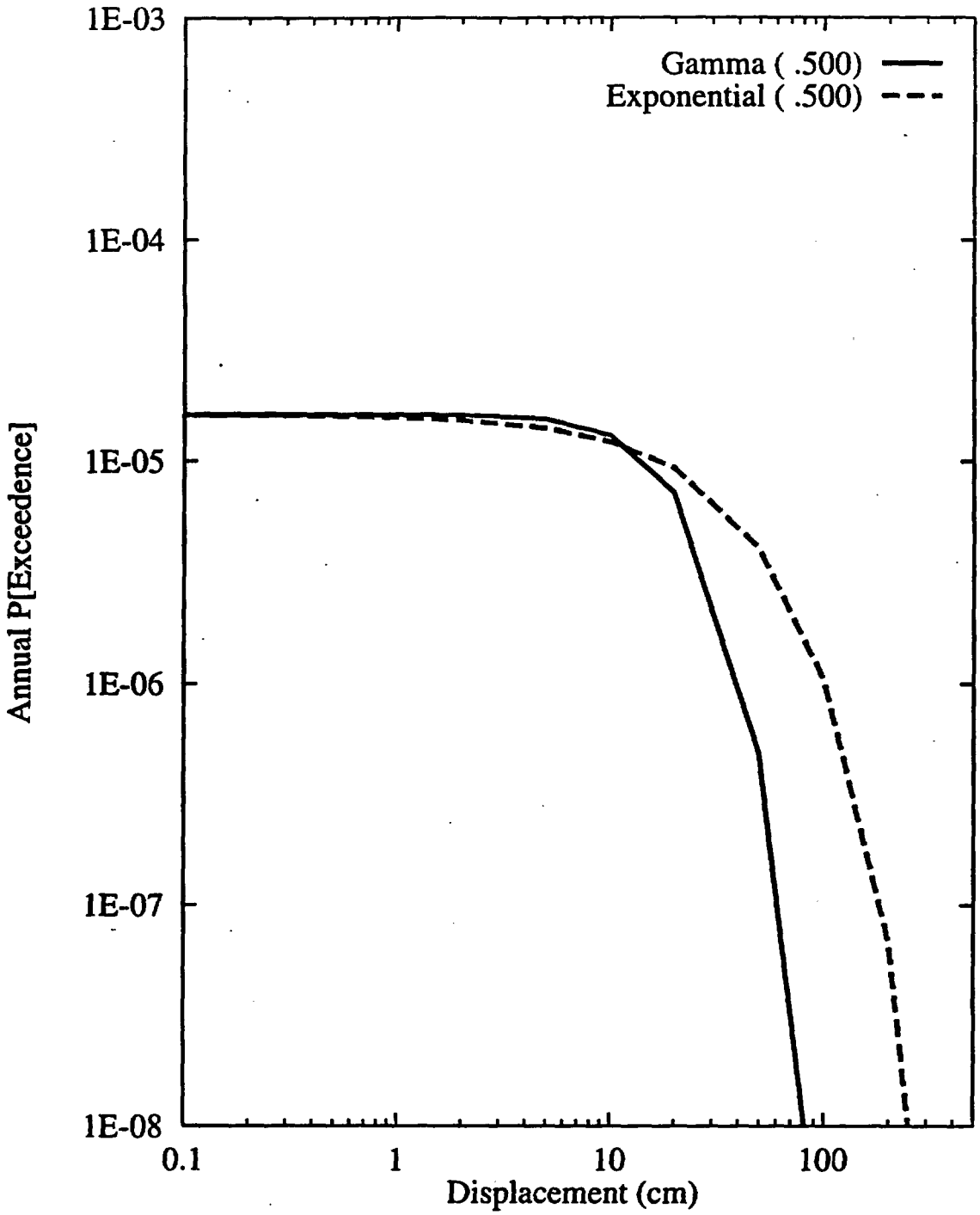

Figure 8-53 Sensitivity of displacement hazard for Site 1 to distribution shape: RYA team, displacement approach

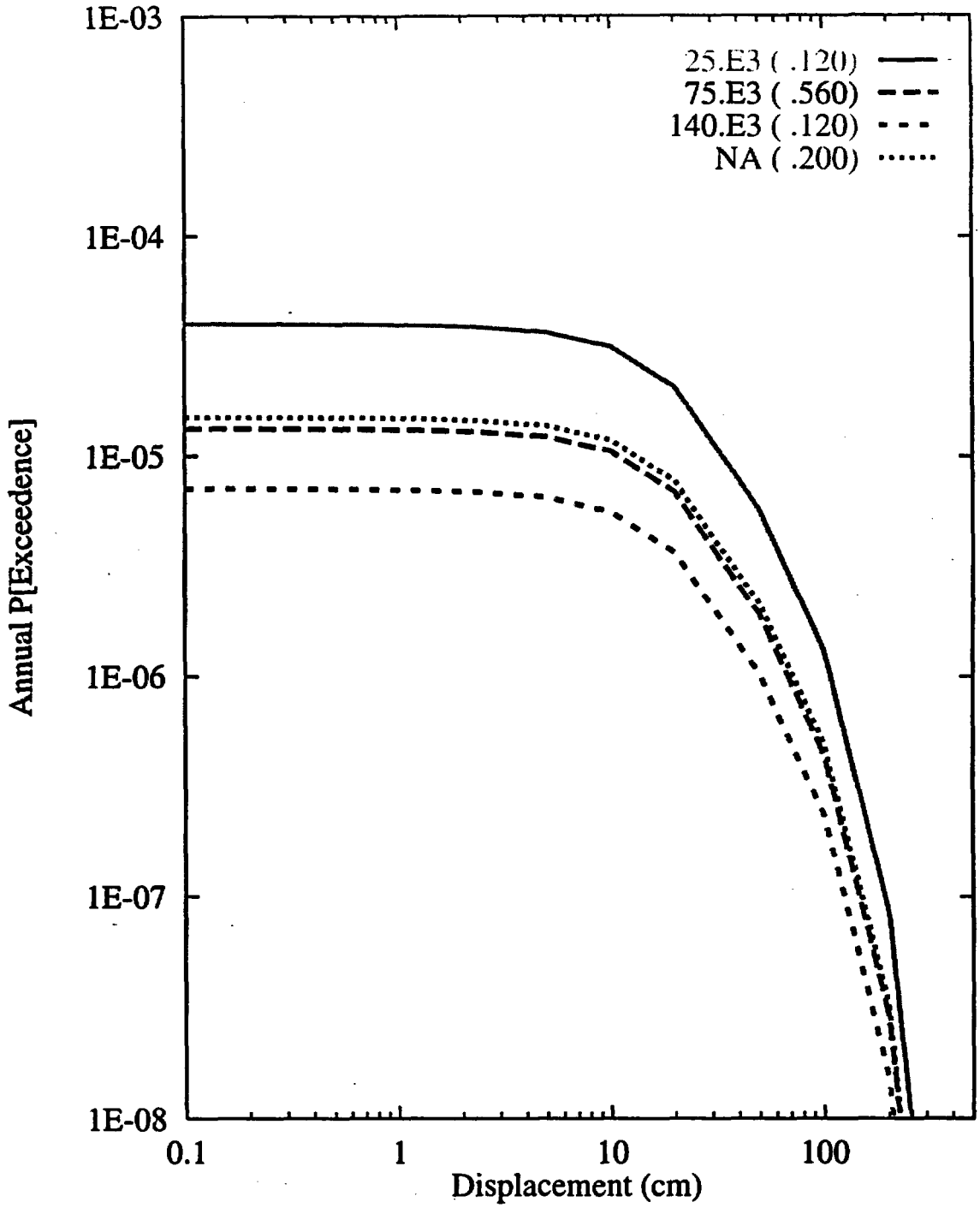

Figure 8-54 Sensitivity of displacement hazard for Site 1 to recurrence interval: RYA team, displacement approach

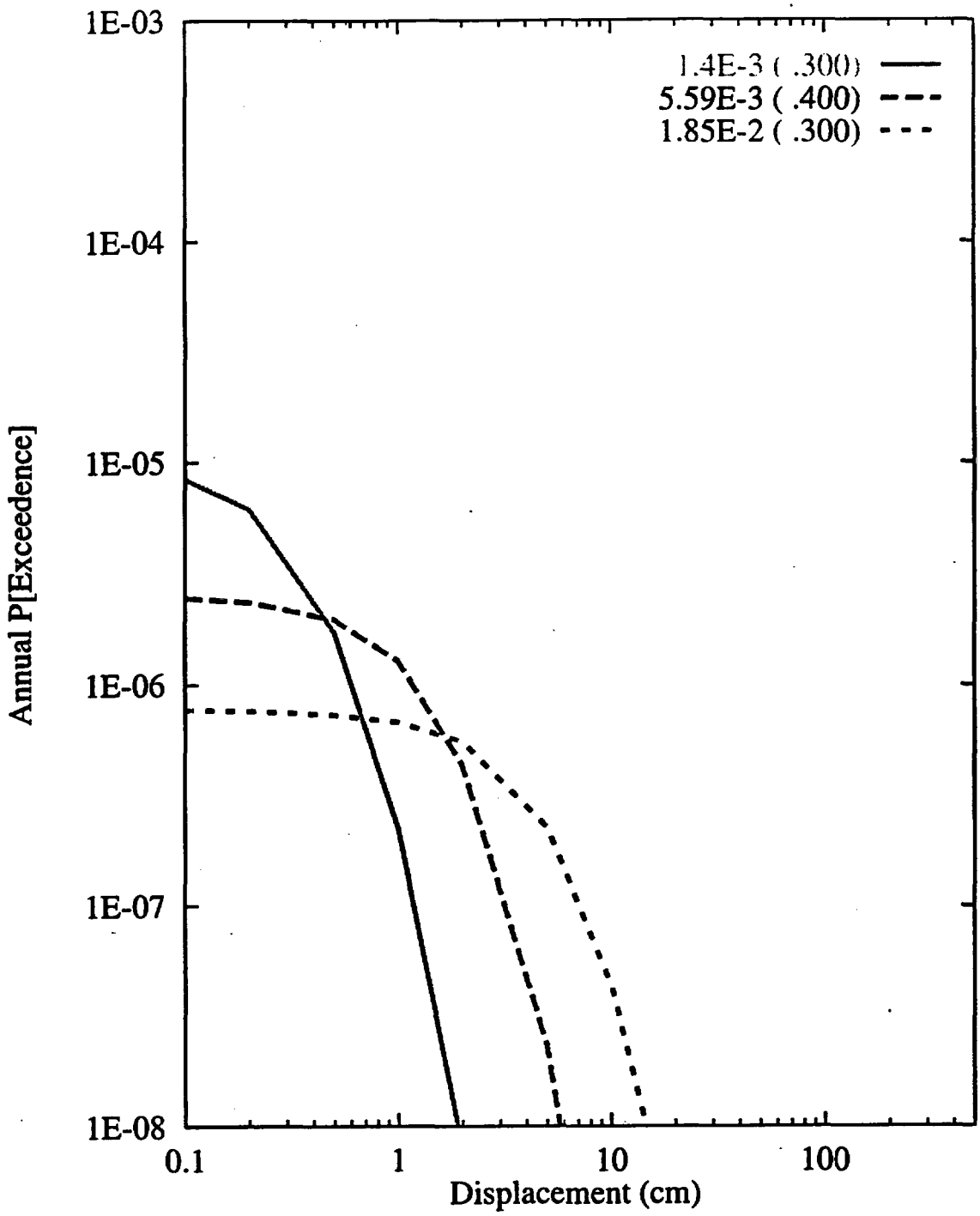

Figure 8-55 Sensitivity of displacement hazard for Site 7a to parameter beta: RYA team, displacement approach

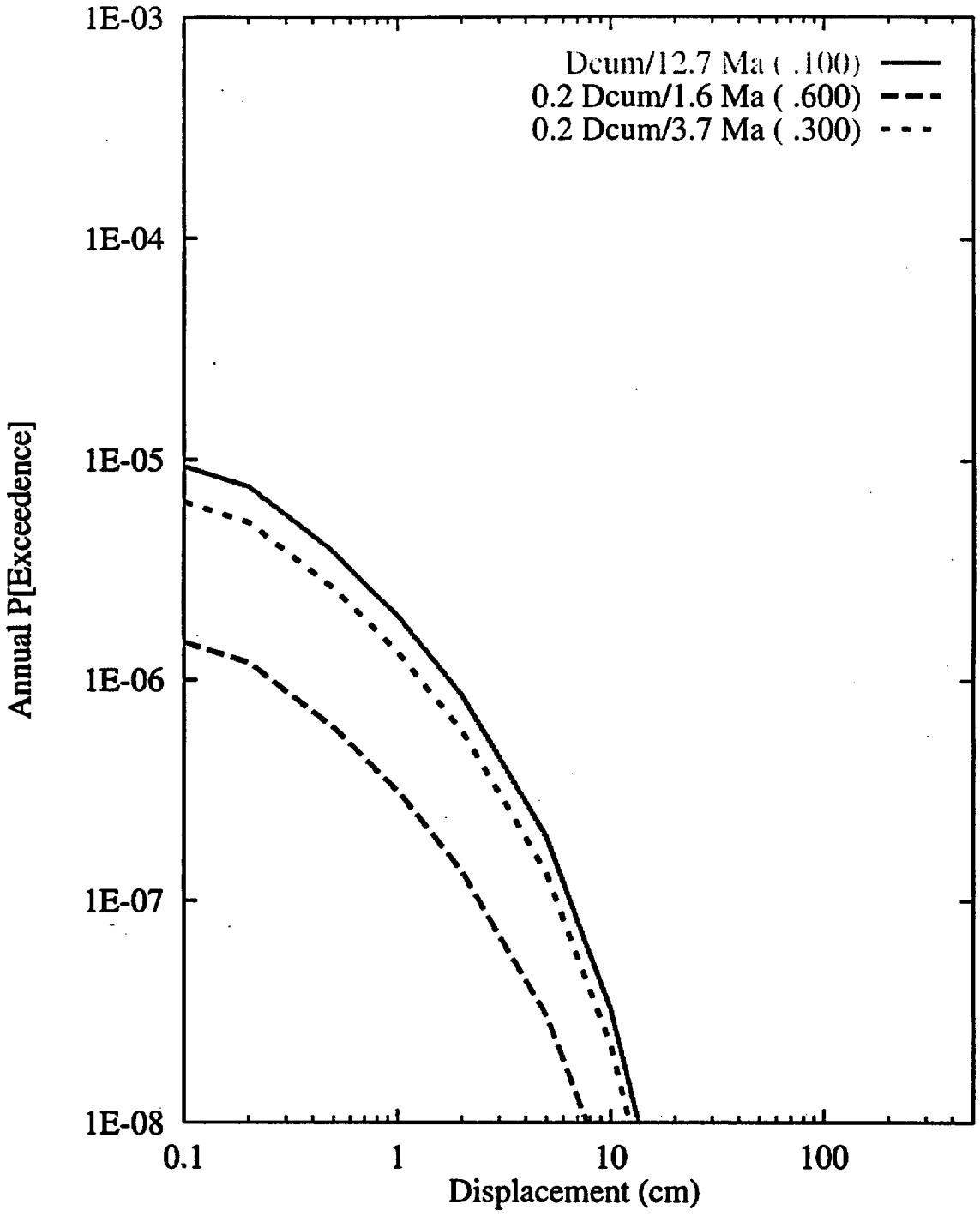

Figure 8-56 Sensitivity of displacement hazard for Site 7a to calculation of slip rate: RYA team, displacement approach

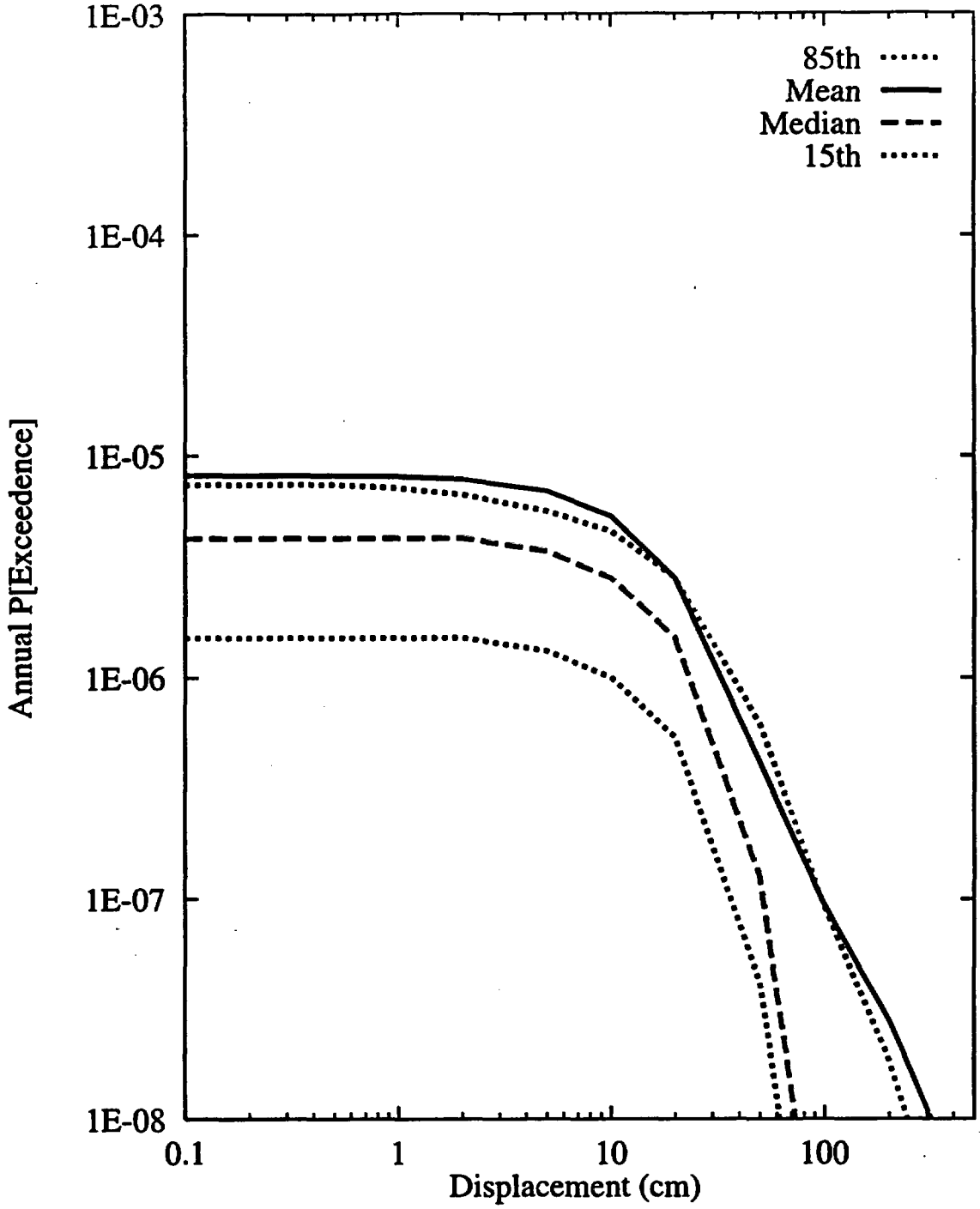

Figure 8-57 Summary hazard curves for Site 1: SBK team, earthquake approach

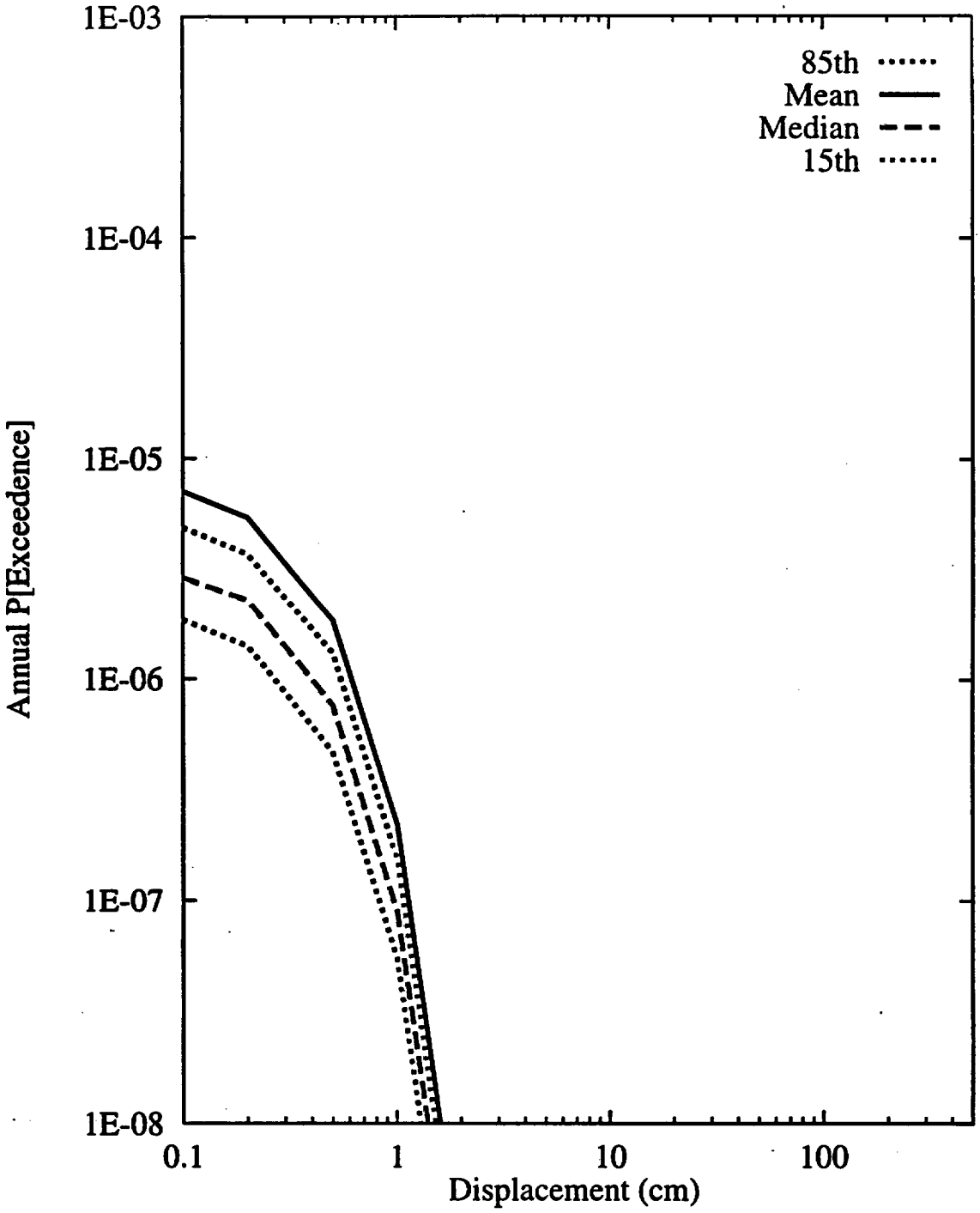

Figure 8-58 Summary hazard curves for Site 7a: SBK team, earthquake approach

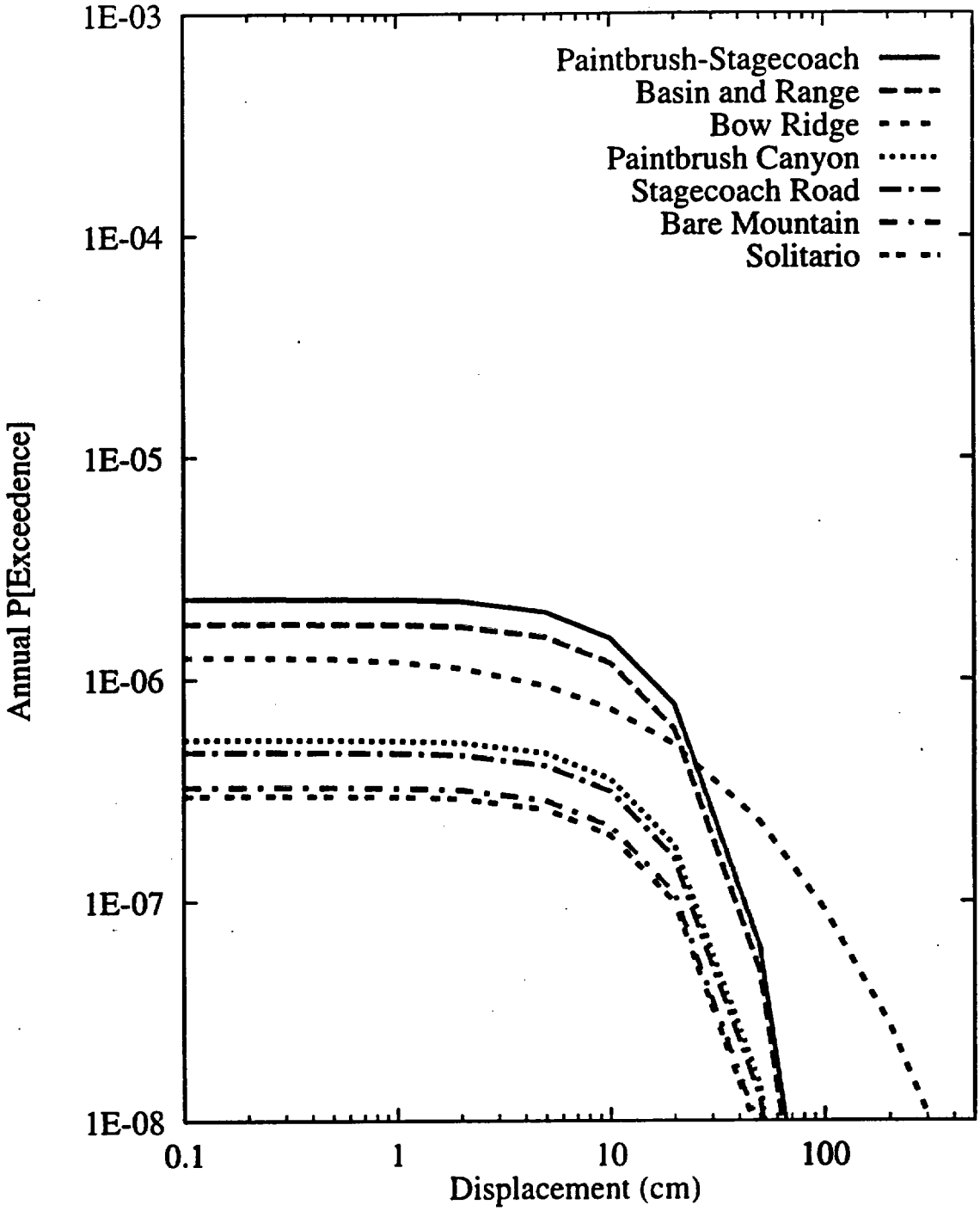

Figure 8-59 Mean hazard curves by source for Site 1: SBK team, earthquake approach

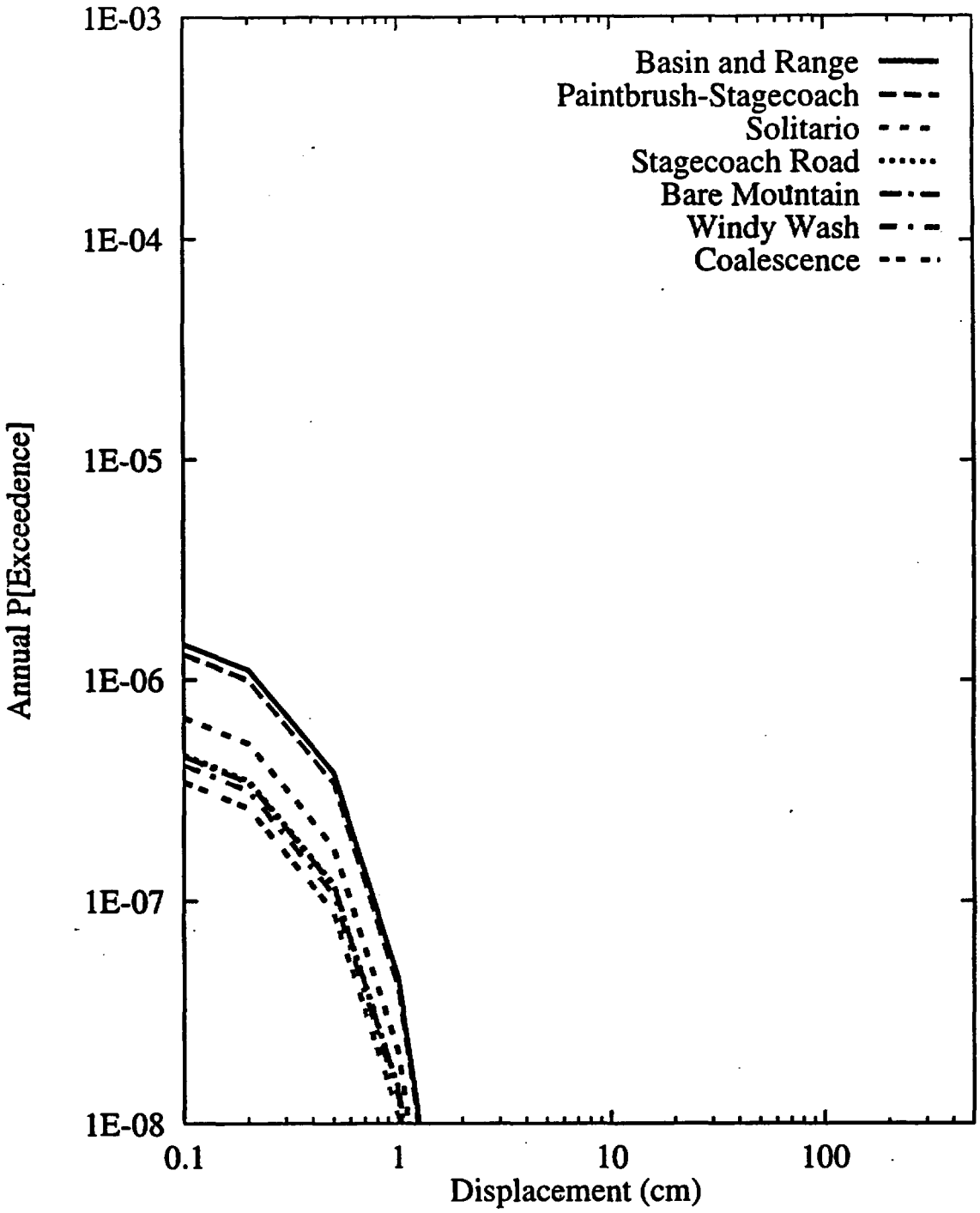

Figure 8-60 Mean hazard curves by source for Site 7a: SBK team, earthquake approach

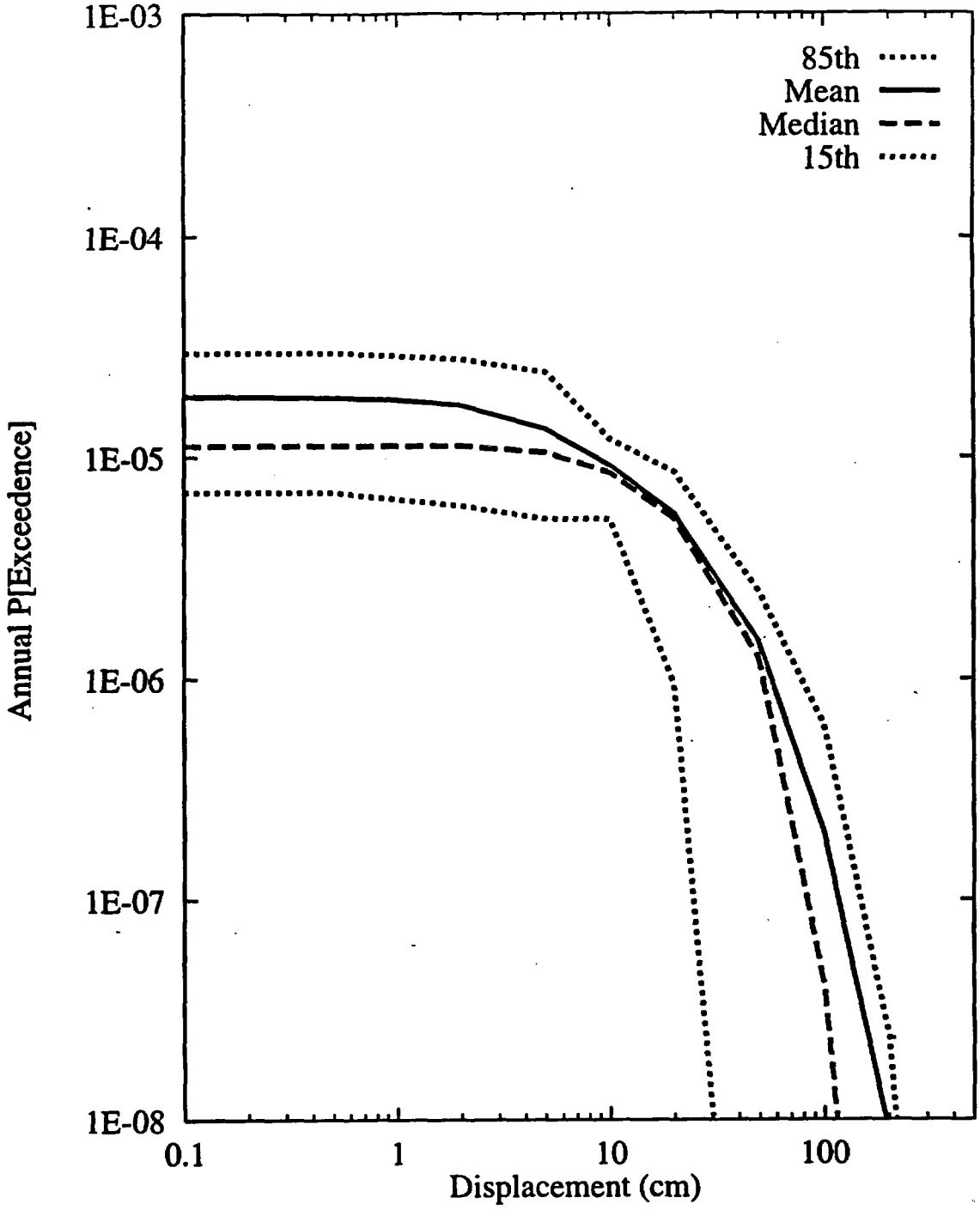

Figure 8-61 Summary hazard curves for Site 1: SBK team, displacement approach

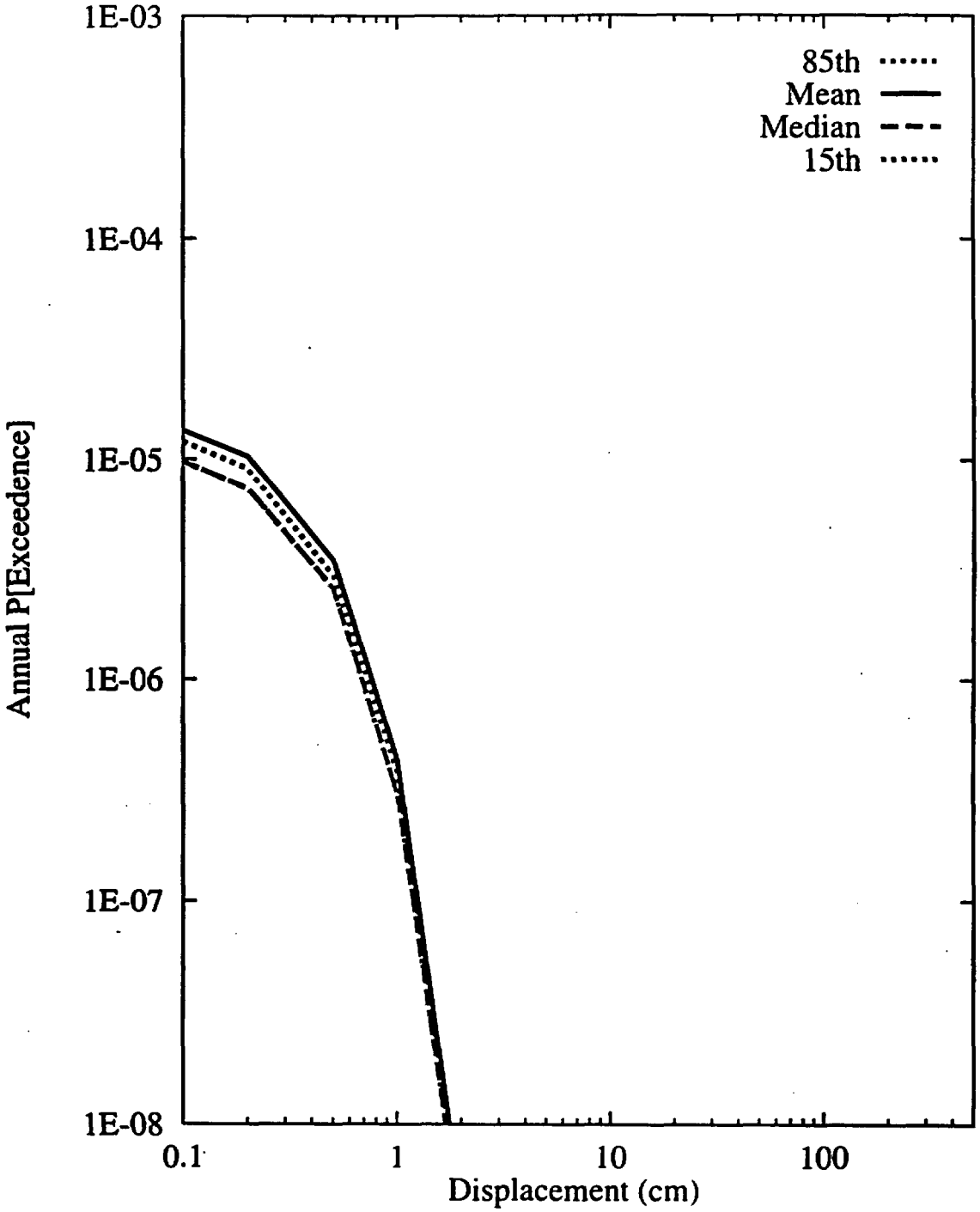

Figure 8-62 Summary hazard curves for Site 7a: SBK team, displacement approach

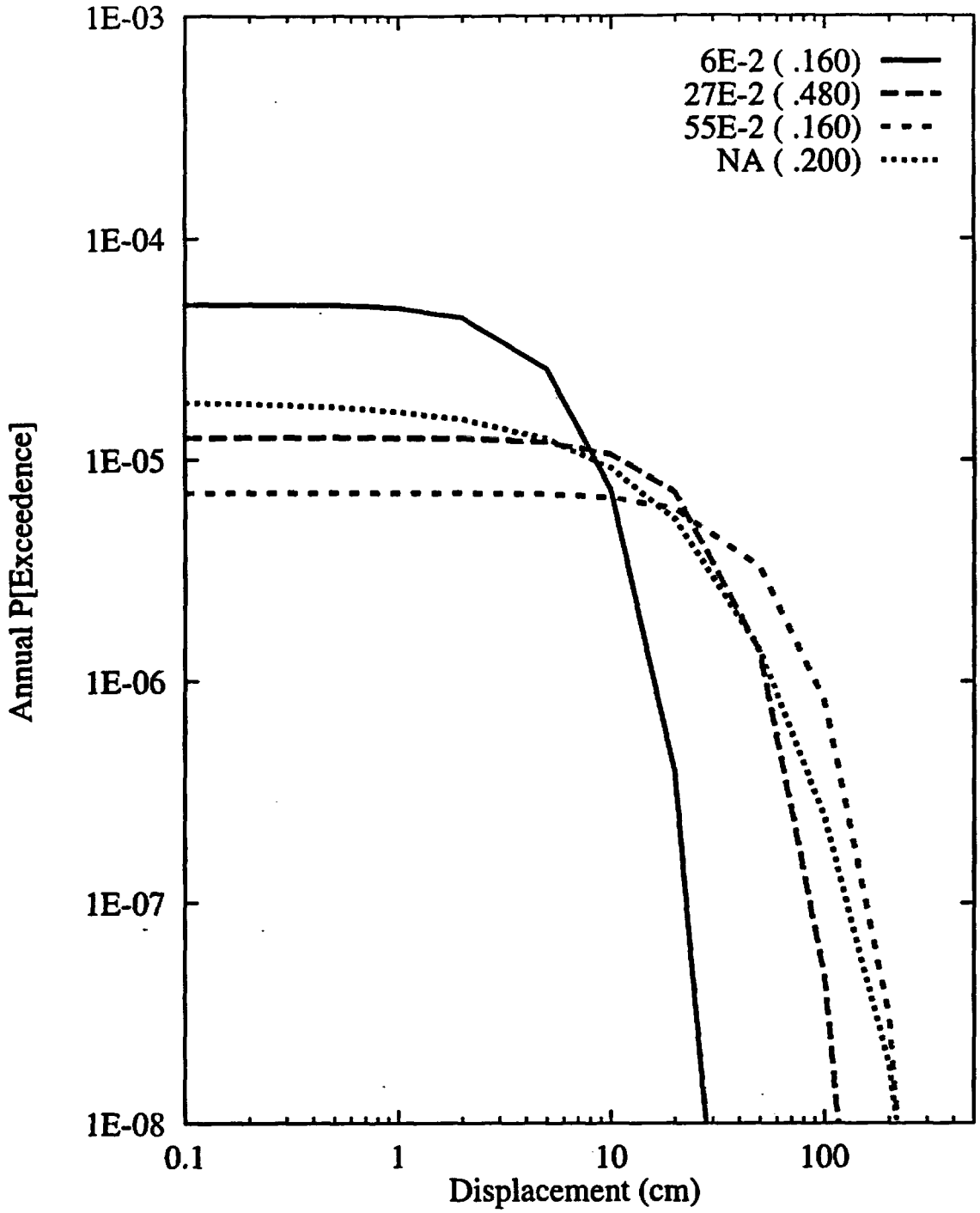

Figure 8-63 Sensitivity of displacement hazard for Site 1 to average displacement per event (m): SBK team, displacement approach

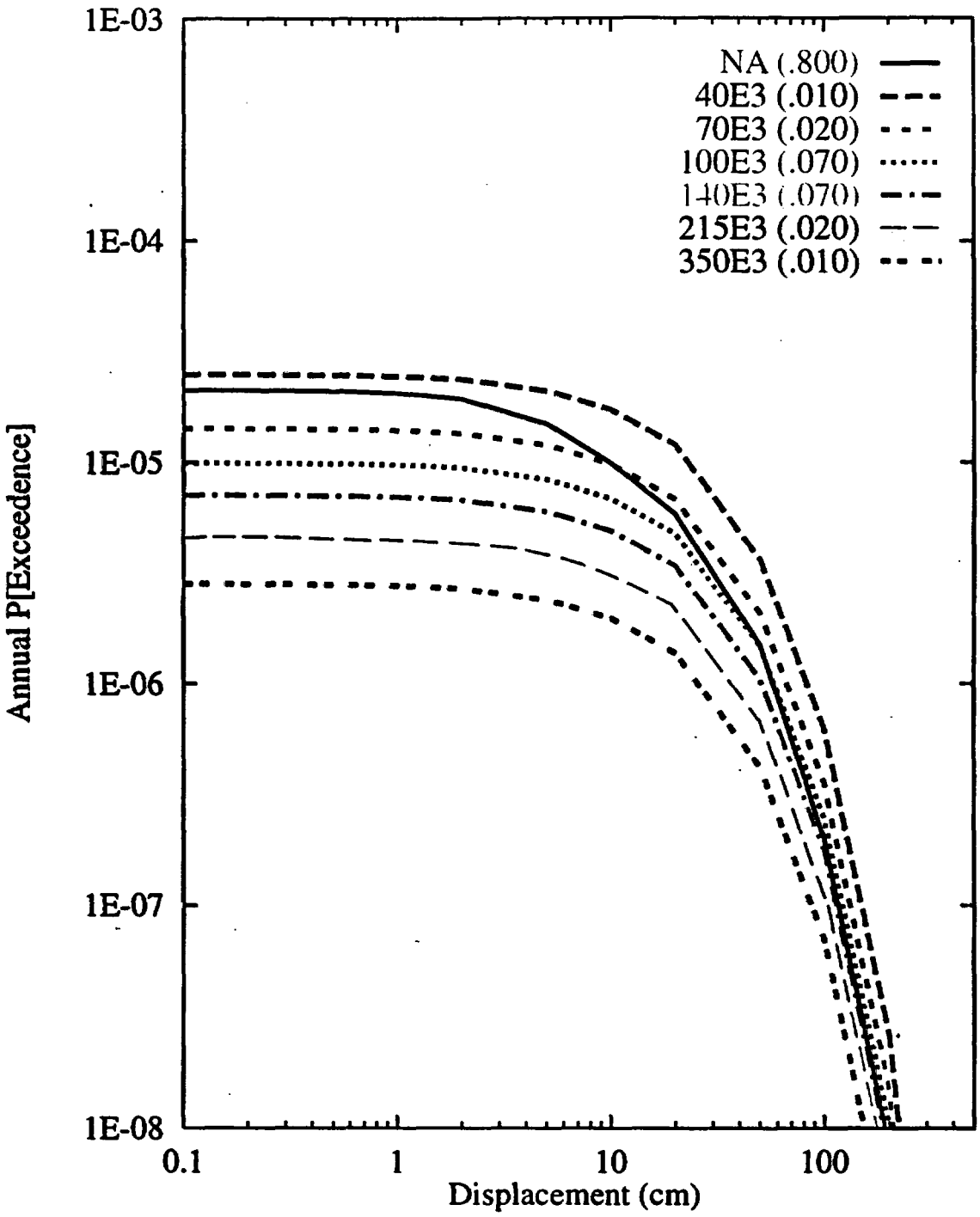

Figure 8-64 Sensitivity of displacement hazard for Site 1 to recurrence interval (yr): SBK team, displacement approach

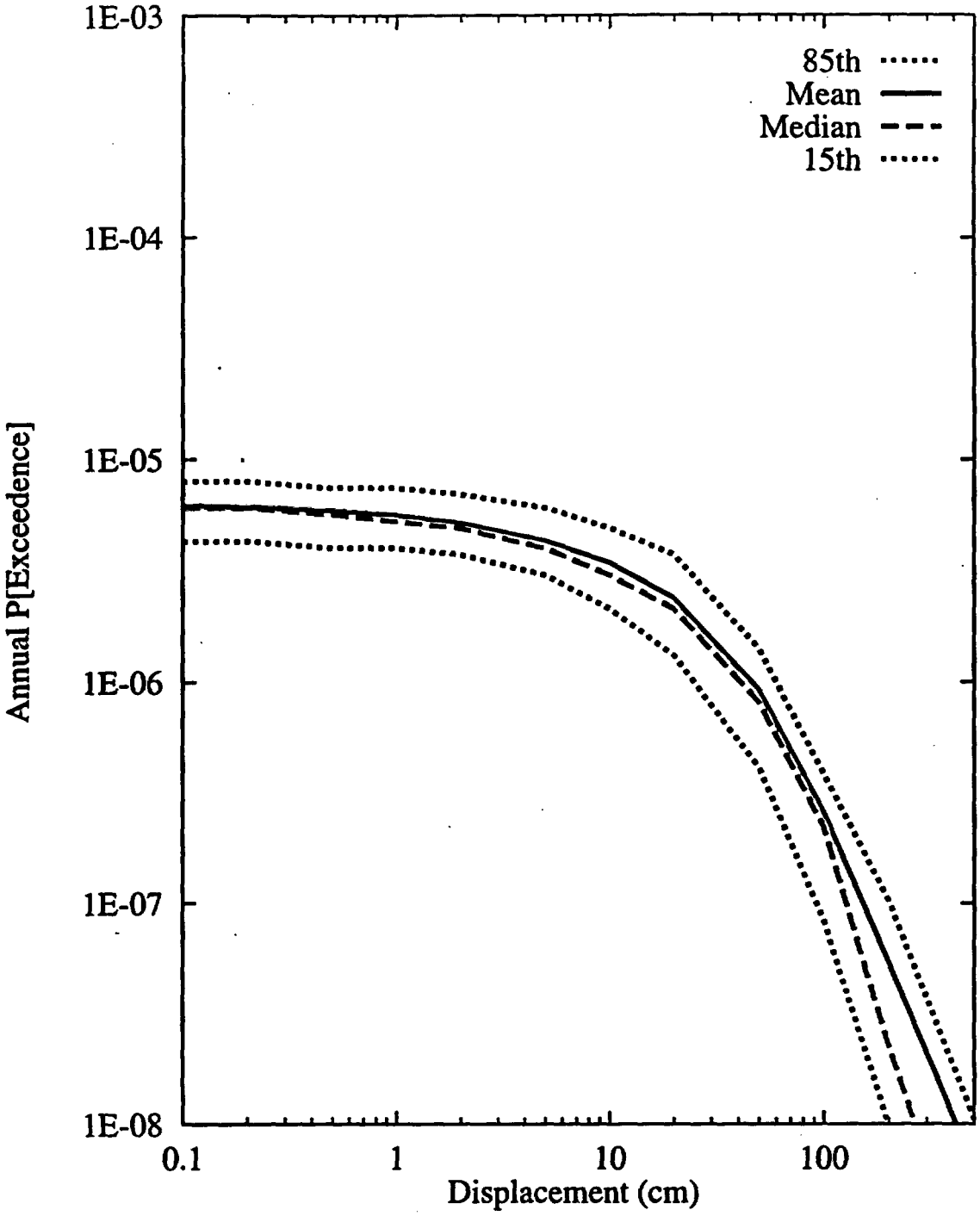

Figure 8-65 Summary hazard curves for Site 1: SDO team, earthquake approach

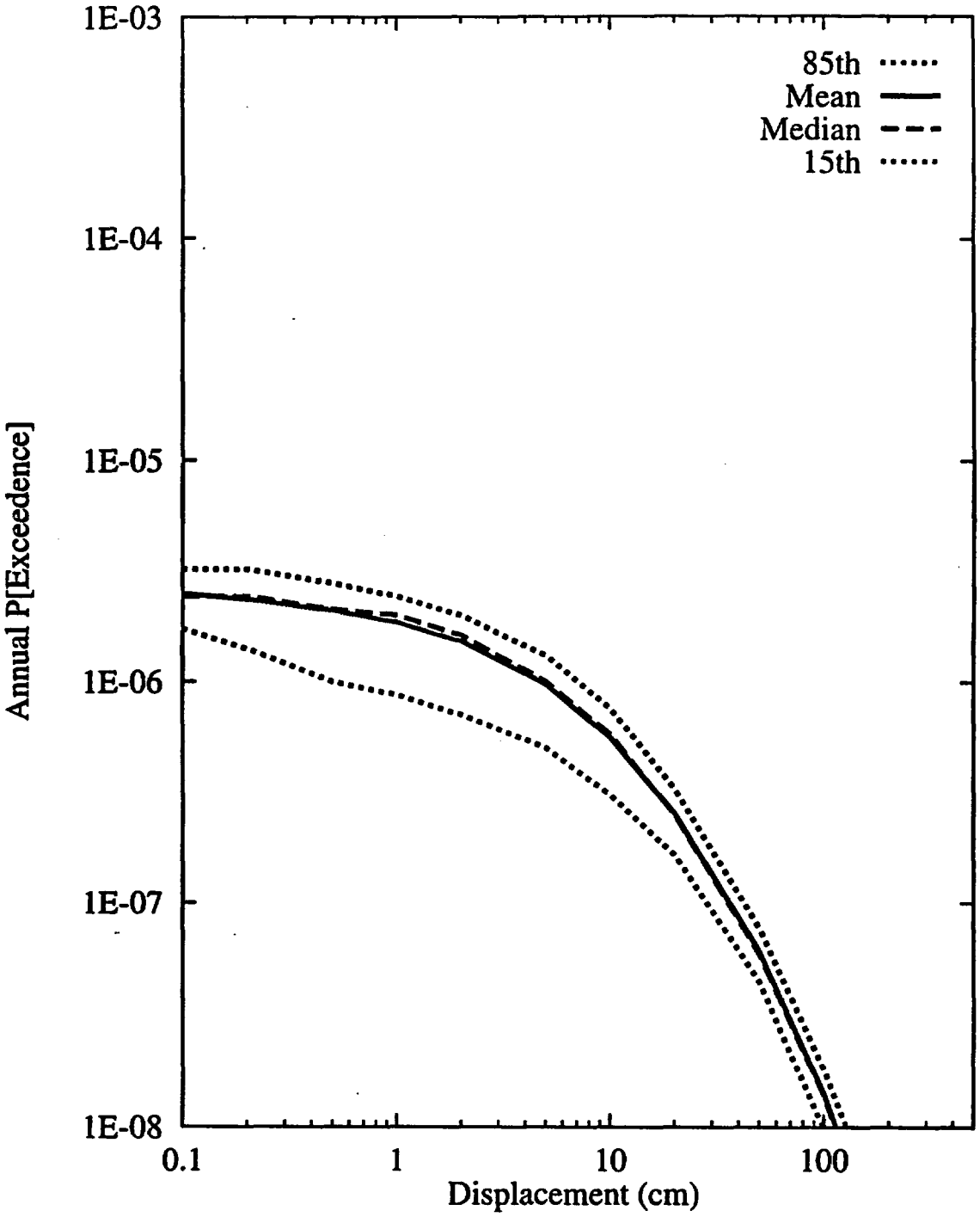

Figure 8-66 Summary hazard curves for Site 7a: SDO team, earthquake approach

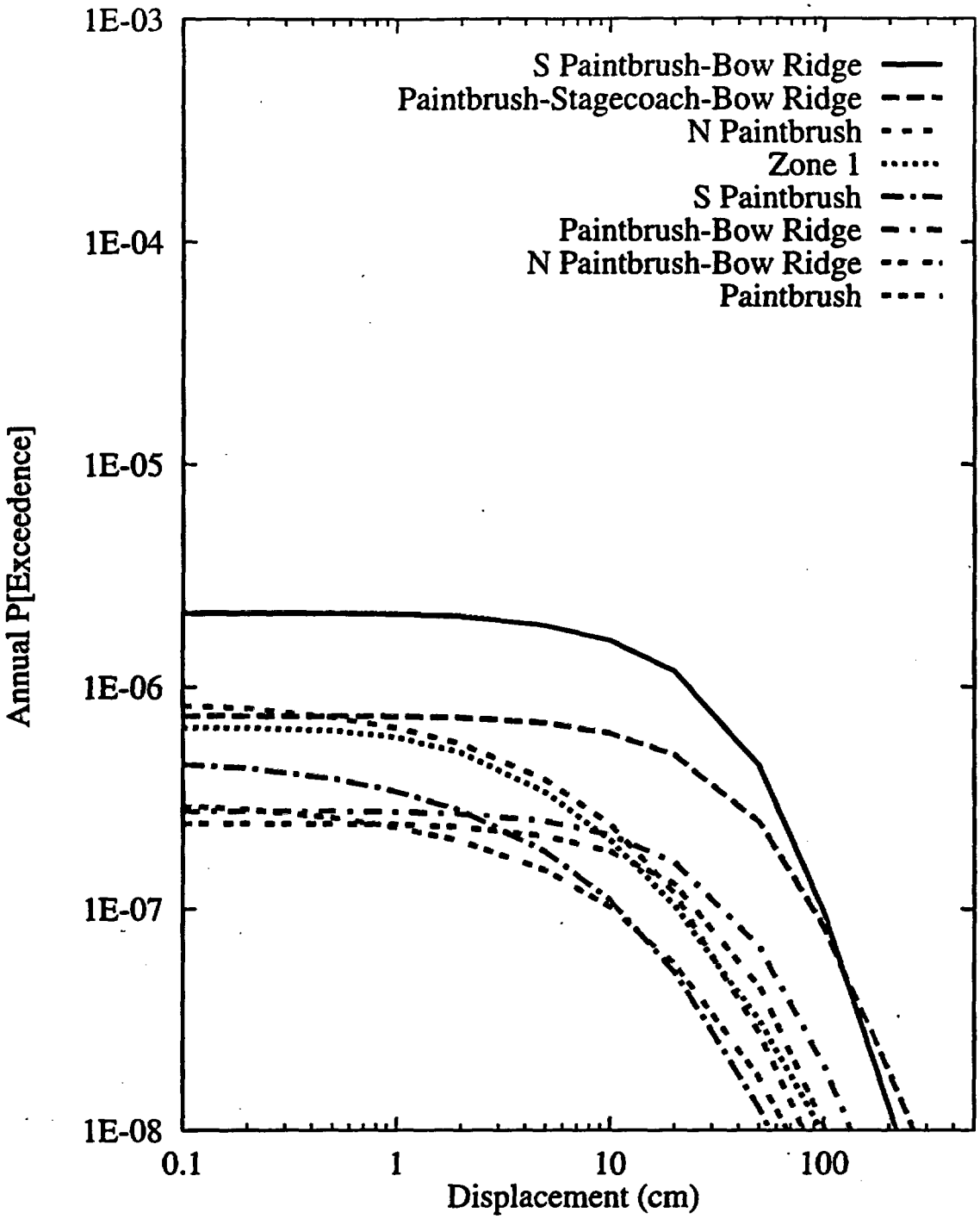

Figure 8-67 Mean hazard curves by source for Site 1: SDO team, earthquake approach

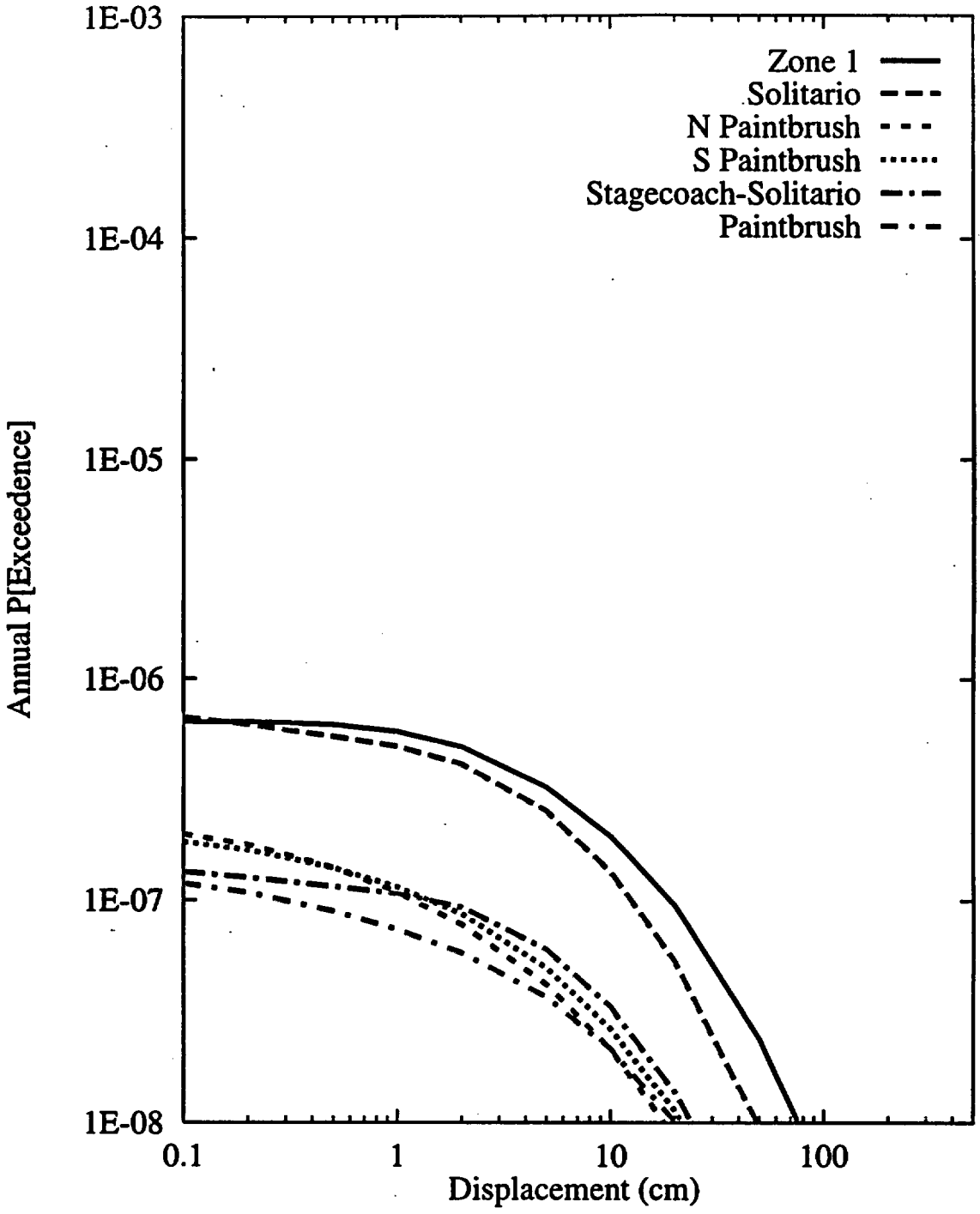

Figure 8-68 Mean hazard curves by source for Site 7a: SDO team, earthquake qpproach

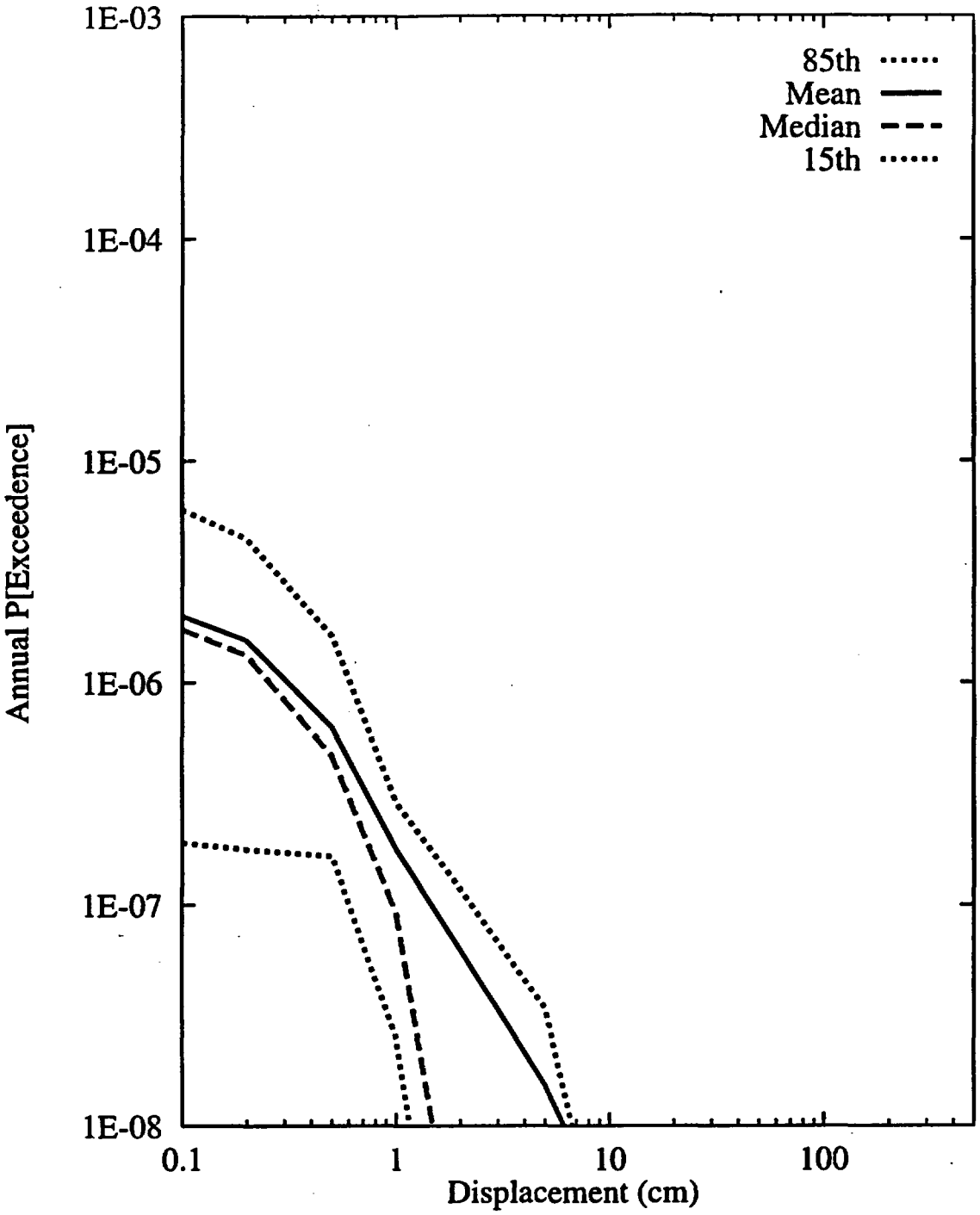

Figure 8-69 Summary hazard curves for Site 7a: SDO team, displacement approach

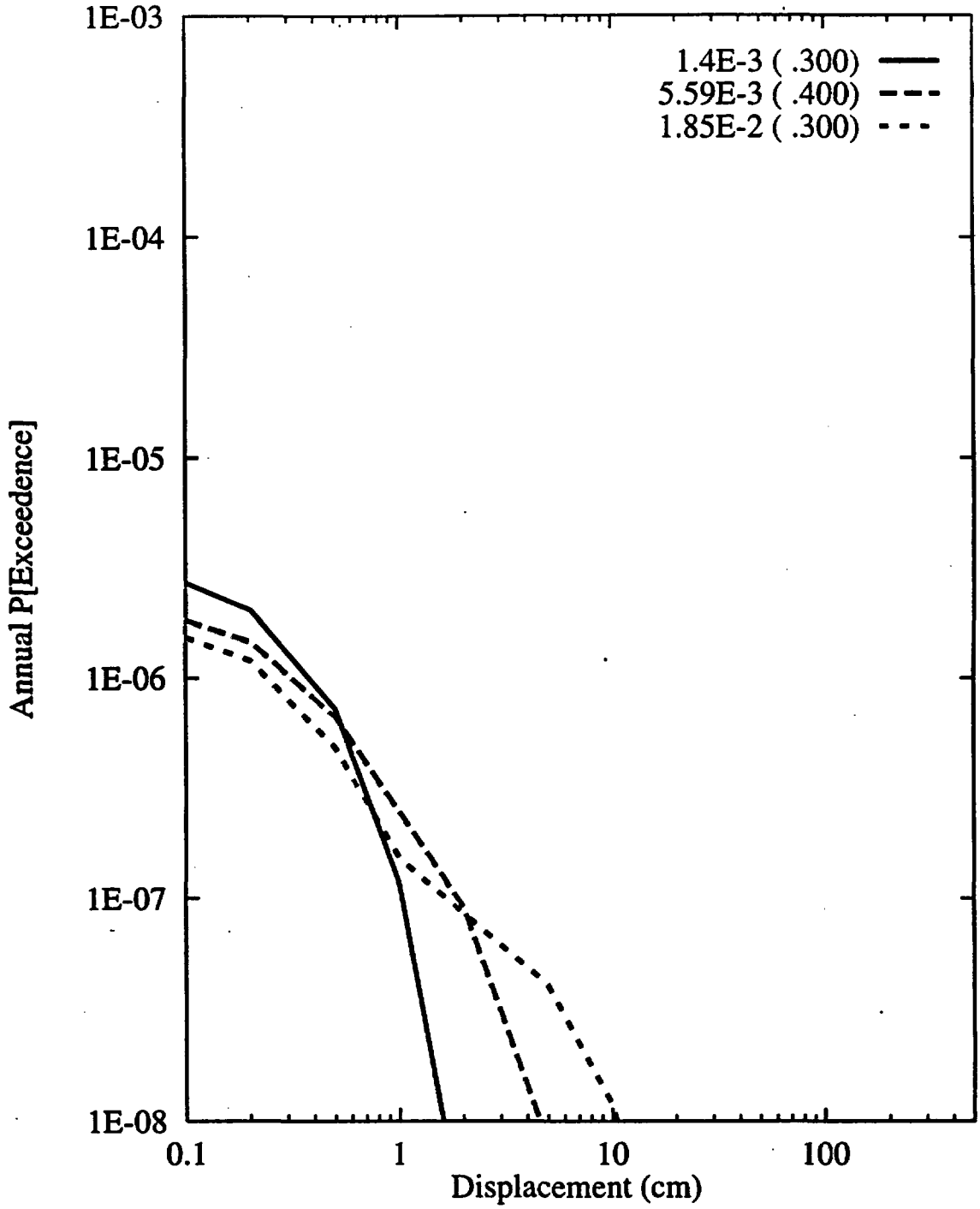

Figure 8-70 Sensitivity of displacement hazard for Site 7a to parameter beta: SDO team, displacement approach

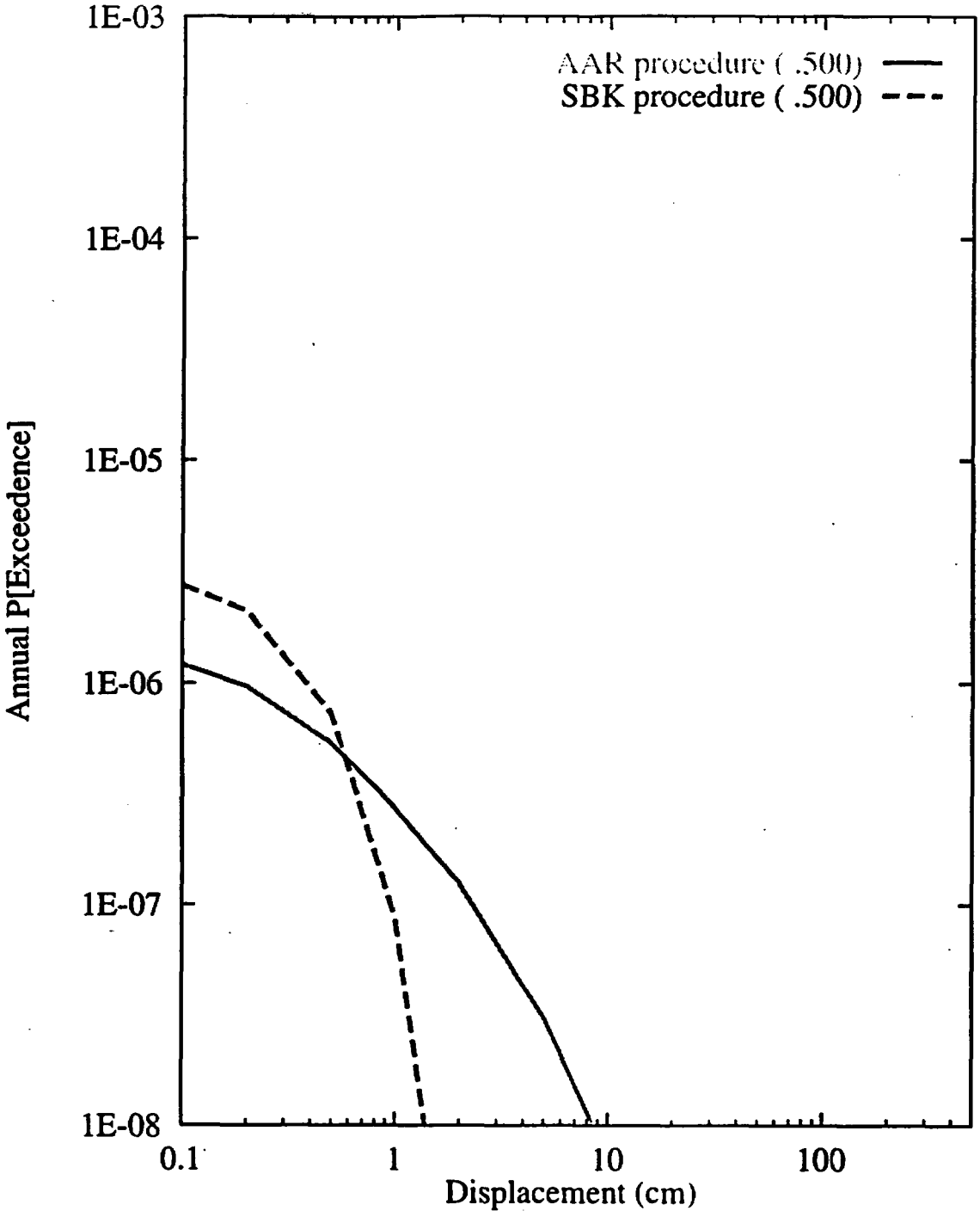

Figure 8-71 Sensitivity of displacement hazard for Site 7a to calculation of average displacement per event: SDO team, displacement approach

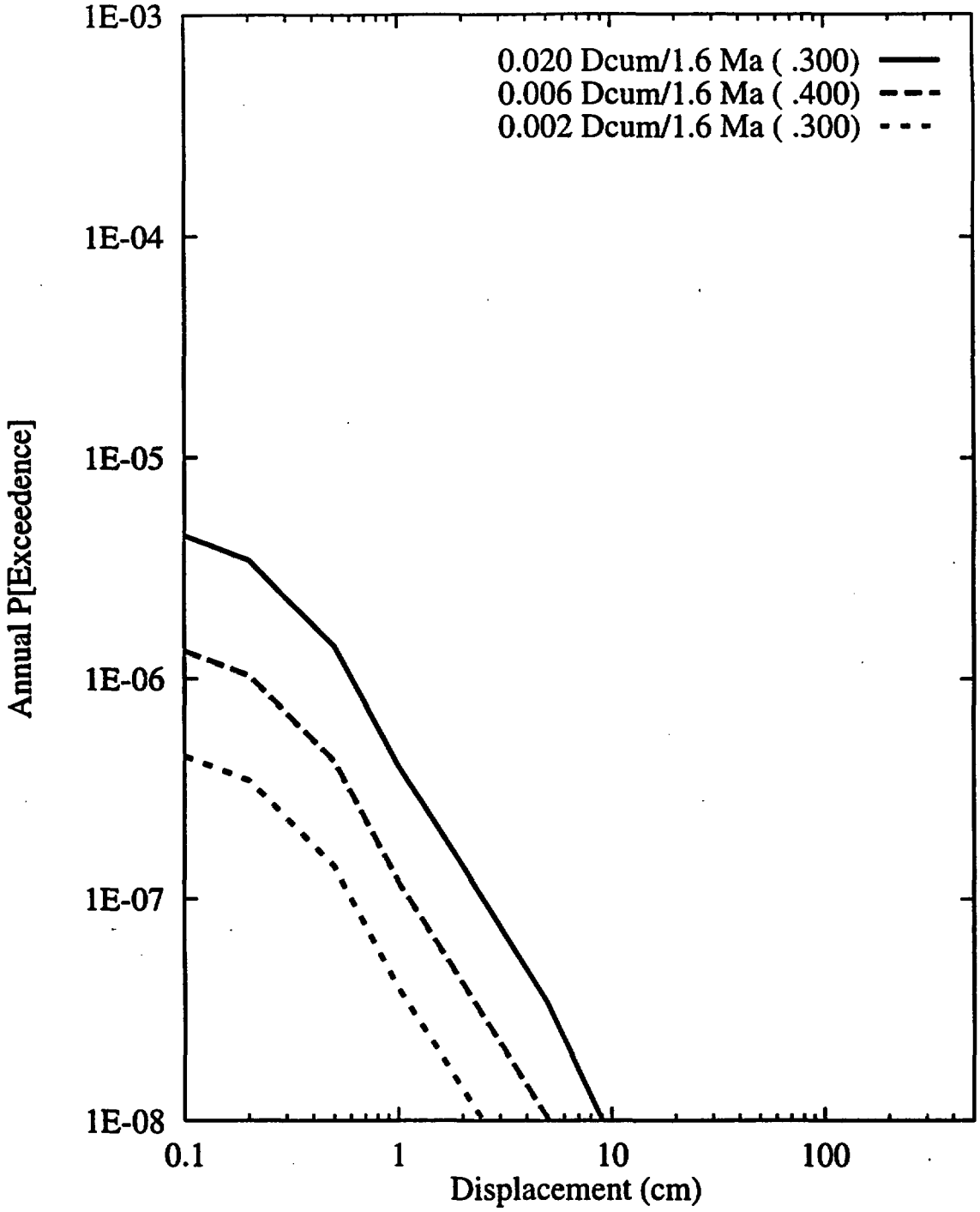

Figure 8-72 Sensitivity of displacement hazard for Site 7a to calculation of slip rate: SDO team, displacement approach

9.0

REFERENCES

Abrahamson, N.A., and Silva, W.J., 1997, Empirical response spectral attenuation relations for shallow crustal earthquakes: Seismological Research Letters v. 68, p. 94-127.

Anderson, J.G., 1979, Estimating the seismicity from geological structure for seismic risk studies: Bulletin of the Seismological Society of America, v. 69, p. 135-158.

Anderson, R.E., Buckman, R.C., Crone, A.J., Haller, K.M., Machette, M.N., Personius, S.F., Barnhard, T.P., Cecil, M.J., and Dart, R.L., 1995a, Characterization of Quaternary and suspected Quaternary faults, regional studies, Nevada and California: U.S. Geological Survey Open-File Report 95-599, 56 p. plus appendices.

Anderson, R.E., Crone, A.J., Machette, M.N., Bradley, L.A., and Diehl, S.F, 1995b, Characterization of Quaternary and suspected Quaternary faults, Amargosa area, Nevada and California: U.S. Geological Survey Open-File Report 95-613, 41 p. plus appendices.

Anderson, J.G., Wesnousky, S.G., and Stirling, M.W., 1996, Earthquake size as a function of fault slip rate: Bulletin of the Seismological Society of America, v. 86, p. 683-690.

Boore, D.M., Joyner, W.B., and Fumal, T.E., 1994, Estimation of response spectra and peak accelerations from western North American earthquakes: An interim report, part 2: U.S. Geological Survey Open-File Report 94-127, 40 p.

Boore, D.M., Joyner, W.B., and Fumal, T.E., 1997, Equations for estimating horizontal response spectra and peak acceleration from western North American earthquakes: A summary of recent work: Seismological Research Letters, v. 68, p.128 - 153.

Campbell, K.W., 1981, A ground motion model for the central United States based on near-source acceleration data, *in* Proceedings, Conference on Earthquakes and Earthquake Engineering: The Eastern United States: Ann Arbor, Michigan, Ann Arbor Science Publishers, v. 1, p. 213-232.

Campbell, K.W., 1990, Empirical prediction of near-source soil and soft-rock ground motion for the Diablo Power Plant site, San Luis Obispo County, California: Report prepared for Lawrence Livermore National Laboratory by Dames & Moore, 110 p.

Campbell, K.W., 1993, Empirical prediction of near-source ground motion from large earthquakes, *in* V.K. Gaur, ed., Proceedings, International Workshop on Earthquake Hazard and Large Dams in the Himalaya: New Delhi, India, Indian National Trust for Art and Cultural Heritage (INTACH), p. 93-103.

Campbell, K.W., 1997, Empirical near-source attenuation relationships for horizontal and vertical components of peak ground acceleration, peak ground velocity, and pseudo-absolute acceleration response spectra: Seismological Research Letters, v. 68, p. 154-179.

Campbell, K.W., and Bozorgnia, Y., 1994, Near-source attenuation of peak horizontal acceleration from worldwide accelerograms recorded from 1957 to 1993: 5th U.S. Nat. Conf. on Eq. Eng., Chicago, IL, July 10-14.

Civilian Radioactive Waste Management System Management and Operating Contractor (CRWMS M&O), 1994, Seismic design inputs for the Exploratory Studies Facility at Yucca Mountain: Prepared for the U.S. Department of Energy, variously paginated.

Civilian Radioactive Waste Management System Management and Operating Contractor (CRWMS M&O), 1997a, Seismic source and fault displacement characterization project: Prepared by Geomatrix Consultants, Inc., for the U.S. Geological Survey, variously paginated.

Civilian Radioactive Waste Management System Management and Operating Contractor (CRWMS M&O), 1997b, Ground motion characterization at Yucca Mountain, Nevada: Prepared by N. Abrahamson and A. Becker for the U.S. Geological Survey, variously paginated.

Civilian Radioactive Waste Management System Management and Operating Contractor (CRWMS M&O), 1998, Probabilistic seismic hazard calculations for Yucca Mountain, Nevada: Prepared by Risk Engineering, Inc., for the U.S. Geological Survey, variously paginated.

Coats, D.W., and Murray, R.C., 1984, Natural phenomena hazards modeling project: Seismic hazard models for U.S. Department of Energy sites: Lawrence Livermore National Laboratory Report UCRL-15910.

Coppersmith, K.J., and Youngs, R.R., 1986, Capturing uncertainty in probabilistic seismic hazard assessment within intraplate tectonic environments, *in* Proceedings, Third U.S. National Conference on Earthquake Engineering: Earthquake Engineering Research Institute, v. 1, p. 301-312.

Cornell, C.A., 1968, Engineering seismic risk analysis: Bulletin of the Seismological Society of America, v. 58, p. 1583-1606.

Cornell, C.A., 1971, Probabilistic analysis of damage to structures under seismic loads, *in* Howells, D.A., Haigh, I.P., and Taylor, C., eds., Dynamic Waves in Civil Engineering: London, John Wiley.

Cornell, C.A., and Van Marke, E.H., 1969, The major influences on seismic risk, *in* Proceedings, Third World Conference on Earthquake Engineering, Santiago Chile: v. A-1, p. 3-14.

dePolo, C.M., 1994, The maximum background earthquake in the Basin and Range: Bulletin of the Seismological Society of America, v. 84, p. 466-472.

Electric Power Research Institute (EPRI), 1986, Seismic hazard methodology for the central and eastern United States: NP-4726, v. 1-10.

Electric Power Research Institute (EPRI), 1988, Seismic hazard methodology for the Central and Eastern United States: NP-4726-A (revised), v. 1-10.

Electric Power Research Institute (EPRI), 1989, Probabilistic seismic hazard evaluations at nuclear plant sites in the Central and Eastern United States, Resolution of the Charleston Earthquake Issue: NP-6395-D.

Electric Power Research Institute (EPRI), 1993, Guidelines for determining design basis ground motions: TR-102293, v. 1-5.

Frankel, A., 1995, Mapping seismic hazard in the central and eastern United States: Seismological Research Letters, v. 66, p. 8-21.

Frankel, A., Mueller, C., Barnhard, T., Perkins, D., Leyendecker, E.V., Dickman, N., Hanson, S., and Hopper, M., 1996, National seismic-hazard maps—documentation: U.S. Geological Survey Open-File Report 96-532, 110 p.

Gutenberg, B., and Richter, C.F., 1954, Seismicity of the earth and associated phenomena: Princeton, New Jersey, Princeton University Press, 310 p.

Gutenberg, B., and Richter, C.F., 1956, Earthquake magnitude, intensity, energy, and acceleration: Bulletin of the Seismological Society of America, v. 46, p. 105-145.

Hanks, T.C., and Kanamori, H., 1979, A moment-magnitude scale: Journal of Geophysical Research, v. 84, p. 2348-2350.

Hosmer, D.W. Jr., and Lemeshow, S., 1989, Applied logistic regression: New York, John Wiley & Sons, 307 p.

Idriss, I. M., 1993, Procedures for selecting earthquake ground motions at rock sites: Report to National Institute of Standards and Technology.

Johnston, A.C., Coppersmith, K.J., Kanter, L.R., and Cornell, C.A., 1994, The earthquakes of stable continental regions, v. 1—Assessment of large earthquake potential: Report prepared for the Electric Power Research Institute (EPRI), TR-102261-V1.

Joyner, W. B., and Boore, D. M., 1993, Methods for regression analysis of strong-motion data: Bulletin of the Seismological Society of America. v. 83, p. 469-487.

Keefer, D.L., and Bodily, S.E., 1983, Three-point approximations for continuous random variables: Management Science, v. 29, p. 595-609.

Keefer, W.R., and Pezzopane, S.K., 1996, Quaternary faults in the Yucca Mountain region, *in* Seismotectonic Framework and Characterization of Faulting at Yucca Mountain, Nevada: U.S. Geological Survey Report to U.S. Department of Energy, Chapter 3, p. 3-1 to 3-34.

Kulkarni, R.B., Youngs, R.R., and Coppersmith, K.J., 1984, Assessment of confidence intervals for results of seismic hazard analysis, *in* Proceedings, Eighth World Conference on Earthquake Engineering: v. 1, p. 263-270.

McGarr, A., 1984, Scaling of ground motion parameters, state of stress, and focal depth: Journal of Geophysical Research, v. 89, p. 6969-6979.

McGuire R.K., 1976, FORTRAN Computer Program for Seismic Risk Analysis: U.S. Geological Survey Open-File Report 76-67.

McGuire R.K., 1978, FRISK: Computer program for seismic risk analysis using faults as earthquake sources: U.S. Geological Survey Open-File Report 78-1007.

McKaque, H.L., Stamatakos, J.A., and Ferrill, D.A., 1996, Type I faults in the Yucca Mountain region: Prepared by Center for Nuclear Waste Regulatory Analyses for Nuclear Regulatory Commission, Report CNWRA 96-007, variously paginated.

Meyer, M.A., and Booker, J.M., 1991, Eliciting and analyzing expert judgment: A practical guide: San Diego, California, Academic Press Inc., , 452 p.

Miller, A., and Rice, T., 1983, Discrete approximations to probability distributions: Management Science, v. 29, p. 352-362.

Morris, A., Ferrill, D.A., and Henderson, D.B., 1996, Slip-tendency analysis and fault reactivation: Geology, v. 24, p. 275-278.

Parzen, E., 1962, Stochastic processes: San Francisco: Holden-Day

Pezzopane, S.K., 1996, Relevant earthquake sources, *in* Seismotectonic Framework and Characterization of Faulting at Yucca Mountain, Nevada: U.S. Geological Survey Report to U.S. Department of Energy, Chapter 11, p. 11-1 to 11-44.

Pezzopane, S.K., and Dawson, T.E., 1996, Fault displacement hazard: A summary of issues and information, *in* Seismotectonic Framework and Characterization of Faulting at Yucca Mountain, Nevada: U.S. Geological Survey Report to U.S. Department of Energy, Chapter 9, p. 9-1 to 9-160.

Pezzopane, S.K., Whitney, J.W., and Dawson, T.E., 1996, Models of earthquake recurrence and preliminary paleoearthquake magnitudes at Yucca Mountain, *in* Seismotectonic Framework and Characterization of Faulting at Yucca Mountain, Nevada: U.S. Geological Survey Report to the U.S. Department of Energy, Chapter 5, variously paginated.

Piety, L., 1995, Compilation of known or suspected Quaternary faults within 100 km of Yucca Mountain, Nevada and California: U.S. Geological Survey Open-File Report 94-112, variously paginated, 2 plates, scale 1:250,000.

Rogers, A.M., Woulett, G.M., and Covington, P.A., 1977, Seismicity of the Pahute Mesa area, Nevada Test Site, 8 October 1975 to 30 June 1976: U.S. Geological Survey Report 474-184.

Sabetta, F., and Pugliese, A., 1996, Estimation of response spectra and simulation of nonstationary earthquake ground motions: Bulletin of the Seismological Society of America, v. 86, p. 337-352.

Sadigh, K., Chang, C-Y., Abrahamson, N.A., Chiou, S.J., and Power, M.S., 1993, Specification of long-period ground motions: Updated attenuation relationships for rock site conditions and adjustment factors for near-fault effects, *in* Proceedings, ATC-17-1 Seminar on Seismic Isolation, Passive Energy Dissipation, and Active Control: v. 1, p. 59-70.

Sadigh, K., Chang, C.-Y., Egan, J.A., Makdisi, F., and Youngs, R.R., 1997, Attenuation relationships for shallow crustal earthquakes based on California strong motion data: Seismological Research Letters, v. 68, p. 180-189.

Schneider, J.F., Abrahamson, N.A., and Hanks, T.C., 1996, Ground motion modeling of scenario earthquakes at Yucca Mountain: Final Report for Activity 8.3.1.17.3.3, variously paginated.

Senior Seismic Hazard Analysis Committee (SSHAC), 1997, Recommendations for probabilistic seismic hazard analysis: Guidance on uncertainty and use of experts: U.S. Nuclear Regulatory Commission (NRC) NUREG/CR-6372, Washington, D.C.

Siddharthan, R., Anderson, J.G., Bell, J.W., and dePolo, C.M., 1993, Peak bedrock acceleration for State of Nevada: Final Report to Nevada Department of Transportation, 51 p.

Silverman, B.W., 1986, Density estimation for statistics and data analysis: Monographs on Statistics and Applied Probability 26, Chapman and Hall, New York.

Spudich, P., Fletcher, J.B., Hellweg, M., Boatwright, J., Sullivan, C., Joyner, W.B., Hanks, T.C., Boore, D.M., McGarr, A., Baker, L.M., and Lindh, A.G., 1996, Earthquake ground motions in extensional tectonic regimes: U.S. Geological Survey Open-File Report 96-292, 351 p.

Spudich, P., Fletcher, J.B., Hellweg, M., Boatwright, J., Sullivan, C., Joyner, W.B., Hanks, T.C., Boore, D.M., McGarr, A., Baker, L.M., and Lindh, A.G, 1997, SEA96 -- a new predictive relation for earthquake ground motions in extensional tectonic regimes: Seismological Research Letters, v. 68, p. 190-198.

Toro, G.R., Abrahamson, N.A., and Schneider, J.F., 1997, A model of strong ground motions from earthquakes in Central and Eastern North America: Best estimates and uncertainties: Seismological Research Letters, v. 68, p. 41-57.

URS/John A. Blume & Associates, 1986, Ground motion evaluations at Yucca Mountain, Nevada, with applications to repository conceptual design and siting: Prepared for Sandia National Laboratories, 140 p.

URS/John A. Blume & Associates, 1987, Technical basis and parametric study of ground motion and surface rupture hazard evaluations at Yucca Mountain, Nevada: Prepared for Sandia National Laboratories, 98 p.

U.S. Department of Energy (DOE), 1995, Principles and guidelines for formal use of expert judgment by the Yucca Mountain site characterization project: Office of Civilian Radioactive Waste Management, Yucca Mountain Site Characterization Office, May, 10 p.

U.S. Department of Energy (DOE), 1996, Topical Report YMP/TR-003-NP: Preclosure Seismic Design Methodology for a Geologic Repository at Yucca Mountain, Rev. 1: U. S. Department of Energy, Office of Civilian Radioactive Waste Management, Las Vegas, NV.

U.S. Department of Energy (DOE), 1997a, Topical report YMP/TR-002-NP: Methodology to assess fault displacement and vibratory ground motion hazards at Yucca Mountain, Revision 1: Civilian Radioactive Waste Management System Management and Operating Contractor .

U.S. Department of Energy (DOE), 1997b, Topical report YMP/TR-003-NP: Preclosure seismic design methodology for a geologic repository at Yucca Mountain, Revision 2: Civilian Radioactive Waste Management System Management and Operating Contractor.

U.S. Geological Survey (USGS), 1996, Seismotectonic framework and characterization of faulting at Yucca Mountain, Nevada (Whitney, J.W., Coordinator): U.S. Geological Survey Report to the Department of Energy, v. 1-4, variously paginated.

U.S. Nuclear Regulatory Commission (NRC), 1988, Safety evaluation review of SOG/EPRI report, "Seismic Hazard Methodology for the Central and Eastern United States": Washington, DC.

U.S. Nuclear Regulatory Commission (NRC), 1991, Individual Plant Examination of External Events (IPEEE): Generic Letter No. 88-20, Supplement 4.

U.S. Nuclear Regulatory Commission (NRC), 1992, Staff technical position on investigations to identify fault displacement hazards and seismic hazards at a geologic repository: NUREG-1451.

U.S. Nuclear Regulatory Commission (NRC), 1994, Staff technical position on consideration of fault displacement hazards in geologic repository design: NUREG-1494.

U.S. Nuclear Regulatory Commission (NRC), 1996, Branch technical position on the use of expert elicitation in the high-level radioactive waste program: NUREG-1563, Washington, D.C.

U.S. Nuclear Regulatory Commission (NRC), 1997a, Recommendations for probabilistic seismic hazard analysis: Guidance on uncertainty and use of experts: NUREG/CR-6372, Washington, DC.

U.S. Nuclear Regulatory Commission (NRC), 1997b, Identification and characterization of seismic sources and determination of safe shutdown earthquake ground motion: Regulatory Guide 1.165.

Veneziano, D., and van Dyck, J., 1985, Statistical discrimination of "aftershocks" and their contribution to seismic hazard, *in* Seismic hazard methodology for nuclear facilities in the eastern United States: EPRI Research Project No. P101-29, Appendix A-4, p. A121-A186.

Weichert, D.H., 1980, Estimation of the earthquake recurrence parameters for unequal observation periods for different magnitudes: Bulletin of the Seismological Society of America, v. 70, p. 1337-1346.

Wells, D.L., and Coppersmith, K.J., 1993, Likelihood of surface rupture as a function of magnitude: Seismological Research Letters, v. 64, p. 54.

Wells, D.L., and Coppersmith, K.J., 1994, New empirical relationships among magnitude, rupture length, rupture width, rupture area, and surface displacement: Bulletin of the Seismological Society of America, v. 84, p. 974-1002.

Wesnousky, S.G., Scholz, C.H., Shimazaki, K., and Matsuda, T., 1983, Earthquake frequency distribution and the mechanics of faulting: Journal of Geophysical Research, v. 88, p. 9331-9340.

Westaway, R., and Smith, R.B., 1989, Strong ground motion in normal-faulting earthquakes: Geophysical Journal, v. 96, p. 529-559.

Wheeler, R.L., 1989, Persistent segment boundaries on Basin-Range normal faults, *in* Proceedings, Conference XLV-Fault Segmentation and Controls on Rupture Initiation and Termination, D.P., Schwartz and R.H. Sibson, eds.: U.S. Geological Survey Open-File Report 89-315, p. 432-444.

Wong, I.G., Pezzopane, S.K., Menges, C.M., Green, R.K., and Quittmeyer, R.C., 1996, Probabilistic seismic hazard analysis of the Exploratory Studies Facility at Yucca Mountain, Nevada, *in* Proceedings, Methods of Seismic Hazards Evaluation, Focus '95: American Nuclear Society, p. 51-63.

Wong, I.G., Pezzopane, S.K., Abrahamson, N.A., Green, R.K., Sun, J.I., and Quittmeyer, R.C., 1998, A preliminary assessment of earthquake ground shaking hazard at Yucca Mountain, Nevada, and implications to the Las Vegas region, *in* Proceedings, Seismic Hazards in the Las Vegas Region Conference: Nevada Bureau of Mines and Geology Special Publication (in press).

Youngs, R.R., and Coppersmith, K.J., 1985, Implications of fault slip rates and earthquake recurrence models for probabilistic seismic hazard estimates: Bulletin of the Seismological Society of America, v. 75, p. 939-964.

Youngs, R.R., Swan, F.H. III, Power, M.S., Schwartz, D.P., and Green, R.K., 1987, Probabilistic analysis of earthquake ground-shaking along the Wasatch front, Utah, *in* Hays, W.W., and Gori, P.L., eds., Assessment of Regional Earthquake Hazards and Risk Along the Wasatch Front, Utah: U.S. Geological Survey Open-File Report 87-585, v. II, p. M-1 through M-110.